Vol. 273, No 1–2, February 15, 1993
Complete in one issue

ISSN 0003-2670

Special issue
PAPERS PRESENTED AT THE FOURTH EUROPEAN CONFERENCE ON ELECTROANALYSIS (ESEAC '92), NOORDWIJKERHOUT, THE NETHERLANDS, MAY 31–JUNE 3, 1992

ANALYTICA CHIMICA ACTA

An international journal devoted to all branches of analytical chemistry

ELSEVIER

ANALYTICA CHIMICA ACTA

Scope. *Analytica Chimica Acta* publishes original papers, preliminary communications and reviews dealing with every aspect of modern analytical chemistry. Reviews are normally written by invitation of the editors, who welcome suggestions for subjects. Preliminary communications of important urgent work can be printed within four months of submission, if the authors are prepared to forego proofs.

Submission of Papers

Americas

Prof. Harry L. Pardue
Department of Chemistry
1393 BRWN Bldg, Purdue University
West Lafayette, IN 47907-1393
USA
Tel:(+1-317) 494 5320
Fax:(+1-317) 496 1200

Computer Techniques

Prof. J.T. Clerc
Universität Bern
Pharmazeutisches Institut
Baltzerstrasse 5, CH-3012 Bern
Switzerland
Tel:(+41-31) 654171
Fax:(+41-31) 654198

Other Papers

Prof. Alan Townshend
Department of Chemistry
The University
Hull HU6 7RX
Great Britain

Tel:(+44-482) 465027
Fax:(+44-482) 466410

Prof. Willem E. van der Linden
Laboratory for Chemical Analysis
Department of Chemical Technology
Twente University of Technology
P.O. Box 217, 7500 AE Enschede
The Netherlands
Tel:(+31-53) 892629
Fax:(+31-53) 356024

Prof. Paul Worsfold
Dept. of Environmental Sciences
University of Plymouth
Plymouth PL4 8AA
Great Britain

Tel:(+44-752) 233006
Fax:(+44-752) 233009

Submission of an article is understood to imply that the article is original and unpublished and is not being considered for publication elsewhere. *Anal. Chim. Acta* accepts papers in English only. There are no page charges. Manuscripts should conform in layout and style to the papers published in this issue. See inside back cover for "Information for Authors".

Publication. *Analytica Chimica Acta* appears in 14 volumes in 1993. The subscription price for 1993 (Vols. 267–280) is Dfl. 4214.00 plus Dfl. 462.00 (p.p.h.) (total approx. US$ 2816.75). *Vibrational Spectroscopy* appears in 2 volumes in 1993. The subscription price for *Vibrational Spectroscopy* (Vols. 4 and 5) is Dfl. 700.00 plus Dfl. 66.00 (p.p.h.) (total approx. US$ 461.50). The price of a combined subscription (*Anal. Chim. Acta* and *Vib. Spectrosc.*) is Dfl. 4592.00 plus Dfl. 528.00 (p.p.h.) (total approx. US$ 3084.25). All earlier volumes (Vols. 1–266) except Vols. 23 and 28 are available at Dfl. 259.50 (US$ 156.25), plus Dfl. 18.00 (US$ 10.75) p.p.h., per volume. The Dutch guilder price is definitive. The U.S. dollar price is subject to exchange-rate fluctuations and is given only as a guide. Subscriptions are accepted on a prepaid basis only, unless different terms have been previously agreed upon.
Our p.p.h. (postage, packing and handling) charge includes surface delivery of all issues, except to subscribers in the U.S.A., Canada, Australia, New Zealand, China, India, Israel, South Africa, Malaysia, Thailand, Singapore, South Korea, Taiwan, Pakistan, Hong Kong, Brazil, Argentina and Mexico, who receive all issues by air delivery (S.A.L.–Surface Air Lifted) at no extra cost. For Japan, air delivery requires 25% additional charge of the normal postage and handling charge; for all other countries airmail and S.A.L. charges are available upon request.

Subscription orders. Subscription orders can be entered only by calendar year and should be sent to: Elsevier Science Publishers B.V., Journals Department, P.O. Box 211, 1000 AE Amsterdam, The Netherlands. Tel: (+31-20) 5803 642, Telex: 18582, Telefax: (+31-20) 5803598, to which requests for sample copies can also be sent. Claims for issues not received should be made within six months of publication of the issues. If not they cannot be honoured free of charge. Readers in the U.S.A. and Canada can contact the following address: Elsevier Science Publishing Co. Inc., Journal Information Center, 655 Avenue of the Americas, New York, NY 10010, U.S.A. Tel: (+1-212) 6333750, Telefax: (+1-212) 6333990, for further information, or a free sample copy of this or any other Elsevier Science Publishers journal.
Advertisements. Advertisement rates are available from the publisher on request.

Detailed "Instructions to Authors" for *Analytica Chimica Acta* was published in Volume 256, No. 2, pp. 373–376. Free reprints of the "Instructions to Authors" of *Analytica Chimica Acta* and *Vibrational Spectroscopy* are available from the Editors or from: Elsevier Science Publishers B.V., P.O. Box 330, 1000 AH Amsterdam, The Netherlands. Telefax: (+31-20) 5862845.

US mailing notice – Analytica Chimica Acta (ISSN 0003-2670) is published biweekly by Elsevier Science Publishers (Molenwerf 1, Postbus 211, 1000 AE Amsterdam). Annual subscription price in the USA US$ 2816.75 (subject to change), including air speed delivery. Second class postage paid at Jamaica, NY 11431. *USA Postmasters*: Send address changes to Anal. Chim. Acta, Publications Expediting, Inc., 200 Meacham Av., Elmont, NY 11003. Airfreight and mailing in the USA by Publication Expediting.

ANALYTICA CHIMICA ACTA

An international journal devoted to all branches of analytical chemistry

(Full texts are incorporated in CJELSEVIER, a file in the Chemical Journals Online database available on STN International; Abstracted, indexed in: Aluminum Abstracts; Anal. Abstr.; Biol. Abstr.; BIOSIS; Chem. Abstr.; Curr. Contents Phys. Chem. Earth Sci.; Engineered Materials Abstracts; Excerpta Medica; Index Med.; Life Sci.; Mass Spectrom. Bull.; Material Business Alerts; Metals Abstracts; Sci. Citation Index)

VOL. 273 NO. 1–2 CONTENTS FEBRUARY 15, 1993

Papers presented at the Fourth European Conference on Electroanalysis, Noordwijkerhout, The Netherlands, May 31–June 3, 1992

(Continued overleaf)

Contents (continued)

(Continued overleaf)

Contents (continued)

ANALYTICA CHIMICA ACTA
VOL. 273 (1993)

ANALYTICA CHIMICA ACTA

An international journal devoted to all branches of analytical chemistry
Revue internationale consacrée à tous les domaines de la chimie analytique
Internationale Zeitschrift für alle Gebiete der analytischen Chemie

Anal. Chim. Acta, Vol. 273 (1993)

ELSEVIER, Amsterdam–London–New York–Tokyo

0003-2670/93/$06.00

This issue is printed on acid-free paper.

PRINTED IN THE NETHERLANDS

SPECIAL ISSUE

PAPERS PRESENTED AT THE FOURTH EUROPEAN CONFERENCE ON ELECTROANALYSIS (ESEAC '92), NOORDWIJKERHOUT, THE NETHERLANDS, MAY 31–JUNE 3, 1992

Analytica Chimica Acta, 273 (1993) 1
Elsevier Science Publishers B.V., Amsterdam

FOREWORD

The *Fourth European Conference on Electroanalysis (ESEAC'92)* was held in Noordwijkerhout, The Netherlands, May 31–June 3, 1992. This series of biannual European meetings was started in 1986, with a conference held in Dublin (Ireland) where Professor Malcolm Smyth was in charge. The second conference was organized by Professor Ari Ivaska in Turku (Finland) in 1988. Professors Paulino Tuñón Blanco and Lucas Hernández Hernández organized the third conference in Gijon (Spain) in 1990. ESEAC'92 continued the success story of the first three conferences: about 180 persons from more than 30 countries contributed an excess of 130 contributions to the scientific program. The interest shown in the various topics indicates the vitality and maturity of electroanalytical chemistry as a science.

This volume of *Analytica Chimica Acta* contains a large number of the papers which were presented at the conference in Noordwijkerhout.

An important goal of the organizers was to open up the conference to scientists from East-European countries who have a long tradition in electrochemistry and electroanalytical chemistry. These people, who are now able to travel and communicate freely were, nevertheless, faced with the problem of financing their visit to ESEAC'92. More than 15 grants were awarded by the organizers to scientists from these countries. We hope that the situation will improve in the near future and that the organizers of future conferences will continue this initiative.

The organizers would like to take the opportunity to thank the Royal Dutch Chemical Society, the exhibitors and the industrial sponsors for their support in arranging the conference. We would, however, especially like to thank the participants.

The organizers of ESEAC'92 were proud to receive many positive post-conference reactions indicating that their primary goal: organizing a "stimulating analytical conference" had been realized.

The next conference, ESEAC'94, will be held near Venice (Italy) in 1994.

Wouter P. van Bennekom
(Chairman)

Analytica Chimica Acta, 273 (1993) 3–11
Elsevier Science Publishers B.V., Amsterdam

Stripping analysis at mercury microelectrodes in the absence of supporting electrolyte

Salvatore Daniele and Gian Antonio Mazzocchin

Department of Physical Chemistry, University of Venice, Calle Larga S. Marta 2137, I-30123 Venice (Italy)

(Received 1st June 1992; revised manuscript received 27th August 1992)

Abstract

Anodic stripping voltammetry of cadmium and lead in pure water, of conductivity as low as 0.6 μS, was studied at a mercury microelectrode obtained by ex situ deposition of mercury on a 10-μm radius platinum disc electrode. The anodic stripping peaks were investigated in detail to verify the influences of the solution resistance and migration on peak position (E_p), peak width at half-height ($W_{1/2}$) and peak current. The results showed that the presence of a small ohmic drop leads to larger $W_{1/2}$ values than those obtained in the presence of supporting electrolyte, while the peak position varied slightly as a consequence of a change in the liquid junction potential. For concentrations of the metal ion higher than 0.1 μM, a contribution due to migration added to the diffusion current when the samples were examined in the absence of supporting electrolyte. The results were also compared with theoretical predictions; in particular, the effects of migration were studied and transferred to a quantitative basis.

Keywords: Stripping voltammetry; Cadmium; Lead; Mercury microelectrodes; Water

Anodic stripping voltammetry (ASV) is inherently a very sensitive technique and it has been widely used for the trace analysis of heavy metals [1]. When coupled with mercury microelectrodes, a number of advantages can be achieved in comparison with larger traditional hanging mercury drop electrodes (HMDE) and mercury film electrodes (MFE). Fast steady-state mass transport by non-planar diffusion obviates the need for stirring during the preconcentration step, leading to improved precision and faster analysis times. The low *iR* drop at microelectrodes has enabled measurements to be performed in solutions of high resistance [2,3] and aqueous media of low ionic strength [4–10]. For ultratrace analysis, microelectrodes are well suited as the addition of the supporting electrolyte is not required and therefore minimizes possible contamination from external chemicals and further avoids alterations of the existing chemical equilibria. This is of particular interest when investigations on speciation have to be performed.

The tolerance of microelectrodes towards low electrolyte levels for most electrode reactions has been explained theoretically [11] and it is due to the fact that the ionic content close to the electrode surface is enriched with respect to the bulk. The low concentration or, as a limiting case, the absence of supporting electrolytes, may induce migration, however, which leads to diffusion as the transport mechanism for the electroreactant. This aspect has been treated in a number of papers [11–16]. A study of this series has been concerned with cylindrical electrodes [13] where no true steady-state develops, unlike micro-disc and micro-hemispherical electrodes used in this work [11,12,14,15,16], where a true steady state may be obtained at least theoretically. Among the

Correspondence to: S. Daniele, Department of Physical Chemistry, University of Venice, Calle Larga S. Marta 2137, I-30123 Venice (Italy).

studies on these last types of electrodes the most straighforward theoretical method is that of Oldham [11]. None of these studies, however, takes into account the typical experimental conditions of stripping analysis, e.g., diluted solutions of the electroreactant.

ASV measurements with microelectrodes carried out with no deliberately addition of supporting electrolyte have been reported; these studies were concerned with the method of in situ plating mercury film [7–10] and therefore mercury ions were added to the solutions along with the investigated species.

In contrast, in this paper a study is presented in which stripping measurements were carried out under the particular conditions of pure water spiked only with the salts of the heavy metal cations studied. A comparison was also made with the case in which the solutions contained large amounts of a non-electroactive current carrier with the aim to ascertaining the effects on the stripping peaks caused by the solution resistance and the migration contribution to the mass transport. The features of the voltammograms were examined on the basis of existing theory and results compared with theoretical predictions. This study represents a model for determining heavy metals in ultrapure water samples by ASV.

EXPERIMENTAL

Instrumentation and reagents

Most of the experiments described were done with a Model 273 potentiostat/galvanostat (EG&G PARC), controlled with an Olivetti M 380 personal computer via EG&G PAR 270 software. Cyclic voltammograms to estimate the radius of the platinum microelectrode were done in a two-electrode cell configuration and the waveform was generated by a PAR 175 function generator; in this instance a Keithley 485 picoammeter served as a current-measuring device and data were plotted with a *X–Y* recorder (Hewlett-Packard 7045B). The cell for experiments was maintained in a Faraday cage made of sheets of aluminium. Unless stated otherwise, the reference electrode was a saturated calomel electrode (SCE), which was separated from the cell by a bridge containing the same solution as in the cell or pure water, depending on whether the measurements were performed with or without supporting electrolyte, respectively.

All chemicals were of analytical-reagent grade and used as received. All the solutions were prepared with water purified with a Milli-Q system (Millipore). Nitrogen (99.99%) was used to remove oxygen from the test solutions.

The stripping measurements were carried out on Milli-Q-purified water having the same characteristics as that used to prepare stock solutions of the reagents. To about 20 ml of this sample, the solutions of heavy metals were added in appropriate amounts. The electrochemical cell was a laboratory-made PTFE cup which was cleaned before the experiments using recommended procedures for trace analysis [17]. All measurements were made at room temperature.

Microelectrode preparation

Working mercury microelectrodes were prepared, in a separate cell different from that used for ASV, by electrodeposition of mercury on a platinum micro-disc electrode of 10 μm radius fabricated by sealing a 10-μm wire into glass. The platinum microelectrode was polished with alumina powder (0.05 μm) on a polishing microcloth. Its effective radius was determined periodically by recording the steady-state limiting current from a 1 mM ferrocene solution in acetonitrile and verifying that the experimental value was equal to that predicted by the equation [18]

$$i_d = 4nFDCr \quad (1)$$

where r is the radius of the micro-disc and the other symbols have their usual meanings.

Deposition of mercury was carried out under potentiostatic conditions at high overpotential: the working potential employed was in the range -0.1 to -0.2 V vs. a mercury pool. The plating solutions consisted of a 12.5 mM $Hg_2(NO_3)_2$ solution at pH < 1 (acidified with nitric acid). Under these conditions, an increase in the current was observed and the chronoamperometric curve was linear with time for $t > 5$ s and the equation

describing this behaviour has the form i (nA) = 97.4 + 0.511t (s) with a correlation coefficient of 0.999; from ten replicates the R.S.D.s for the intercept and slope were within 6 and 10%, respectively. This behaviour agrees with data reported by others [4,19] for platinum disc electrodes larger than 2 μm in diameter. The geometry of the deposit obtained is that of spherical segments with varying height (h) and constant base, that is, the radius of the substrate electrode. From the plating charge the height (h) of the deposits can be calculated [19]. The charge corresponding to the amount of mercury deposited ranged from 13.8 to 34.9 μC and the thicknesses of the deposits varied from about 10 to about 20 μm, respectively. By visual inspection with a Wild Leitz M8 microscope at $\times$256 magnification, it was observed that the mercury film deposited covered the metal substrate completely. Mercury microelectrodes with the above characteristics were employed for stripping measurements.

After the mercury electrode had been prepared, it was removed from the plating solution, rinsed carefully with ultrapure water and then transferred to the cell for the stripping analysis. The samples were kept quiescent during the preconcentration step and no rest period was employed before the anodic scan; in this last step linear-sweep voltammetry (LSV) was employed. The anodic stripping measurements were carried out on samples containing cadmium and lead.

RESULTS AND DISCUSSION

Conductivity and pH of the samples

The conductivity of pure water, free from carbon dioxide, should be 0.056 μs cm^{-1} if estimated by the equation

$$k = (F^2/RT)\sum_i z_i^2 D_i c_i^b$$

where k is the conductivity in μS cm^{-1}, z_i is the charge number and the other symbols have their usual meanings [11]. The conductivity of Milli-Q-purified water samples employed in this work had a value not greater than 0.1 μS cm^{-1} at the source, from the Millipore apparatus. However, measurements of conductivity performed in situ in the electrochemical apparatus on the degassed samples, displayed, on average, a value of 0.6 μS cm^{-1}. The frit at the end of the bridge of the reference electrode compartment should avoid sensible contamination from leakage of electrolyte from the reference electrode. To ascertain this fact the conductivity of the system, maintained under a nitrogen atmosphere, was monitored with time over about 90 min (a period of time which exceeds largely an experimental ASV sequence in this work). It was observed that the conductivity of the system increased up to about 20% with respect to its initial value. This means that contamination takes place mainly from the environment. Tests by ASV, for the heavy-metals blank levels were also performed before each series of experiments. The preconcentration step was carried out at -1 V for 25 min and in the anodic scan LSV at 30 mV s^{-1} was employed; these were typical ASV conditions used for the more dilute solutions examined in this work and only those samples which did not give stripping peaks were considered for further experiments.

A check of the pH was also made in order to verify whether deviations from neutrality took place on addition of the investigated cations; it was found that the pH was 7 ± 0.2 for the concentration levels investigated here.

Effects of the solution resistance on the ASV peaks

The static resistance of the solution in contact with a hemispherical electrode is given by $R = \frac{1}{2}\pi kr$, where k is the conductivity of the solution and r is the radius of the hemispherical electrode [11]. The values calculated with this equation depend on the concentrations of the species investigated; however, even for the more concentrated solution employed (0.5 μM), the calculated resistance are of the order of tens of MΩ. It follows that the shape of the stripping voltammograms could be affected by ohmic polarization. This point was investigated by evaluating the parameters that characterize the processes, in particular the peak position E_p and the peak width at half-height ($W_{1/2}$).

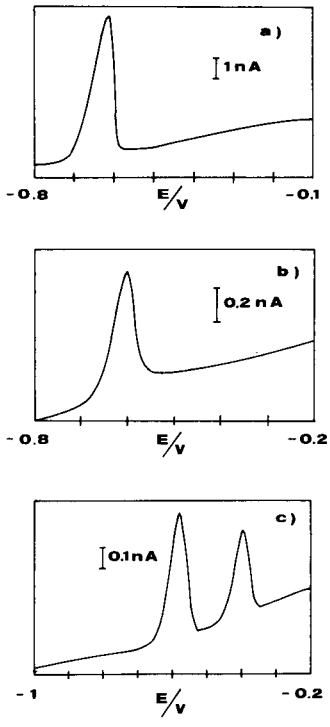

Fig. 1. Anodic stripping voltammograms recorded at mercury microelectrodes in pure water: (a) sample spiked with 5 μM Cd^{2+}, deposition for 120 s; (b) sample spiked with 1 μM Cd^{2+}, deposition for 240 s; (c) sample spiked with 0.02 μM Cd^{2+} and 0.01 μM Pb^{2+}, deposition for 900 s. Scan rate, 30 mV s^{-1}.

Figure 1 shows a series of stripping voltammograms for solutions containing different concentrations of Cd^{2+} and Pb^{2+}; the $W_{1/2}$ values and the peak potentials obtained are given in Table 1 without a supporting electrolyte and compared with those obtained in the presence of a supporting electrolyte. From Table 1 it appears that in the absence of supporting electrolyte the $W_{1/2}$ values are larger than those recorded in the presence of the supporting electrolyte. They increase with increase in the currents of the stripping peaks; for very low concentrations, however, the trend is reversed probably owing to the faster increase in the resistance with respect to the current. These results indicate the presence of an ohmic drop in the absence of supporting electrolyte, but to a lesser extent of that predicted from the static resistance (given by the above equation) and the current recorded experimentally. For instance, for an electrode process yielding 5 nA, occurring in a solution characterized by $R = 10$ MΩ, the iR drop is of 0.05 V. None of the voltammograms obtained in this work at scan rates lower than 1 V s^{-1} had such a large ohmic overvoltage. The tolerance towards the low electrolyte levels has been explained [11] by the fact that for reactions that generate an increase in

TABLE 2

Comparison of peak potentials for ASV of 0.5 μM Cd^{2+} solutions with and without supporting electrolytes (LSV at 30 mV s^{-1})

Supporting electrolyte	$-E_p$ (V)	Supporting electrolyte	$-E_p$ (V)
None	0.615	0.1 M $LiClO_4$	0.632
0.1 M HNO_3	0.630	0.01 M HCl	0.634
0.1 M $HClO_4$	0.633	0.1 M acetate buffer	0.652

TABLE 1

Comparison between characteristic ASV parameters obtained for solutions containing Cd^{2+} and Pb^{2+} at different concentrations with and without deliberate addition of a supporting electrolyte (LSV in the anodic scan 30 mV s^{-1})

Cation	$c(\mu M)$	t_d(s)	$W_{1/2}$ [a](V)	$-E_p$ [a](V)	i_p [a] (nA)	$W_{1/2}$ [b](V)	$-E_p$ [b] (V)	i_p [b] (nA)
Cd^{2+}	5	120	0.058	0.615	7.1	0.039	0.630	2.53
	1	240	0.048	0.610	1.5	0.038	0.629	1.09
	0.5	360	0.043	0.614	0.63	0.039	0.630	0.49
	0.01	900	0.055	0.589	0.15	0.040	0.628	0.16
Pb^{2+}	0.5	300	0.047	0.430	1.4	0.038	0.450	1.10
	0.1	600	0.042	0.420	0.31	0.035	0.440	0.29
	0.01	900	0.043	0.434	0.098	0.039	0.450	0.25
	0.001	1200	0.045	0.426	0.064	0.040	0.440	0.13

[a] Without supporting electrolyte. [b] With 0.1 M HNO_3 for Cd^{2+} and 0.01 M HCl for Pb^{2+}.

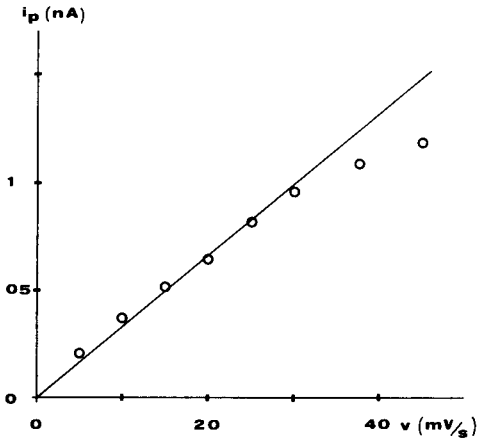

Fig. 2. Plot of the anodic stripping peak current vs. scan rate for 1 μM Cd^{2+} in pure water. Deposition for 240 s.

ionic strength at the microelectrode interface (as is the case for the stripping process), a redistribution of ions takes place, the counter ions will be brought into the neighbourhood of the electrode so effectively that a very low electrolyte concentration can behave as an excess of supporting electrolyte and consequently the ohmic drop is predicted to diminish.

With no deliberate addition of supporting electrolyte, the peak potentials change slightly with variation in the concentration of the metal ions, probably owing to a change in liquid junction potential. Compared with the corresponding values obtained in the presence of supporting electrolyte, the E_p values for Cd^{2+} are generally less negative (see Table 2). Similar effects, although to a lesser extent, are observed for Pb^{2+}.

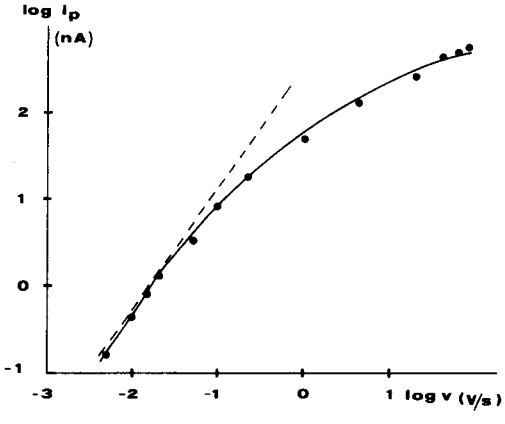

Fig. 3. Plot of log i_p vs. scan rate for 5 μM Cd^{2+} in 0.1 M HNO_3. Deposition time for 120 s.

The effect of scan rate (v) on the ASV peaks in the absence of deliberately added supporting electrolyte was also studied and Fig. 2 shows the trend of the peak current (i_p) against v for 1 μM Cd^{2+}. The trend is linear in the range 0.005–0.03 V s^{-1} and the correlation coefficient obtained was 0.999; for higher scan rates a deviation from linearity was observed. Similar findings were obtained for more concentrated and more diluted solutions. For comparison, a series of measurements were also made in the presence of a supporting electrolyte. Figure 3 shows the log i_p vs. log v plot obtained in this last case up to 80 V s^{-1}, from which a departure from linearity with increasing scan rate is apparent from about 50 mV s^{-1}, indicating that this deviation is not due to the absence of the supporting electrolyte. To verify whether at the highest scan rates employed linear diffusion occurs, i_p was plotted against $v^{1/2}$. A poor correlation coefficient (0.963) was found for the trend i_p vs. $v^{1/2}$, indicating that mixed spherical–linear diffusion conditions probably occur.

The experimental results can be compared with theoretical predictions. The model is that for ASV at an inlaid micro-disc mercury film [20] and the simple expressions describing the anodic stripping peaks are valid for small values of the dimensionless parameters of the thickness of the mercury film (H) and of the electrode radius (p), given by $H = nFl^2v/RTD_R$ and $p = (nFvr^2/D_o)^{1/2}$, where l is the thickness of the film, v the scan rate, D_R the diffusion coefficient of the reduced species in mercury and D_o the diffusion coefficient of the reactant. In particular for H and p smaller than 0.12, the following relationships hold [20]:

$$i_p = 0.367n^2(F^2/RT)Alc_R^0v \quad (2)$$

$$W_{1/2} = 2.32RT/nF \quad (3)$$

$$n(E_p - E_{1/2}) = -1.48RT/F + 1.15(RT/F)\log H \quad (4)$$

TABLE 3

Effects of scan rate on $W_{1/2}$ and peak potential for 1.5 μM Cd^{2+} solutions with and without deliberate addition of supporting electrolyte.

v (mV s^{-1})	$W_{1/2}$ [a] (±1 mV)	E_p [a] (±0.002 V)	$W_{1/2}$ [b] (±1 mV)	E_p [b] (±0.002 V)
10	47	0.638	36	0.645
20	48	0.627	37	0.638
25	49	0.623	38	0.634
30	49	0.619	38	0.631
50	52	0.602	42	0.624
100	55	0.600	47	0.616

[a] Without supporting electrolyte. [b] With 0.1 M HNO_3.

where A is the electrode surface area, c_R^0 is the concentration of the reduced species in mercury and the other symbols have their usual meanings.

Under the experimental conditions used here, by considering $l = h = 10$ μm and $v = 30$ mV s^{-1}, the parameters H and p have values of 0.129 and 0.563, respectively, which are higher than those for which Eqns. 2–4 hold. This could explain why at $v > 50$ mV s^{-1} the current departs from linearity and why the behaviour of the mercury microelectrode tends towards that for larger electrodes, i.e., linear diffusion against spherical diffusion. Actually, also for scan rates lower than 30 mV s^{-1} the parameter p exceeds 0.12 (at 5 mV s^{-1} for the experimental electrode, $p = 0.22$); nevertheless, i_p varies linearly with v. It must be noted that the equation is developed for a flat electrode whereas the experimental electrode is hemispherical and the approximation was made of considering the height of a spherical segment as that of a homogeneous film.

The effect of the scan rate on $W_{1/2}$ and peak position is reported in Table 3. The theory [20] predicts that $W_{1/2}$ is constant as a function of the scan rate for low H and p. Conversely, the experimental results display a dependence with a slight increase in the values both in the presence and in the absence of the supporting electrolyte and in both instances are larger than the theoretical value of 29.7 mV. The values recorded in the presence of the supporting electrolyte are closer to those predicted for a large MFE (37.5 mV) [21], in agreement with expectation for both a large H and a large p. Larger $W_{1/2}$ values can also be explained by the circumstance that the theoretical model differs not only with respect to the sphericity of the electrode but also in the presence in the solution of the oxidized material during the anodic scan [22].

Migration effects on the preconcentration step

Figure 4 shows the trend observed for the experimental current function (i_p/v) against the scan rate for 5 μM $CdCl_2$ solutions either containing or not the supporting electrolyte. The ordinate is labelled S because the current function is also normalized for the charge (Q) spent during plating the mercury on the substrate electrode, in order to account for differences in the surface area of the electrode, which are related to Q. From Fig. 4 it appears that the stripping current function is strongly affected, regardless of the scan rate, by whether the solution contains or not an additional current carrier other than that of the investigated species. In the absence of supporting electrolyte, S is about three times larger than that observed when a supporting electrolyte is present in the solution. On decreasing the concentration of the metal ion this behaviour is still present but to a different extent. Figure 5 depicts the ratios of the unsupported to the supported anodic peak current (i_{pm}/i_{pd}) observed for Cd^{2+} at different concentrations. For the above ionic samples the migration current makes as important contributions to the total current, as

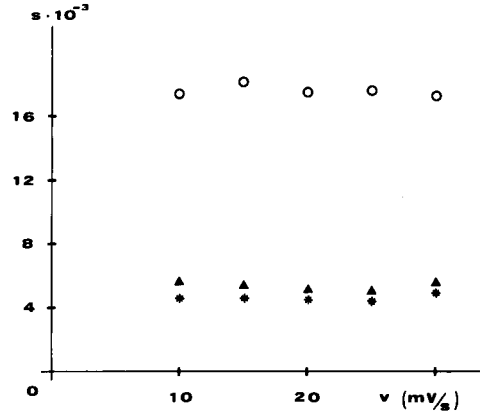

Fig. 4. Plot of experimental current function ($S = i_p / vQ$) as a function of scan rate for 5 μM Cd^{2+} in (○) pure water, (▲) 0.1 M HNO_3 and (*) 0.1 M $HClO_4$. Deposition time, 120 s.

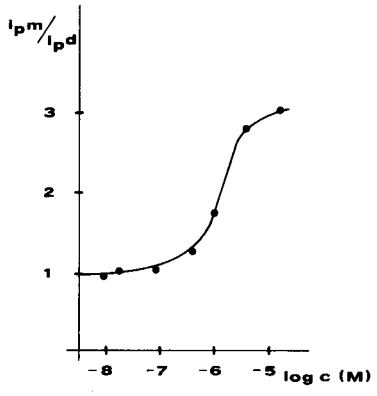

Fig. 5. Plot of i_{pm}/i_{pd} vs. log c for Cd^{2+} solutions. Scan rate, 30 mV s^{-1}.

does the diffusion current. The cations can migrate to the working electrode as the species are positively charged and are reduced at a negatively charged electrode. The migration current, in contrast to the diffusion current, is very sensitive to changes in electrolyte concentration. It is therefore likely that the data reported in Figs. 4 and 5 can be explained in terms of migration which adds to diffusion during the deposition step. This point can be placed on a quantitative basis by predicting the overall current associated at the mercury electrode in the case of combined diffusion–migration mass transport. The method of Oldham [11] will be applied for this purpose.

Consider the local flux J_i of the species S_i in the direction of the radial coordinate r, then, in accordance with the law of mass transport,

$$J_i = D_i \frac{\partial c_i}{\partial r} - z_i D_i c_i \frac{F}{RT} \frac{\partial \phi}{\partial r} \qquad (5)$$

where ϕ is the local electric potential in the solution; the other symbols have already been defined. Because in the preconcentration step steady-state conditions can be assumed to occur, using Faraday's law for a hemispherical electrode Eqn. 5 becomes

$$i\nu_i/2\pi r^2 nF = -D_i \, dc_i/dr - z_i D_i c_i F/RT \, d\phi/dr \qquad (6)$$

where i is the steady-state current (taken as negative when the microelectrode works as the cathode) and ν_i is the stoichiometric coefficient of the species S_i. The charge numbers of the participating ions, both electroactive and electroinactive, are important parameters in studies involving migration, but here we shall treat theoretically only the idealized case (not far from that employed experimentally) relative to solutions made from a divalent electroactive cation (M^{2+}) and a univalent anion (L^-), such as Cl^- or NO_3^-. Moreover, in view of the fact that the concentrations of the metal ions in ASV analysis are comparable to or less than, by orders of magnitude, those of the ions coming from the autoprotolysis of water, H^+ and OH^- are also considered as current carriers along with M^{2+} and L^-. The species considered, with the subscripts used in the equations, and the parameters characterizing each species are given in Table 3. Assuming that electroneutrality is maintained, Eqn. 6 can be solved analytically to give the concentration profiles for each species. At sufficient overpotentials, as usually applies in the deposition step, complete polarization of M^{2+} will occur and the steady-state limiting current will be given by

$$i_{lm} = 4\pi F D_1 r \left[c^b - 2\left(c_3^b c_4^b + c_3^b c_5^b \right)^{1/2} \right] \qquad (7)$$

where c^b is the total concentration of the ions in the solutions. The two limiting cases of Eqn. 7 are of interest. When $M^{2+} \gg H^+$, Eqn. 7 reduces to

$$i_{lm} = 12\pi F D_1 r c_1^b \qquad (8)$$

The other limit corresponds the case when the supporting electrolyte is in excess, when Eqn. 7 reduces to the well known relationship for a

TABLE 4

Parameter assignments for MCl_2 [or $M(NO_3)_2$] reduction in pure water [a]

S_i	z_i	ν_i	c_i^b
M^{2+}	+2	1	c_1^b
M^0	0	−1	0
H^+	+1	0	c_3^b
Cl^-	−1	0	c_4^b
OH^-	−1	0	c_5^b

[a] c_i^b refers to the bulk concentration of each species; see the text for the other parameters.

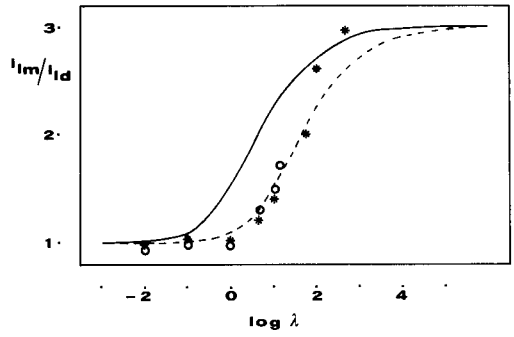

Fig. 6. Plots of i_{lm}/i_{ld} vs. log λ. Full line = theoretical prediction; * = experimental for Cd^{2+}; ○ = experimental for Pb^{2+}; dashed line = fit between theoretical and experimental data.

hemispherical microelectrode under diffusion-control mass transport:

$$i_{ld} = 4\pi F D_1 r c_1^b \qquad (9)$$

Comparison of Eqns. 8 and 9 shows that in the totally unsupported case, the limiting current is three times as large as the diffusion current. To discuss the conditions of the intermediate cases, it is useful to define the parameter λ describing the excess of the electroreactant species with respect to the electroinactive species: $\lambda = c_1^b/c_3^b$ (c_3^b is here H^+). By considering this last parameter and Eqn. 9, Eqn. 7 becomes

$$i_{lm} = i_{ld}\left[3 + 2/\lambda - 2\left(2/\lambda + 1/\lambda^2\right)^{1/2}\right] \qquad (10)$$

The theoretical curve obtained from the plot of i_{lm}/i_{ld} against log λ is reported in Fig. 6 (full line). This figure shows that the contribution of migration to the total current is still about 10% for $\lambda = 0.1$, that is, when the M^{2+} concentration is about 0.01 μM.

The anodic peak currents reported in Figs. 4 and 5 are not exactly the currents considered in the above discussion. Provided that Eqn. 2 holds they are linked through c^0, which in turn depends on the current flowing during the deposition step. However, the steady-state currents associated with the mercury microelectrode in the deposition step can be determined from the electrical charge q associated with the anodic stripping peaks by

$$q = i_l\left[t_d + (E_p - E_d)/v\right] \qquad (11)$$

where t_d is the preconcentration time, E_p and E_d are the peak and deposition potentials, respectively, and v is the scan rate; the additive term in brackets represents the scanning period during which plating of the metal continues. From Eqn. 11 and the experimental charge, i_{lm} can be evaluated. The diffusion limiting current, i_{ld}, can be obtained from Eqn. 11 and from the charge of the anodic peaks recorded with excess of a supporting electrolyte; i_{ld} can also be evaluated from Eqn. 9 by inserting the bulk concentration and the diffusion coefficient of M^{2+}. This last equation was used to calculate i_{ld} for the solutions of M^{2+} less than 0.05 μM because the experimental values often greatly exceeded i_{lm}, probably as a result of the contamination of the samples on addition of the supporting electrolytes.

Equation 11 is valid provided that a linear dependence exists between i_l and t_d. This aspect was studied by using solutions of 2 and 0.5 μM Cd^{2+}, where migration should occur; and 0.01 μM Pb^{2+}, where migration should be negligible; the preconcentration times were varied over the intervals 120–480, 200–600 and 300–900 s, respectively. Linear relationships were obtained between i_p and t_d with correlation coefficients, slopes and intercepts of 0.992, 1.5 pA s^{-1} and 165 pA; 0.999, 2 pA s^{-1} and 65 pA; and 0.999, 4 pA s^{-1} and 53 pA for Cd^{2+} and Pb^{2+}, respectively.

Finally, the experimental i_{lm}/i_{ld} ratios can be calculated and plotted against the logarithm of experimental λ values. These last parameters were calculated by dividing the c^b of M^{2+} by 0.1 μM, which is the concentration of H^+ at pH 7. The points in Fig. 6 are the experimental plots for Cd^{2+} and Pb^{2+}. The agreement between experimental data and theoretical prediction is satisfactory for both high and low concentrations of M^{2+}; whereas there are differences for the intermediate concentrations. In particular, from the experimental plots one would say that migration ceases to be an important factor for values of λ less than 1, where the theory predicts that its contribution is about 50% of that of the diffusion current. This apparent disagreement can be explained by considering that the backgrounds of the samples investigated were not that of pure water. The experimental conductivity determined

is in fact about ten times higher than that estimated by the theory, indicating the presence of ionic impurities in the solutions. It follows that, at a given concentration of M^{2+}, the λ values are lower than those estimated assuming only H^+ as electroinactive current carrier and the theoretical curve will be shifted to the right on the abscissa. A rough fit with the experimental curves (see the dashed line in Fig. 6) leads to an overall ionic content which is about ten times higher than that of pure water.

This discussion has important analytical consequences for the procedure for quantification of blank levels. No problems arise when very low concentrations are involved in that the migration term does not contribute to the steady-state current in the deposition step. This was proved by the fact that calibration graphs constructed, for instance, for Pb^{2+} solutions without supporting electrolyte, gave a linear trend over the range 0.001–0.05 μM with a correlation coefficient of 0.998. As standard addition is usually employed for quantification when the matrix is unknown from a chemical point of view, care must be taken in spiking the samples. Spikes of standards may raise the concentration to levels at which the migration contribution is present, so leading to non-linear calibration graphs.

It must be considered that natural waters characterized by a low ionic strength ($I < 0.001$ M) usually contain enough salts to avoid migration effects. This aspect was investigated by performing stripping measurements on samples of rain and melted snow with conductivities of 41 and 24 $\mu S\ cm^{-1}$, respectively. Spikes of Pb^{2+} and Cd^{2+} up to 0.8 μM did not give any migration effect, the relevant calibration graphs being linear over the range 0.1–0.8 μM, with average correlation coefficients of 0.996 and 0.995, respectively, both with and without supporting electrolyte. These results agree with others obtained with analogous samples [6].

The authors thank Mr. Danilo Rudello for skilful technical assistance. Financial aid from the Italian National Research Council (CNR) and MURST (Rome) is gratefully acknowledged.

REFERENCES

1 J. Wang, Stripping Analysis: Principle, Instrumentation and Application, VCH, Deerfield Beach, FL, 1985.
2 J. Wang and P. Tuzhi, Anal. Chim. Acta, 197 (1987) 367.
3 J. Wang, P. Tuzhi and J. Zadeii, Anal. Chem., 59 (1987) 2119.
4 Z. Stojek and J. Osteryoung, Anal. Chem., 60 (1988) 131.
5 S. Daniele, M.A. Baldo, P. Ugo and G.A. Mazzocchin, Anal. Chim. Acta, 219 (1989) 9.
6 S. Daniele, M.A. Baldo, P. Ugo and G.A. Mazzocchin, Anal. Chim. Acta, 219 (1989) 19.
7 D.K.Y. Wang and A.G. Ewing, Anal. Chem., 62 (1990) 2697.
8 R.R. De Vitre, M.L. Tercier, M. Tsacopoulos and J. Buffle, Anal. Chim. Acta, 249 (1991) 419.
9 M. Wojciechowski and J. Balcerzak, Anal. Chim. Acta, 249 (1991) 433.
10 L. Nyholm and G. Wikmark, Anal. Chim. Acta, 257 (1992) 7.
11 K. Oldham, J. Electroanal. Chem., 250 (1988) 1.
12 A.M. Bond, M. Fleischmann and J. Robinson, J. Electroanal. Chem., 172 (1984) 11.
13 C. Amatore, M.R. Deakin and R.M. Wightman, J. Electroanal. Chem., 225 (1987) 49.
14 J.B. Cooper and A.M. Bond, J. Electroanal. Chem., 315 (1991) 143.
15 D.R. Baker, M.W. Verbrugge and J. Newman, J. Electroanal. Chem., 314 (1991) 23.
16 J.D. Norton, H.S. White and S.W. Feldberg, J. Phys. Chem., 94 (1990) 6772.
17 H.W. Nurberg, Anal. Chim. Acta, 164 (1984) 1.
18 K. Aoki and J. Osteryoung, J. Electroanal Chem., 122 (1981) 1.
19 Z. Stojek and J. Osteryoung, Anal. Chem., 61 (1989) 1305.
20 M. Penczek and J. Stojek, J. Electroanal. Chem., 191 (1985) 91.
21 W.T. de Wries and E. van Dalen, J. Electroanal. Chem., 14 (1967) 315.
22 M. Penczek, Z. Stojek and J. Osteryoung, J. Electroanal. Chem., 170 (1984) 99.

Analytica Chimica Acta, 273 (1993) 13–25
Elsevier Science Publishers B.V., Amsterdam

Flow-through anodic stripping coulometry and anodic stripping coulometry with collection for the simultaneous absolute determination of copper, lead, cadmium and zinc

Ernest Beinrohr [1] and Peter Tschöpel

Max-Planck-Institut für Metallforschung, Laboratorium für Reinststoffanalytik, Bunsen-Kirchhoff-Strasse 13, D(W)-4600 Dortmund 1 (Germany)

Günther Tölg

Max-Planck-Institut für Metallforschung, Laboratorium für Reinststoffanalytik, Bunsen-Kirchhoff-Strasse 13, D(W)-4600 Dortmund 1; and Institut für Spektrochemie und angewandte Spektroskopie, Bunsen-Kirchhoff-Strasse 11, D(W)-4600 Dortmund 1 (Germany)

Michal Németh

Department of Analytical Chemistry, Slovak Technical University, CS-812 37 Bratislava (Czechoslovakia)

(Received 3rd April 1992; revised manuscript received 3rd August 1992)

Abstract

Flow-through electrochemical cells with porous working electrodes made of crushed reticulated vitreous carbon and plated with mercury were used for the absolute determination of copper, lead, cadmium and zinc by anodic stripping coulometry and anodic stripping coulometry with collection in a flow system. The system consisted of a peristaltic pump, pneumatic pulse damper, electrochemical flow-through scrubber to remove impurities and dissolved oxygen from the flowing electrolyte, sample injection port and two serial flow-through cells with porous working electrodes. Trace metals from the injected sample volume were deposited at the working electrode of the first cell, then stripped by scanning the potential to positive values and finally collected at the second cell. Both the stripping and collection currents were registered and integrated. The conditions for a quantitative deposition, stripping and collection were investigated.

Keywords: Coulometry; Flow system; Stripping voltammetry; Cadmium; Copper; Lead; Zinc

The absolute determination of traces of metals in aqueous sample solutions with relatively high salt contents is difficult. Of the known methods, coulometry exhibits the most suitable features for this purpose. The problem in the coulometry of trace elements is the proper separation of the low net Faradaic current from the background currents. As bulk electrolysis is used, the duration of the electrolysis is another parameter to be taken into account. An alternative to commonly used batch techniques is flow electrolysis utilizing flow-through coulometric cells. Exhaustive electrolysis in the flowing sample can only be achieved by cell designs that ensure high mass-transfer

Correspondence to: E. Beinrohr, Department of Analytical Chemistry, Slovak Technical University, CS-81237 Bratislava (Czechoslovakia).

[1] On leave from Department of Analytical Chemistry, Slovak Technical University, CS-812 37 Bratislava, Czechoslovakia.

rates of the electroactive species to the electrode surface. Flow-through thin-layer cells and cells with porous working electrodes proved to be suitable for this purpose.

Reticulated vitreous carbon (RVC) has been used as electrode material in various flow-through cell designs [1–11] owing to its excellent electrical, chemical and mechanical properties. Coulometric flow-through cells have proved to be useful for detection in liquid chromatography and flow-injection analysis (FIA) [3,4,8,10,12,13], absolute electrochemical determination of traces of copper [11] and lead [14], cleaning of flowing electrolytes [6,11], continuous removal of dissolved oxygen [6,11] and preconcentration of trace metals [5,9,15].

Flow-through cells with large-surface-area working electrodes ensure high electrochemical conversion and exhibit correspondingly high sensitivity. However, the large electrode surface leads to high background currents due to electrode surface reactions, charging currents and electrochemical reactions of the supporting electrolyte. In anodic stripping voltammetry with collection (ASVWC) by using the rotating disc–ring electrode assembly, the charging currents can be simply eliminated: the elements deposited at the disc electrode are stripped and subsequently collected at the ring electrode [16]. As the ring electrode is set to a constant potential, no charging currents arise. A similar approach but using a flow system was described by Schieffer and Blaedel [17,18]. They made use of two tubular working electrodes in series: the analyte was deposited at the first electrode from the flowing sample solution, then stripped after applying a potential scan to the electrode and the stripped species were immediately collected at the second tubular electrode with a suitable constant potential imposed.

The same principle but in a coulometric arrangement was used by Fujinaga and co-workers [19,20] and recently by Beinrohr et al. [14] for the determination of traces of lead by anodic stripping coulometry with collection (ASCWC). Two coulometric cells with porous working electrodes were coupled in series. The analyte from the flowing sample solution was quantitatively deposited at the first, "upstream" cell, then dissolved by applying a positive potential scan or step and the stripped metal ions were quantitatively collected at the constant potential "downstream" cell. Owing to the exhaustive character of all the electrochemical steps, the integrated signal (coulombic content of the stripping or collection peaks) could be related to the absolute amount of the analyte entering the system according to the simple Faraday law. Owing to the more favourable signal-to-background ratio, the collection signal measurement was preferred.

Flow-through anodic stripping coulometry (ASC) and anodic stripping coulometry with collection (ASCWC) may provide more information than the corresponding voltammetric methods with non-exhaustive electrolysis, namely direct information about the absolute amount of the analyte in the flow system. The objectives of this work were to investigate the possibility of the simultaneous absolute determination of trace amounts of copper, lead, cadmium and zinc by making use of the flow system described previously [14] for ASC and ASCWC. Work was carried out to elucidate the influence of potential scan, volumetric flow-rate, composition of the supporting electrolyte, etc., on the conversion of electrochemical processes, stripping parameters, sensitivity and signal resolution.

EXPERIMENTAL

Flow system

The flow-through electrochemical cells and the single-line flow system were similar to those described previously [11,14] (Fig. 1). The system consisted of a peristaltic pump (P), pneumatic pulse damper (PD), permeable tube oxygen deoxygenator (D1), electrochemical scrubbing cell (SC, cell design C in [11]), four-way sampling valve (SV), preconcentrator (cell 1) and collector (cell 2) cells. The sampling loop (D2) also served as a deoxygenator for the sample solution. The potential of the scrubber cell was controlled by the potentiostat PS and the voltamperometers VA1 and VA2 served for signal generation. The working electrodes of the cells (Fig. 1, top) were prepared from RVC crushed to a particle size of

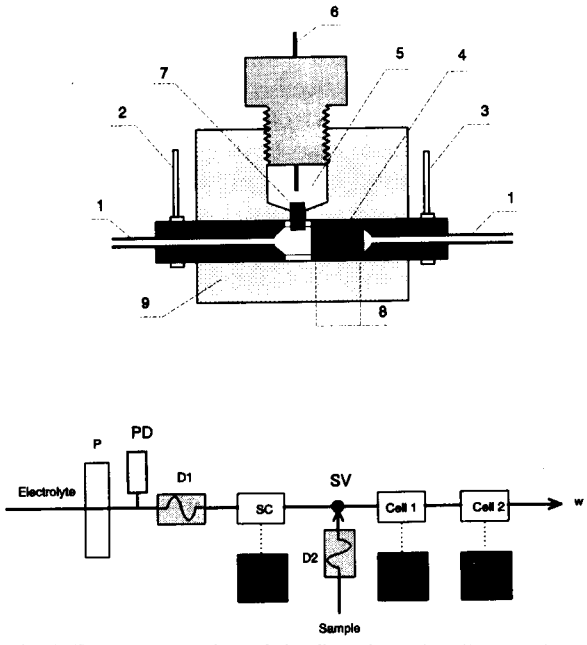

Fig. 1. Top: cross-section of the flow-through cell. 1 = Inlet/outlet PTFE tubes; 2 = lead to the graphite counter electrode; 3 = lead to the working electrode; 4 = crushed RVC electrode; 5 = saturated KCl solution; 6 = Ag electrode; 7 = porous graphite diaphragm; 8 = polyethylene frits; 9 = Plexiglas body. Bottom: schematic diagram of the flow system.

20–100 μm. The working electrodes of the upstream and downstream cells were 6 and 5 mm in diameter and 3 and 2 mm in length, respectively. The porosity of the electrodes was $\epsilon = 0.7$ and the specific surface area was about 590 $cm^2\ cm^{-3}$. The surface areas of the working electrodes in the upstream and downstream cells were estimated to be about 50 and 23 cm^2, respectively.

Equipment

The voltammetric measurements were made on a Polarecord E 506 equipped with a VA Scanner E 612 (Metrohm, Herisau, Switzerland). The other equipment used included a peristaltic pump (Gilson Minipuls 2), a potentiostat (Jaissle 1000 T-B), a digital integrator (VIDAR 6300) and a pH meter (E 350B; Metrohm). The potentials in this work are expressed versus the saturated Ag/AgCl electrodes used in the cells. The integrated values of the stripping and collection signals are given in coulombs.

Reagents

Solutions were prepared from deionized, doubly distilled water and analytical-reagent grade chemicals. The electrolyte solutions for the preparation of the sample solutions were purified by purging them through the scrubber cell adjusted to -1.5 V at a flow-rate of 1–2 ml min^{-1}. The pH of the solutions was adjusted either with dilute acids or with acetate buffer solutions. Standard sample solutions were prepared from Titrisol stock solutions (Merck, Darmstadt). All the solutions were prepared and stored in polypropylene bottles.

Coating the cells

The working electrodes of the cells were coated with 100 ml of 1×10^{-4} M $Hg(NO_3)_2$ solution in 0.1 M KNO_3 supporting electrolyte at a flow-rate of 2.5 ml min^{-1}, a coating potential of -1.6 V and a current of about -0.9 mA. Portions of 25 ml of the deaerated coating solution were pumped through the cells alternately in forward and backward directions. The same coating was used throughout the whole lifetime of the working electrode.

Procedure

The supporting electrolyte, while deaerated by purging an inert gas through it in the reservoir, was pumped through the flow system at a constant flow-rate in the range 1–2.5 ml min^{-1}. The potential of the working electrode of the electrochemical scrubber cell was set at -0.5 to -0.8 V and at -0.8 to -1.2 V for solutions with pH = 2–4 and with pH > 4, respectively. The sample solution, deaerated by purging nitrogen through it in the sample reservoir, was filled into the sampling loop. When using a non-deaerated sample solution it was allowed to stay in the sampling loop for at least 2 min before injection. The deposition and collection potentials were imposed on the upstream and downstream cells, respectively and the sample was injected into the carrier electrolyte. After eluting the sample from the sampling loop, the injection valve was switched back to the loading position. After 2 min the deposited trace elements were stripped and collected by either continuous or step-by-step

stripping. In continuous stripping, the potential of the upstream cell was scanned at a fixed rate to positive values, ensuring dissolution of all the deposited elements. Both the stripping and collection signals were recorded and integrated. In step-by-step stripping, the potential of the upstream cell was shifted to a starting value and a potential ramp with a scan rate of 40–500 mV s^{-1} was applied. The starting and final values of the potential ramp were chosen to dissolve selectively one element only (Table 1). The corresponding collection peak current was registered and integrated. On finishing the integration the potential of the upstream cell was shifted to the starting dissolution potential of the next element with a more positive stripping peak potential and the procedure was continued.

RESULTS AND DISCUSSION

The flow system used in this work (Fig. 1), incorporating two electrochemical cells in series with large-surface-area porous electrodes and continuous removal of oxygen, was described and characterized in detail in a recent paper [14]. The volume and the corresponding surface area of the working electrode in the downstream cell were made as small as possible to minimize the background currents. Those of the upstream cell were made larger to ensure exhaustive electrodeposition also at extremely low analyte concentrations in the sample.

To minimize background currents, the whole surface of the porous working electrode should be covered with mercury as completely as possi-

TABLE 1

Deposition, stripping and collection potentials for selective determination of elements in various electrolytes by the step-by-step stripping procedure

Element	Electrolyte [a]	pH	Deposition potential (V)	Stripping scan (V)		Collection potential (V)
				Start	Stop	
Cu	a	2–4	−1.0 to −0.4	−0.2	+0.2	−0.8 to −0.4
	a	5.4	−1.3 to −0.4	−0.2	+0.2	−1.2 to −0.4
	b	2–4	−1.0 to −0.4	−0.2 to −0.1	+0.2	−0.6 to −0.4
	b	4.8	−1.4 to −0.6	−0.2 to −0.1	+0.2	−0.6 to −0.4
	c	2–3.5	−1.0 to −0.6	−0.42 to −0.40	−0.2	−0.8 to −0.4
	d	2–3.5	−1.0 to −0.6	−0.6	−0.50 to −0.45	−0.8 to −0.6
Pb	a	3–4	−1.3 to −0.6	−0.60 to −0.55	−0.40 to −0.35	−0.8 to −0.6
	a	5.4	−1.3 to −0.6	−0.60 to −0.55	−0.40 to −0.35	−1.2 to −0.6
	b	2–4	−1.0 to −0.6	−0.6	−0.40 to −0.35	−1.0 to −0.55
	b	4.8	−1.4 to −0.6	−0.6	−0.40 to −0.35	−1.0 to −0.6
	c	2–5	−0.8	−0.7 to −0.6	−0.45 to −0.40	−0.8 to −0.6
	d	2–4	−1.0 to −0.6	−0.6 to −0.5	−0.35 to −0.30	−0.8 to −0.6
Cd	a	3–4	−1.0 to −0.9	−0.8	−0.55	−0.8
	a	5.4	−1.3 to −0.8	−0.8	−0.60 to −0.55	−1.2 to −0.8
	b	2–4	−1.1 to −0.8	−0.8	−0.55 to −0.50	−0.85 to −0.80
	b	4.8	−1.3 to −0.8	−0.8	−0.5 to −0.4	−0.8
	c	5.4	−1.2 to −0.8	−0.8	−0.55 to −0.50	−1.0 to −0.8
	d	2–3.5	−1.0 to −0.8	−0.8	−0.6	−0.8
	d	5.4	−1.4 to −0.8	−0.8	−0.6	−1.2 to −0.8
Zn	a	5.4	−1.4 to −1.3	−1.3 to −1.2	−0.8	−1.2
	b	5.4	−1.4 to −1.3	−1.3 to −1.2	−0.8	−1.2
	c	5.4	−1.4 to −1.3	−1.3 to −1.2	−0.8	−1.2
	d	5.4	−1.4 to −1.3	−1.3 to −1.2	−0.8	−1.2

[a] a = 0.2 M Na_2SO_4; b = 0.1 M KNO_3; c = 0.1 M KCl; d = 0.2 M KSCN.

ble, which can be achieved by plating the electrodes with the plating solution flowing alternately from both directions through the electrode. The average thickness of the mercury-film coating was found to be about 0.03 and 0.06 μm for the upstream and downstream cells, respectively [14]. Owing to this extremely low mercury-film thickness, diffusion rates of the deposited metals in the mercury film can be neglected and possibly have no adverse effect on stripping peak widths and selectivity. The plating potential was kept as negative as possible to avoid the formation of Hg(I) species. However, plating currents higher than 2–3 mA caused rapid deterioration of the electrochemical properties of the cells. The lifetime of the coating depended on the currents flowing in the cells and on the properties of the electrolytes. By using carefully deaerated solutions and applying potentials below +0.2 V (−0.1 V in the presence of chlorides and thiocyanates) and currents lower than 1 mA, the same coating could be used for up to 1 week. After this period broadening of stripping and the corresponding collection peaks was observed, especially at electrolyte concentrations below 0.1–0.2 M. Attempts to restore the deteriorated selectivity by electrochemical removal and repeated deposition of the mercury coating failed; new electrode material and a fresh coating had to be used to obtain the original selectivity.

The flow system consisting of two serial coulometric cells could provide up to four types of analytical signals after the analyte deposition step and under favourable circumstances ensuring exhaustive electrolysis each of them corresponds to the absolute amount of the analyte entering the cells. Figure 2 illustrates such signals for Zn, Cd and Pb in sodium sulphate supporting electrolyte. With the continuous stripping procedure the first signal to be obtained is the stripping signal from the upstream cell (Fig. 2a), followed by the corresponding collection signal from the downstream cell (Fig. 2b). The collection signals for the treated elements can also be obtained separately by using the step-by-step stripping mode (Fig. 2c), in which the potential is scanned in a suitably chosen range to strip selectively one element only. On completing the integration of the collection signal, the next, more electropositive element is stripped and collected. The last signal possibly to be obtained after completing a stripping/collection run is a stripping signal from the downstream cell (Fig. 2d) corresponding to the re-oxidation of collected elements. This signal is virtually the same as the stripping signal from the upstream cell and it could serve to check the previous procedures.

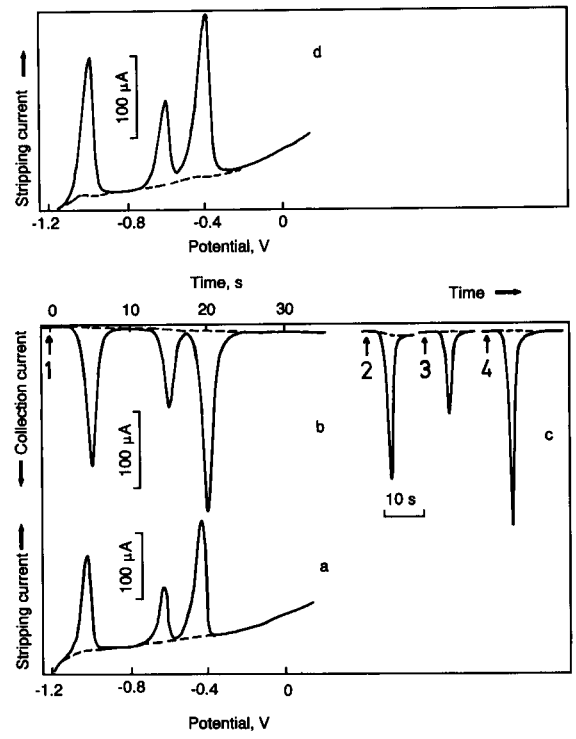

Fig. 2. (a) Stripping and (b) the corresponding collection signals of the upstream and downstream cells, respectively, obtained after a potential scan from −1.2 V to +0.2 V (1). (c) Collection signals of Zn, Cd and Pb after applying consecutively potential ramps from −1.2 to −0.8 V (2), from −0.8 V to −0.58 V (3) and from −0.58 V to −0.35 V (4). Collection potential, −1.2 V. (d) Stripping signal of the downstream cell obtained after collecting the stripped elements from the upstream cell. Potential scan rate, 40 mV s^{-1}; Volumetric flow-rate, 2.5 ml min^{-1}; supporting electrolyte, 0.25 M Na_2SO_4 at pH 5.4; sample volume, 2.4 ml; concentrations, Zn 7.64×10^{-7}, Cd 4.5×10^{-7} and Pb 1.0×10^{-6} M.

The influence of factors such as potential scan rate at stripping, volumetric flow-rate of the sample and the supporting electrolyte and the character, concentration and pH of the supporting

TABLE 2

Symbols and abbreviations used

a	Cross-sectional area of the electrode (cm^2)
ASC	Anodic stripping coulometry
ASCWC	Anodic stripping coulometry with collection
α	Empirical constant
b	Empirical constant
c	Concentration (mol l^{-1})
E_p	Peak potential (V)
$E^{0\prime}$	Formal potential (V)
ϵ	Porosity
F	Faraday constant (96484.6 C eq^{-1})
i_p	Peak current (A)
l	Mercury-film thickness (cm)
R	Gas constant (8.3144 J mol^{-1} K^{-1})
R_{conv}	Conversion efficiency
R.S.D.	Relative standard deviation (%)
T	Absolute temperature (K)
v	Linear potential scan (V s^{-1})
v_f	Volumetric flow-rate (cm^3 s^{-1})
V	Volume (cm^3)
z	Number of electrons per molecule

electrolyte was investigated next. To avoid interactions of Cu with Zn (see later), the synthetic samples treated contained simultaneously either Zn, Cd and Pb or Cd, Pb and Cu.

Potential scan

The stripping peak current for a mercury-coated flow-through porous electrode can be expressed by the following simple expression [2]:

$$i_p = kz^2 v c_{samp} V_{samp} R_{conv} \quad (1)$$

where values of the constant k of 1.1157×10^6 [21] and 1.382×10^6 [22] were given (for symbols, see Table 2). This equation is valid for stirred solutions and for thin mercury films where the diffusion rate of deposited metal can be neglected.

The peak potential for thin mercury-film electrodes derived by Roe and Toni [22] can be modified for porous electrodes as follows:

$$E_p = E^{0\prime} + 2.3[RT/(zF)] \times \log\left\{\left[zF(a\epsilon)^{\alpha} lv\right]/\left(RTbv_f^{\alpha}\right)\right\} \quad (2)$$

The experimental constants α and b for porous electrodes made of crushed RVC determined by Beinrohr et al. [11] were 0.4 and 0.01, respectively. Hence, the peak potential at a given mercury film thickness is influenced by the potential scan and volumetric flow-rate and an increase in the former should shift the peak potential to positive and an increase in the latter to negative values.

Experimentally obtained results mostly confirmed the above assumptions. Except for the coulombic content, the position, height and width of the stripping and collection signals were dependent on the potential scan rate.

According to Eqn. 2, the E_p vs. log v dependence should be linear with a slope of +0.0296 for a two-electron process. Experimentally obtained potential values fit such a theoretical dependence for scan rates up to 5–10 mV s^{-1} for Zn, and up to 20–30 mV s^{-1} for Cd and Pb. At higher scan rates the peak maxima appear at more positive potentials then theoretically predicted. As high scan rates are accompanied by high currents, an uncompensated *iR* drop may be responsible for these irregularities.

The dependence of the stripping peak current on the potential scan rate is depicted in Fig. 3. A levelling off is observed at potential scan rates above 10–20 mV s^{-1}, and moreover the slope in log–log coordinates is slightly smaller than unity as predicted by Eqn. 1: slopes of 0.91, 0.90 and

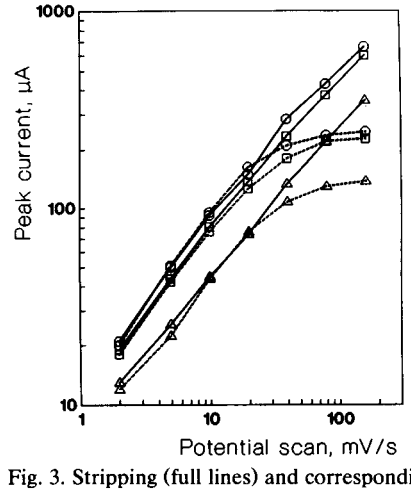

Fig. 3. Stripping (full lines) and corresponding collection peak heights (dashed lines) at various potential scans for (□) Zn, (△) Cd and (○) Pb. Sample and flow parameters as in Fig. 2.

0.96 were obtained for potential scan rates of 2–10 mV s^{-1} for Zn, Cd and Pb, respectively. The deviation from the theoretical value may be related to limited reversibility of the electrode reaction and to *iR* drop effects due to high currents at higher scan rates. A more significant deviation from theory (0.68) was observed with mercury-coated RVC electrodes [2] and other thin-film electrode techniques [17,23]. Values of 1.15×10^6, 1.11×10^6 and 1.01×10^6 were found for the proportionality coefficient k in Eqn. 1 for Zn, Cd and Pb, respectively, in satisfactory agreement with the value given by de Vries and van Dalen [21].

For scan rates below 10 mV s^{-1}, the stripping peak half-widths were near to the theoretical value of 37.7 mV [21]. At higher scan rates the peaks became broader, which can be attributed to the enhanced *iR* drop effects.

The collection peak currents (Fig. 3) were in fact the same as the currents of the "parent" stripping peaks up to potential scan rates of 20–30 mV s^{-1}. Above these values the collection peaks increased much more slowly with the scan rate than the corresponding stripping peaks. The signal half-widths increased considerably while the signal resolution deteriorated. The resolution of the collection signals can be improved either by increasing the volumetric flow-rate of the electrolyte in the stripping/collection process or by decreasing the potential scan rate. In the former instance the highest volumetric flow-rate is limited by the collection efficiency of the downstream cell. The latter approach improves the resolution but the peak-height sensitivity deteriorates as the deposited elements are dissolved slowly in the flowing electrolyte while producing highly dilute solutions entering the collector cell.

High peak-height sensitivity and high resolution of the collection signals even at lower volumetric flow-rates in the stripping process can be ensured by stripping the deposit step-by-step through suitably chosen potential steps ensuring selective dissolution of only one element at a time (Fig. 2c). The highest sensitivity for the collection signal is achieved with dissolution after a potential step and at high flow-rates, as the deposited analyte atoms are dissolved in a minimum volume of the flowing electrolyte giving rise to a zone with high analyte concentration which enters the cell with a high mass flow-rate. Applying consecutively potential steps with different starting and final potential values it is possible to determine selectively the deposited elements. This step-by-step technique is more tedious than linear sweep stripping, but it can easily be automated. Experimental parameters for the tested elements and electrolytes are summarized in Table 1.

The enhanced sensitivity of the stripping process with large-surface-area porous electrodes arising from exhaustive electrolysis in the preconcentration step is accompanied by enhanced background currents. Although the stripping signal sensitivity can be enhanced by increasing the potential scan rate (Eqn. 1), this increase is offset by an increase in the background signal slope. This slope varies with potential, electrode history and solution pH. The signal evaluation at high background slopes brings uncertainty into the background correction and signal integration. Therefore, when choosing the optimum potential scan rate for the stripping process, the ratio of the peak current to the background slope may be an important criterion (Fig. 4). An increase in the scan rate above 20–40 mV s^{-1} gave no significant improvement of this ratio.

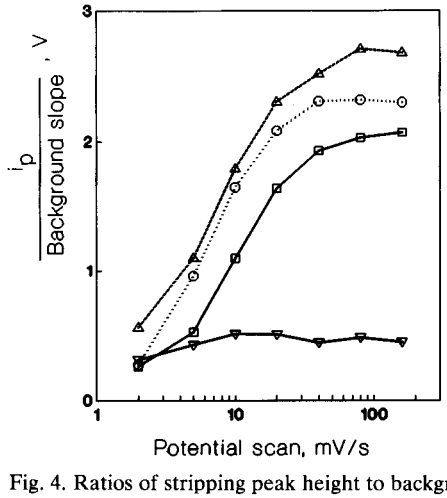

Fig. 4. Ratios of stripping peak height to background slope for (□) Zn, (△) Cd, (○) Pb and (▽) Cu at various stripping potential scans. Analyte concentration, 5×10^{-7} M; other parameters as in Fig. 2.

The background currents of the collection signal were, as expected, much lower and more reproducible than those in the stripping mode. Owing to the constant collection potential, no charging currents can arise, and moreover the electrode surface reactions decay to a minimum and constant value. A potential sweep in the upper cell influences the background signal of the lower cell, however. This influence may be partly attributed to some electric contact between the cells through the thin connecting tube containing the electrically conducting supporting electrolyte. Trace concentrations of electroactive soluble impurities such as oxygen and Fe(II)/Fe(III) may also contribute to this interaction, as their mass flow to the downstream cell and the corresponding current are influenced by the potential of the upstream cell.

Electrolyte flow-rate

The flow-rate of the carrier electrolyte had little influence on the stripping parameters except for the recovery of the stripping signal, but the collection parameters, i.e., peak heights, peak widths and collection recoveries, were all influenced by it.

Recoveries up to 100% were observed for Pb, Cd and Zn for flow-rates as high as 2–2.5 ml min^{-1} for both stripping and collection signals (Fig. 5). At higher flow-rates a decrease in recovery was observed whereas the collection recovery decreased more than that due to the stripping process. This observation can be explained by the smaller volume and the correspondingly smaller electrode surface of the collector cell causing lower recoveries at higher flow-rates. The flow-rate dependence of the collection and stripping conversion efficiency of copper was more complex (see later).

On increasing the flow-rate the observed peak potentials were shifted slightly to negative values in accordance with Eqn. 2. The E_p vs. log v_f dependence is linear with slopes of -0.0129, -0.0124 and -0.0120 for Zn, Cd and Pb, respectively (correlation coefficients 0.90–0.97). These values agree satisfactorily with the theoretical slope of -0.0118 predicted by Eqn. 2. The potential shift can be accounted for by faster removal

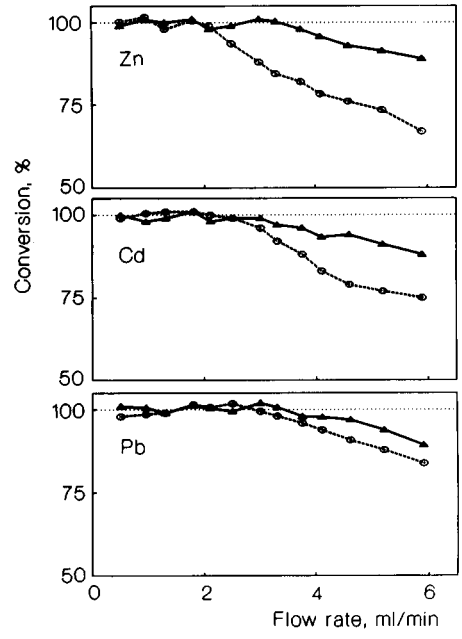

Fig. 5. Influence of flow-rate on the stripping (full lines) and collection recoveries (dashed lines) of Zn, Cd and Pb. Supporting electrolyte, 0.2 M Na_2SO_4 at pH 5.4; deposition and collection potentials, -1.3 and -1.2 V, respectively; sample, 2.4 ml; concentrations, Zn 4.5×10^{-7}, Cd 2.3×10^{-7} and Pb 7.8×10^{-7} M.

of re-oxidized species from the electrode surface at higher flow-rates causing a decrease in the activity of the oxidized form of the treated element.

The stripping peak currents are influenced only slightly by changes in flow-rate (Fig. 6). The slight decrease with increase in flow-rate is probably due to a decrease in conversion efficiency (Fig. 5). The peak widths are not influenced by changes in flow-rate in the range 0.5–6 ml min^{-1}.

The collection peak currents (Fig. 6) and peak widths, on the other hand, are significantly influenced by the volumetric flow-rate. In accordance with the mass flow-sensitive and with the concentration-sensitive character of flow-through coulometric cells, the collection peak current is controlled both by the analyte concentration entering the collector cell and by its mass flow-rate. The former depends on the stripping rate of the deposited analyte from the upstream cell and on the dispersion of the dissolved ions in the flowing

electrolyte solution. At a given analyte concentration the latter parameter is controlled by the volumetric flow-rate. At low flow-rates the dissolved analyte is additionally diluted owing to the axial diffusion causing enhanced dispersion of the analyte zone. As a consequence, the collection peaks become broader and the signal resolution deteriorates. Owing to the low mass flow-rate, the observed collection current is lower than that at higher flow-rates (Fig. 6). An increase in the flow-rate above 2.5 ml min^{-1} caused neither a significant enhancement of the peak current nor a further improvement of the peak widths.

After the preconcentration step the plated elements can also be re-oxidized at the upstream cell with a stopped flow of the carrier electrolyte. The stripping peak potentials are shifted slightly to more positive values compared with those observed with flowing electrolytes. Owing to the minute distances between the small carbon particles in the working electrode, the cells exhibit properties inherent to thin-layer cells [24]. As a consequence, the stripped elements can be deposited again completely at the same electrode by scanning the potential back to negative values. The coulombic contents of the deposition (cathodic) peaks are in fact the same as the corresponding stripping peaks. Moreover, the differences between the corresponding peak potentials are small, about 71, 65 and 100 mV for Pb, Cd and Cu, respectively, at a scan rate of 40 mV s^{-1}, and at lower scan rates even smaller values can be observed.

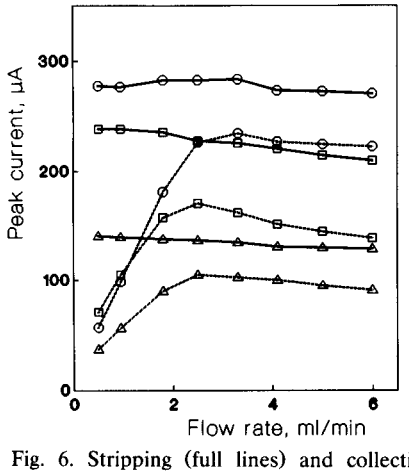

Fig. 6. Stripping (full lines) and collection peak currents (dashed lines) at various volumetric flow-rates for (□) Zn, (△) Cd and (○) Pb. Potential scan rate, 40 mV s^{-1}; other parameters as in Fig. 2.

TABLE 3

Stripping peak potentials in various electrolytes at pH 5.4 [a]

Electrolyte	Stripping peak potential (V)			
	Cu	Pb	Cd	Zn
0.25 M KSCN	−0.51	−0.44	−0.63	−1.03
0.10 M KCl	−0.15	−0.42	−0.61	−1.00
0.10 M KNO_3	+0.01	−0.41	−0.59	−0.99
0.25 M Na_2SO_4	+0.02	−0.42	−0.62	−1.02

[a] Potential scan rate, 40 mV s^{-1}; analyte concentration, 2×10^{-7} M.

Carrier electrolyte

The properties of the supporting electrolyte used as the carrier liquid significantly influence the stripping and collection parameters through redox reactions, formation of complex compounds and poorly soluble compounds readily adsorbing on the electrode surface and frits used in the cells. The supporting electrolytes tested were KNO_3, KCl, KSCN and Na_2SO_4. The stripping peak potentials of the investigated elements in these supporting electrolytes are given in Table 3.

Copper. In potassium nitrate carrier electrolyte the stripping and collection recoveries expressed for a two-electron process were between 50 and 96%, depending on the flow-rate and potential scan rate. A decrease in the stripping potential scan rate below 10–50 mV s^{-1} caused a drop of the recoveries to 50% while the collection signal area was slightly larger than that for the stripping signal. The cyclic voltammograms of the deposited copper with stopped flow exhibited some anomalous features. At scan rates below 5 mV s^{-1} "negative" anodic peaks were observed, whereas the counter peak remained "normal". The coulombic content of the anodic and cathodic peaks corresponding to oxidation of the deposited copper atoms and their subsequent reduction did not fit the theoretically expected values corresponding to a $Cu^{2+}+2e^{-}=Cu$ stoichiometry. At lower scan rates much larger reduction (counter) peaks were registered, as ex-

pected for a two-electron reduction process. As oxygen was carefully removed, an active role of the supporting electrolyte could be expected for the anomalous electrochemical properties of copper [25]. Nitrate ions may be reduced by Cu(I) species which are possibly formed while oxidizing electrochemically the deposited metal at a slow potential scan. The reduced nitrate species, e.g., nitrite, may further be reduced electrochemically, which could explain the origin of the "negative" stripping peaks at low scan rates. During the backward reduction sweep the freshly reduced and in mercury negligibly soluble metallic copper may catalyse the reduction of nitrate ions, as observed earlier with copper electrodes [26], while giving rise to enhanced cathodic currents.

In potassium chloride and potassium thiocyanate carrier electrolytes, both the stripping and collection signal peak areas corresponded to the $Cu(I) + e^- = Cu$ stoichiometry. However, the resolution between the Cu and Pb collection signals in 0.25 M KSCN carrier electrolyte was insufficient owing to the vicinity of the stripping peak potentials and the slow transport of the stripped Cu(I) species to the detector cell. To achieve a better resolution in the ASCWC mode, the potential scan at stripping had to be lowered to at least 10 mV s^{-1}, which caused a significant decrease in collection peak heights. Using the step-by-step stripping procedure at suitably chosen potential steps (Table 1), satisfactory resolution and recoveries were achieved for Cu and Pb. The experimentally obtained results are listed in Table 4. The background of the collection signal of copper in the KSCN electrolyte with respect to other electrolytes is extremely low: on sweeping the potential of the upstream cell from −0.6 to −0.49 V to strip the deposited copper, the background current enhancement of the collection signal was < 0.2 μA. A disadvantage of the KCl and KSCN electrolytes was the slow transport of the stripped Cu(I) species to the collector cell, probably caused by the low solubility of the copper(I) chloride and thiocyanate.

TABLE 4

Figures of merit of ASCWC by using the step-by-step stripping procedure in 0.25 M KSCN carrier electrolyte at pH 3.3 [a]

Element	Added (mol l^{-1})	Found (%)	R.S.D. [b] (%)
Cu	1.6×10^{-7}	99.4	4.8
Pb	1.0×10^{-7}	98.7	2.6
Cd	8.9×10^{-8}	77.5	3.3

[a] Flow-rate, 2.5 ml min^{-1}; potential scan rate, 100 mV s^{-1}; other parameters as given in Table 1. [b] $n = 6$.

The stripping peak shape of Cu in the sodium sulphate carrier electrolyte was significantly dependent on the amount of copper deposited. At concentrations above 10^{-7} M the peak was relatively narrow, but at lower concentrations the peak became broader and split. Owing to the high and irreproducible background slope, no reliable quantification of the stripping signal was possible below this concentration. The determination of Cu through the collection signal was accurate down to concentrations of 5×10^{-7} M in a 2.4-ml sample solution. For lower analyte concentrations a decrease in recovery to about 50% was observed (Fig. 7). Moreover, at lower copper concentrations and with correspondingly lower signals the integration was complicated by the background current enhancement at the collector cell when shifting the potential of the upstream cell from −0.2 to +0.2 V. This background current increase of about 6–7 μA can be attributed to soluble electroactive species in the supporting electrolyte not removed by the scrubber cell. The nature of this interference, also observed by Schieffer and Blaedel [18], was not studied. The deposition of copper ions from the sample solutions, as checked by analyses of the effluent solutions by electrothermal atomic absorption spectrometry, was complete over the whole concentration range investigated. The lower electrochemical yields at copper concentrations below 5×10^{-7} M could partly be attributed to sorption effects inherent to copper ions at carbon surfaces: copper ions may be partly adsorbed on the electrode surface, especially on carbon particles not completely covered with mercury.

Lead. The stripping and collection behaviour of Pb in potassium nitrate supporting electrolyte have recently been investigated [14]. Similar results were also observed with the other investigated carrier electrolytes.

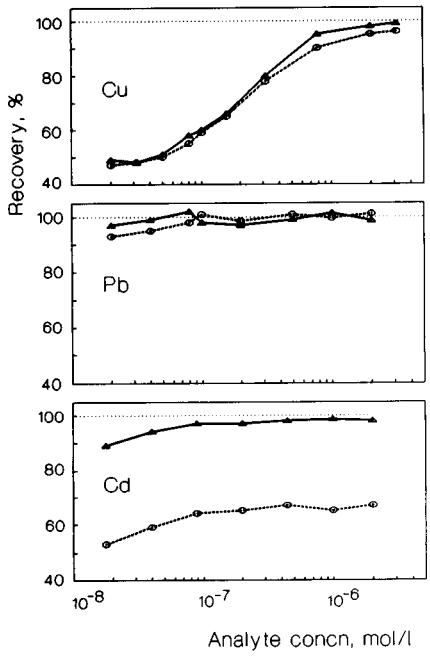

Fig. 7. Collection recoveries for Cu, Pb and Cd at various analyte concentrations in 0.2 M Na_2SO_4 supporting electrolyte at pH 3.3. Volumetric flow-rate, 0.95 ml min^{-1} (full lines) and 2.5 ml min^{-1} (dashed lines); deposition and collection potentials, −1.0 and −0.8 V, respectively.

Cadmium. While the stripping signal of Cd in the potassium nitrate carrier electrolyte was normal, the shape of the corresponding collection signal depended significantly on the collection potential. On applying a collection potential more negative than −0.9 V, the observed collection peak was much larger than theoretically expected, and moreover the signal did not return to its original background value until the deposited Cd was removed from the electrode surface by a positive potential scan. The high currents during Cd collection are probably due to the reduction of nitrate ions to nitrite ions catalysed by the underpotential reduction of Cd [27]. In the other carrier electrolytes no such catalytic currents were observed.

Zinc. The stripping signal area in each tested electrolyte corresponded to the theoretical value but the signal evaluation was complicated by the reduction wave of hydrogen. The collection signal for Zn in potassium nitrate carrier electrolyte was accompanied by a much higher background signal than observed in the other electrolytes.

The best results for the simultaneous determination of Zn, Cd and Pb by ASC and ASCWC were obtained in sodium sulphate carrier electrolyte. Its concentration in the range 0.02–0.3 M did not influence the recoveries of the tested elements in neither the stripping or collection mode. The stripping peak potentials were slightly shifted to positive values on decreasing the electrolyte concentration. Significant broadening of the stripping and the corresponding collection peaks was observed at electrolyte concentrations below 0.1 M. Both the potential shift and the signal broadening may be attributed to *iR* drop effects enhanced by the higher ohmic resistance of the dilute electrolyte solutions.

The pH of the supporting electrolyte influences the deposition efficiency and the shape of the collection signal. The pH of the sample during the preconcentration step should be chosen to be as low as possible to avoid hydrolysis and sorption of the analyte ions on the tube walls and frits used in the cells and at the same time it should ensure quantitative electrodeposition. During the stripping/collection procedure the carrier electrolyte should facilitate rapid transport of the stripped elements and their subsequent quantitative deposition at the collector cell. It is relatively easy to find such a pH range for individual elements, but it is difficult for a simultaneous determination of elements with different electrochemical and sorption properties. At pH values lower than 4.5–4.8 and especially at higher flow-rates the recoveries of Cd (Fig. 7) and mainly of Zn are low owing to the negative redox potential of these elements. At higher pH values the elution of the stripped Pb and especially Cu species is extremely slow. Hence, for the simultaneous determination of Pb, Cd and Zn by ASCWC the pH of the supporting electrolyte should be adjusted to 5.3 − 5.6 and for the determination of Cu the pH should be 2–4. In the ASC mode only when using the upstream cell with a larger electrode surface area can a broader pH range from 5 to ca. 7 for the supporting electrolyte be used for the simultaneous determination of the four elements. Here, the elution rate of reoxidized species need not be taken into account. The pH of the sample solution should be in the range 5–5.5 to avoid sorption of the

analyte ions and to ensure their quantitative deposition at the upstream cell.

By using the optimum experimental parameters, accurate and reproducible results can be obtained over a broad concentration range of Zn, Cd and Pb. The correlation between ASC and ASCWC signals and analyte concentration is shown in Fig. 8. An excellent fit with the theoretical values was observed, especially for Cd and Pb. In the ASCWC mode at lower Zn concentrations slightly lower recoveries (87–94%) were observed at the given flow-rate. On decreasing the flow-rate to 2 ml min^{-1} recoveries of 95–99% were observed. The reproducibilities of the methods expressed as relative standard deviation (R.S.D.) varied with analyte concentration (Table 5) and for a given analyte concentration the ASCWC procedure provided more reproducible results than the ASC mode, especially for Zn, in accordance with the more favourable background signal in the ASCWC mode.

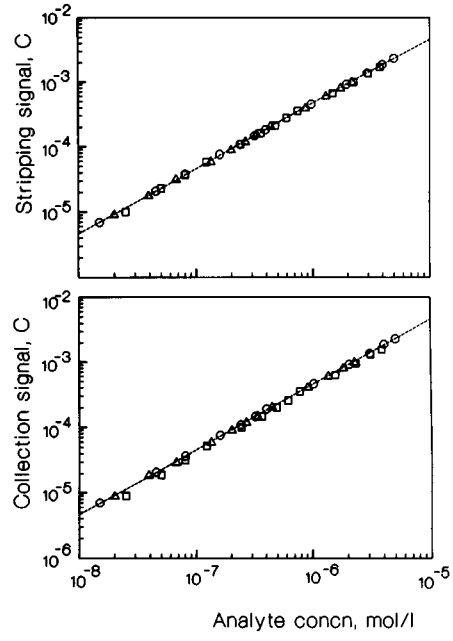

Fig. 8. Correlation of (top) the stripping and (bottom) the collection signals with the concentrations of (□) Zn, (△) Cd and (○) Pb in 2.4 ml of sample solution obtained with the continuous stripping procedure. Broken lines: theoretical dependences calculated as $Q_{calc} = zFc_{samp}V_{samp}$. Carrier electrolyte, 0.25 M Na_2SO_4 at pH 5.4; flow-rate, 2.5 ml min^{-1}; deposition and collection potentials, −1.3 and −1.2 V, respectively; potential scan rate, 40 mV s^{-1}.

Interference of copper

The stripping signal of Zn was broader in the presence of Cu in the samples and lower recoveries than theoretical were obtained. The adverse effect of Cu on the signals of Zn is evident at molar rations of Cu to Zn higher than 1. The signals of Pb and Cd were virtually not influenced by the presence of Cu.

The flow system used here could be utilized for the effective removal of the above interferences due to formation of Cu–Zn intermetallic compounds, but only in the ASC mode [6]. During the preconcentration step the potential of the upstream cell was set to a value ensuring deposition of Cu ions only, e.g., to −0.4 V in sodium sulphate supporting electrolyte. The more electronegative elements passed through the upstream cell and were deposited at the downstream cell kept at −1.2 V. On finishing the preconcentration step, the deposited elements at the downstream cell were stripped and measured without any interfering effect from Cu. Copper deposited at the upstream cell could also be

TABLE 5

Reproducibility of the determination of Zn, Cd and Pb at various analyte concentrations by using the continuous stripping procedure [a]

R.S.D. (%)	Zn (mol l^{-1})		Cd (mol l^{-1})		Pb (mol l^{-1})	
	ASC	ASCWC	ASC	ASCWC	ASC	ASCWC
< 1	–	$> 5 \times 10^{-7}$	$> 3 \times 10^{-7}$	$> 2 \times 10^{-7}$	$> 4 \times 10^{-7}$	$> 2 \times 10^{-7}$
5	2×10^{-7}	9×10^{-8}	6×10^{-8}	4×10^{-8}	9×10^{-8}	4×10^{-8}
10	1×10^{-7}	4×10^{-8}	3×10^{-8}	2×10^{-8}	4×10^{-8}	2×10^{-8}

[a] Calculated from five repeated analyses; investigated concentration range, 10^{-8}–10^{-5} M; for experimental parameters, see Fig. 8.

stripped and determined. In this way Zn at a concentration level of 10^{-7} M was accurately determined in the presence of a 10–50-fold excess of Cu.

Influence of dissolved oxygen in the sample

Neither the stripping nor the collection signals of Cd, Pb and Cu were influenced by oxygen present in the sample solution during the preconcentration step. The signals for Zn, however, were only 57–68% of the theoretical values for the stripping and collection processes in the presence of oxygen in the sample solution. As a consequence, for the reliable determination of Zn oxygen has to be removed from the sample solution before injecting it into the flow system. The oxygen-permeable sampling loop used in this work permitted simple and effective oxygen removal even without purging the sample solution with an inert gas if the sample was kept in the loop for at least 2 min before injecting it to the carrier electrolyte [14].

Conclusions

Anodic stripping coulometry and anodic stripping coulometry with collection have proved to be suitable for the simultaneous absolute determination of Cu, Pb, Cd and Zn. To achieve accurate and reproducible results the following parameters are decisive: potentials in the deposition, stripping and collection procedures; potential scan rate during stripping; volumetric flow-rate; and pH, concentration and properties of the carrier supporting electrolyte.

The advantages of ASC are from its simplicity, high selectivity and its lower dependence on experimental parameters such as volumetric flow-rate and solution pH. ASCWC, on the other hand, owing to the constant potential of the collector cell, exhibits much lower background currents, especially for Zn, Cd and Pb, facilitating signal processing. Its selectivity at higher stripping scan rates is lower than that for ASC, but this disadvantage can be overcome by using the step-by-step stripping/collection procedure.

The main features of the investigated methods are the absolute character and the closed and self-cleaning flow system, ensuring low contamination risks and high reproducibility [14]. Future analytical applications of these methods include analyses of pure reagents, reference materials and environmental and biological samples and trace element speciation analysis.

The award of a research fellowship to E. Beinrohr by the Humboldt Foundation, Bonn, enabling this research to be carried out is gratefully acknowledged.

REFERENCES

1 W.J. Blaedel and J. Wang, Anal. Chem., 51 (1979) 799.
2 W.J. Blaedel and J. Wang, Anal. Chem., 51 (1979) 1724.
3 G.W. Schieffer, Anal. Chem., 52 (1980) 1994.
4 G.W. Schieffer, Anal. Chem., 53 (1981) 126.
5 J. Wang and H.D. Dewald, J. Electrochem. Soc., 130 (1983) 1814.
6 J. Wang and H.D. Dewald, Anal. Chem., 55 (1983) 933.
7 T.P. Tougas and D.J. Curran, Anal. Chim. Acta, 161 (1984) 325.
8 J. Wang and H.D. Dewald, J. Chromatogr., 285 (1984) 281.
9 D.A. Ogaram and R.D. Snook, Analyst, 109 (1984) 1597.
10 D.J. Curran and T.P. Tougas, Anal. Chem., 56 (1984) 672.
11 E. Beinrohr, M. Nemeth, P. Tschöpel and G. Tölg, Fresenius' J. Anal. Chem., 343 (1992) 566.
12 K. Stulik and V. Pacakova, CRC Crit. Rev. Anal. Chem., 14 (1984) 297.
13 K. Stulik and V. Pacakova, Electroanalytical Measurements in Flowing Liquids, Horwood, Chichester, 1987.
14 E. Beinrohr, M. Nemeth, P. Tschöpel and G. Tölg, Fresenius' J. Anal. Chem., in press.
15 J.R. Pretty, E.H. Evans, E.A. Blubaugh, W.-L. Shen, J.A. Caruso and T.M. Davidson, J. Anal. At. Spectrom., 5 (1990) 437.
16 D.C. Johnson and R.E. Allen, Talanta, 20 (1973) 305.
17 G.W. Schieffer and W.J. Blaedel, Anal. Chem., 49 (1977) 49.
18 G.W. Schieffer and W.J. Blaedel, Anal. Chem., 50 (1978) 50.
19 T. Yamada, S. Okazaki and T. Fujinaga, Bull. Inst. Chem. Res. Kyoto Univ., 53 (1975) 452.
20 R. Nakata, S. Okazaki and T. Fujinaga, Nippon Kagaku Kaishi, (1980) 1615.
21 W.T. de Vries and E. van Dalen, J. Electroanal. Chem., 14 (1967) 315.
22 D.K. Roe and J.E.A. Toni, Anal. Chem., 37 (1965) 1503.
23 T.M. Florence, J. Electroanal. Chem., 27 (1979) 273.
24 A.L. Bard and L.R. Faulkner, Electrochemical Methods, Wiley, New York, 1980, p. 406.
25 M. Stulikova, Talanta, 38 (1991) 805.
26 A.G. Fogg, S.P. Scullion and T.E. Edmonds, Analyst, 116 (1991) 573.
27 X. Xing and D.A. Scherson, Anal. Chem., 59 (1987) 962.

Analytica Chimica Acta, 273 (1993) 27–34
Elsevier Science Publishers B.V., Amsterdam

Square wave adsorptive stripping voltammetry on mercury film electrodes

Anastasios Economou and Peter R. Fielden

Department of Instrumentation and Analytical Science, UMIST, P.O. Box 88, Manchester M60 1QD (UK)

(Received 1st June 1992)

Abstract

In this paper the relative advantages of using square wave adsorptive stripping voltammetry in combination with a mercury film electrode as the working electrode were assessed. It was found that the resulting technique is fast, sensitive, offers excellent discrimination against the background current and can be used without deoxygenation of the sample; the analytical applications of the technique are demonstrated for the determination of Ni(II) with a limit of detection of 0.85 nmol l^{-1} and a linear range of 3 orders of magnitude (for 60 s preconcentration) and for the determination of Cu(II) in the nmol l^{-1} concentration level in the presence of dissolved oxygen.

Keywords: Stripping voltammetry; Mercury film electrodes

Over the last decade adsorptive stripping voltammetry has attracted a great deal of attention, owing to its inherent sensitivity for both organic and inorganic surface active species [1,2].

Square wave adsorptive stripping voltammetry (SWAdSV) involves a stripping step carried out by using a square wave time–potential waveform imposed on the working electrode [3], as opposed to differential pulse adsorptive stripping voltammetry (DPAdSV) and linear sweep adsorptive stripping voltammetry (LSAdSV). The advantages of using a square wave for the stripping step include higher sensitivity (especially for reversible reactions) [4,5], effective discrimination against the capacitive current [3], speed of analysis [3] and insensitivity to dissolved oxygen in the sample [6,7].

Mercury film electrodes – which are prepared by electroplating a thin mercury film on a suitable substrate [8] – have found wide application in anodic stripping voltammetry (ASV) [9]. However, it seems that they are equally suitable for adsorptive stripping voltammetry for several reasons: transport to the electrode surface is precise and easily controlled (by employing either a rotating disk or a flow-stream electrode) [8], the electrode itself is robust and easy to maintain (thus it is ideal for industrial applications) [10], the electrode can be easily incorporated into an automated flow system for continuous monitoring applications and finally the electrode surface can be readily and quickly regenerated by plating a new mercury film.

This work is concerned with some initial applications of SWAdSV on MFEs in order to investigate and establish the advantages of the technique.

Correspondence to: P.R. Fielden, Department of Instrumentation and Analytical Science, UMIST, P.O. Box 88, Manchester M60 1QD (UK).

EXPERIMENTAL

Reagents

All reagents used were at least of analytical-reagent grade. Doubly distilled water was used

throughout. The 10 mmol l^{-1} standard stock solutions of Ni(II) and Cu(II) were prepared once and a 1 mmol l^{-1} standard riboflavin solution was prepared daily; more dilute solutions were prepared by serial dilution. The supporting electrolytes were NH_3/NH_4Cl buffer (0.1 mol l^{-1} total NH_3 and NH_4^+, pH 9) for Ni(II), 0.01 mol l^{-1} PIPES buffer (pH 6.8) for Cu(II) and 0.01 mol l^{-1} NaOH (pH 12) for riboflavin. 0.1 mol l^{-1} standard solutions of dimethylglyoxime (DMG) and 8-hydroxyquinoline (oxine) – as complexing agents for Ni(II) and Cu(II) respectively – were prepared in 95% ethanol and 0.45 mol l^{-1} HCl, respectively.

The mercury plating solution was 1 mmol l^{-1} Hg(II) in 0.1 mol l^{-1} KNO_3/0.01 mol l^{-1} HNO_3.

Instrumentation

The analytical set-up included: A three electrode Potentiostat (PARC Model 273) controlled by a 286 Proturbo PC. A rotating disk electrode (RDE) assembly (PARC Model 616) comprising a glassy carbon (3 mm o.d.) working electrode, a Ag/AgCl reference electrode and a Pt counter electrode. Argon gas for purging the solutions. A 50 ml analytical cell. A Roland plotter connected to the computer was used for obtaining hard copies of the data and pH values were measured with a Kent 7045 pH meter calibrated with standard buffers at pH 4, 7 and 9.

Procedure

The mercury film was plated from the 1 mmol l^{-1} Hg(II) solution at 600 s^{-1} rotation speed and at −1.0 V (vs. Ag/AgCl) for 2 min.

Then the electrode was transferred to the sample solution (which had already been spiked with the appropriate complexing ligand and purged with Ar for 10 min, unless otherwise stated), the analytical species was preconcentrated on the mercury film for a fixed time under rotation of the electrode, then the rotation was stopped, a rest period of 10 s followed and the square wave time-potential was initiated while the data (voltammogram) were saved on the hard disk of the computer.

The mercury film was regenerated either in situ (by keeping the electrode potential at −1.2 V (vs. Ag/AgCl) for 1–2 min) or by plating a fresh mercury film.

The conditions used for the measurements are given in Table 1.

TABLE 1

Conditions used for the SWAdSV measurement of different analytes

Analyte	Ni(II)	Cu(II)	Riboflavin
Preconcentration potential (V)	−0.7	0	0
Preconcentration time (s)	60	20	80
Electrode rotation speed (r.p.m.)	600	600	600
Square wave frequency (Hz)	40	40	40
Square wave pulse height (mV)	10	10	5
Square wave scan increment (mV)	2	2	2
Supporting electrolyte	NH_3/NH_4Cl buffer pH 9	PIPES buffer pH 6.8	0.01 M NaOH pH 12
Electrode cleaning	in situ	Fresh film	in situ
Complexing agent	1 mM DMG	0.05 mM oxine	–

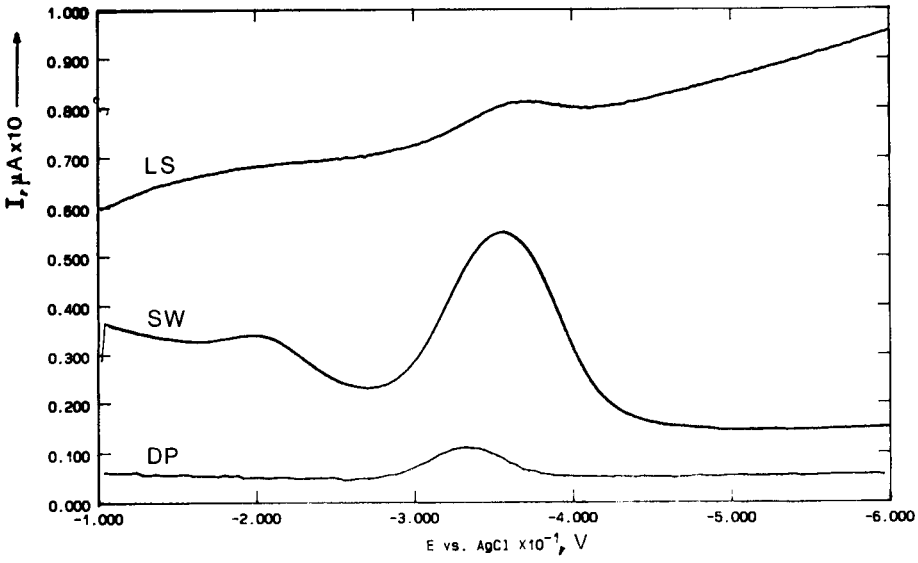

Fig. 1. Comparison between square wave (SW), differential pulse (DP) and linear sweep (LS) stripping for 20 nmol l^{-1} Cu(II) adsorbed on a MFE as the Cu–oxine complex. Conditions: (SW) as in Table 1; (DP) scan rate 10 mV s^{-1}, pulse height 20 mV, pulse width 50 ms, drop time 0.4 s; (LS) scan rate 80 mV s^{-1}.

RESULTS AND DISCUSSION

Sensitivity–background rejection

The theoretical treatment of square wave (SW) stripping of adsorbed species [4,5] indicates a sensitivity proportional to the degree of reversibility of the electrochemical reaction, which means that species that undergo reversible reactions benefit more by the application of SW than species that undergo quasi-reversible or totally

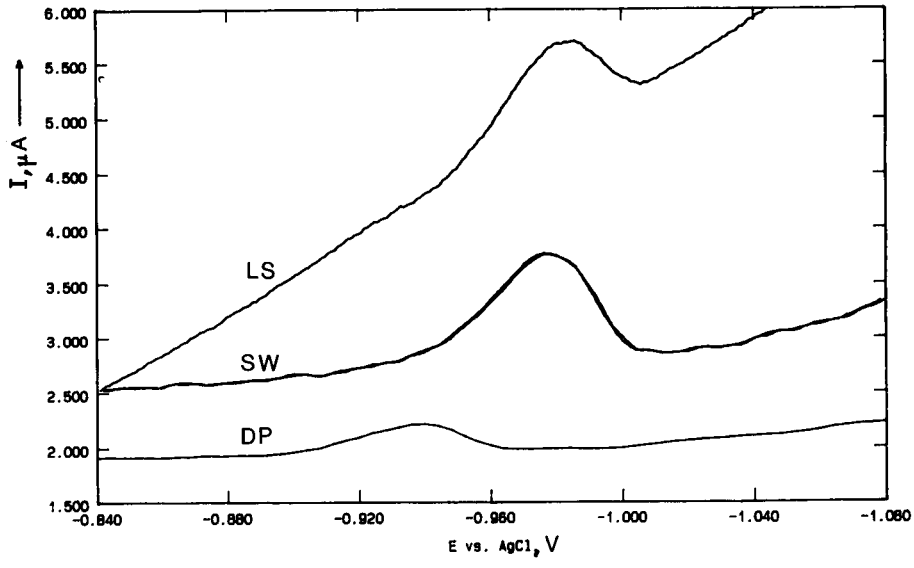

Fig. 2. Comparison between square wave (SW), differential pulse (DP) and linear sweep (LS) stripping for 20 nmol l^{-1} Ni(II) adsorbed on a MFE as the Ni(II)–DMG complex. Conditions: (SW) as in Table 1; (DP) scan rate 10 mV s^{-1}, pulse height 30 mV, pulse width 25 ms, drop time 0.4 s; (LS) scan rate 80 mV s^{-1}.

irreversible reactions. This prediction agrees with the observed behaviour; for the Cu(II)–oxine reduction, which is reversible [11], SW is at least 6 times more sensitive than linear sweep (LS) stripping – both carried out at the same effective scan rate – (Fig. 1) while for the Ni(II)–DMG reduction, which is a less reversible reaction, SW is no more sensitive than LS (Fig. 2). Differential pulse (DP) stripping is inherently limited by the low scan rates that must be used which result in a lower sensitivity than either SW or LS (Fig. 2 and Fig 1). This shortcoming of DP compared with SW and LS stripping becomes more serious considering that only an average scan rate of 80 mV s^{-1} is used for SW and LS stripping in both Fig. 2 and Fig. 1; when it comes to high scan rates of several hundred mV s^{-1} (that can be easily implemented for both SW and LS) DP is put to an even more serious disadvantage in terms of relative sensitivity.

In terms of background rejection LS gives the most sloping baselines to the point that at low concentrations the measurement of the peak height becomes difficult (Fig. 1 and Fig. 2); SW competes with DP for background rejection ability, with DP having a small advantage in that respect. In practice, what small disadvantage SW might have in terms of background discrimination, it more than makes up with superior sensitivity.

Speed

The fact that both SW and LS stripping can easily operate at high scan rates benefits, not only the sensitivity of these techniques as discussed above, but also the analysis time.

For SW an effective scan rate can be calculated by multiplying the square wave frequency by the square wave scan increment, with typical values of the effective scan rate ranging from 40 to 500 mV s^{-1}. On the other hand, in LS stripping of adsorbed species the ratio of the analytical faradaic current to the undesired capacitive current is not affected by the scan rate [12,13], so that high scan rates can be used with no additional background current introduced (as, for instance, in the case of diffusion-controlled voltammetry [13]; typical values for LS are 50–1000 mV s^{-1}.

Under these considerations and the fact that DP cannot usually operate with scan rates higher than 10 mV s^{-1}, a further disadvantage of DP stripping comes to light: it takes from 4 to 50 or even 100 times longer to complete the stripping

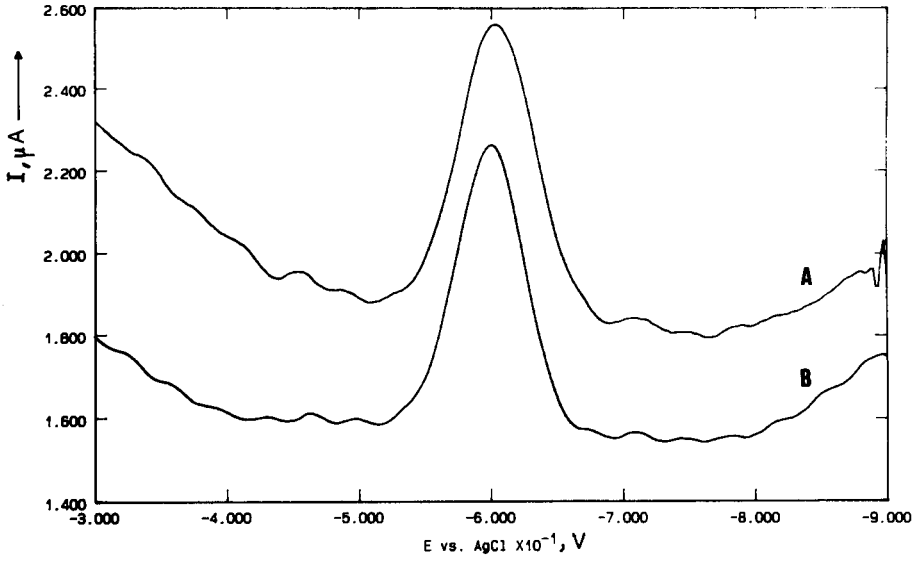

Fig. 3. SW stripping voltammograms for 20 nmol l^{-1} riboflavin adsorbed on a MFE (A) before and (B) after deoxygeneration for 10 min. Conditions as in Table 1.

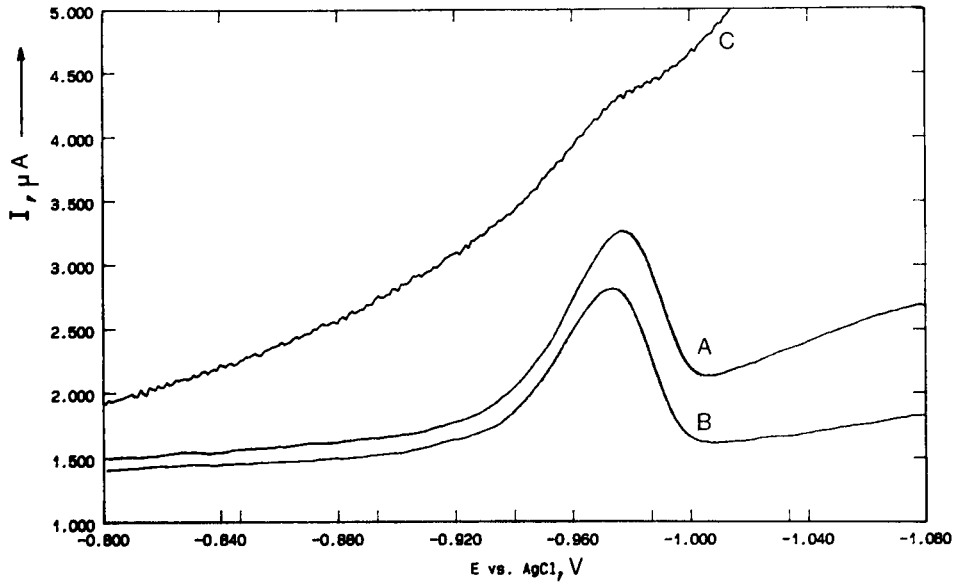

Fig. 4. Stripping voltammograms for 20 nmol l^{-1} Ni(II) adsorbed on a MFE as the Ni(II)–DMG complex (A) square wave stripping before deoxygenation, (B) square wave stripping after deoxygenation for 5 min (C) linear sweep stripping before deoxygenation. Conditions as in Table 1, linear sweep scan rate 80 mV s^{-1}.

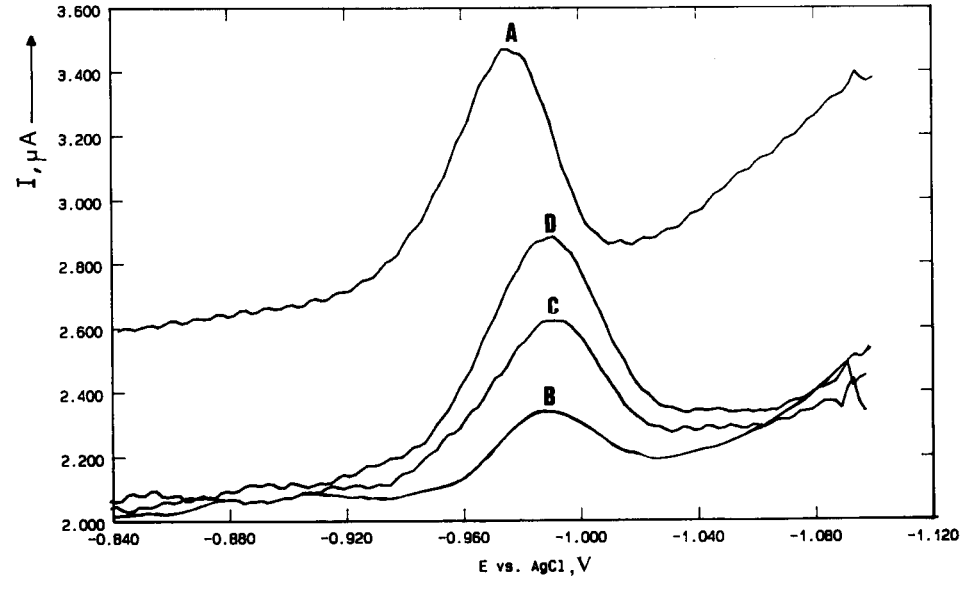

Fig. 5. SW stripping voltammograms for 20 nmol l^{-1} Ni(II) adsorbed on a MFE as the Ni(II)–DMG complex (A) in the absence of Triton X-100; (B) in the presence of 0.1 mg l^{-1} Triton X-100; (C) and (D) as (B) but after standard additions of 10 and 20 nmol l^{-1} Ni(II), respectively, with in situ electrode cleaning at −1.2 V for 1 min between measurements. Conditions as in Table 1.

step of an experiment with DP than with SW or LS.

Insensitivity to oxygen

As the reduction of oxygen is a totally irreversible reaction, the SW waveform is expected not to respond to it [6,7], thus providing a means of carrying out the analysis without deoxygenating the sample.

An example is shown in Fig. 3 where riboflavin (whose reduction is reversible) was measured both before and after deoxygenation of the sample with identical sensitivity. A similar comparison was made for Ni(II) as shown in Fig. 4. In that case oxygen interfered more with the measurement, probably because the Ni(II)–DMG reduction occurs near the second ($H_2O_2 \rightarrow H_2O$) oxygen reduction wave, but SW stripping was again much more sensitive than LS stripping.

Cleaning of the electrode

In some cases it is possible to clean and refresh the mercury film in situ by electrochemical means. In the case of Ni(II)–DMG or riboflavin adsorption the electrode potential was kept at -1.2 V (vs. Ag/AgCl) for 1 min. This cleaning procedure has a twofold function: (a) Any remaining adsorbed analyte on the mercury film is quantitatively reduced, thus any memory effects are minimised, and (b) any surfactants adsorbed on the electrode during the preconcentration step are stripped off at -1.2 V as their adsorption is not favoured at such a negative potential.

So it is possible to carry out the analysis in the presence of surfactants by introducing a cleaning step between stripping cycles. In Fig. 5 (traces B, C and D) standard additions for Ni(II) are shown in the presence of 0.1 mg l^{-1} of Triton X-100. Without the electrochemical cleaning step no increase in the response is observed under standard additions (on the contrary a decrease takes place as eventually all the active electrode surface is saturated with Triton X-100).

Another advantage of using electrochemical cleaning is the excellent reproducibility of the measurements, usually around 3% in terms of percent relative standard deviation.

Unfortunately there are cases where the in situ

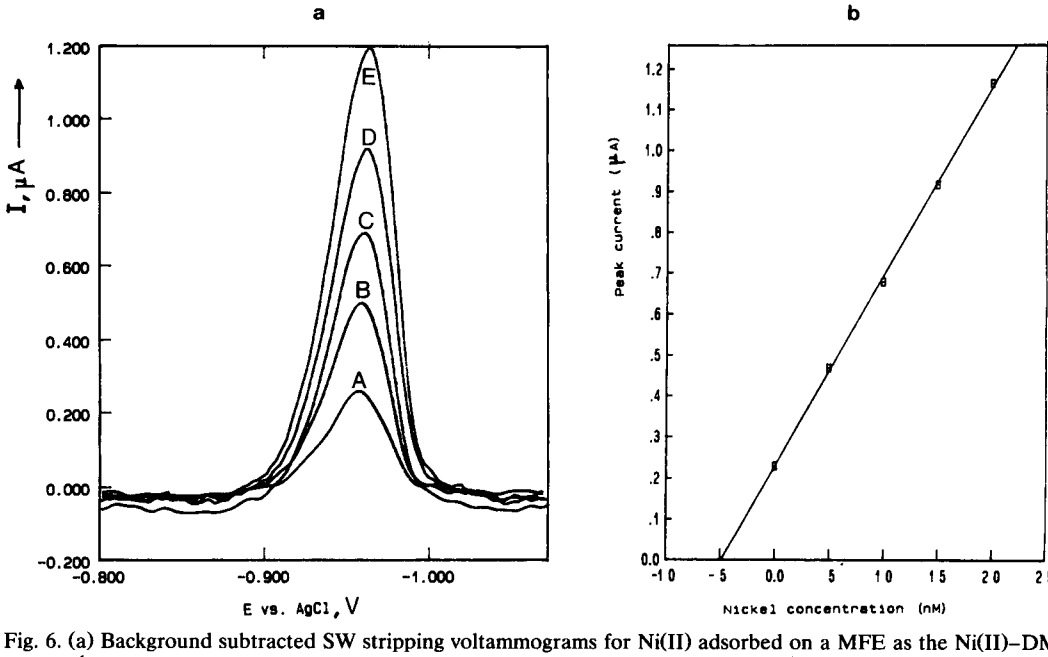

Fig. 6. (a) Background subtracted SW stripping voltammograms for Ni(II) adsorbed on a MFE as the Ni(II)–DMG complex: (A) 5 nmol l^{-1} Ni(II); (B), (C), (D) and (E) standard additions of 5, 10, 15 and 20 nmol l^{-1} Ni(II), respectively. Conditions as in Table 1. (b). Standard additions plot for the standard additions of Fig. 6(a).

cleaning is not possible. For example, if a cleaning step at −1.2 V (or for that matter at any potential more negative than the Cu(II)–oxine reduction potential) is used in the determination of Cu(II), Cu(II) is reduced to metallic copper that, instead of diffusing away of the electrode, amalgamates with Hg. This means that, when a preconcentration step is initiated at 0 V for the next measurement, the amalgamated copper remaining from the previous measurement is reoxidised to Cu(II) and complexes with oxine, thus contributing to the actual response in the form of a memory effect. In that case the cleaning step is self-defeating and a new mercury film has to be plated for each measurement. This brings to light a further disadvantage, lower reproducibility around 15% in terms of percent relative standard deviation and is probably due to irreproducible mercury plating. Nevertheless, by using an automated flow system it was shown that a reproducible film can be generated [14,15].

Analytical applications

Ni(II) can be easily determined at the nanomolar level by SWAdSV after adsorption of its complex with dimethylglyoxime on a MFE. For 60 s preconcentration the linear part of the calibration graph can be expressed by the equation:

$$(I_p/\mu A) = 8.8 \times 10^6 \left(C_{Ni(II)}/\text{mol } l^{-1}\right) + 0.14$$

Linearity holds from the limit of detection (in that case 0.85 nmol l^{-1} at the 3σ level) to 0.8 μmol l^{-1}; at higher concentrations, saturation of the electrode occurs. The limit of detection can be further decreased by using purer chemicals, longer deposition times and by employing the background subtraction approach.

SW voltammograms for the determination of 5 nmol l^{-1} Ni(II) are shown in Fig. 6a, where a computer based background subtraction approach was implemented resulting in an extremely flat baseline. In Fig. 6b the resulting standard additions plot is shown.

Cu(II) can be also determined by SWAdSV after adsorption of its complex with 8-hydroxyquinoline (oxine) on a MFE at the nanomolar level even in the presence of oxygen. SW voltammograms for the determination of 5 nmol l^{-1} Cu(II) in an undeoxygenated sample are shown in Fig. 7a. The same determination was carried out

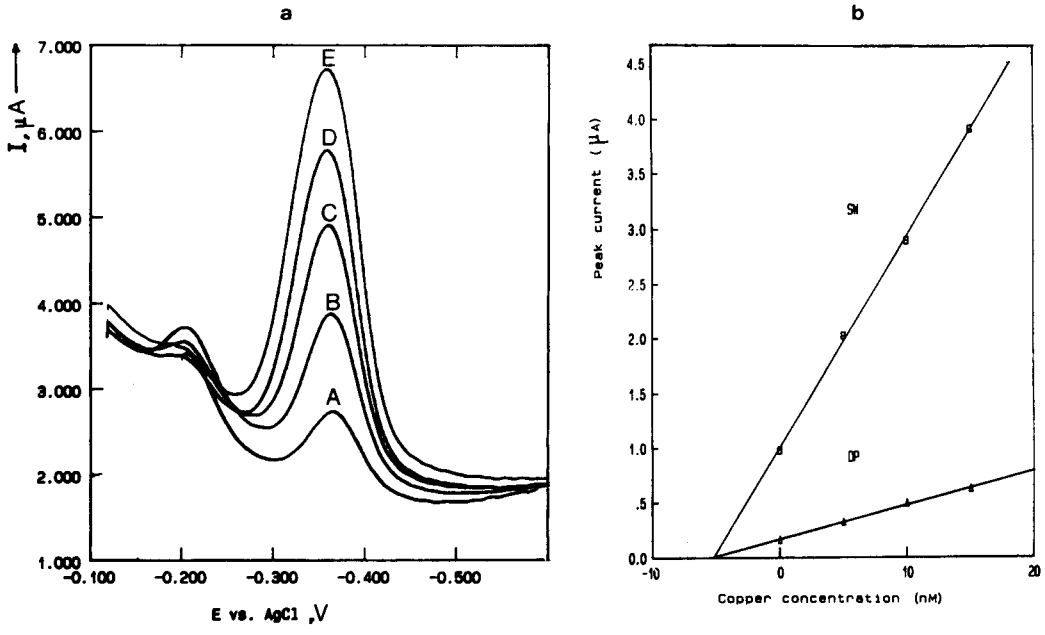

Fig. 7. (a): Stripping voltammograms for Cu(II) adsorbed on a MFE as the Cu(II)–oxine complex in the presence of oxygen; (A) blank; (B) 5 nmol l^{-1} Cu(II); (C), (D) and (E) standard additions of 5, 10 and 15 nmol l^{-1} Cu(II), respectively. Conditions as in Table 1. (b) Standard additions plot for the standard additions of Fig. 7(a) for both SWAdSV and DPAdSV. Conditions for DP are as in Fig. 1.

by using DP stripping and the corresponding standard additions (after subtraction of the blank) are shown in Fig. 7b, where the much higher sensitivity of SW compared with DP is demonstrated.

Conclusions

In this work it has been demonstrated that SWAdSV in conjunction with MFEs is a potentially interesting development in the field of adsorptive stripping analysis. The sensitivity, speed, good background rejection and insensitivity to oxygen of SWAdSV combined with the robustness, precise mass transport and renewable surface of a MFE make the technique very attractive for the trace determination of various species in continuous-monitoring industrial applications. Further work in that direction is being carried out in order to assess the applicability of the technique in flowing streams.

The authors gratefully acknowledge the support of AE by the Royal Society of Chemistry, through provision of a SAC Studentship.

REFERENCES

1 J. Wang, in A.J. Bard (Ed.), Electroanalytical Chemistry, Vol. 16, Marcel Dekker, New York, pp. 1–88.
2 R. Kalvoda and M. Kopanica, Pure Appl. Chem., 61 (1987) 97.
3 J.C. Osteryoung and R.A. Osteryoung, Anal. Chem., 57 (1985) 101A.
4 M. Lovric and M. Branica, J. Electroanal. Chem., 226 (1987) 239.
5 M. Lovric and S. Komorsky-Lovric, J. Electroanal. Chem., 248 (1988) 239.
6 P. Ostapczuk, P. Valenta and H.W. Nürnberg, J. Electroanal. Chem., 214 (1986) 51.
7 M Woljciechowski, W. Go and J. Osteryoung, Anal. Chem., 57 (1985) 155.
8 J. Wang, Stripping Analysis, VCH, Deerfield Beach, FL, 1985, pp. 69–75.
9 J. Wang, Stripping Analysis, VCH, Deerfield Beach, FL, 1985, pp. 109–146.
10 G.E. Batley and T.M. Florence, J. Electroanal. Chem., 55 (1974) 23.
11 C.M.G. van den Berg, J. Electroanal. Chem., 215 (1986) 111.
12 A.J. Bard and L.R. Faulkner, Electrochemical Methods, Wiley, New York, 1980, pp. 220, 522.
13 A.J. Bard and L.R. Faulkner, Electrochemical Methods Wiley, New York, 1980, p. 218.
14 C. Hua, D. Jagner and L, Renman, Anal. Chim. Acta, 197 (1987) 265.
15 H. Eskilsson, C. Haraldsson and D. Jagner, Anal. Chim. Acta, 175 (1985) 79.

Analytica Chimica Acta, 273 (1993) 35–40
Elsevier Science Publishers B.V., Amsterdam

Present potentials and limitations in the determination of trace elements by potentiometric stripping analysis

Peter Ostapczuk

Institute of Applied Physical Chemistry, Research Center (KFA) Jülich, P.O. Box 1913, D-5170 Jülich (Germany)

(Received 1st July 1992)

Abstract

The determination of trace elements such as Zn, Cd, Pb, Cu, Ni, Co, Tl, Bi and Sn by potentiometric stripping analysis (PSA) in various matrices is described. With natural water samples only simple acidification to a pH of about 2 is sufficient to liberate the trace elements. In more complex matrices like waste waters, whole blood or other liquid samples the pH, time and deposition potential play an important role for the liberation of some trace elements. The data of interlaboratory comparisons about the determination of lead in whole blood and wine samples by PSA after simple sample preparation are presented.

Keywords: Potentiometry; Stripping voltammetry; Beverages; Blood; Trace elements; Waters

Potentiometric stripping analysis (PSA) is an electroanalytical technique in which the trace elements (or ions) are preconcentrated by potentiostatic deposition on an electrode. After this preconcentration, the potentiostatic circuitry is disconnected and the elements are re-oxidized (or reduced) by some oxidant or by current (constant current potentiometry). During reoxidation (or reduction) the potential of the electrode is sampled at high-frequency. The need for high sampling rates has hampered the commercial development of PSA for a long time. The performance and price of present personal computers have improved the situation significantly. The dt/dV vs. potential curve recorded has the form of a stripping voltammetry curve. The sample solution may contain an oxidant, or oxidants, which vary in nature depending on the sample. The oxidants most frequently exploited hitherto have been mercury(II) ions and dissolved oxygen. With the mercury film electrode it is possible to determine the following elements by PSA: Bi, Cd, Cu, Ga, In, Pb, Mn, Tl, Zn, Co, Ni, Fe and Se. With a gold electrode it is possible to determine mercury, silver, arsenic, antimony and tin. The detection limit depends on the determined element and matrix as well as on the electrolysis time. The detection limit for the determination of cadmium in seawater is 1 ng l^{-1} but for manganese in the same matrix only 1 μg l^{-1}.

In contrast to anodic stripping voltammetry (ASV), PSA is not so sensitive to some organic compounds present in the sample solution. In the determination of trace elements in liquid samples (various water samples, body fluid, liquid food samples) the main problem is the choice of an appropriate supporting electrolyte to obtain all the determined elements free from complexing reagents.

The aim of this work is to present current knowledge about the possibilities of determining some trace elements in various matrices by PSA.

Correspondence to: P. Ostapczuk, Institute of Applied Physical Chemistry, Research Center (KFA) Jülich, P.O. Box 1913, D-5170 Jülich (Germany).

EXPERIMENTAL

Instrumentation

TraceLab™ and SAM20 sample station (Radiometer, Copenhagen) were used in connection with a Vectra 286/12 computer (Hewlett-Packard, Palo Alto, CA). The potentials in PSA were sampled at a frequency of 30 kHz. A Model SAC80 sample changer and a Model ABU93 Triburette (both from Radiometer) were employed for the routine cadmium and lead determinations in all samples. The Tap2 software package was used to carry out the analysis. For ASV after high pressure digestion with nitric acid in an HPA system (Hans Kürner, Rosenheim), the Model 384B polarographic analyzer from EG &G (PAR, Princeton, NJ) was applied.

All glassware, pipette tips, and vessels were cleaned several times with 10-fold diluted nitric acid. All operations of sample preparation and determination were done in a laminar flow hood with a high efficiency particle accumulator filter (Karl Blaymehl, Jülich).

Chemicals

A mercury plating solution with 8 g l^{-1} or 800 mg l^{-1} Hg(II) in 1.3 mol l^{-1} hydrochloric acid was prepared from Hg_2Cl_2 (p.a., Merck, Darmstadt) and hydrochloric acid (30%, Suprapur, Merck); alternatively, the plating solution (No. S2201) supplied by Radiometer was used.

TABLE 1

Detection limits and plating materials

Metals	Detection limit [a] ($\mu g\ kg^{-1}$)	Plating material
Bismuth	0.5	Mercury
Cadmium	0.001	Mercury
Copper	0.1	Mercury
Gallium	0.5	Mercury
Indium	0.1	Mercury
lead	0.001	Mercury
Manganese	1	Mercury
Thallium	0.1	Mercury
Zinc	0.1	Mercury
Arsenic	0.1	Gold
Cobalt	0.1	Mercury
Iron	0.1	Mercury
Mercury	0.1	Gold
Nickel	0.1	Mercury
Silver	0.1	Gold
Antimony	0.1	Gold
Selenium	0.5	Mercury
Tin	0.5	Gold

[a] Under optimal analysis conditions at 30 min deposition time.

RESULTS AND DISCUSSION

Natural water samples

Natural water samples are the most convenient samples for the electrochemical determination of trace elements. In the case of voltammetric determination, a sample digestion by UV-irradiation is necessary. With PSA determination, simple acidification with hydrochloric acid is sufficient to liberate trace elements from the complexing agents. It is possible to determine zinc, cadmium, lead, copper, thallium and bismuth in different waters by PSA after simple sample preparation.

For zinc determination only short deposition times can be used. Zinc and copper (normally present in all samples) can react in the mercury film and form intermetallic compounds. In this case, a decrease of sample size or deposition time is necessary. Thallium determination can be done at a pH of about 4.5 after the addition of EDTA to mask the lead [7]. Copper and bismuth can be determined in strongly acidified solutions (1–5 mol l^{-1} HCl). It is difficult to clean the electrodes and the cell from adsorbed Bi^{3+} ions. Table 1 presents the detection limits for some elements determined by PSA in natural water samples collected in our environmental specimen banking program.

Tin determination in the presence of lead can be done by PSA only after the addition of surfactant [8] or by constant current potentiometry (CCP) [9–11]. It is difficult to determine tin if very high concentrations of lead and copper are present in the sample.

The concentration of mercury in natural water samples is very low and can be determined on a gold electrode (or a glassy-carbon rod plated with gold) only after a longer deposition time (< 30

min). Mercury from the electrode can be stripped by constant current potentiometry or chemically by gold ions present in the solution. For some natural water, UV-digestion of the sample is necessary to determine the total mercury content.

Constant current potentiometry is used for selenium, nickel and cobalt determination. For these elements a decomposition of organic matter in the water samples by UV-digestion is necessary. In some cases a non-linear calibration curve is observed (e.g. Se or Ni and Co at higher concentrations).

The determination of heavy metals in atmospheric depositions is of interest in the studies of the biogeochemical cycles of trace elements and can give us some information about heavy metal input from the atmosphere. PSA was used for the routine determination of cadmium and lead in rainwater samples. Figure 1 presents the cadmium and lead found in rainwater samples collected in 1992 in three different regions of Germany.

Table 2 presents the results of zinc, cadmium and lead determinations in waste water samples from Hoechst AG by PSA without sample digestion and by voltammetry after sample digestion (HPA). The results obtained by PSA after simple sample acidification to pH 2 agree very well with results obtained by voltammetry after digestion. The precipitate present in these samples has no influence on the results obtained by PSA and voltammetry. This indicated that after acidification all the determined elements are also remobilized from the precipitate and that the filtration of the samples before the determination step is not necessary. In some cases, depending on sample composition (high concentration of complexing agents), the pH needed for remobilization of determined elements must be lower and then zinc determination by PSA can be difficult.

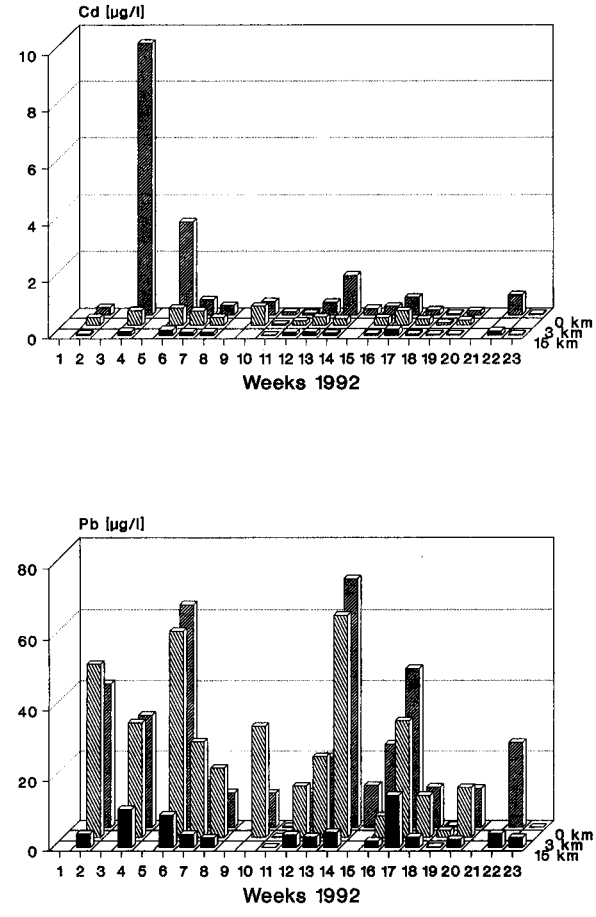

Fig. 1. Cadmium and lead concentration in rainwater collected downwind from the lead plant in the prevailing wind direction.

Body fluids

For the routine determination of cadmium and lead in body fluids only a few analytical methods

TABLE 2

Comparison between PSA and voltammetry (V) for the determination of Zn, Cd, Pb in waste water samples

Sample No.	Zn (mg kg^{-1})		Cd (µg kg^{-1})		Pb (µg kg^{-1})	
	PSA	V	PSA	V	PSA	V
1	3.65 ± 0.07	3.50 ± 0.05	0.12 ± 0.02	0.13 ± 0.02	5.30 ± 0.10	5.15 ± 0.18
2	7.23 ± 0.12	7.98 ± 0.04	0.10 ± 0.02	0.14 ± 0.03	3.22 ± 0.31	3.94 ± 0.43
3	–	–	176 ± 1	162 ± 4	76.1 ± 1.5	76.8 ± 3.1

can be used due to the low concentrations of the elements observed (especially for cadmium). For the determination of lead and cadmium by PSA only dilution of blood sample with appropiate supporting electrolyte (0.5 M HCl) is sufficient. The detection limit changes with deposition time and volume of blood sample used. For 1 ml of blood and 1 min deposition time, the detection limit is equal to 1 ng ml^{-1} for both elements. If the deposition time increases to 10 min cadmium determination is possible at the normal level (detection limit (< 0.1 ng ml^{-1}).

Interlaboratory comparison (ILC)

Our laboratory participates in the Danish External Quality Assessment Scheme (DEQAS) which is a proficiency testing scheme designed to evaluate the quality of results of measurements from a group of laboratories, i.e. ensuring a homogeneous quality of workplace analyses by rendering analytical results comparable and independent of the laboratory performing the analysis [12]. Table 3 presents results obtained by our laboratory in the ILC Round 5 (lead in human whole blood). These results were obtained by using the sample changer with automatic standard addition. Only in one case was the value found to be lower than expected.

In other body fluids, like urine, saliva or sweat, it is also possible to determine Cd, Pb and Cu after simple sample preparation. For other elements a digestion of sample prior to the determination step is necessary.

Liquid food samples

Determination of trace elements in wine and beverages may in the future become an exclusive field of application of PSA. Elements like Cd, Pb, Tl, Cu, and Bi can be determined by PSA after dilution with appropriate supporting electrolyte. The sensitivity in the case of the determination of lead is significantly higher than that of electrothermal atomization–atomic absorption spectrometry (ET–AAS). It is possible to determine 1

TABLE 3

Results of ILC Round 5: "Lead in human whole blood"

All participants		Population			
Sample No.	Results received	$Mean_{pop}$ μ (μmol l^{-1})	$S.D._{pop}$ (μmol l^{-1})	$C.V._{pop}$ (%)	$Outliers_{pop}$
1	18	0.173	0.020	11.460	3
2	18	0.563	0.063	11.220	0
3	18	0.993	0.157	15.800	0
4	18	1.428	0.176	12.330	1
5	18	2.319	0.163	7.010	3

PSA (KFA Jülich)				Acceptance [a]			
Sample No.	Result y (μmol l^{-1})	Ratio y/μ	Deviation $[(y-\mu)/\mu]$ (%)	R	O_{pop}	MEF	$RMSE^{1/2}$
1	0.160	0.926	7.410	+	+	+	+
2	0.579	1.029	2.890	+	+	+	+
3	0.845	0.851	14.920	+	+	+	+
4	1.404	0.983	1.700	+	+	+	+
5	2.273	0.980	1.980	+	+	+	+

[a] Acceptance of each result is given by (+), non-acceptance by (−). A sample is not accepted if: (i) the results from the laboratory were not received (R). (ii) The observation is demonstrated to be an outlier (O_{pop}); (iii) The estimated method evaluation function (MEF) exceeds the specified 95% confidence interval at the actual concentration level. The method evaluation function is only accepted if all the concentration levels are approved. (iv) The square rot of the estimated relative mean square error ($RMSE^{1/2}$) exeeds the 95% tolerance limit.

TABLE 4

Results of the European Community–USA–Canada intercomparison of methods for the analysis of Pb in wine, May 1992

Sample [a]	PSA ($n = 5$) ($\mu g\,l^{-1}$)	ET–AAS ($n = 5$) ($\mu g\,l^{-1}$)
A	70.1 ± 2.5	79.4 ± 1.4
B	990 ± 26	1007 ± 35
C	71.2 ± 1.8	71.5 ± 1.9
D	148 ± 3	148 ± 3
E	43.3 ± 2.0	42.2 ± 1.0

[a] A = acidified Pb solution; B = EPA Reference Material Pb solution; C = naturally contaminated dry white wine; D = naturally contaminated sweet white wine; E = naturally contaminated dry red wine.

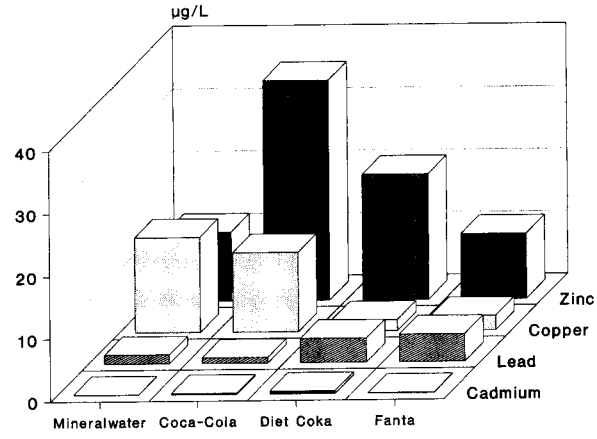

Fig. 2. Trace elements in beverages.

ng ml^{-1} lead in wine by PSA without any changes in procedure. The positive experience with the determination of lead by PSA led us to use this method in an interlaboratory comparison organized in October 1991 by the Bureau Central de Références (BCR) for the determination of lead in wine. The results of this comparison have been published [13]. Table 4 presents the results obtained by direct determination in wine (PSA and ET–AAS) done in our laboratory in the next round organized by BCR in May 1992 (European Community–USA–Canada intercomparison of methods for the analysis of Pb in wine). The values found by both methods agree satisfactorily. Also in other beverages with a higher alcohol content (rum, vodka) it is possible to determine lead, cadmium and copper by PSA but the determination sensitivity decreases with increasing alcohol concentration in the solution.

In soft drinks, including those with high sugar content, some elements can be determined by PSA after acidification. Figure 2 presents the concentration of zinc, cadmium, lead and copper found in some soft drinks. PSA was also used for the determination of some trace elements in sugar after simple dissolution of appropriate amounts of sugar in water at pH 2.

Solid samples

For all the solid samples digestion of the sample is necessary prior to determination. May digestion methods are established in routine analytical work. If voltammetry is used for the determination of trace elements, high pressure digestion (HPA) is the method of choice. If PSA is used for Cd, Pb and Cu determination other digestion systems like digestion in PTFE bombs or microwave digestion can be used. Figure 3 presents the sample path before determination of the trace element used in our routine work. Experience gained from routine determinations of Cd and Pb in environmental samples has demonstrated that PSA can be used with success for the determination of these elements in samples with very small concentrations of them like eggs, milk powder or meat. Figure 4 presents the reproducibility obtained in the determination of cadmium and lead in digested (HPA) filter samples using a sample changer and automatic standard addition. In this case, most human errors are eliminated and a

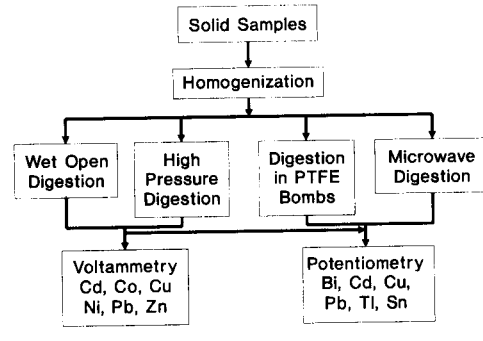

Fig. 3. Solid sample preparation path prior to trace element determination.

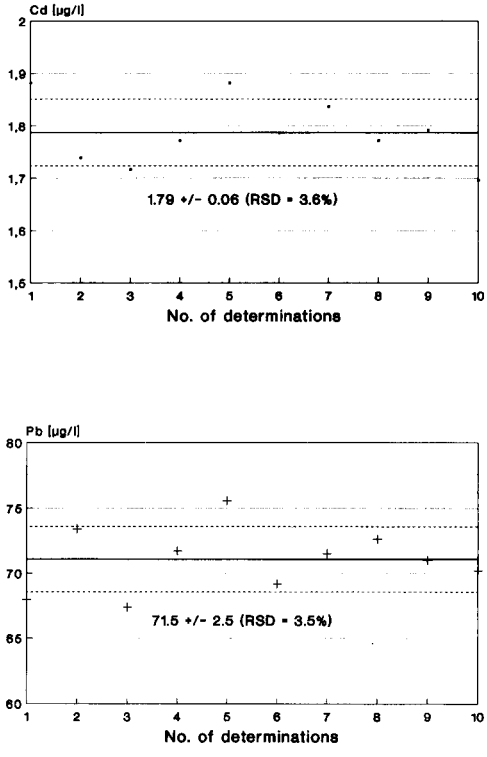

Fig. 4. Reproducibility of Cd and Pb determination in digested rainwater filter.

very good reproducibility is obtained. Some results of element determinations in environmental samples by PSA have been published [14].

Conclusions

In comparison with voltammetry PSA has the following advantages: (1) determinations can be done in undeaerated solution because oxygen is used in the chemical oxidation step (time for a single determination is reduced to about 3 min), (ii) cadmium and lead can be determined directly in the water samples, after simple sample preparation (if the content of organic substances in water samples is very low, the addition of some surfactants may avoid any effect on the analytical signals), and (iii) the sensitivity of PSA is better than that of differential pulse with a static mercury drop electrode when the same deposition time is used.

Analytical experience has demonstrated that parallel to a decrease of determination time direct determination by PSA in liquid samples eliminates the risk of contamination from sample handling and reduces the manpower needs for glassware cleaning.

Use of the sample changer with automatic standard addition significantly improves the reproducibility. Constant current potentiometry has the same disadvantages as voltammetry. For Ni and Co determination, it is necessary to digest the sample and to remove the dissolved oxygen from the solution. Additionally, due to the complicated properties of the mercury film electrode some conditioning steps are needed before determination.

REFERENCES

1 P. Ostapczuk, Lab. Praxis, 6 (1991) 460.
2 L. Almestrand, D. Jagner and L. Renman, Talanta, 33 (1986) 991.
3 P. Ostapczuk, Clin. Chem., in press.
4 L.G. Danielsson, D. Jagner, M. Josefson and S. Westerlund, Anal. Chim. Acta, 127 (1981) 147.
5 M. Rozali bin Othman, J.O. Hill and R.J. Magee, Fresenius' Z. Anal. Chem., 326 (1987) 350.
6 A. Hu, R.E. Dessy and A. Graneli, Anal. Chem., 55 (1983) 320.
7 R. Cleven and L. Fokkert, ESEAC '92, 4th European Conference on ElectroAnalysis, Noordwijkerhout, June 1992.
8 J.H. Mendez, R.C. Martinez and M.E.G. Lopez, Anal. Chim. Acta, 138 (1982) 47.
9 J. Wang and J. Zadeii, Talanta, 34 (1987) 909.
10 C.M.G. van den Berg, S.H. Khan and J.P. Riley, Anal. Chim. Acta, 222 (1989) 43.
11 C.M.G. van den Berg and S.H. Khan, Analyst, 116 (1991) 585.
12 DEQAS, Second Edition, 1992 Danish National Institute of Occupation Health, AMI, DK-2100 Copenhagen.
13 C. Marin and P. Ostapczuk, Fresenius' J. Anal. Chem., 343 (1992) 881.
14 P. Ostapczuk and M. Froning, in M. Rossbach, D. Schladot and P. Ostapczuk (Eds.), Specimen Banking, Springer-Verlag, Berlin, 1992, pp. 153–165.

Analytica Chimica Acta, 273 (1993) 41–51
Elsevier Science Publishers B.V., Amsterdam

Anodic stripping voltammetry of copper at ex situ-formed mercury-coated carbon fibre microelectrodes in the presence of low concentrations of supporting electrolyte

Leif Nyholm

Department of Analytical Chemistry, Uppsala University, P.O. Box 531, S-751 21 Uppsala (Sweden)

Gunnar Wikmark

Radiation, Materials and Chemical Technology, Nuclear Systems, ABB Atom AB, S-721 63 Västerås (Sweden)

(Received 1st June 1992; revised manuscript received 27th August 1992)

Abstract

The anodic stripping voltammetry of copper at ex situ-formed mercury-coated carbon fibre microelectrodes was studied in the presence of low concentrations of supporting electrolyte. Determinations can be carried out in the absence of a deliberately added electrolyte but are affected by changes in the ionic strength. The addition of a small amount of $NaNO_3$ was found to increase the reproducibility in the determinations, particularly in the differential-pulse mode; 5×10^{-10} M Cu^{2+} could be determined with a deposition time of 1800 s in the presence of 2.5×10^{-6} M $NaNO_3$. The stripping peak shapes and potentials also depend on the electrolyte concentration and this dependence cannot be explained by ohmic drop, migration or contamination effects. A dependence of the stripping kinetics on the electrolyte concentration, due to double-layer effects, appears to be a more likely explanation. The stripping peak currents also depend on the nature of the mercury film but this dependence is probably caused by supersaturation of the coatings. The dependence of the copper stripping peak currents on the deposition potential, deposition time, copper concentration and the stripping technique employed (pseudo-staircase, differential-pulse or square-wave stripping voltammetry) in the presence of low electrolyte concentrations is discussed. Some results for lead are also presented.

Keywords: Stripping voltammetry; Carbon fibre microelectrodes; Copper; Mercury-coated carbon fibre microelectrodes

Stripping voltammetric determinations with microelectrodes offer some interesting advantages. One is that the enhanced rate of diffusion to microelectrodes [1–7] makes stirring dispensable during the deposition step. This results in better defined hydrodynamic conditions which are expected to increase the reproducibility in stripping voltammetric determinations [3–5]. Another, perhaps more important, advantage of employing microelectrodes is the possibility of carrying out measurements in solutions with low conductivities [8–16]. As a supporting electrolyte does not need to be added prior to the measurements, the use of microelectrodes helps to minimize the risk of contaminating or otherwise changing the speciation of the sample. Microelectrodes are, therefore, well suited for in situ monitoring of trace elements, especially as it has been shown [17–21] that the determinations can be carried out also in solutions containing oxygen. Daniele et al. [12,22] employed differential-pulse anodic stripping voltammetry (DPASV) at microelectrodes to determine copper, lead, cadmium and zinc in rain and sea water while Wang and co-workers [8,13]

Correspondence to: L. Nyholm, Department of Analytical Chemistry, Uppsala University, P.O. Box 531, S-751 21 Uppsala (Sweden).

discussed stripping voltammetry in poorly conducting solutions and the use of microelectrodes for metal speciation studies in aqueous solutions of low ionic strengths. Iridium-based mercury film electrodes were recently employed by De Vitre et al. [16] to determine trace metals (Pb^{2+} and Cd^{2+}) in low ionic strength lake water.

Inspired by the above papers, we recently tried to determine copper with ex situ-formed mercury-coated carbon fibre microelectrodes in the presence of low concentrations of supporting electrolyte [23]. The experiments showed, however, that the copper peaks were broad and non-symmetrical when the electrolyte concentration was less than ca. 10^{-6} M, despite the fact that well defined stripping peaks were still obtained for lead. The differential-pulse responses for copper increased with increasing electrolyte concentration whereas the staircase responses remained virtually constant. Because the behaviour did not appear to be immediately coupled either to the low solubility of copper in mercury or to the tendency of copper to form intermetallic compounds with, for instance, zinc, the effect is apparently not directly related to the complications often observed in copper determinations at larger electrodes [24–28]. Both mentioned complications are, however, expected to be more pronounced for mercury-coated microelectrodes than for larger mercury film electrodes as the amount of mercury present on the electrode is smaller in the former instance. As only a few workers [10,12,22,29,30] appear to have studied the stripping voltammetry of copper at mercury-coated microelectrodes, it is difficult to say what impact this has on copper determinations.

Although microelectrodes, as already mentioned above, may allow measurements also in the presence of only low concentrations of electrolyte, such measurements are not necessarily straightforward. Migration effects, which normally are of little importance at higher ionic strengths, may have to be considered, in addition to shifts in the peak potentials due to changes in the electrolyte concentration [31–39]. In very dilute solutions, the thickness of the double layer may also become comparable to that of the diffusion layer and the mass transport can then be enhanced or inhibited depending on whether the analyte is attracted or repelled by the charge of the electrode [40,41]. Likewise, double layer effects are probably more pronounced at low electrolyte concentrations [42] and problems associated with relatively high pH values near the electrode may also arise. For low electrolyte concentrations, it is generally more important to know something about the speciation of the sample than when the measurements are carried out after addition of, e.g., HCl or HNO_3 as supporting electrolyte.

The aim of this paper is twofold. First, the possibilities of employing anodic-stripping voltammetry (ASV) at ex situ-formed mercury-coated carbon fibre microelectrodes for the determination of copper in solutions with low conductivity are discussed. This is, for instance, interesting in connection with in situ monitoring of $\mu g\ l^{-1}$ levels of copper in the high-purity water employed in nuclear facilities. The second aim was to investigate the influence of the electrolyte concentration on the stripping peaks for copper. It is shown that this effect is unlikely to be caused by changes in the ohmic drop or in the liquid junction potential, and that the complications, which are most pronounced in the differential-pulse and square-wave modes, are more likely to be due to double-layer effects. The dependence of the anodic stripping peak currents and peak potentials for copper on parameters such as deposition potential, deposition time, copper concentration and the stripping technique employed (i.e., pseudo-staircase, differential-pulse or square-wave) is also discussed for low electrolyte concentrations.

EXPERIMENTAL

A previously described [43,44], microcomputer-controlled voltammetric analyser system was used. The software was modified along previous lines [45] in order to allow the simultaneous recording of pseudo-staircase (SC), differential-pulse (DP) and square-wave (SW) stripping voltammograms. A description of the potential programme and current sampling scheme is given in Fig. 1. The results of the current samplings S_1, S_2

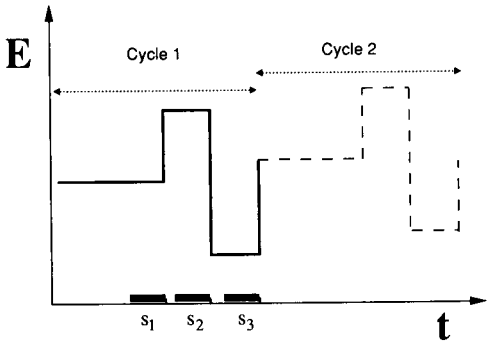

Fig. 1. Potential programme. S_1, S_2 and S_3 denote the three current sampling periods discussed in the text.

and S_3 are stored separately and can be evaluated either individually or as a difference between two samplings. The stripping evaluation mode (i.e., SCASV, DPASV or SWASV) is selected by the appropriate combination of the three current samplings, as is further described below.

Mercury-coated cylinder or disc microelectrodes were manufactured by first heat sealing 25-μm thick platinum wires (from Johnson Matthey) or 8-μm thick carbon fibres (from Sigri Elektrographit, Meitingen, Germany) in a polypropylene matrix and then coating the electrodes with mercury in an ex situ process [23]. The reference electrode was a saturated Ag/AgCl electrode and a bridge containing 10 mM HNO_3 was always used together with this electrode. The counter electrode consisted of a platinum wire.

To minimize systematic errors in the peak currents and peak potentials due to possible contamination by the solution in the reference electrode bridge, the measurements were generally carried out in a pseudo-random order. Unless stated otherwise, the instrumental parameters were as follows: deposition potential, −900 mV: potential range, −900 to +300 mV; pulse amplitude, 50 mV; sweep rate, 28.8 mV s^{-1}; cycle time, 200 ms; pulse duration, 30 ms; and deposition time, 760 s. The number of cycles used for each voltammogram was 208. Further details on the experimental procedures can be found in the previous paper [23].

RESULTS AND DISCUSSION

Figure 2a shows the current sampled during the three current sampling periods (S_1, S_2 and S_3) as a function of the potential for a solution containing 0.9 M $NaNO_3$, 1×10^{-7} M Cu^{2+} and 1×10^{-7} M Pb^{2+}. Note that curve I is, in fact, a pseudo-staircase stripping voltammogram and that the differences between curves II and I, and

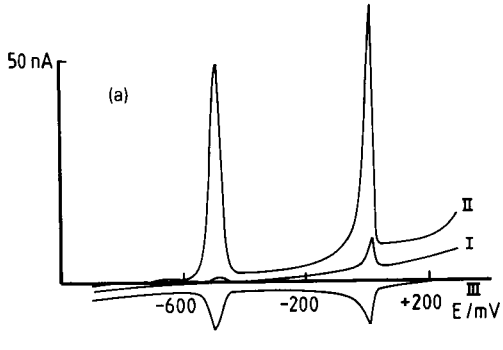

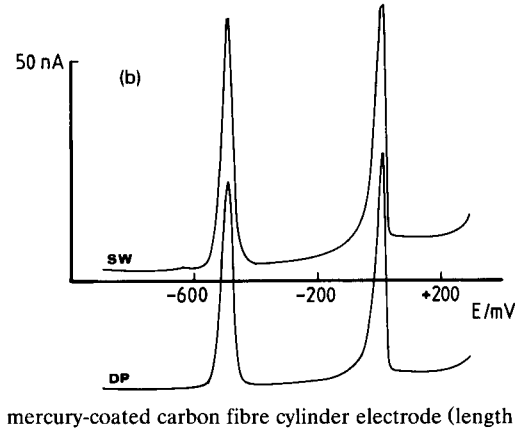

Fig. 2. (a) Anodic stripping currents obtained with an ex situ-formed mercury-coated carbon fibre cylinder electrode (length 50 μm) during the three sampling periods S_1 (I), S_2 (II) and S_3 (III). (b) Pseudo-differential-pulse (DP) and square-wave (SW) stripping voltammograms constructed by taking the difference between curves II and I and between curves II and III in (a) (the DP and SW curves have been shifted vertically for clarity). The solution contained 0.9 M $NaNO_3$, 1×10^{-7} M Cu^{2+} and 1×10^{-7} M Pb^{2+}.

between curves II and III, will yield a pseudo DP and a pseudo-SW stripping voltammogram, respectively. As the reverse currents (i.e., the third sampling responses) are small, it is not surprising that the square-wave evaluation mode yields only slightly larger stripping peaks (see Fig. 2b) compared with the differential-pulse peaks (note that the significantly higher sensitivity often claimed for the square-wave technique is due principally to the shorter pulses employed in this technique). The small reverse currents are in good agreement with earlier findings that the replating efficiency at microelectrodes is lowered by the enhanced diffusion of the ions away from the electrode [6]. The degree of replating was also found to increase when the duration of the pulses was decreased. Shorter pulse durations are therefore required in order to make use of the potentially higher sensitivity offered by the square-wave technique when microelectrodes are employed. The use of shorter pulse durations (i.e., higher frequencies), however, demands more of the electrochemical system as any kinetic complications will be intensified under such conditions. Moreover, decreased signal-to-noise ratios may be encountered as the use of shorter pulse durations may rule out the use of mains noise reduction by integrations during a full period of the mains frequency.

As was observed previously [23], and as is further illustrated in Fig. 3, the stripping voltammetric behaviour for copper (and to a smaller extent also for lead) depends on the concentration of the supporting electrolyte. Note especially the too small and distorted DP peaks and that an anodic rather than a cathodic reverse current is obtained for copper at the lower electrolyte concentration. Distorted reverse currents have been described previously [21,46–48] and it has been shown [20] that the phenomenon depends on the nature of the mercury coating. This is in agreement with our findings because the complications were most pronounced for electrodes with small amounts of mercury on them. As the copper responses are affected more than the lead responses, and as the reactions can be made more reversible by increasing the electrolyte concentration, it is clear, however, that kinetic considerations also are important for a full understanding of the effect.

Split peaks were occasionally observed for both copper and lead. The cause of the split peaks does not appear to be of a kinetic nature, however, as the shapes of the DP peaks were independent of the pulse durations in the range 30–150 ms. The split peaks were still seen after the addition of HNO_3 (to give a pH of ca. 2) and the effect is therefore unlikely to be linked to the speciation of the metals. A more likely explanation is that the appearance of the split peaks is coupled to the state of the mercury film as proposed by Cushman et al. [49].

It should be pointed out that although low concentrations of supporting electrolyte were em-

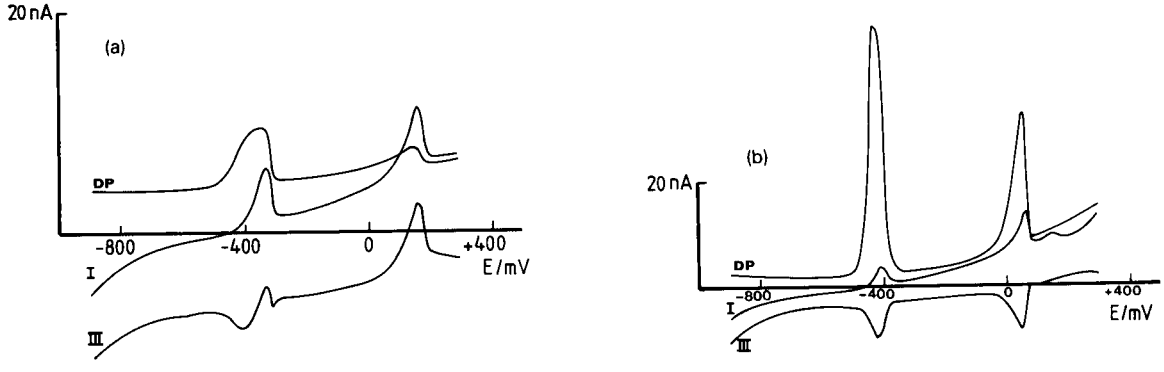

Fig. 3. Pseudo-differential-pulse (DP), staircase (I) and reverse currents (III) obtained with an ex situ-formed mercury-coated carbon fibre disc electrode in a solution containing 4.0×10^{-8} M Cu^{2+} and 4.0×10^{-8} M Pb^{2+}, (a) prior to and (b) after the addition of 7.3×10^{-4} M HNO_3.

ployed in this work, the even lower metal concentrations ensured that the electrolyte was present in an excess in most of the experiments, at least during the deposition step (this could, in fact, be the case even in the absence of an added electrolyte owing to the auto-protolysis of water).

In Fig. 4, the DP and SC stripping peak currents for copper are plotted as a function of the logarithm of the $NaNO_3$ concentration. The DP peak height increases with increasing electrolyte concentration but the SC response remains virtually constant. The DP stripping peaks also became sharper with increasing electrolyte concentration. Although similar supporting electrolyte concentration effects were occasionally seen for lead, the effect was generally more pronounced for copper except when the amount of mercury on the electrode was small. In such instances, the copper peak currents were generally very small and almost independent of the electrolyte concentration. The electrolyte concentration effect illustrated in Fig. 4 was also seen with mercury-coated platinum electrodes. The copper responses obtained with these electrodes were,

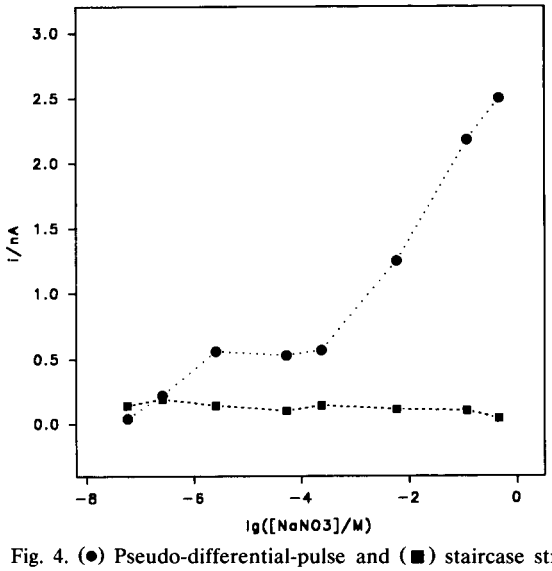

Fig. 4. (●) Pseudo-differential-pulse and (■) staircase stripping peak currents for copper as a function of the logarithm of the added $NaNO_3$ concentration. The voltammograms were recorded with a deposition time of 610 s employing an ex situ-formed mercury-coated carbon fibre disc electrode. The copper concentration was 4.0×10^{-8} M.

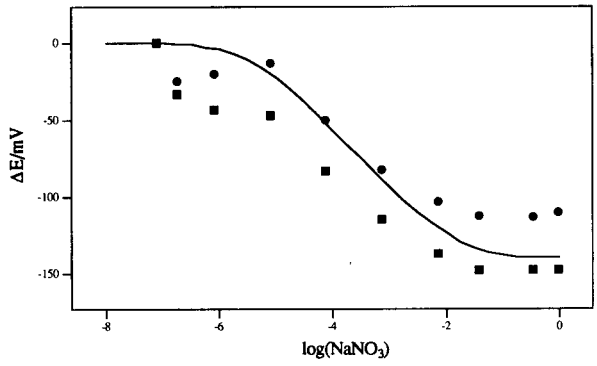

Fig. 5. (●) Pseudo-differential-pulse and (■) staircase peak potential shifts for copper as a function of the logarithm of the added $NaNO_3$ concentration. The potential shifts were calculated by subtracting the peak potentials obtained prior to the $NaNO_3$ additions. The solid line represents the estimated shifts due to changes in liquid junction potentials (see the text). The electrode was an ex situ-formed mercury-coated carbon fibre disc electrode. Other experimental conditions as in Fig. 4.

however, less satisfactory, as described previously [23]. Experiments in which HNO_3 rather than $NaNO_3$ was employed as the electrolyte indicated that the electrolyte effect is most likely connected with the nitrate concentration and is not due to a change in the pH in the vicinity of the electrode. For the highest HNO_3 concentrations, the stripping peak currents were, however, significantly smaller and the background at potentials more positive than that of the copper peak considerably larger than in the $NaNO_3$ experiments. The mercury films generally appeared to be less stable in these HNO_3 solutions, perhaps as a result of the (inevitable) hydrogen evolution during the deposition step.

As is seen in Fig. 5, the stripping peak potentials for copper were shifted in the negative direction when the $NaNO_3$ concentration was increased. A similar shift was also seen for lead and, therefore, appears to stem from either an ohmic drop or a liquid junction effect. Shifts due to the formation of nitrate complexes can be ruled out on the basis of their small stability constants. The size of the shifts did not depend on the magnitude of the current and the shifts therefore cannot be explained by an ohmic drop effect either. Estimations of the changes in the

liquid junction potentials based on the Henderson equation [42], on the other hand, showed that these calculated shifts were in good agreement with the experimental shifts (compare the experimental points in Fig. 5 with the calculated solid line). Smaller shifts were also seen when a 0.1 mM HNO_3 solution was employed instead of a concentration of 10 mM and when an $NaNO_3$ rather than an HNO_3 solution was employed in the reference bridge. These observations are likewise consistent with a liquid junction potential effect.

The liquid junction potential effect cannot explain, however, the dependence of the DPASV current on the $NaNO_3$ concentration. This dependence also cannot be explained by the dependence of the diffusion coefficients on the ionic strength [34], migration effects [31–39], copper impurities in the $NaNO_3$ solution or ohmic drop effects [32,33,35–39]. Instead, the experimental results suggest that the complications are connected with the kinetics of the stripping reaction. It is well known [50–54] that the electrochemical reactions of copper are affected by double-layer effects [42,55] even at high supporting electrolyte concentrations (i.e. 10^{-3}–1 M). As the double-layer effects become even more pronounced when the electrolyte concentration is decreased, it is likely that the dependence on the $NaNO_3$ concentration, seen in Fig. 4, is due to such an effect. Double-layer effects could also explain the decreased mercury stripping peaks obtained by Wong and Ewing [15] in the absence of a deliberately added electrolyte.

The "classical" double-layer effects discussed here should not be confused with those described by, for instance, Norton et al. [40] and Amatore and Lefrou [41] for situations in which the double layer and the diffusion layer are of comparable thicknesses at very small microelectrodes. In the latter cases, enhanced or inhibited steady-state fluxes and distorted voltammograms may be observed.

In the presence of "classical" double-layer effects the relationship between the apparent rate constant k^0 and the true (or corrected) standard rate constant k_t^0 is given by the following expression [42]:

$$k^0 = k_t^0 \exp[(\alpha n - z)F\phi_2/RT] \quad (1)$$

where α, n and z are the charge-transfer coefficient, the number of electrons transferred in the reaction and the charge of the species undergoing reduction or oxidation, respectively, and ϕ_2 denotes the potential drop between the electrode and the outer Helmholtz plane (where the reaction is assumed to take place).

As ϕ_2 depends on the difference $E - E_{pzc}$ [42,55] (where E_{pzc} is the potential of zero charge) and generally is positive at potentials positive of the pzc, it is not surprising that the effects are more pronounced for copper than for lead know-

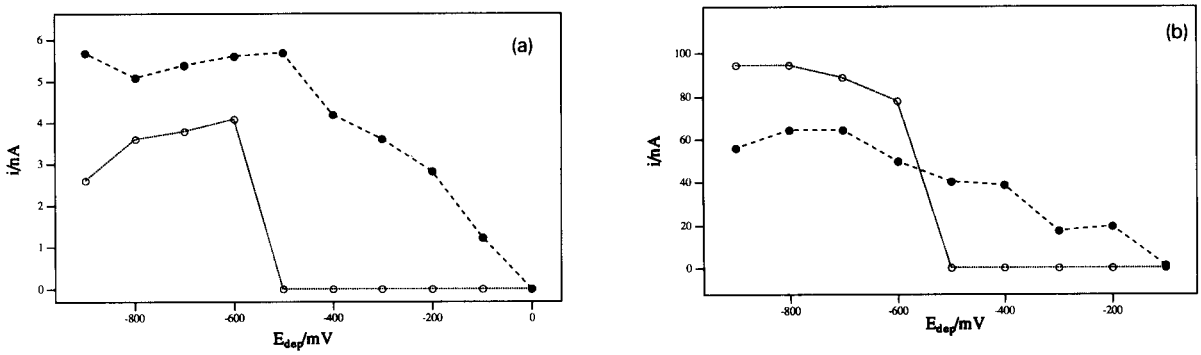

Fig. 6. Pseudo-differential-pulse anodic stripping peak currents for (●) copper and (○) lead as a function of the deposition potential, E_{dep}. (a) 4.0×10^{-8} M Cu^{2+}, 4.0×10^{-8} M Pb^{2+} and 1×10^{-7} M $NaNO_3$; (b) 1.0×10^{-7} M Cu^{2+}, 1.0×10^{-7} M Pb^{2+} and 0.9 M $NaNO_3$. The electrode was an ex situ-formed mercury-coated carbon fibre disc electrode.

ing that the latter metal should be stripped at a potential closer to the pzc and that k_t^0 is higher for lead than for copper.

The dependence of the responses on the $NaNO_3$ concentration can be explained by the decrease in the absolute ϕ_2 value with increasing electrolyte concentration [42,55]. Because the stripping of copper takes place on the positive side of the pzc at a mercury electrode, an increase in the nitrate concentration should result in an increase in the apparent rate constant. This would explain the increase in the DPASV currents and the improved peak shapes obtained with increasing electrolyte concentration. The DP peak currents should be more affected by double-layer effects than the SC currents as the SC measurements are carried out at longer times (i.e., in a time domain in which the reaction behaves more reversibly). The fact that the stripping peak currents were almost independent of the electrolyte concentration when electrodes with small amounts of mercury on them were employed suggests that the double-layer effects influence the stripping of the copper amalgam rather than the stripping of copper metal on the carbon fibre. It should be noted that mercury-coated carbon fibre electrodes have been reported [3,6,23,56,57] to consist of tiny mercury droplets rather than of a conventional film.

The kinetic effects discussed so far have been restricted to the stripping step. Figure 6, however, shows that also kinetic complications are involved during the deposition step at sufficiently positive deposition potentials. As can be seen, the dependence of the peak current on the deposition potential is different for copper and lead for both electrolyte concentrations. Note that the curves for copper are much more drawn-out than those for lead and that the shapes of the copper curves are similar for both nitrate concentrations, even though much larger peaks are obtained for the higher $NaNO_3$ concentration. It therefore appears as if the deposition of copper is kinetically controlled, at least for deposition potentials more positive than ca. −500 mV. As a deposition potential of −900 mV was used throughout this work, it is unlikely, however, that the dependence of the stripping currents on the electrolyte concentration seen in Fig. 4 was due to variations in the deposition step.

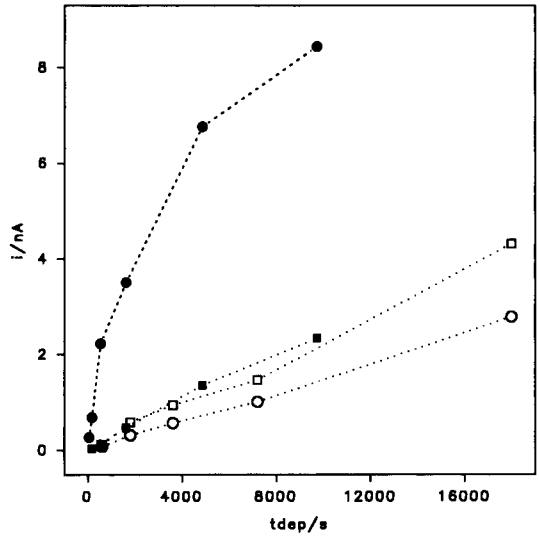

Fig. 7. (○, ●) Pseudo-differential-pulse and (□, ■) staircase stripping peak currents for copper as a function of the deposition time, t_{dep}, for a solution containing (open symbols) 2×10^{-7} M and (closed symbols) 6.3×10^{-3} M $NaNO_3$. The copper concentration was 3.9×10^{-8} M and the voltammograms were recorded with an ex situ-formed mercury-coated carbon fibre disc electrode.

An increasing influence of copper metal deposition with increasingly negative deposition potentials is an unlikely explanation for the shape of the stripping current versus deposition potential curve for copper as the stripping peak potential was almost independent of the deposition potential. A co-deposition of metallic copper is expected to cause a positive shift of the stripping peak potential. The different shapes of the copper and lead curves in Fig. 6 are more likely due to the lower k_t^0 value for copper. Double-layer effects may, however, also be involved as the apparent rate constant k^0 should increase with increasingly negative potentials.

The dependence of the SC and DP stripping peak currents for copper on the deposition time for two different supporting electrolyte concentrations is shown in Fig. 7. As in Fig. 4, the DP peak current increased significantly when the nitrate concentration was increased. Note, however, that the increased electrolyte concentration

resulted in a relationship between the peak current and the deposition time which is far from linear. The reasons for the curvature appear to be kinetic and specific to copper as linear DP plots were still obtained for lead under the same experimental conditions. The latter conclusion is also supported by the observed anodic shifts in the copper stripping peak potential with increasing deposition time and by the broad and distorted DPASV peaks seen for the longest deposition times. Another point, illustrated in Fig. 7, is that the ratio between the DPASV and the SCASV peak currents is lower than expected for low electrolyte concentrations (see also Fig. 4). The SC peak current in Fig. 7 is actually larger than the DP current for the lowest electrolyte concentration. As the SC stripping current was linearly dependent on the deposition times even after the DP plot had become curved the complications are most likely coupled to the stripping step. In fact, it seems as if the DPASV response only represents some of the deposited material but that this measurable fraction increases with increasing electrolyte concentration. We therefore propose that the stripping of the copper deposit is quasi-reversible on the time scale of DPASV but almost reversible on that of SCASV when the electrolyte concentration is low.

The curved DPASV curve in Fig. 7 probably stems from the increased tendency to saturate the mercury coating with copper with increasing deposition times (the solubility of copper in mercury is only ca. 0.006 at.% [24]). Saturations of mercury films with respect to copper are well known for mercury film electrodes of larger dimensions [24–28] and can be expected to be more pronounced for mercury-coated microelectrodes owing to the smaller amount of mercury present on such electrodes (saturation effects for mercury-coated microelectrodes have, for instance, been reported for lead and cadmium [3,15,49,56]). The observed positive shifts in the peak potentials for long deposition times and the sharp descending edge of the peaks are also in agreement with a saturation phenomenon [27,58]. As was indicated earlier, the reactions involving copper metal appear to be slow and also almost independent of the electrolyte concentration.

In the case of a saturation effect, the results should depend on both the copper concentration and the amount of mercury coating present on the electrode. Experiments were therefore undertaken employing electrodes with various amounts of mercury on them. It was found that the DP current increased and that the peak potential shifted negatively with an increase in the amount of mercury coating. The shift in the peak potential cannot be explained on the basis of the theoretical expressions for thin films [59–61] and a more likely explanation for the observations is, therefore, that the stripping reaction becomes more reversible as the amount of mercury coating on the electrode increases. Such an effect would also explain the concurrent changes in the shape of the stripping peaks. With small amounts of mercury on the electrode a memory effect was seen which caused the currents to depend not only on the deposition time but also on the history of the electrode. This memory effect, which was ascribed to the inability to strip all the copper during the stripping step, disappeared when the amount of mercury coating on the electrode was increased or when the mercury deposition was carried out in situ. The more reversible behaviour in the latter instances was also manifested by the fact that the copper peak potentials were found to be almost independent of the deposition time.

When the copper concentration was increased the stripping peak potentials were found to be shifted positively, as shown in Fig. 8, and the peaks also became broader. The effects were again most pronounced when the amount of mercury coating on the electrode was small and the observations are, consequently, also consistent with a saturation of the mercury film, as is the almost linear relationship between the peak potential and the logarithm of the copper concentration for copper concentrations higher than ca. 10^{-8} M in Fig. 8. Despite the apparent saturation, linear calibration graphs were still obtained for copper concentrations up to at least 5.0×10^{-8} M (see the inset in Fig. 8) [the DPASV plot has a slope of 6.4×10^{-2} ($s = 4 \times 10^{-3}$) A mol^{-1} dm^3 and an intercept of 4.0×10^{-10} ($s = 0.9 \times 10^{-10}$) A, while the corresponding values for the SCASV

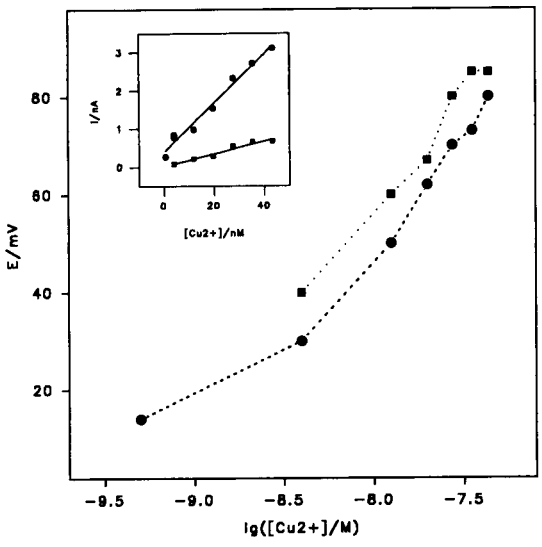

Fig. 8. (●) Pseudo-differential-pulse and (■) staircase stripping peak potentials for copper as a function of the logarithm of the copper concentration. The inset shows the pseudo-differential-pulse and staircase peak currents as a function of the copper concentration. An ex situ-formed mercury-coated carbon fibre disc electrode was employed and 2.5×10^{-6} M $NaNO_3$ was used as electrolyte. The deposition time was 1800 s.

curve are 1.6×10^{-2} ($s = 1 \times 10^{-3}$) A mol^{-1} dm^3 and 1.8×10^{-11} ($s = 4.0 \times 10^{-11}$) A; the numbers in parentheses are estimated standard deviations and the regression coefficients for these lines are 0.979 and 0.966, respectively]. A similar observation was also made by Golas and Osteryoung [3], who obtained linear calibration graphs for lead for up to eight times supersaturated mercury films. Although a nitrate concentration of 2×10^{-6} M was used in our experiments, it should be pointed out that successful determinations of traces of copper can also be achieved in the absence of a deliberately added electrolyte, provided that longer deposition times are employed.

In the presence of 2×10^{-6} M $NaNO_3$ it is possible to determine 4.8×10^{-10} M copper with a deposition time of 1800 s. The detection limit is, at present, mainly set by the sensitivity of the current-to-voltage converter and a current-measuring device more suitable for microelectrode work should most likely allow this limit to be decreased, and the use of shorter deposition times. The latter would save time and decrease the risk of mercury coating saturation and of contamination.

Electrode performance and stability

As described previously [23], the stripping responses for ex situ-formed mercury-coated electrodes were generally found to increase with time initially. At the same time the shape of the peaks generally became better defined. The reasons for these changes with time are still not fully understood but the effects could be connected to a redistribution of many small mercury droplets to form larger drops. Such a redistribution could explain the changes in the peak heights and shapes, as saturation of the films should be less likely for coatings consisting of larger drops. The influence of the nature of the mercury coating on the risk of obtaining supersaturated films has been discussed by, for instance, Stojek et al. [27] and changes in the spreading of mercury on a mercury-coated platinum microelectrode have also been proposed [62] as an explanation for positive shifts in the pzc with time.

The condition of the mercury film is, as already indicated, reflected in the magnitude and shape of the stripping peaks. In situ-prepared mercury films sometimes give rise to sharper and larger stripping peaks than ex situ-formed films, probably owing to the loss of some of the mercury on the transfer of the ex situ-formed electrodes. For small amounts of mercury on the electrode the stripping peak potentials are too anodic and the responses for lead are generally larger than those for copper (it should be mentioned that the presence of metallic copper on electrodes has been reported [63] to give rise to increased lead peaks). The ratio between the DP and SC peaks for copper is also often significantly smaller for ex situ-formed electrodes than for in situ-deposited electrodes.

The lifetime of the ex situ-prepared electrodes is mainly determined by the gradual loss of the mercury coating [23]. The formation of HgO [56] due to the oxidation of the mercury should not give rise to any significant losses of mercury at pH values above ca. 4, owing to the low solubility of HgO under these conditions and the fact that

any HgO present should be reduced to Hg at potentials more negative than ca. +300 mV. A more likely cause of loss of mercury, apart from mechanical detachment, is the dissolution of mercury; the solubility of mercury in water is ca. 3×10^{-7} M [64].

The reproducibility, particularly in the DP results, was generally increased when the supporting electrolyte concentration was increased, probably owing to the reduced sensitivity of the DP peak current to changes in the electrolyte concentration. The reproducibility of the measurements was also found to be higher when the ex situ-formed mercury coated electrodes were kept in the same electrolyte solution between the measurements and when the handling of the electrode was kept to a minimum. The latter was probably partly a result of the reduced risk of loosing the mercury deposit on transfer of the electrode [23]. It is also well known that quantitative stripping voltammetric measurements are best carried out employing the standard addition technique. The present results suggest that experiments with ex situ-formed mercury coatings should be carried out with flow cells, in which the handling of the electrode and the contamination can be minimized. According to some preliminary experiments (in which the Ag/AgCl or the platinum counter electrode was used as a combined counter–reference electrode), the copper measurements can also be done in a two-electrode cell without any significant loss of performance.

Conclusions

Ex situ-formed mercury-coated carbon fibre electrodes can be used in anodic stripping voltammetric determinations of trace amounts of copper in solutions with low conductivity but the determinations are complicated by double-layer effects. As the magnitude of the effect depends on the electrolyte concentration, determinations of copper in, e.g., rain water should be carefully planned as some additional information about the ionic strength of the sample is, in fact, generally required. Standard additions should, for instance, be performed in such a way that the ionic strength of the sample remains unaltered. The kinetic complications which are most pronounced in techniques such as square-wave and differential-pulse stripping voltammetry can be minimized by the use of longer pulse durations or by small additions of a supporting electrolyte.

With small amounts of mercury present on the electrode the risk of supersaturating the coatings with respect to copper is increased. This complication does not appear to be too serious, however, because the saturation primarily is a problem for high copper concentrations and as it should be possible to avoid the problems by employing shorter deposition times, provided, of course, that the small stripping currents can still be measured. The latter should be facilitated by the development of instrumentation specially designed for microelectrode work.

OKG (Oskarshamn Power Company) and ABB Atom are acknowledged for financial funding of this project. L.N. also acknowledges financial support from the Swedish Natural Science Research Council (NFR) during the preparation of the manuscript.

REFERENCES

1 M. Fleischmann, S. Pons, D.R. Rolison and P.P. Schmidt, Ultramicroelectrodes, Datatech Systems, Morganton, NC, 1987.
2 T.E. Edmonds, Anal. Chim. Acta, 175 (1985) 1.
3 J. Golas and J. Osteryoung, Anal. Chim. Acta, 186 (1986) 1.
4 K.R. Wehmeyer and R.M. Wightman, Anal. Chem., 57 (1985) 1989.
5 A.S. Baranski, Anal. Chem., 59 (1987) 662.
6 J.P. Sottery and C.W. Anderson, Anal. Chem., 59 (1987) 140.
7 A.R. Harman and A.S. Baranski, Anal. Chim. Acta, 239 (1990) 35.
8 J. Wang and P. Tuzhi, Anal. Chim. Acta, 197 (1987) 367.
9 B. Scharifker and G. Hills, J. Electroanal. Chem., 130 (1981) 81.
10 J. Wang, P. Tuzhi and J. Zadeii, Anal. Chem., 59 (1987) 2119.
11 Z. Stojek and J. Osteryoung, Anal. Chem., 60 (1988) 131.
12 S. Daniele, M.A. Baldo, P. Ugo and G.A. Mazzocchin, Anal. Chim. Acta, 219 (1989) 19.
13 J. Wang and J.M. Zadeii, J. Electroanal. Chem., 246 (1988) 297.
14 M. Ciszkowska, Z. Stojek and J. Osteryoung, Anal. Chem., 62 (1990) 349.

15 D.K.Y. Wong and A.G. Ewing, Anal. Chem., 62 (1990) 2697.
16 R.R. De Vitre, M.-L. Tercier, M. Tsacopoulos and J. Buffle, Anal. Chim. Acta, 249 (1991) 419.
17 A.R. Fernando and J.A. Plambeck, Anal. Chem., 61 (1989) 2609.
18 M. Wojciechowski and J. Balcerzak, Anal. Chem., 62 (1990) 1325.
19 M. Wojciechowski, W. Go and J. Osteryoung, Anal. Chem., 57 (1985) 155.
20 S.P. Kounaves and W. Deng, J. Electroanal. Chem., 306 (1991) 111.
21 M. Wojciechowski and J. Balcerzak, Anal. Chim. Acta, 249 (1991) 433.
22 S. Daniele, M.A. Baldo, P. Ugo and G.A. Mazzocchin, Anal. Chim. Acta, 219 (1989) 9.
23 L. Nyholm and G. Wikmark, Anal. Chim. Acta, 257 (1992) 7.
24 J. Wang, Stripping Analysis, VCH, Deerfield Beach, FL, 1985.
25 R. Neeb, Inverse Polarographie und Voltammetrie, Verlag Chemie, Weinheim, 1969.
26 F. Vydra, K. Stulik and E. Julakova, Electrochemical Stripping Analysis, Wiley, New York, 1976.
27 Z. Stojek, B. Stepnik and Z. Kublik, J. Electroanal. Chem., 74 (1976) 277.
28 H. Gunasingham and R.R. Dalangin, Anal. Chim. Acta, 246 (1991) 309.
29 A.S. Baranski and H. Quon, Anal. Chem., 58 (1986) 407.
30 G. Schulze and W. Frenzel, Anal. Chim. Acta, 159 (1984) 95.
31 C. Amatore, B. Fosset, J. Bartlelt, M.R. Deakin and R.M. Wightman, J. Electroanal. Chem., 256 (1988) 255.
32 K.B. Oldham, J. Electroanal. Chem., 250 (1988) 1.
33 A.M. Bond, M. Fleischmann and J. Robinson, J. Electroanal. Chem., 172 (1984) 11.
34 C. Amatore, M.R. Deakin and R.M. Wightman, J. Electroanal. Chem., 220 (1987) 49.
35 J.B. Cooper and A.M. Bond, J. Electroanal. Chem., 315 (1991) 143.
36 S.M. Drew, R.M. Wightman and C. Amatore, J. Electroanal. Chem., 317 (1991) 117.
37 M.J. Pena, M. Fleischmann and N. Garrard, J. Electroanal. Chem., 220 (1987) 31.
38 S. Bruckenstein, Anal. Chem., 59 (1987) 2098.
39 B.D. Pendley, H.D. Abruna, J.D. Norton, W.E. Benson and H.S. White, Anal. Chem., 63 (1991) 2766.
40 J.D. Norton, H.S. White and S.W. Feldberg, J. Phys. Chem., 94 (1990) 6772.
41 C. Amatore and C. Lefrou, J. Electroanal. Chem., 296 (1990) 335.
42 A.J. Bard and L.R. Faulkner, Electrochemical methods, Wiley, New York, 1980.
43 P. Baecklund and R. Danielsson, Anal. Chim. Acta, 154 (1983) 61.
44 P. Baecklund, L. Nyholm and G. Wikmark, Anal. Chem., 56 (1984) 1209.
45 L. Nyholm and G. Wikmark, Anal. Chem., 59 (1987) 2383.
46 K. Wikiel and J. Osteryoung, Anal. Chem., 61 (1989) 2086.
47 C. Wechter and J. Osteryoung, Anal. Chem., 61 (1989) 2092.
48 C. Wechter and J. Osteryoung, Anal. Chim. Acta, 234 (1990) 275.
49 M.R. Cushman, B.G. Bennett and C.W. Anderson, Anal. Chim. Acta, 130 (1981) 323.
50 G. Piccardi and R. Guidelli, J. Electroanal. Chem., 90 (1978) 173.
51 J.L. Anderson and I. Shain, Anal. Chem., 48 (1976) 1274.
52 J.L. Anderson and I. Shain, Anal. Chem., 50 (1978) 163.
53 A.W. Verkroost, M. Sluyters-Rehbach and J.H. Sluyters, J. Electroanal. Chem., 47 (1973) 311.
54 A.W.M. Verkroost, M. Sluyters-Rehbach and J.H. Sluyters, J. Electroanal. Chem., 47 (1973) 323.
55 Southampton Electrochemistry Group, Instrumental Methods in Electrochemistry, Horwood, Chichester, 1990.
56 J. Golas and J. Osteryoung, Anal. Chim. Acta, 181 (1986) 211.
57 M. Ciszkowska and Z. Stojek, J. Electroanal. Chem., 191 (1985) 101.
58 H. Gunasingham, K.P. Ang and C.C. Ngo, J. Electroanal. Chem., 215 (1986) 123.
59 S.P. Kounaves, J.J. O'Dea, P. Chandresekhar and J. Osteryoung, Anal. Chem., 59 (1987) 386.
60 M. Penczek and Z. Stojek, J. Electroanal. Chem., 213 (1986) 177.
61 S.P. Kounaves and J. Buffle, J. Electroanal. Chem., 239 (1988) 113.
62 A.R. Harman and A.S. Baranski, Can. J. Chem., 66 (1988) 1036.
63 H. Gunasingham and R.R. Dalangin, Anal. Chim. Acta, 246 (1991) 309.
64 W. Stumm and J.J. Morgan, Aquatic Chemistry, Wiley, New York, 1981, p. 434.

Analytica Chimica Acta, 273 (1993) 53–57
Elsevier Science Publishers B.V., Amsterdam

Anodic stripping voltammetric determination of total copper in blood plasma

Jorge E. Tahán and Romer A. Romero

Laboratorio de Instrumentación Analítica, Facultad Experimental de Ciencias, Universidad del Zulia, Maracaibo (Venezuela)

(Received 1st June 1992; revised manuscript received 14th September 1992)

Abstract

Blood plasma specimens from renal patients and healthy control subjects were mineralized by microwave irradiation for subsequent determination of total copper by differential-pulse anodic stripping voltammetry (DPASV). Graphite furnace atomic absorption spectrometry (GFAAS) was used for accuracy evaluation purposes. An excellent correlation between the two techniques was obtained: [DPASV] = 0.977[GFAAS] − 0.822, $r = 0.998$, $n = 30$, $p < 0.001$. The detection limit of the electrochemical method was 0.2 μg Cu l^{-1}. Mean concentrations (± 1 S.D.) of 1261 ± 126 and 760 ± 33 μg Cu l^{-1} were found for azotemic individuals and controls, respectively. The proposed DPASV-based method represents an important and inexpensive analytical alternative for the clinical chemistry laboratory.

Keywords: Stripping voltammetry; Blood; Copper; Plasma

In recent years there has been a considerable increase in interest in the study of essential trace elements in humans. It is well known that several metals may exercise a definite influence on the control of biological functions affecting the normal development and growth of different body tissues [1–3]. Incorporations or depletions of metals may occur during the haemodialysis treatment of patients with chronic renal failure (CRF), thus altering their concentrations in the blood and tissues and inducing severe pathological manifestations [4]. Copper is essential for various metabolic processes. However, deviations from the normal range of blood plasma copper concentrations (ca. 96–1200 μg l^{-1}) may produce different toxic effects, mainly associated with accumulation of the metal in organs, e.g., copper fever [5], Wilson's disease [6] and primary sclerosing cholangitis [7]. To assess the extent of the possible harmful effect of copper in azotemic subjects, data are required on the total metal concentrations in blood plasma, assuming that they reflect tissue accumulation or depletion [4].

Differential-pulse anodic stripping voltammetry (DPASV) with a hanging mercury drop electrode (HMDE) has been used to determine low concentrations of total copper (ca. < 10 μg l^{-1}) in medical samples, with detection limits comparable to those of graphite furnace atomic absorption spectrometry (GFAAS) [8]. However, the direct DPASV determination of total copper in blood plasma is interfered with by the presence of organic ligands, especially proteins [9]. They bind copper, modifying the metal speciation and, therefore, its electrolability. Hence, the first step in the electrochemical determination of the total metal concentration in materials with high organic matter content is to remove the organic compounds. Consequently, the samples must be suitably mineralized to eliminate these interferents and to produce a single labile metal species that can subsequently be determined by DPASV.

Correspondence to: R.A. Romero, Apartado Postal 15202, Las Delicias, Maracaibo, Zulia 4003-A (Venezuela).

With this approach, the copper determined by DPASV in blood plasma, or any other metal electrochemically measured in this matrix or in any sample material regardless of its complexity, will produce quantitative data statistically similar to those obtained by using techniques such as GFAAS, frequently employed for the purpose of total metal determination. Otherwise, serious underestimations of the metal will be obtained [10].

In a previous paper, Tahán et al. [11] reported the determination of total soluble copper in haemodialysis water with a high organic content, which was mineralized by using high-pressure bomb decomposition to allow subsequent DPASV analysis. The same group [10] also described the determination of total soluble aluminium in haemodialysis water with a high organic matter-content, mineralized by microwave irradiation and subsequently analysed by differential-pulse polarography.

The aim of this work was to develop a closed-vessel microwave mineralization method for the decomposition of blood plasma specimens from patients with CRF and healthy control subjects. This procedure was tested for its suitability to allow the subsequent determination of total copper by DPASV with the HMDE. Copper was also determined by a GFAAS-based method [12] for accuracy evaluation purposes.

EXPERIMENTAL

Apparatus

The DPASV experiments were done using a Model 174A polarographic system [Princeton Applied Research (PAR)] in conjunction with a PAR Model 303 SMDE electrode assembly and a Houston Omnigraphic RE0089 *X–Y* recorder. A large drop size was used with the static mercury drop electrode device throughout this work. During the deposition step, samples were stirred by means of a PAR Model 305 stirrer. DPASV determinations were done at 20°C under oxygen-free nitrogen.

A Perkin-Elmer Model 2380 atomic absorption spectrophotometer with a Perkin-Elmer Model HGA-500 graphite furnace atomizer were used for GFAAS determinations of copper in the unmodified blood plasma samples, according to the method reported by Parra and Romero [12]. A laboratory microwave oven (CEM Model MDS-81D) with a closed-vessel digestion system (with pressure relief valves) was utilized for blood plasma mineralization.

Reagents and samples

All solutions were prepared with grade I ASTM triply distilled, deionized water. A copper stock standard solution (ca. 1000 mg l^{-1}) was prepared from $Cu(NO_3)_2 \cdot 3H_2O$ (Merck). Copper working standard solutions were prepared daily by serial dilution of the stock standard solution with 0.01 M nitric acid. Concentrated nitric acid (Fisher Scientific), with a metal content below the GFAAS detection limit (< 0.2 μg Cu l^{-1}) [12], was used. The supporting electrolyte was 0.01 M nitric acid. Concentrated perchloric acid (Merck) was used for the microwave mineralizations.

Blood specimens were obtained from CRF patients and healthy volunteers at the Dialysis Unit of the University Hospital (Maracaibo, Venezuela) by venipuncture using 5-ml metal-free disposable polystyrene syringes. The test portions of blood were transferred into metal-free polypropylene tubes, which contained sodium heparin, spun and the plasma fractions carefully separated from the red blood cells and introduced into metal-free polypropylene tubes. Blood plasma samples were stored at 4°C until analysed (within 2 days of collection).

Closed-vessel microwave mineralization of blood plasma specimens

A test portion of blood plasma (ca. 1 ml) and 5 ml of concentrated nitric acid were transferred into the PFA microwave digestion vessel, which was capped automatically, placed on the turntable, inserted in the microwave oven and irradiated for six 5-min periods (at 30, 60, 80, 100, 100 and 100% of total power; 100% power is equivalent to 600 W and 2450 MHz). After cooling to ambient temperature, a 2-ml aliquot was taken from the vessel, transferred into another PFA digestion vessel containing 5 ml of concen-

trated perchloric acid and heated again by microwave irradiation for six 5-min periods with the same power settings as above. Finally, 3 ml of the mineralized solution were diluted to 10 ml with 0.01 M nitric acid and placed in the SMDE sample cell for the DPASV determination of the total copper content. Blanks were prepared with the same reagents, without the samples, and subjected to a similar decomposition treatment.

Statistical analysis

Statistical comparisons of data obtained sequentially by DPASV and GFAAS were done by repeated measurements of analysis of variance [13]; significant F values were tested with Tukey's test with the help of a commercial statistical package (Statgraphics, STSC, Rockville, MD); values of $p < 0.05$ were considered significant.

RESULTS AND DISCUSSION

As reported previously [11], the deposition potential, deposition time, potential scan rate, drop size and nitrogen purge time were optimized with synthetic copper samples to yield the following results: −0.50 V, 1 min with stirring (plus 40 s quiescent), 5 mV s^{-1}, large (equivalent to ca. 2.5 mm^2) and 2 min with stirring, respectively. These experimental conditions were applied in the DPASV analysis of real samples of blood plasma.

In previous work, Tahán and co-workers [8–11] demonstrated that only a small fraction (ca. < 30%) of the total metal content present in organic matter-containing haemodialysis water was electrolabile. For this reason, the direct DPASV determination of total copper in blood plasma was not quantitative. Therefore, a microwave mineralization procedure was developed in order to remove concomitant substances and produce mineralized blood plasma samples. The electrochemical results for total copper in blood plasma were verified by the direct GFAAS analysis of the undigested samples [4,12]. Initial microwave mineralization experiments were done without the addition of any oxidizing reagent at several microwave power settings and with different volumes of blood plasma; unfortunately, the samples were incompletely mineralized and a large amount of carbon residues was observed after mineralization.

The addition of nitric acid to the blood plasma under microwave heating increased the electrolabile fraction of the total copper. Hence, 5 ml of concentrated nitric acid, added to 1 ml of blood plasma test portion, were used in a first digestion step intended to mineralize the largest fraction of the organics. Several microwave irradiation programmes were applied; the best results were obtained by using a total irradiation time composed of six cumulative 5-min microwave heating periods, the first period being at 30%, the second at 60%, the third at 80% and the fourth, fifth and sixth at 100% of total power. Cooling and venting intervals of about 10 min, intended to restore the atmospheric pressure inside the microwave vessels, were intercalated between each irradiation period. A second microwave mineralization with perchloric acid was required in order to ensure an efficient destruction of the organic interferents for the subsequent electrochemical determination of total copper in the mineralized blood plasma samples. Under these conditions the DPASV copper concentrations correlated statistically with the results obtained by GFAAS. It should be pointed out that the DPASV determination of copper after the first mineralization programme, with nitric acid only, was not quantitative [recovered copper was 55–70% lower than the total copper and the reproducibility was 5.7% (R.S.D.)]. Sulphuric acid and hydrogen peroxide were tried, but unsuccessfully. After the microwave mineralization, no further sample treatment was required and the copper oxidation peak appeared at a potential of −0.2 V (Fig. 1) in the pH range 1.0–3.0, as reported previously for the DPASV determination of copper in haemodialysis water [11].

Linear calibration graphs were obtained up to 60 μg Cu l^{-1}. The blood plasma test portions analysed were within this linear range. The current, i (μA), was found to be linearly related to the concentration, C (μg Cu l^{-1}), by the equation $i = 0.0175C - 0.0066$ (the standard deviation of the slope and intercept were 0.001 and 0.028, respectively, for ten six-point calibration graphs;

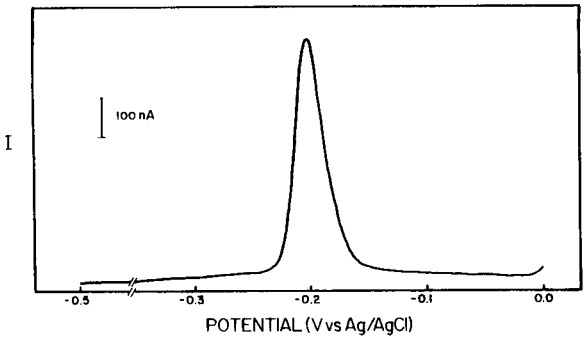

Fig. 1. Typical DPASV trace for copper in blood plasma after mineralization of the sample by microwave irradiation as proposed. Deposition potential, −0.5 V; deposition time, 1 min with stirring (plus 40 s quiescent); potential scan rate, 5 mV s^{-1}.

correlation coefficient = 0.998). The standard addition method was also employed for quantification purposes and provided similar results to those given by the calibration graphs. This implied the absence of interferences in the DPASV determination of copper in blood plasma after adequate microwave mineralization as proposed, and the alternative possibilities of employing either the calibration graphs or the standard addition method for quantification.

Copper concentrations obtained by DPASV analysis of the mineralized blood plasma were compared with those obtained by GFAAS on the same undigested plasma samples. The correlation between the two methods was excellent: $y = 0.977x - 0.822$, $r = 0.998$, $n = 30$, $p < 0.001$, where y and x are the copper concentrations determined by DPASV and GFAAS, respectively. The standard error of the estimate ($S_{y \cdot x}$) is 36.9 μg Cu l^{-1} and the standard deviations of the intercept and slope are 36.6 μg Cu l^{-1} and 0.034, respectively.

TABLE 1

Recovery of copper added to real blood plasma samples from two CRF patients and one control subject (six analyses on each sample)

Blood plasma	Cu added ($\mu g\, l^{-1}$)	Cu found ($\mu g\, l^{-1}$)	Cu expected ($\mu g\, l^{-1}$)	Recovery (%)
CRF 1	10	29	30	97
CRF 2	15	28	27	104
Control	20	45	46	98

The accuracy of the proposed DPASV-based method was also tested by analysing the standard reference material CONTOX (Trace Metal Serum Control A, Level II) supplied by Kaulson Laboratories (West Caldwell, NJ), with a target copper concentration of 1500 ± 300 $\mu g\, l^{-1}$; the concentration found for copper using the proposed method was 1548 ± 240 $\mu g\, l^{-1}$. This mean concentration did not differ significantly ($p > 0.01$) from the certified value. The reliability of the method was further assessed through a recovery study. This was done (Table 1) by six replicate DPASV determinations of copper in three real samples of blood plasma (two from CRF patients and one from a control individual). The average recovery was 99.7% (range 97–104%).

The within- and between-run precisions for the electrochemical determination of blood plasma copper in three real samples are shown in Table 2. Analysis of four replicates of each sample were done (six runs each) using the microwave mineralization procedure. The standard

TABLE 2

Precision of the determination of total copper in blood plasma by DPASV [a]

Sample [b]	Mean Cu concentration [c] ($\mu g\, l^{-1}$)	Within-run		Between-runs	
		S.D. ($\mu g\, l^{-1}$)	R.S.D. (%)	S.D. ($\mu g\, l^{-1}$)	R.S.D. (%)
1	20	0.2	1.0	1.2	5.0
2	17	0.4	2.4	0.8	4.7
3	23	0.4	1.7	0.3	1.3

[a] Four replicate analyses of each sample were done; six runs each. [b] Randomly collected from CRF patients at the University Hospital (Maracaibo). [c] In the diluted blood plasma samples.

deviation ranges were 0.2–0.4 μg Cu l^{-1} (within-run) and 0.3–1.2 μg Cu l^{-1} (between-runs). These results can be considered adequate for this type of analysis and show that the proposed mineralization method is highly reproducible.

The detection limit of the electrochemical method, defined as three times the standard deviation of a blank solution, was 0.2 μg Cu l^{-1} in the diluted blood plasma test portions. This value is similar to that of the GFAAS method [12] and to that reported by Tahán et al. [11] for the DPASV determination of copper in haemodialysis water mineralized in high-pressure reactors.

The proposed method has been used successfully to evaluate the total copper concentration of blood plasma samples from CRF patients receiving haemodialysis treatment at the University Hospital of Maracaibo City. It has been also applied to the analysis of blood plasma specimens from healthy individuals acting as controls. Results of a survey of fifteen azotemic individuals and fifteen controls gave mean blood plasma copper concentrations (± 1 S.D.) of 1261 ± 126 and 760 ± 33 μg l^{-1}, respectively.

It is concluded that the DPASV-based method described is sensitive, accurate and precise, and can be applied to a wide range of copper concentrations. Further, it represents an important and inexpensive analytical alternative, as reliable as GFAAS, for the clinical chemistry laboratory.

This research was partially supported by grant F-142 from the Consejo Nacional de Investigaciones Científicas y Tecnológicas (CONICIT). The authors are grateful to Janeth A. Navarro and Víctor A. Granadillo for helpful discussions on this paper. Financial assistance from FUNDAYACUCHO is also acknowledged.

REFERENCES

1 A.P.S. Narang, H. Masood, M.S. Kamili, I.A. Bhat and A.W. Banday, Trace Elem. Med., 5 (1988) 170.
2 J.A. Navarro, V.A. Granadillo, B. Rodríguez-Iturbe, R. García, O. Salgado and R.A. Romero, Clin. Nephrol., 35 (1991) 213.
3 G. Faa, C. Liguori, A. Columbano and G. Díaz, Hepatology, 7 (1987) 838.
4 R.A. Romero, J.A. Navarro, B. Rodríguez-Iturbe, R. García, O.E. Parra and V.A. Granadillo, Trace Elem. Med., 7 (1990) 176.
5 W.H. Lyle, J.E. Payton and M. Hui, Lancet, i (1976) 1324.
6 E. Aadland, J. Aaseth, K. Dahl, B. Radziuk and Y. Thomassen, J. Trace Elem. Electrolytes Health Dis., 4 (1990) 233.
7 J.B. Gross, J. Ludwig, R.H. Wiesner, J.T. McCall and N.R. LaRusso, Gastroenterol., 89 (1985) 279.
8 A.J. Moronta, J.E. Tahán, J.A. Navarro and R.A. Romero, in B. Momcilovic (Ed.), Trace Elements in Man and Animals, Vol. 7, Institute for Medical Research and Occupational Health, University of Zagreb, Zagreb, 1991, pp. 33-8 to 33-9.
9 C.M. Van der Berg, K. Murphy and J. Riley, Anal. Chim. Acta, 188 (1986) 177.
10 R.A. Romero, J.E. Tahán and A.J. Moronta, Anal. Chim. Acta, 257 (1992) 147.
11 J.E. Tahán, A.J. Moronta and R.A. Romero, Anal. Chim. Acta, 236 (1990) 449.
12 O.E. Parra and R.A. Romero, At. Spectrosc., 8 (1987) 105.
13 S. Wallenstein, C.L. Zucher and J.L. Fleiss, Circ. Res., 47 (1980) 1.

Analytica Chimica Acta, 273 (1993) 59–70
Elsevier Science Publishers B.V., Amsterdam

Carbon fibres as electrode materials for the construction of peroxidase-modified amperometric biosensors

Elisabeth Csöregi, Lo Gorton and György Marko-Varga

Department of Analytical Chemistry, University of Lund, P.O. Box 124, S-221 00 Lund (Sweden)

(Received 1st July 1992)

Abstract

Electrocatalytic reduction of hydrogen peroxide can be brought about through an apparent direct electron transfer between various electrode materials and the active centre of immobilized peroxidases. A hydrogen peroxide-selective amperometric microbiosensor can be constructed by immobilizing horseradish peroxide (HRP) using various carbon fibres as electrode material. The effects of surface pretreatment and enzyme immobilization techniques were investigated. Heat-pretreated graphite fibre (Sigrifil) with covalently immobilized HRP using carbodiimide as the coupling reagent was found to be the best amperometric biosensor for the detection of hydrogen peroxide. Detection can be effected within the optimum potential range (−200 to 0 mV vs. SCE). A linear response range was obtained between 80 and 2500 μM hydrogen peroxide. An apparent Michaelis–Menten coefficient of 1.2 mM was calculated from the slope of the Eadie–Hofstee plot.

Keywords: Amperometry; Biosensors; Carbon fibres; Enzyme electrodes; Hydrogen peroxide

In the last few years, an apparent direct electron transfer has been reported to occur between different electrode materials [carbon black, glassy carbon, carbon paste, graphite epoxy resin, spectrographic, edge oriented pyrolytic and high-density ultra-pure graphite, tin(IV) oxide and platinum] and the active site of various immobilized peroxidases [horseradish peroxidase (HRP), fungal peroxidase, cytochrome *c* peroxidase, lactoperoxidase and microperoxidase] [1–11]. The peroxidase-modified electrodes can be used in the batch mode or in various flow systems as a detection unit for hydrogen peroxide. Detection could be effected within the optimum potential range (−200 to 0 mV vs. SCE) where the background current, the noise levels and the contribution to the response signal from molecular oxygen and from electrochemically easily oxidized compounds common in biological applications, e.g., uric acid, ascorbic acid and paracetamol, are minimal. By co-immobilizing a hydrogen peroxide-producing oxidase with the peroxidase a biosensor can be made with selectivity for the substrate of the oxidase [3,6,7,12–14].

The needs and challenges of miniaturization of detectors and detection devices have been recently addressed [15,16]. Miniaturized biosensors are particularly attractive in connection with various ex vivo and in vivo clinical applications including monitoring of local chemical events in special regions of an organ and measurements of extremely small volumes. Microelectrodes with possible use as sensors in microflow systems were recently reviewed in a special issue of Electroanalysis [17].

Successful attempts to construct enzyme–carbon fibre microelectrodes have been reported in only a few instances. A lactate sensor based on

Correspondence to: L. Gorton, Department of Analytical Chemistry, University of Lund, P.O. Box 124, S-22100 Lund (Sweden).

lactate dehydrogenase immobilized on a pyrolytic carbon fibre [19], glucose sensors based on immobilized glucose oxidase either in polyderivative redox hydrogels on bevelled carbon fibres [20] or on rhodium-modified carbon fibres [21] and an acetylcholine sensor based on acetylcholinesterase and choline oxidase co-immobilized on carbon fibres [22] have recently been presented. A flow cell having a glucose oxidase-modified platinized carbon fibre as the working electrode has also been described [23]. Carbon fibre microelectrodes with millisecond response times for hydrogen peroxide based on immobilized HRP with the biotin–avidin–biotin coupling technique were also presented using a soluble mediator [24].

The electroanalytical applications of carbon fibres have been reviewed by Edmonds [25]. Carbon fibres possess three especially attractive features from an electrochemical point of view. First, they have small dimensions (5–15 μm diameter) and consequently when operated as a single micro-disc electrode perpendicular diffusion to the surface of the electrode is only a small component of the flux of the analyte and the edge effects become significant [26]. Second, the material is carbon, the surface of which is densely populated with oxygen-containing groups. These can play a key role in the electron-transfer processes [8]. Last, they are cheap, readily available and many studies have been carried out on their surface characteristics [27].

According to previous studies [28], the electrochemical response of the microelectrodes is dramatically different from that of electrodes of conventional size, owing to their small surface area. With decreasing size, the "edge effect"/radial diffusion becomes increasingly important and dominates the response of these very small electrodes, even at times of 1 s or less. The high radial diffusion, on the other hand, causes rapid diffusion away from the electrode surface of the products (e.g., H_2O_2) generated by the catalytic reaction of the enzyme immobilized on the microelectrode, even when the enzyme is strongly bound to the electrode surface [29].

Carbon fibres are manufactured by a wide range of suppliers and are available in a wide variety with different properties. They can be classified into three broad categories, presented in Table 1 [27], viz., low, medium and high modulus, depending on the manufacturing process, also influencing the degree of order of the carbon layers. The surface of a high-modulus carbon fibre perpendicular to the fibre axis, is stated to have a high degree of edge orientation and Faradaic electron transfer processes have been shown to occur preferentially at the edge orientation of ordered graphite. Type I (or high-modulus type) carbon fibre is the most suitable for electrochemical work because of the low porosity and better ordered graphite-like structure [26,30].

The activation of the electrode surface is of great importance. It removes contaminants from the electrode surface, increases the concentration of surface functional groups (which may mediate the electron transfer process), increases the surface area by increasing the surface roughness and exposes fresh edge planes, microparticles and defects, which may also be mediating sites for the electron-transfer process [31]. The most commonly used activation techniques are mechanical polishing and electrochemical, chemical and thermal treatment. Oxidative treatments are known to improve the fibre-bonding characteristics [32].

TABLE 1

Characteristics of carbon fibres

Fibre type	Ultimate tensile Strength (GN m^{-2}) [a]	Young's modulus (GN m^{-2}) [a]	Comments
Type I	2.6	340 (high)	High density, low porosity, well ordered linear microfibrils
Type II	2.9	240	Highly microporous, large number of 0.1–5-μm pores
Type III	2.6	190 (low)	Highly microporous, large surface area, microfibrils distorted, poorly ordered

[a] Units are given according to [27].

TABLE 2

Carbon fibres investigated

Carbon fibre	Diameter (μm)	Specifications
Hyfil-130	7.3	?% C, no sizing
Kureha KGF-200 T-201 S	14.5	99% C, no sizing
Kureha KCF-100 T-101 S	14.5	95% C, no sizing
Kureha KCF-100 T 101-T	18.0	95% C, no sizing
Modmor II-S	8.0	?% C, sized?
Polycarbon LGR 10 ply Z-twist (P-type)	15.0 [a]	99% C, 1% ash content, graphite coated
Sigrifil (S-type)	6.0 [a]	Graphite fibre
Toray 800 HB-12000-40 B	–	1% size (epoxy coated)
Toray 700 SC-12000-50 C	–	1.1% size (epoxy coated)
Toray M40 JB-6000-50 B (M40 type)	–	State to be of higher modulus type than the other two Toray fibres

[a] The diameter was determined from scanning electron micrographs.

In all the papers referred to above regarding enzyme-modified carbon fibres, the fibres were pretreated, mainly by electrochemical oxidation, prior to enzyme immobilization.

In this paper the immobilization of HRP on a variety of carbon fibres with the aim of optimizing the electrocatalytic reduction of hydrogen peroxide within the optimum potential range is reported. Batch experiments were therefore made with different carbon fibres in order to see whether the catalytic effect of the reduction of hydrogen peroxide could be observed with these HRP-modified carbon fibres microelectrodes. The effects of the structure of the fibres, the electrode pretreatment and the enzyme immobilization technique on the electrocatalytic behaviour of the microelectrodes were studied.

EXPERIMENTAL

Reagents

Horseradish peroxidase (HRP, E.C. 1.1.11.7, Type VI, cat. no. P 8375, obtained as a powder, 270 U mg^{-1}) and glutaraldehyde (GA, cat. no. G 5882, 25% aqueous solution) were provided from Sigma. 1-Cyclohexyl-3-(2-morpholinoethyl)carbodiimide metho-*p*-toluenesulphonate (denoted carbodiimide, cat. no. 11.136.78) was provided by Janssen Chimica. All solutions were prepared with doubly distilled water. All chemicals were used as received, except GA, which was purified in order to remove polymeric material by shaking with active carbon followed by centrifugation. The clear supernatant containing unreacted GA was kept below −18°C until used.

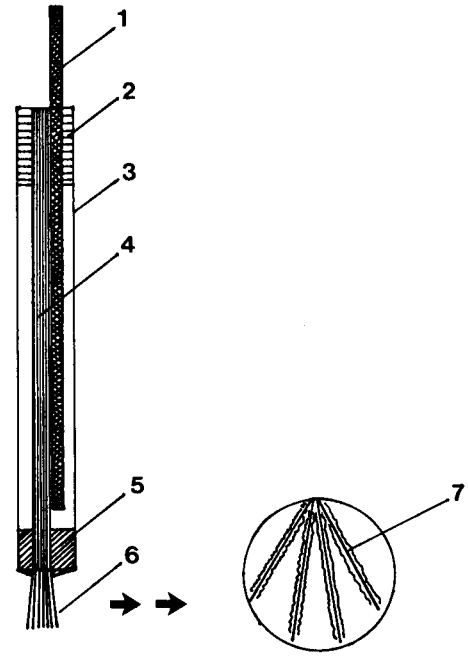

Fig. 1. Schematic diagram of the microelectrode. 1 = copper wire; 2 = conductive carbon cement; 3 = glass microcapsule (50 μl); 4 = carbon fibres; 5 = sealing resin; 6 = unsealed carbon fibres (4–5 mm length) exposed to HRP; 7 = HRP immobilized on the carbon fibres.

TABLE 3

Pretreatment methods applied

Pretreatment	Operating conditions
Heating	At 700°C in a muffle furnace oven for 5, 10, 15, 20, 30, 45 or 60 s
Electrochemical	(a) Cycling between 0 and +1.8 V vs. SCE (v = 50 mV s^{-1}) in a 0.1 M phosphate buffer at pH 7.0 for 5 or 10 min
	(b) At a stationary potential of +1.4 V for 5, 10, 20, 30 or 60 s
	(c) At a stationary potential of +0.8 V for 30 s

Electrode preparation

The various carbon fibres investigated are listed in Table 2 together with the manufacturers' specifications. A bundle of about 5–20 carbon fibres was inserted in a 5-μl microcapsule (Drummond Science), leaving about 4–5 mm outside. Figure 1 shows a schematic diagram of the microelectrode. For sealing several resins were tested. The best was found to be a low-viscosity, rapidly sealing resin (Hylo Gel, Swedish Techno Chemie). Sealing was accomplished by allowing a droplet of the resin at the end of the glass tube for capillary rise. Electrical contact was provided with a copper wire and a droplet of a conducting carbon paste (Leit-C conductive carbon cement from Neubauer Chemikalien), dissolved in xylene to obtain the desired viscosity, was applied at the other end of the microelectrode. Precautions were taken not to contaminate the electrode surface with the resin used. All results presented are an average values for five equivalently prepared electrodes.

Electrode pretreatments

The carbon fibre microelectrodes were pretreated in various ways, either before or after the electrode preparation. Some carbon fibres (P-type, Hyfil) were pretreated both before and after the electrode preparation whereas others (S-type, M40) were only pretreated after inserting the fibres into the glass tubing (see Results and Discussion). Table 3 presents the methods and operating conditions applied.

Enzyme immobilization

The unsealed part of the carbon fibres was modified by dipping the electrode into a solution containing HRP (270 U mg^{-1}, 20 mg ml^{-1} in phosphate buffer at pH 6.0). The various procedures tested are described in Table 4.

TABLE 4

Enzyme immobilization techniques applied

Enzyme immobilization technique	Operating conditions
Adsorption	At room temperature for 10 min
Covalent coupling on carbodiimide-treated fibre	The electrode was allowed to react for 1 h with 4.2 mg of carbodiimide dissolved in 300 μl of 0.05 M acetate buffer at pH 4.8 (under continuous agitation) and then dipped into the HRP-containing solution for 10 min
Covalent coupling on carbodiimide-treated fibre in combination with cross-linking using GA	25% GA aqueous solution was added to the HRP solution (concentration 0.12%) just after the carbodiimide modification, otherwise similar conditions to above
Electrodeposition without and with cross-linking with GA (according to [18])	The enzyme was deposited on the electrode surface from HRP solution (20 mg ml^{-1} in 0.1 M phosphate buffer at pH 7) at +200, +500 and +800 mV vs. SCE under continuous agitation for 1 or 2 min. When cross-linked with GA, the electrode was dipped into a GA solution (2.5% in 0.1 M phosphate buffer at pH 7.0) for 30 min, rinsed and dried before the electrodeposition

Apparatus

Batch experiments with unmodified and HRP-modified carbon fibre electrodes were performed in 0.1 M phosphate buffer at pH 6.0 (volume 20 ml) with the carbon fibre electrode connected to a three-electrode potentiostat (Zäta-Elektronik, Lund, Sweden) having a platinum net as the counter electrode and a saturated calomel electrode (SCE) as the reference electrode. The output of the potentiostat was displayed on a strip-chart recorder (Kipp & Zonen, Model BD 111). Scanning electron micrographs (SEM) of unmodified and HRP-modified carbon fibre surfaces were obtained using a ISI Model 100 A scanning electron microscope.

RESULTS AND DISCUSSION

HRP is a small glucoprotein (M_w 40 000) containing ferroprotoporphyrin IX as the strongly bound cofactor. The oxidation of the native form of the HRP can only be brought about by hydrogen peroxide and some small peroxidases. In a single two-electron ($2e^-$) process the native form of HRP is oxidized by hydrogen peroxide to form water and an oxidized form of HRP, denoted compound I:

$$\text{HRP(native form)} + H_2O_2 \rightarrow \text{compound I} + H_2O \quad (1)$$

The reduction of compound I back into the native form of HRP occurs in two separate $1e^-$ steps:

$$\text{compound I} + e^- \rightarrow \text{compound II} \quad (2)$$

$$\text{compound II} + e^- \rightarrow \text{HRP(native form)} \quad (3)$$

Virtually any reducing agent may act as the electron donor in this respect. When HRP is immobilized on the surface of carbon electrodes, the necessary two electrons (reactions 2 and 3) can be donated from the electrode to compound I and compound II. Whether it is a true direct electron-transfer process or a mediated one brought about by surface functionalities has been discussed in previous papers [1,3,4,8,13].

Influence of the fibre structure

A series of electrodes were prepared from each carbon fibre material and investigated for electrocatalytic properties for hydrogen peroxide reduction when modified with adsorbed HRP. A strong correlation was observed between the electrocatalytic behaviour of the HRP-modified carbon fibres and their structures. No catalytic effect for hydrogen peroxide reduction could be found with HRP-modified fibres (adsorbed HRP) with a "smooth" surface (all Kureha fibres studied), on either unpretreated or heat-pretreated fibres. Carbon fibres with a "spaghetti-like" rough surface (Hyfil, Modmor) displayed a very small catalytic effect, but their surfaces could be activated by heat and electrochemical pretreatments, re-

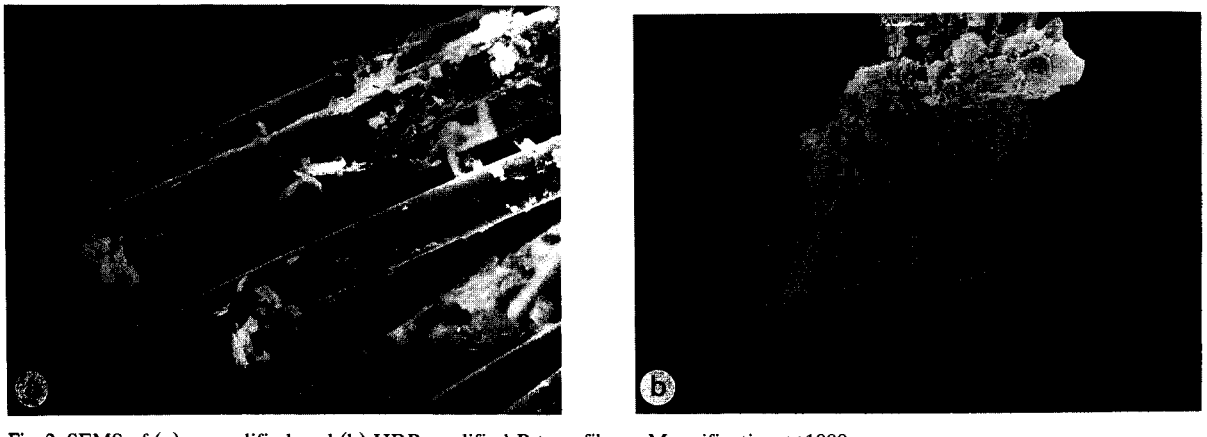

Fig. 2. SEMS of (a) unmodified and (b) HRP-modified P-type fibres. Magnification ×1000.

sulting in an increased catalytic current. The registered currents were still small compared with those obtained with P- (electrochemically oxidized at +0.8 mV vs. SCE for 30 s) and S-type fibres (heated at 700°C for 30 s), which gave the highest catalytic currents for the reduction of hydrogen peroxide (1.6 and 1.9 μA, respectively, at 160 μM hydrogen peroxide). Figures 2 and 3 present SEMs of (a) unmodified and (b) enzyme-modified unpretreated P- and S-type electrodes, respectively. A close examination of the P-type fibre reveals "flakes" of graphite particles on the naked fibres and "enzyme aggregates" round the graphite particles (Fig. 2a and b, respectively). The S-type has a rough surface (so have Hyfil and Modmor) and presents a fairly uniform enzyme layer covering the fibre when modified with HRP (see Fig. 3a and b, respectively). An increase in the fibre diameter could be observed (10–20% increase) after adsorption of the enzyme. The observed structural changes are attributed to an immobilized layer of the enzyme on the fibres studied. No SEMs were taken on Toray 700 and 800 fibres because of the small catalytic currents obtained for the reduction of hydrogen peroxide, explained partly by the epoxy coating covering the fibres.

A series of equivalently prepared P-type electrodes showed different electrocatalytic behaviours. The heterogeneous/random graphite coating could be a possible explanation of the observed phenomena (see Fig. 2a). The pure graphite S-type was found to be much more reproducible, also displaying higher electrocatalytic activity for higher hydrogen peroxide concentrations. The "higher modulus" M40 type was expected to give even higher signals according to the theoretical aspects in the literature [26,30]. In contrast, the currents obtained were small, which could possibly be explained by the epoxy coating applied to the fibres during the manufacturing process. A heat pretreatment of the fibres could be expected to give higher catalytic currents, because of a possible removal of the coating.

Only the P-, S- and M40-type fibres were further tested for the construction of hydrogen peroxide biosensors as the first two fibres gave initially the highest response for hydrogen peroxide reduction and the last one was expected to give the highest catalytic currents according to the literature [26,30]. The dependence of the current response on the applied potential for the S-type fibre (naked and HRP-modified) in 0.5 mM hydrogen peroxide solution is shown in the hydrodynamic voltammogram in Fig. 4. For the naked electrode a small anodic current is observed at +600 mV vs. SCE, attributed to direct oxidation of hydrogen peroxide. As the potential is made more negative, only at +200 mV does a very small current appear for the direct reduction of hydrogen peroxide, which is slightly increased when the applied potential is made more negative. For the HRP-modified fibre anodic currents were observed at +600 mV, but smaller than

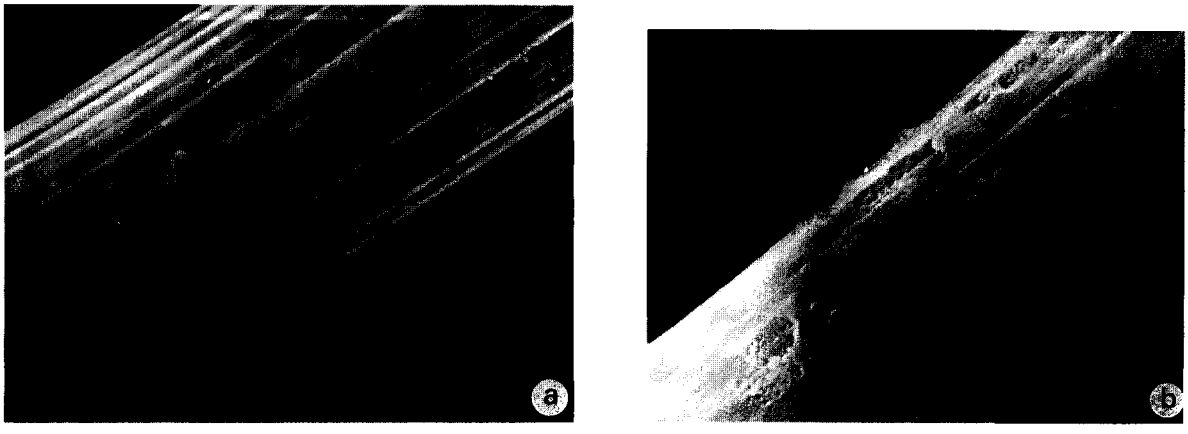

Fig. 3. SEMs of (a) unmodified and (b) HRP-modified S-type fibres. Magnification ×10000.

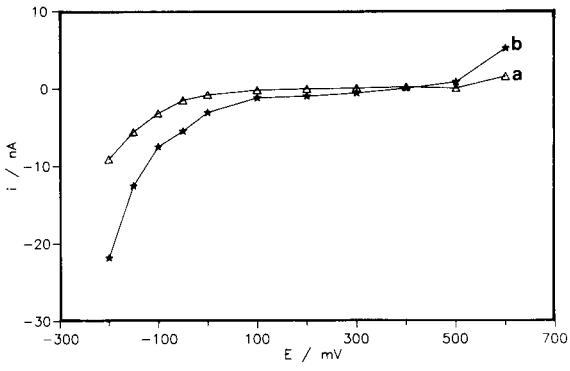

Fig. 4. Hydrodynamic voltammograms for (a) naked and (b) HRP-modified S-type electrodes. Hydrogen peroxide concentration 0.5 mM in 0.1 M phosphate buffer at pH 7.00.

those for the naked carbon fibre. The electrocatalytic reduction of hydrogen peroxide promoted by the adsorbed HRP starts at +400 mV and increases rapidly as the applied potential is made more negative. As expected from previous experiments with HRP-modified solid graphite and carbon paste electrodes, an enhanced current response to hydrogen peroxide (an increase of about 20% at 0 mV compared with the naked fibre) was obtained for the enzyme-modified electrode. A working potential of 0 mV was chosen for further experiments as a compromise between the current response obtained and an applied potential suitable for practical applications.

Unfortunately, there is no information from the manufacturers on whether the investigated carbon fibres are of "high-modulus" type or not, except for the Toray M40 type, which is stated to be of higher modulus than the other Toray fibres tested here. A comparison between the results obtained here and other reports on enzyme-modified carbon fibres cannot be done at this stage. The papers mentioned above on enzyme-based carbon fibres [19–24] contained no specifications regarding the structural characteristics of the carbon fibres used. However, in those reports the electrochemical reaction is either based on the reaction of a soluble product formed in the enzymatic reaction or via a soluble mediator. In contrast, in this investigation the structural characteristics of the electrode surface are of great importance as the electrochemical detection is based on what at least appears to be a direct electron transfer from the electrode to the immobilized peroxidase.

Effect of the electrode pretreatment

Various electrode pretreatment methods were applied to the carbon fibres both before and after the carbon fibres had been inserted into the glass tubing in order to see whether the electrocatalytic properties of the fibres could be improved. The pretreatment applied to the glass-sealed fibres (only electrocatalytic pretreatment) and to the fibres only inserted in glass microcapsules and unsealed (only heat pretreatment) showed a higher degree of surface activation resulting in higher currents for electrocatalytic reduction of hydrogen peroxide than those which were pretreated before the electrode preparation. The lower current responses obtained for these electrodes are believed to be caused by contamination effects when handling the fibres during the fabrication of the microelectrodes. All effects of pretreatment presented below refer to further experiments with electrodes already mounted in glass tubing. As a general effect an increased background current for all fibre types was noted for all pretreated electrodes.

For the P-type fibres heat pretreatment did not result in enhanced catalytic activity but rather a decreased current response was observed with an increase in heating time. SEMs of these electrodes (not presented) showed a decreased number of graphite particles after higher heating temperatures, suggesting a correlation between the visible "flake-like" graphite coating and electrocatalytic reduction at the HRP-modified electrodes. The graphite coating of the P-type electrodes is believed to be the explanation of the high rate of electrocatalytic reduction of hydrogen peroxide observed for this type of fibres and that the heat pretreatment probably caused partial removal of the graphite coating, resulting in a decreased current for hydrogen peroxide reduction. The surface of the P-type fibres could, however, be activated by electrochemical pretreatment. An oxidation at a stationary potential of +0.8 mV vs. SCE for 30 s was found to be the most efficient (see Table 5).

Both electrochemical oxidation and heat pretreatment were found to be powerful methods for increasing the electrocatalytic activity of the S-type fibres (see Table 5). A combination thereof, however, did not result in a further improvement. SEMs taken on both electrochemically and heat-pretreated S-type fibres (not presented) showed that the roughness of the surface was increased by the pretreatment, the effect being more pronounced with the heat pretreatment. The effect of the heating time is presented in Fig. 5. According to our previous results [8], heat pretreatment is supposed to introduce mediating functionalities of quinone type on the electrode surface. Figure 5 reveals that heating for 5 s is not sufficient for obtaining maximum coverage of mediating groups on the surface of the electrode, whereas too long a heating time may result in creating other, non-

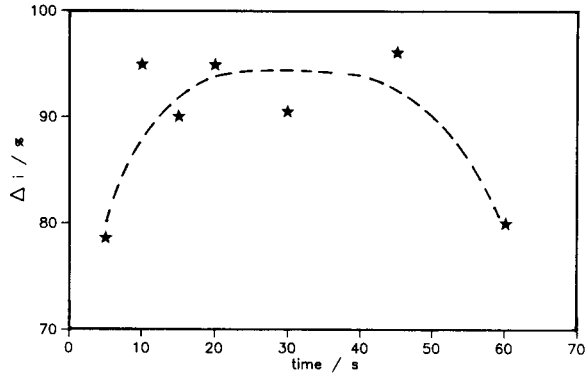

Fig. 5. Effect of the heating time (at 700°C) on the electrocatalytic activity of S-type fibres. Δi denotes the difference between the catalytic current at 2.5 and 0 mM hydrogen peroxide concentration.

TABLE 5

Characteristics of P- and S-type carbon fibre microelectrodes

Fibre type	Pretreatment applied	Enzyme immobilization	i_0–$i_{1.2}$ [a] (nA)	Deactivation concentration (μM H_2O_2)	Slope (log–log plot)	Linear range (μM H_2O_2)
P-type	Electrochemically pretreated (+0.8 mV vs. SCE for 30 s)	Adsorption for 10 min	3.40–18.00	40	0.25	2–20
	As above	Covalent coupling (carbodiimide)	2.50–26.00	160	0.38	2–40
	Electrochemically pretreated (+1.4 mV vs. SCE for 30 s)	Adsorption for 10 min	2.40–53.00	80	0.57	2–10
	Heated (at 7000°C for 5 s) and electrochemically pretreated (at +1.4 mV vs. SCE for 30 s)	Adsorption for 10 min	0.30–1.52	160	0.66	640–2560
	None	Electrodeposition at +500 mV vs. SCE, agitated for 2 min, cross-linked with GA	2.30–7.10	160	0.38	320–2560
S-type	Electrochemically pretreated (at +0.8 mV vs. SCE for 30 s)	Adsorption for 10 min	1.80–8.50	80	0.42	160–2560
	Heated at 700°C for 10 s	Adsorption for 10 min	0.25–4.90	640	0.60	80–2560

[a] Denote the current measured at 0 (i_0) and 1.2 ($i_{1.2}$) mM hydrogen peroxide concentration.

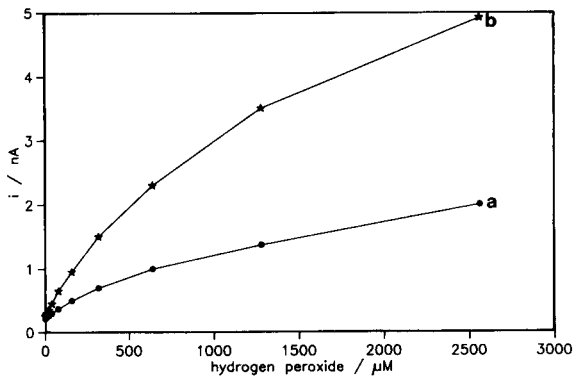

Fig. 6. Calibration graphs for (a) unpretreated and (b) heat-pretreated (at 700°C for 30 s) HRP-modified S-type fibres. Working potential 0 mV vs. SCE.

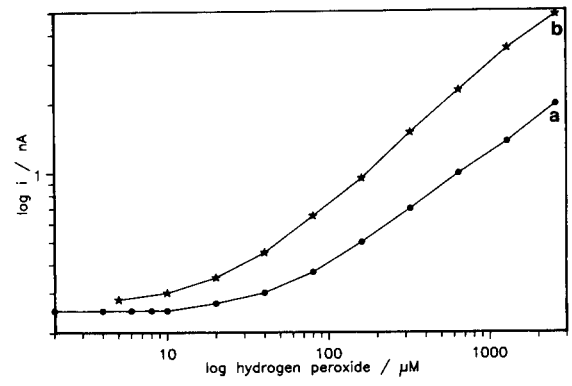

Fig. 7. Log–log plots of the calibration graphs depicted in Fig. 6.

mediating functionalities. A heating time of 30 s was chosen for further experiments as it seemed to be the optimum time to obtain good electrocatalytic results (see Fig. 5). Figure 6 shows the calibration graphs for (a) unpretreated and (b) heat-pretreated HRP-modified S-type electrodes. The heat pretreatment caused a 100% increase in the current response to hydrogen peroxide. Figure 7 shows the log–log plots of the calibration graphs depicted in Fig. 6 [(a) unpretreated and (b) heat-pretreated]. The slopes of these log–log plots were 0.44 and 0.60, respectively, and an increase of 26% in the slope of the linear part of the calibration graph was obtained with the heat-pretreated electrodes.

Experiments made with heat-pretreated M40 fibres showed a drastically increased current response with an increased heating time, reflected in the calibration graphs for hydrogen peroxide depicted in Fig. 8A and B. The effect of the heating time on the difference between the responses obtained at 2.5 mM and 0 mM hydrogen peroxide of these fibres is depicted in Fig. 9. An accentuated increase was observed for heating times longer than 20 s whereas for heating times longer than 50–60 s a decrease was observed. The slope of corresponding log–log plots showed a continuous increase for heating times longer than 20 s, reaching a maximum value for a heating time of 45 s. The linear range varied with the heating time, having the largest value for a heating for 45 s (see Table 6). It is not clear if the experiments with heat pretreatment are sufficient for the total removal of the epoxy coating and if the observed positive effect can be explained by

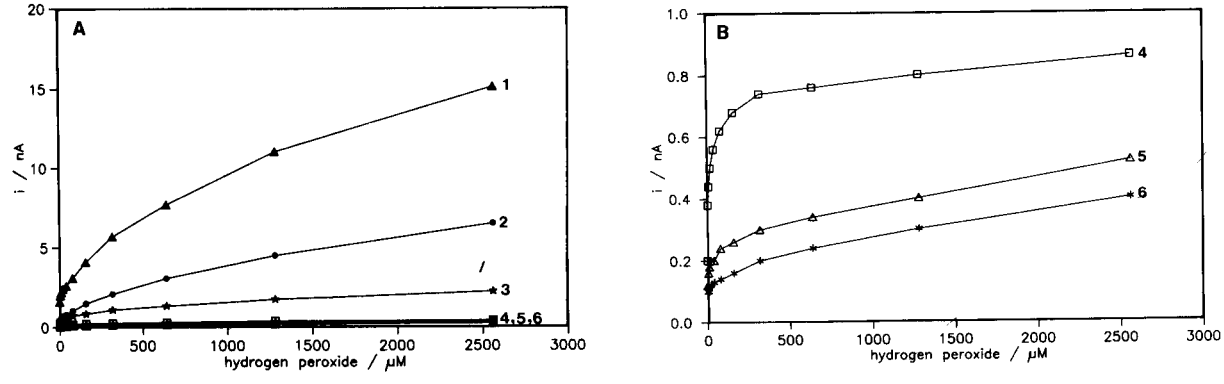

Fig. 8. Calibration graphs for heat-pretreated (700°C) Toray M40 fibres. (A) Heated for (1) 60 s, (2) 45 s, (3) 30 s and (4) 20 s; (B) heated for (4) 20 s and (5) 10 s and (6) unheated.

TABLE 6

Effect of heating time on the current response for M40 fibres

Heating time (s)	$i_0-i_{2.5}$ [a] (nA)	Slope (log–log plot)	Linear range (μM H_2O_2)	Regression coefficient
0	0.14– 0.48	0.19	20–1280	0.995
5	0.10– 0.40	0.32	40–2560	0.990
10	0.12– 0.52	0.19	40–1280	0.996
20	0.12– 0.42	0.24	80–1280	0.994
30	0.30– 2.25	0.35	160–1280	0.999
45	0.40– 6.50	0.51	40–2560	0.999
60	1.60–15.10	0.46	80–2560	0.999

[a] Denote the current values registred at a concentration of 0 (i_0) and 2.5 ($i_{2.5}$) mM hydrogen peroxide.

the removal (partial or total) of the epoxy coating or by the introduction of oxygen-containing functionalities (see Fig. 9). Further studies will be made.

Effect of the enzyme immobilization

SEMs taken on naked and HRP-modified P- and S-type fibres (Fig. 2) reveal substantial changes for the enzyme-modified electrodes as compared with the unmodified electrodes. The observed changes caused by the adsorption of the enzyme on the surface of the fibres were presented above. All results referred to above are based on fibres on which the enzyme was immobilized by simple adsorption. All these electrodes

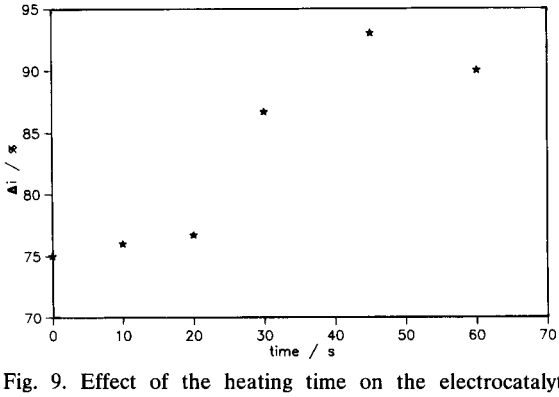

Fig. 9. Effect of the heating time on the electrocatalytic activity of M40-type fibers. Δi denotes the difference between the catalytic current measured at 2.5 and 0 mM hydrogen peroxide concentration.

showed an unstable response behaviour in the presence of hydrogen peroxide. It was noticed that a decrease in the response with time to hydrogen peroxide reduction could be observed and that it was more accentuated for higher hydrogen peroxide concentrations (> 40 μM for the electrochemically pretreated P-type fibre and $>$ 320 μM for the heat-pretreated S-type fibre). The reason for this is not clear but may be attributed to a deactivation of the adsorbed HRP for higher concentrations of hydrogen peroxide whereby an enzymatically inactive form of HRP, compound III, is formed [33].

In order to see whether the stability could be increased, some methods of immobilization of HRP other than simple adsorption were tested for the P-type fibres, such as electrodeposition and covalent coupling using carbodiimide as the coupling reagent. Table 5 presents the best current responses recorded with P-type fibres using different pretreatments and various enzyme immobilization techniques.

Electrodeposition of the enzyme on the electrode at various positive stationary potentials was investigated as it is expected to result in an increased stability because of electrostatic interactions between the negatively charged enzyme (at pH 7.00) and positive applied potentials at the electrode surfaces. However, electrodeposition of the enzyme (both with and without the addition of GA) did not result in improved current responses compared with those obtained with the enzyme only immobilized by adsorption. The decline in the response to hydrogen peroxide reduction was shifted, however, to higher concentrations of hydrogen peroxide than for those with the enzyme only adsorbed on the electrode surface (> 160 μM).

As expected from previous results with HRP immobilized in carbon pastes [13], covalent immobilization using carbodiimide as a coupling reagent improved the operational stability of the electrodes. Further, an increase in the current response of about 60% was observed and a decline in the response to hydrogen peroxide reduction was noted at concentrations higher than 160 μM. The additional use of GA as a cross-linking agent in combination with covalent immobiliza-

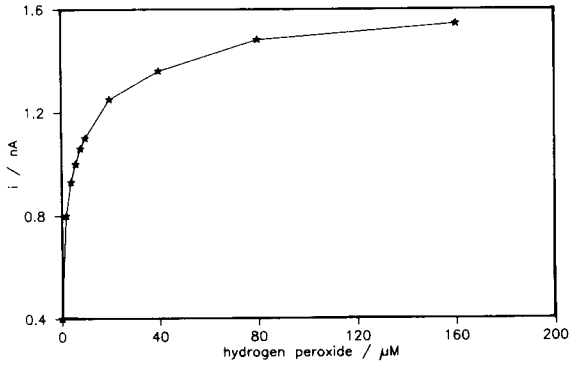

Fig. 10. Calibration graph for electrochemically pretreated (at +0.8 mV vs. SCE for 30 s) and HRP-modified P-type electrodes.

tion using carbodiimide did not enhance the current response.

Sensor characteristics

For simplicity, only adsorption was used as the immobilization method in the investigation of the sensor characteristics of the P-, S- and M40-type electrodes, even though the carbodiimide-activated fibres gave the most stable HRP-modified electrodes. The sensor characteristics were evaluated for the P- and S-type electrodes only, as electrodes prepared from these materials gave the highest response for hydrogen peroxide and it is not clear if a heating time of 45 s is sufficient for the total removal of the epoxy coating of the M40-type fibres. Figures 10 and 6b present typical calibration graphs for pretreated HRP-modified P- and S-type fibres respectively, operated at 0 mV vs. SCE. The linear range for the best P- and S-type electrodes (electrochemically oxidized and heated, respectively) was found to be between 2 and 40 μM (for the P-type) and between 80 and 2500 M hydrogen peroxide (for the S-type). The linear range of the electrodes and the slopes of the log–log plots were found to shift with the pretreatments used (see Table 5). The heat-pretreated S-type fibre was found to be the best sensor giving the highest current response for the reduction of hydrogen peroxide and the largest linear range. An apparent Michaelis–Menten constant of 1.2 mM was evaluated from an electrochemical Eadie–Hofstee plot, with a slope of 0.60 (log–log plot) and a linear range of the calibration graphs as mentioned above. The background current of the electrode was 0.25 nA and the detection limit of the sensor was 20 μM (calculated as twice the signal-to-noise ratio).

No efforts were made to prepare a single carbon fibre microelectrode because using the normalized current response good comparisons could be made between the different carbon fibre electrodes although the number of fibres varied. All results presented above are average values for five equivalently prepared electrodes.

The results obtained open up possibilities for the future use of this kind of microbiosensor in various microflow systems (micro liquid chromatography, micro flow injection, capillary electrophoresis), and the possible construction of various other microbiosensors, by co-immobilizing a hydrogen peroxide-producing oxidase with HRP on the surface of the microelectrodes.

The authors thanks the Swedish National Board for Industrial and Technical Development (NUTEK) and the Swedish Natural Research Council (NFR) for financial support, Mrs. Birgitta Svensson, Department of Chemical Technology, University of Lund, for taking the SEMs, Mr. Hans Roos (R&K, Danderyd), Professor Daniel Jagner (Chalmers Technical University, Gothenburg) and Mr. Sven Olsson, ISOAB (Gothenburg) for their generous gifts of carbon fibres.

REFERENCES

1 A.I. Yaropolov, V. Malovik, S.D. Varfolomeev and I.V. Berezin, Dokl. Akad. Nauk SSSR, 249 (1979) 1399.
2 G. Jönsson and L. Gorton, Electroanalysis, 1 (1989) 465.
3 J. Kulys and R.D. Schmid, Bioelectrochem. Bioenerg., 24 (1990) 305.
4 R.M. Paddock and E.F. Bowden, J. Electroanal. Chem., 260 (1989) 487.
5 U. Wollenberger, V. Bogdanovskaya, S. Bobrin, F. Scheller and M. Tarasevich, Anal. Lett., 23 (1990) 1795.
6 L. Gorton, M. Bardheim, G. Bremle, E. Csöregi, B. Persson and G. Pettersson, in R.D. Schmid (Ed.), Flow Injection Analysis (FIA) Based on Enzymes and or Antibodies [Gesellschaft für Biotechnologische Forschung (GBF) Monographs, Vol. 14], VCH, Weinheim, 1991, p. 305.

7 L. Gorton, G. Bremle, E. Csöregi, B. Persson and G. Jönsson-Pettersson, Anal. Chim. Acta, 249 (1991) 43.
8 E. Csöregi, G. Jönsson-Pettersson and L. Gorton, J. Biotechnol., submitted for publication.
9 T. Tatsuma and T. Watanabe, Anal. Chem., 63 (1991) 1580.
10 L. Gorton, E. Csöregi, E. Domínguez, J. Emnéus, G. Jönsson-Pettersson, G. Marko-Varga and B. Persson, Anal. Chim. Acta, 250 (1991) 203.
11 U. Wollenberger, J. Wang, M. Ozsoz, E. Gonzalez-Romero and F. Scheller, Bioelectrochem. Bioenerg., 26 (1991) 287.
12 G. Jönsson-Pettersson, Electroanalysis, 3 (1991) 741.
13 L. Gorton, G. Jönsson-Pettersson, E. Csöregi, K. Johansson and G. Marko-Varga, Analyst, 117 (1992) 1235.
14 K. Johansson, V. Kacaniklic, G. Marko-Varga, L. Gorton, G. Jönsson-Pettersson and E. Csöregi, J. Biotechnol., in press.
15 D.S. Bidra, Y. Zhang, G.S. Wilson, R. Sternberg, D.R. Thevenot, D. Moatti and G. Reach, Anal. Chem., 63 (1991) 1692.
16 C. Cronenberg, B. van Groen, B. de Beer and H. van den Heuvel, Anal. Chim. Acta, 242 (1991) 275.
17 Microelectrodes, Special Issue, Electroanalysis, Vol. 2 (1990).
18 K.W. Johnson, J.J. Mastrototaro, R.J. Morff and C.C. Andrew, Proceedings of the 3rd International Meeting of Chemical Sensors, Cleveland, OH, Sept. 24–26, 1990, p. 168.
19 M.F. Saud-Chagny and F.G. Gonon, Anal. Chem., 58 (1986) 412.
20 M.V. Pishko, A.C. Michael and A. Heller, Anal. Chem., 63 (1991) 2268.
21 J. Wang and L. Angnes, Anal. Chem., 64 (1992) 456.
22 E. Tamiya, Y. Sugiura, E.N. Navera, S. Mizoshita, K. Nakajima, A. Akiyama and I. Karube, Anal. Chim. Acta, 251 (1991) 129.
23 J. Wang, R. Li and M.S. Lin, Electroanalysis, 1 (1989) 151.
24 P. Pantano, T.H. Morton and W.G. Kuhr, J. Am. Chem. Soc., 113 (1991) 1832.
25 T.E. Edmonds, Anal. Chim. Acta, 175 (1985) 1.
26 T.E. Edmonds, E.M. Palshis and P. Rushton, Analyst, 113 (1988) 705.
27 J.B. Donnet and R.C. Bansal, in International Fibre Science and Technology, Vol. 3: Carbon Fibers, Dekker, New York, 1984.
28 K. Kinoshita, in Carbon, Electrochemical and Physicochemical Properties, Wiley, New York, 1988.
29 A.C. Michael J.B. Justice, Jr., and D.B. Neill, Neurosci. Lett., 56 (1985) 365.
30 M.A. Dayton, J.C. Brown, K.J. Stutts and R.M. Wightman, Anal. Chem., 52 (1980) 946.
31 S. Sarangapani, J.R. Akridge and B. Schumm (Eds.), Proceedings of the Workshop on the Electrochemistry of Carbon, August 17–19, 1983, Vol. 84-5, Case Western University, Cleveland, OH, The Electrochemical Society, Pennington, NJ, 1984.
32 J.X. Feng, M. Brazell, K. Renner, R. Kasser and R.N. Adams, Anal. Chem., 59 (1987) 1863.
33 S.A. Aderian and A.M. Lambeir, Eur. J. Biochem., 186 (1989) 571.

Analytica Chimica Acta, 273 (1993) 71–80
Elsevier Science Publishers B.V., Amsterdam

Mathematical modelling of the chronoamperometric response of an array of rectangular microelectrodes

Spas D. Kolev [1], Jo H.M. Simons and Willem E. van der Linden

Laboratory of Chemical Analysis, Department of Chemical Technology, University of Twente, P.O. Box 217, 7500 AE Enschede (Netherlands)

(Received 13th August 1992)

Abstract

A general mathematical model describing the response of an array of flat amperometric electrodes with arbitrary size and spatial distribution at the bottom of a measuring cell with rectangular walls and finite dimensions is outlined. It is based on the three-dimensional diffusion equation with initial and boundary conditions corresponding to the physical situation which was numerically solved by the implicit alternating-direction finite-difference method. The accuracy of the numerical solution was confirmed by theoretical and experimental results obtained by other authors. By comparing the chronoamperometric curves of the individual electrodes and by examining the spatial concentration distribution in the measuring cell conclusions can be drawn concerning the mutual influence of the individual electrodes for a given geometry of the array and the dimensions of the measuring cell. This will allow the designing of arrays and selecting the proper measuring cell dimensions resulting in minimal sensor interferences. Chronoamperometric curves show the time required for attaining quasi steady state and the corresponding current value. Illustrative examples are presented.

Keywords: Amperometry; Chronoamperometry; Mathematical modelling; Microelectrode arrays

In static solutions microelectrodes exhibit a number of advantages related to their size (e.g., in vivo measurements [1]) and electrochemical properties [2–24] in comparison with conventional macroelectrodes. The most important electrochemical properties are the following: (i) enhanced current densities due to non-linear diffusion [2–13] which results in a rapid establishment of the quasi steady-state in chronoamperometry [6–8,11,12], sigmoidal cyclic voltammograms with reversible couples for moderate scan rates [2,14–17], and increased sensitivity to small deviations from reversibility, allowing the measurement of high rate constants (e.g., up to 400 cm s^{-1} [18]); (ii) low ohmic potential drop which allows measurements to be performed in highly resistive media [19–24]; (iii) reduced double-layer capacitance due to the small surface area which, together with the low ohmic drop, allows measurement of faradaic currents at very short times and the extension of cyclic voltammetry to high scan rates [21].

The currents measured by microelectrodes, despite the non-linear diffusion effects, remain substantially lower in absolute values (e.g., down to the order of femtoamperes) than those of conventional macroelectrodes. This drawback, though not crucial in view of the modern instrumentation available nowadays, can easily be overcome by using ensembles of microelectrodes connected in parallel [25–29]. Depending on the method of manufacturing, (ultra)microelectrode arrays can

Correspondence to: W.E. van der Linden, Laboratory of Chemical Analysis, Department of Chemical Technology, University of Twente, P.O. Box 217, NL-7500 AE Enschede (Netherlands).

[1] Permanent address: Faculty of Chemistry, University of Sofia, 1 James Bouchier Ave., BG-1126 Sofia (Bulgaria).

have regular (e.g., microlithography [27]) or irregular (e.g., composite electrodes [29]) geometry. In addition to the valuable properties of single microelectrodes mentioned above the arrays of microelectrodes offer some additional advantages worth mentioning. It has been established both theoretically and experimentally that an array of microelectrodes in the long-time range (i.e., when the non-linear diffusion fields of the individual microelectrodes overlap) behaves like a macroelectrode (Cottrellian diffusion) with an area equal to the total geometric area of the array, not only to the sum of the areas of the individual microelectrodes comprising the electroactive area of the array [30–34,36–38]. This effect results on one hand in a considerable improvement in the signal-to-noise ratio of the array because despite the fact that the faradaic signal is proportional to the total geometric area (electroactive and non-electroactive area), the noise remains proportional only to the electroactive area of the array [34,39,40]. On the other hand it allows a considerable economy of the electroactive material which very often is a nobel metal [26–28]. The possibility to address individually each microelectrode in an array can be used for simultaneous multicomponent analysis or for study of reaction mechanism by simultaneously detecting the participating species in the reaction. The effectiveness of this approach can be further enhanced by modifying the individual microelectrodes in order to improve the selectivity.

For better understanding of the processes occurring at ensembles of microelectrodes and for their optimal design an adequate mathematical model is required. Models based on analytical [30,32,37] and numerical [31,33–36] solution of the partial differential equation expressing Fickian diffusion to arrays of disk, ring or square microelectrodes under various simplifying assumptions have been proposed before. Lindemann and Landsberg [30] assumed uniform distribution of microdisk electrodes in a rigid hexagonal array. They reduced the diffusion problem for such an ensemble to the diffusion to an array of non-interacting semi-infinite contiguous cylindrical unit cells with a concentrically situated circular active site at their bases. The equation derived for the diffusion current was based on the Cottrell equation [40] in which the term for the diffusion layer was corrected according to the results of Smythe [41]. However, those results are valid for steady-state conditions only and their application to the transient problem of chronopotentiometry resulted in discrepancies between theory and experiment [30]. Levart et al. [31] treated the diffusion to an array of periodically distributed square active sites under steady-state conditions and the results obtained are similar to those of Lindemann and Landsberg [30]. Gueshi et al. [32] developed a model using a representation of the microelectrode array similar to that of Lindemann and Landsberg [30] and assumed a steady-state radial diffusion. The resulting system of differential equations with their initial and boundary conditions corresponds exactly to that for an electron transfer preceded by a first-order chemical reaction. The analytical solution of the model gives accurate results for the current at short (i.e., semi-infinite linear diffusion to the electroactive area) and long (i.e., semi-infinite linear diffusion to the total geometric area) times. For intermediate times (i.e., non-linear diffusion to the individual microelectrodes) the predicted current was found to be too low, the deviation increasing with decreasing the fraction of the electroactive area. Reller et al. [33] numerically solved the model proposed by Gueshi et al. [32] taking into consideration the transient character of radial diffusion by an explicit finite-difference technique. Good agreement between reported experimental data [30] and results based on the simulation for the whole time range was observed. Weisshaar and Tallman [34] derived a model for carbon-based composite electrodes assuming that they consist of two ensembles of microelectrodes with different geometrical dimensions behaving independently of one another so that the total electrode current was simply a weighted summation of the two contributions, each described by the equation of Gueshi et al. [32]. Shoup and Szabo [35] numerically solved the problem treated in literature [30,32,33] using the hopscotch algorithm. They derived an empirical expression based on the equation for the current at an isolated microdisk electrode [6], which accu-

rately reproduced the results of the simulations for all times and for all fractional coverages. The authors found that for very short times ($t \rightarrow 0$) the ensemble current should not coincide with the Cottrell results [30–33] but be displaced from them by $\pi/4$. No experimental or simulation proof for this theoretical prediction can be found in the literature. Cassidy et al. [36] extended the problem treated in literature [30–34] to the case of a reversible simple electron-transfer reaction so that the concentrations of the reduced and the oxidized species at each electroactive disk surface were coupled by the Nernst equation. The orthogonal collocation method was used for the solution of the corresponding diffusion equations for the electroactive species. The simulation results agreed fairly well with those of Reller et al. [33] and those of Shoup and Szabo [35], and with the experimental data presented [30]. Scharifker [37] developed a simple analytical approach for calculating the time-dependent diffusion current to square, hexagonal and random arrays of microdisk electrodes using only the analytical expressions for the non-linear diffusion current to a single microdisk electrode [3] and the Cottrell equation [40]. The approach is based on considering the overlap of equivalent diffusion zones defined by the author as the circular area incorporating a microdisk electrode to which linear diffusion will produce the same effect as the actual non-linear diffusion to the same electrode. The overlap was calculated through the corresponding exact geometrical constructions in the case of square and hexagonal arrays or by applying the Avrami–Kolmgorov theorem in case of random arrays. Despite the substantial simplifying assumptions introduced by the author the analytical expressions obtained are in fairly good agreement with the theoretical results of Shoup and Szabo [35] and the experimental data presented by Gueshi et al. [32].

All the models mentioned above possess several drawbacks limiting their generality, the most important of them being the following:

(1) Only ordered arrays with a high degree of symmetry (e.g., square and hexagonal geometry) are considered which allows the more complicated diffusional problem to an array to be simplified to the case of diffusion to a single electrode. The equation of Scharifker [37] for the diffusion current at randomly distributed overlapping microdisk electrode arrays has not been experimentally confirmed and due to the considerable simplifications made in its derivation it is difficult to predict its validity for real random arrays. Modern microlithographic techniques allow the manufacturing of arrays with various geometries and different degrees of symmetry which cannot be described mathematically by the existing models.

(2) Only microdisk arrays have been considered except for reference [31] where the treatment of non-linear steady-state diffusion to an ordered array of square microelectrodes is reported.

(3) The arrays are assumed to be infinitely wide and long with constant concentration of the electroactive species far from their surface. These simplifying assumptions do not allow to take into account the effects of the walls of real electrochemical measuring cells on the response of the arrays in them, i.e., the models are not suitable for the description of chronocoulometric measurements accompanied by depletion of the electroactive species in the whole volume of the measuring cell or to predict to what extent a real measuring cell can be miniaturized without affecting the chronoamperometric response. Together with point 1, this assumption excludes any interference in the responses of the individual microelectrodes, i.e., the electrodes should exhibit identical responses. For this reason shielding effects of electrodes, where because of the geometry of the array the access of the electroactive species is restricted, cannot be taken into account.

In the present paper the development of a model overcoming the drawbacks of the models existing in the literature mentioned above is reported.

DEVELOPMENT OF THE MATHEMATICAL MODEL

The mathematical model proposed in the present study is based on the following assumptions:

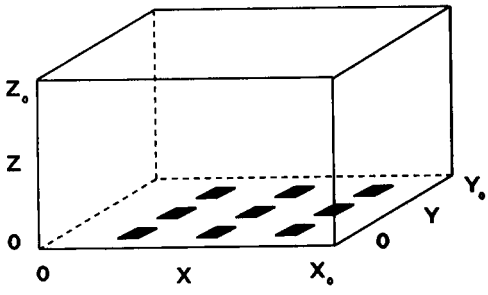

Fig. 1. Scheme of the measuring cell with an array of 9 rectangular electrodes at its bottom.

(i) the mass transfer is the result only of Fickian diffusion, i.e., no migration effects are considered; (ii) the walls of the measuring cell, which are assumed to be rectangles, are impermeable to the electroactive species inside it (Fig. 1); (iii) the depletion of the chemical species is a result only of the heterogeneous electrochemical reaction taking place at the electrodes which are situated at the bottom of the measuring cell (Fig. 1); (iv) a simple reversible charge-transfer reaction is considered and the potentials applied at all microelectrodes, which are not necessarily the same, are assumed to deviate from the formal potential E_0 to such an extent that either the anodic or the cathodic reaction predominates; (v) the microelectrodes were assumed to be rectangular in shape and to lie at the same level as the bottom of the measuring cell.

The mathematical model consists of the dimensionless Fick's second law (Eqn. 1). The symbols and their definitions are given in Table 1.

$$\frac{\partial C}{\partial \theta} = \frac{\partial^2 C}{\partial^2 X} + \frac{\partial^2 C}{\partial^2 Y} + \frac{\partial^2 C}{\partial^2 Z} \tag{1}$$

The initial conditions of Eqn. 1 are

$$C(0, X, Y, Z) = 1 \text{ for } 0 \le X \le X_0;$$
$$0 \le Y \le Y_0 \text{ and } 0 \le Z \le Z_0 \tag{2a}$$

The boundary conditions for the walls of the measuring cell excluding the electrodes are:

$$\left(\frac{\partial C}{\partial X}\right)_{X=0} = 0 \text{ for } 0 \le Y \le Y_0 \text{ and } 0 \le Z \le Z_0 \tag{2b}$$

$$\left(\frac{\partial C}{\partial X}\right)_{X=X_0} = 0 \text{ for } 0 \le Y \le Y_0 \text{ and } 0 \le Z \le Z_0 \tag{2c}$$

$$\left(\frac{\partial C}{\partial Y}\right)_{Y=0} = 0 \text{ for } 0 \le X \le X_0 \text{ and } 0 \le Z \le Z_0 \tag{2d}$$

$$\left(\frac{\partial C}{\partial Y}\right)_{Y=Y_0} = 0 \text{ for } 0 \le X \le X_0 \text{ and } 0 \le Z \le Z_0 \tag{2e}$$

$$\left(\frac{\partial C}{\partial Z}\right)_{Z=0} = 0 \text{ for } (X, Y) \notin S \tag{2f}$$

$$\left(\frac{\partial C}{\partial Z}\right)_{Z=Z_0} = 0 \text{ for } 0 \le X \le X_0 \text{ and } 0 \le Y \le Y_0 \tag{2g}$$

where S is the electroactive area of the array. The boundary conditions for the electrodes in the case of slow or moderate rate of the heterogeneous charge transfer with respect to the mass-transfer rates are given by Butler–Volmer equation:

$$\left(\frac{\partial C}{\partial \theta}\right)_{Z=0} = C_{Z=0} K_0 \exp\left[\frac{\alpha n F}{RT}(E - E_0')\right]$$
$$\text{for } (X, Y) \in S \tag{2h}$$

while if the reaction is very fast the concentrations at the electrodes can be assumed as 0, i.e.,

$$C_{Z=0} = 0 \text{ for } (X, Y) \in S \tag{2i}$$

The dimensionless current (I_i) monitored at each individual electrode and for the whole array (I) can be calculated by

$$I_i = \int_{s_i}\int \left(\frac{\partial C}{\partial Z}\right)_{Z=0} \mathrm{d}X\, \mathrm{d}Y \Big/ \int_{s_i}\int \mathrm{d}X\, \mathrm{d}Y \tag{3}$$

where s_i is the area of the ith microelectrode.

$$I = \sum_{i=1}^{i=N} I_i \tag{4}$$

NUMERICAL SOLUTION OF THE MODEL

The implicit alternating-direction finite-difference method [42] has been successfully applied

TABLE 1

Symbols and definitions

a	Coefficients defined in Table 3
b	Coefficients defined in Table 3
c	Concentration (mol m^{-3})
c_0	Initial concentration (mol m^{-3})
C	$= c/c_0$. Dimensionless concentration
d	Step coefficient (Table 2)
D	Diffusion coefficient (m^2 s^{-1})
E	Potential (V)
E_0'	Formal potential (V)
F	= 96486.332. Faraday constant (C mol^{-1})
i_i	Current at the ith microelectrode (A)
I_i	$= i_i L/nFDs_i c_0$. Dimensionless current of the ith electrode
I	$= \Sigma I_i$. Dimensionless current of the array
J_i	$= I_i s_i / L$. Normalized current of the ith microelectrode (m)
J	$= \Sigma J_i$. Normalized current of the array (m)
k_0	Standard heterogeneous rate constant (s^{-1})
K_0	$= L^2 k_0 / D$. Dimensionless standard heterogeneous rate constant
L	Characteristic length (m)
M	Total number of grid points in X (M_x), Y (M_y), or Z (M_z) direction of the spatial grid (defined in Table 3)
n	Number of electrons exchanged
N	Number of grid points in X (N_x), Y (N_y), or Z (N_z) direction in a uniform or non-uniform region of the spatial grid
R	= 8.3145. Gas constant (J K^{-1} mol^{-1})
s_i	Area of the ith microelectrode (m^2)
S	Electroactive area of the array (m^2)
t	Time (s)
T	Absolute temperature (K)
x, y, z	Directed distances in a cartesian coordinate system (m)
X, Y, Z	$= x/L,\ y/L,\ z/L$. Dimensionless directed distances in a cartesian coordinate system [a]

Greek letters

α	Transfer coefficient in Butler–Volmer equation
$\Delta\theta$	Dimensionless time increment
$\Delta\phi_0$	Dimensionless spatial increment in the uniform space grid region
ΔX_i	Dimensionless spatial increment in X direction (Table 2)
ΔY_i	Dimensionless spatial increment in Y direction (Table 2)
ΔZ_i	Dimensionless spatial increment in Z direction (Table 2)
θ	$= D\,t/L^2$. Dimensionless time

[a] The subscripts of X, Y, and Z are explained in Figs. 1 and 2.

for the numerical solution of partial differential equations describing multidimensional mass transfer [43,44]. The method is unconditionally stable and the corresponding sets of implicit difference equations in the X, Y, and Z directions have tridiagonal matrices and allow straightforward solution by a Gaussian elimination method [42]. The characteristic length of an array (L) was defined as the shorter length of the smallest rectangle in which all the individual microelectrodes of the array are confined. For the solution of Eqn. 1, which is a three-dimensional transient diffusion equation, a modification of the two-dimensional implicit alternating-direction method [42], proposed by Brian [45], was chosen. In order to reduce the computation time, a mixed uniform/non-uniform space grid was used. In the area where the electrodes were situated, i.e., $X_1 \le X \le X_2$, $Y_1 \le Y \le Y_2$, $Z \le Z_1$ (Fig. 2), an isotropic and in all three directions uniform space grid was used. The spatial increment ($\Delta\phi_0$) was selected in such a way that the edges of the electrodes coincide as much as possible with the grid lines. Outside this area spatial increments along all the three coordinate axes increase with distance from the area where the electrodes are located (Fig. 2). The size of the individual increments was determined as elements of an arithmetic progression with a basic element equal to the spatial increment ($\Delta\phi_0$) in the uniform-grid region and step coefficients, d_x, d_y, and d_z chosen in such a way so that X_1, Y_1 and $Z_0 - Z_1$ (Fig. 2) are subdivided by an integer number of grid points, N_x^0, N_y^0, and N_z^1, respectively (Table 2). The finite-difference formulas for the first- and second-order derivatives necessary for constructing the implicit finite-difference equations were obtained from the Taylor expansion [42]. The finite-difference formulas for the X derivatives are given in Table 3 and they are similar to those in the Y and Z directions. The non-uniform space grid outlined above allows the description of the concentration field to be made in greater detail closer to the electrodes and in lesser detail at a greater distance from them where the variations in the concentration gradients are smaller and less grid points are necessary for their accurate determination.

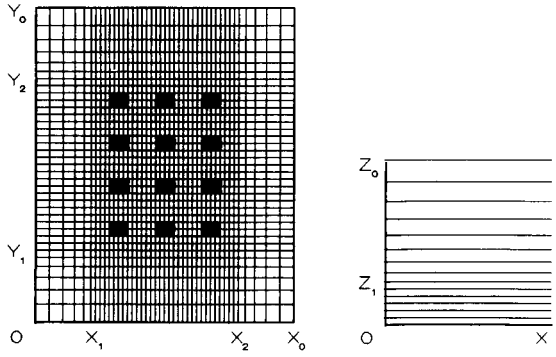

Fig. 2. Spatial grid in the measuring cell. Left: XY plane at $Z = 0$; right: XZ plane at arbitrary Y.

The double integral in Eqn. 3 was calculated by the consecutive application of Simpson's rule [42].

An important step in the model simulation is the accurate calculation of the flux of the electroactive species towards the surface of the microelectrodes, i.e., $(\partial C/\partial Z)_{Z=0}$ at $(X, Y) \in S$. This task could pose severe difficulties because it is well known that numerical differentiation is an inherently less accurate process than numerical integration utilized for solving Eqn. 1. Another reason to be cautious in this particular case is the fact that the concentration gradient in the Z direction (Eqn. 3) changes very rapidly with Z in the neighbourhood of the microelectrodes. Two different approaches for calculating $(\partial C/\partial Z)_{Z=0}$ at $(X, Y) \in S$ were investigated for finding the most appropriate one. According to the first approach the function $C(X, Y, Z) = f(Z)$ was smoothed in the uniform space grid region (i.e., $Z \leqslant Z_1$, Fig. 2) by the Savitzky–Golay algorithm [46] using a quadratic polynomial. The derivative $(\partial C/\partial Z)_{Z=0}$ was obtained by subsequent analytical differentiation of the least-square quadratic polynomial. The second approach was based on approximating the function $C(X, Y, Z) = f(Z)$ with an interpolating polynomial of nth degree [42]. To decide whether the flux should be calculated by a smoothing or interpolating polynomial and with what degree a comparison was made

TABLE 3

Finite-difference representation of $(\partial C/\partial X)$ and $(\partial^2 C/\partial X^2)$ in the case of non-uniform space grid
(Subscripts j and k are omitted for simplicity)

X	Finite-difference formulas
$0 \leq X \leq X_0$	$(\partial C/\partial X)_{X=X_i} = (C_i - C_{i-1})/\Delta X_i$
$X = 0$ [a]	$(\partial^2 C/\partial X^2)_{X=0} = 2(C_1 - C_0)/(\Delta X_1)^2$
$0 < X < X_0$	$(\partial^2 C/\partial X^2)_{X=X_i} = (a_i C_{i-1} - 2C_i + b_i C_{i+1})/(\Delta X_i\, \Delta X_{i+1})$
$X = X_0$	$\partial^2 C/\partial X^2)_{X=X_0} = 2(C_{M_x-1} - C_{M_x})/(\Delta X_{M_x-1})^2$
where	$a_i = 2\,\Delta X_{i+1}/(\Delta X_i + \Delta X_{i+1})$
	$b_i = 2\,\Delta X_i/(\Delta X_i + \Delta X_{i+1})$
	$M_x = N_x^0 + N_x^1 + N_x^2$

[a] Refers only to inactive area of the array where $(\partial C/\partial X)_{X=0} = 0$.

TABLE 2

Calculation of the X, Y, and Z increments in the mixed uniform/non-uniform spatial grid

	Number of points		Region	Increment
i	0	$N_x^0 - 1$	0–X_1	$\Delta X_{i+1} = [1 + (N_x^0 - i - 1)d_x]\,\Delta\phi_0$
X	N_x^0	$N_x^0 + N_x^1 - 1$	X_1–X_2	$\Delta X_{i+1} = \Delta\phi_0$
	$N_x^0 + N_x^1$	$N_x^0 + N_x^1 + N_x^2 - 1$	X_2–X_0	$\Delta X_{i+1} = [1 + (i - N_x^0 - N_x^1)d_x]\,\Delta\phi_0$
j	0	$N_y^0 - 1$	0–Y_1	$\Delta Y_{j+1} = [1 + (N_y^0 - j - 1)d_y]\,\Delta\phi_0$
Y	N_y^0	$N_y^0 + N_y^1 - 1$	Y_1–Y_2	$\Delta Y_{j+1} = \Delta\phi_0$
	$N_y^0 + N_y^1$	$N_y^0 + N_y^1 + N_y^2 - 1$	Y_2–Y_0	$\Delta Y_{j+1} = [1 + (j - N_y^0 - N_y^1)d_y]\,\Delta\phi_0$
k	0	$N_z^0 - 1$	0–Z_1	$\Delta Z_{k+1} = \Delta\phi_0$
Z	N_z^0	$N_z^0 + N_z^1 - 1$	Z_1–Z_0	$\Delta Z_{k+1} = [1 + (k - N_z^0)d_z]\,\Delta\phi_0$

with an existing analytical solution for the flux. As such Cottrell's equation [40] was chosen.

$$I = (\pi\theta)^{-1/2} \quad (5)$$

To meet the conditions under which Eqn. 1 is valid, this equation was solved under the assumption that the entire bottom of the measuring cell was electroactive. The smoothing of $C(X, Y, Z) = f(Z)$ for $(X, Y) \in S$ was done using the concentration in the first 2–5 grid points from the bottom of the measuring cell in the Z direction. The quadratic approximating polynomial utilized for calculating $(\partial C/\partial Z)_{Z=0}$ was of the order 1–5. In all cases very good agreement was observed for longer times while at short times the accuracy of the different approaches for calculating the flux differed. The lowest values of the mean relative error and the square root of the mean squared error between the chronoamperometric curves calculated by Cottrell's equation (Eqn. 5) and the numerical solution of Eqn. 1 were obtained in the case of 4th order polynomial approximation.

By varying the length of the spatial increment ($\Delta\phi_0$) while keeping the time increment constant (i.e., $\Delta\theta = 6.17 \times 10^{-5}$ corresponding to $\Delta t = 0.05$ s) it was found that the numerical and analytical solutions are practically indistinguishable from each other for $\Delta\phi_0 \leq 0.012$ (Fig. 3).

It should be taken into consideration that the values of the dimensionless currents (I_i) of the individual microelectrodes in an array depend on the characteristic length (L). This fact may cause misunderstandings when chronoamperometric curves of arrays with different characteristic length are compared in figures. To avoid this problem, the socalled normalized current defined as $J_i = I_i s_i / L$ and which does not depend on L is used in the the present paper for graphical representation of the calculated current–time dependences.

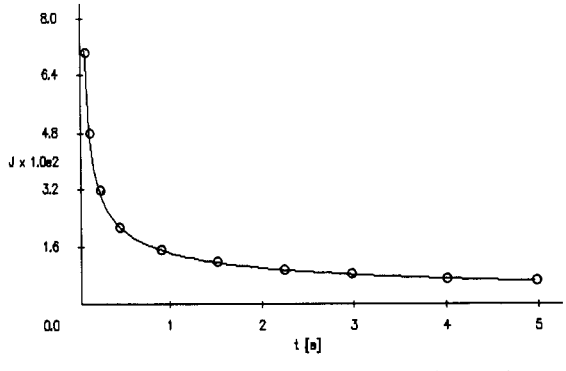

Fig. 3. Normalized chronoamperometric curve (———) calculated by numerical solution of Eqn. 1 with approximating polynomial of order 4 and (○) results obtained by Cottrell's equation ($D = 1.0 \times 10^{-9} m^2\ s^{-1}$).

The computer program solving numerically Eqn. 1 was written in ANSI C and run on VAX/VMS. A program written in Microsoft® QuickC® Version 2.0 was developed for graphical representation of the simulated chronoamperometric results and the concentration distribution of the electroactive species as contour or three-dimensional plots. Outputs of this program will be presented below.

VERIFICATION OF THE MODEL

As was already mentioned above the current measured by an array of microelectrodes at short times can be calculated by the equation assuming semi-infinite linear diffusion to the electroactive area of the array (Eqn. 5). For sufficiently long times the current–time dependence also obeys Cottrell's equation (Eqn. 5) if the whole geometric area of the array is considered as electroactive. These theoretical results [30–37], confirmed experimentally by various authors, were used for checking the validity of the model outlined in the present paper. The chronoamperometric curve for an ordered square distribution array of 16 square-shaped microelectrodes with an area of 10 μm^2 each was determined by numerical solution of the model. The results presented in Fig. 4 exactly follow the theoretically and experimentally established behaviour of microarray electrodes. This result together with the excellent agreement between the chronoamperometric curves calculated by Cottrell's equation and by numerical solution of the model in the case of a single electrode confirm the validity of the model presented in the present study.

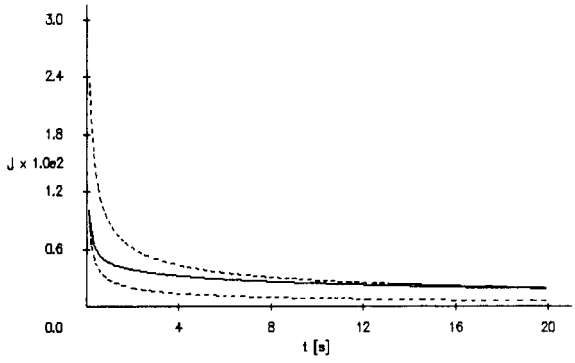

Fig. 4. Normalized chronoamperometric curves for a microelectrode array of 16 square distributed square microelectrodes calculated by (— — —) Cottrell's equation using the electroactive and the total area of the array and (———) by the model proposed in this study ($D = 1.0 \times 10^{-9} m^2\ s^{-1}$).

ILLUSTRATIVE EXAMPLE

One of the conditions for proper performance of arrays of amperometric microelectrodes used for multicomponent analysis is minimal interference between the individual microelectrodes. This condition will hold if the distance between the electrodes with respect to their size and the diffusion coefficients is big enough. Leaving too big a distance, however, will hamper the miniaturization of the arrays which is usually aimed at in their construction. Thus, the determination of the optimal distance between the electrodes appears to be a key parameter in the designing of the corresponding arrays. This can be performed by constructing electrodes with various geometrical dimensions and testing them experimentally. Obviously this is a costly and time consuming approach. The model outlined above is an appropriate tool for the fast and inexpensive solution of this problem. For illustrating this fact the chronoamperometric curves of the individual electrodes of two square distributed arrays with equal total electroactive area but with different total area (Fig. 5) were calculated. For simplicity it was assumed that the electrodes were poised at a potential where the charge-transfer reaction is very fast and the current generation is diffusion controlled. The results from the simulations are presented in Fig. 6. It can be seen that for array A (Fig. 5) there is a clear interference effect resulting in different quasi steady-state currents for the different individual electrodes while for array B (Fig. 5) there is an equal accessibility of the electroactive species to all the electrodes resulting in identical chronoamperometric curves. From the contour (Fig. 5) and the three-dimensional (Fig. 7) plots of the concentration field taken at the end of the chronoamperometric numerical experiment at the bottom of the measuring cell, i.e., $Z = 0$, it can be seen that in the case

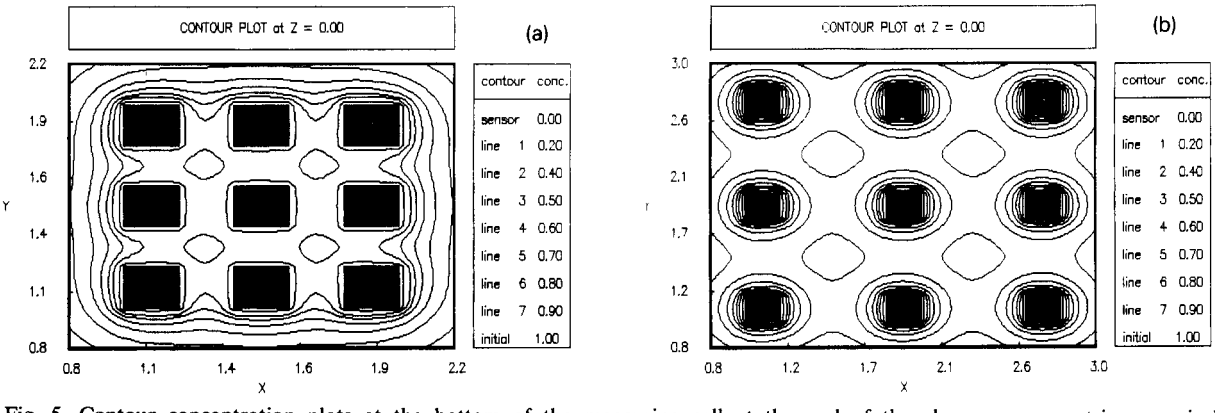

Fig. 5. Contour concentration plots at the bottom of the measuring cell at the end of the chronoamperometric numerical experiment ($t = 50$ s). (a) Array A; (b) array B ($D = 1.0 \times 10^{-9} m^2\ s^{-1}$). (It should be taken into consideration that the microelectrodes of the two arrays are of the same size while the interelectrode gaps differ considerably in size.)

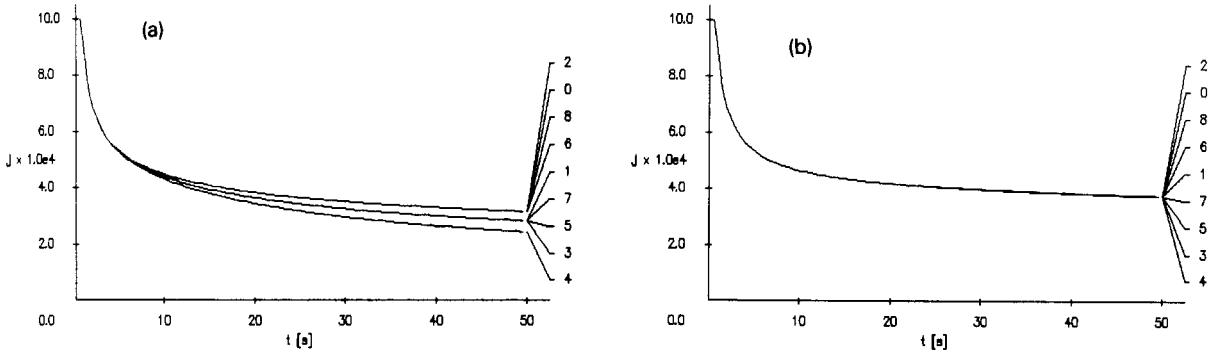

Fig. 6. Normalized chronoamperometric curves for the individual electrodes. Conditions are the same as in Fig. 5.

of array A there is very high degree of overlapping of the diffusion fields of the individual microelectrodes. For array B only a slight overlapping takes place far from the microelectrodes and it can hardly affect under the conditions of the experiment their behaviour as isolated microelectrodes giving the same amperometric response.

Conclusions

A general mathematical model describing the response of an array of amperometric electrodes with arbitrary distribution placed at the bottom of a measuring cell with rectangular walls and finite dimensions is outlined. It consists of the three-dimensional isotropic diffusion equation with boundary conditions corresponding to impermeable walls of the measuring cell and a charge-transfer reaction with either the anodic or the cathodic reaction predominating at the microelectrodes. The model allows to take into consideration the influence of the depletion of the electroactive species in the finite volume of the measuring cell on the response of the individual electrodes. This feature of the model extends its applicability also to chronocoulometry not treated in the present study. Shielding effects due to non-uniform accessibility of the electroactive species to the individual electrodes can be predicted and geometries causing such effects in real arrays can be prevented. The simulated chronoamperometric curves show the time required for attaining quasi steady-state current and its value for a given array and measuring cell, thus supplying the necessary information on the duration and sensitivity of analysis.

Though in the present study only rectangular

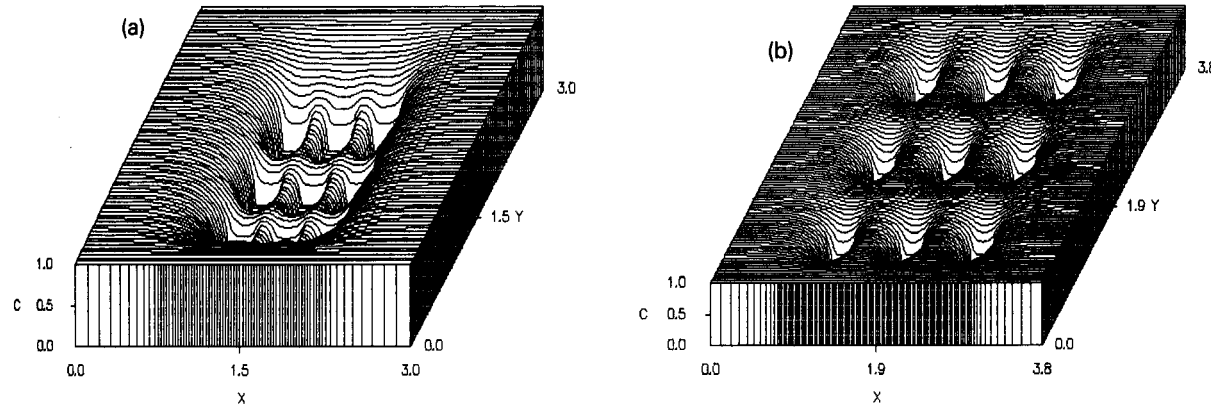

Fig. 7. Three-dimensional concentration plots. Conditions are the same as in Fig. 5.

microelectrodes were considered this fact does not confine the model only to this geometrical shape. The response of arrays with microelectrodes of any shape which can be represented as a combination of rectangles can be modelled. The model considers only the case of either the anodic or the cathodic reaction predominating which limits its application only to electroanalytical techniques working under such conditions (e.g., chronoamperometry, chronocoulometry) but there are no principle obstacles of extending it to reversible and quasi-reversible charge-transfer reactions or to more complex kinetics.

REFERENCES

1 A.G. Ewing, M.A. Dayton and R.M. Wightman, Anal. Chem., 53 (1981) 1942.
2 R.M. Wightman, Anal. Chem., 53 (1981) 1125A.
3 K.B. Oldham, J. Electroanal. Chem., 122 (1981) 1.
4 K. Aoki and J. Osteryoung, J. Electroanal. Chem., 122 (1981) 19.
5 J. Heinze, J. Electroanal. Chem., 122 (1981) 73.
6 D. Shoup and A. Szabo, J. Electroanal. Chem., 140 (1982) 237.
7 B. Speiser and S. Pons, Can. J. Chem., 61 (1983) 156.
8 K. Aoki and J. Osteryoung, J. Electroanal. Chem., 160 (1984) 335.
9 H. Ikeuchi, M. Sato and G.P. Satô, J. Electroanal. Chem., 162 (1984) 321.
10 S. Coen, D.K. Cope and D.E. Tallman, J. Electroanal. Chem., 215 (1986) 29.
11 K. Aoki, K. Tokuda and H. Matsuda, J. Electroanal. Chem., 225 (1987) 19.
12 K. Aoki, K. Tokuda and H. Matsuda, J. Electroanal. Chem., 230 (1987) 61.
13 J.C. Myland and K.B. Oldham, J. Electroanal. Chem., 288 (1990) 1.
14 J.F. Cassidy, S. Pons, A.S. Hinman and B. Speiser, Can. J. Chem., 62 (1984) 716.
15 K. Aoki, K. Akimoto, K. Tokuda and H. Matsuda, J. Electroanal. Chem., 171 (1984) 218.
16 M.R. Deakin, R.M. Wightman and C.A. Amatore, J. Electroanal. Chem., 215 (1986) 49.
17 K. Aoki and K. Tokuda, J. Electroanal. Chem., 237 (1987) 163.
18 P. Bindra, A.P. Brown, M. Fleischmann and D. Pletcher, J. Electroanal. Chem., 58 (1975) 31.
19 K.R. Wehmeyer, M.R. Deakin and R.M. Wightman, Anal. Chem., 57 (1985) 1913.
20 J. Newman, J. Electrochem. Soc., 113 (1966) 501.
21 J.O. Howell and R.M. Wightman, Anal. Chem., 56 (1984) 524.
22 S. Bruckenstein, Anal. Chem., 59 (1987) 2098.
23 A.M. Bond, M. Fleischmann and J. Robinson, J. Electroanal. Chem., 172 (1984) 11.
24 C. Amatore, M.R. Deakin and R.M. Wightman, J. Electroanal. Chem., 220 (1987) 49.
25 N. Sleszynski, J. Osteryoung and M. Carter, Anal. Chem., 56 (1984) 130.
26 W. Thormann, P. van den Bosch and A.M. Bond, Anal. Chem., 57 (1985) 2764.
27 T. Hepel and J. Osteryoung, J. Electrochem. Soc., 133 (1986) 752.
28 R.M. Penner and Ch.R. Martin, Anal. Chem., 59 (1987) 2625.
29 S.L. Petersen and D.E. Tallman, Anal. Chem., 62 (1990) 459.
30 J. Lindemann and R. Landsberg, J. Electroanal. Chem., 30 (1971) 79.
31 E. Levart, D. Schauhmann, E. Contamin and M. Etman, J. Electroanal. Chem., 70 (1976) 117.
32 T. Gueshi, K. Tokuda and H. Matsuda, J. Electroanal. Chem., 89 (1978) 247.
33 H. Reller, E. Kirowa-Eisner and E. Gileadi, J. Electroanal. Chem., 138 (1982) 65.
34 D.E. Weisshaar and D.E. Tallman, Anal. Chem., 55 (1983) 1146.
35 D. Shoup and A. Szabo, J. Electroanal. Chem., 160 (1984) 19.
36 J. Cassidy, J. Ghoroghchian, F. Sarfarazi and S. Pons, Can. J. Chem., 63 (1985) 3577.
37 B.R. Scharifker, J. Electroanal. Chem., 240 (1988) 61.
38 H. Reller, E. Kirowa-Eisner and E. Gileadi, J. Electroanal. Chem., 161 (1984) 247.
39 J. Cassidy, J. Ghoroghchian, F. Sarfarazi, J.J. Smith and S. Pons, Electrochim. Acta, 31 (1986) 629.
40 F.G. Cottrell, Z. Physik. Chem., 42 (1903) 385.
41 W.R. Smythe, J. Appl. Phys., 24 (1953) 70.
42 B. Carnahan, H.A. Luther and J.O. Wilkes, Applied Numerical Methods, Wiley, New York, 1969.
43 S.D. Kolev and W.E. van der Linden, Anal. Chem. Acta, 247 (1991) 51.
44 S.D. Kolev and W.E. van der Linden, Anal. Chem. Acta, 257 (1992) 331.
45 P.L.T. Brian, AIChEJ., 7 (1961) 367.
46 A. Savitzky and M.J.E. Golay, Anal. Chem., 36 (1964) 1627.

Analytica Chimica Acta, 273 (1993) 81–91
Elsevier Science Publishers B.V., Amsterdam

Reduction of acids at a platinum ultramicroelectrode: application to "in situ" acid number control of fluid lubricants (phosphate esters)

M. Perdicakis, C. Piatnicki, M. Sadik, R. Pasturaud, B. Benzakour and J. Bessière

Laboratoire de Chimie et d'Electrochimie Analytique, Faculté des Sciences, Université de Nancy I, B.P. 239, 54506 Vandoeuvre-lès-Nancy Cédex (France)

(Received 10th July 1992, revised manuscript received 24th September 1992)

Abstract

The strength of acids, their charge and possibly their behaviour as polyacids can be deduced by comparing their limiting currents at a platinum ultramicroelectrode in the absence and presence of an excess of supporting electrolyte. Acid–base reactions in tributyl phosphate can be followed without deliberately added supporting electrolyte even if their dielectric constant is low. The acidity of phosphate esters resulting from their hydrolysis can be monitored by amperometry at a platinum ultramicroelectrode.

Keywords: Amperometry; Voltammetry; Acid strength; Lubricants; Phosphate esters; Platinum ultramicroelectrodes

The use of ultramicroelectrodes (UMEs) allows the characterization of a solute by its voltammetric curve in media of low conductivity [1–6]. The small size of the electrode (diameter < 50 μm) leads to a significant decrease in the ohmic drop because of the very low currents. The presence of ionic impurities even at a low level will be sufficient to allow the recording of voltammetric curves without deliberate addition of electrolyte. The transport of electroactive species by migration plays a determining role in modifying the limiting current of charged species and sometimes of neutral species [7–9]. Further, because of the very large flux by diffusion, the convection effects tend to be less apparent than at electrodes of conventional size. This is advantageous for the monitoring of fluids because it limits the flow-rate dependence.

The possibility of characterizing electroactive species using an ultramicroelectrode in solvents of low conductivity can be applied to the analysis of equilibria or chemical analysis. It is certainly an important field of investigation in analytical chemistry.

The first purpose of this paper is to show the influence of migration on the electrochemical behaviour of acids and to obtain information on their charge, dissociation and reactivity towards uncharged bases. Studies were realized in water, acetonitrile–water (95 + 5, v/v) and in phosphate esters. The first two media were selected for analysing the behaviour of strong acids, charged weak acids and dibasic acids. The phosphate esters were chosen because of their poorly conducting character, which hinders conventional voltammetric studies. It is important to know if the results obtained in more dissociation-enhancing

Correspondence to: J. Bessière, Laboratoire de Chimie et d'Electrochimie Analytique, Faculté des Sciences, Université de Nancy I, B.P. 239, 54506 Vandoeuvre-lès-Nancy Cédex (France).

solvents such as acetonitrile are still applicable and if the analysis of chemical reactions in industrial solvents of importance in liquid–liquid extraction [e.g., tributyl phosphate (TBP)] [10] and in lubrication [11] can be realized.

The second purpose is to emphasize the interest of ultramicroelectrochemical methods for the remote measurement of acids and bases present in phosphate esters of low dielectric constant which can be used as lubricants in the primary pump motor of nuclear plants.

THEORETICAL

The development of electrochemistry at UMEs in solvents with no supporting electrolyte added renews interest with regard to the migration effects that were investigated during the initial development of the theoretical fundaments of electrochemistry [7,12–14].

The different approaches for evaluating the ratio between the limiting current of an electroactive species without (i) and with supporting electrolyte (i_d) lead to the same results for some redox systems but are in contradiction for others. Amatore et al. [15] proposed a new model applicable to the UMEs for explaining the migration effect on the limiting current assuming the equality of the diffusion coefficients of the species that participate in the electrochemical reaction at the electrode (reactants and products):

$$i/i_d = 1 + Z\{1 + (1 + |Z|)(1 - Z/n) \times \ln[1 - 1/[(1 + |Z|)(1 - Z/n)]]\} \quad (1)$$

where Z is the charge of the electroactive species and n represents the number of electrons exchanged (the sign used is negative for $n > Z$ and positive for $n < Z$).

Unfortunately, according to the authors, this model cannot be applied to electrochemical systems involving solids or hydrogen ions. In addition, only singly charged counter ions associated with the electroactive species are considered.

For strong acids, the equations proposed by Vetter [14] lead to the equation

$$i/i_d = 1 + (1/|Z_a|) \quad (2)$$

This relationship shows that the migration effect decreases when the charge Z_a of the counter ion associated with the proton increases. These predictions could not previously be fully confirmed experimentally owing to the iR drop limitation in classical methods. However, Eqn. 2 does not allow the prediction of the electrolyte effect when the acid is anionic, because in this instance the unfavourable migration decreases the amount of the anionic acid at the cathode.

A critical analysis of the different theories led to the proposal of a more general equation in which the equivalent conductivity of the ions [16] is considered. For acid reduction, the following expression is established:

$$i/i_d = 1 + (|Z_{ac}/Z_{ci}|) / [(\lambda_{ac}/\lambda_{ci})(1 \pm |n/Z_{ac}|) + 1] \quad (3)$$

where the subscripts ac and ci represent the acid particle and the counter ion, respectively, λ_{ac} and λ_{ci} being their equivalent conductivities. The + and − signs refer to the reduction of an anionic or a cationic acid. For an acid HA^-, the relationship is then

$$i/i_d = 1/(\lambda_{ac}/\lambda_{ci} + 0.5)$$

if the counter ion is singly charged. Equations 2 and 3 give the same results for strong acids.

For analysing the migration effect with systems involving the reduction of several species, as for a polyacid whose first dissociation step corresponds to a strong acid and the second to a weak acid, Eqns. 2 and 3 are no longer suitable. Therefore some simplifying assumptions are proposed for a semi-quantitative evaluation of the migration effect [9,17]. First, it is assumed to a first approximation that the absolute mobilities are equal. This means that the mobilities of ionic species are dependent only on their charge and that the diffusion coefficients are the same with or without an electrolyte. Second, it is assumed that the ionic species present are the only ones carrying the current (the contribution of ionic species eventually formed at the electrode is neglected). The following equation results from these assumptions:

$$i/i_d = (|Z_{anion}| + Z_{cation}) / (|Z_{anion}| + Z_{cation} \pm |n|) \quad (4)$$

where the − sign corresponds to a favourable migration for the transport of the electroactive species and the + sign to the opposite case.

For the reduction of acids, Eqn. 4 leads to the same results as Eqns. 2 and 3 for strong acids, and Eqn. 3 for an anionic acid (AH^-, X^+) if the equivalent conductivities are considered to be equal. These simplifying assumptions, even if they lead to approximate predictions, allow a simple schematic illustration of the transfer of matter by diffusion and migration for all systems.

This representation is particularly interesting for the analysis of systems involving several steps or for understanding the exaltation effect of the migration currents due to the presence of two electroactive species in solution [9]. For instance, if one considers the behaviour of sulphuric acid in water, the transfer of matter can be explained as follows. The migration of H^+ and SO_4^{2-} ions carries the current necessary for the reduction of protons arriving by diffusion at the electrode. Assuming equality of the absolute mobilities of ions, the sulphate species carries twice as much charge per unit time as the proton. The migration of one H^+ and one SO_4^{2-} provides only two charges from the three involved, the proton consuming one charge for its own reduction. If one considers the diffusion of four H^+, a contribution of four charges by migration is necessary for their reduction, which is ensured by the displacement of two H^+ and two SO_4^{2-} in the solution. Hence, in the absence of supporting electrolyte, six H^+ arrive at the electrode and are responsible for the current i. Adding an electrolyte suppresses the contribution of the transfer by migration, and only the diffusion of four H^+ which is responsible for the current i_d has to be considered.

The schemes corresponding to the reduction of charged acids in cases of favourable and unfavourable migration are shown in Fig. 1.

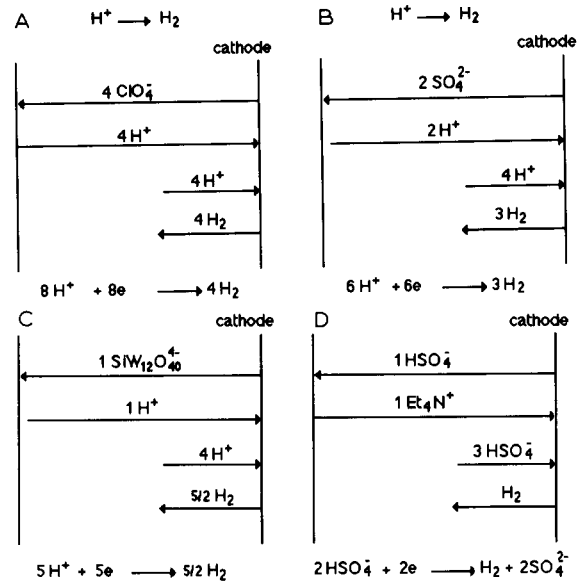

Fig. 1. Schematic representation of the migration and diffusion contributions in electrochemical reduction of charged acids. (A) $HClO_4$; (B) H_2SO_4; (C) $H_4SiW_{12}O_{40}$; (D) Et_4NHSO_4.

EXPERIMENTAL

Reagents

Experiments in aqueous medium were carried out in demineralized water ($\rho < 10^{-7}\ \Omega^{-1}\ cm^{-1}$), with HNO_3, $HClO_4$ and H_2SO_4 of Suprapur grade from Merck and $H_4SiW_{12}O_{40}$ of analytical-reagent grade from Fluka. These acids were titrated by NaOH standard solution from Merck. The supporting electrolyte used in aqueous medium was KNO_3 of Normapur grade from Prolabo.

For experiments in water–acetonitrile (5 + 95, v/v) mixture, the water was distilled, demineralized and the acetonitrile was from SDS (Purex grade). The acids were the same as in aqueous medium and also tetraethylammonium hydrogensulphate (Et_4NHSO_4) (puriss.) from Fluka was used. The supporting electrolyte in this medium was tetrabutylammonium perchlorate (Bu_4NClO_4) (puriss.; electrochemical grade) from Fluka.

For the experiments in tributyl phosphate (TBP), this solvent was of 99% grade from Aldrich and the acids were H_2SO_4, $HClO_4$ and HNO_3 of Normapur grade from Prolabo, titrated with NaOH standard solution from Merck. Tetrabutylammonium perchlorate, dibutylphosphoric acid, (DBPA) and diphenylphosphoric acid (DPPA) were of purum. grade from Fluka, tributylamine of puriss. grade from Fluka and NH_3 of Suprapur grade from Merck.

Industrial lubricants (Fyrquel VPF and Fyrquel 150) from Stauffer were used as received and were stored in the dark.

Instrumentation

The experiments were done in a Faraday cage with a Model 174A polarographic analyzer (EG& G PAR), and data were plotted with an Kipp & Zonen BD90 *X–Y* recorder.

The reference electrode was a saturated calomel electrode (SCE) in a vessel equipped with a diaphragm and containing a solution of the same composition as that studied in order to avoid contamination by KCl (an aqueous SCE was used for the experiments in water and acetonitrile and an SCE in methanol for those in phosphate esters).

The platinum disc UMEs (diameter ca. 10 μm) used were MEPT 10 MI from Tacussel and GO 225 from EG&G PAR.

RESULTS AND DISCUSSION

Electrolyte effect in water and acetonitrile

The analysis of the migration effects on the behaviour of the strong acids $H_4SiW_{12}O_{40}$, H_2SO_4 and $HClO_4$ was done in water. In the presence of electrolyte, all the solutions give the same limiting current i_d when their H^+ concentrations are the same (Fig. 2). Without electrolyte, the limiting current i decreases when the charge of the counter ion increases. The i/i_d values are in accordance with the Eqns. 2 and 4. Progressive addition of KNO_3 leads to a decrease in the limiting current. The i/i_d ratio for a 1 + 1 acid is 2 when the electrolyte concentration is about ten times higher than that of the acid [16].

The study of the weak acids and dibasic acids is easier in acetonitrile with a 5% water content because of its larger electroactivity range compared with water. The curve obtained with H_2SO_4 (Fig. 3) in the presence of Bu_4NClO_4 as electrolyte shows that the dissociation in the first step corresponds to that of a strong acid whereas that in the second step corresponds to that of a weak acid. H^+ and the HSO_4^- ions have very similar diffusion coefficients ($D_{H^+}/D_{HSO_4^-} = 0.9$). Without electrolyte, the voltammogram is strongly modified; virtually only one wave appears, the intensity of which is double that of the first wave obtained in the presence of Bu_4NClO_4. For the first reduction wave, the result is consistent with that for a strong monobasic acid.

At lower potentials, according to the simplifying hypothesis, HSO_4^- reduction at the cathode is impossible because in the first reduction step, as soon as it arrives by diffusion, it immediately moves away from the electrode by migration to ensure H^+ reduction. The absence of the second wave would be due to the fact that the diffusion coefficients of H^+ and HSO_4^- are approximately the same in this medium (see Fig. 4).

The behaviour of HSO_4^- is in accordance whith the theoretical prediction: the addition of electrolyte leads to a 20% increase in the cathodic current instead of the 33% that would be expected if the equality of the equivalent conductivities for the ions is considered (Eqn. 3). The experimental values are in accordance with the equation given by Amatore et al. [15] even if it does not theoretically apply to the reduction of acids (observed value for $i/i_d = 0.82$ and calculated value = 0.85).

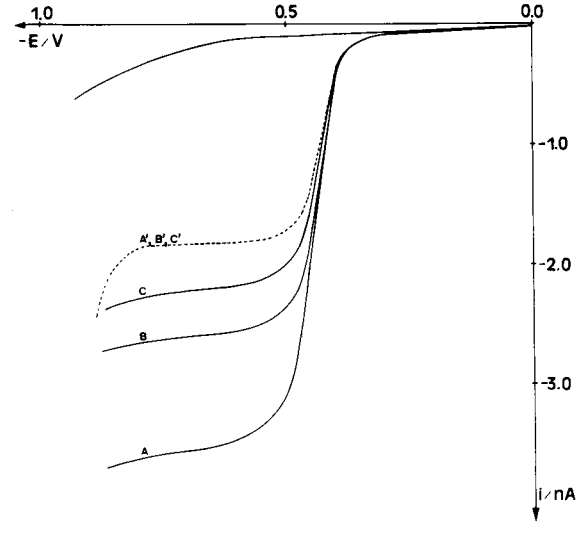

Fig. 2. Voltammograms of aqueous acid solutions 1 mM in H^+ in water. (A) $HClO_4$, (B) H_2SO_4 and (C) $H_4SiW_{12}O_{40}$ without supporting electrolyte and (A'), (B') and (C') with 0.1 M KNO_3 (dashed line). Scan rate, 1 mV s^{-1}.

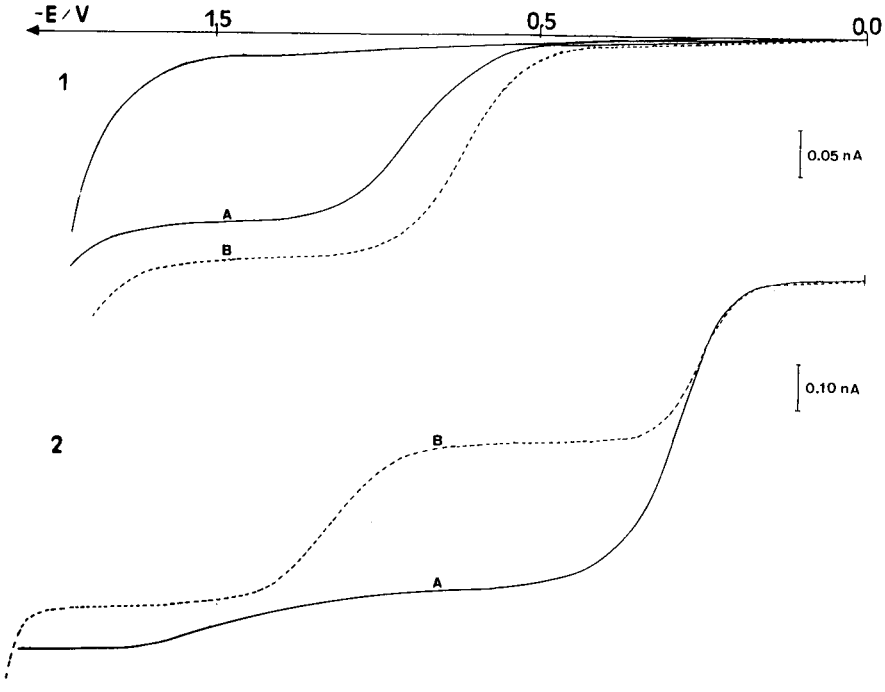

Fig. 3. Voltammograms of (1) 1 mM tetraetylammonium hydrogensulphate and (2) 1 mM sulphuric acid in water–acetonitrile (5 + 95, v/v) without supporting electrolyte (curves A) and with 0.1 M Bu_4NClO_4 added to the solution (curves B). Scan rate, 1 mV s^{-1}.

For $HClO_4$ (Fig. 5), the i/i_d ratio relative to the first wave of H_2SO_4 reaches 1 when the electrolyte concentration is ten times higher than that of the acid (Fig. 4). The electrolyte effect on $H_4SiW_{12}O_{40}$ is the same as that observed in water.

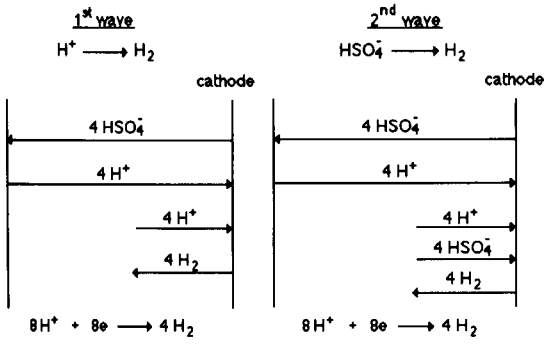

Fig. 4. Schematic representation of the migration and diffusion contribution in electrochemical reduction of sulphuric acid in water–acetonitrile (5 + 95, v/v).

Electrolyte effect in tributyl phosphate

Despite its significance as an industrial solvent in liquid–liquid extraction of uranium [18] and acids [19], TBP has not been extensively studied

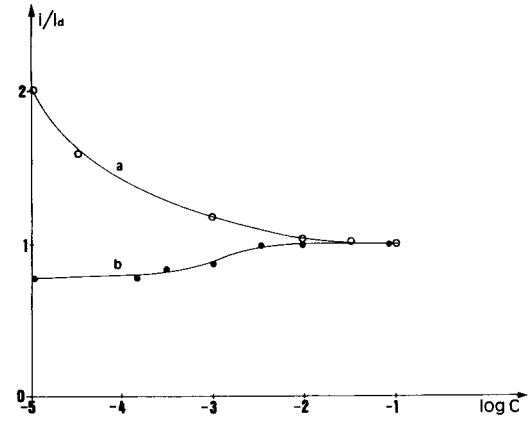

Fig. 5. Electrolyte effect (Bu_4NClO_4) on limiting currents of (a) 1 mM perchloric acid and (b) 1 mM tetraetylammonium hydrogensulphate in water–acetonitrile (5 + 95, v/v).

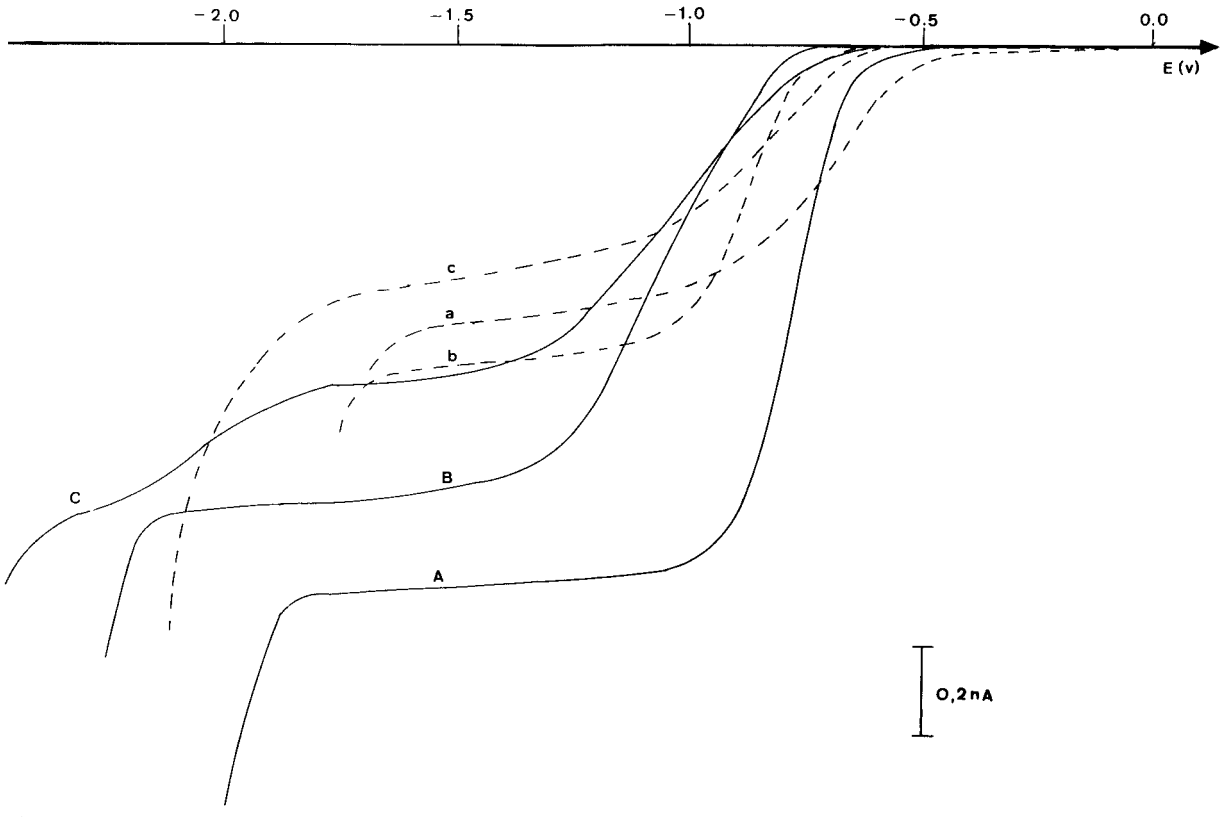

Fig. 6. Electrolyte effect on limiting currents relative to acids in water-saturated TBP. (A) 3.7 mM $HClO_4$; (a) 3.7 mM $HClO_4$ + 150 mM Bu_4NClO_4; (B) 3.7 mM HNO_3; (b) 3.7 mM HNO_3 + 150 mM Bu_4NClO_4; (C) 3.7 mM H_2SO_4; (c) 3.7 mM H_2SO_4 + 150 mM Bu_4NClO_4. Scan rate, 5 mV s^{-1}.

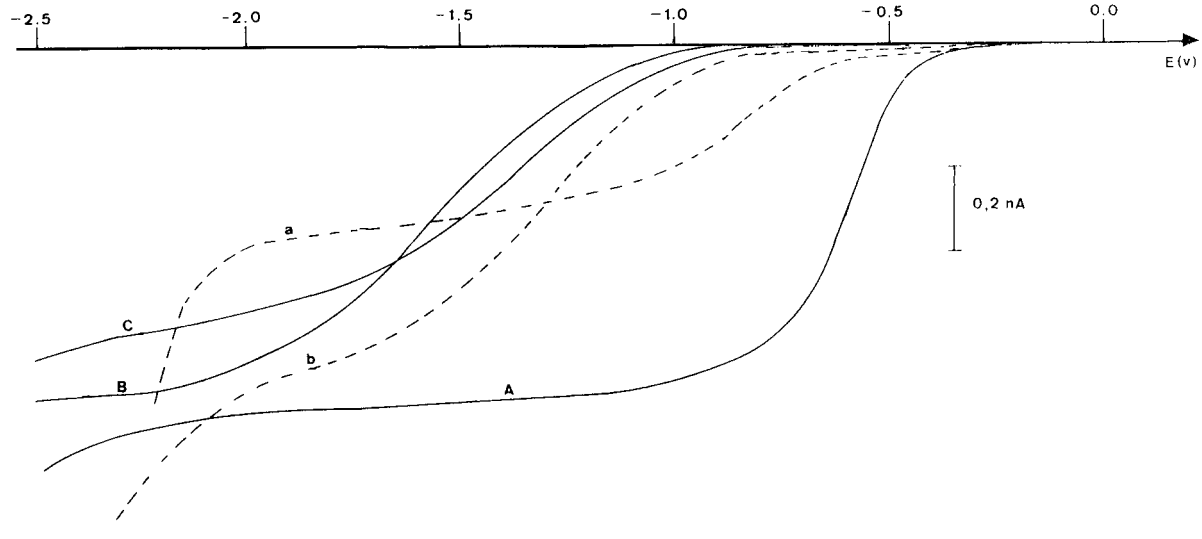

Fig. 7. Electrolyte effect on limiting currents relative to acids in TBP containing 10 mM water. (A) 3.7 mM $HClO_4$; (a) 3.7 mM $HClO_4$ + 100 mM Bu_4NClO_4; (B) 3.7 mM HNO_3; (b) 3.7 mM HNO_3 + 100 mM Bu_4NClO_4; (C) 3.7 mM H_2SO_4. Scan rate, 5 mV s^{-1}.

by means of electrochemical methods [20]. Its dielectric constant is low ($\epsilon = 8.0$), even when water saturated ($[H_2O] = 3.5$ M) ($\epsilon = 10.0$). Its resistive character ($\rho = 1.2 \times 10^{-9}$ Ω^{-1} cm^{-1}) is higher than that of acetonitrile ($\rho = 2.0 \times 10^{-8}$ Ω^{-1} cm^{-1}), the dielectric constant of which is 37.5. It is important to know whether a UME allows both the direct analysis of equilibria in the organic phase of water–TBP biphasic systems and the titration of electroactive species by amperometry.

Other phosphate esters are already used as lubricant in gas turbines on pipelines and their use is envisaged in primary pumps of nuclear plants [11,21]. These fluids, with low dielectric constants, partially hydrolyse and release acids that can cause corrosion of the pump materials. Their use needs strict control of the acidity liberated by the hydrolysis for setting up a preventive treatment. For limiting these disturbances, basic additives such as amines are added to the lubricant. It is interesting to follow their evolution with time.

These two objectives stimulated an examination of the behaviour of acids and amines in TBP. Most of the previous studies realized with UMEs in the absence of a supporting electrolyte have been carried out in solvents with dielectric constants higher than 30. It is important to know what happens in much less dissociation-enhancing solvents ($\epsilon < 10$).

Behaviour of acids

Voltammetric curves relating to the acids studied are dependent on their charge and on the water content of TBP (Figs. 6 and 7).

$HClO_4$ is strong in water-poor TBP ($[H_2O] = 0.01$ M) [22]. The voltammetric curve is well de-

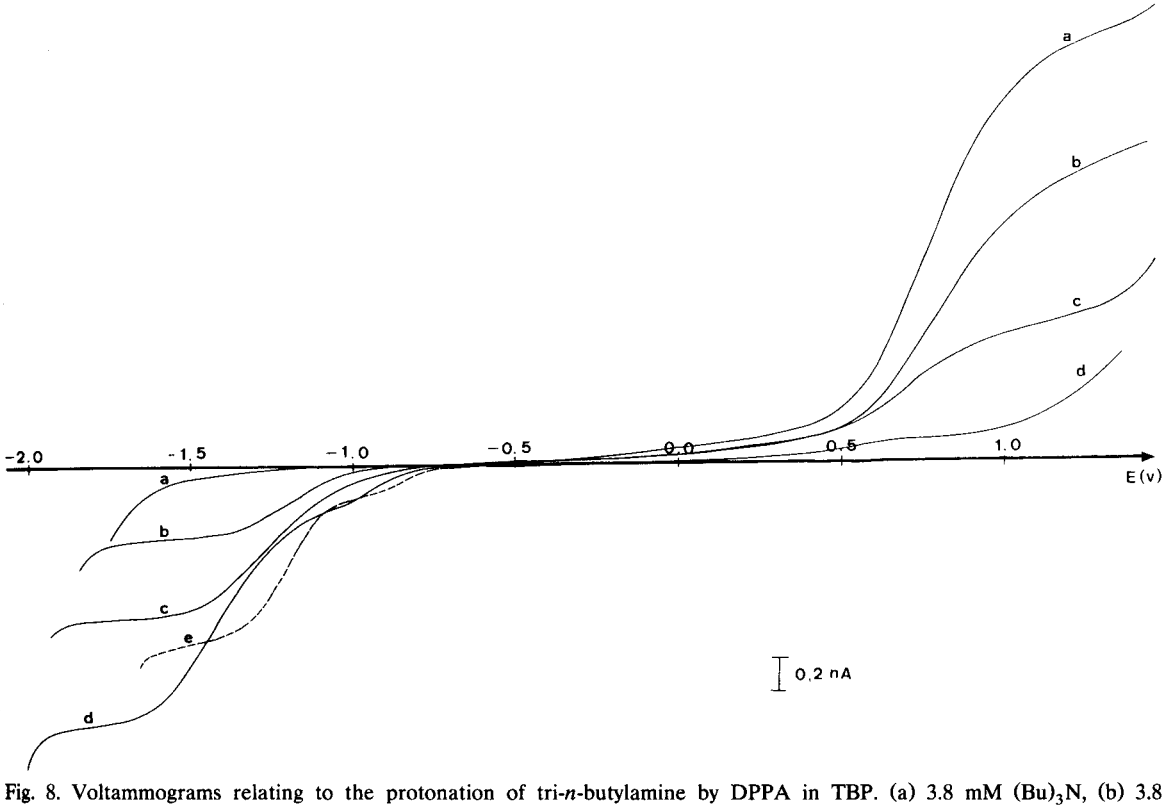

Fig. 8. Voltammograms relating to the protonation of tri-*n*-butylamine by DPPA in TBP. (a) 3.8 mM $(Bu)_3N$, (b) 3.8 mM $(Bu)_3N$ + 1.0 mM DPPA, (c) 3.8 mM $(Bu)_3N$ + 3.3 mM DPPA, (d) 3.8 mM $(Bu)_3N$ + 4.4 mM DPPA, (e) 3.8 mM $(Bu)_3N$ + 4.4 mM DPPA + 150 mM Bu_4NClO_4. Scan rate, 5 mV s^{-1}.

fined and the addition of Bu_4NClO_4 causes a decrease in the limiting current by a factor of 2. $HClO_4$ in TBP thus exhibits the same behaviour as in a dissociation-enhancing solvent. On the other hand, the two acidic functions of H_2SO_4 are weak and there is no effect of the electrolyte on the current as H_2SO_4 is in its molecular form.

In water-saturated TBP, the behaviour of H_2SO_4 is similar to that observed in acetonitrile, except that the first acidic function is not entirely strong. The second wave is slightly larger than in acetonitrile. In the presence of electrolyte, two waves of equal height appear.

HCl and HNO_3 are also molecular in water-poor TBP and significant ohmic drops take place. The addition of an electrolyte (or of water) makes the slopes of the curves steeper without decreasing the limiting currents.

In water-saturated TBP, HNO_3 is partially ionized as electrolyte addition decreases the current; the same result is observed with acetic acid in water [16]. As with acetonitrile, the diffusion coefficients of the molecular acids are twice those of hydrogen ions.

DBPA and DPPA, which result from the hydrolysis of the corresponding phosphate esters, are also present in their molecular form in TBP. In the presence of water, the limiting currents increase linearly with increasing DPPA concentration, but the ohmic drops persist.

Behaviour of amines and ammonia

Tertiary amines. Tertiary amines such as tri-*n*-butylamine and tri-*n*-ethylamine are stable in TBP and give an anodic response corresponding to the exchange of one electron [23], as in other solvents. The current is proportional to the amine concentration and independent of the electrolyte addition, which makes the slopes of the curves steeper only because of the decrease in the ohmic drop (Fig. 8). The progressive addition of DPPA quantitatively decreases the anodic signal and a cathodic wave appears corresponding to the protonated tri-*n*-butylamine. The addition of electrolyte at the equivalence point decreases the cathodic current because of the positive charge of Bu_3NH^+. Meanwhile, the decrease of the current is lower than that predicted (50%). This is proba-

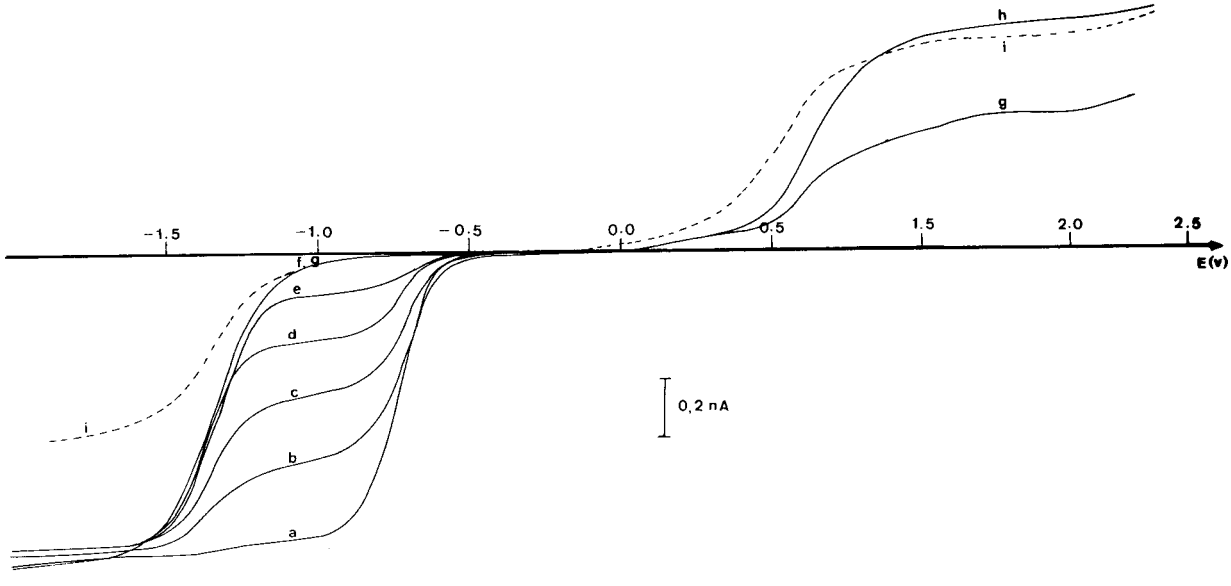

Fig. 9. Voltammograms relating to the neutralization of perchloric acid by tri-*n*-butylamine in TBP. (a) 1.1 mM $HClO_4$, (b) 1.1 mM $HClO_4$ + 0.2 mM $(Bu)_3N$, (c) 1.1 mM $HClO_4$ + 0.4 mM $(Bu)_3N$, (d) 1.1 mM $HClO_4$ + 0.6 mM $(Bu)_3N$, (e) 1.1 mM $HClO_4$ + 0.8 mM $(Bu)_3N$, (f) 1.1 mM $HClO_4$ + 1.0 mM $(Bu)_3N$, (g) 1.1 mM $HClO_4$ + 1.2 mM $(Bu)_3N$, (h) 1.1 mM $HClO_4$ + 1.4 mM $(Bu)_3N$, (i) 1.1 mM $HClO_4$ + 1.4 mM $(Bu)_3N$ + 150 mM Bu_4NClO_4. Scan rate, 5 mV s^{-1}.

bly due to the existence of interactions by hydrogen bonds between $(ArO)_2POO^-$ and Bu_3NH^+ ions, leading to the partial formation of a neutral ion pair. Such a heteroconjugation frequently occurs in aprotic media [24]. This example illustrates the interest in using UMEs for following "in situ" the behaviour of basic additives with acids resulting from their hydrolysis.

The titration of perchloric acid by tri-*n*-butylamine in TBP with a low water content gives voltammetric curves where the ohmic drops are limited because of the presence of ionic species during the titration (Fig. 9). The addition of an electrolyte at the end-point leads to a decrease in the current of about 50%. This result is in accordance with prediction because the perchlorate ion does not participate in hydrogen bonds and heteroconjugation does not take place.

Primary amines and ammonia. *N*-Ethylamine and *n*-butylamine react with TBP [25]: their anodic signal quickly disappears to give a complex cathodic response relative to the degradation products. It is possible to stabilize them by protonation. Thus, the cathodic current relative to ethylammonium perchlorate is well defined.

The influence of electrolyte addition on the limiting currents relative to the ammonium salts gives information on their stability (Fig. 10): the cathodic current of ammonium perchlorate is half that in the presence of electrolyte whereas it remains constant with ammonium acetate. The slope of the curve is steeper only because of the decrease in ohmic drop. This phenomenon is due to the decomposition of ammonium acetate in ammonia and acetic acid. Acetic acid is present in its molecular form and the corresponding curve is not well defined, compared with that for ammonium perchlorate. The effect of electrolyte can thus be used to give information on the progress of the reaction; this effect appears when the molecular species RNH_2 and HA react together. It is also clear that ion-pair formation or hetero-

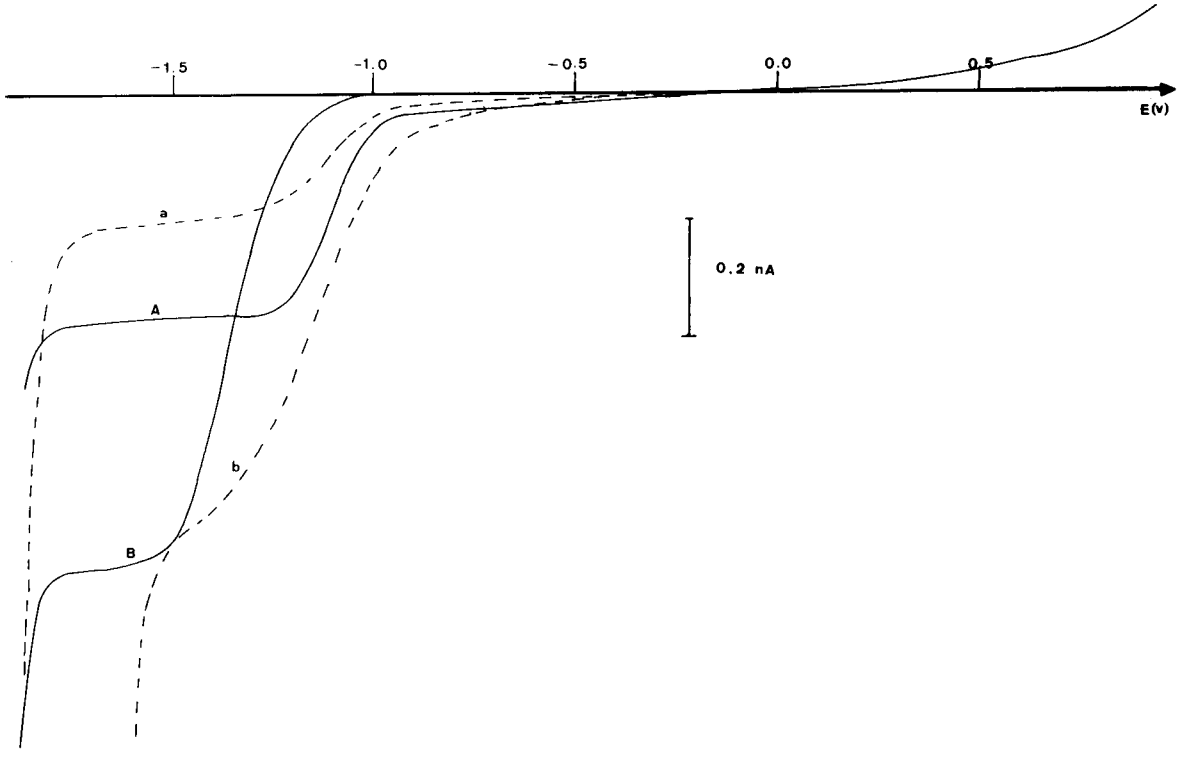

Fig. 10. Electrolyte effect on ammonium salts in TBP. (A) 1.1 mM NH_4ClO_4; (a) 1.1 mM NH_4ClO_4 + 150 mM Bu_4NClO_4; (B) 8.3 mM NH_4COOCH_3; (b) 8.3 mM NH_4COOCH_3 + 150 mM Bu_4NClO_4. Scan rate, 5 mV s^{-1}.

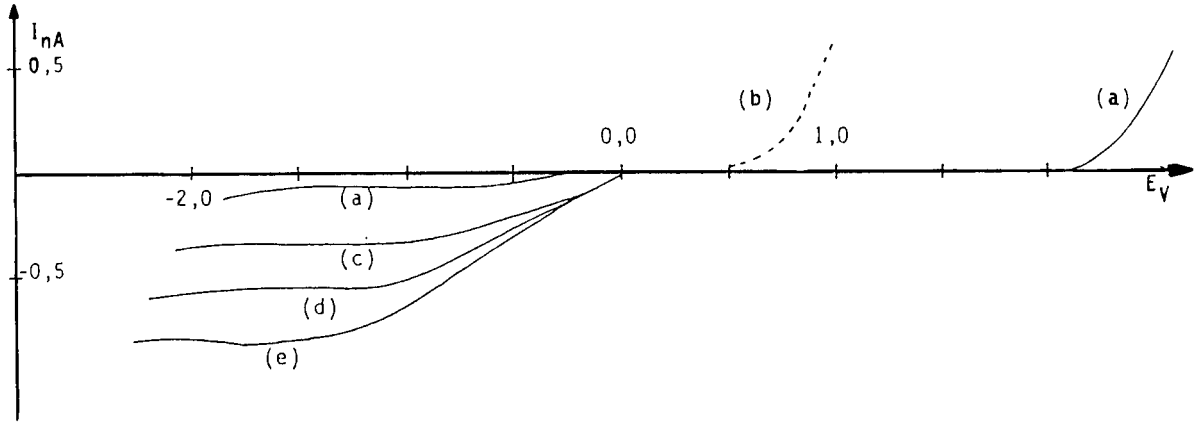

Fig. 11. Voltammetric curves for Fyrquel lubricants. (a) Fyrquel 150 without additives; (b) Fyrquel VPF with additives; increasing amounts of DPPA in Fyrquel 150: (c) 2.6×10^{-4} M; (d) 5.0×10^{-4} M; (e) 7.5×10^{-4} M.

conjugation reactions can render the interpretation of results very complex, as demonstrated with TBP–alkane mixtures [26].

Application to monitoring the lubricant Fyrquel VPF

This study was initiated after a number of lubricating oil (mineral oil) fires occurred in nuclear plants. Previous studies had identified phosphate esters as substitute fluids having adequate lubricating qualities and good fire resistance [11]. Under certain conditions these fluids may degrade, making the solution more acidic. The objective is to monitor the acidity resulting from hydrolysis of the phosphate ester lubricant:

$$(ArO)_3P{=}O + H_2O \rightarrow \underset{\text{(DPPA)}}{(ArO)_2POOH} + ArOH$$

to avoid corrosion of the primary pump motor in nuclear plants.

The industrial requirements are as follows: measurements must be realized continuously in a radioactive zone of the plant for an 18-month period and with no fluid pollution; conventional periodic sample analysis cannot be used; compatibility with an unfavourable environment (vibrations, radiation, strong electric and magnetic fields) has to be observed; remote control is needed.

The characterisics of the chosen lubricant Fyrquel VPF (terbutylated triphenyl phosphate) are a very low conductivity ($< 0.016\ \mu\Omega^{-1}\ cm^{-1}$), low dissociating power ($\epsilon = 7.0$) and high viscosity [468 SUS (Saybolt Universal Seconds) at 21°C]. The medium contains anticorrosion additives.

Traditional methods such as electrical resistivity measurements, absorption spectrometry and optical detection of corrosive attack of copper are not acceptable under industrial conditions [21]. Previous studies in TBP and triphenyl phosphate (TPP) allow suitable conditions for acidity detection to be specified. Two-electrode amperometry with a constant potential difference applied between a platinum UME and a zinc electrode has been applied [27].

Without supporting electrolyte, the cathodic currents increase linearly with increasing DPPA concentration (Fig. 11). There is no effect of the kind of supporting electrolyte on the DPPA wave height. Electroactive additives are anodically detected. Amperometric detection, which requires a controlled temperature (± 1°C), gives reproducible current measurements that have a low flow-rate dependence. Its continuous use is satisfactory.

The amperometric ultramicroelectrochemical device constructed for EDF (Electricité de France) gave the expected results in industrial site testing.

Conclusion

The analysis of the effect of the addition of a supporting electrolyte on the limiting currents of acids at an ultramicroelectrode gives information

about their charge, dissociation and polyacidic character. It is possible to follow acid–base equilibria in TBP without deliberate electrolyte addition, and a means is provided for analysing reactions in the organic phase during liquid–liquid extraction processes. The influence of water content on the acid strength and the protonation of tertiary amines by organophosphoric acids has been demonstrated. "In situ" detection with no disturbance of the medium by electrolyte addition can be successfuly applied to the determination of acidity in industrial phosphate esters used as lubricants.

REFERENCES

1 A.M. Bond and P.A. Lay, J. Electroanal. Chem., 199 (1986) 285.
2 J.O. Howell and R.M. Wightman, J. Phys. Chem., 88 (1984) 3915.
3 J. Cassidy, S.B. Khoo, S. Pons and M. Fleischmann, J. Phys. Chem., 89 (1985) 3933.
4 A.M. Bond and T.F. Mann, Electrochim. Acta, 32 (1987) 863.
5 A.M. Bond, M. Fleischmann and J. Robinson, J. Electroanal. Chem., 168 (1984) 299.
6 M.J. Pena, M. Fleischmann and N. Garrard, J. Electroanal. Chem., 220 (1987) 31.
7 J.J. Lingane and I.M. Kolthoff, J. Am. Chem. Soc., 61 (1939) 1045.
8 C. Amatore, M.R. Deakin and R.M. Wightman, J. Electroanal. Chem., 225 (1987) 49.
9 M. Perdicakis, B. Benzakour and J. Bessière, Bull. Electrochem., 7 (1991) 573.
10 W.W. Schulz and J.D. Navratil, Science and Technology of Tributyl Phosphate, Vol. I, CRC Press, Boca Raton, FL, 1984, p. 2.
11 Evaluation Test of Improved Fire-Resistant Fluid Lubricants for Water Reactor Coolant Pump Motors, Vol. 1, NP-1447, Project 893-1, Electric Power Research Institute (EPRI), Palo Alto, CA, 1980.
12 J. Heyrovsky and J. Kuta, Principles of Polarography, Academic, New York, 1966, p. 67.
13 G. Charlot, J. Badoz-Lambling and B. Trémillon, Les Réactions Électrochimiques, Masson, Paris, 1959, p. 15.
14 K.J. Vetter, Electrochemical Kinetics, Academic, New York, 1966, p. 175.
15 C. Amatore, B. Fosset, J. Bartelt, M.R. Deakin and R.M. Wightman, J. Electroanal. Chem., 256 (1988) 255.
16 M. Perdicakis, C. Piatnicki and J. Bessière, J. Chim. Phys. Phys-Chim. Biol., 89 (1992) 2067.
17 (a) M. Perdicakis, B. Benzakour, L. Mignano and J. Bessière, Communication No. 11,7 in the 4th European Conference on Electroanalysis, Noordwijkerhout, May 1992. (b) M. Perdicakis, B. Benzakour and J. Bessière, to be published.
18 W.W. Schultz, L.L. Burger and J.D. Navratil, Science and Technology of Tributyl Phosphate, Vol. III, Applications of TBP in Nuclear Fuel Reprocessing, CRC Press, Boca Raton, FL, 1991.
19 W.W. Schultz, J.D. Navratil and S.T. Kertes, Science and Technology of Tributyl Phosphate, Vol. IV, Extraction of Acids by TBP, CRC Press, Boca Raton, FL, 1991.
20 V. Gutmann, Coordination Chemistry in Non-Aqueous Solvents, Springer, Vienna, 1968, pp. 148–152.
21 Remote Detection of Degradation of Fire-Resistant Fluid Lubricant, NP-2543, Project 893-1, Electric Power Research Institute (EPRI), Palo Alto, CA, 1982.
22 E. Hesford and H.A.C. McKay, J. Inorg. Nucl. Chem., 13 (1960) 156.
23 A.A.J. Bard and H. Lund, Encyclopedia of Electrochemistry of the Elements, Organic Section, Vol. XV, Dekker, New York, 1984, pp. 93–100.
24 G. Charlot and B. Tremillon, Les Réactions Chimiques dans les Solvants et les Sels Fondus, Gauthier-Villars, Paris, 1963, p. 373.
25 R.F. Dopo and C.K. Mann, Anal. Chem., 35 (1963) 667.
26 M. Perdicakis, R. Pasturaud and J. Bessière, to be published.
27 J. Bessière, and M. Perdicakis, US Pat. Appl., 375 578 (1989).

Analytica Chimica Acta, 273 (1993) 93–99
Elsevier Science Publishers B.V., Amsterdam

Utilization of a silica-modified carbon paste electrode for the direct determination of todralazine in biological fluids

Ramón J. Barrio, Zuriñe Gomez de Balugera and M. Aranzazu Goicolea

Department of Analytical Chemistry, Faculty of Pharmacy, University of País Vaso, 01007 Vitoria-Gasteiz (Spain)

(Received 1st June 1992; revised manuscript received 30th September 1992)

Abstract

Todralazine [ethyl 2-(-1-phthalazinyl)hydrazinecarboxylate] was determined by using a carbon paste electrode modified with silica. Todralazine is adsorbed on the electrode and determined in 0.1 mol l^{-1} KNO_3 (pH 1.8) by differential-pulse voltammetry. The adsorption can be carried out in open circuit or by applying a fixed potential (0.8 V vs. Ag/AgCl). The detection limits are about 4×10^{-7} and 3×10^{-8} mol l^{-1}, respectively. The method can be applied to the determination of todralazine in human urine. It is possible to determine directly 2.3 μg ml^{-1} of todralazine in urine with a relative standard deviation of 1.1% ($n = 5$)

Keywords: Voltammetry; Carbon paste electrodes; Pharmaceuticals; Silica-modified electrodes; Todralazine; Urine

Voltammetric determinations of pharmaceutical products in biological fluids generally need a preceding extraction process so that the multiple interferences caused by this complex matrix in classical electrodes such as Hg, Pt, Au or C can be eliminated. However, the extraction increases the time and expense of analysis.

Recently, the use of carbon paste electrodes modified with several adsorbents has been reported [1–4]. The advantage of this kind of electrode is that drugs can be determined in biological fluids without prior separation. In general, the most sensitive electroanalytical technique is adsorptive stripping voltammetry, using a static mercury electrode for the reduction process or a carbon paste electrode for the oxidation process [5–8]. However, not all compounds can be previously adsorbed on the electrode surface. In order to improve the adsorption capacity of the carbon paste electrode, substances such as bentonite [9], sepiolite [10], hectorite [11] and Bondapak C_{18} [12] have been used.

This paper describes the determination of the antihypertensive agent todralazine [ethyl 2-(1-phthalazinyl)hydrazinecarboxylate] using a carbon-paste electrode modified with silica, by adsorption on the surface of the electrode followed by differential-pulse or cyclic voltammetry.

The electrochemical behaviour of azomethine and hydralazine groups present in the todralazine molecule has been reported previously [13,14]. Also, studies have been carried out which confirm that todralazine is weakly adsorbed on a hanging mercury drop electrode whereas it is not adsorbed on carbon electrodes [15,16].

EXPERIMENTAL

Apparatus and reagents

Two kinds of carbon electrode were used: a Metrohm Model 6.0802.000, with a calibrated

Correspondence to: R.J. Barrio, Department of Analytical Chemistry, Faculty of Pharmacy, University of País Vasco, 01007 Vitoria-Gasteiz (Spain).

precision glass tube, silicone coated and with a diameter of the active front surface of 8.0 mm; and a Metrohm Model 6.0807.000 mini carbon paste electrode with a diameter of the active zone of 3.0 mm and a volume of 14.14 mm^3. The former was used in experiments in which the electrode surface is actually renewed and the latter when the renewal is of a chemical or electrochemical nature only.

The carbon paste was prepared with a graphite base of Ultra "F" purity (Ultra Carbon) and mineral oil (Aldrich) at a graphite to mineral ratio of 2:1 (w/v). The carbon paste was mixed with silica (10%) from Bond-Elut cartridges (Analytichem International) and introduced into the glass or PTFE tube of the electrode.

Three cells were employed. In one of them the solution to be studied was preconcentrated, the second contained a suitable supporting electrolyte in which the electrochemical measurements were made and the other contained the cleaning solution.

Voltammetric curves were obtained by the linear-sweep and differential-pulse methods with a Metrohm E-506 Polarecord and a Metrohm E-613 scanner coupled an Linseis LY-1800 *X–Y* recorder.

All studies were done using an Ag/AgCl/KCl (3 mol l^{-1}) reference electrode and a platinum counter electrode.

A General Radio type 1656 impedance bridge was used for electrode resistance measurements.

A stock solution (10^{-3} mol l^{-1}) of todralazine (Sigma) was prepared in distilled, deionized water. KNO_3 solution (0.1 mol l^{-1}) was used as the supporting electrolyte. Na_2HPO_4 solution (0.2 mol l^{-1}) was used for cleaning and regerating the surface of the electrode.

Procedures

The silica-modified carbon paste (SMCP) electrode is placed in the preconcentration cell containing 20 ml of the given solution of todralazine. The solution is stirred at 500 rpm (under open- or closed-circuit conditions) for a defined time. The electrode, first washed with water, is then placed in the measuring cell containing 0.1 mol l^{-1} KNO_3 at a selected pH. The voltammograms are recorded between 0.8 and −0.1 V with a pulse amplitude of −80 mV and a sweep rate of 6.7 mV s^{-1}.

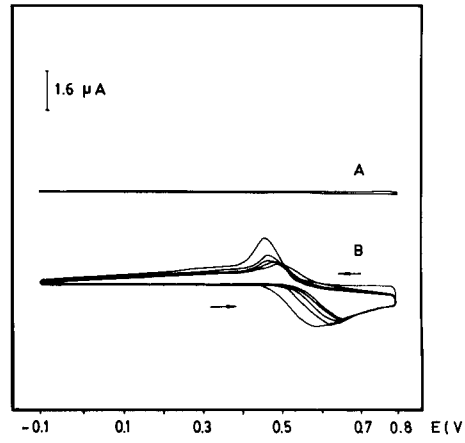

Fig. 1. Response of the SMCP electrode without prior treatment: (A) Blank. (B) Successive cyclic voltammograms for 10^{-5} mol l^{-1} todralazine. t_{acc} = 2 min at open circuit; scan rate = 100 mV s^{-1}; E_{start} = 0.8 V.

Regeneration of the electrode surface is achieved by keeping the SMCP electrode in 0.2 mol l^{-1} Na_2HPO_4 solution after each measurement, with constant stirring. After 5 min the surface is completely regenerated.

RESULTS AND DISCUSSION

Activation and regeneration of the electrode surface

The response of the SMCP electrode without prior treatment is not good. The results obtained (Fig. 1) show that the residual current is very low, but the signal is small and the peak potential is not reproducible. Therefore, the electrode was activated by placing it in 0.1 mol l^{-1} KNO_3 as supporting electrolyte and applying two potentials of −1.2 and 1.6 V, each for 4 min. Under such conditions a good analytical signal was obtained, with a minimum variation in the residual current and with a reproducible peak potential (Fig. 2).

The reproductibility of a voltammetric method is based on the production of identical electrode surfaces for each measurement. When the SMCP electrode is used the oxidation–reduction prod-

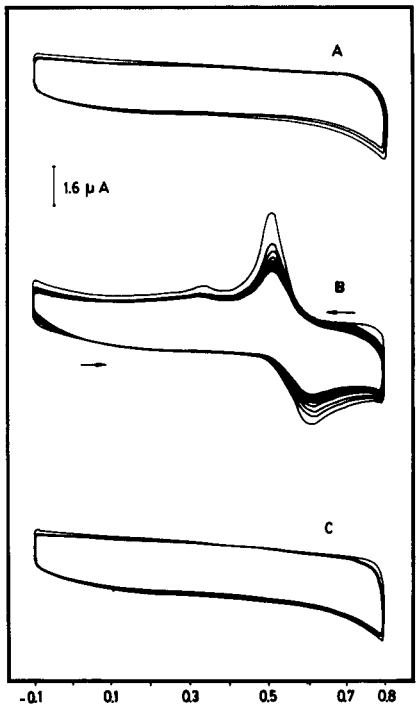

Fig. 2. Response of activated SMCP electrode. (A) Blank. (B) Successive cyclic voltammograms for 10^{-5} mol l^{-1} todralazine. (C) Blank after cleaning in 0.2 mol l^{-1} Na_2HPO_4. t_{acc} = 2 min at open circuit; scan rate = 100 mV s^{-1}; pH in preconcentration cell, 5.6; pH in measuring cell, 1.8; E_{start} = 0.8 V.

ucts of todralazine and also the parent drug itself, remain adsorbed on the electrode, modifying the effective surface. Three different methods were used to regenerate this surface: mechanical regeneration, cutting of a thin layer of the carbon electrode after each measurement; electrochemical regeneration, applying extreme potentials or successive scans; and chemical regeneration, using a cleaning solution capable of desorbing the products from the electrode surface.

In the first instance the reproducibility is worse than 11%. In the second, the application of successive scans does not allow the substances to be desorbed completely, whereas the alternate application of potentials of −1.1 and 1.6 V causes an increase in the residual current. With this method no reproducible measurements were obtained.

With the third method different substances such as ethanol, Britton–Robinson buffer, citrate buffer, KNO_3 and Na_2HPO_4 were employed as chemical regenerators. The best results were obtained using a cleaning solution of 0.2 mol l^{-1} Na_2HPO_4 with constant stirring (5 min). With this process of chemical regeneration, series of 15–20 measurements could be made without a decrease in reproducibility. Thereafter the silica–carbon paste of the electrode has to be renewed and activated again.

Accumulation, stripping and electroanalytical behaviour

The cyclic voltammogram of todralazine with the SMCP electrode (10% silica in carbon paste) recorded at 100 mV s^{-1} with 0.1 mol l^{-1} KNO_3 (pH 1.8, adjusted with HNO_3) shows a reduction

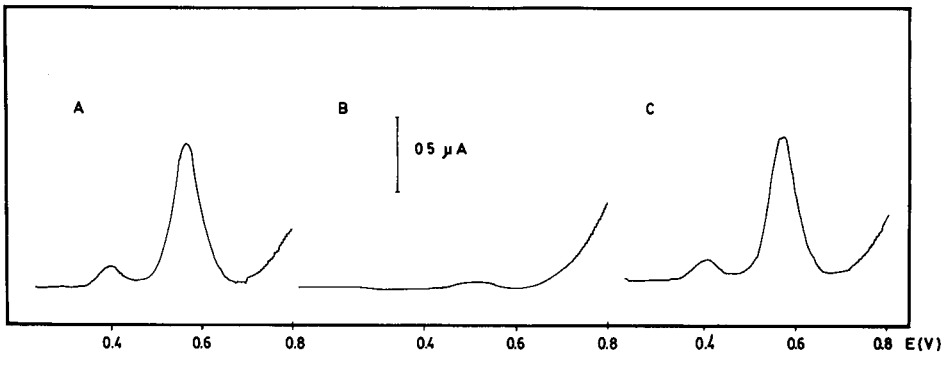

Fig. 3. Voltammetric curves obtained for the determination of 10^{-5} mol l^{-1} todralazine at open circuit. (A) First scan. (B) Blank after cleaning in 0.2 mol l^{-1} Na_2HPO_4. (C) Second scan. Pulse amplitude, 80 mV; t_{acc} = 2 min; t_{clean} = 5 min; scan rate = 6.7 mV s^{-1}; E_{start} = 0.8 V; for other conditions, see text.

peak in the first cathodic scan (Fig. 2B); in the reverse sweep an oxidation peak is observed. In successive sweeps, both the anodic and cathodic peaks decrease in intensity owing to the slow depletion of the species adsorbed on the surface electrode, but do not disappear completely.

The reduction peak is attributed to reduction of the azometline group, whereas the peak of the reverse sweep is attributed to oxidation of the hydralazine group, in agreement with the results found in other studies [13–16]. The reduction peak was chosen for this work because it represented the best electroanalytical response.

When differential-pulse voltammetry was used, the shape of the voltammograms was as shown in Fig. 3. If the electrode is kept for 2 min in a 10^{-5} mol l^{-1} solution of todralazine at open circuit and the voltammograms are recorded in a cell with 0.1 mol l^{-1} KNO_3 solution at pH 1.8, a well defined wave appears that has maximum intensity at a peak potential of 0.59 V. After the cleaning process with 0.2 mol l^{-1} Na_2PHO_4, the new voltammogram is also as shown in Fig. 3.

The adsorption process exhibited a strong dependence on the applied potential (Fig. 4). When a potential was applied, an increase in signal compared with accumulation at open circuit was observed. The i_p was maximum for accumulation around 0.8 V vs. Ag/AgCl.

The influence of pH was studied in the preconcentration and measuring cell (Fig. 5). Well defined waves are obtained in the preconcentration cell at pH 5.6 modified with either NHO_3 or KOH, when using a measurement cell containing 0.1 mol l^{-1} KNO_3 as the supporting electrolyte. If the todralazine solution is prepared for preconcentration on the electrode in a buffered medium (citrate–phosphate, Britton–Robinson), some new waves and splitting of the main wave appear. This can be explained by the simultaneous adsorption of drug and substances originating from the buffers. In addition, the peak intensity, assigned to the reduction of todralazine, decreases compared with the current obtained for an experiment in which accumulation is carried out in the absence of a buffered solution. This decrease in the amount of drug adsorbed can be attributed to the occupation of the adsorption sites on the

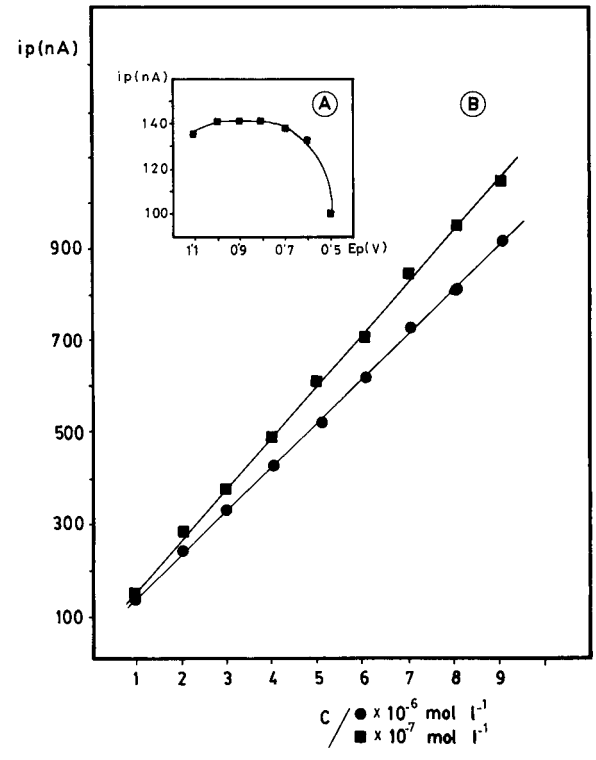

Fig. 4. Variation of i_p of todralazine with (a) accumulation potential and (b) accumulation potential and concentration. (■) Applied potential 0.8 V; (●) open circuit. Other conditions as in Fig. 3.

electrode by the organic components in the buffer. Therefore, the use of buffered solutions in the preconcentration phase should be avoided, using a solution adjusted to pH 5.6 with either HNO_3 or KOH.

In the measuring cell the highest peak intensity occurs when the pH is 1.8; it decreases at higher pH. A considerable change in the peak potential was observed (Fig. 5B). Various supporting electrolytes were investigated at different concentrations adjusted to pH 1.8 ($NaClO_4$, NaCl, KNO_3). In general, concentrations above 0.5 mol l^{-1} lead to a serious decrease in peak intensity (Fig. 6). Similar results have been obtained with a mercury electrode [15].

The percentage of silica in the carbon paste affects of accumulation step. The peak intensity decreases for percentages lower than 5% whereas the response remains constant in the range 6–

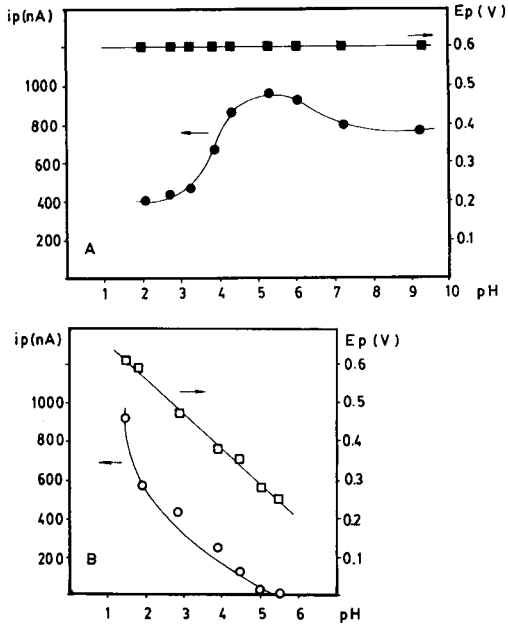

Fig. 5. Influence of pH on (A) the preconcentation cell and (B) the measuring cell. (■, □) Variation of E_p with pH; (●, ○) variation of i_p with pH. Todralazine concentration, 5×10^{-5} mol l^{-1}; t_{acc} = 2 min at open ciruit.

10%. Use of electrodes with higher proportions (25%) led to a decrease in peak intensity owing to the increase in the residual current that distorts the reduction wave of todralazine. This high residual current may be due to the increase in the electrode resistance (10%, 13.5 Ω; 25%, 20.8 Ω). The decrease in current can also be attributed to a decrease in the real active surface area of the electrode, but this cannot explain the high residual current.

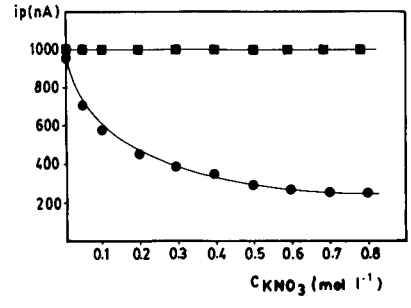

Fig. 6. Influence of ionic strength on i_p of 5×10^{-5} mol l^{-1} todralazine. Supporting electrolyte, KNO_3. (■) Preconcentration cell; (●) measuring cell.

Different instrumental parameters affect the voltammetric response and especially the shape and resolution of the peaks. The peak height was found to increase linearly with increasing pulse amplitude between 40 and 100 mV; 70 mV was chosen because at higher values the wave becomes wider, decreasing the resolution.

The height of the peak was also found to vary linearly with the potential scan rate:

$$i_p\ (\text{nA}) = 255.1 + 14.2\ \Delta E\ (\text{mV s}^{-1})$$

$$(r = 0.9945)$$

for a 10^5 mol l^{-1} concentration of todralazine, under the optimum conditions.

The stirring speed during the accumulation was varied between 500 and 3000 rpm and the best results with respect to current enhancement were obtained with a stirring speed of 3000 rpm.

The determination of todralazine is based on the linear dependence of the peak current on concentration. The accumulation by adsorption at open circuit permits the determination of todralazine at concentrations ranging from 6×10^{-7} to 5×10^{-5} mol l^{-1} using differential-pulse voltammetry with a preconcentration period of 2 min. The linear calibration plot corresponds to the equation

$$i_p\ (\text{nA}) = 0.65 + 1.9\times10^6\ [\text{TOD (mol l}^{-1})]$$

$$(r = 0.9920)$$

Ten replicate measurements on a standard solution were performed to determine the precision of the method. The relative standard deviation at a concentration level of 10^{-6} mol l^{-1} is 4.82% with a detection limit of 4×10^{-7} mol l^{-1}.

Applying a controlled-potential accumulation step (0.8 V) increases the signal 100-fold with respect to the adsorption in open circuit, for concentrations of the order of 10^{-6} mol l^{-1}. In this instance the calibration line corresponds to the equation

$$i_p\ (\text{nA}) = 1.10 + 2.4\times10^8\ [\text{TOD (mol l}^{-1})]$$

$$(r = 0.9974)$$

between concentrations of 5×10^{-8} and 5×10^{-6} mol l^{-1}. The detection limit is 3×10^{-8} mol l^{-1} and the relative standard deviation at a concentration level of 10^{-7} mol l^{-1} is 4.48% ($n = 10$).

Obviously the adsorption peaks vary with the accumulation time, as shown in Fig. 7. The saturation times of the electrode surface are 310 s in the case of open circuit ($c_{TOD} = 10^{-6}$ mol l^{-1}) and 540 s using the controlled-potential accumulation process ($c_{TOD} = 10^{-7}$ mol l^{-1}).

Application to samples of human urine

In this instance no potential was applied in the preconcentration step, because there are some substances in the matrix that can be adsorbed on the surface of the electrode (Fig. 8, curve 1).

The urine sample was spiked with a known amount of todralazine. Urine (1 ml) was diluted to 20 ml and the SMCPE was introduced directly into this solution for the accumulation step (5 min). The solution was stirred continuously by rotation of electrode at open circuit. The electrode was first washed with water and then placed in the measuring cell containing 0.1 mol l^{-1} KNO_3 at pH 1.80. The voltammograms were recorded under the optimum instrumental conditions.

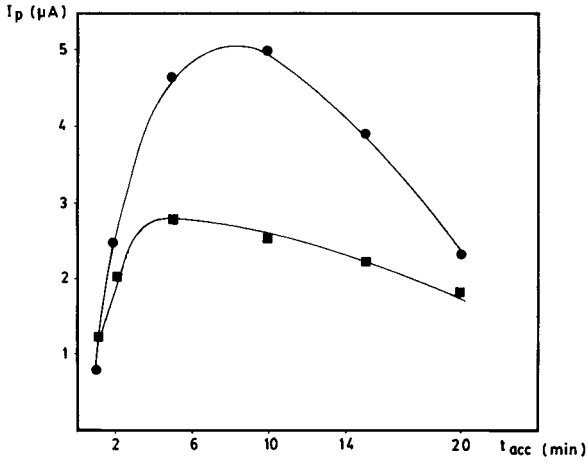

Fig. 7. Variation of i_p of todralazine with accumulation time. (■) Preconcentration at open circuit. Time period for saturation of electrode surface, 310 s; $c_{TOD} = 10^{-6}$ mol l^{-1}. (●) Preconcentration at 0.8 V. Time period for saturation of electrode surface, 540 s; $c_{tod} = 10^{-7}$ mol l^{-1}.

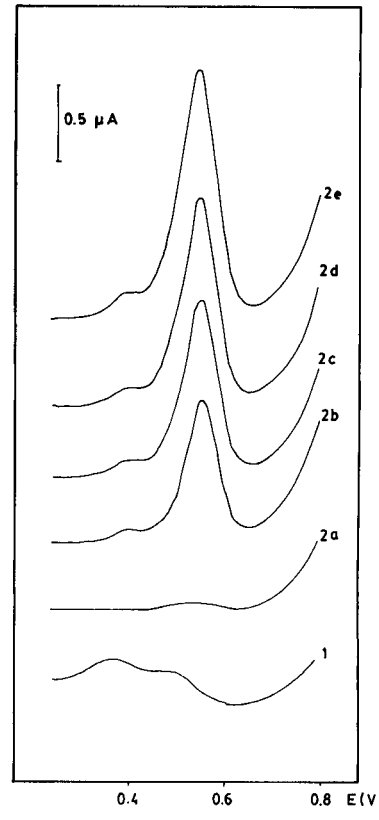

Fig. 8. Voltammetric curves obtained for the determination of todralazine in human urine. (1) Interference of the matrix when accumulation with the controlled-potential method (at 0.8 V) is used (blank); (2a) blank at open circuit; (2b) urine spiked with todralazine (2.56 μg ml^{-1}); (2c–e) standard additions of 200 μl of 268.7 μg ml^{-1} todralazine. For (2), $t_{acc} = 5$ min at open circuit; $t_{clean} = 5$ min in 0.2 mol l^{-1} Na_2HPO_4.

In this direct determination a 6% decrease in the peak intensity with respect to the standard solution was observed when urine samples were analysed. Therefore, the standard addition method was used as shown in Fig. 8.

The detection and determination limits of the method according to the ISO/IUPAC criterion (see, e.g., [17]) are 2.3 and 2.7 μg ml^{-1}, respectively.

A todralazine recovery of 99.7% is obtained, with a relative standard deviation of 1.1% for five successive measurements on spiked urine (5 μg ml^{-1}).

The detection limits are not as low as those found with mercury electrodes (using an adsorp-

tive stripping–differential-pulse voltammetric technique). Nevertheless, they are sufficient to determine the expected todralazine concentrations in urine with prolonged treatments (of the order of 60 μg ml^{-1}) [18]. The detection limits could be decreased considerably by increasing the accumulation time. On the other hand, emitting the separation process and the deoxygenation of the solution facilitates the determinations and shortens the experimental time.

REFERENCES

1 D. Cahen, G. Degan, Y. Mirovski, G. Hodes, W. Giriat and M. Lubke, J. Electrochem. Soc.., 132 (1985) 483.
2 K.J. Bachman, S. Menezes, R. Kotz, M. Fearheily and H.J. Lewerenz, Surf. Sci., 132 (1984) 475.
3 R. Menezes, H.J. Lewerenz and K.J. Bachmann, Nature (London), 305 (1983) 615.
4 L. Hernández, P. Hernández and E. Lorenzo, Electroanalysis, 2 (1990) 643.
5 R. Kalvoda and M. Kopanika, Pure Appl. Chem., 61(1) (1989) 97.
6 J. Wang, Am. Lab., 4 (1985) 41.
7 L. Hernández, A. Zapardiel, J. Pérez and E. Bermejo, Analyst, 112 (1987) 1149.
8 R.J. Barrio, L. López de la Torre, J. F. Arranz and A. Arranz, Talanta, 36 (1989) 501.
9 L. Hernández, P. Hernández, M.H. Blanco and E. Lorenzo, Analyst, 113 (1988) 1719.
10 H. Lund, in M.M. Baizer and H. Lund (Eds.), Organic Electrochemistry, Dekker, New York, 1983, Chap. 8.
11 L. Hernández, P. Hernández and E. Lorenzo, Analyst, 113 (1988) 621.
12 E. González, P. Hernández and L. Hernández, Anal. Chim. Act, 228 (1990) 265.
13 R.M. Jimenez, R.M. Alonso and L. Hernández, in M.R. Smyth and G. Vos (Eds.), Electrochemistry, Sensors and Analysis. Proceedings of the International Conference "Electroanalysis na h'Eireann", Ireland, 1986, Elsevier, Amsterdam, 1986, p. 391.
14 J.P. Hart, M.R. Smyth and W.F. Smyth, Analyst, 106 (1981) 146.
15 Z. Gomez de Balugera, R.J. Barrio, A. Goicolea and J.F. Arranz, Electroanalysis, 3 (1991) 423.
16 R.J. Barrio, Z. Gomez de Balugera, J.F. Arranz and M.A. Goicolea, Electroanalysis, 3 (1991) 429.
17 R. Caulcutt and R. Boddy, Statistics for Analytical Chemistry, Chapman and Hall, London, 1983.
18 Z. Fijalek and E. Szyszko, Acta Pol. Pharm., 39 (1982) 403.

Analytica Chimica Acta, 273 (1993) 101–109
Elsevier Science Publishers B.V., Amsterdam

Adsorptive stripping voltammetry on mercury-coated carbon fibre ultramicroelectrodes

J. Amez del Pozo, A. Costa García and P. Tuñón Blanco

Departamento de Química Física y Analítica, Universidad de Oviedo, 33071 Oviedo, Asturias (Spain)

(Received 27th July 1992)

Abstract

The conditions for the electrodeposition of mercury on the surface of carbon fibres to permit the sensitive and reproducible voltammetry of folic acid and mitoxantrone (MXT) were investigated. The accumulation behaviour of both molecules on a mercury film ultramicroelectrode was studied and the possibility of carrying out a.c. adsorptive stripping analysis using mercury-coated carbon ultramicroelectrodes was demonstrated. Optimum conditions for both the deposition of mercury and a.c. monitoring are described. This procedure gave rise to a linear calibration graph from 5.0×10^{-10} to 2.0×10^{-8} M, a detection limit of 5.0×10^{-10} M and a relative standard deviation (R.S.D.) of 5.05% at 5.0×10^{-9} M ($n = 10$) for the determination of MXT. For folic acid a linear calibration graph from 1.0×10^{-9} to 5.0×10^{-8} M, a detection limit of 9.0×10^{-10} M and an R.S.D. of 1.44% at 4.0×10^{-8} M ($n = 10$) were found. Both compounds can be determined directly in biological samples at physiological levels without any separation or clean-up procedure.

Keywords: Stripping voltammetry; Adsorptive stripping; Biological samples; Carbon fibre microelectrodes; Electrodeposition; Folic acid; Mercury-coated microelectrodes; Mitoxantrone; Pharmaceuticals

Special electroanalytical advantages can be obtained by using carbon fibre electrodes [1]. Following their initial use for in vivo studies, the use of carbon fibres as a surface for mercury deposition and subsequent stripping analysis of metals has been widely reported [2–9]. It has been demonstrated that in anodic stripping analysis, carbon fibre microelectrodes [1] with thin mercury films offer an attractive alternative to the conventional-sized mercury film electrodes [10–12]. As stated by Wojciechowski and Balcerzak [13], the small size of these microelectrodes and their enhanced mass transport properties, due to non-planar diffusion, allow anodic stripping voltammetric (ASV) determinations to be made on micro sample volumes using quiescent solutions [14,15]. Also, the negligible effects of ohmic drops, due to the small currents generated by these microelectrodes, make it possible to carry out ASV in non-aqueous media [16].

The characteristic of mercury film carbon fibre electrodes in differential pulse (DP) or square-wave (SW) ASV have also been reported [7,10,14]. Golas and Osteryoung [7] attempted to indicate the limitations of carbon fibres for mercury deposition, and found that the number of active sites at which mercury could be reduced depended strongly on the applied potential. In addition, the film thickness and the most reproducible film formation increased with increasing negative potential. Only a few examples of organic analyses using mercury-coated carbon fibres could be found, and they mainly dealt with potentiometric stripping analysis [17].

Correspondence to: P. Tuñón Blanco, Departamento de Química Física y Analítica, Universidad de Oviedo, 33071 Oviedo, Asturias (Spain).

It has been shown previously that mercury film electrodes, in general terms, give increased resolution compared with the hanging mercury drop electrode (HMDE) [18], and this has also been demonstrated using adsorptive stripping voltammetry of folic acid [19]. As carbon fibre electrodes exhibit a very small background current, it seemed desirable to combine these two properties in order to widen the analytical applications of such devices.

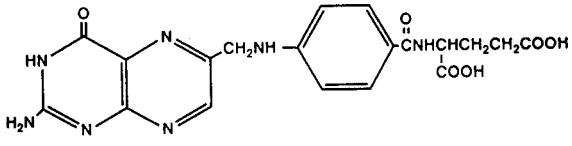

(I)

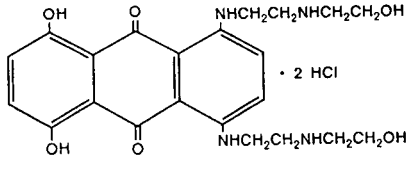

(II)

The purpose of this work was to evaluate the conditions that would allow the formation of the mercury film necessary for adsorptive stripping voltammetric studies. As probe compounds, two biologically important molecules, folic acid (I) and mitoxantrone (II), were chosen. This study constituted an attempt to provide a more concrete voltammetric basis for new analytical applications of thin mercury films deposited on carbon fibres using adsorptive stripping voltammetry of both compounds. Both molecules were adsorbed strongly on mercury surfaces and their electrochemical behaviour has already been reported [19–21].

The conditions for mercury film deposition that provided the best a.c. stripping signals were determined. Excellent reproducibility of the analytical signals was achieved by careful monitoring of the activation conditions. Subsequently, accumulation curves for both molecules on a mercury-coated carbon fibre ultramicroelectrode were obtained and excellent calibration graphs were also achieved. Finally, using the proposed electrode system, an analytical approach for the direct determination of both molecules in biological fluids was developed.

EXPERIMENTAL

Apparatus

All experiments were done using a Metrohm Model E-506 Polarecord in conjuction with a Metrohm Model VA-663 voltammetric stand. A 20-ml electrochemical cell, with the working electrode, reference electrode (Ag/AgCl), platinum wire auxiliary electrode and nitrogen delivery tube inserted trough its Plexiglas cover, was used throughout. The electrolyte solutions were purged prior to voltammetry using nitrogen for 10 min and, after deaeration, a blanket of nitrogen was kept over the solutions.

Carbon fibre microelectrodes were prepared from carbon fibres (Donnay Belgium Sport Tennis, Brussels) having a nominal diameter of 7.5 μm. The fibres were immersed in 10% nitric acid, rinsed with distilled water, soaked in acetone, rinsed with distilled water and finally dried in an oven at 70°C. A single fibre was inserted into a 100-μl standard micropipette to a length of ca. 2 cm and sealed with low-viscosity resin (A.R. Spurr, CA). The pipette was filled with mercury and electrical contact was established with a copper wire. A layer of epoxy resin was then placed over the mercury to prevent any leakage from the microelectrode assembly. Further details can be found in a previous paper [22]. Carbon fibre electrodes of length 0.5 mm were used throughout.

Reagents

Stock solutions (1.0×10^{-3} M) of folic acid (Sigma) in 0.01 M NaOH were prepared daily. The solutions were stored in the dark at 4°C. Sodium acetate buffers of pH 5.00 were used as background electrolytes. MXT was kindly supplied by Lederle Laboratories Division as a sterile, aqueous solution containing mitoxantrone hydrochloride equivalent to 2 mg ml^{-1} mitoxantrone free base. Stock solutions of MXT were

prepared daily by dilution of the ampoule with the background electrolyte solution (0.1 M perchloric acid). The samples were stored in the dark at room temperature to prevent their photochemical decomposition.

Analytical-reagent grade chemicals and deionized water obtained by passing distilled water trough a Millipore Milli-Q purification system were used for in the preparation of all solutions.

The biological materials examined consisted of pools of human urine (or serum) from healthy individuals. Samples consisted of aliquots of 0.5 ml of pooled biological fluids spiked with appropiate amounts of folic acid or MXT to achieve the desired final concentration.

Procedure

In order to obtain stable and well coated mercury films, a preliminary activation of the carbon fibre was necessary. Several pretreatments including electrochemical activation of the fibres were studied [23]. In contrast to some other recommendations [24], careful chemical treatment of the electrode surface was found to be more effective. The final procedure consisted in placing the working electrode for 5 min in a test-tube containing chromic acid mixture and after 5 min washing with nitric acid, then rinsing with distilled water. Figure 1 shows the good characteristics of the film when it was anodically stripped.

When mitoxantrone is being studied, both electrodeposition of the film and stripping analysis can be done in the same electrolytic cell. In contrast, when folic acid is under study, both steps must be done separately in order to prevent mercury salt formation, and two cells are necessary. In that event, when transferring the mercury-coated ultramicroelectrode form one solution to another, the mercury film size decreased. This was attributed to either oxidation of the mercury or mechanical removal of the film during the transfer procedure, which must be done as quickly as possible (within 10 s) [7].

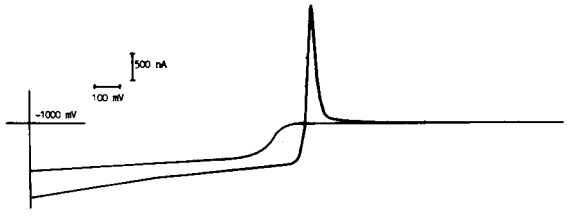

Fig. 1. Typical cyclic voltammogram for the anodization of a mercury film formed under optimum conditions. Scanning rate, 50 mV s^{-1}.

The procedure to obtain good and reproducible analytical signals of both compounds is also different. For folic acid, as the same film must be used for recording different voltammograms, an electrochemical activation step was followed between each measurement by holding the electrode at −1.5 V in quiescent solution for 120 s. MXT analysis can be performed by generating the mercury film in situ. For this reason, different films are used for recording different voltammograms. Between each measurement the film was removed by applying a potential of +0.74 V for 30 s and then a new one can be formed for the next measurement. Both approaches showed excellent reproducibility and allowed the overall stripping procedure to be performed rapidly. Normally, a carbon fibre could be used for 1–2 months before a decline in the sensitivity of the stripping response necessitated a change of fibre.

RESULTS AND DISCUSSION

Initial considerations

A strong dependence of the background electrolyte composition on the the a.c. adsorptive stripping voltammetric signals of both compounds was observed. In fact, whereas with folic acid a supporting electrolyte composed of mercury(II) nitrate–hydrochloric acid was found to be more suitable, a supporting electrolyte composed of mercury(II) nitrate–perchloric acid was more suitable when MXT was studied. On the basis of this qualitative observation, a search for the best preplating conditions was followed and the results obtained for both molecules are outlined separately in the following sections. The optimum film preplating conditions were considered to be those which provided the maximum a.c. stripping signal of the probed compounds.

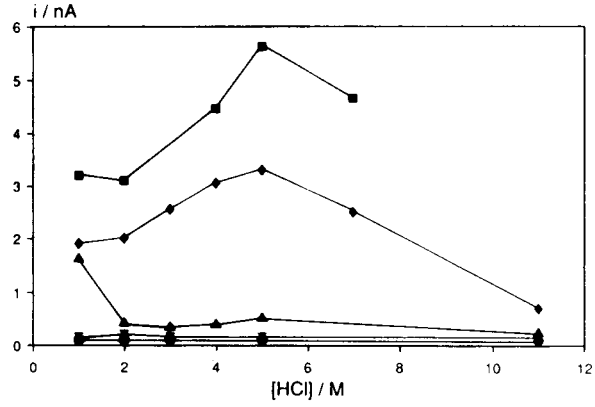

Fig. 2. Optimization of mercury film conditions: influence of the supporting electrolyte composition on the a.c. stripping voltammetric response of 4.0×10^{-8} M folic acid. For more details, see Experimental. $Hg(NO_3)_2$ concentration: ● = 1×10^{-5}; ⧗ = 1×10^{-4}; ▲ = 1×10^{-3}; ◆ = 0.01; ■ = 0.1 M.

Folic acid preplating conditions

The dependence of the a.c. stripping signal of 4.0×10^{-8} M folic acid in acetate buffer (pH 5.0) on the composition of the supporting electrolyte is shown in Fig. 2. From the figure, optimum concentrations of 5 M hydrochloric acid and 0.1 M mercury(II) nitrate can be obtained. The mercury film formation was performed by applying a potential of −0.2 V. The other conditions, such as deposition time and preplating potential, affecting the a.c. stripping signal are shown in Fig. 3. In subsequent studies a deposition time of 30 s and a holding potential of −0.2 V were chosen as the most suitable.

Following the activation procedure indicated above, the possibility of using a single mercury-coated fibre for different determinations was checked. The reproducibility reached in terms of relative standard deviation (R.S.D.) was 1.23% ($n = 10$). When a second film was deposited on the same carbon fibre an R.S.D. of 1.44% ($n = 10$) was observed. In both instances a concentration of folic acid of 4.0×10^{-8} M was used.

MXT preplating conditions

As mentioned before, mercury films can be deposited on the carbon fibre in the presence of the analyte. As the best medium for the voltam-

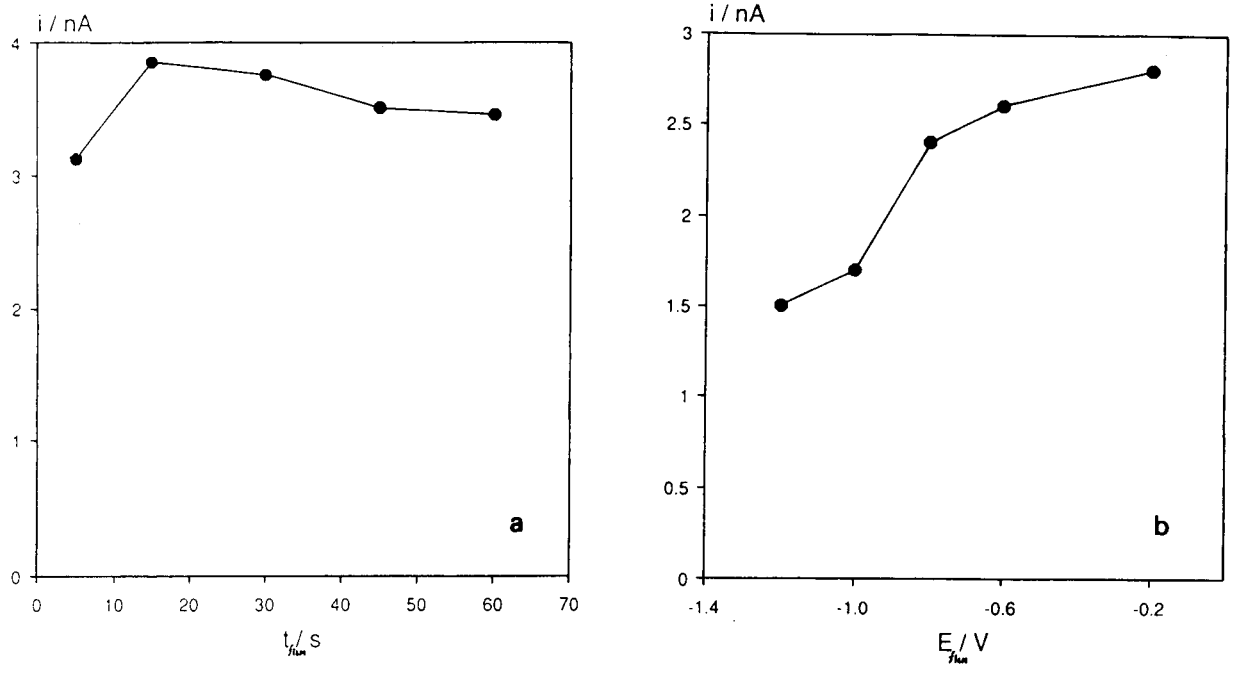

Fig. 3. Effect of (a) the deposition time (t_{film}) with $E_{film} = 0.2$ V vs. SCE and (b) the preplating potential (E_{film}) on the a.c. stripping voltammetric response of folic acid. 0.1 M Hg(II) in 5 M HCl.

metric response of MXT has been reported to be 0.1 M perchloric acid [21], Fig 4 shows the dependence of both mercury salt concentration and deposition time on the a.c. stripping signal of 4.0×10^{-8} M MXT using the optimum preplating potential shown in Fig. 5. As a result of these studies, the optimum preplating conditions allowing good reproducibility of the analytical signal were found to be a mercury salt concentration of 1.0×10^{-4} M and deposition potential of -1.2 V for 60 s. These parameters were adopted in subsequent studies. Excellent reproducibility (R.S.D. = 5.05%, $n = 10$) was found for an MXT concentration of 5.0×10^{-9} M.

Optimization of a.c. monitoring parameters

Phase-selective a.c. voltammetry was used as a stripping step because for both compounds the electrochemical reduction processes are almost reversible. Both compounds formed reversible couples with the reactant and the product was strongly adsorbed on conventional mercury electrodes [20,21] and, as is well known, an enhancement of sensitivity can be expected when the voltammogram is recorded in the a.c. mode [25,26]. For this reason, parameters such as the amplitude of the superimposed voltage (ΔE), and the phase angle were studied. The frequency could not be studied as the apparatus only worked at a fixed frequency of 75 Hz.

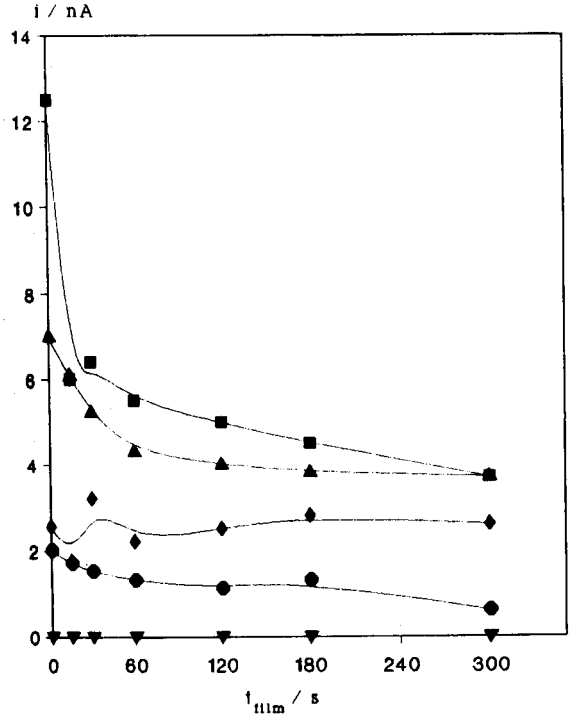

Fig. 4. Optimization of mercury film conditions: influence of the mercury salt concentration on the a.c. stripping voltammetric response of 4.0×10^{-8} M MXT at different deposition times (t_{film}). For more details, see text. $Hg(NO_3)_2$ concentration: ● = 1×10^{-6}; ♦ = 1×10^{-5}; ▲ = 1×10^{-4}; ■ = 1×10^{-3}; ▼ = 0.01 M.

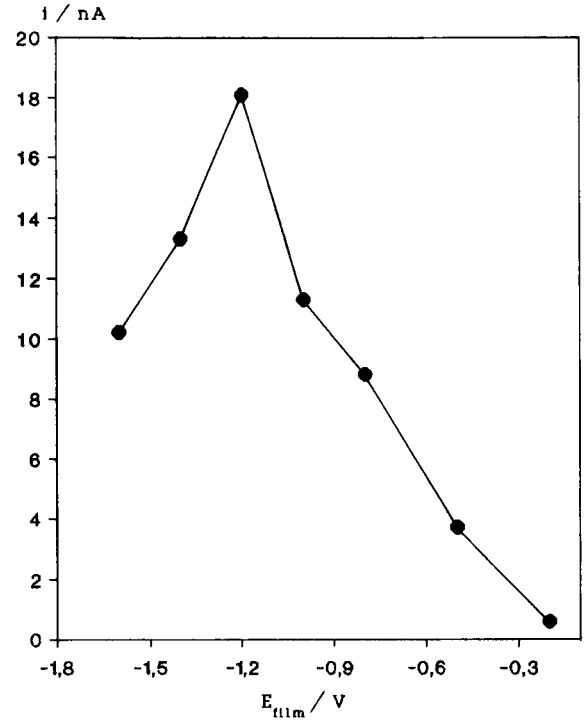

Fig. 5. Influence of the preplating potential (E_{film}) on the a.c. stripping voltammetric response of MXT.

As expected, the current recorded varied linearly with increased amplitude of the superimposed voltage according to the following equations:

$$i\ (\text{nA}) = 0.136\Delta E\ (\text{mV}) + 0.132$$
$$r = 0.9990\ (n = 4)$$

when folic acid was studied and

$$i\ (\text{nA}) = 0.1905\Delta E\ (\text{mV}) + 0.278$$
$$r = 0.9925\ (n = 4)$$

when MXT was studied. In the following work, values of ΔE of 15 and 25 mV were chosen as most suitable for folic acid and MXT, respectively, because with these values the ratios of peak height to peak width at half-height are more favourable. This gives a good balance between sensitivity and selectivity.

Different behaviour was observed when the variation of the phase-selective current with the detection angle was studied. Folic acid gave approximately the same intensity currents for detection angles close to 0° or 90° whereas MXT produced the maximum current at about 90°, it being negligible at 0°. This different behaviour can be explained by taking into account their adsorption behaviour as indicated below. In subsequent work, angles of 4° and 90° for folic acid and MXT detection, respectively, were chosen. At 4° the best discrimination of the faradaic charge against capacity current was obtained for folic acid, whereas the measurement of MXT at 90° was necessary. Although most of the current measured is capacitive, reproducible signals and excellent calibration graphs were obtained, as shown later. The behaviour of MXT can be explained by taking into account that the adsorption of both the reduced and the oxidized forms is strong, as has been reported previously, and that the electrochemical reaction is rapid, in such a way that the faradaic impedance becomes purely capacitive [25].

Accumulation curves and calibration plots

Owing to the steady-state diffusional mass transport characteristics exhibited by these microelectrodes, the need for stirring the solutions during the accumulation time was eliminated. However, during the deposition period it was necessary to hold a potential of −0.2 V (starting scanning potential) in order to keep the film of mercury stable. Accumulation curves at different concentrations of both molecules were obtained by plotting the currents measured at different accumulation times (Figs. 6 and 7). Only MXT showed the expected behaviour; folic acid showed different behaviour to that previously observed on conventional mercury electrodes [19,20]. In fact, as shown in Fig. 6, a negligible accumulation

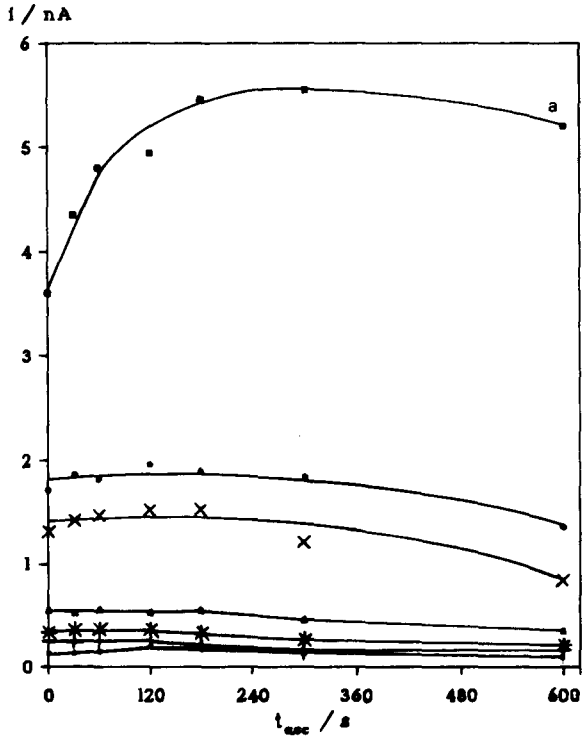

Fig. 6. Accumulation curves for folic acid. For conditions, see text. Concentration: ■ = 1×10^{-9}; + = 2×10^{-9}; * = 3×10^{-9}; ▲ = 4×10^{-9}; × = 1×10^{-8}; ● = 2×10^{-8}; ■, marked a = 4×10^{-8} M.

of folic acid is observed for concentrations of acid below 1.0×10^{-8} M and no saturation is reached as the currents observed increased with increasing concentration. Above these concentrations a very slightly increasing slope can be shown at the beginning of the curves followed by an slight decline of the curves. Again no saturation can be demonstrated as the currents increased with increasing concentration. This behaviour can be explained in terms of a very weak adsorption and the semi-diffusional behaviour of the molecule on this kind of electrode. In spite of this, using an accumulation period of 60 s an excellent linear calibration graph from 1.0×10^{-9} to 2.5×10^{-8} M was obtained. The adjusted equation of the calibration graph was

$$i\ (\text{nA}) = 6.575\times10^{7}C_{\text{folic acid}}(\text{M}) - 0.0305$$

$$r = 0.9994,\ n = 10$$

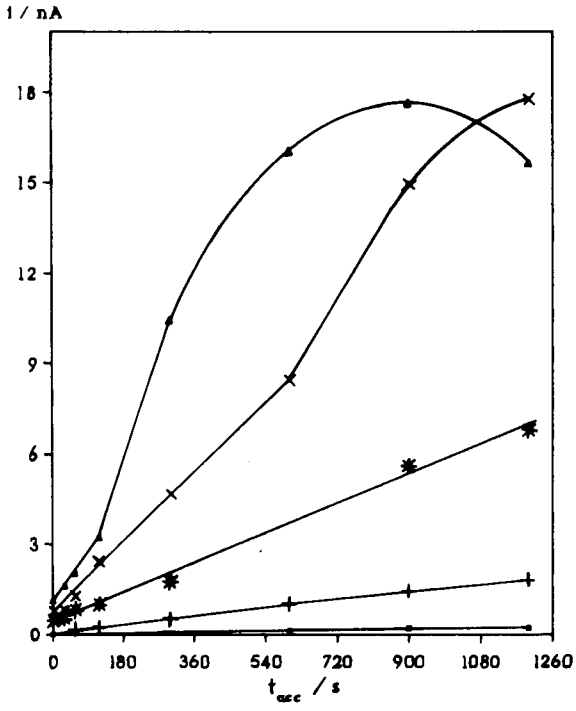

Fig. 7. Accumulation curves for MXT. For conditions, see text. Concentration: ■ = 1×10^{-10}; + = 1×10^{-9}; * = 2×10^{-9}; × = 5×10^{-9}; ▲ = 1×10^{-8} M.

MXT accumulation showed a typical adsorptive behaviour corresponding to an electrochemical system in which both forms, reduced and oxidized, are strongly adsorbed. As shown in Fig. 7, the current measured increased linearly with the accumulation time (t_{acc}) when the MXT concentration assayed was below 5.0×10^{-9} M and no saturation of the surface electrode can be observed. For higher concentrations the initial linear portion of the graph was maintained, showing slopes still proportional to the concentration studied. When the MXT concentration was larger at a certain stage of the accumulation period, the cathodic stripping peak shifted a few millivolts to more negative potentials and became sharper. This caused a strong change in the slope, as shown in Fig. 7. The increase in slope became faster as the concentration of the bulk solution increased. This behaviour can be explained in terms of interactions among adsorbed molecules [26]. By using an accumulation time of 3 s wider range of concentrations can be calibrated. The equation of the linear graph covering three orders of magnitude was

$$i\ (\text{nA}) = 5.349\times10^{8}C_{\text{MXT}}(\text{M}) + 0.147$$

$$r = 0.9991,\ n = 9$$

Analytical approach for analysis of real samples

The influence of some surfactants on the preconcentration–stripping of both compounds was studied in order to determine the optimum experimental conditions for carrying out adsorptive stripping measurements in the presence of large excesses of surface-active materials. This was relevant to their application for the solving of real problems relating to their determination in complex and real samples, e.g., serum, urine. Gelatine (a mixture of soluble proteins) and a cationic (cetyltrimethylammonium chloride; CTAC), an anionic (sodium lauryl sulphate; SLS) and a nonionic (Triton X-100) surfactant were studied. The results were again different, confirming once more the weak adsorption exemplified by folic acid. In fact, all the surfactants affected the a.c. stripping signal of 4.0×10^{-8} M folic acid in such a way that an amount of CTAC 100 times higher totally suppressed the signal, in the same way as did Triton X-100 when its concentration was 50 times higher. SLS decreased the original signal by up to 20% when it was present in the cell in an amount 600 times higher. Gelatine produced less interference, when it was present in an amount 100 times higher the signal was reduced by up to 80%.

In contrast, 1.0×10^{-8} M MXT was more resistant to such interferences. Only Triton X-100 affected the stripping signal when its concentration was about 2222 times higher. The other surfactants had negligible effects on the signal unless their concentrations were much larger.

Both results improved on previous studies carried out with conventional mercury electrodes [20,21], in such a way that the next step consisted in trying to assess their performance for direct analysis of real biological samples. The results obtained were as follows.

Determination of folic acid in human serum

In previous work, adsorptive stripping analysis was demonstrated to be a suitable method for the

determination of folic acid in serum [27]. As surface-active substances from serum competed strongly for adsorption on actives sites on the mercury surface, a simple clean-up procedure was necessary before stripping measurement. Following the procedure indicated above, serum samples spiked with folic acid were diluted with 20 ml of the background electrolyte and a standard addition method was followed. A serum sample containing 4.0×10^{-5} M folic acid was analysed with a relative error of 7.7% ($n = 3$). When this procedure was followed for analysing different samples also containing different amounts of the acid serious errors (over 100%) were found, coupled with the fact that irreproducible measurements were obtained with the calibration graph. This might be attributed to the slow and progressive distortion of the mercury film by the serum. Also, the fibre itself was seriously damaged in such a way that it was almost impossible to form a new and stable film of mercury on its surface. The possibility of using different fibres for each sampling measurement was discarded owing to the time required for both film generation and transfer steps, which also introduced some sources of error. However, the minimum amount of folic acid that could be determined following the established procedure was 6.8×10^{-6} M.

Determination of MXT in urine samples

Taking into account the advantage of the possible generation of the mercury film in situ together with the proved resistance of MXT to surface-active interferents, the determination of MXT in complex matrices seemed to have more potential. A first attempt to determine MXT directly in serum failed because the amounts of drug that can be detected were above the the normal range of physiological concentration. For this reason, the method was applied to the determination of MXT in urine samples. Following the procedure indicated above, the maximum and minimum amounts that could be determined by the standard addition method were found to be 4.0×10^{-6} and 5.0×10^{-7} M, respectively. A sample spiked with a known amount of MXT was diluted with 20 ml of the supporting electrolyte which also contained the mercury salt. Once the film had been formed, successive standard additions of MXT were made. Good calibration graphs were obtained in the overall range of concentrations allowed, i.e., for a urine sample containing 7.0×10^{-7} M, MXT the standard addition graph (four additions) followed the equation

$$i\ (\mathrm{nA}) = 7.1 \times 10^{6} C_{\mathrm{MXT}}(\mathrm{M}) + 0.124$$

$$r = 0.995,\ n = 3$$

and the relative error was 3.8%.

Conclusions

The design of an analytical strategy to make good mercury film-coated carbon fibre microelectrodes has been developed. The devices showed good performance, allowing their use for the adsorptive stripping analysis of organic compounds. Good reproducibility of the measurements can be achieved if a careful procedure of pretreatment and activation of the electrode surface is followed. The compounds under examination (folic acid and MXT) showed different adsorption behaviours. Special advantages can be taken into account when MXT is under examination. Then the mercury film can be generated in situ, allowing a rapid and simple method for the determination of the drug. When these devices are applied to real samples, their use seems to be more resistant to potential surface-active interferents than conventional mercury electrodes. For this reason their use in flow cells promises to be an interesting research area. Work is in progress to develop new flow-injection methods where miniaturization coupled with automation will offer special analytical advantages of simplicity and low cost in order to establish alternative methods for determining drugs in biological fluids. Finally, coupling of these microelectrodes with liquid chromatography seems to be possible in the near future, improving electrochemical detection based on reduction processes.

The authors are indebted to DGICYT, Spain (project No. PB-87-1031), for financial support.

REFERENCES

1 T.E. Edmonds, Anal. Chim. Acta, 175 (1985) 1.
2 K.R. Wehemeyer and R.M. Wightman, Anal. Chem., 57 (1985) 1989.
3 C.W. Sottery and J.P. Anderson, Anal. Chem., 59 (1987) 140.
4 J. Wang and J.M. Zadeii, J. Electroanal. Chem., 246 (1988) 297.
5 J. Wang, P. Tzuhi and J. Zadeii, Anal. Chem., 59 (1987) 2119.
6 A.S. Baranski and H. Quon, Anal. Chem., 58 (1986) 407.
7 J. Golas and J. Osteryoung, Anal. Chim. Acta, 181 (1986) 211.
8 A.S. Baranski, Anal. Chem., 59 (1987) 662.
9 W. Wojciechowski and J. Balcerzak, Anal. Chem., 62 (1990) 1325.
10 M.R. Cushman, B.G. Bennet and C.W. Anderson, Anal. Chim. Acta, 130 (1981) 323.
11 G. Schulze and W. Frenzel, Anal. Chim. Acta, 159 (1984) 95.
12 M. Ciszkowska and Z. Stojek, J. Electroanal. Chem., 159 (1985) 101.
13 M. Wojciechowski and J. Balcerzak, Anal. Chim. Acta, 237 (1990) 127.
14 M. Wojciechowski and J. Balcerzak, Anal. Chim. Acta, 249 (1991) 433.
15 K. McLaughlin, J.R. Barreira Rodriguez, A. Costa García, P. Tuñón Blanco and M.R. Smyth, Electroanalysis, in press.
16 J. Wang and P. Tuzhi, Anal. Chim. Acta, 197 (1987) 367.
17 Chi Hua, D. Jagner and L. Renman, Talanta, 35 (1988) 525.
18 M. Stulikova, J. Electroanal. Chem., 48 (1973) 33.
19 J. Amez del Pozo, A. Costa García, A.J. Miranda Ordieres and P. Tuñón Blanco, Electroanalysis, 3 (1991) 124.
20 J.M [a]. Fernández Alvarez, A. Costa García, A.J. Miranda Ordieres and P. Tuñón Blanco, J. Electroanal. Chem., 225 (1987) 241.
21 J. Cortina Villar, A. Costa García and P. Tuñón Blanco, Talanta, in press.
22 A.L. Suárez Fernández, J.A. García Calzón, A. Costa García and P. Tuñón Blanco, Electroanalysis, 3 (1991) 413.
23 T.J. O'Shea, A. Costa García, M.R. Smyth and P. Tuñón Blanco, J. Electroanal. Chem., 307 (1991) 63.
24 F.G. Gonon, C.M. Fombarlet, M.J. Buda, and J.F. Pujol, Anal. Chem., 53 (1981) 1386.
25 E. Laviron, J. Electroanal. Chem., 97 (1979) 135.
26 E. Laviron, J. Electroanal. Chem., 100 (1979) 263.
27 J.M [a]. Fernández Alvarez, A. Costa García, A.J. Miranda Ordieres and P. Tuñón Blanco, J. Pharm. Biomed. Anal., 6 (1988) 743.

Analytica Chimica Acta, 273 (1993) 111–121
Elsevier Science Publishers B.V., Amsterdam

Voltammetric information from arrays of individually controlled electrodes: their potential for industrial process measurements

P.R. Fielden and T. McCreedy

Department of Instrumentation and Analytical Science, University of Manchester, Institute of Science and Technology, Manchester M60 1QD (UK)

(Received 17th July 1992; revised manuscript received 20th October 1992)

Abstract

The construction, control and operation of an array of electrodes used to obtain voltammetric information in a wall-jet geometry is described for flow-stream analysis. The array consisted of a ring-disk arrangement, where the ring is composed of eight radially-spaced 1-mm glassy carbon disks. The ring array surrounds a 3-mm glassy carbon disk in the centre, impinged by a perpendicular 0.3-mm inlet diameter jet. Independent electrode control and monitoring were achieved through a computer-based multi-electrode potentiostat, designed to operate with single reference and counter electrodes. The flow cell was characterised through variation of the inlet jet separation from the planar ring-disk array and control of inlet volume flow-rate. Optimum conditions were chosen with stability as the primary criterion. A jet separation of 7.25 mm and a flow-rate of 1.5 cm^3 min^{-1} ensured wall jet behaviour at the central electrode and planar behaviour at the ring array. These conditions were maintained throughout subsequent experiments which demonstrated the feasibility of utilising the array of electrodes for voltammetric monitoring of simple mixtures of metal ions, with or without prior separation. The potential of this approach for industrial process monitoring is discussed with a view of maximising information recovery and enhancing data reliability.

Keywords: Chromatography; Flow system; Voltammetry; Industrial process measurements; Wall-jet geometry

Electrode arrays is a term that is usually applied to electrode units made up of an ensemble of microelectrodes. Microelectrodes are connected in parallel to combine the benefits of hemispherical diffusion with working electrode currents that are usually associated with conventional macroscopic electrodes (i.e., those with a surface area of the order of mm^2). A range of construction methods have been employed to fabricate such electrode assemblies. Carbon fibres, either as a bundle [1] or as an array of individual fibres laid in an orderly fashion [2] may be sealed in epoxy resin and interconnected to generate such arrays. It has also been shown feasible to convert macroscopic electrodes into microelectrodes by micromachining. For example, a block of glassy carbon may be cut with fine grooves which are subsequently filled with epoxy resins to generate a fine array of parallel longitudinal microelectrodes [3].

This work is concerned with arrays of independent electrodes operated in such a way that each electrode monitors a representative portion of the sample under measurement. This is most conveniently achieved by flow-injection techniques, where the electrode array is constructed in a suitable flow cell. Wang et al. [4] have

Correspondence to: P.R. Fielden, Department of Instrumentation and Analytical Science, University of Manchester, Institute of Science and Technology, P.O. Box 88, Manchester M60 1QD (UK).

reported a thin layer cell in which four chemically modified amperometric electrodes have been positioned with downstream reference and auxiliary electrodes. Although described as an array, the electrodes were monitored sequentially by a conventional three-electrode potentiostat. Liquid chromatography detectors consisting of a dual electrode measurement cell have been shown to offer improved selectivity [5,6]. When used parallel to the flow stream, simple two-component monitoring has been demonstrated. A pair of serial electrodes offers the possibility of redox cycling, where a transient species generated at the upstream electrode may be monitored by the downstream electrode. This second approach may enable specific discrimination of an analyte that would be masked through interference at a single electrode. An alternative approach has involved the application of rapidly scanned waveforms, such as those used in square wave voltammetry [7]. In this case the voltammetric measurement is made at a single electrode. Whilst attractive in terms of the information retrieved through this latter approach, it does impose significant restriction on the allowable rate of change of composition in the flow stream. Dual interdigitated microelectrode arrays have also been demonstrated in flowing stream measurements with either liquid chromatography or flow-injection analysis (FIA) [8]. An extension of this approach has resulted in the construction of two microelectrode arrays, of 16 and 80 electrodes respectively, in which the applied potential was incremented for each electrode of a linear array. This enabled the generation of three-dimensional FIA results of current vs. time vs. applied potential [9]. In the field of liquid chromatography, a commercially available 16-electrode coulometric array detector has been reported. Rizzo et al. [10] reported the determination of neurochemicals in biological fluids. It was shown possible to determine several compounds after direct injection of a plasma sample, illustrating the potential selectivity of electrode array detectors. The coulometric array detector, however, consists of 16 serially connected self-contained electrode cells, each with its own reference and counter electrodes. Recent work by Hoogvliet et al. [11] has made a significant advance through the design of a multielectrode potentiostat which offers independent control of up to 16 electrodes. This design offers versatile control of both current offset and current range, with the option of low-pass filtering. The performance of a radial thin layer flow cell comprising 16 glassy carbon disc electrodes was demonstrated for the detection of separated catecholamines. In our laboratory, we have reported preliminary results of an electrode array detector developed for liquid chromatography [12,13]. In this work we investigate its properties and potential as a flow-stream monitor suitable for industrial process analysis.

THEORETICAL BASIS

It is important to establish the relationship between a number of key parameters in the design of any electrochemical flow cell. This requirement becomes more important where the flow cell is designed to accommodate arrays of macroscopic electrodes. The electrode arrangement selected was based on a variable geometry wall jet cell where the inlet jet could be accurately positioned relative to the plane of the electrodes. The behaviour of the wall-jet geometry is described by the steady-state equation [14]:

$$I_{\text{lim}} = KnFR^{3/4}a^{-1/2}CD^{2/3}\nu^{-5/12}U^{3/4} \qquad (1)$$

where I_{lim} is the limiting current; K a constant; n the number of electrons in a given electron transfer reaction; F is the Faraday constant; R is the radius of the working electrode; a is the inlet jet diameter; C is the bulk concentration of the analyte; D is the diffusion coefficient; ν is the kinematic viscosity; and U is the volume flow-rate. In this arrangement the incoming solution impinges perpendicularly onto the surface of the electrode and spreads radially over the surface with the hydrodynamic boundary layer developing from the point of impact.

Planar geometry is described by the steady-state equation [15]:

$$I_{\text{lim}} = KnFCD^{2/3}\nu^{-1/6}U^{1/2}A/b^{1/2} \qquad (2)$$

where A is the electrode area; and b the channel

height (i.e., distance between the electrode plane and the parallel face of the jet orifice plate in a wall-jet design). In this arrangement the solution is made to flow over the surface of the electrode in a parallel direction with the hydrodynamic boundary layer developing from the point of entry.

As the inlet jet is brought close to the electrode plane, the jet orifice plate will interfere with the developing hydrodynamic boundary to give a restricted flow geometry. In this circumstance, plate electrode behaviour would be expected, which is described by the steady-state equation [16]:

$$I_{lim} = KnFC(AD/b)^{2/3}U^{1/3} \quad (3)$$

For a flow-injection experiment, a fixed volume probe analyte injected upstream of the electrochemical cell, will give rise to an asymmetric peak typical in flow-injection analysis. The area of such a peak will be related to the total charge passed due to electron transfer between the probe analyte and the electrode under investigation, while the FIA peak passes through the flow cell. Providing that all other parameters are maintained constant, a series of simple relationships between charge and volume flow-rate may be obtained by integration of Eqs. 1–3. The result of such a study would assume the following relationships [17]:

Wall-jet geometry, $Q \propto U^{-1/4}$ (4)

Planar geometry, $Q \propto U^{-1/2}$ (5)

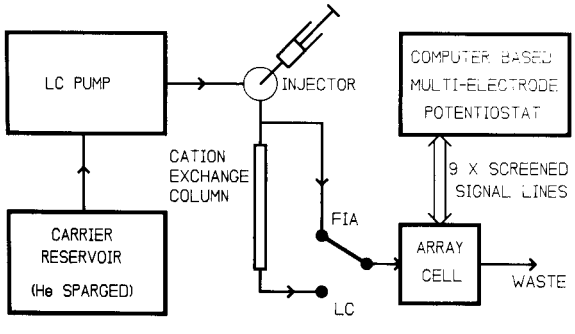

Fig. 1. Schematic diagram to show the experimental arrangement for studies based on flow-injection analysis (FIA) and liquid chromatography (LC).

Plate geometry, $Q \propto U^{-2/3}$ (6)

Hence flow-rate experiments, where the FIA peak area is monitored as a function of volume flow-rate would be expected to yield log–log plots where the slope represents the exponent term in Eqs. 4–6. In this way, the exact hydrodynamic behaviour may be characterised for each electrode in a planar array that is irrigated from a single jet inlet at different inlet to electrode spacings.

EXPERIMENTAL

FIA–LC apparatus

The schematic diagram (Fig. 1) shows the basic flow system utilised for this study. The carrier, an aqueous electrolyte, was contained in a covered reservoir and sparged with helium for a period before experimentation commenced, and during the execution of any experiment. This ensures the successful removal of dissolved gases (particularly oxygen) to prevent bubble formation in the electrochemical cell. The pump employed in this work was a Kontron 420 LC pump, which was near pulse free and of constant volume flow for both FIA and LC experiments. Flow-rates in the range 1 to 5 $cm^3\ min^{-1}$ were used for flow-injection studies, and 1.5 $cm^3\ min^{-1}$ for the LC ion separation. The injector used for this work was a Rheodyne 7125 front port syringe loaded LC injector, fitted with a 20-μl loop.

Electrode array flow cell

The flow cell used in this work is shown in Fig. 2. It consists of three main components: the cell base (containing the planar electrode array); the cell body; and the counter electrode/inlet jet assembly. The cell base, comprising a disk of Kel-F, was fixed to the cell body by three equidistanced bolts, the seal between the two halves formed by a small O-ring (Fig. 2a). The array was constructed from 3 mm (central disk electrode) and 1 mm (array of 8 satellite electrodes forming a segmented ring) rods of glassy carbon (Ringsdorff Carbon Co.). These were secured as a push-fit and sealed with epoxy potting compound.

Electrical connections were made to each electrode with fine wire (single core wire wrap) and silver-loaded conducting paint. The overall connection assembly was potted in a block of epoxy potting compound to give mechanical strength to the electrical connections. Connections were terminated in a nine-pin D-type plug, with gold-plated contacts.

The upper half of the cell was constructed in two sections, where the counter electrode/inlet jet assembly was held in position by a screw thread of 1 mm pitch, such that a complete turn of the assembly would advance the jet-to-electrode array distance by 1 mm (Fig. 2b). In this way, precise spacing between the inlet jet and electrode array could be ensured. The counter electrode was a stainless-steel rod that was machined to a slightly tapering hole to enable a push-fit PTFE tube to act as the inlet and jet. The jet diameter was thus controlled through the selection of the tubing of an appropriate internal diameter (for this work 0.3 mm i.d. × 1.5 mm o.d. was selected). The counter electrode was tapped to accept a brass screw to permit electrical connection. The Kel-F screw mechanism was joined to the counter electrode rod by a push-fit, secured by a single compression pin to prevent rotation. The seal between the counter electrode and the main cell body was maintained by a pair of tight-fitting O-rings fitted into recesses in the main cell body. The reference electrode was either a commercial sealed reference electrode (BAS, MW-2021; Biotech Instruments) or equivalent gel-filled Ag/AgCl unit constructed in-house. The reference electrode was held in place by a stainless-steel holder that completed the seal through a compression O-ring arrangement.

Multi-electrode potentiostat

An important feature of this work has been the development and construction of a versatile potentiostat that would afford independent control and monitoring of each electrode in an array, with a common reference/counter electrode pair. The reduction from dedicated reference/counter pairs for each working electrode to a common

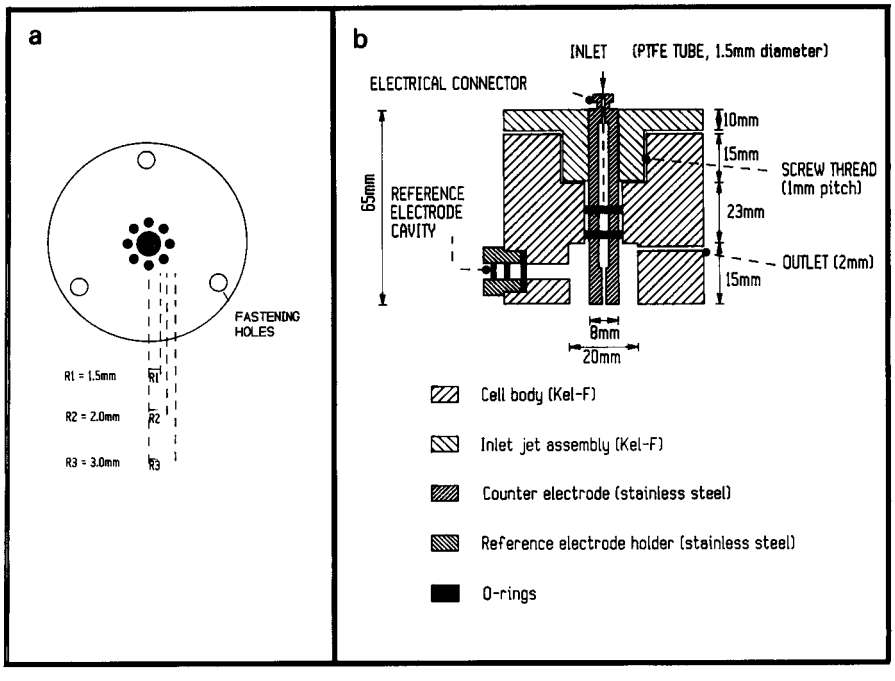

Fig. 2. Scaled diagram of the electrode array flow cell comprising the cell base incorporating the working electrode array (a) and the cell body which accommodates the inlet jet; counter and reference electrode pair; and the flow outlet (b).

pair is important to maintain simplicity in the cell design and to reduce the maintenance and costs to a minimum.

A conventional bi-potentiostat, as typically used for dual electrode measurements [5,6] is based upon a conventional three-electrode potentiostat, to which a second working electrode has been added. In this dual electrode mode, the primary working electrode is maintained at ground potential by means of a current follower held at virtual ground input [5]. The applied potential E^1_{app} is mirrored in the reference electrode, which is controlled by the counter electrode such that it is maintained at a potential $-E^1_{app}$ at the point of contact with the sample solution. In this way, the primary working electrode experiences an apparent potential difference of E^1_{app}, with respect to the reference electrode. The current through the primary working electrode is monitored by the current follower holding it at ground potential. The counter electrode provides a source or sink for any current flow through the working electrode. The addition of a secondary working electrode is realised by controlling its potential relative to the potential of the primary working electrode. If the required operating potential for the secondary working electrode is E^2_{app}, then the secondary working electrode is held at a potential of $(E^2_{app} - E^1_{app})$ through a second current follower. In this way it is possible to control both working electrodes independently, regardless of the current drawn by either, with respect to a single reference/counter electrode pair. In principle, this approach may be extended to accommodate more than two working electrodes (Fig. 3a), where each of the secondary working electrodes is raised to the potential $(E^n_{app} - E^1_{app})$, where E^n_{app} is the required applied potential for the nth working electrode, by an additional current follower stage. This principle has been demonstrated for the independent control of a microelectrode array [9], where a simple resistor network provided an array of working electrodes, each raised by a fixed potential difference to either of its nearest neighbours. Such an approach to the problem has its disadvantages. First, it is inconvenient to have to generate the difference potentials $(E^n_{app} - E^1_{app})$. If analogue circuitry were used, this would increase the complexity of the potentiostat design. An

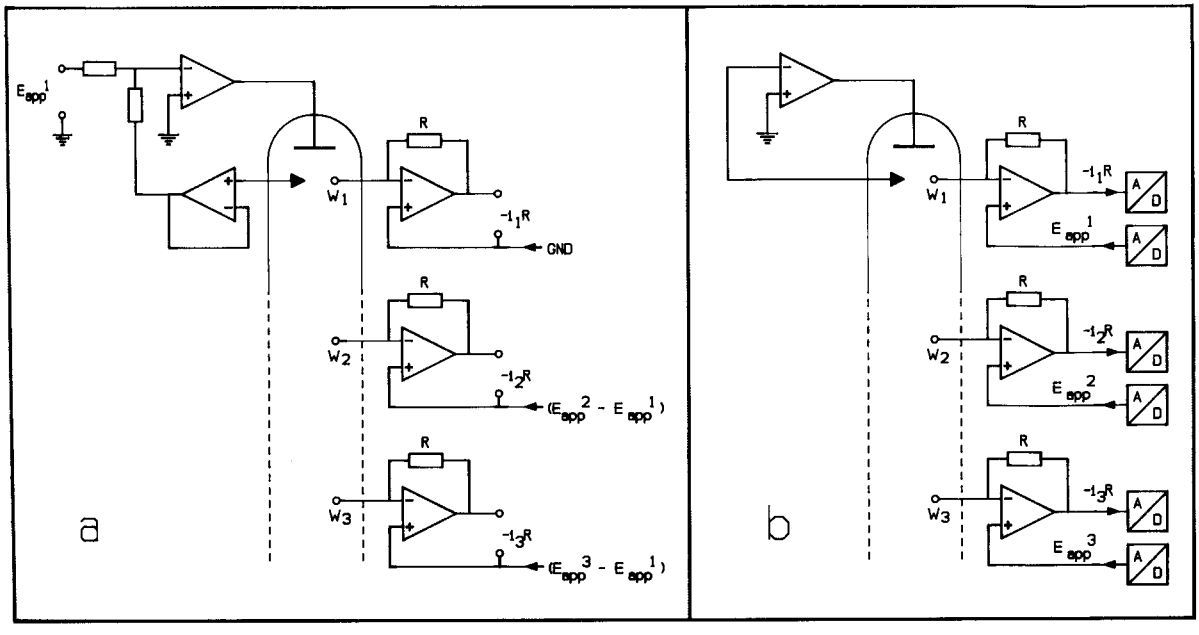

Fig. 3. Schematic representation of the principles of construction used in multielectrode potentiostats: the extended bipotentiostat (a); and the computer-controlled potentiostat designed for this work (b).

alternative is to use a computer to control the potential applied to each working electrode via a digital-to-analogue converter (DAC), where it would be possible to compute the difference potentials. But this may limit the generation frequency where changing waveforms, such as a dc ramp, were required. A second problem encountered on a four-electrode prototype, is the increase in system noise and instability as a function of the number of electrodes. It was considered that further pursuit of this approach should be abandoned for an alternative that overcame the problems observed.

In principle, there is no reason why any working electrode need be held at system ground. In the case of single working electrode measurements, there is some advantage in maintaining the working electrode at virtual ground in order to reduce electronic noise. For multiple working electrode systems, however, this is not necessarily so, since the majority of the working electrodes, except the primary working electrode, would usually be held at potentials away from virtual ground. An elegant solution is to adopt a multi-electrode cell where the reference electrode is maintained at virtual ground by the action of the counter electrode responding to the current demand of the array of working electrodes. This is readily achieved, as shown in Fig. 3b. The control element of the potentiostat consists of an extended voltage follower scheme, with the counter and reference electrodes forming the feedback loop. The whole follower is linked to signal ground, such that the reference electrode/solution contact is also at signal ground. Each working electrode (W_1, W_2, W_3...) is then polarised relative to the reference electrode so that the actual potential (E^1_{app}, E^2_{app}, E^3_{app}...) is used directly rather than a difference potential, as was the case in Fig. 3a.

The remaining hardware consists of individual 12-bit digital-to-analogue converters (DAC) for each array element, to provide the necessary polarisation potential. Multiplexed analogue-to-digital conversion (ADC) is used to monitor the outputs of the current followers over a range of potentials corresponding to a range of electrode currents. For the sake of simplicity, simple fixed resistors (designated R in Fig. 3) were selected for the proposed operating range of the potentiostat. This limited the current range to about three orders of magnitude using the range of a 12-bit ADC. A more versatile design would include provision for switched resistors to offer an extension of the current range. Such a design has been reported by Hoogvliet et al. [11], where a common auxiliary/reference electrode pair were used in conjunction with independently controllable working electrodes. The basic principle of maintaining the reference electrode at system ground was adopted, with flexible control and monitoring of each working electrode in the array. A double 12-bit DAC was utilised to provide the polarisation potential and an input current offset. Furthermore, a sensitivity selector was included to enable current ranges between 1 mA and 1 nA (7 decades) to be realised.

In this work, a computer controlled potentiostat with a capacity for up to 16 working electrodes has been constructed, based on this same principle of operation but without the same degree of flexibility as the system of Hoogvliet et al. [11]. A PC-type computer (Compac 386-20) was used in conjunction with Turbo Pascal control and monitoring routines, which included the necessary data acquisition and processing to generate current vs. time plots for the electrode array.

Reagents and samples

All reagents and samples were made up using Analytical Grade reagents and singly distilled water. Solutions were degassed by sparging with helium prior to use. For ion separation, a Spherisorb 5 μm SCX (15 cm $\times$ 4.6 mm i.d.) column was employed.

Electrode preparation

After initial construction, the electrode array was polished using a range of silicon carbide abrasive papers (grades 120–1000) until a flat surface was generated. A mirror finish on the glassy carbon was obtained by hand polishing first with 1-μm Dialap paste and then by using three successive grades of alumina (0.3, 0.075 and 0.015 μm) in a water based slurry. After polishing, the electrodes were electrochemically pre-treated by

imposing potentials of +1.3 V (vs. Ag/AgCl) for 5 min, followed by −0.6 V (vs. Ag/AgCl) for 5 min. Unless the array had become significantly deactivated after an experimental run, it was unnecessary to repolish the electrodes. Regular electrochemical cleaning between experiments ensured repeatable results.

Flow cell characterisation

FIA was used with a carrier solution of 0.1 M KCl. A sample solution of potassium hexacyanoferrate(II), 0.1 mM and 1 mM for the central satellite electrodes of the array respectively, was injected to provide an electrochemical probe. The electrodes in the array were maintained at 1.05 V (vs. Ag/AgCl), on the diffusion limited plateau region for the probe. The experiment was carried out over a range of jet inlet to electrode array plane distances from 0.25 mm to 10.0 mm, with a fixed jet diameter of 0.3 mm. The flow-rate was varied over the range 1–5 cm^3 min^{-1} in order to obtain plots of log peak area vs. log volume flow-rate.

Metal ion determination

Calibration solutions of Cd(II), Cu(II) and Pb(II) were made up in the range 1–5 mM using the appropriate nitrate dissolved in 0.5% nitric acid. A mixture was also prepared, consisting of 1 mM each of the three cations in 0.5% nitric acid. This mixture was used for both the flow injection and the liquid chromatographic separation.

The liquid chromatographic separation used a mobile phase consisting of 0.1 M KCl and 0.1 M citric acid, whereas the flow-injection carrier was 0.1 M KCl alone. For both experiments a jet inlet to electrode plane separation of 7.25 mm was used, as was a fixed flow rate of 1.5 cm^3 min^{-1}.

RESULTS AND DISCUSSION

Flow cell characterisation

In the characterisation of electrode systems in a flow stream, a plot of log charge (Q) (for these experiments Q = peak area) vs. log flow-rate (U) should yield straight line data within experimental limits. This was found to be so over the flow range 1–5 cm^3 min^{-1} for the cell configuration described, with a 0.3-mm jet inlet diameter. The slopes obtained from such plots should identify the type of flow behaviour. These will not necessarily be exact slopes, but will lie in certain ranges. It is generally accepted [17] that such an experiment will yield slopes as follows for given flow behaviour types: wall-jet, −0.23 to −0.33; planar, −0.48 to −0.58; and plate (thin layer), −0.65 to −0.74.

For a jet to electrode separation of 8 mm the slopes obtained were −0.31 for the central electrode and −0.55 for the satellite array electrodes. From these data it may be concluded that the central electrode is behaving as a true wall jet electrode, whilst the satellite array electrodes are clearly behaving as planar electrodes.

As the jet to electrode separation is reduced, there is a change in behavioural characteristics from one flow mode to another. For example, at a jet to electrode separation of 0.25 mm, the slopes obtained were −0.62 for the central electrode and −0.72 for the satellite array. In this case, the satellite array electrodes are clearly behaving as plate (thin layer) electrodes, which might be expected due to the restricted geometry imposed by the parallel spaced and close proximity of the counter electrode. It is relatively simple to explain this phenomenon in terms of a restriction of boundary layer development by the counter electrode. The central electrode, however, does not fit any of the accepted ranges, but lies between planar and plate behaviour. It is feasible to assume that at close jet to electrode separation, a complex combination of flow types exists with a small region of wall jet character in the centre and plate character towards the edge, as the developing boundary layer comes in contact with the counter electrode. Although these studies are interesting in themselves, their purpose is to determine stable operating conditions in terms of the flow behaviour over the electrode array. To this end, a plot of peak vs. jet to electrode separation (Fig. 4) at a fixed flow-rate of 1.5 cm^3 min^{-1} reveals a distinct curve for a typical satellite electrode in the array. At separations below 1 mm, the peak area rises rapidly, indicating an enhanced sensitivity when operating

under restricted geometry condition, where the satellite electrodes adopt plate electrode behaviour. As the separation is increased, the response curve plateaus above 6 mm separation, where true planar behaviour is established. The conditions selected for further experiments were at a flow-rate of 1.5 cm^3 min^{-1} and with a jet to electrode separation of 7.25 mm. This maintains the flow cell under stable operating conditions, with the central electrode behaving as a wall jet device, and the satellite array electrodes behaving as true planar electrodes. It could be argued that there is a significant compromise in terms of sensitivity, but the benefit is stable operation which will tolerate a degree of variation in the cell geometry without affecting sensitivity. This requirement for stable operation is more important than sensitivity for many industrial process measurement applications. The reliable day-to-day operation is ensured under these conditions, even though some sensitivity is forfeited.

Metal ion determination, by separation

The separation of the sample mixture containing 1 mM each of Cu(II), Cd(II) and Pb(II) is relatively simple. Resolution of Cd(II), with a retention time of 158 s is complete. Resolution of the Cu(II) and Pb(II) with retention times of 219 s and 244 s respectively, is adequate for quantitation. The array chromatogram (Fig. 5) shows the response of six of the satellite electrodes maintained over a range of reductive potentials between −0.3 and −0.9 V (vs. Ag/AgCl). Apart from the selectivity imparted by the chromatography, useful selectivity is also gained electrochemically. It is clear that the Cu(II) response is free from electrochemical interference on the electrode held at −0.3 V (D6). All the other electrodes (D5 to D1) respond to at least two of the cations, with electrodes D2 and D1 responding to all three. Herein lies the potential benefit of the electrode array. A simple subtraction, whereby the signal from the electrode held at −0.8 V (D2) is subtracted from the signal held at −0.9 V (D1) according to:

$$\{D2\} - k\{D2\} \quad (7)$$

where { } indicates the data acquisition set for a given electrode. k is a simple constant to correct for sensitivity differences between the electrodes; in this case determined by the ratio of the responses to Cu(II). Figure 6 shows the results of the subtraction, indicating successful correction for the Cu(II) and Pb(II) components to a degree that is better than 80%. The nature of the disturbances corresponding to the start of the Cu(II)

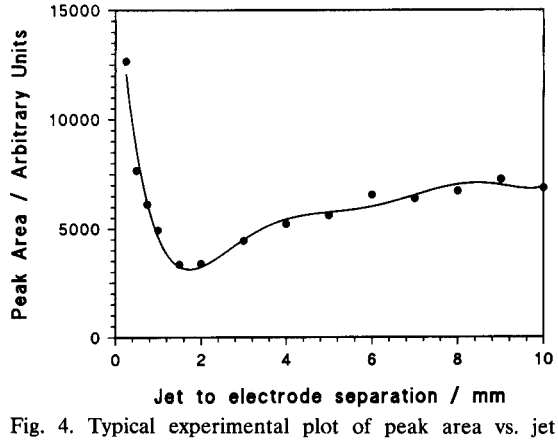

Fig. 4. Typical experimental plot of peak area vs. jet to electrode separation for FIA measurements of 1 mM Fe(II) (as hexacyanoferrate) in 0.1 M KCl for a satellite array electrode with the following operational parameters: Flow-rate, 1.5 cm^3 min^{-1}; inlet jet diameter, 0.3 mm; and applied potential 1.05 V (vs. Ag/AgCl).

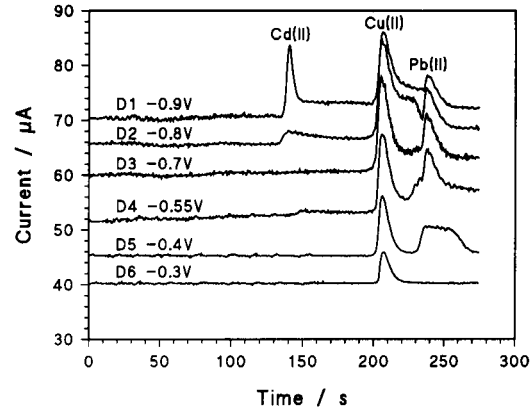

Fig. 5. Simultaneous array chromatogram for the separation of 1 mM each of Cu(II), Cd(II) and Pb(II) in a mobile phase consisting of 0.1 M KCl and 0.1 M citric acid. Six of the satellite array electrodes were monitored (D1 to D6) with applied potentials in the range −0.9 to −0.3 V (vs. Ag/AgCl). Sample injection occurs at 0 s.

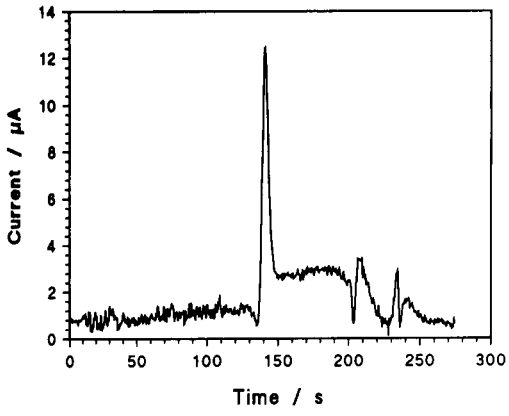

Fig. 6. Chromatogram generated after subtraction between electrodes polarised at −0.9 and −0.8 V (vs. Ag/AgCl). This corresponds to a subtraction of the responses indicated as D1 and D2 respectively in Fig. 5.

and Pb(II) peaks was not fully understood until further subtractions were attempted; this time to resolve the Pb(II) response, by subtracting the common response to Cu(II). Figure 7 shows the basic subtraction:

$$\{D4\} - k\{D6\} \quad (8)$$

where k is determined by the ratio of the responses of the two electrodes towards Cu(II). The

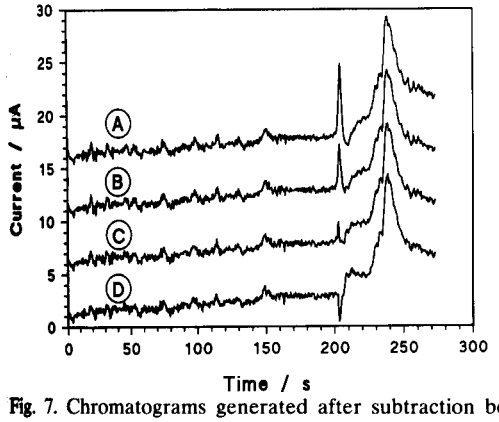

Fig. 7. Chromatograms generated after subtraction between electrodes polarised at −0.55 and −0.3 V (vs. Ag/AgCl). These subtractions represent a series whereby the data sets corresponding to the response, indicated as D4 and D6 respectively in Fig. 5, have been shifted relative to each other prior to subtraction. The data set {D6} is advanced as follows for the four chromatogram subtractions: A, 0; B, 1; C, 2; and D, 3.

subtraction is achieved, albeit with a sudden shift in baseline as the Pb(II) peak elutes. However, a significant feature is the spike generated at the time corresponding to the emergence of the Cu(II) peak. Visual inspection of the data sets associated with each electrode reveals that there is a discrepancy between the exact time at which the sharp rise of the Cu(II) peak occurs. If the normalised D6 set is advanced by two data points relative to the D4 set prior to subtraction, the spike is reduced. A further advancement of the normalised D6 set to a total of three data points relative to the D4 set, followed by subtraction, yields a small negative spike. It is clear that the occurrence of this spike, and also the disturbances noted in Fig. 6, are due to slight discrepancies between data sets as far as exact peak position is concerned. This effect is particularly noticeable at the initial rise of a given peak, rather than during its tail. Such behaviour would be expected, since the relative rate of change on the rising edge of a peak is greater than on its tail. The source of this discrepancy is unlikely to be due to differences in the actual time of data acquisition, even though the current is monitored for all electrodes by a single multiplexed analogue-to-digital converter. Data acquisition is complete in less than 1 ms for each data point, whereas the data acquisition rate in this work is 2 Hz for each channel. A likely explanation is that imperfection in the flow geometry is the cause. If the inlet jet impinges off the geometric centre of the array, there would be a significant difference in exact arrival time of the analyte plug at each electrode in the array. This in turn would account for the observed phenomenon of a spike coincident with the rise of the Cu(II) peak. Two possible courses of action to overcome this effect would be to either increase the data acquisition rate such that a better match between electrode data sets could be invoked or to improve the quality of the jet component and so ensure that it impinges at the geometric centre of the electrode array. Similar effects of this phenomenon were noticed for other electrode pairs, although the example given in Fig. 7 is the most severe for this experiment. The Figs. 5–7 have not been filtered, either at the analogue processing stage within the

potentiostat, or by using digital filtering post data acquisition. The noise level is significant for the current range explored. Although detailed signal analysis has not been carried out, it is probable that much of the noise is an artefact of two features. First, the resolution of the analogue-to-digital converter is compromised by the fixed current gain design, which was frequently operating with a significant background current. Second, since the design is a bench prototype, insufficient attention to shielding of the analogue circuitry from the digital circuitry had been made. A future modification to the potentiostat design would incorporate some of the flexible features described in the work of Hoogvliet et al. [11], to overcome the current range and current offset limitations of the authors potentiostat. Proper application of shielding techniques would be expected to reduce the noise significantly, with further reductions of high frequency components being possible through digital filtering.

In principle, this approach could be extended to larger arrays where several electrodes were used to monitor a single component in a separated mixture. Improved precision in this method of selective monitoring may be possible if the data from several electrodes in an array were fitted to a simple voltammetric model. For example, the Heyrovsky–Ilkovic equation may be used as a working model to describe the voltammetric response of a single component, or may be extended to include a simple mixture of components [18]. PC-based computing should be able to accommodate data fitting to a model in real time, which would further strengthen the case for utilising the selective power of electrode arrays.

Metal ion determination, by direct injection

Industrial process analysis requires robust, reliable monitoring devices with low maintenance. The application of LC techniques to process analysis, although feasible, is not attractive in terms of these basic requirements. The potential selectivity of the electrode array, as demonstrated for the determination of a separated mixture of metal ions, could be used directly for the monitoring of a mixture of electroactive species after direct injection. For this work, the FIA mode of the flow apparatus was adopted. This time, the same test mixture, used for the separation experiments, was injected directly onto the electrode array monitor. Figure 8 shows the results for just three electrodes in the array, polarised at −0.3 V, −0.4 V and −0.9 V respectively (vs. Ag/AgCl). Prior to this, the three electrodes were calibrated using single ion standard solutions containing Cd(II), Cu(II) and Pb(II) in the range 1–5 mM. This yielded linear calibrations with all three electrodes responding to Cu(II); the electrodes polarised at −0.4 V and −0.9 V responding to Pb(II); and the electrode polarised at −0.9 V responding to Cd(II) alone. From the three FIA peak areas, shown in Fig. 8, for the respective electrodes, the following subtractive calculations were made:

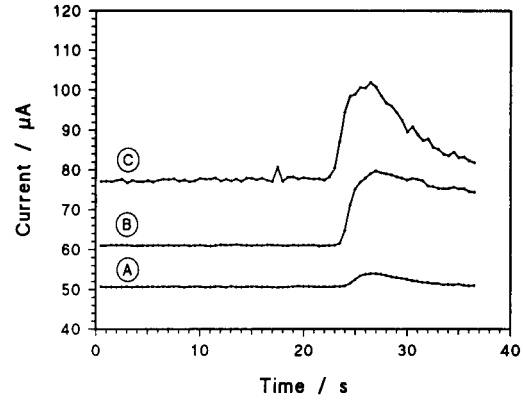

Fig. 8. FIA response for three satellite array electrodes polarised at: A, −0.3 V; B, −0.4 V; and C, −0.9 V (all vs. Ag/AgCl). A sample containing a mixture of Cd(II), Cu(II) and Pb(II) each at 1 mM in a carrier of 0.1 M KCl, at a flow-rate of 1 cm^3 min^{-1}. Injection occurred at 0 s.

(i) The Cu(II) concentration was computed using the electrode polarised at −0.3 V. Following this, the area response due to Cu(II) was subtracted from the remaining two electrode peak responses.

(ii) The Pb(II) concentration was computed using the electrode polarised at −0.4 V and the area response corresponding to Pb(II) subtracted from the area response of the electrode polarised at −0.9 V.

(iii) The Cd(II) concentration was computed from the area response of the electrode polarised

at −0.9 V, from which the contributions due to Pb(II) and Cu(II) had been subtracted.

The results of this operation indicated the following experimental concentrations for a mixture that was 1 mM with respect to each metal ion: Cu(II), 0.89 mM; Pb(II), 1.08 mM; and Cd(II), 0.86 mM. For three electrodes, used to determine three components, the agreement is acceptable (16% deviation from the nominal value of the Cd(II) concentration is the worst case). This clearly demonstrates the potential application of the electrode array for the monitoring of simple mixtures. An aim of this work was to indicate the feasibility of applying electrode arrays to simple industrial process analysis. Since many process analytical measurements are concerned mainly with the monitoring of variation in well defined samples, there is some scope for utilising the technique described for metal ion analysis. This work has been limited to a fixed size glassy carbon array, but it would be quite feasible to utilise a range of electrode materials within a single array and to adopt more powerful means of electroanalytical measurement, such as pulsed amperometry. The limitations lie in the fact that this approach relies upon well defined and consistent hydrodynamic conditions within a flow cell. It would be optimistic at this stage of development to suggest the possibility of true in-stream monitoring, although future work may well move towards that goal. The present system may be applied to a limited range of monitoring applications involving simple mixtures of electroactive components in aqueous media. There is still the requirement for on-line sampling preconditioning, such as sample filtration. However, this system is ideally suited to a FIA approach which has been shown to be a useful process analytical interfacing tool between industrial process lines and measurement equipment that requires a controlled chemical environment with constant physical parameters, such as flow rate and temperature. A further feature of any array detector is the inbuilt information redundancy, which offers the possibility of enhanced reliability as far as the data are concerned. There are many avenues to pursue, but these are the subject of future papers that will build upon the feasibility demonstrated in this work.

Tom McCreedy was supported by SERC. The authors gratefully acknowledge the assistance of ICI Engineering, Northwich in manufacturing the cell components used in this work.

REFERENCES

1 F. Belal and J.L. Anderson, Analyst, 110 (1985) 1493.
2 W.L. Caudill, J.O. Howell and R.M. Wightman, Anal. Chem., 54 (1982) 2532.
3 J.L. Magee and J. Osteryoung, Anal. Chem., 61 (1989) 2124.
4 J. Wang, G.D. Rayson, Z. Lu and H. Wu, Anal. Chem., 62 (1990) 1924.
5 D.A. Roston, R.E. Shoup and P.T. Kissinger, Anal. Chem., 54 (1982) 1417A.
6 C.E. Lunte, P.T. Kissinger and R.E. Shoup, Anal. Chem., 57 (1985) 1541.
7 R.A. Osteryoung and J. Osteryoung, Philos. Trans. Roy. Soc., London, A302 (1981) 315.
8 A. Aoki, T. Matsue and I. Uchida, Anal. Chem., 62 (1990) 2206.
9 T. Matsue, A. Aoki, E. Ando and I. Uchida, Anal. Chem., 62 (1990) 407.
10 V. Rizzo, G. Melzi D'eril, G. Achilla and G.P. Cellevino, J. Chromatogr., 536 (1991) 229.
11 J.C. Hoogvliet, J.M. Reijn and W.P. van Bennekom, Anal. Chem., 63 (1991) 2418.
12 T.H. Brearley, A.K. Doshi and P.R. Fielden, Anal. Proc., 26 (1989) 389.
13 P.R. Fielden, J. Chromatogr. Sci., 30 (1992) 45.
14 J. Yamada and H. Matsuda, J. Electroanal. Chem., 44 (1973) 189.
15 V.G. Levich, Physicochemical Hydrodynamics, Prentice Hall, Englewood Cliffs, NJ, 2nd edn., 1962, p. 20.
16 H. Matsuda, J. Electroanal. Chem., 15 (1967) 325.
17 J.M. Elbicki, D.M. Morgan and S.G. Weber, Anal. Chem., 56 (1984) 978.
18 P.R. Fielden, R.N. Carr and C.F. Oduoza, in M.R. Smyth and J.G. Vos (Eds.), Electrochemistry, Sensors and Analysis (Analytical Chemistry Symposia Series, Vol. 25), Elsevier, Amsterdam, 1986, p. 55.

Analytica Chimica Acta, 273 (1993) 123–137
Elsevier Science Publishers B.V., Amsterdam

Mercury films on a glassy carbon support: attributes and problems

Wolfgang Frenzel

Institut für Technischen Umweltschutz, Technische Universität Berlin, Strasse des 17. Juni 135, D-1000 Berlin 12 (Germany)

(Received 28th August 1992)

Abstract

The main problems associated with the preparation and application of mercury film electrodes on a glassy carbon support (MFGCE) are outlined. The role of the GC support material and in particular of the surface condition (microstructure and polishing procedure) for deposition of homogeneous mercury films and the proper performance of the resulting MFGCE in stripping voltammetric measurements is exploited. Highly polished electrodes without surface defects were found to be unsuitable because elemental mercury does not adhere to the GC surface. Instead, defined roughening of the GC support is proposed and is shown to yield mechanically stable films with excellent electrochemical characteristics. It is further shown that properly prepared MFGCEs may quickly lose their performance characteristics owing to fouling. The main reasons can be attributed to mechanical deterioration, formation of surface layers of insoluble mercury(I) compounds, adsorption of polymeric organic compounds and oversaturation with the mercury film by elements that form irreversible amalgams or intermetallics. The respective interferences are manifested in decreased sensitivity, increased background currents, loss of hydrogen overvoltage, impairment of peak resolution of adjacent signals or even totally erratic behaviour. The advantages of flow-through stripping voltammetry in minimizing or even avoiding these kinds of interferences are emphasized.

Keywords: Stripping voltammetry; Glassy carbon electrodes; Mercury film electrodes

Stripping voltammetry (SV) is one of the most powerful techniques for trace metal determinations [1–3]. In most applications mercury electrodes in the form of a hanging drop (HMDE) or a thin film (MFE) are employed. For the latter type of electrode several different support materials have been suggested, but generally glassy carbon (GC) is claimed to be most favourable [4–9]. In particular, the in situ deposition of mercury on the glassy carbon surface (MFGCE), as originally proposed by Florence [5], has found widespread application and appears to be the ultimate choice for trace and ultratrace determinations of heavy metals [6,7,9–11]. The simple preparation, high sensitivity and excellent resolution of neighbouring signals offered by this type of electrode are unrivalled properties. Reasons for these unique features have been attributed on the one hand to the support material itself, which exhibits low background currents over a wide potential range, high hydrogen overpotential, low porosity, extreme hardness and high chemical inertness [4–6,12,13]. On the other hand, mercury plated on GC is not contaminated by reaction (i.e., amalgamation) with the support material, does not diffuse into the support material and is said to form very thin films (typically 1–10 nm) that are uniformly distributed over the electrode surface [5]. The latter has, however, been disproved by several workers [14–16] in that small

Correspondence to: W. Frenzel, Institut für Technischen Umweltschutz, Technische Universität Berlin, Strasse des 17. Juni 135, D-1000 Berlin 12 (Germany).

droplets are formed rather than a homogeneous film.

In the course of experimental work with SV and related techniques over a period of nearly 10 years [17–21], MFGCs have been successfully applied, but more than once electrode failure has also been observed even when recommended procedures for electrode preparation [5,7,22] have been followed exactly. Unfortunately, such failure, which became apparent in loss of sensitivity with time, irreproducible results, decreasing resolution of adjacent peaks, unusually high background currents, lowering of hydrogen overpotential with time and spurious signals, did not occur consistently with one particular electrode or in a particular electrolyte but appeared irregular. Even electrodes that had worked well for long periods suddenly exhibited erratic performance. Resurfacing of the GC support and replating of the mercury film were sometimes successful, but often failed to restore the initial perfect response.

Indications that similiar observations must have been made by other workers also were found by a thorough perusal of the literature [5,10,11,14,16, 22–32]. Unfortunately, shortcomings and unsuccessful experiments are usually not extensively described and have to be deduced. Florence [26] reported that anodic polarization in chloride media seriously degrades the electrode performance owing to structural changes of the surface. In a paper by Dieker and Van der Linden [24] the occurrence of a small peak located just after the copper dissolution signal was mentioned and was attributed to formation of mercury(I) ions. Clem et al. [23,25], Zakharchuk et al. [27] and Filanovskii et al. [29] observed a cathodic peak in chloride-containing electrolytes which severely and irreproducibly altered the electrode behaviour. In other papers exposure of the electrode to air or the presence of dissolved oxygen was found to give spurious signals and reduced sensitivity [14,30,32]. Alteration of the electrode performance was also reported after excessive hydrogen evolution [28] or when working in solutions of high redox potential [16]. It is interesting that in many other papers none of these failures were mentioned (either because they did not occur or they were thought to be artifacts not worth reporting), although the experimental conditions were probably the same in several instances.

In informal discussions on MFGCEs at conferences, etc., it has been widely admitted that erratic behavior of this type of electrode is a common phenomenon, but no conclusive explanations could be offered. Differences in the quality of GC raw materials, physical and chemical variations of the electrode surface, adsorption of surfactants on the GC surface or the mercury film, oxidation of the mercury surface with concomitant formation of insoluble films (e.g., calomel, oxide layers) have, for instance, been put forward. Accordingly, the curative procedures employed were mainly governed by trial and error.

The paper is organized in three parts, dealing with the exploitation of the surface structure of the support material, mercury deposition on GC surfaces and the fate of mercury films in different analytical situations. With respect to the last aspect, frequent reasons for electrode failure will be discussed and some helpful measures to overcome these problems will be given. In this context the particular advantages of flow-through measurements will be outlined.

EXPERIMENTAL

Apparatus

Voltammetric stripping measurements were performed with a Model 174 A polarographic analyser in combination with a Model 315 A electroanalysis controller (both from EG&G PARC, Princeton, NJ) and a Houston Omniscribe X–Y recorder. Batch experiments were made with a purpose-made electrochemical cell consisting of a 50-ml glass beaker covered with a Perspex plate. Holes were drilled into the cover to accept the electrode holder of the Metrohm rotating disc electrode unit (Type E 628; Metrohm, Herisau, Switzerland), the Ag/AgCl (3 mol l^{-1}) reference electrode, the platinum wire counter electrode and a PTFE tube for sample deaeration. Static electrodes were used in combination with a magnetic stirrer placed under the glass beaker. The flow-through cell was that used in previous work (Fig. 1 in [19]). The flow-injec-

tion system comprised a peristaltic pump (Type IPS-8, Ismatec, Zurich), a PTFE rotary valve (Besta, Heidelberg) and PTFE tubing of 0.5 mm i.d.. Working electrodes used included several commercially available GC electrodes and about 40 laboratory-made electrodes. GC raw materials of different qualities and sizes were obtained from various manufacturers. In Table 1 is given a compilation of all the different electrodes employed. For comparative reasons an HMDE (Model 303; EG&G PARC, Princeton, NJ) and an epoxy resin-impregnated graphite electrode described elsewhere [33] were used.

For the preparation of the laboratory-made electrodes rods about 1–2 cm long were heat-sealed into PTFE tubes. Care was taken to obtain a tight fit between the GC and PTFE material without irregular edges. Most of the electrodes were made to suit both the Metrohm rotating electrode assembly and the wall-jet flow-through cell. The surfaces of the electrode tips were successively polished with emery paper of progressively lower grain size and with metallurgical diamond paste (Winter Diaplast, Hamburg) of decreasing particle size. Usually the final polishing was done with 0.05-μm diamond dust on wet velvet. After each polishing step the electrodes were carefully rinsed with water to prevent carry-over of larger particles. At the end of the polishing procedure the tips were cleaned ultrasonically with acetone and water four about 3 min each. This was found necessary to remove from the electrode surface organic residuals that are present in the polishing paste and the small GC particles abraded. When not in use the electrodes were stored dry in a clean atmosphere. If required, resurfacing of electrodes was done repeating the last step of the polishing procedure only.

For optical inspection of the GC surfaces and the mercury films formed on them, a stereomicroscope (Olympus) was used. Scanning electron microscopy (SEM) and microprobe analysis were applied in surface studies of the GC electrodes. Details of the instrumental settings of these two methods can be found elsewhere [34].

Measurements of the pH of the electrolyte solution and in the close vicinity of the electrode surface were made with a flat-membrane combination electrode (Type 403-S7, Ingold, Urdorf)

TABLE 1

Compilation of commercially available glassy carbon electrodes and raw materials used for the preparation of laboratory-made electrodes as applied in this work

Manufacturer	Type of electrode	GC grade	HTT (°C) [a]	Diameter (mm)
Metrohm	EA 286			3
	EA 276			5
EG&G PARC	R2/112 GC			
	GO 197			
Bioanalytical Systems	MF 2012			
Elektrokohle Lichtenberg				3 and 5
CTI	Prototype material [b]		2500	1 and 3
Carbone Lorraine		V 10	1000	3 and 5
		V 25	2500	1, 3, 5 and 6
Sigri		Sigradur K	1100	1, 3 and 5
		Sigradur G	2200	1, 2, 3, 5 and 7
Tokai		GC-10	1000	3
		GC-20	2000	3
		GC-30	3000	3, 5 and 6
		GC-20S [c]	2000	3
		GC-30S [c]	3000	3 5 and 6

[a] Heat treatment temperature during fabrication of GC raw material. [b] CTI materials are now commercially available in various sizes and qualities. [c] S = high-purity grade.

connected to a research ion-meter (Model 645, Knick, Berlin).

Chemicals and solutions

Metal ion standards were prepared by appropriate dilution of Titrisol stock solutions (Merck, Darmstadt). The reagents used were of Suprapur quality and triply distilled water was used throughout. Usually, 0.1 mol l^{-1} potassium nitrate solution adjusted to pH 2 with nitric acid was used as the base electrolyte. The mercury nitrate solution used for preplating and in situ plating of the electrode was generally 10 mg l^{-1} Hg^{2+}. Acetate buffer (pH 4.5) was prepared from acetic acid and gaseous ammonia.

Experimental procedure for mercury plating and stripping conditions

In batch experiments mercury deposition was generally performed in situ [5]. About 20 ml of electrolyte spiked with mercury(II) ions to give a concentration of 5 mg l^{-1} and appropriate concentrations of the metal ions were filled into the glass beaker. The solution was purged with high-purity argon for about 10 min while electrode rotation was initiated to prevent accumulation of air bubbles at the surface. After that time the plating potential (usually -1.0 V vs. Ag/ AgCl) was applied for 3 min followed by a linear sweep to $+0.2$ V. This first scan was used as indicator for proper electrode performance. In further measurements the plating potential was applied for desired length of time with electrode rotating at 1500 rpm. In order for the stripping step to proceed in quiescent solution, electrode rotation was stopped exactly 15 s before starting of the anodic scan. At the end of the deposition period the stripping voltammogram was recorded while the potential was linearly scanned at a rate of 100 mV s^{-1}. Electrochemical oxidation of mercury was prevented by terminating the scan at $+0.1$ V and ensuring that potential control was never left off (as occurs when the cell circuit is disconnected). Between successive scans and during working breaks a potential of -0.2 V was applied. The same mercury film was often used for many repetitive measurements. When required, however, the utilized mercury film was wiped off with a wet tissue and the GC surface was conditioned by repolishing with 0.05-μm diamond paste for a few seconds.

In flow-injection measurements the carrier electrolyte containing 5 mg l^{-1} Hg^{2+} was continuously pumped through the system at a rate of 1 ml min^{-1}. Prior to use the carrier solution was carefully deaerated with argon and measures were taken [35] to prevent re-aeration during transportation through PTFE tubing. Mercury deposition at a plating potential of -0.7 V was done in situ for the desired length of time (at least 3 min). Shortly before sample injection the potential was switched to $+0.1$ V for a few seconds to strip any metal contaminants that may have been accumulated during the plating step. Simultaneously with sample introduction the deposition potential of -1.0 V was imposed and kept to the working electrode until the sample plug had completely passed the flow cell. With a sample volume of typically 0.5 ml this lasts less than 1 min. Then the stripping curve was recorded under the same conditions as used in batch experiments. Usually, the stripping step was performed in flowing electrolyte but stopped flow [19] was also applied.

RESULTS AND DISCUSSION

Glassy carbon support

The term glassy carbon (GC) was introduced by Yamada and Sato [36] for a gas-impermeable carbon material made from phenolic resins by heating in an inert atmosphere. The combination of unique properties of this material [4,37–39] has stimulated manufacture of glass-like (or vitreous) carbon materials by several companies. As a result, glass-like carbon materials are now available that differ significantly in their mechanical, thermal and electrical properties and in their microstructure and contamination level [37,39,40]. Therefore, it is obviously not possible to define an absolute GC surface state as is possible with platinum, gold, mercury and other metallic electrodes. The GC materials most commonly used in electroanalytical work and particularly as a support for mercury film electrodes are those which offer low porosity, high conductivity, chemical

inertness and hardness. Although these properties have been quantified in terms of apparent porosity, gas permeability, shore hardness, resistivity, etc., there are obviously only a few data available that correlate any of these properties of the raw material with their electrochemical behaviour [41]. A further variable that makes it in fact difficult to compare results obtained, even when the same starting material is used, is the polishing procedure employed to obtain a suitable working electrode for electroanalytical purposes. The actual procedures used by various workers are often not adequately described and may differ considerably. Surface functionalities already present in the raw material or introduced intentionally or accidentially by pretreatment procedures [42–46] further complicate any generalization about the behaviour of GC as an electrode material. From the point of view of application as a support for mercury films, it would be desirable if the GC itself would not contribute to the electrochemical response of the electrode. In other words, ideally the MFGCE should resemble a true mercury electrode. As mentioned by Nürnberg et al. [22], the surface quality is crucial in this respect and according to their experience only a very low degree of roughness secures the deposition of an almost homogeneous mercury film.

Having found that SV with MFGCEs even when a highly polished GC support is employed can be troublesome (see Introduction), the role of the support material was investigated in detail, particularly the microscopic homo- or heterogeneity and the chemical purity of the GC surfaces. For this purpose the electrodes listed in Table 1 were subjected to identical polishing procedures and the electrode surfaces were examined by optical microscopy, SEM and microprobe analysis. As the comprehensive results of this study will be published separately, only some of the important findings will be presented here. As found by others [4], the microstructures of different electrode surfaces vary significantly. Even electrodes cut from the same rod do not exhibit identical surface structures. Most of the electrodes show randomly scattered surface defects in the form of small craters, ruts and pits. The dimensions of these defects are in the nm to lower μm range and cannot be removed by repolishing. They are obviously due to inclusions that result from the fast heating during the fabrication of the raw materials [47]. Some electrodes had totally irregular surfaces, others only few defects of random size and only two materials (3-mm Tokai 30 S and 1- and 3-mm CTI prototype material) were virtually free from any defects. Microprobe analysis of the electrode surfaces revealed that the smooth parts of the electrode were pure carbon whereas many metals (e.g., Fe, Mg, Al, Si, V, Ni and Cr) can be found in craters and micropores. In general, the smoothness of the GC surfaces increased with decreasing diameter of the rods and increasing heat treatment temperature during fabrication, but the starting resin material is also an important factor [34].

Application of the various electrodes in SV could give no clear evidence, however, of what role the microstructure of the GC surface plays. Taking into account the different sizes of the electrodes, comparable values for the background currents and hydrogen overpotentials were usually observed. When plated with mercury most of the electrodes yielded stripping peaks for cadmium and lead which, with respect to sensitivity and resolution, agreed well with literature data. In some instances, however, the sensitivity was much lower, the peak potentials were shifted to more negative values, the resolution between Cd and Pb was significantly worse and double peaks and shoulders occurred. Although not entirely consistent, it seemed that electrode failure was related to the surface quality, but opposite to expectations the electrodes with higher surface roughness and irregularities were those which gave more reproducible results. Particularly surprising, at least at this stage of the investigation, was the fact that the two totally smooth electrodes (see above) were the most troublesome. With these electrodes reproducible results could never be obtained. It was conspicous, however, that the stripping peaks for Cd and Pb at these particular electrodes were always shifted to negative potential values and had the form of doublets (see Fig. 1a). Almost identical peak shapes were obtained in SV at bare GC electrodes. The dou-

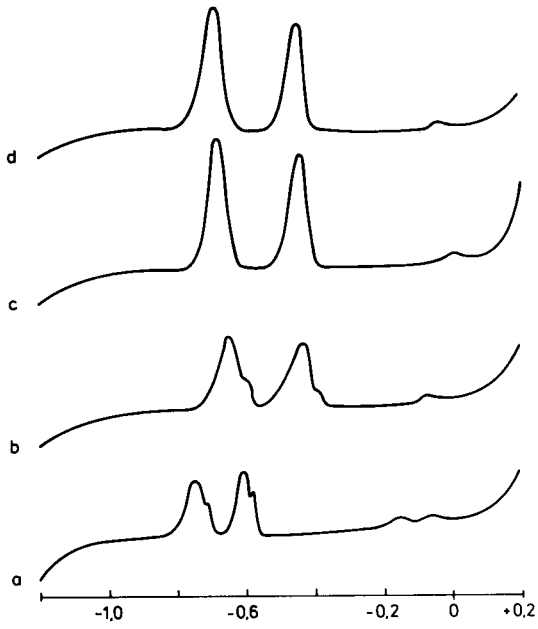

Fig. 1. Typical stripping voltammograms as obtained with (a) perfectly smooth electrode, (b) electrode with surface defects, (c) roughened electrode and (d) composite electrode [33]. In all instances a sample containing 100 $\mu g\ l^{-1}$ each of cadmium and lead was spiked with 5 mg l^{-1} mercury ions and after in situ deposition for 5 min the scans were performed at 100 mV s^{-1}.

ble peaks are due to differences of the stripping potential of metals from adatom deposition and from the monolayer [4]. This prompted a further examination of mercury film formation on GC surfaces.

Deposition of mercury and film formation on GC surfaces

When a sufficiently negative potential is applied to a GC electrode, mercury ions in solution are reduced at the electrode surface and elemental mercury is deposited. Although it is generally assumed that a thin film of mercury is formed, there is strong evidence that the mercury is actually present in the form of droplets [14–16]. According to Stulikova [15], nucleation preferentially occurs at active sites of the GC material and adatom deposition leads to droplet formation. Nothing was said, however, about the nature of the active sites. Dunsch [48] has shown that at oxidized GC surfaces the formation of mercury–carbon bonds may be blocked and the deposition only takes place at locations virtually free from oxygen-containing groups. Laser and Ariel [49] found that the growth of mercury drops is coupled with discontinuities in the electrode surface. In other work [50], increased surface activity of GC electrodes was observed on scratching and was attributed to the rupture of C–C bonds.

Studies were initiated in order to investigate mercury film formation at GC electrodes of different quality and size that had previously been characterized by SEM and microprobe analysis. As all the electrodes were polished in an identical manner and the plating and stripping conditions were also identical, it was hoped to obtain some insights into the relationship between surface structure and film formation. The plating time, deposition potential and mercury ion concentration were varied and optical examination of the electrode surfaces was done after each experiment.

At electrodes with surface defects (either scratches or metallic inclusions), the deposition of mercury (in the form of droplets) preferentially occurred at these sites. Similiar behaviour has also been reported for nickel deposition at GC surfaces [51] and was found by Stojek [52] when laboratory made GC materials with different levels of metallic contaminants were used as supports for mercury film formation. In order to improve the quality of mercury coating, Brainina et al. [16] modified the electrode surface with zinc adatoms, which is a further indication that activation of the GC surface is advantageous for mercury plating. Another result of this study was that with prolonged electrolysis times and increasing mercury ion concentration, the drop size increased before any mercury deposition at the smooth parts of the surface took place. Coalescence of droplets could frequently be seen along scratches and at closely adjacent surface defects. Another finding was that the mercury drop size distribution is strongly related to the size of the surface defects. Comparatively large droplets (1–10 μm diameter) were present in larger cavities and ruts whereas only minute droplets (< 0.2 μm) could be discerned on the remaining part of

the surface. At extremely smooth parts no mercury was deposited and the bare GC surface became visible.

Such electrodes in some respect resemble multi-array microelectrodes [53,54] with variable size of the individual electrodes. As the stripping peak potential of individual elements depends on electrode size [55] (the smaller the electrode the more negative is the potential), it is not surprising that when using such electrodes doublet peaks and shoulders have been observed and the resolution of adjacent peaks deterioted. A typical voltammogram is shown in Fig. 1b for an electrode that exhibited a very irregular surface structure, i.e., a few large craters in the range 10–40 μm, many small pits in the range 1–5 μm and some areas without irregularities. Re-examination of the voltammetric behaviour of many of the electrodes prepared confirmed the relationship between surface structure and quality of the stripping curves.

Particular attention was paid to the behaviour of the extremely smooth electrodes without any surface defects (see above). From plating currents it could unambigiously be shown that mercury ion reduction took place. Optical inspection, however, revealed that independent of plating time and mercury ion concentration, virtually no elemental mercury was present at the surface of the electrode. In few instances some small droplets accumulated at the edge between the GC material and the PTFE housing. Obviously, the elemental mercury formed does not adhere to the highly polished GC surface. Electroreduction of mercury without deposition was also observed by Yoshida and Kihara [56], who studied the deposition of mercury from very dilute solutions. According to that work, monolayer formation and adatom deposition are only possible if the concentration in the double layer is sufficiently high, otherwise elemental mercury readily diffuses into the bulk solution. In the light of these observations one might ask what makes the elemental mercury adhere to the GC surface. Chemical interactions between mercury and carbon are very weak [4,57] so that adhesion is the most probable mechanism. The high surface tension of mercury together with the low contact area available at highly polished and smooth electrode surfaces are obviously very unfavourable conditions. It is therefore assumed that the mercury droplets simply dislodge. Support for this assumption is the reduced likelihood of mercury deposition under conditions of forced convection. Jagner and Aren [58] have reported rupture of mercury droplets from the electrode surface at high rotation speeds and we have repeatedly seen that in flow-through applications with wall-jet electrodes the impinging liquid has removed part of the mercury from the GC surface. Renman [59] pursued the deposition of mercury at GC fibre electrodes during electrolysis by microscopic examination and observed occasional drop-off of some of the mercury droplets formed. In order to improve the adhesive strength mercury and GC, roughening of the electrode surface appeared to be a logical consequence [32] and was tested with a set of electrodes.

Rough electrodes were prepared either by terminating the common polishing procedure at various steps or by successive roughening of formerly highly polished electrodes. In general, the results obtained did not differ very much but the latter procedure, even more time consuming was found to give better reproducibility. Hence, the remainder of the work was done with a 3-mm CTI GC electrode (see Table 1). The roughness of the electrodes can most easily be defined by the particle size of the diamond paste finally used. GC surfaces treated with 1–10-μm paste lost their shiny appearance. On deposition of mercury it could be seen by eye that uniform coverage were obtained almost independently of the quality and size of the raw material. Microscopical examination of the surfaces revealed a highly homogeneous distribution of mercury droplets, the size of which was of the same order of magnitude as the surface roughness. Similiar observations were made by Abdullah et al. [32] with roughened graphite electrodes. At a surface roughness of 1–5 μm and with sufficiently high mercury deposition, the small drops eventually coalesced and formed a true film.

Electrodes prepared in this manner are mechanically stable even when applied at high rotation speed or in flow-through measurements with

high linear flow velocities. Removal of the mercury film, however, is still possible with a wet tissue, as is common practice with polished GC electrodes [5]. Resurfacing of the GC substrate can simply be performed with polishing paste of the desired particle size.

The electrochemical behaviour of roughened GC electrodes appeared to be slightly different from that of the polished electrodes. In the absence of a mercury film the background currents were consistently higher and the hydrogen overvoltage decreased. This is in agreement with other papers [41,44,50,60] and has been explained by an increase in the electrode surface and introduction of oxygen functionalities, respectively. When covered with mercury the electrodes behaved much like a true mercury electrode (as could be shown by comparison with an HMDE), which means that the support itself does not contribute to the electrochemical response.

The application of the roughened MFGCE in SV of heavy metals revealed substantial advantages. When compared with the highly polished MFGCE the reproducibility of successive scans at the same film was significantly improved, as was the reproducibility of current calibration factors (μA l μmol^{-1}) when day-to-day and within-day data were taken. High resolution of neighbouring signals was attained with the peak width at half-height being in close agreement with the theoretical value [61]. In Fig. 1c this is shown as an example for the stripping of Cd and Pb. Interestingly, the results obtained with the roughened MFGCE compare very well with so-called composite electrodes [33,62–64] where the formation of microdroplets at active sites of the carbon surface is also assumed and a homogeneous size distribution is attained. A typical stripping curve as obtained with such an electrode (see Apparatus [33]) is shown in Fig. 1d.

Electrode failure

The intruduction of the in situ plating procedure of MFGCEs [5] has repeatedly been appreciated as a major development in SV. In addition to the convenience of preparation improved precision has been obtained [11,16] in comparison with formerly used preplated electrodes [65]. In his pioneering paper, Florence [5] stated that it is difficult to prepare preplated films of consistent and uniform thickness, and even more difficult to preserve them in an active state for any length of time. With respect to the lifetime of preplated and in situ plated MFGCEs significant discrepancies exist as far as the relevant literature reveals. Some workers claim that a mercury film once prepared may be used for days or even a week [35,66,67], others deem it necessary to prepare a new film with each sample [5,22,68]. According to our experience, both opinions may be right since in several instances the excellent performance of a properly prepared MFGCE (see above) can be maintained for long periods but it may also happen that electrode failure occurs after one plating/stripping cycle only. In the following the main reasons for electrode failure will be outlined and precautions required for protection of MFGCEs will be given.

Mechanical deterioration. The mercury film (or more precisely the assemblage of small mercury droplets) is very sensitive to mechanical destruction. Touching the film immediately leads to removal of part of the mercury and possible coalescence of the remaining droplets. Although much less pronounced with the roughened version of the MFGCE proposed in the present paper, similiar effects can also occur when the electrode rotates at high speeds or when a liquid stream is directed towards the electrode surface. During sample deaeration gas bubbles may pass the surface and deteriorate the uniformity of the film. The same holds for excessive hydrogen evolution during deposition from acidic sample solutions. Optical inspection before and after use of MFGCEs in acidic solution clearly revealed the formation of fewer drops of larger size instead of more drops of smaller size formerly present. In SV the change in the film homogeneity becomes apparent in a decreased sensitivity (due to the lower surface-to-volume ratio), an increase in the residual current and a loss of hydrogen overvoltage. Removal of the electrode from the solution has also been reported to produce patchiness in the texture of the film due to coalescence of droplets [32].

Beside many other advantages, the application of flow-through SV is a suitable approach to prevent or minimize some of the problems mentioned. Once installed in the flow cell the electrode is generally not removed and hence cannot be touched. Sample deaeration is not required because of the matrix exchange procedure inherent in flow systems [66] and purging of the carrier solution is done in the reservoir. Hydrogen formation can effectively been avoided when the (acidic) sample is buffered. This can be done conveniently on-line using the merging zone approach [19]. The ability to analyse samples successively without removing the electrode from the flow system prevents the electrode from being exposed to air between analysis. It is probably for that reason that preplated films are often successfully used in flow systems [64,66,67] which fail to work properly in batch procedures [11].

Oxidation of elemental mercury and formation of insoluble mercury(I) compounds. Oxidation of mercury may occur when potentiostatic control is lost (switching off the cell or removal of the electrode from solution) or the potential is scanned too far positively. Oxidizing agents generally present in solution are traces of oxygen and mercury(II) ions added for in situ film formation. In the presence of chloride calomel is readily formed at the electrode surface, leading to high base currents and erratic performance [5]. The occurence of a cathodic indentation in chloride media at about −0.4 V has previously been observed [23] and excessively studied by Russian electrochemists [27,29,69,70]. In Fig. 2 repetitive background scans are shown as obtained with a properly prepared MFGCE (curve a) and with the same electrode after switching off the cell for 30 s (curve b). The chloride concentration in this experiment was 10 mM. Scans c and d were successively recorded without disconnecting the circuitry. Although the large cathodic peak in the first scan after cell disconnection quickly decreases in successive scans, it is obvious that the initial baseline has not been reached and the hydrogen overvoltage became slightly worse. In order to restore the electrode, excessive polishing is required, as was also found by Florence [26]. Attempts to remove calomel together with elemental mercury by electrochemical oxidation (i.e., application of a positive potential for some time) and plating of a new film also failed to restore the initial response. The reason for this is most likely the alteration of the GC support material due to introduction of surface functionalities [43,44,50].

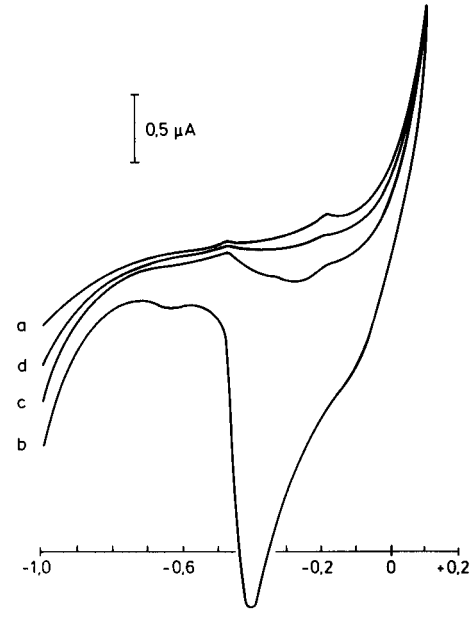

Fig. 2. Electrode failure due to calomel formation. Repetitive background scans are shown as obtained at a properly prepared MFGCE (curve a) and at the same electrode after switching off the cell for 30 s (curve b). Scans shown as curves c and d were run successively without delay.

The likelihood of calomel formation depends on the concentration of chloride in solution and the electrode potential applied. A particular problem may arise in the presence of relatively high chloride concentrations where stripping of copper requires a potential at which calomel already starts to be formed. Matrix exchange is an obvious solution to this problem. However, in the absence of chloride (or other halides) oxide layers may also be formed at the electrode surface [14] when potential control is lost or the electrode is exposed to air, both of which cannot be avoided when the electrode is transfered from the sample into the stripping solution.

The use of flow-through SV is advantageous in this respect as matrix exchange can be conve-

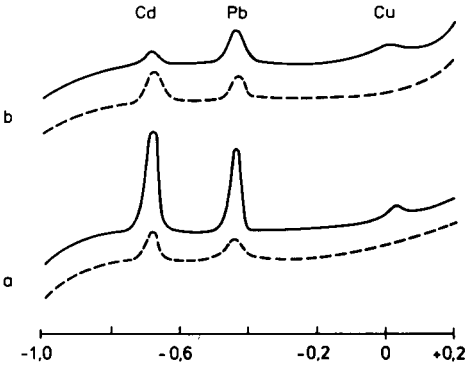

Fig. 3. Stripping voltammograms as obtained for the simultaneous determination of cadmium and lead in (a) aqueous solution and (b) spiked urine samples. The solid and dashed lines are response curves without and with dialysis, respectively. A 1-ml volume of acidified sample (pH 2) spiked with 500 $\mu g\ l^{-1}$ each of Cd^{2+} and Pb^{2+} was injected and deposition was performed at −1.0 V for 1 min. Other conditions were as given under Experimental.

niently performed without electrode transfer [66]. By an appropriate choice of the carrier (or stripping solution if not the same) and downstream location of the reference electrode, the presence of chloride during the stripping step can be totally avoided. The same holds for dissolved oxygen when carefully deaerated carrier solutions are used and measures are taken to prevent reaeration through the connecting tubing [35]. During passage of the sample solution (non-deaerated and containing chloride) the deposition potential is applied and calomel or mercury oxide cannot be formed.

Adsorption phenomena. A serious limitation in the applicability of SV, in general, is the strong interference of polymeric organic materials (e.g., surfactants, humic acids, proteins) which tend to adsorb at the electrode surface [1–3]. Adsorption of surface active compounds on the working electrodes strongly inhibits the deposition of trace metals (leading to reduced sensitivity) or even causes complete fouling of the electrode [71]. In Fig. 3 typical voltammograms are shown as obtained in flow-injection measurements on aqueous standard and urine samples, both spiked with identical concentrations of cadmium and lead Clearly, the peak currents are strongly depressed in the urine matrix. In subsequent scans (not shown) the signals became progressively smaller with total disappearance of the two peaks after the fifth injection (corresponding to about a 5-min exposure of the electrode to urine). Similiar results have also been obtained in the analysis of serum, waste water and surface waters with high value of the chemical oxygen demand.

A variety of methods have been developed for the destruction of organic material prior to SV, but these methods generally suffer from a high risk of contamination, possible interference of the digestion acid (e.g., excessive hydrogen evolution) and considerable lengthening of the analytical procedure. Simple acidification as proposed by Jagner et al. [72] for analysis of biological fluids using potentiometric stripping analysis and the application of the standard addition method [73] have been tested but were found to be of limited utility in SV. A very promising approach is the use of membrane-coated GC electrodes [74–77], which are transparent for ions but retard organic compounds. Dialysis membranes, although very effective in the prevention of organic interferences [74,75], require comparatively long equilibrium times and the membrane becomes the limiting factor to mass transport of the analytes. The successful application of one-line dialysis under dynamic flow conditions [78–80] encouraged us to investigate a similiar technique for SV. As a result of this study [81] a simple wall-jet dialysis cell was developed. As shown schematically in Fig. 4, a small disc of a suitable dialysis membrane (Spectra/Por 1000 MWCO; Kleinfeld,

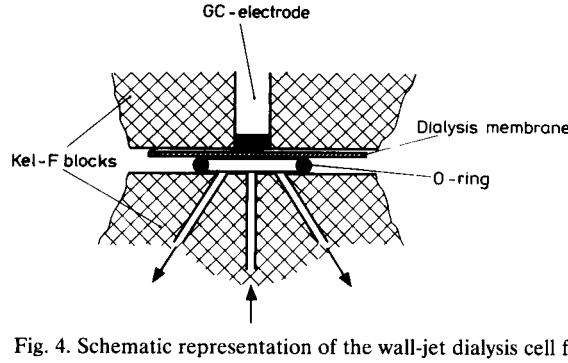

Fig. 4. Schematic representation of the wall-jet dialysis cell for stripping voltammetric measurements. Counter and reference electrodes (not shown) are positioned in the outlet channel. The two Kel-F blocks are held together by means of a clamp.

Hannover) is placed in front of the GC surface. The mercury film is deposited through the membrane as described in previous work [77]. Comparison of stripping signals for cadmium and lead with and without the dialysis membrane in place and otherwise identical conditions shows significantly reduced sensitivity for the coated electrode (see Fig. 3). The reproducibility of peak currents in successive runs, however, was comparable to measurements without the membrane, which clearly indicates that the controlled hydrodynamics in a flow-through system render the attainment of equilibrium unnecessary. In order to prove the feasibility of this novel approach the analysis of the above urine samples (spiked with Cd and Pb) was repeated. As can be seen in Fig. 3, no significant differences in the peak currents, stripping potentials and peak shape exist when aqueous standards and urine samples are compared. The direct determination of trace metals in soil extracts, surface and waste waters and serum samples has also been performed and accurate results have been obtained, as was shown by comparison with atomic absorption spectrometry and SV after sample digestion [81].

The lifetime of the dialysis membrane is in the order of days (which means that hundreds of samples can be run) without a considerable decrease in the mass transport of analytes. Care must be taken, however, to prevent exposure to air or loss of potential control as the mercury film may otherwise undergo the same changes as discussed above. Membrane exchange and preparation of a new mercury film are simple and take only a few minutes.

Oversaturation of the mercury film and intermetallic compound formation. Mercury is preferentially used as an electrode material in SV as many metals form reversible amalgams. The solubility of several metals in mercury is limited, however, and a separate crystalline phase of pure metal is formed when the solubility is exceeded [82]. This generally leads to a decrease in stripping peak currents and the occurrence of a second peak owing to dissolution of the non-amalgamated metal. SV can also be complicated by the formation of intermetallic compounds between metals deposited at the mercury electrode [1–3]. Owing to the minute volume and concomitantly high concentration of metals in the mercury phase, this kind of interference is particularly severe when MFGCEs are applied. Much work has been conducted [1–3,82–85] to study intermetal compound formation and to overcome the interference by proper choice of plating conditions or in making use of the "third" element effect [85]. It is outside the scope of this paper to review interferences due to intermetallic compound formation, but the deterioration of MFGCEs on irreversible deposition of intermetallics and amalgams will be discussed.

As long as all the metals deposited (either as amalgam, pure metal or intermetallic compound) are completely removed from the electrode during the stripping step, the interferences involved are only relevant to the particular sample being analysed. If, however, metals remain at the electrode surface the electrode characteristics may alter. This was in fact found during an investigation of the effects of metals that form irreversible amalgams in the determination of lead and cadmium. Nickel, cobalt and manganese were taken as representatives for such elements. Solutions of the respective elements were injected into the flow injection system and a plating potential was applied at which deposition occurs. After scanning the potential to +0.1 V a new sample was injected containing Cd and Pb only. In Fig. 5 the change in the stripping curves for Cd and Pb before and after deposition of nickel is shown. Obviously, the overpotential decreased and peak shapes are distorted. This picture did not change

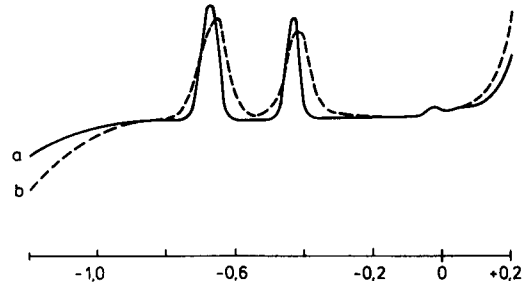

Fig. 5. Alteration of electrode performance due to deposition of metals that form irreversible amalgams. Scans a and b were obtained before and after, respectively, the deposition of Ni. For explanation, see text.

significantly when the waiting time at +0.1 V was prolonged, so it is assumed that nickel cannot be totally removed from the mercury film. In order to obtain the initial response, removal of the mercury film and preparation of a new MFGCE was required.

Flow-through measurements do not provide many advantages as far as the avoidance of intermetallic compound formation is concerned. However, the ability to adjust the chemical environment during deposition and stripping in a simple way is noteworthy. Two-line manifolds permit samples to be mixed on-line with suitable complexing agents (citrate and cyanide have been used, for instance, to prevent deposition of Ni and Cu, respectively [32,86]) and after matrix exchange the stripping step can be performed in a medium where interferences are further reduced. More sophisticated manifolds with automatic control of switching valves [87] offer even higher flexibility in the choice of sequence with which respective solutions are propelled through the system so that each step can be performed under optimum conditions.

pH effects. Most commonly the deposition potential in SV is not set more cathodic than −1.4 V, as this allows many of the relevant elements to be deposited and more negative potentials cause excessive hydrogen evolution. In acidic solution the hydrogen overpotential is considerably decreased and hydrogen evolution can only be avoided when the sample is adequately buffered. As mentioned before, the gas bubbles may distort the mercury film leading to increased base currents, lowering of the overpotential and decreased reproducibility. In Fig. 6 the effects of performing SV in acidic solution are shown. Plating and stripping cycles were carried out alternately in neutral and acidic media using the same MFGCE in flow-through measurements. Evidently, the initial response obtained in neutral solution (curve a) is not restored when the electrode has been used in acidic solution for some time and hydrogen has been evolved. The overpotential drastically decreased (curve c) and the precision deteriorated. Microscopical inspection of the electrode surface, however, did not show noticeable alterations so that chemical transformation of the GC support material might be responsible for the observed effects.

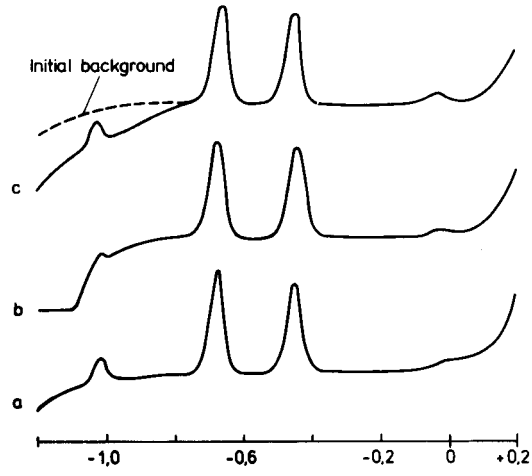

Fig. 6. Effect of hydrogen evolution on the background current of MFGCEs. Scans a, b and c were successively performed in neutral, acidic and neutral solution, respectively. For clarity, the initial baseline of curve a is drawn again in curve c (dashed line). For further details, see text.

The electrochemical reduction of dissolved oxygen poses many problems in voltammetric measurements. High residual currents and the formation of species (e.g., H_2O_2 and OH^-) that can seriously interfere in the deposition and stripping step have been exhaustively discussed [1–3,88]. Significant pH changes in the vicinity of the electrode may occur when neutral and unbuffered samples are analysed. In such cases metal ion precipitation with a concomitant decrease in the amount of metal deposited is possible and the elemental mercury may also undergo reactions in alkaline medium. In order to examine the actual pH changes, a flat-membrane pH electrode was positioned opposite the GC surface, leaving a space of only about 0.5 mm between the two surfaces. In non-deaerated neutral solution pH values as high as 9.4 were measured after a few minutes when the plating potential was set to −1.0 V. On sample deaeration only a slight increase in the pH could be detected. In acidic solutions (pH 2) and buffered electrolyte (ammonium acetate, pH 4.5) no pH change has every been observed. The influence of different conditions during the plating step (i.e., with and

without deaeration, buffered and unbuffered samples) was investigated in flow-injection SV with the stripping conditions kept constant. In contrast to recent work [89], a significant decrease in the stripping current for Cd and Pb was seen when non-deaerated and unbuffered solutions were analysed. Moreover, the MFGCE appeared slowly to lose its excellent performance under these conditions, which can be attributed to the formation of mercury oxides in alkaline medium.

Owing to the observed effects, it is highly recommended that both excessive evolution of hydrogen and the possibility of creating an alkaline environment should be precluded by adequate buffering of the sample solution. This can be conveniently done on-line in a flow system using the merging zone approach [19]. Although metal contamination introduced by the buffer used in our study (see Experimental) is low (< 0.7 $\mu g\ l^{-1}$ Cd and Pb), the constant level allows for proper background correction [90] when ultratrace determinations are envisaged.

Conclusions

Examination of various GC materials revealed significant differences in the microstructure. Gas inclusions and metallic contamination are usually present, leading to surface defects in the form of ruts and pits that cannot be removed by polishing procedures. Only a few materials are virtually free from surface irregularities.

When highly polished the latter materials are totally unsuited as supports for mercury films as elemental mercury fails to adhere to the smooth surface. Renunciation of mirror-like finishing (commonly believed to be a major requirement for the preparation of MFGCEs) is therefore proposed and instead the electrode surface is roughened in a defined manner. By this means a highly homogeneous distribution of mercury droplets of equal size is obtained and the resulting MFGCEs furnish evidence of outstanding performance in SV.

The excellent performance of such electrodes, however, may quickly been lost owing to electrode fouling. The main reasons can be attributed to the formation of insoluble calomel and mercury oxide layers on contact with chloride ions and oxygen, respectively, adsorption of polymeric organic materials and the deposition of elements that form irreversible amalgams or intermetallics. Electrode failure, which becomes apparent in a loss of sensitivity, decreased resolution of adjacent peaks, increase in the base current and lowering of the hydrogen overpotential, generally cannot be cured so that a new MFGCE must be prepared.

Application of flow-through SV is shown to reduce significantly the chances of electrode distortion because on the one hand the electrode is always kept in solution and on the other a suitable chemical environment can easily be created to which the electrode is exposed during deposition and stripping (matrix exchange). Failure due to adsorption has been prevented by the introduction of a simple wall-jet dialysis cell.

In conclusion, it is hoped that the results of this work may help to convert the difficulties that sometimes occur when working with MFGCEs into an outstanding enterprise.

The preparation of this paper was aided by discussions with many workers. Zbigniew Stojek, Joe Wang, Janet Osteryoung, Khiena Brainina and Daniel Jagner are particularly thanked. Thanks are also due to P. Schubert (Hahn-Meitner-Institut, Berlin) for making microscopic, SEM and microprobe measurements. The generous gift of glassy carbon materials from CTI and Deutsche Carbone is highly appreciated.

REFERENCES

1 F. Vydra, K. Stulik and E. Julakova, Electrochemical Stripping Analysis, Horwood, Chichester, 1976.
2 J. Wang, Stripping Analysis – Principles, Instrumentation and Applications, VCH , Deerfield Beach, FL, 1985.
3 G. Henze and R. Neeb, Elektrochemische Analytik, Springer, Berlin, 1986.
4 W.E. van der Linden and J.W. Dieker, Anal. Chim. Acta, 177 (1980) 1.
5 T.M. Florence, J. Electroanal. Chem., 27 (1970) 273.
6 W. Lund and M. Salberg, Anal. Chim. Acta, 76 (1975) 131.
7 L. Sipos, T. Magjer and M. Branica, Croat. Chem. Acta, 46 (1974) 35.

8 T.R. Copeland, J.H.Christie, R.A. Osteryoung and R.K. Skogerboe, Anal. Chem., 45 (1973) 2171.
9 P. Valenta, L. Mart and H. Rützel, J. Electroanal. Chem., 82 (1977) 327.
10 L. Mart, H.W. Nürnberg, P. Valenta and M. Stoeppler, Thalassia Jugosl., 14 (1978) 171.
11 G.E. Batley and T.M. Florence, J. Electroanal. Chem., 55 (1974) 23.
12 H.E. Zittel and F.J. Miller, Anal. Chem., 37 (1965) 200.
13 H. Monien, H. Specker and K. Zinke, Fresenius' Z. Anal. Chem., 275 (1967) 342.
14 S.P. Perone and K.K. Davenport, J. Electroanal. Chem., 12 (1966) 269.
15 M. Stulikova, J. Electroanal. Chem., 48 (1973) 33.
16 K.Z. Brainina, E.A. Vilchinskaya and R.M. Khanina, Analyst, 115 (1990) 1301.
17 W. Frenzel, Thesis, Technical University of Berlin, Berlin, 1984.
18 G. Schulze and W. Frenzel, Anal. Chim. Acta, 159 (1984) 95.
19 W. Frenzel and P. Brätter, Anal. Chim. Acta, 179 (1986) 389.
20 W. Frenzel and P. Brätter, in P. Brätter and P. Schramel (Eds), Trace Element Analytical Chemistry in Medicine and Biology, Vol. 4, de Gruyter, Berlin, 1987, p. 337.
21 W. Frenzel, G. Welter and P. Brätter, in M.R. Smyth and J.G. Vos (Eds.), Electrochemistry, Sensors and Analysis, Elsevier, Amsterdam, 1987, p. 77.
22 H.W. Nürnberg, P. Valenta, L. Mart, B. Raspor and L. Sipos, Fresenius' Z. Anal. Chem., 282 (1976) 357.
23 R.G. Clem, G. Litton and L.D. Ornelas, Anal. Chem., 45 (1973) 1306.
24 J. Dieker and W.E. van der Linden, Fresenius' Z. Anal. Chem., 274 (1975) 97.
25 R.G. Clem, Anal. Chem., 47 (1975) 1778.
26 T.M. Florence, Anal. Chim. Acta, 119 (1980) 217.
27 N.F. Zakharchuk, N.A. Valiskeva and I.G. Yudelevich, Zh. Anal. Chem., 35 (1980) 1708.
28 J. Wang and B. Greene, Anal. Chim. Acta, 144 (1982) 137.
29 B.K. Filanovskii, L.A. Butyrskaya and M.A. Sokolov, Zh. Anal. Chem., 42 (1987) 1440.
30 M. Wojciechowski and J. Balcerzak, Anal. Chem., 62 (1990) 1325.
31 M. Mlakov and M. Lovric, Analyst, 115 (1990) 45.
32 M.I. Abdullah, B. Reuschberg and R. Klimek, Anal. Chim. Acta, 84 (1976) 307.
33 K. Sykut, I. Cukrowski and E. Cukrowska, J. Electroanal. Chem., 115 (1980) 137.
34 W. Frenzel and P. Schubert, unpublished results.
35 J.A. Wise, W.R. Heineman and P.T. Kissinger, Anal. Chim. Acta, 172 (1985) 1.
36 S. Yamada and H. Sato, Nature (London), 193 (1962) 261.
37 G.M. Jenkins and K. Kawamura, Polymeric Carbons – Carbon Fibre, Glass and Char, Cambridge University Press, Cambridge, 1976.
38 L. Dunsch, Z. Chem., 14 (1974) 463.
39 S. Yamada, A Review of Glasslike Carbons, Defense Ceramic Information Centre, Battelle Memorial Institute, Columbus Laboratories, Columbus, OH, 1986.
40 M. Gross and J. Jordan, Pure Appl. Chem., 56 (1984) 1096.
41 L. Bjelica, R. Parsons and R.M. Reeves, Croat. Chem. Acta, 53 (1980) 211.
42 D. Laser and M. Ariel, J. Electroanal. Chem., 52 (1974) 292.
43 R.C. Engstrom, Anal. Chem., 54 (1982) 2310.
44 J. Wang and L.D. Hutchins, Anal. Chim. Acta, 167 (1985) 325.
45 J.-F. Hu, D.H. Karweik and T. Kuwana, J. Electroanal. Chem., 188 (1985) 59.
46 T. Nagooka and T. Yoshino, Anal. Chem., 58 (1986) 1037.
47 D.E. Weishaar and T. Kuwana, Anal. Chem., 57 (1985) 378.
48 L. Dunsch. Z. Chem., 19 (1979) 77.
49 D. Laser and M. Ariel, J. Electroanal. Chem., 52 (1974) 474.
50 H. Gunasingham and B. Fleet, Analyst, 107 (1982) 896.
51 D.E. Weisshaar and T. Kuwana, J. Electroanal. Chem., 163 (1984) 395.
52 Z. Stojek, University of Warsaw, personal communication.
53 N. Sleszynski, J. Osteryoung and M. Carter, Anal. Chem., 56 (1984) 130.
54 J. Wang and J.M. Zadeii, J. Electroanal. Chem., 249 (1988) 339.
55 M. Penczek and Z. Stojek, J. Electroanal. Chem., 191 (1985) 91.
56 Z. Yoshida and S. Kihara, J. Electroanal. Chem., 95 (1979) 159.
57 I. Morcos, J. Electroanal. Chem., 66 (1975) 250.
58 D. Jagner and K. Aren, Anal. Chim. Acta, 100 (1978) 375.
59 L. Renman, University of Göteborg, personal communication.
60 R.E. Panzer and P.J. Elving, J. Electrochem. Soc., 119 (1972) 864.
61 Z. Stojek and Z. Kublik, J. Electroanal. Chem., 105 (1979) 247.
62 W.R. Matson, D.K. Roe and D.E. Carritt, Anal. Chem., 37 (1965) 1594.
63 J.E. Anderson, D.E. Tallman, D.J. Chesney and J.L. Anderson, Anal. Chem., 50 (1978) 1051.
64 J. Wang, A. Brennsteiner, L. Angnes, A. Sylwester, R.R. LaGasse and N. Bitsch, Anal. Chem., 64 (1992) 151.
65 D.K. Roe and J.E.A. Toni, Anal. Chem., 37 (1965) 1503.
66 J. Wang, H.D. Dewald and B. Greene, Anal. Chim. Acta, 146 (1983) 45.
67 C. Wechter, N. Sleszynski, J.J. O'Dea and J. Osteryoung, Anal. Chim. Acta, 175 (1985) 45.
68 H. Gunasingham, B.T. Tay and K.P. Ang, Anal. Chem., 58 (1986) 1578.
69 N.F. Zakharchuk, N.A. Valisheva, I.G. Yudelevich and A.I. Zebrova, Zh . Anal. Khim., 36 (1981) 650.
70 K.Z. Brainina, Elektrohimiya, 16 (1980) 678.

71 R.B. Reust and A.M. Bond, Anal. Chim. Acta, 162 (1984) 389.
72 D. Jagner, M. Josefson and S. Westerlund, Anal. Chim. Acta, 128 (1981) 155.
73 C. Brihaye and G. Duyckaerts, Anal. Chim. Acta, 146 (1983) 37.
74 E.E. Stewart and R.B. Smart, Anal. Chem., 56 (1984) 1131.
75 J. Wang and L.D. Hutchins-Kumar, Anal. Chem., 58 (1986) 402.
76 G. Hoyer, T.M. Florence and G.E. Batley, Anal. Chem., 59 (1987) 1608.
77 B. Hoyer and T.M. Florence, Anal. Chem., 59 (1987) 2839.
78 M. Valcarcel and M.D. Luque de Castro, Non-Chromatographic Continuous Separation Techniques, Royal Society of Chemistry, Cambridge, 1991.
79 E. Martins and G. Johansson, Anal. Chim. Acta, 167 (1985) 111.
80 J.F. Van Staden and A. Van Rensburg, Analyst, 115 (1990) 1049.
81 W. Frenzel, unpublished results.
82 K.Z. Brainina and E.Y. Neiman, Solid Phase Reactions in Electroanalytical Chemistry, Khimia, Moscow, 1982.
83 T.R. Copeland, R.A. Osteryoung and R.K. Skogerboe, Anal. Chem., 46 (1974) 2098.
84 M.S. Shuman and G.P. Woodward, Anal. Chem., 48 (1976) 1979.
85 E.Y. Neiman, L.G. Petrova, V.I. Ignatoy and G.M. Dolgopolova, Anal. Chim. Acta, 113 (1980) 277.
86 A.L.B. Marques and G.D. Chierice, Talanta, 38 (1991) 735.
87 L. Renman, D. Jagner and R. Berglund, Anal. Chim. Acta, 188 (1986) 137.
88 G.G. Wallace, Trends Anal. Chem., 4 (1985) 145.
89 A.R. Fernando and J.A. Plambeck, Anal. Chem., 61 (1989) 2609.
90 J. Wang and H.D. Dewald, Anal. Chem., 56 (1984) 156.

Analytica Chimica Acta, 273 (1993) 139–144
Elsevier Science Publishers B.V., Amsterdam

Chemically modified field-effect transistors; potentiometric Ag^+ selectivity of PVC membranes based on macrocyclic thioethers

Zbigniew Brzozka, Peter L.H.M. Cobben and David N. Reinhoudt

Department of Organic Chemistry and MESA Research Institute, University of Twente, Enschede (Netherlands)

Jilles J.H. Edema, Jan Buter and Richard M. Kellogg

Department of Organic Chemistry, University of Groningen, Groningen (Netherlands)

(Received 17th June 1992)

Abstract

A chemically modified field-effect transistor (CHEMFET) with satisfactory Ag^+ selectivity is described. The potentiometric Ag^+ selectivities of CHEMFETs with plasticized PVC membranes based on macrocyclic thioethers have been determined. All the macrocyclic thioethers tested showed silver response and a selectivity towards Ag^+ and Hg^{2+} versus other interfering cations. The highest Ag^+ selectivity was obtained for a 14-membered cyclic tetrathioether with an exocyclic methylene group.

Keywords: Ion-selective electrodes; Potentiometry; CHEMFETs; Macrocyclic thioethers; PVC membranes; Silver

Macrocyclic thioethers have the ability to discriminate between closely related heavy metal ions based on the relative fit of the ligand cavity size to the metal ionic radius [1]. Taking advantage of their ion-discriminating ability, macrocyclic thioethers have been used as neutral carriers in ion-selective electrodes (ISE), especially for silver [2–5] and mercury [3,6]. However, there is no report of Ag^+-selective sensors based on chemically modified field-effect transistor (CHEMFET) devices. A CHEMFET combines the principle of detection by a membrane ISE with the solid-state integrated-circuit (IC) technology [7–11]. We have developed a CHEMFET technology based on a chemically attached poly(2-hydroxyethyl methacrylate) (polyHEMA) hydrogel interlayer between a hydrophobic membrane and the ISFET gate oxide insulator layer. This solves the problem of the thermodynamically ill-defined membrane/gate oxide interface and suppresses interference from carbon dioxide [10].

In this study, we have determined the potentiometric Ag^+ selectivities of CHEMFETs with plasticized PVC membranes containing macrocyclic thioethers. The effects of the membrane matrix, e.g, type of ionophore, amount of lipophilic salt, and different plasticizers have been investigated in detail. The structures of the ionophores used are depicted in Fig. 1.

Correspondence to: D.N. Reinhoudt, Department of Organic Chemistry and MESA Research Institute, University of Twente, P.O. Box 217, 7500 AE Enschede (Netherlands).

EXPERIMENTAL

Chemicals

High-molecular-weight PVC, bis(2-ethylhexyl)-phthalate (DOP), *o*-nitrophenyl octyl ether (*o*-

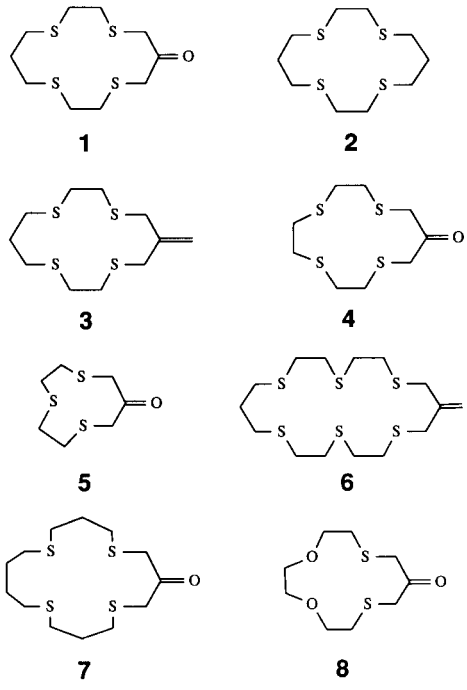

Fig. 1. Structures of the macrocyclic thioethers (ionophores **1–8**).

NPOE) and potassium tetrakis(4-chlorophenyl)-borate (KTpClPB) were obtained from Fluka. Tetrahydrofuran (THF) was freshly distilled from benzophenone–sodium before use. The nitrates of cadmium, calcium, copper, lead, mercury, potassium and silver used were of analytical-reagent grade (Merck). All solutions were made with doubly distilled and deionized water. Compounds **1, 4, 5, 7, 8** [12,13] and **2, 3, 6** [14] were prepared according to literature methods.

CHEMFETs

The ISFETs were fabricated as described previously [8]. The CHEMFETs used in this study contain an intermediate hydrogel layer of poly-HEMA between the gate oxide and the sensing membrane. The polyHEMA layer was anchored chemically to the gate oxide as described before [10,15]. CHEMFETs were encapsulated with epoxy resin (Hysol). Subsequently, the hydrogel layer was conditioned by immersion in buffered (pH 4) 0.1 M aqueous silver nitrate solution for 3–6 h prior to solvent casting. The membranes were made by solvent casting of a mixture of 33 mg of PVC, 65 mg DOP or *o*-NPOE, 2 mg of ionophore and 0.1–2 mg of KTpClPB (10–100 mol% with respect to the ionophore) in 1 ml of THF on mounted CHEMFETs and the THF was allowed to evaporate overnight. Before the measurements were started the membranes had been conditioned in 0.1 M aqueous silver nitrate solution for one night.

CHEMFET measurements

The CHEMFETs were measured in a constant drain-current mode ($I_d = 100\ \mu A$), with a constant drain-source potential ($V_{ds} = 0.5$ V) [16]. This was achieved using a source-drain follower type ISFET amplifier. The developed membrane potential was compensated by an equal and opposite potential (ΔV_{gs}) via the reference electrode. A saturated calomel electrode (SCE) was used as reference with a double junction containing 1.0 M potassium nitrate. Four CHEMFETs were monitored simultaneously and the data were collected and analyzed using an Apple IIe microcomputer. All experiments were performed in a dark and grounded metal box to eliminate interference by static and photosensitivity of the CHEMFETs. The potentiometric selectivity coefficients, $K_{i,j}^{pot}$, were determined by the Fixed Interference Method (FIM) [17]. The constant background concentrations of all interfering ions were 0.01 M at a constant pH 4. All concentrations were converted to activities using the extended Debye–Hückel equation [18]. The obtained response characteristics were analyzed according to the Nicolsky–Eisenman equation [19]

$$E = E^{o} + S \log\left[a_i + \sum K_{i,j}^{pot} a_j^{z_i/z_j}\right],$$

$$S = 2.303\ RT/z_i F$$

where all the symbols have their conventional meanings.

RESULTS AND DISCUSSION

The "real" blank membranes (only plasticizer and PVC) showed no selectivity at all for the ions used for interference studies. Two plasticizers

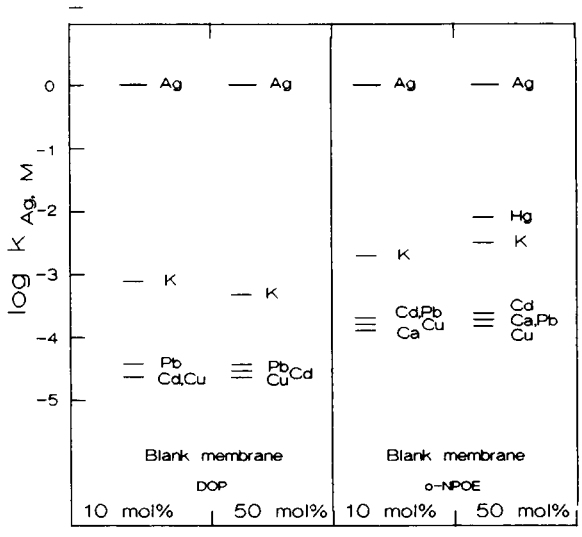

Fig. 2. Selectivity coefficients, log $K_{Ag,M}$, of blank membranes with different plasticizers and amounts of KT_pClPB.

were tested: the less polar di(2-ethylhexyl)-phthalate (DOP) and more polar *o*-nitrophenyl octyl ether (*o*-NPOE). Both types of membranes showed anionic response in case of Hg^{2+} titration with slopes of about 20 and 10 mV, respectively.

Blank (without ionophore) membranes but with lipophilic salt [potassium tetrakis(*p*-chlorophenyl)borate] gave good Ag^+ selectivity (Fig. 2). The selectivities versus divalent cations are almost the same for all membranes with different amounts of KTpClPB salt. The highest Ag^+ selectivities were found for membranes with the less polar plasticizer (DOP), because this will favour the extraction of monovalent rather than divalent cations. The CHEMFET responses were linear over about 1 decade (DOP) or 2 decades (*o*-NPOE) of silver activity with slopes of around 25–30 and 34–45 mV, respectively.

All tested macrocyclic thioethers showed silver response and a selectivity towards Ag^+ and Hg^{2+} versus other interfering cations. A typical silver response of a CHEMFET with a PVC membrane containing a 14-membered macrocyclic tetrathioether (**3**) is given in Fig. 3.

The size of the macrocyclic ring influences the Ag^+ selectivity although this effect is moderate. Based on the three thioethers with a carbonyl group in the ring, the small 10-membered trithioether (**5**) showed the highest Ag^+ selectivity versus al tested cations (Fig. 4). This conclusion is still preliminary because the number of sulphur atoms in the rings is different. Casabo et al. [4] have presented impressive Ag^+ selectivities of membrane ISE for Ag^+ versus Hg^{2+} with small macrocyclic thioethers in the membrane. A 17-membered tetrathioether (**7**) showed responses only for membranes with 50 mol% KTpClPB and even then its Ag^+ selectivity was only slightly better than of the 14-membered macrocy-

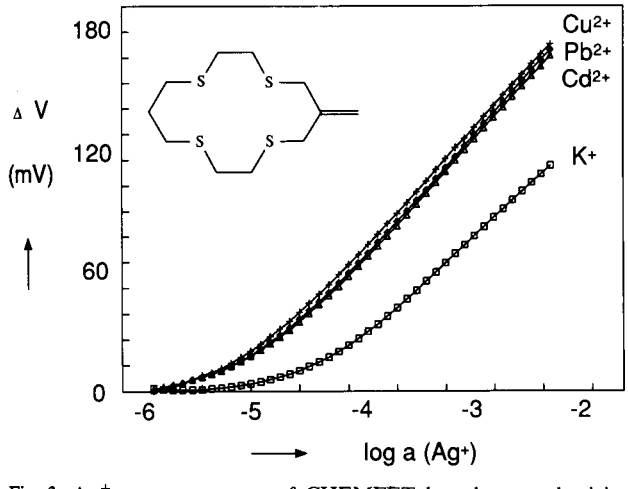

potentiometric selectivity

log $K_{i,j}$

K^+ 0.01	-3.2
Ca^{2+} 0.01	-4.5
Cu^{2+} 0.01	-4.8
Cd^{2+} 0.01	-4.8
Pb^{2+} 0.01	-4.7

Fig. 3. Ag^+-response curves of CHEMFET based on a plasticized PVC membrane containing 14-membered thioether **3** with respect to different interfering cations.

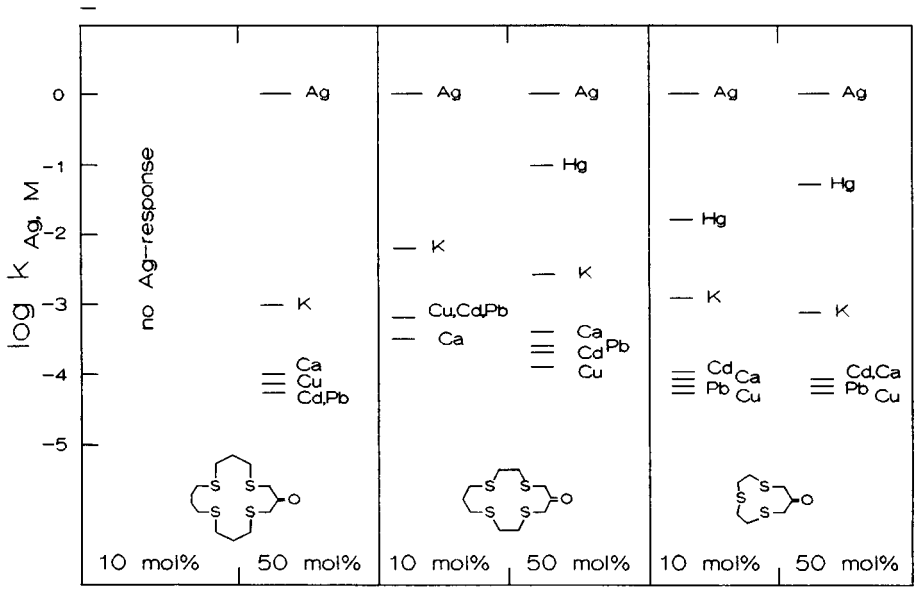

Fig. 4. Selectivity coefficients log $K_{Ag,M}$, of membranes based on macrocyclic thioethers with various ring size (ionophores **1**, **5**, and **7**) and different amounts of KTpClPB.

cle (**1**). The 13-membered ionophore (**4**) gave better Ag^+ selectivity versus tested cations, apart from potassium (Fig. 5), than the 14-membered macrocyclic (**1**).

Ionophores with a carbonyl group exhibited preference for Ag^+ over Hg^{2+}, but introduction of a carbonyl group lowers Ag^+ selectivity with respect to all the tested cations (Fig. 5). The

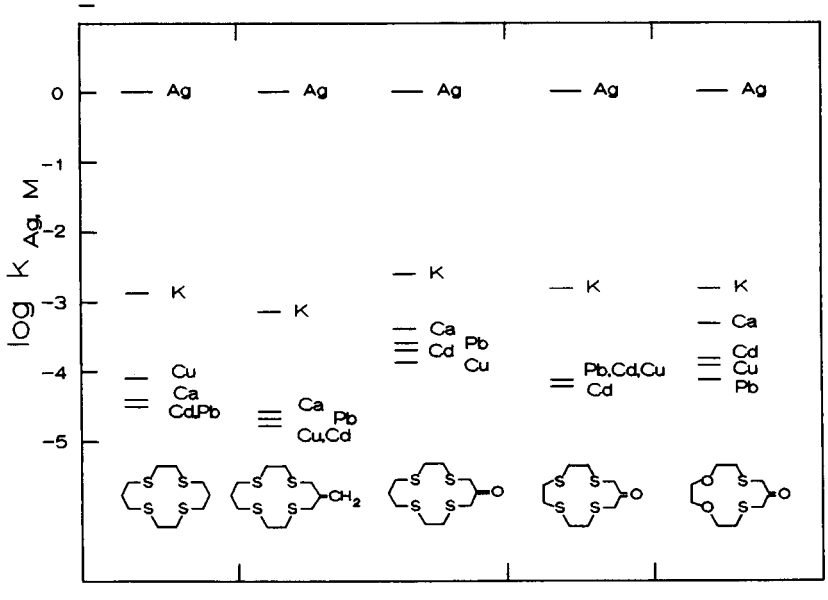

Fig. 5. Selectivity coefficients, log $K_{Ag,M}$, of membranes based on macrocyclic thioethers **1**, **2**, **3**, **4** and **8**. Membranes with 50 mol% of KTpClPB.

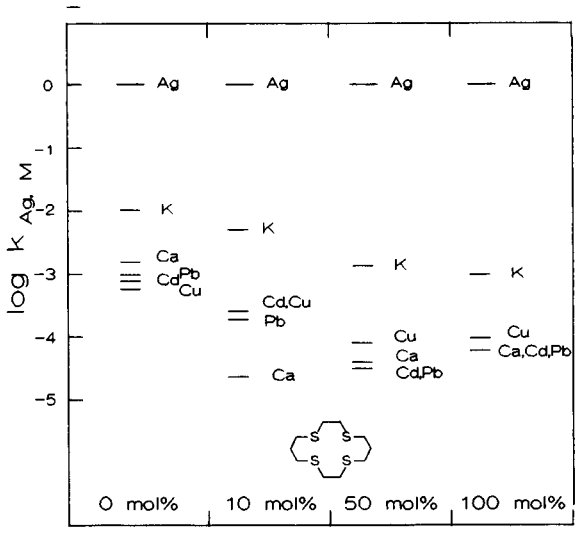

Fig. 6. Selectivity coefficients, log $K_{Ag,M}$, of membranes based on macrocyclic thioether **2** with different amounts of KTpClPB.

highest Ag^+ selectivity was obtained for the 14-membered tetrathioether (**3**) with an exocyclic methylene group. This group seems to cause the superior selectivity but an explanation for this phenomenon would need more variation in the macrocyclic thioether structures.

Substitution of two sulphur atoms in the ring by oxygen changes the behaviour of the ionophore significantly. The Ag^+ selectivity of ionophore **8** (Fig. 5) becomes worse, especially versus calcium, which has a preference for harder basic oxygen atoms.

Optimal CHEMFET composition

The amounts of lipophilic salt in the membranes does not have a significant influence on the Ag^+ selectivity (except for potassium), but it has a beneficial effect on the stability of the CHEMFET response. The membranes with 50 mol% of KTpClPB showed stable response values in measurements over 9 h contrary to the membranes containing 10 mol%. This indicates that the lipophilic salt is leaching from the membrane. It appears that the amount of lipophilic salt does not influence the Ag^+/Hg^{2+} selectivities.

In order to find the optimal membrane composition we have tested membranes with the 14-membered tetrathioether (**2**) in DOP and with different amounts of KTpClPB (0, 10, 50, 100 mol% with respect to the ionophore). The selectivity coefficients log $K_{Ag,M}$, are presented in Fig. 6. The best values were obtained with membranes that contain 50 mol% of KTpClPB.

Conclusions

Satisfactory Ag^+-selective CHEMFETs based on PVC membranes and macrocyclic thioethers have been realized. All tested macrocyclic thioethers show good Ag^+ sensitivity but not always a Nernstian response to the activity changes of Ag^+. An important role of lipophilic salt in the membrane with respect to its Ag^+ selectivity was observed. The presented macrocyclic thioethers are still unsufficiently lipophilic for long term applications of the designed sensors.

The authors thank the Technology Foundation (STW), Technical Science Branch of the Netherlands Organization for Advanced and Pure Research (NWO) for the financial support.

REFERENCES

1 R.D. Hancock and A.E. Martell, Chem. Rev., 89 (19989) 1875.
2 M. Oue, K. Akama, K. Kimura, M. Tanaka and T. Shono, Anal. Sci., 5 (1989) 165.
3 M.T. Lai and J.S. Shih, Analyst, 111 (1986) 891.
4 J. Casabo, L. Mestres, L. Escriche, F. Teixidor and C. Perez-Jimenez, J. Chem. Soc. Dalton Trans., (1991) 1969.
5 M. Oue, K. Akama, K. Kimura, M. Tanaka and T. Shono, J. Chem. Soc. Perkin Trans. 1, (1989) 1675.
6 J. Casabo, C. Perez-Jimenez, L. Escriche, S. Alegret, E. Martinez-Fabregas and F. Teixidor, Chem. Lett., (1990) 1007.
7 E.J.R. Sudhölter, P.D. van der Wal, M. Skowronska-Ptasinska, A. van den Berg and D.N. Reinhoudt, Sensors Actuators, 17 (1989) 189.
8 P.D. van der Wal, M. Skowronska-Ptasinska, A. van den Berg, P. Bergveld, E.J.R. Sudhölter and D.N. Reinhoudt, Anal. Chim. Acta, 231 (1990) 41.
9 D.N. Reinhoudt and E.J.R. Sudhölter, Adv. Mater., 2 (1990) 23.
10 E.J.R. Sudhölter, P.D. van der Wal, M. Skowronska-Ptasinski, A. van den Berg, P. Bergveld and D.N. Reinhoudt, Anal. Chim. Acta, 230 (1990) 59.
11 D.N. Reinhoudt, Sensors Actuators B, 6 (1992) 179.
12 J. Buter, R.M. Kellogg, F. van Bolhuis, J. Chem. Soc. Chem. Commun., (1990) 282.

13 J.J.H. Edema, J. Buter, F. van Bolhuis, A.L. Spek and W.J.J. Smeets, J. Org. Chem., submitted for publication.
14 J. Buter, R.M. Kellogg and F. van Bolhuis, J. Chem. Soc. Chem. Commun., (1991) 910.
15 E.J.R. Sudhölter, M. Skowronska-Ptasinska, P.D. van der Wal, A. van den Berg and D.N. Reinhoudt, Eur. Pat. Appl., 285, 591 (1986).
16 P. Bergveld, Sensors Actuators, 1 (1981) 17.
17 G.G. Guiltbault, Ion-Sel. Electrode Rev., 1 (1979) 139.
18 P.C. Meier, Anal. Chim. Acta, 136 (1982) 363.
19 W.E. Morf, The Principles of Ion-Selective Electrodes and of Membrane Transport, Studies in Analytical Chemistry 2, Elsevier, Amsterdam, 1981, p. 247.

Analytica Chimica Acta, 273 (1993) 145–152
Elsevier Science Publishers B.V., Amsterdam

Cyclic voltammetric experiments with plasticized PVC membranes

Viola Horváth and George Horvai

Technical University of Budapest, Institute for General and Analytical Chemistry, Gellért tér 4, 1111 Budapest (Hungary)

(Received 1st June 1992)

Abstract

Cyclic voltammetry, which is widely used in studying liquid/liquid interfaces, was applied to plasticized PVC-based membranes in order to understand the nature of ion transfer processes at the interfaces of the membrane. Dummy membranes containing a lipophilic salt additive (tetrahexylammonium tetraphenylborate) were examined with this method. By varying the tetrahexylammonium concentration of the bathing solution from 0 to 10^{-3} M, different behaviours of the interfaces could be observed with symmetric and asymmetric bathing.

Keywords: Voltammetry; Ion-selective membranes; Poly(vinyl chloride) membranes

The interface of two immiscible electrolyte solutions (ITIES) has been subject of much research recently. Theoretical studies were done in order to describe the equilibrium properties of the interface and the kinetics of ion transfer [1–4]. Much attention has been paid to the transfer of different alkali and alkaline earth metal ions facilitated by neutral carriers through the water/nitrobenzene interface [5–12]. These systems can serve as a model in the understanding of neutral carrier ion-selective electrode (ISE) performance. The working principles of liquid ion-exchanger membranes have also been studied on the basis of the ITIES theory [13,14]. However, the polarity of nitrobenzene differs considerably from that of conventionally used plasticizers and PVC–plasticizer systems. The stability of the nitrobenzene/water interface is also poor. It would therefore be more appropriate to study the ISE membrane/water interface directly. Recently several workers have used nitrobenzene solidified with PVC or agar-agar as the organic phase [15–17]. Sawada et al. [18] studied ion transfer across an oil/water interface, where the oil-phase solvent contained commonly used plasticizers, e.g., *o*-nitrophenyl octyl ether. It was separated from the aqueous phase by a hydrophilic membrane. These were better models for the ISE than the water/nitrobenzene interface.

The most frequently used electrochemical technique for studying ion transfer and for determining metal ion or carrier concentration in this way has been cyclic voltammetry (CV). Osakai et al. [19] used CV to study ion transfer across a polymer gel/liquid interface.

In this work, linear cyclic voltage scans were applied across plasticized PVC membranes. In this case both serially connected interfaces are polarized simultaneously but in opposite directions. Although the quantitative interpretation of the results becomes more difficult, the cyclic

Correspondence to: G. Horvai, Technical University of Budapest, Institute for General and Analytical Chemistry, Gellért tér 4, H-1111 Budapest (Hungary).

voltammograms resemble those of redox electrodes or ITIES and can be qualitatively interpreted.

The results presented in this paper are part of a study which was conducted in order to elucidate the behaviour of neutral carrier ion-selective membranes. This paper describes CV experiments with dummy membranes that contain no neutral carrier. In order to reduce the bulk resistance of these membranes, a lipophilic salt, tetrahexylammonium tetraphenylborate, was added during their preparation. This kind of salt (both the cation and the anion are lipophilic) was proposed by Horvai et al. [20] as an additive to neutral carrier ion-selective membranes to reduce bulk resistance. This type of salt is also widely used as the base electrolyte in the organic phase in experiments with ITIES.

EXPERIMENTAL

Apparatus

A Solartron—Schlumberger (Farnborough, Hampshire) Model 1286 electrochemical interface was used to carry out CV on the plasticized PVC based membranes in a two-electrode system. The IR drop of the membrane was compensated for by positive feedback. Large surface area Ag/AgCl electrodes were used as reference electrodes on both sides of the membrane. The data from the CV measurements were either recorded on a Hewlett-Packard (Santa Clara, CA) Model 7470A plotter or stored in the memory of an IBM AT compatible PC. Cyclic voltammograms were obtained by recording several cycles. In all the experiments a stationary state was reached after one or two cycles. The curves shown in the figures represent this stationary state.

Chemicals

The plasticizer *o*-nitrophenyl octyl ether (oNPOE), tetrahexylammonium chloride (THexACl), tetraphenylarsonium chloride (TPAsCl) and sodium tetraphenylborate (NaTPB) were obtained from Fluka (Buchs, Switzerland). The PVC powder used was Corvic S704 (ICI). Tetrahexylammonium tetraphenylborate (THexATPB) was prepared by precipitation from solutions of THexACl and NaTPB. Tetraphenylarsonium te-

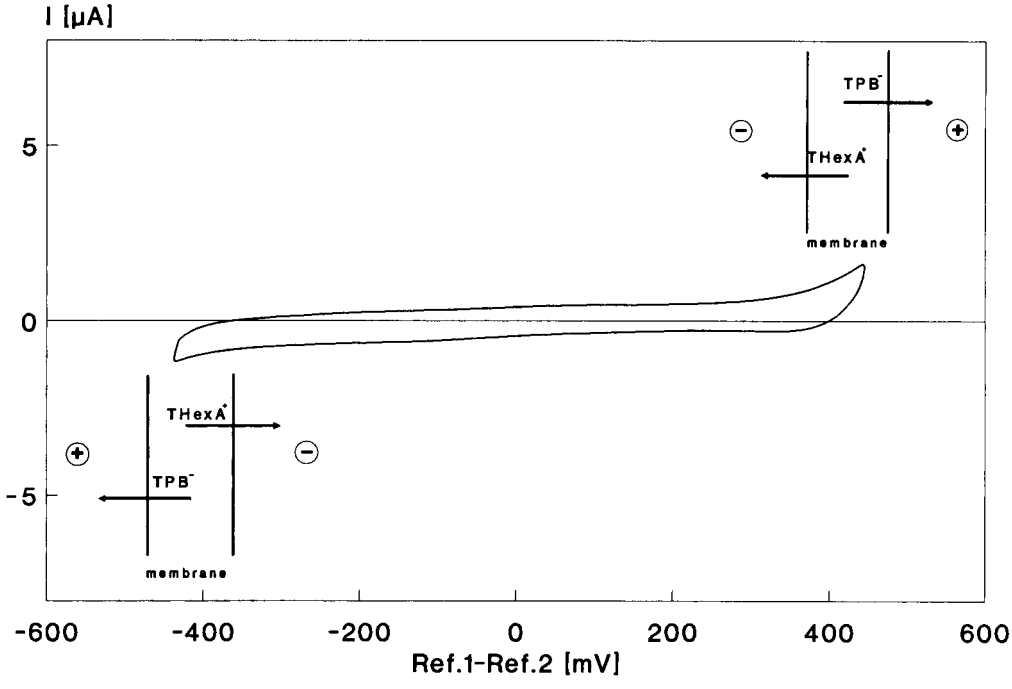

Fig. 1. CV curve of a dummy membrane in 10^{-3} M LiCl solution. Polarization rate: 10 mV s^{-1}.

traphenylborate (TPAsTPB) was prepared in the same way from the corresponding salts. All other chemicals were obtained from Reanal (Budapest) and were of analytical-reagent grade. Solutions were prepared using doubly distilled water.

Membranes

Dummy membranes were prepared by a small modification of the method of Craggs et al. [21]. The composition of the membranes was 33 mg of PVC, 66 mg of oNPOE and 0.6–0.7 mg (ca. 10^{-2} M) of lipophilic salt (THexATPB or TPAsTPB). The components were dissolved in 2 ml of tetrahydrofuran and were cast into a PTFE ring for drying for 1 day. The diameter of the membranes was 19 mm. The dry membranes were glued to the end of a PVC tube (Cole-Parmer, i.d. 15 mm, o.d. 21 mm) with tetrahydrofuran.

RESULTS AND DISCUSSION

The dummy membrane as an ideally polarizable electrode

The dummy membrane may be regarded, to a first approximation, as a thin layer of organic solvent with THexATPB dissolved in it at a concentration of about 10^{-2} M. From ITIES electrochemistry it was expected that both membrane/aqueous interfaces behave as ideally polarizable electrodes if the membrane is bathed symmetrically in a hydrophilic salt solution, e.g., 10^{-3} M LiCl. Hence the membrane as a whole is expected to behave as an ideally polarizable electrode. This expectation was confirmed as described in the next section and shown in Fig. 1.

A dummy membrane was bathed in 10^{-3} M LiCl on both sides. The resulting cyclic voltammogram and a schematic representation of the ion-transfer processes are shown in Fig. 1. The curve is completely flat in the range from ca. −400 to +400 mV. Only capacitive current flows through the membrane. At the two ends of the potential window the current starts to increase drastically. This current corresponds to the transfer of the ions of the lipophilic salt additive ($THexA^+$ and TPB^- ions) from the membrane phase to water. This was proved experimentally in the following way. A dummy membrane containing TPAsTPB was soaked in 10^{-3} M LiCl on both sides (TPAsTPB was used instead of THexATPB, because $TPAs^+$ is more convenient to determine). A constant current (+10 μA) was forced through the membrane for 15 min. After the current had been turned off, the TPB^- and $TPAs^+$ ion concentrations in the soaking solutions were determined spectrophotometrically. The total number of moles of the two ions found in the aqueous phases was equivalent to the charge carried by the current during the experiment.

The CV curve in Fig. 1 was rationalized as follows. The e.m.f. of the symmetrical cell is zero. The relationship between the interfacial potential and the activity of the ions in the organic and aqueous phases is given by the Nernst equation:

$$E^{w-o} = E_0^{w-o} + (RT/zF)\ \ln(a_o/a_w)$$

where E^{w-o} denotes the potential of the aqueous phase relative to the organic phase, E_0^{w-o} is the standard Galvani potential of the ion and a_o and a_w are the activities of the ion in the organic and aqueous phase, respectively (at the standard Galvani potential, the activity of the ion is identical in both phases). At the e.m.f., i.e., at zero polarization voltage, there are orders of magnitude less $THexA^+$ and TPB^- in the aqueous phase than in the organic phase because the interfacial potential is far from the standard Galvani potential of both ions. If the membrane is polarized with a small voltage, the potentials on either side of the membrane are still very far from the standard potentials but on one side of the membrane it moves closer to the standard potential of $THexA^+$ and on the other side to that of TPB^-. This means that some $THexA^+$ ions must be released to the aqueous phase on one side of the membrane and some TPB^- ions on the other. The concentration of these ions is still very low in the aqueous phase, and the faradaic current is negligible. When the polarization voltage approaches in either a positive or negative direction the sum of the absolute values of the standard Galvani potentials of $THexA^+$ and TPB^-, the current starts to increase dramatically and this will determine the size of the potential window.

The dummy membrane as a reversible electrode

Instead of the hydrophilic salt LiCl one could symmetrically soak the dummy membrane in aqueous solutions of a lipophilic salt having a common ion with the membrane electrolyte, e.g., in NaTPB or THexACl. If the concentration of the lipophilic ion in the aqueous phase is sufficiently high (e.g., 10^{-3} M), one can expect both interfaces to behave as reversible electrodes. This was indeed confirmed by the following experiments.

A dummy membrane was soaked in 10^{-3} M THexACl symmetrically. A cyclic voltammogram of this system and a schematic diagram of the ion-transfer processes are shown in Fig. 2. The polarization voltage was also applied symmetrically from −50 to +50 mV. The e.m.f. of the cell is zero. On the cyclic voltammogram the current increases almost linearly with increasing polarization voltage. The interfaces behave reversibly and $THexA^+$ ions can cross them freely without any apparent kinetic limitations. The $THexA^+$ ion concentration in each phase is fairly high so there is no mass transfer control either. The only factor that limits the current is the remaining ohmic resistance of the cell (the *iR* drop compensation never reaches 100%, because it would cause oscillation of the system). This results in the observed linear current–voltage dependence of the CV curve.

Current limited by diffusion in the aqueous phase

In the previous experiments it was found that the dummy membrane behaves as an ideally polarizable electrode if symmetrically bathed by a hydrophilic salt (LiCl) solution. Conversely, it shows reversible electrode behaviour when symmetrically bathed by relatively concentrated (10^{-3} M) THexACl. A logical next step would be to see if diffusion-limited current peaks can be obtained by lowering the concentration of THexACl.

This experiment was again done with symmetrical bathing at three different concentrations of THexACl. The resulting voltammograms are depicted in Fig. 3. Two peaks appeared around 0 mV, one during the forward and the other during

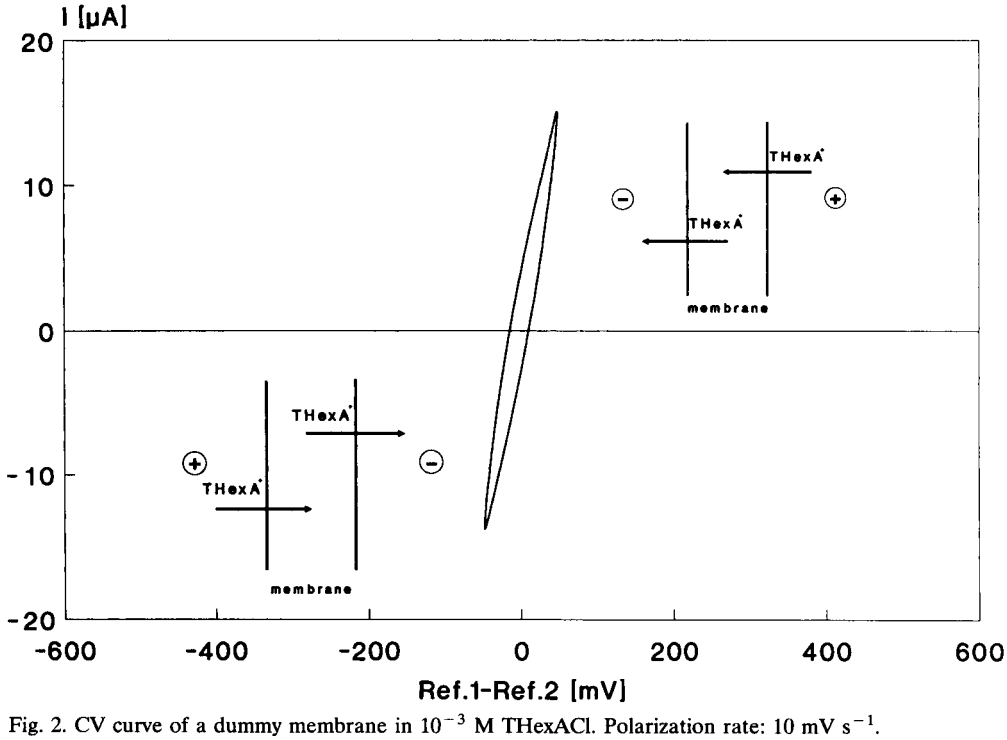

Fig. 2. CV curve of a dummy membrane in 10^{-3} M THexACl. Polarization rate: 10 mV s^{-1}.

the backward scan. The peaks were symmetrical and the peak heights depended linearly on the $THexA^+$ concentration. The peak heights also showed a linear dependence on the square root of the polarization voltage. Stirring the aqueous phase on both sides greatly increased the peaks. From these observations, it was concluded that $THexA^+$ ions entered the membrane phase at very low polarization voltages and their diffusion in the aqueous phase towards the surface of the electrode membrane limited the current.

The observations can be explained as follows. When equal concentrations of $THexA^+$ ions are added to the LiCl solution on both sides, the e.m.f. of the cell will remain zero. On the other hand, the equilibrium interfacial potential (the potential of the aqueous phase relative to the organic phase) on both sides shifts to a substantially more negative value, i.e., much closer to the standard Galvani potential of the $THexA^+$ ion. When the membrane is polarized with a small voltage, the potential at one of the interfaces shifts to a value which corresponds to a lower $THexA^+$ ion concentration than in the bulk water phase, while on the other side of the membrane the potential corresponds to a higher $THexA^+$ concentration since the two interfaces are connected in series with opposite polarity. This causes current to flow across the membrane. As the $THexA^+$ concentration in the aqueous phase is low (10^{-6}–10^{-4} M), after a short time the diffusion of $THexA^+$ in the aqueous phase towards the surface of the membrane will limit the current. On the other interface where $THexA^+$ ions move out to the aqueous phase, the current is not limited because the $THexA^+$ concentration in the membrane is fairly high.

Asymmetric bathing with one reversible interface

Based on the foregoing experiments, it appears feasible to study the diffusion-limited current at one side of the membrane only. This might be

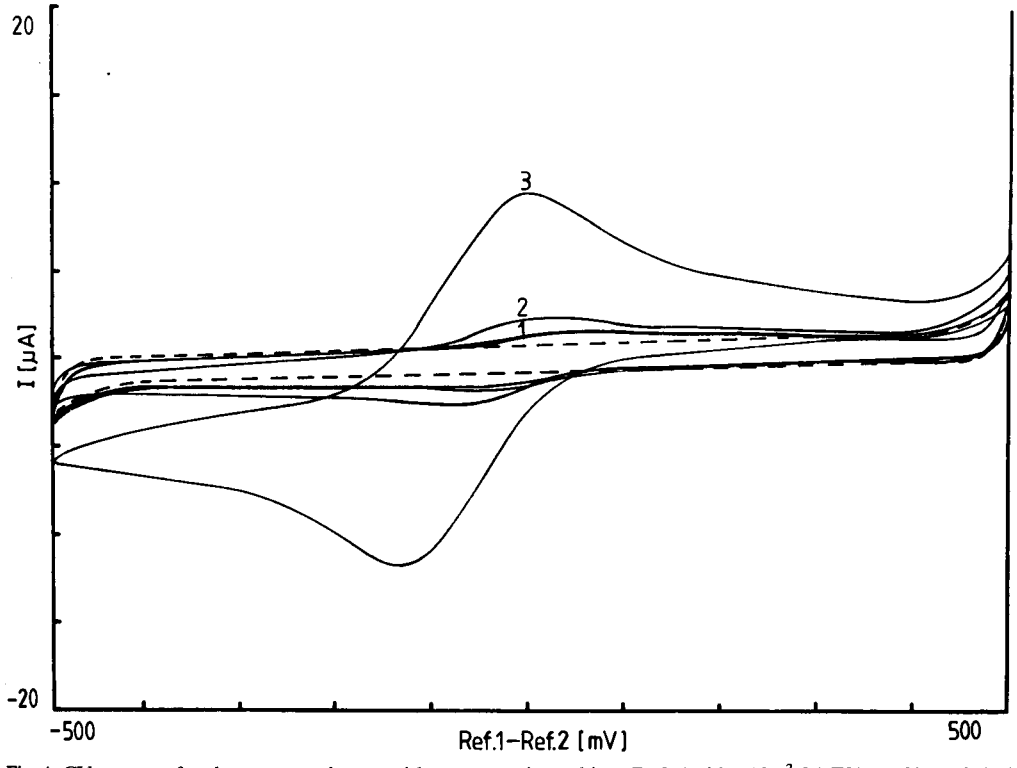

Fig. 4. CV curves of a dummy membrane with asymmetric soaking. Ref. 1 side: 10^{-3} M THexACl. Ref. 2 side: 1 (dashed curve), 10^{-3} M LiCl; 2, 10^{-3} M LiCl + 10^{-5} M THexACl; 3, 10^{-3} M LiCl + 5×10^{-5} M THexACl; 4, 10^{-3} M LiCl + 10^{-4} M THexACl. Polarization rate: 10 mV s^{-1}.

achieved by making the other side reversible. In other words, the membrane would be soaked asymmetrically. On one side of the membrane one would have high concentration (10^{-3} M) of a lipophilic salt, e.g., THexACl, to form a non-polarizable interface. On the other side the concentration of THexACl would be kept low enough to make the current diffusion limited.

Such an experiment was carried out with three different concentrations of THexACl in the base electrolyte (Fig. 4, solid lines). To be able to interpret the results, another experiment with no THexACl on the LiCl side was also performed and the result is shown in Fig. 4 (dashed line). Interestingly, the latter voltammogram is very similar to the other three. The current increases drastically when the THexACl solution is positive compared with the LiCl solution. The current remains low in the other polarization direction until ca. −540 mV is reached, then it starts to increase again. In this direction at −180 mV a peak can be observed even with pure LiCl. Stirring the pure LiCl solution during the sweep eliminates this peak and the membrane behaves as a polarizable electrode down to −540 mV. In contrast, when THexACl containing LiCl is stirred during a scan, the peak observed at −180 mV increases. The explanation of these experimental findings is described as follows.

The interface with high THexACl concentration in the aqueous phase behaves reversibly. When polarizing this side positively, $THexA^+$ ions enter the membrane from the 10^{-3} M THexACl solution and at the other interface $THexA^+$ ions of the membrane are released into the water, thus the current increases dramatically. Because during a half cycle they have insufficient time to diffuse away from the surface into the bulk of the aqueous phase, their concentration near the surface is high. Reversing the potential

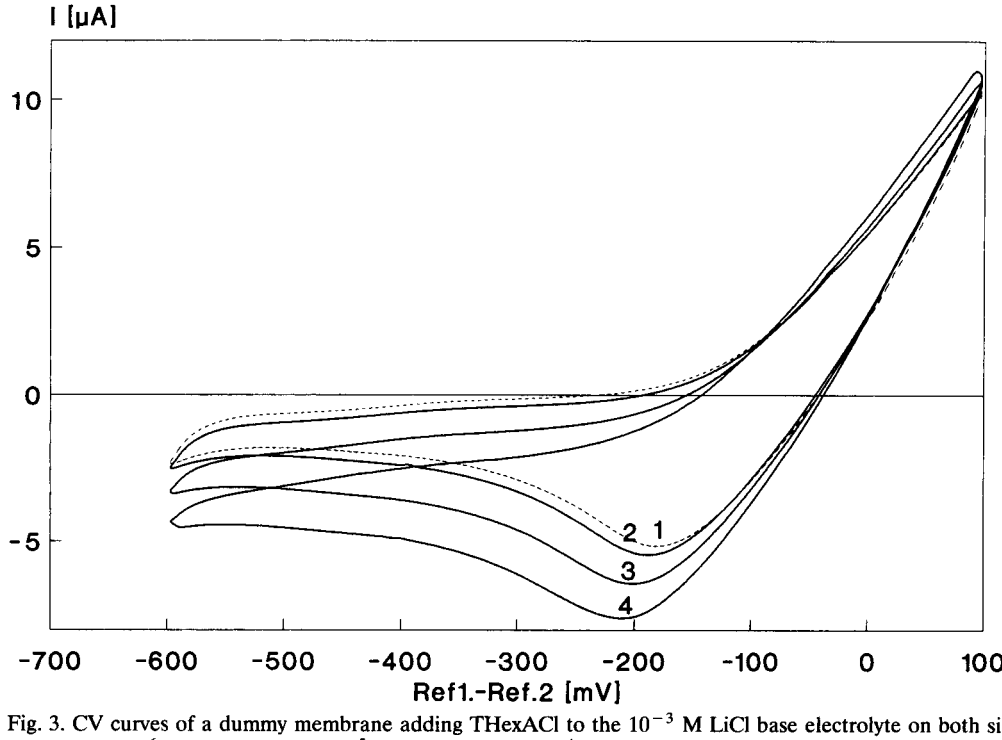

Fig. 3. CV curves of a dummy membrane adding THexACl to the 10^{-3} M LiCl base electrolyte on both sides. Dashed curve 10^{-3} M LiCl; 1, 10^{-6} M THexACl; 2, 10^{-5} M THexACl; 3, 10^{-4} M THexACl. Polarization rate: 20 mV s^{-1}.

scan, at low polarization voltages these accumulated $THexA^+$ ions go back into the membrane. They give a diffusion-controlled peak on the reverse scan even if there were no $THexA^+$ ions present in the LiCl before.

Adding small amounts of THexACl solution to the LiCl increases the peak which appears at ca. −180 mV. Now the bulk $THexA^+$ concentration of the LiCl solution combines with the accumulated $THexA^+$ to give a higher peak.

The results of this experiment show that the presence of a non-polarizable interface on one side of the membrane interacts with the processes on the other side. This interaction could be avoided if the membrane were polarized in only one direction, e.g., in the above experiment only in the direction with $THexA^+$ entering from the low-concentration side. Such experiments have no yet been done.

Asymmetric bathing with one ideally polarizable interface

One can now consider another type of asymmetric bathing: an ideally polarizable interface on one side of the membrane and a diffusion-limited system on the other.

Figure 5 shows the results with 10^{-3} M LiCl on one side of the dummy membrane and 10^{-3} M LiCl + 10^{-4} M NaTPB on the other. The effect of stirring on either side is also shown. At low polarization voltages TPB^- ions enter the membrane from the TPB^- solution, giving a diffusion-controlled peak. Stirring the aqueous solution on this side of the membrane increases the peak as expected (Fig. 5, curve 2). At the same time, TPB^- ions leave the membrane on the other side and accumulate near the surface. Only a small portion of them can diffuse away during a half cycle. During the reverse scan these ions go

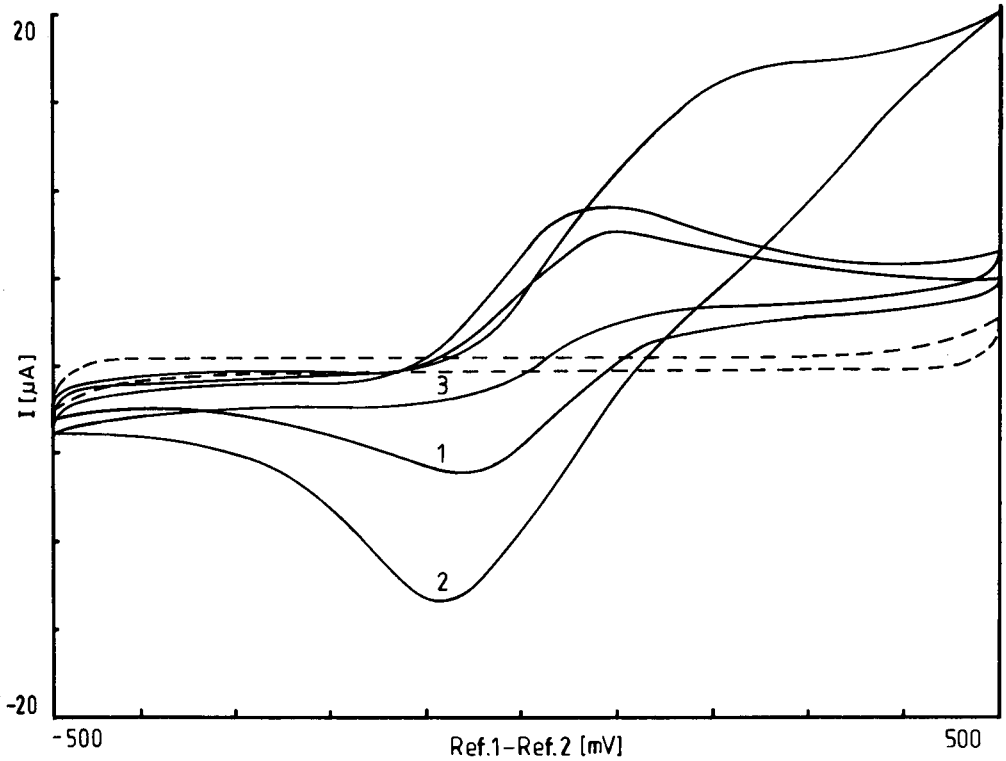

Fig. 5. CV curves of a dummy membrane in NaTPB. Ref. 1 side: 10^{-3} M LiCl. Ref. 2 side: 1, 10^{-3} M LiCl + 10^{-4} M NaTPB; 2, 10^{-3} M LiCl + 10^{-4} M NaTPB, stirring in Ref. 2 side; 3, 10^{-3} M LiCl + 10^{-4} M NaTPB, stirring in Ref. 1 side. Polarization rate: 10 mV s^{-1}.

back into the membrane, giving a current peak of reversed polarity. Stirring the solution on this side of the membrane prevents accumulation of the TPB^- ions near the surface so that the reverse peak disappears (Fig. 5, curve 3).

Conclusion

Plasticized PVC membranes identical in composition with ISE membranes can be studied by cyclic voltammetry. In this work a membrane composition without neutral carrier or ion exchanger (a dummy) was investigated. By changing the composition of the bathing solutions on either side of the membrane, CV curves characteristic of ideally polarizable, reversible or diffusion-limited electrodes could be obtained. The processes at the two interfaces are connected by the constraint that the absolute value of the current density must be identical on both sides. The observed CV curves could be qualitatively interpreted despite this difficulty. This work will also serve as a basis for the interpretation of ISE selectivity based on CV experiments. Work is in progress and results will be reported later. Similar problems are discussed in an article by Armstrong and Marcos [22], which was published while this paper was being reviewed.

REFERENCES

1 L.Q. Hung, J. Electroanal. Chem., 115 (1980) 159.
2 Z. Samec, J. Electroanal. Chem., 99 (1979) 197.
3 Z. Samec, Y.I. Kharkats and Y.Y. Gurevich, J. Electroanal. Chem., 204 (1986) 257.
4 H.H. Girault and D.J. Schiffrin, J. Electroanal. Chem., 195 (1985) 213.
5 M. Seno, K. Ivamoto and Q. Chen, Electrochim. Acta, 35 (1990) 127.
6 S. Kihara and Z. Yoshida, Talanta, 31 (1984) 789.
7 D. Homolka, L.Q. Hung, A. Hofmanova, M.W. Khalil, J. Koryta, V. Marecek, Z. Samec, S.K. Sen, P. Vanysek, J. Weber and M. Brezina, Anal. Chem., 52 (1980) 1606.
8 V. Marecek and Z. Samec, Anal. Chim. Acta, 151 (1983) 265.
9 Z. Sun and E. Wang, Talanta, 35 (1988) 673.
10 E. Wang and Y. Liu, J. Electroanal. Chem., 214 (1986) 459.
11 P. Vanysek, W. Ruth and J. Koryta, J. Electroanal. Chem., 148 (1983) 117.
12 T. Kakutani, Y. Nishiwaki, T. Osaki and M. Senda, Bull. Chem. Soc. Jpn., 59 (1986) 781.
13 T. Kakiuchi and M. Senda, Bull. Chem. Soc. Jpn., 57 (1984) 1801.
14 T. Kakiuchi, I. Obi and M. Senda, Bull. Chem. Soc. Jpn., 58 (1985) 1636.
15 V. Marecek and M.P. Colombini, J. Electroanal. Chem., 24 (1988) 133.
16 O. Dvorak, V. Marecek and Z. Samec, J. Electroanal. Chem., 284 (1990) 205.
17 H. Ji and E. Wang, Analyst, 113 (1988) 1541.
18 S. Sawada, T. Osakai and M. Senda, Bunseki Kagaku, 39 (1990) 539.
19 T. Osakai, T. Kakutani and M. Senda, Bunseki Kagaku, 33 (1984) E371.
20 G. Horvai, T.A. Nieman and E. Pungor, in E. Pungor (Ed.), Proceedings of the 4th Symposium on Ion-Selective Electrodes, Elsevier, Amsterdam, 1984, p. 439.
21 A. Craggs, G.J. Moody and J.D.R. Thomas, J. Chem. Educ., 51 (1974) 514.
22 R.D. Armstrong and M.L. Marcos, Electrochim. Acta, 37 (1992) 1021.

Analytica Chimica Acta, 273 (1993) 153–163
Elsevier Science Publishers B.V., Amsterdam

Barium ion-selective electrode based on a new neutral carrier complex

A.A. Bouklouze, J.-C. Viré and V. Cool

Free University of Brussels (ULB), Institute of Pharmacy, B-1050 Brussels (Belgium)

(Received 1st June 1992; revised manuscript received 4th September 1992)

Abstract

Three derivatives of a new class of ionophores belonging to the binaphthyl polyethers and exhibiting high lipophilicity were synthesized and evaluated as neutral carriers for the fabrication of a barium ion-selective electrode. The influence of the length of the ether side-chain and of the substitution of the amido group ending this side-chain on the complexing capability of barium ion is discussed. The ion-selective membrane was constructed by incorporating the selected ionophore in an ethylene–vinyl acetate copolymer which was previously dissolved in tetrahydrofuran. Nitrophenyl octyl ether was used as a plasticizer and a small amount of sodium tetraphenylborate was added as a lipophilic anion. The influence of the nature of the plasticizer and of the amount of incorporated ionophore on the characteristics of the electrode is discussed. The response of this electrode is linear in the range $0.1–3 \times 10^{-6}$ M with a slope of 30 mV per decade. The potential is not affected by pH modifications in the range 1.6–8.1. Selectivity coefficients determined for both monovalent and divalent cations show negligible interference from most of them. The electrode exhibits excellent potential stability and an operational lifetime of more than 5 months. Moreover, this electrode is not poisoned by copper(II) ions, in contrast with an ion-exchanger liquid membrane electrode, which exhibits a potential shift, or with a PVC membrane electrode, which requires in this instance a long recovery time. This electrode was applied successfully to the determination of sulphate ions in commercial mineral waters using potentiometric titration.

Keywords: Ion selective electrodes; Potentiometry; Titrimetry; Barium; Ethylene–vinyl acetate copolymer; Waters

Ionophore-impregnated polymer membranes [typically plasticized poly(vinyl chloride) (PVC) membranes] are widely used for the preparation of potentiometric ion-selective electrodes [1–4]. Considerable attention has been paid to the synthesis and characterization of ionophores in order to improve both the selectivity and detection limits [5,6]. Crown ethers synthetized first with structures similar to those of naturally occurring antibiotics have been used to prepare ion-selective membrane electrodes [7,8]. Two wide classes of neutral carrier ionophores are generally recognized: acyclic [5,9,10] and cyclic [11,12] molecules. It appears from the literature that several acyclic diamide and dioxadiamide ionophores have been extensively investigated for use in cation-selective electrodes, some of them exhibiting high selectivity [13–16]. Among these neutral lipophilic organic complexing agents [17,18], different molecules showing a higher affinity for barium ions than for alkali and other alkaline earth metal cations have been proposed for the preparation of barium-selective electrodes, including ion-pair materials [19–21].

In this study, three derivatives (I–III) of a new class of ionophores belonging to the naphthyl polyether family have been synthetized and incorporated in an ethylene–vinyl acetate copolymer

Correspondence to: J.-C. Viré, Free University of Brussels (ULB), Institute of Pharmacy, Campus Plaine, C.P. 205/6, Bd. du Triomphe, B-1050 Brussels (Belgium).

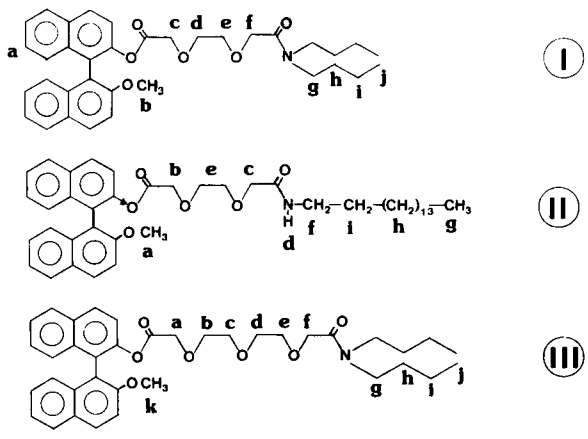

to be evaluated for the potentiometric analysis of barium ions. The electrode was applied to the determination of sulphate ions in commercial mineral waters using potentiometric titration.

EXPERIMENTAL

Reagents

The ethylene–vinyl acetate (EVA) used (Levapren 400, Bayer) contains 40% (w/w) of the vinyl acetate monomer.

2-Nitrophenyl octyl ether (NPOE) and bis(1-butylphenyl) adipate (BPA) (Fluka), bis(2-ethylhexyl) sebacate (EHS) and dioctylphenyl phosphonate (DOPP) (Aldrich), nitrobenzene (NB) and dioctyl phthalate (DOP) (Janssen) were evaluated as plasticizers. Sodium tetraphenylborate (TPB) and tetrahydrofuran (THF) (Merck) were used as lipophilic salt and solvent, respectively.

Metal cations, selected as chloride salts, were dissolved in water purified with a Milli-Q system (Millipore) and standard solutions were prepared from 1 M stock solutions by sequential dilution with Milli-Q-purified water.

Synthesis of the ionophores

Infrared spectra were recorded with a Perkin-Elmer Model 237 spectrometer. ^{1}H NMR spectra were recorded with a Bruker VM 250 spectrometer at 250 MHz; tetramethylsilane (TMS) was used as internal standard in $CDCl_3$ solutions. Mass spectra were recorded using a VG Micromass 7070 F mass spectrometer. Thin-layer chromatography (TLC) was carried out on Polycram Sil G/UV 254 0.25-mm plates. Flash chromatography was effected using Fluka Kieselgel (40–63 μm).

Solvents and reagents were purified as described previously [22]. Organic extracts were dried with magnesium sulphate and concentrated by using a rotary evaporator.

The following spectral data are given: NMR, chemical shift in ppm (multiplicity [singlet, doublet, triplet, multiplet, AB], number of protons, proton type); and MS, *m/z* (relative intensity, %).

8-Amido-N,N-dibutyl-3,6-dioxaoctanoic acid (A). Under nitrogen at −20°C, 100 ml of anhydrous THF and 12.1 ml of 4-*N*-methylmorpholine are mixed slowly, then 13.1 ml ethyl chloroformate and 19.6 g of 3,6-dioxaoctanedioic acid [23] dissolved in 125 ml of THF are added. The mixture is heated at 20°C for 10 min and cooled at −40°C before addition of 18.5 ml of di-*n*-butylamine. Stirring is maintained for 20 h at room temperature. After reaction, 250 ml of ethyl acetate are added. The organic layer is washed with 5% (v/v) HCl. The HCl solutions are washed three times with 50 ml of ethyl acetate. The organic layer is extracted three times with 50 ml of 5% (v/v) $NaHCO_3$, which after acidification is extracted with diethyl ether. After removal of the solvent, 15.21 g of A are obtained (yield 48%).

8-Amido-N-hexadecyl-3,6-dioxaoctanoic acid (B). The same procedure as for A gives B in 15% yield.

11-Amido-N,N-dibutyl-3,6,9-trioxaundecanoic acid (C). The same procedure as for A gives C in 16% yield.

8-Amido-N,N-dibutyl-3,6-dioxactanoic acid, (2'-methoxy-1',1''-binaphthyl-2') ester (ionophore I). A 5.5-mmol amount of A is dissolved in 5 ml of THF. Under nitrogen at −15°C and with stirring are added successively 0.77 ml of triethylamine and 0.53 ml of ethyl chloroformate. After stirring for 10 min, 5.5 mmol of 2-hydroxy-2'-methoxy-1,1'-binaphthyl dissolved in 3 ml of THF

are added. After 2 days, the reaction mixture is extracted with diethyl ether in the presence of 5% (v/v) sodium carbonate and water. After washing the ether phase, removal of the solvent gives 527 mg of ionophore I after column chromatographic purification [$CHCl_3$–diethyl ether (19:1); $R_F = 0.23$]. The yield is 17%.

^{1}N NMR: 7–8 (m, 12H, aromatic H), 4.10 and 4.05 (AB, $J = 16$ Hz, 2H, f), 3.85 and 3.71 (AB, $J = 16$ Hz, 2H, c), 3.72 (s, 3H, b), 3.43 and 3.41 (AB, $J = 4$ Hz, 2H, d or e), 3.28 (t, $J = 7.4$ Hz, 2H, g and d or e), 1.49 (m, 4H, h), 1.28 (m, 4H, i), 0.91 (t, $J = 7.2$ Hz, 3H, j), 0.90 (t, $J = 7.2$ Hz, 3H, j).

MS ($C_{35}O_6NH_{41}$): 571 ($M^{+\cdot}$, 1), 313 (2), 301 (35), 300 (100), 293 (15), 285 (23), 272 (36), 269 (18), 268 (52), 257 (14), 244 (84), 239 (36), 229 (16), 228 (17), 226 (20), 216 (100), 215 (25), 167 (21), 156 (28) 149 (100).

IR (neat, cm^{-1}): 3020 (C–H arom.), 2900 (C–H aliph.), 1760 (CO ester), 1625 (CO amide), 1593, 1440 (ring C=C), 1250 (C–O–C asym.), 1100–1160 (C–O–C sym.), 803, 742 (C–H).

TLC: $R_F = 0.23$ [$CHCl_3$–diethyl ether (19:1)].

8-Amido-N-hexadecyl-3,6-dioxaoctanoic acid, (2"-methoxy-1',1"-binaphthyl-2') ester (ionophore II). The same procedure as for ionophore I gives ionophore II in 18% yield.

^{1}H NMR: 7–8 (m, 12H, aromatic H), 4.13 and 3.90 (AB, $J = 4.7$ Hz, 2H, c), 3.87 and 3.68 (AB, $J = 17$ Hz, 2H, b), 3.83 (s, 1H, d), 3.74 (s, 3H, a), 3.32 (t, $J = 4.4$ Hz, 2H, f), 3.20 (m, 2H, e), 3.0 (m, 2H, e), 1.4 (m, 2H, i), 1.26 (m, 26H, f), 0.88 (m, 3H, g).

MS ($C_{43}O_6NH_{57}$): 685 ($M^{+\cdot}$ +2.1), 684 ($M^{+\cdot}$ +1.6), 683 ($M^{+\cdot}$ 13) 457 (2), 429 (6), 384 (3), 357 (8), 356 (33), 354 (4), 327 (17), 326 (19), 325 (9), 324 (6), 301 (23), 300 (100), 298 (12), 268 (33).

IR (neat, cm^{-1}): 3340 (N–H amide I), 3020 (C–H arom.), 2820–2900 (C–H aliph.), 1795 (CO ester), 1645 (CO amide II), 1593 (ring C=C), 1100 (C–O–C), 740, 803 (C–H).

TLC: $R_F = 0.14$ [$CHCl_3$–diethyl ether (19:1)].

11-Amido-N,N-dibutyl-3,6,9-trioxaundecanoic acid, (2"-methoxy-1',1"-binaphthyl-2') ester (ionophore III). The acyl chloride of C (4.2 mmol) is prepared by the action of oxalyl chloride (with one drop of triethylamine) in CH_2Cl_2 for 24 h. The solvent must be removed without heating (rotary evaporator) and the freshly prepared acyl chloride is dissolved in 10 ml of CH_2Cl_2. This solution is added to a 50 ml CH_2Cl_2 solution of 2-hydroxy-2'-methoxy-1,1'-binaphthyl (7.2 mmol) at −10°C. After stirring for 24 h at room temperature, 1 ml of triethylamine is added. The reaction mixture is treated as for ionophore II. Flash chromatography gives ionophore III (829 mg) in 32% yield.

^{1}H NMR: 7–8 (m, 12H, aromatic H), 4.15 (m, 2H, f), 3.84 and 3.69 (AB, $J = 17$ Hz, 2H, a), 3.74 (s, 3H, k), 3.57 (m, 4H, c and d), 3.49 (m, 4H, g), 3.32 (m, 2H, b), 3.06 (m, 2H, e), 1.58 (m, 4H, h), 1.31 (m, 4H, i), 0.92 (t, $J = 7.2$ Hz, 6H, j).

MS ($C_{37}O_7NH_{45}$, chemical ionization with NH_3): 633 ($MH^{+\cdot}$ + NH_3, 2), 617 ($MH^{+\cdot}$ + 1.3), 586 (1), 570 (3), 488 (2), 484 (10), 483 (8), 482 (26), 465 (15), 464 (48), 462 (5), 448 (9), 446 (10), 438 (8), 420 (10), 385 (6), 376 (4), 360 (5), 341 (12), 300 (37), 299 (23), 290 (6), 276 (8), 130 (100).

IR (neat, cm^{-1}): 3020 (C–H arom.), 2860, 2920 (C–H aliph.), 1765 (CO ester), 1720 (CO amide), 1590 (ring C=C), 1250 (C–O–C asym.), 1110 (C–O–C sym.), 803, 742 (C–H).

Electrode fabrication

The polymeric membranes were constructed by dipping the end of a micropipette tip into the polymeric solution prepared as follows: EVA (30 mg), plasticizer (1 ml), individual binaphthyl neutral carrier (7–21 mg) and TPB (0.5–1 mg) were dissolved in 0.5 ml of THF and the solution was sonicated to ensure homogeneity. After drying for about 2 h, the micropipette was filled with 0.1 M barium chloride as the internal reference solution and a silver wire coated with silver chloride was used as the internal reference electrode. Before use, the electrode must be conditioned overnight by soaking it in 0.1 M barium chloride solution in order to ensure equilibrium at the membrane–water interface [22,24].

Potential measurements

Potentiometric measurements were performed at room temperature using a Tacussel Minisis 6000 millivoltmeter, against a saturated calomel

reference electrode (SCE). The representative electrochemical cell is:

Ag/AgCl	0.1 M $BaCl_2$	polymeric membrane	sample	SCE

The response of the neutral carrier electrode assembly was examined according to a previously described procedure [25]. Unbuffered solutions and solutions buffered at pH 7 using 0.1 M tris(hydroxymethyl)aminomethane hydrochloride were investigated. Calibration graphs were plotted as observed potential against the logarithm of the primary ion activity (Fig. 1).

The activity coefficients were evaluated by means of the Debye–Hückel equation [26,27]:

$$-\log \gamma_i = \frac{AZ^2\mu^2}{1 + Bb\mu^{1/2}}$$

where A and B were taken to be 0.51 and 0.33, respectively ($T = 25°C$, water) [27], and b is the ion size parameter, which is the effective diameter of the hydrated ion in angströms.

The LC determination of the sulphate content of mineral water samples was performed using a Wescam liquid chromatograph equipped with an Anion/HS 269-013 column and a Wescam 213 A conductimeter. The integrator was a Hewlett-

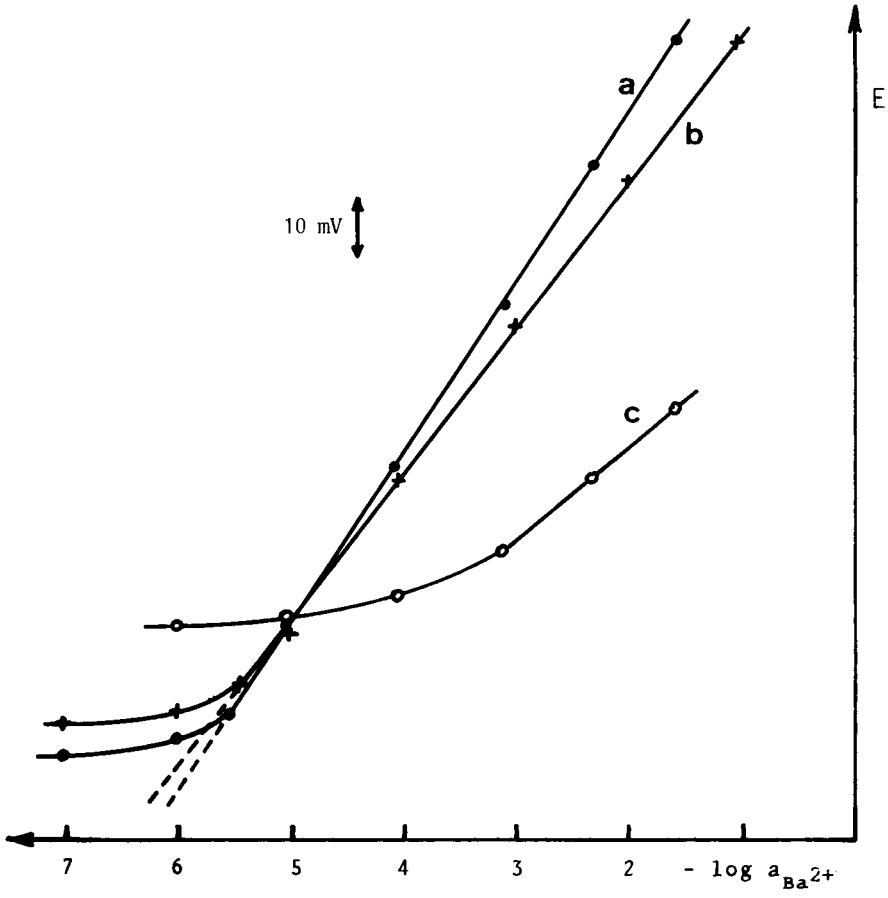

Fig. 1. Calibration graphs for the ionophore I-based electrode. (a) Unbuffered solution with TPB; (b) buffered solution (0.1 M Tris–HCl) (pH 7) with TPB; (c) unbuffered solution without TPB.

Packard Model 5880 A GC terminal. The eluent was 4×10^{-3} M potassium hydrogenphthalate solution prepared with Milli-Q-purified water. A calibration graph was plotted between 4.0 and 60.0 mg l^{-1} of sulphate ions.

RESULTS AND DISCUSSION

Owing to its low glass transition temperature and the wide range of solvents in which it can dissolve, the use of ethylene–vinyl acetate copolymer has been proposed previously as a membrane matrix for the construction of calcium ion-selective electrodes [25] and for the fabrication of potentiometric sensors selective to local anaesthetic compounds [28]. An improved selectivity over copper and zinc ions has been pointed out, other characteristics, i.e., sensitivity, slope and pH effects, being similar to those observed with a PVC membrane. These results suggested the selection of this copolymer for the barium-selective electrode described here.

Optimization of membrane composition

The influence of the nature of the plasticizer on the performances of the three electrodes based on the neutral carriers I, II and III was investigated first. Four types of plasticizers were tested: NPOE, as the phenyl ether mediator; DOP, EHS and BPA, representing the diester derivatives; DOPP, belonging to the phosphate compounds; and NB, which is a nitroaromatic molecule. The response characteristics of each electrode are given in Table 1.

It appears that the ionophore I-based electrodes exhibit the widest linearity ranges, the lowest detection limits and, in most instances, a Nernstian response. Comparing the activities of the plasticizers, the best performances were obtained using NPOE, DOPP and NB. Electrodes containing ester solvents also provide good sensitivity and detection limits but only a nearly Nernstian response; those containing EHS give poor and erratic responses.

By incorporating ionophore II, each electrode exhibits acceptable results but poorer than those observed with ionophore I. A similar evolution of the slope as a function of the nature of the plasticizer is observed with the ionophore I- and II-based electrodes. The last set of electrodes, which contain ionophore III, provide no response, except those associated with the DOPP plasticizer, which exhibit a low slope and a restricted linearity range. Moreover, this last sensor gives a Nernstian response (29 mV per decade) to calcium ions activity changes in the range 10^{-4}–0.1 M.

The above results can be interpreted in terms of the structure and solubility of the neutral carrier in the plasticizer. Ionophore I, which is freely soluble in all the mediators investigated, provides higher performances than ionophore II, which is only slightly soluble. The erratic response observed with EHS may result from its specific interaction with ionophore I.

The influence of the structure of the three ionophores on the characteristics of the electrodes can be interpreted by the capability of binding barium ions reversibly and transporting

TABLE 1

Characteristics of the electrodes based on ionophores I, II and III with various plasticizers [a]

Plasticizer	Ionophore I				Ionophore II				Ionophore III			
	S	LR	DL	*r*	*S*	LR	DL	*r*	*S*	LR	DL	*r*
NPOE	30.0	$0.1–3 \times 10^{-6}$	2×10^{-6}	0.9999	26.0	$0.1–1 \times 10^{-5}$	6×10^{-6}	0.9990	No response			
NB	31.0	$0.1–3 \times 10^{-6}$	3×10^{-6}	0.9999	28.7	$0.1–4 \times 10^{-5}$	2×10^{-5}	0.9941	No response			
DOPP	28.9	$0.1–6 \times 10^{-6}$	3×10^{-6}	0.9996	23.5	$0.1–1 \times 10^{-4}$	2×10^{-5}	0.9976	15.0	$0.1–1 \times 10^{-4}$	2×10^{-5}	0.9961
BPA	22.0	$0.1–6 \times 10^{-6}$	3×10^{-6}	0.9957	20.6	$0.1–7 \times 10^{-4}$	5×10^{-4}	0.9974	No response			
EHS	Poor and erratic response				22.4	$0.1–4 \times 10^{-5}$	2×10^{-5}	0.9964	No response			
DOP	23.0	$0.1–6 \times 10^{-6}$	4×10^{-6}	0.9989	24.5	$0.1–1 \times 10^{-3}$	2×10^{-4}	0.9932	No response			

[a] *S* = slope (mV per decade); LR = linear range (M); DL = detection limit (M) (determined by *S* log 2 [25]); *r* = correlation coefficient.

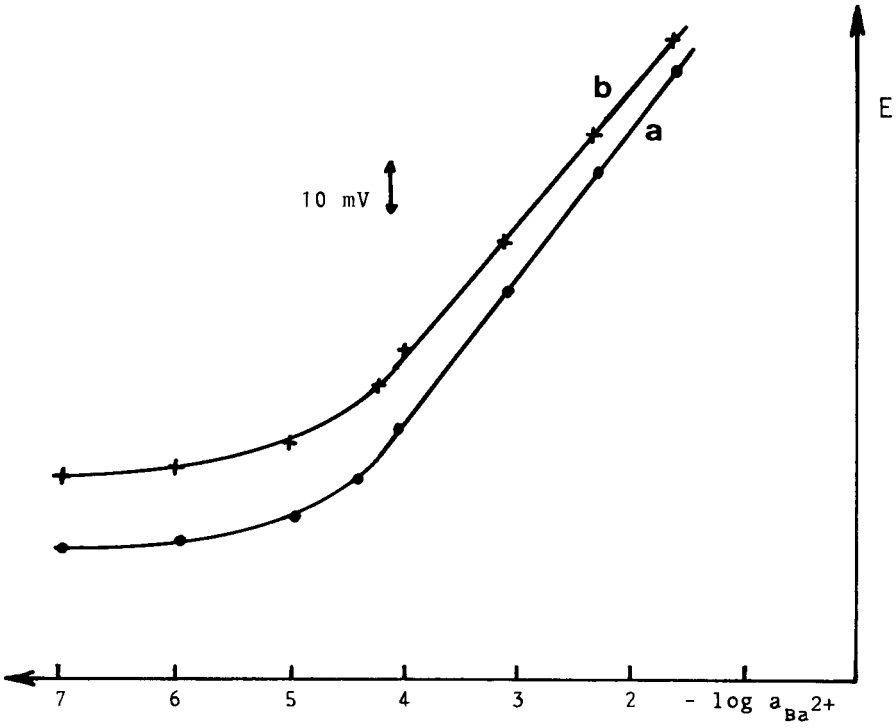

Fig. 2. Calibration graphs for the ionophore II-based electrode. (a) Unbuffered solution with TPB; (b) unbuffered solution without TPB.

them across the organic membrane by carrier translocation. From the above results, and considering the length of the ether side-chain and the substitution of the amido group ending this side-chain, the structure of ionophore I is convenient for achieving this property and making the membrane permeable to barium ions only.

The addition of sodium tetraphenylborate to an ion-selective membrane phase was shown to be favourable in many respects, giving rise to a reduction in the interferences from lipophilic sample anions, an increase in the potentiometric selectivity for divalent over monovalent cations and a reduction in the response time and in the membrane electric resistance [5,29–31]. Tetraphenylborate seems to work as an ion-transfer catalyst which lowers the activation energy for the ion-transfer process between the aqueous phase and the membrane phase [32].

Figs. 1 and 2 show the potential response to barium ions of electrodes based on ionophores I and II, with and without TPB. It appears that the

TABLE 2

Influence of ionophore I concentration on the characteristics of the barium ISE (NPOE plasticizer)

Parameter	Amount of ionophore I (mg)			
	0.9	3.0	7.0	21.0
Slope (mV per decade)	18.5	27.5	30.0	30.0
Linear range (M)	$0.1–1 \times 10^{-4}$	$0.1–1 \times 10^{-4}$	$0.1–3 \times 10^{-6}$	$0.1–3 \times 10^{-6}$
Correlation coefficient (r)	0.9998	0.9995	0.9999	0.9999

membranes devoid of the lipophilic salt provide lower performances (slope and linear range) and a less stable potential.

The above examination of the membrane composition indicates that the combination of ionophore I with the NPOE plasticizer and TPB, incorporated in the EVA matrix, can be regarded as the optimum system for barium determination and this membrane was studied in greater detail.

The effect of the amount of neutral carrier incorporated in the membrane on the electrode characteristics was investigated. Increasing the ionophore concentration generally enhances both sensitivity and selectivity [33,34]. This was also verified here.

Table 2 shows that the performance of the electrode is improved by increasing the amount of the incorporated ionophore to 7 mg (see the polymeric solution preparation in *Electrode fabrication* above). A further increase (21 mg) does not modify these characteristics and the amount of 7 mg was selected for further investigations. The calibration graphs shown in Fig. 1 were established using the above conditions, demonstrating that this sensor can cover a wide linear range in both buffered (0.1 M Tris–HCl, pH 7) and unbuffered solutions.

Table 3 summarizes the characteristics of the electrode described and compares them with those of previously reported barium sensors, including a commercial ISE (EDT Analytical). Each parameter of our electrode can be favourably compared, especially with those of the commercial electrode. However, similarities appear when comparisons are made with an ionophore-based electrode [17].

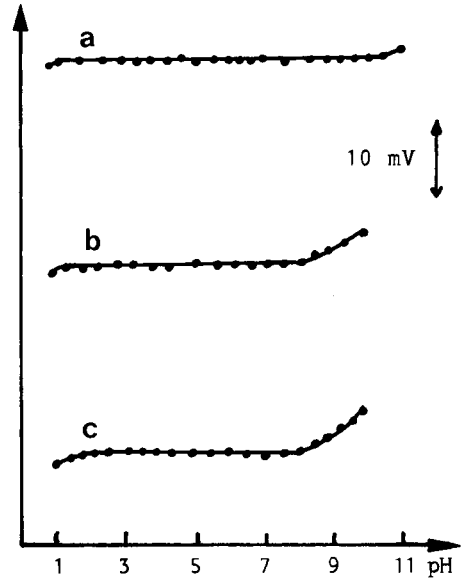

Fig. 3. Influence of pH on the EVA–I–NPOE electrode response in buffered solution. $BaCl_2$ concentration: (a) 0.1 M; (b) 0.01 M; (c) 0.001 M.

The response time of the EVA–I–NPOE electrode is very rapid. Stabilization of the potential is observed after several seconds in the $0.1–10^{-4}$ M range and does not exceed 1 min in more dilute solutions.

For analytical purposes, the sensitive membrane should have as long a lifetime as possible. The lifetime is generally related to the lipophilicity of the ion carrier and of the plasticizer [33].

TABLE 3

Characteristics of the ionophore I barium ISE compared with those of other barium-selective electrodes

Parameter	Electrode					
	EVA–I–NPOE (this study)	Electrodes reported (ref.)				
		[21]	[19]	[20]	[17]	EDT [a]
Lower limit of linear range (M)	3×10^{-6}	2×10^{-5}	1×10^{-5}	9×10^{-6}	8×10^{-6}	7×10^{-5}
Slope (mV per decade)	30.0	58.9	26.6	28.0	32.0	
pH range	1.6–8.1		2–10	1.5–10	2–8	5–9
Detection limit (M)	2×10^{-6}		3×10^{-6}			5×10^{-5}

[a] Commercial electrode from EDT Analytical (London).

Our electrode exhibits an operational lifetime of more than 5 months, indicating the high lipophilicity of ionophore I and of the NPOE plasticizer. It should be noted that, while exhibiting similar performance (Table 1), the use of the NB mediator greatly decreases the lifetime of the electrode. The electrode response is reproducible from day to day, with a potential drift of less than 0.06 mV h^{-1}.

Effect of pH. The influence of pH on the electrode potential was investigated using 0.1–0.001 M solutions. The pH was adjusted by adding small volumes of concentrated hydrochloric acid to the initial buffered solution. The results in Fig. 3 indicate that the electrode potential is not affected by pH in the range 1.6–8.1.

Selectivity of the electrode. In order to investigate the selectivity of this new polymeric electrode, the response of the sensor was assessed in the presence of various foreign cations. Potentiometric selectivity coefficients, $k^{pot}_{Ba^{2+},X^{z+}}$, were evaluated by both the mixed solutions method in 0.1 M Tris–HCl buffer and by the separate solutions method in unbuffered medium. The former is recommended by IUPAC as the most accurate and has been described previously [25]. The latter was performed in order to compare the selectivity coefficients of this electrode with those reported in the literature. Selectivity coefficients determined according to this last method were calculated using the following equation [19]:

$$\log k^{pot}_{Ba^{2+},X^{z+}} = \frac{E_2 - E_1}{S} - \log a_{X^{z+}}^{2/z} + \log a_{Ba^{2+}}$$

where a are the ion activities, S is the slope of the calibration graph, E_1 is the response to barium ions (0.1 M $BaCl_2$) and E_2 is the response to the interferent ion (X^{z+}) (0.1 M of the chloride salt of the investigated cation).

Among the factors that may influence the selectivity, the nature of the plasticizer must be first considered [35]. As has been pointed out (Table 1), the best characteristics are developed by ionophore I-based membranes incorporating

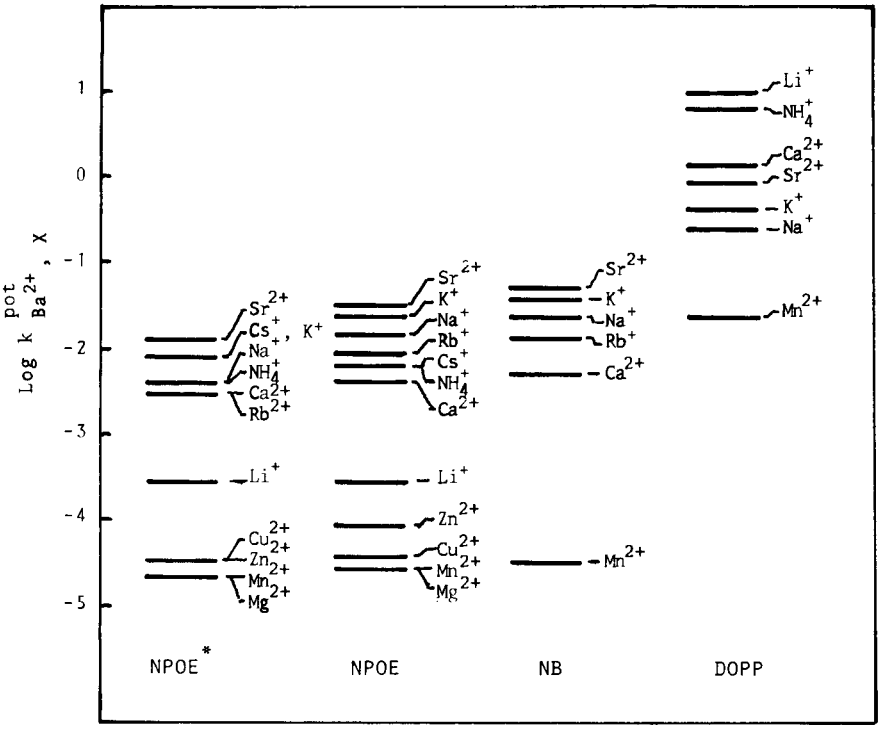

Fig. 4. Selectivity coefficients of the EVA–I–NPOE electrode for different plasticizers. Separate solutions method. Unbuffered solutions.

NPOE, NB or DOPP as plasticizer. These electrodes were considered for selectivity investigations.

The selectivity coefficients (log values) displayed in Fig. 4 show that the use of DOPP gives rise to severe interferences from common cations. NB and NPOE provide high selectivity but the NB-based electrode must be discarded owing to its short lifetime and NPOE remains the most appropriate plasticizer.

Increasing the polarity of the mediator improves the selectivity towards divalent over monovalent cations [20,35]. This is in agreement with our results, as shown from a comparison between the selectivity coefficients related to divalent and monovalent cations for NPOE and NB, more polar than DOPP (Fig. 4).

The concentration of the neutral carrier also plays a significant role with regard to selectivity. Increasing the amount of the ionophore will increase the selectivity of the membrane towards inorganic cations, as shown in Fig. 5. Moreover, small amounts (below 7 mg) give rise to strong interference from the Tris–HCl buffer and no calibration graph can be established in such an instance. This interference is suppressed by increasing the amount of ionophore to 7 mg or more, as illustrated by the small difference between the slopes of the calibration graphs plotted in buffered and unbuffered media (Fig. 1, curves a and b).

Fig. 6 compares the selectivity coefficients determined with the EVA–I–NPOE electrode described here with those reported for other bar-

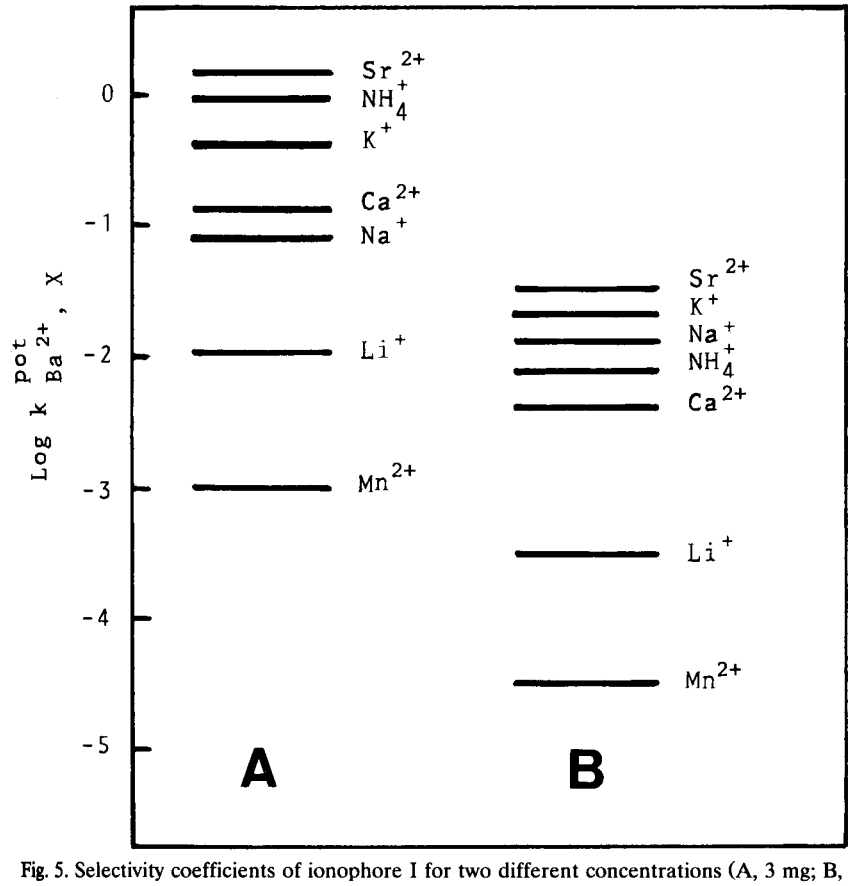

Fig. 5. Selectivity coefficients of ionophore I for two different concentrations (A, 3 mg; B, 7 mg) for the EVA–I–NPOE electrode. Unbuffered solutions.

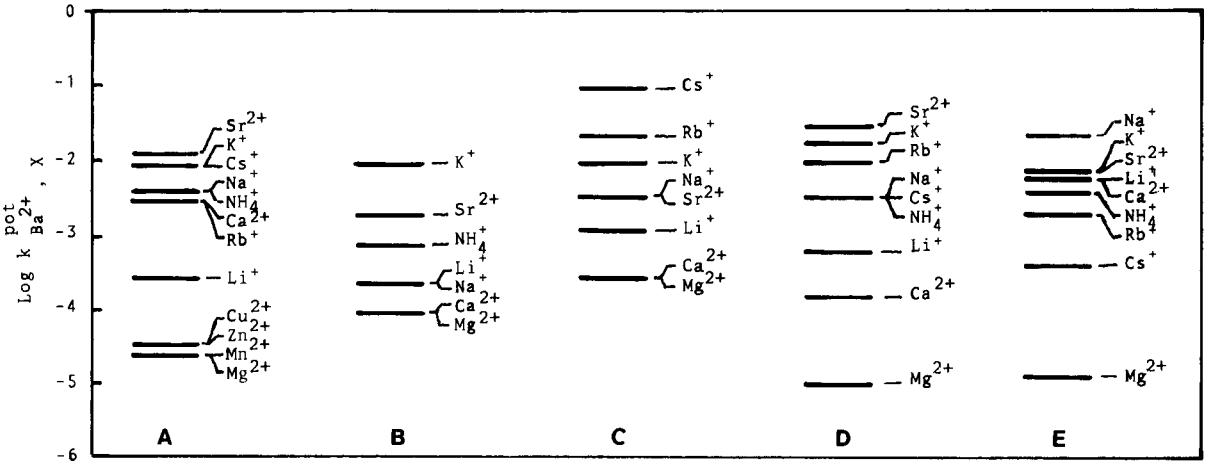

Fig. 6. Comparison of the selectivity coefficients of the EVA–I–NPOE electrode with those of other reported barium selective electrodes. (A) This work, ionophore I, NPOE, EVA; (B) [19], nonylphenoxypoly(ethyleneoxyethanol), 4-nitroethylenebenzene, liquid membrane; (C) [20], nonylphenoxypoly(ethyleneoxyethanol), bis(2-nitrophenyl) ether, PVC; (D) [17], *N,N,N',N'*-tetraphenyl-3,6,9-trioxaundecanediamide, NPOE, PVC; (E) [18], bis(*N,N*-dicyclohexyl)-1,2-phenylenebis(oxy-1,2-ethanediyl)bis(oxyacetamide), NPOE, PVC.

ium-selective electrodes. Except for small differences in the distribution of some cations in the selectivity scale, the present results are similar to those reported for electrodes based on the same scheme (ionophore and NPOE) [17,18] and for a liquid membrane electrode which includes an ion pair [19].

In addition to these selectivity criteria, this new electrode is not poisoned by copper(II) ions in contrast with the ion-exchanger liquid membrane electrode which exhibits a potential shift [19] or with the PVC membrane electrodes which require in this case a long recovery time [20]. This improvement is attributed to the copolymer EVA, as previously demonstrated [25].

Analytical application

Barium ion-selective electrodes find little application for actual barium determination, but they can be used as indicator electrodes for the titration of various anions that form precipitates with barium ions [36,37]. They should also find application in the indirect determination of sulphur in organic compounds that can be oxidized to sulphate ions [17,20].

To investigate the applicability of this electrode, the sulphate contents of different commercially available mineral waters were determined by potentiometric titration using a 0.1 M barium chloride solution without any pretreatment of the sample. The performance of the indicator electrode was first confirmed by the titration of a 0.01 M manganese sulphate solution with the same reagent. The equivalence point was determined graphically as described previously [38].

The data in Table 4 are in good agreement with the nominal values labelled by the manufacturer and are better than those resulting from the LC analysis, this method exhibiting a higher standard deviation. A mean recovery of 102.8% and a relative standard deviation of 1.6% demonstrate

TABLE 4

Potentiometric determination of sulphate ions in commercial mineral waters

Sample No.	Sulphate concentration ($g\ l^{-1}$)				
	Nominal	Found [a]		Recovery (%)	R.S.D. (%)
		LC	Potentiometric		
1	1.192	1.108	1.210	101.5	0.50
2	0.306	0.305	0.318	103.9	2.36
3	0.372	0.422	0.383	103.2	1.95
				Mean: 102.8	1.60

[a] Average of three determinations.

the usefulness of the EVA membrane barium electrode for analytical purposes.

Conclusion

Three derivatives of a new class of ionophores were synthetized and tested as ethylene–vinyl acetate membrane electrodes for the selective potentiometric determination of barium ions. Neutral carrier I with NPOE as plasticizer exhibits good sensitivity and significantly high selectivity, the latter parameter being comparable to that of other barium-selective electrodes. The proposed barium ISE is simple to prepare, inexpensive, easy to use and has a long lifetime. This electrode has been successfully applied to the potentiometric determination of sulphate ions in mineral waters.

The authors are grateful to Professor G. Geuskens (ULB) for the generous gift of the EVA copolymer and to Miss M.-C. Koob of the ULB Department of Oceanography (Professor R. Wollast) who performed the LC measurements. Thanks are also expressed to Professor H. Hurwitz, through whose intermediacy we received the ionophores, to the Fonds National de la Recherche Scientifique (FNRS, Belgium) for help to one of us (J.-C.V.) and to the SPPS (Belgium Politic Research, ARC), Contract No. 86/91–89.

REFERENCES

1 G.J. Moody, B.B. Saad and J.D.R. Thomas, Sel. Electrode Rev., 10 (1988) 71.
2 M.E. Mayerhoff and W.N. Opdycke, Adv. Clin. Chem., 25 (1988) 1.
3 U. Oesch, D. Amman and W. Simon, Clin. Chem., 32 (1986) 1448.
4 J.D.R. Thomas, Anal. Chim. Acta, 180 (1986) 289.
5 D. Amman, W.E. Morf, P. Anken, P.C. Meier, E. Pretsch and W. Simon, Ion-Sel. Electrode Rev., 5 (1983) 3.
6 D. Amman, Ion-Selective Microelectrodes. Principles, Design and Applications, Springer, Berlin, 1986.
7 V.P.Y. Gadzekpo, G.J. Moody, J.D.R. Thomas and G.D. Christian, Ion-Sel. Electrode Rev., 8 (1986) 173.
8 M. Yamanchi, A. Jyd and N. Ishibashi, Anal. Chim. Acta, 136 (1982) 399.
9 R.Y. Xie, V.P.Y. Gadzekpo, A.M. Kadry, Y.A. Ibrahim, J. Ruzicka and G.D. Christian, Anal. Chim. Acta, 184 (1986) 259.
10 V.P.Y. Gadzekpo, G.J. Moody and J.D.R. Thomas, Analyst, 110 (1985) 1381.
11 V.P.Y. Gadzekpo and G.D. Christian, Anal. Lett., 16 (1983) 1371.
12 S. Kitazawa, K. Kimura, H. Yano and T. Shono, Analyst, 110 (1985) 295.
13 E. Metzger, D. Amman, U. Schefer, E. Pretsch and W. Simon, Chimia, 38 (1984) 440.
14 E. Metzger, R. Aeschimann, M. Egli, G. Suter, R. Dohner, D. Amman, M. Dobler and W. Simon, Helv. Chim. Acta, 69 (1986) 1821.
15 O. Dinten, U.E. Spichiger, N. Chaniotakis, P. Gehrig, B. Rustrholz, W.E. Morf and W. Simon, Anal. Chem., 63 (1991) 596.
16 D. Erne, D. Amman, A.F. Zhukov, F. Behm, E. Pretsch and W. Simon, Helv. Chim. Acta, 65 (1982) 538.
17 M. Güggi, E. Pretsch and W. Simon, Anal. Chim. Acta, 91 (1977) 107.
18 M.W. Läubli, O. Dinten, E. Pretsch and W. Simon, Anal. Chem., 57 (1985) 2756.
19 R.J. Levins, Anal. Chem., 43 (1971) 1045; 44 (1972) 1544.
20 A.M.Y. Jaber, G.J. Moody and J.D.R. Thomas, Analyst, 101 (1976) 179.
21 K. Suzuki, K. Thoda, H. Sasakura and S. Tsuneo, Anal. Lett., 20 (1987) 39.
22 D.D. Perrin, W.L.F. Armarego and D.R. Perrin, Purification of Laboratory Chemicals, Pergamon, Oxford, 1966.
23 B. Dietrich, J.M. Lehn, J.P. Sauvage and J. Blanzat, Tetrahedron, 29 (1973) 1629.
24 A.A. Bouklouze, A. El Jammal, J.-C. Viré and G.J. Patriarche, Anal. Chim. Acta, 257 (1992) 41.
25 A. El Jammal, A.A. Bouklouze, G.J. Patriarche and G.D. Christian, Talanta, 38 (1991) 929.
26 J.N. Butler, Ionic Equilibria, Addison-Wesley, Reading, MA, 1964.
27 J. Kielland, J. Am. Chem. Soc., 59 (1937) 1675.
28 A.A. Bouklouze, A. El Jammal, G.J. Patriarche and G.D. Christian, J. Pharm. Biomed. Anal., 9 (1991) 393.
29 W.E. Morf, The principles of Ion-Selective Electrodes and of Membrane Transport, Elsevier, Amsterdam, 1981.
30 E. Lindner, E. Graf, Z. Niegreisz, K. Töth, E. Pungor and R. Buck, Anal. Chem., 60 (1988) 295.
31 P.C. Meier, W.E. Morf, M. Läubi and W. Simon, Anal. Chim. Acta, 156 (1984) 1.
32 P. Gehrig, W.E. Morf, M. Welti, E. Pretsch and W. Simon, Helv. Chim. Acta, 73 (1990) 203.
33 U. Oesch and W. Simon, Anal. Chem., 52 (1980) 692
34 K. Kimura, T. Miura, M. Matsuo and T. Shono, Anal. Chem., 62 (1990) 1510.
35 A. Lewenstam and A. Hulanicki, Sel. Electrode Rev., 12 (1990) 161.
36 D.L. Jones, G.J. Moody, J.D.R. Thomas and M. Hangos, Analyst, 104 (1979) 973.
37 G.J. Moody and J.D.R. Thomas, Lab. Pract., 28 (1979) 125.
38 S. Srianujata, W.R. White, T. Higuchi and L.A. Sternson, Anal. Chem., 50 (1978) 232.

Analytica Chimica Acta, 273 (1993) 165–174
Elsevier Science Publishers B.V., Amsterdam

Steady-state model for an organic conducting salt NADH enzyme electrode

Koon Weng Sim

Centre for Biotechnology and Department of Chemistry, Imperial College, London SW7 2AY (UK)

(Received 1st June 1992; revised manuscript received 26th October 1992)

Abstract

An enzyme electrode which uses the organic conducting salt *N*-methylphenazinium tetracyanoquinodimethane (NMP TCNQ) is reported. A steady-state model for the electrode is used to identify the rate-limiting step of the device. Kinetic parameters of the electrode are also obtained from this model. The model described here is used to assess the process which controls the current produced by the sensor. This amperometric biosensor uses yeast alcohol dehydrogenases as the enzyme for ethanol detection. Linear responses for ethanol in the range of 10 μM to 10 mM and a response time of 2–5 min are obtained. The device also responds to butan-1-ol and propan-2-ol. The system is optimised with regard to NAD^+ concentration in solution, the enzyme concentration behind the membrane and the pore size of the membrane covering the electrode.

Keywords: Biosensors; Kinetic methods; Enzymatic methods; Conducting salt; Enzyme electrode; NADH; Steady-state model

In the past decade, enzymes have been coupled with a variety of electrochemical sensors to generate a group of analytical tools known as enzyme electrodes. The most common application is the quantification of substrate by detecting the amount of product produced by the enzyme acting on the substrate. Enzyme activators or inhibitors can also be detected with enzyme electrodes. Addition of an activator or inhibitor to a sample containing a known amount of substrate will enhance or diminish the response of the electrode.

Nicotinamide adenine dinucleotide (oxidized form NAD^+, reduced form NADH) is an important biological oxidation/reduction cofactor and serves in numerous analytical procedures for substrates of enzymatic reactions. These methods usually involve measuring the cofactor produced or consumed spectrophotometrically. Several reports concerning the electrochemistry of NADH have indicated that the reduced cofactor is electroactive at a variety of solid electrode materials [1,2]. This observation has led to attempts to incorporate amperometric detection of NADH, thus providing an alternate means of determining dehydrogenase substrate concentrations.

In this paper, an enzyme electrode constructed from an organic conducting salt, NMP TCNQ (*N*-methylphenazinium tetracyanoquinodimethane), is reported. Oxidation of NADH on NMP TCNQ electrodes is observed at -0.2 V [3]. The half-wave potential of NADH oxidation on the organic salt is shifted towards more negative potentials by 0.4–0.6 V as compared with the oxidation potential of the same compound on carbon or platinum electrode. High overpotentials are required on these electrodes thereby raising the possibility of other biological materials present in samples being oxidised. This often results in foul-

Correspondence to: K.W. Sim, Xenova Ltd., 545 Ipswich Road, Slough, Berkshire SL1 4EQ (UK) (Present address).

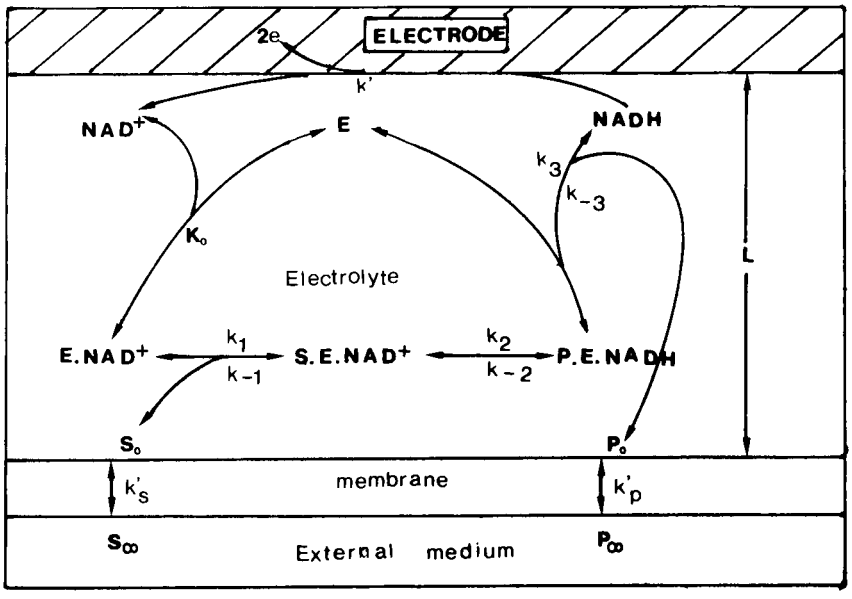

Fig. 1. Reaction scheme for the NADH enzyme electrode.

ing of the electrode. By operating the conducting organic salt electrode at a low overvoltage for NADH oxidation, many new avenues have been opened for the construction of successful enzyme electrodes.

The model to determine the steady-state response of the ethanol enzyme electrode is described below. The response of ethanol enzyme electrode in which the enzyme is entrapped at the electrode surface behind a membrane, can be determined by any one of a number of kinetic steps. It is possible to unravel these steps and then develop a simple model for the electrode response. The advantage of this is that it allows the rate-limiting step to be identified. This means that rational steps can be taken to optimise the electrode performance and design.

STEADY-STATE MODEL

Figure 1 illustrates the enzyme electrode and the kinetic scheme. The kinetic scheme for the NADH enzyme electrode can be written as follows:

$$E + NAD^+ \overset{K_0}{\rightleftharpoons} E \cdot NAD^+$$

We assume that the kinetics of binding of the enzyme to NAD^+ are sufficiently rapid for equilibrium to be established between E and $E \cdot NAD^+$. Following this,

$$S + E \cdot NAD^+ \overset{k_1}{\underset{k_{-1}}{\rightleftharpoons}} S \cdot E \cdot NAD^+ \overset{k_2}{\underset{k_{-2}}{\rightleftharpoons}}$$

$$P \cdot E \cdot NADH \overset{k_3}{\underset{k_{-3}}{\rightleftharpoons}} E + NADH + P + H^+$$

and at the electrode:

$$NADH \xrightarrow{k'} NAD^+ + H^+ + 2e$$

Under these circumstances, assuming there is no product in the external solution, we obtain the following expression for the flux, j [4],:

$$\frac{e_\Sigma}{j} = \frac{1}{Lk_{cat}}\left[1 - \frac{j}{k'_s s_\infty}\right] + \frac{K_M}{Lk_{cat}s_\infty}$$

$$+ \frac{je_\Sigma}{k'_p k' K_{TD} s_\infty [NAD^+]} + \frac{j^2}{k'_p k' K_{TD} s_\infty [NAD^+]}$$

$$\times \left[\frac{1}{k_{-1}} + \frac{K_2}{k_{-1}} + \frac{1}{k_{-2}}\right] + \frac{e_\Sigma}{k'_s s_\infty}$$

where now $K_{TD} = K_0K_1K_2K_3$ describes the overall position of equilibrium between S + NAD^+ and P + NADH + H^+. In the equation k'_s and k'_p are mass transfer constants of the substrate and product through the membrane, respectively. L is the thickness of the electrolyte layer between the electrode and membrane. s_∞ is the substrate concentration in the external medium. The total enzyme concentration is given by:

$$e_\Sigma = [E \cdot NAD^+] + [S \cdot E \cdot NAD^+] + [P \cdot E \cdot NADH]$$

where we have assumed that the concentration of free enzyme is negligible compared to that of $E \cdot NAD^+$.

The expressions for k_{cat} and K_M/k_{cat} are:

$$\frac{1}{k_{cat}} = \frac{1}{k_2} + \frac{1}{K_2k_3} + \frac{1}{k_3}$$

and

$$\frac{K_M}{k_{cat}} = \frac{1}{k_1} + \frac{1}{K_1k_2} + \frac{1}{K_1K_2k_3}$$

which has been discussed by Albery and Knowles [5].

EXPERIMENTAL

Solutions and reagents

All solutions were prepared from doubly distilled water. The standard supporting electrolyte was 0.5 M glycine buffer, pH 9.0 (Sigma) with 50 mM sodium chloride and 24 mM semicarbazide to remove the acetaldehyde formed in the reaction. Solid preparations of yeast alcohol dehydrogenase (YADH, EC 1.1.1.1) and nicotinamide adenine dinucleotide (NAD^+) (both from Sigma) were stored desiccated at −20°C. All other chem-

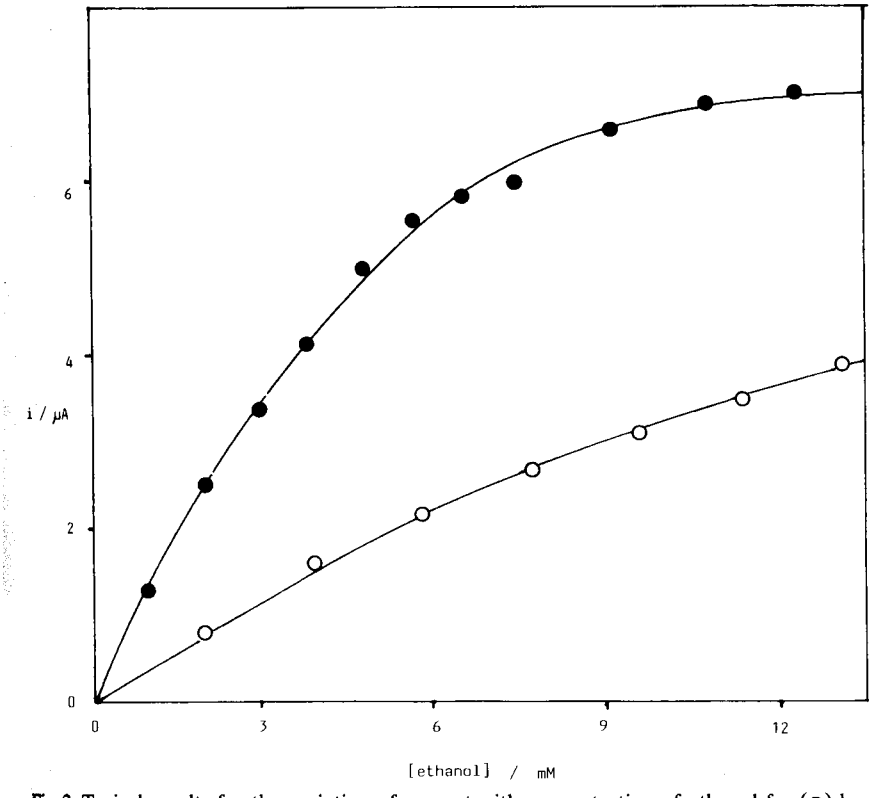

Fig. 2. Typical results for the variation of current with concentration of ethanol for (○) low enzyme loading and (●) high enzyme loading.

icals and solvents were reagent grade. Stock solutions of 17 mM NAD^+ in buffer and 200 mM ethanol were prepared daily. Stock solutions of butan-1-ol (200 mM) and propan-2-ol (2 M) were freshly prepared when required.

Electrode preparation

In the organic conducting salt electrode sensor, a three-electrode system is used as described previously [6]. In the development work, an old batch of NMP TCNQ was used to make drop-coated electrodes. In the final work, a new batch of the conducting salt was synthesized and used to pack the cavity working electrode. The counter electrode is a platinum ring and the working electrode (radius 0.1 cm), an organic conducting salt packed cavity electrode. The reference electrode is a silver/silver chloride reference electrode.

Yeast alcohol dehydrogenase (80 U dissolved in 20 μl of the glycine buffer solution with NAD^+) was placed on top of the electrode and fixed by means of a membrane. The membranes used were: (a) Visking 36/32 (Spectrum Industries, molecular mass cut-off, 12000–14000); (b) benzoylated dialysis membrane (Sigma, molecular

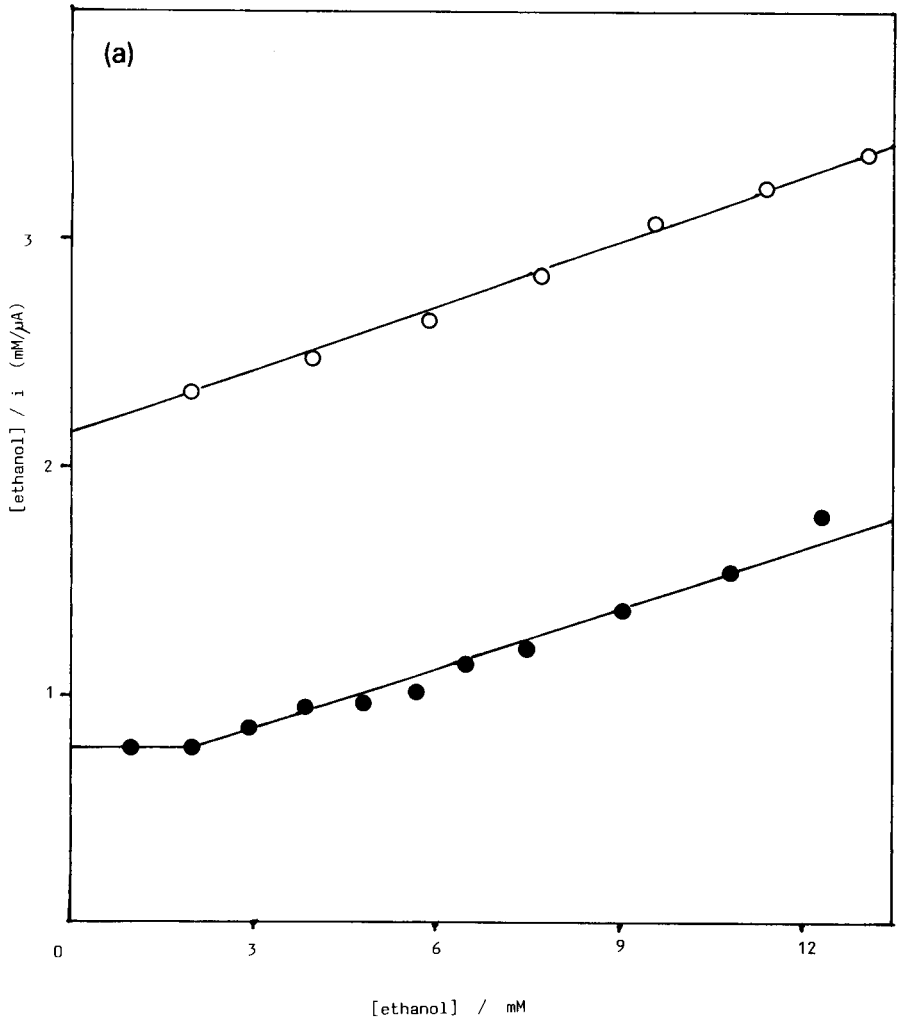

Fig. 3. (a) Hanes plots of ethanol electrode with (○) low enzyme loading and (●) high enzyme loading. (b) The data from Fig. 1 plotted as rho plots.

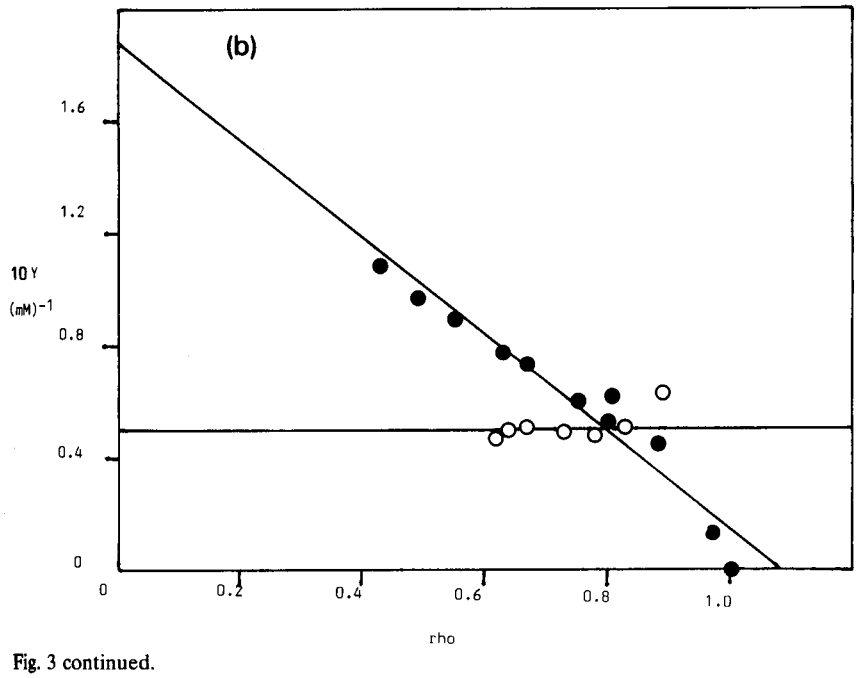

Fig. 3 continued.

mass cut-off, 2000); (c) ultrafilter membrane (Amicon, molecular mass cut-off 500); and (d) duralon membrane (Millipore, 1 μm pore size, 140 μm thick).

The device is then placed in an electrochemical cell which could be thermostatted. The cell held a volume of 2 cm^3 buffer into which alcoholic solutions could be introduced. The working electrode was held at 0.0 V with respect to a silver/silver chloride reference electrode. Background currents obtained settled to a region of approximately 0–3 μA.

Once prepared, the electrode can be used for periods up to 5 h [6] using the same enzyme and membrane before degradation of the enzyme begins to affect the electrode response. The electrode can be taken apart, washed and reassembled with fresh enzyme solution ready to be used again.

In using the electrode as a sensor, the same procedure was followed. A volume of sample was diluted, if necessary, to bring the ethanol concentration into the range 1–10 mM. Aliquots of this solution (20 μl) were then injected into the cell and the rise in the steady-state current was then measured. After measuring three or four samples the buffer solution was replaced and the electrode was calibrated with a sample taken from a standard solution that was 10% (v/v) ethanol and diluted twenty-fold.

TABLE 1

Typical kinetic parameters of the ethanol enzyme electrode with low and high enzyme loadings [a]

Enzyme loading (U cm^{-3})	K_{ME} (mM)	k'_{ME} (cm s^{-1})
1500 (low)	20.00	7.7×10^{-5}
3500 (high)	5.55	12.9×10^{-5}

[a] k'_{ME} is obtained from the intercept on the y-axis in the Hanes plot. K_{ME} is obtained from the intercept on the y-axis in the rho plot.

RESULTS AND DISCUSSION

Optimisation of enzyme concentration

A series of electrodes was prepared in which the concentration of yeast alcohol dehydrogenase behind the membrane ranged from 400–5000 U cm^{-3}. At low enzyme concentrations, it has been

shown that the response is limited by the rate of enzyme kinetics [4]. At high enzyme concentrations, the response can be limited by the diffusion of substrate through the membrane. Typical results are shown in Fig. 2. Application of the usual analyses [7] give the Hanes plots shown in Fig. 3a and the rho plots shown in Fig. 3b. k'_{ME} can be obtained directly from the intercept at the y-axis in the Hanes plot, by converting i, the current, at [ethanol] = 0, to j, the flux with the equation:

$$i/nFA = j$$

where F is the Faraday (96487 C mol^{-1}), n the number of electrons and A the surface area of the working electrode (see Fig. 3a).

In the rho plot (see Figure 3b) (i) where enzyme loading is low, enzyme kinetics are rate-limiting and (ii) where enzyme loading is high, transport of substrate through the membrane is rate-limiting. In (ii), the intercept on the x-axis is close or equal to unity. The kinetic parameters that can be obtained from the rho plot [7] are: (1) K_{ME}, Michaelis constant for the electrode (mM); (2) k'_{ME}, electrochemical rate constant for the enzyme electrode at low substrate concentration (cm s^{-1}); and (3) k'_s, rate constant for transport of substrate across membrane (cm s^{-1}).

The relationship between K_M and k'_{ME} in the enzyme electrode is

$$\frac{1}{k'_{ME}} = \frac{K_M}{e_\Sigma L k_{cat}} + \frac{1}{k'_s}$$

The kinetic parameters for this electrode are shown in Table 1.

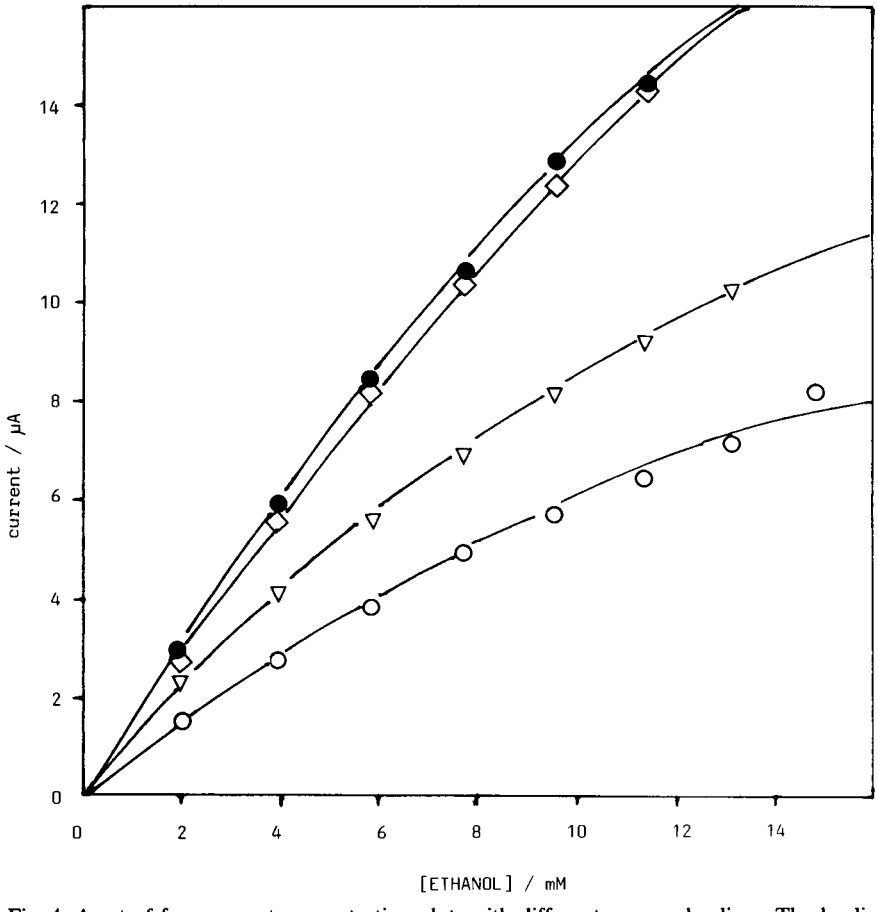

Fig. 4. A set of four current concentration plots with different enzyme loadings. The loadings in units cm^{-3} were as follows: ○, 697; ▽ 2250; □, 3300; ●, 4600.

The same conclusion may be reached in a different way by considering the set of data shown in Fig. 4. Four sets of experiments were carried out at successively higher enzyme loadings where in each set the current was measured as a function of substrate concentration. At the two highest enzyme loadings the response is nearly linear in substrate concentration and independent of enzyme loading. Under these conditions, transport of the substrate through the membrane is rate-limiting. In the saturated region of the graphs, the rate-limiting step is enzyme kinetics as opposed to electrode kinetics.

For analytical purposes, it is desirable that substrate transport across the membrane should be the rate-limiting process. For this reason the sensor is operated with high enzyme concentration of 4000 U cm^{-3}; this concentrations that which saturates the buffer solution. Under these conditions both sensitivity and response time have their optimum values.

Calibration plot for ethanol

The calibration graph for ethanol spans the concentration range 1 μM to 50 mM. Response to ethanol concentrations of 0–1 μM were not significantly above the noise level, typically about 0.01 μA, and were not quantifiable. The least squares regression line of current on concentration at the linear range is:

$y = 0.59 + 0.91x$

where y = current in μA and x = concentration of ethanol in mM. At concentrations above 10 mM the system starts to saturate; hence the present sensor can measure ethanol concentrations in the range 1 μM to 10 mM. The linear range can be extended to higher concentrations by using a less permeable membrane. Reproducibility of response to ethanol solutions was characterised with regard to the performance of the sensor after complete disassembly and replacement of the membrane, enzyme and NAD^+. From a set of five different experiments the standard deviation was found to be 3.5%.

The electrode also responds to higher alcohols such as propan-2-ol and butan-1-ol [8]. This is not surprising as these are also substrates for the enzyme (Fig. 5). In the absence of selective membranes enzyme electrodes can only be as selective as the enzyme used.

Influence of NAD^+ concentration

The sensitivity dependence of the electrode on NAD^+ concentration was determined. Concen-

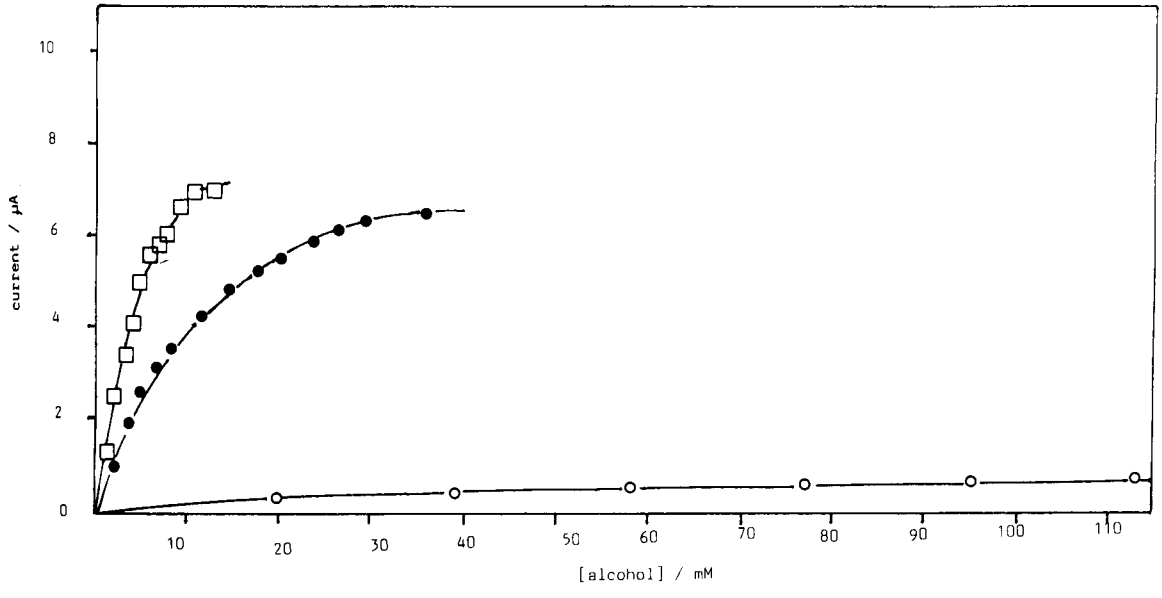

Fig. 5. Typical plots of current against alcohol concentrations for ethanol (□); butan-1-ol (●); propan-2-ol (○).

trations of NAD^+ between 2–30 mM were tested. The response to 9.52 mM ethanol with varying NAD^+ concentration is shown in Fig. 6. An optimum NAD^+ concentration of about 17 mM is obtained. Beyond this concentration, the sensitivity of the device decreased. The sensor was then operated with the optimum NAD^+ concentration of 17 mM.

Effect of different membranes

Ideally the membrane covering the electrode should retain the coenzyme NAD^+ with a molecular weight of 663, but allow the substrate and product to diffuse into and out of the electrode. In practice this is difficult to achieve satisfactorily because those membranes membranes with low molecular weight cut-off slow down the diffusion of substrate so much that the electrode response becomes very sluggish (Table 2). For this reason, ordinary dialysis membranes represent the best

TABLE 2

Effect of membrane on electrode responses

Membrane	Molecular mass cut-off	Sensitivity ($\mu A\ mM^{-1}$)	Response [a] time (min)
Ultrafiltration YCO5	500	2.3×10^{-3}	46
Millipore [b] duralon	–	0.4	6
Benzoylated membrane	2000	0.6	18
Ordinary dialysis	13000	1.2	2

[a] Time to reach 95% of steady-state value. [b] Pore size 1 μm.

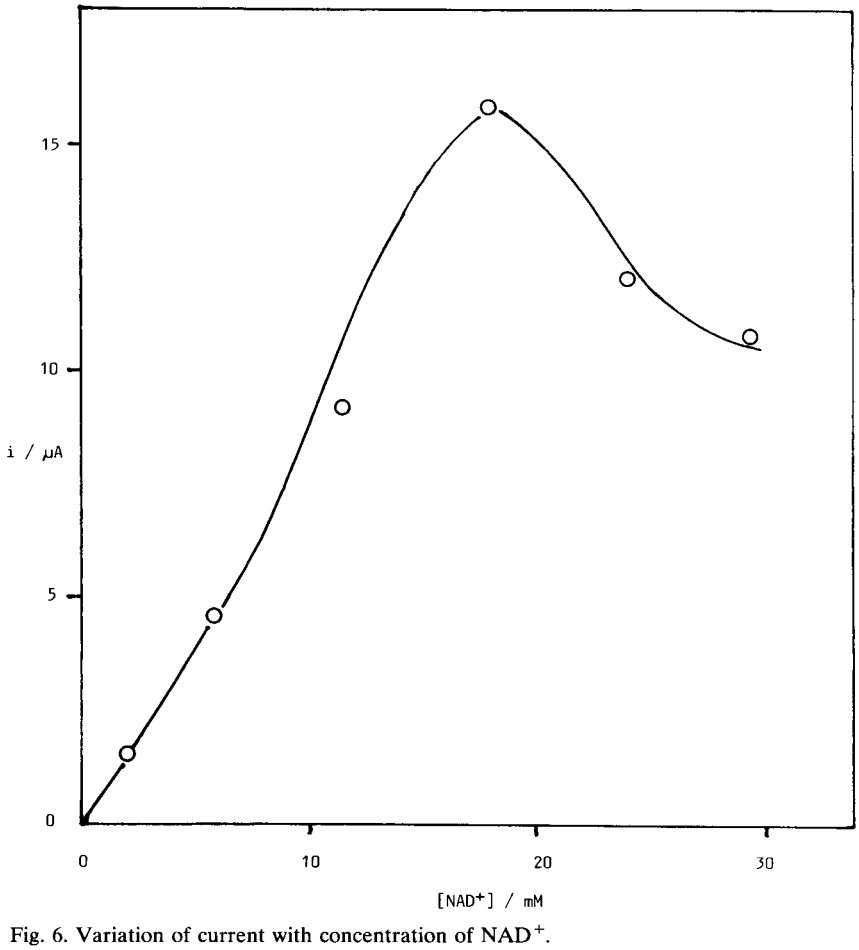

Fig. 6. Variation of current with concentration of NAD^+.

compromise at present. The search for a suitable thin membrane that will trap NAD^+ continues.

Use of the enzyme electrode as a sensor

In collaboration with the Laboratory of the Government Chemist, 15 samples listed in Table 3 were tested with the sensor. A reasonable correlation is found between the results from the enzyme electrode and those from the classical procedure as shown in Fig. 7. The gradient of the line is 0.97 ± 0.04. The ethanolic content determined by the classical procedure takes approximately 3 h. The assay using the enzyme electrode requires just the injection of the sample and takes a matter of minutes.

TABLE 3

List of samples tested

A	Industrial perfume
B	Low alcohol lager
C	Liquid cleanser
D	Apple aroma
E	Bubble bath
F	Breton cider
G	Skin lotion
H	Champagne
J	Red vermouth
K	Chinese wine
L	Fortified wine
M	Cream liqueur
N	Irish liqueur
P	Ouzo
Q	Composite brandy

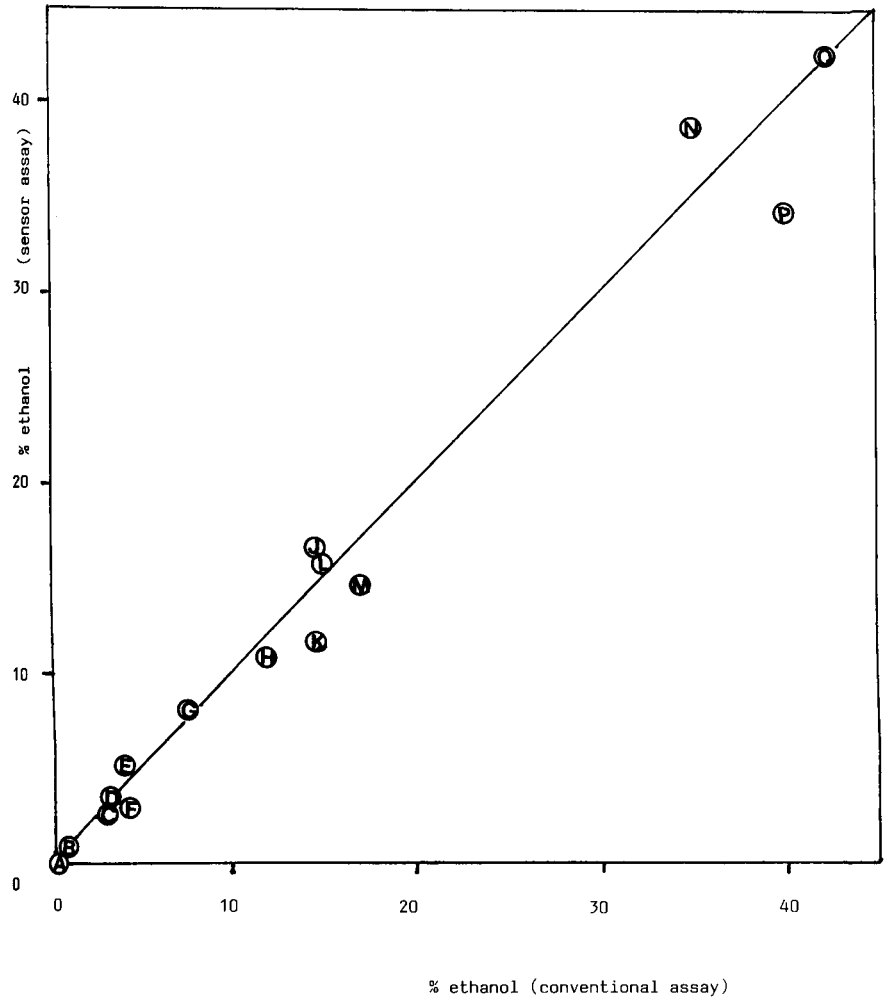

Fig. 7. Comparison of results from the ethanol sensor (y-axis) with those from the conventional assay (x-axis). The concentrations are reported as % (v/v). The samples are listed in Table 3.

I am especially grateful to Professor W.J. Albery, Drs. Tony Cass and Phil Bartlett for their helpful discussions. I also wish to thank the University of London for a postgraduate studentship and ICST Centre for Biotechnology and SERC for financial support. The 15 samples listed in Table 3 were provided by the Laboratory of the Government Chemist.

REFERENCES

1 W.J. Blaedel and R.A. Jenkins, Anal. Chem., 47 (1975) 1337.
2 J. Moiroux and P.J. Elving, Anal. Chem., 51 (1979) 346.
3 J.J. Kulys, Enzyme Microb. Technol., 3 (1981) 344.
4 W.J. Albery, P.N. Bartlett, A.E.G. Cass and K.W. Sim, J. Electroanal. Chem., 218 (1987) 127.
5 W.J. Albery and J. Knowles, Biochemistry, 15 (1976) 5631.
6 K.W. Sim, Biosensors Bioelectronics, 5 (1990) 311.
7 W.J. Albery and P.N. Bartlett, J. Electroanal. Chem., 194 (1985) 211.
8 K.W. Sim, Biosensors Bioelectronics, 6 (1991) 317.

Analytica Chimica Acta, 273 (1993) 175–186
Elsevier Science Publishers B.V., Amsterdam

Biopolymer-modified electrodes in the voltammetric determination of nucleic acids and proteins at the submicrogram level

E. Paleček, F. Jelen and C. Teijeiro

Institute of Biophysics, Czechoslovak Academy of Sciences, 612 65 Brno (Czechoslovakia)

V. Fučík

Institute of Molecular Genetics, Czechoslovak Academy of Sciences, 166 10 Prague (Czechoslovakia)

T.M. Jovin

Max Planck Institute for Biophysical Chemistry, W-3400 Göttingen (Germany)

(Received 1st June 1992)

Abstract

Nucleic acid- and protein-modified mercury and carbon electrodes can be prepared by immersing the electrode in a 5-μl drop of nucleic acid or protein solution. The biomacromolecule is strongly and irreversibly adsorbed at the electrode, resisting subsequent washing. The electrode is then transferred into a background electrolyte (not containing any biomacromolecule) followed by voltage scanning. This procedure is called adsorptive transfer stripping voltammetry (AdTSV). Nanogram amounts of nucleic acid can be determined with graphite electrodes, including the highly oriented pyrolytic graphite frequently used as a support in scanning probe microscopes, at relatively short waiting times without stirring of the solution. Even smaller amounts of nucleic acids are sufficient for analysis with the mercury electrode. Adsorption of DNA from different denaturing media produces DNA cyclic voltammetric peaks of different heights, suggesting that the arrangement of the DNA molecules at the electrode is influenced by the adsorption event and persists even after the electrode transfer to a non-denaturing medium. AdTSV with the mercury and graphite electrodes can be used for studies of virus suspensions producing DNA and protein signals, providing information about the virus particle degradation.

Keywords: Stripping voltammetry; Adsorptive transfer stripping voltammetry; Biopolymer-modified electrodes; DNA; Nucleic acids; Proteins

Modern polarographic (voltammetric) methods have been successfully applied in nucleic acid research [reviewed in 1–4]. For more than two decades these techniques were among the most sensitive physico-chemical methods of nucleic acid analysis [5], yielding early evidence of DNA premelting and structural polymorphy of the DNA double helix [6]. In the last decade, DNA research has concentrated on studies of well defined DNA samples with known nucleotide se-

Correspondence to: E. Paleček, Institute of Biophysics, Czechoslovak Academy of Sciences, 612 65 Brno (Czechoslovakia).

quences isolated from natural sources or synthesized chemically. The preparation of these samples in larger amounts is usually laborious and/or expensive, hence their analysis requires more sensitive techniques that operate with smaller sample amounts. Application of adsorptive stripping in combination with cyclic (CV) [3,7] or a.c. voltammetry [8] and the stationary mercury electrode resulted in recent years in a decrease in detection limits of the nucleic acids by several orders of magnitude (ranging from hundreds to a few nanograms of DNA per ml). While this detection limit is highly satisfactory in comparison to other methods, the volume of sample analysed (usually 1–2 ml) is large.

To decrease the volume requirement, a simple preparation of a DNA-modified mercury electrode requiring only 5–20 μl of nucleic acid solution was proposed [4,9,10]. Instead of performing the voltammetric measurements with the electrode immersed in the analyte solution, the DNA-modified electrode was first prepared by immersing it in a drop of the analyte solution for a short period of time, during which the nucleic acid was irreversibly adsorbed on the electrode. The latter was then washed and transferred to the background electrolyte (not containing DNA) in which the voltammetric measurements were performed. This procedure is called adsorptive transfer stripping voltammetry (AdTSV).

In this paper it is shown that AdTSV is widely applicable to various kinds of nucleic acid and protein studies, AdTSV signals due to oxidation of nucleic acids and proteins can be obtained if graphite electrodes are applied instead of the hanging mercury drop electrode (HMDE) and AdTSV appears to be potentially useful in the analysis of virus suspensions.

EXPERIMENTAL

Materials

Calf thymus and plasmid ColE1 DNAs were isolated as described previously [11,12]. DNA was denatured by heating at 100°C for 6 min with subsequent cooling in an ice-bath. Deoxyoligonucleotides $d(G–A)_{20}$ and $d(C–T)_{20}$ were kindly donated by Dr. F. Azorin. Single-stranded polyribonucleotides poly(A) and poly(A,G,U) were supplied by Sigma (St. Louis, MO). Lysozyme was obtained from Sigma, pancreatic ribonuclease from Reanal (Budapest), trypsin from Leciva (Prague) and bovine serum albumin from US Biochemical (Cleveland, OH).

Bacteriophage PZA [13] was grown in *Bacillus subtilis* 168 SpoOA as the host. The lysate was concentrated by 10% (w/v) polyethylene glycol, purified in a CsCl gradient and dialysed against 0.1 M NaCl–10 mM $MgCl_2$–50 mM Tris–HCl (pH 7.8) (TMS, storage medium). The suspension contained 10^{13} plaque-forming units ml^{-1}. For the electrochemical experiments, the solution was usually diluted fivefold which corresponded roughly to a concentration of 190 $\mu g\ ml^{-1}$ calculated from the absorbance at 260 nm.

Methods

The nucleic acid- and protein-modified mercury electrodes were prepared as described [10]. The HMDE was submerged for a time t_A in a drop (5–10 μl) of the solution to be analysed (deposited on Parafilm). The HMDE was then removed from the solution, washed with distilled water and the background electrolyte solution and placed in the usual voltammetric cell containing 5 ml of previously deoxygenated background electrolyte. Argon was bubbled through the solution for a time t_B (usually 100 s), after which the circuit was closed and the solution left at rest for t_C (15 s). The voltammetric measurements were then performed. In some instances, adsorption of DNA was carried out from the usual voltammetric cell with a closed current circuit and the HMDE charged to a potential E_A. To prepare the biopolymer-modified graphite electrodes 5 μl of the solution to be analysed was pipetted on top of the electrode to spread the solution over the entire electrode surface. After expiration of the time t_A the solution was removed and the electrode washed and treated in the same way as with the HMDE.

For CV measurements wither a Princeton Applied Research (PAR, Princeton, NJ) PAR 362 scanning potentiostat or a PAR 174 polarographic analyser with a PAR 175 universal pro-

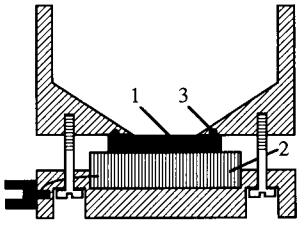

Fig. 1. Plexiglas voltammetric cell for the highly oriented pyrolytic graphite electrode (HOPGE). A 10×10 mm piece of HOPG (1) is placed on a copper plate (2) and held tightly by means of screws and an O-ring (3). This cell was used for both AdTSV and conventional voltammetry.

grammer was used at the following settings: initial potential (E_i) −0.1 V (if not stated otherwise), switching potential (E_s) −1.85 V and scan rate 0.2 V s^{-1}. A.c. voltammetric measurements were performed with a PAR 174A instrument coupled to a Model 174/50 polarographic analyser interface and a PAR 5208 two-phase lock-in analyser. Phase-selective a.c. measurements were carried out with a modulation voltage of 230 Hz and 30 mV peak-to-peak amplitude. A phase angle of 0° with respect to the applied voltage was employed so as to measure the in-phase component. The initial potential E_i was −1.6 V and the scan rate 10 mV s^{-1}. Differential-pulse voltammetry (DPV) was done with the same PAR 174 polarographic analyser and settings of pulse amplitude 25 mV and current sampling at 0.5-s intervals. In voltammetric measurements either an HMDE (Metrohm, Type E 410, area 2.2 mm^2), a pyrolytic graphite electrode (PGE) (geometric surface area 12.5 mm^2) or a highly oriented pyrolytic spectroscopic graphite electrode (HOPGE) (geometric surface area 28 mm^2) (Union Carbide, Cleveland, OH) was used as the working electrode. In experiments with the HOPGE, a 10 mm × 10 mm piece of HOPG was mounted in a simple cell (Fig. 1). In all measurements described a three-electrode system was used with a reference saturated calomel electrode and a platinum wire counter electrode. Except for a.c. voltammetry, the solutions were deoxygenated by passage of a slow stream of pure argon. All voltammetric measurements were done at room temperature.

RESULTS AND DISCUSSION

Nucleic acids

DNA-modified mercury electrode

AdTSCV and a.c. voltammograms of native double-stranded and thermally denatured single-stranded calf thymus DNAs (Fig. 2) show different signals for native and denatured DNAs, in agreement with the previous a.c. voltammetric [8] and CV measurements [7]. In AdTSV, DNA can be immobilized at the electrode by adsorption from various solutions and transferred to the optimum medium for voltammetric analysis. Preliminary results suggested that the DNA voltammetric signals are dependent on the conditions under which DNA is adsorbed at the electrode [4 and unpublished work].

Calf thymus DNA at a concentration of 35 μg ml^{-1} was adsorbed at the electrode either from a

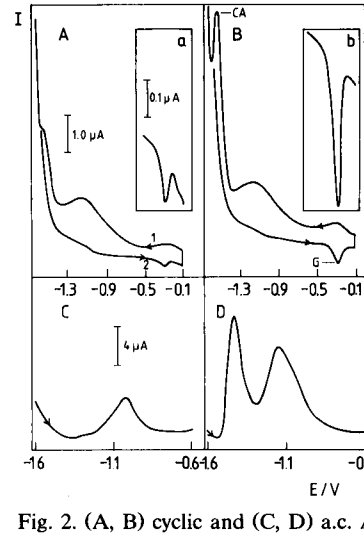

Fig. 2. (A, B) cyclic and (C, D) a.c. AdTS voltammograms of (A, C) native and (B, D) denatured calf thymus DNA at a concentration of 35 μg ml^{-1}. (a, b) Detail of part of CV curves with anodic peak G. Adsorption at the HMDE was performed from 0.2 M NaCl—20 mM sodium phosphate (pH 7.0). CV: $E_A = -0.1$ V; switching potential, $E_s = -1.85$ V; scan rate, 200 mV s^{-1}; $t_A = 60$ s at E_A −0.1 V; 1 = forward scan; 2 = reverse scan; background electrolyte, 0.6 M ammonium formate–0.1 M sodium phosphate (pH 6.8). A.c. voltammetry: scan rate, 10 mV s^{-1}; voltage scanned from −1.6 V in the anodic direction; background electrolyte, 0.5 M NaCl–Britton–Robinson buffer (pH 7.8).

neutral non-denaturing medium [0.2 M NaCl–50 mM sodium phosphate (pH 7.0)] in its double helical form or from an alkaline denaturing medium (0.2 M NaOH) in its single-stranded form. The electrode with the immobilized DNA was transferred to the neutral (non-denaturing) background electrolyte in which it was subjected to CV. DNA adsorbed from the alkaline medium produced a voltammogram very similar to that produced by thermally denatured DNA (not shown), i.e., with cathodic peak CA and anodic peak G substantially higher than those of double-stranded DNA adsorbed from neutral medium (Fig. 2A and B). A.c. voltammetry (Fig. 2C and D) produced similar results.

Adsorption of single-stranded calf thymus DNA from various denaturing media. DNA can be denatured under various conditions which may significantly influence the properties of the DNA molecule (e.g., owing to protonation and deprotonation of DNA bases) and consequently its adsorption at the electrode surface. We were interested as to whether the conformations adopted by DNA under different conditions of adsorption would persist at the electrode even after its immersion in the neutral, non-denaturing background electrolyte.

Single-stranded DNA was prepared by thermal denaturation and adsorbed on the electrode under non-denaturing neutral conditions and under denaturing conditions, including acidic and alkaline media, 65% formamide and 65% formamide containing 8 M urea. The DNA-modified electrode was transferred into 0.3 M ammonium formate–50 mM phosphate (pH 6.9). Adsorption of ssDNA at a concentration of 10 μg ml^{-1} at $t_A = 120$ s and open current circuit resulted in different AdTSCV peak G heights depending on the medium from which the DNA was adsorbed. The highest peak G was yielded by DNA adsorbed from formamide and neutral media and the lowest from alkaline and acidic media. The dependences of the heights of peak G on the concentration of DNA adsorbed at $E_A = -0.1$ V from four different media are shown in Fig. 3. The slopes of the initial linear portions of the curves and the limiting current values obtained at the full electrode coverage were different. The

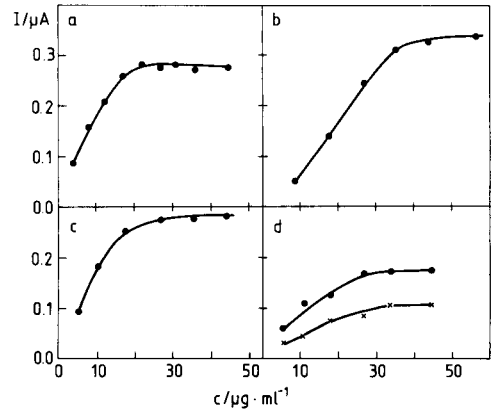

Fig. 3. Dependence of AdTSCV peak G on concentration of thermally denatured calf thymus DNA adsorbed from (a) 0.2 M NaCl–50 mM sodium phosphate (pH 7.0); (b) 0.2 M NaCl–Britton–Robinson buffer (pH 2.4); (c) 65% formamide; (d) 0.2 M NaOH at $t_A = 120$ s and $E_A = (\bullet) -0.1$ and $(\times) -0.7$ V. HMDE, scan rate 200 mV s^{-1}, switching point -1.85 V; background electrolyte, 0.3 M ammonium formate–50 mM sodium phosphate (pH 6.9).

largest limiting values result from adsorption from acidic (pH 2.4) medium (Fig. 3b) and the smallest from the adsorption from alkaline medium (Fig. 3d). The latter values decreased if the adsorption from the alkaline medium was performed at a more negative potential ($E_A = -0.7$ V). Such an effect may be due to the repulsion between the DNA carrying negative charges both on the phosphate groups and some base residues and the negatively charged electrode. Adsorption from the other three media (Fig. 3a–c) at $E_A = -0.7$ V (not shown) had little influence on the DNA current values compared with those after adsorption at $E_A = -0.1$ V. These results suggest that the AdTSV signal of single-stranded DNA strongly depends on the history of the experiment, specifically on the medium from which DNA was adsorbed. The different slope of the curve might indicate differences in the rate of transportation of DNA to the electrode surface (e.g., due to changes in the shape of the DNA molecules in solution), whereas differences in the limiting values might reflect particular arrangements of the DNA molecules at the electrode surface. The current values obtained at both full and partial electrode coverage can also be influ-

enced by differences in the orientation of the electroactive groups and other factors.

Supercoiled and linear plasmid DNA. Linearized ColE1 DNA at a concentration of 10 μg ml^{-1} was adsorbed at open current circle for $t_A = 120$ s at the electrode either from neutral or alkaline (denaturing) media. The electrode was then transferred to a 0.6 M ammonium formate–0.1 M sodium phosphate (pH 6.8) solution (not containing DNA) and the CV peak G was measured. DNA adsorbed from the neutral medium yielded a peak with a height which was about one fifth of that produced by DNA adsorbed at the electrode from the alkaline medium. In the same experiment performed with supercoiled covalently closed circular double-helical (cccd) DNA, the height of the peak G was 9% smaller than that of linear DNA if adsorbed from alkaline medium, but it almost disappeared if the adsorption was performed from neutral solution. In addition, DNA adsorbed from the alkaline medium produced a well developed cathodic peak CA (Fig. 2B) that was virtually absent in AdTSC voltammograms of DNA adsorbed under neutral conditions. For the measurement of the cathodic peak CA, higher DNA concentrations were used.

These results suggest that restoration of the double-helical structure of the covalently closed circular DNA that was adsorbed at the electrode in a melted state (from alkaline medium) does not occur if the denaturing conditions are removed. It is interesting that the heights of peak G produced by linear and cccd DNA differed only slightly. This might be due to a strong fixation of bases to the electrode surface preventing even partial reformation of the duplex structure. A more detailed consideration of this phenomenon will be reported elsewhere. Several years ago a method for the determination of cccd DNA in plasmid samples based on conventional CV was proposed [14]. It can be expected that application of AdTSCV for the same purpose will simplify the procedure and decrease the amount of sample required for the analysis.

Adsorption of DNA from Zn^{2+}-containing solutions. Various metal ions, including Zn^{2+}, Ni^{2+} and $[Co(NH_3)_6]^{3+}$, strongly influence the DNA structure [15,16]. Polarographic (voltammetric)

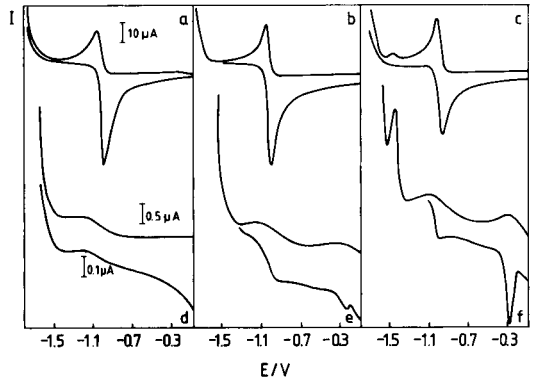

Fig. 4. (a–c) Conventional CV and (d–f) AdTSCV of (b, e) native and (c, f) thermally denatured calf thymus DNA at a concentration of 55 μg ml^{-1} at an HMDE; (a, d) without DNA. Conventional CV was performed in 1.5 mM $ZnCl_2$–0.3 M ammonium formate–10 mM Tris–HCl (pH 6.9); the same medium was used for the adsorption of DNA in AdTSCV; $t_A = 60$ s at $E_A = -0.1$ V. For other conditions, see Fig. 3.

measurements of some metals and their complexes have been used in studies of their interactions with DNA [17–24]. However, determination of the DNA signals in the presence of these metals is not possible by conventional voltammetric methods owing to relatively large metal peaks overlapping smaller signals of DNA. Using AdTSV the interference of the metals is easily removed by washing the electrode (Fig. 4), but the effect of the metal on the DNA structure in solution may be retained by the electrode during the adsorption process.

DNA was used in its native and denatured forms at a concentration of 55 μg ml^{-1} in 0.3 M ammonium formate–10 mM Tris–HCl (pH 6.9), with 1.5 mM $ZnCl_2$, and this solution was subjected to conventional AdSCV. Figs. 4b and c show voltammograms of native and denatured DNAs in which the DNA peak G is absent owing to the presence of very high peaks of Zn. The metal peaks in the case of native DNA were almost the same as those observed with solution not containing DNA (Fig. 4a). However, the Zn peaks observed with denatured DNA solution were significantly smaller (Fig. 4c), suggesting that an appreciable amount of the divalent cation was bound by the DNA. In the same solutions studied by AdTSV, no Zn peaks were observed (Fig.

4d–f) and the peaks of native (Fig. 4e) and denatured DNAs (Fig. 4f) are well developed. Preliminary results (unpublished) suggest that at the Zn/DNA ratio used in the experiment described above (Fig. 4) the peaks of DNA are not influenced by Zn. At higher Zn/DNA ratios, changes in the DNA peak heights can be observed.

Oligonucleotides. In the last 10–15 years, chemically synthesized deoxyoligonucleotides have become available in the amounts and purity necessary for physical and chemical experiments. However, only a few papers dealing with their electrochemical analysis have been published [25–28]. Recently, it has been shown that a self-complementary B-DNA decamer can be analysed by different voltammetric techniques, including AdSCV, which makes it possible to measure this oligonucleotide at subnanomolar concentrations [28]. Here single-stranded oligonucleotides were studied to find out whether they are adsorbed at the electrode with sufficient strength to be analysed by AdTSV.

The oligonucleotides $d(G–A)_{20}$ and $d(C–T)_{20}$ at molecular concentrations of 0.24 and 0.20 μM, respectively, were adsorbed at the electrode from 0.1 M NaCl–10 mM Tris–HCl (pH 7.0), with $ZnCl_2$ at a concentration corresponding to 10Zn/1P. With $d(G–A)_{20}$, an anodic peak G at −0.30 V appeared in addition to a cathodic peak at −1.53 V (Fig. 5c), for which reduction of adenine residues is responsible. In contrast, $d(C–T)_{20}$ yielded only a cathodic peak at −1.53 V due to reduction of cytosine residues (Fig. 5b). Adsorption of these oligonucleotides from Zn-containing solutions yielded voltammograms free of zinc peaks, in agreement with the results for AdTSCV of calf thymus DNA (Fig. 4), and did not change the potentials of the peaks G and A or C from those obtained after oligonucleotide adsorption from a solution not containing Zn^{2+}. Preliminary data (unpublished) suggest that AdTSCV is able to reflect the formation of double- and multi-stranded structures of oligonucleotides formed in neutral Zn^{2+}-containing solutions as well as in acidic solutions not containing the cation.

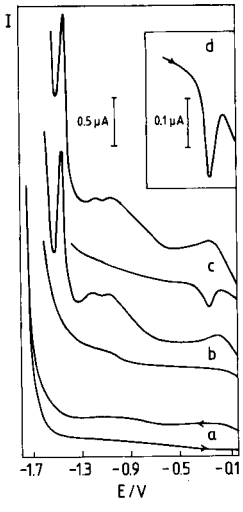

Fig. 5. AdTS cyclic voltammograms of synthetic deoxyoligonucleotides at an HMDE. (a) 0.1 M NaCl–Tris–HCl (pH 7.0)–2.4 μM $ZnCl_2$; (b) 0.20 μM $d(C–T)_{20}$ in 0.1 M NaCl–Tris–HCl (pH 7.0)–2.0 μM $ZnCl_2$; (c) 0.24 μM $d(G–A)_{20}$ in 0.1 M NaCl–Tris–HCl (pH 7.0)–2.4 μM $ZnCl_2$; (d) peak G of 0.24 μM $d(G–A)_{20}$ obtained at a higher instrument sensitivity. Samples were adsorbed at the electrode for $t_A = 60$ s at open current circuit; for other conditions, see Fig. 3.

Nucleic acid-modified graphite electrodes

In the past few years substantial progress has been made in the study of surfaces at very high resolution even down to the atomic level [29]. The surface topography of nucleic acids attached to HOPG has been studied by scanning tunnelling microscopy (STM) and atomic force microscopy (AFM) [29,30]. Voltammetric studies of nucleic acid oxidation have been limited mainly to wax-impregnated and PGEs immersed into the nucleic acid solutions; to our knowledge, no attempt has been made to use HOPG as an electrode in the voltammetric analysis of nucleic acids. Here it is shown that a HOPG electrode (HOPGE) can be used for AdTSV similarly to the usual PGE.

Adenine and guanine residues in nucleic acids are oxidizable at carbon electrodes [31,32] and methods using PGE, paraffin wax-impregnated spectroscopic graphite and glassy carbon electrodes for the analysis of DNA and RNA have been developed [33–35]. We measured the biosynthetic polyribonucleotides poly(A) and poly (A,G,U) using DPV in combination with PGEs and HOPGEs. In agreement with the results ob-

tained by Brabec and Dryhurst [32], poly(A) produced at a PGE a single AdSDPV oxidation peak at 1.1 V. Poly(A,G,U) at a concentration of 0.1 mM in 0.2 M sodium phosphate (pH 6.8) yielded a peak at the same potential and, in addition, another peak at 0.9 V (Fig. 6a); the latter peak is due to oxidation of guanine residues [31]. Under the same conditions both peaks were also observed in voltammograms obtained by AdTSDPV at a PGE (Fig. 6b) and a HOPGE (Fig. 6c). Peaks obtained by means of AdTSDPV (Fig. 6b and c) were better developed than those obtained by conventional AdSDPV (Fig. 6a). The dependence of the guanine peak on poly(A,G,U) concentration is shown in Fig. 7. At $t_A = 5$ min poly(A,G,U) was detectable at a 1 μM monomer concentration and limiting current values were reached at ca. 5 μM concentration. Considering that only 5 μl of solution were used for the polynucleotide analysis, less than 10 ng of poly(A,G,U) was sufficient to obtain the highest guanine peak (at 0.9 V) without stirring the solution.

At a 0.7 μM concentration, $d(G–A)_{20}$ and $d(C–T)_{20}$ were analysed under the same conditions by AdTSDPV at a PGE. As expected, $d(C–T)_{20}$ did not produce any oxidation peak (owing to absence of oxidizable purine bases) whereas $d(G–A)_{20}$ produced two peaks at potentials corresponding to those of the poly(A,G,U) peaks (Fig. 6). In contrast to the results obtained with poly(A,G,U), the peaks of $d(G–A)_{20}$ at the HOPGE were less well developed. The results obtained with calf thymus single-stranded DNA and preliminary data obtained with other nucleic acids suggest that the composition and ionic strength of the solution from which the nucleic acid is adsorbed may significantly influence the resulting signals. An additional factor may be topography of the electrode surface.

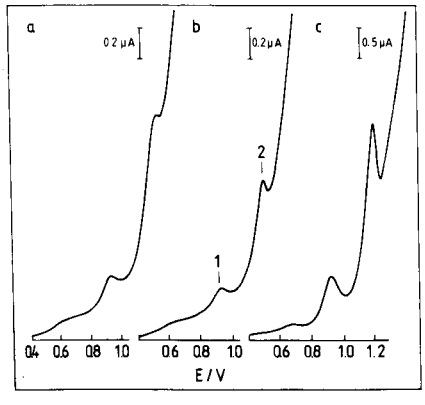

Fig. 6. (a) Conventional and (b, c) AdTS differential-pulse voltammograms of poly(A,G,U) at graphite electrodes. 0.1 mM (mononucleotide) poly(A,G,U) in 50 mM sodium phosphate–0.1 mM EDTA (pH 7.0) was adsorbed at open circuit at an (a, b) PGE and (c) HOPGE for $t_A = 2$ min. Background electrolyte, 0.2 M sodium phosphate (pH 6.7). The area of the PGE was 12.5 mm^2 and that of the HOPGE 28 mm^2; scan rate, 10 mV s^{-1}; pulse amplitude, 25 mV.

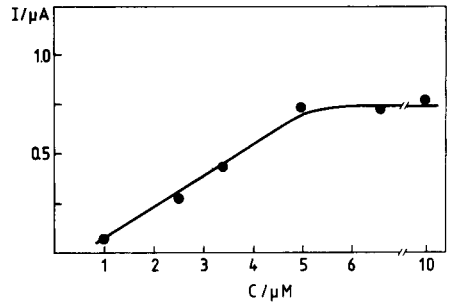

Fig. 7. Dependence of guanine AdTSV peak on the concentration of poly(A,G,U). Poly(A,G,U) in 0.15 M NaCl–15 mM sodium citrate (pH 7.0) was adsorbed at a PGE for $t_A = 5$ min. For other conditions, see Fig. 6.

The results suggest that HOPG is suitable for AdTSV of nucleic acids including single-stranded oligonucleotides. Hence simple voltammetric experiments at a HOPGE may help to find optimum conditions for scanning probe microscopy such as STM and AFM, e.g., with respect to the nucleic acid adsorbability.

Proteins

Protein-modified mercury electrode

Reduction of the disulphide bonds. Disulphide bonds in protein molecules can be reduced at the mercury electrode (reviewed in [1]). Recently Wang et al. [36] have shown that trypsin and chymotrypsin can be determined by means of AdSV in HCl (pH 0.9) at submicromolar concentrations. AdTSDPV was applied to trypsin solutions under the conditions used by Wang et al. [36], that is, trypsin was adsorbed from dilute HCl

and the electrode was transferred to the same electrolyte not containing trypsin) and curves were obtained differeing only slightly from those yielded by conventional AdSDPV.

Protein catalytic currents. In cobalt-containing solutions, proteins produce catalytic polarographic currents involving cysteine sulphydryl groups that have been widely applied in protein analysis [reviewed in [1]]. In AdTSV, proteins can be adsorbed at the electrode from a solution optimum for the given protein and the electrode with the immobilized protein transferred to the cobalt-containing background electrolyte. Examples of the application of AdTSV in studies of bacteriophage proteins will be shown below.

Protein-modified graphite electrodes

More than 10 years ago it was shown that proteins can yield voltammetric oxidation peaks at carbon electrodes [35,37–40]. Irreversible oxidation of tyrosine and tryptophan is responsible for these peaks. Voltammetric analysis of proteins can yield information about accessibility of the electroactive tyrosine and tryptophan residues for the electrode process.

Figure 8A shows a voltammetric curve of 7.1 μM lysozyme obtained at a PGE by means of conventional AdSDPV. The shoulder at about 0.6 V is due to tyrosine and the peak at about 0.95 V to tryptophan oxidation. The curve obtained with lysozyme-modified PGE (Fig. 8A, 2) and HOPGE (Fig. 8A, 3) produced AdTSDPV peaks at the same potentials. This result suggests that lysozyme is irreversibly adsorbed at both PGE and HOPGE. Similar results were obtained with other proteins including pancreatic ribonuclease. Treatment of lysozyme and ribonuclease by chemical agents that attack tryptophan and/or tyrosine resulted in marked changes in the AdTS voltammograms. Figure 8B shows lysozyme treated with potassium permanganate, an agent which degrades both tyrosine and tryptophan residues (unpublished work), in which a decrease in both peaks compared with the untreated control is clearly visible. Treatment of lysozyme with osmium tetraoxide and 2,2′-bipyridine, which forms an osmate ester with tryptophan by addition to the 2,3-position of the indole ring [41], but does not react with

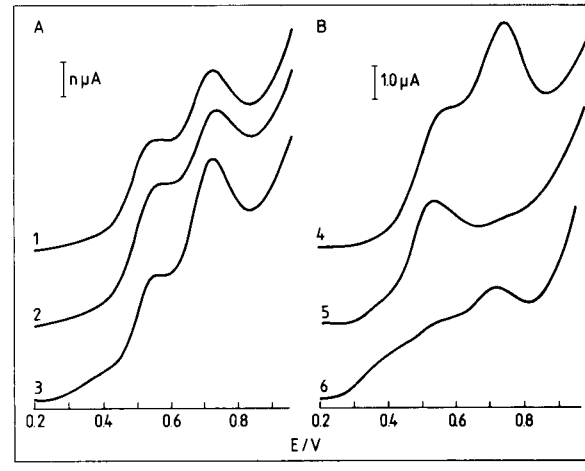

Fig. 8. (A) (1) Conventional and (2,3) AdTS differential-pulse voltammograms of 7.1 μM lysozyme in 7.5 mM NaCl–0.75 mM sodium citrate (pH 7.0) adsorbed at (1, 2) a PGE and (3) a HOPGE at $t_A = 120$ s. Measurements were performed at two instrument sensitivities: for (1, 2) $n = 1.0$ μA and for (3) $n = 0.2$ μA; HOPGE area, 5 mm^2. (B) AdTS voltammograms of (5, 6) chemically modified and (4) unmodified lysozyme at a PGE. Lysozyme (35 μM) was treated with (5) 4 mM osmium tetroxide and 2,2′-bipyridine (forming an osmate ester with tryptophan by addition to the 2,3-position of the indole ring) or (6) 4 mM potassium permanganate (which degrades both tryptophan and tyrosine) for 2 h at 37°C. The lysozyme solutions were thoroughly dialysed against 7.5 mM NaCl–0.75 mM sodium citrate (pH 7.0) prior to voltammetric measurements (performed at full coverage of the electrode). Background electrolyte, 20 mM Na_2CO_3 (pH 10.5). For other conditions, see Fig. 6.

tyrosine, resulted in the elimination of the tryptophan peak but not of that of tyrosine.

Virus particles

Simple viruses, which can be considered as complexes of nucleic acid with proteins, represent an attractive object for electrochemical studies. With the exception of the RNA-containing tobacco mosaic virus (TMV) [1,42–45], little has been done in this area. In principle, methods of electrochemical analysis may yield information about the redox properties of groups located at the surface of the virus particle, the adsorptivitiy of the particle at the electrode and the changes in the particle structure due to its interaction with electrically charged interfaces. These techniques

can also provide information on degradation of the particle induced by various physical, chemical and biological agents.

AdTSV was used to study a bacterial virus (bacteriophage PZA) [13,46,47] composed of a single linear DNA molecule (19366 base pairs) [46,47] and six structural proteins constituting the phage head, head fibres, tail, upper and lower collars and appendage. The aggregate relative molecular mass of the particle is 29×10^6. Using an HMDE we measured (a) a CV peak G that yields information about the accessibility of DNA for the electrode process and (b) a catalytic peak of proteins in cobalt-containing background electrolyte. In addition, a PGE was used to measure tyrosine and tryptophan protein peaks.

A HMDE was immersed in the drop of phage suspension for $t_A = 120$ s in different media including (a) 0.1 M NaCl–10 mM $MgCl_2$–50 mM Tris–HCl (pH 7.8) (TMS, the storage medium in which the particle is stable), (b) TMS containing 0.1 M EDTA, (c) 1 mM $[Co(NH_3)_6]^{3+}$ in 0.1 M NH_4Cl–0.1 M NH_3 (pH 9.5) (background electrolyte for protein analysis) and (d) 8 M urea (which denatures proteins). The electrode was washed and immersed in a background electrolyte composed either of 0.6 M ammonium formate–0.1 M sodium phosphate (pH 6.9) (to determine DNA by CV) or of 1 mM $[Co(NH_3)_6]^{3+}$–0.1 M NH_4Cl–0.1 M NH_3 (pH 9.5) (to determine proteins).

Figure 9a shows differences in the protein peaks P obtained after immersion of an HMDE for $t_A = 120$ s in different media with suspended phase particles at a concentration of 190 μg ml^{-1}. Adsorption from TMS storage buffer produced a single protein peak P1 at about -1.32 V (Fig. 9a, 1). Adsorption from TMS with EDTA (the suspension was kept in this solution for 30 min at room temperature prior to immersion of the HMDE) yielded a substantially higher peak P1 with an indication of another more negative peak (Fig. 9a, 2). Adsorption from 1 mM $[Co(NH_3)_6]^{3+}$–0.1 M NH_4Cl–0.1 M NH_3 (pH 9.5) produced a smaller but distinct peak P1 and peak P2 at potentials about 150 mV more negative (Fig. 9a, 3). The same two peaks were obtained after immersion of the electrode in a phage

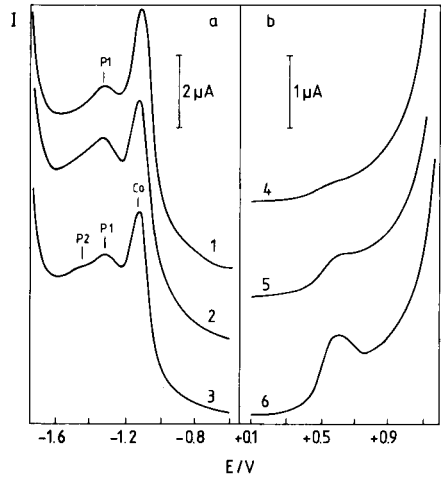

Fig. 9. Protein responses in AdTS voltammograms of the suspension of *B. subtilis* bacteriophage PZA at an (a) HMDE and (b) PGE. Adsorption from (1) TMS, (2) TMS containing 0.1 M EDTA and (3) 1 mM $[Co(NH_3)]_6Cl_3$–0.1 M NH_4Cl–0.1 M NH_3 (pH 9.5) for $t_A = 120$ s. (1–3) D.c. voltammetry; scan rate, 100 mV s^{-1}; background electrolyte, 1 mM $[Co(NH_3)]_6Cl_3$–0.1 M NH_4Cl–0.1 M NH_3 (pH 9.5); bacteriophage at a concentration of 195 μg ml^{-1}. Adsorption from (4) TMS, (5, 6) 8 M urea, for $t_A = 30$ s at a bacteriophage concentration of (4, 5) 390 μg ml^{-1} and (6) 1560 μg ml^{-1}. (4–6) Differential-pulse voltammetry; background electrolyte, Britton–Robinson buffer (pH 8.3). For other conditions, see Fig. 6.

suspension in 8 M urea, in which the phage proteins are denatured.

Transferring the HMDE into 0.6 M ammonium formate–0.1 M sodium phosphate (pH 6.9) allowed the measurement of the DNA CV anodic peak G. After adsorption ($t_A = 30$ s) from TMS no peak G was observed. If, however, the adsorption was performed from EDTA-containing TMS a very small peak G appeared several minutes after addition of EDTA; after 47 min the height of this peak corresponded to about 20% of DNA contained in the phage particles.

In another experiment a PGE was immersed into the phage suspension for $t_A = 300$ s, the electrode was transferred into 0.2 M sodium phosphate (pH 8.3) and DPV measurements were made. If the adsorption was performed using TMS only a small inflection on the DP voltammogram close to 0.6 V was observed (Fig. 9b, 4). If, however, the adsorption was made from the sus-

pension containing 8 M urea a peak was observed at the same potential (Fig. 9b, 5) corresponding to tyrosine oxidation. This peak increased with increasing phage concentration (Fig. 9b, 6). Head fibres and tail proteins with a high prevalence of tyrosine over tryptophan (Tyr/Trp ≈ 6) [46,47] might be mainly responsible for the observed peak. These results show that AdTSV is able to detect degradation of phage particles due to removal of Mg^{2+} ions or protein denaturation by urea and yield specific information about the release of DNA from the particle.

The results of AdTSV experiments with the bacteriophage suspension are basically in agreement with the analysis of TMV protein signals obtained previously by conventional voltammetry with the mercury [44] and graphite electrodes [45]. An important advantage of the AdTSV experiments is that the amount of the virus sample required for the analysis can be substantially reduced. In addition, the adsorption can be performed from the medium of choice and not necessarily from the background electrolyte as is the case in conventional voltammetry, which is not always optimum for virus stability.

Conclusions

It has been shown that nucleic acid- and protein-modified mercury and graphite electrodes can be prepared by immersing the electrode in a drop of solution of a given biomacromolecule. AdTSV with biomacromolecule-modified electrodes have many advantages over conventional voltammetry with mercury and carbon electrodes and some of these have been demonstrated here. It has been shown that owing to the separation of the biopolymer adsorption from the electrode processes (responsible for the voltammetric signals) it is possible to decrease the volume of the analysed sample to 5–10 μl without constructing any special voltammetric cell. Thus nanogram and even subnanogram amounts of nucleic acids and proteins can be used for the analysis. Nucleic acids and proteins were adsorbed mainly from their unstirred solutions. Stirring can substantially increase the sensitivity of AdTSV. Previously it was shown [10] that the stirring of a drop can be accomplished by placing the drop on a vibrating support or by introducing a thin vibrating glass rod into the drop.

It has also been shown that the biomacromolecule can be adsorbed on the electrode from a solution that is optimum for the given macromolecule. This choice can be made independently of the conditions required for the voltammetric measurements, i.e., in terms of the nature and concentration of the electrolyte necessary for obtaining well developed reduction or oxidation signals. Thus, the biomacromolecule can be adsorbed either from a solution that is optimum for the native conformation of the biomacromolecule, from a solution that denatures the biomacromolecule producing, for example, single-stranded nucleic acid molecules or from a solution optimum for the adsorption of the biomacromolecule on the given electrode.

DNA interactions with low-molecular mass electroactive substances can be studied by electrochemical methods in various ways. The most common procedure is based on the measurement of potential shifts and the reduced intensities of voltammetric signals due to a large decrease in the diffusion coefficient of the electroactive substance bound non-covalently to DNA [17–24]. Using these techniques it is usually difficult to measure the relatively small signals yielded by double-stranded DNA that may be overlapped by larger signals of the low-molecular-mass substance (Fig. 4a–c). Interference of the latter substances can be cancelled in AdTSV (Fig. 4e and f) and DNA signals can be easily measured. AdTSV may then give information about changes in DNA structure induced by low-molecular mass substances if the conformational state persists on the electrode after washing. Some substances covalently bound to DNA can be used as electroactive markers and DNA structure probes [3,48–50]. It is expected that the combination of conventional and AdTS voltammetry will yield interesting information about DNA structure and interactions.

The ability of nucleic acids and proteins to adsorb strongly and irreversibly on various surfaces has been known for years (reviewed in [1] and [51]). Also, the possibilities have been discussed of adsorbing nucleic acids and proteins

irreversibly on mercury [1,52,53] and carbon [31,40] electrodes. Transfer of the electrode with adsorbed protein into a background electrolyte was utilized in studies of the mechanism of the electrode processes of protein catalytic currents [52,53]. A.c. voltammetry was used to study the desorption of several organic compounds at a mercury electrode [54]; among them, Triton X-100 and tribenzylamine were irreversibly adsorbed on the electrode. To our knowledge, however, no attempt was made until the introduction of AdTSV in 1986 [9] to exploit the irreversible adsorption of nucleic acids and proteins for an improvement of their voltammetric determination. Even recently [55] the irreversible adsorption of thrombin at carbon electrodes was demonstrated without any attempt to exploit voltammetric thrombin signals.

The results presented in this paper and further experience with AdTSV [4,9,10 and unpublished work] suggest that at least in the analysis of biomacromolecules this technique may become as general as conventional voltammetry. The reproducibility and accuracy of AdTSV for nucleic acids and proteins analysed so far do not differ very much from those of conventional AdSV. For example, single-stranded DNA at a concentration of 8 μg ml^{-1} adsorbed at an HMDE from a 20-μl drop at $t_A = 30$ s was determined by AdTSV with a relative standard error of $\pm 2.9\%$ [10], a value not significantly different from that obtained by conventional AdSV [7]. The possibility of adsorbing biomacromolecules from small volumes of almost any solution may be especially attractive to biochemists and biologists who frequently find it difficult to analyse larger volumes of samples in media suitable for conventional voltammetry.

There are a number of possibilities and advantages of AdTSV that have not been exploited in this work. Techniques for DNA and RNA hybridization have been greatly improved in recent years but electrochemical techniques have not significantly contributed to this development [56]. Nucleic acid-modified electrodes may be of use in this field if a single-stranded nucleic acid adsorbed at the electrode can form a duplex with its complementary strand diffusing to it from the bulk of solution. Preliminary results (unpublished) suggest that at least with simple systems such a duplex formation may occur and produce a specific voltammetric response. Adsorption of single-stranded nucleic acids from different media (Fig. 2) may help to arrange properly the nucleic acid molecules on the electrode surface to obtain an optimum yield of the nucleic acid hybridization. Such experiments are in progress.

The electrode potential at which the biomacromolecule is adsorbed can significantly influence its adsorption and conformation on the surface. At moderate ionic strengths, the adsorption of single-stranded DNA is only slightly influenced by the potential of the HMDE within a wide potential range [1,57]. On the other hand, the potential-dependent unwinding of duplex DNA was observed by AdTSV in a narrow potential range of ca. -1.2 V [57]. The influence of the electrode potential and the composition and pH of the solution from which the adsorption is performed may greatly differ in proteins because, compared with nucleic acids, protein conformations and monomer (amino acid) compositions are more variable. Hence it might be useful to search for optimum adsorption conditions for each individual protein. Further, using AdTSV it may be possible to study specific interactions of proteins at the electrode surfaces. These potential interactions include the formation of DNA–protein, enzyme–substrate and antigen–antibody complexes. Protein and nucleic acid interactions in vivo occur in complex environments involving charged interfaces such as membranes and cell walls. Protein- and nucleic acid-modified electrodes may thus represent not only biosensors but also models for studies of biomacromolecule interactions in vivo.

The authors are indebted to Drs. Z. Kozarac, V. Vetterl and O. Vrana for critical reading of the manuscript and to J. Rainers for assistance with its preparation. Technical assistance of Mrs. Irena Postbieglová is gratefully acknowledged.

REFERENCES

1 E. Paleček, in G. Milazzo (Ed.), Topics in Bioelectrochemistry and Bioenergetics, Vol. 5, Wiley, Chichester, 1983, p. 65.

2 H.W. Nürnberg, in G. Milazzo and M. Blank (Eds.), Biochemistry, Vol. 1, Plenum, New York, 1983, p. 183.
3 E. Paleček, Bioelectrochem. Bioenerg., 15 (1986) 275.
4 E. Paleček, Bioelectrochem. Bioenerg., 20 (1988) 171.
5 E. Paleček, Methods Enzymol., 21 (1971) 3.
6 E. Paleček, Prog. Nucleic Acid Res. Mol. Biol., 18 (1976) 151.
7 E. Paleček, P. Boublíková and F. Jelen, Anal. Chim. Acta, 187 (1986) 99.
8 D. Krznaric and B. Cosovic, Anal. Biochem., 156 (1986) 454.
9 E. Paleček and I. Postbieglová, J. Electroanal. Chem., 214 (1986) 359.
10 E. Paleček, Anal. Biochem., 170 (1988) 421.
11 E. Lukášová, F. Jelen and E. Paleček, Gen. Physiol. Biophys., 1 (1982) 53.
12 M. Vojtíšková, E. Lukášová and E. Paleček, Folia Biol., 31 (1985) 248.
13 V. Fučik, R. Grunow, H. Grunnerová, Z. Hostomsky, S. Zadražil, in S. Zadražil and J. Sponar (Eds.), DNA: Recombination, Interactions and Repair, Federation of European Biochemical Societies, Vol. 63, Pergamon, Oxford, 1980, p. 111.
14 P. Boublíková, M. Vojtišková and E. Paleček, Anal. Lett., 20 (1987) 275.
15 L.G. Marzilli, Prog. Inorg. Chem., 23 (1977) 255.
16 A.M. Pyle and J.K. Barton, Prog. Inorg. Chem., 38 (1990) 413.
17 H. Elzanowska and J.H. van de Sande, Bioelectrochem. Bioenerg., 19 (1988) 425.
18 H. Elzanowska and J.H. van de Sande, Bioelectrochem. Bioenerg., 19 (1988) 441.
19 J.M. Sequaris and J. Swiatek, Bioelectrochem. Bioenerg., 26 (1991) 15.
20 M.T. Carter and A.J. Bard, J. Am. Chem. Soc., 109 (1987) 7528.
21 M.T. Carter, M. Rodriguez and A.J. Bard, J. Am. Chem. Soc., 111 (1989) 8901.
22 M.T. Carter and A.J. Bard, Bioconjugate Chem., 2 (1990) 257.
23 M. Rodriguez and A.J. Bard, Anal. Chem., 62 (1990) 2658.
24 M. Rodriguez, T. Kodadek, M. Torres and A.J. Bard, Bioconjugate Chem., 2 (1990) 123.
25 J.W. Webb, B. Janik and P.J. Elving, J. Am. Chem. Soc., 95 (1973) 8495.
26 V. Brabec and A.P. Kavunenko, J. Electroanal. Chem., 237 (1987) 261.
27 V. Brabec, V. Vetterl, V. Kleinwachter and J. Reedijk, Bioelectrochem. Bioenerg., 21 (1989) 199.
28 E. Paleček, V. Kolář, F. Jelen and U. Heinemann, Bioelectrochem. Bioenerg., 23 (1990) 285.
29 A. Engel, Annu. Rev. Biophys. Chem., 20 (1991) 79.
30 V.A. Bloomfield and P.G. Arscott, in F. Eckstein and D.M.J. Lilley (Eds.), Nucleic Acids and Molecular Biology, Vol. 5, Springer, Berlin, Heidelberg, 1991, p. 39.
31 V. Brabec and G. Dryhurst, J. Electroanal. Chem., 89 (1978) 161.
32 V. Brabec and G. Dryhurst, J. Electroanal. Chem., 91 (1978) 219.
33 V. Brabec and G. Dryhurst, Stud. Biophys., 67 (1978) 23.
34 V. Brabec, Biopolymers, 18 (1979) 2397.
35 V. Brabec, Bioelectrochem. Bioenerg., 7 (1980) 69.
36 J. Wang, V. Villa and T. Tapia, Bioelectrochem. Bioenerg., 19 (1988) 39.
37 V. Brabec and V. Mornstein, Biochim. Biophys. Acta, 625 (1980) 43.
38 J.A. Reynaud, B. Malfoy and A. Bere, Bioelectrochem. Bioenerg., 7 (1980) 595.
39 V. Brabec, Rev. Polarogr., 30 (1984) 50.
40 V. Brabec and I. Schindlerová, Bioelectrochem. Bioenerg., 8 (1981) 451.
41 J.S. Deetz and E.J. Behrman, J. Org. Chem., 45 (1980) 135.
42 G. Ruttkay-Nedecký and A. Anderleová, Nature (London), 213 (1967) 564.
43 G. Ruttkay-Nedecký and B. Bezúch, J. Mol. Biol., 55 (1971) 101.
44 G. Ruttkay-Nedecký and E. Paleček, Acta Virol., 24 (1980) 175.
45 G. Ruttkay-Nedecký and V. Brabec, Gen. Physiol. Biophys., 4 (1985) 393.
46 V. Pačes, C. Vlček, P. Urbánek and Z. Hostomsky, Gene, 44 (1986) 115.
47 V. Paces, C. Vlček, J. Šmarda, S. Zadražil and V. Fučík, Gene 54 (1987) 155.
48 E. Paleček, E. Lukásová, F. Jelen, and M. Vojtiškova, Bioelectrochem. Bioenerg., 8 (1981) 497.
49 E. Paleček, Crit. Rev. Biochem. Mol. Biol., 26 (1991) 151.
50 E. Paleček, Methods Enzymol., 212 (1992) 139.
51 J.D. Andrade, in J.D. Andrade (Ed.), Principle of Protein Adsorption in Surface and Interfacial Aspects of Biomaterial Polymers, Vol. 2, Plenum, New York, 1985, p. 1.
52 B.A. Kuznetsov, N.M. Mestechkina and G.P. Shumakovich, Bioelectrochem. Bioenerg., 4 (1977) 1.
53 B.A. Kuznetsov and G.P. Shumakovich, Bioelectrochem. Bioenerg., 2 (1975) 35.
54 H. Sawomoto and Y. Tanoue, J. Electroanal. Chem., 181 (1984) 209.
55 H. Randriamahazaka and J.-M. Nigretto, Anal. Chim. Acta, 257 (1992) 247.
56 M.E.A. Downs, S. Kobayashi and I. Karube, Anal. Lett., 20 (1987) 1897.
57 E. Paleček, Bioelectrochem. Bioenerg., 28 (1992) 71.

Analytica Chimica Acta, 273 (1993) 187–193
Elsevier Science Publishers B.V., Amsterdam

Alkaline phosphatase-modified carbon fibre disc microelectrode for the determination of 4-aminophenyl phosphate

F. Pariente, L. Hernández, H.D. Abruña and E. Lorenzo

Departamento de Química Analítica y Análisis Instrumental, Facultad de Ciencias, Universidad Autónoma de Madrid, 28049 Madrid (Spain)

(Received 1st June 1992; revised manuscript received 23rd September 1992)

Abstract

The construction and response of an alkaline phosphatase-modified carbon fibre disc microelectrode and its use as an amperometric sensor for the determination of 4-aminophenyl phosphate are described. The enzyme was immobilized on the electrode surface using glutaraldehyde and bovine serum albumin as cross-linking agents. The product of the enzymatic reaction, 4-aminophenol, was determined by oxidation at +0.3 V vs. a sodium chloride saturated calomel electrode, yielding a steady-state current directly related to the bulk concentration of the substrate. The response time of this microbiosensor was typically less than 3 s and 4-aminophenyl phosphate could be determined in the range 5.0×10^{-7}–5.0×10^{-3} M.

Keywords: Amperometry; Biosensors; Enzymatic methods; Alkaline phosphatase-modified electrode; Aminophenyl phosphate; Carbon fibre disc microelectrode; Enzyme electrodes

Ultramicroelectrodes have been employed for the detection of small biological molecules and drugs in physiological fluids [1]. They can be fabricated with appropriate dimensions for insertion in a single cell or tissue sample. Microelectrodes have increased mass transport and decreased double-layer capacitance and ohmic loss, resulting in an increased signal-to-noise ratio, a time-independent response and higher sensitivity [2] in comparison with electrodes of conventional size. Selectivity of ultramicroelectrodes can be achieved by modification or functionalization of the surface [3].

Many strategies have been developed for the immobilization of enzymes on electrode surfaces to improve the selectivity of electrochemical measurements [3]. However, very few enzyme-modified electrodes have been constructed that afford both a small probe size (i.e., < 10 μm diameter) and a rapid response time. Platinized microelectrodes utilizing surface-adsorbed enzymes have been reported to have response times of the order of a few seconds [4]. The stability of enzyme-modified electrodes has been improved by covalent attachment of the enzyme either to the electrode surface [5,6] or to redox polymers adsorbed on the electrode surface [7]. Pantano et al. [8] recently reported an enzyme-modified microelectrode constructed by linking horseradish peroxidase via a biotin–avidin–biotin tether to carbon fibre electrodes with a diameter of 8 μm defining the electroactive surface area and a slightly larger total structural diameter. These electrodes had response times of the order of 300

Correspondence to: E. Lorenzo, Departamento de Química Analítica y Análisis Instrumental, Facultad de Ciencias, Universidad Autónoma de Madrid, Madrid 28049 (Spain).

ms. Abe et al. [9] reported an immobilized enzyme glucose electrode with a total tip diameter as small as 2 μm using platinized carbon ring electrodes.

The feasibility of employing enzyme-modified electrodes for the determination of substrates in solution has been demonstrated previously, including the determination of xanthine an hypoxanthine [10] and 4-nitrophenyl phosphate [11]. In addition to general interest in the development of enzymatic electrodes for analytical determinations, we are also interested in the development of electrochemical microprobes [12] for performing determinations in very small samples. This paper describes a simple procedure for the construction of enzyme-modified carbon fibre microelectrodes where the enzyme is immobilized by cross-linking with glutaraldehyde.

EXPERIMENTAL

Reagents and materials

Carbon fibres, 3–5 cm long and of average diameter 7 μm, were obtained from (Donnay Sport Tennis, Belgium). Low-viscosity epoxy resin (Durcupan ACM, Fluka) was prepared according to the manufacturers specifications in 5-ml syringes and stored at −20°C. Alkaline phosphatase (EC 3.1.3.1; type I-S) from bovine intestinal mucose was purchased from Sigma as a lyophilized powder containing 1.6 IU of enzymatic activity per mg of protein. This preparation was stored dry at −20°C. Acetonitrile (SdS) was dried over 0.4-nm molecular sieves. Tetra-*n*-butylammonium perchlorate (TBAP) (G.F. Smith) was recrystallized three times from ethyl acetate and dried under vacuum. 4-Aminophenyl phosphate was synthesized by catalytic hydrogenation of 4-nitrophenyl phosphate (Aldrich) [13,14]. Glutaraldehyde (25% solution) (grade I, Sigma) was stored at −20°C. Water was purified with a Millipore Milli-Q system. All other chemicals were of at least analytical-reagent grade and were used as received.

Apparatus

A conventional three-electrode system in a glass cell fitted with a PTFE cap was used. The working electrode was a carbon fibre microelectrode prepared as described below. A platinum wire was used as the auxiliary electrode and a sodium chloride saturated calomel electrode (SSCE) as the reference electrode. All potentials are referred to the SSCE electrode without taking into account the liquid junction potential. The experiments were performed inside a Faraday cage. Cyclic voltammetric and amperometric studies were done with a BAS CV-27 potentiostat in conjunction with a BAS preamplifier PA-I low-current module. Data were recorded on a Linseys *X–Y/X–t* recorder. Optical microscopy was done using a Nikon Optihot microscope.

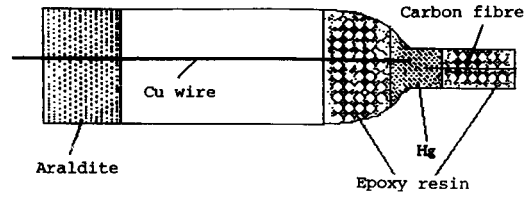

Fig. 1. Schematic diagram of the disc-shaped carbon fibre microelectrode.

Microelectrode fabrication

The carbon fibres were initially conditioned by immersion in distilled water followed by acetone, and were stored in acetone at room temperature. Prior to use, the carbon fibres were immersed in an ethanol–water (1 + 1, v/v) bath. Microelectrodes (see Fig. 1) were prepared by threading an individual carbon fibre through the tip (1 mm diameter) of a Pasteur pipette. The pipette was dried for 2 h at 60°C. A small drop of epoxy resin was carefully applied to the tip of the pipette with a syringe needle until approximately half of the carbon fibre was embedded in resin. The assembly was placed on a horizontal support at 70°C for 48 h to ensure complete polymerization of the resin. The microelectrodes obtained were examined by light microscopy to determine whether the carbon fibre was continuous to the very end of the tip.

Electrical contact to the carbon fibre was established with a copper wire and a drop of mercury. Additional epoxy resin was placed on top of the mercury and polymerized to prevent any leak-

age. The top of the pipette was then sealed with Araldite. Initially the microelectrodes were polished with 600-grit emery paper and subsequently with 10- and 1-μm diamond paste. Prior to experiments the electrodes were polished with 1-μm diamond paste and rinsed with water and acetone.

Microelectrode modification with alkaline phosphatase activity

The proposed modification procedure represents a combination of existing methodologies. The advantages are that owing to the activation and cross-linking procedures, the enzyme is strongly retained yet there are no transport limitations, so that the response time of the sensor is short. Freshly polished carbon fibre electrodes were immersed for 30 min in 2.5% (v/v) glutaraldehyde and 1% (w/v) bovine serum albumin (BSA) solution at 4°C, followed by washing in cold 0.1 M glycine buffer (pH 9.5) for 1–2 min. The electrodes were subsequently dried in air at room temperature. A 2-μl drop containing 0.05–2.0 IU of alkaline phosphatase with 1% (w/v) of BSA in 0.1 M glycine buffer (pH 9.5) was carefully placed on the electrode surface and allowed to dry at room temperature. Prior to use, the enzyme-modified microelectrodes were immersed in cold glycine buffer (pH 9.5) for 30 min to remove any physically entrapped or weakly bonded enzyme. This ensured reproducibility in subsequent measurements. After the experiments the electrodes were soaked in glycine buffer containing 0.01% (w/v) sodium azide and stored at 4°C.

RESULTS AND DISCUSSION

Characterization of enzyme-modified electrode

The microelectrodes exhibit good electrochemical performance. Well developed sigmoidal voltammograms for the oxidation of ferrocene in acetonitrile containing 0.1 M TBAP are observed

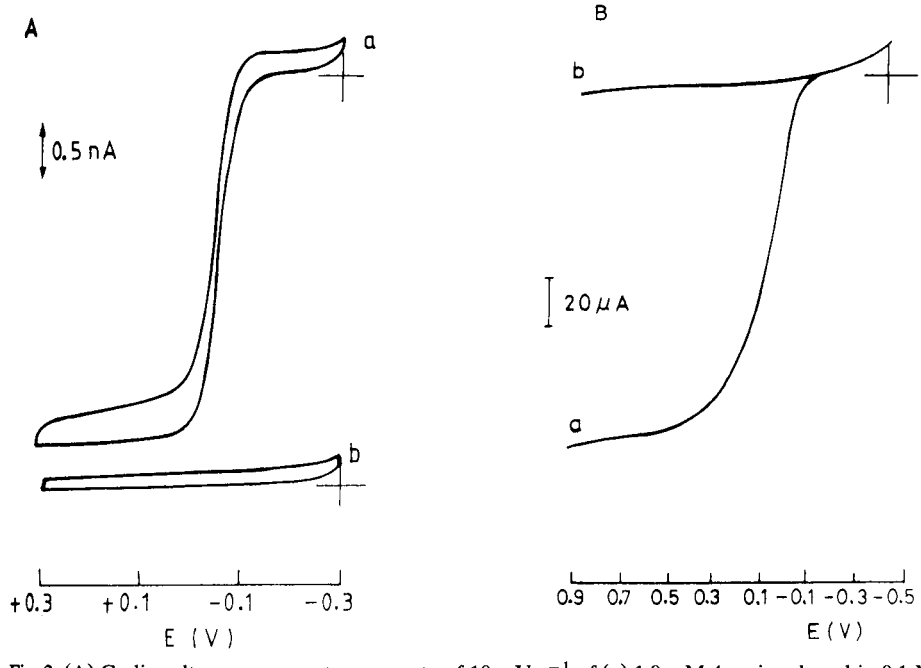

Fig. 2. (A) Cyclic voltammograms at a scan rate of 10 mV s^{-1} of (a) 1.0 mM 4-aminophenol in 0.1 M glycine with 0.1 M KCl buffer (pH 9.5) at a 4.5-μm diameter carbon fibre electrode and (b) blank. (B) Anodic current vs. potential applied to a 0.3-mm diameter glassy carbon electrode with a rotation speed of 2500 rpm for (a) 1.0 mM 4-aminophenol in 0.1 M glycine with 0.1 M KCl buffer (pH 9.5) and (b) blank. The potential was scanned at 50 mV s^{-1}.

for sweep rates from 5 to 500 mV s^{-1}. The slope calculated from the plot of E vs. $\log[i/(i_L - i)]$ was found to be 60 ± 2 mV, which is very close to the value of 59 mV expected for a reversible one-electron reaction [15].

The steady-state or limiting current for microelectrodes of disc geometry is expected to follow the equation

$$I = 4nFDC_r^* r \quad (1)$$

were r is the radius and the other symbols have their usual meanings. Precise values of the electrode radii were calculated from values of the steady-state voltammetric limiting currents for the oxidation of ferrocene in acetonitrile containing 0.1 M TBAP and using the reported value for the diffusion constant of ferrocene in acetonitrile (2.4×10^{-5} cm^2 s^{-1}) [16]. Diameters in the range 4–10 μm were obtained. Optical measurements were also made of the radii of the electrodes and these values correlated well with those derived from voltammetric measurements.

Electrode response

The microsensor response is based on the amperometric detection of 4-aminophenol, which is the product of the hydrolysis of 4-aminophenyl phosphate ester by alkaline phosphatase. A detailed study of this substrate for alkaline phosphatase determinations using conventional electrodes has been the subject of previous work [17].

Figure 2 shows the voltammetry of 4-aminophenol at (A) a 4.5-μm diameter carbon fibre electrode and (B) a 0.3-cm diameter rotated glassy carbon disc electrode. The voltammogram obtained with the carbon fibre electrode is sigmoidal (steady-state), as expected for a microvoltammetric electrode. The half-wave potential (−0.05 V vs. SSCE) is similar to that for 4-aminophenol oxidation at larger glassy carbon electrodes (see Fig. 2B) and the voltammetric wave appears to be kinetically reversible. The slope of the wave calculated from the plot of E vs. $\log[i/(i_L - i)]$ was found to be 30 ± 1 mV. This value is very close to that expected for a reversible two-electron reaction [15]. The diffusion coefficient of 4-aminophenol was calculated from Eqn. 1 using values of the steady-state voltammetric limiting current for the oxidation of 4-aminophenol in 0.1 M glycine buffer (pH 9.5) and using the value of the electrode radius calculated from the voltammetric response for the oxidation of ferrocene in acetonitrile containing 0.1 M TBAP. It was found that the diffusion coefficient is 9.8×10^{-6} cm^2 s^{-1}. This values agrees well with that obtained in previous work with a 0.3-cm diameter rotated glassy carbon disc-shaped electrode under similar conditions [17].

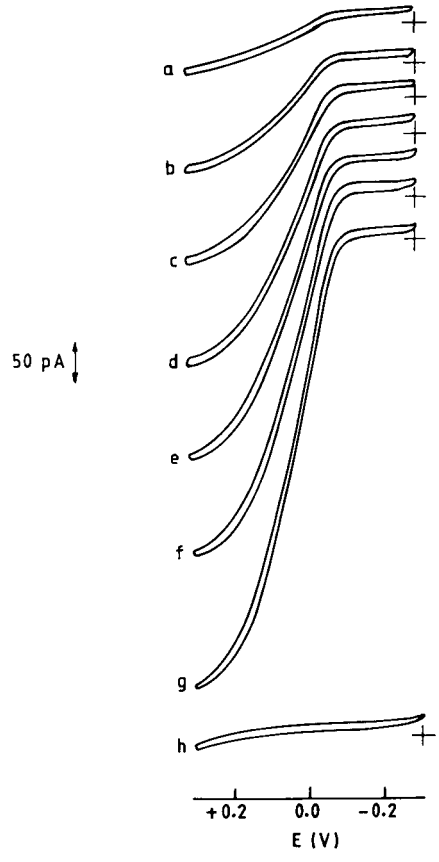

Fig. 3. Voltammetric response of a 4.5-μm diameter alkaline phosphatase carbon fibre microelectrode in 0.1 M glycine buffer (pH 9.5) to increasing amounts of 4-aminophenyl phosphate (PAPP): (a) 0.2, (b) 0.4, (c) 0.6, (d) 0.8, (e) 1.0, (f) 1.2 and (g) 1.4 mM and (h) blank. Scan rate, 10 mV s^{-1}.

Figure 3 shows the voltammetric response obtained when a carbon fibre microelectrode modified with 0.25 IU of alkaline phosphatase activity is immersed in a solution containing increasing

amounts of 4-aminophenyl phosphate in glycine buffer (pH 9.5). The steady-state voltammograms observed correspond to the oxidation of the enzymatically generated product, 4-aminophenol. Therefore, in subsequent experiments the electrode was poised at +0.3 V vs. SSCE (to ensure transport limited oxidation of the 4-aminophenol generated) and the anodic current was monitored continuously with time. A steady-state value was typically reached in less than 3 s and the currents obtained for various concentrations of the substrate were employed in constructing the response curves for 4-aminophenyl phosphate. These results are shown in Fig. 4.

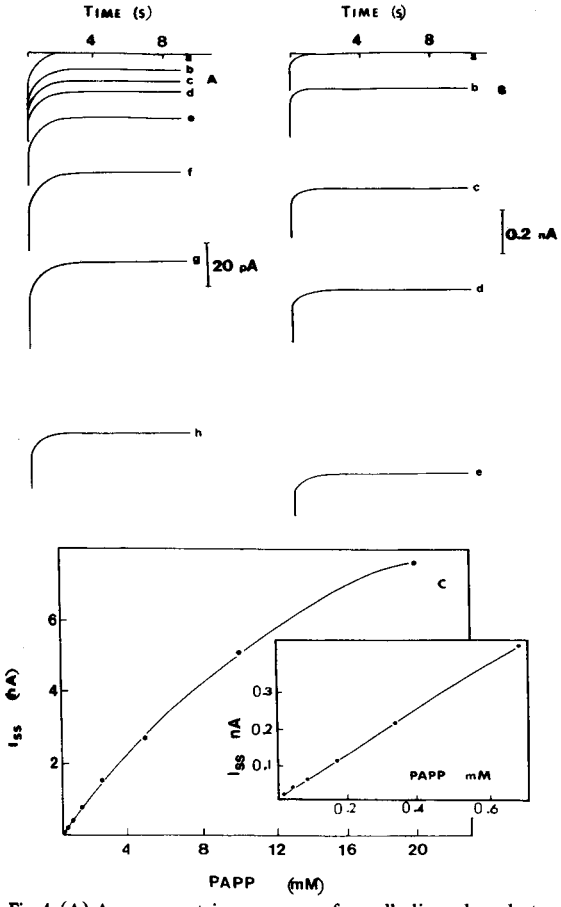

Fig. 4. (A) Amperometric response of an alkaline phosphatase modified carbon fibre electrode in 0.1 M glycine buffer at pH 9.5 to increasing quantities of PAPP. (a) 0, (b) 5, (c) 10, (d) 21, (e) 42, (f) 84, (g) 168 and (h) 337 μM. (B) (a) 0, (b) 0.675, (c) 1.25, (d) 2.5 and (e) 5.0 mM. (C) Steady-state currents vs. PAPP concentration. The linear response region is given in the inset.

In previous work [17], a conventionally sized electrode modified with alkaline phosphatase was found to exhibit a linear response range over more than three orders of magnitude of 4-aminophenyl phosphate concentration. The enzyme microelectrode reported here displayed a linear response range of over four decades in the substrate concentration. The sensitivity in the linear response region of the calibration graph reached 1.4×10^3 nA l mol^{-1}, with a detection limit of 5×10^{-7} M. These results confirm that the enzyme-modified ultramicroelectrodes can be employed in analytical determinations without loss of sensitivity and, in fact, with enhanced sensitivity. The relative standard deviation was 3% ($n = 5$) for a 1 mM substrate solution, hence the system has high reproducibility.

Shu and Wilson [18] suggested that for an enzymatic reaction that is catalytically controlled, the apparent Michaelis–Menten constant (K'_m) can be calculated for the immobilized enzyme by amperometric methods using a Lineweaver–Burk-type plot constructed according to the equation

$$1/i_{ss} = (K'_m/i_{max})(1/C_S) + 1/i_{max}$$

where i_{ss} is the steady-state current, i_{max} is the current measured under conditions of substrate saturation for the enzymatic product detection and C_S is the substrate concentration. A plot of $1/i_{ss}$ vs. $1/C_S$ gave a straight line with a slope (K'_m/i_{max}) of 1.40 mM nA^{-1} and an intercept ($1/i_{max}$) of 0.18 nA. The i_{max} and K'_m values obtained from the Lineweaver–Burk plots were of 6.2 nA and 250 μM, respectively. This value of K'_m agrees well with that obtained previously under conditions of low diffusional resistance (high electrode rotation speed) [17].

The correlation between the enzymatic activity incorporated on the electrode and the limiting current response for a 2.0 mM concentration of substrate was studied using electrodes with diameters between 2.0 and 6.0 μm and different units of immobilized enzyme. Figure 5 depicts the radius-normalized limiting current response versus the incorporated enzymatic activity. The relative

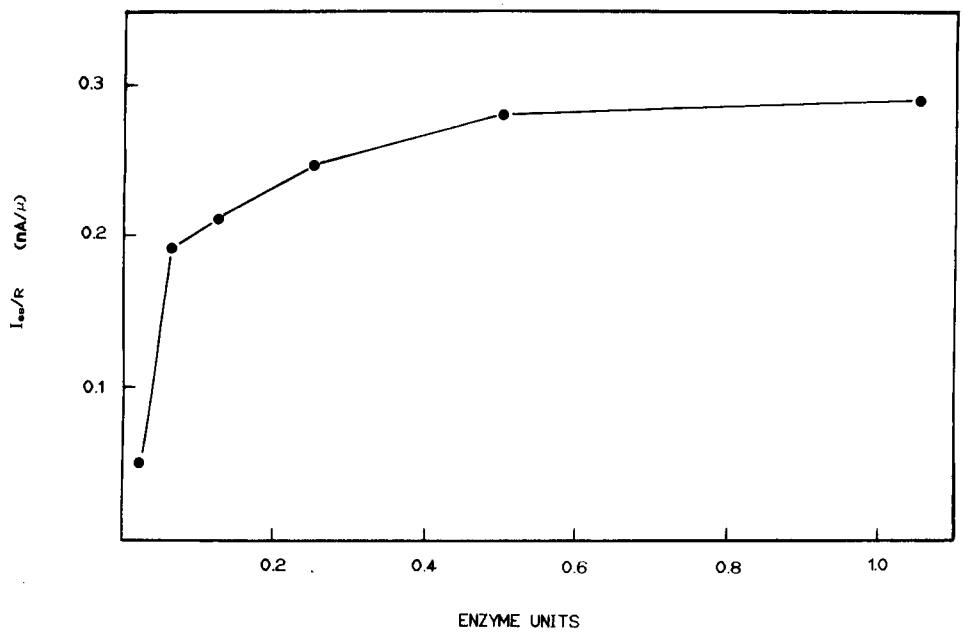

Fig. 5. Plot of radius normalized limiting current vs. incorporated enzyme activity.

i_L response increases with increasing alkaline phosphatase incorporated on the electrode and then levels off so that an optimum response could be obtained with relatively small amounts of immobilized enzyme.

In previous work the pH profile for this system was determined [17] and it was found that the sensor exhibited maximum activity in the pH range 9.5–10.5, as would be expected from solution measurements. Hence the immobilization process does not affect the behaviour profile of alkaline phosphatase.

An important consideration in the use of microelectrodes for direct measurements on real samples is the effect of the supporting electrolyte concentration on the electrode response. Figure 6 shows a plot of the average amperometric signal obtained with an alkaline phosphatase microsensor placed in 1.0 mM 4-aminophenyl phosphate ester solution at various supporting electrolyte (KCl) concentrations. When the concentration of KCl is reduced from 0.2 M to 25 mM the amperometric response is relatively unaffected. This suggests that this type of sensor can be used to monitor alkaline phosphatase activity in samples where the ionic strength can vary widely.

The stability of these microsensors was ascertained by observing the amperometric response obtained in solutions containing 1.0 mM 4-aminophenyl phosphate for a period of 72 h. The electrode was stored after each assay as described under Experimental. The decrease in the response over that time period was found to be less than 15%.

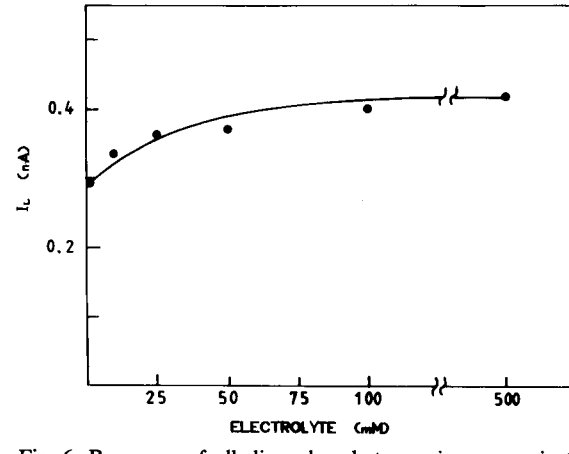

Fig. 6. Response of alkaline phosphatase microsensor in 1.0 mM PAPP solution in 0.1 M glycine buffer (pH 9.5) at various KCl supporting electrolyte concentrations.

The selectivity of this microsensor was checked in amperometric experiments by the addition of other phenol esters typically used in the spectrophotometric detection of alkaline phosphatase such as 4-nitrophenyl phosphate and 1-naphthyl phosphate. No detectable response was observed owing to the significantly higher oxidation potentials of their reaction products. The products of enzymatic hydrolysis of nucleoside monophosphate esters, present in many cellular extracts, have high oxidation potentials. The above results indicate that no interference from such substances would be expected in the use of the alkaline phosphatase-modified microelectrodes in biological samples.

This work was supported in part by the Universidad Autónoma of Madrid, through the Precompetitive Award Programme (E.L.) and the CICYT (Grant No. PB 840152). E.L. acknowledges the CICYT for a Visiting Scientist fellowship at Cornell University. The authors thank E. Gonzalez for assistance with this work.

REFERENCES

1 J.L. Pouchon, R. Cespuglio, F. Gonon and J.F. Pujol, Anal. Chem., 51 (1979) 1483.
2 M. Fleischman, S. Pons, D.R. Robinson and P.P. Schmidt, Ultramicroelectrodes, Datatech. Systems, Morganton, NC, 1987.
3 A.P.F. Turner, I. Karube and G.S. Wilson (Eds.), Biosensors: Fundamentals and Applications, Oxford University Press, Oxford, 1987.
4 Y. Ikariyama, M.A. Yamauchi, T. Yushiashi and H. Ushioda, Bull. Chem. Soc. Jpn. 61 (1988) 3525.
5 R.M. Ianello and A.M. Yacynych, Anal. Chem., 53 (1981) 2090.
6 P. Bianco, J. Haladjian and C.J. Bordillion, Electroanal. Chem., 293 (1990) 151.
7 B.A. Gregg and A. Heller, Anal. Chem., 62 (1990) 258.
8 P. Pantano, T.H. Morton and W.G. Kurh, J. Am. Chem. Soc., 113 (1991) 1832.
9 T. Abe, Y.Y. Lau and A.G. Ewing, J. Am. Chem. Soc., 113 (1991) 7421.
10 E. Gonzalez, F. Pariente, E. Lorenzo and L. Hernández, Anal. Chim. Acta, 242 (1991) 267.
11 E. Lorenzo, E. González, F. Pariente and L. Hernández, Electroanalysis, 3 (1991) 319.
12 R.M. Wightman, Anal. Chem., 53 (1981) 1125A.
13 L.H. de Rimer and L.F. Meares, Biochemistry, 20 (1981) 1606.
14 R.Q. Thomsom, G.C. Barone, H.B. Halsall and W.R. Heineman, Anal. Biochem., 192 (1991) 90.
15 A.J. Bard and L.R. Faulkner, Electrochemical Methods, Wiley, New York, 1980.
16 T. Kuwana, D.E. Bublitz and G. Hoh, J. Am. Chem. Soc., 82 (1960) 5811.
17 F. Pariente, L. Hernández and E. Lorenzo, Biochem. Bioenergy., 27 (1992) 73.
18 F.R. Shu and G.S. Wilson, Anal. Chem., 48 (1976) 1679.

Analytica Chimica Acta, 273 (1993) 195–204
Elsevier Science Publishers B.V., Amsterdam

Voltammetry with carbon paste electrodes containing membrane plasticizers used for PVC-based ion-selective electrodes

Ivan Švancara and Karel Vytřas

Department of Analytical Chemistry, Technical University of Pardubice, CS-532 10 Pardubice (Czechoslovakia)

(Received 1st June 1992; revised manuscript received 24th September 1992)

Abstract

Carbon paste electrodes were prepared by mixing graphite powder with liquids that have been applied as plasticizers for membranes of ion-selective electrodes. In voltammetric measurements, these electrodes exhibited interesting properties such as a wide anodic and cathodic potential range, very low reduction peak of oxygen in the cathodic scan and high extraction and adsorption capabilities. They were shown to be convenient, especially for the selective accumulation of metals in the form of their anionic complexes. Two examples are given. The voltammetric behaviour of gold as its $[AuCl_4]^-$ complex and of bismuth as the $[BiI_4]^-$ anion is discussed.

Keywords: Ion selective electrodes; Stripping voltammetry; Voltammetry; Bismuth; Carbon paste electrodes; Gold; Membrane electrodes; Plasticizers

Carbon paste electrodes (CPEs) and chemically modified carbon paste electrodes have frequently been used in trace analyses for heavy metal ions and organic pollutants and in biological research [1,2]. A wide anodic potential range with low background currents and extraction capabilities are among the unique properties of these electrodes.

Numerous workers have dealt with the question of the relationship between the kind of carbon powder and pasting liquid and the behaviour of CPEs [3–5]. It was stated that despite certain specific properties of the pasting liquid, the choice of this liquid is not especially important in defining the electrochemical and kinetic behaviour of CPEs. Rather, the quality of graphite powder and the ratio between the proportions of graphite and pasting liquid have often been considered to be of major importance in determining electrode properties. However, these conclusions could be influenced by the fact that pasting liquids with similar physico-chemical properties were often used. Most of the pasting liquids, such as Nujol oil, silicone oils, short-chain hydrocarbons, 1-bromonaphthalene and fluorinated hydrocarbons [6], are non-polar and chemically inert.

The plasticizers that are used to prepare membrane ion-selective electrodes [7] represent a group of substances capable of undergoing various interactions with both inorganic and organic ions. The extraction capabilities of liquid plasticizers depend on their polarities. Plasticizers such as dialkyl and trialkyl phosphates, alkyl esters of phthalic acid and nitrated alkyl and aryl esters

Correspondence to: K. Vytřas, Department of Analytical Chemistry, Technical University of Pardubice, CS-532 10 Pardubice (Czechoslovakia).

have been widely used [8]. Substances of the trialkyl phosphate type have also been used to extract some heavy metal ions and lanthanides or actinides. Kalcher et al. [9] have reported on the use of both tributyl phosphate and trioctylphosphine oxide for the modification of CPEs. These electrodes containing 10 and 50% (w/w) of the modifier were exploited to accumulate gold in the form of tetrachloroaurate, $[AuCl_4]^-$, via an extraction mechanism. Gold in the complex was then reduced by imposing a cathodic scan, which resulted in a peak suitable for analytical purposes.

In this paper, it is shown that CPEs containing plasticizers as a pasting liquid exhibit some interesting properties. They can be regarded as a qualitatively new type of CPEs, as these electrodes contain a liquid with properties distinctly different from those of conventionally used pasting liquids. The results of recent work [10] and experience of CPEs based on the plasticizers have shown that the role of a pasting liquid is more important than has been reported in the past. Two examples showing the selectivity to some metal ions, namely gold(III) and bismuth(III), are presented.

Gold(III) is able to form anionic complexes with halides. The formation of $[AuCl_4]^-$ and $[AuBr_4]^-$ anions has been exploited to determine gold. For example, CPEs modified with an alga [11], tertiary alkylamine [12] or chelating resin [13] have been tested for this purpose. Kalcher and co-workers have suggested CPEs containing an ion exchanger [14], dithizone [15], Rhodamine B [16] or organophosphorus compounds [9]. In all instances, it was confirmed that gold was accumulated as $[AuCl_4]^-$.

Bismuth(III) belongs to the ions that can be sensitively determined using differential-pulse anodic stripping voltammetry. Nevertheless, numerous determinations of bismuth(III) suffer from interferences from other ions, especially antimony(III) and copper(II); on the other hand, determinations of antimony(III) and copper(II) are adversely affected by the presence of bismuth(III) [17]. These interferences can be suppressed by using masking agents [18] or by suitable chemical modification of the CPE [19,20].

EXPERIMENTAL

Chemicals and reagents

All chemicals were of analytical-reagent grade. The supporting electrolytes were prepared from doubly demineralized water obtained by passing distilled water through a Milli-Q water-purification system (Millipore). Solutions of heavy metals were prepared at concentrations of 0.01 M. Dilute solutions ($\leq 1 \times 10^{-3}$ M) of Au(III), Bi(III) and other ions were prepared freshly each day.

Apparatus

All measurements were carried out using a PA 3 polarographic analyser connected to an XY 4105 recorder (both from Laboratorní přístroje, Prague). The electrochemical behaviour of Au(III) and Bi(III) ions was monitored by cyclic voltammetry and differential-pulse stripping voltammetry. A three-electrode cell involving a CPE as the working electrode, an Ag/AgCl reference electrode and a platinum counter electrode were used. A mechanical stirrer belonging to the standard equipment of the PA 3 analyser was used. A conventional ohmmeter (Tesla Kolín) was employed to measure the electric resistance of the pastes. Oxygen was removed by passing argon through the electrolyte solution for 10 min. Small volumes of metal ion solutions were introduced into the cell using a Varipipette 3000 microsyringe (Plastomet, Poland).

Carbon paste electrodes

The pastes were prepared by thoroughly mixing graphite powder (CR-2, Tesla Lanškroun) and the selected pasting liquid using a pestle and mortar. Five pastes were prepared: (1) 1.0 g of graphite (C) + 0.4 ml of Nujol oil (Nj) (Merik); (2) 1.0 g of C + 0.4 ml of MV 15 500 silicone oil (SO) (Lučební závody, Kolín); (3) 1.0 g of C + 0.4 ml of tricresyl phosphate (TCP) (Lachema, Brno); (4) 1.0 g of C + 0.4 ml of dioctyl phthalate (DOP) (Aldrich); and (5) 1.0 g of C + 0.4 ml of 2,4-dinitrophenyl *n*-octyl ether (DNPOE) (Crytur, Turnov).

The choice of liquid plasticizers contained in pastes (3)–(5) was made in an effort to test three representative types of membrane plasticizers that have found use in potentiometry [7,8]. Pastes (1)

and (2) served as reference, as Nujol and silicone oils belong amongst the most widely used pasting liquids. The pastes were packed into piston-like electrode holders [2]. A fresh electrode surface was obtained by wiping the paste with a wet filter-paper.

RESULTS AND DISCUSSION

Characterization of carbon paste electrodes containing the plasticizers as a pasting liquid

Electrical resistance of CPEs. The electrical resistance was measured for all the pastes. The piston was adjusted to the same level. The pastes, including those mixed from Nj or SO, had a low resistance from 4 to 10 Ω.

Anodic and cathodic potential ranges of CPEs. Anodic and cathodic potential limits for four CPEs are summarized in Table 1. As expected, the paste containing DNPOE was inapplicable from a voltammetric point of view because this plasticizer comprises electroactive nitro groups. The data show that CPEs with other plasticizers had very positive anodic potential ranges compared with the ordinary CPEs (1) and (2). Especially in a 0.2 M H_2SO_4 medium, both electrodes with plasticizers exhibited an extremely positive potential limit. A high cathodic limit was achieved using the same electrode in a borate buffer. This electrode had also low background currents. Previously, the anodic and cathodic potential limits of CPEs have been considered to be due to the quality of the graphite powder and some workers have proposed various pretreatments to extend both the anodic and cathodic ranges [2,5]. The present results show clearly that the pasting liquid also plays a role.

TABLE 1

Anodic and cathodic potential limits of the four carbon paste electrodes

Carbon Paste	Supporting electrolyte	Anodic potential limit (V)	Cathodic potential limit (V)	Note
C+Nj	0.1 M HCl	+1.10	−0.95	
	0.1 M KCl	+1.20	−1.40	
	0.1 M NaOH	+0.80	−1.50	
C+SO	0.1 M HCl	+1.25	−0.90	
	0.1 M KCl	+1.20	−1.10	
	0.1 M NaOH	+0.85	−1.40	
C+TCP	0.1 M HCl	+1.25	−1.10	From +0.8
	0.2 M H_2SO_4	+1.60	−0.95	to +1.2 V
	0.1 M KCl	+1.45	−1.40	higher
	0.1 M NaOH	+1.25	−1.50	background
C+DOP	0.1 M HCl	+1.35	−1.10	currents
	0.2 M H_2SO_4	+1.65	−0.90	
	0.1 M KCl	+1.30	−1.50	
	0.1 M NaOH	+1.20	−1.50	
	Borate buffer (pH 9.0)	+1.15	−1.65	

Electrochemical and kinetic properties of CPEs. It was found that C + TCP and C + DOP electrodes can be used just like conventional solid electrodes to preconcentrate heavy metals at the electrode surface using differential-pulse anodic stripping voltammetry (DPASV). The peak potentials, E_p, of Pb, Tl, Cu and Hg were found at almost the same values as those obtained at the electrodes with Nj and SO. The sensitivity and reproducibility of the plasticizer-based electrodes were also very similar. Cyclic voltammograms of $[Fe(CN)_6]^{4-}$–$[Fe(CN)_6]^{3-}$ and hydroquinone–quinone systems, often used as model redox couples for electrode testing [3,5], were also obtained. No significant differences between these electrodes and classical CPEs were registered. This is in accordance with previous investigations in which it has frequently been proved that the electrode kinetics are affected mainly by the quality of the graphite and, in some instances, by the graphite-to-pasting liquid ratio [3,5,21].

Reduction of oxygen dissolved in the paste. It is known that during the cathodic scan, both solid carbon and carbon paste electrodes suffer from the reduction of oxygen. Mostly, this is considered to be due to oxygen adsorbed in the pores of graphite, which is difficult to remove [2,6]. Figure 1 shows four curves recorded in 0.1 M HCl solution from which oxygen had been thoroughly removed by bubbling argon through for 15 min. For all these pastes, the voltammograms were obtained under the same conditions, i.e., the same supporting electrolyte solution and identical analyser sensitivity. It is surprising how the type of pasting liquid significantly affected the shape of

the cathodic curve. The recorded baseline for the C + TCP paste suggests that the content of oxygen monitored via its cathodic reduction was markedly lower in comparison with the pastes prepared from Nj and SO. This could be explained by the fact that the plasticizer could cover active absorption sites of the graphite particles [22]. This advantageous property of plasticizer-based CPEs seems to be useful for cathodic redepositions of extracted and adsorbed substances.

Ageing of CPEs. It was observed that both C + TCP and C + DOP electrodes exhibited a substantial change in consistency in time, probably because of the higher volatility of the plasticizer. Thus, desiccated pastes had lost their optimum properties. It was found that the electrode lifetime due to the stability of the paste was about 3 weeks.

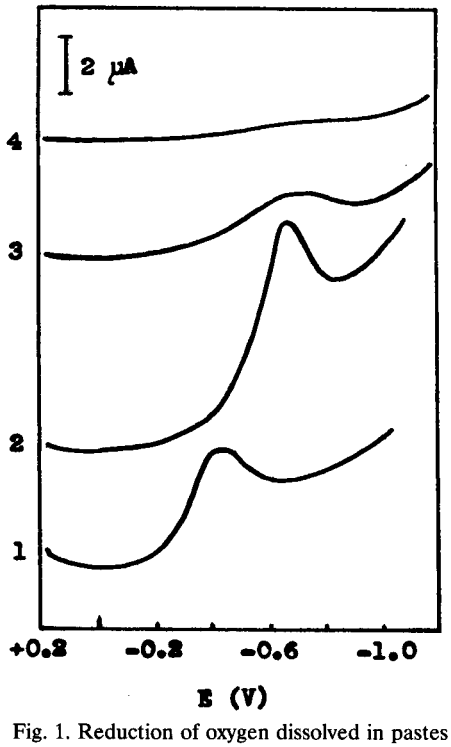

Fig. 1. Reduction of oxygen dissolved in pastes of four carbon paste electrodes: (1) C+Nujol; (2) C+silicone oil; (3) C+ dioctyl phthalate; (4) C+tricresyl phosphate; Measurements carried out in 0.1 M HCl.

Example I: accumulation of gold in the form of $[AuCl_4]^-$

Accumulation mechanism at various carbon paste electrodes. To establish the nature of the accumulated species, it is important to choose optimum voltammetric parameters. After accumulation performed under open-circuit conditions, Au(III) was reduced to Au(0) at $E_p = +0.4$ V vs. Ag/AgCl by imposing a cathodic scan.

The accumulation of gold in the form of an $[AuCl_4]^-$ anionic complex at four different CPEs is shown in Fig. 2. It is clear that with Nj and SO electrodes [set of voltammograms (a) and (b)], the accumulation process differs from the behaviour of plasticizer-based CPEs [(c) and (d)]. Electrodes with the plasticizers showed an increasing current signal depending on the accumulation time, τ_{ac}. This was in contrast to CPEs of type (1) and (2).

Figure 3 shows a plot of i_p vs. τ_{ac}. The experimental data confirm the different accumulation mechanisms at various carbon paste electrodes. The plots for both C + DOP and C + TCP pastes (curves 1 and 2) are similar to those of Wang et al. [23] reported for a study dealing with the extractive accumulation of some organic compounds at a CPE. On the other hand, the i_p vs. τ_{ac} curves for C + Nj and C + SO pastes (Fig. 3) correspond to the general shape of an adsorptive accumulation plot [24]. From the experimental dependences for electrodes with plasticizers in Fig. 2, it is evident that using extremely long accumulation times, i_p increased less than expected. This is in accordance with the fact that a substance extracted into a substantial depth of the paste had to cover a long diffusion path through the interior of the paste in order to participate in the electrode process in the stripping step [23]. This also results in a considerable width of the extraction peak.

It was deduced from these observations that CPEs with plasticizers exhibit "extraction behaviour", whereas the processes at CPEs with Nj and SO correspond to adsorption. It should be mentioned that the extraction capability of electrodes modified with organophosphorus derivatives has already been described by Kalcher et al. [9], who reported on the extraction of ionic asso-

ciates such as $\{[(TBP)_2(H_2O)_nH][AuCl_4]\}$ where TBP is tributyl phosphate and $n = 0$–3.

The adsorption at C + Nj and C + SO electrodes may be due to the electrostatic forces, as it is known that the electrode surface of CPEs polarized in an anodic range contains OH groups [21] that can be protonated, thus attracting $[AuCl_4]^-$ anions.

Finally, the extraction character of the $[AuCl_4]^-$ accumulation at plasticizer-based CPEs was confirmed again by the fact that the response to gold gradually increased when the same electrode surface had been used for successive scans. If the surface layer was always removed prior to a new scan, a reproducibility obtained was very good with a relative error of less than 5%.

Accumulation of other anions of gold. The behaviour of Au(III) in electrolyte solutions of other halides and pseudohalides was also investigated. Useful information can be obtained from the voltammetric curves (Fig. 4) together with the chemical equilibria data on the $[AuX_4]^-$ complexes (where X = F, Cl, Br, SCN and CN) [25]. For instance, the presence of $[Au(SCN)_4]^-$ (stability constant $\log \beta = 43$) and $[Au(CN)_4]^-$ ($\log \beta = 56$) complexes can be predicted directly from the voltammograms, as their peaks were considerably shifted towards more negative po-

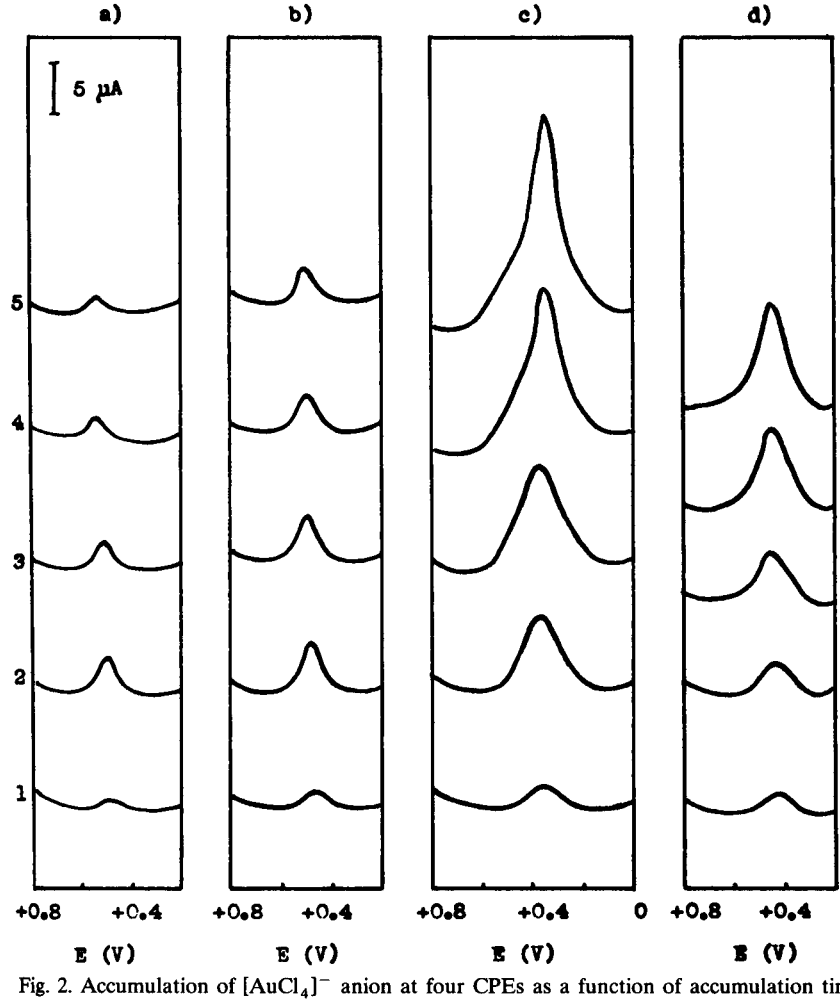

Fig. 2. Accumulation of $[AuCl_4]^-$ anion at four CPEs as a function of accumulation time. (a) C + Nujol; (b) C + silicone oil; (c) C + tricresyl phosphate; (d) C + dioctyl phthalate. Accumulation time: (1) 0; (2) 40; (3) 80; (4) 200; (5) 360 s.

tentials in comparison with the peak of $[AuCl_4]^-$ (log $\beta = 29.6$).

Interferences from other ions and their possible suppression. Table 2 surveys the interference from many ions tested. Negative effects of individual ions are expressed as a number (%) representing the decrease (−sign) or increase (+sign) of the original peak of $[AuCl_4]^-$ taken as 100%. As the CPE with dioctyl phthalate exhibited lower sensitivity, only the electrode with TCP was used for further measurements.

The survey confirms the high selectivity of the CPE with TCP over the other ions. Except for the reducing agents, the other ions did not interfere at concentrations comparable to the concentration of gold. At a higher excess, some ions such as Tl(III), Hg(II), Sb(III), Bi(III) and Fe(III) unfavourably affected the response of gold because all these ions form stable anionic complexes. The above ions gave rise to a response that was superimposed on the peak of gold (see Table 2, +sign). This effect correlated with the stability of their anionic complexes.

Optimum procedure for accumulating gold(III). Optimum conditions for the accumulation of Au(III) at a CPE containing TCP were chosen in concordance with observations described in the previous sections.

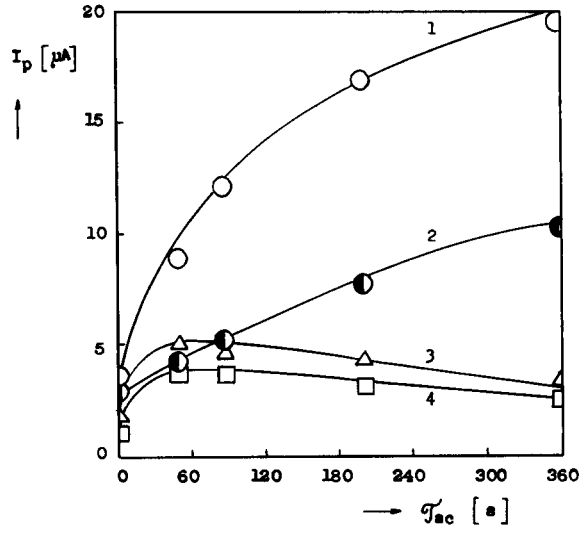

Fig. 3. Relationship between peak height (i_p) and accumulation time (τ_{ac}). $c_{AuCl^-} = 1 \times 10^{-6}$ M. Experimental plots for (1) C+TCP, (2) C+DOP, (3) C+SO and (4) C+Nj.

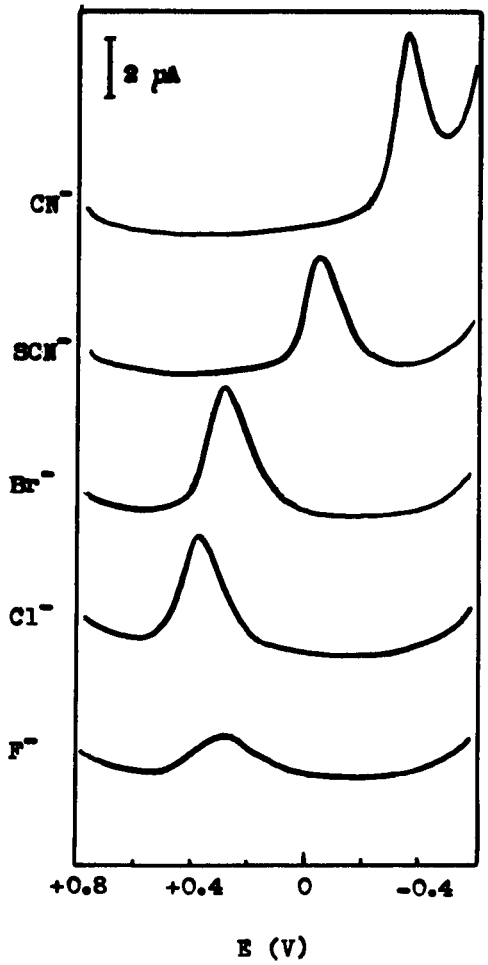

Fig. 4. Behaviour of gold anions at an electrode containing tricresyl phosphate. $c_{AuCl^-} = 1 \times 10^{-6}$ M. Supporting electrolyte: 0.1 M H_2SO_4 + 0.1 M KX (X = F, Cl, Br, SCN, CN).

A 0.1 M HCl medium was used as the supporting electrolyte and accumulation for 40 s was performed without application of potential. The voltammograms were registered by means of a cathodic scan from +0.8 to −0.4 V vs. Ag/AgCl. Each measurement was carried out at a fresh surface of the CPE.

To solve problems associated with interferences from some ions, the theory of chemical equilibria has been exploited. Thus, a suitable masking agent (e.g., EDTA) added to the sup-

porting electrolyte allowed the determination of gold in practical samples with a complex matrix. Using a C + TCP electrode, gold has been determined in samples of gilded electronic components containing also copper and iron that were present at a 100–1000-fold concentration excess [26].

Example II: accumulation of bismuth in the form of $[BiI_4]^-$

Accumulation mechanism. All measurements were carried out with CPEs containing TCP and a mixture of H_2SO_4 + KI was used as the supporting electrolyte. Similarly to the accumulation of $[AuCl_4]^-$, the $[BiI_4]^-$ complex could be accumulated without application of potential. The starting potential for the stripping step had to be chosen as $E_{init} = +0.2$ V vs. Ag/AgCl in order to avoid reduction of iodine. Farsang [4] has reported that the voltammetric curve comprises current contributions corresponding to the reaction $I_2 + 2e^- = 2\,I^-$ in both directions, even if the solution had originally contained only one of the forms, either the reduced or oxidized substance.

For the conditions given above, it was observed that the accumulation of the $[BiI_4]^-$ complex proceeded via the adsorption or electrostatic interaction, respectively, because the i_p vs. τ_{ac} dependence was of the same character as curves 3 and 4 in Fig. 3.

A peak at $E_p = -0.35$ V vs. Ag/AgCl obtained during the cathodic scan was attributed to the reduction of Bi(III) to Bi(0) in the complex. A similar behaviour was observed at CPEs with Nj and SO. However, owing to a large reduction peak of oxygen at the cathodic scan, these electrodes could not be used to monitor the reduction peak of $[BiI_4]^-$, which was obscured by the

TABLE 2

Interferences of other ions on the response of Au(III)

Ion	Concentration excess over Au(III)	Contribution (%) $[i_p(Au) = 100\%]$	Probable reason for interference
Zn(III), Mn(II), Co(II), Ni(II)	50 ×	0	
Pb(II), Cd(II), Tl(I), Ag(I)	50 ×	0	
Cr(III)	50 ×	−30	?
Sb(III)	50 ×	+20	Competitive accumulation of $[SbCl_4]^-$
Bi(III)	50 ×	+30	Competitive accumulation of $[BiCl_4]^-$
Hg(II)	10 ×	+10	Competitive accumulation of $[HgCl_4]^{2-}$
	50 ×	+50	
Pt(IV), Pd(II)	100 ×	0	
Sn(II)	10 ×	−100	Redox reaction between Sn(II) and Au(III)
Fe(II)	10 ×	−100	Redox reaction between Fe(II) and Au(III)
Fe(III)	10 ×	+10	Competitive accumulation of $[FeCl_4]^-$
	100 ×	+100	
Cu(II)	10 ×	0	Overlapping by peak of reduction Cu(II) → Cu(0)
	100 ×	−80	
Tl(III)	10 ×	+50	Competitive accumulation of $[TlCl_4]^-$
	50 ×	+200	
NO_3^-, SO_4^{2-}	1000 ×	0	
ClO_3^-, ClO_3^-	1000 ×	0	
MnO_4^-	1000 ×	0	
Br^-	1000 ×	+50	Accumulation of $[AuBr_4]^-$ instead of $[AuCl_4]^-$
I^-	1000 ×	+500	Redox reaction between I^- and Au(III); reduction of iodine

peak of oxygen. As shown, the electrode containing TCP did not suffer from this reduction of oxygen.

The reduction peak height for $[BiI_4]^-$ was linearly dependent on concentration from 2×10^{-5} to 3×10^{-7} M Bi(III) and the electrode showed reproducibility with a relative error of less than 6%.

Accumulation of other anions of bismuth. Figure 5 illustrates that using an appropriate supporting electrolyte, accumulation of bismuth proceeded in the form of the $[BiX_4]^-$ anion. Reduction of Bi(III) ions transported towards the electrode surface via diffusion could not give rise to these peaks. This is confirmed by the two lower voltammograms that were registered in non-complexing media such as HNO_3 or H_2SO_4. The peak potential and peak height were proportional to the stability constants [25], the values of which increase in the order $[BiCl_4]^-$ ($\log \beta = 6.1$), $[BiBr_4]^-$ ($\log \beta = 8.6$) and $[BiI_4]^-$ ($\log \beta = 15.0$). It was also verified that as a consequence of the hydrolysis of $[BiI_4]^-$ in neutral or basic media, the response decreased or disappeared completely in the supporting electrolyte of higher pH.

Interferences from other ions. Table 3 is analogous to that presented for gold. As expected, the most serious interferents were Tl(III) and Hg(II) ions, forming very stable iodo complexes ($[HgI_4]^{2-}$ with $\log \beta = 29.8$ and $[TlI_4]^-$ with $\log \beta = 35.7$). Nevertheless, at comparable concentration levels, their contribution to the reduction peak of $[BiI_4]^-$ was minimal because of a sufficiently large potential shift.

An important observation was made with the Sb(III) ion, which is a frequently interfering ion in the determination of bismuth. As can be seen in Fig. 6a, the selectivity of the Bi(III) determination depends strongly on the choice of the stripping technique used. Antimony(III) essentially did not influence the reduction peak of bismuth(III) even at a tenfold concentration excess. On the other hand, Fig. 6b shows that the peaks completely overlap after the cathodic preconcentration of antimony and bismuth at the same electrode followed by oxidation in a stripping step

TABLE 3

Interferences of other ions on the response of Bi(III)

Ions	Concentration excess over Bi(III)	Contribution (%) [i_p(Bi) = 100%]	Probable reason for interference
Zn(II), Mn(II), Ni(II), Co(II)	50 ×	0	
Cd(II), Tl(I), Ag(I)	50 ×	0	
Cr(III)	10 ×	0	
Fe(III)	10 ×	0	
Pt(IV), Pd(II)	100 ×	0	
Sn(II)	10 ×	0	
Pb(II)	10 ×	0	Competitive accumulation of $[PbI_4]^{2-}$
	50 ×	+20	
Cu(II)	10 ×	+10	Reaction between Cu(II) and KI
	50 ×	+100	
Hg(II)	1 ×	0	Competitive accumulation of $[HgI_4]^{2-}$
	10 ×	+80	
Tl(III)	1 ×	+10	Competitive accumulation of $[TlI_4]^-$
	10 ×	+50	
Sb(III)	1 ×	0	Competitive accumulation of $[SbI_4]^-$
	10 ×	+10	
	50 ×	+30	

(conventional DPASV). When the preconcentration step was performed at a mercury film, an identical phenomenon was observed.

Optimum procedure for accumulating bismuth. Bismuth was accumulated for 40 s under open-circuit conditions in a supporting electrolyte containing 0.2 M H_2SO_4 + 0.002 M KI. The cathodic scan was started from +0.2 V and stopped at −1.0 V vs. Ag/AgCl. In accordance with the adsorptive character of the accumulation process, it was not necessary to remove the surface layer prior to each scan.

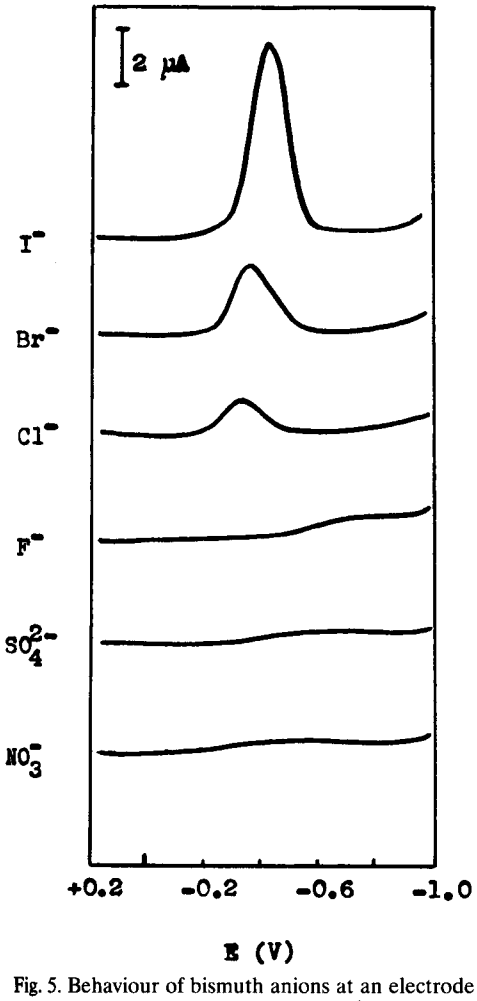

Fig. 5. Behaviour of bismuth anions at an electrode containing tricresyl phosphate. $c_{Bi(III)} = 1 \times 10^{-6}$ M. Supporting electrolyte: 0.2 M H_2SO_4 + 0.1 M KX (X = HSO_4, NO_3, F, Cl, Br) and 0.2 M H_2SO_4 + 0.002 M KI.

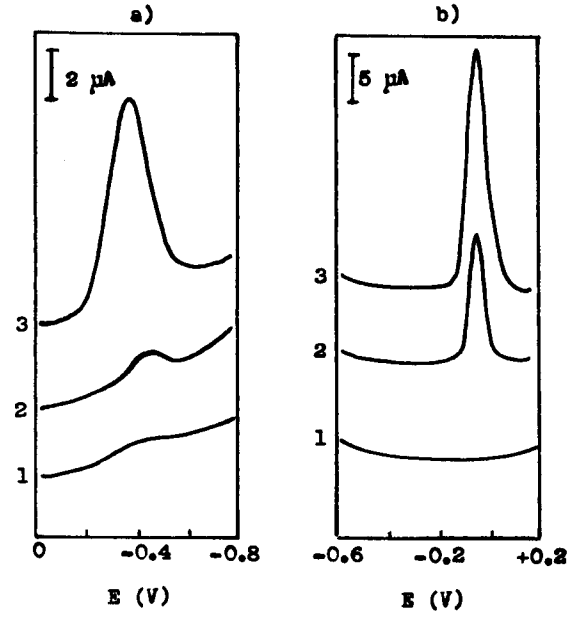

Fig. 6. Behaviour of Bi(III) and Sb(III) ions for two different accumulation processes: (a) accumulation under open-circuit conditions and following cathodic scan; (b) preconcentration at $E_{init} = -0.8$ V vs. Ag/AgCl and following anodic scan. (1) Supporting electrolyte; (2) $c_{Sb(III)}$ = (a) 5×10^{-6} M and (b) 5×10^{-7} M: (3) $c_{Bi(III)}$ = (a) and (b) 5×10^{-7}.

This approach to the determination of bismuth(III) seems to be promising when samples with a higher Sb(III) content have to be analysed. However, the method employing accumulation of the $[BiI_4]^-$ ion does not achieve the detection limit obtainable with chemically modified electrodes [18–20].

The authors thank Mr. Josef Žáček for manufacturing the electrode holders employed.

REFERENCES

1 K. Kalcher, Electroanalysis, 2 (1990) 419.
2 I. Švancara, K. Vytřas, F. Renger and M.R. Smyth, Sb. Ved. Pr. Vys. Sk. Chemickotechnol., Pardubice, 56 (1992/93) 5.
3 J. Lindquist, J. Electroanal. Chem., 52 (1974) 37.
4 G. Farsang, Acta Chim. Hung. Sci., 45 (1965) 163.
5 C. Urbaniczky and K. Lindström, J. Electroanal. Chem., 176 (1984) 169.
6 R.N. Adams, Rev. Polarog., 11 (1963) 71.

7 J. Veselý, D. Weiss and K. Štulík, Analysis with Ion-Selective Electrodes, Horwood, Chichester, 1978, p. 52.
8 K. Vytřas, Ion-Sel. Electrode Rev., 7 (1985) 77.
9 K. Kalcher, H. Greschonig and R. Pietsch, Fresenius' Z. Anal. Chem., 325 (1986) 181.
10 I. Švancara, K. Vytřas, F. Renger and M.R. Smyth, Electrochim. Acta, 37 (1992) 1355.
11 J. Gardea-Torresday, D. Darnal and J. Wang, J. Electroanal. Chem., 252 (1988) 197.
12 T. Peng, Q. Shi and R. Lu, Yingyong Kexue Xuebao, 8 (1990) 366.
13 Z. Gao, P. Li, S. Dong and Z. Zhao, Anal. Chim. Acta, 232 (1990) 367.
14 K. Kalcher, Anal. Chim. Acta, 177 (1985) 175.
15 K. Kalcher, Fresenius' Z. Anal. Chem., 325 (1986) 181.
16 G. Koelbl, K. Kalcher and A. Voulgaropoulos, Fresenius' J. Anal. Chem., 342 (1992) 83.
17 R. Neeb, Inverse Polarographie und Voltammetrie, Akademie Verlag, Berlin, 1969.
18 W. Szczepaniak and M. Ren, Talanta, 31 (1984) 212.
19 J. Lexa and K. Štulík, Talanta, 32 (1985) 1027.
20 K. Kalcher, Fresenius' Z. Anal. Chem., 325 (1986) 186.
21 M.E. Rice, Z. Galus and R.N. Adams, J. Electroanal. Chem., 143 (1983) 89.
22 J.M. Kauffmann, personal communication.
23 J. Wang, B.K. Deshmukh and M. Bonakdar, J. Electroanal. Chem., 194 (1985) 339.
24 L. Novotný, personal communication.
25 S. Kotrlý and L. Šůcha, Handbook of Chemical Equilibria in Analytical Chemistry, Horwood, Chichester, 1985, pp. 112–114, 135–141.
26 I. Švancara, K. Vytřas, F. Renger, M. Srey, R. Vaňková and M. Hvízdalová, Collect. Czech. Chem. Commun., submitted for publication.

Analytica Chimica Acta, 273 (1993) 205–212
Elsevier Science Publishers B.V., Amsterdam

Chemically modified electrode for the simultaneous determination of trace metals and speciation analysis

R. Agraz, M.T. Sevilla and L. Hernández

Department of Analytical Chemistry and Instrumental Analysis, Autónoma University of Madrid, 28049 Madrid (Spain)

(Received 1st June 1992; revised manuscript received 29th September 1992)

Abstract

A modified carbon paste electrode was used for the simultaneous determination of Zn, Cd, Pb, Cu and Hg. Trace metal preconcentration was effected by selective retention on Amberlite IRC 718 chelating resin as an electrode modifier, with subsequent measurement by differential-pulse voltammetry. Peak potentials for he reoxidation of these metals occur at −1.05, −0.80, −0.48, −0.24 and 0.06 V, respectively, allowing determinations at the $\mu g\ l^{-1}$ level. Several metal ratios were studied in order to determine the influence of each metal on the determination of the others. The influence of other substances was also studied to determine the potential of the method for speciation analysis studies.

Keywords: Voltammetry; Cadmium; Carbon paste electrode; Copper; Lead; Mercury; Preconcentration; Speciation; Trace metals; Zinc

The determination of trace metals in the environment is increasingly important. Zinc, cadmium, lead, copper and mercury concentrations are some of the most interesting parameters in this environmental control. Also, the determination of their chemical forms in aquatic systems is of interest because of the relationship with their bioavailability to aquatic living organisms [1].

The use of chelating resins for trace metal preconcentration has been extensively applied to environmental samples [2,3]. The possibility of the preconcentration and separation of trace metals from complex matrices with low contamination risks [4,5] has been a decisive factor for the use of these resins in the determination of many trace elements in a wide variety of samples.

In this work, the advantageous characteristics of chelating resins were combined with the sensitivity and selectivity of differential-pulse voltammetry, allowing the determination of Zn, Cd, Pb, Cu and Hg at the $\mu g\ l^{-1}$ level.

A carbon paste electrode modified with a chelating iminodiacetate-type resin has been used previously for the determination of lead [6] and cadmium [7], with good results for water analysis. This work showed an improvement in the results with regard to simultaneous determination. Other chelating ligands used as chemical modifiers have also been reported for trace analyses, such as dimethylglyoxime [8], 1,10-phenanthroline [9,10] and diethyldithiocarbamate [11], and also other chelating resins with different functional groups, allowing the determination of trace metals with good selectivity and sensitivity.

Trace level determinations of these metals can be achieved by anodic stripping voltammetry at a hanging mercury drop electrode (HMDE) or mercury film electrode [12], but several problems

Correspondence to: M.T. Sevilla, Department of Analytical Chemistry and Instrumental Analysis, Autónoma University of Madrid, 28049 Madrid (Spain).

have been reported [13,14]. The addition of a buffer solution to the sample is necessary for pH and ionic conductivity adjustment, but may lead to sample contamination and changes in the speciation forms of the metals [15,16]. The improvement obtained using the chemically modified electrode described here means that no addition of a buffer system of the sample is necessary, as the measurement step is done in an independent measurement cell and no correction is needed for the ionic conductivity of the sample. Preconcentration at natural pH and ionic strength can be applied by any natural sample.

Adsorption of organic ligands present in natural waters on a mercury electrode may lead to a decrease in sensitivity and may cause interference problems [16–18]. These effects are avoided when the chemically modified electrode is used because of the selective trace metal preconcentration and the use of a clean supporting electrolyte in the measurement step.

In this work, preconcentration of trace metals was done "in situ" on a chelating resin previously attached to the electrode. The chelating resin Amberlite IRC 718 is an iminodiacetate-type resin; the capability for retention of trace metals on this type of resin has been extensively studied [19–21]. This chelating resin shows a good ability for metal preconcentration at pH > 4, with the highest adsorption at pH ≈ 8–9; this fact and the low alkali and alkaline earth metal interferences reported [7] make this resin a very good sorbent for trace metal preconcentration in natural waters.

However, naturally occuring organic ligands and colloids can cause serious interferences owing to their complexation ability [2,22], competing with active sites in the resin for metal complexation. These interferences are avoided through UV irradiation, destroying the interfering organic matter without any addition of reagent [2,23]. This approach has been used extensively to develop speciation analysis schemes based on the ability of the resin to retain only free or "labile" complexed metal [24].

This paper describes the simultaneous determination of zinc, cadmium, lead, copper and mercury using a carbon pase electrode modified with the chelating resin Amerblite IRC 718 and its analysis of tap water.

EXPERIMENTAL

Reagents

Ultrapure water obtained with a Milli–Q–Milli-RO system (Millipore) was used throughout. All reagents were of analytical-reagent grade. Cadmium, mercury and lead stock solutions were prepared by dissolving the nitrates in 0.1 M nitric acid, and copper and zinc stock solutions by dissolving the metals in the minimum amount of nitric acid. The Amberlite IRC-718 chelating resin was purified by successive washing with methanol, 5% hydrochloric acid and water. All solutions were stored in polyethylene containers, except mercury solutions, which were stored in glass bottles.

Apparatus

A Metrohm 646 VA processor was used for differential-pulse voltammetric studies and a BAS CV-27 voltammograph for preliminary cyclic voltammetric studies. A Perkin-Elmer Model 372 atomic absorption spectrometer equipped with an HGA graphite furnace controller and a Metrohm Model 654 pH meter were also used.

Preparation of the modified electrode

Modified carbon pastes were prepared by placing 0.3 g of spectrographic graphite powder, 0.2 g of powdered chelating resin and the necessary amount of paraffin oil in an agate mortar, then mixing them for 10 min until a uniform paste was obtained. Unmodified carbon paste was prepared in the same way but without the resin powder. The carbon paste obtained was packed in the ending pool of a PTFE tube provided with an inner copper contact.

General procedure

The electrode was first activated by successive sweep until a reproducible current was obtained. The electrode was then immersed in a 50-ml preconcentration cell containing the sample and allowed to preconcentrate the trace metal at open

circuit in the stirred solution for a given period of time. The electrode was removed, rinsed with water and placed in the measurement cell containing the supporting electrolyte (0.1 M hydrochloric acid). No deaereation of the electrolyte solution was required. A reduction potential of −1.45 V was applied for 90 s and then an anodic potential scan was performed with a scan rate of 30 mV s^{-1} and a pulse amplitude of 90 mV, producing different anodic peaks of the preconcentrated metals. Regeneration of the electrode surface was done by application of a potential of 1.00 V for 2 min in the stirred supporting electrolyte.

RESULTS AND DISCUSSION

The capability of the Amberlite IRC-718 resin for trace metal preconcentration was deduced from the values of its distribution coefficients towards these metals; these values were calculated through the batch method and using atomic absorption spectrometry for the measurement of the remaining metal concentration in solution, and showed quantitative retention of the trace metals from pH ⩾ 4. This agrees with theoretical calculations of the conditional constants with the iminodiacetate ligand in solution, showing their maximum values for neutral to slightly basic pH. The presence of this resin at the electrode surface can easily be realised by mixing it with the carbon paste, giving the electrode surface the characteristics of selectivity and great affinity to trace metals; the subsequent differential-pulse voltammetric determination of these metals preconcentrated on the electrode surface leads to very low detection limits. Analytical and instrumental parameters were optimized. Oxidation peaks of these metals under the optimum conditions were obtained at −1.05, −0.80, −0.48, −0.24 and 0.06 V (vs. Ag/AgCl) for zinc, cadmium, lead, copper and mercury, respectively (Fig. 1). The better sensitivity for lead and copper is obtained because of their greater retention on the chelating resin compared with the other metals.

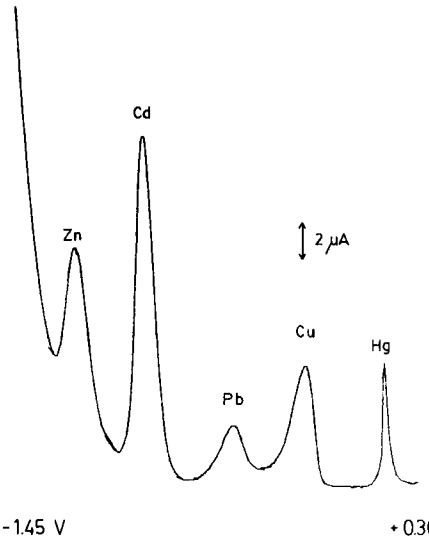

Fig. 1. Differential-pulse voltammogram after a 5-min preconcentration time. Reduction time, 90 s; scan rate, 30 mV s^{-1}; pulse amplitude, 90 mV. Concentrations are of Zn, Cd, Pb, Cu and Hg: 25.0, 12.5, 1.2, 1.2, 50.0 μg l^{-1}, respectively.

Analytical parameters

Owing to the characteristics of aquatic samples, pH adjustment is not necessary as these samples have pH ⩾ 4 (in most instances ca. 8); this is an optimum pH for trace metal preconcentration with the modifier chosen; in addition, this is advantageous for future applications to speciation studies were the addition of any reagent to the sample is undesirable. Previous studies on the amount of modifier incorporated showed that the best results were obtained for resin contents between 35 and 45%, where the signal-to-noise ratio is adequate and the physical stability of the electrode surface is satisfactory ; a compromise value of 40% was chosen for subsequent studies.

Instrumental parameters

Once the trace metal has accumulated on the electrode surface, the subsequent voltammetric measurement of the amount of preconcentrated metal is done by differential-pulse voltammetry. Previous studies on the modified electrode using cyclic voltammetry showed that these metals possess a broad reduction wave and a sharp and large oxidation peak, making this latter peak more suitable for the determination of these metals. In

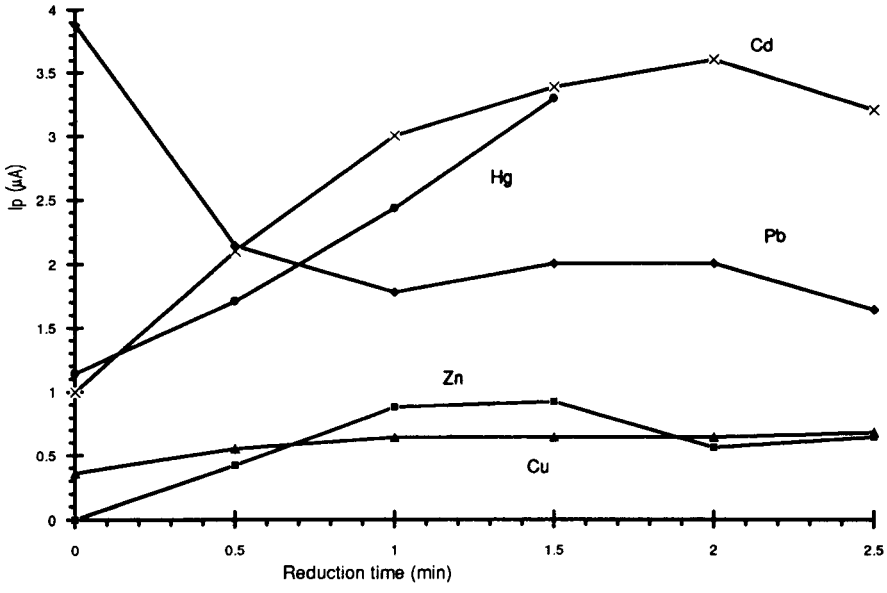

Fig. 2. Influence of reduction time on trace metal signal. Other conditions as in Fig. 1.

order to obtain the maximum efficiency in the reduction step, the reduction potential and reduction time were studied. The selection of the reduction potential depends on the zinc signal, as this metal has the most negative redox potential. A reduction potential of −1.45 V was chosen because it gives the best zinc signal; more negative potentials lead to a higher zinc signal but the

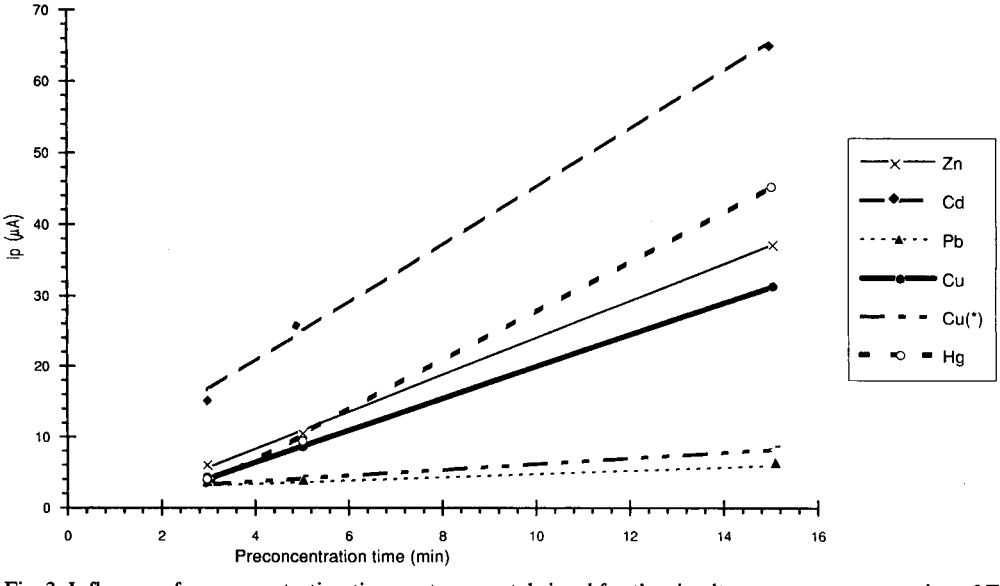

Fig. 3. Influence of preconcentration time on trace metal signal for the simultaneous preconcentration of Zn, Cd, Pb, Cu and Hg at 25.0, 12.5, 1.2, 1.2 and 50.0 $\mu g\ l^{-1}$, respectively, and [Cu(*)] for the preconcentration of 1.2 $\mu g\ l^{-1}$ Cu alone. Other parameters as in Fig. 1.

electrode surface became damaged because of hydrogen evolution. Time reduction is also governed by the zinc and cadmium signals as they are the most affected by this parameter. Different reduction times from 0 to 180 s were studied; the results are shown in Fig. 2. A reduction time of 90 s was chosen as most metals show a maximum close to that value except lead, but owing to its better sensitivity a compromise value of 90 s was considered acceptable.

After the reduction step, the anodic scan was done in order to obtain the oxidation waves of these metals. The pulse amplitude and sweep rate were varied to obtain the best results. A pulse amplitude of 90 mV was chosen, because it gives good sensitivity for all the metals without any resolution problems and the $w_{1/2}$ obtained was suitable for peak evaluation. A scan rate of 30 mV s^{-1} showed good sensitivity for all the metals and the signal-to-noise ratio was the most advantageous.

Intermetallic effects

With these optimized instrumental parameters, the preconcentration time was varied from 0.5 to 15 min. Results are shown in Fig. 3 for the simultaneous preconcentration of 25.0 $\mu g\ l^{-1}$ Zn, 12.5 $\mu g\ l^{-1}$ Cd, 1.2 $\mu g\ l^{-1}$ Cu and Pb and 50.0 $\mu g\ l^{-1}$ Hg, and their respective slope values were calculated (Table 1). The slope values obtained in this study are representative of the sensitivity of this technique for each metal. From these values, it could be concluded that the sensitivity for copper is better than that for lead (m_{Cu}/m_{Pb} = 9.8 for the same concentration level). The reason for this is the presence of zinc in the preconcentration medium, because during the reduction step zinc and copper form an amalgam which is

TABLE 1

Slope values for the evolution of the signals with preconcentration time for the simultaneous preconcentration of Zn, Cd, Pb, Cu, Hg at 25.0, 12.5, 1.2, 1.2 and 50.0 $\mu g\ l^{-1}$, respectively, and for the preconcentration of 1.2 $\mu g\ l^{-1}$ Cu alone (other conditions as in Fig 1)

Metal	Slope ($\mu A\ min^{-1}$)
Zinc	2.62
Cadmium	4.08
Lead	0.23
Copper	2.26
Copper alone	0.27
Mercury	3.50

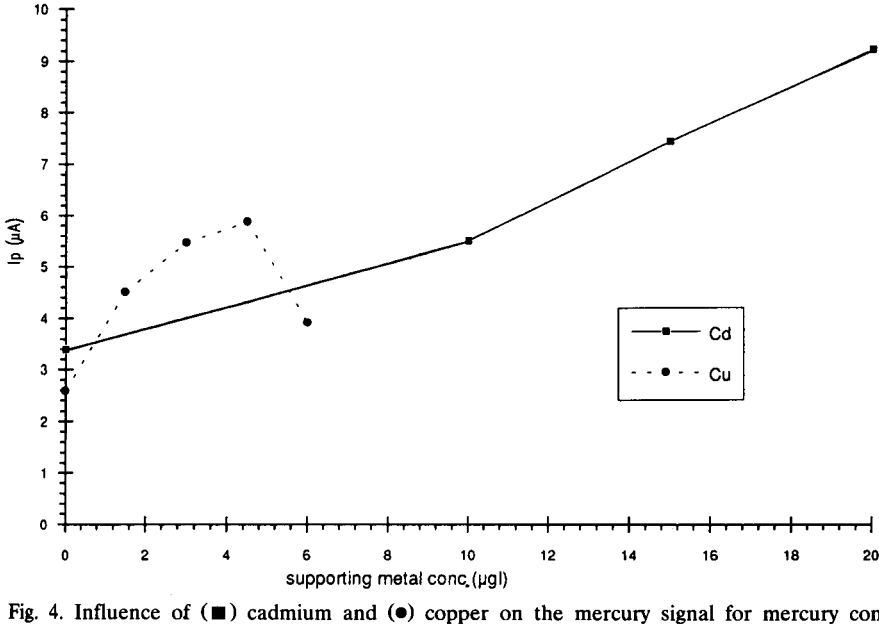

Fig. 4. Influence of (■) cadmium and (●) copper on the mercury signal for mercury concentrations of 0.2 and 0.1 $\mu g\ l^{-1}$, respectively. Other conditions as in Fig. 1.

oxidized at a potential very close to the copper wave. The final effect is an increase in the copper signal and a decrease in the zinc signal. This also explains the smaller value of the slope for zinc compared with cadmium although it is present at a higher concentration ($m_{Cd}/m_{Zn} = 1.6$). When copper preconcentration is done in a medium in which zinc is absent, its slope is close to the value for lead for the same concentration level. This intermetallic effect has been reported previously [25] in the determination of zinc and copper on a thin mercury film electrode or an HMDE, the intermetallic compound formation being more intense in the former electrode.

There is another important effect to be taken into account in the determination of mercury, namely the so-called "support effect" in the deposition of a mercury film on a glassy carbon electrode [26], involving an increase in mercury deposition when trace amounts of cadmium or copper are present in the sample. This effect was observed here, leading to a decrease in the detection limit of mercury from 0.1 to 0.05 mg l^{-1} when traces of these metals are present. However, the effect of the concentration increase of these "supporting" metals on the mercury signal is not as great as in the deposition of a mercury film on a glassy carbon electrode, as the detection limit is also influenced by the retention coefficient on the modifier. With this in mind, it is easy to understand that an increase in copper concentration from 3 $\mu g\ l^{-1}$ can cause a decrease in the mercury signal owing to the competition for the active sites at the electrode surface, as can be seen in Fig. 4. The mercury slope value (Table 1) shows a poorer selectivity than for the other metals as its concentration is higher.

These intermetallic effects can be seen in Fig. 5; an increase in the mercury peak and a decrease in the zinc peak (for the same concentration level) occurs when the copper concentration in the preconcentration cell increases.

Linearity and applications

Detection limits for each metal for a 5-min preconcentration period and linearity functions in the presence of measurable amounts of other metals are shown in Table 2. An example is also shown in Fig. 5. All these detection limits can be improved by employing longer preconcentration periods. It is important to note that the improvement obtained through this method in the determination of mercury that the detection limit obtained with a much shorter preconcentration period is comparable to that reported for deposition on a glassy carbon electrode with a 20-min depo-

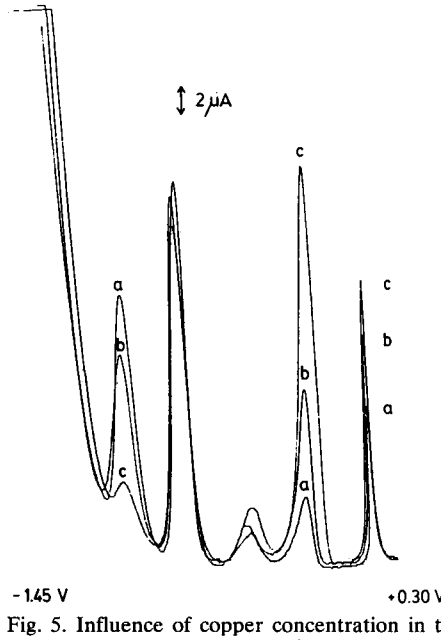

Fig. 5. Influence of copper concentration in the presence of 25.0, 12.5, 1.2 and 50.0 $\mu g\ l^{-1}$ Zn, Cd, Pb and Hg, respectively, for (a) 1.2, (b) 2.5, and (c) 5.0 $\mu g\ l^{-1}$ of copper.

TABLE 2

Calibration and statistical study for the determination of each metal in the presence of Zn, Cd, Pb, Cu or Hg at 25.0, 12.5, 1.2, 1.2 and 50.0 $\mu g\ l^{-1}$, respectively (other conditions as in Fig. 1)

Metal	Linearity range ($\mu g\ l^{-1}$)	Slope ($\mu A\ l\ \mu g^{-1}$)	Detection limit ($\mu g\ l^{-1}$) (3σ)	Determination limit ($\mu g\ l^{-1}$) (10σ)	S.D. (%)
Zn	10.0– 50.0	0.59	7.1	15.6	4
Cd	5.0– 20.0	2.12	3.2	7.4	6
Pb	1.2– 5.0	1.40	1.1	2.1	9
Cu	1.2– 5.0	6.17	1.0	2.0	9
Hg	25.0–125.0	0.23	25.0	40.5	5

sition period. It is also advantageous that the addition of thiocyanate or other ligands is not necessary for the determination of mercury [27], thus avoiding the noise increase and contamination that it may cause.

The method was applied to tap water analysis, obtained a zinc value of 0.31 mg l^{-1} in the sample after a 5-min preconcentration period for a diluted sample; this value agrees well with that of 0.29 mg l^{-1} obtained by the standard HMDE method. A 0.5 μg l^{-1} copper concentration with a 15-min preconcentration period was also obtained. This value is close to the detection limit for copper in the standard HMDE method. Cadmium, lead or mercury were not detected with either the modified electrode or the HMDE method.

Effects of other substances

Inorganic and organic substances present in the sample can interfere in trace metal determination owing to their capability to accompany the metal in the accumulation step. Inorganic ions such as chloride, nitrate, carbonate, phosphate or ammonia only interfere when present at high concentrations ($> 10^{-2}$ M). Alkali metal cations, such as sodium and potassium, do not interfere; alkaline earth metal cations, such as calcium and magnesium, can interfere but only when present in high concentrations, owing to their low retention coefficients in the Amberlite IRC 718 chelating resin. Organic ligands present in natural water samples can interfere depending on the stability constants and the dissociation kinetics of the metal complexes formed [1]. Amino acid-type ligands have little influence owing to their faster dissociation kinetics, but fulvic acid-type ligands show larger interferences owing to their slower dissociation kinetics. Strong complexing agents such as nitrilotriacetic acid cause serious interference. Results are shown in Table 3.

TABLE 3

Influence of other substances on the copper signal for a 2 μg l^{-1} copper concentration and a 1×10^{-6} M ligand concentration

Ligand	Copper signal (μA)
None	5.7
Glycine	5.3
Cysteine	4.9
Fulvic acid	1.2
Nitrilotriacetic acid	0

This approach can be used for trace metal speciation analysis in aquatic systems; further work on this subject is in progress.

The authors thank the Ministry of Education and Research of Spain (DGIC & T, project PA86-0367) and the Comunidad Autónoma of Madrid (project C-09091) for financial support of this work and for a research grant to R. Agraz.

REFERENCES

1 J. Buffle (Ed.), Complexation Reactions in Aquatic Systems, Horwood, Chichester, 1988.
2 K. Terada, Anal. Sci., 7 (1991) 187.
3 H.D. Gesser, Talanta, 37 (1990) 491.
4 T.M. Florence and G.E. Batley, Talanta, 23 (1976) 179.
5 R.T. Clen and A.T. Hogdson, Anal. Chem., 50 (1978) 102.
6 M.T. Sevilla, J. Rodriguez, J.M. Pinilla and L. Hernández, Int. J. Environ. Anal. Chem., 37 (1989) 107.
7 R. Agraz, M.T. Sevilla, J.M. Pinilla and L. Hernández, Electroanalysis, 3 (1991) 393.
8 R.P. Baldwin, J.K. Christensen and L. Kryger, Anal. Chem., 58 (1986) 1790.
9 Z. Gao, P. Li and Z. Zhao, Fresenius' Z. Anal. Chem., 339 (1991) 137.
10 S.V. Prabhu, R.P. Baldwin and L. Kryger, Anal. Chem., 59 (1987) 1074.
11 A.R. Guadalupe and H.D. Abruña, Anal. Chem., 59 (1987) 142.
12 T.S. West (Ed.), The Determination of Trace Metals in Natural Waters, Blackwell, Oxford, 1988, p. 123.
13 J. Wang, Stripping Analysis, VCH, New York, 1985.
14 T.M. Florence and K.J. Mann, Anal. Chim. Acta, 200 (1978) 305.
15 E.A. Schonberger and W.F. Pickering, Talanta, 27 (1980) 11.
16 H.K. Powell and T.M. Florence, Anal. Chim. Acta, 228 (1990) 327.
17 J. Buffle, J. Electroanal. Chem., 125 (1981) 273.
18 R.B. Smart and E.E. Stewart, Environ. Sci. Technol., 19 (1985) 137.
19 D. Votusa, C. Samara, K. Fytianos and Th. Kovimtzis, Fresenius' Z. Anal. Chem., 330 (1988) 596.
20 T.M. Florence and G.E. Batley, Talanta, 22 (1975) 201.
21 R.E. Sturgeon, S.S. Berman, A. Desaulniers and D.S. Russel, Talanta, 27 (1980) 85.
22 T.M. Florence, Analyst, 111 (1986) 489.

23 T.M. Florence, Anal. Chim. Acta, 141 (1982) 73.
24 P. Figura and B. McDuffie, Anal. Chem., 52 (1980) 1433.
25 M.S. Shuman and G.P. Woodward, Jr., Anal. Chem., 48 (1976) 1979.
26 P. Kiekens, M. Mertens, M. Bogaert and E. Temmerman, Analyst, 109 (1984) 909.
27 R. Bilewicz, S. Stojek and Z. Kublik, J. Electroanal. Chem., 96 (1979) 29.

Analytica Chimica Acta, 273 (1993) 213–218
Elsevier Science Publishers B.V., Amsterdam

Investigation of the batch injection analysis technique with amperometric biocatalytic electrodes using a modified small-volume cell

A. Amine and J.-M. Kauffmann

Université Libre de Bruxelles, Institut de Pharmacie, Campus Plaine, CP 205 / 6, 1050 Brussels (Belgium)

G. Palleschi

Dipartimento di Scienze Tecnologie Chimiche, Università di Roma "Tor Vergata", via O. Raimondo, 00173 Rome (Italy)

(Received 14th July 1992; revised manuscript received 23rd October 1992)

Abstract

The performance of the recently developed batch injection analysis (BIA) technique was investigated with regard to the behaviour of enzyme-immobilized electrodes. Glucose oxidase and xanthine oxidase sensors were prepared by casting the enzyme-immobilized membranes on the electrode surface. The measurements are based on the amperometric detection of the product of the enzymatic reaction: hydrogen peroxide at +650 mV vs. Ag/AgCl (GOx) or the reduced form of methylene blue at +50 mV vs. Ag/AgCl (XOD). The enzyme glutamate dehydrogenase was incorporated in the carbon paste and the direct and phenazine methosulphate-mediated detection of NADH was followed at the enzyme electrode. The major characteristics observed were simplicity of the equipment, a high sampling rate and limited consumption of the carrier, i.e., reagents such as the mediator and cofactor. The repeatability of the manual injection of the sample was shown to be the critical step in the BIA mode. A new BIA cell design, allowing semi-continuous solution draining, is reported.

Keywords: Amperometry; Enzymatic methods; Flow injection; Batch injection analysis; Biocatalytic electrodes; Enzyme electrodes; Glucose; Xanthine

Batch injection analysis (BIA) is a recently developed method that consists in injecting a sample from a micropipette tip towards a nearby detector immersed in a large volume (stirred solution) of a batch wall-jet cell [1]. Owing to the difficulty of solution handling in BIA, the use of a detector allowing high selectivity is of prime importance. In this respect, enzyme electrodes may be regarded as appropriate probes allowing selective and sensitive measurements in BIA [1]. In this work, the performance of various amperometric enzyme immobilized electrodes inserted in a new BIA configuration is described. It was of interest to investigate BIA in small volumes (ca. 35 ml) by designing a cell that allows rapid solution draining and switching from BIA to flow injection analysis (FIA), and vice versa, by simple turning and adjusting the cover of the cell (Fig. 1). Oxidase and glutamate dehydrogenase enzymes were investigated; the former was chemi-

Correspondence to: J.-M. Kauffmann, Université Libre de Bruxelles, Institut de Pharmacie, Campus Plaine, CP 205/6, 1050 Brussels (Belgium).

cally immobilized and cast on the platinum electrode and the latter was mixed within a carbon paste electrode.

EXPERIMENTAL

Apparatus and equipment

Amperometric measurements were made with a BAS CV 37 voltammograph (Bioanalytical Systems, Fullerton, CA). The output of the current was recorded with a Linseis L6512 recorder. A three-electrode cell was used throughout. The cell was made of Plexiglas with a diameter of 4 cm, a height of 6 cm and a volume capacity of ca. 35 ml. A schematic diagram of the cell is given in Fig. 1.

The working electrode was inserted through a hole drilled in the bottom of the cell. The cell cover contained four holes and can be switched from the BIA to the FIA mode (see Fig. 1 and [2]). In the BIA mode, one hole was located exactly opposite the surface disc of the working electrode and served for accommodating the standard pipette (Pipetman from Gilson). The tip of the pipette was fixed at a selected distance from the electrode surface (this distance may be adjusted by moving the electrode up or down through the PVC adaptor seal). Two other holes were used to support the counter and reference electrodes. The inlet and outlet allow the drainage of the solution without removing the electrode. The cell drainage may be utilized in the event of background current instability due to the increase in analyte concentration and/or ionic strength in the solution. The fourth hole served for sample and reagent addition in the steady-state mode. The solution was stirred with a magnetic rod at ca. 250 rpm. The reference electrode was an Ag/AgCl electrode (BAS) and a stainless-steel chromatographic tube served as the counter electrode (Supelchem, Milan). A platinum disc from BAS (3 mm diameter) and a carbon paste electrode (laboratory made, 3 mm diameter) modified

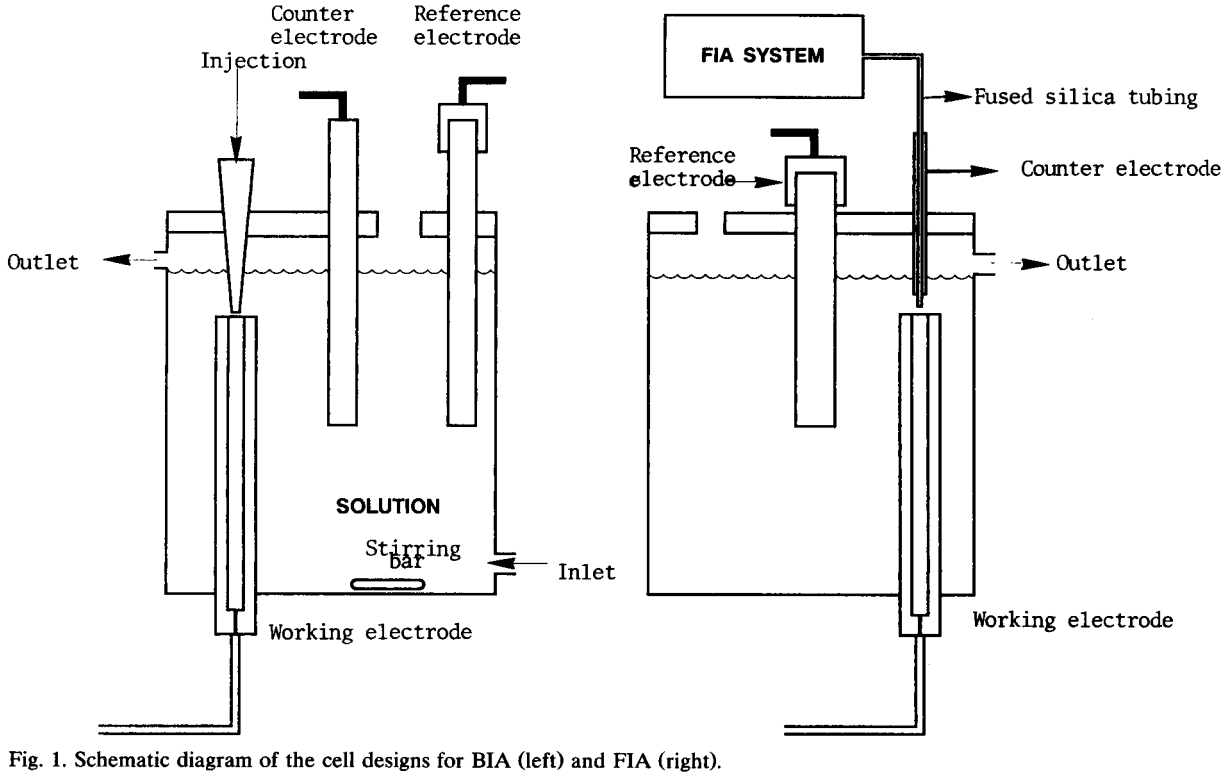

Fig. 1. Schematic diagram of the cell designs for BIA (left) and FIA (right).

as described below served as the working electrode. The carbon paste (EA 207C) was from Metrohm (Herisau, Switzerland). The pH of the solutions was measured with a pH meter (HI 8418) from Hanna (Milan). All experiments were done at room temperature (23 ± 1°C).

Reagents

The solutions were prepared with distilled water. The enzymes glucose oxidase (GOx), type VII-S (EC 1.1.3.4, 200 U mg^{-1} solid, lyophilized), xanthine oxidase (XOD), type X-4376 (EC 1.1.3.22, 0.07 U mg^{-1} solid, lyophilized) and L-glutamate dehydrogenase (GlDH) from bovine liver (EC 1.4.1.3, 24 U mg^{-1} solid, lyophilized) were from Sigma. All reagents were of analytical-reagent grade. The buffer used was either a physiological buffer (Dulbecco, pH 7.4) or 0.1 M phosphate buffer (K_2HPO_4–KH_2PO_4, pH 7.0).

Electrode preparation

The platinum electrode was covered with three membranes, viz., GOx immobilized on nylon net and sandwiched between a permselective cellulose acetate membrane [the molecular weight cut-off (MWCO) was ca. 100] [3–5] and a polycarbonate membrane (Nuclepore, porosity 0.08 μm). The same electrode, but without the cellulose acetate membrane, was also tested in BIA experiments.

The enzyme immobilization on nylon has been described previously [6]. Briefly, it consisted in functionalization of the nylon by immersing it in boiling dimethyl sulphoxide. After washing, a lysine arm was linked to the membrane, which was again reacted with the bifunctional reagent glutaraldehyde. The final step consisted in linking the soluble enzyme to the membrane via the glutaraldehyde terminal part. The hydrogen peroxide produced in the enzymatic reaction was measured at +650 mV in Dulbecco buffer.

The platinum electrode was coated with 10 μl of a xanthine oxidase mixture [5 mg of XOD in 150 μl of 0.02 M phosphate buffer (pH 7.0) + 30 μl of 0.5% glutaraldehyde solution]. The mixture was allowed to dry at room temperature for 2 h, then the electrode was covered with a 0.08-μm polycarbonate membrane and washed with a large amount of distilled water. The electrode was poised at +50 mV in 0.1 M phosphate buffer (pH 7.0).

The modified carbon paste electrode (MCPE) was prepared by thoroughly mixing, in a mortar, carbon paste and GlDH (5%, w/w). The MCPE was covered with a dialysis membrane (MWCO 12000) (Thomas, Philadelphia PA) to prevent problems of mechanical instability due to paste swelling and erosion phenomena [7]. The electrode was poised at +50 mV in Dulbecco buffer.

RESULTS

Glucose oxidase

The response of the electrodes with the enzyme chemically attached on nylon net is illustrated in Fig. 2. As expected, the signal decreases if an additional cellulose acetate membrane is placed in front of the platinum disc (line A). The presence of this additional cellulose membrane increases the peak width at half-height from 32 to 36 s. It is also interesting that the current peak intensity is quasi-independent of the sample volume injected because of the presence of the membranes on the enzyme electrode (lines A and B). Also, the current peak intensity does not change significantly on varying the distance separating the pipette tip and the electrode surface from ca. 0.5 to 3 mm. Further experiments were done by injecting 30 μl of sample volume with a distance from the electrode to the pipette tip of ca. 1 mm.

The repeatability of the measurements was calculated by several injections ($n = 10$) of a 5 mM glucose solution. With both electrodes the relative standard deviation was 5.0%. The sampling frequency for the glucose analysis was about 40 h^{-1}.

The magnitude of the electrode response for a 0.5 mM glucose solution under steady-state conditions was compared with that given by batch injection of 0.5 mM glucose. The signal observed with the latter mode was ca. 30% of the former, indicating that a large proportion of the glucose injected (ca. 70%) is not detected and is lost in

the solution owing to the washing out effect (see below).

It is noteworthy that no response was observed at the cellulose acetate-covered electrode when 100 mg l^{-1} of acetaminophen were injected. This is in contrast to the results obtained previously using the same membrane under batch conditions [5] and may be attributed to the slow diffusion of acetaminophen through the membranes and rapid washing out of the electrode by the stirred solution.

Xanthine oxidase

The chemically immobilized enzyme electrode was tested in the BIA system by poising the electrode at +50 mV. This potential allows the detection of the superoxide produced [8]. The response of the electrode in the presence of increasing xanthine concentrations is shown in Fig. 3, line a. The low responses observed may be attributed to the short lifetime of the superoxide radical [8]. In order to improve the electrode signal, measurements were made in the presence of methylene blue (0.5 mM) in the analysed solution. Methylene blue has been reported to be a judicious mediator for the oxidative regeneration of xanthine oxidase cofactor [9]. The monitoring of the reduced form of methylene blue was made by poising the enzyme electrode at +50 mV. As shown in Fig. 3, the response is markedly improved for xanthine and hypoxanthine (lines b and c). The relative standard deviation calculated for eleven repetitive injections of 0.1 mM hypoxanthine was 5.4%. The electrode retains 100% of its activity over 4 weeks if stored at 4°C after measurements. The frequency of analysis was ca. 50 h^{-1}.

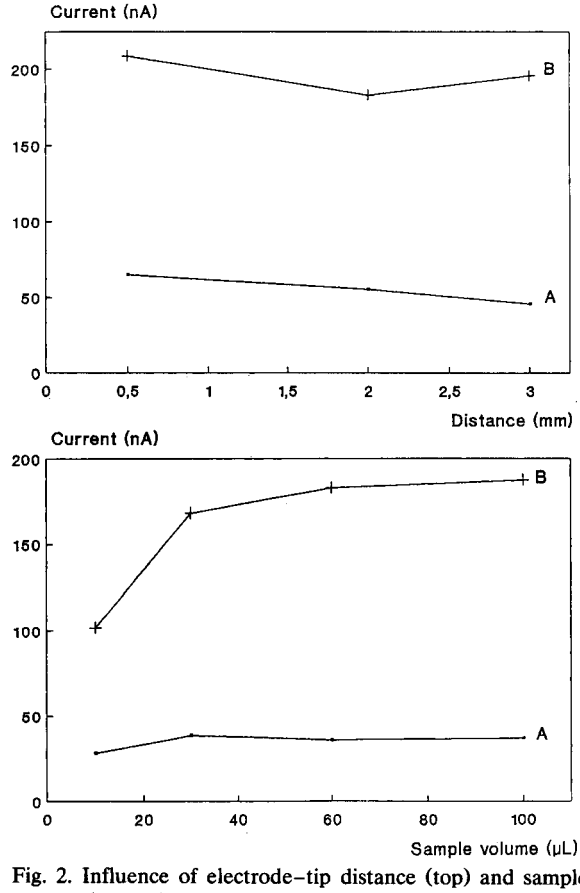

Fig. 2. Influence of electrode–tip distance (top) and sample volume (bottom) on the BIA response of 5 mM glucose. (A) Pt electrode with GOx sandwiched between cellulose acetate and polycarbonate membranes; (B) the same, but without the cellulose acetate membrane. Dulbecco buffer, potential +0.65 V.

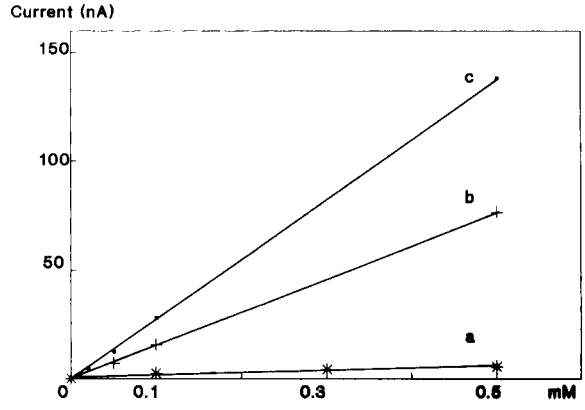

Fig. 3. Calibration graphs at the XOD electrode. (a) Xanthine without mediator; (b) xanthine + mediator; (c) hypoxanthine + mediator. Potential, +50 mV; phosphate buffer (pH 7.0); 0.5 mM methylene blue.

Glutamate dehydrogenase

NADH determination. As dehydrogenase enzymes use NADH as cofactor, its oxidation was studied first. The BIA injections were made in the presence of the redox mediator phenazine methosulphate (PMS^+) at +50 mV (Fig. 4A) and in the absence of PMS^+ at +200 mV (direct

oxidation of NADH) (Fig. 4B). Figure 4 shows that the response of NADH in a stirred solution (a and b) at the platinum electrode is fast. In the presence of the mediator, the response time (including baseline recovery) was 45 s, allowing a sample injection rate of 80 h^{-1}. Under unstirred conditions (c and d) the direct detection of NADH was perturbed by surface problems, as suspected from the asymmetry (low wash-out) of the oxidation peak (Fig. 4B, c). This surface problem may be attributed to the adsorption of NADH oxidation products [10–13]. Varying the stirring rate has no effect on the intensity of the response in the presence of mediator (Fig. 4A, b and d).

A typical calibration graph for NADH oxidation in the presence of PMS^+ at pH 7.4 is shown in Fig. 5 (points +). A linear relationship was obtained between 0.1 μM and 1 mM NADH. It is of importance to note the advantages of the BIA technique over FIA. Indeed, in BIA, the reduced form of the mediator which is not oxidized at the electrode was readily oxidized by dissolved oxygen [14]. This allows recycling of the mediator, in contrast to FIA, where the mediator is wasted. This also eliminates any risk of memory effects due to the progressive increase in reduced mediator concentration (by repetitive injections). This was confirmed by performing BIA under identical conditions as in Fig. 5 (points +), but with 0.1 mM NADH in solution (Fig. 5, points △). The

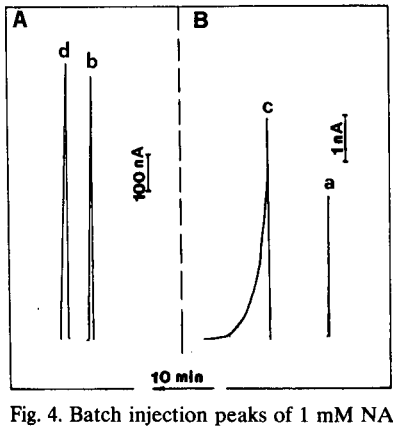

Fig. 4. Batch injection peaks of 1 mM NADH at the platinum electrode: (A) +50 mV, 0.5 mM PMS^+; (B) +200 mV without PMS^+. (a, b) Stirred solution; (c, d) unstirred solution. Dulbecco buffer.

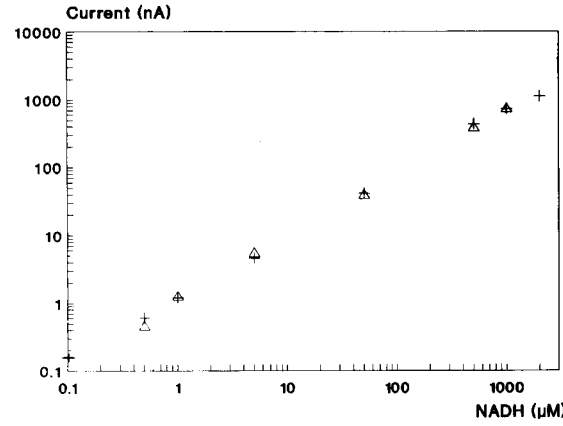

Fig. 5. Typical calibration graphs for NADH at the platinum electrode in stirred solution at +50 mV. + = Dulbecco buffer, 0.5 mM PMS^+; △ = the same, but in the presence of 0.1 mM NADH (deliberately added to the solution).

overlap of the two calibration graphs suggested that NADH (solution and spiked NADH) has been totally oxidized by PMS^+ and that the reduced form of the latter was reoxidized by dissolved oxygen [14]. These observations, i.e., no drift with prolonged spiking, justify the use of cells of low capacity (ca. 35 ml).

Glutamate determination. The experiments on glutamate were made by using the enzyme glutamate dehydrogenase incorporated in the carbon paste. The MCPE response was tested in the presence of 0.5 mM PMS^+ and 1 mM NAD^+ at +50 mV. The background current of the resulting probe was 1 nA. A linear relationship between peak current intensity and glutamate concentration was obtained between 1 and 500 μM [equation: y (nA) = 0.48 (nA) + 0.133 (nA μmol^{-1})x; $r = 0.999$]. In this instance, the batch injection technique allowed a frequency of analysis of ca. 40 h^{-1}.

Conclusion

Enzyme electrodes have been shown to perform well in BIA systems. The electrode response is fast owing to the proximity of the injection tip and the sensor surface and to the washing out phenomena. The risk of baseline deterioration due to the increase in the analyte concentration

can be avoided by using a cell design allowing semi-continuous draining (e.g., glucose, xanthine) or by using a redox mediator readily regenerated by dissolved oxygen.

REFERENCES

1 J. Wang and Z. Taha, Anal. Chem., 63 (1991) 1053.
2 L.J. Nagels, J.-M. Kauffmann, C. Dewaele and F. Parmentier, Anal. Chim. Acta, 234 (1990) 75.
3 A. Amine, G.J. Patriarche, G. Marrazza and M. Mascini, Anal. Chim. Acta, 242 (1991) 91.
4 P. Taylor, E. Kmetec and J.M. Johnson, Anal. Chem., 49 (1977) 789.
5 G. Palleschi, N. Rahni, M.A. Lubrano, J.N. Ngwainbi and G.G. Guilbault, Anal. Biochem., 159 (1986) 114.
6 M. Mascini, G. Palleschi and M. Iannello, Anal. Chim. Acta, 156 (1983) 135.
7 A. Amine, J.-M. Kauffmann, G.J. Patriarche and A.E. Kaifer, Anal. Lett., 24 (1991) 1293.
8 O. Doblhoff-Dier and G.A. Rechnitz, Anal. Lett., 22 (1989) 1047.
9 M. Dixon, Biochim. Biophys. Acta, 226 (1971) 269.
10 A. Amine and J.-M. Kauffmann, Bioelectrochem. Bioenerg., 28 (1992) 117.
11 P.J. Elving, W.J. Bressahan, J. Moiroux and Z. Samec, Bioelectrochem. Bioenerg., 9 (1982) 365.
12 B. Persson and L. Gorton, J. Electroanal. Chem., 292 (1990) 115.
13 L. Gorton, J. Chem. Soc., Faraday Trans. 1, 82 (1986) 1245.
14 T.E. King, J. Biol. Chem., 238 (1963) 4032.

Analytica Chimica Acta, 273 (1993) 219–227
Elsevier Science Publishers B.V., Amsterdam

Direct determination of lead by bioaccumulation at a moss-modified carbon paste electrode

J.A. Ramos, E. Bermejo, A. Zapardiel, J.A. Pérez and L. Hernández

Department of Analytical Chemistry and Instrumental Analysis, Autonoma University of Madrid, E-28049 Madrid (Spain)

(Received 1st June 1992; revised manuscript received 28th October 1992)

Abstract

Mosses are known to accumulate metals by an ion-exchange mechanism. The present work describes the application of a carbon paste electrode modified by Sphagnum Sp. for the determination of lead(II) in natural and drinking waters by anodic stripping differential pulse voltammetry. The preconcentration step is performed under open circuit conditions and the response is evaluated with respect to electrolyte, pH, ionic strength, preconcentration time and lead concentration. The electrode composition, voltammetric waveform and other variables have also been taken into account. For the preconcentration step, the best conditions were acetate buffer of pH 5.0 and 0.01 ionic strength. The supporting electrolyte was acetate buffer of pH 6.0 and 0.7 ionic strength. The modified electrode contained 10% moss. The electrode surface can be regenerated by immersion in 0.05 M perchloric acid for 60 s. The effect of various water components on the voltammetric response was also evaluated. The detection limit was 2 ng ml^{-1} (15 min preconcentration time). The relative standard deviation was 4.8% for a series of ten measurements of 20 ng ml^{-1} samples. Direct determination of lead in natural and drinking waters is possible using the standard addition method.

Keywords: Anodic stripping voltammetry; Differential pulse voltammetry; Lead; Moss-modified electrode; Waters

Research of chemically modified electrodes (CMEs) has experienced a quick development in the last years, especially in electroanalysis [1–3]. Since they allow preconcentration of the analyte prior to its electrochemical quantification, use of chemically modified electrodes enormously improves selectivity and sensitivity in determinations.

Among the methods used for the incorporation of modifiers to the electrodes are irreversible adsorption [4], covalent binding [5], coating with ion-exchange polymers [6], electrochemical polymerization [7] and direct incorporation of the modifier by mixing it with the carbon paste [8]. As for the mechanisms producing analyte accumulation on the electrode surface, they vary widely; among the most common mechanisms we can mention ion exchange [3], precipitation [8], complexation [9–11] and, recently, bioaccumulation [1,2,12,13]. Success in their analytical applications depends mainly on the choice of modifier.

The ability of certain microorganisms such as bacteria [14], yeasts [15], fungi [1,516], lichens [17], mosses [18,19] and water plants [20] for metal bioaccumulation has been known for quite a long time.

Accumulation can occur both in living and dead organisms in which two different metal in-

Correspondence to: L. Hernández, Department of Analytical Chemistry and Instrumental Analysis, Autonoma University of Madrid, E-28049 Madrid (Spain).

corporation mechanisms can be distinguished [21]: one independent of metabolism and the other dependent on it.

The former (metabolism-independent binding of metals) occurs both in living and dead cells and generally comprises two stages, a quick one up to saturation of the active binding positions on the cellular membrane and a second one where bioaccumulation stops or proceeds at a very low rate.

An NMR study on ^{113}Cd [22] (accumulated on a chlorella alga) revealed that metal binds to carboxylic groups belonging to the long polycarboxylic chains on the cellular membrane. Metabolism-dependent binding takes place only in living cells, able to accumulate metals through physico-chemical mechanisms: synthesis of metabolites capable of chelate formation with metal, diffusion through the cellular membrane or creation of a microenvironment around the cell allowing metal deposition or precipitation on the membrane. Deposition is usually a slow process, the metals that pass through the membrane settling in cellular organelles (vacuoles, chloroplasts, etc.) or staying in the citoplasm bound to proteins.

Mosses are plants with one-cell-wide leaves and lacking a cuticle, which means the chlorofilic cells are permanently exposed to changes in the composition of the surrounding medium, sometimes due to contamination episodes.

The ability of mosses from the species Sphagnum to accumulate cations from a solution was first observed in 1936 [23]. The moss has a modifying matrix consisting of non-esterified polyuronic acids [24,25]. As a result, it exhibits a high ability for ion exchange at polyuronic acid levels comprised between 10 and 30% of the moss dry weight [26]. Ions with a higher charge are more easily incorporated to the structure than those with less charge [27].

Wang et al. [1] have recently published a series of experiments carried out with algae-modified electrodes in order to study incorporation of cationic and anionic complexes to the electrode.

Gardea-Torresdey et al. [2,12] performed voltammetric measurements with carbon paste electrodes modified by algae, which allowed them to preconcentrate Cu(II) and Au(III). Connor et al. [13] described the development of carbon paste electrodes modified by lichens for the detection of Pb(II) and Cu(II).

This paper reports on the behaviour and use of a carbon paste electrode modified by a moss. The selected moss belongs to the species Sphagnum and allows selective preconcentration of lead coming from diluted solutions. A study of the experimental and instrumental conditions appropriate for direct determination of lead in natural and fresh waters by means of this electrode is included.

EXPERIMENTAL

Apparatus, electrodes and reagents

Measurements by atomic absorption spectrometry were carried out using a Perkin-Elmer 372 spectrophotometer equipped with a lead hollow cathode lamp and a HGA-2200 graphite furnace. Differential pulse voltammetry measurements were performed with a Metrohm Polarecord E-506 polarograph.

Cyclic voltammetric scans were made with a BAS CV-27 and a three-electrode system (consisting of a moss-modified carbon paste electrode, a platinum disk electrode and a saturated calomel electrode as reference electrode) was used for all voltammetric experiments.

All potentials were referred to the SCE. A magnetic stirrer with a 1.0-cm magnetic stirring bar was used for the preconcentration and/or the electrode regeneration step.

Three 50-ml cells were used, the preconcentration cell containing the sample to be evaluated, the measurement cell containing the supporting electrolyte and the regeneration cell containing a 0.05 M perchloric acid solution. Unless indicated otherwise, the differential pulse voltammograms were made with a 20 mV pulse amplitude, a 15 mV s^{-1} scan rate and a 0.8 s repetition time. Measurements were made at room temperature (22 ± 1°C).

The modified carbon paste electrodes (10% moss by weight) were prepared by mixing 0.1800 g of graphite powder of spectroscopic quality (42

μm maximum particle diameter) with 0.0200 g of sphagnum moss, the moss having been previously dried at 110°C for 60 min, grounded and sieved to a maximum diameter of 150 μm. Vaseline oil was then added to form a paste which is the basis of the modified electrode and which was introduced into a polypropylene tube (2 mm i.d.) where a copper wire was inserted to establish electric contact. Different amounts of graphite and moss were used in order to assess the influence of modifier percentage.

Activation of the electrode was achieved by subjecting it to cyclic high rate scans between −1.0 and +1.0 V for 30 min and then to measuring and regenerating processes (between 5 and 10 cycles) until reproducible behaviour was observed.

All lead solutions were prepared just before use by diluting a lead chloride solution of 9.8×10^{-4} M concentration stored in a polyethylene container. Deionized water was obtained with a Milli-Q and Milli-RO (Millipore) system. All chemicals were analytical grade reagents.

Atomic absorption spectrometry

Lead chloride solutions of 2.9×10^{-4} M concentration were prepared and the pH adjusted between 1 and 6 using hydrochloric acid and sodium hydroxide. 15 mg of moss were then added to 5 ml of the solution and the contact moss solution was maintained for 30 min under constant stirring. After that, the moss was filtered off and the lead remaining in the solution was analyzed, the amount of lead bound to the moss being calculated as the difference between the initial concentration and the one obtained after the moss-solution contact.

Measuring procedure

Each measuring cycle was done according to the following procedure. The electrode was rinsed with water and placed in the lead solution contained in the preconcentration cell for a variable time (preconcentration time), the preconcentration being carried out under constant stirring and at open circuit. The lead solution was buffered to pH 6.0 with 0.02 M acetic acid–sodium acetate.

The electrode was then taken out of the preconcentration solution, rinsed with water and transferred to the measurement cell containing acetate buffer of pH 6.0 and ionic strength 0.70. A constant potential was applied, usually −0.950 V (reduction potential), for 60 s in order to reduce the lead accumulated on the electrode surface followed by an oxidation scan by differential pulse voltammetry, usually between the applied reduction potential (−0.950 V) and −0.400 V.

Once the voltammogram had been obtained, the electrode was rinsed with deionized water and transferred to the regeneration cell, containing 0.05 M perchloric acid, thus eliminating any lead still remaining on the electrode surface, which was then ready for the next measuring cycle.

RESULTS AND DISCUSSION

Moss from the species Sphagnum was selected because the studies carried out by Mazimpaka et al. [28] prove they have a strong affinity towards lead as compared to moss from other species.

Figure 1A shows the ability of the Sphagnum moss to bioaccumulate lead as a function of pH, evaluated by atomic absorption spectrometry. The percentage of lead retained by the moss increases as the pH increases. pH values higher than 4 result in total lead retention. Such a behaviour could be explained by postulating a lead adsorption process due to ionic exchange. Lead competes with protons for the negative charges of the carboxylic groups coming from glucuronic acids in the moss membrane cell. At pH levels higher than 4, the proton concentration is not large enough to compete with lead incorporation to the moss. A possible regeneration route for the moss surface can be deduced from Fig. 1A, since a low pH will cause lead to leave the binding positions in the moss membrane.

In order to study the voltammetric properties of lead on the electrode surface, the 10% moss-modified carbon paste electrode was submerged for 3 min in a stirred 4.8×10^{-6} M lead(II) chloride solution buffered at pH 5.0 with acetic

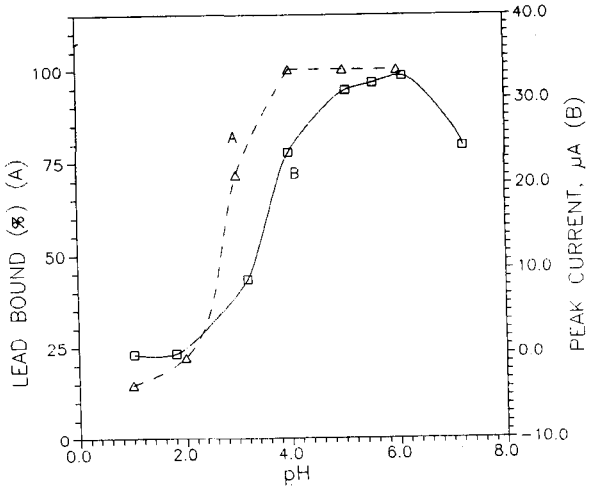

Fig. 1. (A) Effect of pH on the binding of lead(II) to the Sphagnum moss. The profile was obtained using a solution containing 3 mg ml^{-1} Sphagnum, 2.9×10^{-4} M lead(II), and 30 min contact time. (B) Effect of pH on the preconcentration/voltammetric response of a 6% moss-modified electrode. Lead concentration, 4.8×10^{-6} M; preconcentration time, 210 s; scan rate, 10 mV s^{-1}; repetition time, 0.8 s; pulse amplitude, 70 mV; reduction potential, −1.000 V; reduction time, 60 s; supporting electrolyte, 0.2 M acetate buffer of pH 5.0.

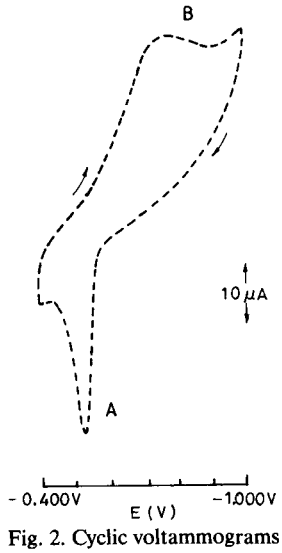

Fig. 2. Cyclic voltammograms obtained with a 10% moss-modified electrode in acetate buffer (pH 6.0 and ionic strength 0.70); preconcentration time, 3 min; lead concentration, 4.8×10^{-6} M; scan rate, 100 mV s^{-1}; reduction potential, −1.000 V; reduction time, 48 s.

acid–sodium acetate of 0.01 ionic strength. The electrode was then transferred to the measurement cell containing, as supporting electrolyte, acetate buffer of pH 6.0 and ionic strength 0.70; a potential of −1.000 V was applied for 48 s and the cyclic voltammograms were obtained (beginning with the anodic scan) between −1.000 and −0.400 V.

Figure 2 shows one of the voltammograms obtained. It has two visible peaks, a big, well-defined anodic one at −0.520 V and a second less intense and more poorly defined cathodic peak at −0.780 V.

The anodic process is reversible, as can be observed from the difference of 28 mV between peak and half-peak potentials. The difference between peak potential and half-peak potential in a reversible system is $59\times n^{-1}$ mV, n representing the number of electrons exchanged [29].

In view of the results obtained, the anodic peak was chosen for lead quantification.

Different measuring techniques can be used in anodic stripping voltammetry. In the present work both differential pulse and linear scans have been applied. One of the voltammograms obtained for each technique is shown in Fig. 3.

Taking into account the peak current obtained, the magnitude of the background current

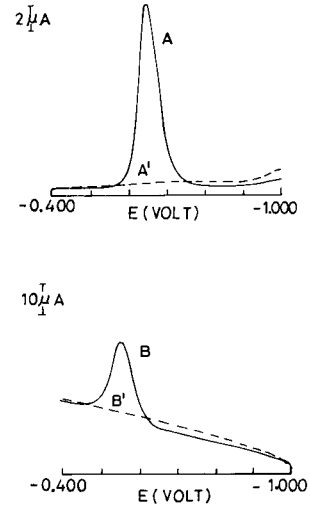

Fig. 3. Comparison of voltammetric responses in the determination of lead. (A) Pulse differential voltammogram. Scan rate, 15 mV s^{-1}; pulse amplitude, 70 mV. (B) Linear-sweep voltammogram. Other conditions as in Fig. 2.

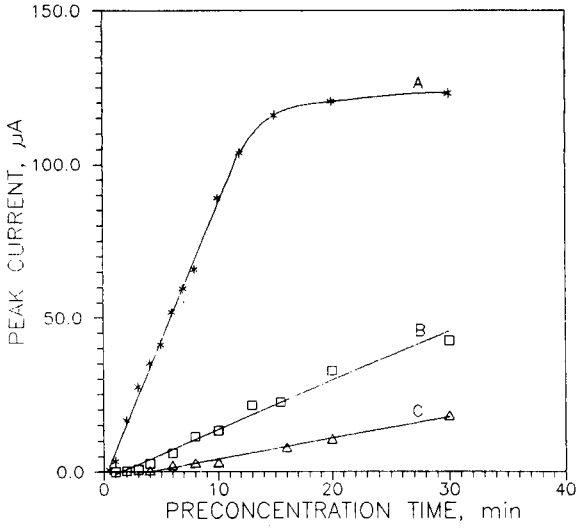

Fig. 4. Dependence of peak current on the preconcentration time. Lead concentration, (A) 4.8×10^{-6} M, (B) 9.7×10^{-7} M, (C) 3.9×10^{-7} M; pulse amplitude, 70 mV; scan rate, 15 mV s^{-1}. Other conditions as in Fig. 2.

and the reproducibility, differential pulse voltammetry was chosen.

Figure 3 also shows the electrode responses after the regeneration treatment had been applied (curves A′ and B′). Renovation of the electrode surface is easily achieved by dipping the electrode in 0.05 M of perchloric acid for 60 s. The subsequent voltammetric scan shows no lead peak.

Influence of pH, ionic strength and preconcentration time were all studied in the preconcentration cell.

Figure 1B shows pH influence on lead preconcentration on the electrode surface. A similar behaviour to that of the moss added to the solution (Fig. 1A) was observed. Moss incorporation to the electrode does not vary its ability for lead preconcentration. The pK_a value of the acid groups on the moss cellular membrane can also be deduced from Fig. 1B. The value obtained (3.7) accords with the usual pK_a values for carboxylic acids.

pH values higher than 6 cause a decrease in peak current due to formation of hydroxylic lead complexes that prevent lead incorporation to the electrode. In order to obtain the highest peak current, acetate buffer was chosen as electrolyte in the preconcentration cell.

The study of the influence of ionic strength on lead bioaccumulation proved that the analytical signal was not influenced for ionic strengths equal to or lower than 0.01. Higher values provoke an exponential decrease of signal height, making it advisable to set the ionic strength in the preconcentration cell at 0.01 or lower.

Figure 4 shows the influence of preconcentration time on peak current for various lead(II) concentrations. A linear dependence of peak current on preconcentration time is established for all concentrations. Electrode saturation for preconcentration times longer than 12 min occurs for a 4.8×10^{-6} M lead(II) chloride solution.

Influence of pH and ionic strength were also studied in the measurement cell. The pH study was carried out using, as supporting electrolyte, 0.40 M potassium nitrate in the first instance and acetate buffer (pH 4–7) and acetic acid–sodium perchlorate (pH 2–3) of ionic strength 0.70 in the second.

Variation in peak potential with varying pH for the two supporting electrolytes mentioned above is shown in Fig. 5, while a summary of the

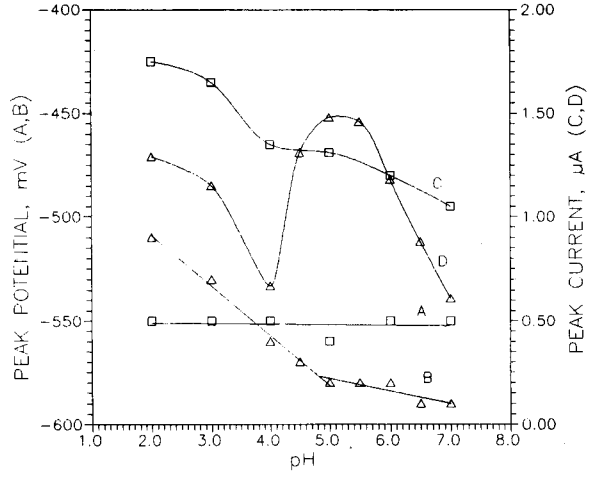

Fig. 5. Dependence of (A, B) peak potential and (C, D) peak current on the pH in the measurement cell. Supporting electrolytes: (B, D) acetate buffer (ionic strength 0.70) and (A, C) 0.4 M potassium nitrate. Lead concentration, 4.7×10^{-7} M; preconcentration time, 8 min; pulse amplitude, 20 mV; scan rate, 15 mV s^{-1}. Other conditions as in Fig. 2.

variation zones in peak potential is given in Table 1.

From the slopes obtained for peak potential variation with pH and taking into account that the process representing the anodic wave behaves as a reversible system, the number of protons involved in the electrochemical reaction can be estimated. The processes taking place in the measurement cell when acetate buffer is used are the following.

Reduction of lead accumulated on the electrode:

$$Pb^{2+} \begin{matrix} \nearrow {}^{-}OOC \\ \searrow {}^{-}OOC \end{matrix} (el) + 2X^{+}(s) + 2e^{-} \longrightarrow$$

$$Pb^{0}(el) + \begin{matrix} X^{+-}OOC \\ | \\ X^{+-}OOC \end{matrix} (el)$$

X^+ = counterion of the moss.

Anodic stripping process:

(1) pH values lower than 4.8:

$$Pb^{0}(el) + HAc(s) \longrightarrow$$

$$PbAc^{+}(s) + H^{+}(s) + 2e^{-}$$

(2) pH values higher than 4.8:

$$Pb^{0}(el) + Ac^{-}(s) \longrightarrow PbAc^{+}(s) + 2e^{-}$$

The pH at the intersection of the two lines (Fig. 5, curve B) corresponds to the pK_a of the acetic acid; under the conditions described, pK_a value is 4.8_4.

When the supporting electrolyte was potassium nitrate, the anodic stripping process consisted of:

$$Pb^{0}(el) + NO_3^{-}(s) \longrightarrow PbNO_3^{+}(s) + 2e^{-}$$

TABLE 1

Variation of peak potential with pH in the measurement cell

Supporting electrolyte	pH range	Straight line equation	Number of protons
Acetate buffer	2.0 < pH < 4.8	−0.457 − 0.026 pH	1
Acetate buffer	pH > 4.8	−0.549 − 0.006 pH	0
Potassium nitrate	2.0 < pH < 7.0	−0.539 − 0.002 pH	0

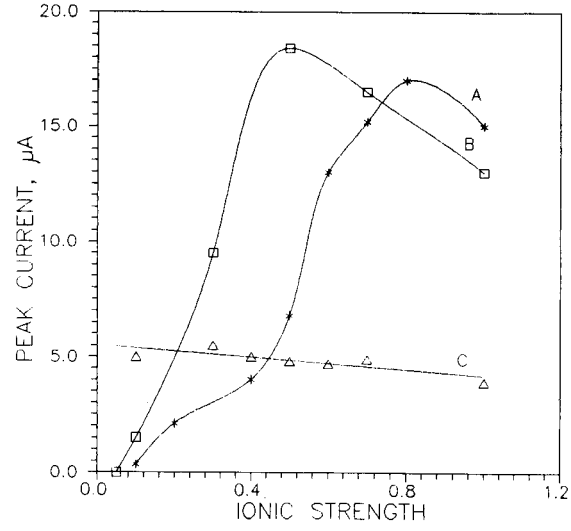

Fig. 6. Influence of the ionic strength on the peak current. Supporting electrolytes: (A) acetate buffer (pH 6.0); (B) sodium nitrate; (C) sodium perchlorate. Lead concentration, 4.7×10^{-7} M; preconcentration time, 8 min; scan rate, 10 mV s^{-1}; pulse amplitude, 70 mV. Other conditions as in Fig. 2.

Figure 5 also shows dependence of peak current on pH. The differences observed are basically due to the differences in acid–base behaviour of the two electrolytes. An acidic pH results in an increase in peak current, since the protons' ability to displace lead from the binding positions is added to the ability of nitrate or acetate to form complexes with lead(II).

The effect of the ionic strength in the measurement cell is shown in Fig. 6. If adjusted with sodium perchlorate, ionic strength has no effect on peak current. When potassium nitrate is used, however, an ionic strength of 0.40 achieves the greatest response, while 0.70 affords the same effect with acetate buffer. The difference in behaviour is due to the fact that, while both the acetate and nitrate ions form weak complexes with Pb^{2+} [30], thus facilitating lead dissolution from the electrode surface, the perchlorate ion does not form complexes with lead. In view of these results, acetate buffer at pH 6.0 and ionic strength 0.70 was chosen as supporting electrolyte in the measurement cell, in order to obtain the highest analytical signal.

A study of the influence of potential and reduction time prior to the recording by anodic

stripping voltammetry proved that the maximum values in the voltammetric response are obtained with potentials between −0.900 and −1.00 V and reduction times of 60 s.

Table 2 shows the values obtained when electrodes with different Sphagnum percentages were used. The best analytical response was obtained with the one containing 10% of dried moss. Higher percentages cause signal reduction, probably due to a decrease in the electrode conductivity.

The influence of pulse amplitude and scan rate was studied. For pulse amplitude values lower than 55 mV, the half-peak width remains constant, 45 mV ($90.4 \times n^{-1}$ mV for a reversible system) and the potential varies linearly with a slope 0.54 (n^{-1} for a reversible system) [31]. These results suggest that the electrode reaction is reversible. A pulse amplitude of 20 mV was chosen, since it affords the highest signal-to-noise ratio.

As for the scan rate, the response rises linearly with increasing scan rate. A scan rate of 15 mV s^{-1} was chosen, with a repetition time of 0.8 s.

Under such conditions, and for a 15-min preconcentration time, the peak current varies linearly with lead concentration between 5 and 150 ng ml^{-1}.

$$I_p\ (\mu A) = 0.0(\pm 0.1) + 0.042(\pm 0.004) \times C\ (\text{ng ml}^{-1})$$

Figure 7 shows differential pulse voltammograms for different lead concentrations. The detection limit (3σ) was 1.9 ng ml^{-1}, the mean relative error 4.4% and a series of ten consecutive measures of a 20 ng ml^{-1} solution gave a peak current of 0.85 μA, with a range comprised between 0.78 and 0.90 μA and a relative standard deviation of 4.8%.

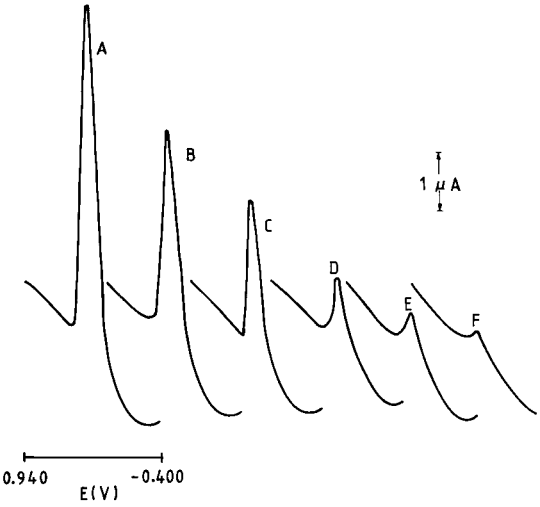

Fig. 7. Differential pulse voltammograms obtained with different lead concentration, (A) 100 ng ml^{-1}, (B) 70 ng ml^{-1}, (C) 50 ng ml^{-1}, (D) 25 ng ml^{-1}, (E) 10 ng ml^{-1}, (F) 5 ng ml^{-1}. Preconcentration time, 15 min; pulse amplitude, 20 mV; scan rate, 15 mV s^{-1}, reduction potential, −0.940 V. Other conditions as in Fig. 2.

TABLE 2

Influence of paste composition on the peak current

Moss content (%)	Peak current (μA)
0	0
3	5.1
6	16.4
10	23.0
15	8.4
20	2.3

Interference study

The ions (anions and cations) present in natural and fresh waters were examined as possible sources of interference.

A 50 ng ml^{-1} lead(II) solution was used for the preconcentration, with increasing concentrations of the interferents until the usual concentrations in water were reached. The preconcentration time was 10 min. Anions do interfere because of a series of reactions with lead (precipitation, complexation, etc.) which prevents its accumulation to the electrode surface later on. Cations interfere because they are potentially competing for the binding sites. In both cases the peak current coming from the lead accumulated on the electrode is reduced. Below, concentrations shown in brackets are the highest assayed.

The following anions do not interfere: chloride (500 mg l^{-1}), sulphate (500 mg l^{-1}), nitrate (200 mg l^{-1}), nitrite (20 mg l^{-1}), fluoride (20 mg l^{-1}),

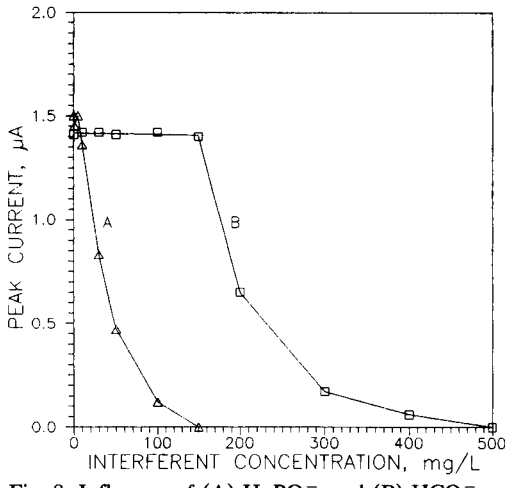

Fig. 8. Influence of (A) $H_2PO_4^-$ and (B) HCO_3^- concentration on the voltammetric response. Lead concentration, 50 ng ml^{-1}; preconcentration time, 10 min; scan rate, 15 mV s^{-1}; pulse amplitude, 20 mV; reduction potential, −0.9940 V. Other conditions as in Fig. 2.

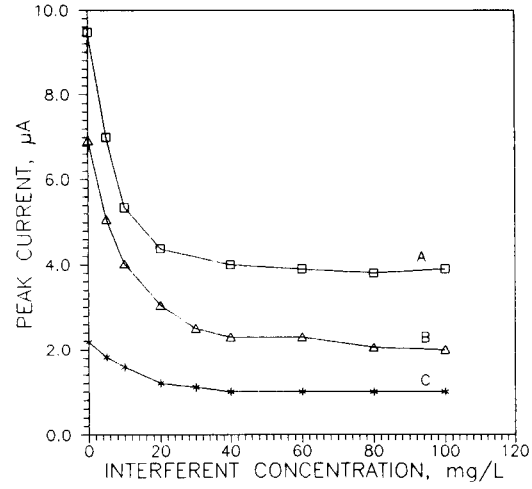

Fig. 9. Influence of (A) magnesium and (B, C) calcium concentration on the peak current. Lead concentration, (A) 50 ng ml^{-1}, (B) 40 ng ml^{-1}, (C) 25 ng ml^{-1}. Pulse amplitude, 90 mV. Other conditions as in Fig. 8.

bromide (20 mg l^{-1}), iodide (20 mg l^{-1}), thiocyanate (20 mg l^{-1}) and arsenate (200 mg l^{-1}).

Figure 8 represents the influence of carbonate and phosphate.

As for cations, sodium (250 mg l^{-1}), potassium (400 mg l^{-1}), zinc(II) (5 mg l^{-1}), copper(II) (5 mg l^{-1}), iron(III) (8 mg l^{-1}), silver(I) (250 μg l^{-1}), and mercury(II) (5 μg l^{-1}) do not interfere nor do cadmium(II), chromium(III), nickel(II), cobalt(II), antimony(III) and vanadium(V) as long as their concentrations are equal to the concentration of lead.

Figure 9 shows calcium and magnesium interference. Presence of bicarbonate or phosphate at concentrations usually found in fresh water does not affect the direct determination of lead. Calcium and magnesium at high concentration reduce the signal thus lowering the sensitivity of the determination.

If the standard addition method is used for quantification, a direct determination can be performed.

Application to lead determination in natural and fresh waters

The method was applied to various samples of natural and fresh waters. None of them revealed detectable lead concentrations, so standard additions were made starting from 10 ng ml^{-1}. Figure 10 shows the result obtained. The sensitivity values obtained were: (A) deionized water: 0.042 μA ml ng^{-1}; (B) running water from the laboratory tap: 0.026 μA ml ng^{-1}; (C) water from the

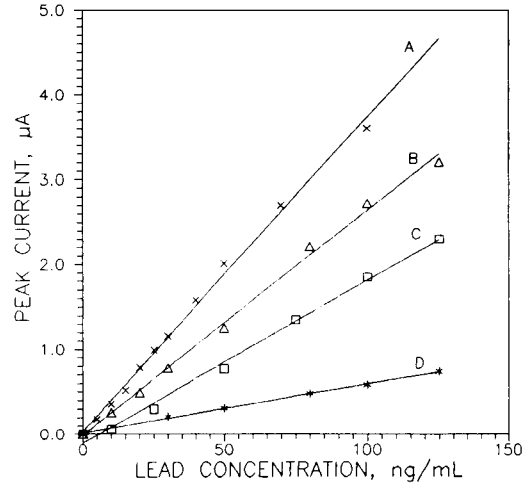

Fig. 10. Effect of lead concentration on the peak current for different water samples. Preconcentration time, 15 min. Samples: (A) deionized water (for comparison), (B) running water from the laboratory tap, (C) water from the Cega river taken at Navafría (Segovia, Spain), (D) marketed calcium bicarbonated mineral water. Other conditions as in Fig. 8.

Cega river taken at Navafría (Segovia): 0.020 μA ml ng^{-1}; (D) marketed calcium bicarbonated mineral water: 0.0058 μA ml ng^{-1}.

Waters with high concentration of the interferents calcium, magnesium and bicarbonate (hard waters), such as sample D, were observed to produce low sensitivities, while relatively soft waters (low concentration of the interferents), as samples B and C gave higher ones. A deionized water sample has been included to allow comparison.

To certify the correctness of the analytical method, a running water sample from the laboratory tap was spiked with 20 ng ml^{-1} of lead and it was analyzed by the described method and by flameless atomic absorption spectroscopy. The results obtained were: voltammetric method, lead concentration 22 ng ml^{-1}; flameless AAS, lead concentration 21 ng ml^{-1}.

The agreement between the above results confirms the validity of this method for lead analysis in water samples.

The results obtained prove the feasibility of the determination of lead in samples of natural or fresh waters. Presence of lead-selective binding sites with respect to alkaline earth cations is a decisive factor for application of the method to direct determination of lead in natural and fresh waters.

The authors thank the Comunidad Autonoma de Madrid for financial support (Proyect CAM No. C 090/91) and for a research fellowship to J.A. Ramos.

REFERENCES

1 J. Wang, T. Martinez and D. Darnall, J. Electroanal. Chem., 259 (1989) 295.
2 J. Gardea-Torresdey, D. Darnall and J. Wang, Anal. Chem., 60 (1988) 72.
3 J. Wang and T. Martinez, Electroanalysis, 1 (1989) 167.
4 W.J. Albery, M.J. Eddowes, H.A.O. Hill and A.B. Hillman, J. Am. Chem. Soc., 103 (1981) 3904.
5 K.J. Stutts and R.M. Wightman, Anal. Chem., 54 (1983) 1576.
6 G. Nagy, G.A. Gerhardt, A.K. Oke, M.E. Rice and R.N. Adams, J. Electroanal. Chem., 188 (1985) 85.
7 A.R. Guadalupe, L.M. Wier and H.D. Abruña, Am. Lab., 18 (1986) 102.
8 R.P. Baldwin, J.K. Christensen and L. Kryger, Anal. Chem., 58 (1986) 1790.
9 Z. Gao, P. Li, S. Dong and Z. Zhao, Anal. Chim. Acta, 232 (1990) 367.
10 R.P. Baldwin, J.K. Christensen and L. Kryger, Anal. Chem., 58 (1986) 1790.
11 S.V. Prabhu, R.P. Baldwin and L. Kryger, Anal. Chem., 59 (1987) 1074.
12 J. Gardea-Torresdey, D. Darnall and J. Wang, J. Electroanal. Chem., 252 (1988) 197.
13 M. Connor, E. Dempsey, M.R. Smith and D.H.S. Richardson, Electroanalysis, 3 (1991) 331.
14 M.L. Simoes Gonçalves, L. Sigg and M. Reutlinger, Sci. Total Environ., 60 (1987) 105.
15 N. Nakajima dn T. Sakaguchi, Appl. Microbiol. Biotechnol., 24 (1986) 59.
16 A. Demon, M. De Bruin and H.T. Wolterbeek, Environ. Monit. Assess., 13 (1989) 21.
17 R.P. Becket and D.H. Brown, New Phytol., 97 (1984) 301.
18 D.H. Brown and G.W. Buck, Cryptogam.: Briol. Lichenol., 6 (1985) 279.
19 D.H. Brown and R.P. Becket, Lichenologist, 16 (1984) 173.
20 F.E. Chigbo, R.W. Smith and F.L. Shore, Environ. Pollut., Ser. A, 27 (1982) 31.
21 d. Khummongkol, G.S. Canterford and C. Fryer, Biotechnol. Bioeng., 24 (1982) 2643.
22 D.A. Laude, Jr. and J.A. Holcombe, Environ. Sci. Technol., 24 (1990) 1309.
23 K.J. Williams and T.G. Thompson, Int. Rev. Gesamten Hydrobiol. Hydrogr., 33 (1936) 271.
24 R.S. Clymo, Ann. Bot. (London), 27 (1963) 309.
25 J.S. Cragie and W.S.G. Maas, Ann. Bot., 30 (1966) 153.
26 R.S. Clymo, Proceedings of the International Biological Program Symposium, 1967, Amsterdam, p. 273.
27 J. Toffet, C.R. Hebd. Séances Acad. Sci., Ser. D, 274 (1972) 2175.
28 V. Mazimpaka, S. Lara, V. Bermejo and J.A. Hernández, J. Bryol., submitted for publication.
29 A.J. Bard and L.R. Faulkner, Electrochemical Methods: Fundamentals and Applications, Wiley, New York, 1980, p. 219.
30 D. Inczédy, Analytical Applications of Complex Equilibira, Wiley, New Yok, 1976, p. 319.
31 A.J. Bard and L.R. Faulkner, Electrochemical Methods: Fundamentals and Applications, Wiley, New York, 1980, p. 190.

Analytica Chimica Acta, 273 (1993) 229–236
Elsevier Science Publishers B.V., Amsterdam

Ion-exchange voltammetry of copper ions in chloride media at glassy carbon electrodes modified with polycationic ionomers

Paolo Ugo, Ligia Maria Moretto and Gian Antonio Mazzocchin

Department of Physical Chemistry, University of Venice, Calle Larga S. Marta 2137, I-30123 Venice (Italy)

(Received 1st June 1992)

Abstract

Perfluorinated polycationic polymers (Tosflex) were applied for preparing polymer-modified electrodes able to preconcentrate anionic complexes of Cu^+ electrogenerated in situ at the electrode/polymer interface by reducing Cu^{2+} solutions in the presence of chloride ions. The species incorporated into the polymeric coating, namely $CuCl_2^-$, was detected by a suitable linear sweep voltammetric reoxidation scan. The dependence of the reoxidation peak current on experimental parameters such as amount of modifier, electrogeneration–preconcentration time and solution concentrations of Cu^{2+} and Cl^- was studied. The possibility of applying Tosflex-modified electrodes to copper speciation studies was also examined. In particular, the influence on the ion-exchange voltammetric responses of some amino acids such as histidine, glycine and glutamic acid which, at the pH employed in this study, carry positive, neutral and negative ionic charges, respectively, is discussed. Some of the advantages and limitations of Tosflex-modified electrodes compared with Nafion-coated electrodes and the hanging mercury drop electrode are critically evaluated.

Keywords: Copper; Glassy carbon electrodes; Polycationic ionomer coatings; Speciation

The use of ion-exchanger-coated electrodes to preconcentrate and detect electroactive species is a rapidly growing field which has given rise to the technique of ion-exchange voltammetry [1].

Cation-exchange voltammetry usually employs electrodes modified with Nafion, a perfluorinated ionomer whose popularity is mainly due to the ease with which stable modified electrodes can be prepared from commercially available solutions of the polymer. Recently, ion-exchange voltammetry at Nafion-coated electrodes has been applied for detecting electroactive cations, such as biologically active organics [2–4] or *f*-element cations [5–7], for which classical anodic stripping methods are not applicable.

Concerning anion exchangers, since the pioneering work of Oyama and Anson [8], the most often studied polycationic modifier is polyvinylpyridine which, however, presents some problems such as non-ideal permselectivity [9,10] and the need for stabilization by chemical cross-linking [11,12].

Correspondence to: P. Ugo, Department of Physical Chemistry, University of Venice, Calle Larga S. Marta 2137, I-30123 Venice (Italy).

Recently, a new class of perfluorinated ionomeric membranes named Tosflex (Tosoh Soda Manufacturing, Kanagawa) has become commercially available. As shown by the structural formula:

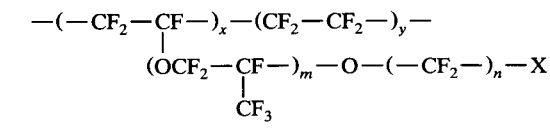

where $m = 0–1$, $n = 1–5$, X = anion-exchange unit, including the counter anion. This polymer can be considered as the anion-exchanger analogue of Nafion and, in principle, it can constitute a valid alternative to polyvinylpyridine, as shown experimentally by recent reports concerning electrodes modified with this [13] and similar ionomers [14].

The use of electrodes modified with anion exchangers seems particularly relevant for developing methods for the direct analysis of complex samples such as natural waters or body fluids, where many trace metals can be present in the form of anionic species [15–17]. Such anion complexation has to be taken into account when polymer-modified electrodes are applied to metal speciation analysis studies [18–20]. In this context, it is worth noting that in the presence of chloride, copper(I) electrogenerated from Cu^{2+} solutions is stabilized mainly in the form of the anionic $CuCl_2^-$ complex [21,22], which can be preconcentrated and detected at electrodes modified with anion exchangers such as quaternary polyvinylpyridine [23]. Considering that in principle the Tosflex polymer can also be used to preconcentrate such an electrogenerated anionic complex, in this work the electrochemical behaviour of copper at Tosflex-modified electrodes in chloride-containing media was examined. In addition, considering the possibility of applying Tosflex-modified electrodes to copper speciation studies, the effect of the presence of other competing ligands was also examined. In particular, as the electrode modifier is a positively charged polyelectrolyte, the influence of some amino acids such as histidine, glycine and glutamic acid, which, at the pH employed in this work carry positive, neutral and negative ionic charges, respectively [24], on the ion-exchange voltammetric behaviour was investigated.

EXPERIMENTAL

Chemicals

All chemicals were of analytical reagent grade. Triply distilled water was used throughout to prepare solutions.

Aqueous–alcoholic solutions (water–methanol–2-propanol, 1:1:1) of Tosflex IE-SA 48 polymer were prepared from the thick solid membrane, obtained from Tosoh Soda Manufacturing, using the method of Dunsch et al. [13]. The filtered solution had a concentration of about 2.5% (w/v). 2.5% (w/v) Nafion solutions were prepared by 1:1 dilution with methanol of Nafion solutions commercially available (Aldrich, 5% (w/v) solution of Nafion 117 in a mixture of lower aliphatic alcohols and 10% water).

Apparatus and procedures

All electroanalytical measurements were made at room temperature (22 ± 1°C) under a nitrogen atmosphere, using a single-compartment three-electrode cell. Electrode potentials were measured versus a saturated calomel electrode (SCE); a platinum coil was used as the counter electrode.

Electrochemical measurements were done with an Amel Model 553 potentiostat connected to an Amel Model 568 function generator or with an EG&G PARC Model 273 programmable potentiostat controlled by a personal computer via EG&G PARC M 270 software; anodic stripping voltammetry was performed using an EG&G PARC Model 303A mercury drop electrode.

Tosflex-coated electrodes were prepared by droplet evaporation of microvolumes (usually 3 μl) of 2.5% (w/v) Tosflex solution deposited on a mirror-polished glassy-carbon electrode (area 0.2 cm^2). The thickness of the coating was measured with an Alfa Step profilometer (Tencor Instruments, Mountain View, CA).

Nafion-coated electrodes were prepared by micropipetting 3 μl of 2.5% (w/v) Nafion solution on to the same glassy carbon electrodes as described above.

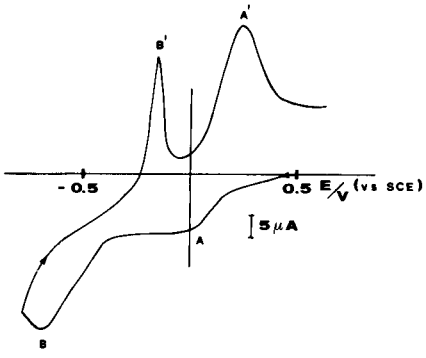

Fig. 1. Cyclic voltammogram of 5×10^{-4} M Cu^{2+} at a Tosflex-coated glassy carbon electrode in 0.5 M NaCl–0.1 M acetate buffer (pH 5.0). Scan rate, 50 mV s^{-1}.

RESULTS AND DISCUSSION

Electrochemical behaviour at Tosflex-modified electrodes

When a Tosflex-modified electrode is dipped in a Cu^{2+} solution containing chloride as the supporting electrolyte, the voltammetric pattern shown in Fig. 1 is recorded. In the forward cathodic scan two broad reduction peaks, A and B, are observed, with which the sharper reoxidation peaks A′ and B′ are associated.

As shown in Fig. 2, when the cathodic scan is stopped at potentials less negative than peak B, e.g., −200 mV, and the electrode is kept at this potential value for a short time before reversing the scan direction, an increase in the current of peak A′ proportional to the duration of the polarization step is observed.

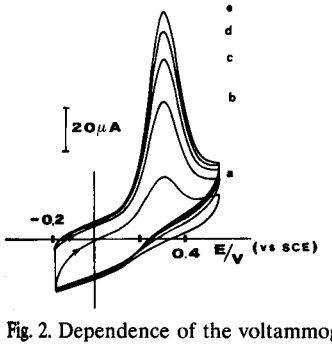

Fig. 2. Dependence of the voltammograms on the duration of the electrogeneration–preconcentration step at −200 mV. Step duration: (a) 0; (b) 60; (c) 120; (d) 180; (e) 240 s. Other experimental conditions as in Fig. 1.

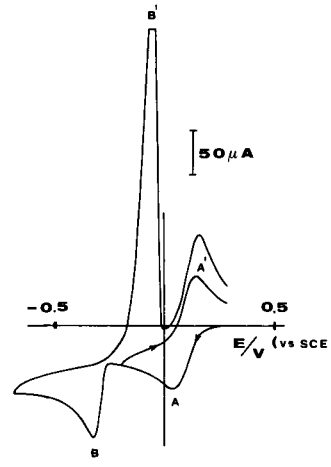

Fig. 3. Cyclic voltammogram recorded at a bare glassy carbon electrode under the same experimental conditions as in Fig. 1.

These results can easily be understood by comparison with the behaviour observed at a bare glassy carbon electrode and reported in Fig. 3. According to previous findings [21,22], in chloride-containing media a Cu^{+} species stabilized by chloride interaction is electrogenerated at peak A. Such a Cu^{+} complex can be reoxidized to Cu^{2+} at peak A′ in the reverse scan (with $i_{p(A')}/i_{p(A)} = 1$ for 20 mV $s^{-1} \leqslant V \leqslant 200$ mV s^{-1}) or can be further reduced to metallic copper at peak B, such a metal deposit being reoxidized to the Cu^{+} complex at the stripping peak B′. These results confirm that the species preconcentrated at −200 mV and reoxidized at peak A′ at the Tosflex-modified electrode is $CuCl_2^-$.

By comparing Figs. 1 and 3, it is evident that the reduction peak A at the modified electrode is lower than the corresponding peak recorded at the bare electrode, indicating that the presence of the Tosflex coating hinders the access of Cu^{2+} ions to the electrode surface. Considering the polycationic nature of the modifier, this effect can be attributed to the permselectivity of the coating, which causes co-ion exclusion. However, the evidence that the reduction is not completely blocked suggests that the 2+ charge of Cu^{2+} ions is partially neutralized by interaction with the electrolyte solution, e.g., with acetate or chloride ions [25], so allowing the progressive incorporation of the reduction product. It is worth

noting that the relevance of such interactions is influenced by the local ion concentrations inside the coating which, for anions, are much higher than those in solution; however, these parameters cannot be quantified reliably because the ion concentrations inside the coating are ruled by selectivity coefficients which for Tosflex polymers have not yet been determined.

Finally, the negative potential shift observed for peak A at the modified electrode agrees with the fact that the reduction takes place inside a permselective coating [26].

Optimization of preconcentration conditions

Focusing attention on the exploitation of the above-described behaviour for the determination of copper(II) in solution, the influence of typical experimental parameters on the electrogeneration and preconcentration of $CuCl_2^-$ at -200 mV and the subsequent detection of the incorporated species at the reoxidation peak A′ was examined.

Preliminary experiments on the influence of the amount of polymer deposited on the electrode surface indicate that good results are obtained by using 0.32 mg cm^{-2}, corresponding to a wet film thickness of 1.8 μm. On lowering the amount of modifier below this value, a progressive decrease in peak A′ is observed. This observation suggests a thin-layer-like behaviour, the voltammetric response depending on the volume of the coating [27]. On the other hand, an increase in the amount of coating above 0.32 mg cm^{-2} causes a distortion of the reoxidation peak, probably owing to an excessive increase in the ohmic resistence of the coating. The above-reported optimum amount of polymer is the result of a compromise between the need to increase the sensitivity, which is proportional to the film thickness, and the necessity to record undistorted peaks.

The influence of the electrogeneration time, shown in Fig. 2, was examined as a function of the Cu^{2+} solution concentration and the relevant results are shown in Fig. 4. It is evident that the height of peak A′ becomes independent of the electrogeneration–preconcentration time for times longer than 10 min, no matter what the Cu^{2+} solution concentration may be. Moreover,

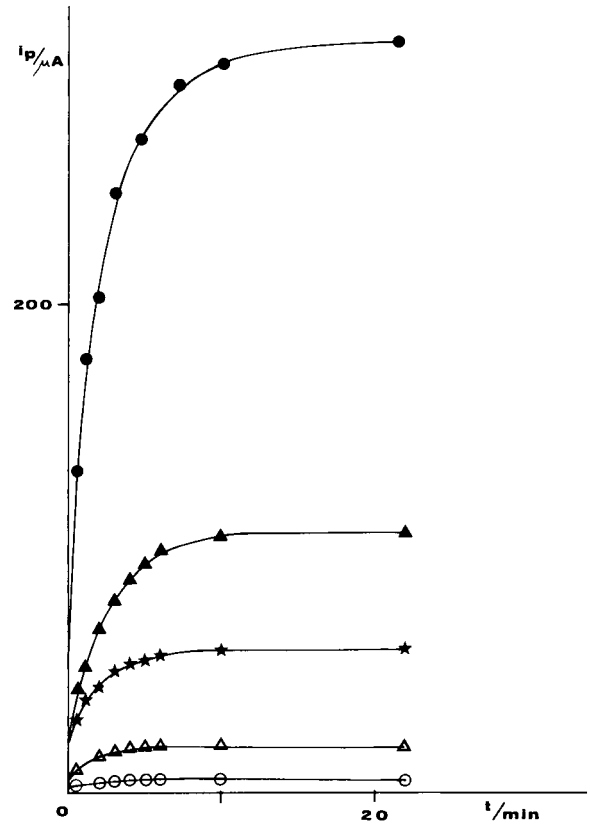

Fig. 4. Dependence of reoxidation current of peak A′ in Fig. 1 on the electrogeneration–preconcentration time at -200 mV for different Cu^{2+} concentrations: (○) 1×10^{-5}; (△) 5×10^{-5}; (★) 1×10^{-4}; (▲) 5×10^{-4} M; (●) 1×10^{-3} M. Other experimental conditions as in Fig. 1.

as shown in Fig. 5, the log–log plots of the current of peak A′ at definite times as a function of the Cu^{2+} concentration are linear even for times shorter than 10 min with a dynamic range extending over ca. three orders of magnitude. These data indicate that quantitative measurements can be carried out even using short electrogeneration–preconcentration times; anyway, when the analysis time is not a limiting parameter, it is suggested that preconcentration time $\geqslant 10$ min are used, when the voltammetric responses do not change significantly even for small variations or errors in the duration of the preconcentration time.

Data characterizing the calibrations graphs using 10 min as the preconcentration time, and

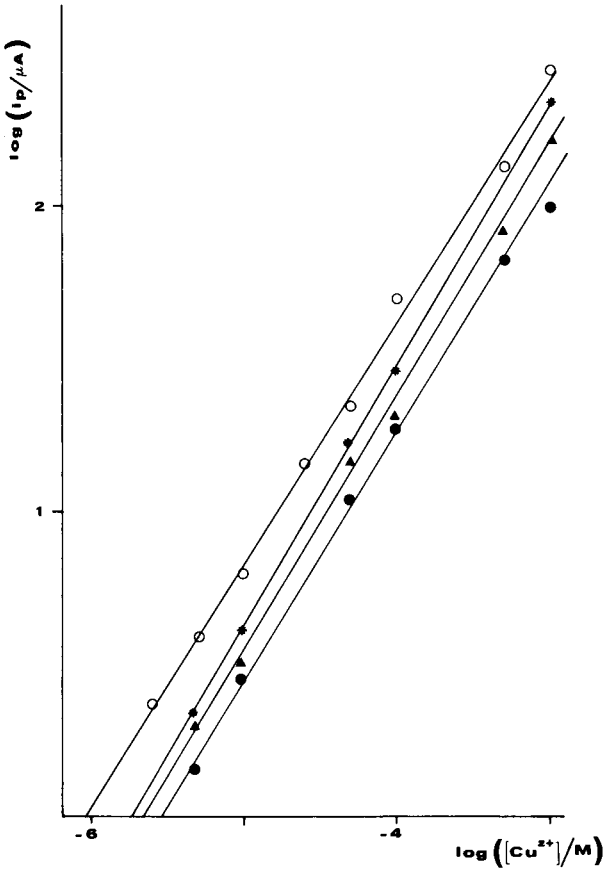

Fig. 5. Dependence of the current of peak A′ in Fig. 1 on the solution concentration of Cu^{2+} for different durations of the electrogeneration–preconcentration step: (●) 0.5; (▲) 1; (*) 5; (○) 10 min. Other conditions as in Fig. 1.

different detection conditions are reported in Table 1. It can be seen that the calibration graphs obtained by using the peak area as the measured quantity are characterized by higher sensitivity and lower detection limits. The best results are obtained at a scan rate of 50 mV s^{-1}, probably as a consequence of the direct dependence of peak height on the scan rate observed in such experiments. The detection limit in this instance is strongly affected by the standard deviation values for the blank and the intercept, the relevant high values reflecting problems connected with noise and reproducibility typical of polymer-modified electrodes.

Data reported in the last line of Table 1, referring to a calibration plot obtained by classical linear-sweep anodic stripping voltammetry at a hanging mercury drop electrode, show that results obtained at the Tosflex-modified electrode are slightly inferior, at least as far as the detection limit is concerned.

An advantage of anion-exchange voltammetry using Tosflex-coated electrodes over classical anodic stripping voltammetry is that the preconcentration can be carried out at far less negative potentials. This is particularly interesting with regard to copper determinations in complex samples containing interferents that can be reduced at potentials more negative than −200 mV vs. SCE.

Finally, it can be noted that the current of

TABLE 1

Statistical data for calibration graphs obtained under different experimental conditions

Electrode [a]	v (mV s^{-1})	i_p [b] (μA)	A [c] (μC)	$m \pm S_m$ [d]	$i \pm S_i$ [e]	S_b [f]	r [g]	DL (μM) [h]
TCE	5	✓		0.016 ± 0.00035	0.0115 ± 0.0125	0.025	0.999	5.4
TCE	5		✓	0.42 ± 0.013	−0.60 ± 0.47	0.42	0.998	4.5
TCE	50	✓		0.082 ± 0.002	0.31 ± 0.06	0.12	0.998	4.9
TCE	50		✓	0.29 ± 0.0015	0.46 ± 0.049	0.30	0.999	3.1
HMDE	50	✓		0.20 ± 0.017	−0.12 ± 0.07	0.003	0.996	1.1

[a] TCE = Tosflex-coated glassy carbon electrode, preconcentration at −200 mV vs. SCE for 10 min; HMDE = hanging mercury drop electrode, preconcentration at −800 mV vs. SCE for 10 min. [b] Peak current is the measured quantity. [c] Peak area is the measured quantity. [d] S_m = standard deviation of the slope, m, $n = 8$. [e] S_i = standard deviation of the intercept, i, $n = 8$. [f] S_b = standard deviation of the blank calculated from ten independent background current determinations at the potential value at which the analyte reoxidation peak is observed. [g] r = correlation coefficient. [h] DL = detection limit, calculated as $DL = 3[S_b^2 + S_i^2 + (i/m)^2 S_m^2]^{1/2}/m$ [28].

peak A′ increases on lowering the chloride concentration in the supporting electrolyte. For instance, for 0.1 M NaCl the current peak A′ is 36% higher than that recorded in 0.5 M NaCl. This trend, which suggests that Cl^- compete with $CuCl_2^-$ in the incorporation, indicates that the proposed method can be particularly useful for analyses of samples that do not contain too high chloride concentrations, e.g., body fluids [24].

Influence of added amino acids

Considering that the efficiency of the preconcentration process depends mainly on the ionic interaction of the species in solution and of the electrogenerated complexes with the membrane, the influence of the presence of added ligands, which introduces other charged species in the electrogeneration–preconcentration process, was examined. In the light of the relevance of copper–amino acid complexes in both biological and environmentals studies, the behaviour of Tosflex-modified electrodes in chloride media in the presence of a 10:1 ([amino acid]/[Cu^{2+}]) excess of histidine, glycine or glutamic acid was studied.

As shown in Table 2, peak A′, which corresponds to $CuCl_2^-$ reoxidation, is dramatically lowered in the presence of an excess of histidine. The peak current decrease related to the presence of amino acid becomes less relevant when the added amino acid is glutamic acid and is almost negligible with glycine. The strong effect on the peak current caused by histidine can be attributed to the high stability in the solution phase of the Cu–histidine complex [29], which under the present experimental conditions is the prevailing copper species. As the complex carries a net positive charge (both the metal and the ligand are positively charged), it is expected to be repelled by the polycationic coating, so lowering drastically the amount of copper that can be reduced and preconcentrated as $CuCl_2^-$.

As far as the influence of glutamic acid is concerned, as this ligand carries a net negative charge, the observed decrease of ca. 30% in peak A′ can be explained by taking into account the competition between the free anionic amino acid present in solution and the electrogenerated $CuCl_2^-$ complex for the ion-exchange sites of the coating. On the other hand, glycine has an almost negligible effect because the formation constant of the Cu^{2+}–glycine complex in solution is not as high as that of the histidine complex [25]; moreover, in this instance the ligand itself is a neutral zwitterion, which is not expected to influence significantly the net charge of the complex species.

As shown in the last column of Table 2, the addition of amino acids causes a slight shift in the peak potentials in the negative direction with histidine and in the positive direction with glycine and glutamic acid. These results could suggest that histidine stabilizes the reoxidation product, i.e., Cu^{2+}, whereas glycine and glutamic acid could interact with $CuCl_2^-$ reoxidation via more complex mechanisms, e.g., a preceding reaction. These suppositions, however, need to be confirmed by a more accurate analysis (examining, for instance, the influence of scan rate), which is beyond the aim of the present study.

TABLE 2

Data corresponding to peak A′ in Fig. 1 at a Tosflex-modified electrode in the presence of 5×10^{-3} M amino acids, 5×10^{-4} M $CuSO_4$, 0.5 M NaCl and 0.1 M acetate buffer (pH 5.0), with electrogeneration–preconcentration step at −200 mV for 10 min

Amino acid [a]	i_p (μA)	E_p (mV)	ΔE (mV) [b]
None	72	350	0
His	9.5	320	−30
Glu	48	365	+15
Gly	66	370	+15

[a] His = histidine; Gly = glycine; Glu = glutamic acid. [b] ΔE = shift in the potential of the reoxidation peak.

Comparison with Nafion-coated electrodes

The above observations on the influence of amino acids on the $CuCl_2^-$ preconcentration on the Tosflex-modified electrodes can be verified by examining the behaviour of the same solutions at an electrode modified with a polyanionic Nafion coating. In fact, the presence on the electrode of a film bearing a negative net charge is expected to have an opposite effect to the presence of the polycationic Tosflex polymer.

In measurements with Nafion coated electrodes, no significant information could be obtained from the reoxidation peak of electrogener-

ated $CuCl_2^-$, as this species is repelled by the polyanionic coating. Therefore, in this instance the reduction current of the Cu^{2+} species present in solution was examined directly. Because of the well proved permselectivity of Nafion coatings [26,30], such a current is related to the fraction of positively charged species that can penetrate the coating.

As shown in Fig. 6 for histidine, the presence of the amino acid can cause dramatic changes in the voltammetric pattern, the largest effect being the shift in peak potentials, which depends on the nature and binding capability of the added ligand. The peak potential values observed with the Nafion-coated electrode and reported in the last column of Table 3 indicate a high stability for histidine and a lower stability for glycine complexes, whereas with glutamic acid it is evident that the species that can penetrate the coating is uncomplexed Cu^{2+}.

The peak currents reported in Table 3 indicate that the presence of histidine now causes a large increase in peak current. The sum of the currents corresponding to the two reduction peaks observed with glycine is almost equivalent to the peak current in the absence of added amino acid. Finally, glutamic acid depresses dramatically the reduction peak. This trend agrees with the charge effect expected for these amino acids. The positively charged Cu^{2+}–histidine complex can penetrate and is incorporated into the coating whereas glutamic acid forms a negatively charged species that is repelled from the coating. In this last instance, only a small fraction of uncomplexed (or labile) Cu^{2+} can arrive at the electrode surface. Glycine seems to complex Cu^{2+} only partially, and the fact that the overall reduction current is roughly unchanged agrees with the effect expected for a neutral free ligand.

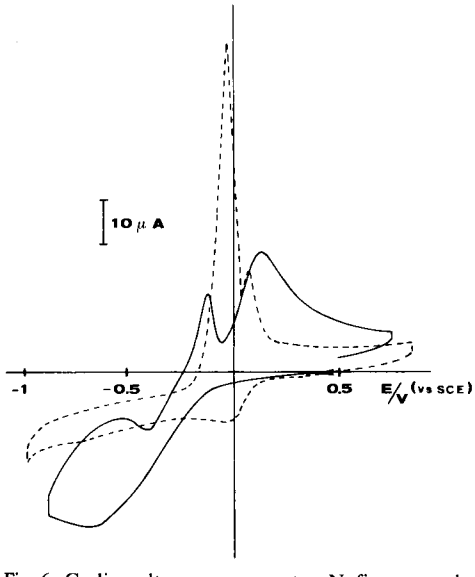

Fig. 6. Cyclic voltammograms at a Nafion-coated glassy carbon electrode after 1 h of equilibration in 5×10^{-4} M Cu^{2+}–0.5 M NaCl–0.1 M acetate buffer (pH 5.0) (dashed line) and after addition of a 10:1 excess of histidine (solid line).

TABLE 3

Data corresponding to reduction of the Cu^{2+} species at Nafion-coated electrodes in the presence of 5×10^{-3} M amino acids, 5×10^{-4} M $CuSO_4$, 0.5 M NaCl, and 0.1 M acetate buffer (pH 5.0).

Amino acid [a]	i_p (μA)	E_p (mV)
None	9	−30
His	35	−670
Gly	6 (4) [b]	−350 (−30) [b]
Glu	2	−30

[a] His = histidine; Gly = glycine; Glu = glutamic acid. [b] With glycine two reduction peaks are observed; data refering to the first peak are given in parentheses.

Finally, it is interesting to compare the preconcentration and detection capabilities of Nafion- and Tosflex-modified electrodes when the copper ions are dissolved in the absence of any added amino acid and is incorporated as Cu^{2+} and $CuCl_2^-$, respectively. Comparison of the data of the first lines of Tables 2 and 3 indicates that Tosflex-modified electrodes display better performances and allow the detection of lower concentration levels than do Nafion-coated electrodes. This less sactisfactory performance of Nafion in preconcentrating simply hydrated ions has already been reported [31,32] and can be attributed to high hydrophobicity of this coating.

Conclusions

Tosflex-modified electrodes have been shown to be suitable for preconcentrating and detecting copper ions from chloride-containing media. The detection levels achievable by applying a simple

electroanalytical technique such as linear-sweep voltammetry are much lower than those obtained with Nafion-coated electrodes, but they are slightly higher than those obtained by classical anodic stripping voltammetry.

However, the peculiar properties of Tosflex-modified electrodes seem worth exploiting, particularly for speciation analysis studies where, when used alone or in association with Nafion-modified electrodes, they open up the possibility of obtaining valuable information on the charges of different competing ligands.

This work was supported by MURST (Rome). L.M.M. is the grateful recipient of a grant from CAPES and CNEN, Brazil.

REFERENCES

1 J. Wang, in A.J. Bard (Ed.) Electroanalytical Chemistry, Vol. 16, Dekker, New York, 1989, p. 53, and references cited therein.
2 G.A. Gerhardt, A.F. Oke, F. Nagy, B. Moghaddam and R.N. Adams, Brain Res., 290 (1984) 390.
3 M.E. Rice and C. Nicholson, Anal. Chem, 61 (1989) 1805.
4 J. Zhou and E. Wang, Anal. Chim. Acta, 249 (1991) 489.
5 P. Ugo, B. Ballarin, S. Daniele and G.A. Mazzocchin, J. Electroanal. Chem., 291 (1990) 187.
6 P. Ugo, B. Ballarin, S. Daniele and G.A. Mazzocchin, Anal. Chim. Acta, 244 (1991) 29.
7 P. Ugo, B. Ballarin, S. Daniele and G.A. Mazzocchin, J. Electroanal. Chem., 324 (1992) 145.
8 N. Oyama and F.C. Anson, J. Electrochem. Soc., 127 (1980) 247.
9 S.M. Oh and L.R. Faulkner, J. Electroanal. Chem., 269 (1989) 77.
10 B. Lindholm, J. Electroanal. Chem., 250 (1988) 341.
11 H. Braun, W. Storck and K. Doblhofer, J. Electroanal. Soc., 130 (1983) 807.
12 B. Lindholm and M. Sharp, J. Electroanal. Chem., 198 (1986) 37.
13 L. Dunsch, L. Kavan and J. Weber, J. Electroanal. Chem., 280 (1990) 313.
14 N. Oyama, T. Ohsaka and T. Okajima, Anal. Chem., 58 (1986) 979.
15 W. Stumm and P.A. Brauner, in J.P. Riley and G. Skirrow (Eds.), Chemical Oceanography, Vol. 1, Academic, London, 1975, Chap. 3.
16 D.R. Turner, M. Whitfield and A.G. Dickson, Geochim. Cosmochim. Acta, 45 (1981) 855.
17 J. Buffle, Complexation Reactions in Aquatic Systems: an Analytical Approach, Horwood, Chichester, 1988.
18 R.D. Guy and S. Namaratne, Can. J. Chem., vol 65 (1987).
19 S.K. Cha and H.D. Abruna, Anal. Chem., 62 (1990) 274.
20 G.M.P. Morrison and T.M. Florence, Electroanalysis, 1 (1989) 485.
21 G. Gunawardena, G. Hills and I. Montenegro, J. Electroanal. Chem., 184 (1985) 357.
22 J. Crousier and I. Bimaghra, Electrochim. Acta, 34 (1989) 1205.
23 J.F. Cassidy and K. Tokuda, J. Electroanal. Chem., 285 (1990) 287.
24 A.L. Lehninger, Biochemistry, Worth, New York, 2nd edn., 1978.
25 R.M. Smith and A.E. Martell, Critical Stability Constants, Vol. 6, Plenum, New York, 1989.
26 R. Naegeli, J. Redepenning and F.C. Anson, J. Phys. Chem., 90 (1986) 6227.
27 A.J. Bard and L.R. Faulkner, Electrochemical Methods, Fundamentals and Applications, Wiley, New York, 1980, p. 406.
28 J.D. Winefordner and G.L. Long, Anal. Chem., 55 (1983) 712A.
29 T.P.A. Kruck and B. Sarkar, Can. J. Chem., 51 (1973) 3563, 3555.
30 C.-F. Shu and F.C. Anson, J. Am. Chem. Soc., 112 (1990) 9227.
31 M.N. Szentirmay and C.R. Martin, Anal. Chem., 56 (1984) 1898.
32 A. Steck and H.L. Yeager, Anal. Chem., 52 (1980) 1215.

Analytica Chimica Acta, 273 (1993) 237–244
Elsevier Science Publishers B.V., Amsterdam

Voltammetric behaviour of thallium(III) on carbon paste electrodes chemically modified with an anion exchanger

W. Diewald, K. Kalcher, C. Neuhold, X. Cai [1] and R.J. Magee [2]

Karl-Franzens Universität Graz, Institut für Analytische Chemie, Universitätsplatz 1, 8010 Graz (Austria)

(Received 12th March 1992)

Abstract

Thallium as tetrachlorothallate(III) can be preconcentrated from hydrochloric acid (10^{-3} M) on to a carbon paste electrode that is chemically modified with an anion exchanger (Amberlite LA-2). This accumulation was performed under open-circuit conditions. The ensuing measurement was done by differential-pulse voltammetry by reducing the thallate(III) ions to Tl(0) during the equilibration period and then re-oxidizing it to Tl(I) when recording the voltammogram. The electrode surface had to be conditioned with different concentrations of hydrochloric acid (1 to 10 and 10^{-3} M) before each accumulation step in order to generate a definite amount of ion-exchanging groups. For repetitive use, the electrode surface could be regenerated with an aqueous solution of ammonia (1 M). The dependence of the current response on the analytical parameters (composition of the paste, preconcentration time, composition of the solutions involved) was investigated. A linear relationship between concentration of Tl(III) and the voltammetric signal was found with the range of 0.1–100 mg l^{-1}. For these concentrations the standard addition method could be applied for analytical evaluations. The influence of other ions interfering in the determination was investigated. The applicability of this method to practical samples (fly ash) was investigated.

Keywords: Voltammetry; Carbon paste electrodes; Fly ash; Thallium

The development of chemically modified electrodes (CME) for electroanalytical applications has been growing rapidly during the last few years [e.g., 1–3]. Functional groups at the surface of the working electrode may increase the selectivity and the sensitivity of common voltammetric methods. In particular, the possibility of preconcentrating electroactive species due to chemical or physico-chemical reactions with the modifier often allows very small amounts of analyte to be detected. Additionally, such accumulations require no applied potential and, therefore, may be performed under open-circuit conditions including a medium exchange preceding the actual measurement. Ion exchangers, in particular, have been widely used as modifiers for the determination of both anionic and cationic species. Many investigations on ion exchangers have been carried out using carbon paste as the electrode material, as it is easy to prepare by directly mixing the modifier with the paste [4]. However, no investigations dealing with the voltammetric behaviour of thallium(III) on a chemically modified carbon paste electrode have been published.

The aim of this work was a basic investigation of the electrochemical behaviour of thallium(III) at a carbon paste electrode chemically modified with Amberlite LA-2, a weakly basic anion exchanger (secondary amine type). The liquid character of the exchanger facilitaties its direct dissolution in the liquid phase of the carbon paste.

Correspondence to: K. Kalcher, Karl-Franzens Universität Graz, Institut für Analytische Chemie, Universitätsplatz 1, 8010 Graz (Austria).
[1] On leave from Hainan University, Hainan (China).
[2] On leave from LaTrobe University, Melbourne (Australia).

Owing to the high affinity of thallium(III) ions for several ligands, particularly the halides, where the trivalent state is normally present as $[TlX_4]^-$, it can be preconcentrated only with cationic functional groups. Thus, the admixed anion exchanger allows the accumulation of Tl(III) directly on the surface of the electrode by immobilizing it there by electrostatic interaction (ion-pair formation). No potential needs to be applied, because the oxidation state of the accumulated species remains unchanged (open-circuit technique). The medium may be exchanged between preconcentration and voltammetric determination, which allows separation of the analyte from interfering species that often show little or no affinity for the ion exchanger. As it is possible to regenerate the surface of the electrode to its initial state, it can be used repeatedly. This leads to a low consumption of carbon paste in combination with higher precision.

EXPERIMENTAL

Apparatus

All voltammetric measurements were made using a PAR 264A polarographic analyzer (Princeton Applied Research). The electrode assembly consisted of a titration vessel (Metrohm 6.1415.220) and a laboratory-constructed cell compartment made of Plexiglas [5]. The reference electrode was a saturated calomel electrode (Ingold 303-NS) that was in contact with the solution via a salt bridge containing KCl (1 M). The auxiliary electrode was a platinum wire. The solution in the cell could be stirred with PTFE-coated stirring bar. A PTFE tube allowed purging of the solution with nitrogen, which was carried out for at least 5 min, after a new solution had been filled into the vessel. During the measurements, nitrogen was passed over the solution. Voltammetric curves were registered on a PAR Model RE 0089 two-channel recorder (Princeton Applied Research) and evaluated manually by the tangent fit method. Cyclic voltammograms were recorded by use of an appropriate interface after A/D conversion of the data in combination with a personal computer [6].

Working electrode

The body of the electrode consisted of PTFE rod (o.d. 10 mm) with a 3 mm deep central hole (diameter 7 mm) for the carbon paste filling. Electric contact to the paste was provided by a platinum wire that was glued into a borehole in the centre of the rod.

The carbon paste was prepared according to Monien et al. [7]. One gram of spectral carbon powder (RWB, Ringsdorff-Werke) was mixed with a solution of Amberlite LA-2 (80 μl) (Fluka) in paraffin oil (0.25 g) (Uvasol, Merck), corresponding to 21 mass-% of modifier in the liquid phase. The paste was filled into the hole of the working electrode, protruding paste was skimmed off and the electrode surface was smoothed by means of a PTFE spatula. An electrode prepared in this way could be used for at least 20 determinations without any notable change in the signal response.

Reagents and solutions

Deionized water was distilled twice in a quartz still and subsequent purified with a cartridge deionization system (Nanopure, Barnstead). Hydrochloric acid and potassium chloride were of Suprapur grade (Merck); all other chemicals were of analytical-reagent grade (Merck). Stock solutions of Tl(III) were prepared by adding HCl (1.0 ml, 10 M) to $TlCl_3$ (1.6526 g, 92%) (Merck) and diluting to a final volume of 1000 ml, which yielded 1000 mg Tl l^{-1} in HCl (0.01 M). Stock solutions with lower concentrations of thallium were prepared freshly by dilution.

Procedure

Conditioning of the electrode. The electrode was immersed in hydrochloric acid (10 M for concentrations of Tl > 10 mg l^{-1}, 1 M for lower concentrations) and a conditioning solution (HCl, 10^{-3} M) for 60 s each, in order to generate a definite amount of ammonium groups. Both solutions were well stirred (300 rpm).

Preconcentration. After conditioning the electrode, it was dipped into the test solution (20 ml, 10^{-3} M HCl) containing thallium(III). Between all medium exchanges, the electrode was rinsed with water for about 0.5 s. During the accumula-

tion period, the solution was stirred with a PTFE-coated stirring bar (30 mm × o.d. 7 mm) at a rate of 300 rpm. After exposure to the test solution for the required time, the electrode was removed, rinsed with water for about 0.5 s, placed into the voltammetric cell and connected to the polarograph.

Voltammetry. The solution for the voltammetric measurements consisted of water (20 ml) containing hydrochloric acid (10^{-3} M) and potassium chloride (0.047 M) as supporting electrolyte. Determinations were performed in the differential-pulse mode (DPV). The potential range was set from −1.2 to −0.5 V vs. SCE in the anodic direction. An equilibration phase of 15 s with the initial potential applied was required in order to settle the solution and to ensure complete reduction of $[TlCl_4]^-$. The pulse height was 50 mV and the scan rate 10 mV s^{-1} with an increment of 2 mV per data point.

Cyclic voltammograms (CV) were recorded from 0.0 to −1.2 V vs. SCE with a scan rate of 20 mV s^{-1}. The equilibration time and scan increment were the same as in DPV.

Regeneration. After recording a voltammogram, the electrode was kept at a potential of −0.2 V vs. SCE for 100 s with the solution of the voltammetric cell being well stirred. Subsequently, the electrode was successively immersed in an aqueous solution of ammonia (1 M) and hydrochloric acid (10^{-3} M) for 60 s each. Both solutions were well stirred (300 rpm). The electrode was rinsed with water between all medium exchanges. The blank curve was recorded with an electrode treated in this way. Freshly prepared, virgin electrodes were conditioned and subsequently immersed in ammonia solution and hydrochloric acid as described, which improved the reproducibility of the results.

Analysis of fly ash. A pulverized sample was dried at 100°C for at least 10 h to constant weight. One gram was suspended in 10 ml of HCl (1 M) and refluxed for 1 h while chlorine gas was passed through the solution. Subsequently the suspension was kept boiling for at least 5 min while nitrogen was bubbled through the solution to remove excess of chlorine. The solution was diluted to a definite volume (25 ml) with water, from which an aliquot of the clear supernatant liquid (1 ml) was taken for analysis. It was transferred into a beaker (50 ml) and diluted with water to 20 ml, after adjustment of the pH to 3 with concentrated ammonia solution. The regenerated electrode was conditioned and then loaded with thallium by exposing it to this solution for 60 s. At least two definite amounts of Tl(III) standards were added and the voltammograms recorded in order to evaluate the concentration of thallium. Each measurement was repeated twice.

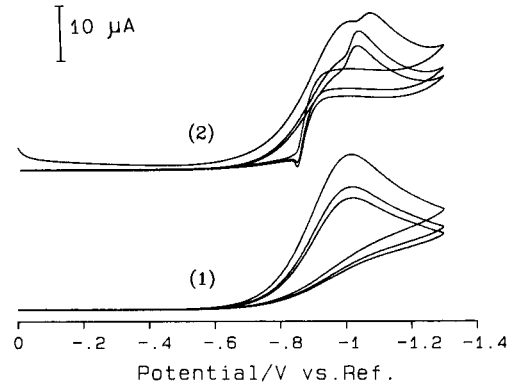

Fig. 1. Three successive cyclic voltammograms of Tl(III) with an unmodified carbon paste electrode. Supporting electrolyte, HCl (10^{-3} M) and KCl (0.047 M). (1) Blank; (2) 5 mg Tl(III) l^{-1}.

RESULTS AND DISCUSSION

As can be seen from the cyclic voltammograms of a solution containing thallium(III) as $[TlCl_4]^-$, the ion may be reduced in acidic solution (HCl) to Tl(0) on carbon paste electrodes at potentials of −1.06 to −1.0 V vs. SCE, overlapping with the reduction of hydronium ions (Fig. 1). At high concentrations of Tl(III), another broad and weak reduction signal may be observed in a more positive region of the voltammogram. This is in good agreement with investigations using glassy carbon electrodes, which yielded only very diffuse signals in the positive potential range if the electrode was not modified (highly irreversible), but which showed a quasi-reversible reduction of Tl(III) to

Tl(I) if the electrode contained an iridium oxide modifier [8].

Therefore, the signal at about −1 V vs. SCE is assigned to the reduction of Tl(I) to its elemental state; this corresponds well with the reduction of Tl^+ on mercury electrodes, which appears at about −0.25 to −0.55 V vs. SCE depending on the supporting electrolyte. The cathodic shift of potential when using carbon paste instead of mercury may be attributed to the fact that the element is precipitated as metal and not as amalgam. The reduction of Tl(I) to Tl(0) was manifested by investigations in which rotating disc glassy carbon electrodes were used instead of carbon paste in order to avoid non-Nernstian responses due to the presence of a pasting liquid. The sigmoidal curve gives a linear $\log[(i_d - i)/i_d]$ vs. E plot with a slope of 60 mV per decade, which supports the assignment of a one-electron process. Thus, at potentials more negative than −1 V vs. SEC, thallium is converted to Tl(0) according to Eqn. 1, which describes the over-all reaction.

$$[TlCl_4]^- + 3\,e^- \rightarrow Tl(0) + 4\,Cl^- \qquad (1)$$

The element is re-oxidized to Tl(I) during the scan in the anodic direction, yielding a sharp signal response at −0.86 V vs. SCE (Fig. 1).

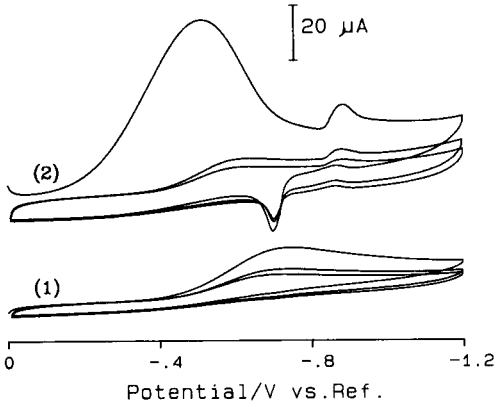

Fig. 2. Three successive cyclic voltammograms of Tl(III) accumulated with a modified carbon paste electrode. Analyte solution, 10^{-3} M HCl, 5 mg Tl(III) l^{-1}; accumulation time, 120 s; supporting electrolyte, HCl (10^{-3} M) and KCl (0.047 M). (1) Blank, (2) 5 mg Tl(III) l^{-1}.

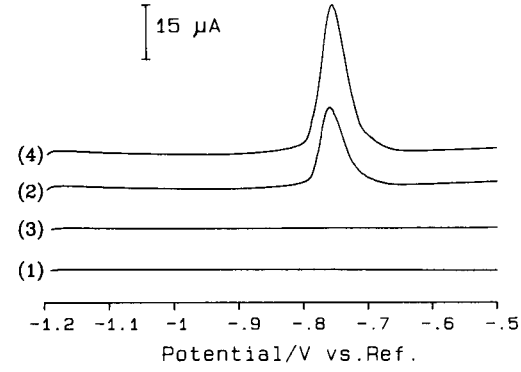

Fig. 3. Differential-pulse voltammograms of Tl(III) with a modified carbon paste electrode. Supporting electrolyte, HCl (10^{-3} M) and KCl (0.047 M); analyte, 10^{-3} M HCl, 5 mg Tl(III) l^{-1} (2) or 10 mg Tl(III) l^{-1} (4). (1) Blank; (3) blank after regeneration.

Tetrachlorothallate(III) is a very stable complex with a formation constant of 2.5×10^{18} in acidic media [9]. This ensures that a reasonable excess of chloride ions converts virtually all of the trivalent cation into its complex anionic form. This anion shows a high affinity for amines with which it combines to give lipophilic ion pairs (e.g., tri-*n*-octylamine [10], and many others) and may be easily extracted with liquid anion exchangers (e.g., Amberlite LA-1 [11,12]).

Thus, a carbon paste electrode modified with a liquid anion exchanger (Amberlite LA-2, secondary amine) is able to extract and preconcentrate tetrachlorothallate(III) on to its surface without application of any potential (open-circuit conditions). The reduction and re-oxidation of thallium can be clearly seen in the cyclic voltammogram of an electrode of this type loaded with $[TlCl_4]^-$ (Fig. 2). Compared with the unmodified electrode, the corresponding peak potentials $E_{p,c}$ and $E_{p,a}$ are shifted in the anodic direction to −0.88 and −0.7 V vs. SCE, respectively, indicating that the species in the adsorbed ion pair is reduced more easily than the free complex in solution.

The signals can be exploited if the voltammograms are recorded in the differential-pulse mode in anodic direction, because the oxidation yields well shaped peaks (Fig. 3). An equilibrium period of 15 s is sufficient to reduce all the accumulated

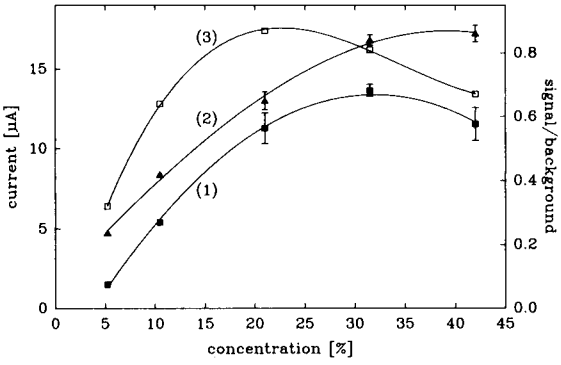

Fig. 4. Dependence of the peak current and the background current on the composition of the paste. Concentration of the modifier given in % (w/w) of the liquid phase of the paste; analyte, 0.1 M HCl, 5 mg Tl(III) l^{-1}; accumulation time, 60 s; supporting electrolyte, HCl (10^{-3} M) and KCl (0.047 M). (1) Signal; (2) background; (3) signal/background.

Tl(III) to the element, which is then re-oxidized during the scan in the anodic direction. Thus, interferences from the reduction of H^+, which are inevitable when polarizing the electrode in the cathodic direction, can be avoided. Hence it is advisable to record voltammograms in the differential-pulse anodic scan mode for quantitative results.

It is obvious that the composition of the paste, with respect to the chemical nature of the modifier and its concentration, is very important for the performance of the electrode. Quaternary ammonium compounds such as Aliquat 336 (tricaprylmethylammonium chloride) produce very large blank currents which decrease the signal-to-background ratio in an unfavourable manner. Tri-*n*-octylamine yields a background current higher than that with Amberlite LA-2. Therefore, the latter seems to be a very useful modifier for the accumulation of thallium. Evidently, the concentration of the modifier in the paste controls the amount of anionic species accumulated at the surface of the electrode (Fig. 4). Up to a concentration of about 30% (w/w) of ion exchanger in the paraffin oil of the paste, the signals in the voltammograms (differential-pulse mode) increase continuously. Higher concentrations result in a decrease which may be due to a loss of hydrophobic properties of the paste. The best signal-to-background ratio is found for a concentration of about 21%, a paste composition which was used for all further investigations in this work.

As the modifier in its native form bears no functional groups, it is necessary to generate them by treating the electrode with acid. A series of studies revealed that exposing the modified paste to two solutions with different concentrations of HCl yields the best results. The more concentrated acid primarily protonates the amine, whereas that with a lower concentration equilibrates the surface for the medium where the electrode is loaded. In a similar way, the functional groups of the modifier may be regenerated after the measurement. Application of a potential of −0.2 V vs. SCE ensures re-oxidation of the thallium at the surface of the electrode; a period of 100 s is sufficient for this purpose. To remove residues of the thallate, which might even migrate from the interior of the electrode to the surface, the electrode is exposed to ammonia, which deprotonates the ammonium groups and decomposes the ion pairs. For repetitive use of the electrode, which is recommended when applying the standard addition method for evaluating thallium concentrations, the procedures for regenerating and conditioning the electrode and for accumulating and measuring thallium may be repeated at least 20 times without any loss of analytical performance of the electrode. It should be stressed that for all measurements that are to be compared with each other, the electrode should not be refilled in between in order to avoid errors resulting from non-equivalent physical conditions of individual fillings (differences in area and smoothness of the paste).

The compositions of the analyte solution, from which thallium is extracted, and the solution in which the electrode is polarized exert a significant effect on the signal response. Optimum signals may be obtained if the concentration of HCl in the solution for the measurements ranges between 10^{-1} and 10^{-3} M. A satisfactory regeneration of the electrode can be achieved only for the lowest concentration of HCl which was, therefore, chosen for these investigations (Fig. 5). To ensure complete complexation, excess of potas-

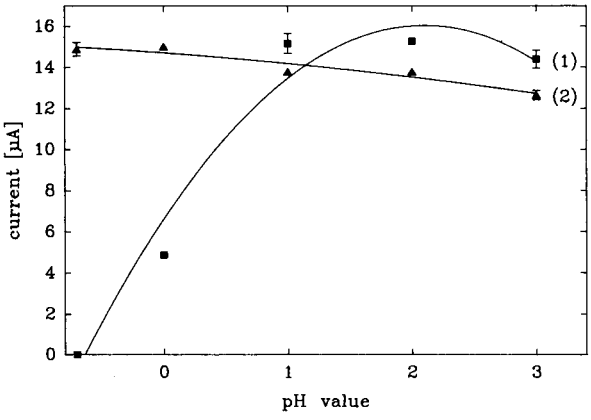

Fig. 5. Dependence of (1) the peak current and (2) the background current on the concentration of supporting electrolyte. Analyte, 0.1 M HCl, 5 mg Tl(III) l^{-1}; accumulation time, 60 s.

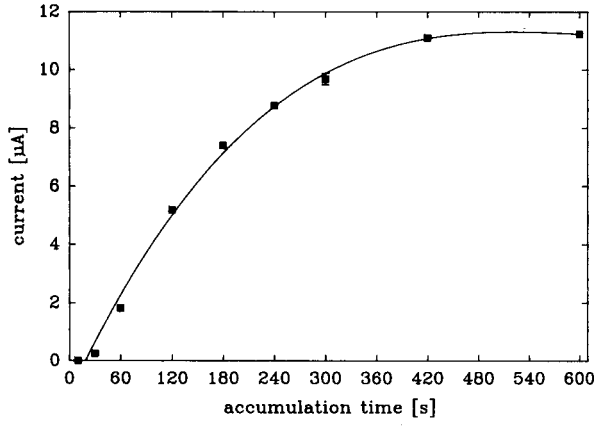

Fig. 7. Dependence of the peak current on the accumulation time. Analyte, 10^{-3} M HCl, 5 mg Tl(III) l^{-1}; supporting electrolyte, HCl (10^{-3} M) and KCl (0.047 M).

sium chloride should be added (the actual amount is not critical). Decreasing the concentration of HCl in the analyte solution from which the thallium is extracted yields a gradual increase in the signal, whereas the background current decreases drastically (Fig. 6). A pH of 3 is the best medium for accumulating the thallate. Lower acidities should be avoided to prevent hydrolysis of Tl(III) and deprotonation of the modifier.

The amount of preconcentrated tetrachlorothallate(III) is dependent on the time during which the electrode is exposed to the analyte solution (Fig. 7). Very short periods (< 10 s) will result in no extraction of thallium (for various concentrations), which implies that the exchange of Cl^- (at the surface of the electrode) versus $[TlCl_4]^-$ (from the solution) needs time to take place. With increasing accumulation time, the amount of preconcentrated thallium increases accordingly. Long periods permit equilibrium conditions to be reached.

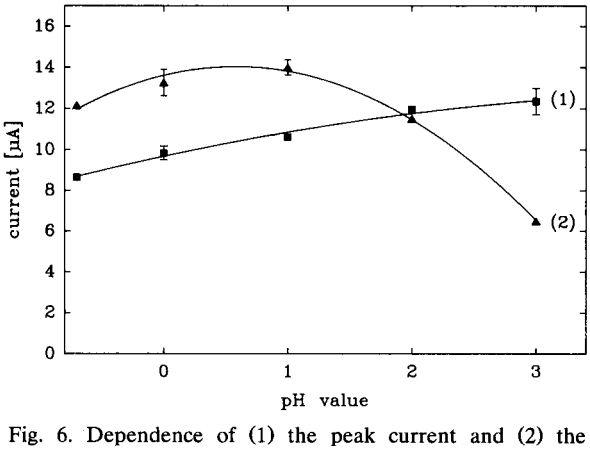

Fig. 6. Dependence of (1) the peak current and (2) the background current on the acidity of the analyte solution. Supporting electrolyte, HCl (10^{-3} M) and KCl (0.047 M); analyte, 5 mg Tl(III) l^{-1}; accumulation time, 60 s.

The dependence of the current on the concentration of thallium is shown in Fig. 8. The relationship between these two parameters is linear up to a concentration of 100 mg Tl(III) l^{-1} if the preconcentration periods are chosen appropriately. The detection limit is about 20 µg Tl(III) l^{-1}. Concentrations significantly higher than 100 mg l^{-1} show deviations from the linear relationship between current and concentration due to saturation. The relative standard deviation (R.S.D.) for the peak current was 0.7% with ten repetitive analyses of a solution containing 5 mg Tl(III) l^{-1}. The determination of 400 µg Tl(III) l^{-1} using two additions of standard solution gave an R.S.D. of 4.4% when each measurement was repeated once.

Table 1 summarizes the influence of other components which may be present in the analyte solution. Severe interferences result from noble metals (platinum metals, gold) which also precon-

centrate on the electrode via negatively charged chloro complexes. Other species such as iodide or hexacyanoferrate(II) affect the determination of Tl(III) by redox reactions. As $[TlCl_4]^-$ is obtained only under oxidizing conditions, these species are usually not present in the analyte solution. Interferences which are not severe (< 20% peak change) usually allow the determination of Tl(III) by this method, because the linear relationship between current and concentration can still be maintained. It is interesting that nitrate, perchlorate and perrhenate increase the signal response significantly. Preliminary investigations of this effect revealed that these species are also extracted from the analyte solution and exert a catalytic action on the electrochemical transformation of Tl when they are immobilized on the surface of the electrode.

The procedure for the determination of thallium described above was applied to evaluate the acid-soluble fraction of the metal in a fly ash with a high content of lead. The overall composition of the ash, determined by classical wet-chemical methods, was SiO_2 7.1, Fe 31.5, Cu 0.85, Zn 1.2,

TABLE 1

Change of the peak current caused by interfering components present in the analyte solution (5 mg Tl(III) l^{-1}, 10^{-3} M HCl; accumulation time 60 s)

Interferent	Added as	Peak current change (%)		Comments [b]
		5 mg l^{-1} [a]	50 mg l^{-1} [a]	
CH_3COO^-	$CH_3COONa-H_2O$	+8	+27	
ClO_4^-	$NaClO_4-H_2O$	+43	+155	A
$H_2PO_4^-$	$NaH_2PO_4-H_2O$	+2	+2	
NO_3^-	KNO_3-H_2O	+30	+107	A
SO_4^{2-}	$K_2SO_4-H_2O$	+26	−5	
F^-	$KF-H_2O$	−3	+22	
Br^-	$NaBr-H_2O$	+15	−20	
I^-	$KI-H_2O$	−90	−100	R
Al(III)	$AlCl_3-H_2O$	+3	+29	
Ga(III)	$Ga_2(SO_4)_3$–HCl	+6	−10	
In(III)	$InCl_3$–HCl	+16	+15	
Pb(II)	$PbCl_2-H_2O$	+46	+15	
As(III)	$NaAsO_2-H_2O$	+1	+1	
As(V)	$Na_2HAsO_4-H_2O$	−2	+40	
Sb(III)	$SbCl_3$–HCl	−21	−56	
Sb(V)	$SbCl_5$–HCl	+163	+114	C
Bi(III)	$BiCl_3$–HCl	+24	+72	P
Cu(II)	$CuCl_2-H_2O$	−2	+36	C
Zn(II)	$ZnCl_2-H_2O$	+0	+28	
Hg(II)	$HgCl_2-H_2O$	+147	+326	B, P
V(V)	$NaVO_3-H_2O$	−67	−75	C
Mo(VI)	$Na_2MoO_4-H_2O$	−21	–	P, B
Mn(VII)	$KMnO_4-H_2O$	−42	−100	P
Re(VII)	$KReO_4-H_2O$	+55	+123	P, A
Fe(II)	$K_4[Fe(CN)_6]-H_2O$	−94	−95	R, D
Fe(III)	$K_3[Fe(CN)_6]-H_2O$	−70	−95	D
Au(III)	$KAuCl_4-H_2O$	+42	−56	P
Ir(III)	$IrCl_3$–HCl	−55	−100	P
Ir(IV)	$(NH_4)_2IrCl_6-H_2O$	−98	−100	P
Pd(II)	$K_2PdCl_4-H_2O$	−46	−100	P, B
Pt(II)	$(NH_4)_2PtCl_4-H_2O$	−98	−100	P
Pt(IV)	$(NH_4)_2PtCl_6-H_2O$	−97	−100	P

[a] Concentration of interferent. [b] A, Catalytic reaction; B, peak broadening; C, change of electrode characteristics; D, competitive concurrent accumulation; P, additional peak; R, redox reaction.

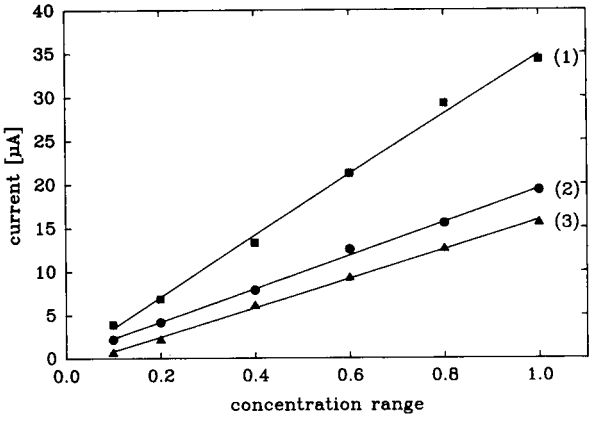

Fig. 8. Dependence of the signal current on the concentration of thallium. Supporting electrolyte, HCl (10^{-3} M) and KCl (0.047 M); analyte, 10^{-3} M HCl. Concentration ranges and accumulation times: (1) 0–100 mg Tl(III) l^{-1}, 15 s; (2) 0–10 mg Tl(III) l^{-1}, 60 s; (3) 0–1 mg Tl(III) l^{-1}; 300 s.

Pb 19.0, As 2.5, S 5.8%. The thallium was extracted from the ash with hydrochloric acid. As lead is one of the main constituents and, additionally, there are minor components that are oxidizable, the use of hydrochloric acid saturated with chlorine is not sufficient to produce Tl(III) quantitatively in the extract. Therefore, a stream of the oxidant had to be passed through the reaction solution to ensure complete oxidation to Tl(III). After appropriate dilution and adjustment of pH, the metal could be determined by the present method. To avoid matrix effects, the internal standard addition method was applied for the evaluation of concentrations. The result of $0.0544 \pm 0.0002\%$ Tl (mean value from two determinations) as acid-soluble fraction agrees well with the result obtained by flame atomic absorption spectrometry. ($0.0545 \pm 0.0001\%$; mean value from two determinations using addition of standards).

If the method described is compared with some other electroanalytical techniques, it presents advantages with respect to interferences. Although inverse voltammetric methods, employing mercury electrodes and exploiting the signal around -0.5 V vs. SCE, possess very low detection limits in the sub-$\mu g\ l^{-1}$ range, which cannot be achieved with the proposed method, the Tl^{+}–Tl(0) redox reaction on mercury suffers strong interferences from lead, tin and larger amounts of cadmium. Owing to its extraction as an anion, these species do not interfere with the determination of Tl in the present method because they are separated off and remain in the sample solution. Compared with atomic absorption spectrometry, the present method possesses a lower detection limit (about 50 ng Tl ml^{-1} for electrothermal atomization and about 250 ng ml^{-1} for flame atomization), but requires a longer time for analysis (about 45 min for a complete analysis).

The authors are indebted to the Austrian Fonds zur Förderung der wissenschaftlichen Forschung for financial support (project number P8538-CHE). C.X. thanks the Austrian government of the grant of scholarship from the North–South Dialogue Programme.

REFERENCES

1 R.W. Murray, in A.J. Bard (ed.), Electroanalytical Chemistry, Vol. 13, Dekker, New York, 1984, p. 191.
2 J.G. Redepenning, Trends Anal. Chem., 6 (1987) 18.
3 S. Dong and Y. Wang, Electroanalysis, 1 (1989) 99.
4 K. Kalcher, Electroanalysis, 2 (1990) 419.
5 K. Kalcher, Fresenius' Z. Anal. Chem., 323 (1986) 238.
6 K. Kalcher and C. Jorde, Comput. Chem., 10 (1986) 201.
7 H. Monien, H. Specker and K. Zinke, Fresenius' Z. Anal. Chem., 225 (1967) 342.
8 J.A. Cox and B.K. Das, Electroanalysis, 1 (1989) 57.
9 A. Alexandrow and A. Dimitrov, Mikrochim. Acta, (1972) 680.
10 I. Tsukahara, M. Sakakibara and T. Yamamoto, Anal. Chim. Acta, 83 (1976) 251.
11 A. Alian, A. El-Kot, A. Haggag, W. Sanad and N. Tadros, J. Radioanal. Chem., 26 (1975) 39.
12 D. Singh, O. Singh and S.N. Tandon, Sep. Sci. Technol., 13 (1978) 625.

Analytica Chimica Acta, 273 (1993) 245–253
Elsevier Science Publishers B.V., Amsterdam

Conductive carbon cement as electrode matrix for cobalt phthalocyanine modified electrodes for detection in flowing solutions

Xinjian Huang and Wim Th. Kok

Laboratory for Analytical Chemistry, University of Amsterdam, Nieuwe Achtergracht 166, 1018 WV Amsterdam (Netherlands)

(Received 1st June 1992)

Abstract

A comparison has been made of the performance of electrodes modified with cobalt phthalocyanine catalyst prepared in different ways for use in flowing solutions. Because of leaching direct adsorption of cobalt phthalocyanine (CoPC) on a glassy carbon electrode surface had little analytical utility. Use of a polystyrene film prevents leaching of CoPC from the electrode surface to some extent, albeit at the expense of sensitivity. A new composite electrode with conductive carbon cement as electrode matrix was found to be comparable to a carbon paste electrode in terms of the electrocatalytic properties of CoPC towards thiol compounds (*N*-acetylcysteine, cysteine, glutathione and dithiothreitol) both in quiescent and flowing solutions, but is obviously superior in terms of long-term stability in flowing solutions. An advantage of the use of conductive carbon cement is that it can be repacked, so that the normal electrode body for carbon paste can be utilized. The modified electrode has been applied in liquid chromatography for the determination of cysteine in urine samples. The decrease of the electrode sensitivity over 5 h was about 5% at a flow-rate of 1.8 ml min^{-1} and a fixed potential of 0.7 V vs. Ag/AgCl.

Keywords: Flow injection; Liquid chromatography; Carbon cement; Cobalt phthalocyanine; Modified electrodes; Thiols; Urine

The chemical modification of electrodes is a growing field of interest in analytical chemistry. Chemically modified electrodes (CMEs) have been developed with three different basic functions: electrodes with a selectively accessible surface for an improved selectivity of detection; electrodes with a modified surface for the preferential accumulation of analytes (preconcentration) and electrodes modified with an electrocatalyst to promote reactions which otherwise have slow electron transfer kinetics. Recent reviews on chemically modified electrodes covering many aspects of the field, provide a key to survey the state of art [1–9].

Electrocatalysis is one of the most important subjects of research on CMEs, directed at the possibility of lowering the overpotential and increasing the rate of certain electrochemical reactions, so that a more sensitive or selective detection can be achieved. Transition-metal phthalocyanines are well known for their catalytic activity in a wide range of redox processes [10]. Among them, cobalt phthalocyanine (CoPC) and its analogues have been intensively studied with respect to their own electrochemical properties [11–23],

Correspondence to: W.Th. Kok, Laboratory for Analytical Chemistry, University of Amsterdam, Nieuwe Achtergracht 166, 1018 WV Amsterdam (Netherlands).

their ability to catalyze the electroreduction of oxygen [23–31], or the electrochemical detection of other compounds [32–42]. It has been found that CoPC exhibits effective electrocatalytic activity in neutral, acidic and basic media. Various methods for the preparation of CoPC modified electrodes have been proposed. Direct deposition of CoPC or analogues on pyrolytic graphite [43,44] or glassy carbon [45] is a simple procedure. Multifunctional CMEs, with combined electrocatalysis and permselectivity, have also been reported [46,47]. CoPC has been mixed with carbon paste [33] and with a carbon–epoxy resin mixture [39] as an electrode matrix.

One of the most important applications of CMEs is in combination with liquid chromatography (LC), which affords a powerful tool for the determination of a wide variety of compounds. However, a key factor which often hinders the successful use of CMEs in flowing solutions is the slow leaching of the modifier from the electrode, owing to vigorous hydrodynamic conditions or the presence of organic components in the mobile phase [5,48,49]. When a CoPC carbon paste electrode was used in LC [33], a decrease in sensitivity was observed due to the leaching and deactivitation of CoPC. It was also reported that a CoPC carbon paste electrode could not be used for determination of glutathione in flowing and stirred solutions mainly due to the leaching of CoPC [39]. Robust and polishable CMEs, based on bulk modification of carbon–epoxy resin electrodes, is another promising alternative for routine analysis [38–42]. However, a disadvantage of epoxy resin is that it cannot be re-packed like carbon paste.

Because of their biological, clinical, pharmaceutical and environmental importance, the development of detection methods for thiol compounds is an area of great interest. Thiols do not have strong chromophores in the UV–visible range, so that pre- or postcolumn derivitization is a prerequisite for spectrometric detection. Due to the sluggish electrode reaction of thiols on a carbon electrode, electrochemical detection is only possible indirectly [50], with mercury (film) electrodes [51,52], or with catalyst-modified electrodes.

In this paper, we compare the performance of different electrode substrates modified with cobalt phthalocyanine catalyst for determination of thiols in flowing solutions. We have investigated a new composite electrode with conductive carbon cement as electrode matrix for electrochemical detection in LC. The modified electrode has been applied in LC for the determination of cysteine in urine samples.

EXPERIMENTAL

Apparatus

Cyclic voltammetry was carried out using a computerized Autolab electrochemical analyzer (ECO Chemie, Utrecht) with a three-electrode configuration. The auxiliary electrode was a platinum plate and the reference was a SCE.

Flow-injection analysis (FIA) and LC were performed using a Gynkotek (Germering) Model 300C pump for solution delivery. Rheodyne 7010 injection valves with 30 μl and 20 μl sample loops were employed for FIA and LC, respectively. Chromatography was performed with a 150 $\times$ 4.6 mm i.d. column slurry packed with Hypersil ODS (5 μm); the column was thermostatted at 24°C. For amperometric electrochemical detection both in FIA and LC, a Model 174A polarographic analyzer (Princeton Applied Research, Princeton, NJ) was operated at constant potential with a Metrohm (Herisau) wall-jet electrochemical detector cell with a Ag/AgCl(KCl sat.) reference electrode and a glassy carbon counter electrode.

The working electrodes (both in static and flow experiments) were a standard Metrohm glassy carbon disk electrode (3 mm diameter, mounted in PTFE) and a carbon paste electrode base (PTFE body, cavity of 3 mm diameter). The latter was packed with either carbon paste or conductive carbon cement (with or without CoPC).

Chemicals and solutions

Cobalt phthalocyanine was obtained from Aldrich (Milwaukee, WI). A polystyrene standard

(M_p = 20 150 000) was obtained from Macherey–Nagel (Düren). Carbon paste was Metrohm E287 and conductive carbon cement (CCC) was from Gerhard Neubauer (Münster). The other chemicals used were all analytical-reagent grade.

To 10 ml of pyridine was added 1–2 mg of CoPC and the mixture stirred till complete dissolution. Polystyrene (PS) was added to the pyridine, the mixture was set aside overnight to dissolve, and gently shaken before use. The diluted CoPC and the mixed CoPC–PS solution (containing 0.12 mg ml^{-1} PS) were prepared from these solutions. The mobile phase was 0.03 M phosphate buffer (pH 2.0) containing 0.1 mM EDTA and 3 mM sodium octyl sulfate and 4% methanol (v/v). The carrier solution for FIA and the mobile phase of LC were de-aerated with helium before use. The thiol standard solutions were prepared with carrier or mobile phase solution. Urine samples were prepared by a method described previously [50].

Preparation of the modified electrodes

Glassy carbon electrodes were polished with alumina on a polishing pad (Antec, Leiden, The Netherlands), sonicated for 10 min, washed with water obtained by sub-boiling and dried with compressed air. To modify the electrodes, 10 μl of a CoPC or CoPC–PS solution was pipetted on to the surface of the bare electrodes and allowed to dry under N_2 flow. Modified carbon paste electrode was prepared by mixing 5% CoPC (w/w) with carbon paste, pressing the mixture into the cavity of the electrode holder with a small spatula, and then further pressing against a computer card. The excess of carbon paste was removed by polishing on the computer card. For the modified conductive carbon cement electrode, conductive carbon cement was mixed with 5% CoPC (w/w). The mixture was packed into the cavity of a carbon paste electrode body and allowed to dry. Then the excess of the mixture was polished off with dry emery (grade P400), then with tissue. The surface layer of conductive carbon cement can be easily removed with a flat-head needle, after immersion in acetone for a while, so that the electrode can be re-packed. All electrodes were washed with water obtained by sub-boiling before use.

RESULTS AND DISCUSSION

Adsorption on glassy carbon electrodes

In contrast to previous reports [46,47,53], we have found that CoPC is poorly soluble in acetone, benzene, toluene, chloroform and methanol. However, pyridine is a good solvent [54]; solubility is 0.15–0.20 mg ml^{-1} and 0.1 mg ml^{-1} solutions were stable for several weeks when stored at 4°C.

Direct adsorption of CoPC on glassy carbon electrodes gave irreproducible results in the electrode preparation. The anodic peak current of 1 mM cysteine (CYS) in cyclic voltammetry was 4 ± 2 μA (n = 14), independent of the amount of CoPC applied (3–30 μg cm^{-2}). This is mainly related to the irreproducible surface status of glassy carbon electrodes [55] and to the fact that CoPC does not form a real film. It was found by microscopy that tiny particles existed on the electrode that can not be washed off by water or methanol except under vigorous hydrodynamic conditions. The applicability of glassy carbon electrode modified with CoPC in flowing solutions was tested in FIA experiments. As shown in Fig. 1 (curve a), after an initial increase of peak heights, a significant steady decrease of the sensitivity of 8% per hour was observed, which was caused mainly by leaching of CoPC. These results indicate that the direct deposition of CoPC on glassy carbon electrode is of little analytical value.

In an attempt to improve the stability of the electrode in flowing solutions, CoPC was mixed with polystyrene to form a film. Polystyrene film has been used before as a support to form a film containing cationic and anionic surfactants [56]. Also, an improvement of the stability of ruthenium-coated electrodes, in FIA by using a non-conductive polymer as support, has been reported [57]. As shown in Fig. 1 (curve b), PS prevents leaching of CoPC from the electrode surface to some extent, thus providing better stability, albeit at the expense of sensitivity. Even so, the elec-

trode still suffered from an unacceptable loss of sensitivity (4% per hour) for quantitative analysis.

Bulk-modified electrodes

Modified-electrode detection is still in the early stages of development and the strategy of preparing CMEs is an active area of research [6]. We have used conductive carbon cement as an alternative matrix material to fabricate bulk-modified electrodes. The property of this new built-in CoPC electrode matrix was compared with the carbon paste approach. Emphasis was laid on its long-term stability in flowing solutions.

The cyclic voltammogram (Fig. 2A) of an unmodified conductive carbon cement electrode immersed in blank phosphate buffer (pH 2.0) shows a low background current. The oxidation of cysteine at this unmodified electrode exhibits a high overpotential. As shown in Fig. 2B, this overpotential was strongly decreased when CoPC was incorporated into the conductive carbon cement matrix. The cyclic voltammogram shows the same electrochemical behaviour during oxidation of cysteine as that with CoPC modified carbon paste electrodes [33], namely: irreversible catalytical waves with no cathodic current on the reverse scan; no simple diffusion-limited peak shapes of cysteine oxidation; anodic current dips in the cathodic potential scan. Note that the reverse anodic dip was irregular in shape, somehow depending on the scan rate and the electrode history, as observed with CoPC carbon paste electrodes. The peak at ca. +0.70 vs. SCE is attributed to the redox reaction Co(II)–Co(III), while the pre-wave-like anodic current at lower potential is considered to be the contribution of Co(I)–Co(II) reaction [33]. The two anodic peaks in the cyclic voltammogram have been also reported for cysteine and glutathione (GSH) with CoPC carbon–epoxy resin electrodes [38,39].

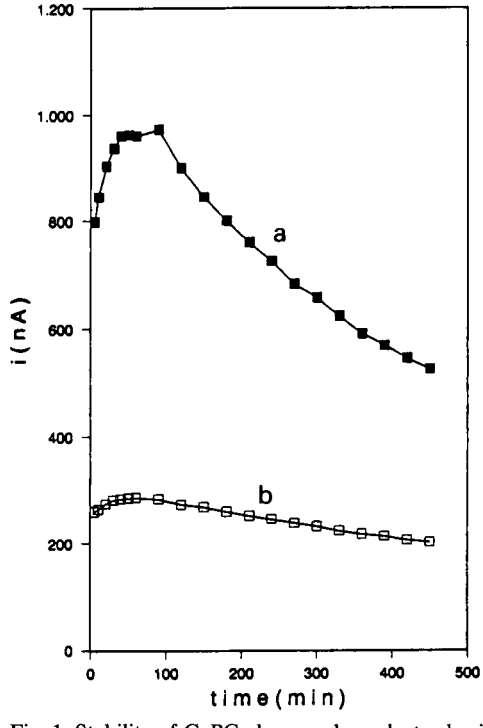

Fig. 1. Stability of CoPC glassy carbon electrodes in FIA with 0.1 mM cysteine. (a) Only CoPC deposited; (b) CoPC–polystyrene deposited. Carrier solution: 0.03 M phosphate buffer (pH 2.0) containing 0.1 mM EDTA and 2% methanol (v/v). Potential: +0.6 V vs. Ag/AgCl, flow-rate: 1.0 ml min^{-1}.

Since our interest lies in developing a CoPC-CME for use in flowing solutions, the electrochemical performance of CoPC conductive carbon cement CME was further examined in combination with LC for the detection of thiol compounds. The experiment was conducted either with CoPC conductive carbon cement electrodes or with CoPC carbon paste electrodes. Hydrodynamic voltammograms (HDVs) obtained for the chosen thiols at these two different CoPC CMEs with LC are shown in Fig. 3. The HDVs are virtually the same for these thiols, with a maximum current at ca. +0.7 V vs. Ag/AgCl and rapid current decrease at higher potentials which probably cause catalyst deactivation. With the CoPC carbon paste electrode lower HDVs were measured. CoPC-CMEs also showed effective electrocatalysis towards (DTT) as shown in Fig. 3, but interestingly, the HDVs of DTT at both electrodes had a lower starting oxidation potential, indicating that DTT is more easily oxidized. This is probably related to the presence of two thiol groups in the DTT. In fact, the unmodified conductive carbon cement electrode showed a maximum potential of ca. 0.70–0.75 V for DTT oxidation, but the anodic current only slightly increased at the examined potential range for N-

acetylcysteine (NAC), CYS and GSH. Figure 4 represents a typical chromatogram of these compounds obtained at the CoPC conductive carbon cement electrode at a potential of +0.70 V. The reproducibility of the electrode preparation was evaluated by measuring chromatograms of standard solutions with seven different electrodes. The results are listed in Table 1. The differences among the electrodes may be mainly associated with their differing surface microstructures. The polishing step may also contribute to these differences.

The stability of a CoPC conductive carbon cement electrode and a CoPC carbon paste electrode was tested over an extended length of time in LC under the same conditions, except that different flow-rates were employed. Every 30 min, a chromatographic injection was performed and the responses at +0.70 V vs. Ag/AgCl towards the thiol compounds were recorded. The results obtained are shown in Fig. 5. The response of the CoPC carbon paste electrode decreased strongly in the first hour, and after that at approximately 5% per hour. This decrease was due to leaching of the CoPC catalyst as well as the carbon paste itself from the electrode body. In contrast, the CoPC conductive carbon cement electrode was stable even at higher flow-rates (1.8 ml min^{-1}). A typical decrease of response of 1% per hour was found, which may be mainly associated with the deactivitation of CoPC in the electrode. Interestingly, the peak current of DTT at the CoPC carbon paste was stable, despite leaching of CoPC. This phenomenon could imply that the oxidation of DTT is less dependent on the catalyst-loading. Calibration plots for the thiol compounds were measured with one CoPC conductive carbon cement electrode. The results are listed in Table 2.

Application to urine samples

Figure 6 shows chromatograms of a urine sample after treatment with DTT using an unmodified and a modified electrode, respectively. It is clear that the modified electrodes gave a much higher response. The standard deviation of the peak height for cysteine was 1.9% for three successive chromatographic runs. An endogenous concentration of 178.5 μM ± 0.8% ($n = 2$) of cys-

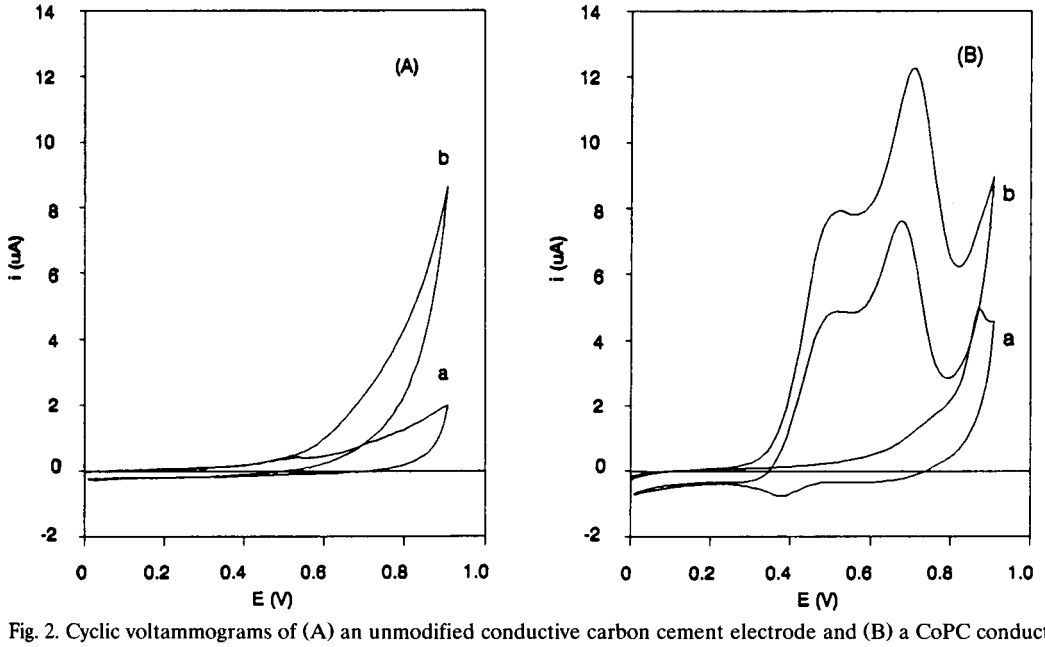

Fig. 2. Cyclic voltammograms of (A) an unmodified conductive carbon cement electrode and (B) a CoPC conductive carbon cement electrode (a) in blank electrolyte, and (b) in 1.0 mM cysteine. Electrolyte: 0.1 M phosphate buffer (pH 2.0); scan rate: 30 mV s^{-1} vs. SCE.

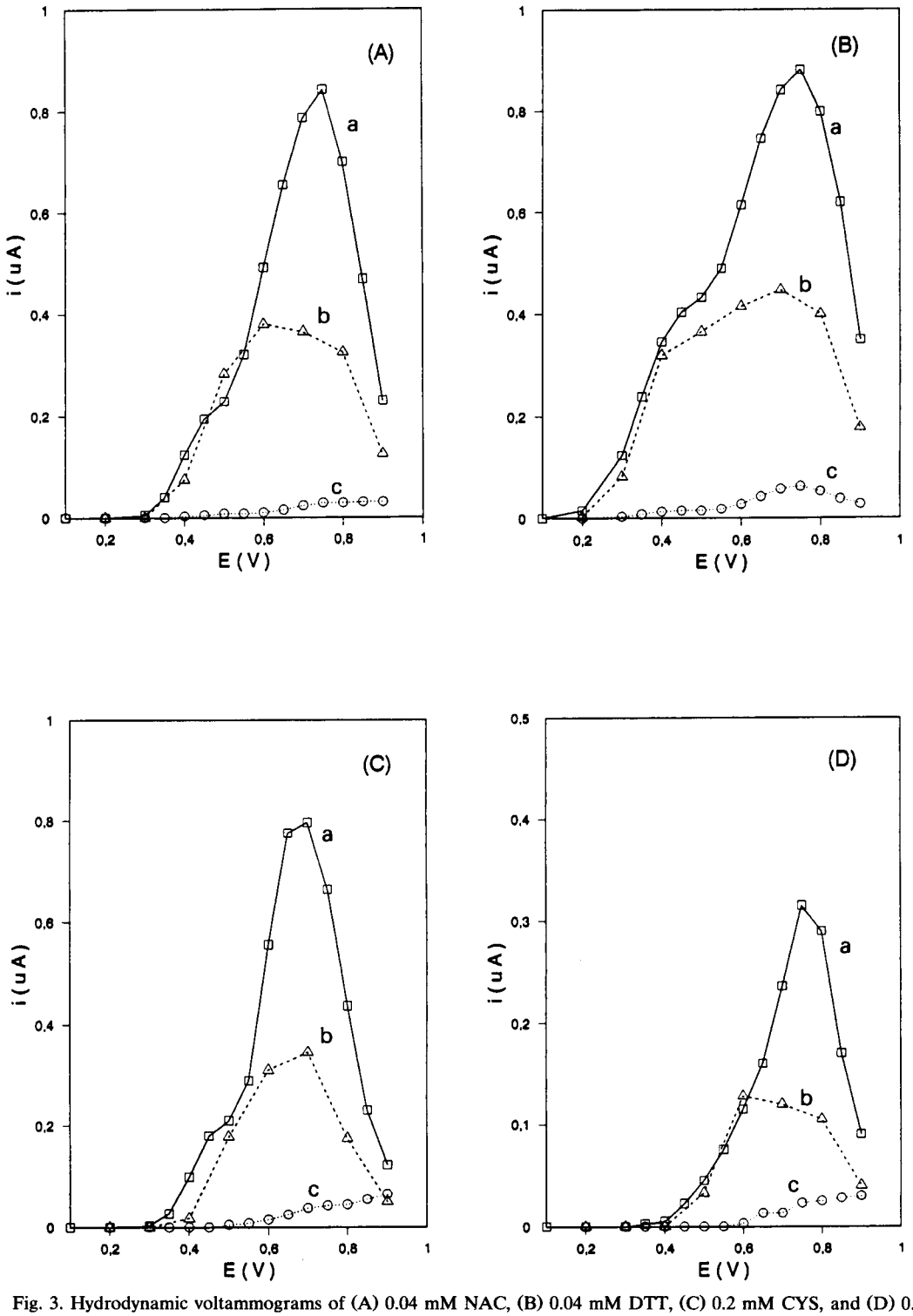

Fig. 3. Hydrodynamic voltammograms of (A) 0.04 mM NAC, (B) 0.04 mM DTT, (C) 0.2 mM CYS, and (D) 0.2 mM GSH at (□) CoPC conductive carbon cement, (△) CoPC carbon paste, and (○) unmodified carbon cement electrodes.

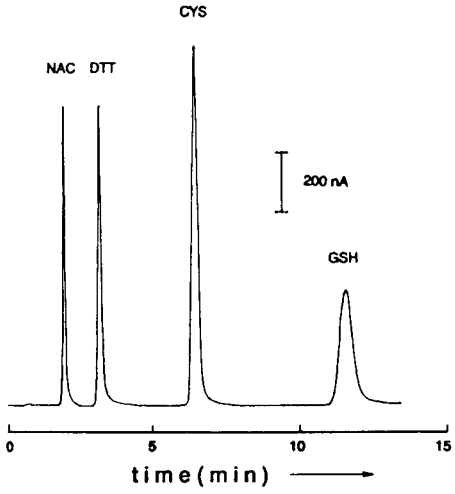

Fig. 4. Chromatogram of *N*-acetylcysteine, dithiothreitol, cysteine and glutathione. NAC and DTT: 0.04 mM; CYS and GSH: 0.2 mM. CoPC conductive carbon cement electrode. Potential: +0.7 V vs. Ag/AgCl. Flow-rate: 1.8 ml min^{-1}.

TABLE 1

Reproducibility of electrode preparation [a]

Electrode No.	Peak height (nA)			
	NAC	DTT	CYS	GSH
1	850	825	1050	375
2	1063	1075	1175	488
3	786	840	795	235
4	655	773	654	187
5	1113	975	1213	500
6	878	1000	990	440
7	1000	1009	1205	390
Mean ± S.D.	906 ± 18%	928 ± 12%	1012 ± 21%	373 ± 32%

[a] Conditions as in Fig. 4.

teine was found in this particular urine sample. The recovery of 20 μM of cysteine which was added to the urine samples was 95.5 ± 6.9% (n = 3). The chromatogram at the modified electrode

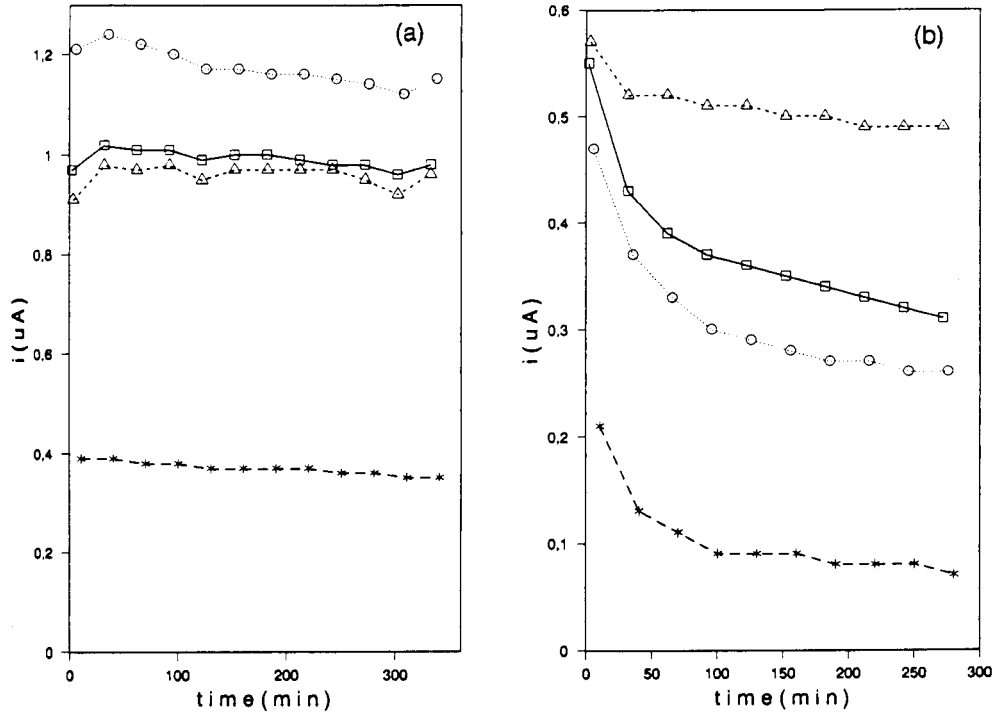

Fig. 5. Stability of (a) CoPC conductive carbon cement electrode and (b) CoPC carbon paste electrode. (□) NAC; (△) DTT; (○) CYS; (*) GSH.

TABLE 2

Calibration graphs of thiol compounds in liquid chromatography [a]

Compound	Concentration range injected (pmol)	Sensitivity (nA $pmol^{-1}$)	Correlation coefficient R ($n = 7$)
NAC	0.4– 200	0.964	0.9995
DTT	2 – 200	0.954	0.9997
CYS	2 – 400	0.212	0.9993
GSH	10 –1000	0.069	0.9933

[a] For experimental conditions see text.

is somehow cleaner than that at the unmodified electrode.

In summary, we have demonstrated that direct adsorption of CoPC on glassy carbon electrode is of little analytical value. The CoPC-containing conductive carbon cement as electrode matrix exhibited much better stability than the CoPC carbon paste electrode for amperometric detection in flowing solutions. We have also found that the stability of the electrode responses is analyte dependent. For DTT a better stability of electrode response was observed with less dependence on electrocatalyst-loading. The CoPC conductive carbon cement electrode has been successfully used in the determination of cysteine in urine samples. The use of conductive carbon cement for the incorporation of other modifiers is now under further investigation in this laboratory.

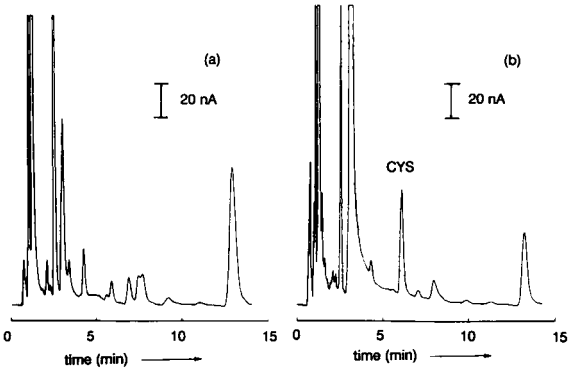

Fig. 6. Chromatograms of a urine sample at (a) unmodified conductive carbon cement electrode and (b) CoPC conductive carbon cement electrode. For experimental conditions see text.

REFERENCES

1 R.W. Murray, in Vol. 13, Electroanalytical Chemistry, A.J. Bard (Ed.), Marcel Dekker, New York, 1984.
2 R.W. Murray, A.G. Ewing and R.A. Durst, Anal. Chem., 59 (1987) 379A.
3 M.D. Imisides, G.G. Wallace and E.A. Wilke, Trans. Anal. Chem., 7 (1988) 143.
4 D.C. Johnson, M.D. Ryan and G.S. Wilson, Anal. Chem., 60 (1988) 147R.
5 S. Dong and Y. Wang, Electroanalysis, 1 (1989) 99.
6 J. Wang, Anal. Chim. Acta, 234 (1990) 41.
7 C.A. Widrig, M.D. Porter, M.D. Ryan, T.G. Strein and A.G. Ewing, Anal. Chem., 62 (1990) 1R.
8 E. Barendrecht, J. Appl. Electrochem., 20 (1990) 175.
9 A. Merz, Top. Curr. Chem., 152 (1990) 49.
10 F.H. Moser and A.L. Thomas, The Phthalocyanines, Vol. 1, CRC Press, Boca Raton, FL, 1983.
11 V.R. Shepard, Jr., and N.R. Armstrong, J. Phys. Chem., 83 (1979) 1268.
12 J.H. Weber and D.H. Busch, Inorg. Chem., 4 (1965) 469.
13 J. Metz and M. Hanack, J. Am. Chem. Soc., 105 (1983) 828.
14 L.D. Rollmann and R.T. Iwamoto, J. Am. Chem. Soc., 90 (1968) 1455.
15 G. Mclendon and A.E. Martell, Inorg. Chem., 16 (1977) 1812.
16 J. Manassen and A. Bar-Ilan, J. Catal., 17 (1970) 86.
17 B.D. Berezin, Russ. J. Phys. Chem., 36 (1962) 258.
18 R. Taube, Pure Appl. Chem., 38 (1974) 427.
19 S.D. Levina, T.I. Andrianova, M.M. Sakharov, O.A. Golovina, K.P. Lobanova and Z.A. Rotenberg, Russ. J. Phys. Chem., 40 (1966) 660.
20 D.J. Cookson, T.D. Smith, J.F. Boas, P.R. Hicks and J.R. Pilbrow, J. Chem. Soc., Dalton Trans., (1977) 109.
21 N.N. Kundo and N.P. Keier, Russ. J. Phys. Chem., 42 (1968) 707.
22 A.B.P. Lever and J.P. Wilshire, Can. J. Chem., 54 (1976) 2514.
23 S. Zecevic, B. Simic-Glavaski, E. Yeager, A.B.P. Lever and P.C. Minor, J. Electroanal. Chem., 196 (1985) 339.
24 A. Bettelhein and R.J.H. Chan and T. Kuwana, J. Electroanal. Chem., 99 (1979) 391.
25 J. Zagal, E. Monoz and S. Ureta-Zanartu, Electrochim. Acta, 27 (1982) 1373.
26 P. Janda, N. Kobayashi, P.R. Auburn, H. Lam, C.C. Leznoff and A.B.P. Lever, Can. J. Chem., 67 (1989) 1109.
27 J. Zagal, P. Bindra and E. Yeager, J. Electrochem. Soc., 127 (1980) 1506.
28 J.M. Green and L.R. Faulkner, J. Am. Chem. Soc., 105 (1983) 2950.
29 R.K. Sen, J. Zagal and E. Yeager, Inorg. Chem., 16 (1977) 3379.
30 J.A.R. Van Veen and C. Visser, Electrochim. Acta, 24 (1979) 921.
31 J.P. Randin, Electrochim. Acta, 19 (1974) 83.
32 K.M. Korfhage, K. Ravichandran and R.P. Baldwin, Anal. Chem., 56 (1984) 1514.

33 M.K. Halbert and Baldwin, Anal. Chem., 57 (1985) 591.
34 L.M. Santos and R.P. Baldwin, Anal. Chem., 58 (1986) 848.
35 L.M. Santos and R.P. Baldwin, Anal. Chem., 59 (1987) 1766.
36 L.M. Santos and R.P. Baldwin, Anal. Chim. Acta, 206 (1988) 85.
37 A.M. Tolbert, R.P. Baldwin and L.M. Santos, Anal. Lett., 22 (1989) 683.
38 J. Wang, T. Golden, K. Varughese and I.E. Rayes, Anal. Chem., 61 (1989) 508.
39 S.A. Wring, J.P. Hart and B.J. Birch, Analyst, 114 (1989) 1563.
40 S.A. Wring, J.P. Hart and B.J. Birch, Analyst, 114 (1989) 1571.
41 S.A. Wring, J.P. Hart and B.J. Birch, Anal. Chim. Acta, 229 (1990) 63.
42 S.A. Wring, J.P. Hart, L. Bracey and B.J. Birch, Anal. Chim. Acta, 231 (1990) 202.
43 J. Zagal, C. Fierro and R. Rozas, J. Electroanal. Chem., 119 (1981) 403.
44 J.H. Zagal and P. Herrera, Electrochim. Acta, 30 (1985) 449.
45 J. Wang and T. Golden, Anal. Chim. Acta, 217 (1989) 343.
46 J. Wang and R. Li, Talanta, 36 (1989) 279.
47 J. Wang, T. Golden and R. Li, Anal. Chem., 60 (1988) 1642.
48 M. Meaney, J.G. Vos, M.R. Smyth and G.G. Wallace, Anal. Proc., 26 (1989) 15.
49 J.N. Barisci, G.G. Wallace, E.A. Wilke, M. Meaney, M.R. Smyth and J.G. Vos, Electroanalysis, 1 (1989) 245.
50 X. Huang and W.Th. Kok, J. Liq. Chromatogr., 14 (1991) 2207.
51 D.L. Rabenstein and R. Saetre, Anal. Chem., 49 (1977) 1036.
52 R. Saetre and D.L. Rabenstein, Anal. Chem., 50 (1978) 276.
53 N. Hu and J.F. Rusling, Anal. Chem., 63 (1991) 2163.
54 Eastman Kodak Co., Kodak Catalog No. 54, New York, 1990, p. 195.
55 G.N. Kaman, Anal. Chim. Acta, 207 (1988) 1.
56 S. Kuwabata, Y. Maida and H.J. Yoneyama, J. Electroanal. Chem., 242 (1988) 143.
57 G.G. Wallace, M. Meaney, M.R. Smyth and J.G. Vos, Electroanalysis, 1 (1989) 357.

Analytica Chimica Acta, 273 (1993) 255–265
Elsevier Science Publishers B.V., Amsterdam

Electrochemically prepared chalcogenide ion-selective membranes as an alternative to conventional pressed-pellet ion-selective electrodes

M.T. Neshkova

Institute of General and Inorganic Chemistry, Bulgarian Academy of Sciences, bl. 11, Sofia 1113 (Bulgaria)

(Received 1st June 1992; revised manuscript received 25th September 1992)

Abstract

Applying cathodic electrodeposition of thin metal chalcogenide (selenide, telluride or arsenide) membranes on an inert electroconductive substrate, all-solid-state ion-selective electrodes (ISEs) were developed for Cu(II), Pb(II), Ag(I) and cyanide. Technologically, the electrochemical approach offers a cost-effective means of in situ membrane preparation which suits best the demand for disposable sensors for environmental and process control. Membranes of very sophisticated composition and strongly defective structure were developed as a result of preliminary membrane composition optimization studies. A brief outline of the optimum electrodeposition conditions for each membrane is given. The major advantage of these sensors as flow-injection potentiometric detectors was demonstrated on the examples of $Cu_{2-x}Se$ and $Ag_{2.40}Se_{0.86}Te_{0.14}$ membranes. A linear Nernstian response was observed down to $n \times 10^{-6}$ M Cu(II) or Ag(I) ($n = 2$–5). Interference of chloride with Cu ISEs can be eliminated with electroplated membranes in the flow-injection mode for Cl concentrations up to 0.5 M, the lower linearity limit still being 5×10^{-6} M Cu(II). It is shown that by switching from the steady-state to the flow-injection mode, separation by rate of the Cu(II) potential-determining processes occurring at the membrane/solution interface in the presence of Cl^- becomes possible. The potential of the electrochemical approach for model response mechanism studies was demonstrated by the example of a Cu ISE. The chemical and phase composition of the $Cu_{2-x}Se$ membrane was varied in the range $0.67 \geqslant x \geqslant 0$ and the Cu(II) electrode function was examined for different x values. Conclusions with regard to the potential-generating reaction and the optimum membrane composition were drawn on this basis.

Keywords: Flow injection; Ion selective electrodes; Potentiometry; Sensors; Chalcogenides; Copper; Cyanide; Lead; Membrane electrodes; Silver

Commercially adopted single-crystal, cast-disc or pressed-pellet membranes of different metal chalcogenides have been the most widely used ion-selective electrodes (ISEs) for metal ions, sulphide and cyanide for the last 20 years. Although great progress has been made in the phenomenological description of their response, no set of principles has been formulated so far regarding the selection of materials that would positively yield membranes with ideal interfacial and bulk properties [1]. The experimental results obtained up to now [2] indicate clearly that the chemical and phase compositions of the membrane are of utmost importance in determining the performances of ISEs, the Cu ISE being the most typical example [3]. Recently, a promising approach has been suggested for pressed-pellet membrane evaluation, focused on their inherent

Correspondence to: M.T. Neshkova, Institute of General and Inorganic Chemistry, Bulgarian Academy of Sciences, bl. 11, Sofia 1113 (Bulgaria).

properties as solid electrolytes of the mixed conductance type [4]. The working ion conductivity, or more precisely its transport number, is assessed as being the most important figure of merit; it depends strongly on the membrane stoichiometry. Hence, model studies which may reveal the relationship between the chemical and phase compositions of the membrane, its electrophysical properties and the electrode performance would be extremely valuable in acquiring a deeper insight into the response mechanisms. The need for such studies is also imposed by the fact that among the chalcogenide materials that might be used as ion-selective membranes there exist a number of single phases or phase compositions that differ significantly in their surface and electrophysical properties. The routine preparation of thick pressed-pellet membranes, with stoichiometry varying over a wide range, seems to be very subjective, and often the mechanical properties of the particular material do not allow the production of compact membrane discs. Accordingly, other, more versatile, techniques for membrane preparation should be sought.

In view of the increasing tendency to incorporate ISEs in flow systems, and especially when transient signals are to be recorded (flow-injection mode), these electrodes have to meet certain additional requirements. Among the parameters essential for flow injection application, the dynamic characteristics of the electrodes and of the potentiometric cell are of the utmost importance [5–7]. Serious deviations from Nernstian behaviour, manifesting themselves in a narrower linearity range and a higher detection limit, have been reported for a number of Cu and Ag membrane and second-kind chalcogenide-based electrodes when applied in the flow-injection mode [8–12]. The observed limitations are too great to be ascribed to dispersion only [8], hence the dynamic response characteristics of the respective electrodes are assumed to be the major reason for this limited response [5,10,11]. Indeed, the results reported for flow-injection analysis (FIA) applications of various Cu ISEs differ considerably depending on the membrane composition. The best performance has been reported for jalpaite membranes [13] and discouraging results for chalcocite [8] and single-crystal $Cu_{1.8}Se$ (Crytur) [12] membranes. Obviously, the search for sensors appropriate for FIA detection is still far from being completed.

Another important reason to look for alternative technological approaches to ISE preparation is the need for inexpensive disposable sensors for application in environmental and industrial monitoring which would preserve all the beneficial features of conventional ISEs

The aim of this work was to elucidate the respects in which electrochemically plated thin chalcogenide-based ion-selective membranes may be considered as a competitive alternative to conventional pressed-pellet metal chalcogenide membranes.

EXPERIMENTAL

Electrochemical preparation of metal chalcogenide membranes

Principle. In the presence of heavy metal ions, the electroreduction of Se(IV), Te(IV) and As(III) is known to proceed to give the corresponding metal selenides, tellurides and arsenides. The essence of this technological approach consists of electrochemical in situ cathodic deposition of the active chalcogenide material on an inert conducting substrate (most often platinum), pre-shaped and sized appropriately as an electrode [14].

Selection of deposition conditions. The choice of the proper electrolytic bath composition and the parameters for membrane electrodeposition was made on the basis of the results obtained from previous voltammetric studies under potentiostatic control for each particular system. The optimum conditions for electrodeposition of the following membranes have been investigated so far in this laboratory: $Cu_{2-x}Se$ ($x = 0.67$) [15–17], CuAgSe and Cu_3As [17] as Cu(II) ISEs; $Ag_{2+\delta}Se$ and Te-doped silver selenide of the general formula $Ag_{2+\delta}Se_{1-x}Te_x$ (where $0.2 < \delta < 0.8$ and $0.2 > x > 0.1$) as CN [18] and Ag ISEs [19]; and Ag-doped PbSe as a Pb ISE [20]. The electrochemical instrumentation and full details of the preparation procedure are given in the references cited.

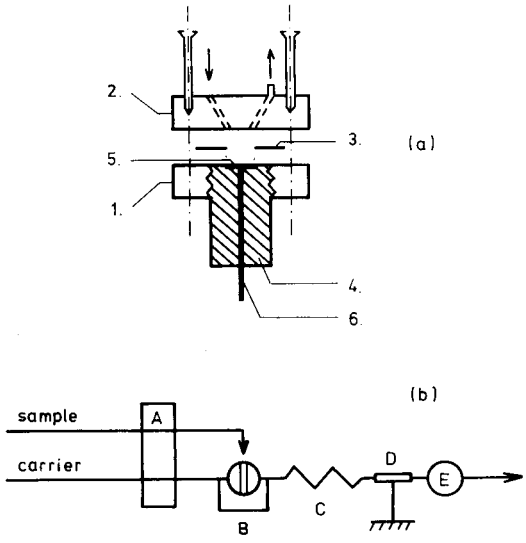

Fig. 1. (a) Schematic diagram of the sandwich-type flow-through cell: 1 = down-side Perspex block; 2 = upper block; 3 = Teflon sheet spacer; 4 = dismountable sensor cylinder; 5 = electroplated chalcogenide membrane on Pt substrate; 6 = inner contact lead. (b) Flow manifold: A = pumps; B = injection valve (85-μl loop); C = dispersion coil (50 cm×0.5 mm i.d. Teflon tube); D = grounding electrode (2 cm×0.5 mm i.d. stainless-steel tube); E = detector cell.

Flow-injection experiments

Construction of flow cell. A sandwich-type detector cell was used (Fig. 1a). The Pt substrate, on which the membrane is electrodeposited, is embedded in a Perspex cylinder screwed into the down-side cell block, thus permitting easy dismantling of the sensor part to have the membrane changed or re-deposited when needed. The carrier solution is fed into the cell through an inlet channel (with i.d. the same as the o.d. of the Teflon tubing) drilled into the upper cell block at an angle of 135° vs. the membrane plane, and leaves the cell through an outlet channel connected to a flow-through Ag/AgCl reference electrode (Radelkis OP-0836P-S). The volume of the sandwich flow-through cell is determined by the surface of the sensor and the thickness of the Teflon sheet spacer (0.15 mm), the typical cell volume used in this investigation being about 8 μl. In this way, a small-volume cell with a thin, controllable layer of solution passing tangentially to the detector surface is obtained.

Flow system. Figure 1b shows a schematic diagram of the optimized single-line flow manifold with connections made of Teflon tubing (0.5 mm i.d.). A Rheodyne Model 5020 injection valve with an 85-μl loop is used. The solutions are propelled with peristaltic pumps (Progress 1, Bulgaria). A 2-cm long earthed stainless-steel tube (0.5 mm i.d.) is inserted just before the detector cell to eliminate the electrostatic action of the peristaltic pumps. The signal is recorded with a ENDIM 621.02 Y–t recorder connected to the cell through a pH meter (OP-208, Radelkis). A typical flow-rate of 4.5 ml min^{-1} is used.

Membrane modelling

Electrode preparation. Cu ISEs with thin electroplated membranes of the general formula $Cu_{2-x}Se$ were prepared as described previously [15] on a Pt substrate. The membrane thickness was varied from 1 to 3 μm. A Radelkis OH-404 coulometric titrator which allowed the quantity of electricity consumed during controlled-potential membrane deposition, Q_{dep}, to be registered was used.

Procedures. The exact stoichiometry of the membrane was determined in the following way. The initially prepared non-stoichiometric $Cu_{2-x}Se$ membrane was rendered stoichiometric (Cu_2Se) by short-circuiting of the galvanic cell

$$Cu/Cu^{2+}_{(sol)}//Cu^{2+}_{(sol)}/Cu_{2-x}Se/Pt/Cu' \quad (I)$$

until reaching e.m.f. zero. In the above galvanic cell a 1×10^{-2} or 1×10^{-3} M $Cu(NO_3)_2$ solution of pH 2 (H_2SO_4) was used as the electrolyte [21]. A thermostated cell (20°C) with a cathodic compartment separated from the anodic compartment was used, deaerated with argon. From the quantity of electricity consumed during membrane deposition, Q_{dep}, and that for the complete membrane reduction in the galvanic cell (I), Q_{red}, the coefficient of non-stoichiometry, x, could be calculated from the equation

$$(Q_{dep} + Q_{red})/8 = Q_{dep}/(8 - x) \quad (1)$$

where 8 is the number of electrons involved in the electrodeposition of the stoichiometric Cu_2Se membrane.

The same galvanic cell (I) was also used to vary the initial composition of the membranes by step reduction in the range $0.7 \geqslant x \geqslant 0$. The phase composition of the membranes was identified by x-ray diffraction. The membrane surface was further characterized by X-ray photoelectron spectroscopy (XPS).

RESULTS AND DISCUSSION

Technological aspects of the electrochemical approach

Table 1 summarizes selected experimental conditions typical for the deposition of different chalcogenide membranes. Full details of the preparation procedures can be found in the references cited.

The ISEs prepared according to this approach should be considered to be of the all-solid-state type [22], denoted in the measuring cell as

$$\mathrm{Cu'/ext.ref.elect./test\ soln./M_{1+\delta}X/Pt/Cu} \quad \text{(II)}$$

(M = metal; X = Se, Te, As) in contrast to the membranes prepared by chemical coating or anodic dissolution of the corresponding metals in the presence of X^{n-} ions (X = Se, Te, As), classified as second-kind electrodes. The mechanism of transfer at the membrane/solution interface for all-solid-state membranes will depend on the nature of the electrical conductivity of the chalcogenide coating. Relative rapidity of electron vs. ion exchange will make the membrane potential dependent on the stoichiometry of the chalcogenide [23,24]. Hence, electrochemically deposited chalcogenide coatings would result in good ISEs only if they meet at least two important requirements: to have a definite chemical and phase composition ensuring reversible potential-determining processes at the two membrane interfaces, and to be compact and of good adherence, mechanically strong and chemically stable to be able to guarantee long-term electrode usage.

A major advantage of this approach over conventional technologies is that, being an in situ technique, it allows ready optimization of the coating composition in view of the above requirements through a simple trial-and-error procedure. This can be easily achieved by varying the composition of the electrolytic bath and by changing the parameters for the electrochemical deposition. The controlled-potential cathodic deposition guarantees further an adequate selectivity of the electrodeposition reaction, resulting in a high reproducibility of the composition of the coating.

As far as the technology of preparation is concerned, electrodeposited thin-layer chalcogenide-based membranes meet the requirements for inexpensive disposable sensors that allow repeated and reproducible re-deposition of the membrane every time it becomes worn out or damaged. The membrane thickness generally

TABLE 1

Selected conditions for metal chalcogenide membrane deposition

ISE	Membrane composition	Electrolytic bath composition	Deposition potential range (mV vs. SCE)	Electricity consumed (mC cm^{-2})	Ref.
Cu	$Cu_{2-x}Se$ ($x = 0.67$) ($Cu_3Se_2 + CuSe$)	0.3 M $CuSO_4$, 5×10^{-2} M Se(IV) 1.3×10^{-2} M KCl, 0.5 M H_2SO_4	+190 to +170	4500	15
Cu	CuAgSe	1×10^{-3} M $AgNO_3$, 1×10^{-2} M $CuSO_4$, 5×10^{-2} M Se(IV), 0.5 M H_2SO_4	+ 70 to + 50	2500	17
CN^-	$Ag_{2.56}Se_{0.84}Te_{0.16}$	2×10^{-3} M $AgNO_3$, 0.1 M Se(IV) 6.7×10^{-3} M Te(IV), 0.5 M H_2SO_4	+ 5 to − 20	1800	18
Ag	$Ag_{2.40}Se_{0.86}Te_{0.14}$	2×10^{-3} M $AgNO_3$, 5×10^{-2} M Se(IV) 6.7×10^{-3} M Te(IV), 0.5 M H_2SO_4	+ 20 to − 5	1600	19

varies within 1–4 μm and the electrodeposition rarely lasts more than 5 min. All this determines the in situ character of the technology.

The conditions under which cathodic co-deposition of compounds of defined stoichiometric composition could be achieved have been treated theoretically by Kroger [25]. In the light of these theoretical considerations, the experimental results obtained so far could be grouped as follows.

First, $Cu_{2-x}Se$, PbSe and Cu_3As membranes are deposited at potentials more positive than that for the corresponding component element [15]. The potential-determining species of this deposition is the chalcogen ion and the limiting current depends on its concentration in the solution (Fig. 2). The electrolytic bath should therefore contain a large excess of the component metal ions over the chalcogene concentration (Table 1).

Second, CuAgSe, $Ag_{2+\delta}Se$ and Te-doped silver selenide membranes are deposited at potentials more negative than or equal to the potential for silver metal deposition or the potential of the

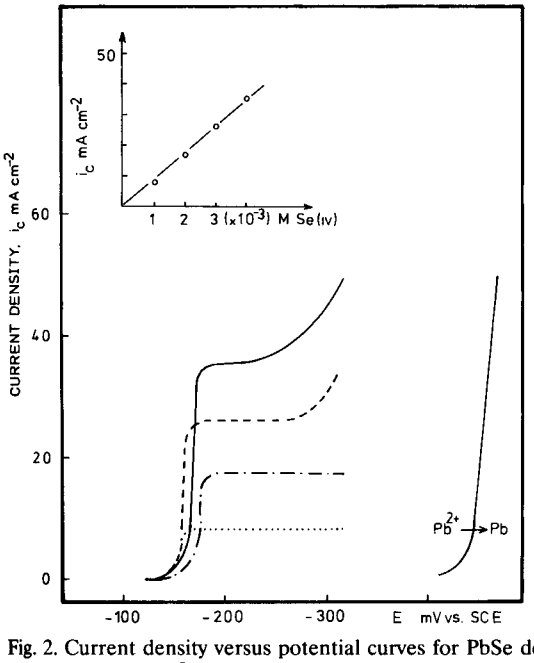

Fig. 2. Current density versus potential curves for PbSe deposition from 2×10^{-2} M $Pb(NO_3)_2$ in 0.75 M HNO_3 and different Se(IV) concentrations: (·····) 1; (·–·–·) 2; (– – – – –) 3; (———) 4 mM. Inset: i_c vs. $C_{Se(IV)}$ at $E_{dep.} = -0.2$ V vs. SCE.

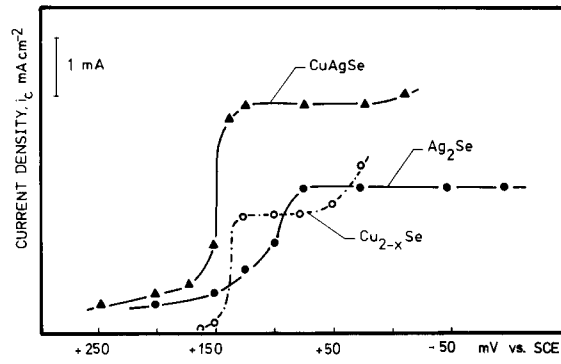

Fig. 3. Comparative current density versus cathode potential curves for (▲) CuAgSe, (○) $Cu_{2-x}Se$ and (●) Ag_2Se deposition on a Pt cathode from 5×10^{-2} M Se(IV) solution in 0.5 M H_2SO_4 containing also (●) 1×10^{-3} M $AgNO_3$, (○) 1×10^{-2} M $CuSO_4$, (▲) 1×10^{-2} M $CuSO_4 + 1\times10^{-3}$ M $AgNO_3$.

corresponding binary chalcogenide (Fig. 3). Thus an Ag^+-diffusion-controlled current is observed and the deposition is carried out in a bath containing a large excess of Se(IV) over the silver ion concentration.

Performance of electroplated chalcogenide membranes as detectors in flow-injection analysis

As established in our previous studies on the steady-state performance of electroplated chalcogenide membranes as ISEs for Cu(II), Ag(I) and cyanide [15,17–20], these membranes prove to be adequate alternatives to conventional ISEs. This section deals with their performance as FIA detectors, with special emphasis on $Cu_{2-x}Se$ and $Ag_{2.40}Se_{0.86}Te_{0.14}$ membranes for Cu(II) and Ag(I) detection.

The flow-through cell and a schematic diagram of the optimized single-line flow manifold are shown in Fig. 1. The flexibility of the electrodeposition technique with regard to membrane shape and size was made use of in designing a flow-through cell with minimum hold-up and optimum washout. As seen from Fig. 1a, it resembles very much the amperometric thin-layer flow cell used in liquid chromatography (e.g., Bioanalytical Systems, USA), preserving the cascade-type arrangement suggested by Hansen et al. [6] for open flow detectors.

Figure 4 shows typical records of the flow-injection signals for Cu(II) and Ag(I) with increas-

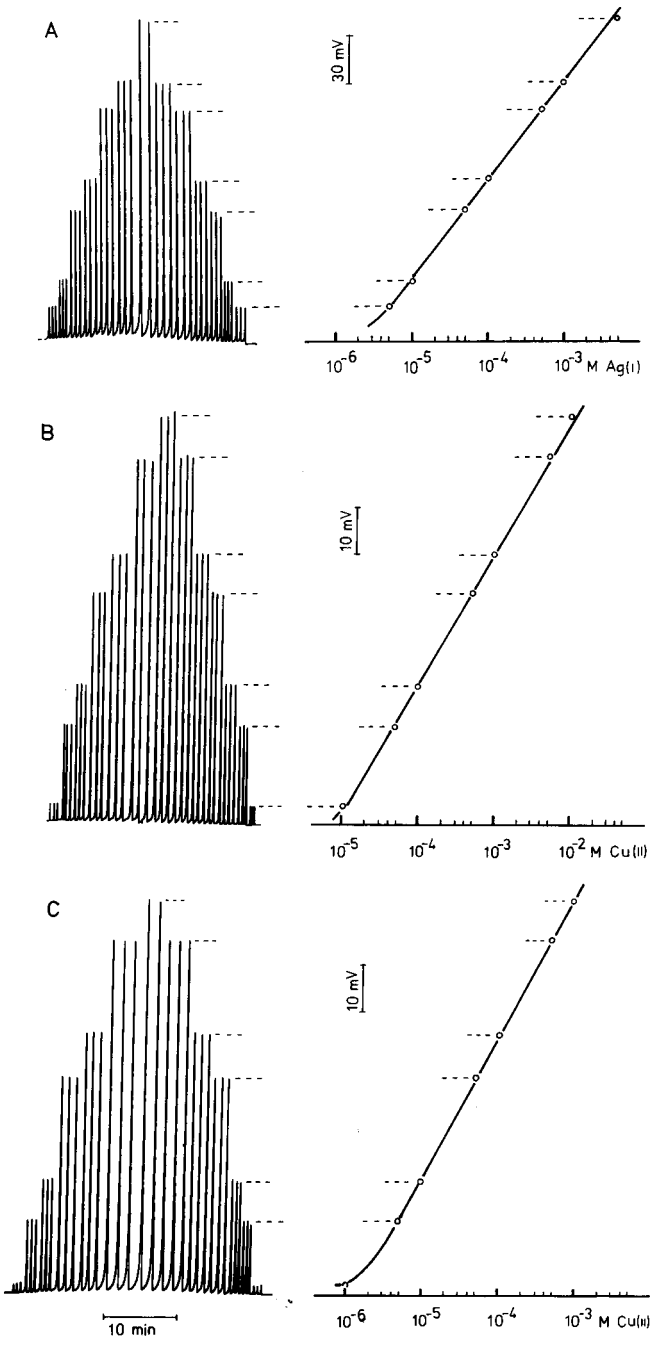

Fig. 4. Calibration runs for Ag(I) and Cu(II) with increasing and decreasing concentrations at a flow-rate of 4.5 ml min^{-1} and with an injected sample volume of 85 μl. (A) $Ag_{2.40}Se_{1.86}Te_{0.14}$ membrane as Ag(I) detector; carrier solution, 0.1 M $KNO_3 + 1 \times 10^{-6}$ M Ag(I). (B) $Cu_{2-x}Se$ membrane as Cu(II) detector; carrier solution, 5×10^{-2} M $KNO_3 + 5 \times 10^{-6}$ M Cu(II). (C) The same detector as in (B); carrier solution, 5×10^{-2} M $KNO_3 + 5 \times 10^{-7}$ M Cu(II).

ing and decreasing concentrations, obtained with the corresponding membranes at different concentrations of the main ion in the carrier solution [13] The first significant result is that a Nernstian type of response is preserved down to $n \times 10^{-6}$ M ($n = 2$–5) concentrations for both metal ions. This corresponds to a decrease in the Nernstian lower linearity range by two orders of magnitude compared with that previously reported for other types of membranes [8–11]. The washout time (i.e., the sample throughput) in the present instance is controlled mostly by the main ion concentration in the carrier solution and improves considerably when it is increased, at the expense of the sensitivity. Still, a fairly satisfactory mean sample throughput (90 h^{-1}) is achieved for sample concentrations varying within three orders of magnitude without changing the main ion concentration (Fig. 4). In contrast to earlier findings [8,11], the magnitude of the signal is virtually independent of the flow-rate within the range 1–5 ml min^{-1}, and is far less dependent on the sample volume injected above the 50-μl limit. The impressive stability of the baseline also deserves special mention. These experimental results are in good agreement with the very fast response recorded for the same membranes under steady-state conditions, and gives support to the suggestion that for low-dispersed systems (D is close to 1 in the present instance) the Nernstian limit of detection is controlled mainly by the dynamic characteristics of the sensor [5,7].

The application of Cu ISEs to natural samples, plating baths and body fluids is known to be greatly restricted by interference from chloride [3,26]. The procedures proposed so far for overcoming this limitation are not applicable to the FIA mode [26–28]. Hence the examination of the flow-injection response of $Cu_{2-x}Se$ electroplated membranes to samples containing chloride is a challenge. A typical illustration of this interference with the steady-state response of electroplated $Cu_{2-x}Se$ membranes is shown in Fig. 5. As can be seen, a deviation from the steady-state Nernstian response for Cu(II) is observed with chloride concentrations above 0.05 M, manifested by an increased calibration slope (up to 60 mV per decade) and poor reproducibility, as also reported for other copper chalcogenide membranes [3].

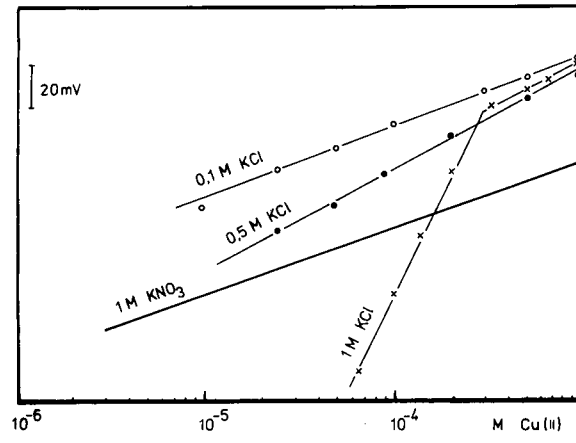

Fig. 5. Cu(II) calibration in the presence of different chloride concentrations with a $Cu_{2-x}Se$ membrane under steady-state conditions. The calibration graph in 1 M KNO_3 gives a Nernstian slope (29 mV per decade).

Under flow-injection conditions, a Cu(II) signal free from chloride interference is observed even in the presence of 0.5 M KCl in the injected

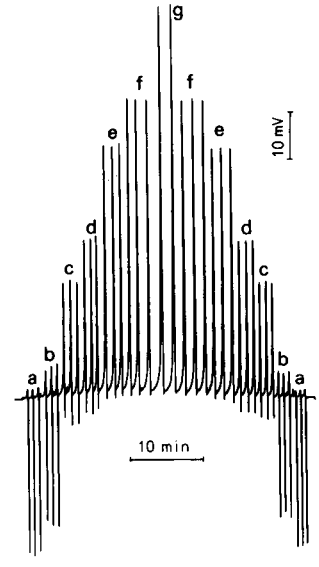

Fig. 6. Typical calibration runs for Cu(II) standards in 0.5 M KCl at a flow-rate of 4.5 ml min^{-1} (85-μl loop) and carrier solution 5×10^{-2} M $KNO_3 + 5\times10^{-7}$ M Cu(II). Standard concentrations from left to right: (a) 5×10^{-6}, (b) 1×10^{-5}, (c) 5×10^{-5}, (d) 1×10^{-4}, (e) 5×10^{-4}, (f) 1×10^{-3} and (g) 5×10^{-3} M and downwards.

samples (Fig. 6). A linear calibration graph with a Nernstian slope of 29 mV per decade is preserved down to 5×10^{-6} M Cu(II) in this instance also, which seems satisfactory for many practical needs. No super-Nernstian response, so typical under steady-state conditions, is observed even in the presence of 1 M KCl, but the limit of the linear Nernstian response is higher in this instance.

The presence of Cl^- in the injected samples is indicated by a negative overshoot in the flow-injection signal, preceding the positive Cu(II) signal (Fig. 6). This negative dip of the signal depends on the [Cu]/[Cl] ratio in the sample and proves to be highly reproducible. Enhanced selectivity due to "kinetic discrimination" of the interfering ions under flow-injection conditions has been reported for the chloride ISE [29,30]. This phenomenon is based on the different response times of the membrane to the primary and interfering ions. The mechanism of chloride interference with Cu ISEs [3] differs significantly from the above common case of interference that can be expressed quantitatively by the selectivity coefficient, K_{sel}. It is assumed that Cl-interferes by modifying the mechanism of the formation of the primary Cu(II) response [16]. Obviously, on passing from the steady-state to the FIA mode, separation by rate of the Cu(II) potential-determining processes in the presence of Cl^- becomes possible. Hence the present experimental results provide a possibility for further elucidation of the mechanism of chloride interference, and such experiments are in progress.

Another flow-injection application of electroplated $Cu_{2-x}Se$ membranes for the indirect determination of Al(III) and U(VI) has been reported recently [31].

Electrochemical modelling of membrane compositions for response mechanism studies

As already mentioned, general electrochemical studies aimed at defining the conditions for metal chalcogenide electrodeposition to be used as ISEs include necessarily the stage of optimization of the membrane composition. Accordingly, this approach allows for differentiation between at least two limiting cases, membrane compositions yielding poor ISE performance and those ensuring ideal Nernstian behaviour. Often intermediate results can also be observed.

Studies of the dependence of the electrode function on membrane stoichiometry varying over a wide range are also possible with electroplated membranes [16]. The results of such investigations undertaken on $Cu_{2-x}Se$ membranes as Cu ISEs (Table 1) are discussed below.

The first step of this investigation included full characterization of the electroplated $Cu_{2-x}Se$ membranes (Table 1) with regard to their stoichiometry, phase composition and surface state. Following the coulometric procedure described under Experimental, a mean value of $x = 0.67$ for the non-stoichiometry coefficient was obtained. Through parallel x-ray diffraction analysis, this value of x was proved to correspond to the co-existence of two phases in the coating: a predominant Cu_3Se_2 (umangite) and an admixture of CuSe (klockmannite). The photoelectron Cu $2p_{3/2}$ spectrum [16] gave evidence for the presence of Cu(I) and Cu(II) at the membrane surface.

This initial stoichiometry of the membrane was further varied in the range $0.67 \geqslant x \geqslant 0$ by a step reduction using the same galvanic cell (I). Figure 7 presents a typical dependence curve of the

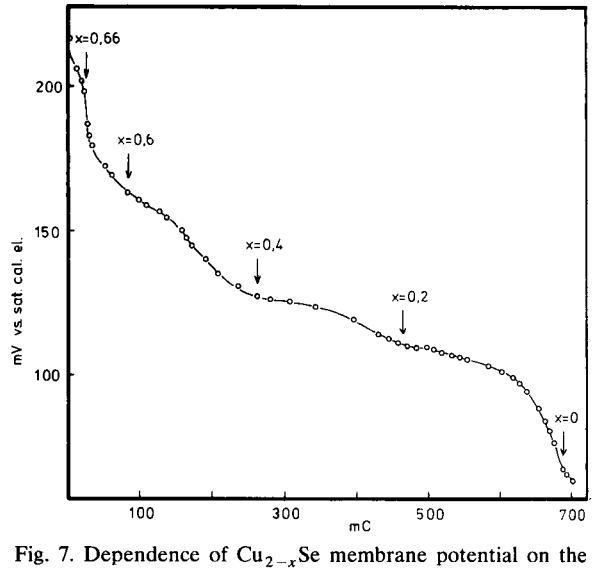

Fig. 7. Dependence of $Cu_{2-x}Se$ membrane potential on the value of x, i.e., the quantity of electricity (mC) consumed during step-by-step reduction in the galvanic cell I.

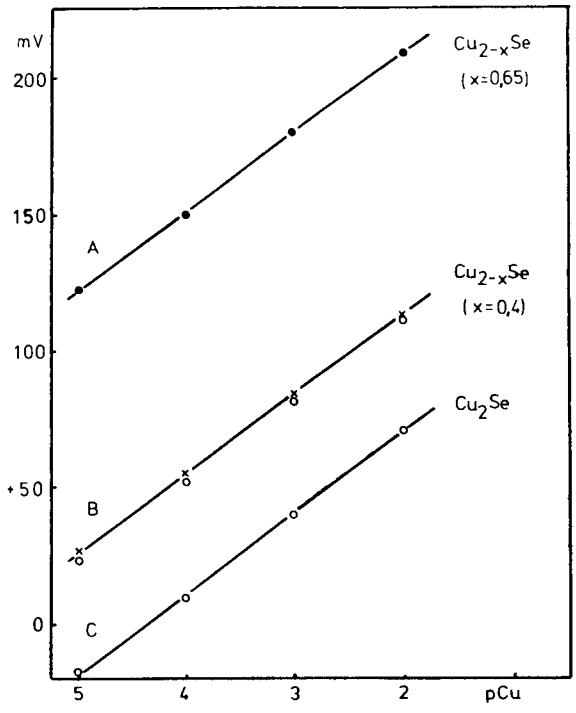

Fig. 8. Calibration graphs for membranes of different composition. (A) Initially prepared membrane; (B) × = partially reduced membrane ($x = 0.4$) and ○ = restructured Cu_2Se membrane; (C) stoichiometric Cu_2Se membrane.

membrane potential at open circuit on its composition. The plateaux registered on the curve correspond to the region of x values for which two phases co-exist in the membrane [21,23]. For $x \leqslant 0.4$ of the plateau region, the co-existence of Cu_3Se_2 (umangite) and $Cu_{1.8}Se$ (berzelianite) was evidenced, and Cu_2Se (monoclinic) and $Cu_{1.8}Se$ (berzelianite) were found for $x \leqslant 0.2$. The change in structure and composition of the membrane also resulted in a change in colour, from ink blue ($x = 0.67$) to light grey ($x = 0$).

The electrode behaviour in Cu(II) standard solutions of a stoichiometric Cu_2Se membrane obtained as a result of complete reduction of the initial membrane in galvanic cell (I) was examined first. Although the stoichiometric membrane responds to Cu(II) in solution, its potential proved to be very unstable with time. The calibration graph C in Fig. 8 represents the initial potential values. The potential changed exponentially with time, tending towards a steady-state value. The time for reaching a stable potential reading proved to depend on the Cu(II) concentration. On shifting towards its steady-state potential value the membrane regained its blue colour and the copper solution became opalescent. It was established by x-ray diffraction that membranes that had reached the equilibrium potential had also undergone some structural changes. Instead of the single cubic phase, Cu_2Se, Cu_3Se_2 and $Cu_{1.8}Se$ were identified, characteristic of the plateau region for $x = 0.4$ (Fig. 7). The membranes thus restructured are characterized by another value of the standard potential (points ○ on line B in Fig. 8) and exhibit a stable electrode performance thereafter. A mixture of Cu(I) and Cu(II) hydroxide species was found by XPS in the precipitate obtained after centrifuging the copper solution.

The observed changes in the membrane and in the solution imply that the following metathesis reaction has taken place:

$$2Cu_2Se + Cu^{2+} = Cu_3Se_2 + 2Cu^{+} \qquad (2)$$

The occurrence of the Cu_3Se_2 phase has also been evidenced in the monocrystal $Cu_{1.8}Se$ membrane after long-term usage in Cu(II) solutions [32]. The present finding explains satisfactorily the reason for the day-to-day potential drift reported for this electrode.

The non-stoichiometric membranes with $x = 0.4$, obtained through partial reduction of the initial membrane ($x = 0.67$), showed a stable potential in Cu(II) solution from the very beginning, and a standard potential identical with that of the stoichiometric membrane after reaching a steady-state potential (line B in Fig. 8).

When immersed in 0.1 M Cu(II) solution, containing also 1×10^{-2} M chloride, the phase transformation of the stoichiometric and partially reduced ($x = 0,4$) membranes was further manifested by an exponential time transient of the potential. On reaching equilibrium, both membranes exhibited a standard potential and phase composition characteristic of the initially prepared $Cu_{2-x}Se$ ($x = 0.67$) (line A, Fig. 8).

In previous studies [33] it was concluded that the response of copper selenide membranes to

Cu(II) is governed by the following exchange reaction proceeding at the membrane/solution interface:

$$Cu_2Se + Cu^{2+} = CuSe + 2Cu^{+} \quad (3)$$

The above results provide further experimental proof of this suggestion. For the membrane to exhibit a stable and reproducible standard potential, a two-phase membrane composition containing both Cu_2Se and CuSe in an appropriate structural arrangement proved to be able to accept the CuSe phase formed as a result of reaction 3 causing no change of the copper activity in the coating [24]. This was not the case with the stoichiometric, Cu_2Se membrane. It had to be restructured first, following reaction 2, before a stable electrode performance could be observed.

The best performance with regard to sensitivity, stability and dynamic response in Cu(II) standards was achieved when using the initially prepared $Cu_{2-x}Se$ ($x = 0.67$) membrane [15–17,31]. This is probably due to the optimum conductivity ensured by this phase composition. While such a correlation has been reported for the ternary CuAgSe membrane [34], no data for the $Cu_{2-x}Se$ membrane are available yet.

Based on the results obtained so far with the other chalcogenide membranes given in Table 1, it is concluded that no stable and reproducible standard potential could be achieved by a single-phase binary metal chalcogenide membrane, arranged in an all-solid-state electrode configuration, whether stoichiometric or non-stoichiometric. This conclusion has not yet found a satisfactory explanation.

Conclusions

Cathodically deposited chalcogenide ion selective membranes appear to be a competitive alternative to the conventional pressed-pellet type in several respects. From a technological point of view, electrodeposition promises an inexpensive in situ technique for the preparation of disposable sensors with optimized membrane composition. From an analytical viewpoint, their major advantage is their fitness for flow-injection detection as far as sensitivity, stability and selectivity of the signal are concerned.

The possibility of extending the range of materials investigated for ISE applications and the potential for modelling of the membrane stoichiometry provide a powerful means for response mechanism studies.

Although best illustrated by the class of chalcogenide membranes, the capacities of the proposed cathodic electrodeposition approach are by no means confined to this type of membrane.

Financial support of this investigation from the National Scientific Research Fund is gratefully acknowledged.

REFERENCES

1 R.P. Buck, in H. Freiser (Ed.), Ion-Selective Electrodes in Analytical Chemistry, Vol. 1, Plenum, New York, 1978, p.1.
2 J. Koryta, Anal. Chim. Acta, 159 (1984) 1; 233 (1990) 1.
3 J. Gulens, Ion-Sel. Electrode Rev., 2 (1980) 117; 9 (1987) 127.
4 V. Young, Solid State Ionics, 20 (1986) 277.
5 K. Toth, J. Fucsko, E. Lindner, Zs. Feher and E. Pungor, Anal. Chim. Acta, 179 (1986) 359.
6 E.H. Hansen, J. Ruzicka and E.A. Zagatto, Anal. Chim. Acta, 88 (1977) 1.
7 E. Pungor, K. Toth and A. Hrabeczy-Pall, Trends Anal. Chem., 3 (1984) 1.
8 M. Trojanowicz and W. Matuszewski, Anal. Chim. Acta, 138 (1982) 71.
9 J.F. van Staden and C.C.P. Wagener, Anal. Chim. Acta, 197 (1987) 217.
10 J.V. van Staden, Fresenius' Z. Anal. Chem., 332 (1988) 157.
11 L.K. Shpigun and O.V. Bazanova, Zh. Anal. Khim., 44 (1989) 1640.
12 Yu.A. Zolotov, L.K. Shpigun, I.Ya. Kolotyrkina, E.A. Novikov and O.V. Bazanova, Anal. Chim. Acta, 200 (1987) 21.
13 W.E. van der Linden and R. Oostervink, Anal. Chim. Acta, 101 (1978) 419.
14 M. Neshkova, Bulg. Pat. 33078 (1976).
15 M. Neshkova and H. Sheytanov, J. Electroanal. Chem., 102 (1979) 189.
16 M. Neshkova, in E. Pungor (Ed.) Ion-Selective Electrodes, 5th Symposium on Ion-Selective Electrodes, Matrafured, 1988, Akadémiai Kiadó, Budapest, 1989, p. 503.
17 M. Neshkova, Thesis, Institute of General and Inorganic Chem., Bulgarian Academy of Sciences, Sofia, 1988.
18 M. Neshkova and E. Pancheva, Anal. Chim. Acta, 242 (1991) 73.
19 M. Neshkova and E. Pancheva, Electroanalysis, submitted for publication.

20 M. Neshkova and R. Banov, in preparation.
21 H.J. Mathieu and H. Rickert, Z. Phys. Chem., 79 (1972) 315.
22 R.P. Buck and V.R. Shepard, Jr., Anal. Chem., 46 (1974) 2097.
23 M. Sato, Electrochim. Acta, 11 (1966) 361.
24 M. Koebel, Anal. Chem., 46 (1974) 1559.
25 F.A. Kröger, J. Electrochem. Soc., 125 (1978) 2028.
26 A. Lewenstam, T. Sokalski and A. Hulanicki, Talanta, 32 (1985) 531.
27 B. Hoyer and M. Loftager, Anal. Chem., 60 (1988) 1235.
28 B. Hoyer, Talanta, 38 (1991) 115.
29 M. Trojanowicz and W. Matuszewski, Anal. Chim. Acta, 151 (1983) 77.
30 L. Ilcheva and K. Camman, Fresenius' Z. Anal. Chem., 322 (1985) 323.
31 M. Neshkova, E. Pancheva, J. Fucsko, G. Nagy and E. Pungor, Anal. Chim. Acta, 259 (1992) 149.
32 J. Siemroth and I. Henning, in E. Pungor (Ed.) Ion-Selective Electrodes 3, Akadémiai Kiadó, Budapest, 1981, p. 339.
33 M. Neshkova and H. Sheytanov, Talanta, 32 (1985) 654.
34 M.I. Agaev, Sh.M. Alekperova and M.I. Zargarova, Dokl. Akad. Nauk Az. SSR 27, No. 5 (1975) 20.

Analytica Chimica Acta, 273 (1993) 267–274
Elsevier Science Publishers B.V., Amsterdam

Investigation of a zirconium electrode as a sensor for fluoride ions

B. Pihlar and Z. Cencič

Department of Chemistry, University of Ljubljana, 61000 Ljubljana (Slovenia)

(Received 1st June 1992)

Abstract

The effect of fluoride ions on the electrochemical behaviour of a zirconium metal electrode was investigated. Since zirconium metal is always covered by a layer of oxide, the anodic characteristic of a Zr/ZrO_2 electrode depends highly on the electrolyte composition. Only in hydrochloric and perchloric acid media was a direct proportionality between fluoride concentration and anodic current density found. In other electrolytes the fluoride ion-induced dissolution of the zirconium metal leads to an increase in ZrO_2 film thickness, and as a consequence, the mass transport of fluoride through the oxide layer is hindered. The mechanism of the zirconium electrode dissolution at low concentrations of fluoride (below 1×10^{-3} M) seems to be different from that at high concentrations. The dependence of the equilibrium potential on the fluoride concentration is far from the Nernstian one, and a zirconium electrode could be successfully applied in the potentiometric mode of operation only as an indicator electrode in titrations. The proportionality between the anodic current density and the fluoride ion concentration in perchloric acid media could be exploited for the amperometric detection of fluoride. With a thin-layer cell and a zirconium metal based indicator electrode, nanogram amounts of fluoride could be detected by a simple flow injection system.

Keywords: Amperometry; Flow injection; Sensors; Fluoride ions; Potentiometric indication; Zirconium electrodes

Since the development of the single crystal lanthanum fluoride membrane electrode by Frant and Ross [1], this ion-selective electrode (ISE) has become the method of choice in analytical practice for the determination of fluoride by potentiometry. The main drawback of this electrode is its relatively short life-time (about one to two years) due to evaporation of the internal filling solution and/or escape of doped europium from the sensor LaF_3 membrane. Restoration of an unresponsive fluoride ISE described by some authors [2–4], requires much skill and in our opinion is applied only exceptionally.

Correspondence to: B. Pihlar, Department of Chemistry, University of Ljubljana, 61000 Ljubljana (Slovenia).

The present paper deals with the investigation of a zirconium metal electrode and the study of its response in aqueous media to fluoride ions. Literature data on research in this field are very scanty. The first report about the response of a zirconium electrode to fluoride ions was published by Magregian [5]. The paper deals with a simple $Zr/F^-/Pt$ galvanic cell similar to that recommended previously by Baker and Morrison [6] and based on an aluminium anode. Deschamps and Bonnaire [7] recommended a zirconium electrode as a convenient pH sensor in acidimetric titrations, and electrochemical investigation of Zr/ZrO_2 electrodes as pH probes, was reported by some authors [8,9].

Since zirconium and its alloys are of considerable importance in nuclear reactor technology

due to their low neutron cross section and great resistence to corrosion, several studies of the electrochemical behaviour of zirconium in aqueous media have appeared [10–13]. The main subject of these papers was the investigation of the passivating ZrO_2 film and the study of its properties and role in the corrosion process. The influence of fluoride ions has not yet been systematically examined. Therefore in the present work we describe some results of our investigation of the effect of fluoride ions on the electrochemical response of a zirconium metal electrode. Some possibilities for the use of such an uncommon sensor for the determination of fluoride ions are suggested.

EXPERIMENTAL

Apparatus and reagents

The indicator electrodes were prepared from a Zr wire (13 mm × 1.25 mm o.d., 99.9% Zr), Zr foil (0.25 mm thick, 1 cm × 1 cm, 99.99% Zr) and a Zr rod (12.6 mm × 6.5 mm o.d., 99% Zr) supplied by Pierce Inorg. B.V. (Rotterdam). The wire electrode was fixed into glass tubing with epoxy resin, and the foil electrode was sealed thermally into polyethylene tubing. The Zr rod electrode was mounted on a standard specimen holder assembly of the K 47 Corrosion Cell System (EG & G Princeton Applied Research, Princeton, NJ). In the flow-through detector (Fig. 7) the Zr rod was fixed into a Perspex body by epoxy resin. The Zr indicator electrodes were polished between measurements by wet grinding with 400 and 600-grit SiC paper. The geometrical surface area actually exposed to the solution was considered in the current density calculation. In potentiostatically controlled measurements a three-electrode system was used, with a Pt wire counter electrode if not stated otherwise. A saturated calomel electrode was used as a reference electrode throughout the work.

A computer controlled potentiostat/galvanostat (EG&G PAR Model M 273) were used in the experiments requiring the control of potential or current during the measurements. For the measurement of the open circuit potential (E_{oc}) and for titrations, a microprocessor controlled pH meter (Iskra Model MA 5740, Ljubljana) coupled to a printer (Iskra Model MA 9150) was used.

Experiments in the flowing mode were done with a thin-layer flow-through cell, constructed in the laboratory. A peristaltic pump (Ismatec Model MS-4/8, Zürich), and a low power potentiostat (Iskra MA 5410) in conjunction with an strip chart recorder (Houston Instrument, Houston, TX, Model B-5000) was used to control the flow-rate of liquids and the potential of the Zr indicator electrode, respectively.

All chemicals were of p.a. grade quality, and the water used for the preparation of the solutions was demineralized twice by ion exchangers and finally purified in the Milli-Q System (Millipore, Bedford, MA). The stock solution of 0.100 M NaF and more diluted working standard solutions of fluoride ions were kept in polyethylene bottles. The acetate buffer (0.5 M CH_3COOH + 0.5 M CH_3COONa) was of pH 4.65, phosphate buffer (1/15 M KH_2PO_4 + 1/15 M Na_2HPO_4) of pH 6.81, and borate buffer (0.05 M H_3BO_3, 0.02 M NaOH) was of pH 9.2. Solutions of HCl, H_2SO_4 and $HClO_4$ were prepared by appropriate dilution of concentrated acids.

Measurements made in acid media (below pH 4) were performed in polyethylene or PTFE (Nalgene, Rochester, NY) vessels. Solutions were deaerated before the addition of fluoride by argon (99.99% Ar), and the experiments were performed in stirred solution (synchronous magnetic stirrer rotated at 750 rpm) at room temperature (20 ± 2°C) if not stated otherwise.

RESULTS AND DISCUSSION

Current–voltage characteristics of the system

Zirconium metal possesses noticeable reductive properties ($E°(Zr^{4+}/Zr) = -1.53$ V) and therefore in aqueous solutions the metal surface is always covered by a passive layer of ZrO_2. The spontaneous formation of a protective ZrO_2 film is accompanied by the evolution of hydrogen and/or the reduction of oxygen. The thickness of the protective film depends on the Zr electrode history, e.g. the mechanical, thermal or chemical

treatment. It is known that a mixture of HF and HNO_3 effectively removes the oxide film. Its formation and the thickness could be closely controlled by anodic oxidation of zirconium metal [14].

A set of polarization curves for the Zr wire electrode in stirred deaerated solutions of different electrolytes is shown in Fig. 1. During anodic polarization of the Zr electrode, oxide formation occurs and the anodic current begins to rise exponentially. It is evident from Fig. 1, that the oxidation proceeds in borate buffer at the lowest overpotential, and in sulphuric acid media, the formation of ZrO_2 occurs at the highest anodic overpotential. The cathodic part of the polarization curves shown in Fig. 1 corresponds to the reduction of hydrogen ions at the $Zr–ZrO_2$ interface. As can be seen from curves 1 to 4, the hydrogen evolution rate is proportional to the concentration of oxonium ions in the solution, with the

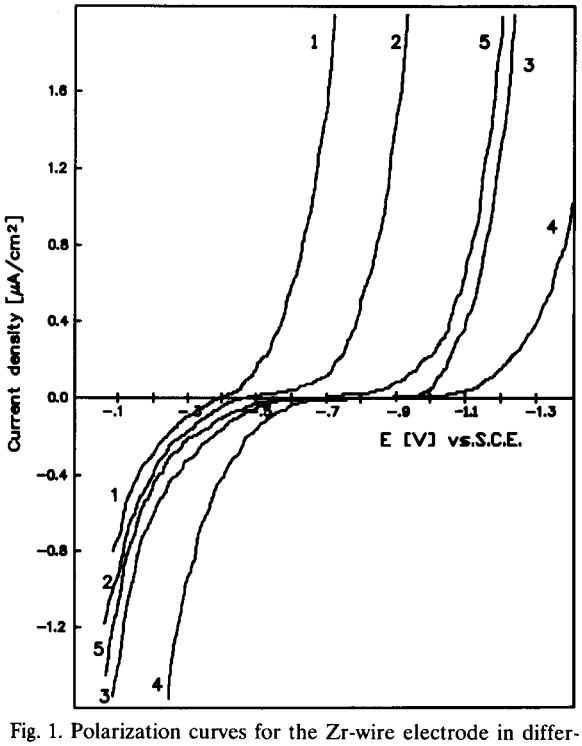

Fig. 1. Polarization curves for the Zr-wire electrode in different electrolytes: (1) 1 M H_2SO_4, (2) 0.1 M acetate buffer of pH 4.65, (3) 0.07 M phosphate buffer of pH 6.8, (4) 0.05 M borate buffer of pH 9.2, (5) 0.1 M NaOH; scan rate 2 mV s^{-1}.

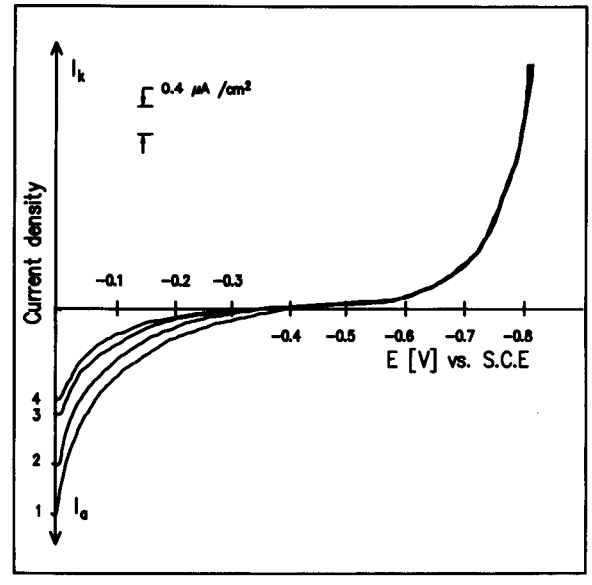

Fig. 2. Polarization curves of Zr electrode in 0.1 M acetate buffer of pH 4.65 at different concentrations of F^- ions: (1) 1×10^{-4}, (2) 1.2×10^{-4}, (3) 2×10^{-4} and (4) 4.8×10^{-4} M; scan rate 2 mV s^{-1}.

exception of 0.1 M NaOH solution, where a remarkable lowering of the overpotential is observed (curve 5 in Fig. 1). This could be ascribed to the solubilization of the oxide layer in the presence of a high concentration of hydroxide ions, and the consequent decrease in the energy required for the reduction process.

It must be mentioned that in the presence of oxygen the cathodic part of the polarization curve changes and due to the reduction of O_2 on the $Zr–ZrO_2$ interface it becomes more or less irreproducible. Dissolved oxygen also affects the exchange current density as well as the open circuit potential.

Another surprising effect on the Zr/ZrO_2 electrode is the decrease of anodic current density with increase in the fluoride ion concentration in solution, as shown in Fig. 2 for the Zr wire electrode in acetate buffer. This phenomenon was observed in sulphuric acid, in the acetate, phosphate and borate buffers and in 0.1 M NaOH, and is in contrast to our expectations, in which the proportionality between anodic current and the concentration of fluoride ion is expected. It

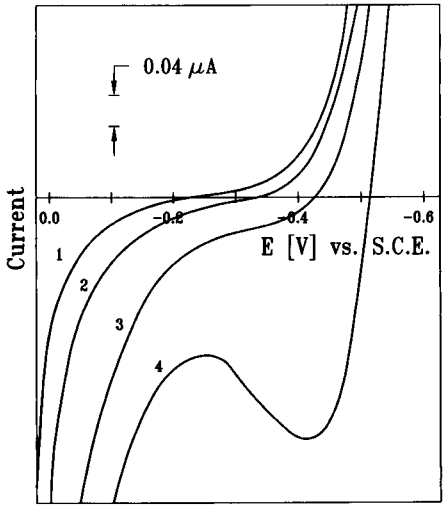

Fig. 3. Current-voltage curves of Zr electrode in 1 M HCl. Concentration of F^-: (1) 2.4×10^{-4}, (2) 2.6×10^{-4}, (3) 2.8×10^{-4} and (4) 3×10^{-4} M; scan rate 2 mV s^{-1}.

should be noted that this effect is observed only at low concentrations of fluoride ions, i.e. below 1×10^{-3} M. It seems that fluoride ions at low concentration promote the dissolution of the zirconium metal which leads to an increase in the ZrO_2 film thickness, and as a consequence there is a decrease in the mass transport of F^- ions through the porous oxide layer.

Quite a different situation appears in hydrochloric and perchloric acid media (Fig. 3). In these electrolytes a direct proportionality between fluoride ion concentration and anodic current density exists even at low concentration (1×10^{-5} M). As is evident from the shape and the position of the polarization curves shown in Fig. 3, with an increase in fluoride ion concentration the exchange current density increases and the corrosion potential (E at $i=0$) is shifted to more negative values. These facts could be exploited for the analytical determination of fluoride ions by amperometry or potentiometry.

ZrO_2 dissolution process

The response of the Zr electrode to fluoride ions in acid media indicates that the fluoride-induced Zr dissolution reaction is a complex process. Since at low pH values only a minor fraction of the total fluoride exists as free F^- species due to the protonation and association reactions (formation of HF and HF_2^-), there must be some other reactions influencing the anodic process. One of them could be the dissolution of the outer ZrO_2 layer by oxonium ions, as mentioned by El-Basiouny et al. [12]

$$ZrO_2\,(s) + H_3O^+ \rightleftharpoons H_2O + ZrOOH^+$$

In perchloric acid media colloidal zirconium-hydroxo perchlorates could be formed and thus the outer oxide film is decomposed. Diminution of the oxide layer thickness enables easier penetration of fluoride species through the inner compact layer, thus triggering the dissolution process. Since in acid media (bellow pH 3) HF is the predominant fluoride species, the solubilization of ZrO_2 should be based on the exchange reaction of HF in the porous layer according to one of the following reactions

$$ZrO_2 + HF \rightleftharpoons ZrO(OH)F + H^+$$

$$ZrOOH^+ + HF \rightleftharpoons ZrO(OH)F$$

At higher concentrations of fluoride, other species such as $ZrOF_2$, $ZrOHF_3$, as well as $ZrF_4,\ldots,ZrF_6^{3-}$, are also formed due to the very high stability of these zirconium fluoride complexes. Adsorption and incorporation of F^- ions into active sites of the ZrO_2 lattice leads to a higher population of structural defects in the inner passive film, and an increase of the rate of the dissolution or corrosion process of the metal.

To confirm the active role of fluoride ions in the dissolution process of the Zr electrode, a set of measurements at higher concentrations of fluoride ions was made. The zirconium rod electrode was exposed in deaerated electrolyte to fluoride ions at concentrations between 1×10^{-3} M and 0.1 M, and the open circuit (corrosion) potential, as well as the polarization resistance R_{pol} (measured at ±10 mV around the E_{oc} at a scan rate of 0.1 mV s^{-1}) was determined. Some results of these measurements are listed in Table 1. It is evident that fluoride ions in weak and strong acid media markedly affect both parameters. The corrosion potential is shifted to more negative values and the polarization resistance decreases when the fluoride concentration in-

creases. The shift of E_{oc} in the cathodic direction is more significant in acetate buffer media than in strong acid media, and the polarization resistance is decreased the most in perchloric acid media. Since the exchange current density (inversely proportional to R_{pol}) was also the highest in acid media at high concentration of F^- ions, it could be concluded that protons play a significant role in the dissolution rate of Zr metal in the presence of fluoride ions.

From the analytical point of view, according to the above cited properties of a Zr metal electrode, there exists the possibility for the amperometric and/or potentiometric determination of fluoride ions especially in aggresive acid media, where other sensors such as the fluoride ISE, and other methods (such as spectrophotometry) fail.

Dependence of E_{oc} on fluoride concentration

In Fig. 4 the dependence of the open circuit potential on the concentration of fluoride ions in 1 M $HClO_4$ and 0.1 M acetate buffer of pH 4.6 is shown. E_{oc} was measured in a stirred solution using the Zr foil electrode. The indicator electrode was polished, etched for 1 min in 0.1 M HF, and immediately after washing placed in the deaerated electrolyte. It is to be noted that in the absence of F^- ions and at its lowest concentration range the potential is shifted after each addition of fluoride to more negative values, and then moves slowly in the anodic direction (about 3 mV min^{-1} in acetate buffer), gradually approaching its limiting equilibrium value. This indicates that the ZrO_2 film is continuously regenerating. Therefore the potential was continuously recorded and when it became stable enough (drift of the signal < 0.5 mV min^{-1}) the value of E_{oc} shown in Fig. 4 was registered. The slope of E_{oc} dependence on the logarithm of fluoride concentration ($\delta E_{(oc)}/\delta \log(c_F)$) at low concentrations of fluoride is near to zero (Fig. 4).

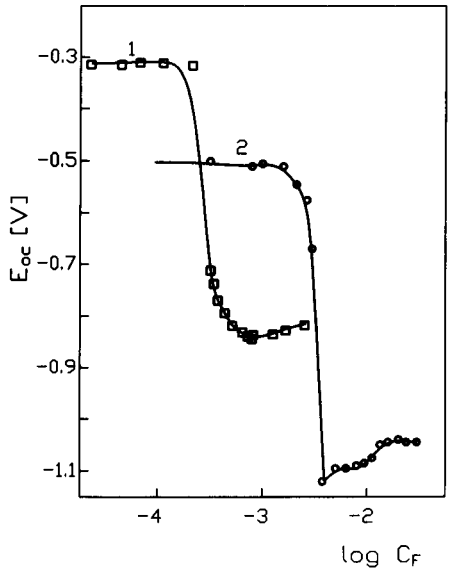

Fig. 4. Open circuit potential dependence of the Zr electrode on the concentration of F^- ions in (1) 1.0 M $HClO_4$ and (2) 0.1 M acetate buffer pH 4.6.

From the shape of the curves shown in Fig. 4 it can be seen that in both media a narrow "breakthrough" concentration range of fluoride exists, at which the ZrO_2 passivating layer could not be fully reconstituted, and E_{oc} rapidly becomes more negative. The transition region starts in perchloric acid at about one order of magnitude lower total concentration of fluoride ions (i.e. at about six orders of magnitude lower concentration of free F^- ions) than that in acetate buffer. Above this region E_{oc} is more or less stable and is slowly shifted in positive direction with the increase of the concentration of fluoride

TABLE 1

Corrosion potential and polarization resistance of a zirconium electrode in different media

Medium	$C(F^-)$ (mol/l)	E_{corr} (V)	R_{pol} (Ω cm^2)
0.1 M $HClO_4$	0	−0.036	–
0.1 M $HClO_4$	0.0033	−0.805	–
1 M $HClO_4$	0	−0.03	1900
1 M $HClO_4$	0.001	−0.565	192
1 M $HClO_4$	0.01	−0.677	3
0.1 M HCl	0	−0.405	–
0.1 M HCl	0.017	−0.881	1000
0.1 M acetate	0.0017	−0.938	3300
buffer (pH 3.6)	0.018	−1.035	330
0.5 M acetate	0	−0.600	–
buffer (pH 4.6)	0.0066	−1.074	–
0.5 M acetate	0.001	−1.138	650
buffer pH 4.6			

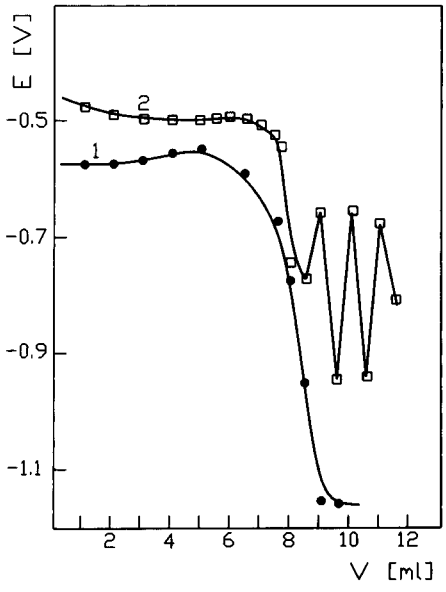

Fig. 5. Titrations of 50 ml 0.156 M $La(NO_3)_3$ with 0.100 M NaF in 0.1 M acetate buffer of pH 4.6; (1) deaerated solution, (2) in the presence of oxygen.

ions in solution. This stepwise change in E_{oc} indicates, that the mechanism of the electrode process at a low concentration of fluoride is different from that at high concentration.

From the nonlinear dependence of E_{oc} on the logarithm of the fluoride ion concentration, it could be concluded that the Zr electrode is an inconvenient sensor for the direct potentiometric determination of fluoride ion activity since its response is far from the Nernstian one. However, it was found that a Zr electrode could be successfully used in the potentiometric mode of operation as an indicator electrode in precipitation (Fig. 5) and complexometric titrations involving fluoride ions. In the absence of oxygen, the titration curve follows the characteristic stepwise dependence of the potential of the indicator electrode, and the end point could be adequately located. Line 2 in Fig. 5 represents the titration curve of lanthanum nitrate with fluoride in the presence of oxygen, and as can be seen, after the equivalence point the potential begins to oscillate, thus preventing a reliable location of the end point. The reason for the unstable potential originates from the slow time dependent transformation of zirconium oxofluoride species into hydrated ZrO_2 on the electrode surface. Dissolved oxygen therefore plays also a significant role in the overall transport of oxygen containing species to the Zr/ZrO_2 reaction zone.

It must be pointed out that a titration using a Zr indicator electrode, due to the large and sharp

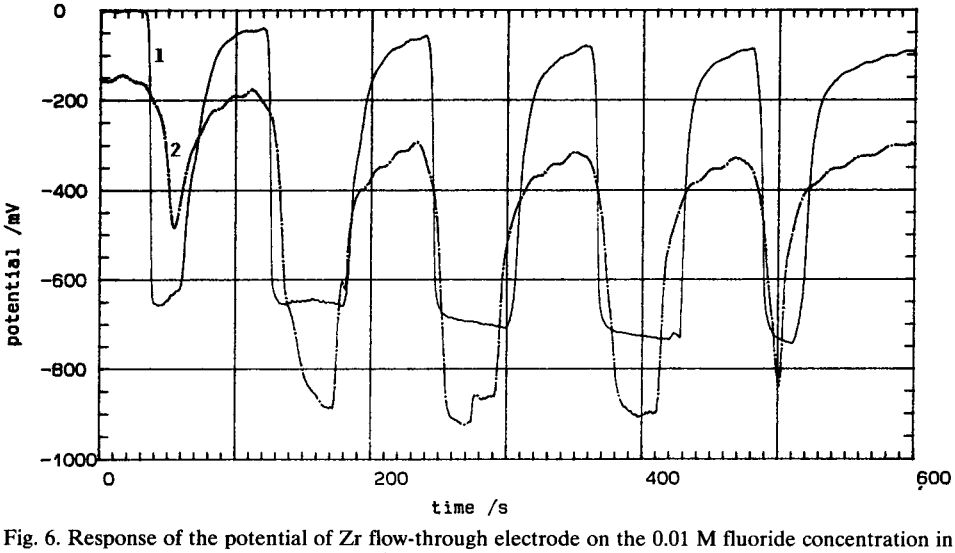

Fig. 6. Response of the potential of Zr flow-through electrode on the 0.01 M fluoride concentration in (1) 0.1 M $HClO_4$ and (2) 0.5 M acetate buffer; flow rate 1.5 ml min^{-1}.

potential step around the equivalence point, gives equally or even more accurate results than a titration using an F^- ISE. Since the manufacture of such a Zr electrode is very easy and inexpensive, in our opinion it could be successfully applied instead of an ISE, especially in acid media.

In Fig. 6 the dynamic response of the Zr electrode potential on the fluoride is shown. For these experiments a thin-layer cell, described below was used, and a 0.01 M concentration of fluoride was periodically aspirated through the cell. It is evident that in perchloric acid media the response of the electrode is much faster than in acetate buffer. This confirms the statements that the thickness of the passive ZrO_2 layer determines the overall rate of the electrochemical dissolution process.

Amperometric response of Zr electrode

The proportionality between the anodic current density and the fluoride ion concentration could be exploited also for the amperometric detection of fluoride. For the continuous and injection mode of operation a thin-layer flow-through cell, schematically shown in Fig. 7, was set up. The potential of the Zr indicator electrode was kept at constant potential (close to the E_{oc}, see Table 1) by means of the potentiostat, and the current flowing through the cell was continuously registered. The volume flow of deaerated carrier solution through the system was controlled by the peristaltic pump, and the fluoride solution was periodically aspirated or injected directly (sample volume 20 μl) into the stream as shown in Fig. 7. In acetate and other buffer solutions of higher pH, the base line was unstable and the response time depended on the F^- ion concentration level. The reason for these artifacts in our opinion originates in the continuous regeneration of the oxide layer after each perturbation caused by injection of F^- into the electrolyte stream. The growing layer of ZrO_2 also affects the sensitivity, which increases markedly when a breakthrough in the outer layer is achieved, and then falls rapidly when no or only a low amount of fluoride was injected.

The best results were obtained in an 0.1 M or 1 M $HClO_4$ carrier solution since the electrode is

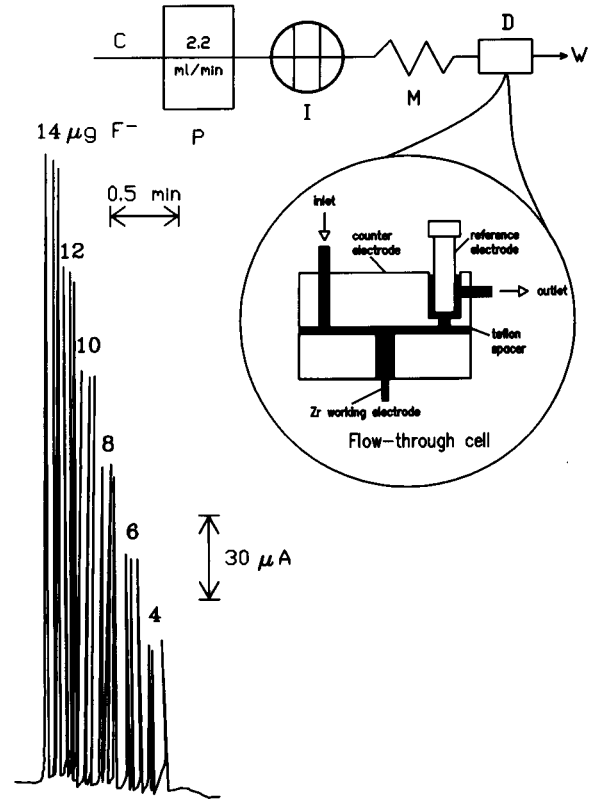

Fig. 7. Scheme of the flow-injection system, zirconium flow-through electrode and its amperometric response. C, 1 M $HClO_4$ carrier solution; P, peristaltic pump; I, injector; M, PTFE mixing coil (50 cm×0.5 mm i.d.); D, amperometric detector; W, waste; potential of Zr electrode −0.5 V vs. SCE.

much better conditioned in acid media, as is evident from its fast response to fluoride ions shown in Fig. 6 and Fig. 7. The response is instantaneous and the current (charge) is directly proportional to the amount of F^- injected. In 1 M $HClO_4$ carrier solution a detection limit of 1×10^{-9} mol of F^- is achieved. This mode of operation should be recommended for the determination of fluoride in samples where direct measurements with a F^- ISE is impossible, e.g. in silicon etching solvents (composed of HF, HNO_3 and H_3PO_4) etc. The most important advantage of a flow-through cell is its capability for continuous monitoring of fluoride, i.e. simple automatization of the measurements at such particular conditions.

REFERENCES

1 M.S. Frant and J.W. Ross, Jr., Science, 154 (1966) 1553.
2 T.A. Fjeldy and K. Nagy, J. Electrochem. Soc., 127 (1980) 1299.
3 J.W. Bixler and L. Solomon, Anal. Chem., 56 (1984) 3004.
4 J. Komljenović, S. Krka and N. Radić, Anal. Chem., 58 (1986) 2893.
5 S. Megregian, Anal. Chem., 29 (1957) 1063.
6 N. Baker and J. Morrison, Anal. Chem., 27 (1955) 1307.
7 P. Deschamps and Y. Bonnaire, Anal. Chim. Acta, 50 (1970) 117.
8 M.J. Madou and K. Kinoshita, Electrochim. Acta, 29 (1984) 411.
9 T.S. Light and K.S. Fletcher, Anal. Chim. Acta, 175 (1985) 117.
10 J.V. Dobson, T. Dickinson and P.R. Snodin, J. Electroanal. Chem., 69 (1976) 215.
11 I. Gardiazabal, R. Schrebler and R. Cordova, J. Electroanal. Chem., 119 (1981) 119.
12 M.S. El-Basiouny, A.A. Mazhar, F. El-Taib Heakal and M.A. Ameer, J. Electroanal. Chem., 147 (1983) 181.
13 J.S.L. Leach and B.R. Pearson, Electrochim. Acta, 29 (1984) 1271.
14 J.S.L. Leach and C.N. Panagopoulos, Electrochim. Acta, 31 (1986) 1577.

Analytica Chimica Acta, 273 (1993) 275–287
Elsevier Science Publishers B.V., Amsterdam

Stripping voltammetry of heavy-metal–(bio)polyelectrolyte complexes

Part 1. Influence of supporting electrolyte

Marc A.G.T. van den Hoop [1] and Herman P. van Leeuwen

Department of Physical and Colloid Chemistry, Wageningen Agricultural University, Wageningen (Netherlands)

(Received 1st July 1992)

Abstract

The association of the heavy metals zinc(II) and cadmium(II) with three commercial humic acid samples has been studied by differential pulse anodic stripping voltammetry for various concentrations of supporting electrolyte. Under the experimental conditions employed, the heavy-metal–humate complexes have been found to be voltammetrically labile over the whole range of metal-to-ligand ratios. Hence, the stability (K) of the complex could be computed taking into account the difference between the diffusion coefficients of the free and the bound metal. The dependence of K on the concentration of supporting electrolyte is of comparable extent for the various metal–humate complexes, but significantly smaller than in the case of the highly charged linear polyelectrolyte poly(methacrylic acid). From this dependency, the competition between monovalent and divalent counterions has been quantified.

Keywords: Anodic stripping voltammetry; Differential-pulse voltammetry; Heavy metals; Humic acids; Polyelectrolytes

Knowledge of the distribution of heavy metals over different physico-chemical forms (metal speciation) is essential to the understanding of many practical properties of natural water systems. The main fraction of natural organic matter, i.e. fulvic and humic substances, is one of the major complexants of metals [1] and plays an important role in their circulation in aquatic systems [2]. Humic and fulvic acids have many functional groups, predominantly carboxylic and phenolic hydroxylic, which are subject to dissociation. Hence these polyacids are generally charged and therefore they are often referred to as (bio)polyelectrolytes.

The association of divalent (heavy) metals with polyelectrolytes is in several ways affected by the presence of monovalent counterions. First, in the case of a large excess of monovalent over divalent counterions, the former ions are mainly responsible for the ionic strength. Hence, they control the magnitude of the Debye–Hückel screening length and thus the resulting effective charge density of the polyelectrolyte. Secondly, due to the electrostatic interaction of monovalent counterions with the polyion, they may compete with divalent counterions and affect the speciation patterns of the metals involved. In natural systems, for example estuaria, where fresh and salt water get mixed, these effects may play an important role in the

Correspondence to: M.A.G.T. van den Hoop, Department of Physical and Colloid Chemistry, Wageningen Agricultural University, Dreijenplein 6, 6703 HB Wageningen (Netherlands).

[1] Present Address: Laboratory for Ecotoxicology, National Institute of Public Health and Environmental Protection, P.O. Box 1, 3720 BA Bilthoven (Netherlands).

distribution of heavy metals over free and bound states.

Voltammetric methods have become quite popular in studying the association of heavy metals with complexing agents in natural waters. This is mainly due to their high sensitivity and the possibility of direct speciation. Furthermore, these electroanalytical techniques allow the use of a wide range of supporting electrolyte concentrations. The interpretation of the voltammetric response of natural samples may be complicated due to (i) the kinetics of the complex association/dissociation reactions involved, (ii) differences between the diffusion coefficients of the free and the bound metal, (iii) possible effects of adsorption of the ligand and the complex at the surface of the electrode and (iv) chemical heterogeneity of the metal-complex system. As a consequence of the large increase in interest from the environmental and ecotoxicological points of view, these aspects nowadays receive attention in theoretical studies [e.g., 3–5]. For example, in the case of simultaneously diffusing metal species with different mobilities, a rigourous treatment, valid for any set of rate constants and diffusion coefficients for the case of ligand excess, has been recently developed [3].

In the case of stripping voltammetry (SV), the mass transport conditions are generally less well-defined than in a dynamic diffusion-controlled direct voltammetric experiment. With labile complex systems, the speciation essentially runs through the analysis of the overall mean diffusion coefficient ($\overline{D}$) of the complex system. In SV the relationship between the response and the diffusion coefficient is not exactly known and it has been proposed to fit the experimental data, obtained under different metal-to-ligand ratios, to the best possible relation with $\overline{D}$ to some power. This semi-empirical procedure has been shown to work satisfactorily well for a number of labile systems [6,7].

The aim of the present paper is to extend our systematic SV study of heavy-metal–polyelectrolyte complexes to systems of natural origin under conditions of different concentrations of supporting electrolyte. We have selected three commercial humic acid samples and studied their complexation characteristics with the heavy metals zinc(II) and cadmium(II) by differential pulse anodic stripping voltammetry (DPASV) in the presence of different concentrations potassium nitrate at a metal concentration level of 10^{-6} mol l^{-1}. The degree of neutralization has been kept constant at 0.8. The results are compared with those for the well-defined linear polyelectrolyte poly(methacrylic acid).

THEORY

In the case of a reversible electrode reaction, the mass transport of metal ions from the bulk solution to the electrode surface characterizes the voltammetric conditions. The simplest complexation scheme in which an electroactive metal ion (denoted as M; charge omitted for simplicity) associates with a ligand or site (L) to form an electroinactive complex (ML) can be presented as

$$\begin{array}{ccc} \mathrm{M} + \mathrm{L} & \underset{k_a}{\overset{k_d}{\rightleftharpoons}} & \mathrm{ML} \\ \Big\uparrow\Big\downarrow ne^- & & \\ \mathrm{M}^0 & & \end{array} \qquad (1)$$

In this complexation scheme, M^0 denotes the metal atom and k_a and k_d are the association and dissociation rate constants, respectively. The complexation equilibrium in the bulk is expressed by the stability K:

$$K = \frac{c^*_{ML}}{c^*_M c^*_L} \qquad (2)$$

where c^*_M, c^*_L and c^*_{ML} denote the bulk concentrations of M, L and ML, respectively. When a large excess of ligand is present [$c^*_L \gg c^*_T (= c^*_M + c^*_{ML})$], the association becomes quasi-monomolecular with a rate constant

$$k'_a = k_a c^*_L \qquad (3)$$

The corresponding stability K' is then the ratio between bound and free metal:

$$K' = \frac{k'_a}{k_d} = \frac{c^*_{ML}}{c^*_M} \qquad (4)$$

The stability can only be obtained from the complexation curve (i.e. the voltammetric response of a metal ion solution as a function of the ligand concentration) under certain conditions. First, the system must be voltammetrically labile. This means that (i) the kinetics of the association/dissociation reactions 1 must be sufficiently fast to maintain equilibrium for any relevant value of the space and time coordinates and (ii) the voltammetric response has to be purely controlled by diffusion. Secondly, there must be a large excess of the complexing agent over the metal. Then, a constant ratio between bound and free metal is achieved over the whole voltammetric diffusion layer. This is necessary to ensure a constant effective diffusion coefficient from the surface of the electrode to the bulk of the solution.

In the dynamic case, the lability criterion for a complexing system with an excess of ligand is given by [3]

$$\frac{k_d^{1/2}\epsilon^{-1/2}(\epsilon^{-1}+K')t^{1/2}}{K'(1+K')^{1/2}} \gg 1 \qquad (5)$$

where ϵ is D_{ML}/D_M (D being the diffusion coefficient) and t is the effective time of the experiment. Equation 5 expresses that the lability of the complex decreases with increasing K at equal effective times of the dynamic experiment, and, hence, the voltammetric conditions have to be changed to obey lability. If the condition in Eqn. 5 is not fulfilled, kinetic effects of the metal-complex system may play a (crucial) role. Then analysis of the voltammetric response becomes quite involved [3]. In the case the I.h.s. of Eqn. 5 becomes $\ll 1$, the system is referred to as non-labile. Under non-labile conditions, the voltammetric response will be purely controlled by the kinetics of the system.

On the same basis, a lability criterion can be derived for the steady-state situation that holds for the usual stripping conditions. The expression parallel to Eqn. 5 is [8,9]

$$\frac{k_d^{1/2}\delta}{D_M^{1/2}K'^{1/2}} \gg 1 \qquad (6)$$

where δ is the thickness of the diffusion layer, which is a function of D_{ML}. In the case of a rotating-disk electrode (RDE) and under conditions that $\epsilon K' \gg 1$, the Levich equation [10] can be used:

$$\delta = 1.61 D_{ML}^{1/3}\omega^{-1/2}\nu^{1/6} \qquad (7)$$

where ω is the angular rotation frequency and ν the kinematic viscosity of the solution. From a theoretical point of view, the planar electrodes (solid or with a thin film of mercury) are preferable to mercury drop electrodes, due to the known hydrodynamic conditions and favourable volume/area ratios. On the other hand, the surface reproducibility is much better for the latter. In this study, we have used the hanging mercury drop electrode (HMDE), and hence we are only able to obtain some estimate of δ (since the relationship between δ and D_{ML} is uncertain).

Voltammetric response

Since the relationship between the voltammetric current and the mass transport properties under stripping voltammetric conditions are not yet well established, it is practically useful to fit the experimentally obtained response to some postulated functionality with respect to the mean diffusion coefficient ($\bar{D}$). Hence, for a labile metal complex system, the pre-electrolysis current (I_e) can be written as

$$I_e \propto \bar{D}^p c_T^* \qquad (8)$$

with

$$\bar{D} = (c_M^*/c_T^*)D_M + (c_{ML}^*/c_T^*)D_{ML} \qquad (9)$$

which actually incorporates the speciation over M and ML. The power p is related to the nature of the mass transport during the pre-electrolysis step. For example, it is 1/2 for semi-infinite linear diffusion and 2/3 for laminar convective diffusion (cf. Eqns. 5 and 6, respectively). For stripping voltammetries the value of p varies with geometrical conditions and the mode of stirring. Usually p is found to be between 1/2 and 2/3 [6]. The concentration of metal in the mercury drop, which is linearly proportional to the reoxi-

dation peak current (I), will be proportional to the pre-electrolysis current and time (t_e):

$$I_e t_e \propto c_{M^0} \propto I \tag{10}$$

Let us define Φ as the ratio between the reoxidation peak current for the complex system and the reoxidation peak current under conditions of no complexation. Combination of Eqns. 2, 8, 9 and 10 then gives

$$\Phi(c_L^*) = \left(\frac{\overline{D}}{D_M}\right)^p = \left(\frac{1+\epsilon K c_L^*}{1+K c_L^*}\right)^p \tag{11}$$

Equation 11 reflects that Φ will decrease with increasing ligand concentration due to increase in K'. It can be mathematically derived that Φ is most sensitive to K if $Kc_L^* \approx 1$ [7]. This implies that the application of the experimental procedure largely depends on the analytically feasible ranges of the concentration of the ligand involved. From Eqn. 11 it is immediately clear that for $Kc_L^* \gg 1$, Φ approaches the limit ϵ^p:

$$\Phi(c_L^*) = \lim_{c_L^* \to \infty} \left(\frac{1+\epsilon K c_L^*}{1+K c_L^*}\right)^p = \epsilon^p \tag{12}$$

Potential shift

In case of a labile complex system, with $\overline{D}$ as the mean diffusion coefficient of the complete set of labile species, the characteristic potential of the metal ion (E_{peak}) will decrease with increasing ligand concentration. The potential shift, ΔE_{peak}, can be related to the stability K [5]

$$(nF/RT)\ \Delta E_{peak} = -\ln\left(\overline{D}/D_M\right)^p - \ln(Kc_L^*) \tag{13}$$

which is the classical DeFord–Hume equation [11], valid in the case of a large excess of ligand over $[M^0]$. In Eqn. 13, n is the number of electrons in the charge-transfer reaction, F the Faraday constant, R the gas constant and T the absolute temperature.

Influence of supporting electrolyte

With respect to the influence of supporting electrolyte on the stability of heavy-metal-polyelectrolyte systems, it is useful to consider first the experimental range of application of stripping voltammetric analysis of these complex systems. Let us therefore recall the condition that, for the present approach, there must be a large excess of complexing agent over the metal, hence $c_L^* \gg c_M^*$. Furthermore, to avoid conductive effects, i.e., to render the transport number of the electroactive species negligibly small, a large excess of supporting electrolyte (in the present study KNO_3) should be added to the system and thus $c_{KNO_3}^* \gg c_M^*$. Finally, in order to exclude possible diffuse double layer effects and to make the ionic strength dependent on $c_{KNO_3}^*$ only, it is necessary that $c_L^* \ll c_{KNO_3}^*$. Typically one therefore has in voltammetric analysis

$$c_{KNO_3}^* \gg c_L^* \gg c_M^* \tag{14}$$

It should be mentioned that for the present study, where [M(II)] is 10^{-6} mol l^{-1} with conditions of a 10–100-fold excess of L over M(II) and a 10–100-fold excess of K^+ over L, it is still possible to study the metal–polyanion interaction over an ionic strength range of some three decades (i.e., from 10^{-3} to 1 mol l^{-1}).

At this point it is useful to consider the dependency of the stability K with respect to the concentration of supporting electrolyte. It has been shown to be necessary to rewrite the association reaction of divalent cations with the polyanion system (reaction 1) by including monovalent counterions [12]:

$$M(II) + K_sL \leftrightarrows M(II)K_{s-\nu}L + \nu K^+ \tag{15}$$

where the subscript s refers to the initial fraction of bound monovalent counterions and ν is the K^+/M(II) exchange ratio. The thermodynamic equilibrium constant K_{th} for the exchange reaction (15) is

$$K_{th} = \frac{a_{M(II)K_{s-\nu}L} a_{K^+}^{\nu}}{a_{M(II)} a_{K_sL}} \tag{16}$$

where a refers to the activity. As long as the concentration of supporting electrolyte is much larger than the concentration of ligand and metal, i.e. when condition 14 obeyed, a_{K^+} is a constant over a whole complexation curve. This condition

is obeyed for all experimental data presented. Hence, it is allowed to rewrite Eqn. 16 into

$$K_c = f(\gamma)K = \frac{a_{ML}}{a_M a_L} = K_{th}\frac{1}{a_{K^+}^{\nu}} \quad (17)$$

where K_c refers to the stability corrected for activity effects and $f(\gamma)$ is some function of activity coefficients. Under the present conditions of large excess of ligand over metal, the degree of coverage, i.e. the number of apparently bound metal ions per charged group on the polyanion, will be very small. Hence, it is assumed that the activity correction is equal for both the complex and the ligand and therefore cancels from Eqn. 17. The remaining activity correction for the heavy metal ion can then be calculated by using expressions for mixtures of electrolytes [e.g., 13].

EXPERIMENTAL

Materials

The humic acids (HA) were commercial samples from Fluka (lot/product number 35069 288/53680), Aldrich (7901816/H1,675-2) and Roth (0411737/7821) and used after pretreatment as described by Van den Hoop et al. [14]. The poly(methacrylic acid) (PMA) solutions, with an average molar mass of 26 000 $gmol^{-1}$, were obtained from BDH, and used without further pretreatment. Concentrations of complexing groups were determined by conductometric titration with hydroxide. Stock solutions were stored in the dark at 4°C to avoid biodegradation. Titrisol potassium hydroxide solutions, potassium nitrate (both from Merck) and nitric acid solutions (Baker) were of analytical-reagent grade. Stock metal standards of 10^{-4} mol l^{-1} for each solution of Cd, Pb and Zn (as nitrates) were prepared by diluting BDH 1000 mg l^{-1} AAS standards. All solutions were prepared using demineralized tap water, produced by a Millipore Super-Q reverse-osmosis system.

Equipment

Voltammograms were obtained using a Metrohm 663 VA stand controlled by a home-made "Quick Step" polarograph attached to a Hewlett-Packard 3497A data acquisition unit and a Hewlett-Packard 85B programmer. The system was also connected to a Metrohm 665 Dosimat for the automatic addition of polyacid solutions and to a Knick Multi-Calimatic pH meter for the pH measurement after each addition. In all cases, working, reference and counter electrodes were HMDE, Ag/AgCl, KCl_{sat} and glassy carbon, respectively. The voltammetric vessel was made of polystyrene. The pulse duration was 25 ms and the pulse height was 50 mV. For the zinc(II) and cadmium(II) systems, the deposition potentials were −1150 and −850 mV, respectively. The pre-electrolysis time and the rest period observed were 2 and 0.5 min, respectively. The scan rate in the stripping step was 4 mV s^{-1}. Purified nitrogen was used for deaeration and blanketing of the sample solutions. The experiments were carried out at 25°C.

Experimental procedure

We will use the procedure recently proposed by Díaz et al. [15], which incorporates the effects of possible losses of metal due to adsorption onto cell material and the protolytic effects in stripping voltammetric titrations of metal–polyacid complexes. The experimental procedure is based on adding the ligand solution to the solution of the metal. The concentration levels should be such that the measured values for Φ all refer to excess ligand while the region $Kc_L^* \approx 1$ is sufficiently covered. In this way, the voltammetric response can be analysed according to Eqn. 12. The total metal concentration should therefore be kept constant over the whole complexation curve. Unavoidable dilution resulting from addition of the ligand solution is accounted for.

(1) The polystyrene vessel and the electrodes are held in contact with a 1 mol l^{-1} nitric acid solution for several hours, in order to desorb all possible adsorbed metal ions.

(2) The metal ion solution, prepared at pH ranging between 3.5 and 4.5, and with a fixed KNO_3 concentration, is placed into the vessel and, after degassing, some voltammetric responses are recorded to establish the blank value and its reproducibility.

(3) The pH is set (by KOH or HNO_3 addition) close to the expected pH of the titration (usually very similar to the pH of the titrant polyacid solution). Then, some voltammetric measurements are done again till the signal becomes reproducible. At this point, the peak potential should coincide with that obtained in step 2 (if not, undesired phenomena such as hydrolysis could be involved). If the currents obtained in step 2 and 3 are equal, adsorption onto the cell material is absent or negligible and the experiment can continue. If the current obtained in step 3 is smaller than in step 2, adsorption onto the cell can be involved.

(4) After each addition of the complexing agent and degassing the solution for at least 1 min, the voltammetric response will be recorded.

(5) To check if the degree of dissociation (α_d) remains constant over the whole complexation curve, pH measurements are performed after each addition. Then, Eqn. 18 is applied to calculate α_d [15]:

$$\alpha_d = \alpha_n + (H^+ - K_w/H^+ + K_w/H_0^+)/c_c \qquad (18)$$

If α_d remains constant, results are valid. If not, the titration must be repeated at a more convenient pH value.

(6) In obtaining the stability of the complex by Eqns. 12 and 13, the intensity and the peak potential values of the heavy metal blank solutions found in step 3, respectively, have to be used.

Fitting procedure

In order to fit the experimental results to theoretical predictions from Eqn. 11, a FORTRAN program was developed. A basic element of the program is the subroutine ZXMIN, taken from the IMSL library [16].

RESULTS AND DISCUSSION

Voltammetric response

In Fig. 1, three sets of differential pulse anodic stripping voltammograms of 10^{-6} mol l^{-1} Zn(II), Cd(II) and Pb(II) are presented for various points along the experimental complexation procedure.

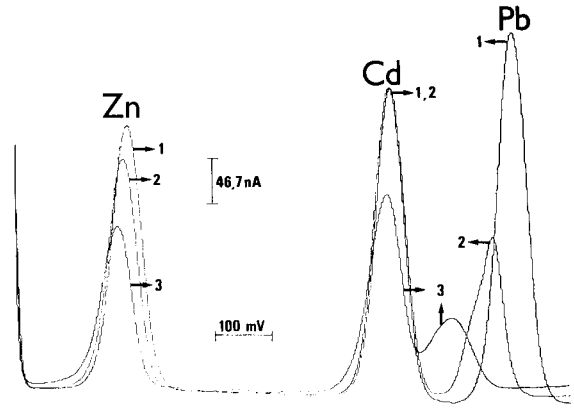

Fig. 1. Differential pulse anodic stripping voltammograms of Zn(II), Cd(II) and Pb(II) for several steps of the experimental procedure. $[M(II)] = 10^{-6}$ mol l^{-1}; $[KNO_3] = 0.03$ mol l^{-1}; $t_e = 1$ min; $V_{scan} = 2.5$ mV s^{-1}. Series 1: pH = 3.75; Series 2: pH = 7.40; Series 3: [Fluka HA] = 10^{-4} mol l^{-1}; $\alpha_n = 0.8$. For further explanation see text.

Series 1 represents step 2 of the experimental procedure and shows the voltammetric responses for the initial metal ion solution at pH = 3.8 and $[KNO_3] = 0.03$ mol l^{-1}. Regular shapes are obtained with $W_{1/2} \approx 60$ mV indicating the reversibility of the electrode process. For the second series the pH was set close to the pH of the Fluka HA solution at $\alpha_n = 0.8$ by adding a small aliquot of KOH (step 3). The resulting pH was 7.4. Except for the Cd(II) peak, the voltammetric responses of both Zn(II) and Pb(II) decrease. The current decrease of the former metal has to be interpreted as a loss of free metal ions due to adsorption onto the cell material [17]. In the case of Pb(II), the potential shift is significant indicating some accompanying complexation, probably with hydroxide. Furthermore, the shape of the voltammogram is seriously affected and hence, the analysis of complexation curves of Pb(II) under these conditions should be done with care. For this reason, we will consider in this study only the Zn(II) and Cd(II)–humate complex systems taking into account the proper procedure to eliminate effects of adsorption. Finally, the addition of Fluka HA results in a decrease in all voltammetric responses due to the association of the heavy metals with the humate polyanion (series 3, step 4). The concentration of the Fluka HA

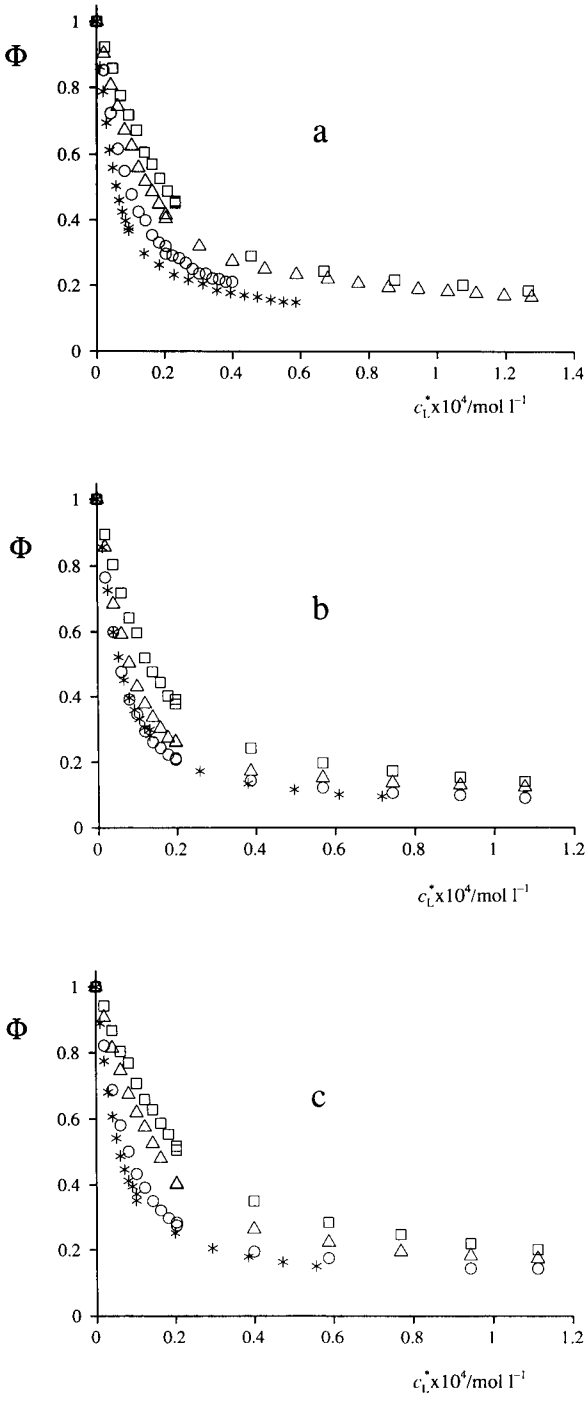

Fig. 2. Stripping voltammetric complexation curves for various Zn(II)–humate systems for different KNO_3 concentrations. [Zn(II)] = 10^{-6} mol l^{-1}; α_n = 0.8. (a) Fluka HA, (b) Aldrich HA and (c) Roth HA. [KNO_3] = (□) 0.1 mol l^{-1}, (△) 0.03 mol l^{-1}, (○) 0.01 mol l^{-1}, (*) 0.003 mol l^{-1}.

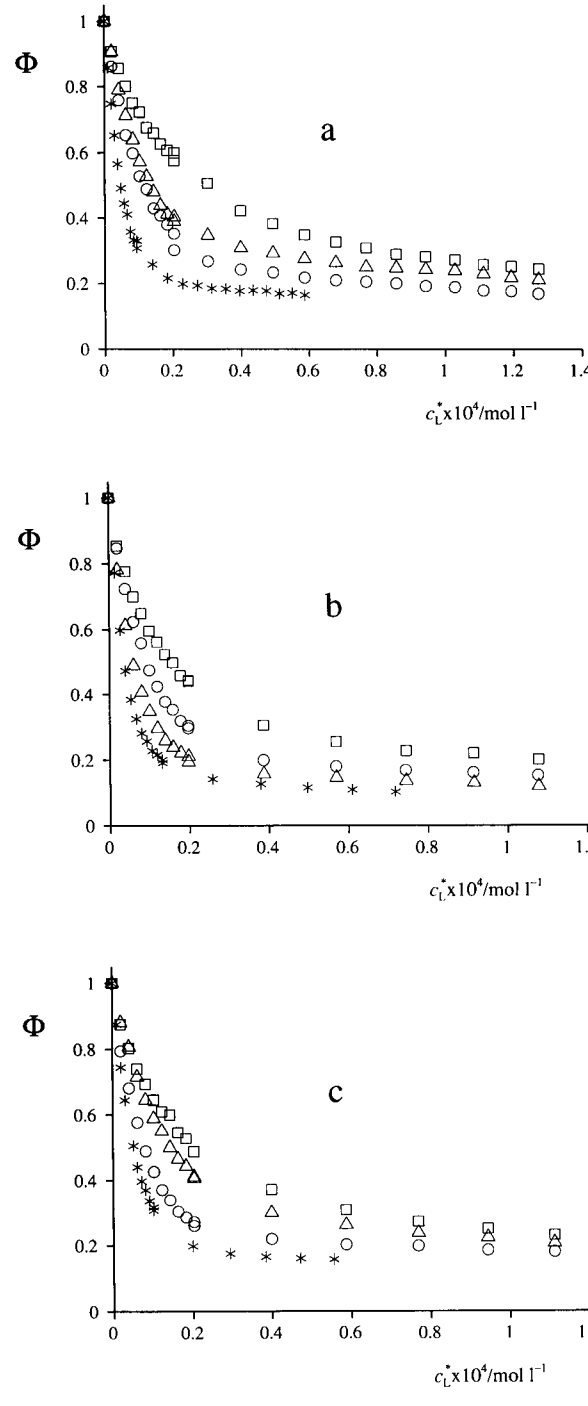

Fig. 3. Stripping voltammetric complexation curves for various Cd(II)–humate systems for different KNO_3 concentrations. [Cd(II)] = 10^{-6} mol l^{-1}; α_n = 0.8. (a) Fluka HA, (b) Aldrich HA and (c) Roth HA. [KNO_3] = (□) 0.1 mol l^{-1}, (△) 0.03 mol l^{-1}, (○) 0.01 mol l^{-1}, (*) 0.003 mol l^{-1}.

equalled 10^{-5} mol l^{-1} (i.e., the volume concentration of deprotonated groups on the HA molecules). According to Eqn. 11, a larger decrease of the peak current at the same Fluka HA concentration indicates a higher stability (K) of the heavy metal–Fluka HA complex involved.

For various Zn(II)–humate and Cd(II)–humate systems, complexation curves are presented for different concentrations of KNO_3 with $\alpha_n = 0.8$ at a metal ion concentration of 10^{-6} mol l^{-1} in Figs. 2a–c and 3a–c, respectively. The subscripts a, b, and c refer to the Fluka, Aldrich and Roth HA samples, respectively. Due to the association of Zn(II) or Cd(II) with the humate polyanion, Φ decreases and reaches a certain plateau value with ever increasing excess of ligand. The latter observation is a clear indication of lability of the metal-complex system on the effective time scale of the stripping voltammetric experiment. In the case of non-lability, Φ would decrease to zero. A second indication of lability of the metal complexes involved is shown by the systematic shift of the peak potential for a sufficiently large excess of ligands (see below). From these results it can be concluded that the Zn(II)–humate and Cd(II)–humate systems are voltammetrically labile under the DPASV conditions employed. Hence, the complexation curves can now be analysed in terms of a stability constant according to Eqn. 11.

In Table 1, the resulting values for the stability K and the diffusion coefficient ratios ϵ are presented for the Zn(II)–humate and Cd(II)–humate complexes studied for $\alpha_n = 0.8$ using $p = 2/3$ in the fitting procedure. The qualities of the fit are given by the values of the correlation coefficient r^2, which are quite satisfying. It should be mentioned that, as a consequence of the uncertainties in the mass transport conditions during the preelectrolysis period, the exact value of p is unknown. However, using $p = 1/2$ the value of the stability is affected by only 0.1 log units (i.e. within the order of the experimental error), which is in agreement with the results of the labile Zn(II)–poly(acrylic acid) system [7].

In this study, we have not used a fixed value of ϵ. The reason for this is two-fold. Some of the complexation curves have not yet reached a con-

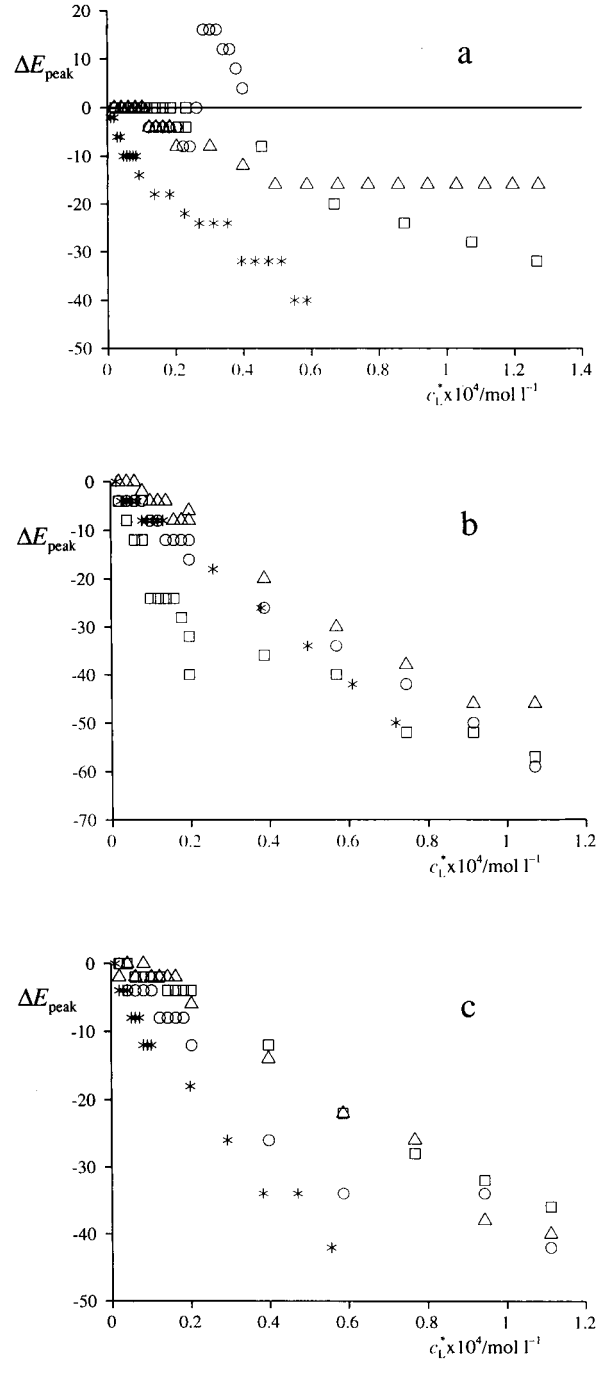

Fig. 4. The shift of the peak potential as a function of ligand concentration for various Zn(II)–humate systems for different KNO_3 concentrations. [Zn(II)] = 10^{-6} mol l^{-1}; $\alpha_n = 0.8$. (a) Fluka HA, (b) Aldrich HA and (c) Roth HA. [KNO_3] = (□) 0.01 mol l^{-1}, (△) 0.03 mol l^{-1}, (○) 0.01 mol l^{-1}, (*) 0.003 mol l^{-1}.

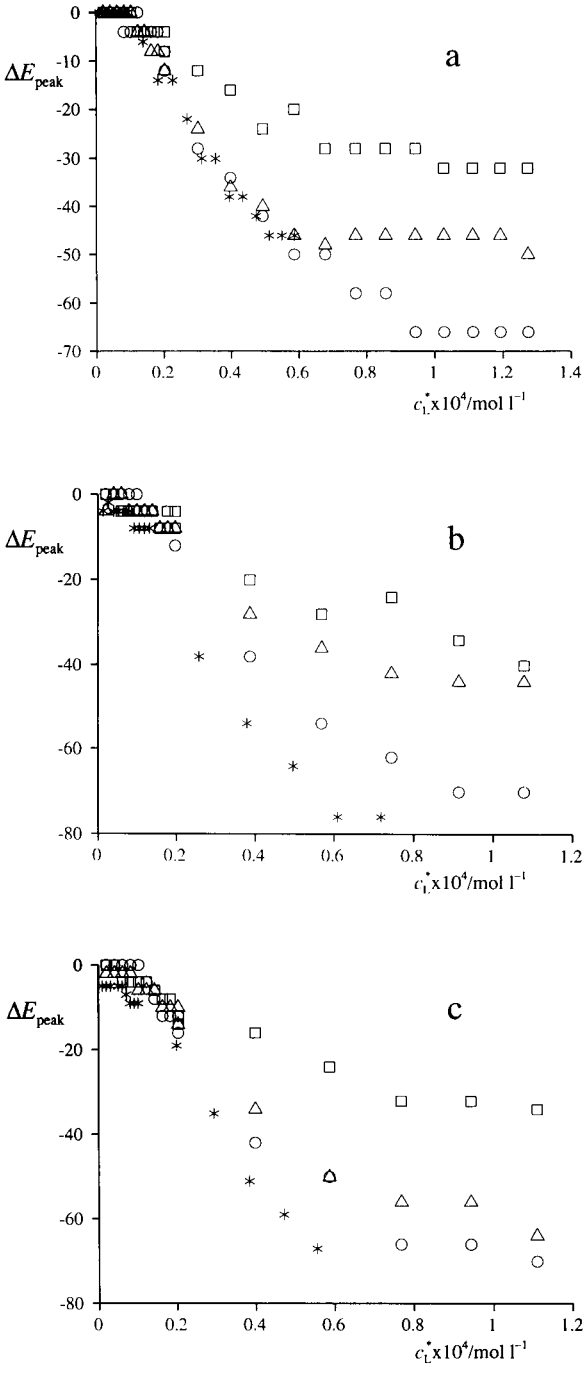

Fig. 5. The shift of the peak potential as a function of ligand concentration for various Cd(II)–humate systems for different KNO_3 concentrations. [Cd(II)] = 10^{-6} mol l^{-1}; $\alpha_n = 0.8$. (a) Fluka HA, (b) Aldrich HA and (c) Roth HA. [KNO_3] = (□) 0.1 mol l^{-1}, (△) 0.03 mol l^{-1}, (○) 0.01 mol l^{-1}, (*) 0.003 mol l^{-1}.

stant limit and thus, estimations of ϵ according to Eqn. 12 are not allowed. Secondly, the diffusion coefficient of the complex may be dependent on the salt concentration as has been shown for Aldrich HA by measuring external mass transfer coefficients [18]. The results in Table 1 show that ϵ tends to go to too small values for the Zn(II)–humate complexes, probably due to the fact that Φ does not yet reach a more or less constant value at the end of the complexation curve. For the Cd(II)–humate complexes, realistic ϵ values are obtained which are in agreement with literature data [19]. However, as compared to the data of Cornel et al. [18], no relationship between ϵ and [KNO_3] is observed. This might be due to the physico chemical complexity of the humate polyanions involved and the relative insensitivity of the procedure for the value of ϵ.

For each type of humate polyanion, the binding of the Zn(II) and Cd(II) ions is approximately equally strong. This is in agreement with the results of Cleven [19]. He studied the association of several heavy metals [Zn(II), Cd(II) and Pb(II)] with the Fluka HA sample as a function of the charge density on the humate polyanion by varying the degree of neutralization (α_n) for [KNO_3] = 0.05 mol l^{-1}. In this polarographic study, comparable stabilities have been observed for the Zn(II)–humate and Cd(II)–humate sample in the range of $0.2 \leq \alpha_n \leq 0.8$, whereas the stability of the Pb(II)–humate complex was significant larger (in the order of two log units) over the whole α_n range employed. On the other hand, Saha et al. [20] have observed a significant difference between the stabilities of the Zn(II)–Fluka humate and the Cd(II)–Fluka humate complex for [KNO_3] = 0.1 mol l^{-1}; the difference increased with increasing pH of the sample solution. These properties might be due to the heterogeneity of the humic acid samples as a consequence of their origin and the kind of pretreatment procedure of the humic acid sample employed (if any).

From Table 1, it can be seen that the stability of the heavy-metal–humate complex decreases with increasing KNO_3 concentration, due to the reduction of the electrostatic component of the metal–polyion interaction. This is the general observation for polyelectrolytic systems with high

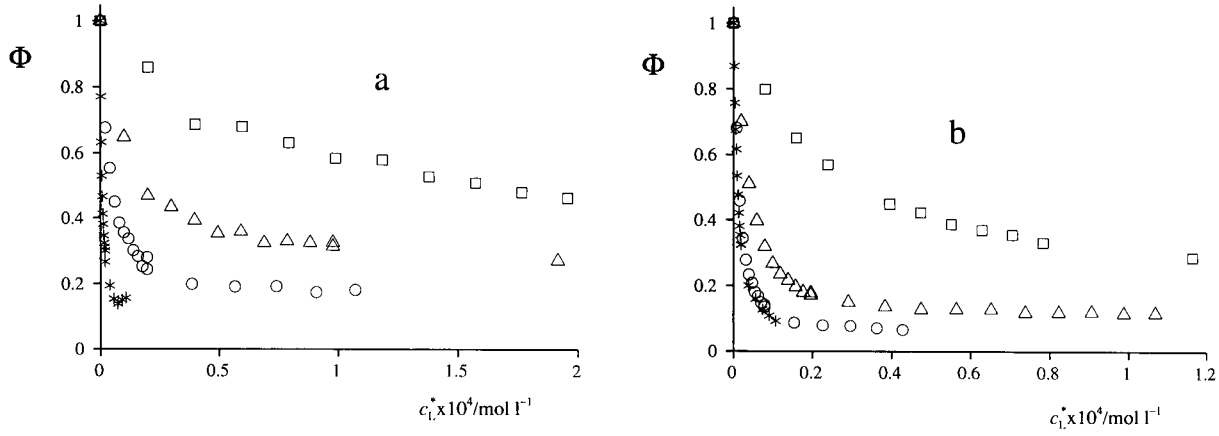

Fig. 6. Stripping voltammetric complexation curves for the (a) Zn(II)–PMA and (b) the Cd(II)–PMA systems for different KNO_3 concentrations. [Zn(II)] = 10^{-7} mol l^{-1}; [Cd(II)] = 10^{-6} mol l^{-1}; α_n = 0.8. [KNO_3] = (□) 0.1 mol l^{-1}, (△) 0.03 mol l^{-1}, (○) 0.01 mol l^{-1}, (∗) 0.003 mol l^{-1}.

polyionic charge densities and can be understood in terms of competition between the monovalent counterions (K^+) and divalent counterions [Zn(II) and Cd(II)] for binding by the humate polyanion. This aspect will be discussed in more detail below. In studies which compare the competitive behaviour with theoretical predictions as in the case of, for example, the Poisson–Boltzmann model or the two-state approximation concept, mainly synthetic model polyelectrolytes such as PMA have been used [e.g., 19,21]. Hence, experimental data of natural systems with respect to the influence of the salt concentration on the stability of the heavy-metal–ligand complex are very scarce. Some 15 years ago, Stevenson [22] studied very briefly the stability of several heavy-metal–

TABLE 1

Stabilities K obtained from Φ values for various Zn(II)–humate and Cd(II)–humate systems as a function of the concentration KNO_3 with α_n = 0.8 and [M(II)] = 10^{-6} mol l^{-1}

[KNO_3] (mol l^{-1})	Zn(II)			Cd(II)		
	log K	ϵ	r^2	log K	ϵ	r^2
Fluka humic acid						
0.1	4.93	< 0.001	0.983	4.80	0.006	0.999
0.03	5.06	< 0.001	0.986	5.16	0.045	0.987
0.01	5.22	0.018	0.990	5.21	0.013	0.990
0.003	5.50	< 0.001	0.993	5.62	0.014	0.981
Aldrich humic acid						
0.1	5.14	< 0.001	0.983	5.09	0.015	0.999
0.03	5.40	< 0.001	0.976	5.31	< 0.001	0.987
0.01	5.58	< 0.001	0.984	5.54	< 0.001	0.990
0.003	5.54	< 0.001	0.975	5.78	0.006	0.981
Roth humic acid						
0.1	4.88	< 0.001	0.987	4.98	0.027	0.999
0.03	5.06	< 0.001	0.985	5.10	0.018	0.992
0.01	4.98	< 0.001	0.987	5.43	0.026	0.977
0.003	5.48	< 0.001	0.989	5.57	< 0.001	0.981

TABLE 2

Stabilities K obtained from ΔE_p values for various Zn(II)–humate and Cd(II)–humate systems as a function of the concentrations KNO_3 with $\alpha_n = 0.8$ and $[M(II)] = 10^{-6}$ mol l^{-1}

$[KNO_3]$ (mol l^{-1})	log K	
	Zn(II)	Cd(II)
Fluka humic acid		
0.1	5.47 ± 0.21	5.59 ± 0.04
0.03	5.23 ± 0.02	6.18 ± 0.04
0.01	[a]	6.93 ± 0.03
0.003	6.28 ± 0.11	6.52 ± 0.08
Aldrich humic acid		
0.1	6.51 ± 0.20	5.75 ± 0.17
0.03	6.22 ± 0.24	6.23 ± 0.10
0.01	6.54 ± 0.31	7.01 ± 0.29
0.003	6.39 ± 0.32	7.34 ± 0.38
Roth humic acid		
0.1	5.59 ± 0.23	5.61 ± 0.16
0.03	5.77 ± 0.25	6.51 ± 0.25
0.01	6.08 ± 0.09	6.14 ± 0.25
0.003	6.21 ± 0.21	6.77 ± 0.47

[a] $\Delta E_{peak} > 0$.

humate complexes as a function of the ionic strength by potentiometric titration. In this qualitative study, an increase in the stability with decreasing ionic strength has been observed too, as in agreement with our results.

Potential shift

In Figs. 4a–c and 5a–c, the shift of the peak potential is presented as a function of humate polyanion concentration for different KNO_3 concentrations and for various Zn(II)–humate and Cd(II)–humate complexes, respectively, with $\alpha_n = 0.8$ and $[M(II)] = 10^{-6}$ mol l^{-1}. Except for the Zn(II)–Fluka HA system with $[KNO_3] = 0.01$ mol l^{-1}, a decrease of the peak potential is observed with increasing concentration of the humate polyanion. The potential shift becomes more pronounced with extremely large excesses of ligand. For the calculation of the stability K from the potential shift, we have used the final five points of the complexation curve to fulfil the condition of having an extremely large excess of ligand over metal. However, this analysis should be done with care, since the condition of excess of ligand is related to the metal atom concentration in the mercury drop. For the present experimental conditions, $[M^0]$ will be increased by a factor of about 100 compared to the total metal ion concentration in solution and thus in the order of 10^{-4} mol l^{-1} (Hg). Considering the fact that the humate polyanion is present in approximately comparable concentrations, the condition of excess of ligand is not rigourously fulfilled. Hence, the calculation of the stability from the potential shift could lead to unreliable results. Just for illustration, the stabilities K as obtained from ΔE_p using Eqn. 13 are presented in Table 2 for the different metal–humate complexes. As can be seen from the value of the standard deviation, the values of K obtained from ΔE_p are less accurate as compared to K values obtained from the decrease of Φ. Furthermore, the results show that K from ΔE_p is in the order of one log unit larger than K from Φ. Except for the Zn(II)–Fluka HA and Zn(II)–Aldrich HA system, K increases with decreasing KNO_3 concentration in agreement with the results from Φ. However, recalling the fact that for the results obtained from ΔE_p the condition of a large excess of the humate polyan-

TABLE 3

Stabilities K obtained from Φ values for the Zn(II)–PMA and Cd(II)–PMA system as a function of the concentration KNO_3 with $\alpha_n = 0.8$ and $[Zn(II)] = 10^{-7}$ mol l^{-1} and $[Cd(II)] = 10^{-6}$ mol l^{-1}

$[KNO_3]$ (mol l^{-1})	Zn(II)–PMA			Cd(II)–PMA		
	log K	ϵ	r^2	log K	ϵ	r^2
0.1	4.15	0.058	0.991	4.81	0.046	0.998
0.03	5.11	0.103	0.993	5.74	0.012	0.979
0.01	5.65	0.045	0.991	5.91	0.051	0.993
0.003	6.45	0.013	0.995	6.25	< 0.001	0.976

TABLE 4

Stabilities K obtained from ΔE_p values for the Zn(II)–PMA and Cd(II)–PMA system as a function of the concentration KNO_3 with $\alpha_n = 0.8$ and $[Zn(II)] = 10^{-7}$ mol l^{-1} and $[Cd(II)] = 10^{-6}$ mol l^{-1}

$[KNO_3]$ (mol l^{-1})	log K	
	Zn(II)–PMA	Cd(II)–PMA
0.1	4.17±0.07	4.76±0.11
0.03	4.93±0.10	5.91±0.04
0.01	5.96±0.18	6.61±0.06
0.003	6.65±0.08	6.26±0.09

TABLE 5

The mean $K^+/M(II)$ exchange ratio ν as resulting from the α_{K^+} dependence of the stability parameters K_c (from Φ) for various M(II)–(bio)polyelectrolyte systems

Polyelectrolyte	ν	
	Zn(II)	Cd(II)
Fluka humic acid	0.26±0.07	0.39±0.10
Aldrich humic acid	0.16±0.08	0.35±0.03
Roth humic acid	0.23±0.17	0.30±0.07
Poly(methacrylic acid)	1.42±0.08	0.81±0.21

ion over the metal atom concentration is not fulfilled, we will consider only the results obtained from Φ in comparison with linear polyelectrolytes.

Comparison with linear polyelectrolytes

In order to compare the results for the metal–humate systems with the properties of a well-defined model polyelectrolyte, some parallel complexation experiments were performed with poly(methacrylic acid). Figure 6a and b shows the voltammetric complexation curves for the Zn(II)–PMA and Cd(II)–PMA systems, respectively, for different concentrations of KNO_3 with $\alpha_n = 0.8$ and $[Zn(II)] = 10^{-7}$ mol l^{-1} and $[Cd(II)] = 10^{-6}$ mol l^{-1}. The resulting stability K and ϵ values are presented in Table 3 using $p = 2/3$. With one exception, realistic ϵ values are found, which seem to be somewhat larger with respect to literature data of 0.023 [6,19]. No clear relationship between the ϵ and $[KNO_3]$ is observed.

Table 4 gives the K values as calculated from five values of the potential shift according to Eqn. 13. In contrast with the metal–humate systems, K values as obtained from ΔE_p are in excellent agreement with K values as obtained from Φ, except for the Cd(II)–PMA system with $[KNO_3] = 0.01$ mol l^{-1}. Considering the fact that the $[Zn(II)] = 10^{-7}$ mol l^{-1} and thus the $[PMA]/[Zn^0]$ ratio varies from approximately 5 to 20, the condition of excess of ligand over metal is reasonably fulfilled for the different Zn(II)–PMA systems. However, performance of the same exercise for the Cd(II)–PMA systems results in $[PMA]/[Cd^0]$ ratios of about 0.1 to 1 and thus comparable to the conditions of the metal–humate complexes. A thorough study is required

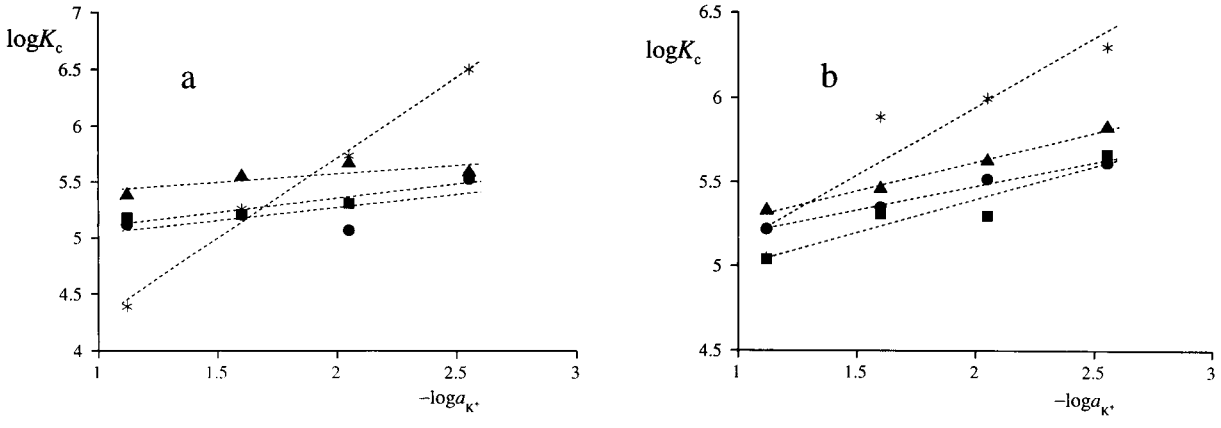

Fig. 7. Dependence of the stability K_c for various M(II)–(bio)polyelectrolytic systems on the activity of the KNO_3 for $\alpha_n = 0.8$ (a) $[Zn(II)] = 10^{-6}$ mol l^{-1} (except for the Zn(II)–PMA system: $[Zn(II)] = 10^{-7}$ mol l^{-1}); (b) $[Cd(II)] = 10^{-6}$ mol l^{-1}; (■) Fluka HA, (▲) Aldrich HA, (●) Roth HA, (*) PMA.

in the understanding of the observed discrepancy.

An important difference with the metal–humate complexes is found in the salt dependency of K. For the Zn(II)–PMA and Cd(II)–PMA system, the dependency of the stability K on $[KNO_3]$ is much stronger than in the case of the corresponding humate complexes, which is visualized in Fig. 7a and b, respectively. As shown in Fig. 7a and b, log K_c (from Φ) and log a_{K^+} are approximately linearly related in agreement with Eqn. 17. The slopes yield $\nu_{K/M(II)}$ values which are presented in Table 5. The exchange ratios for the metal–humate complexes are much lower than for the corresponding metal–PMA systems. This must mean that the interaction of humate polyanion with K^+ counterions is much weaker than in the case of the PMA system. This finding is in accordance with conductometric counterion binding data [14], which show that the electrostatic interaction of K^+ with the humate polyanion is practically absent. This can be understood in terms of a lower charge density for the humate polyanion. For the Fluka HA the mean separation between sites is found to be not less than 1 nm [14], whereas the separation between the individual carboxylate groups on the poly(methacrylate) is about 0.3 nm [23]. The former is well above, the latter is well below the Bjerrum length, which is about 0.7 nm under the present experimental conditions.

The exchange ratios for the Cd(II)–humate systems seem to be somewhat larger than the corresponding Zn(II)–humate systems, whereas for the poly(methacrylate) systems the opposite situation is observed. This cannot be explained from the electrostatic point of view, but may be the result of some chemical interaction, which will not be considered any further here.

It can be concluded that the stability K of labile heavy-metal complexes with (bio)polyelectrolytes can be obtained fairly well from differential pulse anodic stripping voltammetric complexation curves. The results indicate that the polyelectrolytic behaviour of the humic acids studied is very much weaker as compared to the well-defined linear polyelectrolyte PMA. The charge density of the complex (also) plays a key role in the understanding of the association of counterions in polyelectrolytic systems, and this will be subject of a forthcoming study [24].

REFERENCES

1 J. Buffle, Complexation Reactions in Aquatic Systems: An Analytical Approach, Ellis Horwood, Chichester, 1988.
2 J. Buffle, in H. Sigel (Ed.), Metal Ions in Biological Systems, Vol. 18, Natural Organic Matter and Metal-Organic Interactions in Aquatic Systems, Marcel Dekker, New York, 1984, Chap. 6, pp. 165–221.
3 (a) H.G. de Jong, H.P. van Leeuwen and K. Holub, J. Electroanal. Chem., 234(1987) 1.
(b) H.G. de Jong and H.P. van Leeuwen, J. Electroanal. Chem, 234 (1987) 17.
(c) H.G. de Jong and H.P. van Leeuwen, J. Electroanal. Chem, 235 (1987) 1.
(d) H.P. van Leeuwen, H.G. de Jong and K. Holub, J. Electroanal. Chem, 260 (1989) 213.
4 M. Filella, J. Buffle and H.P. van Leeuwen, Anal. Chim. Acta, 232 (1990) 209.
5 H.P. van Leeuwen and J. Buffle, J. Electroanal. Chem., 296 (1990) 359.
6 M. Esteban, H.G. de Jong and H.P. van Leeuwen, Int. J. Environ. Anal. Chem., 38 (1990) 75.
7 M.A.G.T. van den Hoop, F.M.R. Leus and H.P. van Leeuwen, Collect. Czech. Chem. Commun., 56 (1991) 96.
8 W. Davison, J. Electroanal. Chem., 87 (1978) 395.
9 H.P. van Leeuwen, Sci. Total Environ., 60 (1987) 45.
10 V.G. Levich, Physicochemical Hydrodynamics, Prentice-Hall, Englewood Cliffs, NJ, 962.
11 D.D. DeFord and D.N. Hume, J. Am. Chem. Soc., 73 (1951) 5321.
12 H.P. van Leeuwen, Colloids Surf., 51 (1990) 359.
13 E. Guntelberg, Z. Phys. Chem. Leipzig, 123 (1926) 199.
14 M.A.G.T. van den Hoop, H.P. van Leeuwen and R.F.M.J. Cleven, Anal. Chim. Acta, 232 (1990) 141.
15 J.M. Díaz-Cruz, M. Esteban, M.A.G.T. van den Hoop and H.P. van Leeuwen, Anal. Chim. Acta, 264 (1992) 163.
16 IMSL Library, Edition 9.2. IMSL, Houston, TX, 1984.
17 J.M. Díaz-Cruz, M. Esteban, M.A.G.T. van den Hoop and H.P. van Leeuwen, Anal. Chem., 64 (1992) 1769.
18 P.K. Cornel, R.S. Summers and P.V. Roberts, J. Colloid Interface Sci., 110 (1986) 149.
19 R.F.M.J. Cleven, PhD Thesis, Agricultural University, Wageningen, 1984.
20 S.K. Saha, S.L. Dutta and S.K. Chakravarti, J. Indian Chem. Soc., 56 (1979) 1129.
21 J.C. Benegas, S. Paoletti, A. Cesàro, M.A.G.T. van den Hoop and H.P. van Leeuwen, Biophys. Chem., 42 (1992) 297.
22 F.J. Stevenson, Soil Sci., 123 (1977) 10.
23 W.P.T.J. van der Drift, PhD Thesis, State University Utrecht, Utrecht, 1975.
24 M.A.G.T. van den Hoop and H.P. van Leeuwen, in preparation.

Analytica Chimica Acta, 273 (1993) 289–296
Elsevier Science Publishers B.V., Amsterdam

Voltammetry of Cu(II) in the presence of polymethacrylate

José Manuel Díaz-Cruz, Cristina Ariño, Miquel Esteban and Enric Casassas

Departament de Química Analítica, Facultat de Química, Universitat de Barcelona, Av. Diagonal 647, 08028 Barcelona (Spain)

(Received 1st June 1992)

Abstract

A systematic study of the voltammetric reduction of Cu(II) in the presence of polymethacrylic acid (PMA) was carried out by means of sampled direct current, normal pulse, differential pulse and reverse pulse polarography, cyclic voltammetry and differential pulse anodic stripping voltammetry. Titrations of Cu(II) with partially neutralized PMA allow the determination of the apparent formation constant, K, of the Cu–PMA system.

Keywords: Polarography; Stripping voltammetry; Voltammetry; Copper; Metal–polyacid complexes; Polymethacrylate

Determinations of heavy metal ions are of the highest interest in environmental analysis. Voltammetric techniques in general and stripping voltammetry in particular have been extensively used for this purpose, because, in principle, they allow direct determination in natural samples at very low metal concentration levels [1].

Voltammetric determinations of natural systems involves the complexation of metal ions with macromolecular ligands. These studies usually present difficulties derived from the polyelectrolytic and polyfunctional character of the macromolecules. In this respect, model homofunctional polyelectrolytes of known composition and structure have been intensively investigated in order to understand the behaviour of natural polyelectrolytes. Polyacrylic acid (PAA) and polymethacrylic acid (PMA) are among the most popular model polyelectrolytes, and their complexation with several metal ions has been widely studied by voltammetric techniques [2].

Correspondence to: M. Esteban, Departament de Química Analítica, Facultat de Química, Universitat de Barcelona, Av. Diagonal 647, 08028 Barcelona (Spain).

Recently, a rigorous voltammetric model [3] has been developed for the reduction of a metal ion in the presence of a macromolecular ligand, including both the kinetics of complexation and the different mobilities of the species involved. The application of this model to the Cd(II), Zn(II)–PAA, PMA systems [4–6] yielded satisfactory results and further studies improved the experimental methodology [7,8] and the data treatment [9] in order to apply the theoretical model under the optimum experimental conditions. The use of such methodology [10] permitted clarification of some problematic aspects of the Pb(II)–PAA and Pb(II)–PMA systems [4].

Previous polarographic studies of the complexation between Cu(II) and several polyelectrolytes [11] showed rather complex behaviour, with the appearance of pre-waves and post-waves in the polarograms, which were not interpreted.

The aim of this paper is to study the voltammetric reduction of Cu(II) in the presence of the model polyelectrolyte PMA. For this purpose, sampled direct current polarography (DCP), normal pulse polarography (NPP), differential pulse polarography (DPP), reverse pulse polarography

(RPP), cyclic voltammetry (CV) and differential pulse anodic stripping voltammetry (DPASV) were used.

EXPERIMENTAL

Chemicals

Analytical-reagent grade chemicals were used unless otherwise indicated. Polymethacrylic acid (PMA) was obtained from BDH (Poole). The average molecular mass, according to BDH, was 26 000 g mol^{-1}. Stock solutions of ca. 0.1 mol l^{-1} (in monomeric units) were prepared by dilution with water, and the total concentrations of carboxylic groups were determined conductimetrically by acid–base titration. These solutions were stored in the dark at 4°C.

Copper(II) nitrate, potassium nitrate (used as supporting electrolyte), nitric acid and potassium hydroxide (used as a carbonate-free solution) were obtained from Merck (Darmstadt). The water used was purified with a Culligan (Barcelona) water purification system.

Instrumentation

Polarographic and stripping voltammetric measurements were carried out with an Autolab System (EcoChemie, Utrecht) attached to a Metrohm (Herisau) Model 663 VA Stand and to a personal computer by means of the software package GPES2 (EcoChemie). The system was also connected to a Metrohm 665 Dosimat for the manual or automatic addition of PMA solutions and to an Orion (Boston) Model SA 720 pH-meter for pH monitoring during the experiments. In all cases, reference and counter electrodes were Ag/AgCl, KCl_{sat} and glassy carbon, respectively. A static mercury drop electrode (SMDE) or a hanging mercury drop electrode (HMDE) were used as working electrode for polarography or stripping voltammetry, respectively. In the polarographic measurements, drop times of 1 s, pulse durations of 40 ms and scan rates of 4 mV s^{-1} were used when not otherwise indicated. The initial potential was +100 mV for NPP and DPP, and −300 mV for RPP. In DPP measurements, pulse amplitudes of 50 mV were applied. In DPASV measurements, pulse durations of 40 ms, pulse heights of 50 mV, and deposition potentials of −300 mV were used. When not otherwise indicated, the pre-electrolysis time and the rest period observed were 30 and 15 s, respectively, and the scan rate in the stripping step was 8 mV s^{-1}. Glass cells (originally provided by Metrohm) were used in all experiments. Measurements were performed at 25°C. Purified nitrogen was used for deaeration of the sample solutions.

Conductimetric titrations of the PMA solutions were performed at 25°C with an Orion Model 120 conductimeter coupled to a Metrohm Model 665 Dosimat.

Procedures

Titrant solutions of PMA containing 0.1 mol l^{-1} of KNO_3 were prepared to a certain degree of neutralization (α_n) by KOH addition. Solutions of Cu(II) nitrate containing the same KNO_3 concentration were placed in the voltammetric cell, adjusted to the pH of the titrant, by means of KOH or HNO_3 additions, and measured voltammetrically in order to obtain the current, I_0. Aliquots of the titrant PMA solution were added to the metal-ion solution in the cell, and measurements were performed after each addition in order to obtain the current, I [7]. Peak currents were corrected for dilution effects.

RESULTS AND DISCUSSION

General polarographic and voltammetric behaviour

Titrations of 10^{-5} mol l^{-1} Cu(II) and 0.1 mol l^{-1} KNO_3 solutions with partially neutralized PMA solutions, degree of neutralization (α_n) of 0.3, were carried out by DCP, NPP, RPP, DPP and DPASV. During the titrations the degree of dissociation (α_d) of PMA was constant, and equal to the degree of neutralization (α_n) of PMA, and the pH values were ca. 5.4. Under these pH conditions, complications due to losses of Cu(II) by adsorption onto cell materials were negligible [12]. In order to obtain the blank measurements for PMA, analogous experiments were carried out with PMA in the absence of Cu(II).

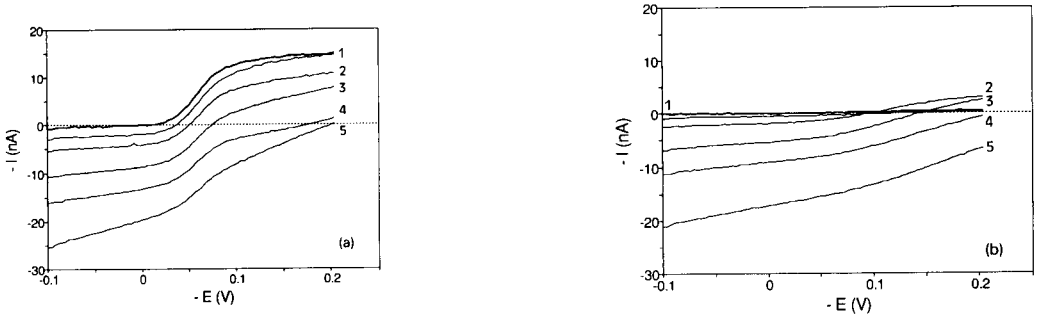

Fig. 1. Direct current polarograms (DCP) obtained for (a) the Cu(II)–PMA system and (b) PMA alone, at different concentrations of carboxylate groups (c_L^*) under the conditions: (a) 10^{-5} mol l^{-1} Cu(II), 0.1 mol l^{-1} KNO_3 and α_d(PMA) = 0.3. Solid lines denote the signals obtained in the absence of PMA. (c_L^* (mol l^{-1}): (1) 2×10^{-5}; (2) 4×10^{-5}; (3) 8×10^{-5}; (4) 1.2×10^{-4} and (5) 2.0×10^{-4}).

The d.c. polarograms of the reduction of Cu(II) obtained in the presence of PMA are of the usual shape (Fig. 1). As the PMA concentration (c_L^*) increases, the baseline progressively shifts towards more anodic currents (Fig. 1a). Similar behaviour is shown by the PMA blanks (Fig. 1b), probably due to the anodic oxidation of the Hg to yield soluble Hg(II)–PMA complexes. The subtraction of the current due to the blank (PMA alone) from the corresponding polarogram obtained for the Cu–PMA solution yields polarograms of the usual shape with a zero current baseline. However, it seems that this procedure is not accurate enough for quantitative calculations, because the blank currents are of the same order of magnitude as those obtained for Cu(II) in the presence of PMA.

Figure 2a shows the slightly deformed NPP signals obtained for the Cu–PMA system, while Fig. 2b shows that PMA, in the absence of Cu(II), yields apparently capacitive signals which explain the deformation of the waves in the presence of Cu(II). The correction of the curves obtained for Cu–PMA by subtraction of the corresponding PMA blanks from the Cu–PMA measurements yields satisfactory results only at low c_L^* values.

RPP waves of the usual shape are obtained for Cu(II) in the presence of PMA (Fig. 3a). However, as c_L^* increases, the baseline becomes progressively deformed and is moved towards higher anodic currents. Figure 3b shows that this may be due to the anodic signals of PMA.

Cyclic voltammograms of Cu–PMA solutions (Fig. 4a) exhibit the first cathodic signal, at ca. −0.05 V, which seems to be due to the Cu(II) reduction. A second signal, due to PMA (Fig. 4b), appears at more negative potentials. The scan rate dependence of this peak (Fig. 4b) indicates

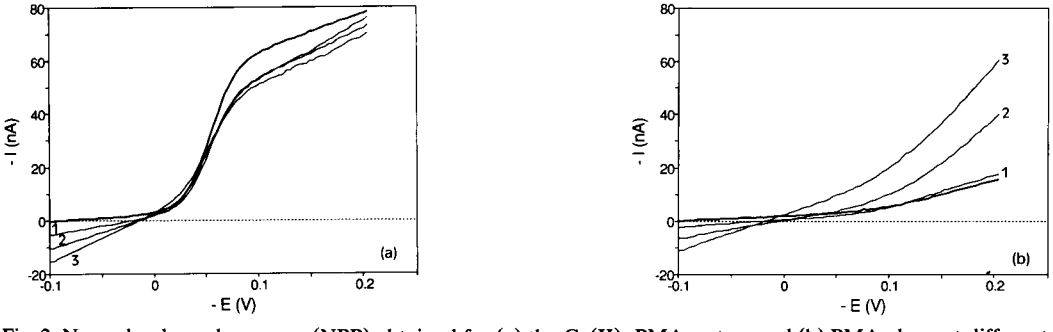

Fig. 2. Normal pulse polarograms (NPP) obtained for (a) the Cu(II)–PMA system and (b) PMA alone at different concentrations of carboxylate groups (c_L^*) under the conditions: (a) 10^{-5} mol l^{-1} Cu(II), 0.1 mol l^{-1} KNO_3 and α_d(PMA) = 0.3. Solid lines denote the signals obtained in the absence of PMA. (c_L^* (mol l^{-1}): (1) 4×10^{-5}; (2) 8×10^{-5} and (3) 1.2×10^{-4}).

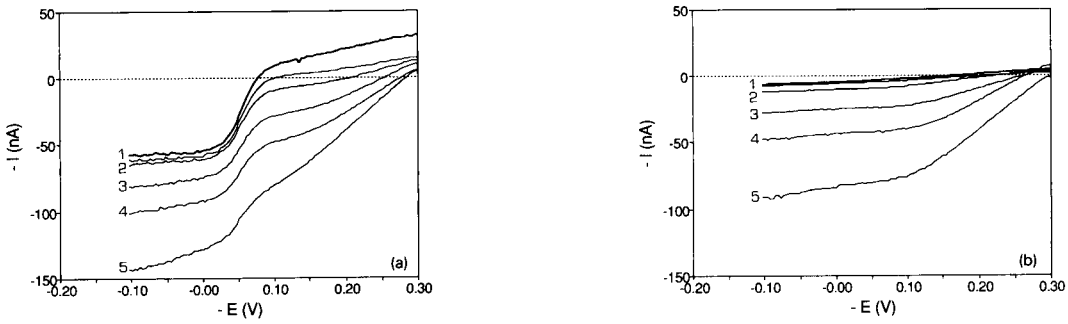

Fig. 3. Reverse pulse polarograms (RPP) obtained for (a) the Cu(II)–PMA system and (b) PMA alone at different concentrations of carboxylate groups (c_L^*) under the conditions: (a) 10^{-5} mol l^{-1}, 0.1 mol l^{-1} KNO_3 and α_d(PMA) = 0.3. Solid lines denote the signals obtained in the absence of PMA. (c_L^* (mol l^{-1}): (1) 2×10^{-5}; (2) 4×10^{-5}; (3) 8×10^{-5}; (4) 1.2×10^{-4} and (5) 2.0×10^{-4}).

its capacitive nature. Attention is drawn to the absence of anodic peaks for PMA.

DPP and DPASV signals of the usual shape were obtained for Cu–PMA, and only flat base lines for the PMA blanks. By both techniques, the width at half-height ($w_{1/2}$) values for Cu–PMA solutions are practically identical to those observed for Cu(II) alone, and they are time-independent. For the Cu–PMA system, linear dependences between peak currents (I_p) and the inverse of the square root of the pulse time (t_p) were reached: $I_p = 1(\pm 1) + 4.2(\pm 0.4)t_p^{-1/2}$ ($r^2 = 0.991$) and $I_p = -60(\pm 20) + 80(\pm 10)t_p^{-1/2}$ ($r^2 = 0.989$), for DPP and DPASV, respectively, I_p is in nA and t_p in ms (in the range 40–200 ms). Furthermore, linear dependence of the DPASV peak current on the pre-electrolysis time (t_{pe}) was found: $I_p = 170(\pm 20) + 5.7(\pm 0.1)t_{pe}$ ($r^2 = 0.9996$), where I_p is in nA and t_{pe} in s (in the range 10–180 s). These findings seem to indicate: (i) the lability of the Cu(II)/PMA complex, at least within the time ranges used in DPP and DPASV; (ii) the possible induced adsorption of Cu(II) on the electrode (as a consequence of PMA adsorption) does not significantly affect the reduction process of Cu(II).

According to the above-mentioned model [3,4], it is useful to define the normalized limiting or peak current ϕ as the ratio between the currents obtained for an M solution in the presence or in the absence of a macromolecular ligand L:

$$\phi = I(\text{with L})/I(\text{without L}) = I/I_0 \qquad (1)$$

For a labile complex and in the presence of a large excess of L, ϕ can be related to the complexation constant K through the equation [3]:

$$\phi = \left(\overline{D}/D_M\right)^p = (1 + \epsilon K c_L^*)^p/(1 + K c_L^*)^p \qquad (2)$$

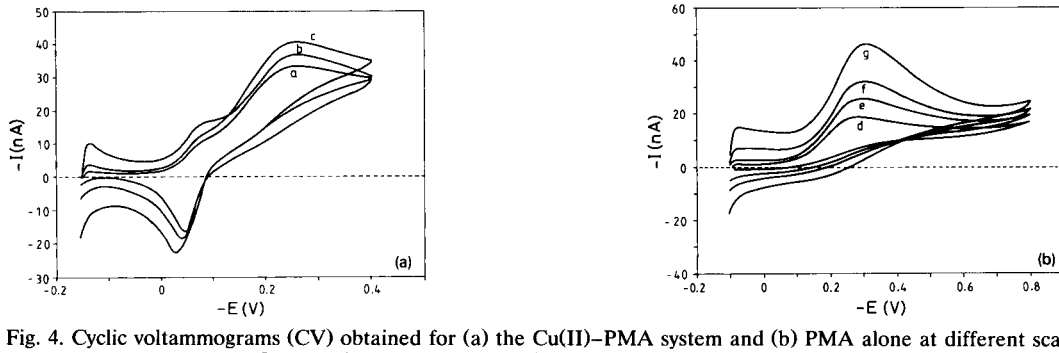

Fig. 4. Cyclic voltammograms (CV) obtained for (a) the Cu(II)–PMA system and (b) PMA alone at different scan rates (v) under the conditions: (a) 2×10^{-5} mol l^{-1} Cu(II), 0.1 mol l^{-1} KNO_3, $c_L^* = 3.8 \times 10^{-4}$ and α_d(PMA) = 0.3. (v (V s^{-1}): (a) 0.01; (b,d) 0.02; (c,e) 0.05; (f) 0.1 and (g) 0.2).

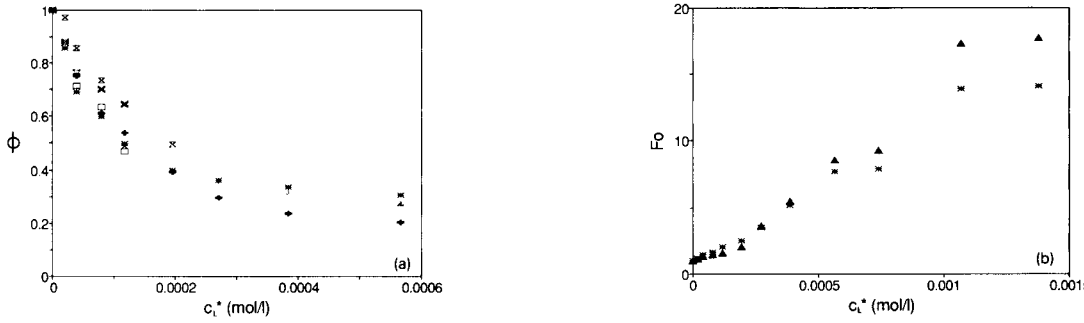

Fig. 5. Experimental plots of (a) ϕ vs. c_L^* and (b) F_0 vs. c_L^* obtained for the Cu(II)–PMA system by means of voltammetric titrations of Cu(II) solutions with PMA using different techniques. The experimental conditions were 10^{-5} mol l^{-1} Cu(II), 0.1 mol l^{-1} KNO_3 and $\alpha_d = 0.3$. (Data from: DCP_{corr} (□); NPP_{corr} (×); RPP_{corr} (×); DPP (+); DPP_{corr} (▲) and DPASV (∗). The subscript "corr" denotes data corrected by substraction of the signals obtained for the PMA alone from the polarograms obtained in the presence of both Cu(II) and PMA).

where $\epsilon = D_{ML}/D_M$, $K = c_{ML}^*/c_M^* c_L^*$, $\overline{D} = (c_M^*/c_T^*)D_M + (c_{ML}^*/c_T^*)D_{ML}$, D_i and c_i^* denote the diffusion coefficient and the bulk concentration of species i, respectively, and $\overline{D}$ is the mean diffusion coefficient of the complex system. The parameter p depends on the nature of the mass transport during the pre-electrolysis step. It was assumed to be 1/2 for semi-infinite linear diffusion and 2/3 for laminar convective diffusion [4]. A recent semi-empirical study has shown that, under the usual hydrodynamic conditions, the values $p = 1/2$ and $p = 2/3$ should be adopted in polarography and stripping voltammetry, respectively [9].

Experimentally, the most convenient procedure to determine ϵ and K by using Eqn. 2 is through successive additions of the ligand L to a metal-ion solution, which yields a set of ϕ vs. c_L^* data. In order to determine the K values, the first part of the complexation curve (low c_L^* values) appears to be the most suitable, whereas to determine ϵ the region at high c_L^* values is the most informative [13].

Figure 5a summarizes the ϕ vs. c_L^* plots obtained in the voltammetric titrations of 10^{-5} mol l^{-1} Cu(II) solutions with PMA at $\alpha_n = 0.3$. The fit of the curves to Eqn. 2 is quite satisfactory, yielding reasonable log K values (Table 1). The ϕ vs. c_L^* plots obtained from DCP, NPP and RPP measurements at relatively low c_L^* values by using blank correction (Fig. 5a) are quite similar to those from DPP or DPASV.

Still for a labile system and with a large excess of L, K can be related to the potential shift of

TABLE 1

Values of log K obtained from current (I) and potential (E) data for the Cu(II)–PMA system [a], at different degrees of dissociation of the polyacid (α_d) and different total concentrations of Cu(II), by means of DPP and DPASV

α_d	10^{-6} mol l^{-1} Cu, DPASV		10^{-5} mol l^{-1} Cu, DPP		10^{-5} mol l^{-1} Cu, DPASV	
	log $K(\phi)$	log $K(F_0)$	log $K(\phi)$	log $K(F_0)$	log $K(\phi)$	log $K(F_0)$
0.2	3.96(±0.06)	3.55(±0.03)	4.24(±0.06)	3.91(±0.04)	4.18(±0.02)	3.79(±0.04)
0.3	4.45(±0.08)	3.74(±0.05)	4.4 (±0.1)	4.42(±0.05)	4.33(±0.08)	4.13(±0.04)
0.4	–	–	4.87(±0.04)	4.60(±0.07)	4.87(±0.05)	4.29(±0.04)

[a] KNO_3, 0.1 mol l^{-1}.

the peak (ΔE_p) through the equation [4]:

$$F_o = \exp\left[-(nF/RT)\Delta E_p - \ln \phi\right] = 1 + Kc_L^* \quad (3)$$

which is written in terms of the Leden Function of order zero, F_0. This expression allows the determination of K from F_0 vs. c_L^* plots.

Fig. 5b shows the corresponding F_0 vs. c_L^* plots obtained by DPP and DPASV, and Table 1 summarizes the results obtained in their fit to Eqn. 3.

These results seem to confirm the lability of the Cu(II)–PMA system and prove the applicability of the theoretical model to DPP and DPASV measurements in such a system. They also suggest that DCP, NPP and RPP measurements agree with the model. However, the mentioned interferences from the anodic and capacitive currents of PMA made them useless for quantitative considerations.

Influence of the degree of dissociation (α_d) of PMA

In order to study the influence of the degree of dissociation (α_d) of the PMA on the complexation constants, DPASV titrations of both 10^{-6} and 10^{-5} mol l^{-1} Cu(II) solutions were carried out with partially neutralized PMA solutions at α_d values in the range 0.2–0.6. In the case of 10^{-5} mol l^{-1} Cu(II) solutions, DPP measurements were also carried out.

Figure 6 shows the ϕ vs. c_L^* plots obtained from the different titrations. At $\alpha_d \leqslant 0.4$ the plots are in good agreement with the theoretical model, but for $\alpha_d \geqslant 0.5$ the curves (especially those obtained by DPASV) show important deformations, with the appearance of minima which cannot be explained in terms of the model. Analogously, F_0 vs. c_L^* plots of the usual shape are obtained at $\alpha_d \leqslant 0.4$, whereas they deform progressively at $\alpha_d \geqslant 0.5$. The reasons for this anomalous behaviour seem to be mainly related to adsorption of Cu(II) onto cell materials, since the mean pH values during the titrations at α_d 0.2, 0.3, 0.4, 0.5 and 0.6 were 5.0, 5.4, 5.6, 5.9 and 6.3, respectively. At pH > 5.5, results can be affected by this

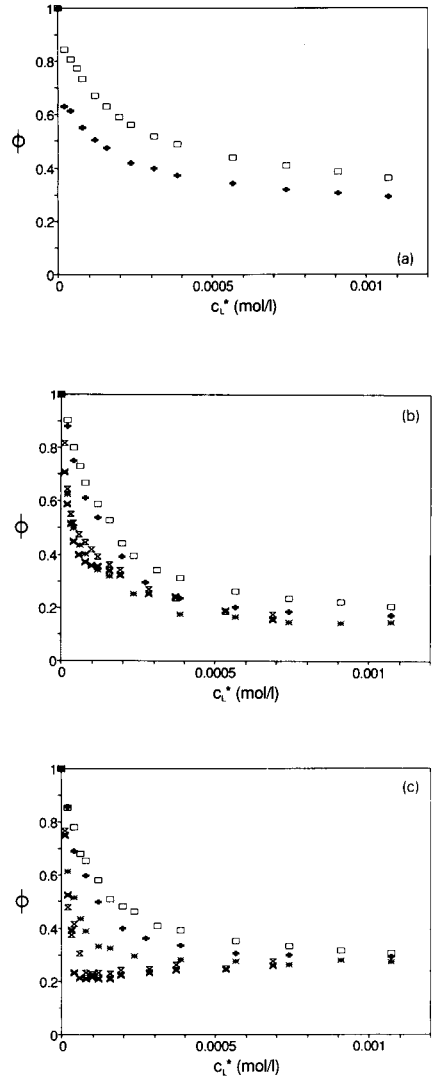

Fig. 6. Experimental plots of ϕ vs. c_L^* obtained for the Cu(II)–PMA system by voltammetric titration of Cu(II) solutions with PMA using DPASV (a,c) and DPP (b). The concentrations used were 10^{-6} (a) or 10^{-5} (b,c) mol l^{-1} Cu(II) and 0.1 mol l^{-1} KNO_3. The degrees of dissociation of PMA (α_d) were: 0.2 (□), 0.3 (+), 0.4 (∗), 0.5 (×) and 0.6 (×).

adsorption [12], while at pH > 6 the hydrolysis of Cu(II) can also play a key role [14].

Table 1 summarizes the log K values obtained in the fit of the regular ϕ vs. c_L^* and F_0 vs. c_L^* plots to Eqns. 2 and 3 respectively, clearly showing the increase in log K values with increasing α_d values. However, the low α_d range within

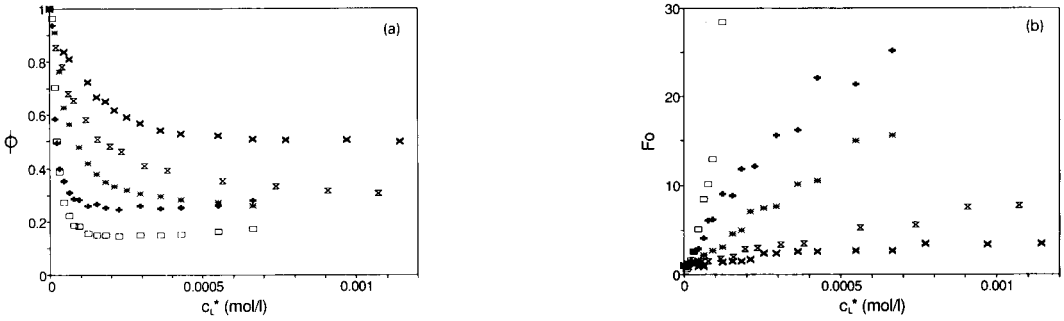

Fig. 7. Experimental plots of (a) ϕ vs. c_L^* and (b) F_0 vs. c_L^* obtained from the Cu(II)–PMA system by means of DPASV voltammetric titrations at a concentration of 10^{-5} mol l^{-1} Cu(II), a degree of dissociation $\alpha_d = 0.2$ and various concentrations of KNO_3. ([KNO_3] (mol l^{-1}): (□) 0.01, (+) 0.02, (*) 0.05, (×) 0.1 and (×) 0.2).

which the observed behaviour follows the model, precludes further conclusions about the log K vs. α_d relationships. Systematically, higher log K values are obtained from ϕ than from F_0, and slightly higher log K values from DPP than from DPASV. The total concentration of Cu(II) does not seem to change the results dramatically, but slightly higher log K values are found at 10^{-5} mol l^{-1} than at 10^{-6} mol l^{-1}.

The formation constant values determined for Cu(II) are slightly lower than those determined for Pb(II) under similar experimental conditions. Thus, for instance log $K = 4.7(\pm 0.1)$ for Pb–PMA system, at $\alpha_n = 0.3$ and pH = 5.4, from ϕ vs. c_L^* plots by means of DPASV, RPP and DPP [10].

Influence of the counterion concentration (c_K)

The DPASV titrations of 10^{-5} mol l^{-1} Cu(II) solutions with partially neutralized PMA solutions at $\alpha_d = 0.2$ (pH 5.0) were carried out at different KNO_3 concentrations. Figures 7a and b show the corresponding ϕ vs. c_L^* and F_0 vs. c_L^* plots respectively, while Table 2 summarizes the log K values found in fitting these plots. Similarly to that observed in the study of the dependence on α_d, log K values determined from ϕ data were slightly higher than those from F_0 data. A rather scattered range of values of ϵ (0.02–0.2) was found in the simultaneous fitting of ϵ and K.

Figure 8 shows the plot of the log K values as a function of log c_K, where c_K denotes the KNO_3 concentration. An increase in log K values with decreasing log c_K values is noticed. In the case of log K values obtained from F_0 data, a well-defined linear relationship is reached: log $K(F_0) = 2.4(\pm 0.4) - 1.4(\pm 0.4)$ log c_K.

TABLE 2

Values of log K obtained from current (I) and potential (E) data for the Cu(II)–PMA system at different concentrations of KNO_3 by means of DPASV [a]

[KNO_3] (mol l^{-1})	log $K(\phi)$	log $K(F_0)$
0.01	5.0 (±0.2)	5.34(±0.04)
0.02	5.1 (±0.1)	4.68(±0.04)
0.05	4.40(±0.07)	4.38(±0.04)
0.1	4.17(±0.02)	3.79(±0.04)
0.2	3.99(±0.06)	3.4 (±0.1)

[a] Cu(II), 10^{-5} mol l^{-1}; $\alpha_n = 0.2$.

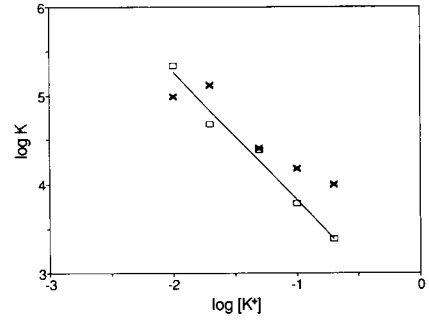

Fig. 8. Values of log K calculated for the Cu(II)–PMA system at $\alpha_d = 0.2$ from (□) current or (×) potential measurements as a function of the logarithm of the concentration of K^+-ion (log K vs. log[K^+] plot).

From a qualitative point of view, the increase in log K with decreasing log c_K is a well-known phenomenon, which can be explained in terms of the competition between monovalent and divalent cations in the complexation process. From a quantitative point of view, linear relationships between log K and log c_K are theoretically expected [15,16]. Experimental results in the literature usually show such a linear relationship. Van Leeuwen [17] points out that the slope of the log K vs. log c_K plots is equal to $-\nu$, where ν is the exchange ratio between monovalent and divalent cations. Recent studies with Zn, Cd, Pb–PAA, PMA systems yielded slope values in the range -1.7 to -2.2 [18], in good agreement with some theoretical predictions [15,16]. Although the slope value of $-1.4(\pm 0.4)$ found for the Cu–PMA system is lower than those obtained for other PMA systems, the limited c_K range within which the results agree with those theoretically expected should be considered.

Conclusions

Under the experimental conditions studied, the Cu–PMA system appeared to be labile. Because of the capacitive currents from PMA, the DCP, NPP and RPP measurements were useless for quantitative studies. In contrast, DPP and DPASV seemed to be very useful for this purpose. Voltammetric titrations, by means of both techniques, at low degrees of dissociation of PMA, yielded results in agreement with those from the theoretical model. The anomalous behaviour (with respect to the model) observed at higher degrees of dissociation can be reasonably attributed to adsorption of Cu(II) onto cell materials and/or hydrolysis of Cu(II).

The financial support of the Spanish Ministry of Education and Science (DGICYT: Project PB90-0821) and of the Institut d'Estudis Catalans is acknowledged.

REFERENCES

1 J. Buffle, Complexation Reactions in Aquatic Systems: An Analytical Approach, Ellis Horwood, Chichester, 1988, Chap. 9.
2 H.P. van Leeuwen, R.F.M.J. Cleven and J. Buffle, Pure Appl. Chem., 61 (1989) 255; and references cited therein.
3 H.G. de Jong, H.P. van Leeuwen and K. Holub, J. Electroanal. Chem., 234 (1987) 1, 17; 235 (1987) 1.
4 M. Esteban, H.G. de Jong and H.P. van Leeuwen, Int. J. Environ. Anal. Chem., 38 (1990) 75.
5 M. Esteban, E. Casassas, H.G. de Jong and H.P. van Leeuwen, Anal. Chim. Acta, 229 (1990) 93.
6 J.M. Díaz-Cruz, C. Ariño, M. Esteban and E. Casassas, Electroanalysis, 3 (1991) 299.
7 J.M. Díaz-Cruz, M. Esteban, M.A.G.T. van den Hoop and H.P. van Leeuwen, Anal. Chim. Acta, 264 (1992) 163.
8 J.M. Díaz-Cruz, M. Esteban, M.A.G.T. van den Hoop and H.P. van Leeuwen, Anal. Chem., 64 (1992) 1769.
9 J.M. Díaz-Cruz, C. Ariño, M. Esteban and E. Casassas, J. Electroanal. Chem., 333 (1992) 33.
10 J.M. Díaz-Cruz, C. Ariño, M. Esteban, E. Casassas and H.P. van Leeuwen, J. Electroanal. Chem., (1992) in press.
11 E. Reisenhofer, A. Cesàro, F. Delben, G. Manzini and S. Paoletti, Bioelectrochem. Bioenerg., 12 (1984) 455.
12 M. Zief and J.W. Mitchell, Contamination Control in Trace Element Analysis, Wiley, New York, 1976.
13 M.A.G.T. van den Hoop, F.M.R. Leus and H.P. van Leeuwen, Collect. Czech. Chem. Commun., 51 (1991) 96.
14 C.F. Baes and R.E. Mesmer, The Hydrolysis of Cations, Wiley Interscience, New York, 1976.
15 M.T. Record, Jr., T.M. Lohman and P. de Haseth, J. Mol. Biol., 107 (1976) 145.
16 G.S. Manning, Q. Rev. Biophys., 11 (1978) 179.
17 H.P. van Leeuwen, Colloids Surf., 51 (1990) 359.
18 J.M. Díaz-Cruz, C. Ariño, M. Esteban and E. Casassas, Biophys. Chem., (1992) in press.

Analytica Chimica Acta, 273 (1993) 297–304
Elsevier Science Publishers B.V., Amsterdam

Semi-empirical full-wave expression for induced reactant adsorption in normal pulse polarography of labile metal–polyelectrolyte systems

Francesc Mas

Departament de Química Física, Facultat de Química, Universitat de Barcelona (UB), C / Martí i Franquès 1, E-08028 Barcelona (Spain)

Jaume Puy

Escola Tècnica Superior d'Enginyeria Agrària, Universitat Politècnica de Catalunya (UPC), Av. Rovira Roure 177, E-25006 Lleida (Spain)

José M. Díaz-Cruz, Miquel Esteban and Enric Casassas

Departament de Química Analítica, Facultat de Química, Universitat de Barcelona (UB), C / Martí i Franquès 1, E-08028 Barcelona (Spain)

(Received 1st June 1992)

Abstract

A semi-empirical expression is proposed for the normal pulse polarographic wave of the reduction of a metal ion in a labile metal–polyelectrolyte system, in the presence of an excess of ligand, and includes both the polyelectrolytic ligand adsorption and the induced adsorption of the metal ion. This expression avoids the need to know the values of the adsorption isotherms of both the complex and the polyelectrolytic ligand as well as their time and potential dependences. A non-linear fitting procedure is performed in order to obtain the parameters of the semi-empirical expression, from which an approximate value of the stability constant of the complex can be estimated. The accuracy of this semi-empirical expression is tested by simulated curves, and it is applied to experimental results for the Cd(II)–polymethacrylate complex, in order to obtain the stability constant of the complex from experimental data in the presence of adsorption phenomena.

Keywords: Polarography; Adsorption; Metal–polyelectrolyte systems; Polyelectrolyte ligands

A model has been recently proposed [1,2] for the interpretation of the normal pulse polarographic (NPP) reduction of a metal ion in a labile metal–polyelectrolyte system, in the presence of an excess of ligand, and includes both the polyelectrolyte adsorption and the induced adsorption of the metal ion. This model has been applied to experimental data of the Cd(II)–polymethacrylate system [3,4].

The model is based on the simple scheme of an electroactive metal ion, M, which is reduced to the metal, M^0, and a ligand L with which M can

Correspondence to: M. Esteban, Departament de Química Analítica, Facultat de Química, Universitat de Barcelona (UB), C/Martí i Franquès 1, E-08028 Barcelona (Spain).

form the electroinactive complex ML. Both L and ML can be adsorbed on the electrode surface:

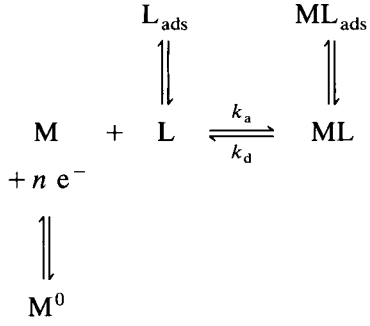

The model yields a general equation (Eqn. 13 in Ref. 1) which allows us to understand and to simulate characteristic NPP curves with induced adsorption phenomena, including the maxima at the onset of the wave and the depletion of the limiting currents. Furthermore, the general expression for the NPP response can be split into two parts: a sigmoidal contribution, $(I_{NPP})_{sigm}$, with a sigmoidal shape of the plot I_{NPP} vs. potential, and a peak contribution, $(I_{NPP})_{peak}$, responsible for the characteristic peaked shape observed in cases with either reactant or induced complex adsorption. These contributions can be expressed as:

$$I_{NPP} = (I_{NPP})_{sigm} + (I_{NPP})_{peak} \quad (1)$$

$$(I_{NPP})_{sigm} \equiv \frac{c(K)\, e^{ax}}{1 + c(K)\, e^{ax}} \{(I_{NPP})_{lim}\} \quad (2)$$

$$(I_{NPP})_{peak} = \frac{c(K)\, e^{ax}}{1 + c(K)\, e^{ax}} \left\{ -nFA \left(\frac{d\Gamma_{ML}}{dt} \right)_{t=t_d} \right\} \quad (3)$$

where $a = nF/RT$, $x = -(E(t_d) - E_0)$, $(I_{NPP})_{lim}$ is the limiting value of the current, and $(d\Gamma_{ML}/dt)_{t=t_d}$ indicates the time variation of the surface concentration of the complex at the drop time (t_d). The parameter $c(K)$ is related to the stability constant, K, of the complex [1] by:

$$c(K) \equiv \sqrt{\frac{D_{M^0}}{D_M}} \frac{1}{\sqrt{(1 + \epsilon K')(1 + K')}} \quad (4)$$

where ϵ is defined as the ratio of diffusion coefficient of the complex to that of the free metal, D_{ML}/D_M, and $K' = Kc_L^*$, c_L^* and K being the bulk concentration of the ligand L and the stability constant of the ML complex, respectively.

The peak contribution, $(I_{NPP})_{peak}$, depends on the stability constant K and on the set of adsorption parameters of the ligand and the complex. Thus, to obtain the value of the stability constant from this contribution, the values of the adsorption parameters and the model for the adsorption isotherms of the complex and of the polyelectrolyte must be known. However, the sigmoidal contribution $(I_{NPP})_{sigm}$, only depends on the stability constant of the complex, because $(I_{NPP})_{lim}$ can be found from the experimental full-NPP wave. A procedure has been described [3] to obtain stability constants and adsorption parameters simultaneously from NPP data recorded in the presence of adsorption phenomena. However, this procedure is time-consuming and requires some computing facilities.

The aim of this work is to develop a simple semiempirical procedure, based on fitting the peak contribution $(I_{NPP})_{peak}$ to a semiempirical expression, in order to obtain an estimate of the stability constant of the complex, K, from NPP data, by means of a simple non-linear regression analysis, requiring only a personal computer.

EXPERIMENTAL

Chemicals and apparatus have been described elsewhere [3]. All calculations were carried out on a PC (a compatible AT with a mathematical coprocessor). Non-linear regression analysis was done by using the ENZFITTER program [5].

RESULTS AND DISCUSSION

As has already been described [1–3], a general rigorous expression has been deduced for the response function of NPP (Eqn. 13 in Ref. 1). Curves of the full-NPP wave can be simulated from this model, as well as the two contributions to the current: $(I_{NPP})_{sigm}$ (Eqns. 20 and 21 in Ref. 1) and $(I_{NPP})_{peak}$ (Eqn. 22 in Ref. 1), when Langmuirian adsorption isotherms for both the ligand and the complex are assumed.

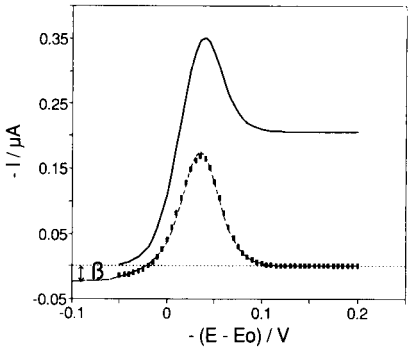

Fig. 1. Comparison between results obtained from the rigorous model and from Eqn. 5 (semi-empirical procedure): Thick solid line and black squares denote the total NPP current and the values of $-nFA\,(d\Gamma_{ML}/dt)_{t=t_d}$, respectively, both calculated by simulation using the rigorous model. Dotted line denotes the curve obtained by fitting the simulated $-nFA\,(d\Gamma_{ML}/dt)_{t=t_d}$ values (black squares) to Eqn. 5, which yields the values $\beta = 0.02(\pm 0.01)$, $p = 20(\pm 10)$, $r = 0.046(\pm 0.002)$ and $s = 0.066(\pm 0.002)$. Data used in the simulation are shown in row 14 of Table 1. Other data used were: $n = 2$, $T = 298.15$ K, $A = 0.52\times10^{-6}$ m^2, $D_M = 7.3\times10^{-10}$ m^2 s^{-1}, $D_{M^0(Hg)} = 20\times10^{-10}$ m^2 s^{-1}, $D_{ML} \approx D_L = 0.168\times10^{-10}$ m^2 s^{-1}, $E^\circ(Cd^{2+}/Cd(Hg)) = -0.3521$ V, $c_L^* = 1.2$ mol m^{-3}, $c_M^* = 1$ mol m^{-3}, and $t_p = 50$ ms.

A semi-empirical expression to reproduce the peak contribution is proposed in order to avoid the need to know the values of the adsorption isotherms of the complex and the polyelectrolyte, as well as their time and potential dependences. The reasoning behind the proposed expression is illustrated by the numerically simulated plots drawn in Fig. 1, which show that the variation of the time derivative of the surface concentration of the complex, $-nFA(d\Gamma_{ML}/dt)_{t=t_d}$, on the applied potential (dashed line) has a similar shape as the full-NPP wave (solid line). As a consequence, because the full-NPP response is the sum of a constant, $(I_{NPP})_{lim}$, and the term $-nFA(d\Gamma_{ML}/dt)_{t=t_d}$, both multiplied by a sigmoidal function, the semi-empirical expression for this derivative term has been chosen as:

$$-nFA\left(\frac{d\Gamma_{ML}}{dt}\right)_{t=t_d} = -\beta + \frac{p\,e^{ax}}{1+p\,e^{ax}}\left\{\beta + \frac{r\,e^{ax}}{(1+s\,e^{ax})^2}\right\} \qquad (5)$$

where β, p, r and s are empirical parameters. In Eqn. 5, the term $r\,e^{ax}/(1+s\,e^{ax})^2$ is the derivative of a sigmoidal function, and it has been chosen because of its peak shape. Furthermore, the term, $-\beta$, which represents the contribution of the time derivative of the complex coverage at potentials close to the base potential ($x \to -\infty$), has been introduced in order to obtain a curve, similar to a full-NPP wave, which begins at $-\beta$ and ends at zero (see dotted line in Fig. 1).

Figure 1 shows a simulated NPP polarogram, from the numerical resolution of Eqn. 13 of Ref. 1, and the derivative contribution of the complex coverage at the drop time. The numerical values of this contribution (black squares in Fig. 1) are used to fit the four parameters of Eqn. 5, using a non-linear least squares curve fit. It can be seen that an excellent agreement is obtained. Therefore, for the full-NPP wave a semi-empirical equation of five parameters is proposed: the four parameters of Eqn. 5, and the parameter c an estimate of the stability constant (K) through the expression $c(K)$ defined in Eqn. 4. Then, the semi-empirical expression can be written as:

$$I_{NPP} = \frac{c\,e^{ax}}{1+c\,e^{ax}}\left[(I_{NPP})_{lim} - \beta + \frac{p\,e^{ax}}{1+p\,e^{ax}}\left\{\beta + \frac{r\,e^{ax}}{(1+s\,e^{ax})^2}\right\}\right] \qquad (6)$$

where $(I_{NPP})_{lim}$ is given by either the numerical or the experimental full wave.

For convergence of the fitting procedure, the parameters included in Eqn. 6 must be independent. In order to ensure this condition, Eqn. 6 can be rewritten in the form:

$$I_{NPP} = \frac{c\,e^{ax}}{1+c\,e^{ax}}\{(I_{NPP})_{lim} - \beta\} + \frac{q\,e^{ax}}{1+q\,e^{ax}}\left\{\beta + \frac{r\,e^{ax}}{(1+s\,e^{ax})^2}\right\} \qquad (7)$$

where the sigmoidal function depending on parameter p is changed by a new sigmoidal function depending on parameter q, which includes the multiplication of the two sigmoidal functions of Eqn. 6, depending on parameters c and p.

The two contributions of the current, Eqns. 2 and 3 can be now identified as:

$$(I_{NPP})_{sigm} \equiv \frac{c\ e^{ax}}{1 + c\ e^{ax}}\{(I_{NPP})_{lim}\} \quad (8)$$

$$(I_{NPP})_{peak} = \frac{c\ e^{ax}}{1 + c\ e^{ax}}\{-\beta\} + \frac{q\ e^{ax}}{1 + q\ e^{ax}}\left\{\beta + \frac{r\ e^{ax}}{(1 + s\ e^{ax})^2}\right\} \quad (9)$$

Figure 2 shows the full-NPP wave as well as these two contributions, whose parameters have been obtained from a non-linear least squares fit of Eqn. 7 to the numerical full-NPP wave of Fig. 1. Thus, if Eqn. 6 is used in the fitting procedure, a value of $c = 1.09 \pm 0.05$ ($\chi_r^2 = 2 \times 10^{-6}$) is obtained, while from Eqn. 7 $c = 0.8 \pm 0.2$ ($\chi_r^2 = 7 \times 10^{-7}$). The value of K assumed in the simulation yields a value of $c(K) = 0.7086$. In this way, the agreement between the simulated and the fitted values of the parameter c is improved.

In order to orientate one as to the choice of the initial values for the empirical parameters, it is of interest to know their influence on the full-NPP wave. Figure 3 shows these dependences; the inflexion point values are affected by c (Fig. 3a) and β (Fig. 3b), the peak current values by q (Fig. 3c), r (Fig. 3d) and s (Fig. 3e), and both the peak potential and the peak width values are affected, diametrically by q (Fig. 3c) and s (Fig. 3e).

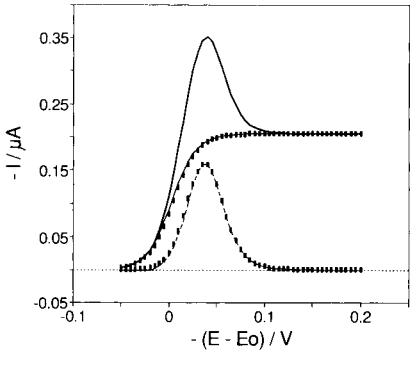

Fig. 2. Comparison between results obtained from the rigorous model and those from Eqn. 7 (semi-empirical procedure): Thick solid line denotes the total NPP current calculated by simulation using the rigorous model. The black squares denote the sigmoidal and the peak components of that simulated NPP current. Solid and dotted lines denote the sigmoidal and peak components, respectively, of the curve obtained by fitting the simulated total current to Eqn. 7. Simulated and fitted parameters are the same as shown in Fig. 1 and row 14 of Table 1.

Since the main object of this work was to determine the stability constant K of the complex, special attention was paid to the $c(K)$ function. A non-linear least squares fit must be performed in order to obtain the empirical parameters of Eqn. 7 and then, from the value of $c(K)$, an estimated value of K. Table 1 shows the results of several fitting procedures applied to numerical full-NPP waves, obtained from Eqn. 13 of Ref. 1, with different values of the adsorption parameters, Γ_m, K_{ML} and K_L (see Eqn. 17 in Ref. 1), and the stability constant K. All the fitting procedures show good agreement between the numerical values and the semi-empirical values obtained from Eqn. 7, as indicated by the satisfactory values of χ_r^2. Figure 4 shows some examples of this fitting procedure with different shapes of the full-NPP wave. In all cases, satisfactory fits are obtained, although not all the c values are in good agreement with $c(K)$ used in the simulation. A detailed study of Table 1 and Fig. 4 suggests that good agreement between $c(K)$ and c is obtained for waves with a smallish peak size, independently of the value of other parameters (e.g., curves 2, 3 and 4 in Fig. 4a and curves 3 and 4 in Fig. 4b). Then, in order to apply the procedure proposed here to the experimental data, smallish peaked waves must be obtained by a suitable choice of c_L^* and pulse time (t_p).

A comment is necessary for cases in which the full wave does not show a peak, even though they are being simulated with non-zero adsorption parameters. While some cases (curves 4 of Fig. 4a and b) can be fitted by Eqn. 7 with five independent parameters (as shown in rows 16 and 20 of Table 1), other cases cannot be fitted (rows 3 and 7 of Table 1) and, therefore, parameters q, r and s must be kept constant because they are directly related to the peak current. Since fixed values for these parameters do not affect the results of the fitting procedure in this last case, they could be taken to be zero. The agreement between the

fitted parameter c and the parameter $c(K)$ used in the simulation is much better for cases in which all five parameters have been fitted from Eqn. (7) than for cases in which q, r and s have not been used in the fitting procedure. This is because in these last cases only the sigmoidal contribution is taken into account, giving similar errors to those shown when the limiting currents are used in order to obtain the stability constant values from expressions without adsorption [3].

This procedure has been applied to the Cd(II)–polymethacrylic acid system in order to obtain experimental values for the stability constant, K, of the 1:1 ML complex, without neglecting the adsorption process, but avoiding the assumption of a certain kind of adsorption

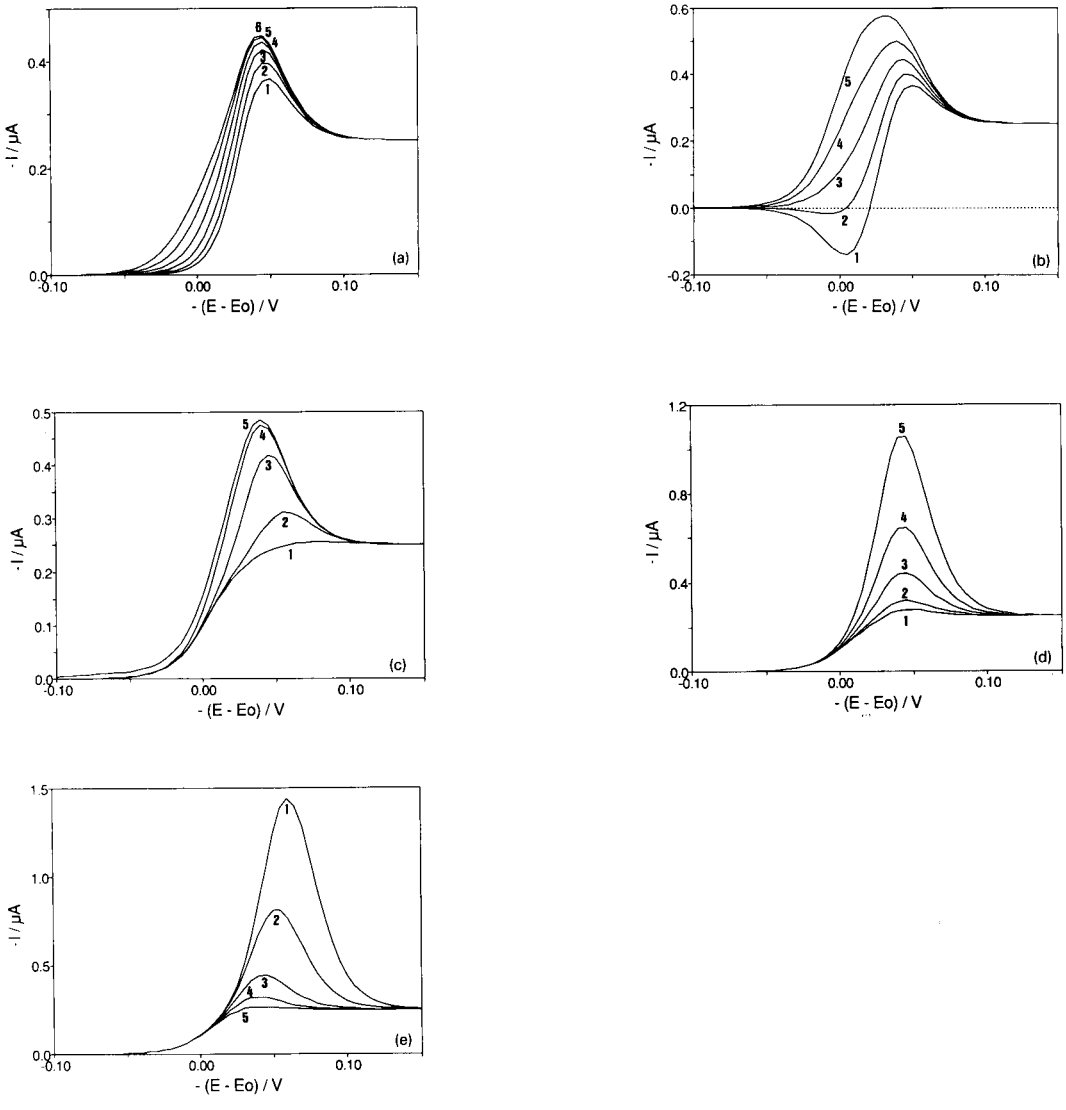

Fig. 3. Influence of the parameters (a) c, (b) β, (c) q, (d) r and (e) s on the NPP current simulated by using Eqn. 7. When not indicated otherwise, the parameters used were: $(I_{NPP})_{lim} = 0.25\ \mu A$, $c = 0.7$, $\beta = 0.01$, $q = 0.2$, $r = 0.05$ and $s = 0.05$. a: Values of c: (1) 0.05, (2) 0.1, (3) 0.2, (4) 0.4, (5) 0.8 and (6) 1.5; b: values of β: (1) 1, (2) 0.5, (3) 0, (4) −0.5 and (5) −1; c: values of q: (1) 0.001, (2) 0.01, (3) 0.1, (4) 1 and (5) 1000; d: values of r: (1) 0.01, (2) 0.02, (3) 0.05, (4) 0.1 and (5) 0.2; e: values of s: (1) 0.01, (2) 0.02, (3) 0.05, (4) 0.1 and (5) 0.2.

TABLE 1

Comparison between the parameters used in the simulation of the NPP curves, by means of the rigorous model assuming Langmuirian adsorption, and the parameters obtained by fitting these curves to the semiempirical Eqn. 7

	Γ_M (mol m^{-2})	K_{ML} (M^{-1})	K_L (M^{-1})	K (M^{-1})	$c(K)$	c	β	q	r	s	χ_r^2
1	10^{-5}	10^4	5×10^2	2400	0.7086	0.7(±0.2)	0.01(±0.04)	0.20(±0.02)	0.174(±0.008)	0.098(±0.003)	5×10^{-6}
2	10^{-6}	10^6	5×10^2	2400	0.7086	0.68(±0.03)	−0.025(±0.005)	2.0(±0.1)×10^{-3}	0.20(±0.04)	0.043(±0.004)	2×10^{-6}
3	10^{-5}	10^4	5×10^4	2400	0.7086	0.843(±0.005)	−4(±2)×10^{-4}	–	–	–	3×10^{-7}
4	10^{-5}	10^6	5×10^4	2400	0.7086	0.25(±0.05)	−0.09(±0.03)	0.049(±0.004)	0.109(±0.006)	0.049(±0.001)	7×10^{-6}
5	10^{-5}	10^4	5×10^2	4500	0.5280	0.3(±0.1)	−0.04(±0.06)	0.07(±0.02)	0.10(±0.02)	0.063(±0.006)	4×10^{-6}
6	10^{-6}	10^6	5×10^2	4500	0.5280	0.41(±0.03)	−0.038(±0.006)	1.1(±0.1)×10^{-3}	0.14(±0.04)	0.028(±0.003)	3×10^{-6}
7	10^{-5}	10^4	5×10^4	4500	0.5280	0.660(±0.007)	−6(±3)×10^{-4}	–	–	–	9×10^{-7}
8	10^{-5}	10^6	5×10^4	4500	0.5280	0.16(±0.06)	−0.06(±0.03)	0.036(±0.004)	0.039(±0.002)	0.023(±0.001)	7×10^{-6}
9	10^{-5}	10^4	5×10^2	8000	0.3896	0.2(±0.1)	−0.02(±0.04)	0.035(±0.007)	0.06(±0.01)	0.040(±0.004)	4×10^{-6}
10	10^{-6}	10^6	5×10^2	8000	0.3896	0.15(±0.01)	−0.062(±0.006)	7.4(±0.5)×10^{-4}	0.05(±0.02)	0.015(±0.002)	2×10^{-6}
11	10^{-5}	10^4	5×10^4	8000	0.3896	0.45(±0.06)	0.2(±0.3)	0.455(±0.005)	2.1(±0.1)×10^{-2}	0.384(±0.006)	1×10^{-9}
12	10^{-5}	10^6	5×10^4	8000	0.3896	0.09(±0.04)	−0.04(±0.02)	0.016(±0.002)	0.023(±0.001)	1.47(±0.05)×10^{-4}	6×10^{-6}
13	1.5×10^{-6}	10^5	10	2400	0.7086	0.34(±0.01)	−0.19(±0.01)	0.016(±0.001)	0.08(±0.02)	0.065(±0.008)	3×10^{-7}
14	1.5×10^{-6}	10^5	10^3	2400	0.7086	0.8(±0.2)	−0.01(±0.04)	3(±3)	0.037(±0.001)	0.056(±0.001)	7×10^{-7}
15	1.5×10^{-6}	10^4	10	2400	0.7086	0.79(±0.06)	0.2(±0.2)	0.80(±0.01)	0.076(±0.001)	0.227(±0.002)	4×10^{-8}
16	1.5×10^{-6}	10^4	10^3	2400	0.7086	0.67(±0.03)	−0.16(±0.04)	0.42(±0.06)	0.09(±0.01)	0.51(±0.04)	7×10^{-8}
17	2×10^{-6}	10^5	10	2400	0.7086	0.17(±0.01)	−0.37(±0.04)	0.020(±0.006)	0.031(±0.008)	0.031(±0.006)	2×10^{-7}
18	2×10^{-6}	10^5	10^3	2400	0.7086	0.2(±0.1)	−0.48(±0.08)	0.07(±0.01)	0.043(±0.004)	0.055(±0.004)	2×10^{-7}
19	2×10^{-6}	10^4	10	2400	0.7086	0.65(±0.06)	−0.17(±0.08)	0.4(±0.1)	0.12(±0.01)	0.22(±0.01)	2×10^{-7}
20	2×10^{-6}	10^4	10^3	2400	0.7086	0.77(±0.04)	0.2(±0.1)	0.80(±0.01)	0.089(±0.002)	0.347(±0.005)	7×10^{-8}

[a] Γ_M, K_{ML}, K_L, K and $c(K)$ are the parameters assumed in the numerical simulation. c, β, q, r and s are the fitted parameters obtained from Eqn. 7. χ_r^2 values of the fittings are also given. The rest of the values used in the simulation are the same as in Fig. 1.

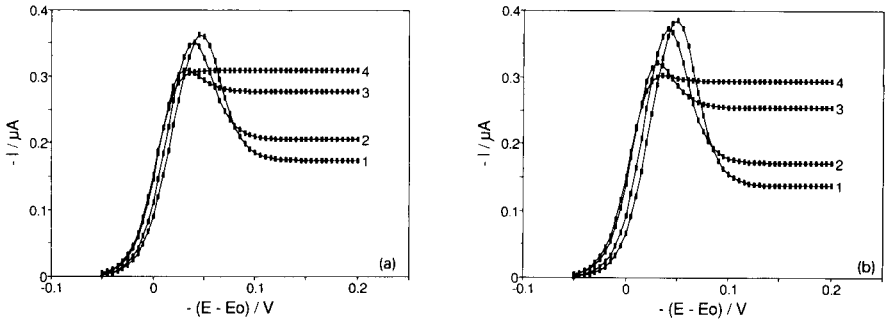

Fig. 4. Comparison between results obtained from the rigorous model and those from Eqn. 7 (semi-empirical procedure): Black squares denote the values of the total NPP current calculated by simulation using the rigorous model, and solid line denotes the curve fitted by using Eqn. 7. The data used in the simulation and the results of the fitting are shown in Table 1. a: rows (1) 13, (2) 14, (3) 15 and (4) 16 of Table 1; b: rows (1) 17, (2) 18, (3) 19 and (4) 20 of Table 1. The rest of parameters were the same as in Fig. 1.

isotherms. The same experimental values of Ref. 3 have been chosen to compare the fitted values of K obtained by the semi-empirical Eqn. 7 with those obtained by the more accurate, but cumbersome, procedure applied in Ref. 3.

Table 2 and Fig. 5 show the results of the fitting procedure. From the estimate of parameter c, for waves with smallish peaks (those yielding the more satisfactory results, as previously mentioned), and using Eqn. 4, it is possible to

TABLE 2

Results of the fit of the experimental NPP currents obtained for the Cd–PMA system to Eqn. 7 [a]

c_T^* (M)	t_p (ms)	c	$\log(K/M^{-1})$	β	q	r	s	χ_r^2
5×10^{-5}	50	0.7(±0.2)	3.62	0.1(±0.3)	0.7(±0.1)	0.0183(±0.0004)	0.0294(±0.0005)	3×10^{-5}
	75	1(±2)	–	0.063(±0.006)	0.37(±0.08)	0.023(±0.003)	0.064(±0.006)	3×10^{-6}
	100	0.5(±0.4)	3.98	0.07(±0.05)	0.51(±0.02)	0.1481(±0.0003)	0.076(±0.001)	2×10^{-6}
1×10^{-4}	50	0.33(±0.06)	4.24	−0.13(±0.04)	0.04(±0.02)	0.05(±0.01)	0.027(±0.004)	3×10^{-5}
	75	1.0(±0.4)	3.22	0.05(±0.02)	0.07(±0.03)	0.08(±0.03)	0.07(±0.01)	2×10^{-5}
	100	0.52(±0.08)	3.88	0(±1)	0.3(±0.1)	0.034(±0.003)	0.075(±0.004)	3×10^{-5}

[a] α_d(PMA) = 0.6, [KNO_3] = 0.1 M, $c_L^* = 10^{-3}$ M.

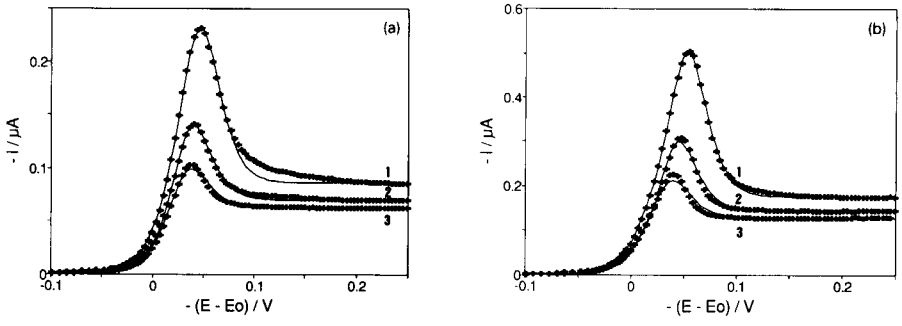

Fig. 5. Fit of the experimental NPP currents obtained for the Cd–PMA system to the semi-empirical Eqn. 7. (α_d(PMA) = 0.6, [KNO_3] = 0.1 M, $c_L^* = 10^{-3}$ M). a: $c_T^* = 5\times10^{-5}$ M, t_p(ms): (1) 50, (2) 75 and (3) 100; b: $c_T^* = 1\times10^{-4}$ M, t_p(ms): (1) 50, (2) 75 and (3) 100.

obtain a mean value of $\log(K/M^{-1}) = 3.6 \pm 0.4$, which is in satisfactory agreement with the numerical, fitted value of $\log(K/M^{-1}) = 3.4 \pm 0.1$ reported in Ref. 3.

Conclusion

A new semi-empirical procedure is proposed for determining stability constant values from NPP data reflecting induced adsorption phenomena. For NPP waves with smallish peaks, this procedure yields satisfactory results, which agree with those obtained from the rigorous, but more cumbersome, procedure previously proposed. Although some additional parameters without physical meaning are obtained during the fitting process, parameter c only contains the information on complexation, which is the main interest of the present approach.

The authors gratefully acknowledge support of this research by the Spanish Ministry of Education and Science (DGICYT: Projects PB 90-0821 and PB 90-0455), and from the Institut d'Estudis Catalans. A personal FPI grant from the Spanish Government to J.M. Díaz-Cruz is also gratefully acknowledged.

REFERENCES

1 F. Mas, J. Puy, J.M. Díaz-Cruz, M. Esteban and E. Casassas, J. Electroanal. Chem., 326 (1992) 299.
2 J. Puy, F. Mas, J.M. Díaz-Cruz, M. Esteban and E. Casassas, J. Electroanal. Chem., 328 (1992) 271.
3 J. Puy, F. Mas, J.M. Díaz-Cruz, M. Esteban and E. Casassas, Anal. Chim. Acta., 268 (1992) 261.
4 J.M. Díaz-Cruz, M. Esteban, E. Casassas, F. Mas and J. Puy, to be published.
5 R.J. Leatherbarrow, ENZFITTER Manual: A Non-linear Regression Data Analysis Program for the IBM PC (and true compatibles), Elsevier, Amsterdam, 1987.

Analytica Chimica Acta, 273 (1993) 305–311
Elsevier Science Publishers B.V., Amsterdam

Modified carbon paste electrodes for the study of metal–humic substances complexation

Z. Navrátilová and P. Kula

Institute of Industrial Landscape Ecology Ostrava, Czechoslovak Academy of Sciences, Hladnovská 9, 710 00 Ostrava 2 (Czechoslovakia)

(Received 1st June 1992; revised manuscript received 25th September 1992)

Abstract

The complexation of copper, zinc, mercury and silver with humic substances was studied by means of carbon paste electrodes modified with these ligands. Six different humic substances were studied. The different behaviour of the copper complexes with solid humic ligands in the electrode were found to correlate with copper complexes formed with ligands in the solution. The complexation reactions of metals are associated with dissolution and dissociation of solid humic substances. The carbon paste electrodes modified with humic substances would be suitable for the study of some soil processes.

Keywords: Voltammetry; Carbon paste electrodes; Copper; Humic substances; Mercury; Silver; Zinc

Chemically modified carbon paste electrodes can serve to enhance the selectivity and sensitivity of voltammetric methods. Modifiers with various characteristics have been used for the purpose of preconcentrating analytes on the surface of electrodes [1]. The use of modified carbon paste electrodes for electrochemical detection in liquid chromatography and flow-injection analysis has been reviewed [2,3]. Modifiers such as clays and zeolites have been studied in recent years [4–6]. New classes of modifying species such as natural ionic polysaccharides [7], enzymes [8] and plants [9] have also been described.

Many organic ligands act as metal-complexing agents when added to carbon paste. Not only organic ligands such as phenanthroline, dimethylglyoxime, crown ethers or dithizone can be used as modifiers, but also substances such as zeolites [4] or clays [6] accumulate some heavy metals. Carbon paste electrodes modified with humic acids improved the determination of mercury [10]. Other metal complexation reactions with humic acids incorporated in the carbon paste have also been reported [11]. This type of electrode is suitable not only for the determination of metals, but also for the study of reactions between metals and humic substances.

This paper deals with carbon paste electrodes modified with various humic substances. The complexation of these humic substances with copper, mercury, zinc and silver is demonstrated. The use of a carbon paste electrode modified with humic matter allows an approach close to natural conditions of metal complexation in soils.

Correspondence to: Z. Navrátilová, Institute of Industrial Landscape Ecology Ostrava, Czechoslovak Academy of Sciences, Hladnovská 9, 710 00 Ostrava 2 (Czechoslovakia).

EXPERIMENTAL

Apparatus

A PA3 polarographic analyser and a Model 4105 *X–Y* recorder (Laboratory Instruments,

Prague) were employed. An electrochemical cell of conventional design was equipped with a three-electrode system: carbon paste, saturated calomel and platinum electrodes.

Modified carbon paste containing humic substances was prepared by ultrasonic mixing of graphite powder with the modifier in hexane. The hexane was then evaporated, 2 g of Nujol were added and the mixture was homogenized in a glass mortar dish for about 2 h. To prepare the electrode, a portion of the paste was inserted in a plastic tube provided with a brass screw that ensured electrical contact and extrusion of the paste. The effective area of the electrode was 3.14 mm^2.

Reagents

Stock standard solutions of Cu(II) and Zn(II) were prepared from Fixanal standards (Riedel-de Haën); Titrisol standard (Merck) was used for Hg(II) solution. A stock standard solution of Ag(I) was prepared from analytical-reagent grade Ag_2SO_4 (Lachema).

Sodium acetate and acetic acid (both of analytical-reagent grade, Lachema) were used to prepare acetate buffers and background electrolytes. Sodium perchlorate (analytical-reagent grade, Lachema) was used for the adjustment of the ionic strength.

Humic substances HS.A, HS.OA and HS.E (Serva) and humic acids HA1, HA2 and HA3 were used as modifiers of the carbon paste.

Humic acids HA1 and HA2 were prepared from commercial preparations of humic acid sodium salts (HA1-Na, Serva; HA2-Na, Aldrich) by the following procedure: an aqueous solution of the sodium salt preparation was filtered, 0.1 M HCl was added and after 24 h the precipitate was filtered and air-dried. Humic acid HA3 was prepared from naturally oxidized North Bohemia lignite (kapucín) as follows: finely crushed lignite was dissolved in 0.1 M NaOH, the solution was centrifuged (6500 *g*), 0.1 M HCl was added and after 24 h the precipitate was filtered and air-dried.

Barium salts HA1-Ba and HA2-Ba were prepared from aqueous solutions of the HA1-Na and HA2-Na preparations by precipitation with $BaCl_2$. The precipitates were filtered and air-dried.

Redistilled water was used throughout. The glassware was cleaned in a Laborcleaner (Labelchem, Czechoslovakia) and with redistilled water (both for 24 h).

Procedures

Differential-pulse voltammetry (DPV) with carbon paste electrodes at a scan rate of 10 mV s^{-1}, a pulse amplitude of 25 mV and a pulse frequency of 5 s^{-1} was applied. A small piece of the paste was extruded from the plastic tube and removed. The fresh surface was polished on a plastic sheet. The cleaning and polishing procedures were repeated before each measurement. The polished electrode was inserted in the electrochemical cell and the voltammogram was immediately recorded. The concentrations of metals and the potential ranges used were as follows: Cu(II), 1.57×10^{-6} M, -1.0 V to $+0.1$ V; Zn(II), 7.65×10^{-6} M, -1.4 V to -0.8 V; Hg(II), 1.25×10^{-6} M, -1.0 V to $+0.4$ V; Ag(I), 9.27×10^{-7} M, -0.6 V to $+0.45$ V.

Cyclic voltammetry (CV) on a hanging mercury drop electrode (HMDE) was carried out at scan rates from 1 to 200 mV s^{-1}. The surface area of the mercury drop was 1.58 mm^2.

When CV on the HMDE and DPV on the unmodified electrode CPE(0) were carried out in a solution of humic substances, the latter were added in the form of sodium salts to the background electrolyte.

RESULTS AND DISCUSSION

Eight types of modified carbon paste electrodes and the unmodified electrode, CPE(0), were prepared. The modified electrodes are denoted by CPE followed by the humic substance in parentheses, e.g., CPE(HA1). All electrodes contained 10% of modifier. The measurements on the modified electrodes were compared with those on the unmodified electrode in the presence of humic substances in the electrolyte.

Because potential shifts have been found with humic acid-containing electrodes [10,11], it is as-

sumed that metal complexes are formed on the electrode surface. Different complexation equilibria were assumed to exist for particular humic substances and the various metals. Therefore, differences in the dependence of the current and potential shift on pH were expected.

Potential shift was calculated as $\Delta E = E_p - E_p^L$, where L specifies the presence of a ligand in the carbon paste electrode or in the solution.

Voltammetry of Cu(II) with CPE(HA1), CPE(HA2) and CPE(HA3) electrodes

The differential-pulse voltammogram of 1.57×10^{-6} M Cu(II) on the humic substances-modified electrode exhibits a well developed peak with a potential E_p shifted with respect to that on the unmodified CPE. As the potential shifts are important parameters in complexation equilibria [12,13], they were examined as a function of pH. The dependence of the current responses on pH were also examined.

Values $\Delta E > 0$ were found on CPE(HA1), CPE(HA2), and CPE(HA3) in the set of acetate buffers of pH 3.6–6.4 with a non-constant ionic strength. The curves $\Delta E = f(\text{pH})$ show a maximum pH at which an apparent release of humic substances from the electrode surface takes place. At the same pH a decrease in the current responses was found to occur. These results for CPE(HA3) are shown in Fig. 1; the dependence on CPE(HA1) and CPE(HA2) showed very similar courses. Similar dependences of current and ΔE on pH were obtained in solutions with a constant ionic strength of $I = 0.2$, except that the values of ΔE were lower. Similar results were obtained with an ionic strength of $I = 0.5$ for both CPE(HA1) and CPE(HA2). The situation is different for CPE(HA3) at $I = 0.5$, where apparently the acid HA3 is not released from the surface of the electrode in the solution. The electrode CPE(HA3) also shows a $\Delta E = f(\text{pH})$ curve with a maximum, but the current response does not decrease rapidly (Fig. 2), in contrast to CPE(HA1) and CPE(HA2).

In general, the current decrease is associated with the release of humic substances from the electrode surface (Table 1). For example, the current response on CPE(HA1-Ba) and CPE

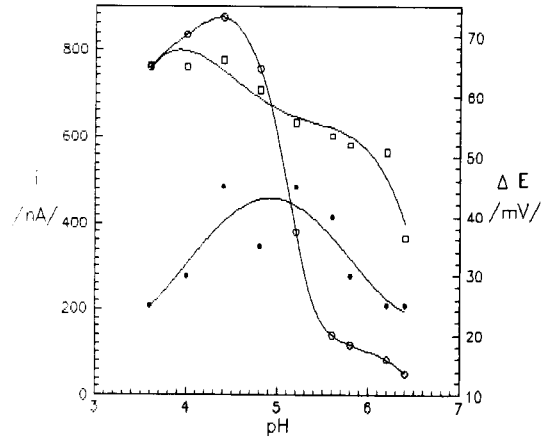

Fig. 1. Influence of pH on the voltammetry of 1.57×10^{-6} M Cu(II) on the CPE(0) and CPE(HA3) electrodes, with acetate buffers, non-constant ionic strength. *i*: ○ = CPE(HA3); □ = CPE(0). ΔE: ● = CPE(HA3).

(HA2-Ba) showed the same dependences on pH as with CPE(0). Potential shifts on CPE(HA1-Ba) and CPE(HA2-Ba) were found, but the compounds HA1-Ba and HA2-Ba were not released from the electrode and a rapid current decrease was not found.

Seemingly the metal complexes with HA1, HA2 and HA3 are formed after the dissolution of humic substances in the solution. However, the potential shifts ΔE were also found on the modi-

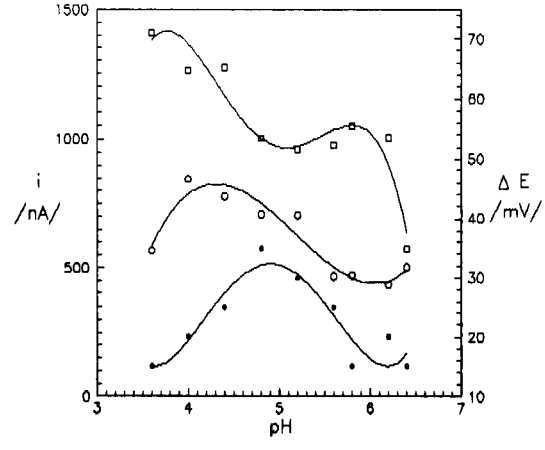

Fig. 2. Influence of pH on the voltammetry of 1.57×10^{-6} M Cu(II) on the CPE(0) and CPE(HA3) electrodes, with acetate buffers, ionic strength $I = 0.5$. Symbols as in Fig. 1.

fied CPEs under conditions of no dissolution of humic substances in the solution. This conclusion is considered to be important because it confirms the earlier presumption about the metal complexations with solid humic substances present on the electrode surface [10,11]. The complex-forming reactions are probably connected with the dissociation of humic substances on the electrode surface in this instance.

Different results were obtained in the voltammetry of 1.57×10^{-6} M Cu(II) on CPE(0) in the presence of humic substances in the solution. The current response decreased uniformly over the whole pH range in the presence of HA3-Na. Also, the dependence of ΔE on pH is different to that on CPE(HA3), although the magnitude of the ΔE values obtained with CPE(0) in the presence of HA3-Na and with CPE(HA3) are comparable. The results obtained in the presence of HA1-Na and HA2-Na are similar to those shown in Fig. 3.

The value $\Delta E'$ represents the corrected value of ΔE according to

$$\Delta E' = \Delta E + 0.03 \log(i/i_L)$$

where i is the metal current response in absence of ligands and i_L is current response in the presence of ligands. This equation follows from the elementary relationships for half-wave potential shifts in the presence of ligands that were postulated in De Ford and Hume's method [13].

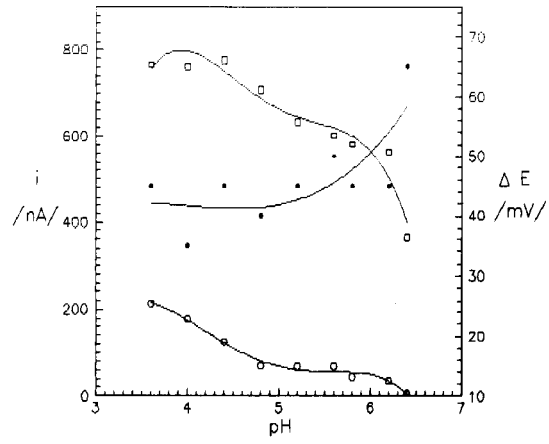

Fig. 3. Influence of pH on the voltammetry of 1.57×10^{-6} M Cu(II) on the CPE(0) electrode in the absence and presence of 16 mg of HA3-Na, with acetate buffers, non-constant ionic strength. i: ○ = CPE(0)+HA3-Na; □ = CPE(0). ΔE: ● = CPE(0)+HA3-Na.

The concept about complexation in the electrode/solution interface is supported by the dependences of ΔE and $\Delta E'$ on pH. Figures 4 and 5 show these dependences for the HA3; other humic substances showed the same results for all the metals examined.

TABLE 1

Influence of ionic strength on the voltammetry of Cu(II) on the modified electrodes in pH range 3.6–6.4

Ionic strength	Effect	pH						
		CPE(HA1)	CPE(HA2)	CPE(HA3)	CPE(HA1-Ba)	CPE(HS.A)	CPE(HS.OA)	CPE(HS.E)
0.015–0.197	Release of humic substances	4.8	4.4	5.2	No release	5.2	5.6	No release
	Current decrease	4.8	4.4	5.2	No decrease	5.2	5.2–5.6	no decrease
	ΔE maximum	4.8–5.2	4.4	5.2	5.2	($\Delta E = 0$)	No maximum	($\Delta E < 0$)
0.2	Release of humic substances	5.2	4.8	5.8	No	5.6	6.2	No release
	Current decrease	4.8–5.2	4.4–4.8	5.8	measurements	5.2–5.6	5.8–6.2	No decrease
	ΔE maximum	5.2	5.2–5.6	5.2		($\Delta E < 0$)	No maximum	($\Delta E < 0$)
0.5	Release of humic substances	5.6	5.2	No release				
	Current decrease	5.2–5.6	4.8–5.2	No decrease	No measurements			
	ΔE maximum	5.2–5.6	5.6	4.8				

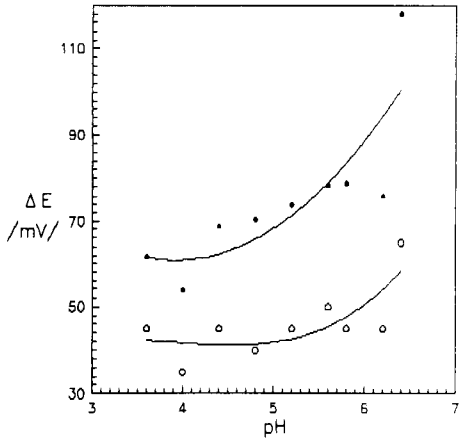

Fig. 4. Dependences of (○) ΔE and (●) $\Delta E'$ on pH on the CPE(0) electrode in the presence of 16 mg of HA3-Na in solutions with non-constant ionic strength, 1.57×10^{-6} M Cu(II).

The dependence of $\Delta E'$ on pH is identical with the dependence of ΔE in the pH range where no release of ligand from the electrode takes place (Fig. 5). It is in the pH range where we assume that complexations take place in the electrode/solution interface. The values of $\Delta E'$ are higher than ΔE in the pH range where ligand is released from the electrode surface, which is equal to the complexation in the solution (Fig. 4). In this pH range complexes are probably formed both near the electrode surface and in the solution. The course of the current corresponds with this idea as the current decreases in this pH range (Fig. 1). The complexes formed in the solution do not contribute to the current response, which is caused by insufficiently rapid attainment of equilibrium between the metal and complex in the diffusion layer of the electrode, so that the metal–humic substances complexes formed in the solution dissociate slowly.

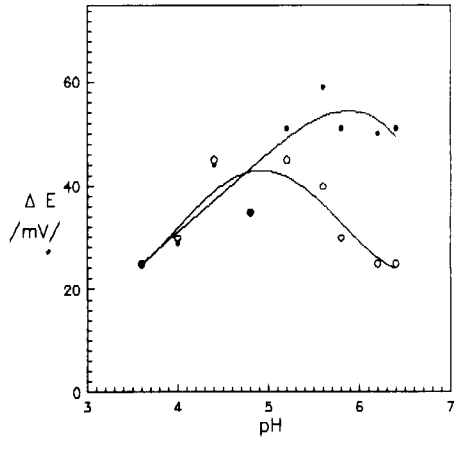

Fig. 5. Dependences of (○) ΔE and (●) $\Delta E'$ on pH on the CPE(HA3) electrode in solutions with non-constant ionic strength, 1.57×10^{-6} M Cu(II).

The complexes formed in the interface contribute to the rapid attainment of equilibrium between the metal and complex in the diffusion layer of the electrode, so these complexes behave as labile, rapidly dissociating species. Because the ligand is not released into the solution, the currents i and i_L are identical and so are the values of ΔE and $\Delta E'$ (Fig. 5), characterizing the complex.

Depending on the dissociation of a complex ML, three types of complexes can be described [12]. If the reaction $ML \rightleftharpoons M + L$ is sufficiently rapid for the attainment of equilibrium between M and ML in the whole diffusion layer on the electrode, the complex ML is said to be labile. If the dissociation of ML is so slow that the complex ML remains unchanged in the diffusion layer, the complex is said to be inert. If the dissociation is slow, but partial equilibrium is achieved within a sufficient distance from the electrode, the complex is said to be slowly dissociating. In order to extract information about metal complexation, the characteristic parameters of the voltammetric curves obtained in the presence of the ligand must be compared with those obtained in its absence. We tried to use this procedure for the evaluation of the complexation by means of the voltammetric parameters in case of voltammetry of Cu(II) on the modified electrodes. The procedure was also used for the voltammetry of Cu(II) on CPE(0) and for cyclic voltammetry on the HMDE.

The complexes Cu–HA1, Cu–HA2 and Cu–HA3 behaved as slowly dissociating species in the pH range 3.6–6.4, as DPV on the unmodified electrode showed. Cyclic voltammetry on the HMDE confirmed this result in the buffers with a non-constant ionic strength and with ionic strengths of $I = 0.2$ and 0.5. It can be said that

the complexes of copper with humic substances are slowly dissociating when they are formed in the solution. This fact proved the above presumption based on the courses of ΔE and $\Delta E'$.

Voltammetry on CPE(HA1), CPE(HA2) and CPE(HA3) gave the following results. In the pH range with no release of ligands from the electrode surface, the complexes Cu–HA1, Cu–HA2 and Cu–HA3 behave as labile complexes. This means that the equilibrium between Cu and the complex is achieved sufficiently rapidly in the diffusion layer. The rapid attainment of equilibrium is probably caused by the presence of ligands at the electrode surface. The complexes behave as slowly dissociating species in the pH range where ligands are released into the solution and where the complexation in the solution is assumed to occur, except for the complexation in the electrode/solution interface. These results are also in agreement with the above presumption about the complexation of Cu with humic substances present on the electrode surface.

Voltammetry of Cu(II) with CPE(HS.A), CPE(HS.OA) and CPE(HS.E) electrodes

The substances HS.A and HS.OA are slightly soluble in water but readily soluble in 0.1 M NaOH. HS.E is soluble only in organic solvents. In the pH range 3.6–6.4 only HS.A and HS.OA are apparently released from the electrode surface. The current response decreased rapidly on CPE(HS.A) at pH 5.2 and on CPE(HS.OA) at pH 5.6; no current decrease was found on CPE (HS.E). A uniform current decrease over the whole pH range was observed with CPE(0) in the presence of HS.A and HS.OA (in the form of their sodium salts).

Different potential shifts were obtained with these electrodes. $\Delta E = 0$ for CPE(HS.A). The peak potential E_p shifts slightly to more negative values and ΔE is small and nearly independent of pH for the CPE(HS.OA). The potential E_p shifts slightly to more positive values and therefore $\Delta E < 0$ for CPE(HS.E). In this instance, the $\Delta E > 0$ only at pH 6.2 and 6.4. Similar results were obtained for measurements with CPE(0) in the presence of sodium salts of HS.A and HS.OA.

Influence of ionic strength on the voltammetric behaviour of Cu(II)

When the ionic strength was increased the humic substances were released from the electrode surface at higher pH (Table 1), in most instance accompanied by a rapid decrease in the current. HA3 was not released at all in the solutions with an ionic strength of $I = 0.5$ and no current decrease could be observed. However, the electrode CPE(HA3) showed the same ΔE vs. pH relationship with a maximum ΔE at pH 4.8.

Generally, the magnitude of ΔE decreased with increase in ionic strength, although its dependence on pH has the same course as in the solutions with lower ionic strength.

These results prove the influence of ionic strength on the release of humic substances from the electrode surface, on their dissolution and on the complex-forming reactions. The influence of the ionic strength is different for various types of humic substances, as has already been stated [12].

Voltammetric behaviour of Zn(II), Hg(II) and Ag(I) on humic substances-modified electrodes

Similar results for the current responses were obtained for Zn and Hg. The release of humic substances from the electrode surface is associated with a rapid decrease in current on the CPE(HA1), CPE(HA2) and CPE(HA3) electrodes. No rapid current decreases were found for either Zn or Hg on the CPE(HS.A), CPE(HS.OA) and CPE(HS.E) electrodes.

The dependences of ΔE on pH for Zn and Hg are different from those for Cu. The highest values of ΔE were obtained for these metals in the pH range where no release of humic substances is observed. It is presumed that the metal complexes are formed on the electrode surface, in the electrode/solution interface.

Voltammetry of Ag(I) on the modified electrodes also exhibited potential shifts. These potential shifts ΔE are very high for CPE(HA3) in comparison with CPE(HA1) and CPE(HA2) and with other metals. Potential shifts $\Delta E > 0$ were also obtained on CPE(HS.A), in contrast to Cu, Zn and Hg, which exhibited $\Delta E = 0$ on this electrode.

The current dependences on pH for Ag are very different for various humic substances. The CPE(HA1), CPE(HS.OA) and CPE(HS.E) electrodes showed the same dependences as CPE(0). The current responses of CPE(HA2), CPE(HA3) and CPE(HS.A) were much lower than those of CPE(0) and they were nearly independent of pH.

Apparent release of HA3 occurred at pH 3.6 for voltammetry of Ag(I), whereas this value was 5.2 for voltammetry Zn, Hg and Cu. Probably the Ag(I) complexes with humic substances in the solid state are formed in a way different to those for Cu, Zn and Hg. The obtained of current and ΔE on pH dependences support this presumption. The voltammetry of Ag(I) on modified electrodes will have to be studied in greater detail; the data presented here are the first experimental results.

These modified electrodes are applicable to the study of the complexation equilibria in which these humic substances are involved. If the hypothesis regarding metal complexation with solid humic substances on the electrode surface can be validated through further investigations, these electrodes will be useful in studies of some soil processes.

This work was supported by the Czechoslovak Academy of Sciences, Grant No. 63603.

REFERENCES

1 K. Kalcher, Electroanalysis, 2 (1990) 419.
2 E. Wang, H.-M. Ji and W.-Y. Hou, Electroanalysis, 3 (1991) 1.
3 J. Wangsa and N.D. Danielson, Electroanalysis, 3 (1991) 625.
4 P. Hernandez, E. Alda and L. Hernandez, Fresenius' Z. Anal. Chem., 327 (1987) 676.
5 A. Fitch, Clays Clay Miner., 38 (1990) 391.
6 J. Wang and T. Martinez, Electroanalysis, 1 (1989) 167.
7 J. Wang, Z. Taha and N. Naser, Talanta 38 (1991) 81.
8 P.D. Hale, L.-F. Liu and T.A. Skotheim, Electroanalysis, 3 (1991) 751.
9 J. Wang, N. Naser, D. Darnall and J. Gardea-Torresdey, Electroanalysis, 4 (1992) 71.
10 Z. Navrátilová and P. Kula, Electroanalysis, 4 (1992) 683.
11 P. Kula and Z. Navrátilová, Proceedings of the Conference on Analytical Chemistry 1991, University of Leipzig, Leipzig, 1991, p. 28.
12 J. Buffle, Complexation Reactions in Aquatic Systems, Horwood, Chichester, 1988, p. 517.
13 D. De Ford and D.N. Hume, J. Am. Chem. Soc., 73 (1951) 5321.

Analytica Chimica Acta, 273 (1993) 313–321
Elsevier Science Publishers B.V., Amsterdam

Indirect tensammetric method for the determination of non-ionic surfactants

Part 2. Investigation and improvement of tolerance to man-made anionic surfactants

Andrzej Szymanski and Zenon Lukaszewski

Technical University of Poznan, Institute of Chemistry, 60-965 Poznan (Poland)

(Received 9th April 1992; revised manuscript received 1st June 1992)

Abstract

Non-ionic surfactants can be determined by means of their lowering effect on the tensammetric peak of ethyl acetate. Representative man-made anionic surfactants were investigated in order to check the tolerance to this group during the determination of non-ionic surfactants. Both the "normal" procedure (recording in the cathodic direction starting from −1.200 V) and "reverse" recording (scanning in the anodic direction starting from −1.400 V) were used. Sodium salts of dodecylbenzene sulphonate (DBS), dodecyl sulphate (DSA), dodecyl sulphonate (DSO) and stearate (S) and the commercial products Kosulfonat 40 (KOS) and Sulforokanol L-3 (lauryl ether sulphate) (LES) were investigated. The interference of the anionic surfactants increases in the order DSA, DBS < LES < DSO, S < KOS with "normal" recording and in the order DSA, DBS, S < LES, DSO < KOS with "reverse" recording. The tolerance to anionic surfactants is substantially better if "reverse" recording is used. On the other hand, the signals of non-ionic surfactants having 1–3 oxyethylene subunits are slightly lower in this case. The real tolerance to anionic surfactants is better than expected presuming additivity of analytical signals. A 2-μg amount of Triton X-100 can be determined in the presence of 20 and 50 μg of DBS with "normal" and "reverse" recording respectively. However, only 2.7 and 7 μg of KOS, respectively, are tolerated under the same conditions.

Keywords: Polarography; Surfactants; Tensammetry

The indirect tensammetric method (ITM) offers new possibilities for the determination of non-ionic surfactants [1]. The method also works in combination with gas stripping separation of non-ionic surfactants from environmental matrices, e.g., surface water. During gas stripping separation non-ionic surfactants are separated and concentrated in an ethyl acetate layer. A small test sample of this ethyl acetate layer is dissolved in a supporting electrolyte to perform the tensammetric measurement. No preconcentration is required. The difference of the heights of the tensammetric peaks of ethyl acetate alone and that in the presence of surfactants is used as the analytical signal. The lowering of the peak of ethyl acetate is caused by competitive adsorption of surfactants with respect to the adsorption of ethyl acetate. ITM is used within a similar range of concentration of non-ionic surfactants to that in Wickbold's method, commonly used for this purpose [2,3]. However, ITM is much simpler and substantially less time consuming and allows the determination of a broader range of ethoxylates. The slopes of the calibration graphs for the various surfactants are much closer to that of the

Correspondence to: Z. Lukaszewski, Technical University of Poznan, Institute of Chemistry, PL-60-965 Poznan (Poland).

surfactant normally used for calibration (Triton X-100) than it is in Wickbold's method.

Man-made anionic surfactants seem to be the most serious source of interferences. These surfactants are usually present in excess over non-ionic surfactants in environmental matrices. Anionic surfactants partially remain in the water phase during gas stripping separation but they partially pass into the ethyl acetate phase. Small analytical signals of anionic surfactants were observed during preliminary experiments. As these signals do not differ from the signals of non-ionic surfactants, they can produce a positive error in determination.

The aim of this work was to study the tolerance of ITM to man-made anionic surfactants, because this tolerance determines the degree of separation that should be achieved. Improvement of this tolerance by using the possibilities offered by tensammetry itself was also an aim of this investigation.

Surfactants representative of the main classes of anionic surfactants were investigated. Attention was focused on sodium dodecylbenzene sulphonate because this surfactant is a dominant product in surfactant manufacture [4] and it is a major constituent in the group of surfactants normally found in environmental samples.

EXPERIMENTAL

A Radelkis OH-105 polarograph was used with a voltage scan rate of 400 mV min^{-1}. The applied amplitude of the alternating voltage was 2 mV. Controlled-temperature hanging mercury drop electrode (HMDE) equipment (Radiometer), having an additional platinum wire auxiliary electrode, was used. All potentials cited were measured versus a saturated calomel electrode (SCE). The beaker of the measuring cell was replaced with a quartz beaker. The ceramic frit on the end of the salt bridge was protected with a polyethylene tube, which reduces the adsorptive loss of surfactant [5].

The following surfactants were used without additional purification: sodium dodecylbenzene sulphonate (DBS), sodium dodecyl sulphonate (DSO), sodium dodecyl sulphate (DSA), sodium stearate (S) (all from BDH); oxyethylated alkylphenols (number of oxyethylene subunits in parentheses): Rokafenol N-1 (1) (ICSO Blachownia, Poland), Rokafenol N-3 (3) (Rokita, Poland), Triton X-100 (9.5) and Triton X-305 (30) (both from Rohm and Haas); oxyethylated oxo alcohols having a C_{10-13} hydrophobic part of the molecule: Oxetal D104 (4) and Oxetal C114 (14) (Zschimmer und Schwarz); oxyethylated alcohols having mainly an n-C_{12} hydrophobic part of the molecule: Rokanol KO-4 (4) (Rokita) and Brij-35 (20) (Atlas); oxyethylated alcohols having a C_{16-18} hydrophobic part of the molecule: surfactant 18-2 (2) (Technical University of Poznan), Marlipal 1618/18 (18) (Hüls) and Rokanol O-30 (30) (Rokita); oxyethylated amines having a C_{16-18} hydrophobic part of the molecule: Rokamin R-3 (3) (ICSO) and Rokamin S-22 (22) (Rokita); oxyethylene–oxypropylene block copolymers: Rokopol 30p5 (5) and Rokopol 30p27 (27) (both

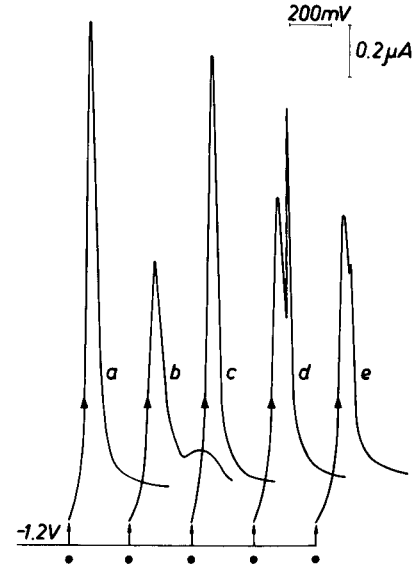

Fig. 1. Tensammetric curves of ethyl acetate in the presence of (b) Triton X-100, (c and d) DBS and (e) KOS with "normal" recording. (a) Tensammetric peak of ethyl acetate alone. Arrows show direction of recording. Concentration of surfactant [μg in the sample (25 ml)]: (a) 0, (b) 25, (c) 25, (d) 75 and (e) 100. Concentration of ethyl acetate: 1.5 ml in the sample (25 ml). (•) Zero of current for respective tensammetric curves.

from Rokita), having an average number of oxypropylene subunits of 30 in both instances. Two commercial products: Kosulfonat 40 (Instytut Chemii Przemyslowej, Poland) (KOS) and sulforokanol L-3 (Rokita) (LES) were used after purification. Kosulfonat 40 is a 2:3 mixture of sodium salts of alkyl sulphate and alkylbenzene sulphonate (having mainly a C_{18} hydrophobic part of surfactant), and Sulforokanol L-3 is the sodium salt of lauryl triethoxy sulphate. Non-ionic impurities of these two surfactants were extracted with ethyl acetate.

Ethyl acetate (POCh, Poland), pure for gas chromatography, was used. The sodium sulphate used for the preparation of the base electrolyte was purified by double recrystallization and heated at 600°C. All solutions were prepared in water triply distilled from quartz. Only freshly distilled water was used. The supporting electrolyte in all the studies was 0.5 M sodium sulphate solution.

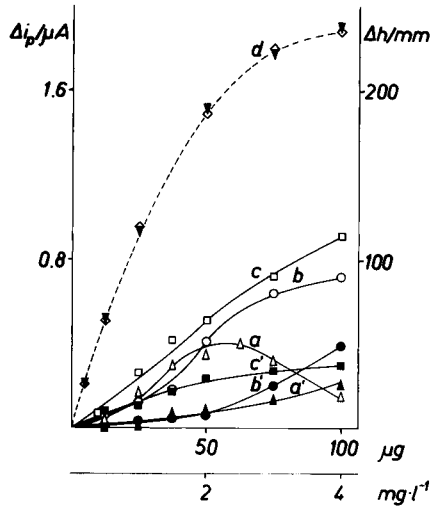

Fig. 2. Dependence of analytical signal on the surfactant concentration for (a and a') DSA, (b and b') DBS, (c and c') LES and (d, dashed line) Triton X-100 with "normal" recording (a–c) and "reverse" recording (a'–c'). Upper scale of concentration shows the amount of surfactant in the sample (25 ml). Concentration of ethyl acetate: 1.5 ml in the sample (25 ml). Initial potential and direction of recording: (a–c) −1.200 V, cathodic direction; (a'–c') −1.400 V, anodic direction.

RESULTS AND DISCUSSION

Analytical signals of anionic surfactants with recording towards the cathodic ("normal") direction

The analytical signals given by representative man-made anionic surfactants were investigated under the same conditions as those used in Part 1 [1]. Under these conditions, the tensammetric curves were recorded towards the cathodic direction usually used in adsorptive stripping tensammetry. This direction of recording is called "normal", in contrast to "reverse" recording. These two terms will be used further in this paper. Sodium salts of DBS, DSA, DSO and S and the commercial products KOS and LES were investigated. Results for Triton X-100 as a representative non-ionic surfactant, used for calibration in ITM, were added. The concentration was varied within the range 2.5–100 μg in the sample, corresponding to 100–4000 $\mu g\ l^{-1}$.

Several tensammetric curves are given as examples in Fig. 1. Curve a shows the peak of ethyl acetate alone and curves b and c show this peak in the presence of 25 μg of Triton X-100 and DBS, respectively. The decrease in the peak height of ethyl acetate is the analytical signal in the reported method. The decrease in the ethyl acetate peak caused by 25 μg of Triton X-100 (expected useful signal) is large whereas that caused by 25 μg of DBS (expected interference) is small, although visible.

The analytical signals of the investigated anionic surfactants within the concentration range 12.5–100 μg in the sample are shown in Figs. 2 and 3, curves a, b and c. Although the signals of most of the investigated anionic surfactants are much lower then that of Triton X-100, they are significant and their presence can be a source of error. These signals increase in the order DSA, DBS < LES < DSO, S < KOS. Fortunately, the most frequently used DBS produces only a weak signal. On the other hand, the signals of KOS and LES, also commonly used surfactants, are high.

Most of the calibration graphs in Figs. 2 and 3 indicate maxima. These maxima are connected with the appearance of specific peaks of anionic

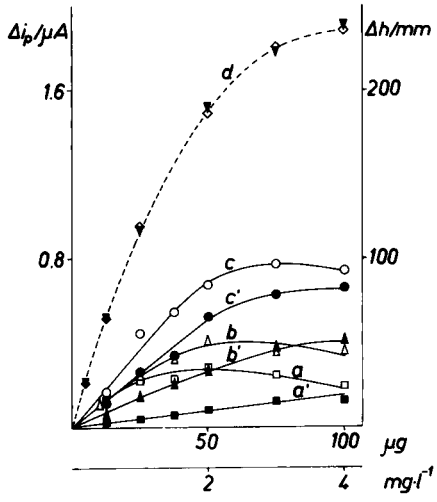

Fig. 3. Dependence of analytical signal on the surfactant concentration for S (a and a'), DSO (b and b'), KOS (c and c') and Triton X-100 (d, dashed line) with "normal" recording (a–c) and "reverse" recording (a'–c'). Upper scale of concentration shows the amount of surfactant in the sample (25 ml). Concentration of ethyl acetate: 1.5 ml in the sample (25 ml). Initial potential and direction of recording: (a–c) −1.200 V, cathodic direction; (a'–c') −1.400 V, anodic direction.

surfactants themselves in addition to the ethyl acetate peak. Examples of such curves having both an ethyl acetate peak and a specific peak of surfactant itself are visible in Fig. 1, curves d and e, for DBS and KOS, respectively. Coincidence of these two peaks leads to irregular behaviour of the analytical signal. It should be stressed that the complication discussed appears only for comparatively high concentrations of anionic surfactants (3–4 mg l^{-1}), and not over the range of usual concentrations of anionic surfactants in surface water. With lower concentrations only the suppressed peak of ethyl acetate appears (compare curves c and d in Fig. 1 for 25 and 75 μg of DBS, respectively).

"Reverse" recording of tensammetric curves

It is obvious from the reported experiments that only a certain excess of anionic over non-ionic surfactants is tolerated in ITM under the conditions used in Part 1 [1], i.e., using an initial potential of −1.200 V vs. SCE. This is not satisfactory. Shifting of the initial potential in the negative direction could be a possible way of improving the tolerance to anionic surfactants, because the range of adsorption of anionic surfactants is narrower than that of non-ionic surfactants. Using a properly selected initial potential it is possible to differentiate between these two groups of surfactants. This effect is shown in Fig. 4, which shows variations in the ranges of adsorption at the cathodic side for the tested non-ionic and anionic surfactants, caused by variations in the concentration of surfactants. In addition to the surfactants tested in this work (bars a–m), the variations in the adsorption range for oxyethylated alcohols, alkylphenols, amines and oxypropylene–oxyethylene block copolymers, i.e., sur-

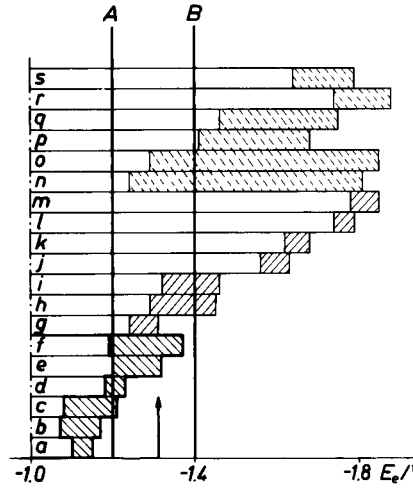

Fig. 4. Fluctuations of adsorption range from cathodic side for anionic (a–f) and non-ionic surfactants (g–s). Lower boundary of adsorption range corresponds to a concentration of surfactant of 200 μg l^{-1} and the higher boundary to a concentration of 1000 μg l^{-1}. Bars corresponding to anionic surfactants: (a) DSA, (b) DBS, (c) DSO, (d) S, (e) LES and (f) KOS. Bars corresponding to non-ionic surfactants: (g) Rokafenol N-1, (h) Rokamin R-3, (i) Rokafenol N-3, (j) Triton X-100, (k) Oxetal C114, (l) Surfactant 18-2 and (m) Marlipal 1618/18, and to groups of non-ionics: (n) oxyethylated alkylphenols (EO 1-30), (o) oxyethylated amines (EO 3-22), (p) oxyethylated oxo alcohols having a C_{10-13} hydrophobic part of the molecule (EO 4-14), (q) oxyethylated *n*-alcohols having mainly a C_{12} hydrophobic part of the molecule (EO 4-20), (r) oxyethylated alcohols having a C_{16-18} hydrophobic part of the molecule (EO 2-30) and (s) oxyethylene–oxypropylene block copolymers (EO 5-27). Vertical line A indicates the initial potential for "normal" recording and line B that for "reverse" recording. Arrow indicates potential of the peak of ethyl acetate.

factants tested in Part 1 [1], have also been included (bars n–s). The adsorption range of a particular surfactant was defined as their range of initial potentials at which a specific peak of the investigated surfactant appears. It is known that the range of adsorption of surfactants is concentration dependent. This is why each surfactant is represented in Fig. 4 by two values: a lower one for a concentration of 200 $\mu g\ l^{-1}$ (5 μg in the sample) and a higher one for a concentration of 1000 $\mu g\ l^{-1}$ (25 μg in the sample). Of course, Fig. 4 is only a rough approximation of real conditions because the boundaries of adsorption indicated were determined in the absence of ethyl acetate. However, Fig. 4 is very useful in explaining the role of the initial potential in minimizing the signal of anionic surfactants. It also explains the effect of the initial potential on the changes in the signals of some non-ionic surfactants.

With "normal" recording using an initial potential of −1.200 V (Fig. 4, vertical line A), all the tested non-ionic surfactants (bars g–s) are still located within the range of their adsorption. These surfactants replace ethyl acetate on the electrode surface, producing an analytical signal in this way. Under these conditions the anionic surfactants DSA (a) and DBS (b) are outside their adsorption range. On the other hand, KOS (f) and LES (e) and partially S (d) and DSO (c) are still located within their adsorption ranges and produce analytical signals.

Shifting the initial potential to more negative value would be desirable for decreasing the interference of anionic surfactants. However, the initial potential used (−1.200 V) is almost a boundary value from the point of view of recording the peak of ethyl acetate ($E_p = -1.31$ V) in the cathodic direction. This is why attempts were made to record the negative peak of ethyl acetate from the opposite side, i.e., from an initial potential more negative than −1.300 V in the anodic direction. The recording of a peak in such a "reverse" manner is possible. An example of such a peak is shown in Fig. 5, curve a, and the dependence of its height on the initial potential is shown in Fig. 6. The results concerning the peak recorded in the cathodic direction ("normal" recording) were also added for comparison. The

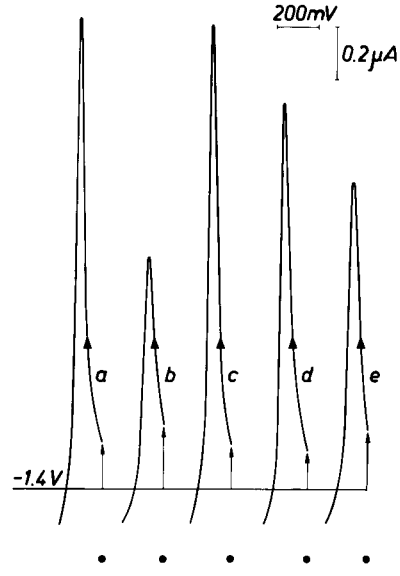

Fig. 5. Tensammetric curves of ethyl acetate in the presence of (b) Triton X-100, (c and d) DBS and (e) KOS with "reverse" recording. (a) Tensammetric peak of ethyl acetate alone. Arrows show direction of recording. Concentration of surfactant [μg in the sample (25 ml)]: (a) 0, (b) 25, (c) 25, (d) 75 and (e) 100. Concentration of ethyl acetate: 1.5 ml in the sample (25 ml). (•) Zero of current for respective tensammetric curves.

heights of the peaks of ethyl acetate obtained with "normal" and "reverse" recording are similar with the exception of the range of initial potentials adjacent to the potential of the peak of ethyl acetate. It should be stressed that the use of

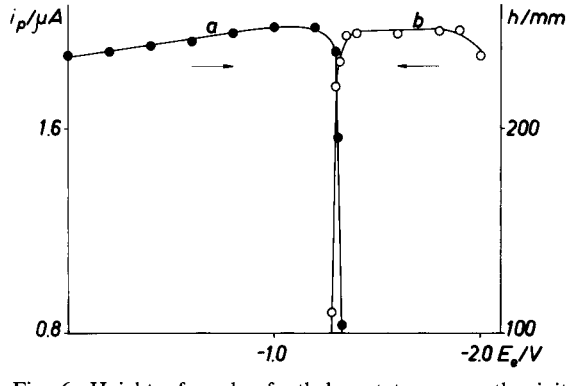

Fig. 6. Height of peak of ethyl acetate versus the initial potential with recording towards (a) cathodic ("normal") and (b) anodic ("reverse") direction. Concentration of ethyl acetate: 1.5 ml in the sample (25 ml).

such a recording with respect to the tensammetric peak located on the cathodic side is a new approach. The recording of a tensammetric curve in the anodic direction is usually used for recording anodic tensammetric peaks.

Analytical signals of anionic surfactants with "reverse" recording

The analytical signals of the same anionic surfactants as in the case of "normal" recording were investigated using "reverse" recording starting from −1.400 V. The concentration was changed within the range 12.5–100 μg in the sample, i.e., 500–4000 μg l^{-1}. Examples of decreasing the peak height of ethyl acetate (recorded in the "reverse" manner) are shown in Fig. 5 and the complete results are shown in Figs. 2 and 3, curves a′, b′ and c′. The calibration graphs obtained with "reverse" recording have been added to the results concerning "normal" recording. The advantage of using "reverse" recording is clearly visible on comparing Figs. 1 and 5. The useful analytical signal, i.e., that represented by Triton X-100, remains almost unchanged (see curves b). The analytical signal of DBS is reduced at both concentrations (curves c and d). With KOS the improvement is smaller (curves e). However, the specific peaks of DBS and KOS disappeared with "reverse" recording (compare curves d and e in Figs. 1 and 5). It is easy to explain this effect by means of Fig. 4. In the case of "reverse" recording (starting from vertical line B) the adsorption ranges of all the anionic surfactants (bars a–f) are almost completely located at the positive side of the ethyl acetate peak.

From Figs. 2 and 3 it is obvious that with "reverse" recording a substantial improvement in tolerance to anionic surfactants, i.e., lowering of their signals, has been achieved for DSA (Fig. 2, curves a and a′) DBS (Fig. 2, curves b and b′) and S (Fig. 3, curves a and a′). With LES (Fig. 2, curves c and c′) this lowering is visible mostly for the higher concentration range, which is less valuable from an analytical point of view. With KOS and DSO (Fig. 3, curves c and c′ and curves b and b′, respectively), the lowering of their signals caused by the change in recording direction is small. The signals of the surfactants increase in the order DSA, DBS, S < LES, DSO < KOS, i.e., in a different sequence than with "normal" recording.

Comparison of "normal" and "reverse" recording in ITM

Results obtained with both recording modes were compared with respect to tolerance to anionic surfactants and with respect to the analytical signals of non-ionic surfactants.

The minimum amounts of the anionic surfactants investigated which cause the appearance of an analytical signal were established for both "normal" and "reverse" recording. This amount should be the minimum concentration interfering in the determination of non-ionic surfactants, presuming additivity of both signals. The minimum amount was defined as that giving a signal corresponding to the standard deviation of the peak height of pure ethyl acetate ($S_r = 0.012$, $n = 7$). This value corresponds to a 3 mm peak height or 24 nA under the conditions used in this work. The results are shown in Table 1. They agree with the conclusions drawn on the basis of Figs. 2 and 3. An improvement of the tolerance to all the investigated surfactants except LES is apparent with "reverse" recording.

TABLE 1

Tolerance to different man-made anionic surfactants with "normal" and "reverse" recording [defined as the amount (μg) of surfactant in the sample (25 ml) producing a signal corresponding to the standard deviation of the ethyl acetate peak (3 mm, $n = 7$)]

Recording mode	Surfactant					
	DSA	DBS	LES	S	DSO	KOS
"Normal"	7.1	6.1	3.7	2.7	2.5	1.7
"Reverse"	19.6	17.8	3.4	14.4	4.6	2.5

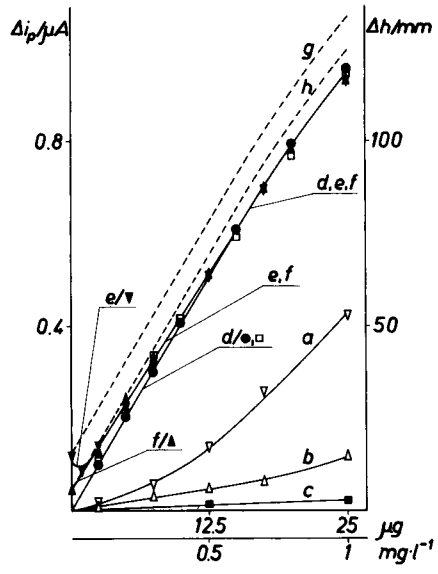

Fig. 7. Dependence of analytical signal on the surfactant concentration for (a–c) DBS and for Triton X-100 (d) alone and (e–h) in the presence of excess of DBS. Dashed curves (g and h) show values of the signal assuming additivity of the signals of Triton X-100 and DBS. Upper scale of concentration shows the amount of surfactant in the sample (25 ml). Concentration of DBS (mg l^{-1}): (e and g) 1.0, (f and h) 2.0. Concentration of ethyl acetate: 1.5 ml in the sample (25 ml). Initial potential (V vs. SCE) and direction of recording: (a) −0.800, cathodic; (b), (d, □), (e) and (g) −1.200, cathodic; (c), (d, ●), (f) and (h) −1.400, anodic direction.

It should be stressed that the amounts determined above can be only roughly considered as a limit of tolerance to anionic surfactants. For a more precise approach the additivity of signals should be checked. The analytical signal of Triton X-100 in the presence of DBS was investigated with this aim. A calibration graph of Triton X-100 was obtained with and without the presence of an excess of DBS "normal" and "reverse" recording were used. The results are shown in Fig. 7. Calibration graphs of DBS obtained using different initial potentials were added for comparison. Dashed lines corresponding to the algebraic sum of the signals of Triton X-100 and DBS were also added. It can be seen that the signal with interfering anionic surfactants is much lower than that expected presuming additivity of signals. That is because of competition between anionic and non-ionic surfactants on the electrode surface, in which the non-ionics are stronger surfactants within the range of potential used. This effect is visible both with "normal" recording of the Triton X-100 signal in the presence of excess of DBS (see Fig. 7e) and with "reverse" recording (Fig. 7d, f and h). With "reverse" recording, the signal of Triton X-100, recorded over the concentration range 50–1000 $\mu g\ l^{-1}$, is only slightly higher in the presence of 2000 $\mu g\ l^{-1}$ of DBS than for Triton X-100 alone (Fig. 7d).

Series of experiments with binary mixtures of Triton X-100 and DBS or KOS were performed with the aim of evaluating the improvement of the tolerance to anionic surfactants. The minimum amounts of DBS and KOS that cause the appearance of interference with the analytical signal of Triton X-100 were determined; DBS represented the most commonly used anionic surfactant and KOS the most troublesome surfactant with the worst tolerance. This minimum amount was defined as that giving a signal corresponding to the standard deviation of the signal of 2 μg of Triton X-100 in the sample (80 $\mu g\ l^{-1}$). This value was determined from seven measurements as 3 mm peak height (24 nA) under the conditions used in this work. In the presence of 2 μg of Triton X-100 in the sample, an increase in the signal by 3 mm requires 20.5 μg of DBS with "normal" recording and 50.0 μg with "reverse" recording, i.e., 2000 $\mu g\ l^{-1}$ of DBS is tolerated if 80 $\mu g\ l^{-1}$ of Triton X-100 are determined using "reverse" recording. From Table 1 it can be seen that a 6.1 μg of DBS alone gives such a 3 mm signal if "normal" recording is used and 17.8 μg with "reverse" recording. Hence the real tolerance to DBS is roughly three times better than that expected presuming additivity of signals. It is of the order of 1:25. A recently reported ratio of non-ionic and anionic surfactants in rivers in West Germany is ca. 1:10 [6]. Hence, the tolerance achieved is better than the expected excess of anionic surfactants in surface water.

The tolerance of KOS is worse. In the presence of 2 μg of Triton X-100 the signal increases by 3 mm if 2.7 μg of KOS are added with "normal" recording and 7.0 μg of KOS with "reverse" recording. This corresponds to 280 $\mu g\ l^{-1}$ of KOS as the tolerated concentration in the deter-

mination of 80 $\mu g\ l^{-1}$ of Triton X-100. From Table 1 it can be seen that 1.7 μg of KOS alone produced a 3 mm signal with "normal" recording and 2.5 μg with "reverse" recording. Although the real tolerance to KOS is also better than that expected presuming additivity of signals, only an excess of 1:3.5 of this surfactant is tolerable under the most favourable conditions. Fortunately, the main anionic surfactant component in surface water is DBS [4] and the fraction of KOS-type surfactants is much smaller.

Comparing the results obtained with "normal" and "reverse" recording, it is clear that an increase in the tolerance to anionic surfactants was achieved by using "reverse" recording. However, variations in the initial potential and in the direction of recording could also change the conditions for the determination of non-ionic surfactants by ITM because with "reverse" recording (initial potential −1.40 V) some of the investigated non-ionic surfactants [Rokafenols N-1 (g) and N-3 (i) and Rokamin R-3 (h)] are also partially located to the positive side of the ethyl acetate peak and their analytical signals are lower (see Fig. 4). Series of experiments with representative non-ionic surfactants using both "normal" and "reverse" recording were performed. Triton X-100 was used for calibration. Oxetal C114 and Marlipal 1618/18, i.e., representative oxyethylated alcohols having a typical oxyethylene chain length, and Rokafenol N-1, Rokafenol N-3, Rokamin R-3 and surfactant 18-2, representative of the group of surfactants having extremely short oxyethylene chains, were investigated. The results are given in Table 2.

The results for Triton X-100, Oxetal C114, Marlipal 1618/18 and surfactant 18-2 remain unchanged with "normal" and "reverse" recording. Some decrease in the analytical signal is visible with Rokafenol N-3 and Rokamin R-3, if "reverse" recording is used, but there is a substantial decrease with Rokafenol N-1. It should be stressed that Rokafenol N-1, Rokafenol N-3, Rokamin R-3 and surfactant 18-2 belong to the group of surfactants which are not determined by the methods currently used [2,3,7]. Certainly it would be better to maintain all advantages of ITM over Wickbold's method. The use of "reverse" recording is justified only with a certain excess of anionic surfactants. "Normal" recording could be used if the separation stage preceding the determination (sublation or extraction) reduces the concentration of anionic surfactants below the level of their influence on the results of determination, i.e., below 50–100 $\mu g\ l^{-1}$. This will be the subject of further work.

TABLE 2

Analytical signal (mm) of non-ionic surfactants with "normal" (N) and "reverse" (R) recording [a]

Surfactant	Recording mode	Concentration of surfactant ($\mu g\ l^{-1}$)								
		100	200	300	400	500	600	700	800	1000
Triton X-100	N	13	26	38	51	64	77	–	99	119
	R	13	26	42	52	–	74	–	95	118
Oxetal C114	N	15	30	43	–	71	80	–	101	122
	R	15	–	44	57	69	81	93	103	119
Marlipal 1618/18	N	13	26	38	50	62	73	–	88	102
	R	13	27	–	49	61	72	–	87	100
Rokafenol N-3	N	12	24	36	47	58	68	–	83	95
	R	13	–	36	47	57	–	–	76	86
Rokafenol N-1	N	10	20	28	36	42	47	–	57	65
	R	5	9	13	–	16	–	20	–	22
Rokamin R-3	N	13	26	38	–	54	–	64	–	77
	R	6	18	25	–	35	–	54	–	68
Surfactant 18-2	N	11	23	36	–	48	–	61	–	72
	R	12	24	37	–	49	–	62	–	74

[a] Initial potential: with "normal" recording −1.200, and with "reverse" recording −1.400 V vs. SCE.

The results obtained also give rough information about the possibility of the determination of anionic surfactants by ITM. It is possible to obtain a substantial analytical signal of DBS by shifting the initial potential towards a less negative value (see Fig. 7c).

This work was supported by the Technical University of Poznan (grant No. R3KB/500/27/8/91).

REFERENCES

1 A. Szymanski and Z. Lukaszewski, Anal. Chim. Acta, 260 (1992) 25.
2 R. Wickbold, Tenside Deterg., 9 (1972) 173.
3 D. Brown, H. de Henau, J.T. Garigan, P. Gerike, M. Holt, E. Keck, E. Kunkel, E. Matthijs, J. Waters and J. Watkinson, Tenside Deterg., 23 (1986) 190.
4 L. Noll, Tenside Surfact. Deterg., 28 (1991) 90.
5 A. Szymanski and Z. Lukaszewski, Anal. Chim. Acta, 231 (1990) 77.
6 H. Hellmann, Tenside Surfact. Deterg., 27 (1990) 318.
7 T.M. Schmitt, M.C. Allen, D.K. Brain, K.F. Guin, D.E. Lemmel and Q.W. Osburn, J. Am. Oil Chem. Soc., 67 (1990) 103.

Analytica Chimica Acta, (1993) 323–327
Elsevier Science Publishers B.V., Amsterdam

Studies on the adsorption of cadmium on hydrous iron(III) oxides in oxic sediments

W. Petersen, K. Wallmann, S. Schröer and F. Schroeder
GKSS Research Centre, Max-Planck-Strasse, D(W)-2054 Geesthacht (Germany)

(Received 17th June 1992; revised manuscript received 20th October 1992)

Abstract

The influence of freshly formed hydrous iron(III) oxides in the oxic layers in sediments on the exchange processes of cadmium between the interstitial and the overlying water was investigated. By the formation of iron oxides as coatings on clay minerals it is possible to measure the dissolved part of cadmium with differential-pulse anodic stripping voltammetry without disturbances of colloidal particles. The results were compared with theoretical calculations using a surface complexing model. The measurements showed that 0.1 mmol of FeOOH coated on the clay mineral kaolinite (1 g) can adsorb up to 95% of the added cadmium (1 μmol l^{-1}). The measured adsorption agreed well with the estimations of the theoretical model. The investigation of the influence of competitive ions (Ca^{2+} and PO_4^{3-}) showed that both ions reduced the proportion of adsorbed cadmium whereas the model postulates higher adsorption with phosphate. The measurements showed that freshly formed hydrous iron(III) oxides may act as a natural barrier to the diffusive flux of toxic trace elements into the overlying water.

Keywords: Stripping voltammetry; Adsorption; Cadmium; Hydrated iron(III) oxides; Sediments; Waters

River sediments can act both as a source and a sink for pollutants. In comparison with the overlying water, the heavy metals in particular are enriched in the interstitial water of the oxic sediment zones and can be transported to the water phase by diffusion processes. On the other hand, freshly formed hydrous iron(III) oxides (HFO) permanently arise in the oxic zone of the sediments owing to diffusion of reduced iron [Fe(II)] from the anoxic layers. These oxides can act as strong adsorbers of heavy metals and other contaminants and thus hinder the diffusive transport of pollutants to the overlying water.

Figure 1 shows the diagenetic model of a typical sediment of the Elbe river with the reactions and distribution of the major anions and cations in the different zones.

Correspondence to: W. Petersen, GKSS Research Centre, Max-Planck-Strasse, D(W)-2054 Geesthacht (Germany).

To investigate the adsorption of heavy metals on freshly formed HFO suspensions differential-pulse anodic stripping voltammetry (DPASV), which allows the continuous direct measurement of heavy metals in suspensions within the range of naturally occurring concentrations, was used. The advantages of voltammetric methods are that, unlike other methods (e.g., atomic absorption spectrometry), they do not require a separation of the solid phase. This circumvents the uncertainties due to problems with contamination or losses (e.g., by adsorption on filters) that often occur at low metal concentrations. Recently, Müller [1] investigated in a similar way the adsorption properties of lead and zinc on an oxide surface (goethite) and suspended particles.

In this work, the adsorption of cadmium in the range 1×10^{-8}–1×10^{-6} mol l^{-1} on coatings of HFO on clay minerals was investigated. The re-

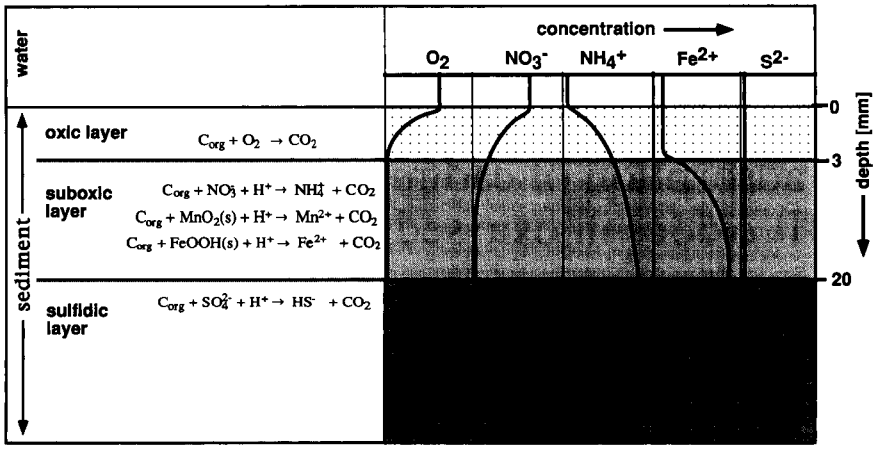

Fig. 1. Diagenetic model of the oxic and anoxic zones in a sediment.

sults of the adsorption on synthetic hydrous iron(III) oxides were compared with theoretical calculations according to the surface complexing model as developed by Schindler and Stumm [2]. The aims were to investigate the possibilities of in situ measurements of the dissolved part of heavy metals in suspensions of hydrous iron(III) oxides with ASV within the natural concentration range of 1×10^{-8}–1×10^{-6} mol l^{-1}, to compare the experimental results with a theoretical model of the adsorption of cadmium on hydrous iron(III) oxides (surface complexing model described by Dzombak and Morel [3]), to examine the influence of competitive ions (Ca^{2+}, PO_4^{3-}) with the specific sites of adsorption and to determine the influence of adsorption on the diffusive exchange of heavy metals between the sediment/water interface.

EXPERIMENTAL

The experimental set-up is shown in Fig. 2. The polarograph (Metrohm VA 646) connected

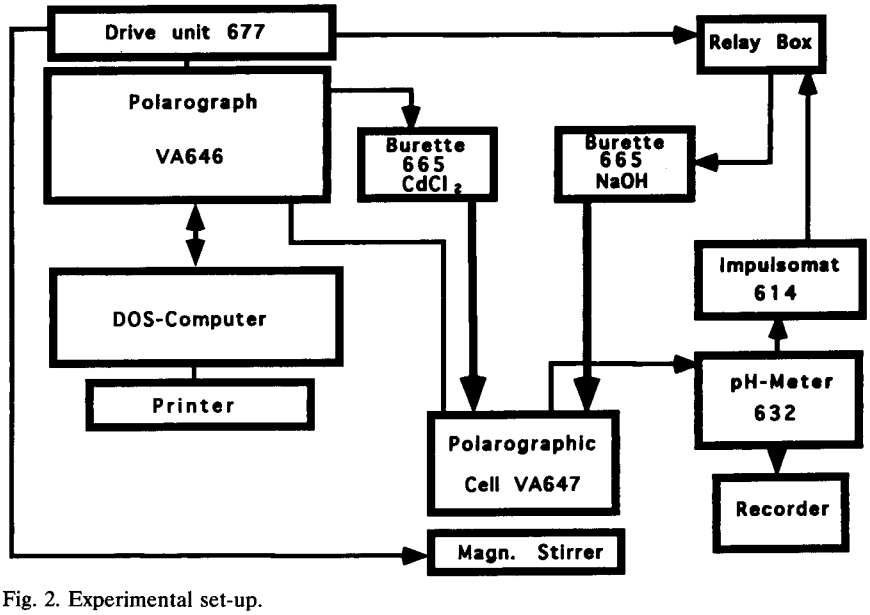

Fig. 2. Experimental set-up.

with the polarographic cell was time-controlled by the computer. In addition, the computer allowed the storage of the data on hard disk for later evaluation. The measuring cell was made from quartz glass to avoid losses by adsorption on the container walls and the temperature was kept constant at 25°C with a thermostat.

To obtain comparable results, the hydrous iron(III) oxides coated on clay minerals were freshly prepared daily by precipitation of 0.1 mmol $Fe(NO_3)_3$ in a suspension of 1 g of kaolinite in 100 ml of water at a constant pH (7.5) within 12 h as described by Van der Woude and De Bruyn [4]. This was carried out directly in the polarographic cell to avoid problems with contamination and/or losses by sorption on different container walls. The ionic strength of the suspension was adjusted to $I = 0.02$ mol l^{-1} with $NaNO_3$. The concentrations of the competitive ions were 1.0×10^{-3} mol l^{-1} calcium or 1.0×10^{-4} mol l^{-1} phosphate.

The pH in the cell was controlled by a pH meter and regulated with a pH-stat (Metrohm Impulsomat 614) with NaOH. Only during measurement was the pH regulation interrupted by the drive unit-controlled relay (Metrohm VA 677) to avoid uncontrolled dosages of NaOH into the unstirred solution. The suspension was continuously bubbled through with nitrogen and, additionally to the stirring device in the polarographic cell, the solution was still stirred with a magnetic stirrer to keep the solid in suspension. Only during the polarographic measurement was the stirrer stopped to allow an undisturbed polarographic measurement. Cadmium was added via a burette (Metrohm 665) controlled by the VA 636 polarograph. After each dosage of cadmium an equilibrium time of 20 min was allowed before starting the polarographic measurement. The following DPASV parameters were used: deposition time, 300 s; deposition voltage, −0.8 V; sweep rate, 10 mV s^{-1}; and amplitude, 50 mV. The data were evaluated automatically by the computer with a program described elsewhere [5].

Surface complexing model

The surface complexing model as derived from Schindler and Stumm [2,3] describes the adsorption as a thermodynamically controlled reaction of metals on the surface of metal oxides. In this instance the sorption can be calculated in the same manner as for calculations of chemical equilibrium among solute and mineral phases. The theory is based on the assumptions that the sorption of ions involves site-specific binding at surface functional groups, the adsorption reactions can be described using mass law equations and the electrostatic effects that influence surface reactions can be accounted for by including in the surface complexation constants a coulombic term derived from electrical double-layer theory. The complexation is shown schematically in Fig. 3.

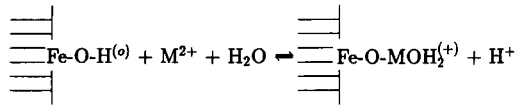

Fig. 3. Schematic diagram of the surface complexation for sorption of a cation M^{2+} on hydrous iron(III) oxide.

Calculations with the surface complexing model were carried out with the program DSURF. This program is a special version of the program MINEQL [6], modified by Dzombak and Morel [3], which calculates the chemical equilibrium composition of an aqueous system. An iron concentration in the same order as was found in sediments from the Elbe river (1 mmol l^{-1}Fe) was used. The sorption of the clay mineral kaolinite was neglected. The calculations showed that the strong binding sites of hydrous iron(III) oxides already become saturated at a Cd concentration of 1 μmol l^{-1} and then at higher concentrations weaker binding sites show much weaker adsorption.

RESULTS AND DISCUSSION

First experiments showed that when FeOOH was formed without any carrier it was impossible to determine the free cadmium owing to a high background current due to colloidal hydrous iron(III) particles. When using a clay mineral as a carrier on which the iron oxides are coated, it was possible to determine cadmium down to very low concentrations even if the peak potential was

shifted to a slightly more negative potential (−20 mV). Measurements under the same conditions showed very good reproducibility of the measured free cadmium, also indicating that the the properties of the suspended hydrous iron(III) oxides were very reproducible. Figure 4 shows plots of the measured dissolved cadmium versus titrated total cadmium in two experiments that were carried out under the same conditions (suspension of kaolinite with HFO and 1 mmol l^{-1} Ca).

The investigations on the adsorption of cadmium on hydrous iron(III) oxides with and without competitive ions and also with the pure kaolinite and a comparison of the results with the calculation according to the surface complexing model are shown in Fig. 5.

The comparison of the measured adsorption with the theoretical adsorption model shows good agreement between the measured and calculated adsorption in solutions of cadmium without other competitive ions. In the presence of ions that are in competition with the sites of adsorption (Ca^{2+} and PO_4^{3-}), the estimations of the theoretical model differ from the experimental values. With calcium, the adsorption of cadmium was decreased to a greater extent than calculated by the model and was even less than with the pure clay mineral. With phosphate, the model estimated stronger adsorption whereas the experiment also showed a decrease in adsorbed cadmium.

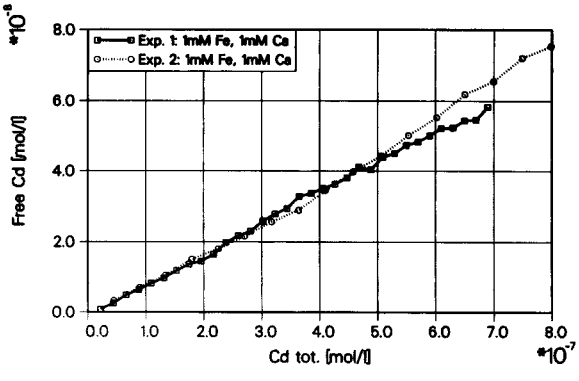

Fig. 4. Reproducibility of measured free cadmium on HFO. Conditions: 1 mmol l^{-1} Fe and 1 mmol l^{-1} Ca. □ = Experiment 1; ○ = experiment 2.

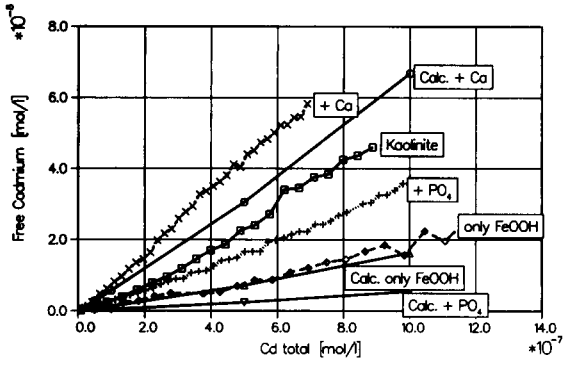

Fig. 5. Comparison between calculated and experimentally determined dissolved cadmium in suspensions of hydrous iron(III) oxides coated on kaolinite. Fe concentration = 10^{-3} l^{-1}; I = 0.02; pH = 7.5; temperature = 20°C.

The adsorption of cadmium in suspensions of kaolinite or of kaolinite coated with hydrous iron(III) oxides (iron to kaolinite ratio = 0.6%) increases in the order kaolinite + HFO + Ca < kaolinite < kaolinite + HFO + PO_4 < kaolinite + HFO.

Conclusion

The adsorption experiments showed that in suspensions of clay minerals the hydrous iron(III) oxides form discrete phases and/or coatings on the clay minerals which allow the direct determination of cadmium in the suspension by DPASV at very low concentrations.

The measured adsorption of about 95% in the range of natural cadmium concentrations showed that freshly formed hydrous iron(III) oxides in river sediments may, with their high adsorption capacity, act as a natural barrier for the diffusive flux of contaminants into the overlying water. On the other hand, it could be shown that in the complex mixture of substances of the interstitial water, the hydrous iron(III) oxides have a significantly weaker affinity to trace metals then would be estimated by data from the literature for pure HFO.

This work was supported by the Ministry of Research and Technology. The authors thank D.A. Dzombak for kindly providing the program DSURF.

REFERENCES

1 B. Müller, PhD Thesis, No. 8988, ETH, Zürich, 1989.
2 P.W. Schindler and W. Stumm, in W. Stumm (Ed.), Aquatic Surface Chemistry, Wiley, New York, 1987, Chap. 4.
3 M.M. Dzombak and F.M.M. Morell, Surface Complexing Modeling Hydrous Ferric Oxide, Wiley, New York, 1990.
4 J.H. van der Woude and P.L. de Bruyn, Clay Miner., 19 (1984) 745.
5 W. Petersen, Anal. Chim. Acta, 248 (1991) 77.
6 J.C. Westall, J.L. Zachary and F.M.M. Morel, MINEQL, a Computer Program for the Calculation of Chemical Equilibrium Composition of Aqueous Systems, Technical Note 18, Department of Civil Engineering, Massachusetts Institute of Technology, Cambridge, MA, 1976.

Analytica Chimica Acta, 273 (1993) 329–334
Elsevier Science Publishers B.V., Amsterdam

Pharmaceutical and biomedical applications of electroanalysis

A critical review

J.-M. Kauffmann and J.-C. Viré

Université Libre de Bruxelles, Institut de Pharmacie, Campus Plaine CP 205 / 6, Boulevard du Triomphe, 1050 Brussels (Belgium)

(Received 7th July 1992)

Abstract

Various aspects of the application of electrochemical techniques in drug analysis are scrutinized. Considerations regarding the adequacy of modern polarographic and voltammetric methods for the determination of drugs in various samples are discussed. A tentative validation scheme for electroanalytical methods is illustrated.

Keywords: Polarography; Voltammetry; Drug analysis

Electrochemical methods cover a large domain of investigation in drug analysis ranging from the classical potentiometric and amperometric titrations to conductimetric and pulsed amperometric detection techniques, and the recent in vivo microelectrode and biosensor developments. The great diversity of electroanalytical methods, along with the refinements realized over the past 10 years in electronics, computers and in electrode design and handling (cleaning) allows the application of electrochemistry to various stages of drug research and development.

SYNTHESIS AND DRUG SCREENING

Electroorganic synthesis can lead to the development of a great number of raw products amenable to further chemical modification into pharmacologically interesting molecules [1]. Actually, despite the definite advantages of electroorganic synthesis, (i) high selectivity due to accurate potential control, (ii) no chemical pollution (no handling of toxic reagents), few applications are encountered in pharmaceutical industries [2]. Renewed interest, however, is expected in this area with the development of new electrode substrates, the use of better ion exchange membranes, and the possible electroregeneration of cofactors, particularly in enzymatic reactions of biotechnological interest [3,4].

In addition to the synthetic approach, electrochemistry can be used at the early stage of drug research for screening the pharmacological activity of a homologous series of newly synthesized molecules. There are several examples in the literature showing the relationship between electrochemical data and the pharmacological properties of drugs [5–8]. Simple and rapid investigation techniques such as cyclic voltammetry [9] can be advantageously applied for predicting the psychotic activity of phenothiazine derivatives (from

Correspondence to: J.M. Kauffmann, Université Libre de Bruxelles, Institut de Pharmacie, Campus Plaine CP 205/6, Boulevard de Triomphe, 1050 Brussels (Belgium).

differences in the stability of the cation radical) [5], the antiinflammatory activity of organoselenides (from differences in the oxidation potential) [6] and the anthelmintic activity of arylethenylpyridinium salts (from differences in the reduction potentials) [7,8]. In drug research, electrochemical techniques may have application to drug–protein [10], and drug–DNA binding studies [11] giving results useful in drug bioavailability and toxicity tests, respectively.

The electrochemical investigation of the redox behavior of xenobiotics can also be of valuable interest for the identification of unstable (toxic) intermediates and for the elucidation of complex reaction pathways [12]. This information may be particularly useful during early studies dealing with biotransformation, since several reports have suggested some parallelism between electrochemical and physiological degradation of xenobiotics [13,14].

BIOTRANSFORMATION STUDIES

As recently illustrated in a review article on xenobiotic metabolisation [15], electroanalytical techniques are well adapted to helping the investigator elucidate the processes occurring within a biological system. The advances observed in microelectrodes, in electronics (rapid scanning techniques) and in the understanding of the relevant theories has prompted several in vivo investigations particularly in the neurosciences [16,17]. Of particular pharmacological interest are studies related to the overall effects of drugs on neurotransmitter release. These experiments can be performed in vivo on freely moving animals or in vitro in tissue samples and recently, also on single intact cells by using microelectrodes [18]. Selectivity in vivo with microelectrodes, however, is limited due to the similar electrochemical properties of numerous compounds and to the ubiquitous matrix interferences at the sensor tip. This requires surface modification strategies which considerably complicate the experimental set-up and leads to difficulties in the interpretation of the results. Hopefully, new impulses are expected with the development of selective miniaturized biosensors (enzyme immobilized electrodes) [19]. Further, the use of modern microdialysis sampling technology (capillary ultrafiltration) coupled to LC–EC (liquid chromatography–electrochemical detection) opens new horizons in the field of on-line monitoring of metabolic changes occurring in vivo in the extracellular space [20–22].

In addition to the "in vivo" mechanistic aspects, electrochemical detectors combined with liquid chromatographic separation (LC–EC) can be advantageously used for the determination of a vast number of xenobiotics in biological media [15,22,23]. In pharmacokinetic studies, LC–EC can be regarded as an alternative or complement to LC–UV for the identification and quantitation of minor-metabolites (generally highly electroactive) and drugs with low absorptivity, for example, successful applications have been observed in the determination of mitomycin C [24], daunorubicin [25], *cis*-platin [26], cycloserine [27], neurotransmitters [28] and acetaminophen [15]. During the past few years, modern EC detector concepts (low volumes), new electrode designs (microelectrodes) and new surface cleaning techniques (potential pulses) have considerably improved the detection limits and enlarged the application fields of drug analysis in biological fluids (see below).

ANALYSIS OF RAW MATERIAL AND DRUG FORMULATION

As far as the assay of drugs in a pure form is concerned, following the pharmacopoeia official monographs, electrochemical investigation modes are mainly concerned with potentiometric titration in non-aqueous media. Amperometric titrations are also reported and few examples of polarography have been mentioned in *USP Pharmacopoeia* since 1975. From review articles dealing with polarography and voltammetric analysis of drugs [29–31] it appears, however, that many drugs are electroactive. By compiling a list of the most frequently occurring drugs (Table 1) [32] and checking the electrochemical literature data [29–31], it was found that most of the drugs listed in Table 1 (presently the benzodiazepines must

TABLE 1

Most frequently occurring drugs in drug formulations as the only active ingredient

Acetylsalicylic acid	Heparin
Acetaminophen [a]	Hydrocortisone [b]
Allopurinol [a]	Isosorbid dinitrate [a]
Ampicillin [a]	Nitrofurantoin [a]
Ascorbic acid [a]	Phenoxymethylpenicillin [a]
Atropin [b]	Prednisolone [b]
Bisacodyl [a]	Prednisone [b]
Chloramphenicol [a]	Retinol [a]
Cyanocobalamine [a]	Tetracycline [a]
Dexamethasone [b]	Triamcinolone [b]
Digoxin [a]	Vincamine [b]
Erythromycin [a]	

[a] Electroactive. [b] Non aqueous media.

be added in the list) can be studied by polarography and/or voltammetry. For the investigation of drug formulations, potentiometric and amperometric titrations, constant current and potential coulometry [29,30,33], ion-selective electrodes [33,34], enzyme, bacterial, and tissular electrodes [35,36], numerous voltammetric techniques [29–31] have been successfully applied with minor sample treatments.

ANALYSIS IN BIOLOGICAL FLUIDS

The application fields of electroanalysis in biological matrixes are broad and the experimental approaches differ depending on the sample and the specific analytical requirements (Table 2). Modern electroanalysis, such as pulsed wave forms and adsorptive techniques, offer, at least under well-defined drug therapy monitoring, the possibility of a direct quantitation of the drug in diluted biological samples. For these assays, it is usually mandatory to isolate the drug and its metabolites from the biological matrix, usually by solvent or solid phase extraction [37]. Some degree of selectivity can be attained by proper adjustment of the electrode potential. However, most of the investigations require the separation of every component from the isolated material. In this respect LC–EC has contributed significantly to the successful analysis of drugs in clinical chemistry [22,38] and in the forensic determination of the drugs of abuse [39]. New impulses have been observed recently with (i) the commercial launching of detection systems applying pulsed and integrated waveforms for the detec-

TABLE 2

Drug analysis application fields

Research and development (pharmacokinetics, metabolization)	
Analysis of raw products (pharmacopoeia monography)	
Analysis of drug formulation	
Analysis in biological fluids:	drug therapy monitoring
	drug intoxication
	drug addiction
	doping

TABLE 3

Examples of solid electrodes in electroanalysis

Classical (A)	Composite (B)	Modified (C)
Platinum	Carbon black/graphite	A or B
Gold	+	+
Graphite	Nujol, Silicone, Teflon	Polymer
Glassy carbon	PEG [a], Epoxy resin, Kel-F, Nafion	Polymer + catalyst
Tin oxide	PVC [b], polystyrene, CA [c]	Conductive polymer
Indium oxide	+	Conductive polymer + catalyst
Ruthenium oxide	Composite + Au, Pt, Ag = Consolidated	Chelator
		Ion-exchanger
		Silicate
		Biocomponent
		Amphiphile

[a] PEG = polyethyleneglycol. [b] PVC = polyvinylchloride. [c] CA = cellulose acetate.

tion of carbohydrates and glycoproteins [40,41], (ii) the refinements in conductivity detection [42], (iii) new postcolumn derivatization strategies (e.g. UV photolysis [43], enzymatic reactors [44]) which allow for the detection of electroinactive drugs, and (iv) the use of microelectrodes in capillary zone electrophoresis [45,46]. Electrochemical immunoassays in flow systems (LC and flow injection analysis) allow much lower detection limits and permit assays on small amounts of physiological fluids [47,48]. As far as microsamples are concerned, the recent commercialization of portable amperometric biosensors for glucose in whole blood [49] has stimulated considerable research on the development of miniaturized (screen printing technology) biosensors for drug control in hospitals (for clinical, and routine use) and in emergency medicine. The disposable sensor strips generally consist of a carbon working electrode and a Ag/AgCl reference electrode with the appropriate enzyme for acetaminophen, salicylate, or theophylline [50]. Since direct determinations of drugs in biological fluids are perturbed by matrix effects and suffer from poor selectivity, research is underway to modify classical electrodes so that the electrode would take on the properties of the modifier [51].

As shown in Table 3, the strategies include (i) conferring on the electrode surface anti-fouling and/or selective properties by means of appropriate membrane barriers (electrostatic and/or hydrophobic phenomena), (ii) increasing the selectivity and enlarging the field of application towards electroinactive drugs by immobilizing a (bio)catalyst and (iii) conferring better selectivity and sensitivity by immobilizing the chelating agents, the ion-exchanger, the lipids etc. Despite the great amount of effort within the last ten years at the academic level, few, if any, modified electrodes for drug analysis are commercially available.

TABLE 4

Tentative recommendations for electroanalysis of drugs

Identification of the electroactivity of the molecule
Identification and study of the degradation product(s)
Identification and study of the metabolite(s)
Selectivity towards structurally related drugs
Influence of the components of the matrix on the EC response
Influence of the side products on the EC response
Comparison with a non-electrochemical method
Calibration curve versus standard addition method
Internal standard (recovery test)
Reproducibility and repeatability of the response (+blank)
Linearity (range and slope)
Detection limit

Conclusions

Electrochemistry is a well established and fast growing area with a number of possible applications in the pharmaceutical field. However, from personal investigations in several drug control laboratories and hospitals, from reports at the pharmaceutical industries level [52,53] and from the content of the monographs of the National and the European Pharmacopea [see also Ref. 54] it appears that polarographic and voltammetric techniques are consistently avoided despite their performance outlined above. Without entering into a speculative description explaining the limited attention given to electrochemistry in routine analysis, one must admit that the requirements of drug analysis are stringent, and, if not well understood and applied, electroanalytical methods may only have limited success. The improvement of quality of life has stimulated considerable research in drug design (high activity at low dose) bioavailability and safety. Thus, in order to achieve these targets, highly sensitive and specific methods of analysis are necessary, e.g., techniques able to differentiate enantiomers. The requirements are such that validation of any analytical measurement is regarded as a prerequisite in drug analysis; a tentative recommendation for drug electroanalysis is given in Table 4 (see also Refs. 55 and 56). Finally, it is hoped that in the near future more attention will be devoted to developing teaching programs dealing with modern electroanalysis, with the emphasis on instrumentation design (automation, flow injection, batch injection [57] software, etc.), electrode shape and design (modified electrode) for the sake of simplicity and the quality of life.

Thanks are expressed to C. Marvin for help in the preparation of this manuscript and to the Fonds National de la Recherche Scientifique.

REFERENCES

1 D.E. Danly and C.J.H. King, in H. Lund and M.M. Baizer (Eds.), Organic Electrochemistry, Marcel Dekker, New York, 1991, p. 1285.
2 Electricité de France (EDF), Electrosynthèse organique, Internal Document, Direction des Études et Recherches, Saint Denis, 1986.
3 L. Campanella, T. Ferri, M.P. Sammartino, W. Marconi and A. Nidola, J. Mol. Catal., 42 (1987) 153.
4 J. Bonnefoy, J. Moiroux, J.M. Laval and C. Bourdillon, J. Chem. Soc. Faraday Trans. 1, 84 (1988) 941.
5 J.-M. Kauffmann, J.-C. Viré, G.J. Patriarche and W.H. Heineman, Analyst, 110 (1985) 349.
6 B. Dakova, J.-M. Kauffmann, M. Evers, L. Lamberts and G.J. Patriarche, Electrochim. Acta, 35 (1990) 1133.
7 P. Kovacic, J.R. Ames, D.L. Rector, M. Jawdosiuk and M.D. Ryan, Free Rad. Biol. Med., 6 (1989) 131.
8 J.R. Ames, J. Pharm. Sci., 80 (1991) 293.
9 C. Amatore, in H. Lund and M.M. Baizer (Eds.), Organic Electrochemistry, Marcel Dekker, New York, 1991, p. 11.
10 J.A. Squella and L.J. Nunez-Vergara, Bioelectrochem. Bioenerg., 11 (1983) 425.
11 O. Vrana and V. Brabec, Bioelectrochem. Bioenerg., 19 (1988) 145.
12 M.Z. Wrona and G. Dryhurst, J. Org. Chem., 52 (1987) 2817.
13 J.-M. Kauffmann, J.-C. Viré and G.J. Patriarche, Bioelectrochem. Bioenerg., 12 (1984) 413.
14 P.W. Crawford, W.O. Foye, M.D. Ryan and P. Kovacic, J. Pharm. Sci., 76 (1987) 481.
15 S.M. Lunte, D.M. Radzik and P.T. Kissinger, J. Pharm. Sci., 79 (1990) 557.
16 R.N. Adams, Progr. Neurobiol., 35 (1990) 297.
17 K. Shibuki, Neurosci. Res., 9 (1990) 69.
18 K.T. Kawagoe, J.A. Jankowski and R.M. Wightman, Anal. Chem., 63 (1991) 1589.
19 E.R. Reynolds and A.M. Yacynych, Am. Lab., 3 (1991) 19.
20 M.C. Linhares and P.T. Kissinger, Trends Anal. Chem., 11 (1992) 171; M.C. Linhares and P.T. Kissinger, Pharm. Res., submitted for publication.
21 B.H.C. Westerink, Trends Anal. Chem., 11 (1992) 176.
22 P.T. Kissinger and D.M. Radzik, Drug Pharm. Sci., 47 (1991) 65.
23 K. Stulik and V. Pacakova, C.R.C., Crit. Rev. Anal. Chem., 14 (1984) 297.
24 U.R. Tjaden, J.P. Langenberg, K. Ensing, W.P. Van Bennekom, E.A. DeBruijn and A.T. Van Oosterom, J. Chromatogr., 232 (1982) 355.
25 C. Akpofure, C.A. Riley, J.A. Sinkula and N.E. Evans, J. Chromatogr., 232 (1982) 377.
26 K. Digua, J.-M. Kauffmann, G.J. Patriarche and G. Ghanem, J. Liq. Chromatogr., in press.
27 K. Digua, J.-M. Kauffmann, G. Caliaro and M. Jans, (1992) unpublished data.
28 M.Z. Wrona, D. Lemordant, L. Lin, C. LeRoy Blank and G. Dryhurst J. Med. Chem., 29 (1986) 499.
29 G.J. Patriarche, M. Chateau Gosselin, J.L. Vandenbalck and P. Zuman, in A.J. Bard (Ed.), Electroanalytical Chemistry, Vol. 11, Marcel Dekker, New York, 1979, p. 141.
30 P.M. Bersier and J. Bersier, in M.R. Smyth and J.G. Vos (Eds.), Analytical Voltammetry (Comprehensive Analytical Chemistry Vol. 27, Series Editor G. Svehla), Elsevier, Amsterdam, 1992, p. 159.
31 G.J. Patriarche and H. Zhang, Electroanalysis, 2 (1990) 573.
32 H.J. Roth and A. Kleeman, Pharmaceutical Chemistry: Drug Synthesis, Vol. 1, Ellis Horwood, Chichester, 1988 p. 13.
33 K. Vytras, J. Pharm. Biomed. Anal., 7 (1989) 789.
34 V.V. Cosofret, Trends Anal. Chem., 10 (1991) 298.
35 G.J. Patriarche, J.-M. Kauffmann and J.-C. Viré, in R.D. Schmid (Ed.), Biosensors International Workshop 1987, GBF Monographs, VCH, Weinheim, 1987, p. 61.
36 Y.J. Fitzgerald, G.W. Hanlon, A.J. Hutt and C.J. Olliff, J. Pharm. Pharmacol., 39 (1987) 149p.
37 J.-C. Viré, J.-M. Kauffmann and G.J. Patriarche, in G.-A. Junter (Ed.), Electrochemical Detection Techniques in the Applied Biosciences, Ellis Horwood, Chichester, 1988, p. 21.
38 D.C. Johnson, S.G. Weber, A.M. Bond, R.M. Wightman, R.E. Shoup and I.S. Krull, Anal. Chim. Acta, 180 (1986) 187.
39 C.M. Selavka and I. Krull, J. Liq. Chromatogr., 10 (1987) 345.
40 M.R. Hardy and R.R. Townsend, Proc. Natl. Acad. Sci., 85 (1988) 3289.
41 D.C. Johnson and W.R. LaCourse, Anal. Chem., 62 (1990) 589A.
42 R.W. Slingsby J. Chromatogr., 371 (1986) 373.
43 L. Dou and I.S. Krull, Anal. Chem., 62 (1990) 2599.
44 G. Marko-Varga and L. Gorton, Anal. Chim. Acta, 234 (1990) 13.
45 T.J.O'Shea, R.D. Greenhagen, S.M. Lunte, C.E. Lunte, M.R. Smyth, D.M. Radzik and N. Watanabe, J. Chromatogr., 593 (1992) 305.
46 R.A. Wallingford and A.G. Ewing, Anal. Chem., 61 (1989) 98.
47 B. Halsall and W.R. Heineman, J. Int. Fed. Clin. Chem., 2 (1990) 179.
48 Y. Xu, B. Halsall and W.R. Heineman, J. Pharm. Biomed. Anal., 7 (1989) 1301.
49 D.R. Matthews, R.R. Holman, E. Bown, J. Steemson, A. Watson, S. Hughes and D. Scott, Lancet, 4 (1987) 778.
50 P.I. Hilditch and M. Green, Analyst, 116 (1991) 1217.
51 R.P. Baldwin and K.N. Thomsen, Talanta, 38 (1991) 1.

52 J.B. Reust, in A. Ivaska, A. Lewenstam and R. Sara (Eds.), Contemporary Electroanalytical Chemistry, Plenum Press, New York, 1990, p. 359.
53 P. Bersier and J. Bersier, Analyst, 114 (1989) 1531.
54 G. Phillips, Anal. Proc., 28 (1991) 420.
55 J.C. Wahlich and G.P. Carr, J. Pharm. Biomed. Anal., 8 (1990) 619.
56 A.R. Buick, M.V. Doig, S.C. Jeal, G.S. Land and R.D. McDowall, J. Pharm. Biomed. Anal., 8 (1990) 629.
57 J. Wang, Microchem. J., 45 (1992) 219.

Analytica Chimica Acta, 273 (1993) 335–338
Elsevier Science Publishers B.V., Amsterdam

Determination of trace amounts of impurities in pharmaceutical preparations by differential-pulse polarography

Part 1. Determination of diisooctyl maleate in the pharmaceutical sodium 1,4-bis(2-ethylhexyl)sulphosuccinate and of maleic acid in fumaric acid

Walenty Szczepaniak and Maria Ren

Department of Instrumental Analysis, Faculty of Chemistry, Adam Mickiewicz University, 60 780 Poznań (Poland)

(Received 1st June 1992; revised manuscript received 16th September 1992)

Abstract

A differential-pulse polarographic procedure is described for the determination of impurities such as diisooctyl maleate and maleic acid in pharmaceutical products. The concentration range for diisooctyl maleate is 1×10^{-6}–30×10^{-6} μg ml^{-1} and the detection limit is 0.2 μg ml^{-1}; for maleic acid the detection limit is 0.15 μg ml^{-1}. It is possible to determine very low concentrations of maleic acid in the presence of fumaric acid by a preseparation by dissolution in water, in which fumaric acid dissolves to only a small extent.

Keywords: Polarography; Voltammetry; Diisooctyl maleate; Fumaric acid; Maleic acid; Pharmaceuticals; Sodium 1,4-bis(2-ethylhexyl)sulphosuccinate

Electrochemical methods, including voltammetry, are widely used in the analysis of drugs [1]. In this present paper, a differential-pulse polarographic (DPP) technique is proposed for the determination of impurities in pharmaceuticals. In the process of drug production, the determination of impurities is an essential analytical problem, which can generally be solved by the DPP technique owing to its high selectivity towards electroactive substances. As a result of this feature, complex media can be examined and this technique has proved to be applicable in trace analysis.

Maleic acid and its derivatives can be readily studied by voltammetry because they contain a double bond that undergoes an electrochemical reduction [2] according to

$$ROOCCH = CHCOOR + 2H^+ + 2e^- \rightarrow ROOCCH_2CH_2COOR$$

where R = H or a radical. This paper gives the results of studies of the determination of diisooctyl maleate (DM) in sodium 1,4-bis(2-ethylhexyl)sulphosuccinate (AOT) and maleic acid (MA) in fumaric acid (FA).

DM is a starting material in the production of sodium 1,4-bis(2-ethylhexyl)sulphosuccinate, which is the active ingredient in the purgative Dipolaxan, and unreacted DM may occur as an impurity in AOT. MA is an impurity occurring in FA and it has been the subject of both polarographic [3,4] and potentiometric [5] studies with

Correspondence to: W. Szczepaniak, Department of Instrumental Analysis, Faculty of Chemistry, Adam Mickiewicz University, 60 780 Poznań (Poland).

the objective of improving the methods used in its determination in admixtures. MA, unlike FA, is toxic both to humans and animals, having a harmful effect on the respiratory system and urinary tract [6]. Therefore, it is necessary to control its content both in FA used in pharmaceuticals and in malonic acid applied in food products

EXPERIMENTAL

Apparatus

For voltammetric measurements, a PA4 polarograph with a Model 4106 *X–Y* recorder (Laboratórní Přístroje, Prague) was used, with an SMDE-1 hanging mercury drop working electrode (HMDE) (Laboratórní Přístroje), a platinum auxiliary electrode and an Ag/AgCl reference electrode.

Reagents and solutions

All standard solutions were prepared using chemicals from Merck, all the samples studied came from Polfa (Poznań). A 0.01 g ml^{-1} standard solution of DM was prepared in a 70% ethanolic solution of borate buffer (pH 10).

Determination of diisooctyl maleate in sodium 1,4-bis(2-ethylhexyl)sulphosuccinate

A 10-ml volume of sample solution was placed in a polarographic cell and deaerated for 10 min with ultrapure argon. The voltammetric response was obtained with initial and final potentials of −0.9 and −1.7 V, respectively, pulse repetition time 0.2 s, amplitude −50 mV and scan rate 10 mV s^{-1}. The concentration of DM in AOT was determined by the multiple standard addition technique.

Determination of maleic acid in fumaric acid

About 80 ml of distilled water were added to 50 g of fumaric acid, mixed, filtered and washed. To the filtrate, another portion of 50 g of fumaric acid was added, mixed, filtered and washed. A 1-ml volume of filtrate obtained was diluted to 10 ml with an appropriate supporting electrolyte. Voltammetric determination was performed as for the determination of DM in AOT, with initial and final potentials of −1.0 and −1.8 V, respectively.

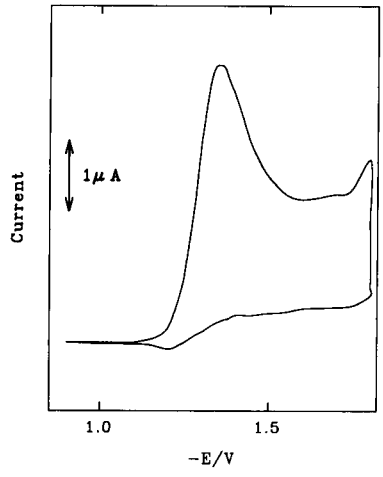

Fig. 1. Cyclic voltammograms for diisooctyl maleate (0.2 mg ml^{-1}) in borate buffer in 70% ethanol. Scan rate, 100 mV s^{-1}.

RESULTS AND DISCUSSION

Diisooctyl maleate in AOT

Attempts were made to obtain the best voltammograms by testing potassium chloride, acetate buffer and borate buffer in 70% ethanol as basic electrolytes. The best results were achieved with a solution containing borate buffer and ethanol. Measuring parameters were established for standard solutions of DM.

Figure 1 shows a cyclic voltammogram obtained on an HMDE for a solution of DM in borate buffer in 70% ethanol. A reduction peak was observed at −1.3 V.

Figure 2 presents differential-pulse voltammograms for solutions of DM of increasing concentration in borate buffer in 70% ethanol (pH 10). The well resolved obtained peak increases with increasing DM concentration.

Linearity between the peak current and DM concentration over the range 1×10^{-6}–30×10^{-6} μg ml^{-1} was obtained (slope 4.84 nA ml μg^{-1}, correlation coefficient 1.000). The detection limit under the conditions of experiment was 0.2 μg ml^{-1}.

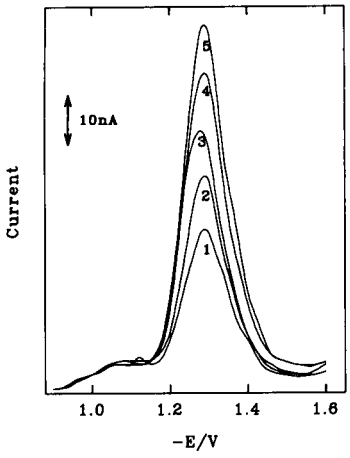

Fig. 2. Differential-pulse voltammograms for diisooctyl maleate: (1) 6; (2) 8; (3) 10; (4) 12; (5) 14 μg ml^{-1}. Pulse repetition time, 0.2 s; amplitude, −50 mV; scan rate, 10 mV s^{-1}.

From the analytical point of view, the most important aspect is the possibility of the occurrence of DM as an impurity in AOT. Figure 3 shows voltammograms obtained for DM contained in AOT and for successive standard additions. A linear dependence between the peak current and the standard concentration was obtained (correlation coefficient 0.9999). The precision of DM determinations in AOT was obtained on the basis of eight parallel determinations of DM in AOT solutions prepared from the same sample. The relative standard deviation was 3.5%.

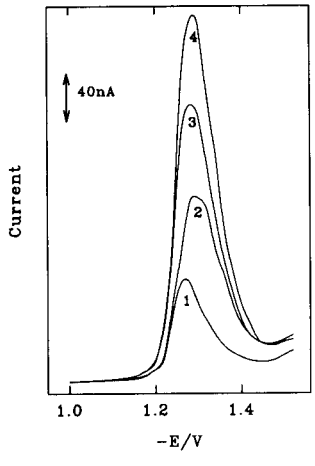

Fig. 3. Differential-pulse voltammograms for (1) DM in AOT and (2–4) after successive additions of DM standard. Scan rate, 10 mV s^{-1}; pulse repetition time, 0.2 s; amplitude, −50 mV.

Maleic acid

In the determination of trace amounts of MA in FA, a large excess of the latter was subjected to preliminary separation. MA dissolves very well in water (78.8 g per 100 ml), whereas fumaric acid dissolves poorly (0.69 g per 100 ml), so it is possible to separate a large excess of FA from trace amounts of MA. After this preliminary separation, there is still a large excess of FA relative to MA, but it is possible to determine MA in the presence of FA. DPP was applied for this determination owing to its relatively high resolution. The behaviour of MA and FA (voltammetric response) in solutions of different basic electrolytes [ammonia buffer (pH 8.2), 0.1 M K_2HPO_4 (pH 8.6) and a solution containing 0.1 M tetraethylammonium chloride and 0.05 M citric acid in 70% dioxane] was tested. The most convenient difference in the positions of the MA and FA peaks was obtained with phosphate buffer.

Figure 4 shows linear-sweep voltammograms of MA and FA in a solution of K_2HPO_4 (MA and FA concentration 0.02 mg ml^{-1}). The reduction peaks for MA and FA were observed at −1.45 and −1.7 V, respectively.

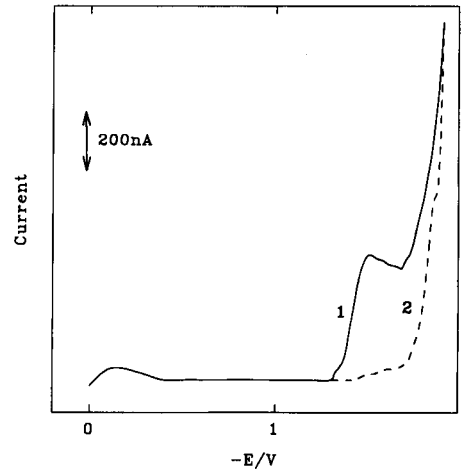

Fig. 4. Linear-sweep voltammograms for (1) maleic and (2) fumaric acids in K_2HPO_4 solution. MA and FA concentrations, 0.02 mg ml^{-1}; scan rate, 100 mV s^{-1}.

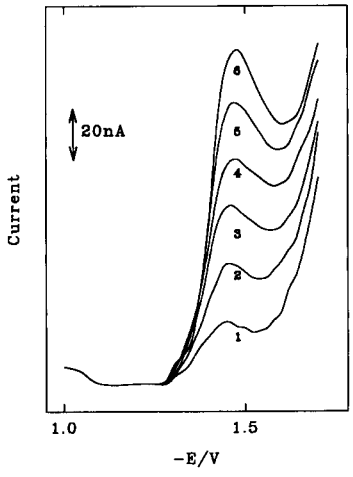

Fig. 5. Differential-pulse voltammograms for standard solutions of maleic acid of concentration (1) 2, (2) 4, (3) 6, (4) 8, (5) 10 and (6) 12 μg ml^{-1}. Pulse repetition time 0.2 s; amplitude, −50 mV; scan rate, 5 mV s^{-1}.

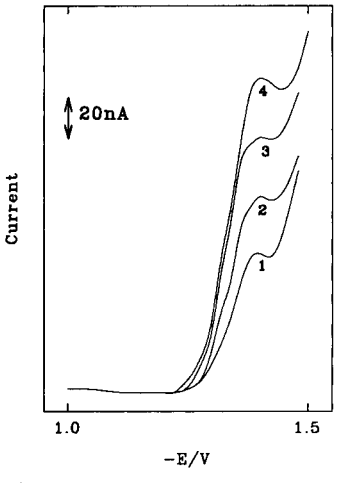

Fig. 6. Differential-pulse voltammograms for (1) maleic acid contained in a sample of fumaric acid and (2–4) for successive standard additions of MA (2, 4 and 6 μg ml^{-1}). Pulse repetition time, 0.2 s; amplitude, −50 mV; scan rate, 5 mV s^{-1}.

Conditions for MA determination and the measuring parameters were established for standard solutions of MA. The peak height was found to be linearly dependent on MA concentration. Figure 5 presents differential-pulse voltammograms for MA solutions of different concentrations. The dependence of the peak current on MA concentration is linear with a slope of 10.14 μA ml mg^{-1} and a correlation coefficient 0.9999. The detection limit is 0.15 μg ml^{-1}.

It is possible to determine MA at very low concentrations relative to a large excess of FA by applying the method of multiple standard additions. Figure 6 presents voltammograms for MA contained in a sample of FA without a reference standard and after subsequent standard additions. A linear dependence between peak current and concentration was obtained (correlation coefficient 0.9999).

The precision of MA determinations was obtained on the basis of parallel MA determinations in five solutions of FA prepared from the same sample. The relative standard deviation was 3.27%.

The examples presented provide good evidence that the method incorporating the DPP technique is successful for determinations of 0.1% of DM in AOT and 0.01% of MA in FA.

REFERENCES

1 G.J. Patriarche and H. Zhang, Electroanalysis, 2 (1990) 573.
2 P.J. Elving and C. Teitelbaum, J. Am. Chem. Soc., 71 (1944) 3916.
3 I. Spiłevska and V. Rekalic, Glas. Hem. Drus., Beograd, 49, No. 2 (1984) 45.
4 I. Spiłevska and V. Rekalic, Glas. Hem. Drus., Beograd, 49, No. 2 (1984) 57.
5 M. Kataoka, R. Naganava, K. Odashima and Y. Umezaria, Anal. Lett., 22 (1989) 1089.
6 M. Nikonorow and B. Urbanek-Karłowska, Toxicological Evaluation of Food Additives, PZWL, Warsaw, 1987.

Analytica Chimica Acta, 273 (1993) 339–342
Elsevier Science Publishers B.V., Amsterdam

Determination of trace amounts of impurities in pharmaceutical preparations by differential-pulse polarography

Part 2. Determination of disodium bis(ethanesulphonato) disulphide in sodium 2-mercaptoethanesulphonate

Walenty Szczepaniak and Maria Ren

Department of Instrumental Analysis, Faculty of Chemistry, Adam Mickiewicz University, 60 780 Poznań (Poland)

(Received 1st June 1992; revised manuscript received 16th September 1992)

Abstract

A differential-pulse polarographic procedure is described for the determination of trace amounts of disulphides in sodium 2-mercaptoethanesulphonate and in pharmaceutical products in which the latter compound is a component. Concentrations of the order of 1 mg ml^{-1} can be determined with a precision of about 3.2%. The lowest concentration of disulphide that could be determined in the mercaptosulphonate and the pharmaceutical product is about 0.1%. No matrix separation is required.

Keywords: Polarography; Voltammetry; Disodium bis(ethanesulphonato) disulphide; Pharmaceuticals; Sodium 2-mercaptoethanesulphonate

(mesna) (Sodium 2-mercaptoethanesulphonate) is an active component of the mucolytic agent Mistabron (Polfa, Poznań). In both the aforementioned products, disodium bis(ethanesulphonato) disulphide ($NaO_3SCH_2CH_2SSCH_2CH_2SO_3Na$), is formed as an undesirable impurity. In controlling the quality of both mesna and Mistabron, it is necessary to determine the disulphide (DS). According to early reports on the polarographic determination of organic disulphides [1] and organic polysulphides [2], these compounds are subject to an electrochemical reduction according to $RSSR + 2H^+ + 2e \rightarrow 2RSH$ yielding well shaped polarographic waves. It was also demonstrated that the analysis is not hindered by sulphides and thiols.

In this paper, the application of differential-pulse polarography (DPP) in the determination of traces of DS as an impurity in mesna and Mistabron is proposed.

Correspondence to: W. Szczepaniak, Department of Instrumental Analysis, Faculty of Chemistry, Adam Mickiewicz University, 60780 Poznań (Poland).

EXPERIMENTAL

Apparatus

In voltammetric measurements, a PA4 polarograph with a Model 4106 *X–Y* recorder (Laboratórní Přístroje, Prague) was used, with an SMDE-1 hanging mercury drop working electrode (Laboratórní Přístroje), a platinum auxiliary electrode and an Ag/AgCl reference electrode.

Reagents and solutions

All standard solutions were prepared using chemicals from Merck and all the samples studied came from Polfa.

Determination of the disulphide in mesna

A 10-ml volume of basic electrolyte (1 M $NaHCO_3$) was placed in a polarographic cell and oxygen was removed from the solution by passing argon for 10 min, then 10 mg of mesna were added, the solution was stirred and argon was passed through it again. The voltammetric response was obtained using a pulse repetition time of 0.2 s, amplitude −50 V and scan rate 5 mV s^{-1}, with initial and final potentials of −0.6 and −1.5 V, respectively.

In the method of multiple standard additions, a known amount of KIO_3 was introduced three times, each time oxygen was removed by passing argon through the solution and then a voltammogram was measured. KIO_3 oxidizes mesna to disulphide and the disulphide thus formed is the standard, e.g., 20 μl of KIO_3 at a concentration of 1.632 mg ml^{-1} oxidizes 0.15 mg of mesna to the disulphide.

Determination of the disulphide in Mistabron

A 9.5-ml volume of basic electrolyte was placed in a polarographic cell, then oxygen was removed and 0.5 ml of Mistabron was added (this amount corresponds to 25 mg of mesna), then again oxygen was removed and a voltammogram was measured.

Measurement of the voltammograms and determination via the method of multiple standard additions were as for mesna.

RESULTS AND DISCUSSION

Organic disulphides can be electrochemically reduced, generating well shaped polarographic waves. Using the DPP method, a clear reduction peak of the disulphide (DS) contained in mesna at a potential of −1.15 V is observed. Its height depends on the concentration, so this peak can be used for analytical purposes. As mentioned under Experimental, a standard solution of DS

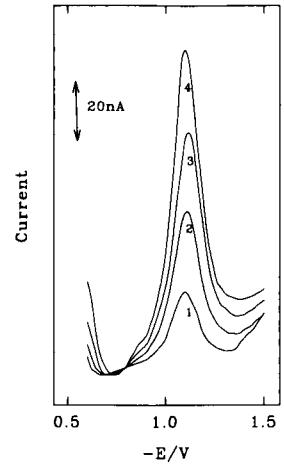

Fig. 1. Differential-pulse voltammograms for disulphide of concentration (1) 0.01, (2) 0.02, (3) 0.03 and (4) 0.04 mg ml^{-1}. Supporting electrolyte, $NaHCO_3$; pulse repetition time, 0.2 s; amplitude, −50 mV; scan rate, 10 mV s^{-1}.

was obtained as a result of oxidation of mesna by a standard solution of KIO_3 according to

$$6RSH + KIO_3 \rightarrow 3RSSR + 3H_2O + KI$$

Figure 1 shows differential-pulse voltammograms of DS with increasing concentration. A linear dependence of the peak current on DS concentration was obtained (slope 24.05 nA per 0.01 mg ml^{-1}, correlation coefficient 0.9999).

The basic solution of the disulphide for this experiment was prepared by oxidizing 10 mg of mesna (in $NaHCO_3$ solution) with a suitable amount of KIO_3. The concentration of disulphide in this solution was 1 mg ml^{-1}. Subsequent solutions were prepared by adding appropriate amounts of the basic solution of disulphide to the supporting electrolyte, then their analytical curves were obtained.

Determination of the disulphide in mesna

The determination of DS in mesna was conducted using the method of standard multiple additions. Figure 2 shows some examples of the voltammograms obtained. A linear dependence between peak current and concentration was obtained (correlation coefficient 0.9994). Standard additions were made by introducing into the solution of mesna a corresponding (increasing)

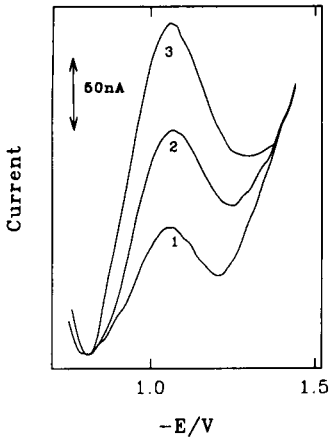

Fig. 2. Differential-pulse voltammograms for (1) disulphide contained in mesna in a solution of mesna (1 mg ml^{-1}) in $NaHCO_3$ and (2 and 3) after successive additions of KIO_3, the resultant concentration of the disulphide formed (as a standard) being 0.015 and 0.03 mg ml^{-1}, respectively.

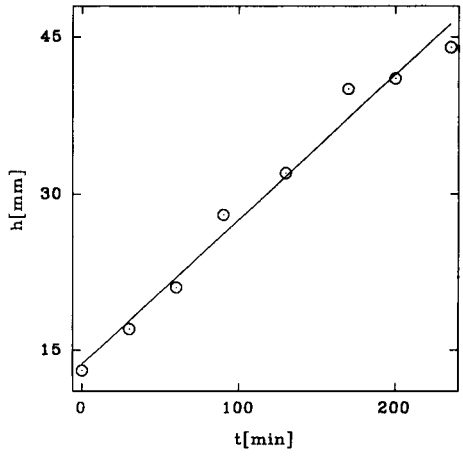

Fig. 3. Dependence of the peak height of disulphide in a solution of mesna exposed to light and air.

amount of the KIO_3 solution, which oxidized mesna and increased the DS concentration. Four successive analyses of the same sample yielded results with a relative standard deviation of 3.2%.

It should be noted, however, that mesna solutions may also be oxidized by atmospheric oxygen according to

$$2RSH + \tfrac{1}{2}O_2 \rightarrow RSSR + H_2O$$

Therefore, for solutions of mesna stored for a long period of time and exposed to light and air, an increasing concentration of DS is observed. Figure 3 illustrates the time dependence of the peak height of the same mesna solution. The peak height of DS increases almost linearly with time. Therefore, only solutions prepared shortly before use should be employed. It is also possible to obtain mesna solutions under an atmosphere of argon, and it was then found that only an insignificant increase in the DS peak took place after 2 h.

Determination of the disulphide in Mistabron

The determination procedure was analogous to that applied for mesna and Fig. 4 presents some voltammograms obtained. A linear dependence between peak current and concentration was obtained (correlation coefficient 0.9999). The relative standard deviation based on four successive analyses of the same sample was 3.5%. The analysis was performed directly after opening a container, as the DS content in an open vessel increased with time.

The lowest concentration of DS determined in mesna and in Mistabron was 0.1%. The results obtained demonstrate that the proposed DPP technique provides a convenient, rapid and precise method for the determination of trace impu-

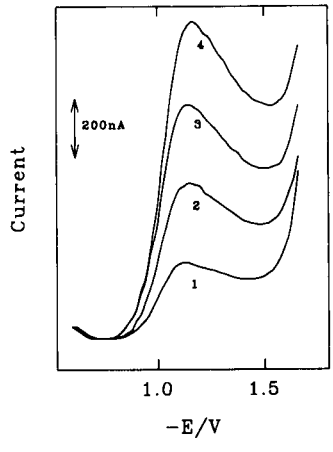

Fig. 4. Differential-pulse voltammograms for (1) disulphide contained in Mistabron (concentration of active ingredient in the solution of Mistabron = 2.5 mg ml^{-1}) and (2 and 3) after successive additions of KIO_3, the resultant concentration of the disulphide formed (as a standard) being 0.075 and 0.15 mg ml^{-1}, respectively.

rities of disulphide in pharmaceuticals based on sodium 2-mercaptoethanesulphonate. An advantage of the method is that thiols do not interfere, hence there is no need to separate the matrix.

REFERENCES

1 M.J. Gerber, Zh. Anal. Khim. USSR, 5 (1950) 262.
2 J.H. Karchmer and T.M. Walker, Anal. Chem., 26 (1954) 271.

Analytica Chimica Acta, 273 (1993) 343–349
Elsevier Science Publishers B.V., Amsterdam

Polarographic study of simazine in micellar and emulsified media

R. Gálvez, M. Pedrero, F.J. Manuel de Villena, J.M. Pingarrón and L.M. Polo

Department of Analytical Chemistry, Faculty of Chemistry, Complutense University of Madrid, 28040 Madrid (Spain).

(Received 19th May 1992; revised manuscript received 23rd July 1992)

Abstract

A polarographic study of the reduction of the herbicide simazine in micellar solutions and oil–water emulsions is reported. The anionic surfactant sodium pentanesulphonate was chosen as the most suitable agent for micellar solutions and emulsions. In micellar solutions two reduction peaks were observed in differential-pulse polarography (DPP) below pH 2.0, whereas only one peak was obtained above pH 2.0. Ethyl acetate was chosen as the organic solvent to form simazine emulsions. Unlike in micellar solutions, DP polarograms of simazine in oil–water emulsions showed only one peak even at pH values lower than 2.0, suggesting that pesticide hydrolysis is hindered in the emulsified medium. The limiting current is diffusion-controlled and the electrode process is irreversible. The diffusion coefficient of simazine in emulsified medium was 8.85×10^{-6} cm^2 s^{-1}, and the αn_a and K_f° values were 0.82 and 8.03×10^{-14} cm s^{-1} respectively. Using DPP, simazine can be determined over the concentration ranges 8.0×10^{-7}–4.0×10^{-5} mol l^{-1}. The limit of detection was 2.2×10^{-7} mol l^{-1}. The effect of the presence of other herbicides belonging to the *s*-triazine family on the simazine reduction peak was studied. The method was applied to the determination of simazine in spiked irrigation water with good recoveries.

Keywords: Polarography; Voltammetry; Herbicides; Simazine; Triazines

s-Triazine derivatives are used extensively in agriculture as herbicides to control weeds in several food crops. They have a long persistence and may be present as pollutants in drinking water [1,2]. Simazine (**I**), a monochloro-substituted derivative belonging to the *s*-triazine family, is widely used in cereal, vine, leguminous and several fruit crops and was the most commonly used triazine in Spain in 1988–89 [3]. It appears among the UK Red List Substances, which are mostly organic compounds, herbicides, insecticides, solvents and chlorinated base compounds liable to be found in rivers and effluents [4]. Consequently, the routine monitoring of simazine levels is necessary.

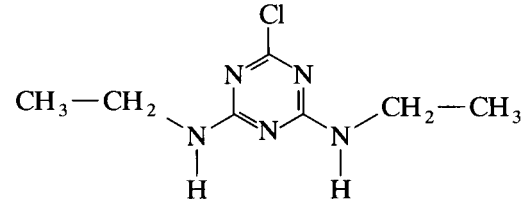

I

Chromatographic techniques, such as thin-layer chromatography (TLC) [5], liquid chromatography (LC) with spectrophotometric [6,7] and electrochemical [1] detection and gas chromatography (GC) [8–11] are the most widespread techniques used for the determination of simazine and other *s*-triazines. In addition, the EPA Method 525 includes the determination of simazine in drink-

Correspondence to: J.M. Pingarrón, Department of Analytical Chemistry, Faculty of Chemistry, Complutense University of Madrid, 28040-Madrid (Spain).

ing water by capillary column chromatography–mass spectrometry after liquid–solid extraction [12]. Electroanalytical techniques were proposed by Stastny et al. [13] and, more recently, by Lippolis and Concialini [14] for the determination of several *s*-triazines by differential-pulse polarography (DPP) in aqueous medium.

The determination of triazines in samples requires their extraction into organic solvents, the most common of which are chloroform [8], ethyl acetate [15] and dichloromethane [5,9]. The well known practical difficulties of using organic solvents in electroanalysis to determine scarcely water-soluble compounds can be overcome by working in oil–water emulsions, as these are predominantly aqueous [16–19].

This paper reports a polarographic study of the simazine reduction process in appropriate emulsions to find the optimum conditions for simazine determination. The proposed method was applied to the determination of simazine in samples of irrigation water.

EXPERIMENTAL

Apparatus

A Metrohm E 506 Polarecord equipped with an E 505 polarographic stand was used. A Metrohm E 612 VA-Scanner, LY 1600 Linseis *X–Y* recorder, Metrohm E 510 pH meter and a P-Selecta Ultrasons ultrasonic bath were used.

Electrodes and electrochemical cell

The electrochemical cell consisted of a Metrohm 6.1230.000 dropping mercury electrode, an Ingold 10-303-3000 saturated calomel reference electrode and a platimum wire counter electrode in a double-walled Metrohm EA 867-20 vessel. A Metrohm AG-9100 combined electrode was used for pH measurements. Cyclic voltammetric measurements were done using a Metrohm 6.1246.020 multimode mercury electrode equipped with a Metrohm 6.1226.030 capillary tube.

Reagents and solutions

Simazine was obtained from Riedel-de Haën. The non-ionic surfactants tested were Triton X-405 and X-305 and Pluronic F-68, F-64 and F-61 (Serva), the cationic surfactants were Hyamine 1622, 2389 and 3500 (Serva), and the anionic surfactants were sodium pentanesulphonate (Aldrich) and sodium dodecyl sulphate (SDS) (Carlo Erba). The organic solvents used were ethyl acetate and methanol (Carlo Erba). All chemicals were of analytical-reagent grade and the water used was obtained from a Millipore Milli-Q purification system.

A 1.0×10^{-3} mol l^{-1} stock solution of simazine in methanol was prepared by weighing. More dilute standards for working in micellar solutions were prepared by suitable dilution with water. A 1.0×10^{-3} mol l^{-1} stock solution in ethyl acetate was also prepared by weighing. More dilute standards for working in emulsified media were prepared by suitable dilution with the same organic solvent. Stock solutions of surfactants were 0.5% (w/v) in water. A Britton–Robinson buffer solution containing each component acid at 0.2 mol l^{-1} was used as supporting electrolyte.

Preparation of micellar solutions and oil–water emulsions

Micellar solutions were prepared by transferring into a 50-ml volumetric flask known volumes of the simazine stock solution and of the surfactant solution (depending on the required final concentrations) and 25.0 ml of the 0.2 mol l^{-1} Britton–Robinson buffer solution, in that order, after which the solution was diluted to the mark with water and the flask was placed in the ultrasonic bath for 1 min.

To prepare emulsions the following procedure was used. To a 50-ml flask a known volume of the simazine stock solution in ethyl acetate, a known volume of this organic solvent (up to 4.0 ml), a known volume of 0.5% sodium pentanesulphonate and 25.0 ml of the 0.2 mol l^{-1} Britton–Robinson buffer were added, in that order. After shaking for a few seconds, the flask was placed in the ultrasonic bath for 3 min.

Polarographic and cyclic voltammetric studies

The micellar solutions and emulsions prepared above were transferred into the electrochemical cell and deaerated by passing an argon stream

through them for 20 min. Polarograms were recorded at 25 ± 1°C keeping an inert atmosphere in the cell, with $\Delta E = -50$ mV, $v = 8.3$ mV s^{-1} and $t = 0.6$ s. The analytical response was measured in all instances against the background current. Cyclic voltammograms were recorded at 20 mV s^{-1}.

Determination of simazine in spiked water by differential-pulse polarography

The samples were obtained by allowing water to seep through agricultural soil and collecting it. Then 50-ml aliquots of these samples were spiked with simazine stock solution at the 4.0×10^{-6} or 2.0×10^{-5} mol l^{-1} level, shaken for a few seconds and filtered. The filtrate was transferred into a 100-ml separating funnel and 50 ml of ethyl acetate were added. The mixture was stirred mechanically for 20 min and the phases were separated. The extraction was repeated with another 50 ml of fresh organic solvent and the combined extracts were concentrated to about 2 ml in a rotatory vacuum evaporator. Finally, the emulsion was prepared from this concentrated extract as indicated above. Simazine was determined by DPP and interpolation of the calibration graph.

RESULTS AND DISCUSSION

Despite the low solubility of simazine in water, some preliminary DPP studies in virtually aqueous solutions (methanol content < 1%) were made. Solutions were prepared from the 1.0×10^{-3} mol l^{-1} simazine stock solution in methanol by dilution with water. In acidic solutions a well defined reduction peak was obtained for 1.0×10^{-5} mol l^{-1} simazine, whose peak current was highest between pH 2 and 3. This peak probably arises from the reduction of the –C=N– bond in the heterocyclic ring, as usual in triazines [13]. The reduction peak disappeared above pH 4.0.

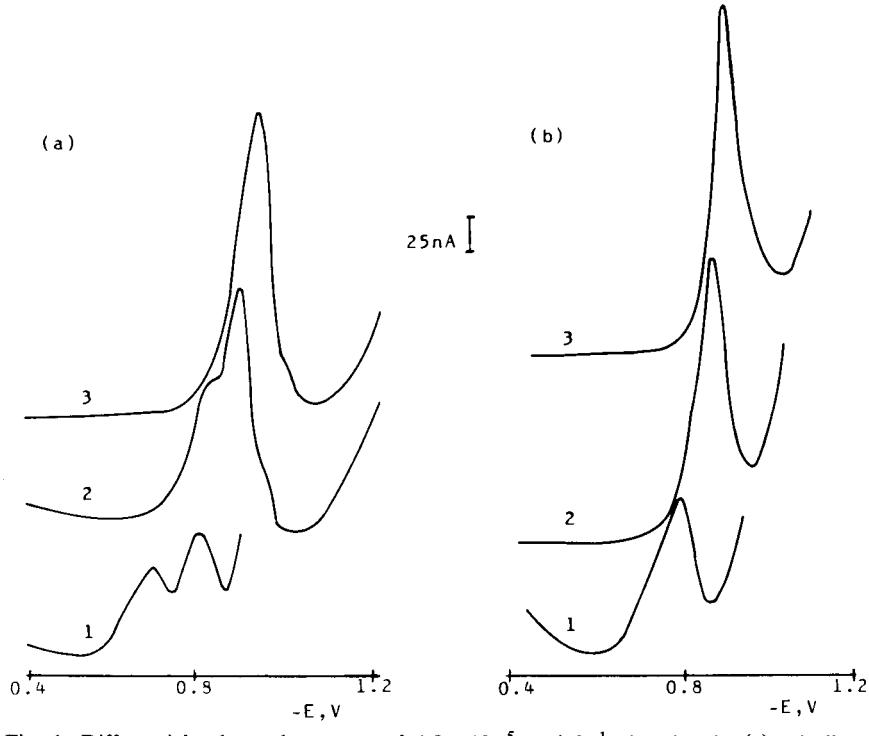

Fig. 1. Differential-pulse polarograms of 1.0×10^{-5} mol l^{-1} simazine in (a) micellar solutions formed with 0.1% sodium pentanesulphonate and (b) oil–water emulsions with 2.0 ml of ethyl acetate as the organic solvent. (1) 1 M $HClO_4$; (2) 0.1 mol l^{-1} Britton–Robinson buffer (pH 1.5); (3) 0.1 mol l^{-1} Britton–Robinson buffer (pH 2.5).

Micellar solutions

As indicated above, the use of oil–water emulsions as working media for the polarographic determination of simazine has some practical advantages because its determination usually involves extraction into organic solvents that can be emulsified. In order to prepare these emulsions, a surfactant must be added as an emulsifying agent. To choose the most suitable surfactant for analytical purposes, micellar solutions of simazine containing different cationic, anionic and non-ionic surfactants were tested by DPP.

The presence of cationic (Hyamine 1622, 2389 and 3500) and non-ionic surfactants (Triton X-305 and X-405 and Pluronic F-61, F-64 and F-68) in acidic solutions of simazine produced a remarkable decrease in simazine i_p values. This peak disappeared at surfactant concentrations higher than 0.01% at all pH values tested.

Anionic surfactants such as SDS and sodium pentanesulphonate exhibited different behaviour. At pH 1.0 and 2.0, SDS concentrations above 0.01% and 0.03%, respectively, inhibited the appearance of the simazine reduction peak, whereas at pH 3.0 this peak was observed for SDS concentrations up to 0.05 %. However, SDS itself exhibited a well defined reduction peak whose potential became more negative with increasing concentration. This resulted in a single overall peak in many instances, which hindered accurate measurement of the simazine peak. On the other hand, sodium pentanesulphonate did not affect the simazine reduction peak at any of the concentrations studied (0.001–0.2%) and at pH values between 1.0 and 4.0. Consequently, this surfactant was chosen as the most suitable for analytical purposes and was used as the emulsifying agent in appropriate oil–water emulsions.

In micellar solutions formed with 0.1% sodium pentanesulphonate, two reduction peaks were observed below pH 2.0, whereas only one peak was obtained at pH $\geqslant$ 2.0 (Fig. 1a). This behaviour may be due to *s*-triazine pesticide hydrolysis below pH 2.0 [13]. The peak current of the main peak was maximum at pH 2.5 and the peak potentials became more negative as the pH increased. Reduction signals were not observed above pH 4.0. At pH 2.5 the simazine reduction peak current was considerably higher than in a water–alcohol medium. For example, a 20% decrease in i_p was obtained for a 1.0×10^{-5} mol l^{-1} simazine solution in methanol–water (30 + 70) with respect to micellar solution.

Linear calibration graphs at pH 2.5 and $\Delta E = -50$ mV were obtained over the concentration ranges 1.0×10^{-6}–1.0×10^{-5} mol l^{-1} ($r = 0.9993$) and 1.0×10^{-5}–4.0×10^{-5} mol l^{-1} ($r = 0.9990$). Deviation from linearity was observed above 4.0×10^{-5} mol l^{-1} simazine, suggesting that simazine is adsorbed on the electrode surface at high concentrations. The relative standard deviation was 3.3% at 4.0×10^{-6} mol l^{-1} simazine ($n = 10$).

Oil–water emulsions

Ethyl acetate was chosen as the organic solvent to form simazine emulsions because of its wide use as a herbicide extracting agent, particularly for the *s*-triazine family [15]. Moreover, this solvent has proved to be highly suitable for the preparation of oil–water emulsions [19].

Optimization of the emulsion variables, such as the percentage of sodium pentane sulphonate, organic solvent–water volume ratio and emulsification time, was carried out by DPP at 1.0×10^{-5} mol l^{-1} simazine, pH 2.0 and $\Delta E = -50$ mV. The volume of organic phase had no significant influence on the simazine reduction peak in the 1.0–4.0-ml range studied, using an emulsification time of 3 min and a sodium pentanesulphonate concentration of 0.1%. Likewise, surfactant concentrations in the range 0.001–0.2% did not significantly affect the simazine peak current or peak potential. Consequently, an organic solvent volume of 2.0 ml and a sodium pentanesulphonate concentration of 0.1% were chosen for further studies.

Emulsions were prepared by ultrasonic treatment, 3 min being sufficient to obtain the maximum i_p values. This peak current remained virtually constant for at least 1 h, indicating that the emulsion was stable from an analytical point of view. Therefore, an ultrasonic treatment of 3 min was chosen for further studies.

Under the above experimental conditions, DP polarograms of simazine showed only one peak even at pH < 2.0 (Fig. 1b), unlike the two peaks

in micellar solutions, suggesting that pesticide hydrolysis is hindered in the emulsified medium. The influence of pH on E_p and i_p, for 1.0×10^{-5} mol l^{-1} simazine, is shown in Fig. 2. The E_p plot shows two linear regions with an intersection point at pH 2.1, which agrees fairly well with the reported simazine pK_a value [20]. The i_p vs. pH plot shows a maximum current at pH 2.0, and consequently this value was chosen as working pH for further studies. The $E_{1/2}$ and i_l results obtained by current-sampled direct current (d.c.) polarography were very similar to those shown in Fig. 2.

Characteristics of the electrode process. The limiting current is diffusion controlled, as deduced from the slope value, 0.67, of the log i_l vs. log h_{corr} plot using current-sampled d.c. polarography for a 1.0×10^{-5} mol l^{-1} simazine concentration, from the value of the temperature coefficient, 1.7%, and from the linear relationship between limiting current and the simazine concentration in the range 5.0×10^{-6}–5.0×10^{-5} mol l^{-1} ($r = 0.9995$).

The diffusion coefficient of simazine in this medium, calculated from the slope of the above

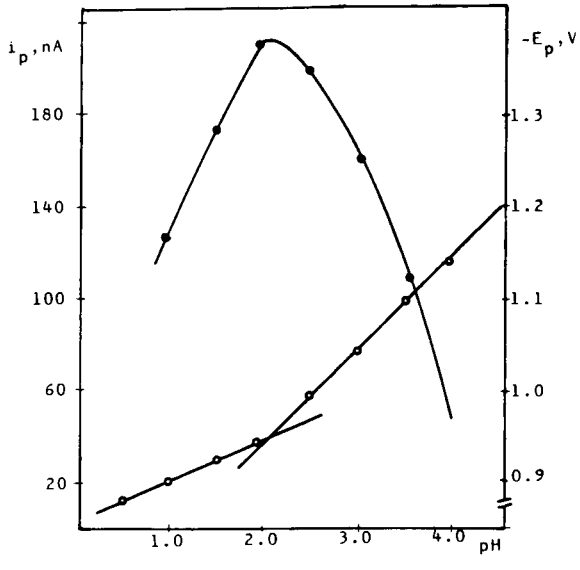

Fig. 2. Effect of pH on (○) E_p and (●) i_p in DPP in emulsified medium: 1.0×10^{-5} mol l^{-1} simazine, 2.0 ml of ethyl acetate, 0.1% sodium pentanesulphonate and 0.1 mol l^{-1} Britton–Robinson buffer.

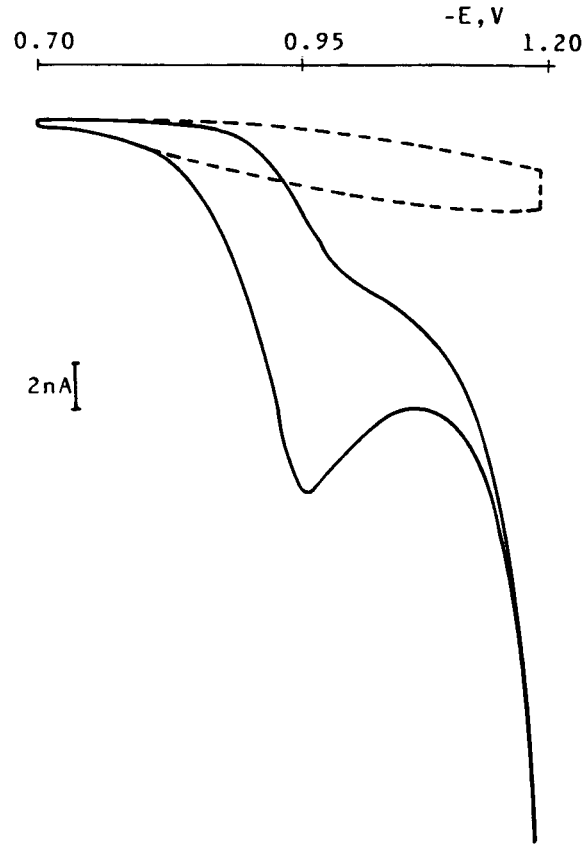

Fig. 3. Cyclic voltammograms of 5.0×10^{-5} mol l^{-1} simazine in emulsified medium. Dashed line, background cyclic voltammogram. 2.0 ml of ethyl acetate, 0.1% sodium pentanesulphonate and 0.1 mol l^{-1} Britton–Robinson buffer (pH 2.0).

i_l vs. concentration plot, 1.32×10^2 μA l mol^{-1} and, assuming a two-electron exchange [13], was 8.85×10^{-6} cm^2 s^{-1}.

Cyclic voltammograms for simazine and for the background electrolyte, obtained at a hanging drop mercury electrode, are shown in Fig. 3. No oxidation peak was obtained in the potential range scanned, indicating the non-reversibility of the polarographic reduction process.

Logarithmic analysis of the sampled-current d.c. polarograms obtained from a 1.0×10^{-5} mol l^{-1} simazine solution yielded a linear plot with slope -0.0695 V. This gives an αn_a value, at 25°C, of 0.78, which is in good agreement with that obtained from the Tafel plot, $\alpha n_a = 0.82$,

and by application of the $E_{3/4} - E_{1/4}$ (−0.062 V) criterion, $\alpha n_a = 0.83$. These αn_a values are consistent with a two-electron exchange in the simazine reduction process, probably involving the formation of the dihydro derivative [21]. The heterogeneous rate constant, K_f°, calculated from the Tafel plot, was 8.03×10^{-14} cm s^{-1}.

Using DPP, no significant dependence between the peak width at half-height and the pulse amplitude was observed. The value of $W_{1/2}$ (90 mV) is appreciably higher than the theoretical $W_{1/2}$ for a reversible system with $n = 2$. Moreover, a non-linear i_p vs. $(\sigma - 1)/(\sigma + 1)$ plot was obtained, where $\sigma = \exp[(nF/RT)\,\Delta E/2]$.

All the above results indicate that the polarographic reduction process of simazine in the emulsified medium is irreversible.

Analytical characteristics of the method. Simazine can be determined in emulsified medium by DPP using $\Delta E = -50$ mV, over the concentration ranges 8.0×10^{-7}–1.0×10^{-5} mol l^{-1} (r = 0.9993) and 1.0×10^{-5}–4.0×10^{-5} mol l^{-1} (r = 0.9990), the slopes of the calibration graphs being $(1.85 \pm 0.07) \times 10^7$ and $(1.57 \pm 0.17) \times 10^7$ nA l mol^{-1}, respectively, and the intercepts being 2 ± 6 and 32 ± 42 nA, respectively. The analytical characteristics of the method using the above calibration graphs were relative standard deviation 2.6% at a concentration level of 5.0×10^{-6} mol l^{-1} and $n = 10$; limit of determination 7.1×10^{-7} mol l^{-1}, according to the 10 × standard deviation criterion [22] and detection limit 2.2×10^{-7} mol l^{-1}, defined as $3s_b/m$ [23], where m is the slope of the lowest calibration graph and s_b is the standard deviation ($n = 10$) of the signal from 8.0×10^{-7} mol l^{-1} simazine.

Interferences. Various herbicides belonging to the *s*-triazine family, such as propazine [2,4-bis(isopropylamino)-6-chloro-*s*-triazine], methoprotryne [2-isopropylamino-4-(3-methoxypropylamino)-6-methylthio-*s*-triazine] and terbutryne [2-(*tert*-butylamino)-4-ethylamino-6-methylthio-*s*-triazine], were tested by DPP in order to check whether they interfere with the simazine reduction peak. Polarograms of these *s*-triazines at pH 2.0 show single reduction peaks whose E_p values are −0.92 V for propazine and −1.0 V for methoprotryne and terbutryne. In the presence of propazine, only one overall peak was obtained for all the interferent-to-simazine molar ratios studied (10:1–0.1:1) (fig. 4) and so propazine is an interferent. However, for 1:1 ratios of both methoprotryne and terbutryne, two overlapping peaks were observed (Fig. 4). The simazine concentrations calculated from the calibration graph mentioned above yielded values within the $2s$ range (equivalent to a relative error of about 5%) for 4.0×10^{-6} mol l^{-1} simazine ($n = 10$) when 0.5:1, 1:1 and 2:1 interferent-to-simazine ratios were used for propazine, methoprotryne and terbutryne, respectively. Although the use of simazine is much more usual than that of the other *s*-triazines, when mixtures of these herbicides are suspected in the sample, separation and identification, mainly in the case of propazine, would be necessary.

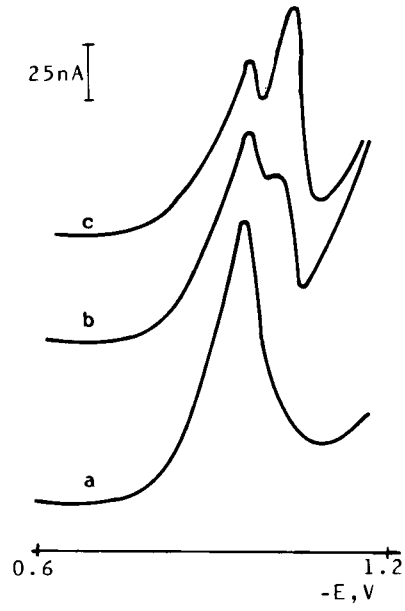

Fig. 4. Differential-pulse polarograms in emulsified medium for 1:1 mixtures: (a) propazine–simazine; (b) methoprotryne–simazine; (c) terbutryne–simazine; 4.0×10^{-6} mol l^{-1} of each *s*-triazine. 2.0 ml of ethyl acetate, 0.1% sodium pentanesulphonate and 0.1 mol l^{-1} Britton–Robinson buffer (pH 2.0).

Determination of simazine in spiked irrigation water. DPP under the experimental conditions mentioned above was used to determine simazine in spiked irrigation water. The pesticide was ex-

tracted into ethyl acetate and then the extract was emulsified. The background in the emulsified medium showed better analytical characteristics (much lower background current) than that obtained directly with the irrigation water at pH 2.0. Moreover, this methodology could minimize potential interferences from other electroactive substances (e.g., metallic ions). Recovery studies on irrigation water containing 4.0×10^{-6} and 2.0×10^{-5} mol l^{-1} simazine yielded the following results for five determinations: simazine found, $(3.7 \pm 0.1) \times 10^{-6}$ mol l^{-1} ($93 \pm 3\%$ recovery) and $(1.92 \pm 0.05) \times 10^{-5}$ mol l^{-1} ($96 \pm 3\%$ recovery), the confidence interval being calculated for a significance level of 0.05, with relative standard deviations of 3.0% and 2.1%, respectively. Similar results, within $95 \pm 2\%$, were obtained using 25-ml aliquots of ethyl acetate in the extraction process. The pH of the irrigation water did not have a significant influence on recoveries between pH 4.0 and 10.0.

Financial support from the Spanish CICYT (project ALI 89-0055) is gratefully acknowledged.

REFERENCES

1 D.S. Owens and P.E. Sturrock, Anal. Chim. Acta, 188 (1986) 269.
2 R. Frank and G. Sirons, Sci. Total Environ., 12 (1979) 223.
3 G. Durand, R. Alonso and D. Barceló, Quim. Anal., 10 (1991) 157.
4 C.D. McPhail and D. Pirie, presented at the Third North Sea Conference, The Hague, 1990.
5 D.C. Abbott, J.A. Bunting and J. Thomson, Analyst, 90 (1965) 356.
6 P. Beilstein, A.M. Cook and R. Hütter, J. Agric. Food Chem., 29 (1981) 1132.
7 V. Pacáková, K. Stulík and M. Príhoda, J. Chromatogr., 442 (1988) 147.
8 K. Ramsteiner, W.D. Hörmann and D.O. Eberle, J. Assoc. Off. Anal. Chem., 57 (1974) 192.
9 W.D. Hörmann, J.C. Tournayre and H. Egli, Pestic. Monit. J., 13 (1979) 128.
10 V. Pacáková and I. Nemec, J. Chromatogr., 148 (1978) 273.
11 B.A. Ripley and H.E. Braun, J. Assoc. Off. Anal. Chem., 66 (1983) 1084.
12 J.W. Eichelberger, T.D. Behymer and W.L. Budde, Method 525, Revision 1.0, 2.0, 2.1 (1988), Environmental Monitoring Systems Laboratory, Office of Research and Development, US Environmental Protection Agency, Cincinatti, OH, 1988.
13 M. Stastny, H. Benadikova, J. Nepozitek and R. Volf, Sb. Vys. Sk. Chem.-Technol. Praze, Anal. Chem., H17 (1982) 69.
14 M.T. Lippolis and V. Concialini, Talanta, 35 (1988) 235.
15 D.C. Muir and B.E. Baker, J. Agric. Food. Chem., 24 (1976) 122.
16 J.M. Pingarrón, A.J. Reviejo and L.M. Polo, J. Electroanal. Chem., 234 (1987) 175.
17 J.M. Pingarrón, A. Gordon, A.J. Reviejo and L.M. Polo, Anal. Chim. Acta, 216 (1989) 231.
18 A. González, J.M. Pingarrón and L.M. Polo, Electrochim. Acta, 36 (1991) 1573.
19 A.J. Reviejo, J.M. Pingarrón and L.M. Polo, Electroanalysis, 4 (1992) 111.
20 J.B. Weber, Residue Rev., 32 (1970) 93.
21 H. Lund and M. Baizer (Eds.), Organic Electrochemistry, Dekker, New York, 1991, p. 736.
22 ACS Committee on Environmental Improvement, Principles of Environmental Analysis, Anal. Chem., 55 (1983) 2210.
23 K. Hasabe and J. Osteryoung, Anal. Chem., 47 (1975) 2412.

Analytica Chimica Acta, 273 (1993) 351–359
Elsevier Science Publishers B.V., Amsterdam

Polarographic behaviour and determination of furaltadone in its formulations, milk and urine by differential-pulse polarography

T. Galeano Díaz and A. Guiberteau Cabanillas

Departamento de Química Analítica, Facultad de Ciencias, Universidad de Extremadura, 06071 Badajoz (Spain)

L. López Martínez

Instituto de Investigaciones Científicas, Universidad de Guanajuato, Guanajuato (Mexico)

F. Salinas

Departamento de Química Analítica, Facultad de Ciencias, Universidad de Extremadura, 06071 Badajoz (Spain)

(Received 19th May 1992)

Abstract

The polarographic behaviour of furaltadone was studied in Britton–Robinson buffer solutions and perchloric acid media. Three well defined reduction waves appear in acidic media (pH < 4) whereas at higher pH the last two peaks overlap. The variation of $E_{1/2}$ or E_p and I_{lim} or I_p with pH was studied. The diffusion-controlled nature of the waves at pH 1.87 (Britton–Robinson solution) and in 0.1 M perchloric acid was established and the irreversibility of the electrode process was verified by different criteria. The mechanism for the reduction is discussed. A method for the determination of furaltadone by differential-pulse polarography which allows 0.025–2.0 μg ml^{-1} (7.7×10^{-8}–6.2×10^{-6} M) of this compound to be determined is proposed and was applied to the determination of furaltadone in its formulations, milk and urine.

Keywords: Polarography; Furaltadone; Milk; Pharmaceuticals; Urine

Furaltadone [5-morpholinomethyl-3-(5-nitrofurfurylideneamino)-2-oxazolidinone] and other nitrofuran derivatives have been used for more than 30 years in medicine, alone or in combination with other drugs, for the treatment of gastrointestinal infections in animals and humans. The use of most nitrofurans is strictly regulated in many countries [1]. Because of this, the determination of nitrofuran derivative residues in body fluids and in foods of animal origin is of great interest.

For these purposes, spectrophotometric, conductimetric and gas and liquid chromatographic methods have been proposed, but less attention has been paid to the polarographic determination of these drugs [2]. In this regard, only two references to the polarographic behaviour of furaltadone were found [3,4]. In one study [3], the interaction between furaltadone or other 2-nitrofuran derivatives and polyvinylpyrrolidone or poly(vinyl

Correspondence to: A. Guiberteau Cabanillas, Departamento de Química Analítica, Facultad de Ciencias, Universidad de Extremadura, 06071 Badajoz (Spain).

alcohol) was investigated by means of polarographic techniques. In the other [4], studies of the polarographic behaviour of various 5-nitrofurfurolhydrazones in different media (aqueous, aqueous–alcoholic and dimethylformamide) by using direct current (d.c.) polarography were described and a mechanism of the electrochemical reduction was proposed. However, no information could be found about the polarographic determination of furaltadone, although there are some reports on the determination of other nitrofuran derivatives in different samples, such as pharmaceutical formulations [5–8], urine [9–12] and feeds [13,14].

In this paper, a study of the polarographic behaviour of furaltadone is described and methods to determine this compound in formulations, urine and milk are proposed.

EXPERIMENTAL

Reagents

Standard solutions of furaltadone (Sigma) in dimethylformamide (DMF) were prepared. A stock Britton–Robinson buffer solution, which was 0.04 M with respect to boric, orthophosphoric and acetic acids, was prepared from analytical-reagent grade reagents. From this stock solution, solutions of various pH were prepared by the addition of 0.1 M sodium hydroxide solution. All other chemicals were of analytical-reagent grade.

Apparatus

A PAR Model 264A polarographic analyser equipped with a PAR Model 303A SMDE cell and a Yokogawa 3020 A4 *X–Y* recorder were

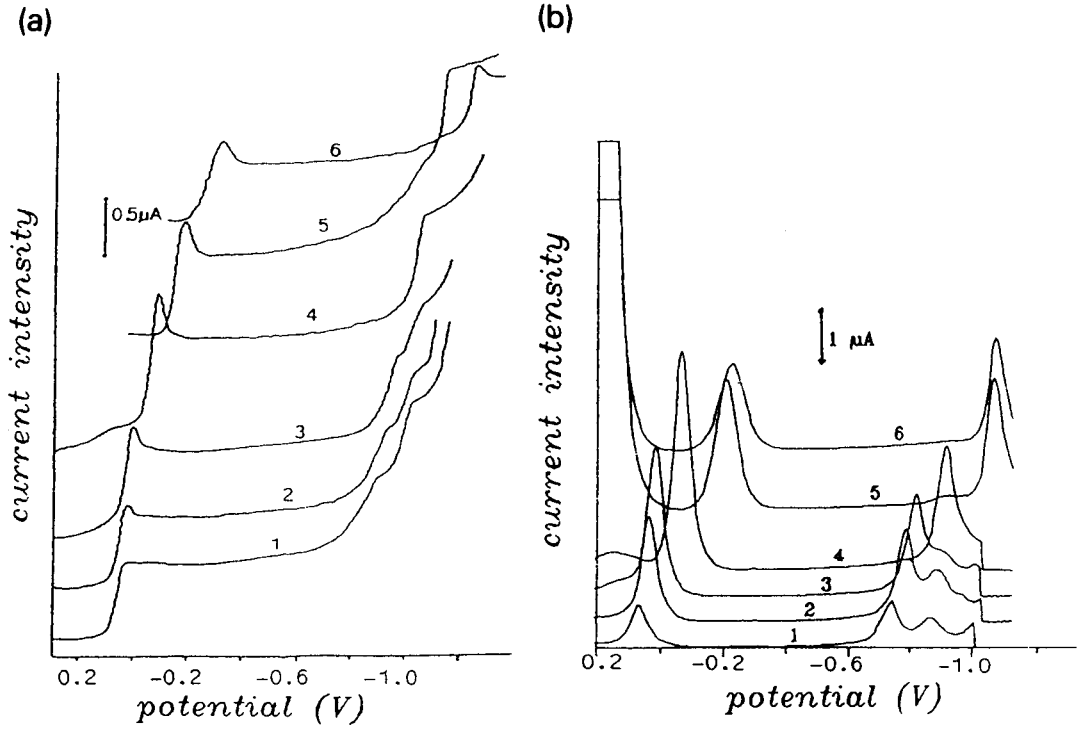

Fig. 1. Voltammograms of 6.20×10^{-6} M furaltadone solutions obtained by using (a) d.c. and (b) DPP techniques without gelatine at different pH values (Britton–Robinson buffers). pH: 1, 2.09; 2, 2.87; 3, 3.76; 4, 5.72; 5, 7.24; 6, 8.36.

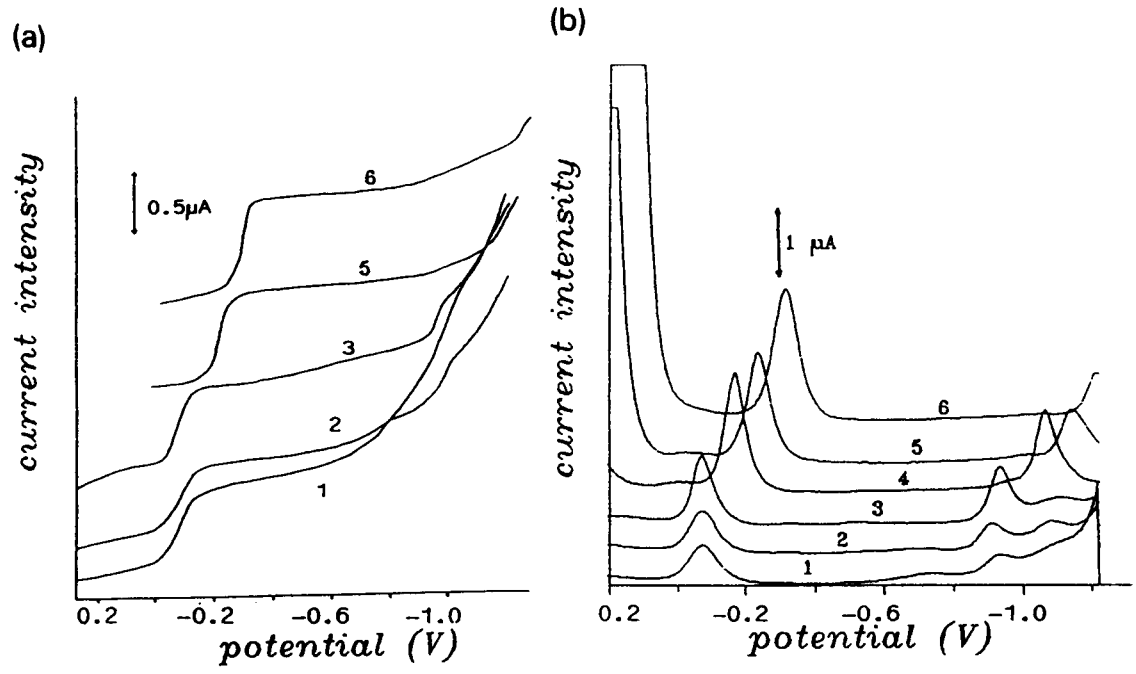

Fig. 2. Voltammograms of 6.20×10^{-6} M furaltadone solutions obtained by (a) d.c. and (b) DPP techniques in the presence of 0.04% of gelatine at different pH values (Britton–Robinson buffers). pH: 1, 2.56; 2, 3.29; 3, 4.10; 4, 6.09; 5, 7.24; 6, 8.95.

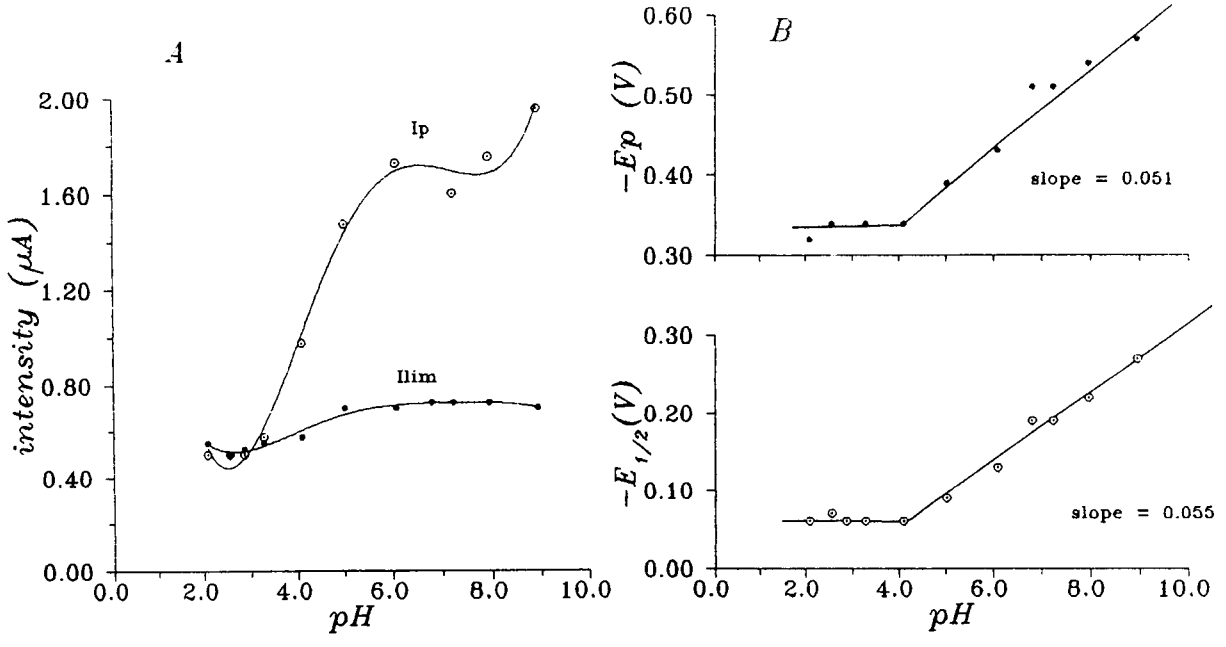

Fig. 3. Effect of pH on (A) I_p or I_{lim} and (B) E_p or $E_{1/2}$ for the first wave of 6.2×10^{-6} M furaltadone solutions in the presence of 0.04% of gelatine.

used. The *Y* recorder input was also connected to an Olivetti M-240 PC by means of a 12-bit PCL-812 analogue–digital converter [15]. A BASIC program allows the acquisition of intensity values and the voltammograms stored as ASCII files for later representation and manipulation with other programs. A Metrohm Polarecord E-506 with a Metrohm 663 VA cell was also used in some studies. Both cells have an Ag/AgCl reference electrode. Solutions were purged with oxygen-free nitrogen for 8 min before recording voltammograms.

Determination of furaltadone in pharmaceutical formulations

Aliquots of formulation (solution or suspension) are dissolved in DMF, filtered if necessary and diluted to a known volume with DMF. Sample solutions are prepared in 10-ml calibrated flasks by mixing the appropriate volumes of the above solutions with reagents so as to give concentrations of 5% of DMF and 0.1 M perchloric acid, and then assayed polarographically.

Determination of furaltadone in urine

Aliquots of 50 ml of urine, previously filtered, are adjusted to pH 6 and then extracted with 50 ml of chloroform. After shaking vigorously, the two phases are allowed to separate. The organic layer is dried with sodium sulphate and a 40-ml aliquot is extracted twice with 10 ml of 0.1 M perchloric acid. The aqueous portions are combined and a 9.5-ml aliquot is mixed with 0.5 ml of DMF and assayed polarographically.

Determination of furaltadone in milk

Aliquots of 50 ml of milk are deproteinated by addition of 3 ml of 60% perchloric acid. The serum is separated by centrifugation, its pH is adjusted to 6 and then it is extracted with 50 ml of chloroform. The above procedure for urine analysis is then followed.

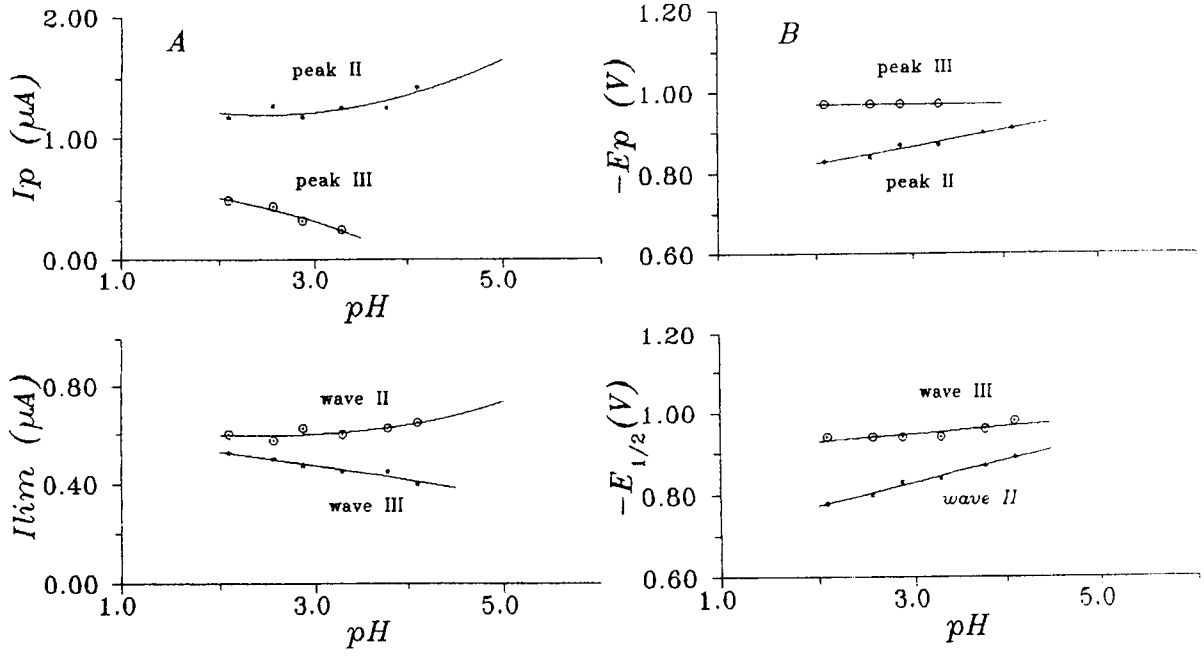

Fig. 4. Effect of pH on (A) I_p or I_{lim} and (B) E_p or $E_{1/2}$ for the second and third waves in the presence of 0.04% of gelatine.

RESULTS AND DISCUSSION

Influence of pH

The influence of pH (2–10) was studied in Britton–Robinson buffers. Furaltadone shows three well defined reduction waves in acidic media (pH < 4). At higher pH, the second and third wave start to overlap and at pH > 5 only two waves appear. On the other hand, the first wave shows a maximum, sharper in weakly acidic medium, which is suppressed by addition of 0.04% of gelatine. The presence of this suppressor also affects the other two waves. In Figs. 1 and 2 some of the d.c. and differential-pulse polarographic (DPP) scans obtained in the presence and absence of gelatine are shown.

The influence of pH on I_{lim} and I_p, corresponding to the first wave in the presence of gelatine, is shown in Fig. 3A and the variation of $E_{1/2}$ and E_p with pH in Fig. 3B. Figure 4A and B show the variation of all these parameters for the second and third waves in the absence of gelatine and in the pH range in which these waves appear separately.

It can be seen that I_{lim} of the first wave increases slightly with increase in pH from 3 to 5, whereas the variation of I_p is much greater. Both E_p and $E_{1/2}$ remain constant up to pH 4 and, at higher pH, change to more negative values, with slopes of 0.055 and 0.051 V $(pH)^{-1}$, respectively.

Influence of other variables

Studies of the influence of instrumental variables such as pulse amplitude, drop time and temperature were made by the DPP technique at pH 1.87 (Britton–Robinson buffer), because of the absence of the first wave maximum at this pH value, with 4.6×10^{-6} M furaltadone solutions.

The first peak was found to be diffusion controlled in this medium, as shown by the linear plots of I_p vs. $t^{2/3}$ and log I_p vs. temperature (temp. coeff. $\omega = 1.68\%$ °C^{-1}). This result is also confirmed by the linearity obtained between I_p and the square root of the scan rate in the cyclic voltammograms. The I_p value of the other waves changes linearly with $t^{2/3}$. $I_{p_{II}}$ (second peak) decreases with increase in temperature and $I_{p_{III}}$ (third peak) shows a similar behaviour at temperatures higher than 25°C. The shapes of these peaks also change irreversibly when the temperature increases. This behaviour could be attributed to adsorption processes or to hydrolysis reactions. The variation of I_p with ΔE is linear up to $\Delta E = 60$ mV for the three peaks. A 50-mV pulse amplitude was selected for this study.

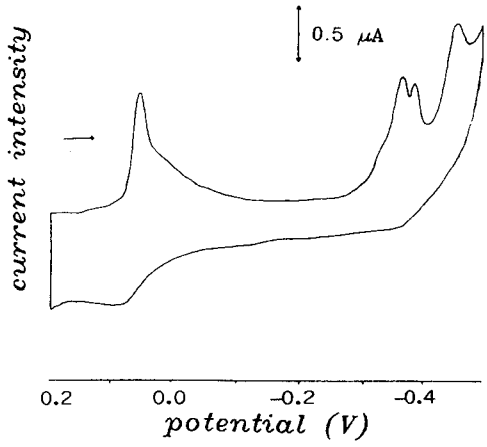

Fig. 5. Cyclic voltammogram of a 4.6×10^{-6} M furaltadone solution [50 mV s^{-1}, pH 1.87 (Britton–Robinson buffer)].

The plot of I_p vs. furaltadone concentration exhibits good linearity for all peaks over the range 7.7×10^{-7}–6.2×10^{-6} M.

Reversibility studies

Several criteria were used to study the reversibility of the electrode reduction processes. When the cyclic voltammogram was recorded (Fig. 5), only reduction peak appeared, illustrating the irreversible character of the reduction processes. This result was confirmed by applying different criteria to d.c. polarograms (such as logarithmic analysis of waves at pH 1.87 and determination of the $E_{3/4} - E_{1/4}$ value) and DPP polarograms (Birke criterion).

Mechanism of the electrode process

The number of electrons involved in the reduction process, corresponding to the first wave, was calculated by controlled-potential coulometry (at $E = -0.2$ V) at pH 1.87. The number of

TABLE 1

Determination of furaltadone in pharmaceutical formulations, urine and milk by differential-pulse polarography

Pharmaceutical formulation	Composition	Furaltadone claimed (mg g^{-1} or mg ml^{-1})	Furaltadone found [a] (mg g^{-1} or mg ml^{-1})
Panotile solution	(per ml)		
	Furaltadone hydrochloride 4.5 mg	4.5	4.70 ± 0.07
	Polymixin B sulphate 10 000 U		
	Neomycin sulphate 3.5 mg		
	Fluorocortisone acetate 1.0 mg		
	Lidocaine hydrochloride 40.0 mg		
Altabactine suspension	(per 200 ml)		
	Furaltadone 4.16 g	19.6	18.96 ± 0.26
	Chloramphenicol 4.16 g		
	Neomycine sulphate 10.0 g		
	Valeramide sulphate 41.50 g		
	Magnesium chloride 16.66 g		
Carfurin	(per ml)		
	Furaltadone 50 mg	50.0	50.60 ± 0.20
	Chloramphenicol 50 mg		
	Dexamethasone 0.1 mg		

Sample	Furaltadone added (μg ml^{-1})	Furaltadone found (μg ml^{-1})	Recovery (%)
Urine	0.80	0.775	97.0
	0.80	0.752	94.0
	0.10	0.091	91.0
	0.10	0.089	89.0
Milk	0.10	0.090	90.0
	0.10	0.091	91.0
	0.013	0.011	84.6
	0.013	0.012	92.3

[a] Each value is the mean of three determinations.

electrons was found to be three. On the other hand, from the logarithmic analysis of the first wave, in the presence of gelatine, an $n\alpha$ value (where n = number of electrons involved and α = transfer coeff.) of 0.91 was obtained. Assuming irreversibility of the process, n must be 2. It was not been possible to calculate the number of electrons corresponding to the second and third waves because these disappear after coulometry at $E = -0.2$ V, but the $n\alpha$ values obtained (0.59 for the second wave and 0.88 for the third wave) and the similar intensity values in the d.c. polarogram for all three waves suggest the same number of electrons for each of these processes.

For the first wave, the variations of $E_{1/2}$ and E_p with pH indicate the participation of one proton in the electrode process ($0.059m/n\alpha = 0.055$, $n\alpha = 0.91$) at pH > 4 (m = number of protons involved).

These results suggest a mechanism of the reduction for furaltadone similar to that proposed by Morales et al. [16] for a very similar compound, furazolidone, which consists of several steps:

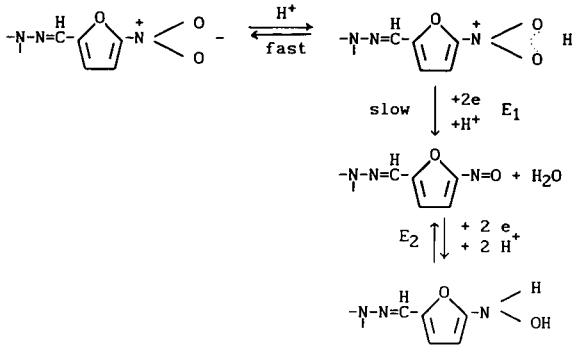

Two electrons and one proton take part in the rate-determining step of the reaction and a nitrous intermediate group is obtained, which is rapidly reduced to hydroxylamine. In the reduction of nitrofuran derivatives, owing to the effect of the donor properties of the substituent, subsequent reactions can follow, giving rise to a highly reducible intermediate imine and primary amine.

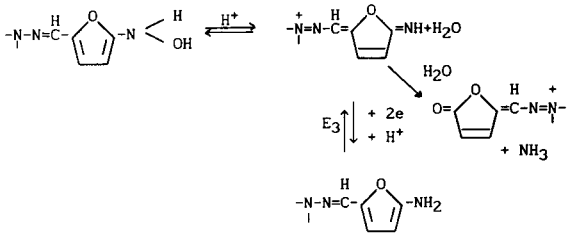

Our results are not concordant with the mechanism of reduction proposed by Stradins and Reihmanis [4] for furaltadone and other 5-nitrofurfurolhydrazones, which involves between four and six electrons.

The processes corresponding to the second and third waves may be as follows, as described for similar compounds:

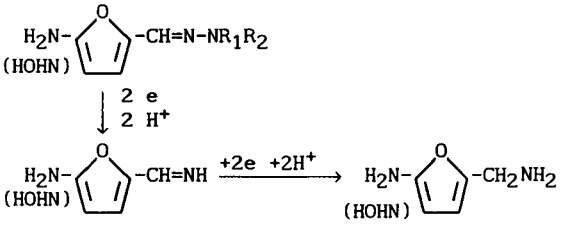

However, in other studies [6,16,17], a reduction wave for similar compounds was attributed to the reduction of the hydroxylamine group to the primary amine. This could explain the disappearance of one of the last waves of furaltadone after a macroreduction process.

Determination of furaltadone

The studies on the influence of pH indicate that an acidic medium is more appropriate for determining furaltadone by DPP, using the first wave, because no maximum appears. Therefore, we propose a perchloric acid medium for this purpose.

I_p remains constant in the perchloric acid concentration range studied (0.05–0.35 M). A 0.1 M perchloric acid concentration was selected. In this medium, a 6.2×10^{-6} M solution of furaltadone is stable for at least for 2 h. The ionic strength does not affect the I_p value up to a sodium perchlorate concentration of 0.15 M; therefore, in the following experiments, we prepared samples without sodium perchlorate. When the fraction of DMF in the samples increases I_p decreases, and we chose 5% of DMF as sufficient.

In 0.1 M perchloric acid, I_p also changes linearly with $t^{2/3}$ and the plot of log I_p vs. temperature is linear up to 30°C ($\omega = 1.15\%$ °C^{-1}). The variation of I_p with pulse amplitude is also linear up to 60 mV and a pulse amplitude of 50 mV was chosen.

Under these conditions, I_p changes linearly with furaltadone concentration in the range 0.025–2.0 μg ml^{-1} (7.7×10^{-8}–6.2×10^{-6} M), the straight-line equation being I_p (μA) = 1.271 (furaltadone) (μg ml^{-1}) + 0.0171 ($r = 0.9988$). For higher furaltadone concentrations the I_p vs. concentration relationship is not linear. The proposed method has a detection limit of 0.008 μg ml^{-1}, calculated, because no blanks were used, on the basis of the variation of the analyte response at low concentrations [18] and defined as the concentration of furaltadone yielding an I_p equal to three times the standard deviation of I_p of a sample containing 0.025 mg l^{-1} of furaltadone. The relative standard deviation ($P = 0.05$, $n = 11$) calculated for 1.0 mg l^{-1} of furaltadone was 2.9%.

Analysis of of formulations, urine and milk for furaltadone

The proposed method was applied to the determination of furaltadone in pharmaceutical formulations, urine and milk and the results are given in Table 1. It must be emphasized that some of the formulations also contain another nitrofuran derivative, chloramphenicol, which shows a peak at −0.13 V under the conditions of the method. This peak appears well differentiated from that of furaltadone, so the simultaneous determination of both nitrofuran derivatives by the proposed method is possible.

To determine furaltadone in urine and milk, and because of the blank signal in acidic media, a prior separation of furaltadone from the matrix is required. For this purpose, we made successive extractions of this compound in chloroform and in an acidic medium (0.1 M perchloric acid) as described for the spectrophotometric determination of furaltadone in milk [19]. This procedure allows furaltadone to be determined in the presence of other nitrofuran derivatives, such as furazolidone and nitrofurantoin, which may be combined with furaltadone in formulations and which show peaks at the same potential value. Furazolidone is not re-extracted by 0.1 M perchloric acid and nitrofurantoin is extracted in chloroform to a much smaller extent than is furaltadone. In this respect, it should be noted that the determination of 0.5 μg ml^{-1} of furaltadone in the presence of equal amounts of furazolidone and nitrofurantoin in urine is possible with errors lower than 10%.

As examples, Figs. 6 and 7 show the polarograms obtained in the analysis of a formulation (Carfurin) and a urine sample.

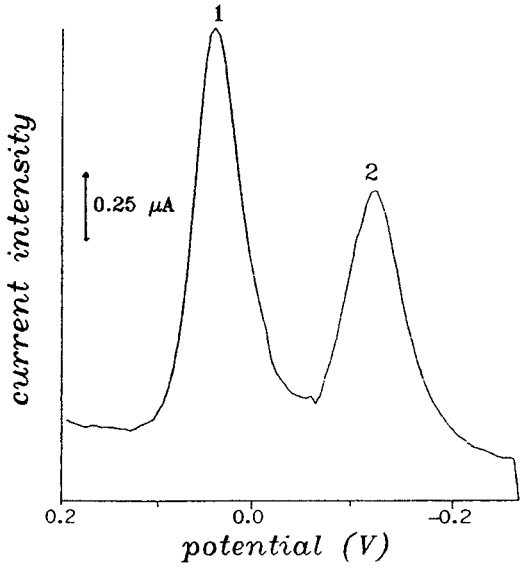

Fig. 6. DPP scan obtained from Carfurin. Peak 1 is due to the furaltadone and peak 2 to chloramphenicol.

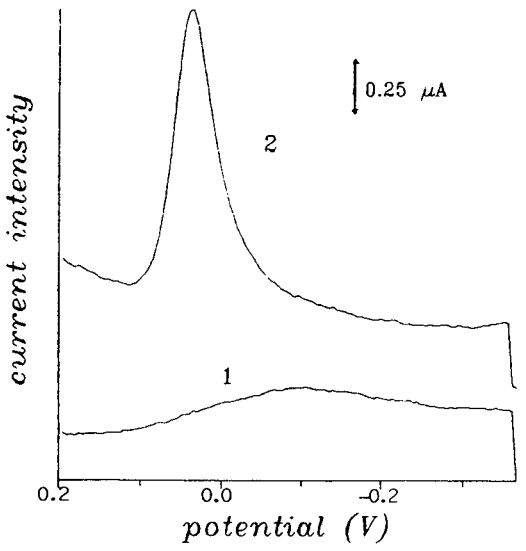

Fig. 7. DPP scans for (1) urine sample without furaltadone and (2) urine sample spiked with 0.8 μg ml^{-1} of furaltadone (according to the procedure described in the text).

The authors gratefully acknowledge financial support from the DGICYT, project PB88-0431. The authors are also grateful to Dr. A. Muñoz de la Peña, of the Department of Analytical Chemistry, for interfacing the microcomputer with the PAR polarograph and the elaboration of the BASIC program for the acquisition of data.

REFERENCES

1 J.J. Laurensen and J.F.M. Nows, J. Chromatogr., 472 (1989) 321.
2 A. Morales, P. Richter and M.I. Toral, Analyst, 112 (1987) 971.
3 A. Queralto and M. Ortega, Galenica Acta, 25 (1971) 3.

4 J. Stradins and G. Reihmanis, Latv. PSR Zinat. Akad. Vestis, Kim. Ser., 2 (1972) 180.
5 P. Surmann and P. Aswakun, Arch. Pharm. (Weinheim, Ger.), 318 (1985) 14.
6 A.K. Mishra and K.D. Gode, Indian Drugs, 23 (1986) 302.
7 P. Kazandzhieva, N. Nin'o and I. Nedelchev, Farmatsiya, 36 (1986) 6.
8 C. Sridevi and S.J. Reddy, Electroanalysis, 3 (1991) 435.
9 J.S. Burmicz, W.F. Smyth and R.F. Palmer, Analyst, 101 (1976) 986.
10 L. Faith and A. Strakova, Cesk. Farm, 32 (1983) 19.
11 A. Morales, M.I. Toral and P. Richter, Analyst, 109 (1984) 633.
12 A. Morales, P. Richter and M.I. Toral, Analyst, 112 (1987) 971.
13 P. Hocquellet and A. Pevendrant, Analusis, 1 (1972) 192.
14 M. Slamnik, Talanta, 21 (1974) 960.
15 PCL-812 Enhanced Multi-Lab Card, Advantech Co., 1989.
16 A. Morales, P. Richter and M.I. Toral, Analyst, 112 (1987) 965.
17 A.K. Mishra and K.D. Gode, Analyst, 110 (1985) 1373.
18 J.A. Glaser, D.L. Foerst, G.D. McKee, S.A. Quave and W.L. Budde, Environ. Sci. Technol., 15 (1981) 1427.
19 P.L. Cox and J.P. Heotis, J. Agric. Food. Chem., 11 (1963) 499.

Analytica Chimica Acta, 273 (1993) 361–368
Elsevier Science Publishers B.V., Amsterdam

Determination of ephedrine in human urine using a glassy carbon electrode

M. Chicharro, A. Zapardiel, E. Bermejo, J.A. Pérez and L. Hernández

Department of Analytical Chemistry and Instrumental Analysis, Universidad Autónoma, 28049 Madrid (Spain)

(Received 1st July 1992; revised manuscript received 16th September 1992)

Abstract

The electrochemical behaviour of ephedrine at a glassy carbon electrode was studied using linear-sweep and differential-pulse voltammetry at a stationary electrode and a rotating disc electrode. The studies were performed using 0.04 M Britton–Robinson buffer (pH 10.0), which allowed the evaluation of the diffusion constant, the charge-transfer coefficient and the conditional charge-transfer rate constant. A method was also devised for the electrochemical determination of ephedrine in human urine samples using differential-pulse voltammetry with prior drug separation. If this separation method is applied, either calibration graphs or standard additions can be used to determine ephedrine at concentrations between 7 and 20 $\mu g\ ml^{-1}$, with relative errors lower than 6.0% and relative standard deviations lower than 5.8%. The presence of norephedrine at levels 20% lower than those of ephedrine has no influence on ephedrine determination.

Keywords: Voltammetry; Ephedrine; Glassy carbon electrodes; Pharmaceuticals; Urine

Ephedrine [(1*R*, 2*S*)-(+)-α-(1-methylaminoethyl)benzyl alcohol] is a sympathomimetic amine obtained by extraction from several plants of the genus *Ephedra* or by synthesis. Ephedrine has a characteristic physiological function and pharmacological action. It stimulates α- and β-adrenergic receptors and is a stimulant of the central nervous system, stimulating cortical, bulbar and mesencephalic centres, including the respiratory system. Ephedrine is used as a drug in therapeutic doses at levels of 15–60 mg to produce peripheral vasoconstriction, to raise blood pressure, to prevent hypotension and to treat allergic states, catalepsy and myasthenic gravis.

Ephedrine has been the subject of numerous analytical studies, including spectrophotometric [1,2], chromatographic [3] and electrochemical with solid electrodes [4–6]. Electrochemical studies established that the characteristics of the voltammetric response depend on the material of which the electrode is made; a graphite electrode makes oxidation easier than a glassy carbon or platinum electrode [4]. Among the different procedures developed for the detection and determination of ephedrine in plasma and urine are gas–liquid chromatography [7–12], radioimmunoassay [13,14], membrane electrode methods [15–17], liquid chromatography (LC) [18–20] and capillary electrophoresis [21].

Once absorbed in the human organism, ephedrine undergoes partial *N*-desmethylation and is converted into phenylpropanolamine (norephedrine), a drug with a sympathomimetic action similar to that of ephedrine. About 60% of ephedrine is excreted free in urine, ca. 10% being metabolized [22,23].

This paper reports an electrochemical study of ephedrine at a glassy carbon electrode. It gives

Correspondence to: L. Hernández, Department of Analytical Chemistry and Instrumental Analysis, Universidad Autónoma, 28049 Madrid (Spain).

redox and kinetic data for the electrodic process, and takes into account the influence of the metabolite (norephedrine). A method for the determination of ephedrine in human urine is proposed.

EXPERIMENTAL

Apparatus and electrodes

All experiments were performed using a Metrohm Model 646 VA processor in conjunction with a Model 647 VA stand. A three-electrode system was used, consisting of an Ag/AgCl/3 M KCl reference electrode, a platinum (65 × 2 mm) auxiliary electrode and a glassy carbon working electrode (Metrohm 6.1204.040). All measurements were made at room temperature (25°C).

Pretreatment of the glassy carbon electrode was done following the recommendations by Engstrom and Strasser [24]. The electrode was cleaned after each measurement by carrying out scans between −0.3 and +1.5 V in 0.04 M (in each acid) Britton–Robinson buffer (pH 10.0).

Reagents

All chemicals were of analytical-reagent grade (Merck). Stock solutions (0.01 M) of ephedrine hydrochloride and norephedrine [(1*S*, 2*R*)-(+)-α-(1-aminoethyl)benzyl alcohol] hydrochloride both from Aldrich (99%), were prepared by dissolving the compounds in purified water (obtained with Milli-Q and Milli-Ro systems; Millipore). The solutions were stored in the dark under refrigeration.

Linear-sweep voltammetry

Voltammograms were obtained between 0.3 and 1.5 V at 60 mV s^{-1} in 0.04 M Britton–Robinson buffer (pH 10.0).

Rotating disc measurements were performed on a rotating disc glassy carbon electrode in the same range of potentials as above and rotating at a frequency between 20.3 and 43.6 Hz, with a scan rate of 20 mV s^{-1}.

Differential-pulse voltammetry

Measurements were made in 0.04 M Britton–Robinson buffer (pH 10.0) with potential scans between 0.3 and 1.2 V at 20 mV s^{-1}, a 75 mV pulse amplitude and a 0.6 s repetition time.

Separation of ephedrine from human urine

Sep-Pak C_{18} (Waters–Millipore) cartridges were used, and the following procedure was followed. The cartridge is rinsed by successively passing 1 ml of methanol and 1 ml of water, activated with 1 ml of methanol and buffered at pH 10.0 with 2 ml of ammonia–ammonium chloride. Then, 10 ml of the urine sample adjusted to pH 9.5 with ammonia–ammonium chloride buffer are passed, the drug finally being eluted with 16 ml of diethyl ether. The organic phase is eliminated with nitrogen; the extract thus obtained is made up to 5.0 ml with 0.04 M Britton–Robinson buffer (pH 10.0). A scan is then made by differential-pulse voltammetry (pulse amplitude 75 mV, repetition time 0.6 s and scan rate 20 mV s^{-1}).

RESULTS AND DISCUSSION

Linear-sweep voltammetry

Electrolyte and pH. The influence of several electrolytes (ammonia–ammonium chloride, carbonate–hydrogencarbonate, Britton–Robinson, Clark–Lubs borate [25], Teorell–Stenhagen [25] buffers, etc.) on the analytical signal was studied.

Figure 1 shows the voltammograms obtained with 1.7×10^{-3} M ephedrine at 20 mV s^{-1} at pH 10.0 in some of the buffers. Only one oxidation peak is observed at 0.92 V, and Britton–Robinson buffer gives the best signal-to-noise ratio.

The influence of pH on current and peak potential in 0.04 M Britton–Robinson buffer is shown in Fig. 2. No oxidation peaks for ephedrine appear at pH < 8.0, whereas at pH > 11.5 the anodic peak current is influenced by the anodic wave of the solvent. The highest peak currents are obtained at pH 10.0–11.0.

The variation of peak potential with pH shows a shift towards less positive values as the pH increases, so that two linear variations with slopes of 20 and 202 mV pH^{-1} are observed, intersect-

ing at pH 9.8, from which a value very similar to the corresponding pK_a value of ephedrine found spectrophotometrically can be calculated [1].

On studying the ionic strength of the medium, the peak current was observed to remain virtually constant for electrolyte concentrations higher than 0.03 M; 0.04 M Britton–Robinson buffer (pH 10.0) was chosen as electrolyte for all subsequent studies.

It was observed that, for ephedrine concentrations between 1.7×10^{-4} and 1.7×10^{-3} M, when the solutions were stirred for periods shorter than

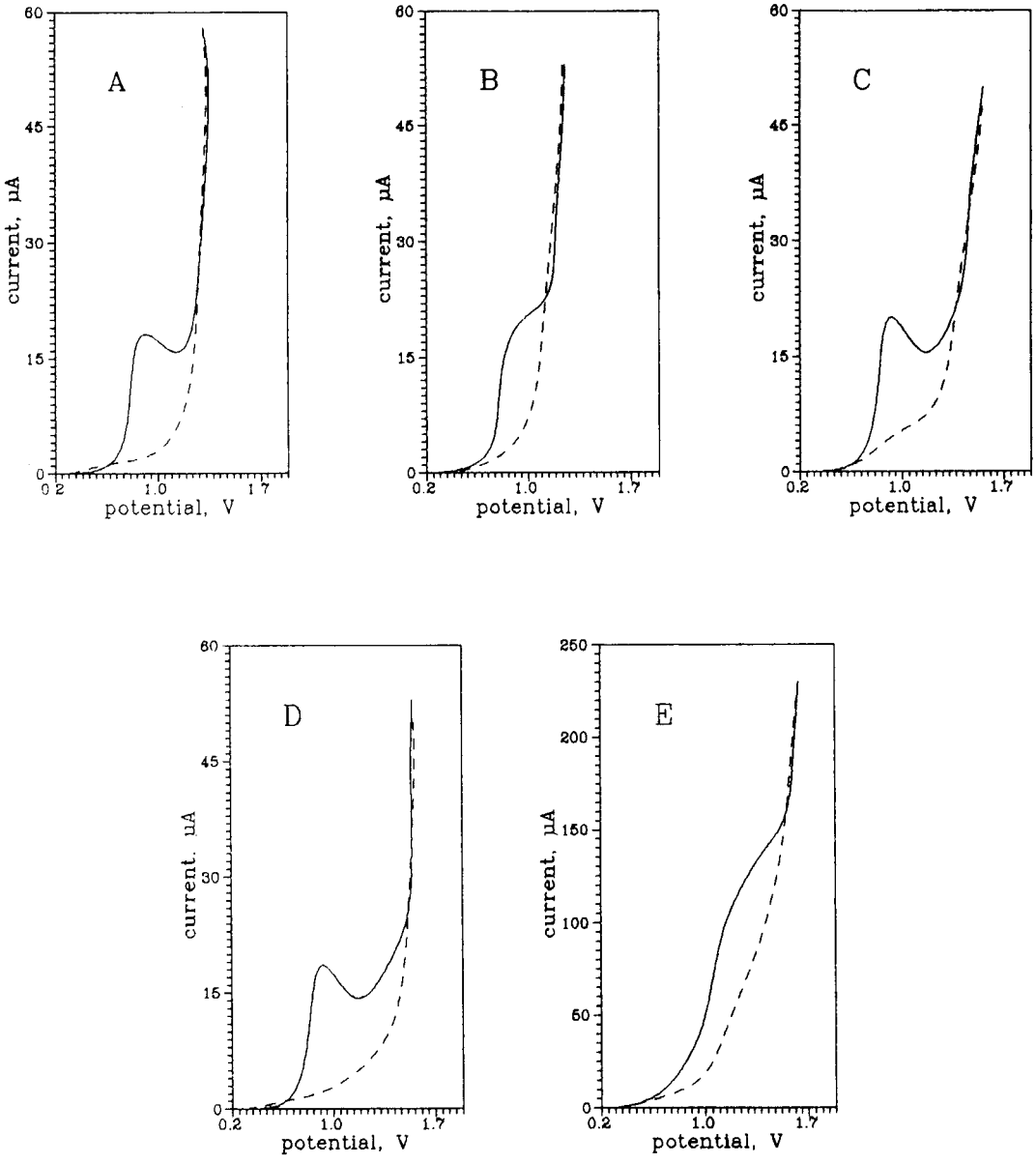

Fig. 1. Linear-sweep voltammograms in different buffers. Ephedrine, 1.7×10^{-3} M; scan rate, 20 mV s^{-1}. Buffers: (A) carbonate, 0.1 M; (B) ammonia–ammonium chloride, 0.1 M; (C) Clark–Lubs borate, 0.1 M; (D) Britton–Robinson, 0.1 M; (E) Teorell–Stenhagen, 0.1 M.

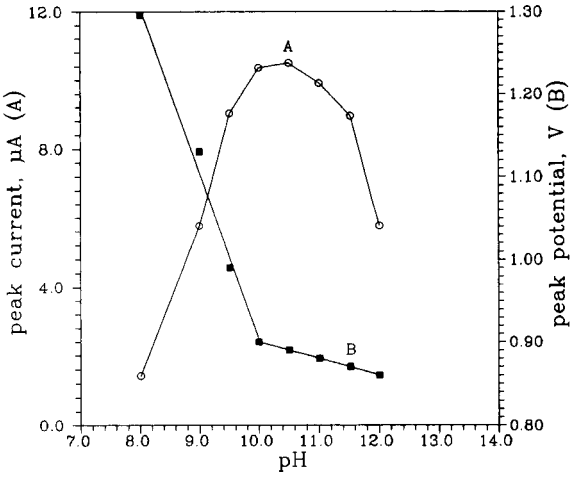

Fig. 2. Dependence of peak current and peak potential on pH. Ephedrine, 1.7×10^{-3} M; scan rate, 20 mV s^{-1}; 0.04 M Britton–Robinson buffer.

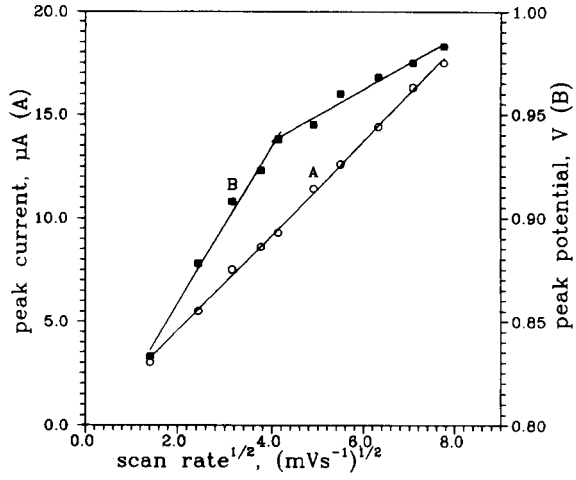

Fig. 3. Dependence of peak current and peak potential on scan rate. Ephedrine, 1.7×10^{-3} M; 0.04 M Britton–Robinson buffer (pH 10.0).

30 min before the potential scan was started, the voltammetric response was constant, which seems to indicate that there is virtually no adsorption of ephedrine on the working electrode.

Nature of the process and kinetic parameters. Studies of the ephedrine oxidation process at several electrodes has been reported [4,5] and on the basis of quantum mechanical studies, different oxidation processes were postulated with an overall loss of two electrons in consecutive one-electron steps. No references could be found either to kinetic studies or to studies with rotating disc electrodes. Figure 3 shows the influence of scan rate on the analytical signal using linear-scan voltammetry. The anodic peak potential is observed to increase when the scan rate increases, indicating an irreversible process. A linear relationship between peak current and square root of the scan rate was observed, which fits the equation

$$I_p(\mu A) = 0.1 + 2.27\left[V(\text{mV s}^{-1})\right]^{1/2};$$

$$r = 0.9991 \ (n = 10)$$

as predicted by Nicholson and Shain's equation [26,27] for a diffusion-governed process.

The behaviour of ephedrine at the rotating disc glassy carbon electrode was studied in order to establish wether it fits Levich's equation [28]

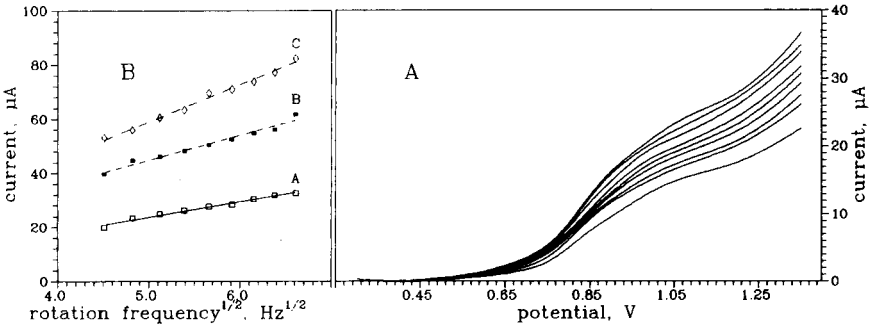

Fig. 4. Dependence of analytical response on rotation frequency. (A) Different ephedrine concentrations: $A = 2.0\times10^{-4}$ M; $B = 3.8\times10^{-4}$ M; $C = 7.6\times10^{-4}$ M. (B) Anodic voltammetric response at different rotation frequencies between 20.3 and 43.6 Hz; ephedrine, 2.0×10^{-4} M. Conditions: 0.04 M Britton–Robinson buffer (pH 10.0); scan rate, 20 mV s^{-1}.

TABLE 1

Calibration graphs in 0.04 M Britton–Robinson buffer (pH 10.0) at two different scan rates

Scan rate (mV s^{-1})	Linear response ($\mu g\ ml^{-1}$)	Equation of calibration graph: $I\ (\mu A) = a + b[C\ (\mu g\ ml^{-1})]$	Correlation coefficient [a]	Limit of determination ($\mu g\ ml^{-1}$)	Limit of detection ($\mu g\ ml^{-1}$)
20	2–240	$I = 0.2 + 0.07C$	0.998	6	2
60	2–180	$I = 0.8 + 0.13C$	0.9991	3	1

[a] Twelve points.

and thus characterizes the nature of the process. Figure 4A shows the voltammograms obtained at the rotating disc electrode for different rotation frequencies between 20.3 and 43.6 Hz, and the variation of the limiting current with the square root of the electrode rotation speed for three ephedrine concentrations is shown in Fig. 4B. Linear variations are obtained, as predicted by the theory. A fit of the ephedrine behaviour to Levich's equation indicates that the oxidation process of ephedrine at the glassy carbon electrodes is governed by diffusion.

Based on Bishop's pattern theory [29] and taking into account the following expressions:

$$K_D = \frac{D_{red}}{\delta_x} = \frac{i_l}{nAFC_{red}}$$

$$\beta = 1 - \alpha = 2.303 \cdot \frac{RT}{nF(E_{f1} - E_{f2})} \cdot \log\left[\frac{f_1(1-f_2)}{f_2(1-f_1)}\right]$$

$$\log K = \log\left(\frac{D_{red}}{\delta_x}\right) + \log\left[\frac{f_1}{(1-f_1)}\right] - \frac{E_{f1} - E_0'}{E_{f1} - E_{f2}} \cdot \log\left[\frac{f_1(1-f_2)}{f_2(1-f_1)}\right]$$

$$E_{f1} - E_0' = E + 0.242$$

where

K_D = mass-transfer rate constant (l cm^{-2} s^{-1});
D_{red} = diffusion coefficient of the reactant (l cm^{-1} s^{-1});
δ_x = apparent diffusion layer thickness (cm);
i_l = limiting current (A);
β = charge-transfer coefficient;
E_{fi} = potential at point i on the i–E curve (V);
f_i = i_i/i_l;
i_i = current at point i on the i–E curve (A);
K = conditional charge-transfer rate constant (l cm^{-2} s^{-1}).

The diffusion constant (K_D), the charge-transfer coefficient (β) and conditional charge-transfer rate constant (K) were calculated for three ephedrine concentrations between 2.0×10^{-4} and 7.5×10^{-4} M, where the process is governed by diffusion. The conditional potential, E_0', cannot be measured and the results are referred to zero potential. The results obtained give a mean value for the diffusion constant of log K_D of -4.86 ± 0.12, for the charge-transfer coefficient of 0.31 ± 0.02 (considering $n = 1$) [4,5] and a mean conditional charge-transfer rate constant of $K = 8.3 \times 10^{-12}$ l cm^{-2} s^{-1}. The values obtained for the conditional charge-transfer rate constant make it possible to state that the oxidation process of ephedrine is slow and irreversible.

On calculating the charge-transfer coefficient for the ephedrine oxidation step with the data from the linear-scan voltammograms at the stationary electrode and using the expression $E_p - E_{p/2} = 0.048/n\beta$, a mean value of 0.39 ± 0.01 is obtained for $n\beta$.

Effect of concentration. The study of the influence of drug concentration on the analytical signal reflects a gradual increase in the signal with increasing ephedrine concentration between 2 and 180 $\mu g\ ml^{-1}$. Table 1 gives the results obtained in 0.04 M Britton–Robinson buffer of (pH 10.0) and two different scan rates, 20 and 60 mV s^{-1}.

Differential-pulse voltammetry

Instrumental parameters. An increase in pulse amplitude causes a linear rise in peak current for amplitudes lower than 90 mV (Fig. 5). Figure 5

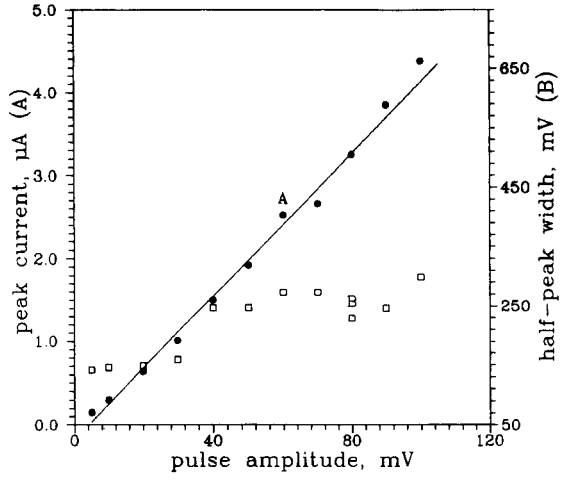

Fig. 5. Dependence of peak current on pulse amplitude. Ephedrine, 2.0×10^{-4} M; 0.04 M Britton–Robinson buffer (pH 10.0); scan rate, 20 mV s^{-1}.

also shows the influence of the pulse amplitude on the half peak width, determined with the difference $E_p - E_{p/2}$.

Influence of concentration. Table 2 gives the equations of the calibration graphs, correlation coefficients and detection and determination limits obtained in the study on the influence exerted by ephedrine concentrations on the analytical signal, performed in 0.04 M Britton–Robinson buffer (pH 10.0) at pulse amplitudes of 50 and 70 mV.

Influence of norephedrine on the analytical signal. Norephedrine has already been identified as the main metabolite of ephedrine, being present at a concentration equivalent to 8–10% of the total amount of ephedrine excreted by the organism [22,23], so its influence on the analytical signal was studied in 33 μg ml^{-1} ephedrine solution in 0.04 M Britton–Robinson buffer (pH 10.0) to which increasing amounts of norephedrine up to 6 μg ml^{-1} (18%) were added. No interference with the analytical signal of ephedrine was observed.

Determination of ephedrine in human urine

As the direct determination of ephedrine in human urine by differential-pulse voltammetry with a glassy carbon electrode is not possible owing to the increase in residual current brought about by the presence in urine of interfering components that mask the analytical signal, it was necessary to develop an extraction method in order to separate ephedrine from urine prior to determination. The method adopted is described under Experimental.

A comparison of the voltammograms obtained in the determination of various amounts of ephedrine in human urine with prior extraction and those obtained for the determination of ephedrine in water is shown in Fig. 6. Although the former voltammograms are lower in current and more poorly defined, they do not prevent the detection of ephedrine at levels higher than 2 μg ml^{-1}.

Table 3 gives the recoveries for several urine samples containing different amounts of ephedrine. The values were calculated by comparing the results obtained when ephedrine-free urine samples were subjected to the separation method and increasing amounts of ephedrine were added to the blank thus prepared with the results obtained for ephedrine-containing urine samples subjected to the same separation process. The mean recovery was $99.8 \pm 1.5\%$.

Application of the separation process described above allows the determination of

TABLE 2

Calibration graphs in 0.04 M Britton–Robinson buffer (pH 10.0) at two different pulse amplitudes

Pulse amplitude (mV)	Linear response (μg ml^{-1})	Equation of calibration graph: I (μA) = $a + b[C$ (μg ml^{-1})]	Correlation coefficient [a]	Limit of determination (μg ml^{-1})	Limit of detection (μg ml^{-1})
50	2–30	$I = 0.17 + 0.05C$	0.996	7	2
75	2–30	$I = 0.21 + 0.08C$	0.998	4	1

[a] Fifteen points.

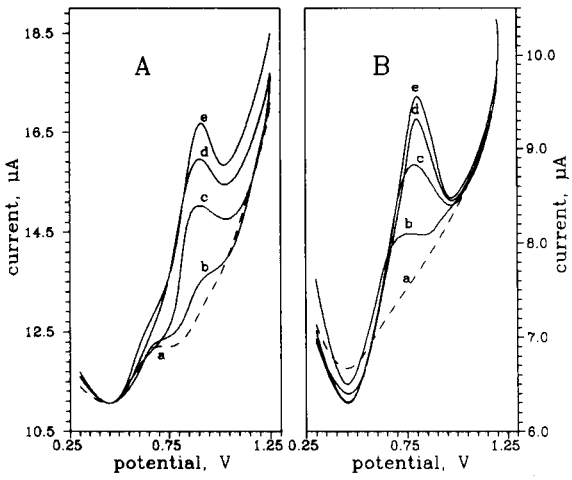

Fig. 6. Voltammograms obtained in the determination of ephedrine. (A) In urine with prior extraction: A = 0.0; B = 2.0; C = 8.0; D = 16.0; E = 20.0 μg ml^{-1}. (B) In water: A = 0.0; B = 2.0; C = 8.0; D = 16.0; E = 20.0 μg ml^{-1}. Conditions: 0.04 M Britton–Robinson buffer (pH 10.0); scan rate, 20 mV s^{-1}; pulse amplitude, 75 mV.

ephedrine in urine at levels between 7 and 20 μg ml^{-1}. The equation for the calibration graph is

$$I_p(\mu A) = 0.30 + 0.03[C(\mu g\ ml^{-1})];$$

$$r = 0.9990\ (n = 10)$$

the limits of detection (3σ) and determination (10σ) being 2 and 7 μg ml^{-1}, respectively.

A statistical study conducted with five samples of each concentration gave a mean relative error that was never higher than 6.0%, with a relative standard deviation of 5.8% ($n = 5$).

The standard addition method proved to be applicable for the determination of ephedrine in urine, as increasing amounts of ephedrine can be successively added to ephedrine-free urine samples subjected to the separation method described and reconstituted with 0.04 M Britton–Robinson buffer (pH 10.0) to obtain the calibration graph:

$$I_p(\mu A) = 0.32 + 0.02[C(\mu g\ ml^{-1})];$$

$$r = 0.991\ (n = 7)$$

under the conditions defined above.

TABLE 3

Recovery for different urine samples

Ephedrine (μg ml^{-1})	n	Donor	Recovery (%)
10	5	A	98.4 ± 2.0
10	5	B	99.5 ± 0.9
10	5	C	99.3 ± 1.5
14	5	A	101.0 ± 2.9
14	5	B	98.6 ± 1.3
14	5	C	102.1 ± 1.9

Conclusions

The electrochemical determination of ephedrine in human urine using a glassy carbon electrode appears to be a reliable method provided that a previous separation of ephedrine is carried out. The proposed separation method uses Sep-Pak C_{18} cartridges and gives recoveries of 99.8 ± 1.5%. The differential-pulse voltammetric method used, with either a calibration graph or standard additions, can be applied to the determination of ephedrine in urine samples at levels higher than 7 μg ml^{-1}.

The authors thank CICYT for financial support for this project (No. Dep. 91-103).

REFERENCES

1 D.J. Smith, J. Assoc. Off. Anal. Chem., 53 (1970) 840.
2 E.B. Leffler, J.M. Spencer and A. Burger, J. Am. Chem. Soc., 73 (1951) 2611.
3 M.C. Salvadory, M.E. Velletri, M.M.A. Camargo and A.C.P. Araújo, Analyst, 113 (1988) 1189.
4 A.M. Gazaliev, S.D. Iazylov, E.P. Sim and M.Zh. Zhurinov, Khim. Prir. Soedin., 4 (1989) 523.
5 M. Masui and S. Ozaki, Chem. Pharm. Bull., 26 (1978) 2153.
6 M. Chicharro, A. Zapardiel, E. Bermejo, J.A. Pérez and L. Hernández, in preparation.
7 L.M. Cummins and M.J. Fourier, Anal. Lett., 2 (1969) 403.
8 E.T. Lin, D.C. Brater and L.Z. Benet, J. Chromatogr., 140 (1977) 275.
9 K.K. Midha, J.K. Cooper and J. McGilveray, J. Pharm. Sci., 68 (1979) 557.
10 S. Sun and M.J. Leveque, J. Pharm. Sci., 68 (1979) 1561.
11 L.Y. Lo, G. Land and A. Bye, J. Chromatogr., 222 (1981) 297.
12 C. Bye, H.M. Hill, D.T.D. Hughes and A.W. Peck, Eur. J. Clin. Pharmacol., 8 (1975) 47.

13 R.G. Kuntzman, I. Tsai, L. Brand and L.C. Mark, Clin. Pharmacol. Ther., 12 (1971) 62.
14 J.T. Warren, R.M. Welch and J.W.A. Findlay, Fed. Proc., Fed. Am. Soc. Exp. Biol., (1978) 725.
15 S.M. Hassan Saad and G.A. Rechnitz, Anal. Chem., 58 (1966) 1052.
16 S.M. Hassan Saad and M.M. Saoudi, Analyst, 111 (1986) 1367.
17 S.M. Hassan Saad, Arab. Gulf. J. Sci. Res., 4 (1986) 127.
18 M. Endo, H. Imamichi, M. Moriyasu and Y. Hashimoto, J. Chromatogr., 196 (1980) 334.
19 Y. Nakahara and Y. Takeda, Chromatographia, 26 (1988) 363.
20 Y. Nakahara and A. Ishigami and Y. Takeda, J. Chromatogr., 489 (1989) 371.
21 A.J.J. Debets, R.W. Frei, K.P. Hupe and W.Th. Kok, J. Chromatogr., 465 (1989) 315.
22 G.R. Wilkinson and A.H. Beckett, J. Pharm. Pharmacol. Exp. Ther., 162 (1968) 139.
23 A.H. Beckett and G.R. Wilkinson, J. Pharm. Pharmacol., 17 (1965) 2611.
24 R.C. Engstrom and V.A. Strasser, Anal. Chem., 56 (1984) 136.
25 K. Diem, Tablas Científicas. Documenta Geigy, Sociedad Alianza de Artes Gráficas, Barcelona, 6th edn., 1965, pp. 320–321.
26 R.S. Nicholson and I. Shain, Anal. Chem., 36 (1964) 706.
27 R.S. Nicholson and I. Shain, Anal. Chem., 37 (1965) 178.
28 B. Levich, Acta Physicochim. URSS, 17 (1942) 257.
29 E. Bishop, Analyst, 97 (1962) 761.

Analytica Chimica Acta, 273 (1993) 369–375
Elsevier Science Publishers B.V., Amsterdam

Adsorptive stripping voltammetric behaviour of sulphaquinoxaline using differential-pulse and square-wave techniques

J.J. Berzas, J. Rodríguez, J.M. Lemus and G. Castañeda

Departamento de Química Analítica y Tecnología de Alimentos, Facultad de Químicas, Universidad de Castilla-La Mancha, 13071 Ciudad Real (Spain)

(Received 1st June 1992; revised manuscript received 16th September 1992)

Abstract

The adsorptive stripping voltammetric behaviour of sulphaquinoxaline (SQX) was studied by both square-wave and differential-pulse techniques, leading to two methods for its determination in aqueous samples and pharmaceutical formulations. The application of the square-wave mode for the stripping of adsorbed SQX proved to be more sensitive, yielding signals fifteen times larger than those obtained by applying a differential-pulse scan. The relative standard deviations obtained for concentration levels of SQX as low as 1.5×10^{-6} M with square-wave and differential-pulse methods were 2.47% and 2.21% ($n = 8$), respectively.

Keywords: Polarography; Stripping voltammetry; Voltammetry; Pharmaceuticals; Sulphaquinoxaline

In both veterinary and medical practice, formulations containing sulphonamides are applied to prevent infections in a variety of situations. They are rapidly absorbed, establishing therapeutic ranges of 30–150 mg l^{-1} in plasma and 500–1000 mg l^{-1} in urine [1]. With their use in veterinary practice, there may be a risk of residues subsequently contaminating food products. In many countries, maximum residue levels for sulphonamides below 1 mg kg^{-1} have been established. Nowadays, pharmaceutical and veterinary products frequently contain a sulphonamide mixed with an excipient or with another drug used to increase the activity of the sulphonamide. Therefore, simple, rapid and economical methods of analysis are required. Spectrophotometric methods on the basis of the Bratton–Marshall reaction are commonly used for determining the total sulphonamide content [2–5]. Derivative spectrophotometric techniques have recently been used for resolving different sulphonamide mixtures, e.g., pyrimethamine and sulphaquinoxaline (SQX) [6].

Kotoucek and co-workers [7,8] investigated the possibility of the direct determination of some sulphonamides by differential-pulse polarography (DPP) and adsorptive stripping voltammetry. An acidic medium was necessary in all these determinations where the reduction procceses had to proceed. An indirect method was reported by Fogg and Ahmed [9] for submicromolar concentrations of sulphonamides using DPP after diazotization and coupling with 1-naphthol. No references to the electrochemical determination of SQX could be found.

Adsorptive stripping voltammetry has been demonstrated to be a useful technique for the

Correspondence to: J. Rodríguez, Departamento de Química Analítica y Tecnología de Alimentos, Faculdad de Químicas, Universidad de Castilla-La Mancha, 13071 Ciudad Real (Spain).

study and determination of many molecules of biological importance [10]. In this work, a study of the electrochemical behaviour of SQX was made, taking into account the possible adsorption of the molecule on mercury, followed by differential-pulse polarography (DPP) and square-wave voltammetry (SWV).

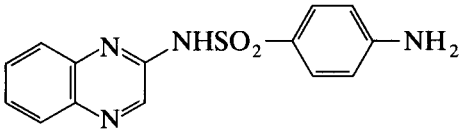

Sulphaquinoxaline (SQX)

In stripping voltammetry, the substance to be determined is concentrated in or on the working electrode by electrochemical means before doing the analysis. With a sufficiently long deposition time, the concentration of the substance will be higher in or at the electrode than in the sample solution. If the electrode potential is then scanned, the substance will be stripped from the electrode, causing an increase in the cell current as this process occurs.

The high sensitivity of adsorptive stripping methods is obviously their greatest advantage. On the other hand, a serious drawback is interferences from other surface-active substances that may be present in the solution. In this event, competitive adsorption usually occurs and leads to a decrease in the measured current or, at very high surface-active substance concentrations, to significant suppressions of the signal. In such instances it is then necessary to employ a suitable separation of interfering compounds.

If the sample contains interfering compounds that are electrochemically active but are not absorbed on the electrode surface, then classical separation procedures are not necessary. Another advantage of stripping analysis is the possibility of working with very dilute samples, with a consequent decrease in interferences in pharmaceutical analysis.

The combination of the adsorptive stripping technique and square-wave measurement provides a very sensitive, selective and rapid approach. The methods proposed here have yielded good results in the determination of SQX in the presence of other components in three different Spanish pharmaceutical products: Anticoccidiosico potenciado [SQX 30 g l^{-1}, pirimethamine (PMT) 9 g l^{-1} and excipient, from Laboratorios Maymó], Coccirex (SQX 44 g l^{-1}, PMT 12 g l^{-1} and excipient, from Laboratorios Revex) and Disulviar potenciado (SQX 33 g l^{-1}, PMT 10 g l^{-1} and excipient, from Laboratorios Sobrino).

EXPERIMENTAL

Materials

All reagents were of analytical-reagent grade unless indicated otherwise. Solutions for voltammetry were prepared in deionized water. Stock solutions of 5 M perchloric acid and sodium perchlorate were prepared using Suprapur-grade reagents. These were diluted 1 + 49 with deionized water and used throughout the voltammetric investigations.

Sulphaquinoxaline (sodium salt) was obtained from Sigma and was used as received. A stock solution (250 mg l^{-1}) was prepared in ethanol–water (1 + 1, v/v).

Apparatus

Voltammograms were obtained with a Princeton Applied Research (PAR) (Princeton, NJ) Model 384B polarographic analyser combined with a PAR Model 303A static mercury drop electrode (SMDE) using an Ag/AgCl reference electrode, a PAR Model 305 magnetic stirrer, a Tandon computer, using 384 B software, and an Epson FX 850 recorder.

A PAR Model 9301 thermostated cell was maintained at 21 ± 1°C in all experiments.

Procedure

For all voltammetric investigations, 0.2 ml of the 5 M $NaClO_4$ and $HClO_4$ supporting electrolyte solution was made up to 10.0 ml with deionized water and purged with oxygen-free nitrogen for 10 min (and for 2 min in subsequent runs). The required accumulation potential (E_{acc}) of −0.050 V was then applied to the electrode for a selected accumulation time (t_{acc}), while the solution was stirred at 400 rev. min^{-1}. After a

10-s rest period, a differential-pulse or a square-wave scan was initiated in the negative direction.

The selection of the acid and the electrolyte ($HClO_4$ and $NaClO_4$) was based on the good background obtained under the selected conditions for the determination of SQX.

RESULTS AND DISCUSSION

The preconcentration of SQX at the SMDE and the application of a subsequent DP potential scan in the negative-going direction gave rise to two stripping peaks. In Fig. 1, the differential-pulse and the square-wave voltammograms are shown for an assayed concentration of 3.1×10^{-7} M. It can be readily seen that a square-wave form applied to the stripping of the adsorbate yields a larger analytical signal ($E_p = -0.32$ V; curve B) than that obtained by applying a differential-pulse wave form ($E_p = -0.28$ V; curve A). Neither the sulphonamide nor the primary amine group of SQX is electroreducible, reduction probably occurring at the C=N bound of the quinoxaline group.

The nature of the electrochemical process was also studied by cyclic voltammetry (CV). Figure 2 shows a cyclic voltammogram for a 1.5×10^{-6} M solution of SQX after a t_{acc} of 60 s. The reduction processes are not accompanied by anodic waves, which seems to indicate a certain degree of irreversibility.

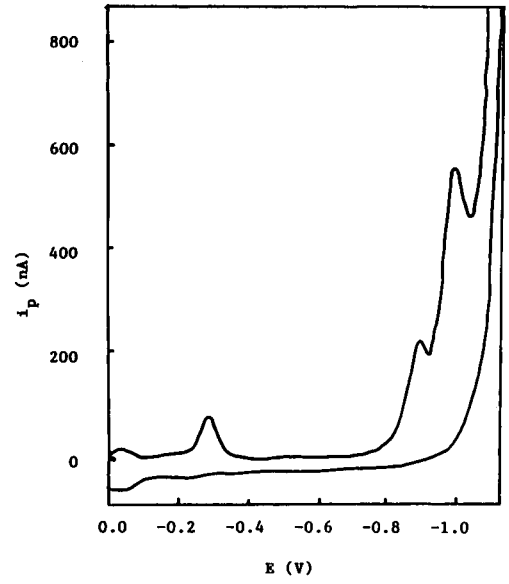

Fig. 2. Cyclic voltammogram obtained from a 1.5×10^{-6} M solution of SQX. Scan rate, 50 mV s^{-1}; $t_{acc} = 60$ s; $E_{acc} = -0.05$ V.

When the potential was scanned at increasing rates from 20 to 500 mV s^{-1} under the same experimental conditions, a linear relationship was

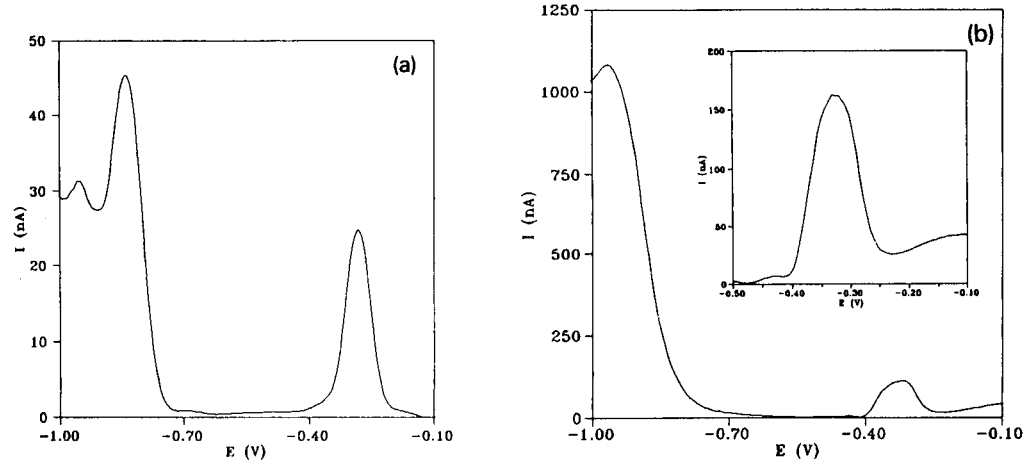

Fig. 1. (a) Differential-pulse and (b) square-wave adsorptive stripping voltammograms from a solution of 3.2×10^{-7} M SQX. For conditions, see Experimental.

observed between the peak intensity and the scan rate (V_b), demonstrating that the phenomenon is adsorption controlled:

$$i_p(\text{nA}) = 0.30[v_b(\text{mV s}^{-1})] + 5.7;$$

$$r = 0.998 \ (n = 6)$$

Apart from this increase in the analytical response originating from the use of higher scan rates, the significant improvement in sensitivity achieved by employing a square-wave scan can be described in terms of the characteristic parameters governing this technique. The application of pulses in the negative and positive directions of potential and the high frequency with which they are repeated result in a better signal compared with the responses obtained when using the differential-pulse mode. Two calibration graphs were obtained for SQX by using the adsorptive and direct DPP modes, obtaining linear ranges from 3.1×10^{-8} up to 5.3×10^{-7} M and from 1×10^{-6} up to 5.5×10^{-5} M, respectively. This shows the high sensitivity of adsorptive stripping methods.

The concentration of $HClO_4$ was varied between 0.02 and 0.25 M and the ionic strength of the supporting electrolyte was studied in the range from 0.05 to 0.25 M $NaClO_4$. A 0.1 M concentration of $HClO_4$ and $NaClO_4$ seemed to yield the largest response for the adsorptive phenomena.

Experiments were made in order to find the optimum conditions for the adsorption step. Several preconcentration–stripping voltammograms were recorded for accumulation potentials varying from +0.1 to −0.2 V and a t_{acc} of 10 s. The reduction peaks obtained with a DP scan under the conditions mentioned under Experimental showed similar intensities for the application of accumulation potentials in the negative and positive regions.

Small additions of ethanol to the cell containing the sulphonamide solution had no influence on the adsorption process of SQX.

Differential-pulse adsorptive stripping voltammetry (DPAdSV)

Experiments carried out for different pulse amplitudes (25–125 mV) demonstrated that there is a linear relationship between peak intensity, i_p, and the applied pulse, ΔE, as expressed by the following equation:

$$i_p\ (\text{nA}) = 0.57[\Delta E(\text{mV})] - 3.9$$

This equation holds for values between 25 and 75 mV. However, the peak width at half-height increased for the larger pulse amplitudes and a pulse amplitude of 50 mV was adopted.

The stripping signal increased with increasing electrode area. As the noise level that accompanied the use of a large electrode surface was not significant, the remainder of the study was carried out using the largest electrode area (0.025 cm^2) that provided the most sensitive signal and best signal-to-noise ratio.

The influence of the scan rate on the analytical signal was studied from two viewpoints. First, the scan increment, Δs, was varied from 2 to 10 mV for a given sampling time (t_{drop} = 1.0 s, constant). The results are given in Table 1. For a fixed sampling time of 1.0 s, an increase in the scan increment from 2 to 10 mV resulted in broader peaks. Thus, the peak width at half-height, $\Delta W_{1/2}$, for a scan increment of 10 mV is 2.63 times larger than that corresponding to 2 mV. Conversely, the peak intensity for a scan increment of 2 mV is 1.60 times larger than that obtained for a scan increment of 6 mV. A small decrease was obtained for scan rates of 8 and 10 mV s^{-1}.

The best signals were achieved for a scan rate of 4 mV s^{-1} obtained with Δs = 4 mV and t_{drop} = 1.0 s. These values were adopted for the remainder of the study.

TABLE 1

Influence of scan rate on the DPAdSV behaviour of sulphaquinoxaline [a]

Δs (mV)	v (mV s^{-1})	$\Delta W_{1/2}$ (mV)	i_p (nA)	$-E_p$ (V)
2	2	57	18.4	0.262
4	4	64	23.5	0.272
6	6	92	29.4	0.280
8	8	120	25.0	0.276
10	10	148	22.4	0.280

[a] [SQX] = 3.1×10^{-7} M; t_{drop} = 1 s.

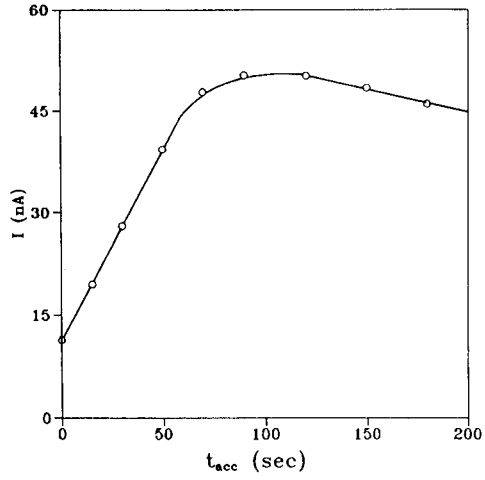

Fig. 3. Effect of accumulation time on the differential-pulse adsorptive stripping signal for a solution of 3.1×10^{-7} M SQX.

Some voltammograms with increasing accumulation times were recorded of a solution containing 3.1×10^{-7} M SQX under the above described conditions. The resulting peaks showed a linear relationship between peak intensity and accumulation time up to 80 s ($n = 7$, $r = 0.99$) with a slope of 0.50 nA s^{-1} (Fig. 3). Owing to saturation of the electrode area, the peak intensity started to decrease but with a smaller slope. Thus, when a certain coverage of the electrode is reached, interactions among the molecules in the adsorbed state become noticeable. The peak potentials undergo a small displacement towards more positive potentials, indicating that lower energy is needed to strip the adsorbate from the electrode. A calibration graph was constructed by using a t_{acc} of 10 s, which is not too high and at the same time is well within the linear range of the accumulation times studied. A linear response was obtained between 3.1×10^{-8} and 5.3×10^{-7} M of the analyte with a slope of 7.8×10^{7} nA mol^{-1} l and a correlation coefficient of 0.9993 ($n = 8$). Another calibration graph was constructed by using a longer accumulation time ($t_{acc} = 40$ s), which is too high to obtain an extensive linear range for the determination of SQX. The reproducibility of the stripping signal expressed in terms of the relative standard deviation for measurements of the height carried out at a concentration level of 1.5×10^{-6} M was 2.21% ($n = 8$).

Square-wave adsorptive stripping voltammetry (SWAdSV)

Considering the larger response obtained in the stripping of SQX by SWAdSV than DPAdSV (Fig. 1), it was felt that this technique might be successfully applied to the determination of this drug. Consequently, the parameters governing this voltammetric mode were studied.

The stripping peak intensity increased very rapidly with increasing pulse amplitude, as indicated by the fact that $\Delta E = 125$ mV gave rise to a response of 9045 nA compared with 1706 nA obtained with $\Delta E = 25$ mV when $t_{acc} = 10$ s and a frequency of 100 Hz were used for a 1.5×10^{-6} M solution of SQX. The analytical signal varied linearly between these two values according to the equation

$$i_p(\text{nA}) = 7.53[\Delta E(\text{mV})] + 1562$$

reaching a plateau at higher pulse amplitude.

Again, the larger the size of the electrode the better is the response obtained, as shown in Table 2.

The dependence of the peak intensity on the frequency follows the equation

$$i_p(\mu\text{A}) = 27.75[f(\text{Hz})] - 139.1$$

The study was done for a constant scan increment of 6 mV, and the results, as expected, showed a linear relationship between peak intensity and frequency for the whole range studied (25–120 Hz). When the scan increment was increased, an increase in the peak intensity was observed but at the same time a progressive

TABLE 2

Influence of electrode area on the SWAdSV behaviour of sulphaquinoxaline [a]

Drop size	Area (cm^2)	i_p (nA)	$-E_p$ (V)
Small	0.010	747	0.276
Medium	0.016	1209	0.276
Large	0.025	2037	0.288

[a] [SQX] = 1.5×10^{-6} M; $t_{acc} = 10$ s.

broadening of the peak took place (e.g., a $\Delta W_{1/2}$ of 56.47 mV was obtained for a scan increment Δs of 2 mV compared with of 63.53 mV for $\Delta s = 10$ mV). It was concluded that a frequency of 75 Hz and a Δs of 6 mV, together with a ΔE of 50 mV, provided analytical signals that were sensitive enough and at a very reasonable scan rate (450 mV s^{-1}). The use of higher Δs values would lead to more distorted peaks, resulting in poorer resolution.

The accumulation curves was obtained for a 1.5×10^{-6} M solution of SQX under the previously optimized conditions. Linearity prevailed for all the values of t_{acc} applied (i.e. up to 10 s) with a slope of 99.6 nA s^{-1} ($n = 5$, $r = 0.997$).

From these studies, the optimum conditions for the determination of SQX were established as $E_{acc} = -0.05$ V, frequency = 75 Hz, drop size = 0.025 cm^2 (large), $\Delta E = 50$ mV, scan rate = 450 mV s^{-1} and accumulation time = 10 s.

Voltammograms at different concentrations of SQX were recorded using the optimum conditions (Fig. 4). From these a linear calibration graph was obtained for SQX between 1×10^{-8} and 2×10^{-6} M, with a slope of 6.17×10^8 nA mol^{-1} l and a correlation coefficient of 0.999 ($n = 10$). The relative standard deviation of the stripping signal was calculated to be 2.47% ($n = 7$, at a concentration level of 1.5×10^{-6} M).

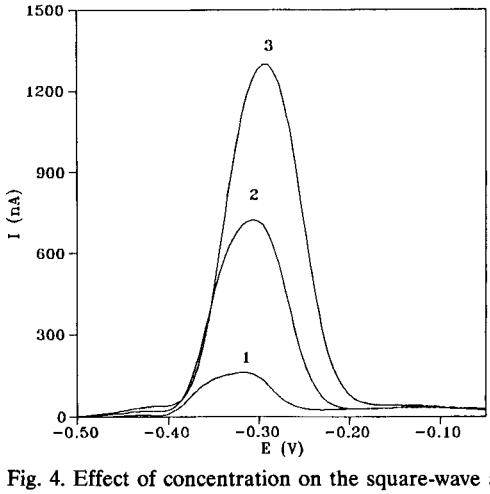

Fig. 4. Effect of concentration on the square-wave adsorptive stripping voltammograms of SQX. $t_{acc} = 10$ s; $\Delta E = 50$ mV; $\Delta s = 6$ mV; $f = 75$ Hz. SQX concentration: (1) 3.1×10^{-7}; (2) 1.2×10^{-6}; (3) 2.1×10^{-6} M.

TABLE 3

Results obtained in the determination of SQX in veterinary preparations

Preparation	SQX recovery (%) [a]		
	Spectrophotometry [b]	SWAdSV	DPAdSV
Coccirex	98	101	98
Disulviar potenciado	101	98	98
Anticoccidiosico potenciado	89	89	90

[a] Averages for three determination. [b] Results published by Berzas Nevado et al. [6].

Applications

Three commercial preparations containing SQX were studied. A 1-ml volume of each preparation was diluted with ethanol–water (1 + 1, v/v) in a 100-ml calibrated flask. Aliquots of 2.5 ml were diluted with deionized water in a 25-ml calibrated flask. To the voltammetric cell were added 0.0025, 0.030 and 0.034 ml of stock solutions of Coccirex, Disulviar potenciado and Anticoccidiosico potenciado, respectively, and the volumes were made up to 10.0 ml with 0.2 ml of $NaClO_4$, 0.2 ml of $HClO_4$ and deionized water. The final concentrations of SQX in the solutions were 3.47×10^{-7} M (Coccirex), 3.07×10^{-7} M (Disulviar potenciado) and 3.6×10^{-7} M (Anticoccidiosico potenciado).

Table 3 shows the recoveries obtained for these pharmaceutical products in the determination of the total content of SQX by the two proposed adsorptive methods and by spectrophotometry as reported by Berzas Nevado et al. [6] using the derivative ratio spectra method [11]. Good results for SQX were found for Coccirex and Disulviar in all instances. The determination of SQX in Anticoccidiosico potentials gave lower recovery values with all the methods.

The authors thank the DGICYT of the Ministério de Educación y Ciencia (Spain) for supporting this study (Project PB 90-0397).

REFERENCES

1 W. Sadee and G.C.M. Beelen, Drug Level Monitoring, Wiley, New York, 1980.
2 A.C. Bratton and E.K. Marshall, J. Biol. Chem., 128 (1939) 537.
3 A. Bye and A.F.J. Fox, Clin. Chem., 20 (1974) 288.
4 M.A. Koupparias and P.I. Anagnostopoulou, Anal. Chim. Acta, 204 (1988) 271.
5 F. Salinas, A. Espinosa Mansilla and J.J. Berzas Nevado, Anal. Chim. Acta, 204 (1988) 271.
6 J.J. Berzas Nevado, J.M. Lemus Gallego and G. Castañeda Peñalvo, J. Pharm. Biomed. Anal., in press.
7 M. Kotoucek, I. Cechova and J. Novakova, Cesk. Farm., 40 (1991) 53.
8 M. Kotoucek, J. Ruzickova and I. Cechova, Mikrochim. Acta, 2 (1989) 109.
9 A.G. Fogg and Y.Z. Ahmed, Anal. Chim. Acta, 70 (1974) 241.
10 J. Wang, in A.J. Bard (Ed.), Electroanalytical Chemistry, Vol. 16, Dekker, New York, 1989, p. 39.
11 F. Salinas, J.J. Berzas Nevado and A. Espinosa Mansilla, Talanta, 37 (1990) 347.

Analytica Chimica Acta, 273 (1993) 377–382
Elsevier Science Publishers B.V., Amsterdam

Simultaneous adsorptive stripping voltammetric determination of riboflavin and folic acid in multivitamin preparations

M.J.F. Villamil, A.J. Miranda Ordieres, A. Costa García and P. Tuñón Blanco

Departamento de Química Física y Analítica, Universidad de Oviedo, 33071 Oviedo, Asturias (Spain)

(Received 27th July 1992)

Abstract

The adsorptive stripping voltammetric behaviour of folic acid and riboflavin was studied at a hanging mercury drop electrode by phase-selective a.c. voltammetry. In 0.1 M sodium acetate buffer (pH 5.0) a cathodic scan gave peaks at −0.29 and −0.55 V vs. Ag/AgCl for riboflavin and folic acid, respectively. The adsorptive stripping response was evaluated with respect to concentration dependence and preconcentration time. Both compounds can be simultaneous determined with a relative standard deviation of 1.4% at 5×10^{-8} M riboflavin and 0.74% at 10^{-8} M folic acid. The method compared favourably with liquid chromatography with UV detection and was succesfully applied to the simultaneous determination of both compounds in multivitamin preparations. The average contents of riboflavin and folic acid were found to be 15.19 mg ± 2.1% and 1.8 mg ± 2.6%, respectively.

Keywords: Stripping voltammetry; Adsorptive stripping; Folic acid; Pharmaceuticals; Riboflavin; Vitamins

Folic acid [*N*-(4-{[(2-amino-1,4-dihydro-4-oxo-6-pteridinyl)methyl]amino}benzoyl)-L-glutamic acid} and riboflavin [7,8-dimethyl-10-(D-ribo-2,3,4,5-tetrahydroxypentyl)isoalloxazine] are part of the vitamin B complex (B_9 and B_2, respectively). Many methods for the determination of water-soluble vitamins using different physical, chemical and biological methods have been published [1–3], but the determination of vitamins in pharmaceutical preparations is often complicated by large excess of other ingredients. A variety of methods for determining riboflavin and folic acid are available. Some depend on the use of liquid chromatography (LC) with UV and fluorescence detection [4,5] and others use adsorptive stripping voltammetry [6–8], but the latter technique has never been used for the simultaneous determination of both vitamins. Various reducible and oxidizable compounds have been measured following their adsorptive accumulation on mercury [8–11] or solid [12–14] electrodes, although only a few attempts have been made towards the simultaneous adsorptive stripping analysis of organic compounds [15].

Folic acid undergoes polarographic reduction showing three waves, which have been studied previously [16,17]. In acidic medium the first reduction wave corresponds to a $2e^-$, $2H^+$ reversible process of conversion of folic acid into 5,8-dihydrofolic acid and the second wave is due to a $2e^-$, $2H^+$ reductive cleavage of the latter dihydro derivative between the C-9 and N-10 positions to give 7,8-dihydro-2-amino-4-hydroxy-6-metylpteridine. Finally, the third wave is due to a $2e^-$, $2H^+$ reduction to the corresponding 5,6,7,8-tetrahydro derivative. The polarographic

Correspondence to: P. Tuñón Blanco, Departamento de Química Física y Analítica, Universidad de Oviedo, 33071 Oviedo, Asturias (Spain).

behaviour of riboflavin has also been studied by Lindquist and Farroha [18], showing a $2e^-$, $2H^+$ reversible reduction process. Cylic voltammetry of folic acid and riboflavin [8,19] shows that both are strongly adsorbed at the electrode surface.

The presence of the aromatic ring system leads to good adsorption of the molecule on the mercury electrode and allows preconcentration on the surface of the electrode and subsequent measurement by stripping of the adsorbed molecules. This technique has proved to be useful for the measurement of biological molecules [20,21], but has seldom been employed to the simultaneous determination of molecules in the presence of electroactive species in solution that can interfere.

Adsorptive stripping voltammetry allows good precision and selectivity. The theory shows that the voltammetric response can be affected by the competitive and simultaneous adsorption of other species, decreasing the linear range. However, for low coverage of the electrode surface, interactions between adsorbed molecules could not be very important and consequently the linear range should not be affected.

In this work, the simultaneous adsorptive stripping voltammetric behaviour of riboflavin and folic acid was studied and both vitamins were determined in multivitamin preparations that contain other species at higher concentrations. The procedure described compared favourably with LC with UV detection.

EXPERIMENTAL

Instrumentation and reagents

A Metrohm (Herisau, Switzerland) E 506 polarograph was used in conjunction with a Metrohm EA-410 hanging mercury drop electrode with a drop area of 2.2 mm^2. Platinum wire was used as the auxiliary electrode and all potentials were measured versus an Ag/AgCl/KCl (sat.) reference electrode.

A Philips PU 4100 liquid chromatograph coupled to a Waters Lambda-Max 481 spectrophotometric detector and equipped with a syringe-loaded loop injection valve was used. A 25×0.4 cm i.d. Spherisorb ODS-2 column (10 μm) was used for reversed-phase chromatography. The chromatograms were recorded on a Philips PU 4815 integrator at a chart speed of 10 mm min^{-1}.

Riboflavin and folic acid were purchased from Sigma. Stock solutions of 0.01 M folic acid in 0.01 M sodium hydroxide and 1×10^{-4} M riboflavin in 0.01 M sodium acetate (pH 5.0) were prepared and stored in the dark at 4°C. Sodium acetate buffer (0.1 M, pH 5.0) was used as the background electrolyte. Analytical-reagent grade chemicals and nitrogen N-48 (S.E.O.) were used. Water was purified in a Milli-Q system (Millipore).

Sample preparation

A tablet was pulverized and a known portion was dissolved in 1% sodium carbonate solution. The precipitate was washed three more times with this solution and acetic acid was added to maintain a low pH because riboflavin is very unstable in alkaline media. The final volume was 100 ml. As many samples had to be analysed, this sample treatment was repeated for three tablets.

Stripping voltammetry

The supporting electrolyte solution (20 ml of 0.1 M sodium acetate buffer) was degassed with nitrogen for 15 min and 60 s before each adsorptive stripping cycle. A preconcentration potential of -0.1 V was applied to the electrode for 30 s under electrolysis while the solution was stirred at 200 rpm. The stirring was stopped and after a 10-s rest period the voltammogram was recorded. Stripping voltammetric experiments in the a.c. mode were done using a fixed frequency of 75 Hz and a superimposed a.c. voltage of 20 mV. The potential was scanned at a rate of 10 mV s^{-1}. For sample analysis 40 μl were injected into the electrochemical cell.

LC procedure

A reversed-phase LC method was developed that resolves riboflavin and folic acid. The mobile phase was methanol–0.025 M sodium phosphate buffer (pH 3.7) (20 + 80, v/v) with a linear gradient between 20 and 50% methanol in 10 min at a flow-rate of 1.0 ml min^{-1}. An internal standard (methotrexate) was added to the standard solu-

tions and samples at a final concentration of 2×10^{-5} M. The volume injected was 20 μl and UV detection was applied at a wavelength of 370 nm.

RESULTS AND DISCUSSION

Factors affecting the adsorptive stripping response

Adsorption processes can be utilized as an effective and simultaneous preconcentration step. Figure 1 shows a.c. voltammograms obtained for (A) riboflavin and (B) folic acid following 30-s adsorptive accumulation in 0.1 M sodium acetate buffer (pH 5.0). Both peaks are well defined at (A) −0.29 and (B) −0.55 V.

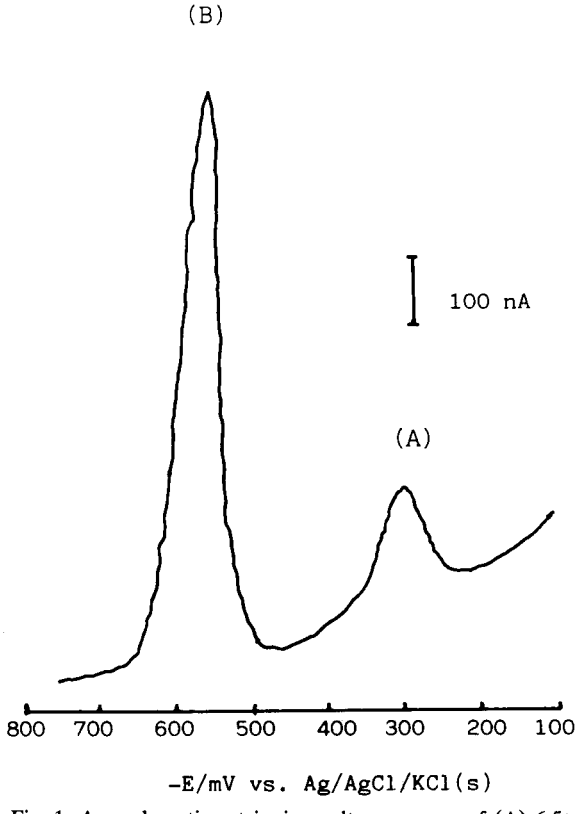

Fig. 1. A.c. adsorptive stripping voltammogram of (A) 6.5×10^{-8} M riboflavin and (B) 4×10^{-8} M folic acid in 0.1 M sodium acetate buffer (pH 5.0). Scan rate, 10 mV s^{-1}; preconcentration potential, −0.1 V; detection angle, 8°; a.c. amplitude, 20 mV; preconcentration time, 30 s; stirring speed, 200 rpm.

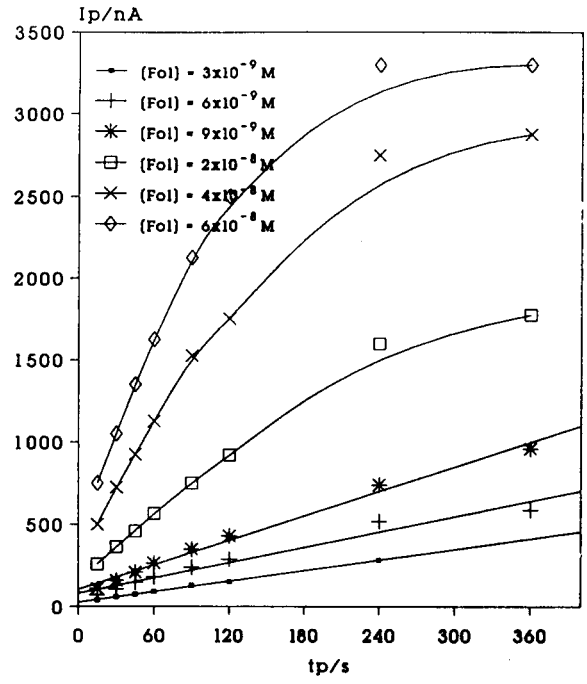

Fig. 2. Effect of preconcentration time on the adsorptive stripping response of folic acid in the presence of 6.5×10^{-8} M riboflavin. Folic acid concentration: ■ = 3×10^{-9}; + = 6×10^{-9}; * = 9×10^{-9}; □ = 2×10^{-8}; × = 4×10^{-8}; ◇ = 6×10^{-8} M. Other conditions as in Fig. 1.

The adsorptive stripping response depends on the composition of the supporting electrolyte. Various electrolytes (NaOH, Britton–Robinson, citrate and acetate buffers, hydrochloric acid) were examined. Optimum signals (in terms of sensitivity) were obtained in 0.1 M sodium acetate buffer (pH 5.0).

As expected, the extent of preconcentration is a function of the accumulation time. Figure 2 shows the dependence of accumulation time on the stripping voltammetric response of folic acid in presence of 6.5×10^{-8} M riboflavin. The peak currents increase linearly with increasing preconcentration time and the growth is faster as the concentration of the bulk solution increases. The slopes of the linear portion are proportional to the solution concentration ($r = 0.9998$), showing the validity of the calibration method. It was also observed that when the concentration and accu-

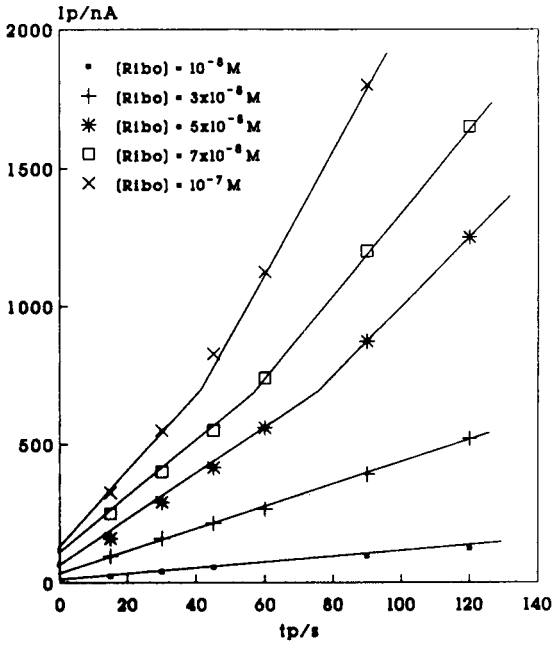

Fig. 3. Effect of preconcentration time on the adsorptive stripping response of riboflavin in the presence of 5×10^{-9} M folic acid. Riboflavin concentration: ■ = 1×10^{-8}; + = 3×10^{-8}; * = 5×10^{-8}; □ = 7×10^{-8}; × = 1×10^{-7} M. Other conditions as in Fig. 1.

mulation time are increased saturation is reached (last portion of the curves).

Figure 3 shows the dependence of preconcentration time on the stripping voltammetric response of riboflavin in presence of 5×10^{-9} M folic acid. The current increases linearly with accumulation time and the growth is faster as the concentration of the bulk solution increases. The slopes of the linear portion are proportional to the solution concentration ($r = 0.9997$).

The observed change in slope is accompanied by changes that affect the morphology of the peaks, which become sharper and are shifted a few millivolts to more negative potentials. This behaviour has been explained by Laviron [22] in terms of interactions among the adsorbed molecules.

For signicant analytical utility the method must exhibit a simultaneous concentration dependence for both compounds. The concentration dependence of folic acid between 1×10^{-9} and 1×10^{-7} M in the presence of 1×10^{-8} and 6.5×10^{-8} M riboflavin was studied. Linearity was obtained and least-squares analysis of the data yielded slopes of 2.20×10^{10} and 2.10×10^{10} nA mol^{-1} l, intercepts of 29.70 and 5.86 nA and limits of detection of 1×10^{-9} and 1×10^{-9} M, respectively.

Similar experiments were done for riboflavin over the concentration range 1×10^{-8} to 1.5×10^{-7} M in the presence of 5×10^{-9} and 5×10^{-8} M folic acid, yielding slopes of 83.98×10^{8} and 62.5×10^{8} nA mol^{-1} l, intercepts of 23.5 and 18 nA and limits of detection of 5×10^{-9} and 6.3×10^{-9} M, respectively.

Deviations from linearity occurred at higher concentrations and longer preconcentration times. For this reason, short preconcentration times must be used to avoid saturation at the hanging mercury drop electrode.

The high sensitivity of adsorptive stripping voltammetry is accompanied by good reproducibility. The precision was calculated from seven successive measurements of a 5×10^{-8} M solution of riboflavin and a 1×10^{-8} M solution of folic acid at −0.1 V with a 30-s preconcentration time. The mean peak currents were of 416.6 and 613.7 nA with relative standard deviations of 1.4% and 0.74%, respectively.

TABLE 1

Results obtained for the LC and the voltammetric determination of the vitamins in a tablet (mean values of five determinations)

Vitamin	Voltammetric method			LC method		
	Mean content (mg)	S.D. (mg)	R.S.D. (%)	Mean content (mg)	S.D. (mg)	R.S.D. (%)
Riboflavin	15.19	0.32	2.1	14.98	0.39	2.6
Folic acid	1.18	0.03	2.6	1.22	0.05	2.5

Analytical application

It was possible to use the adsorptive stripping voltammetric response of folic acid and riboflavin for their simultaneous determination in multivitamin preparations containing 23 components plus excipients. Tablets (Micebrina, Derly) nominally containing 5 mg of riboflavin and 0.4 mg of folic acid per tablet were used. Five samples were analysed following the procedure described under Experimental. The standard addition method was used to determine the contents of the two components required. The results obtained are given in Table 1. Well defined peaks were obtained and no interferences were observed.

The adsorptive stripping voltammetric method was checked by LC as this method is the most frequently used technique in the pharmaceutical analytical control laboratories. Figure 4 shows the LC separation of the active substances. The retention times were 10.1 and 6.22 min for riboflavin and folic acid, respectively. The method shows good reproducibility; the relative standard deviations based on five injections of standards were 1.75% and 1.26% for riboflavin and folic acid, respectively. The LC method used permits the simultaneous separation of riboflavin, folic acid and other vitamins of unknown composition in 10 min.

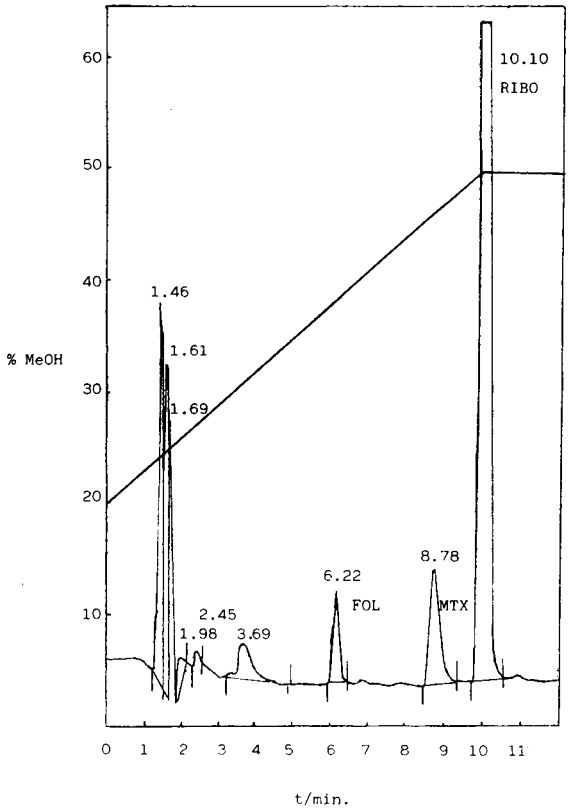

Fig. 4. Liquid chromatogram for a tablet. Conditions: eluent, methanol–0.025 M sodium phosphate buffer (pH 3.7), gradient elution from 20 to 50% methanol in 10 min; volume injected, 20 μl; flow-rate, 1 ml min^{-1}; UV detection at 370 nm.

Both vitamins are determined in the same kind of tablets submitted to the same kind of pretreatment by the internal standard method using methotrexate (MTX) [*N*-(4-{[(2,4-diamino-6-pteridinyl)methyl]methylamino}benzoyl)-L-glutamic acid]. Its retention time under these conditions was 8.78 min. Because of the large difference in the concentrations of folic acid and riboflavin, the sample was diluted for the determination of the latter. The results are also given in Table 1.

Conclusions

Adsorptive stripping voltammetry is a valuable technique for the simultaneous determination of folic acid and riboflavin in the presence of a large excess of electroactive species in solution with good accuracy and precision. The adsorptive stripping voltammetric response shows a linear dependence on concentration when both vitamins are preconcentrated simultaneously for 30 s. This technique was applied to their determination in multivitamin preparations. The results showed good precision of 2.1% and 2.6% for riboflavin and folic acid, respectively. Similar results were obtained using the voltammetric and an LC method, but the former is faster and cheaper.

REFERENCES

1 Y.A. Beltagy and R. Soliman, Zentralbl. Pharm. Pharmakother. Laboratoriumsdiagn., 118 (1979) 1285.
2 E. Elenaey and R. Soliman, Talanta, 26 (1979) 1164.
3 P. Vasileva-Aleksandrova and A. Neicheva, Microchim. Acta, II (1979) 337.
4 R.N. Reingold and M.F. Picciano, J. Chromatogr., 234 (1982) 171.

5 T. Conuella and G. Bichi, Boll. Chim. Farm., 122 (1983) 205.
6 J.M. Fernández Alvarez, A. Costa García, A.J. Miranda Ordieres and P. Tuñón Blanco, J. Electroanal. Chem., 225 (1987) 241.
7 N. Abo el Maali, J.C. Vire, G.J. Patriarche and M.A. Ghandour, Analusis, 17 (1989) 213.
8 J. Wang, D. Luo, P.A.M. Farias and J.S. Mahmoud, Anal. Chem., 57 (1985) 158.
9 C.F. Kolpin and H.S. Swofford, Jr., Anal. Chem., 50 (1978) 916.
10 A. Webber, M. Shah and J. Osteryoung, Anal. Chim. Acta, 154 (1983) 105.
11 J. Wang, D.B. Luo and P.A.M. Farias, J. Electroanal. Chem., 185 (1985) 61.
12 H.Y. Cheng, L. Falat and R.L. Li, Anal. Chem., 54 (1982) 1384.
13 E.N. Chaney and R.P. Baldwin, Anal. Chem., 54 (1982) 2556.
14 J. Wang and B.A. Freiha, Anal. Chem., 55 (1983) 285.
15 P. Tuñón Blanco, J.M. Fernández Alvarez and A. Costa García, in A. Ivaska, A. Lewenstam and R. Sara (Eds.), Contemporary Electroanalytical Chemistry, Plenum, New York, 1990, pp. 329–336.
16 Y. Asahi, Yakagaku Zasshi, 79 (1959) 1548.
17 K. Kretzschmar and W. Jaenicke, Z. Naturforsch., Teil B, 26 (1971) 225.
18 J. Lindquist and S.M. Farroha, Analyst, 100 (1975) 377.
19 E. Jacobsen and M.W. Bjornsen, Anal. Chim. Acta, 96 (1978) 345.
20 J. Wang, Int. Lab., 15 (1985) 68.
21 W.F. Smyth, Electrochemistry, Sensors and Analysis (Analytical Chemistry Symposia Series, Vol. 25), Elsevier, Amsterdam, 1986, p. 29.
22 E. Laviron, J. Electroanal. Chem., 63 (1975) 245.

Analytica Chimica Acta, 273 (1993) 383–390
Elsevier Science Publishers B.V., Amsterdam

Electrochemical detection of anabolics in human plasma and urine

R. Wintersteiger and M.J. Sepulveda

Institut of Pharmaceutical Chemistry, Karl Franzens University Graz, A-8010 Graz (Austria)

(Received 1st June 1992; revised manuscript received 4th November 1992)

Abstract

A new method for the analysis of anabolic hormones by reversed-phase liquid chromatography coupled with electrochemical detection has been developed. Testosterone and androsterone were derivatized into corresponding salicylic esters by treatment with salicylic acid chloride in the presence of 18-crown-6 and potassium carbonate as catalysts. Before derivatization, plasma and urine samples of the hormones were precleaned by solid-phase extraction using also reversed-phase material as a stationary phase. The derivatives were separated from the excess of reagent by column switching and were monitored amperometrically at 1000 mV vs. palladium in the oxidative mode.

Keywords: Liquid chromatography; Anabolic steroids; Androsterone; Pre-column derivatization; Plasma; Urine; Testosterone

The design and development of electrochemical detectors for liquid chromatography (LC) permit determination of trace amounts of electroactive materials. Therefore, electrochemical detection (ECD) can be used after chromatographic separation for the analysis of biological samples containing very low concentrations of analytes. Furthermore, endocrinology is one of the fields of medicine which has shown fast development during recent years. This fast progress would not have been possible without improvements in qualitative and quantitative techniques for hormone assay. Quantification of anabolic steroids represents a branch of steroid analysis with a wide field of applications such as sports [1], horseracing [2], in the residue determination of food from animals [3] and, of course, in biomedical and biochemical investigations [4]. Different methods based on coulometric titration [5], thin-layer chromatography (TLC) [6], gas chromatography [7], liquid chromatography [8] and enzyme-immunoassay [9] have been reported for steroids.

Reversed-phase LC coupled with electrochemical detection offers excellent sensitivity and selectivity for the quantification of compounds possessing a suitable redox center in their structures. Therefore, a four-stage procedure for the determination of testosterone and androsterone in biological matrices involving solid-phase extraction, pre-column derivatization, column switching and amperometric detection has been developed.

To increase the sensitivity and selectivity, salicylic acid chloride (SAC) is used as a new pre-column derivatization agent for the formation of electrochemically active derivatives with electrochemically inactive hormones having alcohols as functional groups.

Correspondence to: R. Wintersteiger, Institute of Pharmaceutical Chemistry, Karl Franzens University Graz, A-8010 Graz (Austria).

EXPERIMENTAL

Chemicals and solvents

Androsterone, testosterone, thionylchloride and 1,4,7,10,13,16-hexaoxacyclooctadecane (18-

crown-6), were purchased from Fluka (Buchs) and sodium salicylate from Herba (Graz). Potassium carbonate and lithium perchlorate trihydrate were of analytical grade from Merck (Darmstadt).

Benzene, methanol, acetone, all molecular sieve dried, glacial acetic acid and petroleum ether were also of analytical grade quality and used without further purification. For preparing mobile phases, water was deionized and distilled twice in a quartz still and further purified with a cartridge purification system (nanopure, Barnstead), specific resistance 18.3 MΩ cm.

Methanol for LC from Loba Chemie (Vienna) was doubly distilled. Plasma and urine from volunteers were stored in polypropylene containers at −20°C. Water and methanol were stored in glass containers. Bond-Elut C18 extraction columns (1 cm^3) were purchased from Analytichem (Harbor City, CA).

Standard solutions

Stock solutions of testosterone and androsterone were prepared in methanol. Working standards were prepared by diluting the stock solutions with methanol. The reagent solutions were prepared in dried benzene and stored in the refrigerator. Under these conditions the solutions were found to be stable for two weeks.

Apparatus

The LC system consisted of an LDC Milton Roy Consta-Metric 3000 solvent delivery system pump with a pulse damper. Manual injection was carried out using a Rheodyne injection valve Model 7125 with a 20-μl loop. The detection was performed with an LKB (Bromma) 2143 electrochemical detector, with a glassy carbon electrode, at +1.0 V vs. palladium. Output signals were monitored by a Perkin Elmer Model 56 recorder.

For column switching an additional LDC Milton Roy miniPump VS metering pump and a Rheodyne switching valve Model 7010 were used. (The Rheodyne Model 7010 was converted to the Model 7000 switching valve by removing the loop.)

The detector is housed in a Faraday cage protected from external influences. For sample clean up a Vac-Elut station from Analytichem was used.

Chromatographic conditions

LC analyses were performed at room temperature on a 5 × 4 mm Knauer pre-column, packed with 35–40 μm RP8 Perisorb from Merck and a Brownlee RP8 analytical column, Spheri 5, 100 × 4.6 mm i.d., cartridge system.

The mobile phase consisted of methanol–water (70:30, v/v), 2 g lithium perchlorate trihydrate and 2 ml glacial acetic acid per litre, a flow-rate of 1.0 ml min^{-1} was employed. The washing phase consisted of methanol–water (30:70, v/v), flow-rate 0.8 ml min^{-1}. Mobile phase and washing phase were filtered through a 0.45-μm Millipore filter and degassed by purging with helium for 5 min and by an ultrasonic bath before use.

Synthesis of salicylic acid chloride (SAC)

27.5 g of freshly distilled thionylchloride were dissolved in 30 ml dried benzene. The solution was cooled with ice and stirred. A tube of calcium chloride was utilized to exclude humidity. 25 g of sodium salicylate were added under stirring and nitrogen atmosphere.

The mixture was kept in an icebath for 1 h, and excess of thionylchloride and benzene were removed by vacuum distillation.

50 ml of dried petroleum ether were added and stirred for 15 min. The mixture was centrifuged and the petroleum phase was separated and evaporated. The residue (SAC) was dissolved in dried benzene.

Derivatization procedure

The derivatization reaction was carried out in 500-μl conical vials containing about 5 mg of potassium carbonate, shaking 50 μl of SAC solution (0.2 M) with 50 μl of 18-crown-6 solution (0.25 M) and with 50 μl of a solution containing the hydroxy compound to be derivatized. The mixture was left to stand at 70°C in a pre-heated oven for 1 h. The reaction mixture was left to cool at room temperature and centrifuged.

RESULTS AND DISCUSSION

Derivatization

To determine steroids with high sensitivity and selectivity it is often necessary to derivatize by

means of appropriate reagents. But many of these substances possess an alcoholic hydroxyl function which is less reactive and electrochemically inactive. To enable electrochemical detection of this important class of compounds we planned to introduce a phenolic hydroxyl group into the molecule as an electrofunctional component. For this purpose salicylic acid chloride was synthesized as a derivatization agent for the quantification of anabolic steroids in biological materials using testosterone and androsterone as model substances. The reaction scheme is given in Fig. 1.

To optimize derivatization conditions with respect to reaction medium, reaction time, temperature, influence of catalyst or excess of reagent, a special procedure explained in the experimental section was carried out. 120 μl of the reaction mixture were evaporated under nitrogen and the residue was redissolved in 100 μl of methanol, or even better in 100 μl of the mobile phase. It was possible to detect picomoles of the testosterone derivative and of the androsterone derivative amperometrically at +1.0 V working potential when 20 μl of this solution were injected.

Column switching

A limiting factor to achieve high sensitivity in derivatization methods is often the requirement of high quantities of reagent compared to the analyte. If very low concentrations of derivatives are to be detected the detector signal has to be strongly amplified, the excess of reagent produces a great peak overlapping the derivative peak. Moreover, overloading of the electrochemical detector may occur, causing problems in the evaluation of the data. Therefore a long time is needed to stabilize the electrode in order to avoid incorrect quantification. The excess of reagent has to be the higher the lower the concentration of the analyte is, otherwise loss of sensitivity is unavoidable. For instance, to derivatize picogram amounts of analyte with nanogram amounts of SAC, a more than 1000-fold excess of reagent is necessary to obtain a sufficient reaction rate. Because it is impossible to separate such enormous

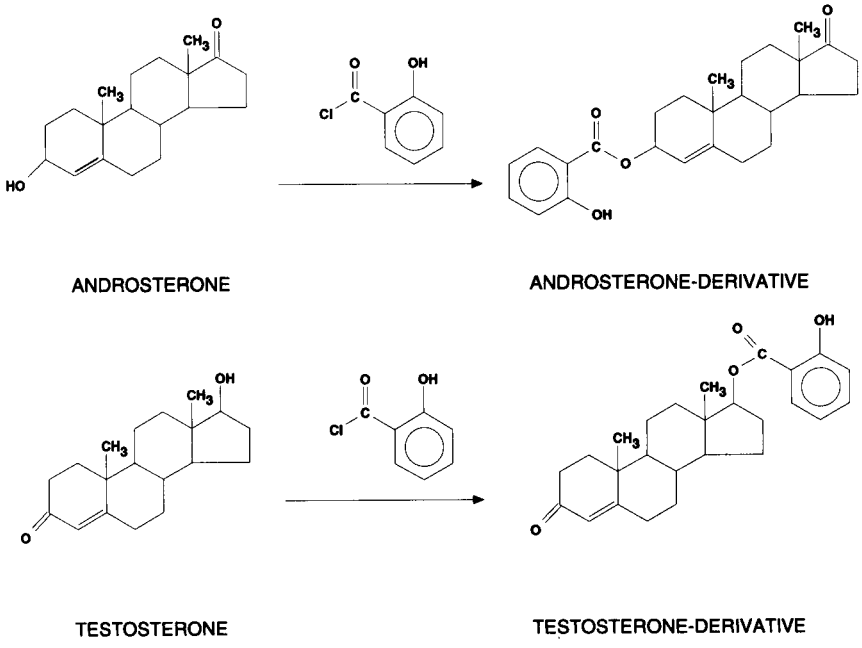

Fig. 1. Reaction scheme for the formation of androsterone- and testosterone-derivative with SAC.

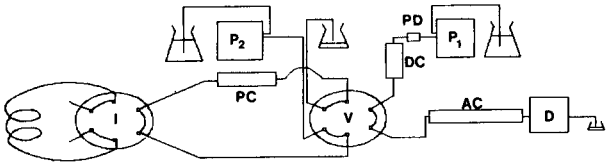

Fig. 2. Scheme of equipment used for column switching. P_1, P_2 = Pumps; PD = pulse damper; DC = pulse dampening column; I = injection valve; V = switching valve; PC = precolumn; AC = analytical column; D = detector.

amounts of reagent from the derivative by classical extraction methods, it was tried to overcome this problem by column switching. Figure 2 illustrates the system used.

The process of column switching consists of four steps: (i) Filling the loop and at the same time cleaning the pre-column with a washing phase, (ii) switching the injection valve from load to inject. The sample is transferred to the precolumn; testosterone and androsterone derivative are retarded and excess of reagent and secondary products are directed to waste, (iii) switching the injection valve after 15–30 s to load position. This is not so important when employing a 20-μl loop, but if for reasons of sensitivity upto 1-ml loops should be used, the volume of washing phase running through the detector cell has to be reduced. Moreover, a great initial peak caused by the difference in polarity between washing and mobile phase may interfere with the chromatographic separation of the analytes, (iv) switching the V-valve after 8 min of washing process. The precleaned sample is transferred onto the analytical column on which the final separation of derivatives and other products is performed.

Using this technique an extremely high molar excess of reagent can be removed almost quantitatively.

Determination in plasma and urine

In order to determine testosterone and androsterone in biological materials an effective sample pretreatment is necessary. Otherwise, numerous electroactive endogenous substances which are also oxidizable at the detection potential may interfere.

Bond-Elut C18 columns were mounted on a specially designed vacuum manifold station which can process ten extraction columns simultaneously. It was convenient to place disposable syringes without plunger on top of the cartridges as reservoirs for sample and washing solutions.

The extraction cartridges were conditioned by washing with 2×0.5 ml of methanol and 2×0.5 ml of water. 1 ml of steroid spiked plasma or urine samples containing the analytes were diluted with 1 ml water and added onto the columns and allowed to adsorb for 2 min before washing twice with 1 ml of water followed by two 1-ml washes with 10% methanol. For collection of probes conic ampules were inserted and 1 ml of methanol was passed through the columns under vacuum. The eluent was carefully dried by a stream of nitrogen.

The residue was redissolved in 50 μl dried benzene for the following derivatization procedure.

For the determination of recoveries calibration curves were prepared by adding working stan-

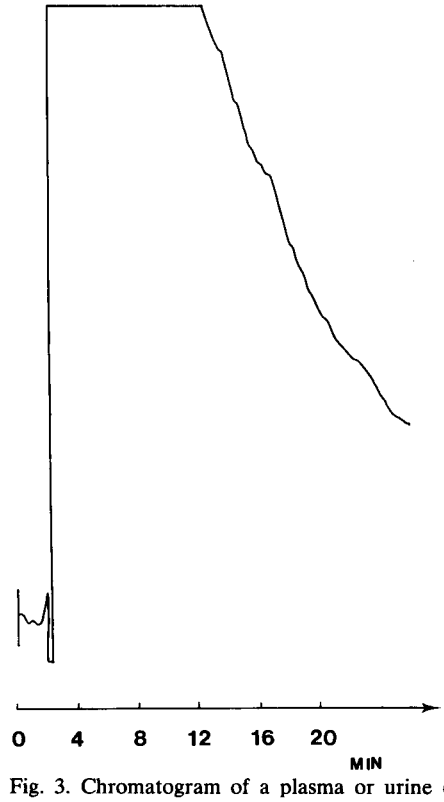

Fig. 3. Chromatogram of a plasma or urine extract without column switching.

TABLE 1

Calibration graphs for the testosterone- and for the androsterone-derivative at a potential of +1.0 V vs. palladium

	Testosterone in plasma			Androsterone in urine		
	Mean	Standard deviation	Standard error	Mean	Standard deviation	Standard error
Slope	0.1651067	6.119402×10^{-4}	3.533038×10^{-4}	0.2977009	8.683715×10^{-4}	5.013545×10^{-4}
y intercept	0.1974963	2.554166×10^{-3}	1.474648×10^{-3}	0.692574	1.983809×10^{-2}	1.145352×10^{-2}
x intercept	1.19621	1.873611×10^{-2}	0.0108173	−2.326448	0.684215	3.950317×10^{-2}

dards (100 μl) to 1.0 ml of plasma or urine diluted with 1.0 ml of water in the range of 12.5–1000 ng ml^{-1} plasma for testosterone and 25–1000 ng ml^{-1} urine for androsterone. For the blank sample 100 μl of dried methanol were added instead of working standards.

As described above, utilizing the column switching technique only the relevant part of the sample is transferred to the analytical column rendering feasibly easy separation of derivatives from byproducts. Figures 3–5 show the difference in the analysis of testosterone and androsterone in plasma and urine with and without column-switching. However, in spite of sample precleaning the working electrode may be fouled by interfering substances from the biological material at the relatively high voltage applied for detection. This results in a gradual decay in detector sensitivity and in long equilibration times. To avoid this effect it is advisable to clean the electrode

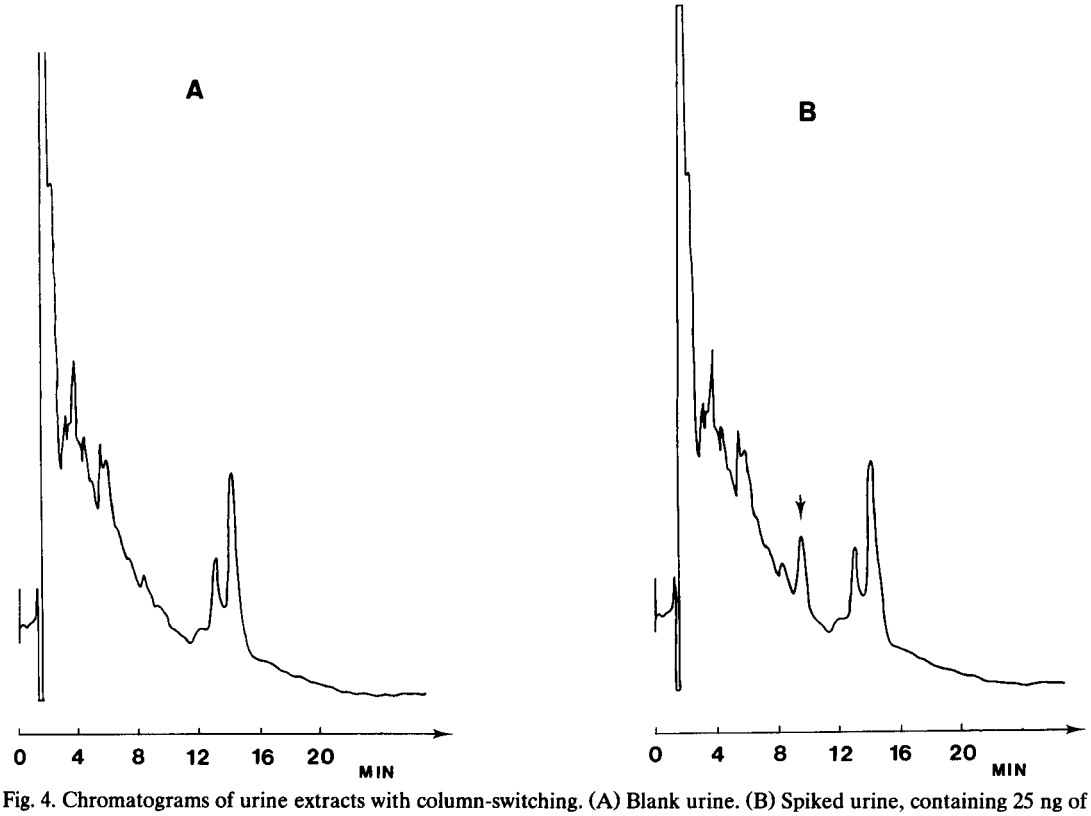

Fig. 4. Chromatograms of urine extracts with column-switching. (A) Blank urine. (B) Spiked urine, containing 25 ng of androsterone per ml.

with a cotton cloth, to wash with dichloromethane and to replace the spacer. This operation takes only a few minutes but several hours are required to obtain a linear baseline. Furthermore, to stabilize the background current it seems recommendable to equilibrate the chromatographic system by recycling with mobile phase for one day before the injection of biological samples.

Calibration and linearity

Table 1 shows the calibrations graphs for the determination of testosterone in plasma and androsterone in urine in the range of 12.5–1000 ng ml^{-1} and 25–1000 ng ml^{-1}, respectively. Each concentration level consisted of replicate determinations ($n = 3$) performed on different days. The calibration curves, based on the electrochemical response and peak-height measurements, were found to be linear with a correlation coefficient of 0.999 for both steroids and with intercepts which were not significantly different from zero. Equations of the calibration lines were $y = 0.1654418x + 0.1946294$ and $y = 0.2986737x +$

TABLE 2

Extraction of testosterone in plasma and androsterone in urine

Testosterone in plasma		Androsterone in urine	
Amount (ng ml^{-1})	Recovery (%)	Amount (ng ml^{-1})	Recovery (%)
1000	96.9	1000	97.1
500	96.4	500	94.5
250	96.1	250	96.3
125	95.5	125	91.7
100	94.1	100	88.6
80	91.6	80	84.2
50	87.5	50	82.3
25	83.3	25	81.6
12.5	85.7	– [a]	– [a]

[a] Detection not possible.

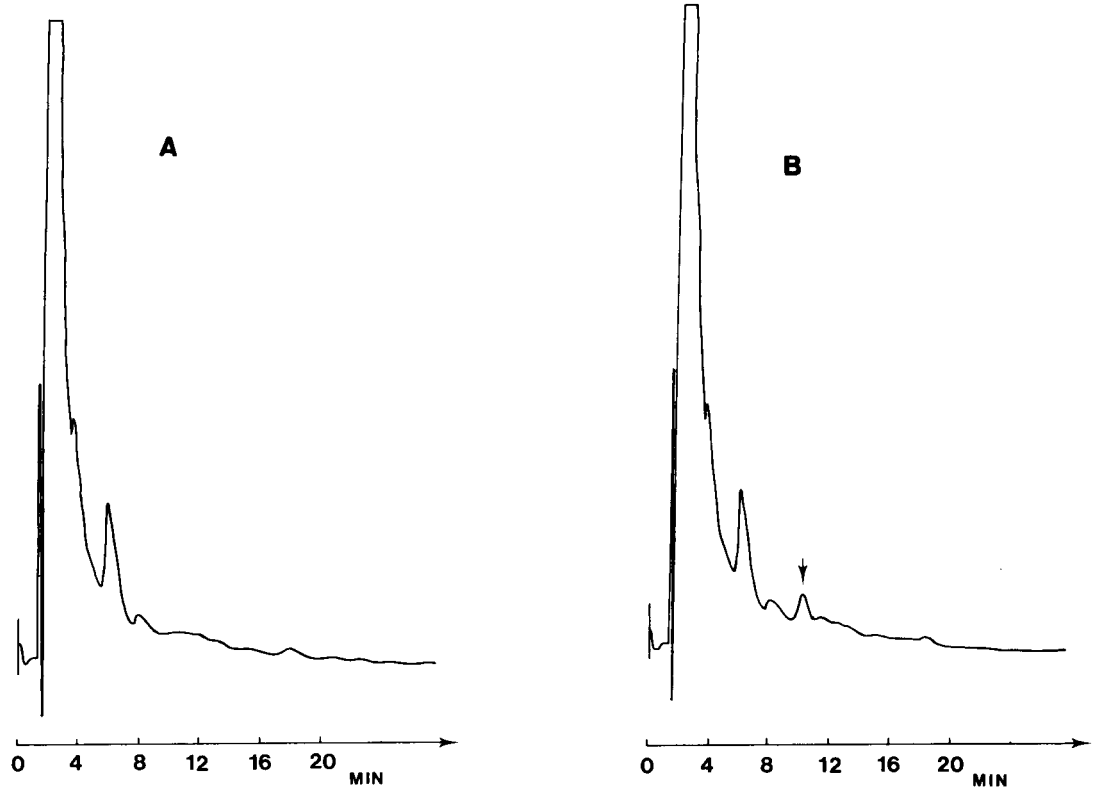

Fig. 5. Chromatograms of plasma extracts with column-switching. (A) Blank plasma. (B) Spiked plasma, containing 12.5 ng of testosterone per ml.

TABLE 3

Intra- and inter-assay variability for the measurement of spiked plasma and urine samples

	Testosterone in plasma ($n = 10$)			Androsterone in urine ($n = 5$)		
	Added (ng ml^{-1})	Found ± S.D. (ng ml^{-1})	C.V. (%)	Added (ng ml^{-1})	Found ± S.D. (ng ml^{-1})	C.V. (%)
Intra-assay	110	112.2 ± 1.45	7.9	120	124.7 ± 3.1	3.2
Inter-assay	125	126.93 ± 1.95	7.8	120	136.2 ± 3.8	4.0

0.6936097 for testosterone and androsterone, respectively.

Recovery

Table 2 presents the recovery of testosterone in plasma, and of androsterone in urine. As indicated in this table, the recovery was not 100%, but high enough to determine the steroids at the nanogram level in biological matrices.

When the columns are washed with a higher percentage of methanol (for example 30% instead of 10%, v/v) or when the washing phase necessary for the column switching has also a higher percentage of methanol, the recovery of the extraction of these steroids decreases significantly. Further decrease of the recovery may be observed, when the time of the washing procedure takes more than 8 min.

Reproducibility and accuracy

The reproducibility and the accuracy were evaluated from spiked control plasma samples with intra- and inter-assay variability. The within- and between-run reproducibility are given in Table 3. The results were obtained by direct comparison of the responses with the calibration curve of the non-extracted standard solutions of testosterone or androsterone. The relative standard deviations are well acceptable for biological samples.

Conclusions

The LC–ECD method has been proposed for the analysis of anabolic steroids in plasma and urine. Testosterone and androsterone were used as model substances and could be transformed by pre-column derivatization into electrochemically active derivatives. SAC, which easily can be synthesized from salicylic acid and thionylchloride, proved to be an appropriate electrophore and a reactive reagent. 300 pg of testosterone and 600 pg of androsterone can be detected per injection.

To minimize the effect of interfering byproducts from the biological matrix, the first step of the procedure contains sample precleaning by solid-phase extraction. Intensive drug binding by primary interaction could be observed with C18 reversed-phase material and after a washing process, elution of anabolics was performed with methanol. Subsequent to derivatization and injection of the reaction mixture, the technique of column switching was utilized successfully to remove excess of reagent which is necessary to derivatize picomole amounts of anabolics. Detection is carried out at 1000 mV vs. palladium in the oxidative mode using an amperometric detector. Detection at higher working potentials may further enhance sensitivity. The application of the present method to the quantification of various hydroxysteroids will be reported in a future paper.

REFERENCES

1 L. Goldberg, E. Bosworth, D. Elliot and R. Bents, New Engl. J. Med., 322 (1990) 775.
2 P. Teale and E. Houghton, Biol. Mass Spectrom., 20 (1991) 109.
3 L.A. van Ginkel, R.W. Stephany, H.J. van Rossum, H.M. Steinbuch, G. Zomer, E. van de Heeft and A.P.J.M. de Jong, J. Chromatogr., 489 (1989) 111.
4 W. Malarkey, R. Strauss, D. Leizman, M. Liggett and L. Demers, Am. J. Obstet. Gynecol., 165 (1991) 1385.

5 K. Nikolic, Pharmazie, 44 (1989) 350.
6 R. Wintersteiger and E. Gamse, Advances in Steroid Analysis, Elsevier, Amsterdam, 1982, p. 453.
7 G. Cartoni, M. Ciardi, A. Giarrusso and F. Rosati, J. High Resolut. Chromatogr. Chromatogr. Commun., 8 (1985) 539.
8 E.H.J.M. Jansen, R.H. van den Berg and R. Both-Miedema, J. Chromatogr., 489 (1989) 57.
9 G. Degand, J. Frere, J. Gosling, W. Abdulabad, G. Maghuinrogister and P. Schmitz, Biochem. Soc. Trans., 17 (1989) 604.

Analytica Chimica Acta, 273 (1993) 391–398
Elsevier Science Publishers B.V., Amsterdam

Electrochemical study of the oxidation of carbidopa and its determination using liquid chromatography with electrochemical detection

P. Tömpe, A.N. Halbauer and L. Ladanyi

EGIS Pharmaceuticals, P.O. Box 100, H-1475 Budapest (Hungary)

(Received 1st June 1992; revised manuscript received 25th September 1992)

Abstract

The electrochemical oxidation of carbidopa [(*S*)-(−)-2-(3,4-dihydroxybenzyl)-2-hydrazinopropionic acid monohydrate] was studied by linear sweep voltammetry, cyclic voltammetry, microcoulometry and preparative electrolysis. An ECCE mechanism with two-electron transfer, followed by two chemical reactions (decarboxylation and hydrolysis), were found, giving carbon dioxide, hydrazine and 3,4-dihydroxyphenylacetone. The final electrochemical step may be a reversible two-electron oxidation process which gives the *o*-quinoidal analogue of the latter. An analogous oxidation mechanism was found when carbidopa was oxidized with $HBrCl_2$ in hydrochloric acid.

Keywords: Liquid chromatography; Voltammetry; Carbidopa; Electrochemical oxidation; Pharmaceuticals

N-Amino-α-amino acids (α-hydrazino acids) are of considerable interest as biologically active amino acid analogues. The conversion of α-methyldopa (AMD) into its hydrazino analogue is an example of such molecules. Carbidopa (I) [(*S*)-(−)-2-(3,4-dihydroxybenzyl)-2-hydrazinopropionic acid monohydrate] (CD) is an aromatic acid decarboxylase inhibitor. It has been used extensively in the therapy of Parkinson's disease as a means of inhibiting the extracerebral metabolism of L-Dopa (LD) and thus decreasing the dosage requirement of LD and possibly therefore decreasing those side effects which are the consequence of too high levels of the amino acid in the periphery [1]. Pharmaceutical preparations containing LD which are used in substitution therapy of Parkinsonism, contain also 10–25% of carbidopa as an adjuvant [Sinemet-275 and Sinemet-Plus tablets (Merck Sharp & Dohme, Hoddesdon, UK), Isicom 25/250 tablets (VEB Isis-Chemie, Zwickau, Germany) and Duellin tablets (EGIS, Budapest)].

Correspondence to: P. Tömpe, EGIS Pharmaceuticals, P.O. Box 100, H-1475 Budapest (Hungary).

CD is absorbed readily but incompletely after oral administration. About 50% of an oral dose is excreted in the urine in 48 h; 60% of the urinary material are metabolites and these are excreted mainly as glucuronide conjugates (Scheme 1). Among the metabolites about 10–14% is 2-(3-hydroxy-4-methoxybenzyl)propionic acid (M_1 in Scheme 1), 10% is 2-(3,4-dihydroxybenzyl)propionic acid (M_3), 10% is 2(3-hydroxybenzyl)propionic acid (M_2) and 5% is 3,4-dihydroxyphenylacetone (DHPA; II) [2].

With some catecholamine derivatives, DHPA can also be formed by chemical oxidation. Slates et al. [3] isolated DHPA formed in the oxidation of α-methyldopa in alkaline solution by hypochlorite. DHPA was possibly formed in this case by *N*-chlorination. Vickers et al. [1], using GC–MS,

also reported the formation of DHPA during the metabolism of CD. In this work, the electrochemical oxidation of carbidopa and its determination by liquid chromatography with electrochemical detection (LC–ED) was studied.

EXPERIMENTAL

Apparatus

The LC–ED system consisted of a Model PU-4010 solvent-delivery pump (Pye Unicam), a

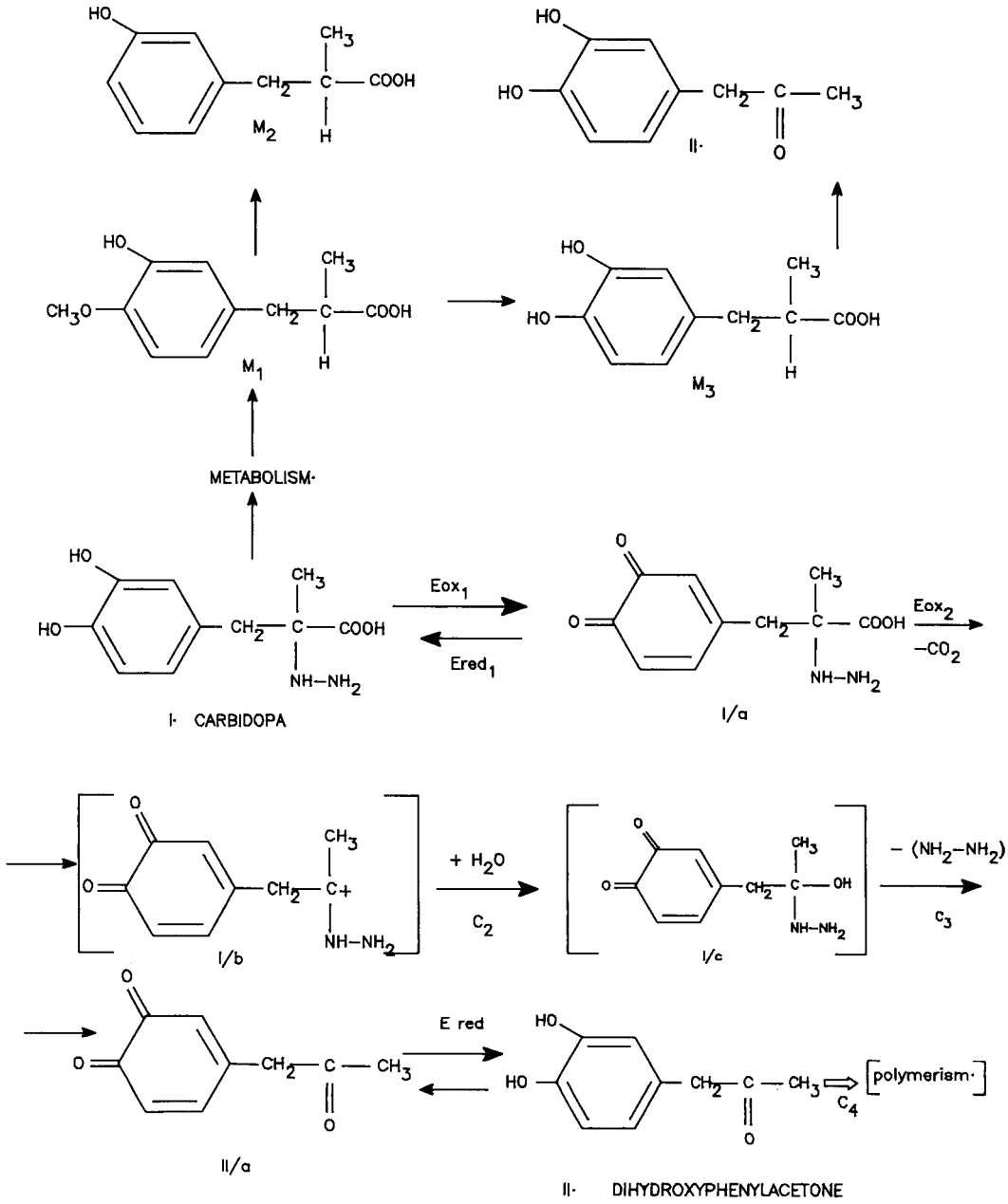

Scheme 1.

Model 7125 syringe sample injector with a 100-μl sample loop (Rheodyne) a Model CC-4 amperometric electrochemical detector (Bioanalytical Systems) and a Model PRG-DEL potentiostat (Tacussel). The columns used were a Pelliguard LC-18, 5 cm (Supelco), as the precolumn and a Nucleosil 5 C_{18}, 125 mm length, 8 mm o.d. and 4 mm i.d. (Macherey–Nagel), as the analytical column. Peak areas and peak heights were calculated using a Model C-R6A integrator (Shimadzu).

Mass spectra were obtained on a Model MS-25-RFA mass spectrometer (Kratos) by direct introduction of the sample using electron impact (EI) and chemical ionization (CI) with isobutanol as reaction gas.

Voltammetric experiments were conducted on a Metrohm system, including a Model 506 and 626 Polarecord, E-608 Programmer, E-612 VA scanner and E-478 Labograph.

The coulometric and preparative electrolysis system consisted of a Model OH-404/C,I potentiostat and Integrator (Radelkis) with a platinum net as the working electrode (geometrical surface area 0.4 dm^2).

Absorbance spectra were measured on an SP8–150 UV–visible spectrophotometer (Pye Unicam).

Chemicals

Unless stated otherwise, all chemicals and reagents were obtained from Merck and were of the highest purity available. 3-(3,4-dihydroxyphenyl)-L-alanine (levodopa, LD), carbidopa (CD) and 3-(3,4-dihydroxyphenyl)-2-methyl-L-alanine (AMD) were obtained from EGIS Pharmaceuticals (Budapest) and 3,4-dihydroxybenzylamine hydrobromide (DHBA) and 3-(3,4-dihydroxyphenyl)propionic acid (hydrocaffeic acid, HCA) from Aldrich.

Stock standard solutions were prepared on a daily basis in doubly deionized water obtained with a Milli-Q system (Millipore). Solutions of lower concentrations were prepared by diluting the stock solutions with an aqueous medium. The LC mobile phase (0.100 M $NaH_2PO_4 \cdot H_2O$–0.020 M citric acid–1.25 mM sodium octanesulphonate–0.150 mM disodium EDTA in 8% methanol; pH adjusted to 3.2 with 10% NaOH) was prepared according to Nissinen and Taskinen [4].

Electrochemistry

Cyclic voltammetry (CV) was performed on 1 mM sample solutions diluted with 0.1 M perchloric acid, using either carbon paste or glassy carbon as the indicator electrode. The product of electrooxidation was strongly adsorbed on the electrode surface, which had to be regenerated after every cycle.

Microcoulometric measurements on carbidopa stock solution were performed with a three-electrode system using a platinum net or carbon paste with a high surface area as the working electrode. The cathode was separated from the main compartment with a glass diaphragm. A Metrohm EA-996–20 electrochemical cell was used.

Constant-potential electrolysis on a platinum net was used to determine the number of electrons involved in the electrode process. Differential-pulse voltammograms were obtained for CD stock solutions over the range 10 μM–10 mM, using a carbon paste working electrode, polarized from -400 to $+1200$ mV.

Electrochemical synthesis of DHPA

DHPA was prepared by electrooxidation of CD in acidic media according to the coulometric method, e.g., with 200 ml of 1 mM CD stock solution being oxidized at $+1200$ mV using a platinum net working electrode. All the CD was oxidized in about 6 h and the formation of the oxidized product was monitored by LC. The electrooxidation product was then extracted from the reaction mixture with dichloromethane and the carbon dioxide formed was detected with barium hydroxide and hydrazine (also formed) with 3,4-dimethylaminobenzaldehyde [5].

Extraction of DHPA. A 100-ml volume of electrolysed stock solution was extracted with 2×25 ml of dichloromethane and the combined organic phase was dried over anhydrous sodium sulphate, then the solvent was evaporated at 20 mmHg. The remaining dried material was identified by mass spectrometry.

Detection of carbon dioxide. A 10-ml [illegible] the aqueous phase was neutr

sodium hydroxide and the hydrocarbonate ions formed were detected with barium hydroxide (formation of barium carbonate).

Detection of hydrazine. A 10-ml volume of 3,4-dimethylaminobenzaldehyde reagent solution, made according to Deutsches Arzneibuch 10.VII.1.1, was added to 50 ml of the aqueous phase. This solution was allowed to stand for 1 h, then the aldazine formed was extracted with 25 ml of dichloromethane. The organic phase was dried, then concentrated to a volume of 1 ml and a 5-μl portion of this was examined by thin-layer chromatography (TLC). Blank and reference solutions (CD, AMD and hydrazine hydrate) were also examined. For TLC, Kieselgel GF_{254} plate (100 × 200 mm) (Merck) was used with benzene–methanol (80 + 20) as the mobile phase and detection with UV radiation at 366 and 254 nm and with Dragendorff reagent, according to DAB 10.VII.1.1. The TLC spots were extracted from the plate with 2 ml of ethanol and the UV absorption spectra of the solutions were measured in a 0.2-cm quartz cell using ethanol as the blank.

Chemical synthesis of DHPA

DHPA can be obtained by chemical oxidation as follows. A 24.4-g (0.10-mol) amount of carbidopa was dissolved in 45 ml of 4 M HCl, then 11.414 g (0.410 mol) of $KBrO_3$ and 16.265 g (0.410 mol) of KBr dissolved in 400 ml of water were added in about 1 h with vigorous stirring and continuous cooling with ice. The reaction mixture was extracted with 2 × 150 ml of ethyl acetate, the organic phase was washed with 2 × 50 ml of water, dried over anhydrous sodium sulphate and evaporated under vacuum. A yellow oily product was obtained (yield 9.13 g = 55%).

Structure identification of DHPA

Structure identification was made by mass spectrometry (positive-ion EI and CI) with electron energy 70 eV, accelerating voltage 4 kV, emission current 100 μA and sample temperature 280°C. For silanization of DHPA 100 mg of DHPA were weighed into a PTFE-stoppered reaction vessel and 3 ml of N,O-bis(trimethylsilyl)-acetamide (BSA) reagent were added. This solution was kept at 70°C for an 1 h. MS identification was made directly on the sample taken from the reaction mixture. Elemental analysis: calculated for $C_9H_{10}O_3$ molecular weight 166.00), C 65.06, H 6.02, O 28.92; found, C 65.11, H 6.22, O 29.02%.

LC conditions

For the investigation of tablets containg LD and CD (Sinemet), for monitoring the formation of DHPA in different dosage forms (tablets and solutions) and for the investigation of the reaction mixture, the LC–ED method of Nissinen and Taskinen [4] was used, with the columns and

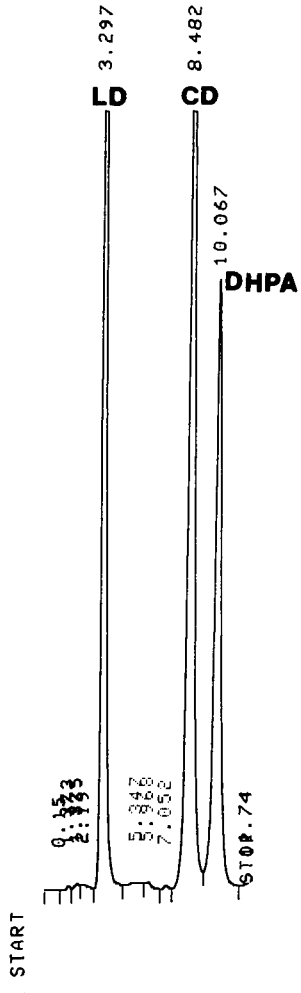

Fig. 1. Typical LC–ED trace for a standard solution of LD, CD and DHPA.

mobile phase specified under Experimental. This procedure can also be used for bioavailibility studies. In this case AMD or DHBA can be applied as an internal standard (see Fig. 2).

RESULTS AND DISCUSSION

Typical LC traces are shown in Figs. 1 and 2.

The cyclic voltammograms of LD, AMD and DHBA correspond to a quasi-reversible, two-electron transfer process (Fig. 3A), whereas that of CD shows irreversible electron transfer with two oxidation peaks (CD_2 and CD_1 in Fig. 3B).

The scan rate of polarization has no effect on the shape of the cyclic voltammograms of CD. On reversing the scan direction after peak I (CD_2), no cathodic peak corresponding to a reversible process was found (Fig. 3B).

The cyclic voltammogram of CD is different from those of analogous catecholamines. Rapid and reversible electrooxidation cannot be observed and, for this reason, the oxidation mechanism must be different from that described by Young and co-workers [6,7].

Figure 4 shows the differential-pulse voltammogram for equivalent concentrations of CD and LD solutions. It seems that the second oxidation process of CD (E_p = +980 mV) (peak II) corresponds to a one-step electrode process (peak I).

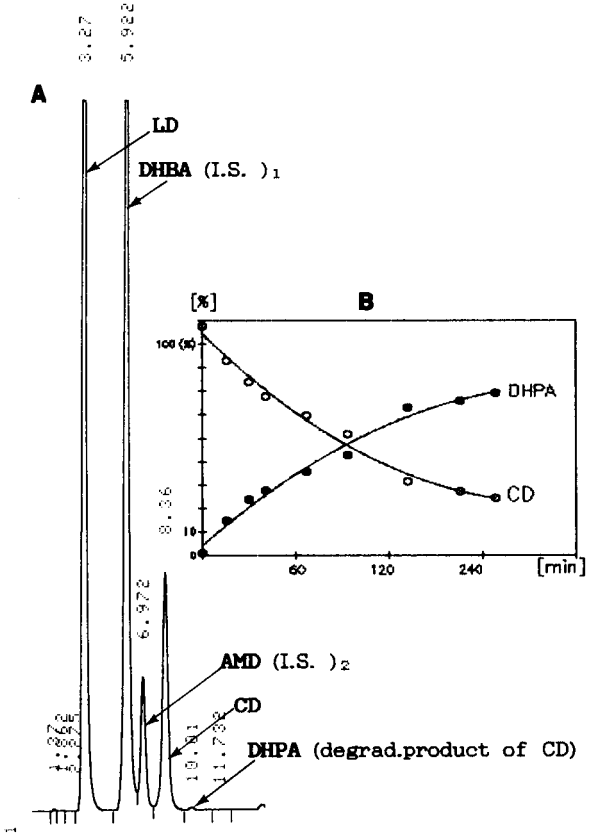

Fig. 2. (A) Typical LC–ED trace for LD, CD, DHBA as $I.S._1$ (internal standard), AMD as $I.S._2$ and DHPA. (B) Detection of decomposition of CD in acetate buffer solution (4×10^{-5} M) at pH 7.40 using LC–ED.

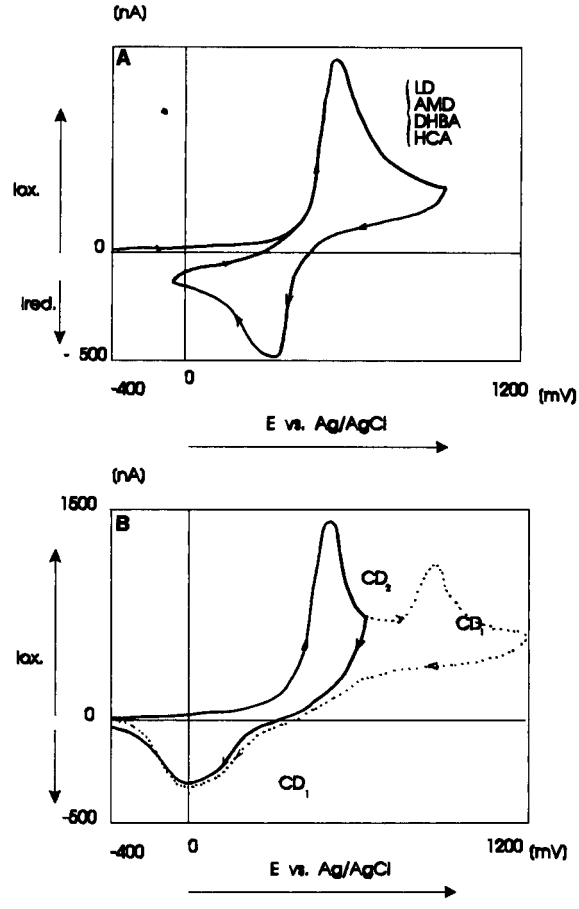

Fig. 3. (A) Cyclic voltammograms of 1 mM LD, DHBA, AMD and hydrocaffeic acid (HCA) and (B) 1 mM CD obtained with a carbon paste electrode. Scan rate, 60 mV s^{-1}; electrolyte, 0.1 M perchloric acid. CD_1, reversal of the scan after second oxidation step (+1200 mV); CD_2, reversal of the scan after first oxidation step (+800 mV).

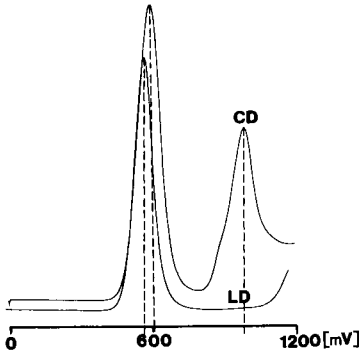

Fig. 4. Differential-pulse voltammogram of 1 mM CD and LD in 0.1 M perchloric acid, obtained with a carbon paste electrode. Scan rate, 10 mV s^{-1}.

The peak height was proportional to the concentration of CD. Linear calibration graphs for *peaks I* and *II* of CD were obtained over the range 10 μM–10 mM with the following regression parameters: for peak I, slope = 355 mAl $mmol^{-1}$, intercept = 5.24 mA, $r = 0.9995$, R.S.D. = 6.7% ($n = 5$); and for peak II, slope = 260 mA l mol^{-1}, intercept = 22.2 mA, $r = 0.9895$, R.S.D. = 7.4% ($n = 5$). Above 100 μM loss of linearity was observed for Peak II, perhaps owing to filming at the electrode surface. This method can be used to determine the amount of CD in the presence of LD.

The second electrochemical oxidation step can be observed on both the cyclic and differential-pulse voltammograms (Fig. 4) and the reaction products DHPA, carbon dioxide and hydrazine can be detected by chemical methods. These products were obtained by potentiostatic preparative electrolysis and the number of electrons involved (four) was measured by coulometry. The positive barium hydroxide test ($BaCO_3$ precipitate formation) proves the formation of carbon dioxide as a result of the decarboxylation process.

The positive test with 3,4-dimethoxybenzaldehyde (colour reaction) and the subsequent TLC test showed that the same product was obtained as formed in the reaction of hydrazine hydrate with 3,4-dimethyl-aminobenzaldehyde (aldazine). The R_F values obtained were as follows: 3,4-dimethylaminobenzaldehyde blank, 0.65 (fluores-

TABLE 1

MS spectral data

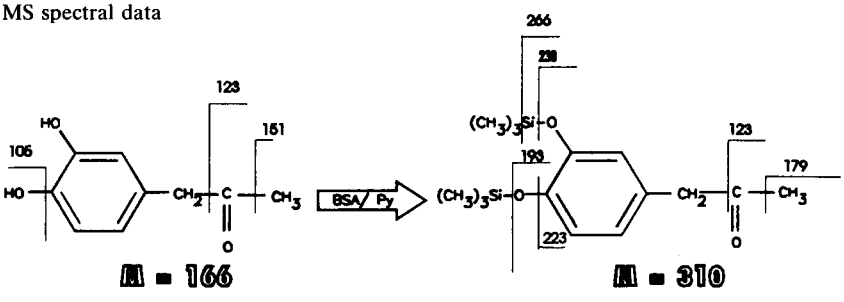

Starting compound			Product		
m/z	Relative intensity [a]		*m/z*	Relative intensity [a]	
	EI	CI		EI	CI
167	2	100	311	–	39
166	12	20	310	17	4
151	2	11	267	68	26
150	< 1	2	239	–	100
123	100	25	238	13	19
105	4	–	223	–	31
			195	30	26
			179	100	30
			123	47	23

[a] Percentage of base peak.

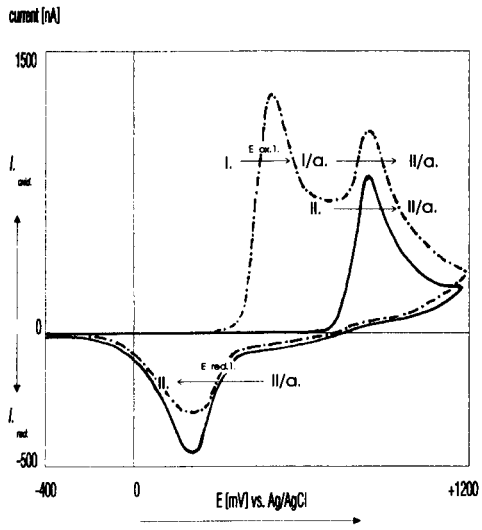

Fig. 5. Cyclic voltammogram of 1 mM DHPA (II) and CD (I) obtained with a carbon paste electrode. Scan rate, 60 mV s^{-1}; electrolyte, 0.1 M perchloric acid.

cence at 254 nm); aldazine reference product, 0.85 (fluorescence at 366 nm); carbidopa reaction product, reference, 0.45 (fluorescence at 254 mn); AMD reaction product, reference, 0.40 (fluorescence at 254 nm); and extracted electrolysis product, 0.85 (fluorescence at 366 nm).

The structure of the organic product obtained by preparative electrolysis was investigated by mass spectrometry and the results are given in Table 1. Identical mass spectra and fragmentation patterns were obtained for the product prepared by chemical oxidation of CD by $HBrCl_2$. The structure of this oxidation product was identified as 3,4-dihydroxyphenylacetone (DHPA).

As can be seen in Fig. 5, DHPA gives an anodic peak at +900 mV (II → IIa) and a cathodic wave at ca. +200 mV (IIa → II), which is probably due to the reduction of DHPA-quinone (IIa). The cyclic voltammogram characterizes an irreversible two-electron charge-transfer process.

The decarboxylation and hydrolysis are rapid chemical reactions, and neither the quinoidal form (Ia) nor 3,4-dihydroxyphenylpropionic acid (M_3 in Scheme 1) can be detected. The latter would present a reversible cyclic voltammogram anyway (Fig. 3). Moreover, it can be assumed that 3,4-dihydroxyphenylpropionic acid was not formed at all because it could not be detected in the reaction mixture.

Instead, a decarboxylation process occurs in the first chemical step (C_1) to give Ib. This theory is supported by the formation of a stable carbocation [8,9]. In this case the carboxyl group is eliminated as carbon dioxide. Water can also react with this carbocation to give the hydroxy compound Ic, from which hydrazine is eliminated giving the quinoidal form of DHPA (IIa in Scheme 1). IIa can also be formed from DHPA (II in Scheme 1) by oxidation (Fig. 5). DHPA, however, is unstable and can easily be polymerized when heated or treated by bases to give a dark melanin-like product. When using $KBrO_3$, KIO_3 or NaOCl as oxidizing agent, polymerized melanin-type products were always obtained.

The chemical and electrochemical oxidations of CD show some similarity to the metabolic pathway. In all instances one of the main products is DHPA or a melanin-like polymerization product of the latter. The mechanism of the enzymatic metabolism (in which the hydrazino group is eliminated before the decarboxylation step giving elementary nitrogen) is different from that of the chemical and electrochemical oxidation [10]. The final product, however, is DHPA in all instances [1].

The formation of a stable quinoidal form as an intermediate (Ia in Scheme 1) cannot be proved owing to the subsequent chemical and electrochemical reactions ($E_{ox.2}$, C_1 and C_2 in Scheme 1). The formation of DHPA from CD is always possible when the latter is metabolized and also when CD is allowed to stand in solution. It was found by LC–ED that manufactured batches of carbidopa always contain about 0.03% of DHPA as an impurity.

REFERENCES

1 S. Vickers, E.K. Stuart, J.R. Bianchine, H.B. Hucker, M.E. Jaffe and R.E. Rhodes, Drug Metab. Dispos., 2 (1974) 9.
2 A.E. Moffat (Ed.), Isolation and Identification of Drugs, Pharmaceutical Press, London, 1986, p. 432.
3 H.L. Slates, D. Taub, C.H. Kuo and N.L. Wendler, J. Org. Chem., 29 (1964) 1424.
4 E. Nissinen and J. Taskinen, J. Chromatogr., 231 (1982) 459.

5 B. Kakac and Z.J. Vejdalek, Handbuch der Photometrischen Analyse Organischer Verbindungen, Band 1, Verlag Chemie, Weinheim, 1974 p. 597.
6 T.E. Young, B.W. Babbitt and L.A. Wolfe, J. Org. Chem., 45 (1980) 2899.
7 T.E. Young and B.W. Babbitt, J. Org. Chem. 48 (1983) 562.
8 N.L. Weinberg, Techniques of Chemistry, Vol. V, Part I, Wiley-Interscience, New York, 1974, pp. 495 and 832.
9 Houben-Weil, Methoden der Organischen Chemie, Band E19c, Thieme, Stuttgart, 1990, p. 66.
10 G.G. Gordon and P. Skett, Introduction to Drug Metabolism, Chapman and Hall, London, 1986, p. 11.
11 N. Dizdar, A. Henriksson and B. Kagedal, J. Chromatogr., 565 (1991) 1.

Analytica Chimica Acta, 273 (1993) 399–407
Elsevier Science Publishers B.V., Amsterdam

4-Aminophenyl acetate as a substrate for amperometric esterase sensors

F. Pariente, L. Hernández and E. Lorenzo

Departamento de Química Analítica y Análisis Instrumental, Universidad Autonoma de Madrid, Cantoblanco, 28049 Madrid (Spain)

(Received 1st June 1992; revised manuscript received 9th October 1992)

Abstract

4-Aminophenyl acetate (PAPA) was applied as a new substrate for esterase activities. Acetylcholinesterase from electric eel (EC 3.1.1.7) was determined using PAPA as an improved substrate. Acetylcholinesterase was covalently bound to a nylon filter mesh using glutaraldehyde and bovine serum albumin as cross-linkers. The modified membrane was subsequently attached to the surface of a glassy carbon electrode. 4-Aminophenol generated by the enzymatic reaction was detected by cyclic voltammetry and amperometry at an activated glassy carbon electrode. A linear current response, proportional to the PAPA concentration, over the range 0.1 μM–0.5 mM was obtained. Optimization of various kinetic parameters of the biosensor is discussed. Acetylcholinesterase was determined in whole human blood using PAPA as substrate.

Keywords: Amperometry; Biosensors; Enzymatic methods; Voltammetry; Acetylcholinesterase; Aminophenyl acetate; Blood; Enzyme electrodes; Esterase activities

Esterase enzymes play an important role in cellular biology because they are responsible for the hydrolysis of acetyl- and butyrylcholine esters in the cholinergic synapses. Acetylcholinesterase (acetylcholine hydrolase, EC 3.1.1.7) is one of these membrane-bound enzymes of great importance in the control of the electrical activity of excitable membranes [1]. This enzyme has been obtained in pure and homogeneous form from electric eel tissue [2,3] and from human erythrocytes [4]. In the presence of acetylcholinesterase (ACE), acetylcholine is rapidly hydrolysed to biologically inactive acetate and choline. When the non-hydrolyzed neurotransmitter remains in the region of the synaptic cleft, the original state of the postsynaptic membrane cannot be re-established. Thus, xenobiotics such as organophosphorus pesticides and carbamates capable of inhibiting ACE can cause great damage to living organisms that have ingested these compounds [5]. For this and other reasons, biosensors based on esterase activities are of great interest in the quantitative measurement of xenobiotic inhibitors.

Acetylcholine sensors have been developed in recent years by using immobilized ACE and choline oxidase [6–8]. The first enzyme hydrolyses the neurotransmitter and the second can oxidize the free choline generated to give, in the presence of molecular oxygen, betaine and hydrogen peroxide. The enzymatic reaction can be monitored with a Clark electrode [6,7] or by amperometric detection of the hydrogen peroxide produced [8]. Similar esterase-immobilized sensors have been used to study the inhibitory effect caused by the presence of organophosphorus pesticides and carbamates using different immobilization techniques and detection methods [9–12].

Correspondence to: E. Lorenzo, Departamento de Química Analítica y Análisis Instrumental, Universidad Autonoma de Madrid, Cantoblanco, 28049 Madrid (Spain).

In these studies, either co-immobilized enzymatic activities must be employed or a redox transfer mediator is utilized instead of one of the enzymatic activities. The design of rapid techniques for the determination of these toxic xenobiotics is of great interest from both chemical and environmental points of view.

Many enzymatic activities have been measured in vitro by using non-natural substrates. In this area of enzymatic analysis, nitrophenyl esters have been used in the determination of a great number of hydrolytic enzymes such as phosphatases [13], proteases [14,15] and esterases [16,17]. In all instances, the enzymatic reaction generates 4-nitrophenol (PNP), which is easily detected by absorption spectrophotometry, Kulys and coworkers [18,19] have established 4-aminophenyl phosphate (PAPP) and 4-aminophenyl-β-D-glucoside as improved substrates for alkaline phosphatase and β-glycosidase, respectively. The product of the hydrolysis of these substances, 4-aminophenol (PAP), can be readily oxidized ($E^{\circ\prime} = 0.00$ V), and thus can be more easily determined than PNP by amperometric methods [20]. This makes these substrates of great interest in some applications in enzymatic analysis.

This paper describes the use of 4-aminophenyl acetate (PAPA) as a substrate for the determination of esterase activities. This material can be easily obtained by reduction of 4-nitrophenyl acetate (PNPA) and used in the determination of ACE in solubilized or immobilized form. Further, an amperometric sensor based on immobilized ACE using PAPA as substrate is described. The response time, pH response, linear range, kinetic parameters and other features of this biosensor are discussed.

EXPERIMENTAL

Reagents

Acetylcholinesterase (EC 3.1.1.7; type III) from electric eel was purchased from Sigma as a solution containing 5 mg of ammonium sulphate per mg of protein and 0.8 U per μl of solution. This enzyme preparation was stored frozen at −20°C. The stability of the enzymatic activity was excellent when frozen. PNPA (M_r 181.15) was obtained from Aldrich and PAPA was synthesized by selective reduction of the nitro group of PNPA as indicated below. PAP was purchased from Merck. Nylon filter meshes of pore size 50 and 150 μm were obtained from Nytal. Deionized water from Milli-Q and Milli-RO systems (Millipore) was used to prepare all solutions. All other chemicals were of analytical-reagent grade and used as received.

Apparatus

Cyclic voltammetric and amperometric studies were carried out with a BAS CV-27 potentiostat and a Linseis *X–Y–t* recorder. Glassy carbon (GC), obtained from BAS, was used as the working electrode and a platinum wire served as the auxiliary electrode. All potentials refer to a sodium chloride saturated calomel electrode (SSCE).

Preparation of 4-aminophenyl acetate

PAPA was synthesized from PNPA by selective reduction of the nitro group [21]. A mixture of 0.01 mol of PNPA and 0.05 mol of $SnCl_2 \cdot 2H_2O$ in 40 ml of absolute ethanol was heated at 70°C under a nitrogen atmosphere. After 60 min the solution was allowed to cool and then poured on to ice. The ethanolic solution was made neutral (pH 6–7) by addition of a 5% (w/v) aqueous sodium hydrogencarbonate solution. The inorganic impurities were removed by centrifugation at 10000 *g* at 4°C. The supernatant was concentrated by rotary evaporation and the PAPA was extracted with ethyl acetate. The organic phase was washed with sodium chloride solution, treated with charcoal and clarified by centrifugation. The solution was dried under vacuum at room temperature. The dark brown solid was stored at 4°C. The yield was 90%.

Preparation and enzyme modification of electrodes

Glassy carbon electrodes were polished using a procedure similar to that recomended by Bruckenstein et al. [22]. Electrodes with no visible scratches were polished with 1-μm diamond paste

(Buehler) and activated by three cyclic voltammetric scans from 0.0 to 1.5 V (vs. SSCE) at 50 mV s^{-1} in 1.0 M NaOH solution. Subsequently, the electrodes were washed with buffer solution. Enzyme immobilization on the nylon filter mesh was carried out as described previously [23].

Amperometric determinations

The enzyme electrode was placed in 3–5 ml of buffer solution at an applied potential of 0.25 V (vs. SSCE). After the background current had decayed to a steady-state value, aliquots of a stock substrate solution were added. After stirring for 60 s the steady-state current in the quiescent solution was recorded. These responses were typically achieved after ca. 90–120 s.

Esterase determinations in human blood

Human plasma and erythrocyte concentrate were obtained from heparinized venous blood from normal volunteers by Ficoll Hypaque (Pharmacia, Uppsala, Sweden) centrifugation. The fractions were collected in the cold in 1-ml aliquots and stored at −80°C. For esterase determinations, 100 μl of the human plasma fraction or 200 μl of the erythrocyte concentrate fraction were added to 3.0 ml of 0.1 M phosphate buffer solution (pH 7.0) containing 2.3 mM PAPA at 25°C. The product of enzymatic reaction, PAP, was detected by cyclic voltammetry at a glassy carbon electrode activated as described above.

RESULTS AND DISCUSSION

Analysis of the synthesized PAPA

In order to report an accurate value of the Michaelis–Menten constant, K_m, for ACE, the exact relative molecular mass of the substrate must be known. As PAPA prepared by reduction of PNAP with $SnCl_2$ has not been previously assessed a complete analysis of the substrate preparation was performed.

The ^1H NMR spectrum (in $CDCl_3$ solution) of the synthesized compound confirmed the presence of two amino protons, which were observed as a singlet at 6.8 ppm and whose integral corresponded to two protons. The presence of the NH_2 group was also supported by IR spectrometry.

Elemental analysis of the synthesized PAPA gave C 63.6, H 5.8, N 9.2, O 21.5%. The percentage of each element and water found in the product yields the empirical formula $C_8H_9NO_2$ (C 63.6, H 5.9, N 9.3, O 21.2%). Hence the preparation of PAPA by reduction of PNPA with $SnCl_2 \cdot 2H_2O$ in a non-aqueous medium gives non-hydrated aminophenyl acetate, which has M_r = 151.2. This value was confirmed by treating a solution containing 10.0 μM PAPA with ACE and following the reaction amperometrically. The maximum signal obtained in the reaction was compared with the signal given by a 10.0 μM solution of PAP under the same conditions, and from these data the M_r of PAPA was calculated to be 145 ± 10. PAPA is stable to atmospheric water when stored below 0°C.

Electrochemical characterization of the product and the substrate

Cyclic voltammetry was used to study the electrochemical properties of the substrate (PAPA) and the product (PAP) of esterase reactions. Detailed studies were carried out in order to obtain the maximum sensitivity for the low levels of these materials produced during the enzymatic reaction. The electrochemical behaviour of PAP at electrochemically activated glassy carbon electrodes has been described previously [23].

A new procedure for the electrochemical activation of glassy carbon electrodes providing excellent results in the determination of catecholamines [24] and NADH [25] has been described recently. Figure 1 shows cyclic voltammograms for 2.0 mM PAP obtained at (A) untreated and (B) electrochemically activated glassy carbon electrodes. At the untreated electrode a well defined anodic peak at 0.15 V and a cathodic peak at 0.0 V are observed. In successive scans, a potential shift to more positive (anodic scan) or more negative potentials (cathodic scan) with a decrease in peak current is observed. This behaviour suggests passivation of the electrode surface, perhaps due to adsorption of the oxidation product of PAP. At the treated electrode, how-

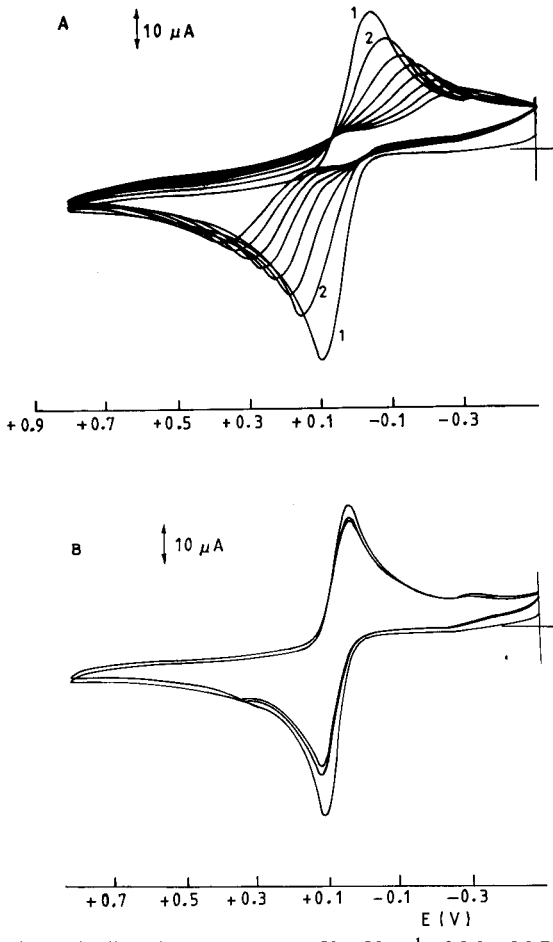

Fig. 1. Cyclic voltammograms at 50 mV s^{-1} of 2.0 mM PAP solution at an (A) untreated and (B) NaOH–activated glassy carbon electrode in 0.1 M phosphate buffer (pH 7.5).

ever, PAP exhibits a well behaved response that is invariant with continuous cycling.

Cyclic voltammograms of 1 mM PAPA at (A) untreated and (B) activated glassy carbon electrodes are shown in Fig. 2. At the untreated electrode PAPA exhibits irreversible oxidation with a peak at 0.7 V. At the activated electrode a well defined cathodic peak at 0.0 V, in addition to the anodic peak at 0.7 V, is observed. In a second anodic scan a new peak at 0.1 V is also observed.

The above results may be indicative of strong adsorption of the oxidation product of PAPA on the electrode surface. Activation of the electrode in NaOH solution results in a functionalized electrode surface that is less susceptible to passivation, giving rise to a nearly reversible response, as was observed for catecholamines [24]. Cyclic voltammetric scans past the oxidation wave of PAPA give an oxidation product which, after hydrolysis and reduction, generates PAP. Because of the large difference in peak potential values, PAPA does not interfere in the determination of PAP, which is the product of the enzymatic reaction.

Enzymatic hydrolysis of PAPA

The catalytic activity of ACE using PAPA as substrate can be followed in solution by cyclic

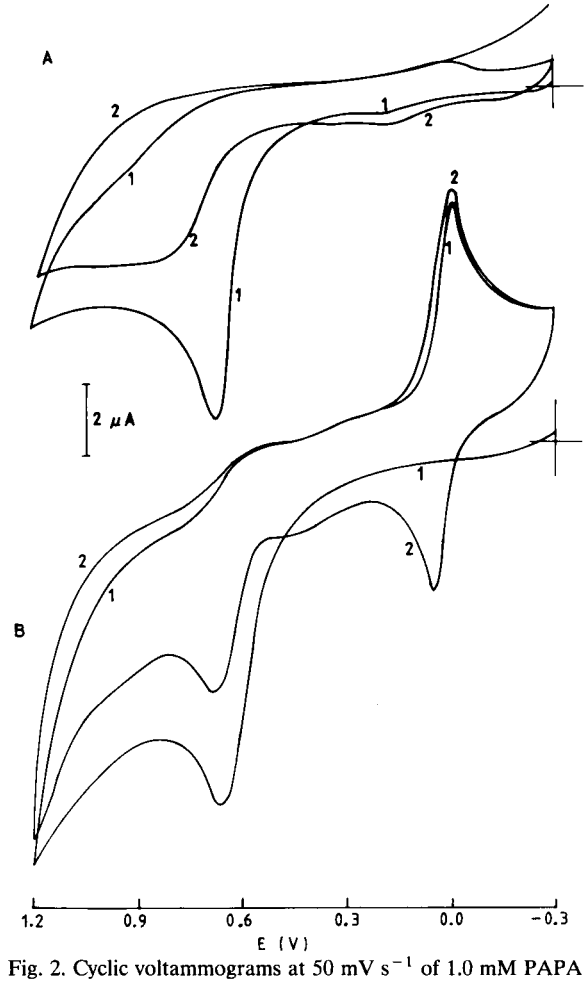

Fig. 2. Cyclic voltammograms at 50 mV s^{-1} of 1.0 mM PAPA solution at an (A) untreated and (B) NaOH–activated glassy carbon electrode in 0.1 M phosphate buffer (pH 7.5).

voltammetry. Figure 3A shows the voltammetric response obtained at various times after immersion of an activated electrode in a solution containing 1.0 U of ACE and 1.0 mM PAPA in 0.1 M phosphate buffer (pH 7.5). As the catalytic reaction proceeds, PAPA is converted into PAP, so that the current for the wave centred at about +0.1 V (which is due to oxidation of the PAP generated by the enzymatic reaction) increases with time. Figure 3B depicts the time dependence of the peak current for PAP oxidation. The plot exhibits the expected logarithmic variation with time. This non-linear response indicates first-order kinetics as typically obtained in enzymatic reactions under no substrate saturation conditions.

In cyclic voltammetry, assuming semi-infinite linear diffusion conditions, the peak current (i_p) resulting from the oxidation of an electroactive species is proportional to the bulk concentration and to the square roof of the scan rate. At 298 K i_p is given by the Randles–Sevcik equation [26]:

$$i_p = 2.69 \times 10^5 n^{3/2} A D^{1/2} v^{1/2} C_R^* \quad (1)$$

where A is the electrode area (cm^2), n is the number of electrons involved in the reaction, D is the diffusion coefficient ($cm^2\ s^{-1}$), v is the scan rate ($V\ s^{-1}$) and C_R^* is the bulk concentration of the electroactive species ($mol\ cm^{-3}$).

For the oxidation of PAP the slope of the plot of i_p vs. C_R^* was determined to be 33 $\mu A\ \mu mol^{-1}\ cm^{-3}$. This is in excellent agreement with the

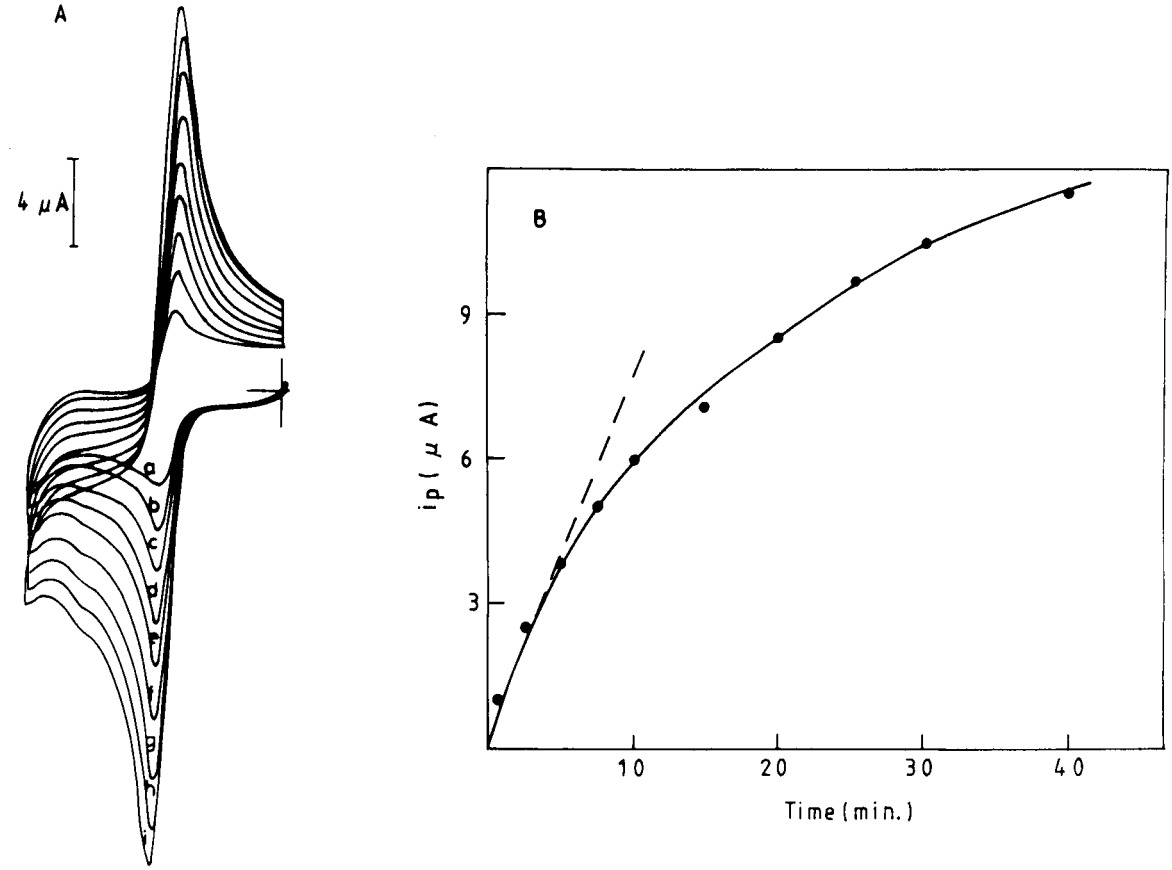

Fig. 3. (A) Catalytic activity of ACE in 0.1 M phosphate buffer (pH 7.5) using PAPA as substrate determined by cyclic voltammetry at 50 mV s^{-1}. Voltammograms were obtained after (a) 1, (b) 2.5, (c) 5.0, (d) 10, (e) 15, (f) 20, (g) 25, (h) 30 and (i) 40 min. (B) Plot of i_p vs. time from the data in (A).

value of 34 μA μmol^{-1} cm^{-3} calculated from Eqn. 1 for an electrode with a geometric area of 0.071 cm^2, a scan rate of 0.05 V s^{-1}, a diffusion coefficient of 7.9×10^{-6} cm^2 s^{-1} [27] and two electrons involved in the electrochemical reaction [27]. Based on these results, the rate of enzymatic hydrolysis of PAPA can be related to the peak current so that the enzyme kinetic constants, K_m and maximum rate, V_{max}, could be determined. For this purpose, the substrate concentrations were varied from 40 μM to 10 mM, with a reaction time for each concentration of 12 min. As is generally done, the initial rate was plotted against the substrate concentration as shown in Fig. 4. As expected, the plot exhibits significant hyperbolic curvature and asymptotically reaches a level slightly above 0.4 μmol min^{-1}. The Lineweaver–Burk plot is linear over a broad range (Fig. 4, inset). From this plot the values of K_m and V_{max} were determined to be 1.3 mM and 0.41 μmol min^{-1}, respectively. These values agree well with those given by Kupta [28] for ACE from bovine erythrocytes for phenyl acetate. Our results indicate that, in phosphate buffer, ACE from electric eel has less affinity for PAPA than for acetylcholine (K_m 90 μM [29]), its natural substrate.

Reaction progress curves (product concentration versus time) for PAPA were obtained using blood preparations and the esterase activities present in each blood fraction determined. Figure 5 shows the esterase activity present in human plasma and in the erythrocyte concentrate fraction. As can be seen, the erythrocyte concentrate has an activity that is four times that of human plasma. This observation can be explained by the high concentration of ACE in the erythrocyte membrane, in contrast to human plasma,

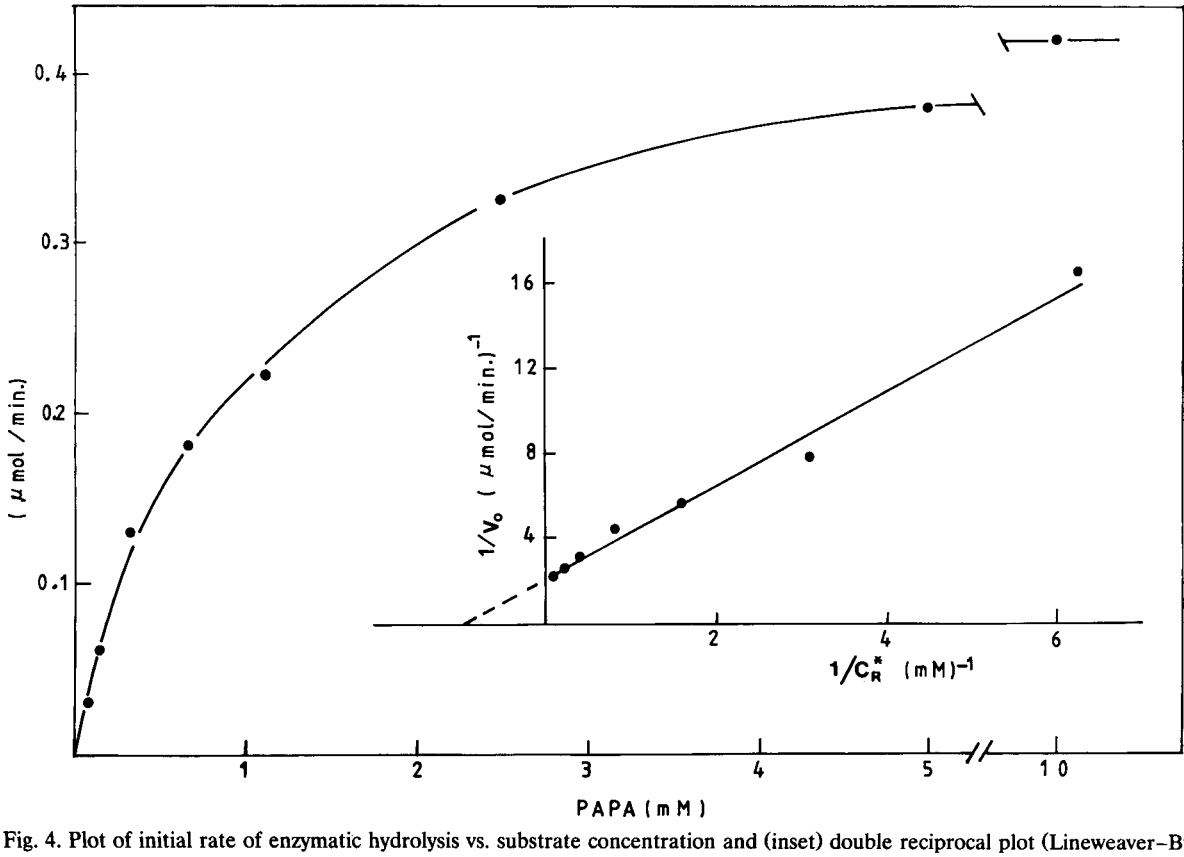

Fig. 4. Plot of initial rate of enzymatic hydrolysis vs. substrate concentration and (inset) double reciprocal plot (Lineweaver–Burk) for PAPA in the presence of 1.0 U of ACE in 2.5 ml of 0.1 M phosphate buffer (pH 7.5).

where the principal esterase activity is the butyrylcholinesterase (also called pseudocholinesterase) [30].

Enzyme electrode response

In order to test the utility of PAPA as a substrate in biosensors based on esterase activities, ACE was immobilized on nylon filter meshes by covalent binding of the enzymes. The membranes were closely attached to the glassy carbon electrode surface. The steady-state currents obtained at 0.25 V (vs. SSCE) for various concentrations of the substrate were employed in constructing response curves for PAPA. These results are shown in Fig. 6. A linear response range of nearly four decades of PAPA concentration and a good linear correlation ($r = 0.998$) were obtained.

The sensitivity in the linear region of the calibration graph is 2.1 nA l μmol^{-1} (see inset in Fig. 6). The system shows high reproducibility with a relative standard deviation of 2% for five replicate measurements of a 100 μM PAPA solution. The above results indicate that PAPA is an excellent substrate for the amperometric determination of ACE activity.

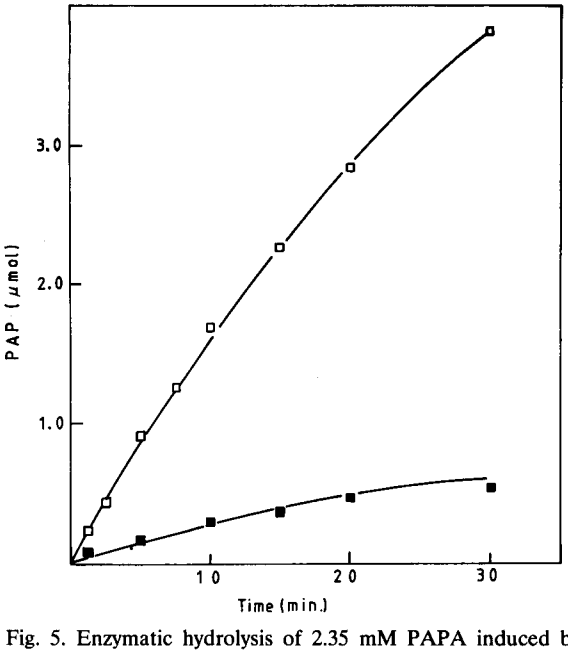

Fig. 5. Enzymatic hydrolysis of 2.35 mM PAPA induced by 100 μl of (■) human serum or (□) human erythrocyte concentrate in 5.0 ml of 0.1 M phosphate buffer (pH 7.5).

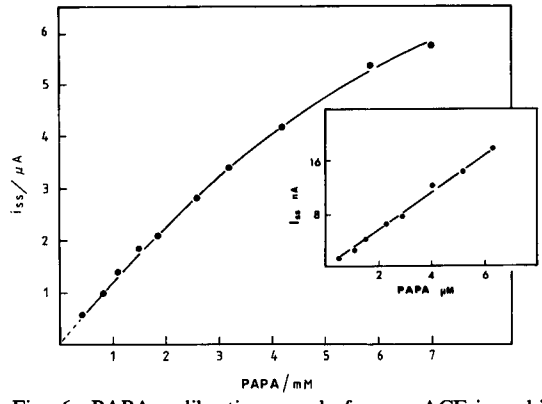

Fig. 6. PAPA calibration graph for an ACE-immobilized electrode. Steady-state currents were measured to +0.25 V (vs. SSCE) in 0.1 M phosphate buffer (pH 7.5).

The process of immobilization of an enzyme on an insoluble support can result in the alteration of its catalytic properties, as compared with the solubilized enzyme. This alteration can manifest itself by changes in the Michaelis–Menten constant and in the pH dependence of the response. Therefore, catalytic parameters were evaluated in order to optimize the electrode response.

The rate of an enzymatic reaction may be either mass transport limited or catalytically controlled. With the immobilization procedure used in this work, the enzymatic reaction is catalytically controlled, as previously demonstrated for alkaline phosphatase [23]. Thus, as Shu and Wilson [31] suggested, the apparent Michaelis–Menten constant (K'_m) can be calculated for the immobilized enzyme by amperometric methods using the Lineweaver–Burk equation:

$$\frac{1}{i_{ss}} = \frac{1}{i_{max}} + \left(\frac{K'_m}{i_{max}} \times \frac{1}{C^*_R} \right)$$

where i_{max} and i_{ss} are the currents measured for the detection of the enzymatic product under conditions of substrate saturation and the steady state, respectively, for a given substrate concentration C^*_R. A double reciprocal plot of i_{ss} vs. C^*_R should be linear with an intercept on the ordinate of $1/i_{ss}$ and on the abcissa of $-1/K'_m$ (Fig. 7). The apparent Michaelis–Menten constant (K'_m) characterizes the enzyme electrode, not the en-

zyme itself. It provides a measure of the substrate concentration range over which the electrode response is approximately linear. For bound ACE, the apparent Michaelis–Menten constant was calculated to be 6.67 mM and i_{max} to be 10.2 μA. This K'_m value is approximately half an order of magnitude greater than the value calculated for the solubilized enzyme. This increase in the magnitude of K'_m extends the upper limit of the linear response.

The effect of pH on the response of the ACE electrode was studied from pH 6.0 to 11.0. A series of 0.1 M phosphate buffers were employed for this purpose. As shown in Fig. 8, the ACE electrode displays maximum response in the pH range 7–8. When compared with the corresponding value for the enzyme in solution, this represents a shift of about 1 pH unit to more acidic values. This might reflect differences in the microenvironment around the enzyme in the immobilized state.

The lifetime of the sensor is ca. 30 days if stored in a refrigerator at 4°C when not in use.

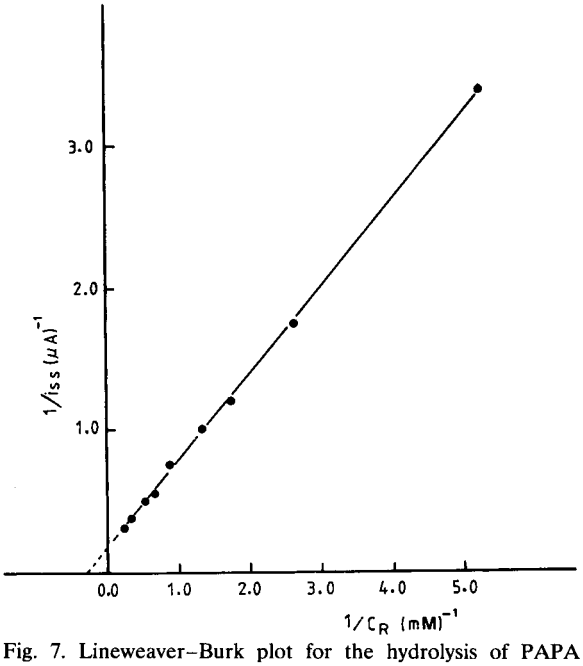

Fig. 7. Lineweaver–Burk plot for the hydrolysis of PAPA produced by an ACE-modified electrode (1.0 U) in 0.1 M phosphate buffer (pH 7.5).

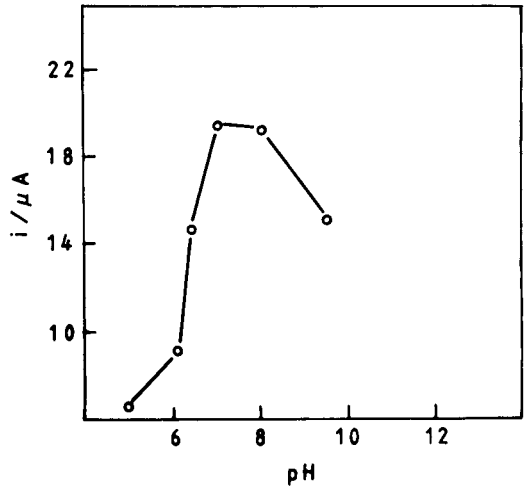

Fig. 8. Effect of pH on the ACE electrode response for the hydrolysis of 1.0 mM PAPA in 0.1 M phosphate buffer solutions.

This value is similar to those reported for other enzymes covalently bound to glassy carbon electrodes [32,33].

Conclusions

It has been demonstrated that PAPA is an excellent substrate for the amperometric determination of esterase activities via oxidation of PAP, the product of the enzymatic reaction. An amperometric biosensor was developed by immobilizing ACE on a nylon mesh membrane and subsequently placing the latter over a previously activated (in NaOH) glassy carbon electrode. Such a sensor exhibits excellent properties with K'_m and i_{max} values of 6.67 mM and 10.2 μÅ, respectively. It also exhibits excellent reproducibility (2%) and long-term (more than 30 days) stability when stored at 4°C when not in use. The substrate PAPA could also be employed in the determination of esterase activity in whole blood and in erythrocyte concentrate. In both instances excellent results were obtained, which suggests that this substrate can be used to measure esterase activities in biological tissues such as liver and kidney.

The use of PAP in detection is advantageous because of its ready oxidation and reversible response. Such behaviour has been previously ex-

ploited in developing a sensor based on alkaline phosphatase activity using 4-aminophenyl phosphate as substrate. The possibility of extending this approach to inhibition studies of esterase activities by natural or xenobiotic agents is currently being explored.

This work was supported in part by the Universidad Autónoma de Madrid, through the Precompetitive Award Program (E.L.) and the DGICyT through grant No. PB 890152.

REFERENCES

1 D. Nachmansohn, Ann. N.Y. Acad. Sci., 137 (1966) 877.
2 W. Leuzinger and A.L. Baker, Biochemistry, 57 (1971) 446.
3 J.D. Berman and M. Young, Proc. Acad. Sci. U.S.A., 68 (1971) 395.
4 K. Sihotang, Biochim. Biophys. Acta, 370 (1974) 468.
5 R.D. O' Brien, Insecticide Action and Metabolism, Academic, New York, 1967.
6 K. Gibson, G.G. Guilbault, Anal. Chim Acta, 86 (1975) 245.
7 L. Campanella, M. Achilli, M.P. Sammartino and M. Tomassetti, Bioelectrochem. Bioenerg., 26 (1991) 237.
8 E. Tamiya, Y. Sugiura, E. Nepomuceno, S. Misoshita, K. Nakajima, A. Akiyama I. Karube, Anal. Chim. Acta, 251 (1991) 129.
9 P. Durand D.J. Thomas, J. Environ. Pathol. Toxicol. Oncol., 5 (1984) 51.
10 C. Tran-Minh, P.C. Pandey and S. Kumaran, Biosensors Bioelectron., 5 (1990) 461.
11 J. Kulys and E.J. D'Costa, Biosensors Bioelectron., 6 (1991) 109.
12 G. Palleschi, M.G. Lavagnini, D. Moscone, R. Pilloton, D. D'Ottavio and M.E. Evangelisti, Biosensors Bioelectron., 4 (1989) 27.
13 O.A. Bessey, O.H. Lowry M.J. Brock, J. Biol. Chem., 164 (1946) 321.
14 F.J. Kezdy and M.L. Bender, Biochemistry, 1 (1962) 1097.
15 P. Manfred, I. Tsai and M.L. Bender, Biochemistry, 18 (1979) 3769.
16 D.J. Escobichon, Can. J. Biochem., 51 (1973) 506.
17 D.J. Escobichon, Can. J. Biochem., 48 (1970) 1359.
18 V.J. Razumas, J.J. Kulys and A.A. Malinauskas, Anal. Chim. Acta, 117 (1980) 387.
19 J.J. Kulys, V. Razumas and A.A. Malinauskas, J. Electroanal. Chem., 116 (1980) 11.
20 R.Q. Thomsom, G.C. Barone, H.B. Halsall and W.R. Heineman, Anal. Chim. Acta, 192 (1991) 90.
21 F.D. Bellamy and K. Ou, Tetrahedron Lett., 25 (1984) 839.
22 S. Bruckenstein, J.W. Sharkey and J.Y. Yip, Anal. Chem., 57 (1985) 368.
23 F. Pariente, L. Hernández and E. Lorenzo, Bioelectrochem. Bioenerg., 27 (1992) 73.
24 D.M. Anjo, M. Kahr, M.M. Khodabakhsh, S. Nowinski and M. Wanger, Anal. Chem., 61 (1989) 2603.
25 E.J. Eisenberg and K.C. Cundy, Anal. Chem., 63 (1991) 845.
26 A.J. Bard and L.R. Faulkner, Electrochemical Methods: Fundamentals and Applications, Wiley, New York, 1976, p. 218.
27 R.N. Adams, Electrochemistry at Solid Electrodes, Dekker, New York, 1969, p. 220.
28 R.M. Kupta, Biochemistry, 3 (1964) 1749.
29 F. Bergmann and J.B. Wilson, J. Biol. Chem., 238 (1963) 1714.
30 D.K. Das and J. Liddell, J. Med. Genet., 7 (1970) 351.
31 F.R. Shu and G.S. Wilson, Anal. Chem., 48 (1976) 2090.
32 R.M. Ianniello, T.S. Lindsay and A.M. Yacynych, Anal. Chem., 54 (1982) 1980.
33 R.M. Ianniello and A.M. Yacynych, Anal. Chem., 53 (1981) 2090.

Analytica Chimica Acta, 273 (1993) 409–417
Elsevier Science Publishers B.V., Amsterdam

Amperometric enzymatic glucose electrode based on an epoxy–graphite composite

F. Céspedes, E. Martínez-Fàbregas, J. Bartrolí and S. Alegret

Departament de Química, Universitat Autònoma de Barcelona, E-008193 Bellaterra (Spain)

(Received 1st June 1992; revised manuscript received 9th October 1992)

Abstract

An inexpensive, robust, polishable and easy to mechanize amperometric transducer showing a long lifetime, based on a composite material made of graphite and non-conducting epoxy resin (Epo-Tek H77), was constructed. This composite was characterised electrochemically using cyclic voltammetry and linear-sweep voltammetry. The applicability of this amperometric transducer was demonstrated in the construction of a glucose biosensor based on the amperometric detection of hydrogen peroxide produced by the catalytic action of glucose oxidase covalently immobilized on a nylon mesh. The sensor shows a linear response range for glucose in the range 10^{-5}–10^{-2} M when a potential of 1150 mV is applied with respect to an Ag/AgCl electrode in a pH 7.00 buffered solution with 0.1 M phosphate and 0.1 M KCl. The resulting biosensor was compared with a commercial glucose analyser.

Keywords: Amperometry; Biosensors; Enzymatic methods; Voltammetry; Enzyme electrodes; Epoxy-graphite composite electrode; Glucose

Analytical methodologies for process monitoring and control are constantly evolving, seeking to increase simplicity, reliability, precision, rapidity and economy in the acquisition of analytical data. In this context, sensors are seen as a viable alternative to complex analytical instruments. Hence great efforts are being made to develop new transducers that are increasingly selective, sensitive, robust, inexpensive, easy to build and amenable to application in the monitoring and control of clinical, environmental and industrial processes.

Polymer technology offers a wide choice of materials suitable for use in a great variety of industrial products, conferring advantageous physical and chemical properties on those products and often making them cheaper to manufacture.

Correspondence to: S. Alegret, Departament de Química, Universitat Autònoma de Barcelona, E-008193 Bellaterra (Spain).

The field of chemical sensors in general, and electrochemical transducers in particular, has taken advantage of the availability of new materials, yielding a generation of composite-based electrodes [1]. Conventional voltammetric electrodes built with a conductor the surface of which has been chemically or physically treated (modified electrodes) can also be considered to belong to this group [2,3].

In this work, a new electrochemical sensing material is reported. This material encompasses the dispersion of electrically conductive material in a non-conductive, plastic phase. This rigid transducing material yields an electrode with features similar to those of carbon paste electrodes that have a mouldable and soft structure [4].

Electrodes constructed using these new, conductive composite materials show several electrochemical advantages over those built using a single conductive phase (platinum, gold, silver, mercury, graphite, etc.). The matrix of the composite

material can accommodate other substances to improve the electrochemical response of the transducer [5,6]. Additionally, the signal-to-noise ratio is higher in composite material electrodes than in single-phase electrodes, allowing for lower detection limits [7].

From the mechanical point of view, an electrode based on a composite material can be renewed by polishing its surface, thus lengthening its lifetime [8], and it can be mechanized as a hard solid. Further, composite materials have technologically appealing features, such as their initial moulding before the polymerization of the plastic phase. This moulding permits the construction of sensors of various sizes and shapes, such as flow-through configurations, and also permits the construction of electrodes by the deposition of conductive tracks on a non-conductive strip, which is a recurrent design in disposable amperometric sensors [9]. This line of research is being pursued at present.

Conductive composite materials have been used to construct ion-selective electrodes (ISEs), where the ion-sensitive membrane is fixed directly to the composite, replacing the usual ISE structure involving an internal reference solution. The performance of these ISEs is encouraging, especially with respect to the lifetime of the sensor, a consequence of the good adhesion of PVC-based membranes to the composite material [10].

In this work, the application of [0,3]-composite materials [11,12] to the construction of disposable electrochemical transducers has been broadened. This matrix has a conductive phase formed by graphite powder and the insulating phase is an epoxy resin. Following their electrochemical characterization (using hydrogen peroxide detection), the applicability of these transducers was demonstrated in the design, construction and evaluation of a conventional first-generation type of amperometric glucose sensor.

EXPERIMENTAL

Apparatus

Voltage–current curves were recorded using a Polarecord E506 recorder (Metrohm, Herisau, Switzerland). Cyclic voltammograms were generated employing a Dacfamov 05.10 CNRS-Microtec unit controlled by an Apple II Computer (CNRS, Toulouse, France). Sensor current was measured with a PRG-DEL amperometric unit (Tacussel, Lyon, France). pH was controlled using a Digilab 517 pH meter (Crison, Barcelona, Spain). Responses were recorded with a Labograph E586 recorder (Metrohm).

Reagents and solutions

To construct the electrodes, graphite powder with a particle size of 1 μm (Merck) and Epo-Tek H77 (Epoxy Technology, Billerica, MA) and Araldit M (Ciba-Geigy) epoxy resins were used. Lysine, glutaraldehyde and dimethyl sulphate were obtained from Fluka. D-(+)-Glucose monohydrate and hydrogen peroxide were obtained from Merck. Glucose oxidase (G-2133 type VII from *Aspergillus niger*) was obtained from Sigma.

The supporting electrolyte was an aqueous solution buffered at pH 7.00 with 0.1 M phosphate and 0.1 M KCl. Hydrogen peroxide solutions were fresh prepared daily. Glucose solutions were prepared from a benzoic acid saturated solution (3 g dm^{-3}) [13].

Auxiliary electrodes

To characterize and evaluate the working electrodes, a platinum auxiliary electrode and a double-junction Ag/AgCl reference electrode (Orion 92-02-00) were used. The external reference solution was 0.1 M KCl.

Construction of the amperometric transducer

The composite material employed was prepared by dispersing graphite powder in Epo-Tek H77 epoxy resin. The mixing proportions were 1:4 parts by weight. Before its mixing with the graphite, the resin was prepared by mixing its two components, part A (the resin proper) and part B (HR hardener), in a 20:3 weight ratio.

Once homogenized, the mixture was applied to one of the openings of a PVC tube (6 mm o.d.). This tube formed the body of the electrode. The composite mixture filled the tube to a depth of ca. 3 mm (Fig. 1). The assembly was kept at 50°C for 48 h to harden the composite. After the

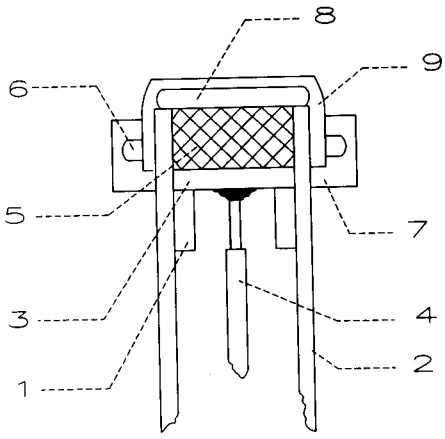

Fig. 1. Construction of the sensors. 1 = Flexible supporting ring; 2 = electrode body; 3 = copper contact; 4 = wire; 5 = conductive and polishable graphite–epoxy resin; 6 = O-ring; 7 = Parafilm; 8 = enzyme membrane; 9 = dialysis membrane. Amperometric transducer, 1–5; glucose biosensor, 1–9.

hardening process, the outer surface of the composite was finely polished using 3-μm alumina paper (polishing strips 301044-001, Orion) moistened with doubly distilled water.

Construction of the biosensor

The glucose biosensor was constructed by applying a nylon 6,6 membrane to the surface of the electrode. Previously, glucose oxidase (GOD) had been immobilized covalently on the nylon surface. The nylon membrane used has 108 threads cm^{-2} and a thickness of 120 μm (A. Bozzone, Appiano Gentile, Milan, Italy).

The immobilization process employed [14,15] consisted of activating the nylon with dimethyl sulphate in order to form an imido ester group. This group was made to react with one of the amino groups from the lysine molecule used as a spacer. The linking of the enzyme to the extender arm was realized using glutaraldehyde. The nylon membrane containing the enzyme was fixed to the electrode by a dialysis membrane and an O-ring and using Parafilm as a sealant (Fig. 1).

Characteristics of the sensing system

The resulting glucose biosensor based on composite materials is of the kind known as a first-generation sensor. These electrodes are identified by the selective biocatalytic generation of an electrochemically active species (hydrogen peroxide) by an enzyme (GOD):

$$\text{D-(+)-glucose} + O_2 \xrightarrow{\text{GOD}} \text{gluconic acid} + H_2O_2 \quad (1)$$

The hydrogen peroxide produced is measured amperometrically by the direct oxidation on the surface of the composite-material electrode when a potential E is applied:

$$H_2O_2 \xrightarrow{E} O_2 + 2H^+ + 2e^- \quad (2)$$

RESULTS AND DISCUSSION

Construction of transducer with epoxy–graphite composite material

Conductivity of the composite material. An amperometric transducer should have a very low resistance. The conductivity of an epoxy–graphite composite is determined by its graphite content. The Epo-Tek H77 resin admitted a maximum of 20% graphite content (sensors made in this manner will be called ET units), while Araldite M resin admitted a 60% graphite content (sensors made in this manner will be called AM units). If the graphite content is reduced for both ET and AM units, a decrease in conductivity and sensitivity will result (Fig. 2).

H_2O_2 oxidation potential. The exact oxidation potential of hydrogen peroxide, somewhere between 1000 and 1200 mV, is difficult to determine because of the proximity of the oxidation potential of the solvent (water). In the linear-sweep voltammogram obtained at a glassy carbon electrode, the typical plateau in the oxidation curve, corresponding to the maximum current, is present (Fig. 3). This plateau is not observed when the voltammogram is recorded using both ET and AM units (Fig. 4).

The system was optimized by calibrating at different potentials between the limits 1000 and 1200 mV. The best compromise between sensitivity and residual current of the system was found at a potential of 1150 mV.

Heterogeneity of the composite material. When doing cyclic voltammetry with a simple, reversible

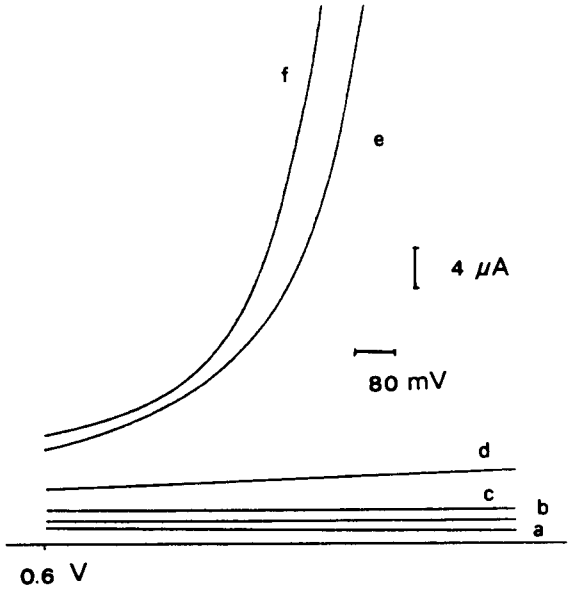

Fig. 2. Linear-sweep voltammogram with a pH 7.00 buffer (0.1 M phosphate–0.1 M KCl). Sweep rate, 10 mV s^{-1}. Graphite content of the composite material: (a) 10; (b) 20; (c) 30; (d) 40; (e) 50; (f) 60%.

redox system, such as Fe(II)–Fe(III), the ET and AM units behaved differently. These differences were observed by determining the maximum cathodic currents (i_{cp}) and maximum anodic currents (i_{ap}) and the potentials at which those currents values were reached (E_{cp} and E_{ap}). These values should be related by

$$i_{cp}/i_{ap} = 1 \quad (3)$$

$$0.059/(E_{ap} - E_{cp}) = n \quad (4)$$

where n is the number of electrons participating in the redox process.

In AM units the ratio between anodic and cathodic currents and the value of n are close to

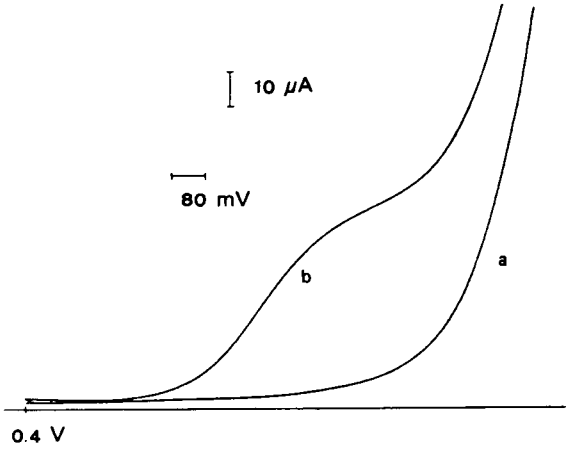

Fig. 3. Linear-sweep voltammogram using a commercially available glassy carbon electrode (2 mm diameter). (a) In pH 7.00 buffer (0.1 M phosphate–0.1 M KCl); (b) in pH 7.00 buffer (0.1 M phosphate–0.1 M KCl) and 1 mM H_2O_2.

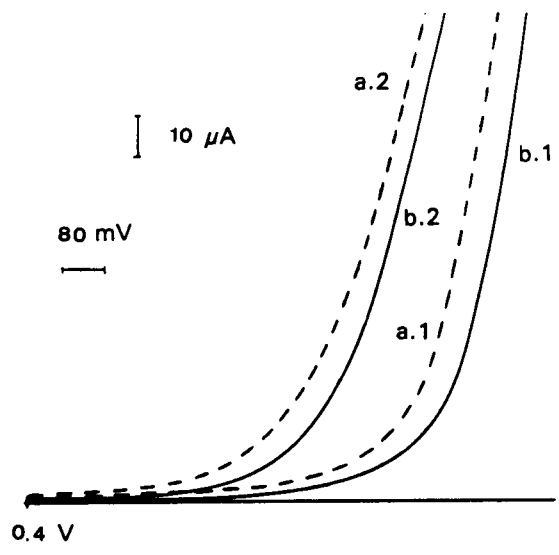

Fig. 4. Linear-sweep voltammograms using (a) AM unit (60% graphite–40% Araldite M epoxy resin) and (b) ET unit (20% graphite–80% Epo-Tek H77 epoxy resin). (1) In pH 7.00 buffer (0.1 M phosphate–0.1 M KCl); (2) in pH 7.00 buffer (0.1 M phosphate–0.1 M KCl) and 5×10^{-4} M H_2O_2.

In AM units the ratio between anodic and cathodic currents and the value of n are close to

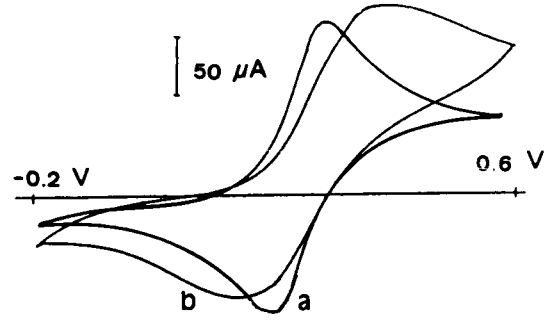

Fig. 5. Cyclic voltammogram using (a) an AM unit (60% graphite–40% Araldite M epoxy resin) and (b) an ET unit (20% graphite–80% Epo-Tek H77 epoxy resin) with 5 mM $K_4Fe(CN)_6$ and 1 M KCl. Sweep rate, 50 mV s^{-1} between −200 and +600 mV.

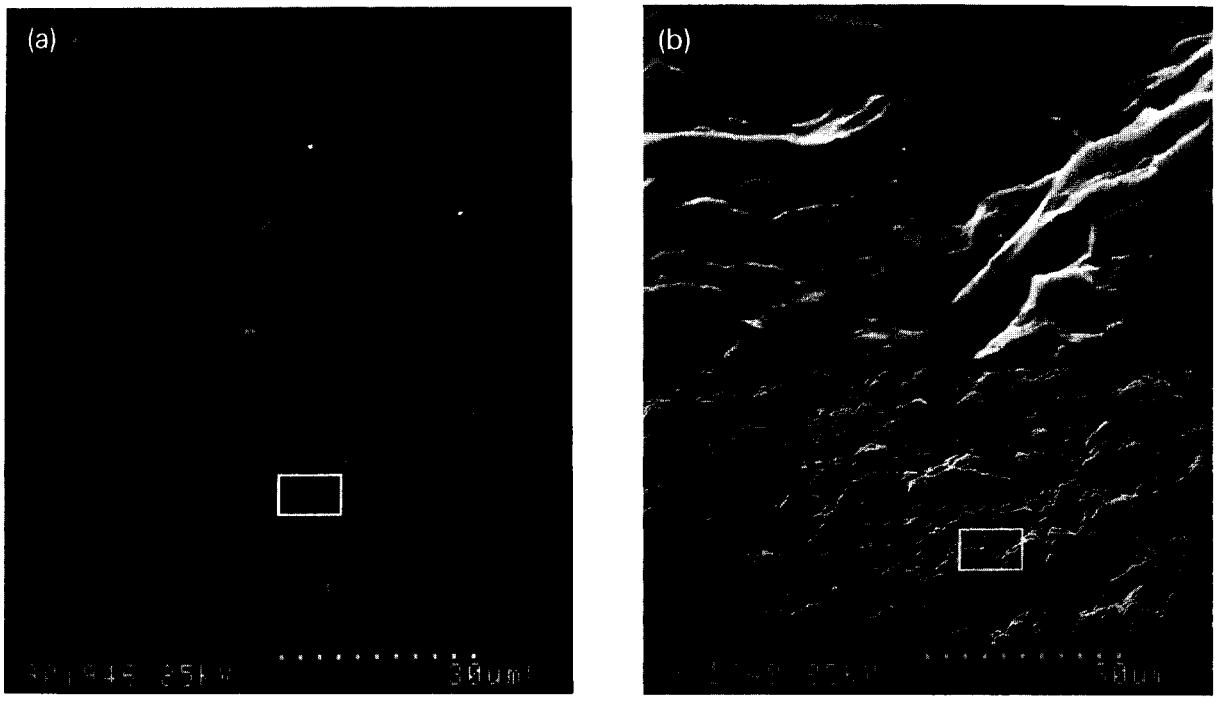

Fig. 6. Surface of composite material electrodes. (a) Composite containing 60% graphite–40% Araldite M epoxy resin; (b) composite containing 20% graphite–80% Epo-Tek H77 epoxy resin. The top micrographs show magnifications of the white boxed areas indicated below.

1. The peaks in the cyclic voltammogram (Fig. 5a) are well defined, indicating that the composite with a high graphite content (60%) is homogeneous. ET units, on the other hand, yield a value of $n = 0.7$, and show ill-defined peaks in the cyclic voltammogram (Fig. 5b). This is due to decreased homogeneity in this type of composite material [16] with a low graphite content (20%). Electrochemical activity is not uniform in the totality of the electrode surface.

Composite materials behave as if they were arrays of very small electrodes. For this reason, non-linear diffusion appears, and mass transport by migration is the dominant phenomenon, generating a steady-state current [17].

The photomicrograph in Fig. 6 shows the distinct surface morphology of these electrodes.

Electrode stability. At first, a better response was expected from electrodes constructed using Araldite M epoxy rather than from those based on Epo-Tek H77 resin. This was expected on the basis of their respective electrochemical responses. However, after repeated calibration runs, AM electrodes showed a loss of linearity, whereas ET electrodes maintained their linearity throughout the concentration range of interest (Fig. 7). The non-linearity of the AM electrodes is proba-

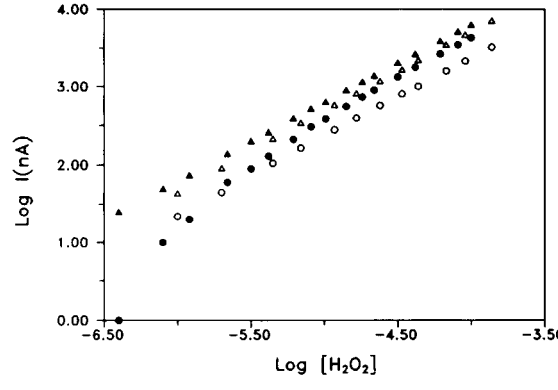

Fig. 7. Stability (○, ●) AM and (△, ▲) ET units. ○, △ = Calibration graphs for freshly built units; ●, ▲ = Calibration graphs for units after being immersed in pH 7.00 buffer (0.1 M phosphate–0.1 M KCl) for 1 week.

bly induced by absorption of water in the AM matrix. This absorption was demonstrated when the linearity recovered after the electrodes had been dried at 40°C for 48 h.

Given the stability shown by ET units, they were chosen as the electrodes to be used in the glucose biosensor.

Evaluation of the ET transducer in H_2O_2

Electrolyte concentration and pH effects. A study of the system was made at different concentrations of the supporting electrolyte. It was observed that at low concentrations of hydrogen peroxide, the linearity diminished significantly, the background noise increased and current instability occurred. All these deleterious effects happened when a buffered solution (pH 7.00, 0.1 M phosphate) was used as the background. When KCl at a concentration of 0.1 M or higher was added, the system became very stable.

The faradaic process described by Eqn. 1 constitutes a proton source. If a low pH is employed, Eqn. 2 will shift to the left, diminishing the value of the current and the overall sensitivity of the system. If a high pH is used, the ensuing proton deficit will provoke a shift of reaction 2 towards proton production, thus oxidizing more hydrogen peroxide and increasing the current considerably (Fig. 8). However, using a high pH also facilitates the oxidation of the solvent, producing an overall detrimental effect. Experimental data confirmed that the optimum working pH was one neighbouring acid–base neutrality.

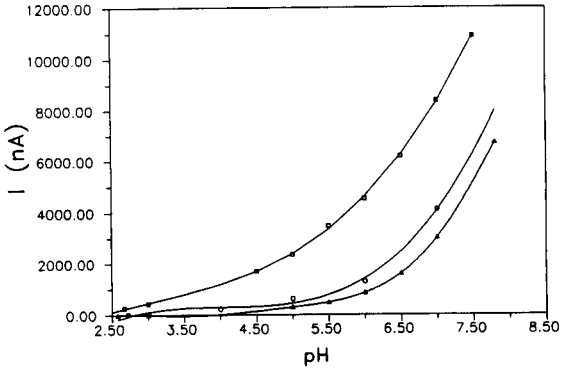

Fig. 8. Effect of pH on the signal of an ET transducer at different concentrations of hydrogen peroxide: ○ = 1×10^{-4}; □ = 1×10^{-3}; ▲ = 0 M.

TABLE 1

Calibration parameters for composite electrodes measuring H_2O_2 concentration

Electrode		$\log[I(\text{nA})] = a + b \log[H_2O_2\,(\text{M})]$		
	Day	a	b	r
ET1	1	7.82	1.03	0.99995
	1	7.91	1.04	0.99992
	4	7.95	1.02	0.99995
	6	7.86	1.01	0.99995
	6	7.81	1.00	0.99998
	11	7.83	1.00	0.99997
	25	7.76	0.98	0.99999
ET2	1	8.02	1.01	0.99996
	5	8.05	1.00	0.99990
ET4	1	7.76	0.99	0.99990
	9	7.79	1.00	0.99992
ET6	1	7.90	1.01	0.99980
	14	7.88	1.02	0.99990
ET8	1	7.77	1.01	0.99995
	21	7.80	1.02	0.99992

Calibration parameters. If the logarithm of the current and the logarithm of hydrogen peroxide concentration are treated by the least-squares method, the experimental data fit a linear equation expressed by

$$\log[I(\text{nA})] = a + b \log[H_2O_2(\text{M})] \qquad (5)$$

where a is the value of $\log[I(\text{nA})]$ at the origin and b is the slope of the straight line. In Table 1, a, b and the correlation coefficient r are given for several electrodes using a working solution of 0.1 M phosphate–0.1 M KCl (pH 7.00). The average values of these parameters ($n = 15$) for a 95% confidence level are $a = 7.9 \pm 0.1$ and $b = 1.00 \pm 0.01$. The concentration range examined was 10^{-6}–10^{-3} M hydrogen peroxide.

Linearity range. The lower limit of the linear response (LLLR) and the upper limit (ULLR) were found graphically using a calibration graph. The linear range of the system is between 10^{-7} and 10^{-3} M hydrogen peroxide. If hydrogen peroxide concentrations of the order of 10^{-7} M are used, the current generated is very close to the

variations of the baseline. The upper limit of the linear response is determined by the ability of the transducer to oxidize the analyte as it comes in contact with its surface. The drift of the residual current generated by the system is 5 nA min^{-1}.

Response dynamics. The 95% response time of the transducer is 13 s when the hydrogen peroxide concentration increases from 0 to 2×10^{-5} M. During ensuing calibrations, the signal is very stable between consecutive additions.

Repetitivity of the signal. For discrete measurements of hydrogen peroxide in separate solutions, with a 4×10^{-6} M concentration, an average error of 1% was found for a 95% confidence level ($n = 8$).

Evaluation of the glucose biosensor

pH effect. The working pH range for glucose oxidase lies between 4.00 and 7.00, with an activity maximum at pH 5.5. However, when the enzyme has been chemically treated for immobilization, the optimum pH depends on the immobilizing system used.

As expected from the results obtained for the hydrogen peroxide system, the current rises with increase in pH. Above pH 9, the signal diminishes owing to enzyme denaturation. For the system described, the working pH range is between 6 and 9 (Fig. 9).

Calibration parameters. When the logarithm of the current and the logarithm of glucose concentration are treated by the least-squares method, the data fit a straight line where a, the value of

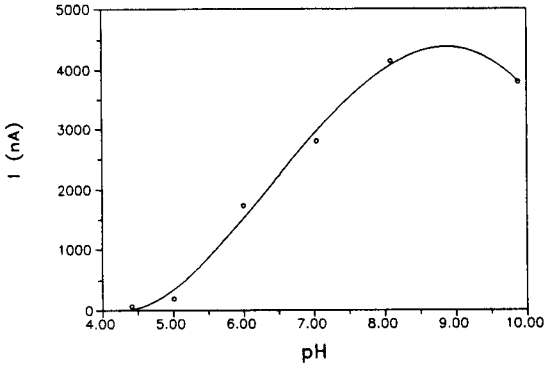

Fig. 9. Effect of pH on the glucose biosensor signal. Glucose concentration, 1 mM.

TABLE 2

Calibration parameters for composite-based glucose biosensors

Biosensor		Log[I(nA)] = a + b log[glucose (M)]		
	Day	a	b	r
ETG4	2	6.73	0.99	0.99995
	3	6.89	1.06	0.99990
	6	6.89	1.02	0.99995
	14	7.13	1.10	0.99992
ETG5	1	6.59	1.04	0.99990
	7	6.64	1.06	0.99995
	10	6.53	1.03	0.99996
	17	6.60	1.06	0.99993
	30	6.46	1.03	0.99995
ETG7	19	6.17	1.06	0.99990
	30	6.12	1.03	0.99995
	33	6.21	1.04	0.99993
	40	6.10	1.02	0.99992
ETG8	20	6.09	1.03	0.99993
	30	6.11	1.04	0.99992

log[I(nA)] at the origin, is 6.13 ± 0.05 and b, the slope, is 1.04 ± 0.01 for a 95% confidence level and $n = 15$. As can be seen in Table 2, the results show low scatter using different electrodes over a period of more than 1 month. The scatter of these results is similar to that shown by the internal epoxy–graphite transducer. When the sensors were not in use, they were kept in 0.1 M phosphate–0.1 M KCl buffered solution (pH 7.00) at 4°C.

Linearity range. The glucose biosensor response is linear between 10^{-5} and 10^{-2} M glucose. This range covers most requirements for glucose measurements in industrial and clinical applications.

Response dynamics. The 95% response time of the glucose biosensor is 32 s when the concentration increases from 0 to 1 mM. This increase in the response time when compared with that of the hydrogen peroxide transducer can be explained by the influence of two factors: enzyme kinetics and the barrier effect of the dialysis membrane. In any event, this lengthening of the response time does not constitute a hindrance to calibration, as the response signal settles rapidly with successive glucose additions.

TABLE 3

Average measurements for three glucose samples measured with the reported biosensor and the YSI glucose analyser

Standard (g/l)	[Glucose] (g/l)	
	ETG biosensor ($n = 3$)	YSI glucose analyser ($n = 4$)
4.58	4.5 ± 0.2	4.46 ± 0.01
9.09	9.1 ± 0.3	8.98 ± 0.01
13.64	13 ± 2	13.4 ± 0.1

Repetitivity of the signal. The dialysis membrane stabilized the signal significantly and increased the reproducibility of the response. For glucose determinations in separate solutions of 10^{-4} M concentration the mean error was 1% for a 95% confidence level and $n = 10$.

Comparison between the glucose biosensor and a commercial biosensor

The Yellow Spring Instruments (YSI) Model 2000 glucose analyser is a semi-automatic system based on the same principle as the biosensor reported here. Its working electrode is a platinum disc with a membrane containing immobilized GOD and other membranes (cellulose acetate and polycarbonate) that help to prevent interferences.

Table 3 compares the results obtained when three different samples (aqueous glucose solutions) were analysed by the composite-based sensor and the YSI glucose analyser. When a correlation diagram is constructed, the line passes through the origin and has a slope very close to unity. Therefore, it can be concluded that the results obtained by the biosensor described are very similar to those given by the commercially available analyser.

Modification of epoxy–graphite composite

Although good results were obtained using the composite material described above, the potential applied for the detection of hydrogen peroxide is high (1150 mV vs. Ag/AgCl), posing several problems such as interferences arising from electrochemically active species and the impossibility of a clear discrimination of the optimum oxidation potential of hydrogen peroxide from the oxidation potential of water. All these aspects are also present in the glucose measurement.

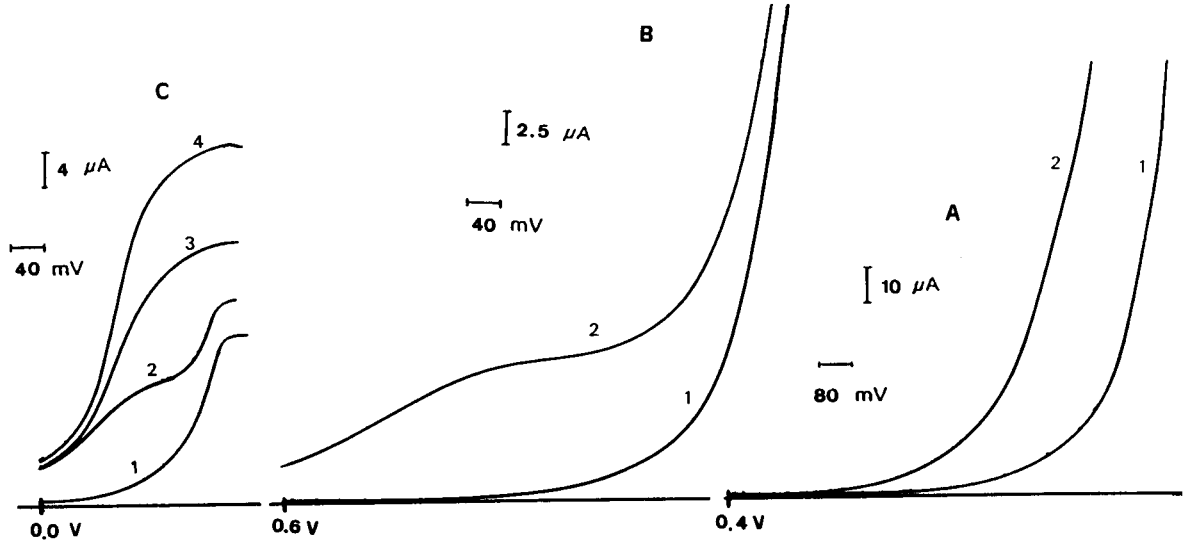

Fig. 10. Linear-sweep voltammetry in a pH 7.00 buffered solution (0.1 M phosphate–0.1 M KCl). (A) Unmodified ET unit. Sweep rate, 10 mV s^{-1}. (1) In supporting electrolyte (SE); (2) in SE + 5×10^{-4} M H_2O_2. (B) Modified ET unit with a 10% Au–Pd catalyst. Sweep rate, 50 mV s^{-1}. (1) In SE; (2) in SE + 4×10^{-4} M H_2O_2. (C) Modified ET unit with 3×5 μl of a tetrathiafulvalene solution in 0.25% acetone and enzyme membrane. Sweep rate, 10 mV s^{-1}. (1) In SE; (2), (3) and (4) in SE + 2.4, 4.4 and 6.4 mM glucose, respectively.

The nature of the composite material allows for the addition of further materials to its matrix and permits the absorption of various substances on its surface owing to its high porosity.

Owing to the above, work is being carried out on the alteration of the composite matrix with a catalyst to promote hydrogen peroxide oxidation. The catalyst employed is made of a mixture of gold and palladium in 3:2 weight proportions [18]. When the electrode was modified with the addition of the catalyst, the hydrogen peroxide oxidation potential was lowered to 900 mV vs. Ag/AgCl. Additionally, the characteristic plateau due to the maximum oxidation intensity of the species can be distinguished very clearly (see Fig. 10). The segregation of the oxidation potentials of hydrogen peroxide and the solvent permits greater signal stability and lower background noise.

However, the problem posed by interference has not been completely solved as the applied potential of 900 mV is still relatively high. Therefore, current work is focused on the development of a second generation of polishable and robust electrodes in which the composite material is modified by a redox mediator (tetrathiafulvalene) capable of establishing electron transfer with the active centres of the glucose oxidase enzyme. In this instance the applied oxidation potential is 150 mV vs. Ag/AgCl (see Fig. 10).

REFERENCES

1 J.E. Anderson and D.E. Tallman, Anal. Chem., 48 (1976) 209.
2 K. Aoki and J. Osteryound, J. Electroanal. Chem., 125 (1981) 315.
3 A.J. Bard, J.A. Crayston, G.P. Kittlesen, T.V. Shea and M.S. Wrighton, Anal. Chem., 58 (1986) 2321.
4 R.N. Adams, Anal. Chem., 30 (1958) 1576.
5 V. Stará and M. Kopanica, Electroanalysis, 1 (1989) 251.
6 J. Wang, Electroanalysis, 3 (1991) 255.
7 S.G. Weber, Anal. Chem., 61 (1989) 295.
8 J. Wang and K. Varughese, Anal. Chem., 62 (1990) 318.
9 W.J. Aston, Biosensors Bioelectron., 7 (1992) 85.
10 S. Alegret and E. Martínez-Fàbregas, Biosensors Bioelectron., 4 (1989) 287.
11 R.E. Newnham, Ferroelectrics, 68 (1986) 1.
12 G.R. Ruschau, R.E. Newnham, J. Runt and B.E. Smith, Sensors Actuators, 20 (1989) 269.
13 J.A. Lott and K. Turner, Clin. Chem., 21 (1975) 1754.
14 W.E. Hornby and D.L. Morris, in H.H. Weetall (Ed.), Immobilised Enzymes, Antigens, Antibodies and Peptides, Vol. 1, Dekker, New York, 1975, p. 141.
15 M. Mascini, M. Iannello and G. Palleschi, Anal. Chim. Acta, 146 (1983) 135.
16 R.C. Engstrom, M. Weber and J. Werth, Anal. Chem., 57 (1985) 933.
17 N. Sleszynski, J. Osteryoung and M. Carter, Anal. Chem., 56 (1984) 130.
18 X. Yang, G. Johansson and L. Gorton, Mikrochim. Acta, 1 (1989) 9.

Analytica Chimica Acta, 273 (1993) 419–424
Elsevier Science Publishers B.V., Amsterdam

Enzyme amperometric sensor for the determination of cholinesterase inhibitors or activators

S.S. Babkina, E.P. Medyantseva, H.C. Budnikov and V.G. Vinter

Department of Biochemistry, Kazan State University, Kazan 420008 (Russian Federation)

(Received 1st June 1992)

Abstract

An enzyme amperometric sensor (EAS) based on immobilized cholinesterase (ChE) sensitive to ChE effectors (both specific and non-specific) is shown to be useful in enzyme immunoassay. For example, a mink autoimmune (Aleutian) disease can be diagnosed with the EAS when an antigen is labelled with a ChE inhibitor. When the ChE-containing membrane is modified by incorporation of the antigen to give an immunoenzyme EAS, this immunoassay can be performed on the basis of the steric shielding of the enzyme active sites with the immunocomplexes formed.

Keywords: Amperometry; Biosensors; Enzymatic methods; Immunoassay; Cholinesterase

The analytical application of the biologically important enzyme cholinesterase (ChE) offers broad possibilities for developing new means of analytical monitoring. In previous papers [1,2] an enzyme amperometric sensor (EAS) was proposed for the determination of various ChE effectors (inhibitors or activators) [1,2]. Two different approaches to the use of the analytical systems on the basis of ChE can be considered: first, the use of the biosensor for the determination of ChE specific effectors; and second, the determination of non-specific effectors which can somehow affect the enzyme reaction (e.g., by creating steric hindrances). Both approaches will be discussed in this paper.

Most of the usual enzyme immunoassay tests are based on spectrophotometric or fluorimetric detection of an enzyme activity (an enzyme can play the role of an antigen or antibody label) [3,4]. Breyer and Radcliff [5] first used an electrochemical technique to investigate the antigen–antibody reaction, the antigen being an azo-protein which was registered polarographically. Heineman and co-workers [6,7] investigated the use of differential-pulse polarography for studying the binding of a hapten marked with an electroactive "tag". A number of reviews show the proliferation of the application of electroanalysis in immunoassays [8–12].

The effectors, or modulators, of enzymes can be used as a label for antigens or antibodies instead of enzymes [4]. Enzyme modulator-mediated immunoassay (EMMIA) has been used for the determination of 2,4-dinitrophenyllysine [13], with horseradish peroxidase serving as the indicator enzyme. The modulator was an antibody to horseradish peroxidase. In another study [14], an antigen (thyroxine) was marked with an organophosphorus inhibitor (modulator) of acetylChE and the immunochemical reaction was monitored spectrophotometrically. The use of the EAS in inhibitor EMMIA using the steric hindrance effect will be discussed.

Correspondence to: S.S. Babkina, Department of Biochemistry, Kazan State University, Kazan 420008 (Russian Federation).

The next step in the development of an electroanalytical technique for immunoassay is an immunoenzyme amperometric sensor (IEAS) in which an antigen or antibodies are the components of the biosensor part of the enzyme electrode. Such systems are promising owing to the possibility of creating compact enzyme immunoanalysers and of automation of the enzyme immunoassay technique. Hence another purpose of this investigation was to devise and use the IEAS for immunoassay.

EXPERIMENTAL

Cyclic voltammetric measurements were performed with a PO-5122/03 polarograph (Russia). The EAS was constructed on the basis of a mercury film-covered silver electrode and a nitrocellulose membrane containing immobilized ChE on the electrode surface [1,15]. This was used as a working electrode. The reference electrode was a saturated calomel electrode (SCE).

All measurements were made at 25.0 ± 0.2°C in borate buffer prepared from high-purity reagents and providing a pH of 9.05. The solutions were deaerated with argon. ButyrylChE (EC 3.1.1.8, horse serum) (denoted ChE in this paper) with an activity of 151 IU mg^{-1} was used. Recrystallized butyrylthiocholine iodide (BuSChI) was used as a ChE substrate. Recrystallized dimethyl-2,2,2-trichloro-1-hydroxyethylphosphonate(chlorophos), hydroxylamine, high-purity organic solvents and 20% glutaraldehyde (Reanal) were also used. Immunoglobulin G (IgG) of 0.8 and 1.5 mg ml^{-1}, produced from blood serum from a sick mink, was previously salted out twice with ammonium sulphate. IgG was isolated by ion-exchange chromatography on a column packed with DEAE-cellulose. Bovine spleen DNA of 0.01 and 0.1 mg ml^{-1} in 0.1 M carbonate–hydrogencarbonate buffer (pH 9.6) were used.

Preparation of sensor part of the IEAS

Cellulose nitrate (0.05 g) was dissolved in toluene–butyl acetate (1 + 1.6) and 0.2 ml of a solution containing 0.018 g of ChE and an antigen (DNA) or antibodies was added. The solution was stirred, then 0.06 ml of 25% glutaraldehyde solution was added. The resulting mixture was cast on a glass plate, dried and a membrane was obtained. The membrane was cut into small pieces (2.5×6.5 cm^2) and immersed in 1% bovine serum albumin in 0.01 M physiological phosphate buffer solution (pH 7.0–7.4) at 25°C for 0.5 h. After washing with borate buffer, a crimped membrane was fixed on the surface of the body of a mercury film-covered silver electrode by means of clamping rings.

Preparation of chlorophos–DNA conjugate

Chlorophos (0.0004 g) was dissolved in 2 ml of 0.1 mg ml^{-1} DNA solution. After stirring the solution for 15 min, glutaraldehyde (0.06 ml) was added.

Performance of diagnosis by inhibitor EMMIA technique using the EAS

To construct a peak current versus concentration plot, 4.3 ml of borate buffer were added to the electrochemical cell equipped with an SCE, then 0.2 ml of the conjugate and 1–10 μl of the γ-globulin fraction prepared from the sick mink blood serum (15 mg ml^{-1}) were injected. After stirring for 15 min, 0.5 ml of standard 1.9×10^{-2} M BuSChI solution was injected and the EAS was immersed in the cell. After deaerating for 15 min, cyclic voltammograms were recorded over the potential range -0.1 to -0.8 V (scanning rate 1 V s^{-1}, continuous polarization mode, triangular scanning). The peak current value at -0.55 V was measured.

To determine the unknown concentration of antibodies the above procedure was repeated with the injection of an analysed blood serum. The peak current value thus obtained was compared with the value for a blank experiment (without a conjugate and specific antibodies) and with that obtained in the presence of the conjugate and healthy mink blood serum.

Performance of diagnosis using the IEAS

To construct a calibration graph, 1–100 μl of 0.8 mg ml^{-1} γ-globulin fraction obtained from sick mink blood serum were added to 0.5 ml of 1.9×10^{-2} M BuSChI solution. The solution was

diluted to 5 ml with borate buffer and then injected into the cell equipped with an SCE and the IEAS. The peak current values for different antibody concentrations were measured as indicated above. The concentration of antibodies in a blood serum aliquot was calculated using a calibration graph.

RESULTS AND DISCUSSION

Enzyme amperometric sensor for inhibitor EMMIA

The determination of specific antibodies was based on the mercury mercaptide electrochemical activity. This compound results from the reaction of a thiol, producted by enzymatic hydrolysis of BuSChI, with the mercury of the electrode and produces a peak on the voltammogram at −0.55 V vs. SCE. The peak current value strongly depends on ChE activity and hence on the presence of its effectors (under the condition of constant concentration of BuSChI). The fact that the signal decreased in the presence of an inhibitor such as chlorophos was used to perform an inhibitor enzyme immunoassay according to the scheme presented in Fig. 1.

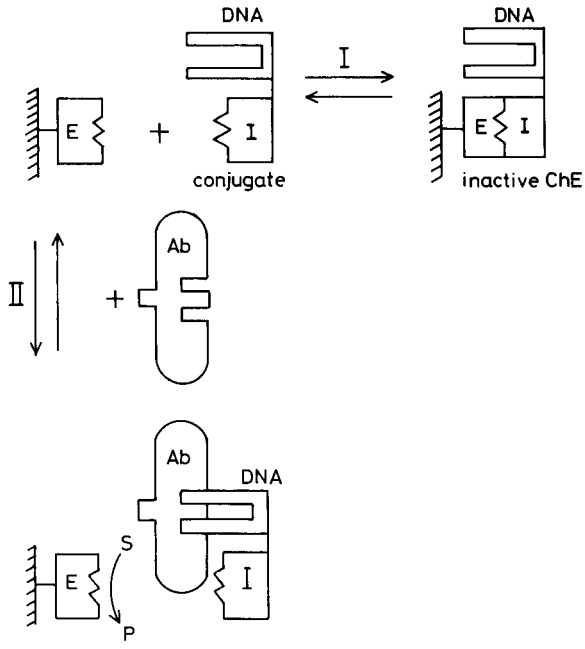

Fig. 1. Inhibitor enzyme modulator-mediated immunoassay using the EAS.

In EMMIA it is important to obtain a conjugate [antigen (antibody)–label couple] which is stable enough and possesses specificity towards corresponding antibodies (antigen). In this work DNA was used as an antigen (Fig. 1) owing to its capability to bind autoantibodies [16]. The use of chlorophos as a second component of the conjugate allows its stable adduct with DNA to be obtained while its inhibiting activity is not reduced.

When specific antibodies are absent from an analyte, the conjugate consisting of an inhibitor reaches the active sites of ChE freely and interacts with them, so preventing a substrate from approaching, i.e., the conjugate acts as an inhibitor (see path I in Fig. 1). This leads to a decrease in the peak current value. When specific antibodies are present, fast binding to DNA of the conjugate takes place (see path II, Fig. 1). As bulky molecules the antibodies in the immunocomplexes shield the inhibitor, so it cannot affect the ChE activity. The peak current value remains constant in this situation.

The proposed variant of inhibitor EMMIA on the basis of the steric hindrance effect was utilized in diagnosing an automimmune disease, Aleutian mink disease, which is characterized by a sharp increase in the level of immunoglobulins. This infection of mink produces a considerable economic loss [17]. The protocol for the diagnosis of such an autoimmune disease by means of this EMMIA variant is as follows: obtaining a control signal (without conjugate and serum); obtaining the analytical signal in the presence of the conjugate and serum free from specific antibodies; plotting the peak current value vs. IgG concentration; and obtaining the analytical signal in the presence of the conjugate and serum containing an unknown amount of specific antibodies.

The peak current vs. IgG concentration plot is presented in Fig. 2. This plot reaches a plateau when the concentration exceeds 1.2×10^{-7} M. This corresponds to the situation where all the inhibitor molecules of the conjugate are completely shielded with bulky immunocomplex

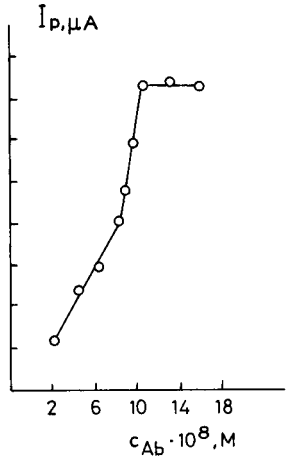

Fig. 2. Peak current value (I_p) vs. specific antibody concentration in blood serum in the presence of chlorophos–DNA conjugate. pH = 9.05; scan rate = 1 V s^{-1}; $E_0 = -0.1$ V.

molecules, thus losing their inhibiting activity. The linear portion of the plot in the range from 10^{-8} to 10^{-7} M in the presence of the chlorophos–DNA conjugate can be used as a calibration graph for the determination of antibodies. This is important for evaluating the gravity of the disease. The results of the determination of specific antibodies are summarized in Table 1.

An animal is considered healthy if the peak current value does not exceed the value obtained for a healthy animal serum plus three times the standard deviation of this value. The animal is regarded as sick when the peak current is above this level but less than a control analytical signal. The total time of analysis is 1.25 h. The obtainment of a control signal and a signal for healthy animals blood serum is not needed in subsequent runs for routine diagnosis by this method. The duration of the diagnosis is thus reduced to 30 min.

TABLE 1

Determination of specific antibodies using the EAS ($n = 5$, $P = 0.95$)

Added (10^8 M)	Found (10^8 M)	R.S.D. (%)
2.0	2.1	3.0
4.0	4.2	2.4
6.0	5.9	1.3
8.0	8.0	1.0

To provide the possibility for repeated use of ChE and the possibility of automation, the conditions for reactivation of the EAS biosensor part were established. When immersed in 2×10^{-2} M hydroxylamine solution for less than 10 min, the sensor demonstrates initial enzyme activity. The assay of a solution containing bovine or horse IgG shows a decrease in peak current as if only the conjugate were present in the system (without specific antibodies). This result confirms the selectivity of the assay.

The assay results were found to be in agreement with those obtained by a usual enzyme immunoassay on microtitration plates with spectrophotometric detection. However, the use of the EAS in EMMIA has several advantages: simplification of the assay by elimination of some steps (e.g., the separation of bound and unbound antibodies has become unnecessary); shortening of the time of assay from several hours to 30 min under routine conditions; a low limit of detection of 2×10^{-8} M specific antibodies provided by amperometric detection and high sensitivity of the enzyme reaction towards inhibitors; and versatility, as not only can various autoantibodies be determined, but also antibodies of many other types can be assayed by using a suitable antigen instead of DNA. The experimental error is less than 4%.

Immunoenzyme amperometric sensor for enzyme immunoassay

The inclusion of an antigen in the sensor part of the EAS allowed an IEAS to be constructed for a separation-free enzyme immunoassay. On the one hand this sensor serves as an immunological solid phase and contains ChE as an enzyme label, and on the other it provides the possibility for electrochemical monitoring of the enzyme activity.

Figure 3 shows the scheme of the enzyme immunoassay using the IEAS. If antibodies do not occur in the analyte, the situation is similar to that when using a simple EAS, namely BuSChI undergoes enzymatic hydrolysis and mercury mercaptide is reduced at the electrode. However,

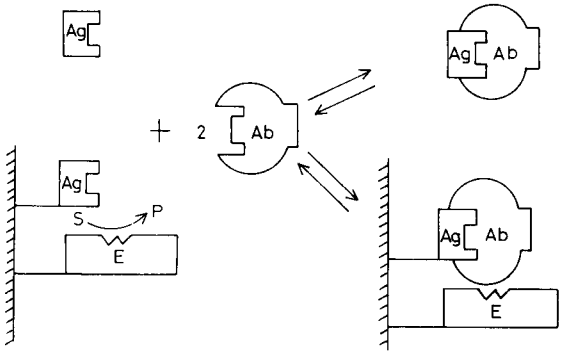

Fig. 3. Enzyme immunoassay using the IEAS.

when specific antibodies are present in the solution they bind rapidly (if there is no transport limitation by stirring the solution) to antigens immobilized in the nitrocellulose film to give antigen–antibody complexes. The complexes so formed produce steric hindrance to the transfer of the substrate molecules to the active sites of ChE, thus reducing the analytical signal. The conformational distortions in the ChE structure caused by immunocomplex formation seem to be another possible reason for the change in the enzyme activity. When unbound antigens are introduced into the system, which compete for binding sites with bound antigens, the extent of inhibition is decreased and the ChE activity is restored. This observation confirms the formation of immunocomplexes.

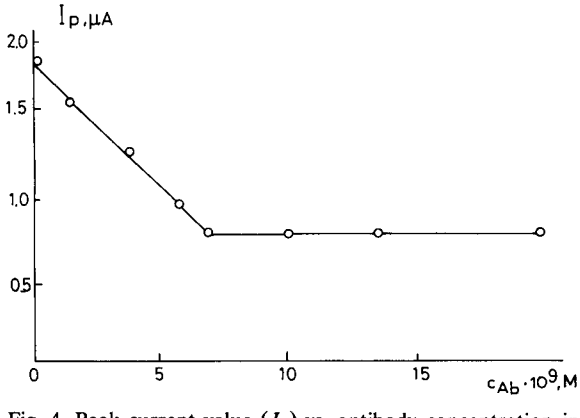

Fig. 4. Peak current value (I_p) vs. antibody concentration in blood serum measured with the IEAS.

TABLE 2

Determination of specific antibodies using the IEAS ($n = 5$, $P = 0.95$)

Added (10^9 M)	Found (10^9 M)	R.S.D. (%)
2.0	2.1	3.5
3.0	3.2	2.8
6.5	6.5	1.5

The IEAS was also utilized in the diagnosis of Aleutian mink disease. The peak current value was plotted against IgG concentration in sick mink blood serum to calculate the unknown concentration of specific antibodies (Fig. 4). The linear portion of this plot over the range 1×10^{-9}–7×10^{-9} M was used as a calibration graph. The limiting concentrations of 7×10^{-9} M may be ascribed to the binding of this amount of antibodies to the maximum possible amount of immobilized antigens, which prevents penetration of the substrate to the active sites of ChE. The peak current observed in this instance refers only to the spontaneous hydrolysis of BuSChI.

The results of the determination of specific antibodies with the IEAS are presented in Table 2. The diagnosis was based on the difference between the peak current in the presence and absence of mink blood serum. When healthy mink blood serum is injected into the cell this difference is not less than 2–3 times greater than the

TABLE 3

Diagnosis of Aleutian mink disease using enzyme immunoassay with (1) an immunoenzyme amperometric sensor and (2) spectrophotometric detection [a]

$I_p(\mu A)$	Absorbance at 492 nm	Result of diagnosis	
		(1)	(2)
1.8	0.414	+	+
0.9	0.423	+	+
2.0	0.010	–	–
1.0	0.344	+	+
1.9	0.034	–	–

[a] For (1), $I_p^0 = 2.0$ μA, $3 \times$ S.D. = 0.13 μA and for (2), $A^0 = 0.035$ (absorption of conjugate + healthy animal serum solution or of non-specific serum solution), $3 \times$ S.D. = 0.105, where I_p^0 is the value of the peak current in the absence of specific antibodies and A^0 is the value of the absorbance in the absence of specific antibodies.

standard deviation (under the present conditions the deviation equals 0.043 μA for five runs).

Some results of diagnosis are presented in Table 3. The results are in good agreement with those obtained by the usual enzyme immunoassay using spectrophotometric detection. The advantages of using the IEAS are the low limit of detection (5×10^{-10} M) arising from the heterogeneous character of the assay and the lack of a need to separate the components owing to the application of the steric hindrance effect. The lack of peak current lowering in the presence of human and bovine IgG shows the selectivity of this sensor. It should be mentioned that antibodies can be introduced into the biosensor part of the device instead of antigens, allowing the determination of corresponding antigens in biological liquids.

REFERENCES

1 H.C. Budnikov, E.P. Medyantseva and S.S. Babkina, J. Electroanal. Chem., 310 (1991) 49.
2 E.P. Medyantseva, H.C. Budnikov and S.S. Babkina, Zh. Anal. Khim., 45 (1990) 1386.
3 C. Blake and B.J. Gould, Analyst, 109 (1984) 533.
4 T.T. Ngo and H.M. Lenhoff (Eds.), Enzyme-Mediated Immunoassay, Plenum, New York, 1985.
5 B. Breyer and F.J. Radcliff, Nature (London), 167 (1951) 79.
6 W.R. Heineman, C.W. Anderson and H.B. Halsall, Science, 204 (1979) 865.
7 K.R. Wehmeyer, H.B. Halsall and W.R. Heineman, Clin. Chem., 28 (1982) 1968.
8 W.R. Heineman and H.B. Halsall, Anal. Chem., 57 (1985) 1321A.
9 J.D. Czaban, Anal. Chem., 57 (1985) 345A.
10 T.T. Ngo (Ed.), Electrochemical Sensors in Immunological Analysis, Plenum, New York, 1986.
11 M.J. Green, Philos. Trans. R. Soc. London, 316 (1987) 135.
12 D.M. Ivnitskiy, I.H. Kurochkin and S.D. Varfolomeev, Zh. Anal. Khim., 46 (1991) 1462.
13 T.T. Ngo and H.M. Lenhoff, FEBS Lett., 116 (1980) 285.
14 P.R. Finley, R.J. Williams and D.A. Lichti, Clin. Chem., 26 (1980) 1723.
15 H.C. Budnikov, E.P. Medyantseva, N.A. Ulakhovich and S.S. Babkina, Invention Certificate No. 1562831 (USSR), 1987.
16 N.E. Yastrebova and N.P. Vaneeva, in Enzyme Immunoassay in Disease Diagnosis, Moscow, 1989, p. 110.
17 I.I. Dukur, V.S. Slugin and V.A. Chizhov, in E.P. Danilov (Ed.), Fur-Bearers' Diseases, Nauka, Moscow, 1984, p. 78.

Analytica Chimica Acta, 273 (1993) 425–430
Elsevier Science Publishers B.V., Amsterdam

Development of amperometric sensors for choline, acetylcholine and arsenocholine

Beatriz Lopez Ruiz [1], Eithne Dempsey, Chi Hua and Malcolm R. Smyth
School of Chemical Sciences, Dublin City University, Dublin (Ireland)

Joseph Wang
New Mexico State University, Las Cruces, NM 88 003 (USA)

(Received 13th February 1992; revised manuscript received 1st June 1992)

Abstract

Immobilisation of acetylcholine esterase (ACE) and choline oxidase (COx) within a polymeric coating on a glassy carbon electrode resulted in the development of a sensor for the important transmitter acetylcholine and its metabolite choline. Anodic detection at +0.25 V vs. SCE is facilitated by the addition of the redox-mediating hexacyanoferrate(III) ion. The influence of various experimental parameters is described. Linearity for acetylcholine and choline responses extended up to 5 mM and 13 mM, with limits of detection of 43 μM and 50 μM, respectively. The simple immobilisation procedure and the rapid reaction kinetics between the mediator and the enzyme, coupled to a fast heterogeneous rate constant, resulted in rapid response times and good precision. An important application of the biosensor was shown for the determination of arsenocholine, using the choline oxidase immobilised electrode, resulting in a response ten times that obtained for choline, with linearity extending up to 0.6 mM and a limit of detection of 10 μM. The high selectivity offered by this sensor was indicated by the lack of interference offered by easily oxidised compounds normally found in serum, because of both the charge exclusion properties of the Nafion polymeric coating and the low operating potential required to re-oxidise the mediator.

Keywords: Amperometry; Biosensors; Sensors; Acetylcholine; Arsenocholine; Choline

Acetylcholine was the first documented transmitter for motor neurons in both the spinal cord and in nerve skeletal junctions in vertebrates. The considerable interest in the determination of levels of this compound has resulted in the development of various biosensors based on immobilised enzymes, with application in different areas of medicine, food and environmental analysis.

Correspondence to: M.R. Smyth, School of Chemical Sciences, Dublin City University, Dublin (Ireland).
[1] Permanent address: Laboratorio de Technicas Instrumentales, Facultad de Farmacia, Universidad Complutense, Madrid (Spain).

Previous methods which permitted the quantitation of acetylcholine include radiolabelling [1,2] and gas chromatographic techniques [3]. Several acetylcholine sensors have since been developed based on enzyme electrodes with potentiometric [4,5] or amperometric detection of oxygen [6,7] or hydrogen peroxide [8–10]. However, the consumption of oxygen may be strongly affected by fluctuations in the ambient oxygen concentration, while, in the case of hydrogen peroxide detection, the applied potential is very high, and hence the method is susceptible to easily oxidisable interferents.

The co-immobilisation of the enzymes acetylcholine esterase (ACE) and choline oxidase (COx) on an alkylamino-bonded silica surface using glutaraldehyde has been incorporated as the enzyme reactor in a liquid chromatographic system for detection of acetylcholine and choline [11]. An ultramicro acetylcholine sensor based on modified carbon fiber electrodes with entrapment of both enzymes within a polyvinyl alcohol–quarternised stilbazole matrix has also been reported recently [12].

Previously published methods for the determination of toxic substances, e.g. organophosphorous and carbamate pesticides, based on the inhibitory effects of these compounds on acetylcholinesterase activity, have made use of pH electrodes which indicate the generation of protons in the cholinesterase-catalysed reaction [13,14]. Choline electrodes for pesticide analysis have also been previously described [15,16]. A screen-printed sensor, based on 7,7,8,8-tetracyanoquinodimethane-modified graphite and immobilised butyrylcholinesterase, was found to be sensitive to non-competitive inhibition by organophosphates in the range 0.06 to 8 ppm [17]. Another recent report of an amperometric biosensor for pesticides was based on a cobalt–phthalocyanine modified carbon paste electrode with a cholinesterase enzyme membrane [18].

Preliminary experiments in our laboratory indicated that the signal-to-noise ratio could be improved by immobilising the enzymes at the surface of the electrode rather than by mixing them directly in the carbon paste electrode. A similar observation was found by Skladal et al. [19] who described the development of a sensor based on the co-immobilisation of ACE and COx on a glassy carbon electrode, permitting the quantitative measurement of acetylcholine and choline. The soluble mediator potassium hexacyanoferrate(III) has been shown to efficiently reoxidise the reduced flavin adenine dinucleotide centres of choline oxidase. An important arsenic complex of choline, namely arsenocholine, found in fish tissue, could be determined using the choline oxidase modified glassy carbon electrode, therefore allowing the development of a novel biosensor for the quantitation of this compound.

EXPERIMENTAL

Apparatus

Amperometric measurements were performed using an EG&G PAR Model 174A polarographic analyser connected to a Philips Model PM 8251 recorder. Cyclic voltammetry was performed with an EG&G PAR Model 264A polarographic analyser and a JJ Instruments Model PL4 recorder. Experiments were carried out in a 10-ml electrochemical cell using a saturated calomel reference electrode, a platinum wire auxillary electrode and a glassy carbon working electrode. A magnetic stirrer and bar provided the convective transport.

Reagents

All chemicals were of analytical grade, and deionised water, obtained by passing distilled water through a Milli-Q water purification system, was used to prepare all solutions. Choline oxidase, acetylcholinesterase and choline were all purchased from Sigma, while acetylcholine and Nafion were obtained from Aldrich. Arsenocholine was obtained as part of a study of arsenic speciation organised by the Bureau of Certified Reference Materials (BCR) of the European Community.

Electrode preparation

Prior to coating, the glassy carbon electrode was polished using an alumina slurry. Modification of the electrode was achieved by applying 5 μl of a choline oxidase solution containing 5 mg ml^{-1} enzyme (12 U mg^{-1}), resulting in an activity of 0.382 U cm^{-2}, for the choline electrode. In the case of the acetylcholine sensor, an additional 0.5 μl of acetylcholinesterase solution containing 1 mg ml^{-1} of enzyme (950 U mg^{-1}) was applied to the surface (resulting in an activity of 0.475 U ACE cm^{-2}) and allowed to dry using a heat gun. 5 μl of a Nafion solution (diluted 1 in 10 with deionised water) was then placed on the enzyme layer and subsequently dried until a stable film was obtained. When not in use, the electrodes were stored at 4°C in phosphate buffer pH 7.0.

RESULTS AND DISCUSSION

Constant potential measurements

Preliminary studies on the amperometric detection of H_2O_2 with the choline oxidase modified electrode was performed in phosphate buffer (0.1 M, pH 6.5). The background transient current was allowed to decay to a constant value before samples of a stock choline solution were injected into the electrolyte. The time required to reach 95% of the amperometric steady state current was typically < 5 s after addition of the choline sample. As was expected in the absence of biocatalytic activity, the unmodified electrode showed no response to choline. Despite the high operating potential (0.85 V) required for monitoring the hydrogen peroxide produced in the enzymatic reaction, favourable signal-to-noise (S/N) ratio characteristics were observed.

However, when the electrolyte contained 1 mM hexacyanoferrate(III) ion, the current density for choline addition was considerably greater, due to recycling of the mediator between the Fe(II) and Fe(III) states.

$$\text{Acetylcholine} \xrightarrow{\text{ACE}} \text{Choline} + \text{Acetate}$$

$$\text{Choline} + 2O_2 + H_2O \xrightarrow{\text{COx}} \text{Betaine} + H_2O_2$$

$$Fe(CN)_6^{3-} + e^- \rightarrow Fe(CN)_6^{4-}$$

Therefore in subsequent experiments, 1 mM potassium hexacyanoferrate(III) was used in solution, and reoxidation of the hexacyanoferrate(II) ion achieved by applying a potential of 0.25 V.

Development of an amperometric electrode for choline

The sensitivity of the choline electrode was affected by various preparation and operational parameters. At low surface loadings of the enzyme the response exhibited the greatest current but the poorest linearity; hence a loading of 0.382 U cm^{-2} electrode surface was chosen as a compromise. The solution pH was found to have a profound effect on the sensitivity (Fig. 1), with a decrease in the response observed with increasing pH. The best S/N ratio was obtained with a solution of pH 6.5 which was subsequently used in further experiments.

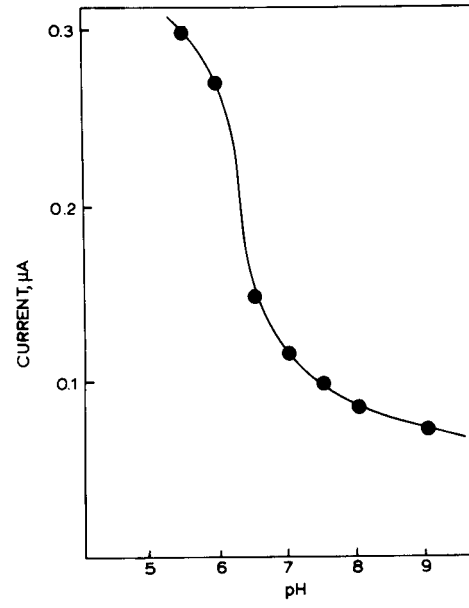

Fig. 1. Dependence of the choline response upon the solution pH. Electrolyte: phosphate buffer (0.1 M) containing 1 mM potassium hexacyanoferrate(III); applied potential, 0.25 V, loading 0.382 U COx cm^{-2}; solution stirring rate, 200 rpm; sensitivity, 2 μA full scale.

Since choline has a pK_a of 13.9, it will be positively charged at pH 6.5, and therefore will partition preferentially into the anionic polymeric Nafion layer. The dependence of the choline response on the concentration of the redox mediating hexacyanoferrate(III) ion is shown in Fig. 2. The catalytic current increases rapidly with mediator concentration up to 1 mM, after which it was not the limiting factor.

A typical response trace of current density vs. time for choline under the optimum conditions outlined above, allows a limit of detection (L.O.D.) (based on three times the standard deviation of the background current) of 50 μM. Calibration curves for 1 mM additions of choline, for two different enzyme loadings can be seen in Fig. 3. In the case of 0.30 U choline oxidase per cm^2 electrode surface, linearity extended between 1 and 10 mM choline with a correlation coefficient $r = 0.999$ and sensitivity of 41.0 nA mM^{-1}. For a loading of 0.382 U cm^{-2}, linearity was observed between 1 and 13 mM ($r = 0.999$) with a sensitivity of 48.0 nA mM^{-1}.

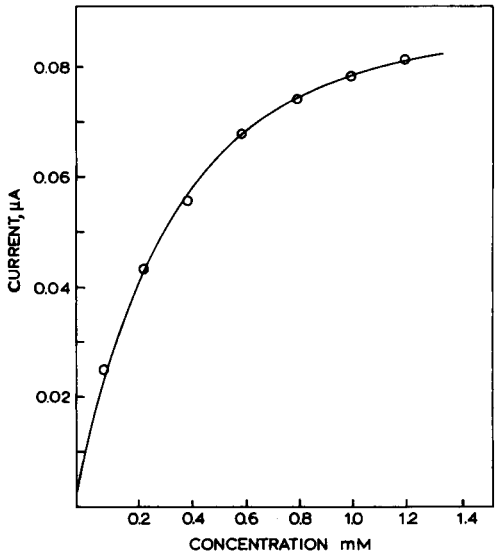

Fig. 2. Optimisation of mediator concentration in solution. Loading, 0.077 U cm^{-2} COx. Injections of 2 mM choline. Conditions as for Fig. 1.

Determination of arsenocholine

A novel application of this sensor was demonstrated in the determination of arsenocholine. The amperometric response to 0.04 mM additions may be seen in Fig. 4. Linearity was found

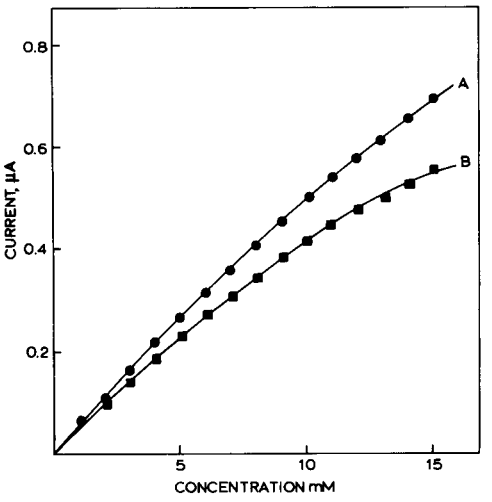

Fig. 3. Calibration curves for two surface loadings of COx (A) 0.382 U cm^{-2} and (B) 0.307 U cm^{-2}. Injection of 1.0 mM choline. Sensitivity, 0.5 μA full scale. Other conditions as for Fig. 1.

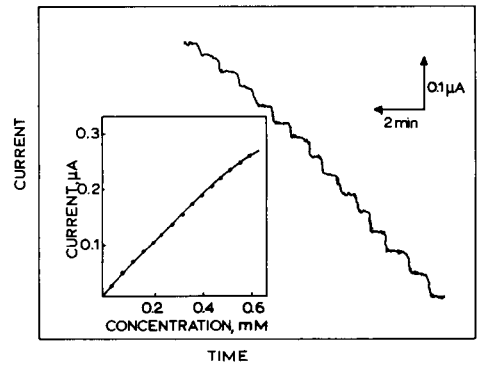

Fig. 4. Current–time response for successive 10 mg l^{-1} injections of arsenocholine. Loading, 0.307 U cm^{-2} COx.

to extend from 0.04 to 0.6 mM with $r = 0.998$ and a sensitivity of 0.44 μA mM^{-1}. The greater sensitivity observed for arsenocholine may be due to interaction with the metal and the enzyme binding site. Substrate specificity of the enzyme was enhanced by the metal complex, which perhaps caused steric modification, thus increasing the affinity of the substrate for the active site.

Development of an acetylcholine sensor

The acetylcholine sensor fabrication involved co-immobilisation of both choline oxidase and acetylcholinesterase, this layer being subsequently covered with the polymeric Nafion coating. The same electrolyte and conditions were employed as for the choline determination. Changes in the surface loading were not found to appreciably modify the amperometric response for either choline or acetylcholine. The amperometric response of this electrode to successive additions of both compounds can be seen in Fig. 5; each addition effecting a 0.5 mM increase in concentration. A shorter linear range was obtained in the case of the acetylcholine response, extending only up to 5 mM with a L.O.D. of 43 μM.

Cyclic voltammetry

Cyclic voltammetry of the hexacyanoferrate(III) ion at a Nafion coated glassy carbon electrode showed a completely reversible behaviour. The current obtained here, however, was lower than that obtained at the bare glassy car-

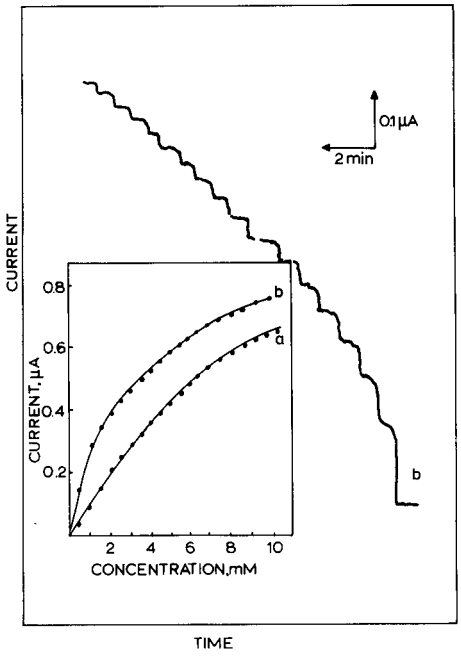

Fig. 5. Amperometric response for successive (a) 0.5 mM additions of choline, (b) 0.5 mM acetylcholine. Loading, 0.382 Units COx and 0.475 U ACE cm^{-2} electrode surface. Sensitivity, 1 μA full scale.

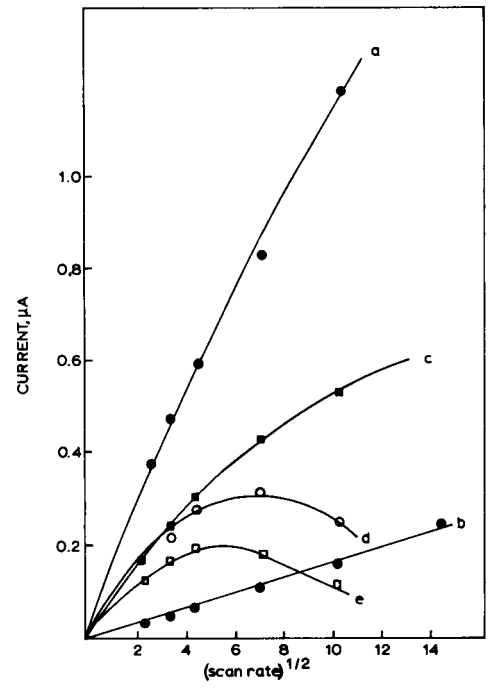

Fig. 6. Steady state current vs. (scan rate)$^{1/2}$ for (a) bare glassy carbon electrode, (b) Nafion modified electrode, (c) Nafion and COx modified electrode, (d) Nafion and ACE modified electrode, (e) COx and ACE (0.382 U COx and 0.602 U ACE per electrode) modified electrode.

bon, perhaps due to some electrostatic repulsion involving the Nafion polymer. When the glassy carbon electrode was modified with both choline oxidase and Nafion, the mediator also exhibited reversible behaviour, and the current was only slightly higher, perhaps due to the ionic interaction between the enzyme and the polymer, resulting in a lower net charge within the film in contact with the solution. The effect of modification with acetylcholinesterase resulted in irreversible behavior for the mediator. The non-linear relationship between i_p and $v^{1/2}$ indicates a slow mass transfer process, probably due to the additional complexity of this film when modified with this enzyme as opposed to choline oxidase. This phenomenon was even more pronounced when the electrode was modified with both enzymes. Figure 6 shows the relationship between current and $v^{1/2}$ for the various modified electrodes. These curves show initial diffusion control followed by limitation due to electron transfer at high scan rates. The potential difference between E_a and E_c increased as the complexity of the film increased, as shown in Table 1.

Apparent Michaelis–Menten constants

The linear response range of the sensors can be estimated from a Michaelis–Menten analysis of different calibration curves (Table 2), using the

TABLE 1

Oxidation and reduction potentials for various modified electrodes [a]

Electrode	E_a (V)	E_c (V)	ΔE (mV)
Bare	0.24	0.15	90
Nafion coated	0.20	0.15	50
COx + Nafion	0.24	0.14	100
ACE + Nafion	0.34	0.05	290
COx/ACE(i) + Nafion	0.31	0.02	290
COx/ACE(ii) + Nafion	0.44	−0.07	520

[a] COx/ACE(i) corresponding to 0.382 and 0.602 U cm^{-2}, and COx/ACE(ii) 0.382 and 0.475 U cm^{-2}, respectively.

TABLE 2

Comparison of apparent Michaelis–Menten constants and I_{max} values for different analytes

Analyte [a]	Apparent K_m (μA mM^{-1})	I_{max} (μA)
(A)		
Choline: 0.30 U	83.60	5.00
0.24 U	51.96	2.50
(B)		
Arsenocholine	1.35	0.87
Choline	67.05	1.20
(C)		
Acetylcholine	1.37	1.14
Choline	11.63	1.33

[a] (A) Different loadings of COx; (B) Arsenocholine and choline responses for the same COx (0.307 U cm^{-2}) electrode; (C) Acetylcholine and choline responses under the same conditions as in Fig. 5.

Lineweaver–Burk plot of $1/i_{ss}$ (μA) vs. 1/(substrate concentration (mM)), where i_{ss} represents the steady state current. The apparent K_m value obtained from the slope of such plots provides a measure of the substrate concentration over which the electrode response is linear, and characterises the enzyme electrode – not the enzyme itself. I_{max} represents the maximum current density measured under conditions of enzyme saturation. The additional diffusional restrictions imposed as a result of increased loading, and therefore complexity on the electrode surface, cause alteration of the basic catalytic properties, together with causes a shift in apparent K_m. In particular, the lower apparent K_m values for the arsenocholine and acetylcholine responses prove the enhanced sensitivity of the sensor towards these compounds.

Conclusion

These results demonstrate the feasibility of constructing an amperometric biosensor for acetylcholine that allows a very fast response time while operating at low applied potentials, where the oxidation of interferents, e.g. ascorbic acid in neurochemical applications and the reduction of oxygen, are minimised. The polymeric Nafion coating enhances the discriminative properties of the electrode surface in that it serves to reject anionic interferences. The high sensitivity of the bienzyme sensor makes it useful for future measurements in biological media. An in vivo acetylcholine sensor would be a powerful tool for elucidating the site of acetylcholine action in the brain. In order to apply this sensor to real life situations, miniaturisation is necessary, together with a lowering of the limit of detection in order to reliably measure actual neurotransmitter release. The sensor system could also be useful in environmental studies related to arsenic accumulation in fish.

B.L.R. gratefully acknowledges financial support from La Communidad Autonoma de Madrid.

REFERENCES

1 M.L. Gilberstadt and J.A. Russell, Anal. Biochem., 138 (1984) 78.
2 D.R. Haubrich, N. Gerber, A.B. Pfueger and M. Zweig, J. Neurochem., 36 (1981) 1409.
3 I. Hanin and R.F. Skinner, Anal. Biochem., 66 (1975) 568.
4 P.D. Hale, L.-F. Liu and T.A. Skotheim, Electroanalysis, 3 (1991) 751.
5 K. Gibson and G.G. Guilbault, Anal. Chim. Acta, 80 (1975) 245.
6 P. Durand, A. David and D. Thomas, Biochem. Biophys. Acta, 527 (1978) 277.
7 L. Campanella, M. Mascini, G. Palleschi and M. Thomasetti, Clin. Chim. Acta, 151 (1985) 71.
8 L. Campanella, M. Tomassetti and M. Sammartino, Analyst, 113 (1988) 77.
9 M. Mascini and D. Moscone, Anal. Chim. Acta, 179 (1986) 439.
10 K. Sode, J. Marty and I. Karube, Anal. Chim. Acta, 228 (1989) 49.
11 R.M. Morelis and P.R. Coulet, Anal. Chim. Acta, 231 (1990) 49.
12 T. Yao, Anal. Chim. Acta, 153 (1983) 169.
13 E. Tamiya, Y. Sugiura, E.N. Navera, S. Mizoshila, K. Nakajiama, A. Akiyama and I. Karube, Anal. Chim. Acta, 251 (1991) 129.
14 R. Gruss and F.W. Scheller, Fresenius' Z. Anal. Chem., 333 (1989) 29.
15 P. Durand, J.M. Nicauld and J. Mallevialle, J. Anal. Toxicol., 8 (1984) 112.
16 R. Kindervater and R.D. Schmid, in A.P.F. Turner et al. (Eds.), Proc. Biosensors, 90 Singapore, May 1990, Elsevier, Amsterdam, pp. 240–241.
17 U. Luffer, U. Wollenberger, F.W. Scheller and W. Gopel, Fresenius' Z. Anal. Chem., 335 (1989) 295.
18 J. Kulys and E.J. D'Coste, Biosensors Bioelectron., 6 (1991) 109.
19 P. Skladal, Anal. Chim. Acta, 252 (1991) 11.

Analytica Chimica Acta, 273 (1993) 431–433
Elsevier Science Publishers B.V., Amsterdam

Determination of 2-chloroethyltrimethylammonium chloride in Retacel by ion-selective electrode potentiometry and capillary isotachophoresis

Jiří Koleček, Václav Říha and Karel Vytřas

Department of Analytical Chemistry, Technical University of Pardubice, 53210 Pardubice (Czechoslovakia)

(Received 1st June 1992)

Abstract

Retacel [chlormequat, 2-chloroethyltrimethylammonium chloride, chlorocholine chloride (CCC)] is used in agriculture in aqueous solution. In such solutions, the 2-chloroethyltrimethylammonium cation can be determined by potentiometric titration using sodium tetraphenylborate and a simple coated-wire plastic membrane electrode. At lower concentration levels, the preparation was analysed by capillary isotachophoresis using sodium acetate as the leading electrolyte and 6-aminocaproic acid as the terminator in a medium buffered to pH 4.5 with citric acid. To determine the CCC concentration, a calibration graph was used. Adsorption of Retacel on sand and soil was also studied and the result indicated that the contamination of ground water is hardly possible.

Keywords: Electrophoresis; Potentiometry; Titrimetry; Chloroethyltrimethylammonium chloride; Herbicides; Ion-selective electrodes; Isotachophoresis

Chlormequat [2-chloroethyltrimethylammonium chloride, known also as chlorocholine chloride (CCC)] is a growth regulator that positively influences the formation of robust straws of corns. It can also be applied in flower and fruit growing. The substance used in such way is able to release ethylene in a concentration having a favourable influence on different biological functions of plants. In Czechoslovakia, the preparation Retacel, containing ca. 60% of the active substance, is available and applied to ca. 600000 ha of corn fields [1]. The possible contamination of drainage or ground water must be monitored because preparations based on CCC are classified as highly toxic irritants.

The determinations of CCC can be performed spectrophotometrically by measuring the absorbance of its dipicrylaminate extracted into dichloromethane [2,3]. A titration procedure based on precipitation of the counter chloride ion with silver nitrate is used by the manufacturer for product quality control [4]. Direct titration of the 2-chloroethyltrimethylammonium cation is also feasible using sodium tetraphenylborate as a titrant and a plastic membrane coated-wire electrode as a simple potentiometric sensor [5]. For lower concentrations, isotachophoresis has been found to be advantageous for the final determination of cationic herbicides [6]. The last two methods were modified and used in the study presented here.

Correspondence to: K. Vytřas, Department of Analytical Chemistry, Technical University of Pardubice, CS-53210 Pardubice (Czechoslovakia).

EXPERIMENTAL

Stock solutions of CCC were prepared from the preparation Retacel (Lučební závody Kolín) and their concentrations were controlled poten-

tiometrically. For the control, sodium tetraphenylborate solution (0.01 M) was prepared by dissolving about 1.71 g of the compound (VEB Jenapharm Laborchemie, Apolda) in water, adjusting the pH to 9 with sodium hydroxide and diluting to 500 ml with water. The sodium tetraphenylborate titrant was standardized potentiometrically against standard 0.01 M thallium(I) nitrate solution.

A Model OP-208/1 digital pH meter (Radelkis, Budapest) was used with a 10-ml burette. The indicator electrode was prepared as described previously [7] by coating an aluminium conductor with a membrane from a solution of poly(vinyl chloride) (0.085 g) and 2,4-dinitrophenyl *n*-octyl ether (0.2 ml) in tetrahydrofuran. A double-junction calomel electrode (RCE-102; Crytur, Turnov) filled with 0.1 M sodium nitrate solution was used as a reference electrode.

Isotachophoretic determinations were done on a CS isotachophoretic analyser (VÚVJF, Spišská Nová Ves), equipped with two capillary columns: a preseparation capillary (200 × 0.8 mm i.d.) and an analytical capillary (200 × 0.3 mm i.d.). The current was set at 300 μA for the separation column and 45 μA for the analytical column. A conductivity detector was used; the zone lengths were measured as distances of two peaks from the derivative record with a scan rate of 0.25 mm s^{-1}. The operational system consisted of 0.01 M sodium acetate as the leading electrolyte and 0.01 M 6-aminocaproic acid as the terminator, both buffered to pH 4.5 with citric acid. Samples (30 μl) were dosed using a capillary stopcock.

RESULTS AND DISCUSSION

Potentiometric titration was found useful for analysing the herbicide preparations if the aqueous solutions are not too dilute with regard to the active substance (ca. 5×10^{-3} M, Fig. 1). For lower concentrations, ion-pair formation with tetraphenylborate anion gives rise to the potentiometric titration curve, the end-point of which can be readily evaluated, but the reproducibility of the results is worse when the concentration of CCC is below ca. 5×10^{-4} M.

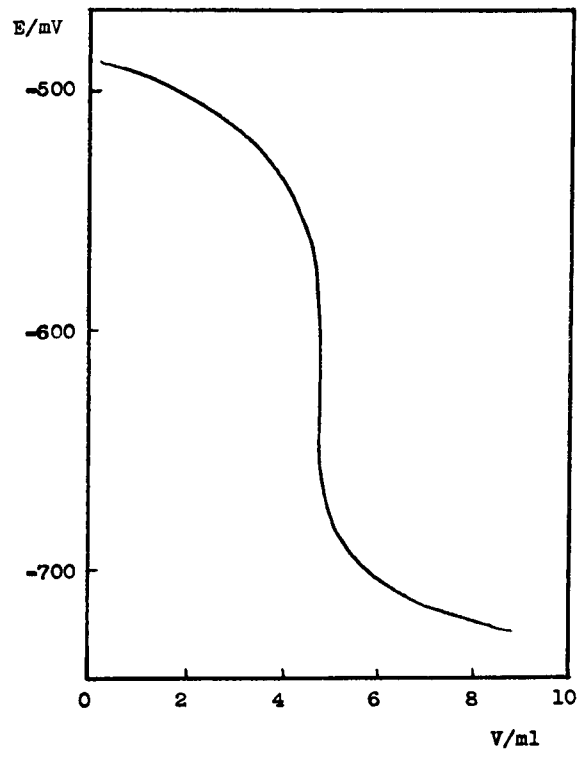

Fig. 1. Potentiometric titration curve for Retacel preparation (80.07 mg in 50 ml) titrated with sodium tetraphenylborate (0.0616 mol l^{-1}).

For more diluted solutions (6×10^{-5}–7×10^{-4} M), isotachophoresis was used, which gave a linear calibration graph (Fig. 2, line 1). Contamination of different soils and sands at the same concentration level was then artificially performed and 50-g samples were taken. For the determination of CCC, the contaminated samples were extracted with water (50 ml). It was found that only ca. 15% of the total amount of CCC was liberated from the soil samples by simple extraction (Fig. 2, line 3). Using repeated extraction, it was confirmed that higher yields can be obtained, but up to ca. one third of the original CCC concentration at most. Treating the samples by Soxhlet extraction at higher temperature also gave low yields. Analysis of the sand samples gave yields for simple extraction of ca. 30% (approximately twice those for the soil samples; see line 2 in Fig. 2).

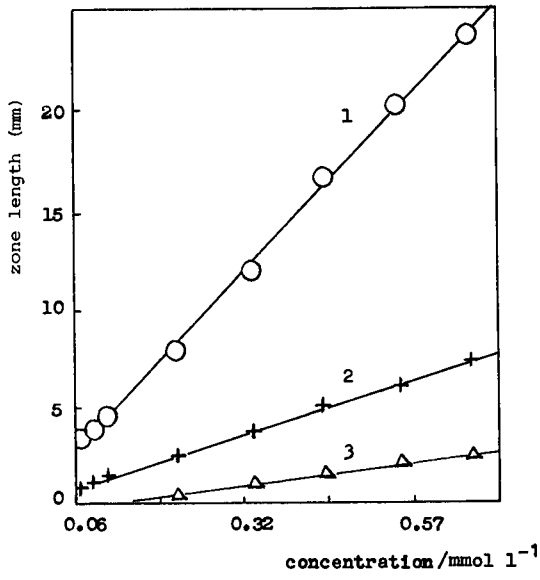

Fig. 2. Calibration graphs for CCC based on capillary isotachophoresis. 1 = Aqueous solutions; 2 = sand extracts; 3 = soil extracts.

It can be concluded that the soils exhibit good adsorption properties with respect to CCC, depending to some extent on the soil quality. Therefore, contamination of ground water is hardly possible, taking into account that the application level of Retacel in agriculture is about 3–8 l ha^{-1}, depending on the kind of crop. In addition, CCC degrades rapidly in soil [1], within 2–3 weeks depending on its biological effectivity. These conclusions were also confirmed by analyses of ground water, in which no detectable amounts of CCC were found.

REFERENCES

1 J. Pilný, Chemické Látky v Zemědělství, VŠCHT, Pardubice, 1988, p. 137.
2 R.P. Mooney and N.R. Pasarela, J. Agric. Food Chem., 15 (1967) 989.
3 J. Jung and G. Henjes, Z. Pflanzenernähr. Bodenkd., 124 (1969) 97.
4 J. Fischer, personal communication.
5 K. Vytřas, M. Dajková and V. Mach, Anal. Chim. Acta, 127 (1981) 165.
6 Z. Stránský, J. Chromatogr., 320 (1985) 219.
7 K. Vytřas, Microchim. Acta, Part III, (1984) 139.

Analytica Chimica Acta, 273 (1993) 435–441
Elsevier Science Publishers B.V., Amsterdam

Electrochemical detection for flow analysis and liquid chromatography: present status and some roads to the future

Karel Štulík

Department of Analytical Chemistry, Charles University, Albertov 2030, 128 40 Prague 2 (Czechoslovakia)

(Received 1st June 1992)

Abstract

The field of flow electroanalysis is briefly surveyed, emphasizing the common hydrodynamic basis of continuous monitoring, continuous flow and flow-injection analysis and liquid chromatography (LC). Examples of recent developments are given for potentiometric and voltammetric detection. Special attention is paid to the use of ion-selective microelectrodes and large-volume wall-jet cells in potentiometric detection, the use of voltammetric microelectrodes for detection in open-tubular column LC, physical, electrochemical and biochemical modification of solid voltammetric electrodes and application of cells with solid polymer electrolytes to amperometric detection in liquids with very low electrical conductivity.

Keywords: Amperometry; Flow injection; Liquid chromatography; Potentiometry; Voltammetry; Electrode modification; Microelectrodes

The importance of flow analytical measurements is steadily increasing, as demonstrated in numerous original and review papers and monographs [1–4]. The field is very broad, ranging from continuous industrial, environmental and clinical monitoring, through continuous-flow (CFA) and flow-injection analysis (FIA), to liquid chromatography (LC). All these methods are based on common hydrodynamic principles and thus the detection techniques are generally applicable, on condition that the design of the detector cell and the selection of experimental conditions take into account the number of theoretical plates (tanks in series) characterizing the analytical system in hand [4,5]. At present, there is extremely rapid progress in electromigration methods and their combinations with other separation methods. Many aspects of flow and electromigration systems are similar; therefore, many detection techniques developed for flow measurements, especially LC, have been successfully applied to electrophoretic measurements [6].

UV–visible spectrophotometry is the workhorse among the methods employed for flow detection and is replaced by other methods only when its sensitivity and/or selectivity are insufficient for a particular analysis. Electrochemical detection is one of the alternatives.

Two classes of electrochemical measurement are employed in flow detection: one class is based on charge transfer between a liquid or gaseous phase containing the analyte(s) and a solid or immiscible liquid phase that is electrically conductive or semiconductive, and includes the most common potentiometric, voltammetric and coulometric detection techniques, and the other class

Correspondence to: K. Štulík, Department of Analytical Chemistry, Charles University, Albertov 2030, 128 40 Prague 2 (Czechoslovakia).

involves the measurement of the electrical properties of liquids, i.e., the electrical conductivity and relative permittivity.

Conductivity detectors are inherently non-selective and find use primarily for continuous monitoring of electrolytes and in ion chromatography. High-frequency measurement of impedance is universal, but suffers from limited sensitivity, high noise and a pronounced signal dependence on temperature. These detectors will not be discussed in detail and attention will be concentrated on charge-transfer detection techniques.

Detection based on charge-transfer reactions is selective and the selectivity can be varied to some extent by judiciously controlling the experimental conditions. The measurement can be made highly sensitive, retaining acceptable precision. On the other hand, problems may arise from the interactions of the electrode surface with the sample (adsorption effects, interfering chemical and electrochemical reactions). However, this inevitable problem, which has so often discouraged many workers from using electrochemical methods, can also be exploited to broaden the scope of the methods, as demonstrated, e.g., in stripping analysis and the dynamic field of electrode modification.

In electrochemical flow measurements it is possible to use all the extensive experience gathered during many decades of study and application of batch measurements, but two important characteristics of flow experiments must always be borne in mind [4]: the active surface of the sensor must be sufficiently mechanically strong to withstand liquid flow, and, except for continuous monitoring, the analyte forms a zone of a certain shape and width in the stream and its residence time in the analytical system is not very long. Therefore, the time constants of all the processes involved, from the sample introduction into the stream to the display of the analytical signal, must be sufficiently small to suppress distortion of the zone profile and of the signal. In addition, the very small cells used in LC exhibit a high impedance and their behaviour deviates from the general theory which is based on the assumption that the cell dimensions are much larger than the diffusion layer thickness. Consequently, the detection conditions should always be derived from measurements performed in the given flow cell and not from the data obtained in large cells and batch experiments.

At present, standard techniques of potentiometric, voltammetric and coulometric detection are firmly established; it is understood that these detectors are really practically advantageous only in certain application areas and these applications are well known. There are many types of measuring cells and procedures, but they generally fall into just a few basic classes. The detectors can be made and modified in the laboratory, but standard electrochemical detectors are available from many manufacturers. Therefore, current research efforts are directed toward further improvements in the sensitivity, selectivity, reliability and versatility of electrochemical detection; in this paper some of the promising trends are discussed.

POTENTIOMETRIC DETECTION

With few exceptions, potentiometric flow detection employs ion-selective electrodes (ISEs) as the sensors. The instrumentation and measurement are simple and thus the method has become popular in continuous monitoring, CFA and FIA [1,4,7]. However, its use in LC is very limited, for two main reasons: the sensors are usually too selective for chromatographic detection and, more important, their response is slow and usually becomes even slower with decreasing activity of the analyte. Nevertheless, there are two examples of chromatographic detection that are promising for the future: ion-selective microelectrodes can be inserted into the end of a capillary LC column, thus obtaining simple detector cells with extremely small effective volumes [8,9]; so far, such detection has been used for the alkali and alkaline earth metal ions; and a pH electrode can be employed as a universal sensor for detection in suppressed ion chromatography and a potassium ISE for detection in replacement ion chromatography, with a sensitivity better than that of conductimetric detection [10].

Chemically sensitive transistors (CHEMFETs) and related semiconductor sensors [11] exhibit a number of very attractive features for flow detection, mainly rapid response, small size, low impedance and the possibility of placing several sensors on a single chip. However, they have so far not lived up to their promise completely, primarily because of technical difficulties in encapsulation and preparation of selective membranes and because their signal is not very stable. There has, however, been some progress in the encapsulation methods which are applicable not only to semiconductor materials, but also to metal and carbon microelectrodes, and include photolithography [12], glass bonding [13], micromachining [14] and electrochemical generation of a poly(oxyphenylene) film [15].

A detailed discussion of the consequences of the slow response of ISEs and related sensors [16] has demonstrated that not only are the sensitivity, precision and sample throughput of flow measurements affected, but that also there is a significant influence on the measuring selectivity. The overall response time of an ISE can be decreased by using higher flow-rates while keeping the measuring cell sufficiently small (below ca. 100 μl); the flow-rate must, however, be optimized from the point of view of the hydrodynamic conditions in the whole flow-through system [17].

Very good results have been obtained using metallic tubular electrodes with a thin coating of an ion-selective material [18–20]; typical response times are below 2 s, relative standard deviations (R.S.D.) are below 2%, the limits of detection are low (e.g., 10 μg Cl^- l^{-1}), the lifetime of the sensor is several months and the ion-selective coating is readily renewed [20].

So far, solid-membrane ISEs have been better suited than liquid-membrane ISEs for flow detection, because of their faster response, greater mechanical strength and longer lifetime. However, there has been great progress in the preparation of plastic membrane ISEs that has led to increasing numbers of applications in flow analysis [21,22]; e.g., photocured polymeric membranes are very suitable for flow detection [23].

It has been found [24] that large-volume wall-jet cells are very advantageous in flow analysis

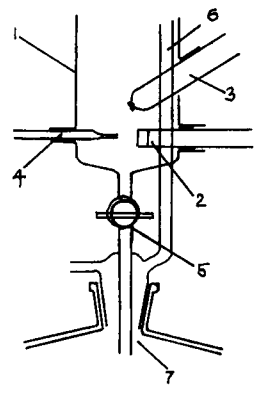

Fig. 1. Large-volume wall-jet cell [24]. 1 = Cylindrical glass vessel; 2 = working electrode; 3 = reference electrode; 4 = nozzle; 5 = solution outlet stopcock; 6 = tube maintaining a constant solution level; 7 = waste bottle.

with ISE detection. This type of cell was originally designed [25,26] for amperometric detection and later also used for potentiometric stripping [27] and potentiometric [28] analysis. The liquid jet issuing from the nozzle remains intact even at distances of the nozzle from the electrode surface of up to ca. 10 mm, the effective working volume of the cell is small, less than the volume of the hydrodynamic boundary layer at the electrode, and the stream of the test solution protects the electrode from the influence of the liquid in the cell.

A design of such a cell [24] is shown in Fig. 1. The horizontal position of the nozzle and the electrode prevents air bubbles from sticking to the electrode surface. This cell permits continuous regeneration of the electrode surface, e.g., an acidic solution of aluminium ions is placed in the cell in the determination of fluoride to remove passivating layers from a fluoride ISE, or a diaminocyclohexanetetraacetic acid (DCTA) solution is used for this purpose in measurements with a chloride ISE. When a sample is pumped through the nozzle, the electrode is shielded by the sample solution from the regeneration solution in the cell and the electrode responds to the sample; between samples, air is pumped through the nozzle, thus stirring the regeneration solution at the electrode and accelerating the cleaning process. In this way, highly reproducible and sensitive determinations can be carried out (e.g.,

limits of detection for fluoride and chloride are 6.3×10^{-8} and 2.3×10^{-7} mol l^{-1}, respectively, with R.S.D. values below 3%, a sample throughput of 90 h^{-1} and the lifetime of the regeneration solution of at least 150 measurements).

VOLTAMMETRIC DETECTION

The standard techniques of amperometric and coulometric detection are now generally known and routinely used. In an effort to improve further the analytical parameters and versatility, research is in progress in several main directions: use of micro- and ultramicroelectrodes; physicochemical and biochemical modification of the electrode surface and use of selective chemical reactions between the analyte and the electrode; rapid-scan techniques, dual- and multi-channel detection; combinations of several detection methods, spectroelectrochemistry and spectrochemical derivatization; membrane electrodes and solid-polymer electrolyte cells; and charge transfer between two immiscible electrolyte solutions. These approaches may further be variously combined in solving analytical problems. Just a few typical examples of this wide research and application field are given below.

Micro- and ultramicroelectrodes [29] have a number of advantages for flow analysis [4]. Their small dimensions make them very attractive for detection in open-tubular capillary LC, as demonstrated on single carbon fibre [30] and microdisc wall-jet [31] detectors. Because of the low-voltage ohmic drops involved, poorly conductive solutions can be used, often in the absence of base electrolyte, which considerably widens the accessible potential range and the selection of solvents. Fast establishment of a steady-state and rapid charging facilitate the use of rapid-scan voltammetric techniques. Microelectrode arrays in flowing streams exhibit an improvement in the signal-to-noise ratio because of edge effects and replenishment of the diffusion layer with the analyte on passage between the individual microelectrodes.

The number of applications to flow detection is rapidly increasing, both in LC (e.g., [32,33]) and in FIA (e.g., [33,34]). Further references can be found in a review [5].

The field of variously modified electrodes [5,35–37] is extremely active and wide; for recent surveys of their use in flow analysis, see [38,39]. Basically, modified electrodes fall into three categories: systems are attached to the electrode surface that selectively interact with the sample components, e.g., through ion exchange, liquid–liquid extraction or size exclusion, thus permitting selective access and possibly also accumulation of analytes at the electrode; the electrode surface contains a submonomolecular or monomolecular layer of species that act as selective catalysts of electrode reactions; and the electrode surface is covered with a polymeric film containing redox catalytic sites.

From the point of view of flow measurements, the response rate and mechanical strength of the sensor must always be considered. Therefore, strongly bound, thin modifying films are often better suited than thick polymeric layers. There are two approaches to the modification of solid electrodes that have the advantages of the possibility of performing the modification procedure in situ and regulating the composition and surface concentration of catalytic sites through control of the experimental conditions, i.e., laser irradiation and electrochemical pretreatment.

These procedures affect the surface concentrations of the catalytic functionalities that are always present at solid electrode surfaces exposed to air, i.e., mixtures of oxides and adsorbed hydroxyl radicals on noble metal electrodes and quinones, phenols, carbonyls, carboxyls and some other species on carbon materials.

Laser irradiation generally leads to the removal of passive layers, a decrease in the amount of chemisorbed oxygen and a slight increase in the surface roughness; the measuring sensitivity is selectively increased for certain compounds. The effect decays with time and is restored by another laser pulse. Virtually the same results are obtained on irradiation in solution [40] and in air [41]. The method has been applied to batch pulse voltammetric measurements [42] and electrochemical detection in LC [43].

Anodic pretreatment of carbon electrodes, ei-

ther potentiostatic [44–46] or galvanostatic [47], leads to an increase in the amount of chemisorbed oxygen. The sensitivity for certain classes of compounds is greatly increased, but the response rate decreases, as the signal enhancement requires preceding adsorption of the analyte on the electrode surface [44,47,48]. Selectivity of LC detection can be considerably enhanced when using a split-disc dual-electrode amperometric cell, with one of the glassy carbon electrodes anodically pretreated and the other untreated [49]. A detailed discussion of mechanical, heat, laser and electrochemical modification of solid electrodes can be found in a review [50].

There has been tremendous development in the field of biosensors, because the enzymatic and immunochemical processes occurring in living organisms exhibit the highest attainable selectivity. The literature is extensive (for surveys, see, e.g., [5,51,52]). In flow measurements, complications may arise from sluggish response of biosensors and sometimes from their poor stability (FIA with biochemical sensors is treated in detail in [53]).

Most amperometric biosensors monitor the consumed or liberated oxygen using a Clark sensor, or use solid electrodes that may be modified to monitor the hydrogen peroxide formed or an enzymatically reduced acceptor. In flow systems, the biochemical agent is either placed directly on the measuring electrode or is deposited in a preceding reactor. Analytical systems with a reactor exhibit greater capacities for the analyte and longer lifetimes; on the other hand, the sample zones are more dispersed. Membrane-covered electrodes (e.g., the Clark sensor) are more resistant toward passivation, but their response is slower and the measuring sensitivity poorer than with bare electrodes [5,54]. Biosensors can be combined to advantage with a simple LC presep-

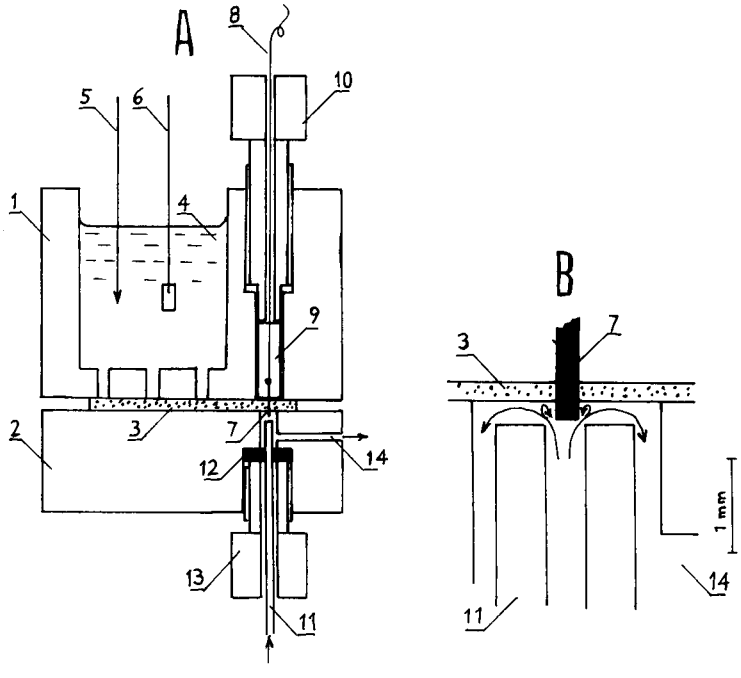

Fig. 2. Amperometric cell with a solid polymer electrolyte membrane [57]. (A) Overall view; (B) expanded view of the detection space. 1,2 = Plastic detector body; 3 = Nafion membrane; 4 = auxiliary electrolyte chamber; 5 = Ag/AgCl reference electrode; 6 = platinum counter electrode; 7 = working electrode; 8 = lead to working electrode; 9 = Plexiglas cylinder; 10 = fixing screw; 11 = PTFE capillary; 12 = silicone-rubber seal; 13 = fixing screw; 14 = sample solution outlet.

aration, as demonstrated, e.g., on a very rapid and simple determination of ethanol in serum [55].

A great limitation of electrochemical detection is the necessity to work in electrically conductive solutions; this is partly alleviated by using microelectrodes. Another approach is based on a cell in which the working, counter and reference electrodes are electrolytically connected other than by means of the liquid stream to be analysed, e.g., by using a solid polymer electrolyte, such as Nafion (DuPont). Two such cells have been designed and tested, one with a large-area platinum electrode obtained by chemical deposition [56] and the other with a platinum wire semi-microelectrode [57], which is depicted in Fig. 2. The cell with the smaller electrode exhibits a better signal-to-noise ratio. The response is reasonably fast (a time constant of 1.5 s at a flow-rate of 0.7 ml min^{-1}), with good linearity (correlation coefficient 0.998), a sufficient linear dynamic range of at least three decades of concentration, a good sensitivity with limits of detection in subnanogram range for common LC sample volumes and a good precision (R.S.D. 1–5%). In this way, the possibilities of amperometric detection are substantially widened, e.g., to normal-phase LC and methods with programmed composition of the mobile phase.

Conclusion

The above few examples demonstrate that there is still great potential for electrochemical flow detection methods and that the future lies primarily in specialized applications in which all the advantages of electrochemistry can be utilized to tailor a highly selective and sensitive analytical system for a particular analytical problem. It seems that the most promising research areas involve micro- and ultramicroelectrodes, variously modified sensors, especially those employing biochemical processes, and multi-channel detection techniques.

REFERENCES

1 J. Růžička and E.H. Hansen, Flow Injection Analysis, Wiley, New York, 2nd edn., 1988.
2 C.F. Poole and S.A. Schuette, Contemporary Practice of Chromatography, Elsevier, Amsterdam, 1984.
3 J. Váňa, Gas and Liquid Analyzers, Elsevier, Amsterdam, 1982.
4 K. Štulík and V. Pacáková, Electroanalytical Measurements in Flowing Liquids, Horwood, Chichester, 1987.
5 K. Štulík and V. Pacáková, Sel. Electrode Rev., 14 (1992) 87.
6 E.S. Yeung and W.G. Kuhr, Anal. Chem., 63 (1991) 275A.
7 M. Valcárcel and M.D. Luque de Castro, Flow-Injection Analysis. Principles and Applications, Horwood, Chichester, 1987.
8 A. Manz and W. Simon, J. Chromatogr. Sci., 21 (1983) 326.
9 S.R. Muller, W. Simon, H.M. Widmer, K. Grolimund, G. Schomburg and P. Kolla, Anal. Chem., 61 (1989) 2747.
10 M. Trojanowicz and M.E. Meyerhoff, presented at International Symposium on Detection in LC and FIA, September 20–22, Córdoba, 1989, paper PII 30.
11 J. Janata, Principles of Chemical Sensors, Plenum, New York, 1989.
12 N.J. Ho, J. Kratochvíl, G.F. Blackburn and J. Janata, Sensors Actuators, 4 (1983) 413.
13 M. Decroux, H.H. Van den Vlekkert and N.F. De Rooij, in Proceedings of the Second International Meeting on Chemical Sensors, Bordeaux, July 7–10, 1986, pp. 403–404.
14 R.L. Smith and S.D. Collins, IEEE Trans. Electron Dev., ED-35 (1988) 787.
15 K. Potje-Kamloth, P. Janata, J. Janata and M. Josowicz, Sensors Actuators, 18 (1989) 415.
16 J.R. Sandifer, Anal. Chem., 61 (1989) 2341.
17 P. Peták and K. Štulík, Anal. Chim. Acta, 185 (1986) 171.
18 L. Ilcheva and K. Cammann, Fresenius' Z. Anal. Chem., 325 (1986) 11.
19 J.F. van Staden, Fresenius' Z. Anal. Chem., 333 (1989) 226.
20 W. Frenzel, Fresenius' Z. Anal. Chem., 335 (1989) 931.
21 J.D.R. Thomas, Anal. Chim. Acta, 180 (1986) 289.
22 A. Lewenstam, M. Maj-Zurawska and A. Hulanicki, Electroanalysis, 3 (1991) 727.
23 T.J. Cardwell, R.W. Cattrall, P.J. Iles and I.C. Hamilton, Anal. Chim. Acta, 204 (1988) 329.
24 J. Lexa and K. Štulík, Talanta, 38 (1991) 1393.
25 G. Horvai, K. Tóth, J. Fekete and E. Pungor, presented at Euroanalysis IV, Helsinki, 1981.
26 H. Gunasingham and B. Fleet, Anal. Chem., 55 (1983) 1409.
27 W. Mattuszewski, M. Trojanowicz and W. Frenzel, Fresenius' Z. Anal. Chem., 332 (1988) 148.
28 J.G. Douglas, Anal. Chem., 61 (1989) 922.
29 M. Fleischmann, S. Pons, D.R. Rolison and P.P. Schmidt (Eds.), Ultramicroelectrodes, Datatech Systems, Morgantown, NC, 1987.
30 L.A. Knecht, E.J. Guthrie and J.W. Jorgenson, Anal. Chem., 56 (1984) 479.
31 M.J.J. Hetem, H.A. Claessens, P.A. Leclercq, C.A. Cramers, V. Pacáková and K. Štulík, in P. Sandra (Ed.), Proceedings of the VIIIth International Symposium on

Capillary Chromatography, Vol. II, Hüthig, Heidelberg, 1987, p. 1122.
32 J.E. Bauer and R.M. Wightman, J. Chromatogr., 482 (1990) 65.
33 T.-Y. Ou and J.L. Anderson, Anal. Chem., 63 (1991) 1651.
34 D.L. Luscombe, A.M. Bond, D.E. Davey and J.W. Bixler, Anal. Chem., 62 (1990) 27.
35 R.W. Murray, in A.J. Bard (Ed.), Electroanalytical Chemistry, Vol. 13, Dekker, New York, 1983, pp. 191–368.
36 K. Kalcher, Electroanalysis, 2 (1990) 419.
37 K. Štulík and V. Pacáková, in J. Zýka (Ed.), Instrumentation in Analytical Chemistry, Vol. 2, Horwood, Chichester, in press.
38 J. Wang, Anal. Chim. Acta, 234 (1990) 41.
39 E.-K. Wang, H.-M. Ji and W.-Y. Hou, Electroanalysis, 3 (1991) 1.
40 M. Poon and R.L. McCreery, Anal. Chem., 58 (1986) 2745.
41 K. Štulík, D. Brabcová and L. Kavan, J. Electroanal. Chem., 250 (1988) 173.
42 M. Poon and R.L. McCreery, Anal. Chem., 59 (1987) 1615.
43 K. Sternitzke, R.L. McCreery, C.S. Bruntlett and P.T. Kissinger, Anal. Chem., 61 (1989) 1989.
44 J.-X. Feng, M. Brazell, K. Renner, R. Kasser and R.M. Adams, Anal. Chem., 59 (1987) 1863.
45 J. Wang and M.S. Lin, Anal. Chem., 60 (1988) 499.
46 L.J. Kepley and A.J. Bard, Anal. Chem., 60 (1988) 1459.
47 J. Mattusch, K.-H. Hallmeier, K. Štulík and V. Pacáková, Electroanalysis, 1 (1989) 405.
48 J.E. Witt, L.A. Larew and D.C. Johnson, Electroanalysis, 2 (1990) 21.
49 J. Mattusch, G. Werner, K. Štulík and V. Pacáková, Electroanalysis, 2 (1990) 443.
50 K. Štulík, Electroanalysis, 4 (1992) 672.
51 G.G. Guilbault, Analytical Uses of Immobilized Enzymes, Dekker, New York, 1984.
52 A.P.E. Turner, I. Karube and G.S. Wilson (Eds.), Biosensors: Fundamentals and Applications, Oxford University Press, Oxford, 1987.
53 R.D. Schmid (Ed.), Flow-Injection Analysis (FIA) Based on Enzymes or Antibodies (CBF Monographs, Vol. 14), Verlag Chemie, Weinheim, 1990.
54 V. Pacáková, K. Štulík, D. Brabcová and J. Barthová, Anal. Chim. Acta, 159 (1984) 71.
55 V. Pacáková, K. Štulík, Kang Le and J. Hladík, Anal. Chim. Acta, 257 (1992) 73.
56 T.W. Kaaret and D.H. Evans, Anal. Chem., 60 (1988) 657.
57 L. Loub, F. Opekar, V. Pacáková and K. Štulík, Electroanalysis, 4 (1992) 447.

Analytica Chimica Acta, 273 (1993) 443–447
Elsevier Science Publishers B.V., Amsterdam

Determination of inert sugars in urine by liquid chromatography with pulsed amperometric detection

S.K. Sanghi [1] and W.Th. Kok

Laboratory for Analytical Chemistry, University of Amsterdam, Nieuwe Achtergracht 166, 1018 WV Amsterdam (Netherlands)

G.C.M. Koomen and F.J. Hoek

Department of Clinical Chemistry, Academic Medical Centre, Meibergdreef 9, 1105 AZ Amsterdam (Netherlands)

(Received 29th June 1992)

Abstract

Liquid chromatography and pulsed amperometric detection with a gold working electrode have been used for the determination of cellobiose and rhamnose in urine samples. A conventional sugar-separation column was used with an acidic mobile phase, and a potassium hydroxide solution was added post-column. Under optimal conditions detection limits of 10 ng were obtained. The method could be used for the assessment of the human intestinal permeability by the determination of the urinary excretion of inert sugars. Limits of determination in urine were 5 mg l^{-1} for cellobiose and 15 mg l^{-1} for rhamnose. Good agreement was found with the results of alternative methods.

Keywords: Amperometry; Liquid chromatography; Intestinal permeability; Sugars; Urine

Alterations of the permeability of the intestine for inert compounds are an indication of the mucosal abnormalities observed in various disorders. The determination of the urinary excretion rate of exogenous compounds after oral administration can be used in the diagnosis and follow-up of, for instance, coeliac disease and Crohn's disease [1]. In particular, the determination of the ratio of the excretion rate of inert monosaccharides and disaccharides finds increasing application in research and clinical practice [2–6].

Although enzymatic methods, quantitative paper chromatography and gas chromatography (GC) are also used for the determination of these sugars in urine samples, liquid chromatography (LC) is now the primary approach for this analysis. The separation can be performed on cation-exchange columns especially designed for this purpose, or, alternatively, on anion-exchange columns operated with a high-pH mobile phase. A third approach is to use a normal-phase [7,8] or reversed-phase [9,10] column for the separation after derivatization of the sugars.

When the often troublesome post- or precolumn derivatization techniques are to be avoided, until recently a refractive index (RI) detector had to be used for the detection of (underivatized) sugars in LC. However, for complex samples such as urine, the sensitivity and selectivity of this detector is in many cases insufficient. A breakthrough in this field was achieved with the development of the pulsed amperometric detection (PAD) technique, using platinum [11,12] or gold

Correspondence to: W.Th. Kok, Laboratory for Analytical Chemistry, University of Amsterdam, Nieuwe Achtergracht 166, 1018 WV Amsterdam (Netherlands).

[1] On leave from the Department of Chemistry, Bhilai Institute of Technology (Seth Balkrishna Memorial), Bhilai House, Durg, MP (India).

[13,14] electrodes. Due to the electrocatalytic activity of these electrode materials, sugars can be oxidized at a moderate potential in alkaline solution. Positive and negative potential pulses are applied in regular cycles during the analysis to keep the electrode surface in an active state. With PAD, detection limits in the low nanogram range can be obtained, while the selectivity is by far superior to RI detection.

While the LC–PAD combination has become a routine method for the determination of sugars in, for instance, food analysis [15], only few clinical applications have been published so far. Fleming et al. [16] have shown that LC–PAD can be used to measure the urinary concentrations of lactulose and mannitol. They report a good agreement with alternative (GC) assays. For the separation of the sugars they used a strong anion-exchange column with a mobile phase of 0.15 mol l^{-1} sodium hydroxide.

A drawback of the method proposed by Fleming et al. is that anion-exchange columns with sufficient efficiency at the high mobile-phase pH which is necessary for the separation, are not generally available. Therefore, we have studied the feasibility of LC–PAD for the determination of exogenous sugars in urine, with a classical sugar-separation column and post-column addition of an alkaline solution. The urinary excretion of the monosaccharide–disaccharide combination rhamnose–cellobiose has been studied. Results have been compared with those obtained with enzymatic and other LC methods.

EXPERIMENTAL

Chromatographic apparatus

The liquid chromatographic system consisted of a Gynkotek (Germering, Germany) Model 300 high-precision pump with pulse-dampener, delivering a flow-rate of 0.5 ml min^{-1}, and a Rheodyne (Berkeley, CA) 7120 valve with a 100-μl loop. Sugars were separated on a Bio-Rad (Richmond, CA) HPX 87-H ion-exclusion column (particle size 9 μm; 300 × 7.8 mm), with a similar guard column. Post-column addition of potassium hydroxide solutions was performed with a Minipulse II pump (Gilson, Villiers-le-Bel, France), which was connected by a T-piece with the analytical column, at a flow-rate of 0.25 ml min^{-1}. The mixing device was a 200 × 0.8 mm single-bead string reactor with 0.6-mm glass beads. Column and mixing reactor were thermostated at 55°C.

A Hewlett Packard 1049 A programmable electrochemical detector, with a gold working electrode and a Ag/Ag/KCl (1 mol l^{-1}) reference electrode was used. The working electrode was cleaned daily with a tissue soaked in methanol. Peak heights were measured for quantitation.

Chemicals and solutions

Cellobiose was obtained from Fluka (Buchs), glucose and rhamnose from Merck (Darmstadt). Other chemicals used were of analytical-reagent grade. Aqueous standard solutions of the sugars were prepared daily from concentrated stock solutions. The mobile phase was 0.01 mol l^{-1} sulphuric acid. A 0.2 mol l^{-1} solution of potassium hydroxide was added post-column, unless stated otherwise. Helium was used to purge the solutions to obtain oxygen-free conditions.

Human urine samples were kept at −20°C. They were diluted with distilled water and filtered through 0.45-μm disposable filters (Millipore, Milford, MA) before injection.

RESULTS AND DISCUSSION

The detector pulse potentials and times have been optimized with respect to the signal-to-noise ratio for glucose, by post-column addition of a 0.2 mol l^{-1} solution of the sugars of potassium hydroxide (detection pH 12.8). Interference by pump noise was avoided using the peristaltic pump at its highest speed with narrow tubes. The optimum parameters are given in Table 1. The values found are similar to those reported in literature. The potentials and duration of the cleaning pulses were not very critical for the signal-to-noise ratios. With the values presented in the table a good long-term stability was obtained, with a decrease in the sensitivity of less than 3% per

TABLE 1

Optimum pulse parameters

Pulse	Duration time, t (s)	E (V vs. SSE)
Measuring	0.4	+0.1
Cleaning-1	0.2	+0.9
Cleaning-2	0.2	−0.9

day. An important parameter is the pH of the final solution after mixing of the mobile phase and the alkaline solution [17]. With a detection pH of 12.0, the sensitivity for glucose was decreased by 25% compared to that at pH 12.8.

The analytical performance of the method under optimal conditions is summarized in Table 2. With standard solutions detection limits below 10 ng are obtained. The method is therefore well suited for the determination of urinary sugars in these permeability measurements, even after dilution of the samples, since usually concentrations between 10 and 100 mg l^{-1} are observed. With one-line systems, using anion-exchange columns, detection limits in the order of 1–5 ng have been reported in literature [13,14]. Linear calibration plots were obtained up to 1 μg/injection (10 mg l^{-1}). Above this concentration the sensitivity rapidly decreased.

The selectivity of the conventional sugar-separation column used in this study was not completely satisfying, especially not for the separation of the monosaccharides. For instance, a baseline separation of the peaks of rhamnose (retention time 12.25 min) and the naturally occurring mannitol (12.0 min) could not be obtained, despite

TABLE 2

Analytical performance

Sugar	t_r (min)	Sensitivity (μA mg^{-1} l^{-1})	LOD [a] (ng)	Peak-height C.V. [b] (%)
Cellobiose	8.60	1.26	8	1.7
Glucose	10.70	1.73	6	0.9
Rhamnose	12.25	1.10	9	3.2

[a] Limit of detection with a signal-to-noise ratio of 3. [b] Coefficient of variation for 5 mg l^{-1}, $n = 6$.

TABLE 3

Recovery of sugars from spiked urine samples (Urine samples were filtered and diluted 1+9 before injection)

Added (mg l^{-1})	Found [a] (mg l^{-1})	
	Cellobiose	Rhamnose
0	0.3±0.5	1.8±1.6
25	25.2±2.0	26.6±1.5
50	49.4±1.9	50.4±3.2
100	106.8±2.1	106.8±2.1

[a] Mean±S.D. for 3 different samples, each analyzed 3 times.

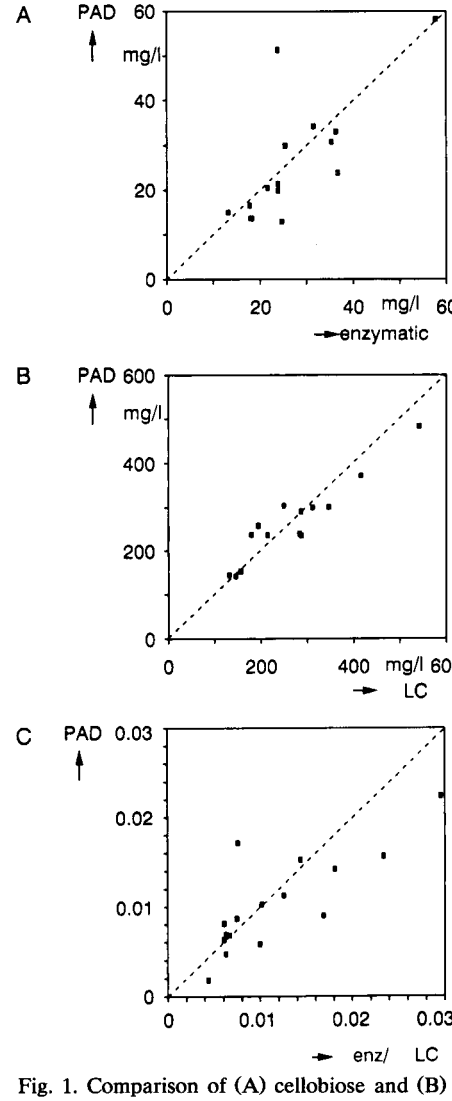

Fig. 1. Comparison of (A) cellobiose and (B) rhamnose concentrations and (C) their ratio as determined by LC–PAD and alternative methods.

variations of the column temperature or the mobile phase composition. Also, some interference can be encountered from other sugars normally present in urine in concentrations in the range 5–50 mg l^{-1}, such as xylose (11.3 min), mannose (11.35 min), galactose (11.4 min), fructose (11.5 min), arabinose (12.5 min) and fucose (13.15 min). The extent of interference was studied by measuring the recovery of the inert sugars from spiked urine samples. Different urine samples collected from healthy persons were spiked with cellobiose and rhamnose in various concentrations. The results are given in Table 3. Generally, a recovery > 100% is found, indicating some interference from the urine matrix. When limits of determination for urine samples of about 5 mg l^{-1} for cellobiose and 15 mg l^{-1} for rhamnose are accepted, this interference is usually negligible.

The method described in this work has been compared with other methods for the determination of cellobiose and rhamnose, as previously employed in the laboratory. Cellobiose was determined as described by Strobel et al. [3], using enzymatic determination of glucose concentrations, before and after the treatment of the urine samples with β-glucosidase. For rhamnose an LC method with precolumn derivatization was used as described by Honda et al. [10]. Urine was collected from healthy volunteers 6 h after the ingestion of a mixture of 10 g cellobiose and 1 g rhamnose. In Fig. 1 the concentrations in urine as found with the alternative assays are compared. Apart from a single outlier for cellobiose, reasonable agreement is found. Correlation coefficients of 0.852, 0.872 and 0.828 are found for cellobiose, rhamnose and the excretion ratio, respectively. The calculated ratios of the urinary excretion of the disaccharide and the monosaccharide (Fig. 1C) fall well within the normal ranges reported for healthy subjects [2,3,5,6].

In Fig. 2 chromatograms are shown of the urine samples of one subject before and after the intake of the inert sugars. An excretion ratio (the ratio of the percentage recovered of cellobiose to

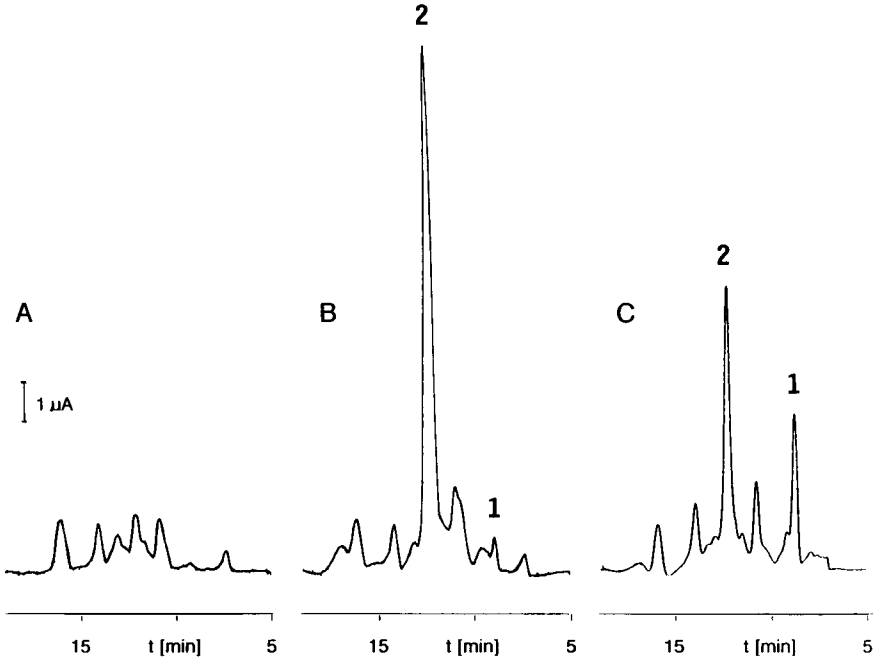

Fig. 2. Chromatograms of urine samples from (A) a healthy volunteer before and (B) 6 h after ingestion of cellobiose and rhamnose and (C) a Crohn's disease patient after ingestion of the sugars. Urine samples are diluted 1:9 with destilled water and filtered before injection. Peaks: (1) cellobiose and (2) rhamnose.

the percentage recovered of rhamnose) of 0.008 was calculated. For comparison, the chromatogram obtained of a urine sample from a patient suspected of Crohn's disease after the intake of the inert sugar mixture, is shown in Fig. 2C. There is clearly a high excretion of cellobiose relative to rhamnose. The excretion ratio for this patient was 0.049. This pattern is typical for abnormal permeability as can be found in active Crohn's disease [2].

Preliminary experiments have shown that the separation system described in this paper can be used for the determination in urine of polyethylene glycol, which is also employed as an indicator of the intestinal permeability [1,5,17]. With urine samples collected from patients and healthy volunteers after ingestion of a polyethylene glycol solution (PEG 400), a clearly defined peak with a retention time of 21.4 min was observed in the chromatograms, well separated from other peaks found in blank urine samples. Further study is required to compare the usefulness of PEG and the cellobiose–rhamnose combination for the diagnosis of intestinal disorders.

REFERENCES

1 J. Peters and I. Bjarnason, Can. J. Gastroenterol., 2 (1988) 127.
2 S.O. Ukabam, J.R. Clamp and B.T. Cooper, Digestion, 27 (1983) 70.
3 S. Strobel, W.G. Brydon and A. Ferguson, Gut, 25 (1984) 1241.
4 T. Delahunty and D. Hollander, Clin. Chem., 32 (1986) 1542.
5 L. Stenhammar, K. Falth-Magnusson, G. Jansson, K.-E. Magnusson and T. Sundqvist, J. Pediatr. Gastroenterol. Nutr., 9 (1989) 281.
6 C. Catassi, P. Pierani, G. Natalini, O. Gabrielli, G.V. Coppa and P.L. Giorgi, J. Pediatr. Gastroenterol. Nutr., 12 (1991) 209.
7 M. Takeda, M. Maeda and A. Tsuji, J. Chromatogr., 244 (1982) 347.
8 C.A. White, S.W. Vass, J.F. Kennedy and D.G. Large, J. Chromatogr., 264 (1983) 99.
9 M. Batley, J.W. Redmond and A. Tseng, J. Chromatogr., 253 (1983) 124.
10 S. Honda, E. Akao, S. Suzuki, M. Okuda, K. Kakehi and J. Nakamura, Anal. Biochem., 180 (1989) 351.
11 S. Hughes and D.C. Johnson, Anal. Chim. Acta, 132 (1981) 11.
12 S. Hughes and D.C. Johnson, J. Agric. Food Chem., 30 (1982) 712.
13 R.D. Rocklin and C.A. Pohl, J. Liq. Chromatogr., 6 (1983) 1577.
14 D.C. Johnson and W.R. LaCourse, Anal. Chem., 62 (1990) 589A.
15 J. van Riel and K. Olieman, Carbohydr. Res., 215 (1991) 39.
16 S.C. Fleming, M.S. Kapembwa, M.F. Laker, G.E. Levin and G.E. Griffin, Clin. Chem., 36 (1990) 797.
17 P.G. Jackson, M.H. Lessof, R.W.R. Baker, J. Ferret and D.M. MacDonald, Lancet i, (1981) 1285.

Analytica Chimica Acta, 273 (1993) 449–456
Elsevier Science Publishers B.V., Amsterdam

Liquid chromatographic determination of acids and anions using liquid membrane ion-selective electrodes in a potentiometric flow-through detector

B.L. De Backer, L.J. Nagels and F.C. Alderweireldt

Chemistry Department, Universitair Centrum Antwerpen, B-2020 Antwerp (Belgium)

P.P. Van Bogaert

Physiology / Biochemistry Department, Universitair Centrum Antwerpen, B-2020 Antwerp (Belgium)

(Received 1st June 1992; revised manuscript received 8th September 1992)

Abstract

The sensitive detection of organic acids in liquid chromatographic (LC) systems remains problematic. The behaviour of a potentiometric detector was studied in this type of analysis, using ion-selective PVC-based liquid membranes. One membrane contained a quaternary ammonium salt as a carrier and another contained a lipophilic macrocyclic pentamine. The selectivity and sensitivity of the two membrane types towards 20 ions was determined using flow-injection experiments. The flow-through detector was of the wall-jet type. The response times of the membranes were evaluated and are discussed with respect to their use in LC and flow-injection analysis (FIA). The response times were compared with these obtained with amperometric wall-jet detectors. The different factors that determine the extent of the response times are discussed. The membranes were used for the sensitive detection of inorganic anions in an LC ion chromatography system. For the separation of organic acids, and Aminex HPX87H ion-exclusion chromatographic column was used. With the potentiometric liquid membrane detector, the detection limits were at least 100 times lower than the values obtained with the low-wavelength UV detector that is normally used in these systems. Typically, a detection limit of 10 ng was measured for acetic acid. The potential and limitations of potentiometric liquid membrane detectors in LC and FIA are discussed.

Keywords: Flow injection; Ion selective electrodes; Liquid chromatography; Potentiometry; Acids; Anion; Membrane electrodes;

Polystyrene-based cation exchangers are mostly used for the LC separation of organic acids. Recently, capillary zone electrophoresis has been shown to give very promising separations [1]. Low-wavelength UV detection was used for the quantitation of these compounds, resulting in high detection limits and interferences from other compounds especially when biological matrices are analyzed. This study will investigate the potential of potentiometric membrane detectors for this purpose.

Interesting potentiometric detection systems have been applied for the LC analysis of organic acids by Haddad et al. [2], and for the LC analysis of ions by Manz and Simon [3]. Little work is done generally however on potentiometric detection in the LC area. It is not clear from the literature whether such detectors can be designed to respond fast enough for LC requirements. Therefore, the dynamic behaviour of these poten-

Correspondence to: L.J. Nagels, Chemistry Department, Universitair Centrum Antwerpen, Groenenborgerlaan 171, B-2020 Antwerp (Belgium).

tiometric detectors was also compared to the dynamics of amperometric detectors which had the same wall-jet construction characteristics.

EXPERIMENTAL

Reagents

Dioctyl phthalate (DOP) and high-molecular-weight poly(vinyl chloride) (PVC) were obtained from Janssen Chimica (Geel, Belgium). Tetrapentylammonium chloride was purchased from Aldrich (Milwaukee, WI). *N*-(2-Hydroxyethyl)-piperazine-*N'*-2-ethanesulphonic acid (HEPES) (Sigma, St. Louis, MO) was used as a buffer. Inorganic salts and acetic, succinic, citric, maleic, oxalic, lactic and L-(+)-tartaric acid were obtained from Merck (Darmstadt). *o*-Coumaric, 4-hydroxybenzoic and caffeic acid were purchased from Fluka (Buchs).

Organic syntheses

The lipophilic macrocyclic pentamine 15-hexadecyl-1,4,7,10,13-pentaazacyclohexadecane (see Fig. 1) was synthesized according to Umezawa et al. [4]. Its structure was verified by NMR, mass and IR spectrometry.

Electrode construction

Two different types of liquid PVC-based membranes were prepared, one type containing a lipophilic macrocyclic pentamine and the other containing a commercial quaternary ammonium salt (92-17-02, Orion Research) as a carrier. The macrocyclic pentamine-based liquid membranes were composed of 6 mg of carrier, 45 mg of PVC, 150 mg of DOP. For the quaternary ammonium salt-based membranes 42.5 mg of PVC and 100 mg of liquid ion exchanger were used. The membrane components were dissolved in tetrahydrofuran (THF). The solution was poured into a glass casting ring (30 mm diameter) on a glass plate and the solvent was allowed to evaporate at room temperature for 24 h. A small disc was cut out of the resulting master membrane and glued on a PVC tube (4 or 1.5 mm i.d.) with THF. The other end of the PVC tube was then connected to a disposable 5-ml medical syringe. The electrodes were filled with a 0.1 M potassium chloride solution containing 1×10^{-3} M tetrapentylammonium chloride. A silver wire coated with silver chloride was used as an internal reference electrode.

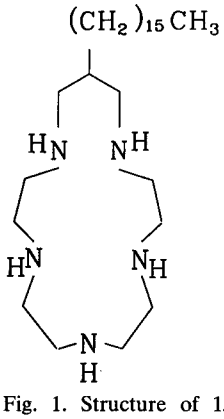

Fig. 1. Structure of 15-hexadecyl-1,4,7,10,13-pentaazacyclohexadecane.

Flow cell

All measurements were done with a laboratory-made large-volume wall-jet type of flow cell [5]. This flow cell can accept both potentiometric membrane electrodes and amperometric electrodes. For potentiometric measurements, a Schott (Hofheim, Germany) B 3510 calomel electrode was used as a reference electrode. For amperometric measurements, a combined counter and reference electrode system (Schotte Pt 62) was applied.

Flow-injection measurements

The flow-injection analysis (FIA) system was constructed from a Spectra-Physics SP 8810 pump, a Rheodyne LC injector and the laboratory-made wall-jet detector. Potentials were measured with a Corning Model 125 pH meter. A strip-chart recorder or an oscilloscope was connected to the pH meter. The response time of the whole system was lower than 200 ms. For amperometric measurements, a laboratory-made three-electrode potentiostat was used, with a response time lower than 100 ms.

RESULTS AND DISCUSSION

Response times of the potentiometric membrane detectors and comparison with amperometric detectors

Many studies have been devoted to measuring the dynamic characteristics (i.e., the ability to follow changes in the concentration of the analyte) of potentiometric flow-through detectors [6,7]. It is still not clear, however, to what extent the response times of potentiometric detectors affect peak broadening under typical LC and FIA conditions (flow-rates between 2 and 0.1 ml min^{-1}). In order to obtain a better idea of the factors governing the behaviour of these detectors in this respect, it seemed logical to compare their behaviour with that of the amperometric detectors, which are far more popular in LC. As far as we know, no detailed studies have appeared on the response times of amperometric detectors. For the latter detectors, cell time constants have been considered in on-line fast-scanning voltammetric applications [8]. The latter cell time constants express the slowness of this detector towards changes in working electrode potential. They are in no way comparable to the response times that express the slowness of the detectors towards the measurements of rapid changes in concentration.

For both amperometric and potentiometric flow-through cells, the response behaviour towards rapidly changing analyte concentrations is dependent on elements that are specific for electrochemical detection methods. These include mass transfer kinetics of the sample molecules in the hydrodynamic boundary layer and diffusion layer and electrode kinetics. For amperometric detectors, special care should be taken to avoid *iR* drop phenomena, which also influence the dynamic behaviour of these detectors.

The above-mentioned effects were evaluated and compared for potentiometric and amperometric large-volume wall-jet detectors. Measurements were performed in a FIA system in which rectangular concentration pulses were injected. The t_{90} response times were taken as an evaluation criterion, where t_{90} is the time required to reach 90% of the signal steady-state value. This definition of response times [6] was preferred over other definitions sometimes used in the literature.

Effects due to the time constants of the electronic or recording equipment are kept to a minimum by an appropriate choice of the equipment or adaptation of the time constant. Deformation of concentration pulses by the tubing connecting the injector to the detector is often overlooked, or may be interpreted as being due to slow detec-

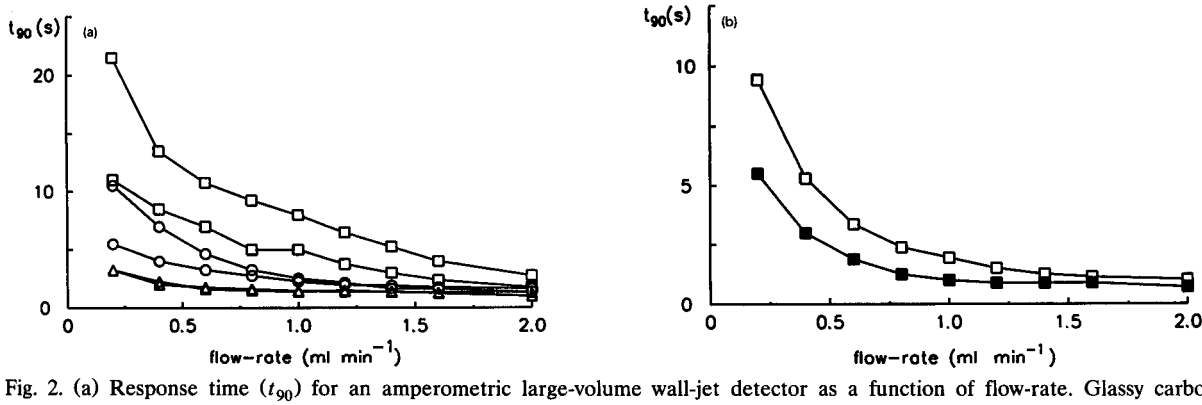

Fig. 2. (a) Response time (t_{90}) for an amperometric large-volume wall-jet detector as a function of flow-rate. Glassy carbon electrode, 3 mm diameter, 0.5 mm jet–electrode distance. Solvent carrier, water. Injection of concentration plugs of 0.1 mM caffeic acid. □ = 0.5 mm i.d. tubing of length 37 cm (upper curve) and 22 cm (lower curve); ○ = 0.25 mm i.d. tubing of length (upper curve) and 22 cm (lower curve); △ = 0.100 mm i.d. capillary of length 45 and 22 cm (overlapping curves). (b) Response time (t_{90}) for a potentiometric (pentamine-based liquid membrane) large-volume wall-jet detector as a function of flow-rate. Electrode diameter, 1.5 mm; jet–electrode distance, 0.5 mm; solvent carrier, water. Injection of concentration plugs of 10 mM KI. 0.25 mm i.d. tubing of length (□) 50 and (■) 37 cm.

tor dynamics. Therefore, tubing effects are treated first below.

Tubing effects. It is not totally correct to describe peak broadening due to injector–detector connecting tubing in terms of "response times". However, this will be done in this paper in order to obtain a simple evaluation of these effects. Figure 2 gives t_{90} response times for (a) an amperometric and (b) a potentiometric large-volume wall-jet detector as a function of flow-rate. In order to evaluate tubing effects, the curves were examined using various tube lengths and inside diameters. A first observation of the results shows a decrease of t_{90} when tubing with large (0.5 mm) to moderate (0.25 mm) i.d. are shortened, especially at low flow-rates. At 0.2 ml min^{-1}, shortening a 0.5 mm i.d. tubing from 37 to 22 cm dramatically decreased the response time from 22 to 11 s. As all variables other than tubing length are kept constant, this reduction is due to deformation of the sample pulse by the Poiseuille flow profile [9]. Analogous results were obtained for the potentiometric detector (see Fig. 2b). Shortening a 0.25 mm i.d. tube length from 70 to 37 cm clearly reduced the measured response times by a factor 2 over the whole flow-rate region. The response times shown in Fig. 2b for the potentiometric detector were smaller than those for the amperometric detector (Fig. 2a), but this is mainly due to the use of a smaller electrode diameter for the potentiometric measurements. (Smaller electrode diameters result in smaller hydrodynamic boundary layers which will yield shorter response times; these effects are discussed below.)

The deformation of the rectangular concentration pulse profile in the tubing was estimated by applying the Taylor–Golay equation. This equation predicts the changes in concentration profile as a concentration plug moves through tubing. As argued by Guiochon and Colin [9], a simplified form of the Taylor–Golay equation can be used to evaluate effects of connecting tubing:

$$\sigma^2 = \pi r^4 lV/24D_m \quad (1)$$

where r is the radius and l the length of the tubing, V is the flow-rate and D is the diffusion coefficient. The calculated response times (not shown) correlated with our measurements in the

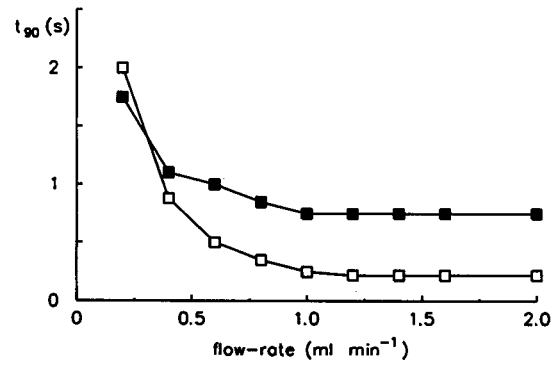

Fig. 3. Response time (t_{90}) as a function of flow-rate for (■) an amperometric detector (1.5 mm diameter glassy carbon electrode) and (□) a potentiometric detector (1.5 mm diameter liquid membrane electrode, quaternary ammonium salt ionophore) using a 0.1 mm i.d. capillary.

higher flow-rate region (1–2 ml min^{-1}). For lower flow-rates, our measurements indicated more extensive peak broadening. Calculation of band broadening in a 100 μm i.d. capillary showed that for such small diameters, Poiseuille flow gives negligible contributions to peak dispersion. This is confirmed in Fig. 2a, where variation of the length of a 100 μm i.d. quartz capillary tubing had almost no influence on the response time. It is advisable to use capillary tubing with an i.d. of 100 μm for detector response time studies if typical analytical LC flow-rates are used (2–0.1 ml min^{-1}). Tubing effects are often neglected in such studies, although the above results show that they contribute significantly to effects that may be wrongly interpreted as detector response times.

Hydrodynamic boundary layer and diffusion layer effects. Figure 3 still shows a decrease in the response time with increasing flow-rate when 100 μm i.d. capillary tubing is used between the injector and detector. As the contribution of Poisseuille flow dispersion to the response time is negligible in this instance, is this observation ascribed to hydrodynamic boundary layer effects: higher flow-rates result in thinner hydrodynamic boundary and diffusion layers. Both the amperometric and potentiometric detectors show resonably fast response times. At 1 ml min^{-1}, the response times are smaller than 0.75 s, which is an acceptable value for a conventional LC sys-

tem. For lower flow-rates (microbore LC and micro-LC), the detector should be modified (shorter jet–electrode distance) to obtain better response times. Note that the potentiometric membrane detector showed a faster response time than the amperometric detector in this experiment. Theoretically, the faster response times of the potentiometric detectors can be partly attributed to the logarithmic nature of the signal versus concentration relationship. However, no dependence of the response time on experimental conditions such as the extent of the concentration steps was observed. Therefore, the measured potentiometric response times can be assumed to be representative. As the jet–electrode distance was 0.5 mm here, still smaller response times could be obtained for both detectors by decreasing this distance. Figure 3 also indicates that in the ml min^{-1} region, large-volume wall-jet detectors should preferably not be used with jet–electrode distances larger than 0.5 mm (contrasting with the measurements of Gunasingham and Fleet [10]).

The dependence of the response time of wall-jet electrode systems on the thickness of the hydrodynamic boundary layer and diffusion layer is also demonstrated in Figs. 4 and 5. Decreasing the electrode diameter from 3 to 1.5 mm resulted in a two-fold decrease in the measured response times for the amperometric system (Fig. 4). Increasing the jet–electrode distance in a potentiometric wall-jet system gives a linear increase in response time (see Fig. 5).

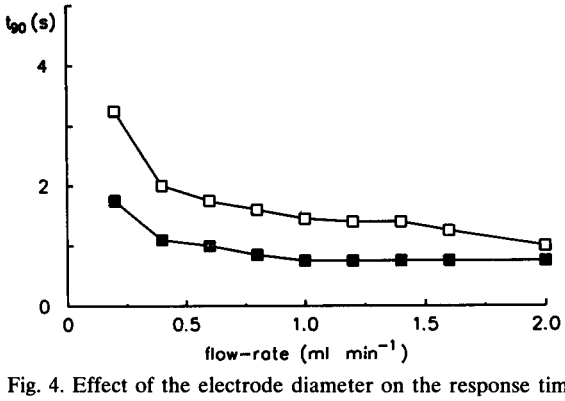

Fig. 4. Effect of the electrode diameter on the response time (t_{90}) for an amperometric detector. Electrode diameter (□) 3 mm and (■) 1.5 mm.

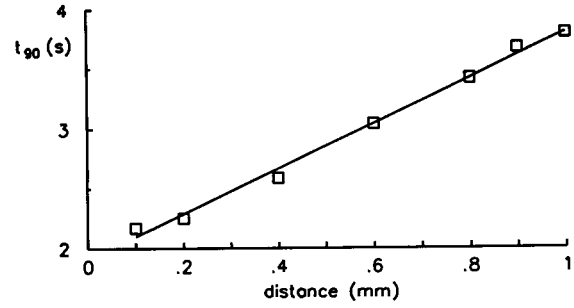

Fig. 5. Response time of a potentiometric detector as function of the jet–electrode distance. Electrode diameter, 4 mm; flow-rate, 1 ml min^{-1}.

The response time caused by the diffusion layer thickness can be estimated. If it is assumed that the actual concentration in the membrane phase determines the response, t_{90} can be estimated by calculating the time required for the analyte concentration at the membrane surface to equal 90% of the concentration in the bulk of the solution. This "response time" was calculated by using (2), which describes the actual concentration at the electrode surface as a function of time [11].

$$\frac{c_i'}{c_i} = 1 - \left(1 - \frac{c_i^0}{c_i}\right) \exp(-t\pi^2 D/4\delta^2) \qquad (2)$$

where c_i^0 is the initial concentration, c_i is the newly introduced concentration at $t = 0$, c_i' is the concentration at the membrane surface at time t, D is the diffusion coefficient and δ is the diffusion layer thickness. The diffusion layer thickness of the wall-jet detector was calculated from Eqn. 3, which was derived by Gunasingham and Fleet [10]:

$$\delta_{dl} = 5.8 k_2 \pi^{3/4} D^{1/3} a^{1/2} \nu^{5/12} R^{5/4} V^{-3/4} \qquad (3)$$

where D is the diffusion coefficient, a the jet diameter, ν the kinematic viscosity, R the radius of the electrode and V the volume flow-rate.

Table 1 gives some of the calculated results obtained when representative values were substitute in Eqns. 2 and 3 ($D = 10^{-5}$ cm^2 s^{-1}, $\nu = 10^{-2}$ cm^2 s^{-1}, $a = 0.1$ mm and $R = 1.5$ mm).

TABLE 1

Comparison of calculated versus measured t_{90} response times as a function of flow-rate for an amperometric detector (glassy carbon electrode, 3 mm diameter)

Flow-rate (ml min^{-1})	t_{90} (calc.) [a] (s)	t_{90} (measured) (s)	
		Jet–electrode distance 100 μm	Jet–electrode distance 500 μm
0.20	2.16	1.40	3.25
0.40	0.96	0.95	2.25
0.60	0.66	0.60	1.60
0.80	0.53	0.50	1.50
1.00	0.47	0.45	1.38
1.20	0.43	0.40	1.50
1.40	0.40	0.40	1.35
1.60	0.38	0.40	1.30
2.00	0.36	0.40	1.30

[a] Theoretical values were computed with Eqns. 2 and 3.

It is clear from the above calculations that the rate diffusion of analyte molecules can only partly explain the extent of the experimentally measured response times for jet–electrode distances larger than 100 μm. For the latter distance, the calculated diffusion effects correspond fairly well to the measured response times. Clearly, for larger jet–electrode distances, other effects such as the increase in the hydrodynamic boundary layer thickness must be involved.

Electrode kinetics. All response times discussed so far were measured in the upward concentration step. In contrast to the amperometric detection mode, the response times of the ion-selective electrodes (ISEs) were dependent on the direction of the concentration change. The conditions for amperometric detection were chosen so as to work under diffusion control: the electroactive molecule used, caffeic acid, reacts rapidly [12], shows good reversibility and gives no adsorption phenomena on glassy carbon electrodes. For the cyclic pentamine-based membranes, the response times were two to three times higher in the downward concentration step. For the quaternary ammonium salt-based membranes, the response times can be as much as ten times higher for the downward concentration change. For membranes based on the latter ionophore, increasing the pulse time from 20 to 120 s resulted in a two-fold higher value of t_{90} (hysteresis effect). The explanation of the difference in behaviour between membranes based on these two types of ionophores can be found in the distribution of the ion-exchange sites in the membrane phase: the commercial liquid ion-exchange membrane (quaternary ammonium ionophore) has active ion-exchange sites distributed over the whole membrane phase. Hence ionic diffusion in the bulk of the membrane electrode can occur as the electrode is exposed to an analyte molecule. With a change to a lower concentration, diffusion of the analyte from the PVC membrane will lead to longer response times. The ISE containing the lipophilic macrocyclic pentamine, on the other hand, is probably built up of the unprotonated, inactive form of the macrocycle in the bulk membrane phase [13]. Only the receptors at the membrane surface are protonated, and thus active. Interaction between the anion and the membrane receptor will only occur at the membrane surface. As there is no diffusion into the bulk of the membrane phase, response times are obtained that are compatible with LC and FIA system.

Selectivity of the ISE membranes

Table 2 shows the response of the macrocyclic pentamine-based potentiometric membrane sensor for a variety of inorganic ions and organic acids. It was measured in an FIA set-up. This type of polymer membrane electrode was sensitive to pH changes. Therefore, a buffered carrier stream was used (0.01 M HEPES buffer, pH 6.6). From the peak heights of a 1 mM sample injection (injection volume 50 μl, flow-rate 1 ml min^{-1}) of monovalent anions, it can be seen that the sensor responds according to a Hofmeister series. Considering di- and trivalent anions, the sensor showed the best performance for maleate and citrate anions. In contrast to the former sensor, the response of the quaternary ammonium salt-based liquid ion-exchange membrane was almost indifferent to pH changes. The FIA experiments were done in HEPES buffer to allow comparison with the sensor containing the macrocyclic pentamine. The liquid ion-exchange ISE also showed a Hofmeister type of behaviour for monovalent anions (see Table 3).

Use of the potentiometric membrane sensors in LC systems

The performance of potentiometric membrane detectors was tested in two commercial systems, one for the determination of anions and the other for the determination of organic acids. Figure 6 shows the analysis for some inorganic anions in an ion chromatographic environment. Ions were separated on an anion-exchange column [AS4A (Dionex), 20 cm × 4.6 mm i.d.], with a CO_3^{2-}–HCO_3^- mixture as eluent. An ion suppressor system was placed after the column to convert carbonate and hydrogen carbonate ions into carbonic acid. The conductivity detector that is normally applied in this system was replaced with the potentiometric large-volume detector. The electrode containing the lipophilic macrocyclic pentamine gave the best performance. Detection limits at the sub-microgram level (injected amounts) were obtained.

TABLE 2

FIA results for the macrocyclic pentamine-based liquid membrane electrode [a]

Ion	Slope (mV per decade)		Peak height (mV) (50 μl of a 1 mM sample)
	Eluent 10 mM HEPES (pH 6.6)	Eluent 10 mM HEPES (pH 6.6)–1 mM KCl	
ClO_4^-	59.4	43.0	78.5
I^-	50.9	47.7	53.3
NO_3^-	33.1	24.5	32.2
Cl^-	32.2	10.5	42.0
$S_2O_3^{2-}$	19.9	16.2	18.6
NO_2^-	22.7	11.5	15.7
SO_4^{2-}	22.4	15.0	8.8
HPO_4^{2-}	25.8	12.0	7.2
Lactate	27.7	4.5	11.0
Acetate	25.2	24.0	10.0
Maleate	25.3	15.5	23.5
Succinate	17.6	16.3	11.1
Oxalate	24.0	15.2	9.5
Malonate	22.0	17.0	8.0
Tartrate	18.0	19.0	4.8
Citrate	31.5		24.5
o-Coumarate	39.1		12.8
Caffeate	24.9		13.0
4-Hydroxybenzoate	36.7		12.4
ATP	23.0	6.0	9.0

[a] Carrier solution, 10 mM HEPES (pH 6.6); flow-rate, 1 ml min^{-1}; injection volume, 50 μl; electrode diameter, 4 mm.

TABLE 3

FIA results for the commercial liquid ion-exchange membrane electrode [a]

Ion	Slope (mV per decade)		Peak height (mV) (50 μl of a 1 mM sample)
	Eluent HEPES (pH 6.6)	Eluent HEPES (pH 6.6)–1 mM KCl	
I^-	48.0	82.8	86
ClO_4^-	55.8	77.6	83
NO_3^-	40.3	42.5	48
SO_4^{2-}	25.2	26.0	41
Cl^-	41.8	21.5	26
$S_2O_3^{2-}$	32.6	19.1	24
NO_2^-	30.0	37.0	17
HPO_4^{2-}	32.0	26.0	15
Acetate	34.5	20.0	9
Lactate	38.7		6
Tartrate	33.9	30.0	32
Succinate	29.2	38.0	26
Maleate	33.6	44.0	21
Oxalate	39.1	29.0	14
Malonate	41.0	46.0	8
Citrate	49.5	46.0	40
o-Coumarate	65.1		68
Caffeate	25.0		22
4-Hydroxybenzoate	17.5		18
ATP	14.0	14.0	3

[a] Carrier solution, 10 mM HEPES (pH 6.6); flow-rate, 1 ml min^{-1}; injection volume, 50 μl; electrode diameter, 4 mm.

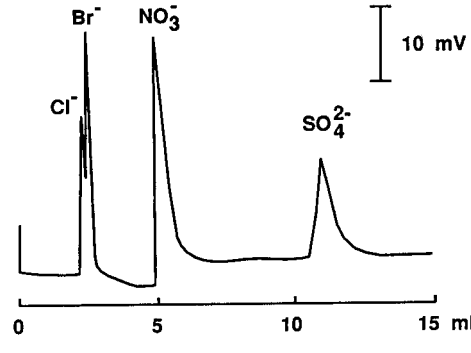

Fig. 6. Chromatogram of inorganic anions using the macrocyclic pentamine-based liquid membrane electrode. Column, Dionex AS4A, 200 mm × 4.6 mm i.d.; eluent, 1.7 mM $NaHCO_3$–1.8 mM Na_2CO_3; flow-rate, 1.5 ml min^{-1}; injected amounts, 30, 40, 60 and 30 nmol of KCl, KBr, $NaNO_3$ and Na_2SO_4, respectively.

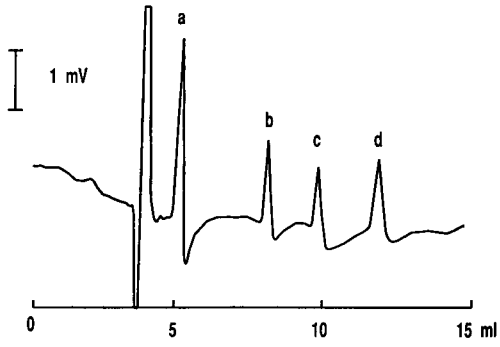

Fig. 7. Chromatogram of carboxylic acids using potentiometric detection with the commercial liquid ion-exchange membrane electrode. Column, Aminex HPX-87H (Bio-Rad), 300 mm × 7.8 mm i.d.; eluent, water; flow-rate; 0.5 ml min^{-1}; injected amounts, (a) 45 ng of lactic acid, (b) 30 ng of acetic acid, 37 ng of propionic acid and (d) 43 ng of butyric acid.

For the chromatographic determination of weak organic acids, conductivity detection is less successful. In these applications, low-wavelength UV detection is still preferred. This results in high detection limits and considerable interference from other classes of compounds. Clearly, a sensitive LC detector for the determination of trace amounts of organic acids in biological media is still lacking. When applying potentiometric detection in this field, good results were obtained with the quaternary ammonium salt-based liquid membrane system (see Fig. 7). Low nanogram detection limits (injected amounts) were found for the separate organic acids. The resuls were very reproducible. The detection limits were 10 and 100 times smaller in comparison with conductivity detection and low-wavelength UV detection, respectively.

Conclusions

Conditions have been established that allow the configuration of rapidly responding wall-jet flow cells for use in potentiometric and amperometric measurements in LC and FIA systems. Potentiometric liquid membrane detectors have response times comparable to those of their amperometric counterparts, under conditions of stepwise increases in concentration. The time constants measured for potentiometric detectors under conditions of a stepwise decrease of analyte concentration depend on the ionophore that is used. The potentiometric detection used in this study shows promising results, especially for the LC determination of organic acids. Further work will be directed towards the synthesis and testing of new ionophores and towards the use of the liquid membranes in miniaturized systems [14], in order to improve membrane response times. Technically, an antilog conversion would further facilitate the interpretation of results obtained with potentiometric detectors in LC [15].

REFERENCES

1 W.R. Jones and P. Jandik, J. Chromatogr., 608 (1992) 385.
2 P.R. Haddad, P.W. Alexander, M.Y. Croft and D.F. Hilton, Chromatographia, 24 (1987) 487.
3 A. Manz and W. Simon, Anal. Chem., 59 (1987) 74.
4 Y. Umezawa, M. Kataoka, W. Takami, E. Kimura, T. Koike and H. Nada, Anal. Chem., 60 (1988) 2392.
5 L.J. Nagels, J.M. Kauffmann, C. Dewaele and F. Parmentier, Anal. Chim. Acta, 234 (1990) 75.
6 K. Stulik and V. Pácáková, in R.A. Chalmers and M. Masson (Eds.), Electroanalytical Measurements in Flowing Liquids, Ellis Horwood, Chichester, 1987, Chap. 2, p. 33.
7 E. Lindner, K. Tóth, E. Pungor, W.E. Morf and W. Simon, Anal. Chem., 50 (1978) 1627.
8 D.O. Wipf, E.W. Kristensen, M.R. Deakin and M.R. Wightman, Anal. Chem., 60 (1988) 306.
9 G. Guiochon and H. Colin, in P. Kucera (Ed.), Microcolumn High-Performance Liquid Chromatography (Journal of Chromatography Library, Vol. 28), Elsevier, Amsterdam, 1984, p. 13.
10 H. Gunasingham and B. Fleet, Anal. Chem., 55 (1983) 1409.
11 E. Lindner, K. Tóth and E. Pungor, Anal. Chem., 48 (1976) 1071.
12 G. Sontag and K. Kral, Microchim. Acta, II (1979) 317.
13 M. Kataoka, R. Naganawa, K. Odashima, Y. Umezawa, E. Kimura and T. Koike, Anal. Lett., 22 (1989) 1089.
14 C. Haber, I. Silvestri, S. Röösli and W. Simon, Chimia, 45 (1991) 117.
15 M. Trojanowicz, T.K.V. Krawczyk and W. Augustyniak, Anal. Chim. Acta, 207 (1988) 325.

Analytica Chimica Acta, 273 (1993) 457–467
Elsevier Science Publishers B.V., Amsterdam

Liquid chromatographic determination of non-volatile nitrosamines by post-column redox reactions and voltammetric detection at solid electrodes. Study of a flow reactor system based on Ce(IV) reagent

G. Favaro, G.A. Sacchetto, P. Pastore and M. Fiorani

Department of Inorganic, Organometallic and Analytical Chemistry, University of Padova, via Marzolo 1, 35131 Padova (Italy)

(Received 1st June 1992)

Abstract

The behaviour of an on-line post-column reactor system based on the use of Ce(IV) reagent in acidic medium for the liquid chromatographic amperometric determination of non-volatile nitrosamines has been investigated in a two-line flow manifold coupled with a flow-through voltammetric detector equipped with twin gold electrodes for both mono- and biamperometric detection modes. The physical dispersion coefficients and the time domain parameters of the current peak responses obtained by flow injections of both Ce(III) and nitrite in aqueous and mixed water–acetonitrile carriers were used to evaluate the performance of the flow reactor elements. Mono- and biamperometric measurements allowed the determination of the linear dynamic ranges, the sensitivities and the detection limits of nitrite under different experimental conditions with respect to the composition of the carrier liquid and the temperature of the reactor system. Peak standard deviations were calculated and used to predict the effects of band broadening and tailing induced by the reactor system on the chromatographic bands.

Keywords: Amperometry; Flow injection; Liquid chromatography; Voltammetry; Nitrosamines

In a previous paper [1] the suitability of Ce(IV) acidic solutions as post-column reagents for the oxidation and electrochemical detection of the nitrite (nitrous acid) produced in the warm acid denitrosation reactions of some classes of nitrosamines was presented. In particular, the electrochemical behaviour of the Ce(IV)–Ce(III) couple in 0.5–2.0 M solutions of sulphuric acid was studied for different electrodic materials such as platinum, gold and glassy carbon. Batch hydrodynamic electrochemical techniques such as rotating disc electrode voltammetry and mono- and biamperometry in stirred solutions were used. Gold was found to be the most suitable electrode material for the oxidative detection of Ce(III) produced by the reaction of nitrite with excess of Ce(IV), mainly because of the lower background current obtainable under the chosen conditions [1]. Further, a more reversible behaviour of the couple, favouring the biamperometric detection mode, and an increase in the signal stability was demonstrated for the gold electrode after it had been submitted to prepolarization at a potential selected in the "oxygen chemisorption" range. The reaction between nitrite and Ce(IV) was also demonstrated to reach completeness in a few seconds [1], which allows any further kinetic complication to the flow reactor processes, which

Correspondence to: G.A. Sacchetto, Department of Inorganic, Organometallic and Analytical Chemistry, University of Padova, via Marzolo 1, 35131 Padova (Italy).

should be governed only by the different denitrosation rates of the nitrosamines, to be excluded, [2].

In this paper, first the design and construction of an on-line post-column reactor (PCR) system coupled to a flow-through voltammetric detector equipped with a twin-gold electrode assembly is described. Then the analyte zone dispersion caused by the reactor and its consequences for the sensitivity of the determination and for the analytical resolution of the eluted chromatographic bands is discussed in the light of experiments performed both by continuous mixing of the Ce(III) analyte solutions with the Ce(IV) reagent and by flow injections of the Ce(III) solutions in a carrier continuously mixed with the Ce(IV) reagent. The analytical efficiency parameters for nitrite determination are then evaluated on the basis of the results of similar flow-injection experiments with nitrite solutions under widely varying experimental conditions, such as the use of aqueous and mixed water–acetonitrile carriers (eluents), the choice of different reactor temperatures and the application of mono- and biamperometric detection modes.

EXPERIMENTAL

Apparatus

The study of the PCR was performed by using the two-channel flow manifold shown in Fig. 1. A Gilson Minipuls 3 peristaltic pump was used to propel both the carrier and the reagent streams, usually at a flow-rate of 0.5 ml min^{-1} in each line. Delivery tubes were made of 0.5 mm i.d. PVC tubing, and 0.5 mm i.d. PTFE tubing was used for the connections throughout the whole manifold. Samples were injected (intercalated) by using a metal-free rotary injection valve (Rheodyne Model 9125) equipped with a 30-μl sample loop. Confluence of the two streams was effected with a Kel-F triple connector (0.5 mm i.d.) (Dionex). The mixed stream then entered a single-bead string reactor (SBSR), consisting of a 25-cm length PTFE tubing (0.5 mm i.d.) filled with 0.25 mm diameter glass beads (Supelco). The stream then passed through a PTFE delay tube (3 m × 0.5 mm i.d.) wound as a three-dimensionally knitted coil (Supelco). Both the SBSR and the delay tube were enclosed in a water-circulating thermostatic chamber, the temperature of which was controlled within ±0.2°C. The delay tube was followed by a tightly coiled PTFE tube (1 m × 0.5 mm i.d., 6 mm coil diameter) cooled by circulating water at room temperature. All the joints were made with plastic fittings having zero dead volume (Dionex).

The electrochemical detector employed was an EG&G Model 400 (Princeton Applied Research) equipped with a thin-layer flow cell of the rectangular channel type having an effective volume of about 3 μl (a 50-μm spacer was generally used). Two flat disc gold electrodes (3 mm diameter) are embedded in one side of the cell, the removable Kel-F block, and they can be used as working electrodes for both mono- and biamperometric detection modes. For the latter mode the upstream electrode must work as the anode and the downstream electrode as the cathode, to avoid a substantial amount of Ce(III) being produced from the Ce(IV) reagent, thus increasing the

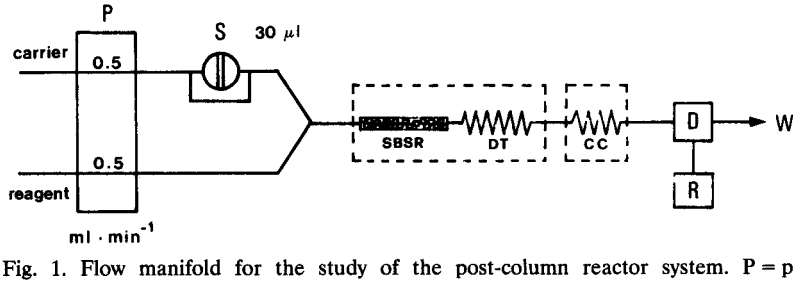

Fig. 1. Flow manifold for the study of the post-column reactor system. P = peristaltic pump; S = sample injection valve; SBSR = single-bead string reactor; DT = delay tube; CC = cooling coil; D = detector; R = recorder; W = waste.

background biamperometric current. The counter electrode is a stainless-steel block bearing the inlet and outlet tubings, and the reference electrode is an Ag/AgCl/3 M NaCl electrode in contact with the flowing stream just before the outlet of the cell. The potential of this electrode was checked against a saturated calomel electrode (SCE) and it was found to be about 60 mV more negative. The potential values in this paper are referred to the SCE as usual.

A DMA 60 digital density meter (Paar) was used for density measurements on the water–acetonitrile mixtures.

Reagents

$(NH_4)_4Ce(SO_4)_4 \cdot 2H_2O$ (analytical-reagent grade, Merck), $Ce_2(SO_4)_3 \cdot 5H_2O$ (Rectapur, Prolabo), KNO_2 (RP Normapur, Prolabo) and acetonitrile (LC grade, Prolabo) were used as received. Solutions of Ce(IV) and Ce(III) were prepared by dissolving the corresponding sulphates in 0.5 M H_2SO_4. The solution of Ce(IV) was checked for the presence of Ce(III), which was found to amount to 1.5–2.0% of the total Ce [1]. An attempt to remove this residual Ce(III) permanently by pre-electrolysis was unsuccessful, as it was found that Ce(III) was formed again in a few minutes. The presence of this small amount of Ce(III) has, however, a certain influence on the background current of the flow experiments, as will be discussed below.

Procedure

The mechanical polishing treatment and the electrochemical cleaning procedures for the gold electrodes were similar to those described previously [1]; care was taken to finish them by anodic prepolarization at the "oxygen chemisorption" potential (1.5–1.6 V), as previously suggested. In biamperometric experiments both gold disc electrodes were treated simultaneously in the same way as above.

RESULTS AND DISCUSSION

Hydrodynamic voltammograms of the Ce(IV)–Ce(III) couple in the flow system

Slow-scan hydrodynamic voltammograms (10 mV s^{-1}) were first obtained with the flow system to confirm the results of the previous batch studies carried out by rotating disc electrode voltam-

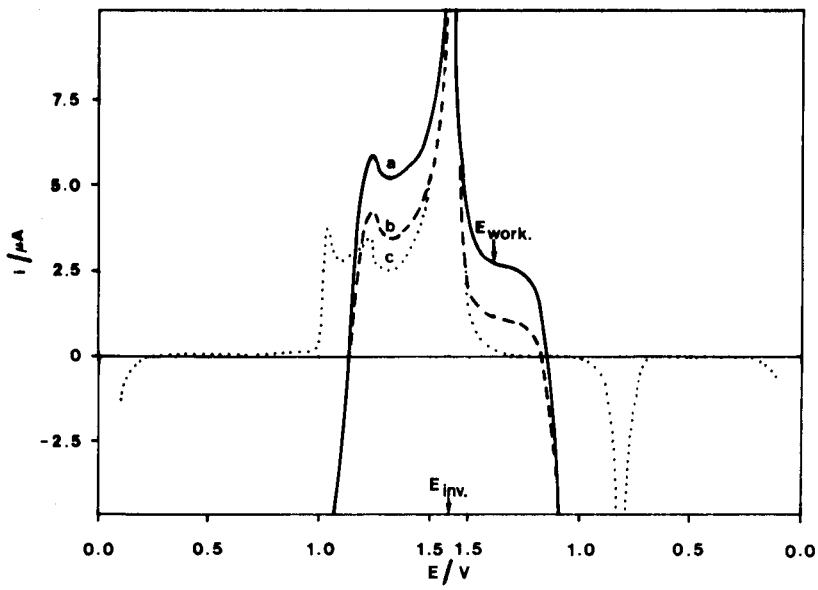

Fig. 2. Hydrodynamic voltammograms with aqueous carrier. (a) Reagent, 1×10^{-3} M Ce(IV) in 0.5 M H_2SO_4; carrier, 1×10^{-4} M Ce(III). (b) Reagent, as for (a); carrier, water. (c) Reagent, 0.5 M H_2SO_4; carrier, water. Scan rate, 10 mV s^{-1}.

metry on the Ce(IV)–Ce(III) system [1]. A 1×10^{-4} M Ce(III) solution was pumped into the carrier line and a 1×10^{-3} M Ce(IV) solution in 0.5 M H_2SO_4 flowed in the reagent line. The flow-rates were 0.5 ml min^{-1} for both streamlines. The resulting voltammogram is shown in Fig. 2, curve a.

The scan was first performed in the anodic direction: the complex wave associated with the oxygen chemisorption process [3] superposed on the Ce(III) oxidation wave is visible. On reversing the scan the wave for the Ce(IV)–Ce(III) system is obtained on the prepolarized gold surface. When only water was pumped into the carrier line a small background current is obtained (curve b), which is due to the presence of Ce(III) in the Ce(IV) reagent (see Experimental). A voltammogram in the absence of Ce(IV) was also run for comparison (curve c). The presence of this background current will be discussed below in connection with the evaluation of the detection limit for nitrite determination. From Fig. 2 the most suitable working potential for monoamperometric measurements is 1.4 V, whereas for a biamperometric determination a ΔE value not lower than 0.3 V should be applied in order to obtain a linear current response vs. Ce(III) concentration, as with this choice the potential of the anode just falls in the limiting current region.

Further voltammograms were measured by pumping into the carrier line a 1×10^{-4} M Ce(III) solution in water–acetonitrile (70 + 30, v/v). This is the most frequently used concentration of organic modifier for the liquid chromatographic (LC) separation of nitrosamines [2]. One of these voltammograms is shown in Fig. 3. The Ce(IV)–Ce(III) couple appears to be slightly less reversible than in the aqueous medium and the potential range of the limiting current for Ce(III) oxidation is slightly restricted. However, a working potential of 1.4 V and ΔE of about 0.3 V are still suitable for mono- and biamperometric determinations, respectively. A noteworthy difference is found in the value of the limiting current, which is lower by about 8% compared with Fig. 2. This can be ascribed to a decrease in the diffusion coefficient of the Ce(III) species, possibly owing to an increase in the kinematic viscosity of the medium.

For a rectangular-channel thin-layer cell, the

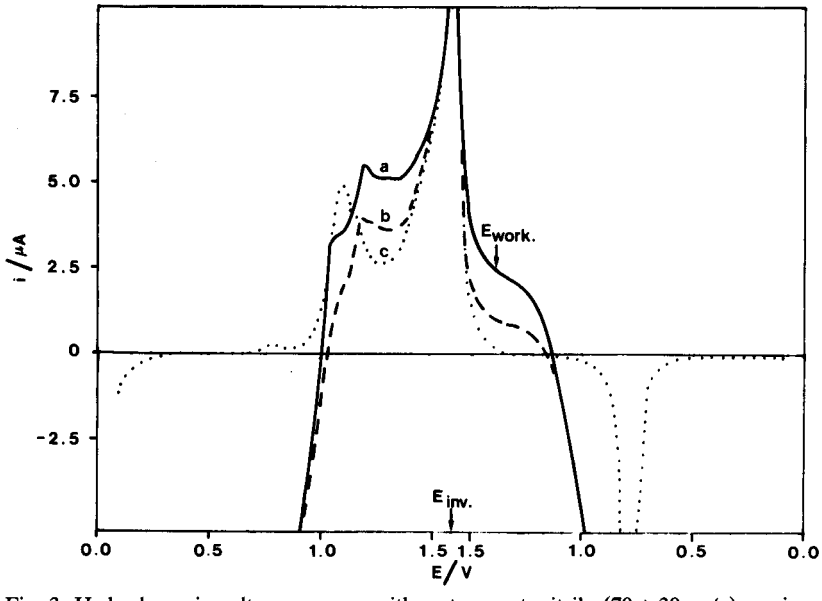

Fig. 3. Hydrodynamic voltammograms with water–acetonitrile (70 + 30, v/v) carrier. (a) Reagent, 1×10^{-3} M Ce(IV) in 0.5 M H_2SO_4; carrier, 1×10^{-4} M Ce(III) in water–acetonitrile. (b) Reagent, as for (a); carrier, water–acetonitrile. (c) Reagent, 0.5 M H_2SO_4; carrier, water–acetonitrile. Scan rate, 10 mV s^{-1}.

following equation holds for the limiting current (see, e.g., [4]):

$$i_{lim} = 1.47nFACD^{2/3}l^{2/3}U^{1/3} \quad (1)$$

where D is the diffusion coefficient, l is the electrode length, U is the flow-rate and the other quantities have their usual meanings. The only parameter that changes from one experiment to another is the diffusion coefficient of the Ce(III) species. As the diffusion coefficient is to a first approximation inversely proportional to the kinematic viscosity ν, an evaluation of the change of this quantity on passing from water to water–acetonitrile (85 + 15, v/v, after mixing with the reagent) was undertaken, by neglecting the presence of 0.25 mol l^{-1} sulphuric acid. Values of the dynamic viscosity η for these mixtures are available [5] and their density ϱ was directly measured.

The kinematic viscosity $\nu = \eta/\varrho$ was calculated and found to increase from 9.0×10^{-3} to 9.8×10^{-3} cm^2 s^{-1} in the above composition range. With due account being taken of the uncertainties inherent in this explanation, and particularly the possible change in the solvation state of the Ce(III) species, the above decrease in the limiting current can be at least partially justified.

Amperometric responses for Ce(III) in the flow system

Mono- and biamperometric responses were measured both for aqueous Ce(III) solutions continuously flowing in the carrier line and for 30-μl sample injections of the same solution in the aqueous carrier. The results of a continuous-flow experiment (steady-state currents) are shown in Fig. 4, where the monoamperometric responses at 1.4 V and the biamperometric responses obtained for $\Delta E = 0.3$ and 0.2 V (curves a, b and c, respectively) are plotted against the Ce(III) concentration in the range $(0.2–1.2) \times 10^{-4}$ M. Curves a and b exhibit a satisfactory linear trend and the biamperometric response agrees within about 5% with the monoamperometric response, an acceptable difference for this kind of measurement (see also [1]). Curve c instead appears to deviate markedly from the expected linear trend for concentrations higher than about 0.5×10^{-4} M, indicating that 0.2 V is insufficient to reach the limiting current region.

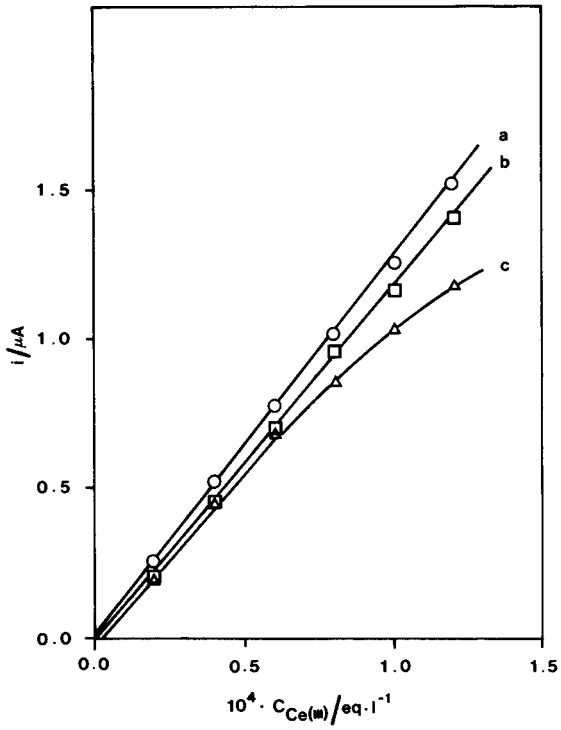

Fig. 4. Steady-state currents for continuous flows of Ce(III) aqueous solutions. Reagent, 1×10^{-3} M Ce(IV) in 0.5 M H_2SO_4. (a) Monoamperometric responses at 1.4 V; (b) biamperometric responses with $\Delta E = 0.3$ V; (c) biamperometric responses with $\Delta E = 0.2$ V.

The results of a flow-injection experiment (peak currents) are shown in Fig. 5, where again the monoamperometric response at 1.4 V and the biamperometric responses obtained for $\Delta E = 0.3$ and 0.2 V (curves a, b and c, respectively) are plotted against the Ce(III) concentration. Again, curves a and b exhibit a satisfactory linear trend with just a 5% difference, whereas curve c deviates, but to a lesser extent than for the steady-state currents. This better result is not unexpected as, owing to the physical dispersion, the true concentrations of Ce(III) in the detector cell are lower than the injected concentrations.

Physical dispersion effects in the PCR

The behaviour of the complete PCR and of its main components, the SBSR reactor and the

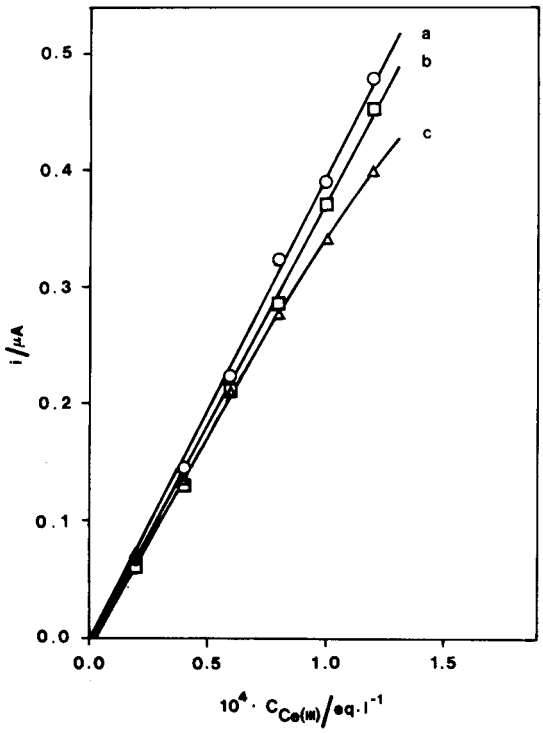

Fig. 5. Peak currents for flow injections of Ce(III) in aqueous carrier. Reagent, 1×10^{-3} M Ce(IV) in 0.5 M H_2SO_4. (a) Monoamperometric responses at 1.4 V; (b) biamperometric responses with $\Delta E = 0.3$ V; (c) biamperometric responses with $\Delta E = 0.2$ V.

delay tube, with respect to the physical dispersion effect of the injected analyte plug has been investigated on the basis of both Ruzicka and Hansen's concept [6] of dispersion coefficient, D_R, and the "exponentially modified Gaussian" (EMG) model for flow-injection analysis peaks by Brooks and co-workers [7,8]. The latter peak analysis not only takes into account the effect of dispersion on the peak height, which influences the analyte determination sensitivity, but allows the peak characteristics in the time domain to be determined. The variance, σ^2, (second statistical moment) accounts in fact for the peak total broadening effects, while the separation into its Gaussian (σ_G^2) and exponential (τ^2) components allows the peak tailing contribution to the total variance to be accounted for. Both kinds of effects are important in controlling the resolution of the bands eluted from the column. The EMG model is particularly suitable for the analysis of peaks produced by this PCR, as their shape approaches more the Gaussian shape of the chromatographic peaks than the skewed shape of the usual flow-injection analysis peaks. Measurements with continuous-flow and with 30-μl injections were made for three concentrations of Ce(III) solution (0.2×10^{-4}, 0.6×10^{-4} and 1.0×10^{-4} M) and for the following geometric configurations of the PCR: (a) PCR without SBSR reactor and delay tube; (b) without delay tube; (c) without SBSR reactor; and (d) complete PCR. A set of current responses obtained for the configurations (a) and (d) is given in Fig. 6.

The proposed procedure allows the contribution of the different reactor elements to the total dispersion of the PCR to be evaluated. The EMG model was first tested to give consistent peak area values from peak widths, w, and asymmetry factors, b/a, derived at four peak heights (10, 25,

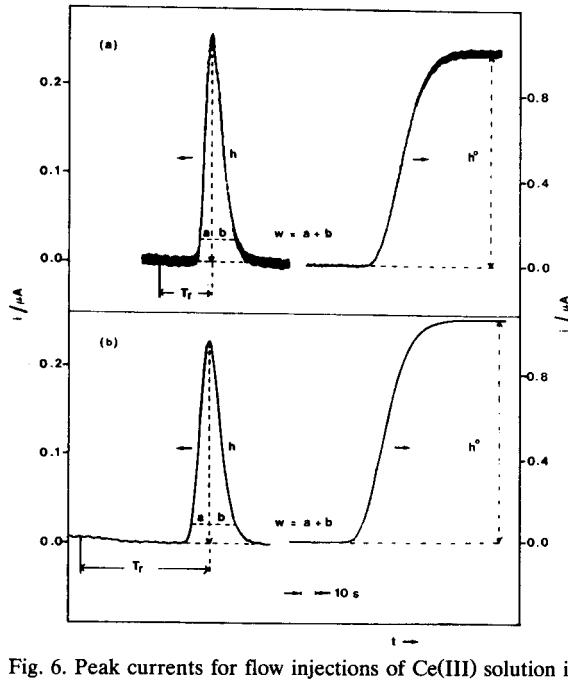

Fig. 6. Peak currents for flow injections of Ce(III) solution in aqueous carrier and steady-state currents for continuous flow of the same solution. Ce(III) concentration, 6×10^{-5} M; reagent, 1×10^{-3} M Ce(IV) in 0.5 M H_2SO_4. (a) PCR without SBSR and delay tube; (b) complete PCR.

TABLE 1

Values of the Ruzicka dispersion coefficient, D_R, the residence time, T_r, and the time domain parameters according to the EMG model (see text): peak variance, σ^2, peak standard deviation, σ, Gaussian component, σ_G, exponential time constant, τ, and their ratio, τ/σ_G, for different geometric configurations of the PCR: (a) PCR without SBSR reactor and delay tube; (b) without delay tube; (c) without SBSR reactor; (d) complete PCR

[Average values and estimates of their standard deviations were calculated from sets of nine samples, three for each concentration (see text)]

Configuration	D_R	T_r (s)	σ^2 (s^2)	σ (s)	σ_G (s)	τ (s)	τ/σ_G
(a)	3.96 ± 0.08	37.1 ± 0.2	66 ± 16	8.1 ± 1.0	3.5 ± 0.2	7.2 ± 1.2	2.0 ± 0.5
(b)	3.90 ± 0.10	40.8 ± 0.3	59 ± 1	7.7 ± 0.1	4.0 ± 0.2	6.5 ± 0.2	1.7 ± 0.1
(c)	4.42 ± 0.13	91.9 ± 0.6	74 ± 6	8.6 ± 0.4	5.0 ± 0.2	7.0 ± 0.6	1.4 ± 0.2
(d)	4.45 ± 0.13	94.0 ± 0.8	69 ± 6	8.3 ± 0.4	5.1 ± 0.2	6.5 ± 0.7	1.3 ± 0.2

50 and 75% of the maximum) [7]. The calculated areas did not deviate by more than ±10% of the mean values in at least 90% of the cases, so that the model can be correctly applied [7]. In Table 1, average values of D_R are reported together with the time domain parameters calculated from peak widths and asymmetry factors at 10% of the peak height, as usual. The value of about 90 s for the residence time in the complete PCR is of the order of the times necessary for good conversion yields of those classes of nitrosamines to be detected by this method [1,2].

Table 1 shows that the main contribution to the dispersion of the PCR is not due to the SBSR reactor and the delay tube, but to the remaining parts of the system (valve, connecting tubes, confluence, cooling coil and detector). The value of $D_R = 3.96$ for configuration (a) indicates a medium-sized dispersion effect, and can be considered as an acceptable loss of sensitivity for the conduit elements involved. The standard deviation of the peak, σ, is more strongly influenced by the exponential time constant term, τ, than by the Gaussian term, σ_G: the ratio τ/σ_G is in fact

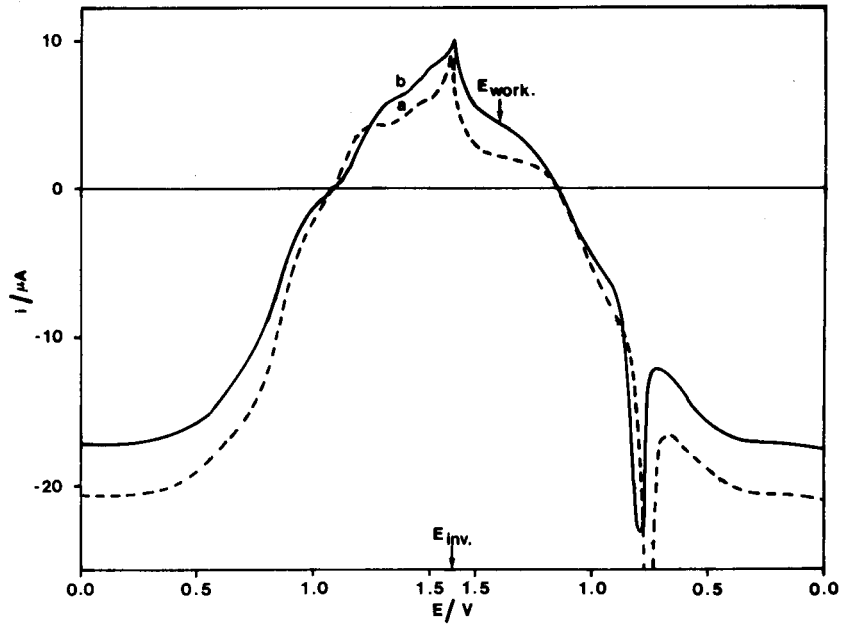

Fig. 7. Hydrodynamic voltammograms with water–acetonitrile (70 + 30, v/v) carrier. (a) Reagent, 1×10^{-3} M Ce(IV) in 0.5 M H_2SO_4; carrier, water–acetonitrile. (b) Reagent, as for (a); carrier, 8×10^{-5} M KNO_2 in water–acetonitrile. Scan rate, 10 mV s^{-1}.

2.0; τ is related to the dispersion caused by the axial convection of the sample plug, whereas σ_G depends mainly on the efficiency of the convective and diffusive radial motions, including secondary flow patterns generated by centrifugal forces in coiled conduits [9]. By introducing the SBSR reactor [case (b)], a short element (T_r increases by only 4 s) with a good mixing efficiency, there is no substantial change in D_R, but a slight decrease in τ and a small increase in σ_G are obtained. The lower asymmetry ($\tau/\sigma_G = 1.7$) and the virtually unchanged value of the standard deviation indicate an improved radial mixing in the sample plug. Alternatively, the introduction of the delay tube [case (c)], a long, three-dimensionally knitted coil, which allows the residence time to be increased by more than 50 s, has a substantial effect on the value of D_R, which increases to 4.42. This is paralleled by a small increase in the standard deviation, but there is also an advantageous decrease in the τ/σ_G ratio to 1.4. Overall, the delay tube is a very efficient conduit element which allows much longer residence times to be obtained (92 s), while peak broadening and tailing are limited. As expected, the complete PCR [case (d)] exhibits comparable values of D_R and T_r (4.45 and 94 s, respectively) and a further useful decrease in the τ/σ_G ratio to 1.3. In conclusion, the peak standard deviation has not been substantially modified by the introduction of the two reactors, whereas a much longer residence time and a more Gaussian shape have been obtained. It is also worth mentioning that a very effective reduction in the noise due to the pumping pulsations was observed after the introduction of the SBSR reactor, possibly owing to the damping effect of the glass microspheres.

Comparison between flow injections of Ce(III) and of nitrite

The voltammogram shown in Fig. 7 was obtained under the same conditions as those in Fig. 2, but by using nitrite in place of Ce(III). The only noteworthy difference is the decrease in the cathodic limiting current [reduction of Ce(IV)] proportional to the concentration of nitrite in the carrier stream. However, this result is not unexpected as it had already been demonstrated [1] that the reaction of nitrite with Ce(IV) is completed in a few seconds.

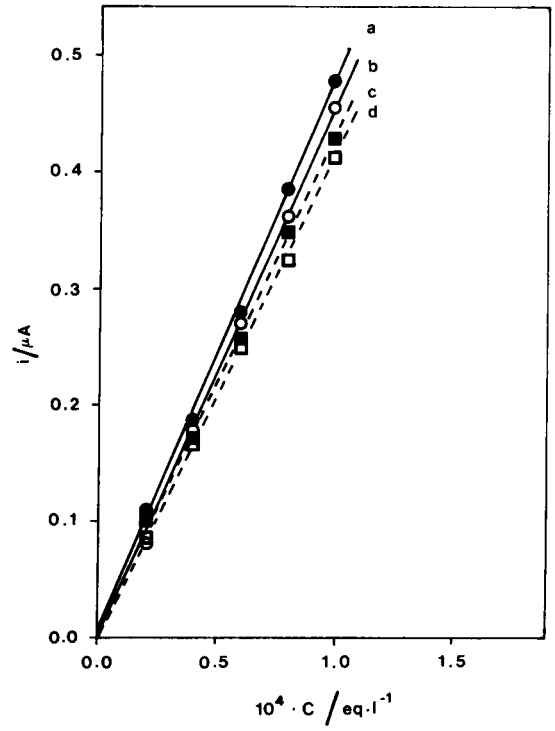

Fig. 8. Peak currents for flow injections of Ce(III) and nitrite in aqueous carrier. Reagent, 1×10^{-3} M Ce(IV) in 0.5 M H_2SO_4. (a) Biamperometric responses with $\Delta E = 0.3$ V for KNO_2; (b) as in (a) for Ce(III); (c) biamperometric responses with $\Delta E = 0.2$ V for KNO_2; (d) as in (c) for Ce(III).

To compare the current responses for flow injections of Ce(III) and nitrite, some biamperometric flow-injection experiments were performed. The peak shapes were found to be the same for both analytes, which confirms that, if the chemical reaction is fast enough, both the heights and the time domain characteristics are the same as for a physical dispersion without chemical reaction [10]. The peak heights are plotted against the concentrations in Fig. 8, as obtained for $\Delta E = 0.3$ and 0.2 V. In this instance also the latter data are satisfactorily fitted by straight lines. The fitting straight lines (a with b and c with d) agree within about 5% (see above).

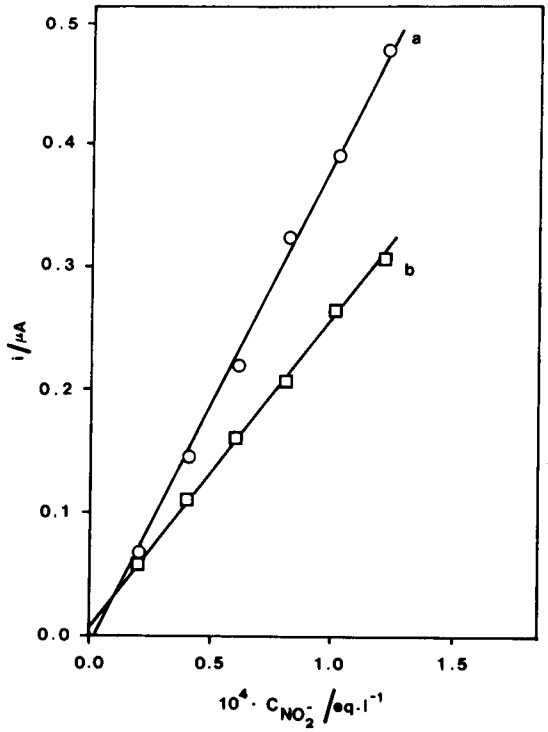

Fig. 9. Peak currents for flow injections of nitrite in aqueous and mixed carriers. Reagent, 1×10^{-3} M Ce(IV) in 0.5 M H_2SO_4. (a) Monoamperometric responses at 1.4 V for nitrite in aqueous carrier; (b) as in (a) for water–acetonitrile (70 + 30, v/v) carrier.

Flow injections of nitrite in water–acetonitrile carrier

A test was made to evaluate the change in sensitivity on changing the carrier from water to water–acetonitrile (70 + 30, v/v). In Fig. 9, the response curve for the mixed carrier (line b) appears to be about 30% lower than that for the aqueous carrier (line a). As the corresponding decrease in the steady-state currents amounts to about 8% (see above), the further decrease of the peak current is due to increased dispersion, as a consequence of the increased viscosity of the carrier. A determination of D_R, however, performed with the PCR at 70°C, gave a change from 3.9 for the aqueous carrier to 4.6 for the mixed carrier. Hence increase in dispersion of almost 20% is expected under the conditions exhibited in Fig. 9. On increasing the carrier viscosity, both the axial dispersion (mainly due to convective contribution) and the radial mass transfer (due to both convective and diffusive contributions) are slowed [11], but from these experiments it appears that the latter factor is more influenced than the former.

Flow injections of nitrite with the PCR at enhanced temperature

As the yields of the acid denitrosation reactions of the nitrosamines are greatly enhanced at temperatures exceeding 40–50°C [2], the optimum conditions for nitrite determination were investigated using water–acetonitrile carrier by maintaining the PCR at 70°C; this was selected as a safe temperature to avoid problems in the flow system, such as bubble formation due to degassing or boiling of the solvent. A set of measurements were then performed under these experimental conditions using both mono- and biamperometric detection modes. An example of plots of peak current vs. nitrite concentration is given in Fig. 10. All the response curves are satisfactorily linear over the whole concentration range. The sensitivity is found to be almost 10% higher than that found with the PCR at 25°C (see for comparison Fig. 9, line b); this finding suggests that a substantial decrease in physical dispersion is promoted by such an increase of temperature. This trend is also supported by the decrease in the Ruzicka dispersion coefficient, which was directly measured for the aqueous carrier at both temperatures: whereas $D_R = 4.5$ at 25°C [see Table 1, case (d)], a value of 3.9 was obtained with the PCR at 70°C (see previous paragraph). The variances and the other time domain parameters were also calculated as described above and are given in Table 2. In Table 2 the data obtained previously for Ce(III) flow injections in the aqueous carrier with the PCR at 25°C are also reported for comparison. Although the carrier is mixed, which involves the drawbacks discussed in the previous paragraph, one finds two beneficial effects of the large increase in temperature: the variance is lowered by about 30% and the peaks exhibit a more Gaussian character, as indicated by the decrease in the τ/σ_G ratio. The decrease in the dispersion effects can be ascribed to both an enhancement of the

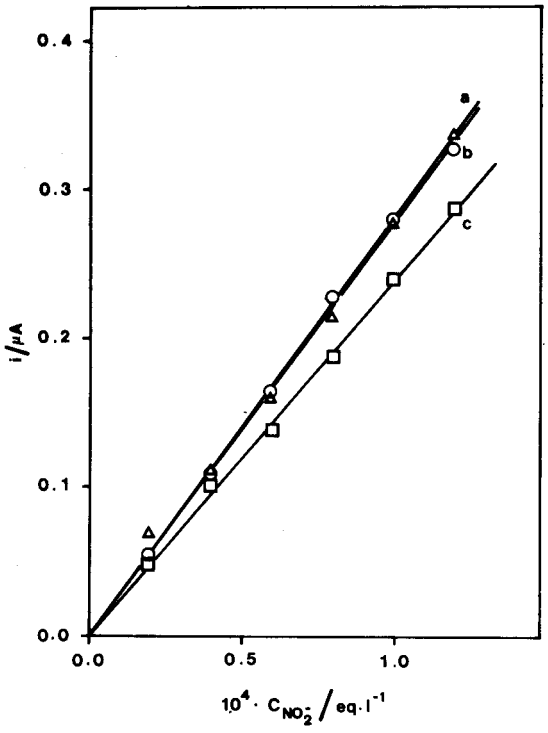

Fig. 10. Peak currents for flow injections of KNO_2 samples in water–acetonitrile (70+30, v/v) carrier with the PCR at 70°C. (a) Monoamperometric responses at 1.4 V; (b) biamperometric responses with $\Delta E = 0.3$ V; (c) biamperometric responses with $\Delta E = 0.2$ V.

radial mass transfer due to a faster molecular diffusion and to a decrease in the viscosity (see previous paragraph). In brief, on increasing the temperature of the PCR one increases the sensitivity of the determination and lowers the additional band broadening and band asymmetry, thus helping to control the degradation of the resolution of the chromatographic bands due to the flow reactor.

Detection limit of nitrite

The measurements by flow injections were also extended to lower nitrite concentrations. Both mono- and biamperometric current responses in the range 10^{-6}–10^{-5} M were found to be consistent with the results for higher concentrations and the sensitivity over the linear dynamic range 10^{-6}–10^{-4} M was 5.6×10^6 nA mol^{-1} 1. Most of the noise is due to the flow-rate pulsations of the pump. By attaching two gas-filled syringes as pulse-damping devices to the connector tubings, the peak-to-trough fluctuations of the background current were controlled to within 0.3 nA. As this noise depends on the magnitude of the background current, which is bound to the residual Ce(III) in the Ce(IV) reagent (see Experimental), an attempt was made to lower the noise by using more dilute reagent solutions. However, with biamperometric detection a tenfold decrease in Ce(IV) concentration reduced both the background current and noise to about one third, but also the sensitivity was decreased in a similar way, so that no improvement in the signal-to-noise ratio was obtained. For a tentative explanation of these findings, one can recall that the Ce(IV)–Ce(III) couple is not a highly reversible electrode system [1]; excessive dilution flattens the rising edge of the cathodic wave and the usual applied ΔE fails to match the limiting current region for Ce(III) oxidation.

Anyhow, an evaluation of the detection limit can be performed by using the following equation:

$$C_{d.l.} = ks/S \qquad (2)$$

where s is the estimate of the standard deviation of the noise, S is the sensitivity and k is a statistical factor usually taken equal to 3. A calcu-

TABLE 2

Values of the residence time, T_r, and of the time domain parameters according to the EMG model (see Table 1) for different carriers and reactor temperatures

[Average values and estimates of their standard deviations were calculated from sets of nine samples, three for each concentration (see text)]

Carrier	t (°C)	T_r (s)	σ^2 (s^2)	σ (s)	σ_G (s)	τ (s)	τ/σ_G
Water	25	94.0 ± 0.8	69 ± 6	8.3 ± 0.4	5.1 ± 0.2	6.5 ± 0.7	1.3 ± 0.2
Water–acetonitrile (70 + 30, v/v)	70	88.6 ± 0.3	45 ± 4	6.7 ± 0.3	4.7 ± 0.4	4.7 ± 0.8	1.0 ± 0.3

lation of s performed on the background current fluctuations gave a value of about 0.1 nA; by taking the value 5.6×10^6 nA mol^{-1} l as the current response sensitivity S, one obtains $C_{d.l.} = 5 \times 10^{-8}$ M, which is the minimum detectable concentration with a 30-μl sample loop. The minimum detectable amount of nitrite under the specified conditions is then 0.1 ng.

Conclusions

The on-line PCR system based on the use of Ce(IV) in 0.5 M sulphuric acid as the reagent solution has been investigated in a two-line flow manifold coupled with a flow-through voltammetric detector. Steady-state currents for continuous-flow and peak currents for flow injections of Ce(III) and nitrite solutions in aqueous and water–acetonitrile carriers were measured under different experimental conditions. Ruzicka dispersion coefficients and time domain parameters of the peaks evaluated with the help of the EMG model showed that the physical dispersion produced by the main elements of the reactor system, the SBSR reactor and the three-dimensional knitted coil delay tube, was very limited, whereas good-quality quasi-Gaussian peaks were obtained for residence times around 90 s, the order of useful reaction times for a good conversion yield of nitrosamines in warm acidic solutions. Wide linear dynamic ranges were determined by both monoamperometric ($E = 1.4$ V) and biamperometric ($\Delta E = 0.3$ V) detection modes.

By changing the carrier to water–acetonitrile a small decrease in sensitivity was found, mainly due to the increased viscosity, which influences both the physical dispersion and the magnitude of the limiting current.

By increasing the reactor system temperature to 70°C a remarkable improvement in both sensitivity and peak characteristics was found, which was ascribed to a favourable balance of radial mass transfer in respect of axial dispersion, induced by decreased viscosity and increased molecular diffusion. The detection limit for nitrite under the optimized conditions, i.e., about 5×10^{-8} M, and the additional peak standard deviation, which is to a few seconds (for residence times around 90 s), indicate that the proposed method is suitable for the determination of nitrosamines under the usual LC conditions of separation. Further work is in progress along these lines.

This work was financially supported by the Italian Consiglio Nazionale delle Ricerche (CNR) and by the Italian Ministero dell'Università e della Ricerca Scientifica e Tecnologica (MURST).

REFERENCES

1 G.A. Sacchetto, P. Pastore, G. Favaro and M. Fiorani, Anal. Chim. Acta, 258 (1992) 99.
2 S.H. Lee and L.R. Field, J. Chromatogr., 386 (1987) 137.
3 R. Woods, in A.J. Bard (Ed.), Electroanalytical Chemistry, Vol. 9, Dekker, New York, 1976, pp. 119 et seq.
4 J.M. Elbicki, D.M. Morgan and S.G. Weber, Anal. Chem., 56 (1984) 978.
5 H. Strehlow and H. Schneider, in J.C. Marchon (Ed.), Non-Aqueous Electrochemistry, Butterworths, London, 1971, p. 341.
6 J. Ruzicka and E.H. Hansen, Flow Injection Analysis, Wiley, New York, 1988, pp. 23 et seq.
7 S.H. Brooks, D.V. Leff, M.A. Hernandez Torres and J.G. Dorsey, Anal. Chem., 60 (1988) 2737.
8 S.H. Brooks and J.G. Dorsey, Anal. Chim. Acta, 229 (1990) 35.
9 R. Tijssen, Anal. Chim. Acta, 114 (1980) 71.
10 J.M. Reijn, H. Poppe and W.E. Van der Linden, Anal. Chem., 56 (1984) 943.
11 J. Ruzicka and E.H. Hansen, Flow Injection Analysis, Wiley, New York, 1988, p. 135.

Analytica Chimica Acta, 273 (1993) 469–475
Elsevier Science Publishers B.V., Amsterdam

Flow-injection analysis with electrochemical detection for determination of salicylic acid in pharmaceutical preparations

M. Neumayr, O. Friedrich and G. Sontag

Institute for Analytical Chemistry, University of Vienna, Währingerstrasse 38, A-1090 Vienna (Austria)

F. Pittner

Institute for General Biochemistry and Ludwig Boltzmann-Forschungsstelle, University of Vienna, Währingerstrasse 38, A-1090 Vienna (Austria)

(Received 10th June 1992)

Abstract

An enzyme-based flow-injection system with electrochemical detection suitable for the determination of salicylic acid in pharmaceuticals is described. The method makes use of the enzyme salicylate hydroxylase (EC 1.14.13.1), which is covalently bound to glass beads and put into the reactor of a flow system. The enzyme catalyses the stoichiometric conversion of salicylic acid to catechol, which can then be detected amperometrically at +0.45 V (vs. $Ag/AgCl/KCl_{sat.}$). The electrode response is linearly proportional to the concentration of salicylic acid between 5 and 150 $\mu g\ ml^{-1}$. The detection limit is 0.4 $\mu g\ ml^{-1}$. This method is simple, rapid and specific. The assayed samples yielded relative standard deviations between 0.5 and 2.0% and recoveries between 93 and 98%.

Keywords: Amperometry; Enzymatic methods; Flow injection; Pharmaceuticals; Salicylic acid

The toxic properties of salicylic acid [1] require the control of its amount in plasma, serum or urine of patients who are therapeutically treated with acetylsalicylic acid [2] or who have ingested an overdose in a suicidal attempt [3]. Further, it has to be determined in dermatological pharmaceuticals and in foods, where it has long been used for preservation purposes [1].

Many methods have been reported for the determination of salicylic acid. Spectrophotometric methods [4,5], although widely used, suffer from interferences from a variety of compounds [2], but spectrofluorimetric methods [6–8] give better results. The possibility of the simultaneous determination of several derivatives of salicylic acid is the main advantage of liquid chromatographic techniques [9–14], which have displaced gas–liquid chromatographic methods [15–19], where derivatization is necessary. Liquid membrane electrodes [20–25], allowing rapid determinations, have been developed, but their selectivity is poor and their lifetime is short. Recently, immunoassays [26,27] have also been reported.

Other approaches for the determination of salicylic acid use the enzyme salicylate hydroxylase (salicylate-1-monooxygenase, EC 1.14.13.1) [28–30], a flavoprotein which catalyses the irreversible hydroxylation of salicylic acid to catechol:

Correspondence to: G. Sontag, Institute for Analytical Chemistry, University of Vienna, Währingerstrasse 38, A-1090 Vienna (Austria).

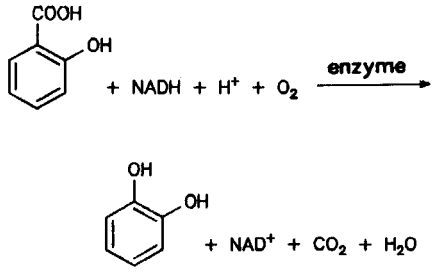

According to this reaction, the determination of salicylic acid is possible by measuring the decrease in NADH [31,32], the decrease in oxygen [33,34], the formation of carbon dioxide [35] or the formation of catechol [36,37]. The electrochemical detection of catechol is the most accurate method. So-called "pseudo-substrates" [29,30], which consist of aromatic compounds with a free carboxyl group, permit to some extent a reduction of the enzyme-bound FAD by NADH in the absence of salicylic acid. This results in the production of hydrogen peroxide and carbon dioxide, thus leading to incorrect results, if NADH, oxygen or carbon dioxide is detected. To make the method cheaper and more efficient, the enzyme is immobilized on electrodes by cross-linking [34] or by inclusion [35,37]. Unfortunately, the lifetime of these electrodes is short.

The aim of this work was the development of a rapid enzymatic method for the determination of salicylic acid, which should be achievable by combining a flow system with an enzyme reactor and an amperometric detector. This system has also been successfully used for the determination of ascorbic acid [38].

EXPERIMENTAL

Apparatus

A schematic diagram of the final flow-injection system is shown in Fig. 1. All components were connected by capillaries made of stainless steel (i.d. 0.01 mm). A Model 330 C LC pump (Gynkotek) was used to deliver the carrier solution. Volumes of 20 μl of the sample could be brought into the carrier stream by a bypass injection valve (Gynkotek). Using a Model 7000 switch valve (Rheodyne), the flow could be directed either to the enzyme reactor (Waters Guard Column 84550, 40 × 4 mm i.d.) containing the glass beads with immobilized enzyme, or to the inactive reactor (23 × 4 mm i.d.) which was filled with silanized glass beads. The latter was used for testing and optimizing the system without biochemical reaction. The amperometric detector was an EA 1096 three-electrode wall-jet cell (Metrohm) with a glassy carbon working electrode, a platinum auxiliary electrode and a silver/silver chloride/saturated potassium chloride reference electrode. The amperometric measurements were made with a Model 174 A polarographic analyser (PAR), which simultaneously applied the desired potential to the working electrode and measured the resulting current. The latter was recorded on an HP 3390 A integrator (Hewlett-Packard) and Servogor 210 recorder (Goerz).

Reagents

All chemicals were of analytical-reagent grade.

The carrier solution, 20 mM phosphate buffer (pH 7.6) containing 1 mM EDTA, was prepared

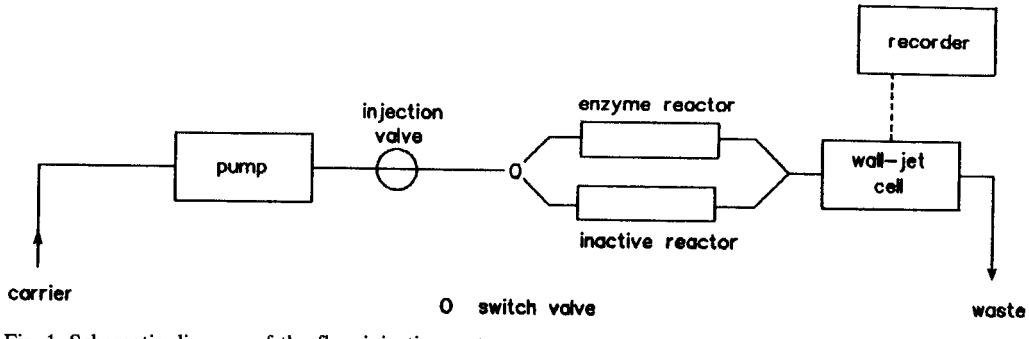

Fig. 1. Schematic diagram of the flow-injection system.

with doubly distilled water and sterilized by filtration (Sterilfilter FP 030/3, 0.2 μm) before use. Standard solutions were prepared with this buffer. The enzyme salicylate hydroxylase was obtained from Sigma. For immobilization, CPG 10 glass beads (24 nm, 120–200 mesh) from Serva were used. Salicylic acid and catechol were obtained from Merck and β-NADH from Merck or Sigma. NADH solutions were prepared fresh daily.

Immobilization

Glass beads were modified with aminosilane and activated with *p*-tetrachloroquinone as described in [39]. Defined amounts (1–7 mg) of the lyophilized enzyme salicylate hydroxylase were dissolved in 4.5 ml of phosphate buffer. A 100-mg amount of the dried activated beads was degassed and added to the enzyme solution. After shaking for 6 h at 4°C, the beads were filtered, washed with buffer and stored in buffer at 4°C.

Photometric characterization of the immobilized enzyme

The photometrically measurable decrease of NADH during the enzymatic reaction served for the evaluation of the activity of the immobilized enzyme. A closed-loop system with a photometric flow-through cell was used. A solution of sodium salicylate (0.1 mM) and NADH (0.18 mM) circulated through the loop (15 ml), driven by a Minipuls 2 peristaltic pump (Gilson), at a flow-rate of 1 ml min^{-1}. After inserting a small MoBiTec column (Gatt), which contained a defined amount of immobilized enzyme, in the closed loop, a time scan lasting 10 min was made, the absorbance at 340 nm being measured. The activity of the immobilized enzyme was calculated as described [32].

Hydrodynamic voltammograms

For measurement of the current–voltage characteristic of the relevant substances, salicylic acid (36 μg ml^{-1}), catechol (5 μg ml^{-1}) and NADH (200 μg ml^{-1}), the path over the inactive reactor of the flow system was used. The current was measured in the range from 0 to +1.1 V in increments of 0.05 V.

Procedure

Before use the flow system was purged with doubly distilled water and with carrier solution over the inactive reactor. The system was operated with a flow-rate of 1 ml min^{-1}. The glassy carbon electrode was polished with aluminium oxide. A potential of +0.45 V (vs. Ag/AgCl/$KCl_{sat.}$) was applied to the working electrode. The enzyme reactor was inserted. The amounts of NADH needed for the biochemical reaction ([NADH]/[salicylic acid] $\geqslant$ 1.8) were added to 3 ml of the salicylic acid standards just before measurements. Volumes of 20 μl of the standard solutions were injected and the peak areas were determined. At the end of all measurements, the enzyme reactor was stored in a refrigerator at 4°C. The system was purged with doubly distilled water and with methanol–water (1 + 1).

Measurement of pharmaceuticals

Drugs were diluted with buffer until their salicylic acid concentration varied between 5 and 50 μg ml^{-1}. For the Pilison sample the solution had to be filtered. Then 163 μl of 12 mM β-NADH solution were added to 3 ml of each sample and standard (5–50 μg ml^{-1}). Starting with low concentrations, each standard was measured twice. Two to four samples were measured within one calibration. Recoveries were studied by spiking the samples with a defined amount (6.7 μg) of salicylic acid and comparing their concentrations with those of unspiked samples.

RESULTS AND DISCUSSION

Optimization of the immobilization procedure

The covalent immobilization of an enzyme to silanized glass beads via *p*-tetrachloroquinone results in a stable linkage [40]. To achieve high activity on a defined amount of beads, the immobilization procedure for salicylate hydroxylase was optimized with regard to the amount of enzyme used. It can be seen (Fig. 2), that the amount of enzymatically active immobilized enzyme increases linearly with the amount of enzyme available during the immobilization until it finally

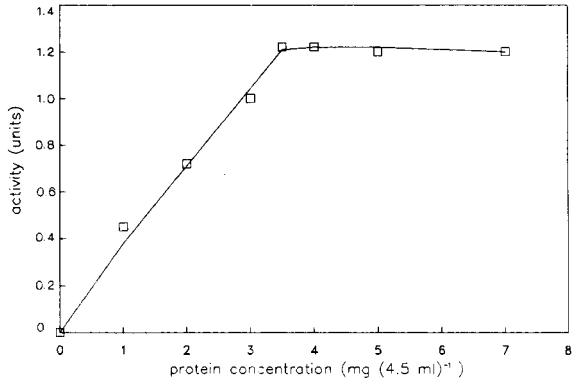

Fig. 2. Effect of protein concentration during immobilization on the activity.

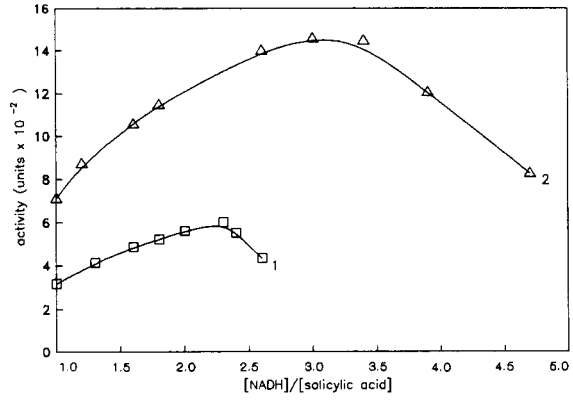

Fig. 3. Influence of NADH concentration on the activity of a defined amount of immobilized enzyme: (1) 14 mg of wet beads with immobilized enzyme; (2) 31.55 mg of wet beads with immobilized enzyme.

reaches a plateau. The optimum amount of the enzyme to be taken for the immobilization lies at the beginning of the plateau, where maximum activity can be achieved with a minimum of resources. Therefore, 3.5 mg of the protein (4 mg of lyophilized powder) should be used for immobilization on 100 mg of activated beads; in this instance, the activity of the immobilized enzyme is 13% of the activity of the enzyme solution.

Characterization of the immobilized enzyme

Various parameters, such as coenzyme concentration and pH, influence the activity of the immobilized enzyme and were investigated by measuring photometrically the decrease in NADH during the enzyme reaction.

Figure 3 shows the effect of various NADH concentrations on the activity. The more immobilized enzyme taken, the higher is the possible ratio of NADH to salicylic acid for an undisturbed reaction. It can be concluded (see also below) that a reactor of length ca. 4 cm contains enough immobilized enzyme to measure salicylic acid in a suitable concentration range without any disturbance by the coenzyme.

The optimum pH of the soluble enzyme has been reported to be 7.6 [30]. For the immobilized enzyme, the optimum pH is broader and lies between 7.3 and 8.3 (Fig. 4). A pH of 7.6 was chosen for all measurements.

An important feature of an immobilized enzyme is its stability under storage and under assay conditions. Therefore, the change in the activity with time was investigated. With storage at 4°C, the immobilized enzyme was stable for more than 1 year. Under assay conditions the activity of a defined amount of beads with immobilized enzyme first decreased, but finally also became stable for more than 1 year (Fig. 5). The initial decrease in activity may be due to intercalation of reactants or leakage of FAD.

Amperometric detection in the flow system

Inactive reactor. To obtain information about the optimum detector potential, the hydrody-

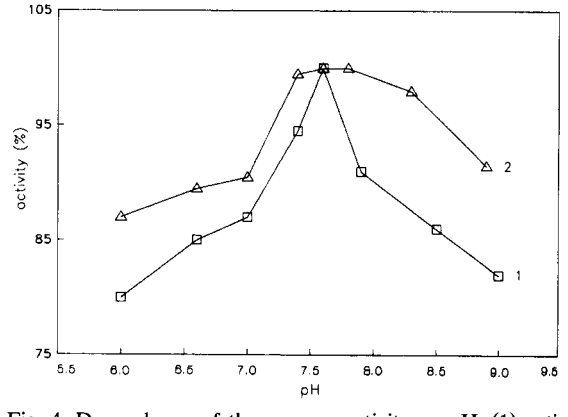

Fig. 4. Dependence of the enzyme activity on pH: (1) native enzyme; (2) immobilized enzyme.

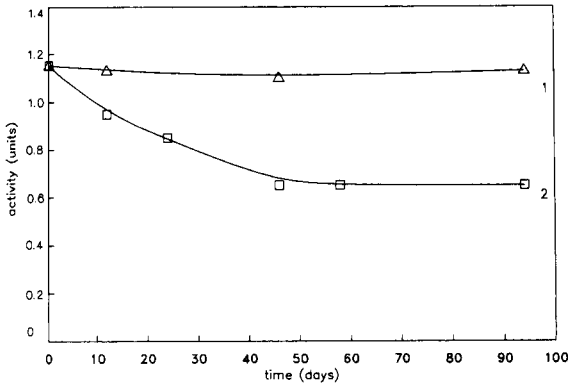

Fig. 5. Stability studies: (1) storage conditions; (2) assay conditions.

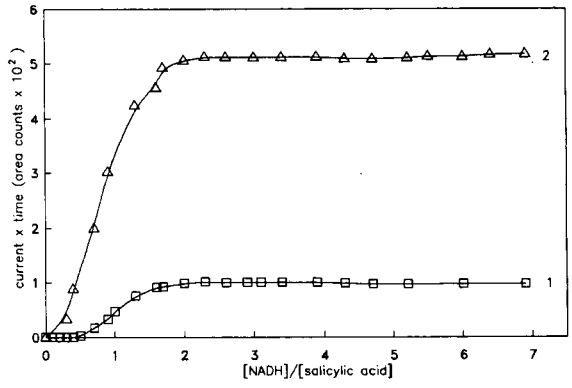

Fig. 7. Effect of NADH concentration on the signal of salicylic acid: (1) 5 μg ml^{-1} salicylic acid; (2) 10 μg ml^{-1} salicylic acid.

namic voltammograms of salicylic acid, catechol and NADH were measured (Fig. 6).

For the detection of catechol a potential of +0.45 V (vs. Ag/AgCl/KCl$_{sat.}$) was chosen, as the current due to the oxidation of catechol is not yet in the limiting range but the response of NADH and electrode contamination by NADH can be minimized. As a consequence, the detection limit of catechol is 50 pg (2.5 ng ml^{-1}). The linear range was restricted to 120 μg ml^{-1} catechol owing to contamination of the electrode by catechol, but it could be expanded to 210 μg ml^{-1} if the electrode was polished with aluminium oxide between measurements.

Enzyme reactor. The molar ratio of NADH to salicylic acid influences the amount of catechol being formed and hence the response of the detector. A constant signal is reached at a ratio of 1.8. The signal did not decrease even for high ratios, thus proving that the reactor was long enough to eliminate disturbances of the enzymatic reaction by high NADH concentrations.

Figure 7 demonstrates that higher concentrations of salicylic acid yield higher signals, but no conclusion could be drawn about the amount of salicylic acid being converted into catechol. By comparison of the signals of known concentrations of salicylic acid and NADH with those of the molar equivalents of catechol, it could be established that salicylic acid is quantitatively

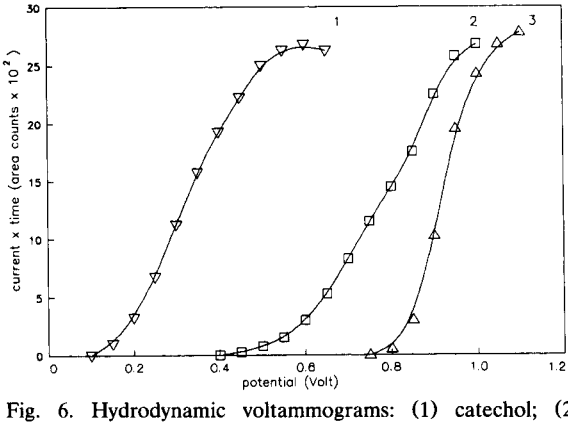

Fig. 6. Hydrodynamic voltammograms: (1) catechol; (2) NADH; (3) salicylic acid.

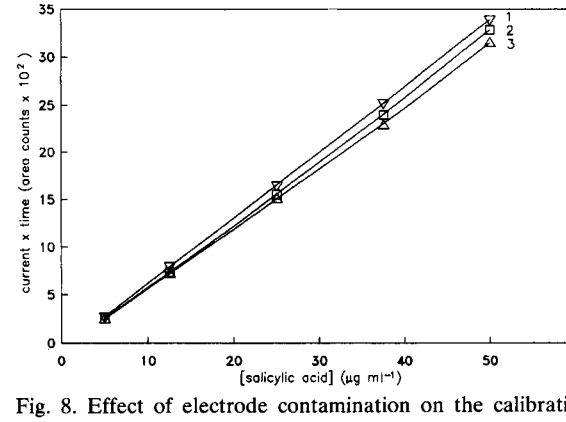

Fig. 8. Effect of electrode contamination on the calibration graph. One calibration graph was measured immediately after the other: (1) first; (2) second; (3) third calibration graph.

TABLE 1

Salicylic acid in pharmaceuticals

Drug	n [a]	Mean concentration found (μg/ml)	R.S.D. (%)	Deviation [b] (%)	Recovery (%)
DDD	6	22.60	2.0	+3.5	98.6
Pilison	4	30.62	0.5	+2.1	98.9
Diprosalic	3	30.32	0.6	+1.4	92.9
Volon A	3	22.55	0.6	+2.2	93.3

[a] Number of different samples, each of which was assayed at least three times. [b] Deviation from the values stated by the manufacturer.

converted into catechol if the molar ratio of NADH to salicylic acid is greater than 1.8.

Simultaneous detection of NADH on the electrode is negligible if the molar excess of NADH to salicylic acid is less than 30, although ratios near 30 lead to tailing of the signal. Ratios greater than 30 result in double peaks because of the broad and flat signal of NADH, which reaches its maximum at the end of the catechol signal. This does not greatly disturb the results, but it lengthens the baseline-to-baseline time and electrode contamination. Therefore, the molar ratio of NADH to salicylic acid should be kept below 30.

The detection limit is significantly higher than for the system without the enzyme reactor and is 8 ng of salicylic acid (0.4 μg ml^{-1}). This is possibly due to the need for a certain amount of substrate and coenzyme necessary for the enzymatic process to start. The linear range begins at 5 μg ml^{-1} salicylic acid and is limited to 150 μg ml^{-1} owing to contamination of the electrode by oxidation products of catechol.

Calibration

If an unknown amount of salicylic acid is to be measured, a certain amount of NADH must be added to all solutions so that the molar ratio of NADH to salicylic acid is 1.8 for the highest and less than 30 for the lowest concentration. Because of this and to minimize the contamination of the electrode at high concentrations, a calibration range from 5 to 50 μg ml^{-1} salicylic acid was chosen for accurate and rapid measurements [41]. The correlation coefficient of the calibration graph is ca. 0.9999. Mainly at the beginning of the measurements electrode fouling can occur, which influences the slope of the calibration graph (Fig. 8). Nevertheless, it is possible to obtain accurate and reliable results by recalibrating the system after several injections.

Salicylic acid in pharmaceuticals

The samples only have to be diluted to the suitable concentration range. Table 1 gives the results of the measurements. The relative standard deviation of the method is between 0.5 and 2.0%. For all samples the determined salicylic acid concentration was higher than stated. Influences on the salicylic acid signal by other components of the sample could be excluded because there was no response from samples passing through the inactive reactor and the recoveries were less than 100%.

The authors thank the Hochschuljubiläumsstiftung der Stadt Wien for supporting this project.

REFERENCES

1 E. Lück, Chemische Lebensmittelkonservierung, Springer, Berlin, 1977, p. 186.
2 E.S. Kang, T.A. Todd, M.T. Capaci, K. Schwenzer and J.T. Jabbour, Clin. Chem., 29 (1983) 1012.
3 K. Alan and M.D. Done, Pediatrics, 26 (1960) 800.
4 P. Trinder, Biochem. J., 57 (1954) 301.
5 U. Saha and K. Baksi, Analyst, 110 (1985) 739.
6 A.M. de la Pena, F. Salinas and I.D. Meràs, Anal. Chem., 60 (1988) 2493.
7 G. Graham and M. Rowland, J. Pharm. Sci., 61 (1972) 1219.
8 M. Kleinerman, Anal. Lett., 10 (1977) 205.
9 S.K. Bakar and S. Niazi, J. Pharm. Sci., 72 (1983) 1020.
10 U. Reidl, J. Chromatogr., 272 (1983) 325.
11 I.M. Jalal and S.I. Sa'sa', Talanta, 31 (1984) 1015.
12 W.D. Mason and R. Gillilan, Anal. Lett., 16 (1983) 903.

13 M. Carlson and R.D. Thompson, J. Liq. Chrom., 10 (1987) 997.
14 C.P. Terweij-Groen and J.C. Kraak, J. Chromatogr., 138 (1977) 245.
15 S.L. Ali, J. Chromatogr., 126 (1976) 651.
16 J.R. Watson, P. Crescuolo and F. Matsui, J. Pharm. Sci., 60 (1971) 454.
17 E.R. Blakley, Anal. Biochem., 15 (1966) 350.
18 M. Rowland and S. Riegelman, J. Pharm. Sci., 56 (1967) 717.
19 L.J. Walter, D.F. Biggs and R.T. Coutts, J. Pharm. Sci., 63 (1974) 1754.
20 K.K. Choi and K.W. Fung, Anal. Chim. Acta, 138 (1982) 385.
21 N.A. Chaniotakis, S.B. Park and M.E. Meyerhoff, Anal. Chem., 61 (1989) 566.
22 H. James, G. Carmack and H. Freiser, Anal. Chem., 44 (1972) 856.
23 S.M. Hassan and M.A. Hamada, Analyst, 113 (1988) 1709.
24 D. Midgley, Anal. Chim. Acta, 182 (1986) 91.
25 Q. Chang and M.E. Meyerhoff, Anal. Chim. Acta, 186 (1986) 81.
26 C.L. Keegan, F. Ungemach, J. Simpson and M. Aden, Clin. Chem., 31 (1985) 942.
27 L. Hendeles and C. Edwards, J. Clin. Pharm. Ther., 13 (1988) 131.
28 S. Takemori, H. Yasuda, K. Suzuki and M. Katagiri, Biochim. Biophys. Acta, 191 (1969) 58.
29 R.H. White-Stevens and H. Kamin, J. Biol. Chem., 247 (1972) 2358.
30 H. Kamin, R.H. White-Stevens and R.P. Presswood, Methods Enzymol., 53 (1978) 527.
31 K.S. You and J.A. Bittikofer, Clin. Chem., 30 (1984) 1549.
32 R.W. Longenecker, J.E. Trafton and R.B. Edwards, Clin. Chem., 30 (1984) 1369.
33 K.S. You, Clin. Chim. Acta, 149 (1985) 281.
34 M.A.N. Rahni, G.G. Guilbault and G.N. de Oliveira, Anal. Chim. Acta, 181 (1986) 219.
35 T. Fonong and G.A. Rechnitz, Anal. Chim. Acta, 158 (1984) 357.
36 S.A.P. Chubb, R.S. Campbell, J.R. Ramsay, P.M. Hammond, T. Atkinson and C.P. Price, Clin. Chim. Acta, 155 (1986) 209.
37 J.E. Frew, S.W. Bayliff, P.N.B. Gibbs and M.J. Green, Anal. Chim. Acta, 224 (1989) 39.
38 O. Friedrich, Dissertation, University of Vienna, 1991.
39 E. Mann-Buxbaum, Dissertation, University of Vienna, 1990.
40 E. Mann-Buxbaum, F. Pittner and T. Schalkhammer, Sensors Actuators, B1 (1990) 518.
41 M. Neumayr, Thesis, University of Vienna, 1991.

Analytica Chimica Acta, 273 (1993) 477–483
Elsevier Science Publishers B.V., Amsterdam

Simplex method for the computation of analytical parameters of potentiometric sensors

Robert Koncki, Stanisław Głab and Adam Hulanicki

Department of Chemistry, Warsaw University, Pasteura 1, 02-093 Warsaw (Poland)

(Received 7th July 1992; revised manuscript received 10th September 1992)

Abstract

The simplex method is proposed for obtaining calibration parameters for potentiometric sensors. As examples an ion-selective electrode, an enzyme substrate electrode, a tissue electrode and a pH–enzyme electrode were chosen. The effectiveness of the method was checked on real experimental data of the different sensors. This procedure shows good convergence and precision. It is especially recommended when the classical least-squares method cannot be used because of non-linearity and non-explicity of theoretical functions.

Keywords: Ion selective electrodes; Potentiometry; Sensors; Calibration; Enzyme electrodes; Simplex optimization

Analytical methods can be divided into two groups: absolute and relative [1]. In both instances the analytical signal (R_A), which is measured in the experiment, is a function of the search for analyte concentration (C_A). The exact values of the parameters in this function may be either known, as in absolute methods (such as gravimetry or coulometry), or unknown, as in relative methods. In the latter instance one has to use calibration to obtain the parameter values before the analysis can be performed. If R_A is a linear function of C_A (e.g., Lambert–Beer law in optical methods, analytical response functions in voltammetry and conductimetry), the classical least-squares method (LSM) can be used for this purpose. Sometimes, however, R_A is a non-linear or non-explicit function of C_A and application of the LSM is more difficult or even impossible. This applies in potentiometry with ion-selective electrodes (ISEs), enzyme substrate electrodes (ESEs) or pH–enzyme electrodes (HEEs). Linear and non-linear regression [2] and optimization techniques [3] have been used only for ISEs. In this paper, a simplex method is proposed for obtaining parameters of all these potentiometric sensors.

Correspondence to: A. Hulanicki, Department of Chemistry, Warsaw University, Pasteura 1, 02-093 Warsaw (Poland).

METHOD OF FITTING

For both ISEs and ESEs the analytical signal is an explicit function of the analyte concentration:

$$R_A = f(C_A, \text{parameters}) \quad (1)$$

For ISEs it has the form of the Eisenmann–Nikolsky equation [4,5]:

$$E_i = E^0 + S \log\left([I]_i + \sum_{J=1}^{n_J} K_J [J]_i + L_d\right) \quad (2)$$

where E^0, S, K_J and L_d are standard potential, slope, selectivity coefficient for the Jth interferent and detection limit, respectively. In many instances with ISEs, the difference between the potentials in the presence and absence of the analyte [$\Delta E = E(C_A) - E(0)$] is taken as the ana-

lytical signal instead of the direct potential $[E(C_A)]$ corresponding to the analyte concentration. Equation 2 then changes to

$$\Delta E_i = S \log\left(\frac{L'_d + [I]_i}{L'_d}\right) \quad (3)$$

where L'_d is a modified detection limit that includes all interference effects, as in the standard multiple addition method the concentrations of the interferents (and their influences) are constant.

For an ESE the explicit function according to Eqn. 1 was obtained by coupling the Eisenmann–Nikolsky equation (Eqn. 2) with the final equation of Morf's model [6]:

$$E_i = E^0 + S \log\left([P_{enz}]_i + [P_{bulk}]_i + \sum_{J=1}^{n_J} K_J[J]_i + L_d\right) \quad (4)$$

where

$$[P_{enz}]_i = \tfrac{1}{2}\left(C_{A_i} + K_V + K_M - \sqrt{(C_{A_i} - K_V - K_M)^2 + 4K_M C_{A_i}}\right) \quad (5)$$

In Eqns. 4 and 5, some kinetic parameters describing the rate of the enzymatic reaction appear: K_M, the Michaelis–Menten constant; K_V the normalized maximum rate constant of enzymatic reaction; and $[P_{enz}]$ and $[P_{bulk}]$, the concentrations of the product of the enzymatic conversion of the substrate and the product concentration being present in the bulk solution, respectively. $[P_{enz}]$ determines the electrode potential that corresponds to the concentration of the substrate (C_A) of the enzymatic reaction in solution (Eqn. 5).

Similarly as for an ISE (Eqn. 3), an equation for the differential measurement can be obtained:

$$\Delta E_i = S \log\left\{\left[L'_d + \tfrac{1}{2}\left(C_{A_i} + K_M + K_V - \sqrt{(C_{A_i} - K_M - K_V)^2 + 4K_M C_{A_i}}\right)\right]/L'_d\right\} \quad (6)$$

For an HEE the analytical signal is a non-explicit function of the analyte concentration:

$$f(R_A, C_A, \text{parameters}) = f(H, C_S, \text{parameters}) = 0 \quad (7)$$

The response function in Eqn. 7, obtained on the basis of a kinetic model [7] of HEE, has the form

$$\left([H]^B - [H]\right)\left[1 + \frac{K_{aW}C_W}{(K_{aW} + [H]^B)(K_{aW} + [H])}\right] + \frac{1}{2}\left(\frac{n_A K_{aA}}{[H] + K_{aA}} - \frac{n_B[H]}{[H] + K_{aB}}\right) \times \left[C_{S_i} + K_M + K_V - \sqrt{(C_{S_i} - K_M - K_V)^2 + 4K_M C_{S_i}}\right] = 0 \quad (8)$$

where n_A and n_B are stoichiometric coefficients of the enzymatic reaction, K_{aA}, K_{aB} and K_{aW} are dissociation constants of the acidic and basic products of the enzymatic reaction and of the buffer, respectively, and $[H]^B$ and C_W correspond to the pH value and concentration of the buffer in the bulk solution, respectively.

To obtain the best fit, the minimization condition for all cases studied has to be defined:

$$R_S = \sum_{i=1}^{n}\left[R_{A_i} - R_A(C_{A_i}, \text{parameters})\right]^2 = \min \quad (9)$$

This condition is identical with the condition in LSM. The latter method, however, requires analytical forms of the minimization condition derivatives for all searched parameters:

$$\frac{\partial R_S}{\partial \text{parameter}_k} = 0 \quad k = 1 \ldots n \text{ parameters} \quad (10)$$

and the solution of the obtained set of equations. Minimization conditions 9 obtained from the analytical function for the ISE (Eqns. 2 and 3), ESE (Eqns. 4–6) and HEE (Eqn. 8) cannot be differentiated. This problem was by-passed using a simplex method [3,8]. The minimization condition (Eqn. 9) was taken as the response function (R_S) described in $(n + 1)$-dimensional response space,

for n parameters, for which minimization is carried out.

The following response functions R_S (Eqn. 9) are suggested for the cases studied:

for ISE (Eqn. 2):

$$R_S = \sum_{i=1}^{n} \left\{ E_i - E^0 - S \log\left([I]_i + \sum_{J=1}^{n_J} 10^{-K_J}[J]_i + 10^{-L_d} \right) \right\}^2 \quad (11)$$

for differential potentiometry with ISE (Eqn. 3):

$$R_S = \sum_{i=1}^{n} \left\{ \Delta E_i - S \log\left(\frac{10^{-L_{d'}} + [I]_i}{10^{-L_{d'}}} \right) \right\}^2 \quad (12)$$

for ESE (Eqns. 4 and 5):

$$R_S = \sum_{i=1}^{n} \left\{ E_i - E^0 - S \log\left\{ \sum_{J=1}^{n_J} 10^{-K_J}[J]_i + 10^{-L_d} + [P_{bulk}]_i + \tfrac{1}{2}\left[C_{A_i} + 10^{-K_M} + 10^{-K_V} - \left(\left(C_{A_i} - 10^{-K_M} - 10^{-K_V} \right)^2 + 4 \times 10^{-K_M} C_{A_i} \right)^{1/2} \right] \right\} \right\}^2 \quad (13)$$

for differential potentiometry with ESE (Eqn. 6):

$$R_S = \sum_{i=1}^{n} \left\{ \Delta E_i - S \log\left(10^{-L'_d} + \tfrac{1}{2}\left[C_{A_i} + 10^{-K_M} + 10^{-K_V} - \left(\left(C_{A_i} - 10^{-K_M} - 10^{-K_V} \right)^2 + 4 \times 10^{-K_M} C_{A_i} \right)^{1/2} \right] \right) / 10^{-L'_d} \right\} \quad (14)$$

Eqns. 11–14 are slightly modified compared with Eqn. 9 for the analytical response of ISE (Eqns. 2 and 3) and ESE (Eqns. 4–6). The proposed modification is based on the introduction of the exponential form for some parameters (e.g., 10^{-L_d} instead of L_d, 10^{-K_V} instead of K_V) and it corresponds to the change in the scale of these parameter axes in the response space from linear to logarithmic. There are two reasons for such modifications. They increase the efficiency of the iteration process as the basic parameters can vary over many orders of magnitude (for real systems K_J and L_d can take values from 10^2 to 10^{-20} and K_M and K_V from 10 to 10^{-7}). The second reason is to prevent movements of the simplex into areas of the response space which do not have any physical meaning (e.g., negative values of these parameters). This modification also protects the numerical process from "illegal" calculations (e.g., logarithm of negative values). This modification complicates only the form of equations, and does not give any problem in the realization of simplex procedure. Such additional non-linearities make the use of LSM impossible.

The HEE case requires additional modifications (in addition to changes in the parameter scale). Because of the non-explicitness of Eqn. 7 it is impossible to define Eqn. 9 directly. Moreover, because pH rather than concentration of hydrogen ions [H] is the analytical response of these sensors, Eqn. 9 should be given in the following form:

$$R_S = \sum_{i=1}^{n} \left[pH_i - pH(C_{A_i}, \text{parameters}) \right]^2 = \sum_{i=1}^{n} \left[\log \frac{[H](C_{A_i}, \text{parameters})}{[H]_i} \right]^2 \quad (15)$$

Calculations of $[H](C_A, \text{parameters})$ in Eqn. 15 for a given set of parameters is equivalent with zeroing the function in Eqn. 8. For this purpose, a modified bisection procedure is an effective method [9]. The scale of some axes in the simplex response space is changed, as for the ISE or ESE. Complicated forms of Eqns. 8 and 15 and their further modifications [10] do not cause any prob-

lems if solved by the simplex method. The use of LSM for such complicated cases is impossible.

It is worth noting that the value of the response function R_S (Eqns. 9 and 11–15) quantitatively defines the fitting quality, as it is the sum of square deviations. It is then recommended to define the standard deviation of the fitting as

$$\text{S.D.} = \sqrt{R_S/n} \quad (16)$$

The so-defined standard deviation is given in mV as units for ISE (Eqns. 11 and 12) and ESE (Eqns. 13 and 14), or in pH units for HEE (Eqn. 15).

CALCULATIONS FOR REAL SYSTEMS

ISE

As an example for ISE, the calibration data for a chloride electrode were chosen (Fig. 1). Fitting was performed for the normal (Eqns. 2 and 11) and differential (Eqns. 3 and 12) modes of potentiometry. In the differential mode (two estimated parameters) values of $S = -58.073$ mV per decade, log $L_d = -5.513$ and S.D. = 0.638 mV were obtained. In the normal mode (three estimated parameters) values of $E^0 = -359.3$ mV, $S = -58.081$, log $L_d = -5.512$ and S.D. = 0.637 mV were obtained.

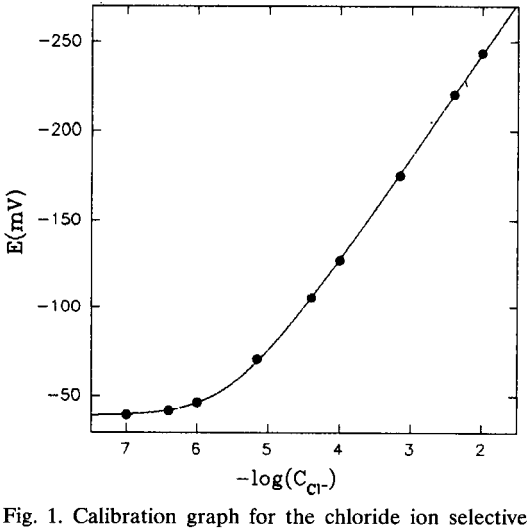

Fig. 1. Calibration graph for the chloride ion selective electrode. Points = experimental data; line = fitted curve.

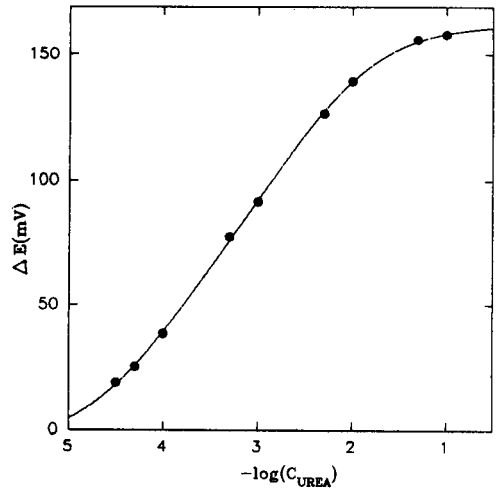

Fig. 2. Calibration graph for the enzyme substrate electrode for urea. Points = experimental data; line = fitted curve.

ESE

As an example for ESE, the calibration data for an ammonium ion-selective electrode enzymatically sensitized for urea [11] (Fig. 2) were used. The results are given in Table 1. First, fitting was done for two parameters, K_M and K_V, with the assumption that the other parameters of the ISE used are known. These results are given in the first row of Table 1. The response

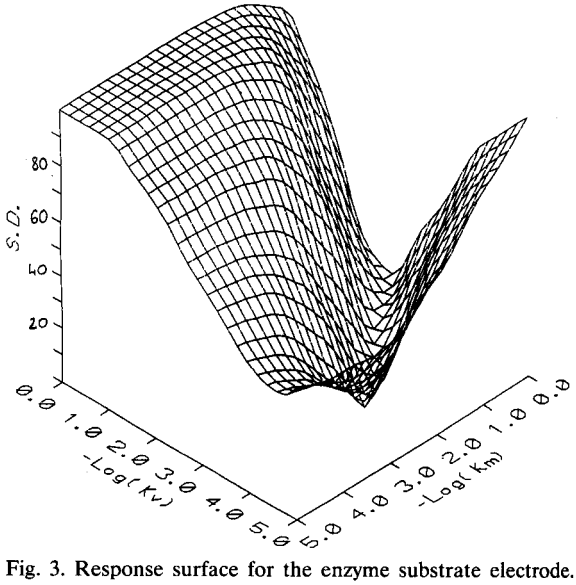

Fig. 3. Response surface for the enzyme substrate electrode.

TABLE 1

Estimated analytical parameters of an enzyme substrate electrode for urea (Estimated parameters are underlined.)

No.	No. estimated parameter	E^0 (mV)	S (mV)	$-\log L_d$	$-\log K_V$	$-\log K_M$	S.D. (mV)
1	2	–	59.15	6.00	3.47	1.85	0.823
2	3	–	59.15	7.46	4.93	1.84	0.815
3	3	–	58.53	6.00	3.44	1.83	0.801
4	4	–	58.62	6.79	4.24	1.83	0.799
5	5	392.4	58.63	6.78	4.23	1.83	0.798

surface dependence of the standard deviation on these two parameters for which minimization was done is shown in Fig. 3. The movements of the simplex on this response surface towards a minimum are shown in Fig. 4. Results for a greater number of parameters (rows 2–5 in Table 1) cannot be illustrated graphically as the response spaces are four or more dimensional. All fittings, except the last one, were done on the basis of Eqns. 6 and 14 (differential potentiometry mode). The results in the last row in Table 1, where minimization was done for all parameters, were obtained by minimization of Eqn. 13 (normal potentiometry mode, Eqns. 4 and 5).

Equations for ESE (Eqns. 4–6) can also be used for tissue-sensitized potentiometric sensors. As an example, fittings to calibration data for carbon dioxide and ammonia electrodes tissue sensitized for urea (soja beans) [12] are shown in Fig. 5. In both instances equations for differential potentiometry (Eqns. 6 and 14) were used to obtain parameter values. $K_M = 3.34$ mmol, $K_V = 3.98 \times 10^{-3}$, $S = 84.73$ mV per decade, log $L_d = -3.77$ and S.D. = 1.362 mV were obtained for the biosensor based on ISE(NH_3) (curve A, Fig. 5), and $K_M = 4.75 \times 10^{-2}$ mmol, $K_V = 9.91 \times 10^{-3}$, $S = 69.20$ mV per decade, log $L_d = -3.28$ and S.D. = 1.043 mV for the biosensor based on ISE(CO_2) (curve B, Fig. 5). The slope is super-Nernstian, as was reported in the paper [12] from which the experimental data were taken. It can be only supposed that this is connected with insufficient buffering capacity of the solution between the pH-sensing membrane and the enzyme layer.

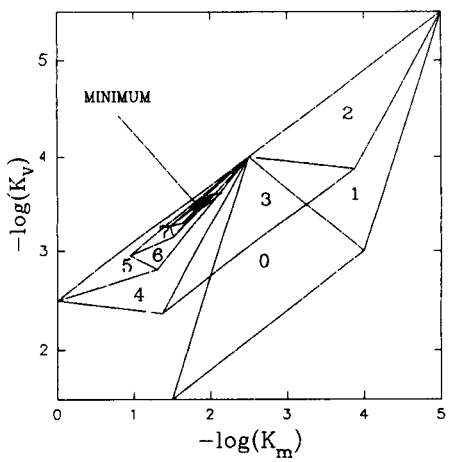

Fig. 4. Movement of the simplex on the response surface (for the case of an enzyme substrate electrode) towards minimum.

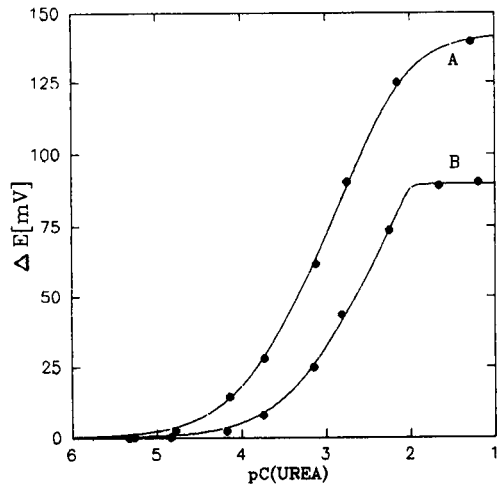

Fig. 5. Calibrations graphs for tissue electrodes for urea. Points = experimental data; lines = fitted curves. (A) NH_3 gas tissue-sensitized electrode for urea; (B) CO_2 gas tissue-sensitized electrode for urea.

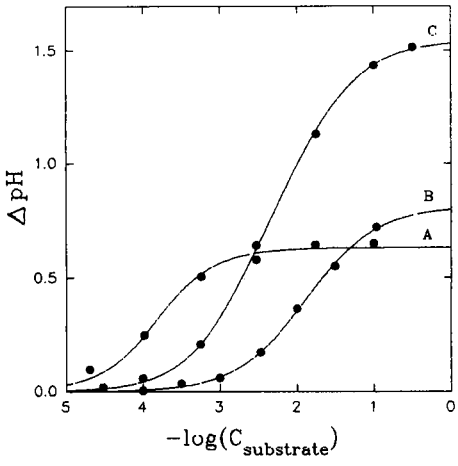

Fig. 6. Calibrations for pH–enzyme electrodes. Points = experimental data; lines = fitted curves. A = acetylcholine; B = glucose; C = urea.

HEE

As examples for HEE, the calibration data for glass pH electrodes sensitized enzymatically [13] for acetylcholine [9], glucose [9] and urea [10] were chosen (Fig. 6). An acetylcholine sensor was calibrated in 0.001 mol l^{-1} Tris buffer (pK_a = 8.08) of pH 7.00, a glucose sensor was calibrated in 0.001 mol l^{-1} phosphate buffer (pK_a = 7.20) of pH 7.00 and a urea electrode was calibrated in 0.005 mol l^{-1} phosphate buffer of pH 6.00. Calculations were done based on Eqn. 8 with the following values of the constants: acetylcholine, pK_{a_A} = 4.73 (acetic acid), n_A = 1, n_B = 0; glucose, pK_{a_A} = 3.77 (gluconic acid), n_A = 1, n_B = 0; and urea, pK_{a_A} = 6.40 (carbonic acid), pK_{a_B} = 9.25 (ammonium ion), n_A = 1, n_B = 2. Calibration data and theoretical curves obtained from Eqn. 8 (by minimization of Eqn. 15) are shown in Fig. 6.

TABLE 2

Estimated analytical parameters of the pH–enzyme electrodes for acetylcholine, glucose and urea

Analyte	K_V	K_M (mol l^{-1})	S.D. (pH)	S.D. (mV)
Acetyl-choline	5.95×10^{-5}	5.97×10^{-5}	0.023	1.36
Glucose	2.94×10^{-4}	7.41×10^{-3}	0.009	0.53
Urea-1	3.05×10^{-3}	1.12×10^{-2}	0.012	0.71
Urea-2	3.83×10^{-3}	1.09×10^{-2}	0.011	0.65

Minimization was done for the parameters K_M and K_V listed in Table 2. The results for urea-2, in contrast to those for urea-1 (see Table 2), take into account the pH dependence of the kinetic parameters of the enzymatic reaction [10].

DISCUSSION

Calibration of the chloride ISE (Fig. 1) shows the usefulness of the application of the simplex method for calculating analytical parameters of such sensors. The standard deviations of the results obtained are similar to those usually encountered for measurements with ISEs. The procedure employing the logarithmic axis for some parameters ($L_{d_1}K_J$) enables parameter values to be obtained after just a few tens of iteration cycles. The simplex method permits the calculation of the analytical parameters of an ISE from the data for several different calibrations (e.g., series of calibrations with different concentrations of different interferents) or data from titration of the main ion with titrant containing an interferent [5], e.g., calculation of the selectivity coefficient of a pH sensor for Na^+ and K^+ ions from data of the titration of HCl with NaOH or KOH, respectively. In the latter instance the most common, graphical method for the evaluation of selectivity coefficients [5] cannot be used. Linear and non-linear regression methods for ISEs also cause problems, especially for data for several different calibrations.

For enzymatic sensors (ESEs and HEEs) regression methods are useful because of the non-linearity and non-explicity (HEE) of the analytical response (R_A) equations.

These problems can be avoided by using non-linear optimization techniques, such as direct search and gradient methods. For ISEs the two direct methods (namely the simplex method and the Hooke and Jeeves method) and the Davidon–Fletcher–Powell gradient search method were examined [3]. The simplex method is 3–4 times quicker (more convergent) than the Hooke and Jeeves method. This gradient method is quicker than the simplex method, but it has the disadvantage of all gradient methods that it re-

quires differentiation of the analytical response functions. This makes its use difficult for ESEs and impossible for HEEs. The noise is another problem with the gradient method. When the signal-to-noise ratio is low, direct search methods can converge more rapidly than the gradient methods [3]. For these reasons the simplex method for calculating parameters for all the sensors described here was used.

For biologically modified potentiometric sensors the chosen method was especially effective. The procedure employing a logarithmic axis for some parameters in the response space increases the efficiency of the iteration process and prevents simplex movement into the areas of the response space which do not have any physical meaning. The response function for ESEs and HEEs have a complicated form, but nevertheless less than 100 iterations are sufficient for fitting two parameters (and less than 1000 iterations are necessary for the estimation of five parameters). The convergence of the simplex method is illustrated for ESEs in Figs. 3 and 4 (tissue sensors and HEEs gave similar results). In all instances very good quality of fitting was obtained (S.D. values in Tables 1 and 2). As shown in Table 1, fitting of a greater number of parameters does not cause an increase in the error. All parameter fittings described in this report required less than 1000 iterations.

Further modifications of the model equations for ESEs and HEEs (e.g., taking into account the pH effects of the kinetics of the enzymatic reaction, Table 2) do not cause any problems. For the example mentioned, modifications did not change the efficiency of the method, but they increased the quality of fitting. The modifications were done according to the Waley's model [7,10]. Non-explicity of the HEE equations (Eqns. 8 and 15) also do not cause any problems. In contrast to the gradient methods, the simplex method can employ procedures for solving non-explicit equations, e.g., the bisection method [9]. For ESEs and HEEs, just as for ISEs, the simplex method can be used for the simultaneous processing of data from several independent calibrations [9,10].

This work was supported by the Committee of Scientific Research (Grant BST 412/3/92).

REFERENCES

1 A. Hulanicki, Anal. Proc., in press.
2 P. Zhao and D. Qi, Anal. Chim. Acta, 258 (1992) 27.
3 R.J. Forster and D. Diamond, Anal. Proc., 28 (1991) 117.
4 B.P. Nikolsky, Zh. Fiz. Khim., 10 (1937) 495.
5 G.G. Guilbault, R.A. Durst, M.S. Frant, H. Freiser, E.H. Hansen, T.S. Light, E. Pungor, G. Rechnitz, N.M. Rice, T.J. Rohm, W. Simon and J.D.R. Thomas, Pure Appl. Chem., 48 (1976) 127.
6 W.E. Morf, Mikrochim. Acta, 2 (1980) 317.
7 S. Głab, R. Koncki and A. Hulanicki, Electroanalysis, 3 (1991) 361.
8 S.N. Deming and R.L. Parker, CRC Crit. Rev. Anal. Chem., 7 (1978) 187.
9 S. Głab, R. Koncki and I. Holona, Analyst, in press.
10 S. Głab, R. Koncki and A. Hulanicki, Analyst, in press.
11 G.G. Guilbault and J.G. Montalvo, J. Am. Chem. Soc., 92 (1970) 2533.
12 J. Deng, Y. Fang and R. Cai, Electroanalysis, 3 (1991) 767.
13 R. Koncki, P. Leszczyński, A. Hulanicki and S. Głab, Anal. Chim. Acta, 257 (1992) 67.

Analytica Chimica Acta, 273 (1993) 485–492
Elsevier Science Publishers B.V., Amsterdam

Metal chelates as membrane active components in liquid-state ion-selective electrodes. Factors affecting the electrode properties and stability

Krzysztof Ren

Department of Instrumental Analysis, Faculty of Chemistry, Adam Mickiewicz University, 60 780 Poznań (Poland)

(Received 1st June 1992; revised manuscript received 6th October 1992)

Abstract

The applicability of solvents in liquid-membrane ion-selective electrodes using chelate metal complex increases with increase in their dielectric constant. It was found that the properties of the electrodes are considerably affected by impurities present in the solvent and in the electroactive compound. The reason for the limited stability of ion-selective electrodes with liquid membranes is penetration of water into the membrane and its adsorption on the surface of capillary walls. The stability of electrodes may be improved by counteracting water adsorption by hydrophobization of the pore surface of the porous membrane carrier.

Keywords: Ion-selective electrodes; Liquid-membrane electrodes; Membrane electrodes; Metal chelates

Ion-selective electrodes with liquid membranes are well known from both the analytical and construction points of view. In spite of their simple structure, it is not so easy to develop new ion-selective electrodes. The difficulty lies in the selection of membrane components so that the analytical parameters such as sensitivity, selectivity and detection limits are satisfactory and remain stable over a long period of time. Usually, from the point of membrane formation, a continuous decrease in the slope of the calibration graph is observed, accompanied by an increasing time of potential stabilization. Owing to these unfavourable effects, the electrode cannot be used for analytical purposes after a certain time.

The objective of this work was to investigate some of the factors affecting the above parameters and thus the stability of ion-selective electrodes with liquid membranes, and to determine the conditions which, when fulfilled, will permit the construction of an electrode with the most satisfactory values of the parameters. The studies were performed with ten different [1–7] liquid-membrane electrodes sensitive to metal cations, in which the following metal cations were used as electroactive compounds:

Ligands:	Cations:
$(C_{10}H_{21}O)\ P(S)S^-$	Tl^+, Pb^{2+}, Cd^{2+}, Ni^{2+}, Cu^{2+}
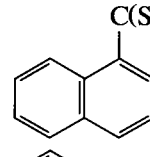	Pb^{2+}, Cd^{2+}
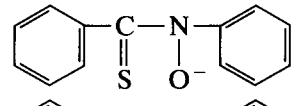	Cu^{2+}
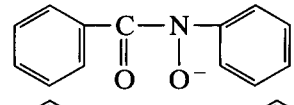	Cu^{2+}
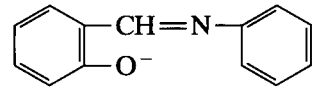	Cu^{2+}

Correspondence to: K. Ren, Department of Instrumental Analysis, Faculty of Chemistry, Adam Mickiewicz University, 60 780 Poznań (Poland).

EXPERIMENTAL

Preparation of the ion exchange membrane

For all the electrodes studied the membrane phase consisted of a 0.01 M solution of metal complexes in the organic solvent. Solutions of the complexes were obtained by extraction with a ligand solution of cations of a corresponding metal from a 0.1 M aqueous solution of its nitrate.

The organic phase containing the complex solution was washed with water and then centrifuged to achieve a good phase separation.

Construction of the electrode

A previously described [8] PTFE body is used for making the electrode. The construction is similar to that of an Orion liquid-state ion-selective electrode. The internal solution of the electrode, including the reference electrode (Ag/AgCl) immersed in it, is separated from the test solution by a porous membrane saturated with the liquid ion exchanger. A 0.01 M solution of a corresponding metal chloride in 0.1 M KCl (saturated with AgCl) was used as the internal solution. The porous membrane was made of cellulose nitrate (Sartorius type SM 11306 and 13306, pore size 0.45 μm, thickness 0.13 mm). To make the porous membranes hydrophobic, the SM 11306 membrane was heated at 80°C for 5 h in a 10% solution of hexamethyldisilazane and then washed with benzene and dried. The measurement cell is of the form shown in Scheme 1.

RESULTS AND DISCUSSION

Effect of the type of organic solvent used in the membrane on the properties of ion-selective electrodes

Four organic compounds to be used as solvents in membranes were selected, differing in dielectric constant, dipole moment and solubility in water. The solvents and their properties are given in Table 1.

TABLE 1

Properties of organic solvents applied in the electrodes studied

Solvent	Dipole moment (D)	Dielectric constant	Solubility in water (%)
o-Xylene	0.62	2.35	0.0076
Chlorobenzene	1.69	5.6	0.05
Chlorocyclohexane	2.3	7.06	0.07
1,1′,2,2′-Tetrachloroethane	1.36	8.08	0.13

For the ten metal complexes studied, electrodes were made in which their solutions in the above-mentioned solvents were applied as membranes. The course of the calibration graph (slope and linear range) was assumed to be the applicability criterion of the solvent. Calibration graphs for some electrodes are shown in Fig. 1, and show that solvents of high dielectric constants are more useful. A high dielectric constant favours better dissociation of the complex in the organic phase, and is responsible for a higher concentration of metal cations which take part in transporting charges through a membrane. A higher concentration of ions in the membrane, and thus also at and near the membrane–aqueous solution phase boundary, favours the rapid establishment of the potential (exchange current increases), as a result of which the electrode becomes less polarizable.

Effect of solvent purity on the properties of ion-selective electrodes

The previous experiment showed that there is a clear relationship between the course of the calibration graph and the dielectric constant of the solvent. This implies that in the applied mem-

Ag/AgCl	0.1 M KCl 0.01 M MCl_2	Membrane 0.01 M ML_2 complex in organic solvent	Test solution	1 M KNO_3	1 M KCl	Ag/AgCl

Scheme 1.

brane solutions the concentration of charge carriers is small. Therefore, it is reasonable to suppose that all foreign substances which may be present in the membrane as impurities and which show the ability to dissociate into ions or to form ion pairs, may modify the properties of the electrode and thus affect its potential. To check the influence of the purity level of the solvent used in the membrane on the properties of the electrode, an experiment with solvents of different purity

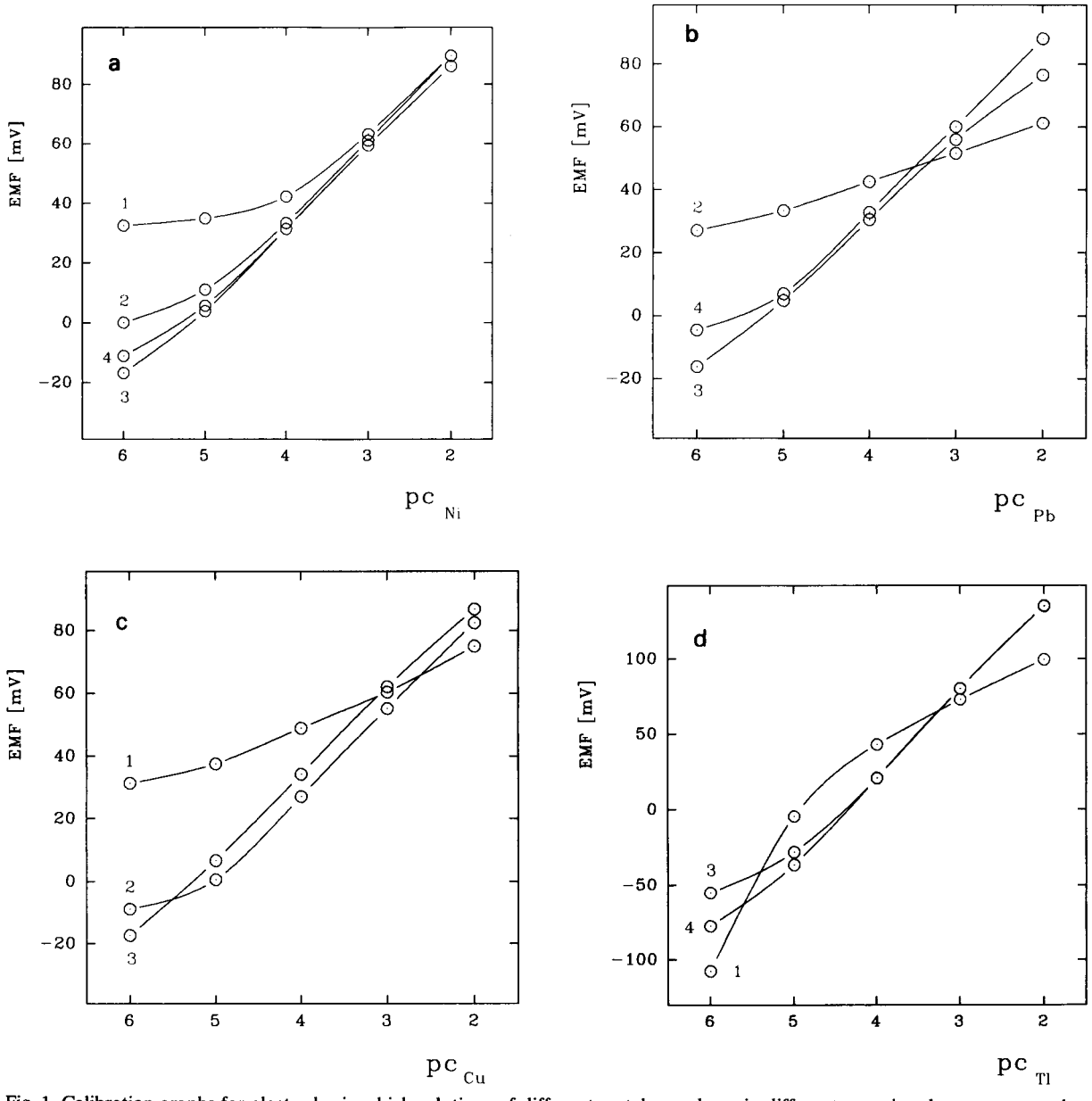

Fig. 1. Calibration graphs for electrodes in which solutions of different metal complexes in different organic solvents were used as membranes. Solvents: 1 = xylene; 2 = chlorobenzene; 3 = tetrachoroethane; 4 = chlorocyclohexane. Metal complexes: (a) Ni(II) didecyldithiophosphate; (b) Pb(II) naphthyldithiocarboxylate; (c) Cu(II) benzoylphenylhydroxylamine; (d) Tl(I) didecyldithiophosphate.

was performed, using the previously mentioned electrodes. The criterion of electrode applicability was assumed to be the course of the calibration graphs.

Figure 2 shows examples of calibration graphs for electrodes in which solvents of a different level of purity were applied. The results of the experiments indicate the necessity for thorough

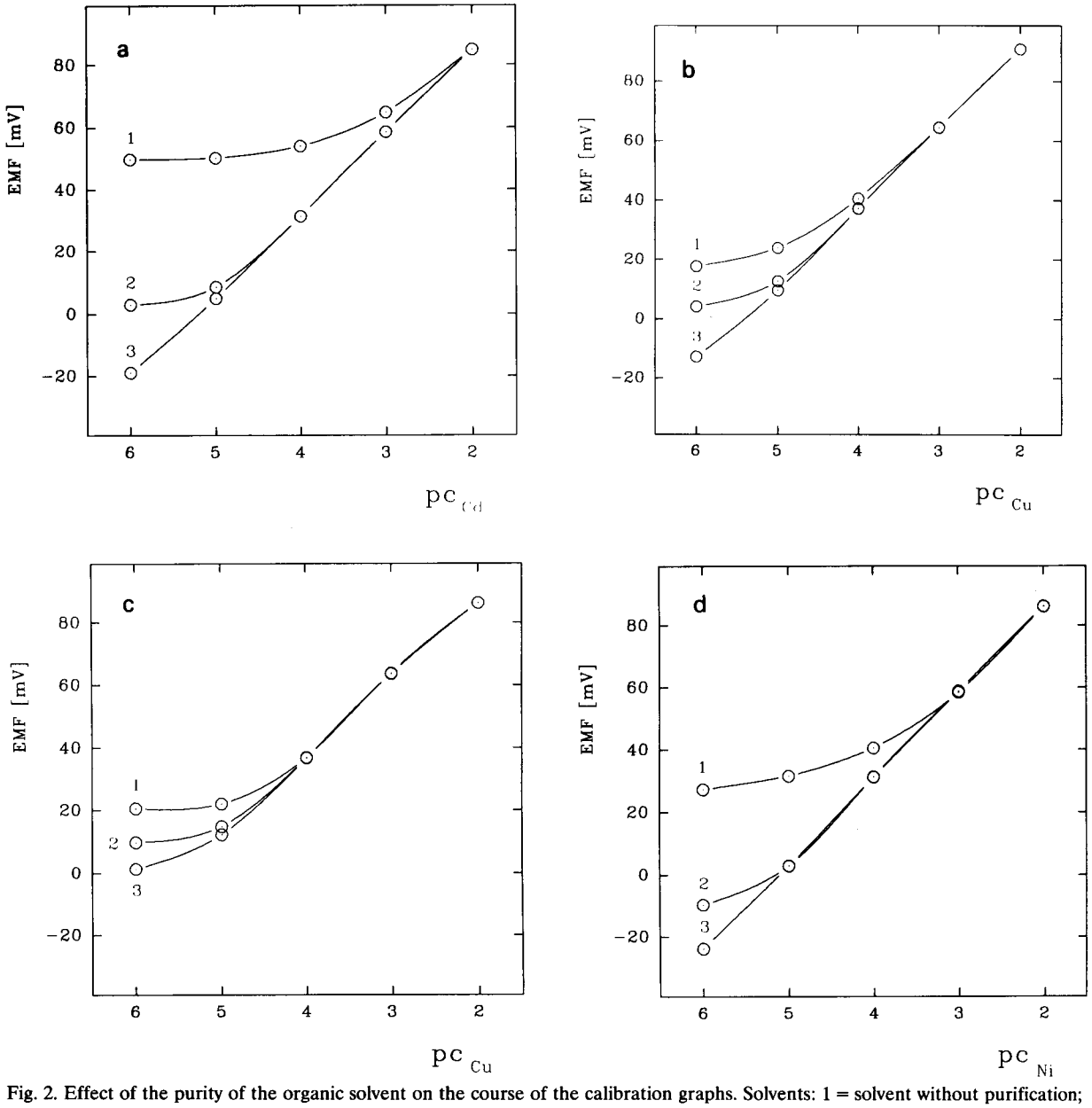

Fig. 2. Effect of the purity of the organic solvent on the course of the calibration graphs. Solvents: 1 = solvent without purification; 2 = solvent distilled at 760 mmHg; 3 = solvent distilled at 760 mmHg and distilled at 20 mmHg. Membranes: (a) Cd(II) naphthyldithiocarboxylate in tetrachloroethane (purum, Fluka); (b) Cu(II) thiobenzoylphenylhydroxylamine in tetrachloroethane (purum, Fluka); (c) Cu(II) thiobenzoylphenylhydroxylamine in chlorobenzene (zur Synthese, Merck); (d) Ni(II) didecyldithiophosphate in tetrachloroethane (purum, Fluka).

purification of the solvents. The influence of impurities is particularly evident with tetrachloroethane, which is the least stable of the solvents applied.

Influence of the purity of the electroactive compound on the properties of ion-selective electrodes

The effect of impurities present in the ligands that are introduced into the membrane on the electrode properties is similar to that of the solvent impurities. Figure 3 shows calibration graphs for electrodes in which electroactive substances of different purity levels were applied. The detection range of the electrodes was clearly dependent on the purity of the electroactive compound.

Sulphur-containing ligands were applied in the electrodes. Under the influence of different factors during synthesis or in the period following it, these ligands may undergo oxidation according to the scheme

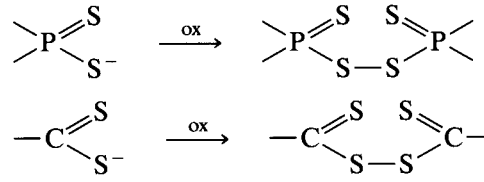

Changes in the courses of the calibration graphs may also be due to competitive reactions of complex formation. An example is the behaviour of the electrodes in which dithiophosphate (DTP) complexes in solutions containing Cu(II) cations are used. The oxidation reaction of DTP to give disulphate at the expense of Cu(II) reduction to Cu(I) [9] may be accompanied by the following reaction [10]:

$$Cu(DTP)_2 + CuX_2 \rightleftharpoons 2CuX(DTP)$$

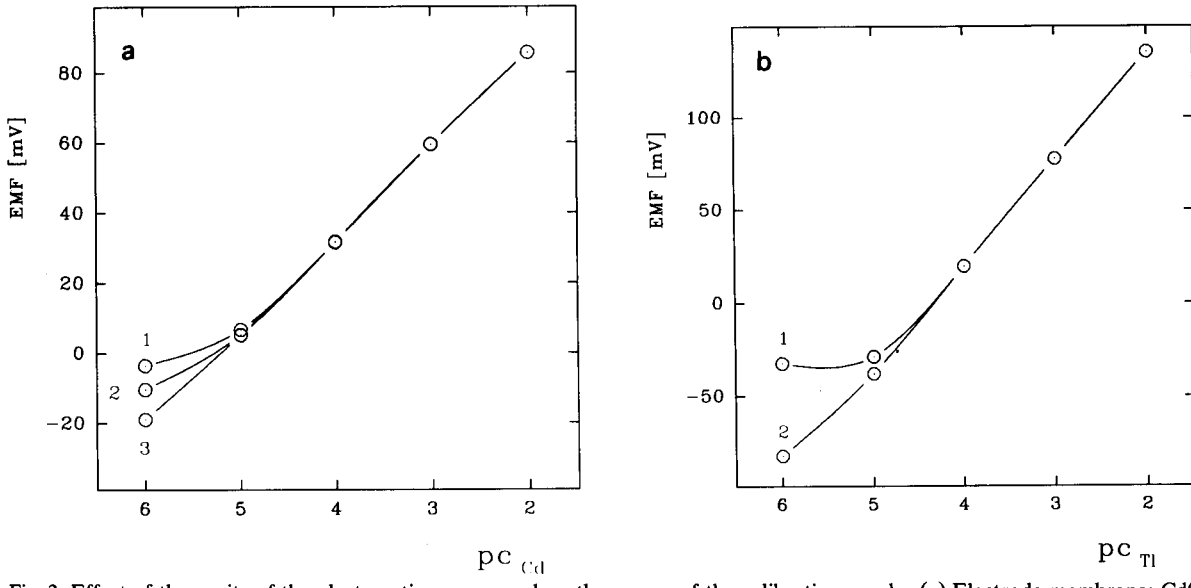

Fig. 3. Effect of the purity of the electroactive compound on the course of the calibration graphs. (a) Electrode membrane: Cd(II) naphthyldithiocarboxylate in tetrachlorethane. Purity of complex: 1 = tetraethylammonium naphthyldithiocarboxylate crystallized once from ethanol; 2 = tetraethylammonium naphthyldithiocarboxylate crystallized twice from ethanol; 3 = Cd(II) naphthyldithiocarboxylate obtained from twice-crystallized tetraethylammonium naphthyldithiocarboxylate and chromatographically purified on a silica column. (b) Electrode membrane: Tl(I) didecyldithiophosphate in chlorocyclohexane. Purity of complex: 1 = Tl(I) didecyldithiophosphate crystallized once from acetone; 2 = Tl(I) didecyldithiophospate crystallized three times from acetone.

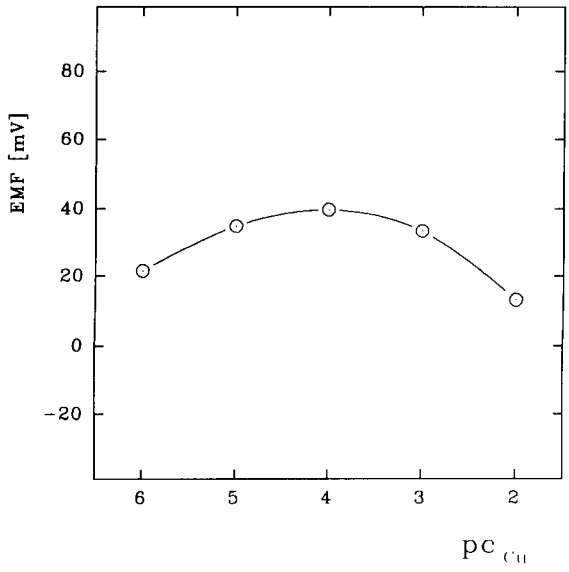

Fig. 4. Callibration graph for a copper electrode with a membrane made from Cu(II) didecyldithiophosphate in tetrachlorethane.

The complex formed may dissociate to form a complexing cation and anion (X^-). This process permits the transport of anions through the interphase, as a result of which the anions may affect the electrode potential. This leads to a decrease in the slope of the calibration graph and a deterioration of the detection limit.

The above processes are illustrated by the course of the calibration graph in Fig. 4 for an electrode in which copper didecyldithiophosphate was applied as the electroactive compound. For low copper concentrations, the electrode has a cationic function which, on increasing the copper concentration in the tested solution [accompanied by an increase in the concentration of the Cu(DTP)X form in a membrane and in the anion concentration in the solution], transforms into an anionic function.

Influence of penetration of water into the porous membrane on the stability of ion-selective electrodes

An important construction aspect of a liquid membrane that influences its geometrical dimensions is a disc made of a porous material. This disc is saturated with a membrane solution kept inside the pores through capillary forces. The porous material must be characterized by suitable parameters such as thickness, pore diameter, mechanical strength and good resistance to the effects of the applied organic solvent and water. The porous materials applied here were cellulose acetate, regenerated cellulose, polyamide, PTFE membrane filters from Sartorius, cellulose nitrate membrane filters from Sartorius, Schleicher and Schüll and Synpor (Czechoslovakia) and glass mi-

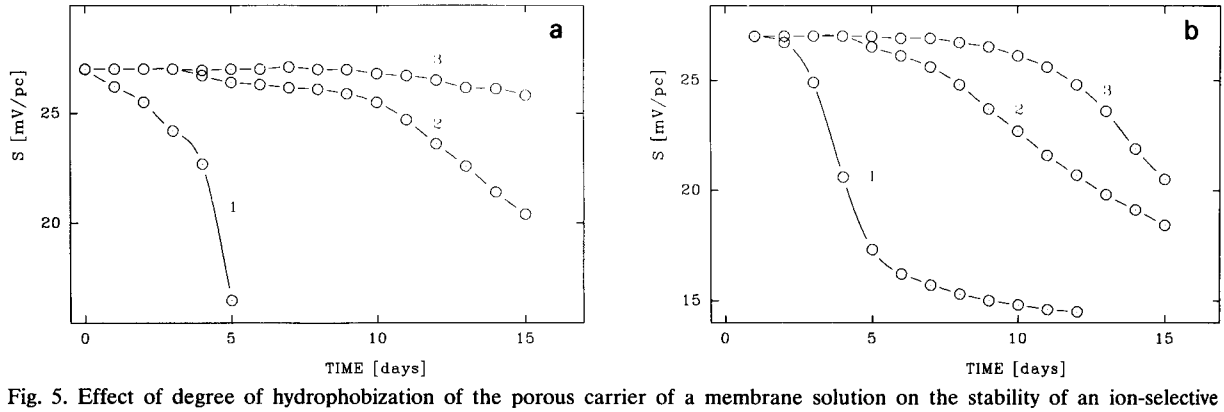

Fig. 5. Effect of degree of hydrophobization of the porous carrier of a membrane solution on the stability of an ion-selective electrode (changes in the slopes of the calibration graphs). 1 = Porous disc from non-hydrophozibed cellulose nitrate (SM 11306); 2 = porous disc from producer-hydrophobized cellulose nitrate (SM 13306); 3 = porous disc (SM 11306) hydrophobized with hexamethyl disilazane. Membranes: (a) made from Pb(II) naphthyldithiocarboxylate in tetrachloroethane; (b) made from Pb(II) naphthyldithiocaboxylate in chlorocyclohexane.

crofibre filters from Whatman. The values of these parameters proved to be most satisfactory for the Sartorius cellulose nitrate filters.

For the ion-selective electrodes under study, porous filters used in the membranes were made of cellulose nitrate with a pore diameter of 0.45–0.6 μm. On the surface of the cellulose nitrate, in addition to nitrate groups there are also OH groups. Both groups are hydrophilic in nature. Therefore, when cellulose nitrate is exposed to an organic solvent saturated with water, first the water on its surface may be absorbed and subsequently the formation may take place of a layer whose properties are similar to those of electrolyte solutions. Water adsorbed on the surface of the capillary pores of the membrane forms an "electrolytic junction" between the inner solution of the electrode and the external, test, solution. As a result of this process, the slope of the calibration graph for the electrode decreases. This unfavourable process may be counteracted by either using suitable hydrophobic materials for making porous membranes or by modifying the surface of pores so as to change the hydrophilic properties into hydrophobic properties (protection of hydrophilic groups of porous materials from the solvent). Figure 5 shows the stability of the potential of lead electrodes whose membranes were made from the solutions of lead(II) 1-naphthyldithiocarboxylate complex dissolved in chlorocyclohexane and tetrachlorethane. In the electrodes, porous discs made of cellulose nitrate with different degrees of hydrophobization were used in addition to unmodified filters of the SM 11306 type, a filter of the SM 13306 type hydrophobized by the producer and a filter of the SM 11306 type hydrophobized by using hexamethyldisilazane. Similar changes in potential were observed for other electrodes with different metal complexes in membranes. The lowest stability of the electrodes was observed for the electrode with a non-hydrophobized porous filter of the SM 11306 type. The process of absorption of water on the capillary walls of the membrane porous material was also confirmed by conductimetric measurements. Figure 6 shows changes in conductivity for the membrane in a lead electrode and for the membrane containing only a

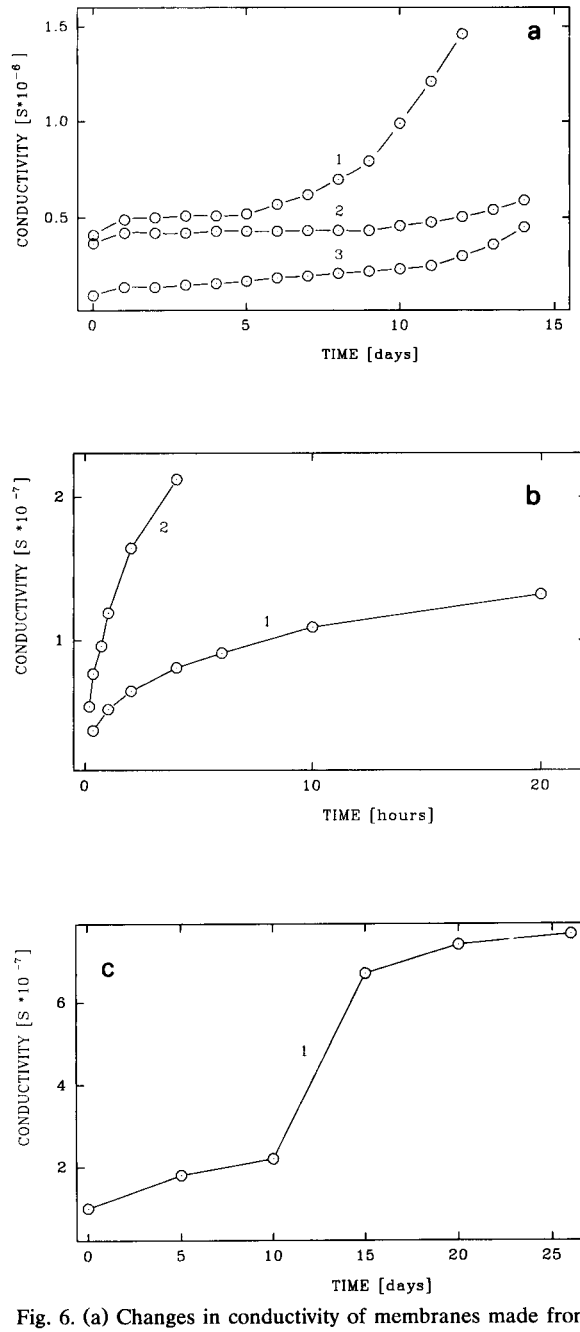

Fig. 6. (a) Changes in conductivity of membranes made from Pb(II) naphthyldithiocarboxylate solution in tetrachloroethane. The porous discs were made from (1) non-hydrophobized SM 11306 filter, (2) SM 13306 filter hydrophobized by the producer and (3) SM 11306 filter hydrophobized with hexamethyldisilazane. (b,c) Changes in conductivity of membranes made from tetrachlorethane. The porous discs were made from: (1) non-hydrophobized SM 11306 filter and (2) SM 11306 filter hydrophobized with hexamethyldisilazane.

solvent (tetrachloroethane) for a long operation time of the electrodes. Membranes with hydrophobized porous material exhibit the lowest changes in conductivity.

REFERENCES

1 W Szczepaniak and K. Ren, Anal. Chim. Acta, 82 (1976) 37.
2 W. Szczepaniak and K. Ren, presented at Ion-Selective Electrodes Symposium, Warsaw, 27–28 October 1976.
3 K. Ren, Chem. Anal. (Warsaw), 35 (1991) 637.
4 K. Ren, Chem. Anal. (Warsaw), 37 (1992) 193.
5 K. Ren, Chem. Anal. (Warsaw), 38 (1993) 1.
6 W. Szczepaniak, M. Ren and K. Ren, Chem. Anal. (Warsaw), 24 (1979) 51.
7 K. Ren, Talanta, 36 (1989) 767.
8 K. Ren and W. Szczepaniak, Chem. Anal. (Warsaw), 21 (1976) 1365.
9 A.I. Busev and M.I. Ivanutin, Zh. Anal. Khim., 11 (1956) 523.
10 N.D. Yordanov, N. Nicolov, A. Shishkov and D. Shopov, Inorg. Nucl. Chem. Lett., 12 (1976) 527.

Analytica Chimica Acta, 273 (1993) 493–497
Elsevier Science Publishers B.V., Amsterdam

Ion-selective electrode control based on coulometrically determined stability constants of biologically important calcium and magnesium complexes

Stanisław Głąb, Magdalena Maj-Zurawska, Paweł Łukomski and Adam Hulanicki

Department of Chemistry, Warsaw University, Pasteura 1, 02-093 Warsaw (Poland)

Andrzej Lewenstam

Department of Analytical Chemistry, Abo Akademi, Biskopsgatan 8, 20500 Abo (Finland)

(Received 17th June 1992)

Abstract

Coulometric titration was used for the determination of stability constants of calcium and magnesium complexes with ligands that may be present in biological fluids. The experimental conditions were the same as in clinical analysers. On the basis of these constants and the content of ionized calcium or magnesium measured with ion-selective electrodes, the total concentrations of both metals may be calculated. The results obtained were in good agreement with expectation.

Keywords: Coulometry; Ion-selective electrodes; Titrimetry; Calcium; Magnesium; Serum; Stability constants

Magnesium and calcium are present in the human body in many chemical forms at relatively high levels. The total concentration of calcium in blood serum varies from 2 to 3 mmol dm^{-3} and of magnesium from 0.6 to 1.1 mol dm^{-3} [1]. About 50–60% of calcium and magnesium are bound to proteins, mainly albumins, and several percent to other ligands, mainly hydrogencarbonate, lactate, oxalate and phosphate. For clinical analysis some other ligands such as citrate (used as anticoagulants) and acetate (used in standards) are also important.

The knowledge of ionized calcium and magnesium fractions and also their total content is essential because of their physiological and biological role. The concentration of ionized calcium and magnesium in blood serum or plasma and in other biological fluids can be determined potentiometrically with the use of the respective ion-selective electrodes. The total concentration of these elements could also be determined potentiometrically when the sample is chemically modified in such a way that all calcium and magnesium complexes are totally dissociated. Calcium and magnesium ion-selective electrodes have to respond properly under the above conditions. When, however, the conditional stability constants of calcium and magnesium complexes are known and the ionized fractions of these cations can be determined potentiometrically, then the total content of both metals can be evaluated. The stability constants of these complexes are not known at an ionic strength $I = 0.15$ mol dm^{-3}

Correspondence to: S. Głąb, Department of Chemistry, Warsaw University, Pasteura 1, 02-093 Warsaw (Poland).

and temperature 37°C, i.e., under the conditions which obtain in clinical analysers.

All the discussed ligands have protolytic properties. This allows the use of the method of determining the stability constants of their calcium and magnesium complexes based on alkalimetric titration of the protonated form of the ligand alone and in the presence of the metal ion [2]. Stability constants of these complexes are low and for their evaluation an accurate and precise method is required. In such a situation, the coulometric generation of titrant instead of the volumetric addition of a strong base in the course of alkalimetric titrations carried out in order to determine ligand protonation constants [3] and complexation constants of their complexes [4] is recommended. The coulometric procedure for the determination of stability constants, in addition to showing high precision and accuracy, also does not need the preparation of standard solutions.

The need to develop potentiometric procedures for the determination of total calcium and magnesium contents in biological fluids has led to the determination of the stability constants of some of the above complexes and protontation constants of the ligands under experimental conditions used in clinical analyzers. The aim of this paper is also to show that the total concentration of calcium or magnesium in a sample containing ligands can be evaluated from the concentration of ionized calcium or magnesium measured potentiometrically using the respective ion-selective electrodes when complexation of these cations is taken into account.

The agreement between the total content of the metal in the sample and the content calculated on basis of the potentiometric determination of ionized calcium and ionized magnesium and coulometrically evaluated stability constants gives additional proof of the reliability of the calcium and, in particular, of the magnesium ion-selective electrodes.

EXPERIMENTAL

Reagents

Analytical-reagent grade reagents were used. Compounds used included acetic, citric, lactic, oxalic, perchloric and phosphoric acid, 2-{[tris(hydroxymethyl)aminomethyl]amino}-1-ethanesulphonic acid (TES), disodium ethylenediaminetetraacetate dihydrate (EDTA), anhydrous calcium chloride, magnesium chloride hexahydrate and sodium chloride.

For the preparation of the membranes for the calcium [5] and magnesium [6] ion-selective electrodes, the following chemicals were used: high-molecular-mass poly(vinyl chloride) (PVC) (Fluka), tetrahydrofuran (Merck), tetrakis(4-chlorophenyl)potassium borate (Fluka), bis(2-ethylhexyl) sebacate (DOS) (Fluka) (Ca electrode), calcium ionophore ETH 1001 (Ca electrode), *o*-nitrophenyl octyl ether (*o*-NPOE) (Fluka) (Mg electrode), chloroparaffine (Scientific Polymer Products) (Mg electrode) and magnesium ionophore ETH 5220 (Mg electrode).

Apparatus

The amperostat was a PAR Model 173 with a Model 179 integrator. A Radiometer PHM-64 pH meter was used with a G202B glass electrode and silver–silver chloride reference electrode. The generating circuit consisted of a platinum electrode with a surface area of about 0.6 cm^2 and a platinum auxiliary electrode with a surface area of about 3 cm^2. All measurements were made at 25 and 37°C in a two-compartment coulometric cell equipped with a magnetic stirrer. The solutions were deaerated and kept under argon.

The calcium [5] and magnesium [6] ion-selective membranes used for ionized calcium and magnesium measurements were placed in a Philips IS 560 electrode body.

Procedures

The anode and cathode compartments of the coulometric cell were separated by two G-4 sintered-glass discs and the space between them was filled with 2% aqueous sodium perchlorate in 2% agar-agar. Both electrodes of the generating system were platinum. The reference electrode of the indicator system was connected through an electrolytic bridge containing 0.15 mol dm^{-3} sodium chloride. A current $i = 5$ mA provides 100% generation efficiency of the base [3].

The solutions titrated coulometrically con-

tained ca. 0.05 mmol of perchloric acid for calibration of the indicator electrode system or 0.05 mmol of protonated ligand for the determination of the protonation constant.

For the determination of stability constants the solutions contained a mixture of protonated ligand (ca. 0.05 mmol) and examined metal ions (ca. 0.5 mmol). The ionic strength of all solutions was adjusted with sodium chloride to 0.15 (the total volume of titrated solutions was 50 cm^3).

Solutions of metal ions were standardized by volumetric complexometric methods [7].

RESULTS AND DISCUSSION

Experimental data obtained in the course of a coulometric titration of the protonated ligand with electrogenerated strong base were used for protonation constant calculations. The protonation constant of a ligand (K_H) is evaluated from the equation [3]

$$\log K_H = -\log[H^+] + \log\left\{\frac{Q_{E.P.} - Q - FV([H^+] - [OH^-])}{Q + FV([H^+] - [OH^-])}\right\}$$

where V is the volume of solution, F is the Faraday constant and $Q_{E.P.}$ is the charge consumed until the titration end-point. The pairs of values Q and $[H^+]$ (or $[OH^-]$) were evaluated from the coulometric titration curve, $E = f(Q)$, of the acid examined. With diprotic acids, when $\log K_{1H} - \log K_{2H} < 2.3$ the constants were calculated from the titration curve using a least-squares procedure [8].

The evaluation of hydrogen ion concentration $[H^+]$ requires calibration of the indicator electrode, according to the relationship

$$\log[H^+] = (E_a^0 - E)F/2.3RT$$

where E_a^0 is a calibration constant [9]. This constant is evaluated from coulometric titration of perchloric acid at a given temperature and ionic strength [3]. Stability constants of metal–ligand complexes, β_{ML}, were calculated from the experimental data obtained in the course of the alkalimetric titration of a solution containing a mixture of protonated ligand and metal ion, using the equation given by Yoshino et al. [10], which was converted into a form directly applicable to coulometric titration [4].

The coulometric method for the determination of stability constants which was checked earlier and was found useful for the evaluation of stability constants of calcium and magnesium complexes [4], is especially valuable when weak complexes are formed. In that event the error of the volumetric titration procedure may become significant and coulometry allows that error to be decreased.

The low value of the stability constants of the examined complexes results in a very small shift of the titration curve in the presence of metal ions in comparison with the titration curve of the ligand alone. A significant excess of metal ions in the titrated metal–ligand mixture (10 : 1) was used in order to obtain a sufficient large shift of these titration curves, which allows the calculation of the stability constant. The protonation constants of ligands examined and the stability constants of their calcium and magnesium complexes, determined at an ionic strength of 0.15 and at 25 and 37°C, are given in Tables 1 and 2. When the literature data for comparable conditions were available the agreement was found to be satisfactory.

TABLE 1

Protonation constants (K_H) of ligands determined by coulometric titration at ionic strength $I = 0.15$ mol dm^{-3} NaCl and 25 and 37°C with literature data [11] in parentheses

Ligand	Log K_H	
	25°C	37°C
Acetate	4.62 (4.56) [a]	4.76 (4.76) [b]
Lactate	3.51 (3.66)	3.70 (3.87) [c]
Oxalate	3.76 (3.81) [a]	3.95 (3.68) [d]
	– (1.37) [a]	– (1.12) [d]
Citrate	5.71 (5.62)	5.75 (5.82) [e]
	4.38 (4.34)	4.42 (4.44) [e]
	2.92 (2.91)	2.98 (2.94) [e]
Phosphate	– (12.3) [a]	– (12.18) [f]
	7.28 (7.2) [a]	7.33 (7.16) [f]
	2.42 (2.16) [a]	2.47 (3.32) [f]

[a] $I = 0.10$. [b] $I \to 0$, 35°C. [c] $I \to 0$, 38°C. [d] $I = 1.0$, 32°C. [e] $I = 0.10$, 30°C. [f] $I \to 0$.

TABLE 2

Stability constants (β_{ML}) of calcium and magnesium complexes determined coulometrically at ionic strength $I = 0.15$ mol dm^{-3} NaCl and 25 and 37°C with literature data [11] in parentheses

Ligand	Log β_{CaL}		Log β_{MgL}	
	25°C	37°C	25°C	37°C
Acetate	0.48 (0.53)	0.57	0.46 (0.51) [a]	0.58
Lactate	0.48 (0.8)	0.61	0.61 (0.93) [b]	0.64
Oxalate	1.46 (1.37) [a]	1.47	2.18 (2.55)	2.39
Citrate	3.17 (3.20)	3.28	3.27 (3.15)	3.24
Phosphate	1.3 (1.33)	1.4 (1.3)	1.9 (2.50) [a]	2.9 (3.4)

[a] $I = 0.1$. [b] $I = 0.2$.

Stability constants of the examined calcium and magnesium complexes, determined under conditions similar to those obtaining in clinical analysers, i.e., ionic strength 0.15 mol dm^{-3} NaCl and 37°C, were used to calculate the total concentration of calcium or magnesium in solutions of the following composition: $CaCl_2$ or $MgCl_2$, 1×10^{-4} mol dm^{-3}; ligand, 1×10^{-3} mol dm^{-3}; NaCl, 0.15 mol dm^{-3}; and pH, 7.4 (TES).

The concentration of ionized calcium or magnesium was measured at 37°C in an argon atmosphere using a calcium or magnesium ion-selective electrode. The results obtained (Table 3) show the agreement between the calcium and magnesium electrode responses and the determined stability constants.

TABLE 3

Total calcium and magnesium concentrations ($C_M = [M] + \beta_{ML}[M]C_L$) calculated using the ionized calcium (magnesium) concentration [M] measured with ion-selective electrodes and the determined stability constants [a]

Ligand	C_{Ca} (mol dm^{-3})	Error (%)	C_{Mg} (mol dm^{-3})	Error (%)
Acetate	9.86×10^{-5}	−1.4	1.01×10^{-4}	+1
Lactate	9.21×10^{-5}	−7.9	9.36×10^{-5}	−6.4
Oxalate	1.06×10^{-4}	+6.0	9.46×10^{-5}	−5.4
Citrate	9.56×10^{-5}	−4.4	1.02×10^{-4}	+2.0
Phosphate	1.04×10^{-4}	+4.0	1.03×10^{-4}	+3.0

[a] C_L is ligand concentration ($C_L = 1 \times 10^{-3}$ mol dm^{-3}). Total concentrations of calcium and magnesium were 1×10^{-4} mol dm^{-3}.

Conclusions

The coulometric method based on alkalimetric titration of solutions containing the protonated form of the ligand alone and in the presence of metal ions is useful for determining the stability constants of weak complexes such as occur in biological fluids. On the basis of the content of ionized calcium or magnesium, measured with ion-selective electrodes, the content of ionized calcium or magnesium, the known concentration of complexing ligands and the stability constants of both metal complexes, the total concentrations of both metals may be calculated. The results obtained were in good agreement with expectation, indicating good functioning of the ion-selective electrodes and proper values of coulometrically evaluated complexation constants.

Stability constants of calcium and magnesium complexes with other ligands, such as carbonate and hydrogencarbonate, heparin and proteins, should be determined. The possibility of calculating the total concentrations of both metal ions in serum could then be tested.

This work was partly supported by the Committee of Scientific Research under Grant BST 14/91 and by KONE Instruments.

REFERENCES

1 J.P. Kokko and R.L. Tannen (Eds.), Fluids and Electrolytes, Saunders, Philadelphia, 1986.
2 J. Inczedy, Analytical Applications of Complex Equilibria, Horwood, Chichester, 1973.
3 S. Głąb, E. Skrzydlewska and A. Hulanicki, Talanta, 34 (1987) 411.
4 S. Głąb, U. Nowicka and A. Hulanicki, Talanta, in press.
5 D. Ammann, R. Bissig, Z. Cimerman, U. Fiedler, M. Guggi, N.E. Morf, M. Oehme, M. Osswald, E. Pietsch and W. Simon, in M. Kessler, L.C. Clarke, Jr., D.W. Lübbers, I.A. Silver and W. Simon (Eds.), Ion and Enzyme Electrodes in Biology, Urban and Schwarzenberg, Munich, 1976.
6 M. Maj-Zurawska and A. Lewenstam, Anal. Chim. Acta, 236 (1990) 331.
7 R. Pribil, Komplexone in der Chemischen Analyse, VEB Deutscher Verlag der Wissenschaften, Berlin, 1961.

8 A. Albert and E.P. Serjeant, The Determination of Ionization Constants, Chapman and Hall, London, 1971.
9 L. Persson, F. Ingman and A. Johansson, Talanta, 23 (1976) 76.
10 T. Yoshino, S. Murakami, M. Kagawa and T. Araragi, Talanta, 21 (1974) 79.
11 A.E. Martell and R.M. Smith, Critical Stability Constants, Plenum Press, New York, London, 1977.

Analytica Chimica Acta, 273 (1993) 499–509
Elsevier Science Publishers B.V., Amsterdam

Optimization of a sample subtraction procedure: potentiometric analysis of bases

Carlo Maccà and Andrea Tapparo

Department of Inorganic, Metallorganic and Analytical Chemistry, University of Padova, Via Marzolo 1, 35131 Padova (Italy)

(Received 1st June 1992)

Abstract

A previously proposed variation of the principle of potentiometric sample subtraction was theoretically and experimentally evaluated using acid–base reactions as model systems. The potential of a glass electrode was measured after addition of two measured aliquots of a standard acid, followed by "subtraction" of a measured volume of sample base. Criteria for optimization of the procedure are discussed. If the ratio between the second and the first addition of standard is large enough ($\geqslant 5:1$) and the analyte in the added sample consumes a major part of the standard reagent (80% or more), very good accuracy and precision, approaching those of titration, can be attained. The theoretical predictions were confirmed by experiments.

Keywords: Optimization methods; Potentiometry; Acidimetry; Sample subtraction

Addition methods are widely used in potentiometric analysis [1–4], particularly with microprocessor-based automated instruments [5,6]. These methods compete in rapidity with direct potentiometry while aiming at improved accuracy and precision. In addition to the popular single standard addition, several procedural variations have been devised in order to handle a variety of samples. When an electrode selective for the analyte, i.e., the sample species to be determined, is not available, sample subtraction, also termed analyte subtraction, is the method of choice [1,4,7].

A variation of the principle of sample subtraction has been proposed [8] that seems particularly suitable for reducing the effects of deviations of the electrode response from the ideal behaviour [7]. The technique depends on three measurements of the e.m.f. of a suitable pair of electrodes, immersed in a known volume of a supporting electrolyte (which ensures constancy of ionic strength and junction potential during the measurements), after the addition of (i) and (ii) two measured aliquots of a standard solution of the primary ion, towards which the indicating electrode is responsive, and (iii) of a known volume of sample containing an analyte that reacts quantitatively with the primary ion. This procedure has been successfully applied to the determination of hypochlorite by reduction with bromide, this ion being monitored with a bromide-selective electrode [8].

The general conditions for the method to perform ideally are the same as for the usual addition and subtraction methods [7]. Among these, the requirement that the reaction be quantitative must be stressed. In addition, optimization of accuracy and precision requires the following two stoichiometric parameters to be taken into account and properly set: first, the ratio between

Correspondence to: C. Maccà, Department of Inorganic, Metallorganic and Analytical Chemistry, University of Padova, Via Marzolo 1, 35131 Padova (Italy).

the second and the first aliquot of primary ion; a ratio 1:1 has been suggested [3,7], but a larger ratio (about 9:1) was found satisfactory in practice [8]; and second, the ratio between analyte and total primary ion added; reasonably, the analyte should subtract, by reacting with it, a major part of the primary ion (without exceeding, of course, the stoichiometric amount). Subtraction of an amount approximately corresponding to the second aliquot of primary ion (90% of the total amount) seemed advisable when the method was first applied [8].

This work was aimed at rationalizing and substantiating with experiments the above criteria, to demonstrate that the method deserves wider application. The determination of strong and weak bases was taken as an example, being of practical interest and fitting the general requirements of an ideal model system.

EXPERIMENTAL

Apparatus

The measured solution was contained in a jacketed cell and stirred with a PTFE-coated magnetic bar and a magnetic stirrer. The e.m.f. of a combination glass electrode with encapsulated Ag/AgCl reference electrode in 3 M KCl and sleeve junction was measured by a digital pH–mV meter with 0.1 mV resolution. Two computer-controlled, motor-driven microburettes (Crison, Barcelona), typically equipped with 1-ml Hamilton syringes (0.4-μl resolution), were used for the additions of standard and sample solutions.

Reagents

Analytical-reagent or higher grade reagents and ultrapure (MilliQ-Plus grade) water were used. HCl solutions were prepared from primary standard acid obtained by azeotropic distillation of an analytical-reagent grade product.

Procedure I

The cell was filled with 25 ml of water or 0.1 M KCl and thermostated when required. The electrode and the tips of the delivery tubes of the burettes were immersed. A volume V_1 of standard solution of the reagent (concentration C_s) was added with a burette and the e.m.f. E_1 was measured. After 30–60 s, a volume V_2 of the same solution was added (typically $V_2 = 9\text{–}10V_1$) and E_2 was recorded. A volume V_3 of sample solution was introduced with a second burette, or a weight W of solid sample was added with a glass or aluminium boat; E_3 was measured. Equation 4 or, for solid samples, Eqn. 9 (see below) was used for the calculation.

Procedure II

The thermostated cell was filled with 25 ml of a C_1 M standard solution of the reagent in 0.1 M KCl. The electrodes and the delivery tubes were immersed, and E_1 was recorded. A volume V_2 of a C_s M standard solution of reagent, suitable to increase the reagent concentration in the cell to $C_2 \gg C_1$, was added with a burette and E_2 was recorded. V_3 ml of sample solution were introduced with a second burette and E_3 was measured. The result was calculated with Eqn. 7 (see below).

PRINCIPLES

Calculation of the sample concentration

The technique is discussed for the subtraction of a base from a strong acid. The conclusions can be simply transposed to the symmetrical subtraction of acid from strong base and to other kinds of reactions. After addition of the first aliquot of V_1 ml of the standard strong acid at concentration C_s to V_0 ml of supporting electrolyte solution, the e.m.f. of the measuring cell is

$$\begin{aligned} E_1 &= E^0 + S \log[H^+] + S \log \gamma_H + E_j - E_{ref} \\ &= E^* + S \log[H^+] \\ &= E^* + S \log C_1 \\ &= E^* + S \log\left[\frac{C_s V_1}{(V_0 + V_1)}\right] \end{aligned} \quad (1)$$

where γ_H is the activity coefficient of hydronium ion, E_j is the junction potential, E_{ref} is the potential of the reference electrode and C_i is the

stoichiometric concentration of acid in the measured solution after the ith addition (C_1 in Eqn. 1). After addition of the second aliquot, V_2, the e.m.f. is (if all the terms included in E^* remain unchanged)

$$E_2 = E^* + S \log C_2$$

$$= E^* + S \log\left[\frac{C_s(V_1+V_2)}{(V_0+V_1+V_2)}\right] \quad (2)$$

If the base, in smaller amount than the total acid, reacts quantitatively, after addition of V_3 ml of sample, containing the base (or the basic function, for polyfunctional bases) at concentration C_x, the e.m.f. becomes

$$E_3 = E^* + S \log C_3$$

$$= E^* + S \log\left[\frac{C_s(V_1+V_2) - C_xV_3}{(V_0+V_1+V_2+V_3)}\right] \quad (3)$$

In fact, the first two measurements with known concentrations of primary ion calibrate the measuring cell. This makes it possible to calculate from the third measurement the concentration C_3 of unreacted acid after the sample subtraction, i.e., after the partial consumption of the primary ion by the analyte; thereby the analyte concentration in the sample is obtained. By combining Eqns. 1–3, one obtains

$$C_x = \frac{C_s(V_1+V_2)}{V_3}\left[1 - \left(1 + \frac{V_3}{V_0+V_1+V_2}\right) \times \text{antilog}\left(\frac{E_3-E_2}{S}\right)\right] \quad (4)$$

or, alternatively,

$$C_x = \frac{C_sV_1}{V_3}\left[1 + \frac{V_2}{V_1} - \left(1 + \frac{V_2+V_3}{V_0+V_1}\right) \times \text{antilog}\left(\frac{E_3-E_1}{S}\right)\right] \quad (4')$$

where

$$S = (E_2-E_1)\left\{\log\left[\frac{(V_0+V_1)(V_1+V_2)}{V_1(V_0+V_1+V_2)}\right]\right\}^{-1} \quad (5)$$

When a large electrode calibration range, as expressed by the ratio Q between the primary ion concentrations made up by the two initial additions of standard reagent,

$$Q = C_2/C_1 \quad (6)$$

is wanted, it may be impractical to add two very different volumes of the same standard solution of primary ion; this ratio is more suitably obtained by preparing a stock solution of acid at C_1. In this instance, E_1 is measured in V_0 ml of the stock solution at C_1 (thus $V_1 = 0$), and only one aliquot V_2 of standard solution is added to increase the primary ion concentration to C_2, where E_2 is measured (see *Procedure II*). The sample concentration is calculated with the equation

$$C_x = \frac{C_1V_0 + C_sV_2}{V_3}\left[1 - \left(1 + \frac{V_3}{V_0+V_2}\right) \times \text{antilog}\left(\frac{E_3-E_2}{S}\right)\right] \quad (7)$$

where

$$S = (E_2-E_1)\left\{\log\left[\frac{C_1V_0 + C_sV_2}{C_1(V_0+V_2)}\right]\right\}^{-1} \quad (8)$$

Lastly, if the sample is solid and causes a negligible volume increase when a weighed amount containing N_x mmol of analyte is dissolved, Eqn. 9 is used:

$$N_x = C_s(V_1+V_2)\left[1 - \text{antilog}\left(\frac{E_3-E_2}{S}\right)\right] \quad (9)$$

where S is given again by Eqn. 5 or (when $V_1 = 0$) by Eqn. 8.

Optimization of experimental parameters

The electrode calibration range Q (Eqn. 6) and (to the extent that the sample concentration is approximately known) the stoichiometric reaction ratio Φ, that is, the fraction of primary ion ideally consumed by the analyte after the third addition (the sample subtraction),

$$\Phi = C_xV_3/C_s(V_1+V_2) \quad (10)$$

are experimental parameters under the operator's control. These parameters must be optimized for

improving both accuracy and precision. For this purpose, the dependence of the error of C_x determination on Φ and on Q must be evaluated. Only the effect of the error of e.m.f. measurement is dealt with in this discussion. Error of volumes, which be appreciable, however, are not considered for simplicity.

The dependence on the value of Φ of the effect of the e.m.f. measurement error on the accuracy of a single determination (for which systematic and random errors are indistinguishable) can be evaluated with simple consideration. Let E_3 be the theoretical value of e.m.f. after the addition of sample, obeying Eqn. 3 with the experimental calibration parameters E^* and S from the first two measurements (additions of standard). Let E_3' be the experimental value. Any deviation of E_3' from E_3, $e_E = E_3' - E_3$, whichever is its origin, causes the concentration C_3' of the primary ion measured by the electrode to be different from the true value C_3, and therefore the calculated value C_x' to differ from C_x. The relative error of C_x, ϵ_{Cx}, is

$$\epsilon_{Cx} = (C_x' - C_x)/C_x \tag{11}$$

From the equations for E_3 and E_3' (see Eqn. 3), we have

$$e_E = E_3' - E_3 = S \log C_3' - S \log C_3$$
$$= S \log\left[\frac{C_s(V_1 + V_2) - C_x'V_3}{C_s(V_1 + V_2) - C_xV_3}\right] \tag{12}$$

and therefore

$$C_x'V_3 = C_s(V_1 + V_2) + [C_xV_3 - C_s(V_1 + V_2)] \times \text{antilog}(e_E/S) \tag{13}$$

By rearranging Eqn. 13 and using eqns. 11 and 10, Eqn. 14 is obtained:

$$\epsilon_{C_x} = \left(\frac{1}{\Phi} - 1\right)\left[1 - \text{antilog}\left(\frac{e_E}{S}\right)\right] \tag{14}$$

by which the relative error of the determination of the sample concentration for a given measurement error e_E can be calculated at variable reaction ratio Φ.

In Fig. 1, ϵ_{Cx}, calculated using an electrode slope $S = 60$ mV, is plotted against Φ for three values of e_E: 0.2, 0.5 and 1.0 mV (the curves for

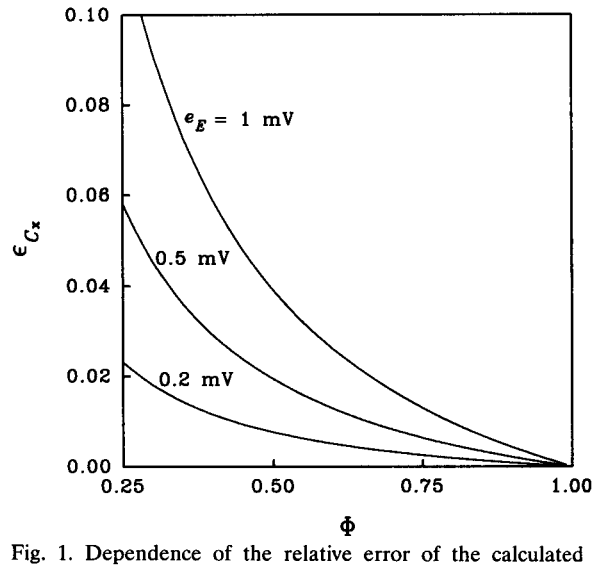

Fig. 1. Dependence of the relative error of the calculated sample concentration C_x on the counter-titration ratio Φ at various levels of error e_E of the measured e.m.f.

$e_E = -0.2$, -0.5 and -1.0 mV are approximately symmetrical with the plotted curves). It is seen that for any Φ larger than 0.5 the method is more accurate than direct potentiometry; indeed, in this technique e.m.f. deviations of 0.2, 0.5 and 1.0 mV cause relative errors of 0.8, 2 and 4%, respectively, in the measurement of the primary ion concentration. The error of the subtraction method becomes smaller than 1% (a respectable performance for a rapid method) at $\Phi > 0.8$ for $e_E = 1$ mV and at $\Phi > 0.43$ for $e_E = 0.2$; it can ideally reach the level wanted in titration (0.1%) at $\Phi = 0.99$ and $\Phi = 0.89$, respectively.

Quantification of the effects of the different causes of systematic errors is beyond the scope of this paper. However, it is easily understood that ion strength, which causes variations of γ_H and E_j, and temperature, which causes variation of E^0, E_{ref} and S, must be kept under some control in order that the parameters of the electrode response, E^* and S (Eqn. 1), remain unaffected. Important aspects have been examined by Midgley [7].

A more complete appreciation of the effect of the choice of both the calibration range Q and the reaction ratio Φ is obtained by evaluating how these variables affect the uncertainty of re-

peated determinations of the sample concentration for a given precision of the e.m.f. measurement. For this purpose the random e.m.f. errors of all the three points must be taken into account. The equations, with their derivation, are given in Appendix I. Some examples are illustrated in Figs. 2 and 3; for convenience, the uncertainty scale is logarithmic.

The solid-line plots in Fig. 2 show the effect of the amplitude of the calibration range on the dependence on Φ of the relative uncertainty of C_x, dC_x/C_x, at a given value of the precision of E ($dE = 0.5$ mV) for $S = 60$ mV. It is seen that increasing the calibration ratio Q from 2 to 5 greatly improves the precision at $\Phi > 0.5$; larger Q values give a moderate improvement, which practically ceases for $Q > 10$.

The other plots in Fig. 2 show the dependence of dC_x/C_x on the reaction ratio Φ at different values of the precision of E ($dE = 1$ and 0.2 mV, respectively) for the calibration range $Q = 10$. In all instances, increasing Φ from 0.5 to 0.9 improves the precision by tenfold. If the e.m.f. can be measured with fairly good precision, a very good precision can be reached at values of Φ that are not critical operationally; indeed, meeting values of Φ in the range 0.8–0.95 should not require trial-and-error procedures, at least with repetitive samples having a moderately narrow composition range.

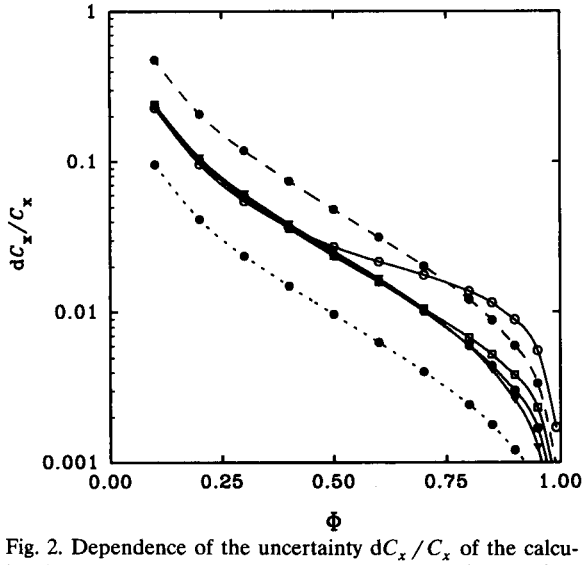

Fig. 2. Dependence of the uncertainty dC_x/C_x of the calculated concentration C_x on the reaction ratio Φ (Eqn. 10) at various values of calibration ratio Q (○, $Q = 2$; □, $Q = 5$; ●, $Q = 10$; ▼, $Q = 100$) for a precision of the measured e.m.f. $dE = 0.5$ mV (solid line), $dE = 1.0$ mV (dashed line) and $dE = 0.2$ mV (dotted line).

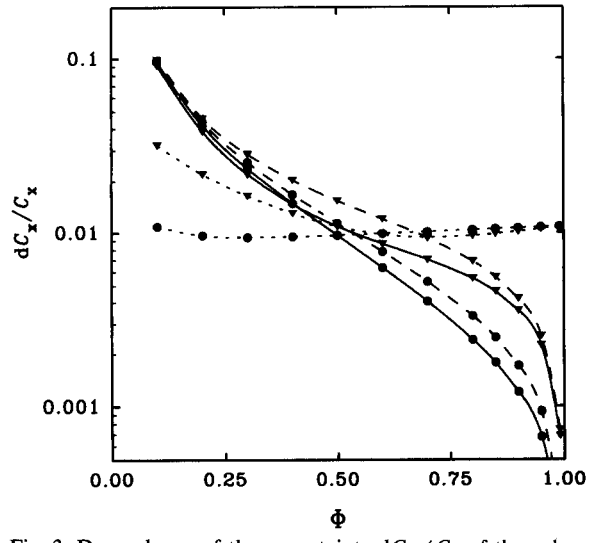

Fig. 3. Dependence of the uncertainty dC_x/C_x of the calculated sample concentration C_x on the reaction ratio Φ at two values of the calibration ratio (▼, $Q = 2$; ●, $Q = 10$) for a precision of the measured e.m.f. $dE = 0.2$ mV. Solid lines, modified sample subtraction (Φ, see Eqn. 10); dashed lines, ordinary sample subtraction ($\Phi = C_x V_3 / C_2 V_0$); dotted lines, direct potentiometry ($\Phi = C_x / C_2$).

The criteria for optimization resulting from the above, i.e., $5 \leqslant Q \leqslant 10$, $\Phi \geqslant 0.8$, are only apparently contrasting with the considerations on which a reaction ratio $\Phi \approx 0.5$ after calibration with $Q = 2$ has been proposed [3,7]. These last values have been suggested as a compromise allowing for increasing bias at increasing Φ. However, working at $Q = 2$, $\Phi \approx 0.5$, although being operationally simpler, does not fully exploit the precision of the method. Therefore, larger values of Q and Φ seem to be advisable when measuring and measured systems behave nearly ideally. As noted by Midgley [7], compensation of the bias originated by deviations of the electrode response from Nernstian behaviour is obtained when $E_3 = E_1$, i.e., with $\Phi \approx 1 - 1/Q$; if these deviations are moderate, the possibility of using

$Q > 2$, $\Phi > 0.5$ should be considered and tested. In contrast, too high values of Φ must be avoided when the uncertainty and the bias affecting E_3 (which in our treatmeant have been considered to be constant) increase considerably with Φ; this occurs, for instance, when the reaction between the primary ion and the analyte is insufficiently quantitative.

In Fig. 3, the modified sample subtraction procedure is compared with ordinary sample subtraction [1,7] and with direct potentiometry (see Appendix I). The calibration concentrations C_1 and C_2 are taken to be the same for the three methods. For consistency, in the ordinary sample subtraction V_3 ml of sample at C_x is assumed to be subtracted from V_0 ml of standard primary ion at concentration $C_s = C_2$; thus $\Phi = C_x V_3 / C_2 V_0$. In direct potentiometry, the primary ion, measured by the electrode, is also the determinand species; in this case, $C_x = C_3$ and $\Phi = C_x / C_2$. In all instances, the analyte concentration in the measured solution increases towards the right-hand side of the plot.

It is seen that similar criteria of optimization of the experimental parameters Φ and Q do hold for both the ordinary and modified subtraction procedures. The advantage of the modified procedure over the usual method of subtraction is moderate if only random errors taken into account. The main benefit is increased protection, due to in situ calibration, against systematic errors [7]. Both sample subtraction methods are seen to be greatly superior to direct potentiometry provided that Φ is larger than 0.5.

Not ideally quantitative reactions: weak bases

An insufficiently quantitative reaction is a cause of systematic negative errors [7]. This can occur when a very weak base is subtracted from a more or less diluted strong acid. The contribution of a non-quantitative reaction to the systematic relative error of the experimental concentration of sample base (having acidity constant K_a) is conveniently calculated with Eqn. 15 for given values of C_2 (the total concentration of standard acid in the measured solution) and Φ (the counter-titration ratio):

$$\epsilon = -K_\alpha / [C_2(1 - \Phi)] \quad (15)$$

The derivation of Eqn. 15 (an approximate equation, obtained by neglecting dilution due to the sample addition) is given in Appendix II. It is seen that the contribution of Eqn. 15 to the systematic error increases more negatively with increasing Φ and decreasing C_2. Equations 16 and 17, obtained by rearranging Eqn. 15, give, respectively, the concentration C_2 at which for a given Φ the result is affected by a specified error ϵ (to which a negative value must be assigned) and the ratio Φ at which, for a fixed C_2, ϵ reaches a specified value:

$$C_2 = K_\alpha / [\epsilon(1 - \Phi)] \quad (16)$$

$$\Phi = 1 + (K_\alpha / \epsilon C_2) \quad (17)$$

These equations help in choosing the experimental conditions for the determination of weak acids.

RESULTS AND DISCUSSION

The modified sample subtraction method discussed above was tested by analysing samples containing single strong or weak bases at concentrations of 0.05 mol l^{-1} or higher. In several instances, the standard procedures described under Experimental were modified in various ways, in order that a larger amount of homogeneous data could be obtained from each experiment. For instance, in some series of experiments the volume of sample corresponding to ca. 95% of the equivalence volume ($\Phi = 0.95$) was subtracted stepwise, by consecutive addition of three aliquots corresponding respectively to about 50% ($\Phi = 0.50$), 30% ($\Phi = 0.80$) and 15% ($\Phi = 0.95$) of the stoichiometric amount. The "true" value of sample concentration was generally obtained by independent potentiometric titration of the standard acid with the sample base; the equivalence volume was calculated by the Gran method [1,9].

Titrations were also used for testing the subtraction method. In this instance, the standard acid to be titrated was introduced into the measuring cell in two or more aliquots, and the e.m.f. was measured after each addition. Subsequently, the acid was titrated by addition of constant volumes of the sample base. The points of the

first part of the titration (i.e., the points in acidic solution) were used all together for finding the equivalence point of the Gran titration (yielding the total alkalinity of the sample [10]); each one of the same points could be used separately for the application of the subtraction method at different selected values of Φ, together with two additions of acid (corresponding respectively to the total amount of acid and to one of the preceding additions).

The experiments were performed by several operators having different degrees of skill. All results, except for accidents of ascertained origin, confirmed that the method can achieve high accuracy and precision, and that conditions for optimization are easily met, in accordance with the theoretical expectations discussed above and with the results previously obtained on a completely different system [8].

The results of a few series of experiments, in which the effects of uncontrolled temperature and ionic strength were also investigated, are summarized in Table 1. The titre of 0.1 M sodium hydroxide was determined by stepwise subtraction after addition of two aliquots of standard 0.10063 M hydrochloric acid. The temperature increased by 0.5°C by effect of additions in series 1, and by less than 0.3°C in series 2, where the initial volume was double. In series 3 the temperature was held constant (within 0.1°C) and the ionic strength was stabilized by addition of 0.2 M KCl. The improvement of the results due to controlled temperature and ionic strength is appreciable. However, when compared with Gran titration (series 5), the results of the subtraction method are always acceptable at $\Phi = 0.8$, and very good at $\Phi = 0.95$. The difference between series 3, $\Phi = 0.95$, and Gran titration is less than 0.2%; it is statistically significant (t-test) only owing to the great precision of the subtraction method. Moreover, this very small difference could be assigned to a possible systematic error of the Gran titration due to a deviation, although small, of the electrode slope from the theoretical value used in calculations. It has also been observed that the results obtained with automatic titrators, using differential methods for the equivalence point, are generally affected by larger systematic and random errors that arise from the inability to resolve the equivalence point of the titration of strong base + carbonate to hydrogencarbonate from the complete titration to carbon dioxide in the presence of this contaminant.

The results of series 4 in Table 1 show that increasing the ratio Q substantially above 10 leads to worse accuracy and precision, because the actual value of $[H^+]$ at C_1, which necessarily becomes very small ($\ll 10^{-4}$), can be appreciably affected by acidic or basic impurities.

Similar results were obtained by using Eqn. 4 with the points of Gran titrations. Figure 4 shows the results of one of the experiments of a series performed to verify the dependence on Φ of the accuracy at different values of Q. The ratio of the sample concentration calculated with Eqn. 4 for single titration points, C_{calc}, to the "true" concentration resulting from the Gran linearization, C_{true}, is plotted against Φ. The error is smaller than 0.1% for $0.75 < \Phi < 0.95$ at $Q \geqslant 5$, whereas at $Q = 2$ the range of extreme accuracy is shorter

TABLE 1

Determination of titre of ca. 0.1 M NaOH by subtraction from standard HCl under different conditions (1–4) and by Gran titration of standard HCl (5) (C_2 and C_x in mol l^{-1})

No.	T (°C)	μ	Log C_2	Q	n	$\Phi = 0.50$		$\Phi = 0.80$		$\Phi = 0.95$	
						C_x	s	C_x	s	C_x	s
1	Const.	0	2.4	10.6	6	0.1096	0.0004	0.11162	0.00017	0.11228	0.00005
2	Const.	0	2.7	10.8	6	0.1106	0.0005	0.11180	0.00011	0.11229	0.00006
3	Const.	Const.	2.4	10.6	6	0.1105	0.0003	0.11173	0.00006	0.11222	0.00005
4	Const.	Const.	3.4	10^2	5	0.1051	0.0005	0.1100	0.0003	0.1118	0.0002
5	Const.	Const.	(Gran)		3	$C_x = 0.11208$		$s = 0.00010$			

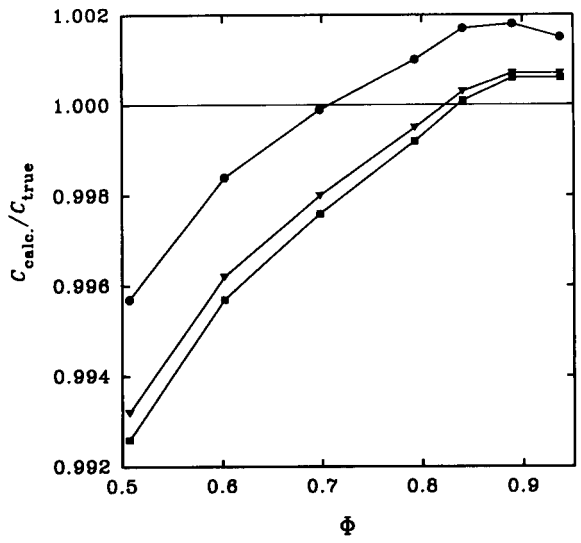

Fig. 4. Determination of the titre of 0.095731 M NaOH with the subtraction method: dependence of the experimental results on the reaction ratio Φ (Eqn. 10) at different values of the calibration ratio Q (●, $Q = 2$; ▼, $Q = 5.2$; ■, $Q = 11.7$) with $C_2 = 10^{-2.4}$.

and displaced towards smaller Φ. Other experiments reproducibly yielded the best accuracy at larger values of Q and Φ.

Determination of the titre of moderately weak bases, reacting quantitatively, gave similar results. For instance, the titre of ca. 0.1 M ammonia solution was 0.0988 ± 0.0003 mol l^{-1} at $\Phi = 0.5$, 0.09984 ± 0.00008 mol l^{-1} at $\Phi = 0.8$, and 0.10004 ± 0.00005 mol l^{-1} at $\Phi = 0.95$ (uncertainty expressed as standard deviation; $n = 5$; experimental conditions as in series 3, Table 1); independent Gran titration yielded 0.09982 ± 0.00013 mol l^{-1}.

With very weak bases, the reaction becomes less and less quantitative as Φ approaches unity. A satisfactory compromise between the quantitativeness of the reaction and the general requirements of the subtraction method can hardly be found, but perhaps at higher concentrations. For instance, by application of Eqn. 16 it is calculated that the reaction of sodium acetate ($pK_a = 4.50$ at 25°C, $I = 0.5$ mol l^{-1}) is 99% quantitative at least up to $\Phi = 0.9$ only for C_2 larger than $10^{-1.5}$ mol l^{-1}. At lower concentrations the optimum range of the subtraction method, $0.8 < \Phi < 1$, cannot be exploited. A test was performed by subtraction of weighed amounts of sodium acetate trihydrate ($M_r = 136.1$) after two additions of 1 M HCl to 0.5 M KCl ($n = 8$, $C_2 = 10^{-1.4}$ mol l^{-1}, $Q = 9.6$, $0.70 < \Phi < 0.81$). Equation 9 gave $M_r = 139.1 \pm 0.7$. Gran titration of ca. 0.1 M solutions obtained by dissolving weighed amounts of the salt in 0.5 M KCl yielded $M_r = 138.6$, a value accounted for by a larger amount of water than the theoretical value. The difference is in good agreement with the value of −0.5% for the systematic error calculated with Eqn. 15 for $C_2 = 10^{-1.4}$ mol l^{-1}, $\Phi = 0.80$.

The determination of strong and weak acids by subtraction from standard base is equivalent in principle. However, alkaline errors of glass electrodes and unpredictable contamination of standard strong base by carbonate make the sample subtraction method perform less well than in the case of the model systems discussed so far. Therefore, the determination of acids has not been thoroughly investigated in this work. However, standard subtraction after calibration by double sample addition [7] can be used as an alternative procedure, able to avoid these difficulties.

Conclusions

Theory and experiments have shown that the method of sample subtraction after in situ calibration by two additions of standard can yield very good accuracy and very high precision in the determination of strong and moderately weak bases by subtraction from standard strong acid, provided that the calibration ratio of the primary ion and the reaction ratio between analyte and primary ion are properly set. Calibration over about 0.5–1 decade of primary ion concentration is advisable. The reaction ratio required for optimization, $\Phi = 0.8$–0.95, is easily met for repetitive samples or after a trial. The short time required for each experiment makes repeated determinations easier, thus helping the statistical evaluation of analyses. With strong or moderately weak bases, the only limit to the application of the method is set by the sample concentration, which must allow the initial concentration C_1 of standard acid in the measured solution to be

larger than about 10^{-4} mol l^{-1}, while satisfying the condition $C_x \gg C_2 \approx (5\text{–}10)C_1$. The results deteriorate only moderately when the temperature and ionic strength are not kept constant; control of these parameters is needed only when the highest accuracy is wanted. With very weak bases, the requirement for quantitative reaction causes the range of application of the method to be narrower; however, the results can still be acceptable when rapidity is a primary requirement.

This variation of the potentiometric sample subtraction method is capable of approaching Gran titration in both accuracy and precision. It compares favourably with the automatic potentiometric titration of base with strong acid using a differential end-point, which are easily affected by systematic and random errors due to contamination of the base by carbon dioxide. It is only moderately superior in theoretical precision to the ordinary sample subtraction; the sample principles hold for optimization of both procedures with systems that give a Nernstian response, the existence of which, the modified procedure offers direct verification.

Owing to the high quality of the results, the method is currently being used for standardizing solutions of strong bases to be used as acidimetric titrants, in place of Gran titration; the latter, however, remains the reference method, also used for controlling the extent of carbonation of bases. Programmable titrators are available whose software is suitable for performing automatically all the steps of the modified sample subtraction procedure, including calculations [11].

APPENDIX I

The expressions of the theoretical precision for three different analytical procedures are obtained on the assumption that volume error and dilution are negligible [in practice, in order that E^* (Eqn. 1) is constant through the additions, it is advisable that all the added volumes are small, although not necessarily negligible, with respect to V_0]. By neglecting dilution, the concentration of the analyte in the measuring cell, C_b, can be expressed by the approximate form of Eqn. 18:

$$C_b = C_x V_3/(V_0 + V_1 + V_2 + V_3) \approx C_2 - C_3 \quad (18)$$

and the titration ratio Φ by the approximate Eqn. 19:

$$\Phi = C_b/C_2 \approx (C_2 - C_3)/C_2 \quad (19)$$

Modified sample subtraction

The dependence of the uncertainty dC_b of the calculated value of analyte concentration in the measuring cell, C_b (Eqn. 18), on the uncertainties of the measured values of e.m.f., dE_1, dE_2 and dE_3, is obtained by applying the equation

$$dC_b^2 = \left(\frac{\partial C_b}{\partial E_1}\right)^2 dE_1^2 + \left(\frac{\partial C_b}{\partial E_2}\right)^2 dE_2^2 + \left(\frac{\partial C_b}{\partial E_3}\right)^2 dE_3^2 \quad (20)$$

to the explicit form of the approximate Eqn. 21:

$$C_b \approx C_2 - C_3 = C_2 - C_2\ \text{antilog}\left(\frac{E_3 - E_2}{S}\right) = C_2\left\{1 - \text{antilog}\left[\frac{E_3 - E_2}{E_2 - E_1}\log\left(\frac{C_2}{C_2}\right)\right]\right\} \quad (21)$$

If it is assumed that the experimental uncertainty of the measured e.m.f. is independent of E, i.e., $dE_1 = dE_2 = dE_3 = dE$, the uncertainty affecting C_b is given by

$$dC_b^2 = \left(\frac{C_3 \ln 10\, dE}{S}\right)^2 \times \frac{(\log C_2/C_1)^2 + (\log C_3/C_1)^2 + (\log C_3/C_2)^3}{(\log C_2/C_1)^2} \quad (22)$$

The relative uncertainties of C_b and C_x are identical. By using Eqn. 19, both of them are expressed by the equation

$$\frac{dC_x}{C_x} = \frac{dC_b}{C_b} = \frac{1-\Phi}{\Phi}\frac{dE \ln 10}{S} \times \frac{[(\log C_2/C_1)^2 + (\log C_3/C_1)^2 + (\log C_3/C_2)^2]^{1/2}}{(\log C_2/C_1)} \quad (23)$$

or, by using also Eqn. 6, by the equation

$$\frac{dC_x}{C_x} = \frac{dC_b}{C_b} = \frac{1-\Phi}{\Phi}\frac{dE \ln 10}{S} \times \frac{[(\log Q)^2 + [\log Q(1-\Phi)]^2 + [\log(1-\Phi)]^2]^{1/2}}{\log Q} \quad (23')$$

Ordinary sample subtraction

In the usual sample subtraction procedure [1,2], a single measurement of e.m.f. in a standard solution is followed by the subtraction of sample in the same solution. The slope of the electrode response, S, is either determined separately by two or more measurements in standard solutions, or the theoretical value is used. For comparison with the modified procedure, the independent evaluation of S (Eqn. 24) is assumed to be done by measurement of E_1' and E_2' in two separate standard solutions at C_1 and C_2, the more concentrated solution having the same concentration as the measured solution before subtraction of sample (all subscripts are chosen to be the same as those of the corresponding steps of the modified sample subtraction; however, the e.m.f. E_2' of the calibration solution at concentration C_2 can be experimentally different from E_2 of the measured solution at the same concentration):

$$S = \frac{E_2' - E_1'}{\log(C_2/C_1)} \quad (24)$$

The uncertainty of the slope is

$$dS^2 = \frac{2\,dE^2}{[\log(C_2/C_1)]^2} = \frac{2\,dE^2}{(\log Q)^2} \quad (25)$$

By indicating with E_3 the e.m.f. measured after subtraction of the sample at concentration C_x, the uncertainty dC_b of the analyte concentration in the measured solution is obtained from

$$dC_b^2 = \left(\frac{\partial C_b}{\partial E_3}\right)^2 dE_3^2 + \left(\frac{\partial C_b}{\partial E_2}\right)^2 dE_2^2 + \left(\frac{\partial C_b}{\partial S}\right)^2 dS^2 \quad (26)$$

By using the form of Eqn. 21 containing S, Eqns. 27 and (with Eqn. 19) 28 are obtained:

$$dC_b^2 = \left(\frac{C_3 \ln 10}{S}\right)^2 \left\{2\,dE^2 + [dS \log(C_3/C_2)]^2\right\} \quad (27)$$

$$\frac{dC_x}{C_x} = \frac{dC_b}{C_b} = \frac{1-\Phi}{\Phi}\frac{\ln 10}{S} \times \left\{2\,dE^2 + [dS \log(1-\Phi)]^2\right\}^{1/2} \quad (28)$$

Direct potentiometry

Direct potentiometry commonly makes use of three independent measurements of e.m.f.: two calibration points in separate standard solutions (C_1, E_1; C_2, E_2) followed by a measurement of E_3 of the sample solution at some intermediate concentration $C_3 = C_b = C_x$ (the primary ion also being the analyte). The analyte concentration being calculated with the equation

$$C_x = C_2 \,\text{antilog}\left[\frac{E_3 - E_2}{E_2 - E_1}\log\left(\frac{C_2}{C_1}\right)\right] \quad (29)$$

the uncertainty dC_x is calculated with Eqn. 31, obtained from Eqn. 30:

$$dC_x^2 = \left(\frac{\partial C_x}{\partial E_1}\right)^2 dE_1^2 + \left(\frac{\partial C_x}{\partial E_2}\right)^2 dE_2^2 + \left(\frac{\partial C_x}{\partial E_3}\right)^2 dE_3^2 \quad (30)$$

$$\frac{dC_x}{C_x} = \frac{dE \ln 10}{S} \times \frac{[(\log C_2/C_1)^2 + (\log C_x/C_1)^2 + (\log C_x/C_2)^2]^{1/2}}{(\log C_2/C_1)} \quad (31)$$

For the comparison of direct potentiometry with the two subtraction procedures, Φ is defined as

$\Phi = C_x/C_2$, and therefore, using Eqn. 6, Eqn. 31′ is obtained:

$$\frac{dC_x}{C_x} = \frac{dE \ln 10}{S} \frac{[(\log Q)^2 + (\log \Phi Q)^2 + (\log \Phi)^2]^{1/2}}{(\log Q)} \quad (31')$$

APPENDIX II

Equation 3 depends on the hypothesis that the sample base B reacts quantitatively with the strong acid HA, as expressed by the balance

$$[H^+] = C_3 = C_a - C_b \approx C_2 - C_b \quad (32)$$

where C_a ($\approx C_2$) and C_b (Eqn. 18) are respectively the concentrations of the reactant and of the analyte prevailing when E_3 is measured; approximations arise from neglecting dilution. By using the approximate expression of Φ (Eqn. 19), $[H^+]$ can be written as

$$[H^+] \approx C_2(1 - \Phi) = C_b[(1 - \Phi)/\Phi] \quad (33)$$

When the reaction

$$B + H^+ \rightarrow HB$$

(charges are omitted for generalization) is not quantitative, the unreacted weak base causes a systematic relative error

$$\epsilon \approx [B]/C_b \quad (34)$$

By using the equations

$$C_b = [HB] + [B] \quad (35)$$

and

$$[H^+][B]/[HB] = K_a \quad (36)$$

the following equation is obtained as the expression of ϵ:

$$\epsilon = -K_a/([H^+] + K_a) \quad (37)$$

Substitution of Eqn. 33 for $[H^+]$ in Eqn. 37 does not affect ϵ substantially; therefore,

$$\epsilon = -\frac{K_a}{K_a + C_2(1 - \Phi)} = -\frac{K_a}{K_a + C_b(1 - \Phi)/\Phi} \quad (38)$$

In the range of application of the method, the condition $[H^+] \gg K_a$ generally holds; therefore, the simpler form Eqn. 15 (see Principles) or 15′ of Eqn. 38 is adequate:

$$\epsilon \approx -K_a\Phi/[C_b(1 - \Phi)] \quad (15')$$

Helpful discussions with Giorgio G. Bombi are gratefully acknowledged. This work was partially supported by CNR, grant 91.03156.CT03.

REFERENCES

1 M. Mascini, Ion-Sel. Electrode Rev., 2 (1980) 17.
2 D. Midgley, Analyst, 112 (1987) 557.
3 D. Midgley and K. Torrance, Potentiometric Water Analysis, Wiley, Chichester, 2nd edn., 1991.
4 J. Koryta and K. Štulík, Ion-Selective Electrodes, Cambridge University Press, Cambridge, 2nd edn., 1983.
5 G.J. Moody and J.D.R. Thomas, Lab. Pract., 28 (1979) 125.
6 S. Ebel and U. Becht, Fresenius' Z. Anal. Chem., 320 (1987) 117.
7 D. Midgley, Analyst, 113 (1988) 997.
8 C. Maccà, Fresenius' Z. Anal. Chem., 326 (1987) 559.
9 G. Gran, Analyst, 77 (1952) 661.
10 F.J.C. Rossotti and H. Rossotti, J. Chem. Educ., 42 (1956) 375.
11 Titrilab Reference Manual; Titrilab Operators Handbook, Radiometer Analytical, Bagvaerd, Denmark.

Analytica Chimica Acta, 273 (1993) 511–519
Elsevier Science Publishers B.V., Amsterdam

Automated iodimetric determination of Cu^{+}, Cu^{2+} and Cu^{3+} in the superconductor YBCO using a modified Gran plot technique

Jan Yperman, An De Backer, Ann Vos, Dirk Franco, Jules Mullens and Lucien C. Van Poucke

Laboratory of Inorganic and Physical Chemistry, Limburgs Universitair Centrum, B-3590 Diepenbeek (Belgium)

(Received 1st June 1992)

Abstract

An automated potentiometric determination of the oxygen content of the superconductor YBCO is described. The end-point of the titration is found using a linear Gran plot technique. Suitable equations are derived by which the number of titration points can be considerably reduced and the titration can be stopped even before the equivalence point is reached. Automation of the iodimetric titration can be performed in an easy manner. During the titration a good estimate of the equivalence volume can be calculated using only two titration points.

Keywords: Potentiometry; Titrimetry; Copper; Gran plots; Iodimetry; Superconductors; YBCO superconductor

The non-stoichiometry of the superconductor YBCO is usually explained by the presence of Cu^{3+}. The determination of Cu^{3+} is carried out using iodimetric titration [1]. A number of papers have been published [2–8] concerning the iodimetric determination of the total Cu content and the amount of Cu^{2+} and Cu^{3+} present in YBCO superconductor. Mostly, the titrations are carried out in a manual or semi-automatic way. The end of the titration is found visually by adding starch indicator just before the equivalence point [2–7]. In one instance [8], using a semiautomatic titration system, the titration is executed until a preset equivalence potential. Mostly the total amount of Cu, Y and Ba is not determined, assuming that these amounts are equal to those in the starting material, e.g., CuO, $BaCO_3$ and Y_2O_3. However, this can be questioned. The determination of all three components Y, Ba and Cu seems to be necessary for defining the oxygen content in the superconductor [9,10].

When classical titration techniques are used, the determination of the equivalence point has always been criticized, because in the neighbourhood of the equivalence point a great relative change in concentration and potential occurs. These potentials are often unstable, which may lead to a less accurate determination of the end-point of the titration based on first or second derivative when the potential jump is not very large. Gran [11] avoided this problem by using titration points at the beginning or end of the titration. These points are better defined and more accurate and, if all conditions are fulfilled (high ionic strength and constancy of temperature), a correct equivalence point can be calculated using the well known Gran plots [12,13].

In this work, a modified version of this technique was used in order to calculate the exact equivalence point of each iodimetric titration.

Correspondence to: J. Yperman, Laboratory of Inorganic and Physical Chemistry, Limburgs Universitair Centrum, B-3590 Diepenbeek (Belgium).

For each sample, the amount of Cu^{2+}, Cu^{3+} or Cu^{+} and the total Cu content can be determined using two different titration conditions. During each titration, a good estimate of the equivalence volume can be calculated from only two titration points. This estimate is used as a criterion to stop the titration even before the end-point is reached.

EXPERIMENTAL

Reagents and solutions

All chemicals were of analytical-reagent grade. Deionized, doubly distilled water was used to prepare stock solutions of $Na_2S_2O_3$, $KBrO_3$, KI and HCl.

Superconducting materials were made in the laboratory as described previously [9,10,14].

Preparation of $NaCuO_2$

The preparation of $NaCuO_2$ has been reported by several workers [15–17]. It was prepared by heating a mixture of Na_2O_2 (> 95%) (Janssen) and CuO (> 96%) (Merck) for 48 h under flowing oxygen at 450°C. A compound containing about 91% of Cu^{3+} was obtained.

Apparatus

All the components of the measurement system are enclosed in a thermostated box maintained at 20.0 ± 0.2°C (see Fig. 1).

The electrodes used are a platinum indicator electrode and an Ingold Argenthal reference electrode (type 363-57) with saturated KCl reference electrolyte, placed in a secondary function chamber with a ceramic diaphragm (type 303-95) filled with 1.5 M KNO_3 solution. The potential difference is measured with a Radiometer PHM 84 precision digital potentiometer. Oxygen-free nitrogen gas is blown into and over the titration solution in order to work in an inert atmosphere.

Three motor-driven Schott T 100 burettes with interchangeable standard cylinder units are used. Burette No. 1, equipped with an anti-diffusion titration tip, contains a freshly prepared $S_2O_3^{2-}$ solution (ca. 0.03 M), burette No. 2, also equipped

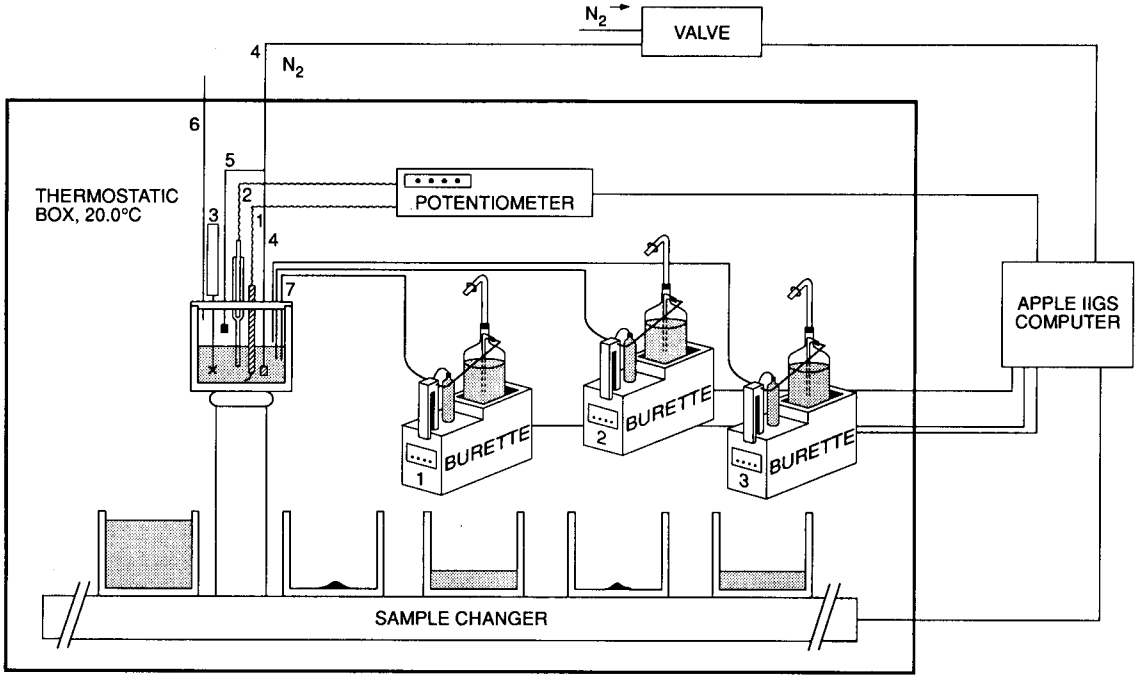

Fig. 1. Apparatus for iodimetric determination. 1 = Pt electrode; 2 = reference electrode; 3 = mechanical stirrer; 4 and 5 = N_2 gas inlets; 6 = gas outlet; 7 = burette tips. Burette contents: No. 1 = ca. 0.03 M $Na_2S_2O_3$ solution; No. 2 = 1.5 M KNO_3 solution; No. 3 = 2.0 M HCl.

with an anti-diffusion titration tip in the solution, contains 0.7 M KI solution and burette No. 3, with a titration tip just above the solution, contains 2.0 M HCl.

The different sample beakers are placed on a Metrohm 624.0030 sample changer and sequentially rotated to the measurement position. All the equipment is controlled by an Apple II GS microcomputer. Specific programs for monitoring the potentiometer, the burettes, the stirrer, the sample changer and the gas inlet system are written in UCSD-Apple Pascal with incorporated UCSD-Apple-Assembler 6502 subroutines. Data handling, evaluation and presentation are carried out by the same program.

Titration procedures and equations

According to Harris and co-workers [6,7] the following modified procedures are followed.

Method A. About 25 mg of YBCO sample are dissolved in 20 ml of 0.7 M HCl and gently boiled for 10 min. After cooling the solution to room temperature, the amount of solution is readjusted to 20 ml by adding the appropriate volume of 0.7 M HCl. The following reaction occurs:

$$2Cu^{3+} + H_2O \longrightarrow 2Cu^{2+} + 1/2O_2 \uparrow + 2H^+ \quad (1)$$

After this procedure, the sample is placed on the sample changer. The procedure is automatically continued when the beaker is rotated to the measurement position by adding from burette No. 2 20 ml of 0.7 M KI solution under a stream of oxygen-free nitrogen bubbling in and above the solution. Then the following reaction takes place:

$$2Cu^{2+} + 5I^- \longrightarrow 2CuI \downarrow + I_3^- \quad (2)$$

While stirring, after equilibration of the electrode pair, the titration with $S_2O_3^{2-}$ is automatically started. Here the following reaction has to be considered:

$$I_3^- + 2S_2O_3^{2-} \longrightarrow S_4O_6^{2-} + 3I^- \quad (3)$$

Method B. About 25 mg of YBCO are weighed into a dry beaker and placed on the sample changer. At the measurement position, 30 ml of 0.7 M KI are added from burette No. 2 automatically under a stream of oxygen-free nitrogen. While stirring, 20 ml of 2.0 M HCl are added by burette No. 3. It was found that two separate solutions of KI and HCl give better results. In addition to reaction 2, the following reaction also occurs:

$$Cu^{3+} + 4I^- \longrightarrow CuI \downarrow + I_3^- \quad (4)$$

After electrode equilibration and after dissolution of the sample, which takes only a few minutes, the titration with the thiosulphate solution starts automatically. In both procedures, one assumes that Cu is present as Cu^{2+} and Cu^{3+}. If, instead of Cu^{3+}, Cu^+ is present, according to method A, the following reaction occurs instead of reaction 1:

$$2Cu^+ + 2H^+ + 1/2O_2 \longrightarrow 2Cu^{2+} + H_2O \quad (5)$$

According to method B, in addition to reaction 2, the following reaction has to be considered:

$$Cu^+ + I^- \longrightarrow CuI \downarrow \quad (6)$$

According to reactions 4 and 6, a different amount of $S_2O_3^{2-}$ will be found and thus a distinction can be made between the two oxidation states of copper. If the amount of I_3^- formed according to method A is a mol and according to method B it is b mol, then

$$a = \text{total moles of Cu}/2 \quad (7)$$

If only Cu^{3+} and Cu^{2+} are present, then it follows that

$$b = (\text{moles of } Cu^{2+}/2) + \text{moles of } Cu^{3+} \quad (8)$$

and if only Cu^+ and Cu^{2+} are present, then

$$b = \text{moles of } Cu^{2+}/2 \quad (9)$$

From Eqns. 7 and 8, the amount of Cu^{2+} and Cu^{3+} can be calculated:

$$\text{moles } Cu^{2+} = 2(2a - b) \quad (10)$$

$$\text{moles } Cu^{3+} = 2(b - a) \quad (11)$$

From Eqns. 7 and 9, the amount of Cu^{2+} and Cu^+ can be calculated:

$$\text{moles } Cu^{2+} = 2b \quad (12)$$

$$\text{moles } Cu^+ = 2(a - b) \quad (13)$$

If both Cu^{3+} and Cu^+ are present, only the difference between Cu^{3+} and Cu^+ is found.

Before the samples are analysed, the thiosulphate solution is standardized against $KBrO_3$. This titration is also executed automatically once at the beginning and once at the end of the analyses. No difference in $S_2O_3^{2-}$ concentration was found.

Determination of the end-point

Determination of the concentration of the $S_2O_3^{2-}$ solution. Before the equivalence point, the potential of the platinum electrode in each iodimetric titration is determined by the following half-cell reaction:

$$I_3^- + 2e \longrightarrow 3I^- \tag{14}$$

resulting in

$$E = E^0_{I_3^-/I^-} + \frac{RT}{2F}\ln\left(\frac{a_{I_3^-}}{a^3_{I^-}}\right) + E_j \tag{15}$$

where $E^0_{I_3^-/I^-}$ is the reduction potential under standard conditions, E_j the diffusion potential and $a_{I_3^-}$ and a_{I^-} the activities of the species I_3^- and I^-, respectively. Instead of activities, it is more convenient to use molar concentrations. Equation 15, then becomes

$$E = E^0_{I_3^-/I^-} + \frac{RT}{2F}\ln\left(\frac{[I_3^-]}{[I^-]^3}\right) + \frac{RT}{2F}\ln\left(\frac{f_{I_3^-}}{f^3_{I^-}}\right) + E_j \tag{16}$$

where $f_{I_3^-}$ and f_{I^-} are the activity coefficients of the species I_3^- and I^-, respectively. As the titration is executed in a solution of high ionic strength and the temperature is held constant (thermostated box, mechanical instead of magnetic stirring), the variables $E^0_{I_3^-/I^-}$, $f_{I_3^-}$, f_{I^-} and E_j can be considered as being constant [11–13]. Therefore, a new function E′ is defined as

$$E' = E^0_{I_3^-/I^-} + \frac{RT}{2F}\ln\left(\frac{f_{I_3^-}}{f^3_{I^-}}\right) + E_j \tag{17}$$

E' is constant under the conditions cited above and Eqn. 16 reduces to

$$E = E' + \frac{RT}{2F}\ln\left(\frac{[I_3^-]}{[I^-]^3}\right) \tag{18}$$

Here the concentration of I^- for each titration point is given by the equation

$$[I^-] = \frac{C_{0,I^-}V_{I^-}}{V_0 + V} \tag{19}$$

where C_{0,I^-} is the molar concentration of the KI solution in burette No. 2, V_{I^-} is the corresponding added volume, V is the volume of thiosulphate added during the titration and V_0 is equal to the sum of volumes: V_{I^-}, $V_{BrO_3^-}$ (the pipetted volume of the standard solution of BrO_3^- with molar concentration C_{0,BrO_3^-}) and $V_{H_2SO_4}$ (the volume of dilute H_2SO_4).

As a function of the progress of the titration, the concentration of I_3^- is given by the equation

$$[I_3^-] = \frac{C_{0,I_3^-}V_0}{V_0 + V} - \frac{2C_{0,S_2O_3^{2-}}V}{V_0 + V} \tag{20}$$

where C_{0,I_3^-} and $C_{0,S_2O_3^{2-}}$ are the starting molar concentration of I_3^- and the molar concentration of $S_2O_3^{2-}$ in burette No. 1, respectively.

At the equivalence point, the following equation is valid:

$$C_{0,I_3^-}V_0 = 2C_{0,S_2O_3^{2-}}V_{eq} \tag{21}$$

where V_{eq} is the equivalence volume. Substitution of Eqn. 21 in Eqn. 20 results in

$$[I_3^-] = 2C_{0,S_2O_3^{2-}}\frac{V_{eq} - V}{V_0 + V} \tag{22}$$

So far $C_{0,S_2O_3^{2-}}$ is still unknown, so Eqn. 22 needs to be expressed as a function of C_{0,BrO_3^-}. The amount of BrO_3^- as a function of the amount of I_3^- can be expressed by the equation

$$3C_{0,BrO_3^-}V_{BrO_3^-} = C_{0,I_3^-}V_0 \tag{23}$$

Combining Eqns. 21 and 23 with Eqn. 20 results in

$$[I_3^-] = \frac{3C_{0,BrO_3^-}V_{BrO_3^-}}{V_0 + V}(1 - V/V_{eq}) \tag{24}$$

Substitution of Eqns. 24 and 19 in Eqn. 18 gives, after some rearrangements,

$$\frac{3C_{0,BrO_3^-}V_{BrO_3^-}(1 - V/V_{eq})(V_0 + V)^2}{(C_{0,I^-}V_{I^-})^3} = \exp[2F(E - E')/RT] \tag{25}$$

By putting $3C_{0,BrO_3^-}V_{BrO_3^-}/(C_{0,I^-}V_{I^-})^3$ equal to Q and by rearranging the terms, the following equation is obtained:

$$\frac{\exp(2FE/RT)}{Q(V_0+V)^2} = \exp(2FE'/RT) - \frac{V}{V_{eq}}\exp(2FE'/RT) \quad (26)$$

This equation, a typical Gran plot expression [11–13], is of the form $y = b - ax$. By plotting $\exp(2FE/RT)/[Q(V_0+V)^2]$ versus V, a linear relationship is found.

When V becomes equal to V_{eq}, y or $\exp(2FE/RT)/[Q(V_0+V)^2]$ becomes zero. Therefore by a simple linear extrapolation technique, using a number of titration points before the equivalence point, V_{eq} can be easily deduced. Equation 26 can be used by the computer program for the automated titration in order to calculate a good estimate of the correct equivalence point by using only two titration points. Indeed, being these points (potential E_1, volume V_1) and (potential E_2, volume V_2), then after some manipulations

$$V_{eq} = \frac{R_2V_1 - V_2R_1}{R_2 - R_1} \quad (27)$$

with $R_i = \exp(2FE_i/RT)/[Q(V_0+V_i)^2]$ for $i = 1$ or 2.

During the titration, in order to compare the amount of added thiosulphate solution with the volume needed to reach the equivalence point, this point (V_{eq}) is calculated after each addition of titrant. If the next amount of thiosulphate is to be added and if the sum of added volumes is greater than the equivalence volume, the titration is stopped even before this last addition took place (see Tables 1, 3 and 5).

It is also found that only a few titration points are needed in order to calculate the correct equivalence point. For example, for a titration containing 32 titration points before the equivalence point and using Eqn. 26, V_{eq} was found to be 4.072 ml of $S_2O_3^{2-}$ with a correlation coefficient (r) of 0.99986. With half the number of titration points (i.e., instead of titration points each 0.100 ml, the titration points were taken every 0.200 ml starting from 1.0 ml of $S_2O_3^{2-}$ added), the equivalence volume now calculated was 4.070 ml, with $r = 0.99986$. Reducing again the number of titration points to 8 (so every 0.400 ml), $V_{eq} = 4.070$ ml with $r = 0.99984$. From this, it can be deduced that with five or six titration points before the equivalence volume, a very good value for the volume of the equivalence point can be obtained.

To be correct, Eqn. 19 needs to be rectified not only for the amount of I^- that is reacting according reaction 3, but also for the reaction of I^- with $KBrO_3$. If this is done, the following equation is found:

$$[I^-] = \frac{C_{0,I^-}V_{I^-}}{V_0+V} - \frac{9C_{0,BrO_3^-}V_{BrO_3^-}}{V_0+V} + \frac{6C_{0,S_2O_3^{2-}}V}{V_0+V} \quad (28)$$

On substituting Eqns. 21 and 23 in Eqn. 28, one obtains, after some rearrangements,

$$[I^-] = \frac{C_{0,I^-}V_{I^-}}{V_0+V} - \frac{9C_{0,BrO_3^-}V_{BrO_3^-}}{V_0+V}(1 - V/V_{eq}) \quad (29)$$

It is clear that the greater V becomes, the smaller the second term of Eqn. 29 will be. It is also found that the first titration points cannot be used in Eqn. 26 (the potential of the platinum electrode did not change much), and this happens to be the area where the greatest corrections in Eqn. 29 are to be made. Substituting Eqns. 29 and 24 in Eqn. 18 results, after some rearrangements, in

$$\frac{\left[C_{0,I^-}V_{I^-} - 9C_{0,BrO_3^-}V_{BrO_3^-}(1 - V/V_{eq})\right]^3}{3C_{0,BrO_3^-}V_{BrO_3^-}(V_0+V)^2} \times \exp(2FE/RT) = \exp(2FE'/RT) - \frac{V}{V_{eq}}\exp(2FE'/RT) \quad (30)$$

This is again an equation of the form $y = b - ax$. By plotting y versus x, i.e., V, one can find V_{eq}. However, one needs an estimate of V_{eq} for calculating y. This estimate is calculated by extrapola-

tion of Eqn. 26 and an iteration procedure. It is found that this iteration converges very fast.

Method A. According to reaction 2, by neglecting the amounts of I^- that are reacting or being formed, one finds Eqn. 19. However, now V_0 is equal to the sum of V_{I^-} and V_{HCl}, where V_{HCl} is the volume of HCl added by burette No. 3. The amount of I_3^- is given by Eqn. 20. Because the concentration of $S_2O_3^{2-}$ is already known, Eqn. 20 can now be converted into a form which is a function of $C_{0,S_2O_3^{2-}}$ instead of C_{0,BrO_3^-}. This results in Eqn. 22. Substituting Eqns. 22 and 19 in Eqn. 18, and rearranging the terms, results in

$$\frac{(C_{0,I^-}V_{I^-})^3}{2C_{0,S_2O_3^{2-}}(V_0+V)^2}\exp(2FE/RT) = V_{eq}\exp(2FE'/RT) - V\exp(2FE'/RT) \quad (31)$$

Again a linear equation of the form $y = b - ax$ is obtained. By plotting y versus x, i.e. V, y becomes zero when V tends to V_{eq}. Eqn. 31 can be converted into Eqn. 27 in order to calculate, during the titration, a good estimate of the real equivalence point by using only two titration points. Therefore, the same procedure is followed as described in the previous section. Using experimental data, it is found that no corrections ought to be made for the amount of I^- that is reacting and is being reformed with a more extended equation like Eqn. 30, i.e.,

$$[I^-] = \frac{C_{0,I^-}V_{I^-}}{V_0+V} - \frac{C_{0,S_2O_3^{2-}}V_{eq}}{V_0+V} - \frac{(3/2)C_{0,S_2O_3^{2-}}(V_{eq}-V)}{V_0+V} \quad (32)$$

resulting in

$$\frac{\left\{C_{0,I^-}V_{I^-} - C_{0,S_2O_3^{2-}}\left[(5/2)V_{eq} - (3/2)V\right]\right\}^3}{2C_{0,S_2O_3^{2-}}(V_0+V)^2}\times\exp(2FE/RT) = V_{eq}\exp(2FE'/RT) - V\exp(2FE'/RT) \quad (33)$$

The same V_{eq} is calculated as found by Eqn. 31 using the same iteration procedure as in the case of Eqn. 30.

Method B. The same conclusions can be derived as for method A.

RESULTS AND DISCUSSION

The program for the automatic analysis of YBCO samples is written in such a way that the following procedure is executed. After automatic rinsing of the burettes and the measurement equipment with water, first the $S_2O_3^{2-}$ solution is standardized using BrO_3^-. Then the YBCO samples are subsequently investigated according to methods A and B. Between each determination, the measurement equipment is cleaned with water. No cross-contamination between solutions was found. If all the samples are analysed, again the thiosulphate solution is standardized using BrO_3^-. No difference was found between the two determinations, although the analyses of all samples can take hours.

Standardization of thiosulphate solution

In Table 1 the experimental results of a standardization titration according to the described method are given. As can be seen, the first two added volumes of $S_2O_3^{2-}$ are large. It was found that the first three titration points could not be used by Eqn. 26, because a non-linear relationship was found. Therefore titration points 0 and 1 result in a meaningless value of V_{eq}. Using titration points 1 and 2, the estimate of V_{eq} is only a

TABLE 1

Results of titration of BrO_3^- with $S_2O_3^{2-}$

Titration point	$S_2O_3^{2-}$ added (ml)	Measured potential (mV)	Estimated V_{eq} (Eqn. 27) (ml)
0	0.00	−330.2	–
1	5.00	−325.3	–
2	7.50	−317.8	10.12
3	7.90	−315.6	9.86
4	8.30	−312.9	9.90
5	8.70	−309.5	9.91
6	9.10	−304.5	9.91
7	9.50	−296.1	9.91
8	9.90	−254.8	9.92

TABLE 2

Cu^{2+} and Cu^{3+} determination in $NaCuO_2$

Sample	Cu_{Total} (mmol)	Cu^{2+} (mmol)	Cu^{3+} (mmol)	Cu^{3+} (%)	O_{active} : Cu ratio
1	0.008256	0.000665	0.007592	92.0	1.46
2	0.008292	0.000725	0.007567	91.3	1.46
3	0.008426	0.000720	0.007707	91.5	1.46
Mean	0.008325	0.000703	0.007622	91.6	1.46
S_x [a]	0.00009	0.00003	0.00007	0.4	–

[a] Standard deviation.

good indicator for the real V_{eq}. The added amounts of 5.00 ml for the first and 2.50 ml for the second titration point are so chosen because no linear Gran plot relationship could be obtained between 0.00 and 7.50 ml and because the expected equivalence volume is greater than 9.00 ml. Hence, starting from titration point 3 good estimates of the equivalence volume can be calculated, as shown in Table 1. From titration point 2, very good estimates of V_{eq}, using Eqn. 27, can be calculated using only two titration points. Using Eqn. 26 and the five last titration points, V_{eq} is found to be 9.91 ml with a correlation coefficient of 0.99985 and resulting in a concentration of $S_2O_3^{2-}$ of 0.03026 M [$C_{0,BrO_3^-} = (1/6) \times 0.0300$ M). The same concentration of $S_2O_3^{2-}$ is found with the second titration of the BrO_3^- solution at the end of the analyses.

Determination of Cu^{3+} compounds

$NaCuO_2$ compounds were prepared in order to test and optimize the above-described iodimetric method. In Table 2 the results are given of the analysis of a sample containing about 91% of Cu^{3+}. The amounts of Cu_{Total}, Cu^{2+} and Cu^{3+} are always normalized, so comparison between the results is possible.

In Table 3 an example of the experimental titration data according to methods A and B is shown. The amounts of sample used in methods A and B were 26.0 and 25.3 mg, respectively.

From Table 3, for both methods A and B, the first added amounts of $S_2O_3^{2-}$ are large. Also in this instance it was found that at the start of this type of titration only small changes in the potential of the electrode pair are measured when small amounts of $S_2O_3^{2-}$ are added. The three first data points could not be used in Eqn. 31, because no linear Gran plot relationship exists for these points. Therefore, added volumes of 1.50 ml for the first point and 0.50 ml for the second point were chosen as a standard in these

TABLE 3

Results with method A (Eqn. 31 using the last five titration points), $V_{eq} = 7.21$ ml and $r = 0.999798$ and with method B (Eqn. 31 using the last five titration points), $V_{eq} = 13.46$ ml and $r = 0.999993$

Method	Titration point	$S_2O_3^{2-}$ added (ml)	Measured potential (mV)	Estimated V_{eq} (Eqn. 27) (ml)
A	0	0.00	−313.1	–
	1	1.50	−311.1	–
	2	2.00	−310.3	7.58
	3	2.70	−308.8	7.21
	4	3.40	−307.1	7.32
	5	4.10	−304.8	7.12
	6	4.80	−302.0	7.20
	7	5.50	−298.0	7.21
	8	6.20	−291.7	7.21
	9	6.90	−277.3	7.22
B	0	0.00	−308.9	–
	1	1.50	−308.2	–
	2	2.00	−307.9	14.44
	3	3.00	−307.3	14.12
	4	4.00	−306.5	13.87
	5	5.00	−305.6	14.14
	6	6.00	−304.4	13.70
	7	7.00	−303.0	13.55
	8	8.00	−301.4	13.68
	9	9.00	−299.2	13.37
	10	10.00	−296.3	13.45
	11	11.00	−292.4	13.47
	12	12.00	−286.2	13.47
	13	13.00	−272.2	13.47

TABLE 4

Cu^{2+} and Cu^{3+} determination in a YBCO sample

Sample	Cu_{Total} (mmol)	Cu^{2+} (mmol)	Cu^{3+} (mmol)	Cu^{3+} (%)	O_{active} : Cu ratio
1	0.005304	0.004117	0.001186	22.4	1.11
2	0.005371	0.004248	0.001123	20.9	1.10
3	0.005319	0.004054	0.001265	23.8	1.12
Mean	0.00533	0.00414	0.00119	22.4	1.11
S_x [a]	0.00004	0.00006	0.00007	1.5	0.01

[a] Standard deviation.

types of titrations. Only the data points starting from 2.00 ml of $S_2O_3^{2-}$ result in a linear form of Eqn. 31. The titrations were always performed with ca. 25 mg of sample and the amounts of Cu were calculated per mg of dry sample.

An important condition in method B is that one must ensure that the whole sample is dissolved. At the beginning of the automation some problems occurred when, in using a sample changer, mechanical stirring was needed instead of magnetic stirring. The sample dissolves much better with magnetic stirring. To overcome this problem, an extra waiting time for dissolution is built into the program. Also, the shape of the stirrer was changed so that better mixing of liquid and solid matter was obtained.

Determination of Cu in YBCO

In Table 4 the results are given of the analysis of a YBCO sample. In Table 5 an example of the experimental titration data according to methods A and B is shown. The amounts of sample used in methods A and B were 25.0 mg and 20.2 mg, respectively. It should be noted that the titration results in Table 5 were obtained on different amounts of YBCO sample, so the small difference in the calculated V_{eq} for the two methods is somewhat misleading.

There is some variation in the calculated percentages of Cu^{3+} presented in Table 4. However, the results for the O_{active} : Cu ratio, are reproducible. In almost all papers dealing with the oxygen content of YBCO superconductor these data are given. Nevertheless, it is believed that the results can be improved if the homogeneity of the samples can be optimized.

Again it is demonstrated that V_{eq} found using Eqn. 31 is not better than the results obtained with the simplified Eqn. 29.

Conclusion

A fully automatic system for precise iodimetric determination has been developed. Using a Gran plot technique, in order to determine the end-point, only a few titration points are needed for the determination of the equivalence point. Because of the automatic set-up, objectivity in the

TABLE 5

Results with method A (Eqn. 31 using the last five titration points), $V_{eq} = 4.47$ ml and $r = 1.00000$, and with method B (Eqn. 31 using the last five titration points), $V_{eq} = 4.42$ ml and $r = 0.999604$

Method	Titration point	$S_2O_3^{2-}$ added (ml)	Measured potential (mV)	Estimated V_{eq} (Eqn. 27) (ml)
A	0	0.00	−305.3	–
	1	1.50	−300.8	–
	2	2.00	−298.6	4.32
	3	2.40	−296.4	4.32
	4	2.80	−293.8	4.40
	5	3.20	−290.5	4.45
	6	3.60	−285.9	4.46
	7	4.00	−278.3	4.47
	8	4.40	−256.5	4.48
B	0	0.00	−290.5	–
	1	1.50	−286.1	–
	2	2.00	−284.0	4.53
	3	2.40	−281.9	4.46
	4	2.80	−279.3	4.48
	5	3.20	−275.9	4.42
	6	3.60	−271.0	4.42
	7	4.00	−262.5	4.41
	8	4.40	−223.2	4.42

end-point determination is ensured. A great number of titrations can be executed in an easy and fast manner.

REFERENCES

1 A.Y. Prokopchik and P.K. Norkus, Russ. J. Inorg. Chem., 4 (1959) 611.
2 J.H. Choy, S.Y. Choi, S.H. Byeon, S.H. Chun, S.T. Hong, D.Y. Jung, W.Y. Choe and Y.W. Park, Bull. Korean Chem. Soc., 9 (1988) 289.
3 J. Novák, P. Vyhlidka, D. Zemanová, E. Pollert and A. Triska, Physica C, 157 (1989) 346.
4 J.T.S. Irvine and C. Namgung, J. Solid State Chem., 87 (1990) 29.
5 E.H. Appelman, L.R. Morss, A.M. Kini, U. Geiser, A. Umezawa, G.W. Crabtree and K.D. Carlson, Inorg. Chem., 26 (1987) 3237.
6 D.C. Harris, M.E. Hills and T.A. Hewston, J. Chem. Educ., 64 (1987) 847.
7 D.C. Harris and T.A. Hewston, J. Solid State Chem., 69 (1987) 182.
8 P. Lanza and S. Rossi, Anal. Chim. Acta, 244 (1991) 253.
9 A. Vos, R. Carleer, J. Mullens, J. Yperman, J. Vanhees and L.C. Van Poucke, Eur. J. Solid State Inorg. Chem., 28 (1991) 657.
10 K. Leroy, J. Mullens, J. Yperman, J. Vanhees and L.C. Van Poucke, Thermochim. Acta, 136 (1988) 343.
11 G. Gran, Acta Chem. Scand., 4 (1950) 559.
12 F.J.C. Rossotti and H. Rossotti, J. Chem. Educ., 42 (1965) 375.
13 M. Mascini, Ion-Sel. Electrode Rev., 2 (1980) 17.
14 A. Vos, J. Mullens, R. Carleer, J. Yperman, J. Vanhees and L.C. Van Poucke, Bull. Soc. Chim. Belg., 10 (1992) 187.
15 J. Pickardt, W. Paulus, M. Schmalz and R. Schölhorn, J. Solid State Chem., 89 (1990) 308.
16 K. Hestermann and R. Hoppe, Z. Anorg. Allg. Chem., 367 (1969) 261.
17 N.E. Brese and M. O'Keeffe, J. Solid State Chem., 83 (1989) 1.

Analytica Chimica Acta, 273 (1993) 521–530
Elsevier Science Publishers B.V., Amsterdam

Triangle programmed coulometric flow titration with potentiometric and optical detection

Zsófia Fehér, Géza Nagy, István Slezsák, Klára Tóth and Ernö Pungor

Research Group for Technical Analytical Chemistry of the Hungarian Academy of Sciences, Institute for General and Analytical Chemistry, Technical University, Gellért tér 4, H-1521 Budapest (Hungary)

(Received 16th March 1992; revised manuscript received 6th August 1992)

Abstract

The application of a flow-through titration technique, the so-called triangle programmed coulometric titration, is presented for acid–base titrations using potentiometric and photometric detection. A flow-through capillary glass electrode–saturated calomel electrode pair was employed for potentiometric detection, and an indicator mixture and a light-emitting diode–phototransistor system was used for photometric detection. In photometric detection the precision of the end-point location was enhanced by the addition of a suitable mixture of Methyl Red and *m*-Cresol Purple acid–base colour indicators. The suitability of the technique was demonstrated for different acid–base titrations. As an example, the determination of the drug content of a nicotinic acid-containing experimental pharmaceutical preparation is described.

Keywords: Coulometry; Flow system; Potentiometry; Titrimetry; UV–Visible spectrophotometry; Nicotinic acid; Pharmaceuticals; Triangle programmed coulometric flow titration

Flow analytical techniques, especially the continuous-flow (CF) and flow-injection (FI) types, are now frequently applied to the analysis of different samples. Although methods employing titration for quantification are generally considered to be more reliable than those using direct detector signal-based evaluation, the application of flow titration is relatively rare.

Flow titrators used mainly for industrial monitoring often employ the feedback controller principle. The reagent influx is controlled by monitoring the instantaneous detector signal and comparing it with a preset value. The instantaneous reagent influx adjusted in this way is the measure of the sample mass flow [1,2]. The other type of flow titrators simply performs single-point titrations [3].

For obtaining a complete titration curve, the mass flow of the titrant has to be changed according to an exact, well defined time programme. The most convenient way to fulfil this requirement is with a linear increase in the mass flow of the titrant while the mass flow of the analyte is kept constant [4]. This is realized, for example, by applying a gradient flow for performing the titrations. In the so-called flow-injection titrations, because of the input function of the system, the titration curves obtained are the transformed forms of the conventional titration curves [4]. In this paper it is intended to focus attention on a widely applicable flow titration technique that is based on recording complete titration curves, the so-called triangle programmed titration tech-

Correspondence to: Z. Fehér, Research Group for Technical Analytical Chemistry of the Hungarian Academy of Sciences, Institute for General and Analytical Chemistry, Technical University, Gellért tér 4, H-1521 Budapest (Hungary).

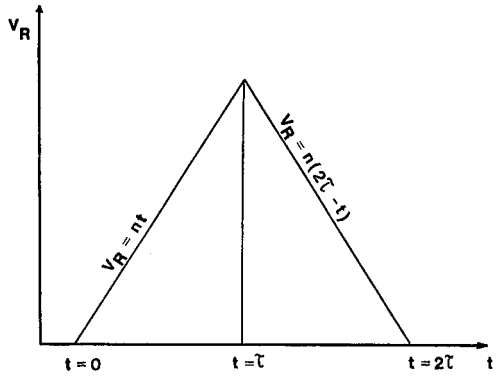

Fig. 1. Reagent mass flow vs. time programme of the triangle programmed titration technique.

nique. A detailed description of this technique and some examples of its capability have been given previously [5–9].

Triangle programmed titrations are performed in a special flow-through analysis channel in which the sample solution flows at a constant rate (v_s). Through a merging point incorporated in the channel, the titration reagent can be introduced at a mass flow V_R. To carry out the titration the reagent mass flow is changed according to an isosceles triangle-shaped time programme (Fig. 1). The degree of completeness of the titration is followed by an appropriate detector placed downstream of the merging point. In this way two titration curves (signal vs. time), connected to each other as mirror images can be recorded. According to simple considerations it was found that the time interval elapsing between the appearances of the two equivalence points (Q) and the concentration of the solution titrated (c_s) have a well defined relationship (it is assumed that the reagent mass flow at a certain point of the titration programme exceeds the stoichiometric equivalence and the recorded curves contain sufficiently long under- and over-titrated sections):

$$Q = 2\tau - \frac{2a}{b} \cdot \frac{v_s c_s}{n} \qquad (1)$$

where 2τ is the time interval of the reagent addition programme and a/b is the stoichiometric factor assuming a titration reaction of the type $aS + bR \rightarrow fP_1 + gP_2$ (S, R, P_1 and P_2 are the sample, reagent and products, respectively).

Controlled-current coulometry offers an easy way to accomplish time-programmed titrant addition. By the use of appropriate reagent-generating solutions and flow-through half-cells, and a suitable current–time programme, a number of different titrants can be prepared in situ and a wide range of components can be determined with the triangle programmed titration technique.

The relationship which is valid in the case of coulometric reagent generation is

$$Q = 2\tau - \frac{2a}{b} \cdot \frac{\mu F \tau v_s}{i_{max}} \cdot c_s \qquad (2)$$

where i_{max} is the maximum value of the reagent generating current, μ is the number of electrons taking part in the reagent generating reaction and F is the Faraday constant.

In practice, the determination of the sample concentration by triangle programmed titrations is performed by using calibration graphs (Q vs. c relationships) rather than by calculation based on the determination of the exact values of the titration parameters (v_s, i_{max}, etc.).

For acid–base titrations, when instrumental end-point detection is considered, potentiometry with a pH-selective glass indicator electrode is in general the method of choice. However, in special cases photometric detection can have advantages over potentiometry.

In this paper, in addition to the potentiometric titration investigations, triangle programmed acid–base titrations with photometric detection are also described.

The applied photometric detection system consisted of a light-emitting diode (LED) as a radiation source and a phototransistor, in the photodiode operation mode, as a detector unit. The first system working on this principle in analytical practice was introduced by Flaschka et al. [10]. Later this kind of detector found applications especially in the analysis of flowing solutions (e.g., [11–16]). The main advantages of their use are their simplicity, high stability, small size, low mass and easy handling. Trojanowicz and the constructors of the simplest device (Worsfold and Clinch)

have published a review [17] on these solid-state photometric devices.

In this work, a system very similar to that described by Worsfold and co-workers [13–15] was used. The important point of the detector is that the solution-carrying PTFE tubes of 0.8 mm i.d. serve as "cuvettes" in the flow-through photometric measurements.

The photometric detector was intended to be used for following the colour of a special indicator mixture in the course of an acid–base titration process. The indicator mixture, similar to that suggested by Mullen and Anton [18], contains Methyl Red and *m*-Cresol Purple. Methyl Red changes colour from red to yellow over the pH range 4.4–6.2 and *m*-Cresol Purple from yellow to purple over the pH range 7.2–8.8. Between pH 6.2 and 7.2 a solution containing these two indicators at appropriate concentrations is yellow. This gives the possibility of the use of the indicator mixture in the photometric detection of acid–base titrations.

In this work the advantages of the flow-through triangle programmed titration technique were intended to be combined with those of the solid-state photometric detector and the indicator mixture mentioned.

EXPERIMENTAL

The scheme of the experimental set-up is shown in Fig. 2. A Model OL-602 multi-channel peristaltic pump (LaborMIM, Hungary) is used to ensure the flow of the sample solution, the reagent-generating solution and the reagent-generating auxiliary solution.

The titrant is generated in a two-compartment flow-through electrolysis cell. The two half-cells, separated from each other by a dialysis membrane, contain the reagent-generating and the auxiliary electrodes, respectively. Platinum wires of 0.3 mm diameter and about 50 mm long coiled to form a loose coil of 3 mm o.d. served for both electrodes.

The generated titrant and the sample solution merged in the titration cell. The titration cell is a cylindrical vessel ca. 5–10 ml in volume, having two inlet tubes of small (< 1 mm) diameter and a sharp end. The dropwise confluence of the solutions (which is the result of the shape and the placement of the inlet tubes) ensures the proper mixing on the one hand, while on the other it separates the reagent-generating electric circuitry from the detector circuitry. In this way the disturbing effect of the reagent-generating electric

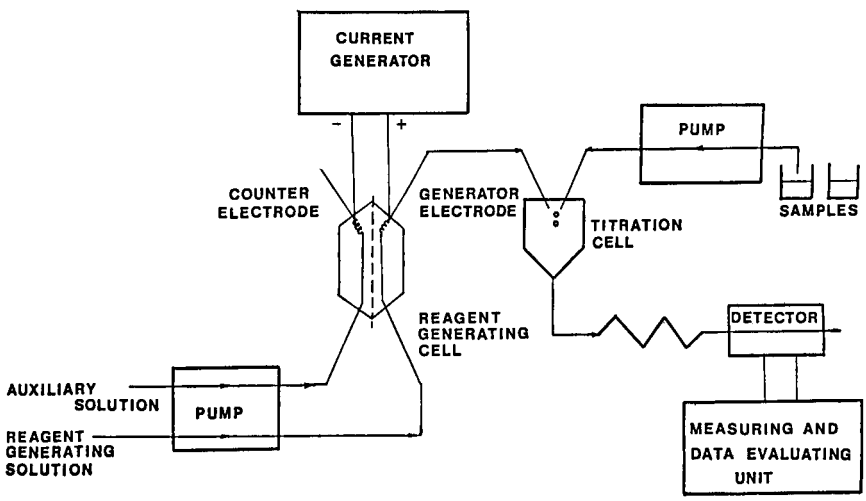

Fig. 2. Schematic diagram of the triangle programmed flow titrator.

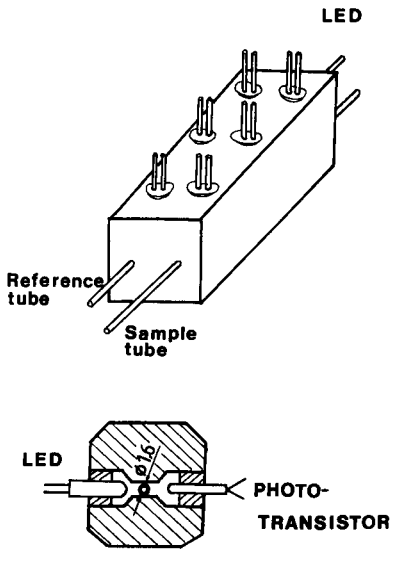

Fig. 3. Diagram of the flow-through photometric detector cell.

field on the detection is avoided. This means that the titration cell can also be considered as a dripping vessel.

A Model OH-409 current generator (Radelkis, Hungary) was used to accomplish the triangle programmed current vs. time function, while a Model OP-208/1 pH–mV meter (Radelkis) served as the measuring instrument when potentiometric detection was selected.

The potentiometric detector cell applied contained a Model OP-0753P micro-capillary pH-sensitive glass electrode (Radelkis) and a Model OP-0837P flow-through type saturated calomel reference electrode (Radelkis).

For performing photometric titrations a laboratory-made detector unit was used. As mentioned earlier, its construction was very similar to that described by Worsfold and co-workers [13–15]. The structure of the "optical part" is shown in Fig. 3. The solid-state photometric detector contains three pairs of LEDs and a phototransistor, in the photodiode operation mode, for sensing the intensity of radiation. The photometer contains red, yellow and green light-emitting diodes (HLMP-3315, HLMP-3415 and HLMP-3517 respectively; Hewlett-Packard. As can be seen, detection at the three different wavelengths (635, 583 and 565 nm) can be performed by the selection of the appropriate LED. For detection a KP 101 phototransistor (Intermetall, Germany) working in a relatively wide wavelength range was used. One of the PTFE tubes serves as the reference channel, the other being used for the sample solution. These parts of the detector are built in an aluminium body. The electronic part of the detector is built in the same unit as the optical part. To achieve high instantaneous light intensities, the LEDs operate in the pulse operation mode. The signal provided by the electronics is linearly proportional to the difference in the transmittance prevailing in the sample and the reference line (see later).

The titration curves were recorded using a Model OH-850 x–t strip-chart recorder (Radelkis). The absorption and the transmission spectra of the indicator mixture at different pH values were recorded using a Specord spectrophotometer (Zeiss).

Although various acids and bases have been titrated, in this paper only those obtained with nicotinic acid as model compound are presented. The drug and an experimental pharmaceutical preparation (nicotinic acid-containing tablet) were a generous gift from Alkaloida Chemical Works (Tiszavasvári, Hungary).

The chemicals used were of analytical-reagent grade and the quality of the drug used corresponded to the requirements of the Hungarian Pharmacopoeia [19].

It should be noted that all the solutions used or studied were prepared using boiled and cooled distilled water to avoid the interfering effect of dissolved carbon dioxide.

RESULTS AND DISCUSSION

Determination of current efficiency of titrant generation

In coulometry, 100% current efficiency is needed for accurate analysis. As mentioned earlier, in triangle programmed titrations calibration graphs can also be used for the evaluation. In that event it is not so important to achieve strictly

100% current efficiency in reagent-generating electrolysis. However, when carrying out triangle programmed titrations, parallel reactions decreasing the efficiency of the reagent-generating electrode reaction must be avoided as much as possible in the range of current density employed.

For checking the current efficiency of the reagent-generating cell in the course of the titration programme, constant current intensities, at different current levels in the range 0.2–5 mA, were forced through the generating electrodes for a given time interval, while the solution flowing through the investigated half-cell was collected (originally 0.1 M potassium nitrate solution) and then titrated. It was found that in the current interval mentioned above, both hydrogen and hydroxide ions are generated with a current efficiency approaching 100%, within the error limit of the determinations.

Potentiometric titrations

A typical triangle programmed potentiometric titration curve indicating the analytical signal (Q) is shown in Fig. 4. As can be seen from Eqn. 1, in the case of fast titration reactions the sensitivity of the determination (the slope of the calibration line) can be adjusted by appropriate selection of the measuring parameters, i_{max}, v_s and 2τ. This means that calibration lines for the precise analysis of solutions of very similar concentration and a rough analysis of solutions of very different concentrations can be constructed.

In Fig. 5 calibration graphs obtained by titration of nicotinic acid solutions are shown. It can be seen that by increasing the maximum value of the reagent-generating current (i_{max}) the slope of the calibration line decreases.

Q vs. c relationships for different sample flow-rates are presented in Fig. 6. The application of relatively high flow-rates results in a high sensitivity. However, in this instance the sample volume needed for the analysis is larger than at lower sample flow-rates.

The time interval of the reagent (titrant) generation, 2τ, also influences the slope of the calibration graph but in the selection of the 2τ value for an analytical determination the rate of the analysis is more crucial. The application of a

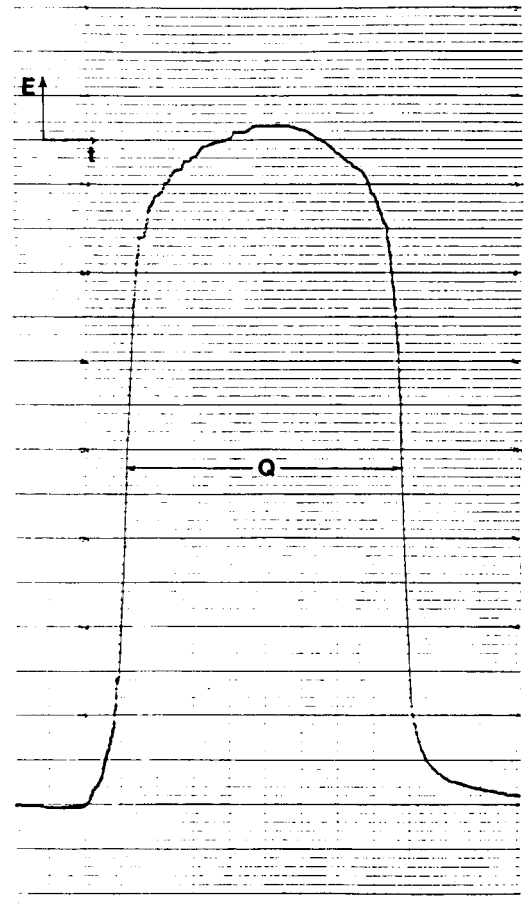

Fig. 4. Typical triangle programmed potentiometric titration curve. Solution, 2×10^{-4} M nicotinic acid; $i_{max} = 2.0$ mA; $2\tau = 120$ s; $v_s = 1.2$ ml min^{-1}.

short reagent-generating time interval can provide an advantageously high speed of analysis, but, too small 2τ values can lead to distorted titration curves. It was found that in potentiometry 40 s is the shortest reagent-generating time interval that still safely provides satisfactorily evaluable titration curves and good reproducibility of the results.

In the concentration range studied in this work (10^{-4}–10^{-3} M) the reproducibility of the results was examined at different concentration levels, and the relative standard deviation of the results was found to be in the range 0.8–1.5% ($n = 7$), depending on the experimental parameters.

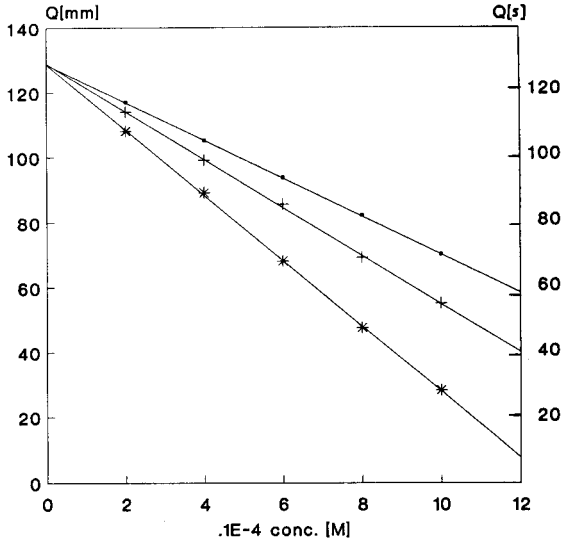

Fig. 5. Q vs. c dependences obtained with potentiometric detection at various i_{max} values: * = 1.5; + = 2.0; □ = 2.5 mA. v_s = 0.8 ml min^{-1}; 2τ = 120 s.

Photometric titrations

Experiments with the indicator mixture. For studying the properties of the indicator mixture, Methyl Red- and *m*-Cresol Purple-containing solutions were prepared with Britton–Robinson buffer solutions of different pH. In these investigations the concentration of the indicator mixture was adjusted to 10^{-5} g per 100 ml. Because the photometric device used measures the transmittance, transmittance vs. wavelength spectra were recorded for the different solutions. In order to study the applicability of the green LED as a light source in photometric end-point detection, from the spectra the transmittance values were determined at 565 nm, which is the intensity maximum of the emission band of this LED.

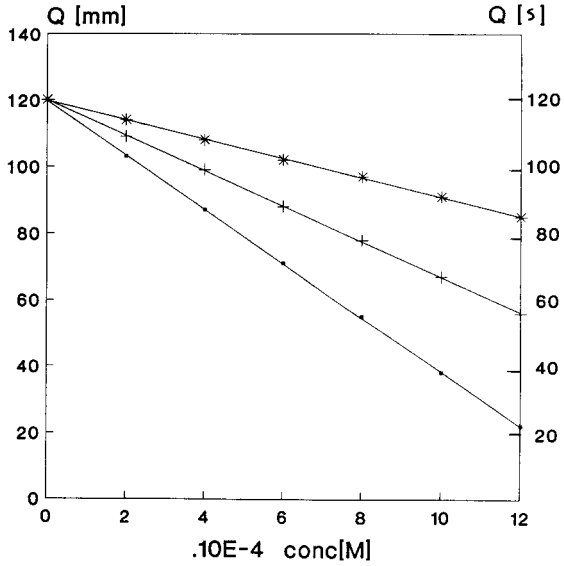

Fig. 6. Potentiometric calibration graphs for nicotinic acid obtained at various sample flow-rates, v_s: □ = 1.8; + = 1.2; * = 0.77 ml min^{-1}. i_{max} = 2.0 mA; 2τ = 120 s.

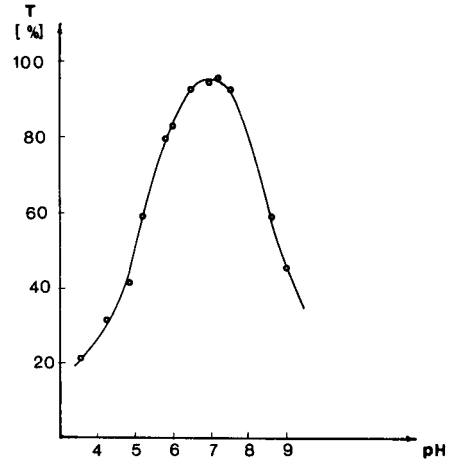

Fig. 7. Transmittance vs. pH relationship obtained with Methyl Red–*m*-Cresol Purple mixed indicator solutions. The concentration of the indicators was 10^{-5} g per 100 ml in each instance. λ = 565 nm.

The transmittance values are plotted against pH in Fig. 7. A similar curve was obtained when the photometric signal vs. pH dependence was investigated using the LED–phototransistor measuring device. From these observations it can be concluded that around pH 7 a very intense and fairly narrow transmittance maximum appears at 565 nm. This means that the equivalence point can be accurately detected photometrically with the indicator mixture if the pH is in the vicinity of 7.

A typical triangle programmed titration curve obtained with the laboratory-made flow-through photometer employing the indicator mixture in the sample solution is shown in Fig. 8. For the titration, 4×10^{-4} M nicotinic acid sample solu-

tion was pumped through the analysis channel at a flow-rate of 0.77 ml min^{-1} with reagent addition programme parameters $2\tau = 120$ s and $i_{max} = 2.5$ mA. It can be seen that two sharp, easy to evaluate maxima appear. These maxima represent the end-points of the two titration curves. As the location of these maxima can be ascertained fairly accurately, the sample solution concentration can be determined knowing the streaming rate and the reagent addition programme parameters.

In order to select the concentration of the acid–base colour indicators, it has to be taken into consideration that the indicators may cause a systematic error because they are also acid–base reagents. The higher the concentration of the indicators, the larger the error can be. However, the photometric signal was found to be linearly dependent on the concentration of the indicator in the low concentration range. A higher signal supports easier, more reliable end-point location. Considering these aspects, an indicator concentration of 10^{-5} g per 100 ml for each titration was selected and applied in further investigations. (The error caused by the presence of indicators can be avoided by the use of calibration graphs for the concentration determination.)

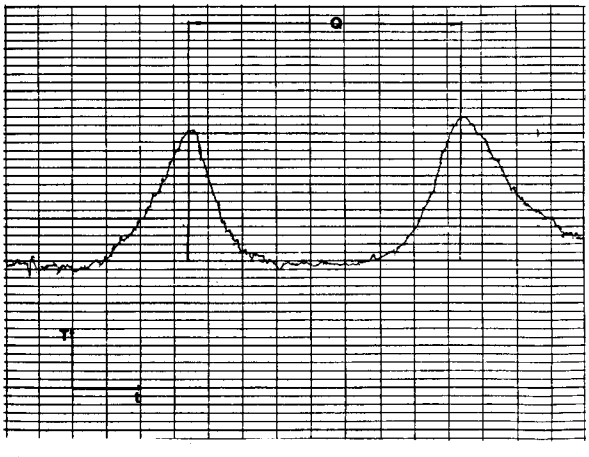

Fig. 8. Triangle programmed photometric titration curve. Solution, 2×10^{-4} M nicotinic acid; $v_s = 0.77$ ml min^{-1}; $2\tau = 120$ s; $i_{max} = 2.5$ mA; indicator, Methyl Red–*m*-Cresol Purple mixture at 10^{-5} g per 100 ml concentration. T is the transmittance in arbitrary units.

TABLE 1

Calculated indicator errors (%) for different K_d values at different sample concentrations

Sample concentration (M)	K_d		
	10^{-4}	10^{-5}	10^{-6}
10^{-3}	+0.01	+0.9	+9.7
10^{-4}	0	+0.7	+9.0
10^{-5}	−0.2	0	+7

It should be noted that the signal of the photometric device is not the transmittance itself but it is proportional to it. In the titrations the change in the transmittance is used for the concentration determination, but if a knowledge of the exact value of the transmittance is needed, it can be obtained by calibration.

For the estimation of the indicator error it has to be kept in mind that the application of the triangle programmed titration technique is especially advantageous when solutions of low concentration have to be analysed. An estimate of the possible error was of special importance. Therefore, in this work the indicator error values were calculated for solutions containing sample components with different dissociation constants at different concentrations. The calculated values are listed in Table 1. It can be seen that the indicator error in the titration of solutions of low concentration is negligible, except with very weak acids or bases ($K_d \leqslant 10^{-6}$) present at very low concentrations.

Investigations were also done to select a suitable ratio of the concentrations of the two indicators. In accordance with expectations, the symmetry of the titration curves is different for the application of different ratios of the two indicators. It was found that dissolving 1 mg of Methyl Red and 1 mg of *m*-Cresol Purple in 100 ml of ethanol (96%) gave an appropriate indicator mixture. A 1-ml volume of this mixture was used for 100 ml of standard or sample solution.

Results obtained with photometric detection. The basic relationships of the triangle programmed titration technique were also studied with photometric detection, again using also nicotinic acid solutions of different concentration. Q vs. c_s de-

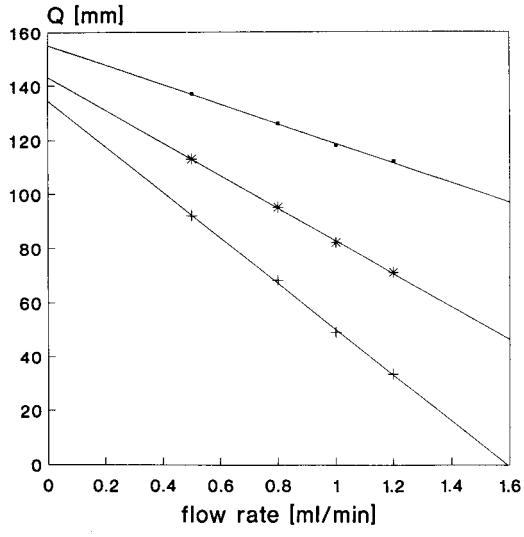

Fig. 9. Q vs. v_s dependences obtained with photometric detection in nicotinic acid solutions of different concentration c_s: □ = 2×10^{-4}; * = 6×10^{-4}; + = 1×10^{-3} M. i_{max} = 2.0 mA; 2τ = 120 s.

pendences measured at different i_{max} values (1.5, 2.0 and 2.5 mA) proved the linear relationship expected from Eqn. 1.

Applying different sample flow-rates, Q vs. c_s lines of different slope were obtained. In Fig. 9 the Q values are plotted against the sample flow-rate for three different sample concentrations. It can be seen that, in agreement with the correlation described by Eqn. 1, these relationships are also linear.

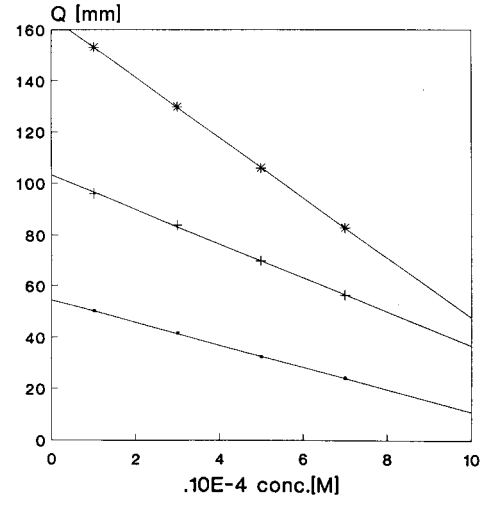

Fig. 10. Photometric calibration graphs for nicotinic acid obtained at various 2τ values: □ = 40 s; + = 80; * = 120 s. i_{max} = 2.0 mA; v_s = 1.2 ml min^{-1}.

In Fig. 10 calibration lines of different slope values and different intercepts on the Q axis, relevant to various reagent-generating time intervals (2τ), are shown.

The reproducibility of the results was tested at different concentration levels and at different measuring parameters with seven parallel measurements in each instance, the relative standard deviation was between 0.3 and 1.5%, depending on the parameters of the experiment. The correlation coefficients of the calibration lines were between 0.9991 and 0.9998 and the residual standard deviation was about 0.5%.

The above results show that the joint application of the special indicator mixture and the solid-state photometric device offers an easy way for detection in acid–base titrations. The simplicity of the evaluation of the photometric titration curves is advantageous mainly when the analysis and the evaluation of the results are not automated.

Determination of the drug content of nicotinic acid-containing tablets

The applicability of triangle programmed titrations with photometric detection was tested in the determination of the nicotinic acid content of an experimental pharmaceutical preparation. The results were compared with those obtained by triangle programmed potentiometric titration and also by classical volumetric acid–base titration using phenolphthalein as the indicator. The declared content of nicotinic acid was 0.05 g.

The photometric calibration graph constructed for the determination of the drug content covered a narrow concentration range (3.6×10^{-4}–4.4×10^{-4} M) and it had a relatively high slope. This was achieved by using the measuring parameters i_{max} = 1.75 mA, 2τ = 120 s and v_s = 1.8 ml min^{-1}. (In the potentiometric titrations the sample flow-rate was 1.2 ml min^{-1}, otherwise the same parameters could be applied.) It is worth mentioning that on the calibration graph a 1 mm difference in the Q values corresponds to a concentra-

tion difference Δc of about 1×10^{-6} M. This means that a reading error of 1 mm would cause far less than a 0.5% concentration difference at the level of the declared concentration in the tablet.

To investigate the influence of tablet ingredients other than nicotinic acid on the titration, solid mixtures containing all the tablet components (nicotinic acid, starch, talc, etc.) were made by weighing. These were dissolved in distilled water and filtered. The filtrates were titrated using the flow titrator and the Q values obtained were compared with those taken from Q vs. c_s calibration graph constructed with standard nicotinic acid solutions prepared using boiled and cooled distilled water as solvent. No significant difference were found between the Q values, indicating that the tablet matrix does not interfere with the nicotinic acid titration.

For the determination of the average drug content (mean value), ten tablets were pulverized and 0.100 g (the mass of one tablet) from the homogenized powder was dissolved in distilled water in a 100-ml volumetric flask. After dissolution it was made up to 100 ml and filtered. A 10-ml volume of the filtrate was diluted to 100 ml with distilled water. This solution was then titrated using the flow-through titration system ($i_{max} = 1.75$ mA, $v_s = 1.8$ ml min^{-1}, $2\tau = 120$ s).

For the determination of the drug content of a single tablet (individual drug content), one tablet was pulverized, dissolved in water and made up to 100 ml. This solution was filtered, diluted and titrated as described above.

The volumetric titrations were carried out according to the prescription of the Hungarian Pharmacopoeia [19], one tablet (individual drug content determination) or 100 mg of the powder obtained by pulverizing ten tablets (determination of the mean value of the drug content) was dissolved in distilled water and then titrated with 0.1 M sodium hydroxide solution using phenolphthalein as the indicator. The results of the drug content determinations are given in Table 2.

The top part of Table 2 shows the reproducibility of the determinations, as the same sample (powder) was analysed in each instance. The relative standard deviations obtained with the three different techniques are very similar. In the bottom part the results of repeated assays of the drug content in one tablet are shown. The relative standard deviations are not larger than in the former instance, which means on the one hand that the drug content in the pharmaceutical preparation is uniform, and on the other that the flow analytical methods applied are as valuable as the classical titrimetric technique.

TABLE 2

Results for the determination of the drug content of a nicotinic acid-containing experimental pharmaceutical preparation

Analysis No.	Volumetric titration	Triangle programmed titration	
		Photometric detection	Potentiometric detection
	Mean drug content of 10 tablets (mg)		
1	47.8	48.0	47.5
2	47.2	46.8	46.5
3	48.0	47.5	47.6
4	47.6	47.0	47.8
5	47.2	47.3	47.5
Mean	47.6	47.3	47.5
R.S.D.	0.4%	0.5%	0.5%
	Results of repeated assays of drug content in one tablet (mg)		
1	47.2	47.2	47.6
2	47.0	46.8	46.8
3	47.4	47.0	46.8
4	47.8	47.2	47.2
5	47.4	47.8	47.5
Mean	47.4	47.2	47.2
R.S.D.	0.3%	0.4%	0.4%

Conclusions

The triangle programmed titration technique can be used advantageously for the reliable and convenient analysis of series of sample solutions. The titrant is generated by controlled-current coulometry. Acid–base titrations were performed applying both potentiometric and photometric detection.

The application of the Methyl Red and *m*-Cresol Purple indicator mixture and the simple solid-state photometric device was demonstrated to be favourable for the titration of acids and

bases at low concentrations. The successful determination of the drug content of a nicotinic acid-containing experimental pharmaceutical preparation has been presented as an example.

REFERENCES

1 W.J. Blaedel and R.H. Laessig, Anal. Chem., 36 (1964) 1617.
2 W.J. Blaedel and R.H. Laessig, Anal. Chem., 37 (1965) 332.
3 O. Aström, Anal. Chim. Acta, 105 (1979) 67.
4 E. Pungor, Zs. Fehér, G. Nagy and K. Tóth, CRC Crit. Rev. Anal. Chem., 14 (1983) 175.
5 G. Nagy, Zs. Fehér, K. Tóth and E. Pungor, Anal. Chim. Acta, 91 (1977) 87.
6 G. Nagy, Zs. Fehér, K. Tóth and E. Pungor, Anal. Chim. Acta, 91 (1977) 97.
7 G. Nagy, Zs. Fehér, K. Tóth and E. Pungor, Anal. Chim. Acta, 100 (1978) 181.
8 Zs. Fehér, G. Nagy, K. Tóth, E. Pungor and A. Tóth, Analyst, 104 (1979) 560.
9 Zs. Fehér, J. Kolbe and E. Pungor, Analyst, 113 (1988) 881.
10 H. Flaschka, C. McKeithan and R. Barnes, Anal. Lett., 6 (1973) 585.
11 D. Betteridge, E.L. Dagless, B. Fields and N.F. Graves, Analyst, 103 (1978) 897.
12 T.J. Sly, D. Betteridge, D. Wibberley and D.G. Porter, J. Autom. Chem., 4 (1982) 186.
13 P.J. Worsfold, J.R. Clinch and H. Casey, Anal. Chim. Acta, 197 (1987) 43.
14 J.R. Clinch, P.J. Worsfold and H. Casey, Anal. Chim. Acta, 200 (1987) 523.
15 J.R. Clinch and P.J. Worsfold, Anal. Chim. Acta, 214 (1988) 401.
16 M. Trojanowicz and J. Szpunar-Lobinska, Anal. Chim. Acta, 230 (1990) 125.
17 M. Trojanowicz, P.J. Worsfold and J.R. Clinch, Trends Anal. Chem., 7 (1988) 301.
18 P.W. Mullen and A. Anton, Anal. Chem., 32 (1960) 103.
19 Pharmacopoeia Hungarica, Medicina Könyvkiadó, Budapest, VIIth edn., 1986.

Analytica Chimica Acta, 273 (1993) 531–537
Elsevier Science Publishers B.V., Amsterdam

Development of a method for oxalate determination by differential-pulse polarography after derivatization with *o*-phenylenediamine

José A. Rodrigues and Aquiles A. Barros

Department of Chemistry, Faculty of Sciences, University of Porto, 4000 Porto (Portugal)

(Received 1st June 1992; revised manuscript received 22nd October 1992)

Abstract

A method for the determination of oxalic acid was developed, based on derivatization with *o*-phenylenediamine. The electroactive product, dihydroxyquinoxaline, was determined by differential-pulse polarography and a linear calibration range from 2×10^{-7} to 2×10^{-5} M was obtained, with a detection limit of 5×10^{-8} M. A study of interferences was undertaken and, although *o*-phenylenediamine can react with a wide variety of other species, it was found that the method is specific for oxalic acid if the amount of interference is not very large. The method was applied successfully to the determination of oxalic acid (oxalate) in three different kinds of products (corks, beer and spinach) using, in each instance, an alternative method of determination to confirm the validity of the results.

Keywords: Polarography; Beer; Corks; Oxalic acid; Spinach

Oxalate assay is of great interest both in clinical diagnosis and in food technology, but considerable improvement is still required in the analytical procedures now available [1]. For instance, the inability to measure oxalate accurately in biological fluids has been a major barrier to a better understanding of oxalate physiology in order to optimize therapy for patients with abnormal oxalate homeostasis [2]. The low concentration of oxalate in plasma and the presence of interfering compounds in biological fluids form the main obstacles. Severe interferences are observed when enzymatic methods of determination of oxalate are used [3].

There are many procedures for the determination of oxalate, including liquid [4], gas [5] and ion [6] chromatography and a variety of enzymatic methods, ranging from spectrophotometric [7,8], to radioenzymatic isotope dilution [9] and immobilized enzyme electrodes [1].

In this paper, a method for the determination of oxalate is proposed in which the oxalate ion is derivatized with *o*-phenylenediamine (OPDA) to the electroactive compound 2,3-dihydroxyquinoxaline (DHQ), which is determined using differential-pulse polarography (DPP). The reaction of cyclic condensation with OPDA is not specific for oxalate and there are, for example, chromatographic methods for the determination of α-keto acids [10] and spectrophotometric methods for the determination of carbohydrates [11] based on a same type of derivatization reaction. Nevertheless, this investigation showed that the interferences in this method for the determination of oxalate are, generally, of minor importance, owing to the inherent selectivity of the detection process.

The method was applied to the determination of oxalate in different products and the results

Correspondence to: J.A. Rodrigues, Department of Chemistry, Faculty of Sciences, University of Porto, 4000 Porto (Portugal).

were compared with those obtained with alternative methods.

EXPERIMENTAL

Instrumentation

Differential-pulse polarographic experiments were done using a Metrohm system including a VA stand (E663), a VA scanner (E612), a VA detector (E611) and a VA controller (E608). This equipment was connected with a *X–Y* recorder (Houston 2000).

A three-electrode system was employed, with a dropping mercury working electrode, a glassy carbon counter electrode and an Ag/AgCl (KCl, 3 M) reference electrode.

A Jenway 6100 spectrophotometer equipped with a 1-cm glass cell was used for the absorbance measurements and a two-resin system [Amberlite IR-120 (H^+) and Dowex 2-X8 (Cl^-)] was used as described elsewhere [12] for the determination of oxalate in beer.

In the ion chromatographic measurements of oxalate in spinach a Dionex 4000i ion chromatograph was used, with a conductimetric detector and connected to a Spectra-Physics SP4290 integrator, as described by Ishii [6].

For the enzymatic determination of oxalate in corks a diagnostic kit from Sigma Diagnostics (Cat. No. 590) was used.

Solution preparation

All chemicals were of analytical-reagent grade. Deionized, distilled water was used for the preparation of solutions. Stock solutions of 1000 μg ml^{-1} sodium oxalate and dihydroxyquinoxaline were prepared weekly. Solutions with lower concentration were prepared by dilution. A 2% OPDA solution was prepared daily in 0.5 M HCl.

Recommended procedure for oxalate

Aliquots of oxalate solution containing from 2 to 200 μg of oxalate and 10 ml of 2% OPDA solution in 0.5 M HCl were introduced into a small beaker (25 ml) and the acidity was adjusted to 0.5 M HCl. This solution was then heated to dryness in a boiling water-bath. The residue was dissolved in 25.00 ml of 1 M HCl and transferred into the polarographic cell; after the deoxygenation process (nitrogen for 10 min) and a rest period of 15 s, a cathodic differential-pulse scan was initiated with a scan rate of 3 mV s^{-1}, a pulse amplitude of -30 mV and a forced drop time of 1 s. The final result was obtained by means of a calibration graph or by addition of known volumes of DHQ standard solution to the polarographic cell (nitrogen for 2 min after each addition).

Determination of oxalate in corks

Oxalate was extracted from groups of five corks of the same batch. Each cork was split into three equal cylinders and each cylinder into four equal pieces. Fragmented corks were introduced into a 300 ml Erlenmeyer flask that was filled with 0.01 M HCl. The solution was mixed magnetically for 2 h and filtered through filter-paper; the cork residue on the filter was washed with 0.01 M HCl solution and the filtrates were added and diluted to 500 ml. Aliquots of 2 ml of this solution were taken and used in the recommended procedure.

Determination of oxalate in beer

Before polarographic analysis, oxalate was extracted from beer using a system of two ion-exchange columns, as described by Alavi and West [12]. A 200-ml sample of beer was boiled gently for 4–5 min to expel CO_2, diluted to 500 ml and passed through the ion-exchange columns at a flow-rate of 3–4 ml min^{-1}. After being washed with 100 ml of water, the columns were separated and oxalic acid was eluted from the second column (Dowex 2-X8), first with 150 ml of 1 M HCl and then with 100 ml of water. The eluates were mixed and diluted to 500 ml. Volumes of 3 ml of this solution were used in the recommended procedure.

Determination of oxalate in spinach

A sample of spinach was washed with water and wiped with paper towels. After being cut in small pieces and homogenized, 5 g of spinach were placed in a small gauze bag and introduced into a 500-ml flask attached to a condenser. A 200-ml volume of water was added and after

boiling for 120 min the suspension was cooled and filtered through filter-paper. The filtrate was diluted to 500 ml and 1 ml of this solution was used in the recommended procedure.

RESULTS AND DISCUSSION

Optimization of the derivatization procedure

The derivatization reaction used in the determination of oxalic acid (OXA) is a particular case of cyclic condensation reactions of aromatic *o*-diamines [13] and can be described by the following equation:

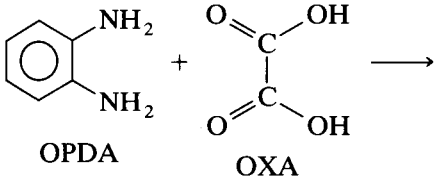

OPDA + OXA

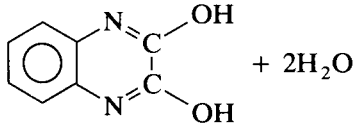

DHQ

Many years ago [14] a procedure based on this reaction was developed for the nearly quantitative production of DHQ. However, this is not true for low concentrations of OXA and the procedure had to be modified in order to obtain completeness of the reaction.

The optimum conditions for the determination of DHQ using DPP were studied. With a pulse amplitude of 30 mV (cathodic pulse), a scan rate of 3 mV s^{-1} and a forced drop time of 1 s, a linear correlation was obtained between the peak height and DHQ concentration over the concentration range 2×10^{-7}–2×10^{-5} M. Least-squares treatment gave a slope of 26.3 nA per 10^{-6} M and a intercept of 1.18 nA, with a standard deviation of the slope and intercept of 5.29 $\times 10^{-2}$ nA per 10^{-6} M and 0.52 nA, respectively, for eight data points.

Comparing the polarographic peak currents obtained with derivatized OXA and with DHQ, the conversion of OXA in DHQ was evaluated as a function of the amount of OPDA used in the derivatization process (Fig. 1).

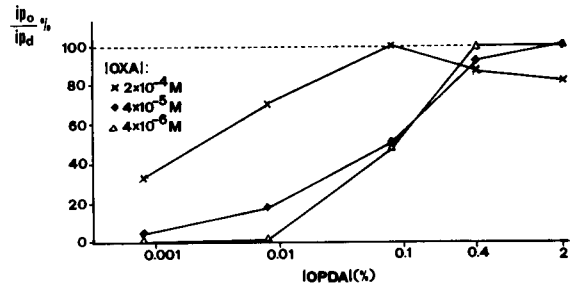

Fig. 1. Conversion of OXA into DHQ as a function of the amount of OPDA used in the derivatization process. i_{p_0} = peak current of derivatized OXA; i_{p_d} = peak current of DHQ. OXA concentration: × = 2×10^{-4}; ◆ = 4×10^{-5}; △ = 4×10^{-6} M.

As OPDA does not interfere in the polarographic determination it is possible to use an amount of this compound up to 2%, leading to quantitative derivatization of OXA for concentrations as low as 10^{-6} M (Fig. 2). The standard deviation for five separate determinations of 2×10^{-6} M OXA is 2.3% (using standard addition of DHQ) and the limit of determination is 5×10^{-8} M. The optimum concentration for the evaluation of OXA is between 1×10^{-6} and 2×10^{-5} M.

Interferences

Interferences in the determination of OXA could be expected taking into account either the

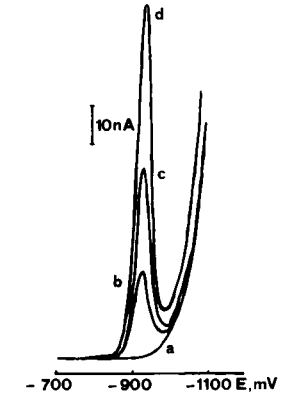

Fig. 2. DPP determination of OXA after derivatization with 2% OPDA. OXA concentration: (a) 0; (b) 1×10^{-6}; (c) 2×10^{-6}; (d) 4×10^{-6} M.

derivatization process or the polarographic method of detection. Of course, all the species that show polarographic activity near the reduction potential of DHQ will interfere and the first compound to be investigated in this context should naturally be the derivatizing agent itself; as stated previously, it was found that OPDA is inactive in that potential region, and this allows the use of large excess of the derivatizing agent, therefore favouring the completeness of the derivatization reaction. Generally, other compounds with reduction potentials similar to that of DHQ are not found in materials that have to be assayed for OXA.

The more likely source of interference comes from those compounds which, being structurally similar to OXA, are often present in several products containing the acid and can derivatize with OPDA in a similar way. The results of an investigation carried out with some of the more common of these compounds, reported in Table 1, showed that, in general, if the amount of compound and of OXA are of the same order of magnitude there is no problem with this kind of interference. In fact, the compounds themselves (or their derivatization products) when active have polarographic peaks at different potentials and only interfere when present at high concentrations, as can be seen in Fig. 3.

TABLE 1

Interferences in the DPP determination of oxalic acid

Species	[OXA] (M)	[Interferent] (M)	[Interferent]/[OXA]	Interference
Nitrate	2.0×10^{-6}	1×10^{-3}	500	No [a]
	2.0×10^{-5}		50	No [a]
Sulphate	2.0×10^{-6}	1×10^{-3}	500	No [a]
	2.0×10^{-5}		50	No [a]
Acetate	2.0×10^{-6}	1×10^{-3}	500	No [a]
	2.0×10^{-5}		50	No [a]
Formic acid	2.0×10^{-6}	1×10^{-3}	500	No [a]
	2.0×10^{-5}		50	No [a]
Pyruvic acid	2.0×10^{-6}	1×10^{-3}	500	No [b]
	2.0×10^{-5}		50	No [b]
Glyoxylic acid	2.0×10^{-6}	1×10^{-3}	500	Yes [c]
	2.0×10^{-5}		50	Yes [c]
Nitrite	2.0×10^{-6}	1×10^{-3}	500	Yes [c]
	2.0×10^{-5}		50	Yes [c]
Phosphate	2.0×10^{-6}	1×10^{-3}	500	No [a]
	2.0×10^{-5}		50	No [a]
Succinic acid	2.0×10^{-6}	1×10^{-3}	500	No [a]
	2.0×10^{-5}		50	No [a]
Malonic acid	2.0×10^{-6}	1×10^{-3}	500	No [a]
	2.0×10^{-5}		50	No [a]
Maleic acid	2.0×10^{-6}	1×10^{-5}	5	No [b]
		1×10^{-4}	50	Yes [c]
	2.0×10^{-5}	1×10^{-4}	5	No [b]
		1×10^{-3}	50	Yes [c]
Fumaric acid	2.0×10^{-6}	1×10^{-4}	50	No [b]
	2.0×10^{-5}	1×10^{-3}	50	Yes [c]
Formaldehyde	2.0×10^{-6}	1×10^{-3}	500	No [a]
	2.0×10^{-5}		50	No [a]
Salicylic acid	2.0×10^{-6}	1×10^{-4}	50	No [a]
	2.0×10^{-5}	1×10^{-3}	50	No [a]
Butane-2,3-dione	2.0×10^{-6}	1×10^{-4}	50	Yes [c]
	2.0×10^{-5}	1×10^{-3}	50	Yes [c]
Ascorbic acid	2.0×10^{-6}	1×10^{-4}	50	Yes [c]
	2.0×10^{-5}	1×10^{-3}	50	Yes [c]

[a] No polarographic wave. [b] Polarographic wave far from DHQ wave. [c] Polarographic wave can interfere with DHQ wave, depending on the relative excess of the interferent.

Applications

The method was applied to the determination of oxalic acid (and oxalates) in three different types of materials (corks, beer and spinach) and in each instance another method was used for comparison.

Determination of oxalic acid in corks. The development of a new method for the determination of OXA started with the need for a process of evaluation of oxalates in corks, a problem that is now concerning an increasing number of institutions related to the wine industry. Oxalic acid is present in the final cork, because this is prepared by a set of physical and chemical treatments of the natural cork, including immersion in a aqueous solution of oxalic acid [15].

A project for an international standard for the determination of OXA in corks is currently in progress, using the enzymatic method with spectrophotometric detection [8], and it was decided to compared this method with that developed here. OXA was extracted from corks using the process proposed by CT Cork, the Portuguese Centre for Cork Technology (unpublished).

The present method proved to be simpler and more reliable than the enzymatic method. There was no need to perform any separation prior to

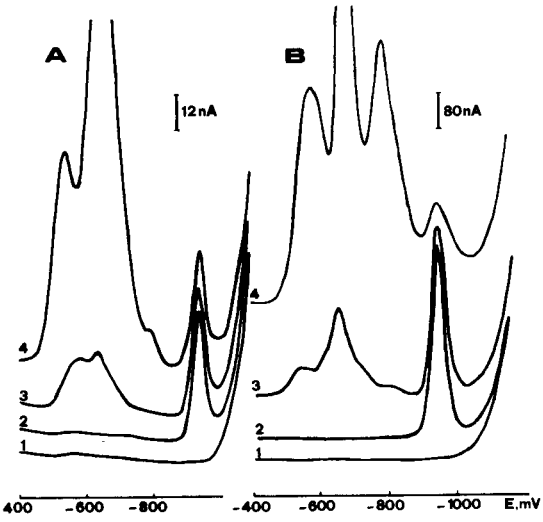

Fig. 3. DPP determination of OXA: (A) 1 = blank; 2 = 2.0×10^{-6} M OXA; 3, 4 = 2.0×10^{-6} M OXA in the presence of 1×10^{-5} and 1×10^{-4} M maleic acid, respectively. (B) 1 = blank; 2 = 2.0×10^{-5} M OXA; 3, 4 = 2.0×10^{-5} M OXA in the presence of 1×10^{-4} and 1×10^{-3} M maleic acid, respectively.

the analysis, a procedure that is essential in the enzymatic method and very prone to several interferences [7]. Although the results obtained with the two methods are in agreement for treated corks, the present method gives a much lower value when natural, untreated, corks are analysed, the amounts of oxalic acid found per natural cork being 0.14 ± 0.03 and 0.36 ± 0.06 mg for the DPP and enzymatic methods, respectively, and per treated cork being 3.15 ± 0.07 and 3.60 ± 0.10 mg, respectively (mean values $\pm$ S.D., $n = 3$). There is no special reason for the appearance of a significant amount of OXA in natural corks and the higher value obtained with the enzymatic method is probably due to interference from other constituents of the corks.

The polarograms obtained in the determination of natural and treated corks are shown in Fig. 4. Although the concentration of OXA in the natural corks is very low (about 0.1 mg per cork), the polarographic signal is clearly measurable.

Determination of oxalates in beer. It is important for breweries to have a method for the determination of oxalate in beer, because the presence of insoluble calcium oxalate crystals can produce haze, sediment and overfoaming in package beer [16]. The amount generally found in normal beer is about 10–20 mg l^{-1} of calcium oxalate and problems can arise when this level exceeds 20 mg l^{-1} [17].

Numerous methods for the determination of oxalate in beer have been published, but none has gained wide acceptance. The present method was compared with a published method [12] in which oxalate is first removed from part of the interferences by passing the beer through a system of two ion-exchange columns, then the oxalate in the eluate is precipitated with 10% calcium chloride to eliminate the interference of formic acid and finally the crystals of calcium oxalate are dissolved in hydrochloric acid and made to react with indole to form a pink to red colour that can be measured by spectrophotometry.

The visible reaction of OPDA with an aliquot of beer, with the formation of a brownish compound, probably due to some kind of oxidation [18], did not allow the direct spectrophotometric analysis of oxalate in beer. The present polarographic method proved to be more straightfor-

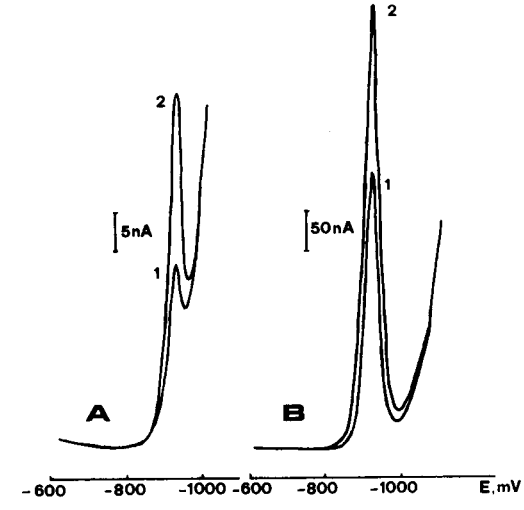

Fig. 4. DPP determination of OXA in corks using a standard addition of DHQ. (A) 1 = natural corks; 2 = addition of 2.5×10^{-6} M DHQ. (B) 1 = treated corks; 2 = addition of 3.0×10^{-5} M DHQ.

ward than the spectrophotometric method, with no need for a precipitation step after the passage through the columns (formic acid does not interfere, as can be seen in Table 1). The efficiency of the precipitation step could even be determined by comparing the polarographic results obtained with and without using it. The results obtained for the analysis of a solution containing 7 mg l^{-1} of OXA were 3.5 ± 1.5 mg l^{-1} by Alavi and West's method [12], and 3.2 ± 1.5 and 6.8 ± 0.2 mg l^{-1} by the DPP method with and without a precipitation step, respectively (mean values ± S.D., $n = 3$). According to these values, it can be predicted that the method proposed by Alavi and West [12] probably gives much lower oxalate values than the real values. This could be expected because for low concentrations of oxalate and in solutions that are not as simple as "oxalate in water", the solubility of calcium oxalate can have a significant value. The only explanation for the large variance of the first two results is a high variability in the amount of calcium oxalate obtained in the precipitation step.

Figure 5 shows the polarograms obtained in the determination of oxalate in beer using a standard addition method. The corresponding amount of oxalate expressed as calcium oxalate was 10.1 $\pm$ 0.3 mg l^{-1}.

Determination of oxalates in spinach. The determination of oxalates in foods is very important. Accumulation of oxalates by crop and pasture plants adversely affects the nutritional quality of foods and feeds; consumption of plants with high oxalate contents can lead to poisoning and death of livestock and high-oxalate diets can increase the risk or renal calcium oxalate formation in certain groups of people and may also affect calcium absorption [19].

The present DPP method was used in the determination of oxalates in spinach and the results were compared with those obtained with the ion chromatographic (IC) method proposed by Ishii [6]. Oxalates were extracted from spinach and the extract was analysed using both methods. The amounts of oxalate found per 100 g of spinach were 1058 ± 32 and 995 ± 45 mg with the DPP and IC methods, respectively (mean values ± S.D., $n = 3$). These similar results confirm the possibility of applying the polarographic method to the determination of oxalates in spinach.

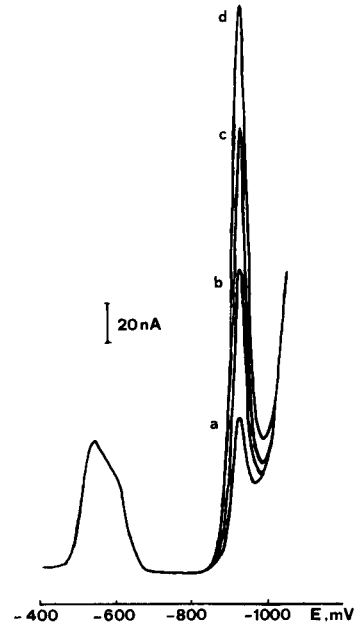

Fig. 5. DPP determination of oxalate in beer: (a) sample of beer; (b), (c) and (d) with standard additions of 4.8×10^{-6}, 9.6×10^{-6} and 14.4×10^{-6} M OXA, respectively.

The authors acknowledge the financial support of INIC (CIQ, linha 3) and J.A. Rodrigues also thanks the Fundação Gomes Teixeira, Porto, for financial support.

REFERENCES

1 C.H. Assolant-Vinet, G. Bardeletti and P.R. Coulet, Anal. Lett., 20 (1987) 513.
3 A.W. Williams and D.M. Wilson, Semin. Nephrol., 10 (1990) 2.
3 M.A. Saka Amini and J.J. Valou, Anal. Chim. Acta, 245 (1991) 129.
4 W. Koolstra, B.G. Wolthers, M. Hayer and H.M. Rutgers, Clin. Chim. Acta, 170 (1987) 237.
5 A.I. Sutikno, D. Suherman and B. Tangendjaja, J. Sci. Food Agric., 39 (1987) 233.
6 Y. Ishii, Anal. Sci., 7 (1991) 263.
7 M.G. Li and M.M. Madappally, Clin. Chem., 32 (1989) 2330.
8 M.F. Laker, A.F. Hofmann and B.J.D. Meeuse, Clin. Chem., 26 (1980) 827.

9 D.J. Bennet, F.E. Cole, E.D. Frohlich and D.T. Erwin, Clin. Chem., 25 (1979) 1810.
10 P.A. David and M. Novotky, J. Chromatogr., 452 (1988) 623.
11 J.C. Towne and J.E. Spikner, Anal. Chem., 35 (1963) 211.
12 Z.I. Alavi and D.B. West, Am. Soc. Brew. Chem. J., 41 (1983) 24.
13 E.H. Rodd, Chemistry of Carbon Compounds, Vol. III, Part A, Elsevier, Amsterdam, 1954, p. 225.
14 M.A. Phillips, J. Chem. Soc., (1928) 2395.
15 M. Borges and C. Cunha, Bol. Inst. Prod. Flor., (1985) 693.
16 M.W. Brenner, Am. Soc. Brew. Chem. Proc., (1957) 5.
17 M. Burger and K. Becker, Am. Soc. Brew. Chem. Proc., (1949) 102.
18 R. Paul, in V. Grignard, (Ed.), Traité de Chimie Organique, Tome XXI, Masson, Paris, 1953, p. 195.
19 B. Libert and V.R. Franceschi, J. Agric. Food Chem., 35 (1987) 926.

Analytica Chimica Acta, 273 (1993) 539–543
Elsevier Science Publishers B.V., Amsterdam

Determination of sulphanilic acid in the presence of tartrazine by differential-pulse polarography after conversion into an azo compound

Aquiles A. Barros, José A. Rodrigues and Paulo J. Almeida

Department of Chemistry, Faculty of Sciences, University of Porto, 4000 Porto (Portugal)

(Received 1st June 1992; revised manuscript received 17th September 1992)

Abstract

The determination of a hydrophilic aromatic amine, sulphanilic acid, in the presence of the water-soluble colouring matter tartrazine was studied. Previously, hydrophobic aromatic amines were determined in water-soluble colouring matter using extraction of the amines into chloroform. With the hydrophilic sulphanilic acid this procedure is not feasible and a polarographic method was developed for the determination of sulphanilic acid in the presence of tartrazine, using a masking agent, gelatin, to suppress the polarographic peak of the colouring matter. Concentrations of sulphanilic acid as low as 0.1 mg l^{-1} could be determined in solutions up to 500 times more concentrated in tartrazine. The method was applied to measure the amount of sulphanilic acid formed in the degradation of tartrazine in 10% sodium hydroxide solution. In contrast with the results obtained when the degradation is carried out in ascorbic acid, virtually no sulphanilic acid was found, indicating a different process of degradation.

Keywords: Polarography; Sulphanilic acid; Tartrazine

The importance of methods for the determination of aromatic amines is largely related to the toxicity of many of these compounds. In fact, aromatic amines are easily absorbed by the skin, which may cause a systematic poisoning [1], and some of them are recognized carcinogens [2]. A method frequently employed for the determination of individual aromatic amines involves diazotization and coupling, with the formation of an intensely coloured azo compound that is easily detected by spectrophotometry [3].

One of the applications of various primary aromatic amines is in the production of synthetic azoic colouring matters, using the above diazotization–coupling procedure. As one of the uses of azoic colouring matters is in the coloration of foods, drugs and cosmetics, it is important to have a method to verify that the amine used in the production of a particular colouring matter was completely removed after the synthesis. Of course, if the usual method of analysis for amines is employed, involving their conversion into azo compounds, the colouring matter itself, structurally similar to the derivatized amine, will interfere in the determination. Therefore, an intermediate separation step between the amine and the colouring matter will be necessary. The spectrophotometric determination of aniline (and other primary aromatic amines) in the colouring matter D&C Red No. 33 has been reported [4], based on the extraction of the amines from an aqueous solution of the colouring matter into chloroform. A similar determination using adsorptive stripping voltammetry in the detection step has been described [5].

Correspondence to: A.A. Barros, Department of Chemistry, Faculty of Sciences, University of Porto, 4000 Porto (Portugal).

In this work, the determination of sulphanilic acid in the presence of the water-soluble colouring matter tartrazine was studied. The extraction of this aromatic amine into a hydrophobic solvent is not possible in this instance owing to the hydrophilic character of the sulphonic group of the amine. Nevertheless, a polarographic method for the determination of sulphanilic acid in the presence of tartrazine (without any extraction step), using gelatin as a masking agent, was developed. In fact the addition of a convenient amount of gelatin before the polarographic analysis results in complete suppression of the polarographic peak of tartrazine [6], and under these conditions it was found that the polarographic activity of the derivatized sulphanilic acid is not greatly affected. Using this masking procedure an amount of sulphanilic acid as low as 0.1 mg l^{-1} was determined in the presence of a 500-fold excess of tartrazine.

EXPERIMENTAL

Differential-pulse polarographic (DPP) experiments were performed using a Metrohm system including a VA stand (E663), a VA scanner (E612), a VA detector (E611) and a VA controller (E608). This equipment was connected with a *X–Y* recorder (Houston 2000).

A three-electrode system was employed, with a dropping mercury working electrode, a glassy carbon counter electrode and a silver/silver chloride (3 M KCl) reference electrode.

pH measurements were made with a combined pH–reference electrode by using a pH537 microprocessor pH meter, both from WTW (Germany).

Reagents and solutions

All chemicals were of analytical-reagent grade. Deionized, distilled water was used for the preparation of solutions.

A stock solution of sulphanilic acid (1000 μg ml^{-1}) was prepared weekly. Solutions with lower concentration were prepared by dilution. The diazotization solution was prepared by dissolution of 50 mg of sodium nitrite in 50 ml of water. The coupling solution was prepared daily by dissolving 50 mg of α-naphthol in 1 M NaOH solution.

Recommended procedure for sulphanilic acid determination

A suitable aliquot of sulphanilic acid solution was placed in a 25-ml beaker and acidified with 10 ml of 0.02 M H_2SO_4, 1 ml of 0.1% $NaNO_2$ solution was added and the mixture was stirred for 5 min. Then 1 ml of α-naphthol in 1 M NaOH solution was added, the final pH was adjusted to 10.0 with 0.2 M NH_4NO_3 and the solution was transferred into a 25-ml volumetric flask and diluted to volume with water. This solution was introduced into the polarographic cell and analysed by DPP as follows: deoxygenation for 10 min with N_2, a rest period of 15 s and then a cathodic differential-pulse scan at a scan rate of 3 mV s^{-1}, a pulse amplitude of 20 mV and a forced mercury drop time of 1 s.

RESULTS AND DISCUSSION

Differential-pulse polarographic determination of sulphanilic acid

A method for the polarographic determination of sulphanilic acid was developed in which the compound was first diazotized with nitrous acid and the diazotization product was coupled with α-naphthol, forming a polarographically active azo derivative. The process can be represented as follows:

1st step, diazotization:

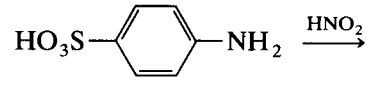

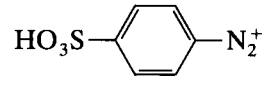

2nd step, coupling:

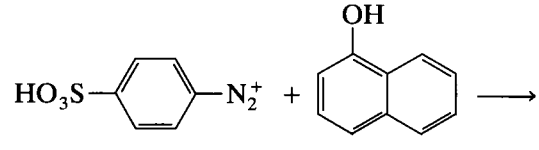

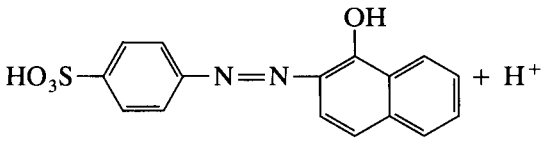

(A)

3rd step, DPP determination of the azo compound A.

The optimization of the conditions led to the procedure described under Experimental. A linear calibration graph for the polarographic determination of sulphanilic acid was obtained over the concentration range 0.1–1.0 mg l^{-1}. Least-squares treatment gave a slope of 48.1 nA l mg^{-1} and an intercept of 0.21 nA, with standard deviations of the slope and intercept of 1.26 nA l mg^{-1} and 0.69 nA, respectively, for eight data points, with a limit of detection well below 0.1 mg l^{-1} (Fig. 1) Even lower limits of detection could be achieved using adsorptive stripping voltammetry with a hanging mercury drop electrode (HMDE), as azo compounds of type A are known to be strongly adsorbed at a mercury drop [7], but the addition of gelatin as a masking agent (see the next section) makes the use of the adsorptive techniques impossible.

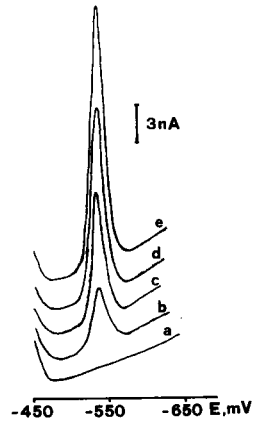

Fig. 1. DPP determination of derivatized sulphanilic acid. Concentration of sulphanilic acid: (a) 0; (b) 0.1; (c) 0.2; (d) 0.3; (e) 0.4 mg l^{-1}.

Determination of sulphanilic acid in the presence of tartrazine

As stated previously, unlike aniline, sulphanilic acid cannot be separated from tartrazine by extraction into a hydrophobic solvent. To avoid polarographic interference of the colouring matter another approach was devised, based on the drastic effect of gelatin on the DPP peak of tartrazine [6].

Figure 2 shows that gelatin virtually suppresses the DPP peak of 10 mg l^{-1} of tartrazine, but still allows the determination of sulphanilic acid at concentrations even less than 0.1 mg l^{-1}. The overall results of the investigation are reported in Table 1, showing that if 0.02% gelatin is added, the peak of tartrazine almost disappears, whereas

TABLE 1

Effect of gelatin on DPP peaks of tartrazine and derivatized sulphanilic acid

Azoic compound	Final concentration (mg l^{-1})	Variation of peak current $(i_p - i_{p_0})/i_{p_0} \times 100$ (%) [a]		
		0.02% gelatin [E_p (tartrazine) = −720 mV; E_p (sulphanilic acid) = −630 mV]	0.05% gelatin [E_p (tartrazine) = −700 mV; E_p (sulphanilic acid) = −630 mV]	0.1% gelatin [E_p (sulphanilic acid) = −630 mV]
Tartrazine (E_{p_0} = −750 mV) [b]	5	−100	−100	−100
	10	−97	−100	−100
	20	−98	−99	−100
	50	−90	−95	−100
Derivatized sulphanilic acid (E_{p_0} = −620 mV) [b]	0.1	+20	−50	−52
	0.2	+16	−51	−60
	0.5	+13	−43	−54
	1.0	+10	−47	−50

[a] i_p and i_{p_0} = peak currents with and without gelatin, respectively. [b] E_{p_0} = peak potential without gelatin.

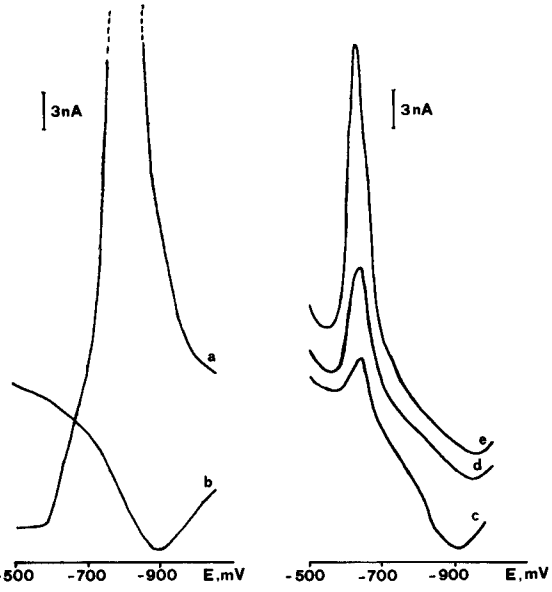

Fig. 2. DPP determination of derivatized sulphanilic acid in the presence of 10 mg l^{-1} of tartrazine. Concentration of sulphanilic acid: (a) 0; (b) 0; (c) 0.1; (d) 0.2; (e) 0.5 mg l^{-1}. Concentration of gelatin: (a) 0; (b)–(e) 0.02%.

the peak of the derivatized sulphanilic acid is only slightly affected. The polarographic determination of derivatized sulphanilic acid in the presence of 0.02% gelatin showed linearity over the concentration range 0.1–1.0 mg l^{-1}. Least-squares analysis gave a slope of 40.1 nA l mg^{-1} and an intercept of 0.91 nA, with standard deviations of the slope and intercept of 2.30 nA l mg^{-1} and 1.30 nA, respectively, for five data points. Under these conditions, owing to the severe decrease in the peak of tartrazine, it is possible to determine sulphanilic acid in solutions with a 500-fold higher concentration of tartrazine.

Degradation of tartrazine

Taking into account the structure of tartrazine (Fig. 3), the formation of sulphanilic acid can be predicted if its degradation proceeds via reductive splitting of the azo group. In agreement with this, it has been demonstrated that sulphanilic acid with a molar yield of more than 50% is produced if tartrazine is degraded in the presence of ascorbic acid [8,9]. Nevertheless, the degradation is very slow and occurs only if conditions of intense heat or light are used. However, in 10% sodium hydroxide, tartrazine can degrade significantly without the need to use such drastic conditions [10].

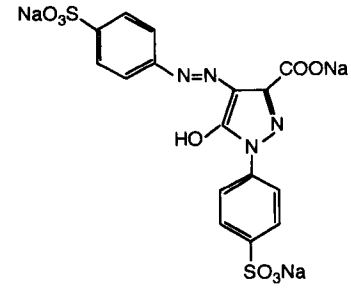

Fig. 3. Structure of tartrazine.

Solutions of 0.1% tartrazine in 10% sodium hydroxide were prepared and the above method was applied to follow the course of degradation of tartrazine and formation of sulphanilic acid in this basic medium. As can be seen in Table 2, although tartrazine was more than 50% degraded after 1 month, the amount of sulphanilic acid found was insignificant. This cannot be explained on the basis of subsequent degradation of sulphanilic acid, because this acid is stable under the conditions of the experiment, as shown in the last column.

Although no references to the mechanism of the alkaline degradation of tartrazine could be found, these results can be understood only by considering the occurrence of different processes of tartrazine degradation in ascorbic acid [8,9] and in 10% sodium hydroxide [10], with and

TABLE 2

Degradation of tartrazine in 10% NaOH

Time (days)	Tartrazine (1000 mg l^{-1}) in 10% NaOH		Sulphanilic acid (50 mg l^{-1}) in 10% NaOH: sulphanilic acid in solution (%)
	Sulphanilic acid in solution (%)	Tartrazine degradation (%)	
1	0.12	0	100
3	0.22	5	98
8	0.6	15	96
15	0.8	31	96
30	1.1	52	94

without the formation of sulphanilic acid, respectively.

The authors acknowledge the financial support of INIC (CIQ, linha 3) and J.A. Rodrigues also thanks the Fundação Gomes Teixeira, Porto, for financial support.

REFERENCES

1 G.D. Christian, Analytical Chemistry, Wiley, New York, 4th edn., 1986, p. 653.
2 K. Venkataraman, The Analytical Chemistry of Synthetic Dyes, Wiley, New York, 1987, p. 571.
3 G. Norwitz and P.N. Keliher, Anal. Chem., 53 (1981) 56.
4 J.E. Bailey Jr., Anal. Chem., 57 (1985) 189.
5 J.A. Rodrigues and A.A. Barros, presented at IX Congreso Iberoamericano de Electroquimica, Resumenes de Conferencias e Comunicaciones, La Laguna, 1990.
6 A.A. Barros, J.O. Cabral and A.G. Fogg, Analyst, 113 (1986) 853.
7 A.G. Fogg, A.A. Barros and J.O. Cabral, Analyst, 111 (1986) 831.
8 A.G. Fogg and A.M. Summan, Analyst, 108 (1983) 1339.
9 A.G. Fogg and A.M. Summan, Analyst, 109 (1984) 743.
10 D.M. Marmion, Handbook of U.S. Colorants for Foods, Drugs and Cosmetics, Wiley, New York, 2nd edn., 1984, p. 50.

Analytica Chimica Acta, 273 (1993) 545–551
Elsevier Science Publishers B.V., Amsterdam

Polarographic determination of *tert*-butylhydroquinone in micellar and emulsified media

A. González Cortés, A.J. Reviejo García, P. Yáñez-Sedeño and J.M. Pingarrón

Department of Analytical Chemistry, Faculty of Chemistry, Complutense University of Madrid, 28040 Madrid (Spain)

(Received 7th May 1992; revised manuscript received 23rd July 1992)

Abstract

A polarographic study of the oxidation of *tert*-butylhydroquinone (TBHQ) in micellar and emulsified media is described. The non-ionic surfactant Pluronic F-68, in Britton–Robinson buffer (pH 9.0), was found to be the most suitable for determining this antioxidant in micellar solutions. The characteristics of the oxidation process were established. Linear calibration graphs were obtained for TBHQ by differential-pulse polarography (DPP) within the ranges 1.0×10^{-6}–1.0×10^{-5} and 1.0×10^{-5}–1.0×10^{-4} mol l^{-1} with a limit of determination (10 × standard deviation) of 6.7×10^{-7} mol l^{-1} TBHQ (0.11 mg l^{-1}). An emulsified medium formed with a mixture of hexane and ethyl acetate (99:1) at pH 8.0 was also used. Linear calibration graphs were obtained by DPP within the ranges 1.0×10^{-6}–1.0×10^{-5} mol l^{-1} and 1.0×10^{-5}–1.0×10^{-4} mol l^{-1} TBHQ. The limit of determination was found to be 8.3×10^{-7} mol l^{-1}. Interferences from *tert*-butylhydroxyanisole, *tert*-butylhydroxytoluene, citric acid, propyl gallate and propylene glycol were tested. Except for propyl gallate, none of them interfered. The proposed method was applied with good results to the determination of TBHQ in spiked edible oils by direct emulsification of the samples.

Keywords: Polarography; Voltammetry; Antioxidants; Butylhydroquinone; Foods

Phenolic antioxidants such as *tert*-butylhydroxyanisole (BHA), *tert*-butylhydroxytoluene (BHT) and *tert*-butylhydroquinone (TBHQ) are commonly added to foods to improve their stability and especially to prevent rancidity in products containing lipids or fats [1]. Legislation in most countries limits the permissible concentrations of these additives. Thus, in the USA, for example, a maximum concentration of 200 mg kg^{-1} TBHQ or TBHQ–BHA or TBHQ–BHT mixtures in fats and oils is allowed [2].

Several methods, usually involving separation steps, used for the determination of antioxidants in different samples, have been reviewed by Robards and Dilli [1]. Regarding electrochemical methods, few applications have been found in this field. As an example, flow-injection methods have been described for the determination of BHA and BHT based on their oxidation processes at a glassy carbon electrode [3]. With respect to TBHQ, its polarographic behaviour in ethanol–water (1 + 1) has been studied [4], and its determination in edible oils at the 50, 100 and 200 mg kg^{-1} TBHQ levels by differential-pulse polarography (DPP) has also been reported using a toluene–ethanol solvent in acetate buffer [5]. Further, TBHQ has been determined by liquid chromatography with amperometric detection [6,7].

In this work, micellar and oil–water emulsified media were used, thus allowing polarographic studies of the TBHQ oxidation process to be

Correspondence to: J.M. Pingarrón, Department of Analytical Chemistry, Faculty of Chemistry, Complutense University of Madrid, 28040-Madrid (Spain).

carried out in predominantly aqueous media where special reference electrodes and solvent purification are not needed [8]. On the other hand, the direct emulsification from the oil samples permits the determination of TBHQ without a previous extraction step with organic solvents.

EXPERIMENTAL

Apparatus

A Metrohm E 506 Polarecord equipped with an E 505 polarographic stand was used. Cyclic voltammetric and coulometric studies with a mercury pool cathode were done using an EG&G PAR 273 potentiostat using the 270 Electrochemical Analysis software. A Metrohm E 510 pH meter and a P-Selecta Ultrasons ultrasonic bath were also used.

Electrodes and electrochemical cell

A Metrohm EA 1019/2 dropping mercury electrode (drop time 6–7 s), an Ingold 10-303-3000 saturated calomel electrode (SCE), a counter electrode consisting of a platinum wire immersed in the solution and a double-walled Metrohm EA 867-20 cell were used for polarographic studies. Cyclic voltammograms were recorded using a Metrohm E 410 hanging drop mercury electrode.

Reagents and solutions

Micellar stock solutions of TBHQ (1.0×10^{-3} mol l^{-1}) were prepared by weighing the product (Aldrich) and dissolving it in 1% (w/v) Pluronic F-68 (Serva) solution by treatment in the ultrasonic bath for 5 min. More dilute standards were prepared by suitable dilution with water and subsequent ultrasonic treatment for 2 min.

Stock solutions of TBHQ (1.0×10^{-3} mol l^{-1}) in hexane–ethyl acetate (99 + 1) were prepared by weighing and dissolution. More dilute standards were prepared by suitable dilution with the same solvent mixture.

Aqueous 1% (w/v) stock solutions of the surfactants Triton X-405, Pluronic F-68, Hyamine 2389 (all from Serva), tetrapropylammonium bromide (Fluka) and sodium dodecyl sulphate (SDS) (Carlo Erba) were prepared by weighing and dilution with water. Buffer solutions were 0.2 mol l^{-1} acetic acid–sodium acetate (pH 4.8), 0.2 mol l^{-1} sodium dihydrogenphosphate–disodium hydrogenphosphate (pH 7.2), 0.2 mol l^{-1} ammonia–ammonium chloride (pH 9.2) and Britton–Robinson containing each component acid at 0.2 mol l^{-1}. These buffers were used as supporting electrolytes. All other chemicals were of analytical-reagent grade. The water used was obtained from a Millipore Milli-Q purification system.

Samples

Edible oils containing no perservatives were analysed. These samples, olive oil, corn oil and sunflower oil, which were purchased in local supermarkets, were spiked with 100 mg kg^{-1} of TBHQ.

Polarography in micellar solutions

A suitable volume of the micellar stock solution of TBHQ was transferred into a 50-ml volumetric flask containing 25.0 ml of 0.2 mol l^{-1} Britton–Robinson buffer solution at the required pH. Then, various volumes of 1% (w/v) Pluronic F-68 stock solution were added, depending on the required final concentration. The solution was diluted to the mark with water and the flask was placed in the ultrasonic bath for 2 min. Finally, the micellar solution was transferred into the electrochemical cell and polarograms were recorded from -0.40 V at $\Delta E = 50$ mV and at a scan rate of 10 mV s^{-1}, after deaeration with a stream of argon for 5 min, while keeping an inert atmosphere in the cell.

Polarography in oil–water emulsions

A suitable volume of the TBHQ stock solution in hexane–ethyl acetate (99 + 1) was transferred into a 50-ml volumetric flask containing 25.0 ml of 0.2 mol l^{-1} Britton–Robinson buffer solution at the required pH and various volumes of 1% (w/v) Pluronic F-68 solution. Then, various volumes of hexane–ethyl acetate (99 + 1) were added and the solution was diluted to the mark with water. After shaking for a few seconds, the flask was placed in the ultrasonic bath for 5 min, shaking manually each minute. The emulsion obtained was transferred into the electrochemical

cell and differential pulse polarograms were recorded from −0.40 V at $\Delta E = 50$ mV and at a scan rate of 10 mV s^{-1}, after deaeration with a stream of argon for 5 min, while keeping an inert atmosphere in the cell.

Determination of TBHQ in spiked oils

About 25 g of oil were accurately weighed with a precision of 0.1 mg into a 50-ml beaker, then 5.0 ml of a 500 mg l^{-1} TBHQ stock solution in hexane–ethyl acetate (99 + 1) were added. The spiked oil was quantitatively transferred into a 100-ml volumetric flask, rinsing with hexane–ethyl acetate (99 + 1), mixing and diluting to the mark with hexane–ethyl acetate (99 + 1). A 1.0-ml aliquot of this solution was transferred into a 50-ml volumetric flask containing 25.0 ml of 0.2 mol l^{-1} Britton–Robinson buffer solution (pH 8.0) and 5.0 ml of 1% (w/v) Pluronic F-68 solution, then diluted to the mark with water. After shaking for a few seconds, the flask was placed in the ultrasonic bath for 10 min, shaking manually each minute. The emulsion obtained was transferred into the electrochemical cell and polarograms were registered after deaeration with a stream of argon for 5 min, while keeping an inert atmosphere in the cell.

TBHQ was determined by using the standard additions method, which involved the addition of 25.0–125 μg of TBHQ from a 500 mg l^{-1} TBHQ stock solution in hexane–ethyl acetate (99 + 1). The intensity of the analytical response was measured against the background current.

RESULTS AND DISCUSSION

Micellar solutions

In order to choose the most suitable surfactant for the polarographic study of TBHQ, various cationic (tetrapropylammonium bromide and Hyamine 2389), anionic (SDS) and non-ionic surfactants (Triton X-405 and Pluronic F-68), all fairly soluble in water, were tested at pH 4.8, 7.2

TABLE 1

DPP in micellar solutions: 4.0×10^{-5} mol l^{-1} TBHQ: 0.2% surfactant; 0.1 mol l^{-1} buffer–background electrolyte: pH 4.8, $HAcO–AcO^-$; pH 7.2, $H_2PO_4^-/HPO_4^{2-}$; pH 9.2, NH_4^+/NH_3

Surfactant	pH	i_p (μA)	E_p (V) (vs. SCE)	Observations
SDS	4.8	0.752	+0.112	One well defined peak. A signal due to the surfactant appears at potentials close to that of TBHQ
	7.2	0.228	+0.016	One peak of low sensitivity
	9.2	0.328	−0.184	One well defined peak
Triton X-405	4.8	0.400	+0.064	One well defined peak. A broad peak due to the surfactant appears at potentials close to that of TBHQ
	7.2	0.332	−0.072	The background peak is higher than at pH 4.8
	9.2	0.296	−0.176	One well defined peak
Pluronic F-68	4.8	0.552	+0.068	One well defined peak. A peak due to the surfactant appears at potentials very close to that of TBHQ
	7.2	0.276	−0.072	The background signal appears at more positive potentials than that of TBHQ
	9.2	0.344	−0.176	One well defined peak
Tetrapropylammonium bromide	4.8	–	−0.080	One shoulder appears which coincides with that of the surfactant
	7.2	–	–	No suitable response was obtained
	9.2	0.264	−0.172	One well defined peak
Hyamine 2389	4.8	–	–	Only one shoulder appears
	7.2	0.272	−0.080	One broad peak appears. A shoulder due to the surfactant appears at potentials close to that of TBHQ
	9.2	0.284	−0.168	One very broad peak appears which virtually coincides with that of the surfactant

and 9.2. The DPP results obtained are summarized in Table 1. Taking into account the analytical characteristics (sensitivity, background signal and reproducibility) of the TBHQ oxidation peak in these media, Pluronic F-68 was chosen as the most suitable.

Effect of pH. The influence of pH on $E_{1/2}$ and the limiting current i_l and on E_p and i_p was examined for a TBHQ concentration of 4.0×10^{-5} mol l^{-1} using current-sampled direct current (d.c.) and differential-pulse polarography, respectively. A 0.1 mol l^{-1} Britton–Robinson buffer was used as the supporting electrolyte between pH 2.0 and 11.0 in these studies.

The results obtained are shown in Fig. 1, where $E_{1/2}$ and E_p values of the surfactant-alone response are also plotted. At pH < 7.0, only an overall wave was observed, including the TBHQ oxidation wave and the surfactant response. The same behaviour was observed in DPP between pH 4.0 and 6.0; however, two peaks could be observed at pH < 4.0, that of TBHQ appearing at more positive potential values. At pH > 7.0 two well separated waves or peaks were obtained, and consequently this zone was chosen as being of analytical interest. The E_p–pH and $E_{1/2}$–pH plots showed linear relationships with very similar slopes (-0.056 and -0.055 V, respectively). It must be pointed out that the peak potentials (or $E_{1/2}$) of overall peaks (or waves) between pH 4.0 and 6.0 fitted these linear plots. The i_p and i_l vs.

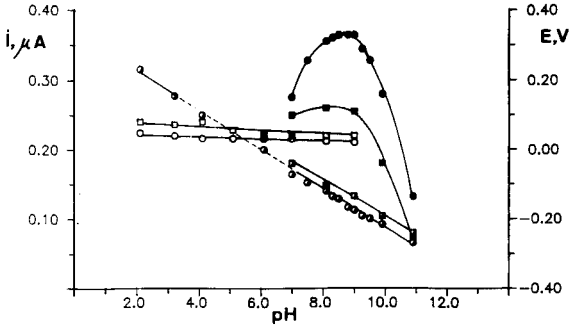

Fig. 1. Effect of pH on i_l, $E_{1/2}$, i_p and E_p: ◪ and ■ = $E_{1/2}$ and i_l in current-sampled d.c. polarography; ◑ and ● = E_p and i_p in DPP; 4.0×10^{-5} mol l^{-1} TBHQ, 0.04% Pluronic F-68, 0.1 mol l^{-1} Britton–Robinson buffer; □ and ○ = $E_{1/2}$ and E_p for 0.04% Pluronic F-68 solutions.

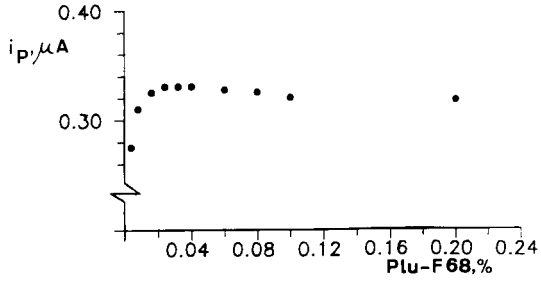

Fig. 2. Effect of Pluronic F-68 concentration on peak current by DPP; 4.0×10^{-5} mol l^{-1} TBHQ, 0.1 mol l^{-1} Britton–Robinson buffer (pH 9.0).

pH plots showed a zone of highest sensitivity between pH 8.0 and 9.0. Taking into account this point and the larger difference between the TBHQ $E_{1/2}$ or E_p and the Pluronic F-68 $E_{1/2}$ or E_p, pH 9.0 was chosen as the most suitable for analytical purposes.

Using DPP, the peak current for TBHQ did not depend on the Pluronic F-68 concentration at levels $> 0.02\%$ (Fig. 2). Also, the TBHQ peak potential remained virtually constant over the whole concentration range of surfactant studied (0.004–0.2%). A Pluronic F-68 concentration of 0.04% was chosen for further studies. The stability of the micellar solution formed at pH 9.0 was tested; a peak current decrease of about 5% was observed after 40 min, so that it is possible to use pH 9.0 as the working pH.

Characteristics of the oxidation process. The slope of the log i_l vs. log h_{corr} plot in current-sampled d.c. polarography, 0.71, suggested a diffusion-controlled limiting current for a TBHQ concentration of 1.0×10^{-4} mol l^{-1}. Logarithmic analysis of this polarogram yielded a linear plot with slope 0.030 V. The application of the $E_{3/4} - E_{1/4}$ criterion gave a value of 0.029 V. Cyclic voltammograms obtained using a hanging drop mercury electrode (Fig. 3) showed well defined oxidation and reduction peaks, the difference between E_{pa} and E_{pc} being 0.030 V. All these data suggested the reversibility of the electrode process with a value of n (number of electrons involved) = 2. This number of electrons was confirmed by controlled-potential coulometry using a mercury pool cathode, and agrees with literature

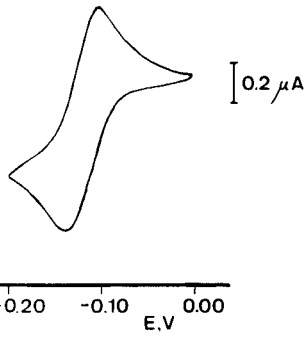

Fig. 3. Cyclic voltammogram in micellar solution at a hanging drop mercury electrode. 1.0×10^{-4} mol l^{-1} TBHQ, 0.04% Pluronic F-68 and 0.1 mol l^{-1} Britton–Robinson buffer, (pH 9.0); scan rate, 20 mV s^{-1}; drop size, 0.52 mm^2; initial potential, −0.20 V.

data for the TBHQ oxidation in other media [4]. Moreover, the number of protons involved in the electrode process is also 2, as deduced from the slope of the $E_{1/2}$ vs. pH plot (−0.055 V), so the oxidation process would be

$$TBHQ \rightleftharpoons TBQ + 2H^+ + 2e^-$$

where TBQ is the corresponding quinone.

Analytical characteristics of the method. TBHQ can be determined by DPP using $\Delta E = 50$ mV over the concentration ranges 1.0×10^{-5}–1.0×10^{-4} and 1.0×10^{-6}–1.0×10^{-5} mol l^{-1} (the r values, slopes and intercepts being 0.9999, $7.5 \pm 0.1 \times 10^3$ μA l mol^{-1}, -0.7 ± 5 nA and 0.9994, $7.2 \pm 0.2 \times 10^3$ μA l mol^{-1}, -0.6 ± 1 nA, respectively). The analytical characteristics of the method using the above calibration graphs were as follows: relative standard deviation, 3.1% at a concentration level of 5.0×10^{-6} mol l^{-1} TBHQ ($n = 10$); limit of determination, according to the 10 × standard deviation criterion [9], 6.7×10^{-7} mol l^{-1}; and detection limit, defined as $3s_b/m$ [10], where m is the slope of the lowest calibration graph and s_b is the standard deviation ($n = 10$) of the signal from 1.0×10^{-6} mol l^{-1} TBHQ, 2.0×10^{-7} mol l^{-1}.

Emulsified medium

Hexane was envisaged as an appropriate organic solvent to form oil–water emulsions because it is the solvent recommended by the AOAC to prepare solutions from oil samples [11]. However, TBHQ is scarcely soluble in this solvent, so a mixture of hexane and a polar organic solvent, such as ethyl acetate, in which TBHQ is highly soluble, was used. An organic phase formed by hexane–ethyl acetate (99 + 1) was chosen in order to have the maximum possible amount of the recommended solvent.

DPP for 4.0×10^{-5} mol l^{-1} TBHQ and pH 9.0 was used to study some parameters in the emulsified medium (surfactant concentration and volume of the organic phase). Using a concentration of Pluronic F-68 of 0.04%, the volume of the organic phase, in the range 1.0–5.0 ml did not have a significant influence on the peak current when a pulse amplitude of 50 mV and an emulsification time of 5 min were used. The effect of the surfactant concentration on the peak current using an organic phase volume of 2.0 ml was similar to that obtained in micellar solutions. Consequently, an organic phase volume of 2.0 ml and a Pluronic F-68 concentration of 0.04% were used for subsequent studies. Under these experimental conditions, the DP polarograms are qualitatively similar to those obtained in micellar solutions being suitable for analytical purposes.

The effect of pH on the DP polarograms was studied for 4.0×10^{-5} mol l^{-1} TBHQ. The results were similar to those shown in Fig. 1 for micellar solutions. However, the i_p vs. pH plot now showed a well defined maximum at pH 8.0, and therefore this pH value was chosen for use in analytical studies. The emulsion formed was stable (the i_p values remained virtually constant) for at least 45 min. As expected, the electrochemical behaviour of TBHQ in the emulsified medium was very similar to that shown in micellar solutions, and then the characteristics of the electrode process discussed above can be extrapolated to the emulsified medium.

Analytical characteristics of the DPP method. The plots of i_p vs. TBHQ concentration were linear (for $\Delta E = 50$ mV) for the concentration ranges 1.0×10^{-6}–1.0×10^{-5} mol l^{-1} ($r = 0.9995$) and 1.0×10^{-5}–1.0×10^{-4} mol l^{-1} ($r = 0.9998$). The slopes of the calibration graphs were $6.5 \pm 0.2 \times 10^3$ and $7.3 \pm 0.4 \times 10^3$ μA l mol^{-1}, with intercepts of -0.004 ± 0.001 and -0.01 ± 0.02 μA, respectively. The analytical characteristics of

the method are as follows: relative standard deviation 3.3% for a concentration level of 5.0×10^{-6} mol l^{-1} TBHQ ($n = 10$); limit of determination, 8.3×10^{-7} mol l^{-1}; and detection limit, 2.5×10^{-7} mol l^{-1}.

Interferences. Different substances commonly present in commercial antioxidants mixtures (BHA, BHT, citric acid, propyl gallate and propylene glycol) were tested by DPP in order to check for interferences with respect to the TBHQ peak. Interferent-to-analyte ratios in the range 1:1–100:1 were studied for a TBHQ concentration of 5.0×10^{-6} mol l^{-1}. Polarograms from solutions of BHA, citric acid and propylene glycol at pH 8.0 did not show any analytical peak in the potential range −0.40 to 0.00 V. Further, the shape of the TBHQ oxidation peak did not change appreciably in the presence of these compounds, which indicates that they do not interfere. In fact, in the presence of a 100:1 interferent-to-TBHQ ratio, the calculated concentrations of analyte using the calibration graph mentioned above yielded values within the 2 standard deviations range for 5.0×10^{-6} mol l^{-1} TBHQ ($n = 10$). However, propyl gallate gave a peak at −0.072 V and interfered even with a 1:1 ratio, leading to a TBHQ oxidation peak much higher than that obtained in the absence of propyl gallate; consequently, the presence or not of this compound must be previously checked.

Determination of TBHQ in oil samples. DPP under the experimental conditions mentioned above was used to determine TBHQ in three types of spiked edible oils: olive oil, corn oil and sunflower oil. First, the commercial oils were tested to check the absence of antioxidants. Thus, the described procedure was applied to a 25-g blank sample. As an example, the polarogram of the corresponding emulsion obtained for corn oil is shown in Fig. 4. As can be observed no peak appeared in the potential range scanned. The addition of TBHQ to this emulsion gave rise to a well defined peak at −0.128 V, which increased with increasing TBHQ concentration (Fig. 4).

Oil samples were spiked with 100 mg kg^{-1} of TBHQ. Following the described procedure, the final TBHQ content in the analytical emulsion was 0.5 mg l^{-1}. The results obtained from five

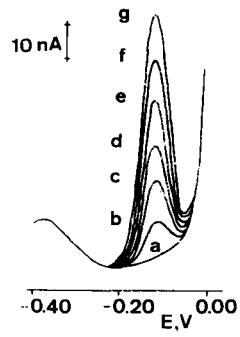

Fig. 4. Differential-pulse polarograms of TBHQ in an emulsion formed with a corn oil sample and hexane–ethyl acetate (99+1). (a) Unspiked sample, 0.1 mol l^{-1} Britton–Robinson buffer (pH 8.0); (b–g) successive additions of 50-μl aliquots of TBHQ stock solution.

samples of each oil type are given in Table 2. The relative standard deviations and the confidence intervals at a significance level of 0.05 were 2.3%, 2.7% and 4.4% and ±0.01 mg l^{-1} (±2%), ±0.01 mg l^{-1} (±3%) and ±0.02 mg l^{-1} (±4%) for olive oil, corn oil and sunflower oil, respectively. The recoveries found are usual for the determination of traces of organic compounds in food samples. Taking into account that in this method

TABLE 2

Recovery studies for TBHQ in spiked oil samples by DPP in emulsified medium

Sample	TBHQ found (mg l^{-1})	Recovery (%)
Olive oil	0.40	80
	0.40	80
	0.40	80
	0.38	76
	0.39	78
	Mean: 0.39	79
Corn oil	0.36	72
	0.39	78
	0.36	72
	0.38	76
	0.37	74
	Mean: 0.37	74
Sunflower oil	0.44	88
	0.42	84
	0.45	90
	0.46	92
	0.46	92
	Mean: 0.45	89

virtually no treatment of the sample is required, the differences in recoveries from the oil samples may be attributed to the different natures of the matrices.

Financial support from the Spanish CICYT (project ALI 89-0055) and the Comunidad de Madrid (project C009/91) is gratefully acknowledged.

REFERENCES

1 K. Robards and S. Dilli, Analyst, 112 (1987) 933.
2 TENOX TBHQ Antioxidant for Oils, Fats and Fat-containing Foods, Publication No. ZG-201G, Eastman Chemical Products, Kingsport, TN.
3 P. Yáñez-Sedeño, J.M. Pingarrón and L.M. Polo Díez, Anal. Chim. Acta, 252 (1991) 153.
4 O. Ryba, J. Petránek and J. Pospisil, Collect. Czech. Chem. Commun., 30 (1965) 843.
5 N. Thunyaudom Tonmanee and V.S. Archer, Talanta, 29 (1982) 905.
6 A.N. Masoud and Y.N. Cha, J. High Resolut. Chromatogr. Chromatogr. Commun., 5 (1982) 299.
7 Y. Kitada, Y. Ueda, M. Yamamoto, K. Shinomiya and H. Nakazama, J. Liq. Chromatogr., 8 (1985) 47.
8 A.J. Reviejo, A. Samprón, J.M. Pingarrón and L.M. Polo, Electroanalysis, 4 (1992) 111.
9 ACS Committee on Environmental Improvement, Principles of Environmental Analysis, Anal. Chem., 55 (1983) 2210.
10 K. Hasebe and J. Osteryoung, Anal. Chem., 47 (1975) 2412.
11 Official Methods of Analysis of the Association of Official Analytical Chemists, AOAC, Arlington, VA, 14th edn., 1984, Procedure 20012, p. 373.

Analytica Chimica Acta, 273 (1993) 553–560
Elsevier Science Publishers B.V., Amsterdam

Diffusion coefficients of oxygen, hydrogen peroxide and glucose in a hydrogel

S.A.M. van Stroe-Biezen, F.M. Everaerts, L.J.J. Janssen and R.A. Tacken

Instrumental Analysis, Chemical Technology, Eindhoven University of Technology, P.O. Box 513, 5600 MB Eindhoven (Netherlands)

(Received 27th May 1992)

Abstract

For the design of a new glucose sensor, a knowledge of the diffusion of all participating compounds is needed. A rotating disc electrode covered with hydrogel layer was used to determine the effective diffusion coefficients (D_{eff}) of oxygen, hydrogen peroxide and hydroquinone in a hydrogel, which is used in the sensor. Measurements were carried out under steady-state conditions. The three compounds appeared to be slowed by the gel to the same extent. A comparison was made between the D_{eff} values of glucose and hydroquinone by simultaneous diffusion through a hydrogel membrane. In this case glucose diffusion was slowed to a larger extent than hydroquinone diffusion. The effect, however, was independent of the degree of cross-linking of the hydrogel.

Keywords: Biosensors; Diffusion coefficient; Glucose; Hydrogel; Hydrogen peroxide; Oxygen

It is important to obtain continuous information about the blood glucose concentration of diabetics and an implantable sensor is a good alternative for regularly analysing blood samples.

A number of glucose sensors have already been developed [1–8]. In most of these sensors glucose reacts with oxygen to yield hydrogen peroxide [1–5]. The reaction is catalysed by the enzyme glucose oxidase (GOD). Hydrogen peroxide is oxidized or reduced at a detection electrode; its detection current is proportional to the glucose concentration. The enzyme is immobilized in a hydrogel by chemical cross-linking with a bifunctional reagent. As blood is low of oxygen, oxygen should be electrochemically produced in the sensor itself.

The disadvantage of existing sensors is that the concentration profiles and the diffusion patterns for oxygen, hydrogen peroxide and glucose in the enzyme-containing layer are not well defined. This can be the cause of a low detection current, as only a part of the hydrogen peroxide will reach the detection electrode.

For a proper design of a glucose sensor, measurement of the diffusion coefficients of all the participating compounds in the hydrogel seems to be essential. The diffusion coefficients of oxygen and hydrogen peroxide have been determined electrochemically, but this method is not useful for glucose. The diffusion coefficient of glucose had to be determined with a diffusion cell. To correlate the data for oxygen, hydrogen peroxide and glucose properly, an additional species, viz., hydroquinone, is used, as this compound is applicable in both the electrochemical and diffusion cell methods.

Correspondence to: S.A.M. van Stroe-Biezen, Instrumental Analysis, Chemical Technology, Eindhoven University of Technology, P.O. Box 513, 5600 MB Eindhoven (Netherlands).

THEORY

A rotating disc electrode (RDE) covered with a hydrogel layer appears to be an accurate means

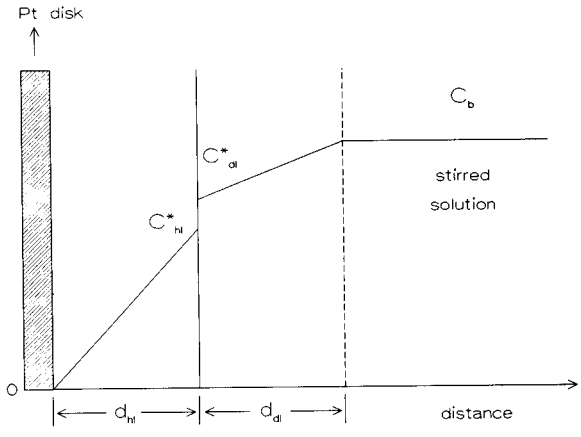

Fig. 1. Schematic profiles for the concentration of electroactive species vs. the distance from the platinum disc surface. Hydrogel layer thickness is denoted by d_{hl} and Nernst diffusion layer by d_{dl}.

of measuring diffusion coefficients of electrochemically active compounds [9,10]. Figure 1 shows schematically the concentration profile for active species.

Under steady-state conditions, the flux J (mol m^{-2} s^{-1}) in both the hydrogel layer (J_{hl}) and the Nernst diffusion layer (J_{dl}) is the same:

$$J = J_{hl} = J_{dl} \tag{1}$$

From the definition for J and assuming a linear concentration profile, it follows that

$$J_{hl} = J_{dl} \Leftrightarrow D_{hl}\frac{\Delta C_{hl}}{d_{hl}} = D_{dl}\frac{\Delta C_{dl}}{d_{dl}} \tag{2}$$

At the hydrogel layer–Nernst diffusion layer interface a jump in the concentration of the active component can take place. The partition coefficient α is defined by

$$\alpha = C^*_{hl}/C^*_{dl} \tag{3}$$

where the asterisk refers to the interface.

The concentration of the electroactive species at the electrode surface will be virtually zero, as a sufficiently high overpotential is applied. In this case, from Eqns. 2 and 3 the following expression is derived:

$$D_{hl}\frac{\alpha C^*_{dl}}{d_{hl}} = D_{dl}\frac{C_b - C^*_{dl}}{d_{dl}} \tag{4}$$

where C_b is the bulk concentration (mol m^{-3}). From Eqn. 4, it follows that

$$C^*_{dl} = \frac{D_{dl}\dfrac{C_b}{d_{dl}}}{\dfrac{\alpha D_{hl}}{d_{hl}} + \dfrac{D_{dl}}{d_{dl}}} \tag{5}$$

As $J = D_{hl}\alpha C^*_{dl}/d_{hl}$ and using Eqn. 4, it is found that

$$J = \frac{\dfrac{\alpha D_{hl}}{d_{hl}}\dfrac{D_{dl}}{d_{dl}}C_b}{\dfrac{\alpha D_{hl}}{d_{hl}} + \dfrac{D_{dl}}{d_{dl}}} \tag{6}$$

The permeabilities P_{hl} and P_{dl} are defined by

$$P_{hl} = \alpha D_{hl}/d_{hl} = D_{eff}/d_{hl} \tag{7}$$

and

$$P_{dl} = D_{dl}/d_{dl} \tag{8}$$

where D_{eff} is the effective diffusion coefficient (m^2 s^{-1}).

Combining Eqns. 6, 7 and 8 and using

$$I_{lim} = nFA_eJ \tag{9}$$

where I_{lim} is the limiting current (A), n the number of electrons involved in the electrode reaction, F the faraday, i.e., the charge on one mole of electrons (C), and A_e the electrode area (m^2), the following equation can be derived:

$$\frac{1}{I_{lim}} = \frac{1}{nFA_eC_bP_{hl}} + \frac{1}{nFA_eC_bP_{dl}} \tag{10}$$

The limiting current depends on two serial diffusion resistances. The total diffusion resistance ($1/k$) is defined by

$$\frac{1}{k} = \frac{1}{k_{hl}} + \frac{1}{k_{dl}} = \frac{1}{P_{hl}} + \frac{1}{P_{dl}} \tag{11}$$

where k is the total mass transfer coefficient (m s^{-1}). The first term ($1/k_{hl}$) is independent of the rotation speed. The second term ($1/k_{dl}$), however, is proportional to the reciprocal of the square root of the angular rotation rate (ω) of the RDE as P_{dl} is inversely proportional to d_{dl}. From

the theory of mass transfer to an RDE [11], it is known that

$$d_{dl} = 1.61(D_{dl}/\nu_{dl})^{1/3}(\nu_{dl}/\omega)^{1/2} \quad (12)$$

and so

$$P_{dl} = \frac{D_{dl}}{1.61(D_{dl}/\nu_{dl})^{1/3}(\nu_{dl}/\omega)^{1/2}} \quad (13)$$

Hence, if the reverse of the limiting current is plotted against the reverse of the square root of the angular rotation rate, a linear plot is obtained, the slope of which and the intercept give information about the permeability of the solution (Levich slope [11]) and the permeability of the hydrogel layer, respectively.

In this way, effective diffusion coefficients of oxygen and hydrogen peroxide can be determined electrochemically. However, glucose is electrochemically inactive and its diffusion coefficient has to be determined by the diffusion cell method. A comparison between the effective diffusion coefficients of hydroquinone (electrochemically determined) and glucose can be made by simultaneous diffusion through a membrane made of the same hydrogel material as used for the RDE experiments, which is strengthened by a filter-paper on each side of the membrane. The concentration profile is shown in Fig. 2. In this method two stirred solutions, A and B, where $C_A \gg C_B$, were separated.

For relatively short times the total flux J through the various layers is constant:

$$J = k\Delta C \quad (14)$$

where $\Delta C = C_A - C_B \approx C_A$ and k is, similarly to Eqn. 11, the total mass transfer coefficient (m s^{-1}).

Again, the diffusion resistance is built up of several terms:

$$\frac{1}{k} = \frac{1}{k_m} + \frac{2}{k_{dl}} + \frac{2}{k_f} = \frac{d_m}{D_{eff}} + \frac{2d_{dl}}{D_{dl}} + \frac{2d_f}{D_f} \quad (15)$$

where the subscripts m, dl and f refer to the membrane, the Nernst diffusion layer and the filter-paper, respectively. Combining Eqns. 14 and 15 gives

$$J = \frac{\Delta C}{\left(\frac{2d_{dl}}{D_{dl}} + \frac{2d_f}{D_f} + \frac{d_m}{D_{eff}}\right)} \quad (16)$$

The total amount of glucose or hydroquinone transported from compartment A to compartment B can now be written as

$$C_B V = JA_m t \quad (17)$$

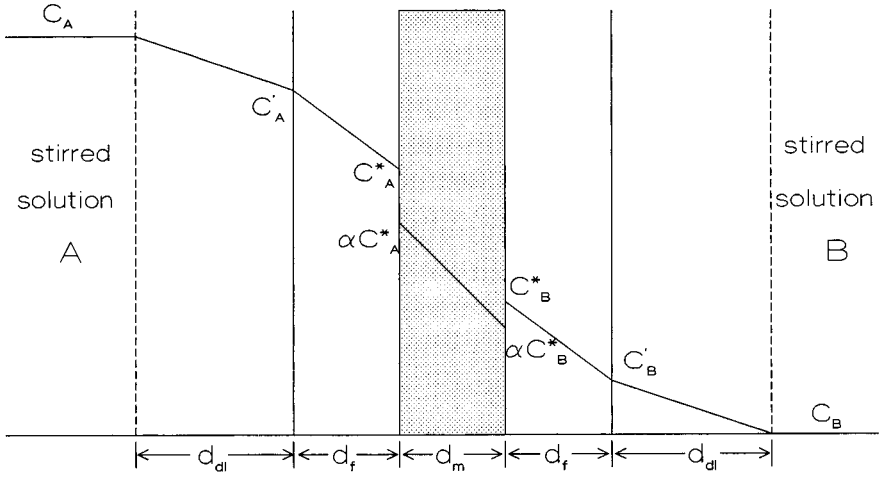

Fig. 2. Concentration profiles through a hydrogel membrane (d_m) with a filter-paper (d_f) on each side, placed between two compartments, A and B. Nernst diffusion layers are denoted by d_{dl}.

and so the rate of increase of the concentration in solution B is

$$\frac{dC_B}{dt} = \frac{JA_m}{V} = \frac{1}{\left(\frac{2d_{dl}}{D_{dl}} + \frac{2d_f}{D_f} + \frac{d_m}{D_{eff}}\right)} \Delta C \frac{A_m}{V} \quad (18)$$

By comparing the slope of the plots of C_B vs. time, the ratio of the effective diffusion coefficients of hydroquinone and glucose in the membrane can be determined. However, first the diffusion resistance of the Nernst diffusion layers and the two filter-papers for both hydroquinone and glucose have to be checked and inserted in Eqn. 18.

In this diffusion cell method, imperfections of the gel do not matter as the two compounds diffuse simultaneously through the same membrane. The thickness and area of the membrane are also of no importance.

EXPERIMENTAL

Reagents

The hydrogel used for these experiments was made of poly(vinyl alcohol) (PVA) from Denka Poval (B24) and cross-linked with glutaraldehyde (25%, w/w, aqueous solution; Merck) and photosensitive DTS-18 (polyazonium salt from PCAS, Longjumeau, France).

$NaH_2PO_4 \cdot 2H_2O$ and $Na_2HPO_4 \cdot 2H_2O$, used for the buffer solution were purchased from Merck. Hydrogen peroxide (30%, w/w, aqueous solution) was obtained from Chempro Pack, hydroquinone from Merck and D-glucose from Janssen Chimica.

Glucose detection was performed with a Sigma glucose kit (No. 635), based on the reaction of glucose with *o*-toluidine, which yields a blue–green complex. All solutions were prepared with demineralized, distilled water.

Instrumentation

For the RDE experiments a Wenking POS 73 potentiostat was used, equipped with a digital multimeter (Fluke 8600 A) and a Motomatic E-550-M stirring motor. Recording was carried out with an *x,y* recorder (Philips 8120). A circulating water-bath (Colora NB-32981) was used for temperature control of the one-compartment cell.

Diffusion cell experiments were performed with a magnetic stirrer in both compartments, which were thermostatically controlled with a Colora NB-32981 circulating water-bath. For the determination of the glucose concentration an LKB Biochrom Ultrospec II Type 4050 spectrophotometer was used for detecting the glucose–*o*-toluidine complex at 635 nm. The same spectrophotometer was used to determine the hydroquinone concentration at 290 nm.

A Talysurf 4 roughness meter from Rank Precision Instruments was used to measure the thickness of the gel layers.

Preparation of gel layers

A 10-g amount of PVA was slowly added to 90 cm^3 of demineralized water and stirred. The solution was heated for 1.5 h at 80°C until all the PVA had dissolved and a homogeneous solution was obtained. The solution was cooled to room temperature. Just before the spinning procedure, 0.20 g (0.2%, w/w) of DTS-18 and 0.16 or 0.40 g of 25% (w/w) aqueous glutardialdehyde were added. With a pipette an aliquot of the resulting solution was placed on the required surface (electrode surface or glass plate). After spinning for 5 s at 1000 rpm and for 25 s at 3000 rpm, the gel layer was dried for 30 min at 40°C. The spinning and drying procedure was repeated until enough layers had been spun on the surface. Thereafter the gel layer was irradiated with UV radiation at room temperature for 90 s. The gel layer was developed in demineralized water for 2 min and unreacted reactants were washed away. Finally, the gel layer was dried for at least 1 h at 60°C.

The thickness of the gel layer on both platinum electrodes and glass plates (control measurement) was measured with a roughness meter, connected with a thermograph. The thickness of a swollen gel layer (after contact with an aqueous solution) could also be measured with this technique.

Procedures

For all electrochemical experiments a polished platinum electrode was used as the working elec-

trode ($A_e = 0.50 \times 10^{-4}$ m^2). Further, a platinum counter electrode with a surface area of 5×10^{-4} m^2 s^{-1} and a saturated calomel reference electrode (SCE) with a Luggin capillary were placed in the one-compartment cell. A circulating water-bath was used to keep the temperature constant. As supporting electrolyte 0.1 M sodium phosphate buffer (pH 6.7) was used with a kinematic viscosity of 0.9×10^{-6} m^2 s^{-1} at 25°C and 0.7×10^{-6} m^2 s^{-1} at 37°C [12].

For oxygen measurements the buffer solution was saturated with oxygen (1 atm) for at least 30 min. This yields an oxygen concentration of 1.1 mol m^{-3} at 25°C and 0.9 mol m^{-3} at 37°C [13]. A voltammogram was recorded from +600 to −650 mV (vs. SCE) at a rotation speed varying from 1 to 49 s^{-1} (Pt electrode experiment) or from 0.5 to 16 s^{-1} (Pt–PVA electrode experiment).

For hydrogen peroxide measurements (7–8 mol m^{-3}) the buffer solution was saturated with argon before adding hydrogen peroxide and voltammograms were scanned from +300 to −650 mV (vs. SCE). The rotation speed for both the Pt electrode and Pt–PVA electrode experiments varied between 1 and 9 s^{-1}.

Hydroquinone studies (2 mol m^{-3}) were performed with an argon-saturated buffer solution with hydroquinone added before saturation. Anodization from −550 to +1200 mV (vs. SCE) was conducted at various rotation rates (Pt electrode 1–36 s^{-1}; Pt–PVA electrode 0.5–9 s^{-1}).

For all three compounds the electrode was rotated at high speed (> 50 s^{-1} for a Pt electrode and > 16 s^{-1} for a Pt–PVA electrode) for about 20 s before a new scan was made. The scan rate varied between 25 and 50 mV s^{-1} for Pt electrode experiments and between 2 and 10 mV s^{-1} for Pt–PVA electrode experiments.

With a diffusion cell containing two compartments, the ratio of the effective diffusion coefficients of glucose and hydroquinone was determined. Compartment A of the cell contained 160 cm^3 of 0.1 M sodium phosphate buffer with 1.00 kmol m^{-3} glucose and 0.100 kmol m^{-3} hydroquinone. Initially compartment B contained only 160 cm^3 of phosphate buffer. Between the two compartments a cross-linked PVA membrane (3.46 cm^2) was placed with a filter-paper (Rotband, Schleicher and Schüll) on each side for solidity purposes. Thereafter both compartments were simultaneously filled with the solution. The concentration increase in compartment B was followed for 5 h, with UV spectrophotometry for hydroquinone and with a glucose kit [14] and visible spectrophotometry for glucose. Although only samples from compartment B were analysed, an equal amount of sample was taken from compartment A to keep the solution levels in both compartments equal and to prevent forced diffusion through the membrane and destruction of the membrane.

The influence of the two filter-papers and the Nernst diffusion layers was checked by conducting a comparative experiment with only the two filter-papers placed between the two compartments.

The temperature was maintained at 25°C with a circulating water-bath for all diffusion cell experiments and both compartments were stirred magnetically.

RESULTS AND DISCUSSION

Properties of the gel layer on an RDE

Several PVA gel layers with different degrees of cross-linking were used to investigate the diffusion behaviour oxygen, hydrogen peroxide and hydroquinone.

In Table 1 properties of gels A–D are given, such as thickness, percentage of glutardialdehyde added and swelling factor after saturation with buffer solution. All gels were made on different days. Although gel solutions A, B and C were

TABLE 1

Properties of the various hydrogels used for diffusion measurements

Gel	No. of layers	Glutardialdehyde added (g)	d_{hl} (dry) (μm)	Swelling factor
A	4	0.16	13.5	2.3
B	2	0.16	8.0	2.3
C	4	0.16	26.0	2.3
D	4	0.40	13.0	2.1

made with the same procedure, the thickness of one spun layer, varied substantially.

If the same gel solution (i.e., gel A) was spun on several surfaces (platinum discs or glass plates), it was found that the spinning and cross-linking procedure provided layers of reproducible thickness and degree of cross-linking. This means that the difference in the behaviour of the gel layers is due to the gel solution preparation.

Determination of diffusion coefficients

Plots of I_{lim}^{-1} versus $\omega^{-1/2}$ gave straight lines, as expected, for measurements with both the Pt electrodes and Pt–PVA electrodes (Figs. 3 and 4).

Table 2 shows the diffusion coefficients in the buffer solution and the effective diffusion coefficients in the gel layer for various gels and at two temperatures (25 and 37°C). The ratio D_{eff}/D_{dl} is also given.

For oxygen, hydrogen peroxide and hydroquinone the D_{eff}/D_{dl} ratios are virtually identical and depend on the properties of the gel and temperature. This means that the ratio of the effective diffusion coefficients for the three compounds in the hydrogel layer is almost identical with this ratio in the buffer solution.

Simultaneous diffusion of glucose and hydroquinone through two filter-papers shows a linear increase of C_B/C_A for both species (Fig. 5). C_B was divided by C_A ($\approx \Delta C$) to correct for the different starting concentrations. The slopes of the lines of glucose and hydroquinone have a

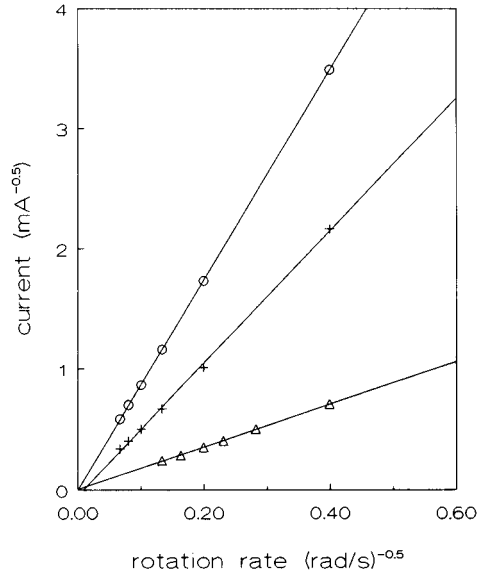

Fig. 3. Rotating disc electrode data with a Pt electrode (T = 25°C) for (△) H_2O_2, (+) O_2 and (○) hydroquinone.

ratio of 0.81. Washburn [12] gave a diffusion coefficient of 0.52×10^{-9} m^2 s^{-1} for glucose in pure water at 15°C and of 0.66×10^{-9} m^2 s^{-1} for hydroquinone. The ratio of the diffusion coefficients under these conditions is 0.79, which makes it acceptable to consider the two filter-papers as a stagnant layer of buffer solution with a diffusion coefficient equal to that in the Nernst diffusion layer. The diffusion resistance of the Nernst diffusion layer and the filter-paper (Eqn. 15) can

TABLE 2

Diffusion coefficients in the buffer solution and effective diffusion coefficients in the various gels for O_2, H_2O_2 and hydroquinone (HQ) at two temperatures

T (°C)		Buffer: D_{dl} (10^{-9} m^2 s^{-1})	Gel A		Gel B		Gel C		Gel D	
			D_{eff} (10^{-9} m^2 s^{-1})	$\frac{D_{eff}}{D_{dl}}$	D_{eff} (10^{-9} m^2 s^{-1})	$\frac{D_{eff}}{D_{dl}}$	D_{eff} (10^{-9} m^2 s^{-1})	$\frac{D_{eff}}{D_{dl}}$	D_{eff} (10^{-9} m^2 s^{-1})	$\frac{D_{eff}}{D_{dl}}$
25	O_2	1.93	0.40	0.21	0.68	0.35	0.55	0.28	0.36	0.19
	H_2O_2	1.43	0.31	0.21	0.50	0.35	0.40	0.28	0.27	0.19
	HQ	0.89	0.20	0.22	0.31	0.35	0.25	0.28	0.18	0.20
37	O_2	2.46	0.60	0.25	0.99	0.40	0.82	0.33	0.54	0.22
	H_2O_2	1.83	0.45	0.25	0.73	0.40	0.58	0.31	0.37	0.22
	HQ	1.17	0.27 [a]	0.23 [a]	0.43 [a]	0.37 [a]	–	–	–	–

[a] Unreliable measurement, gel destroyed.

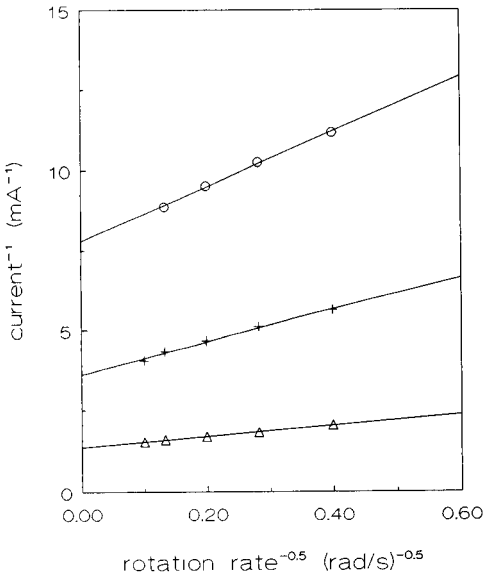

Fig. 4. Rotating disc electrode data with a Pt–PVA electrode (T = 25°C) for (△) H_2O_2, (+) O_2 and (○) hydroquinone.

be considered as one resistance of a buffer solution layer:

$$\frac{2}{k_{dl}} + \frac{2}{k_f} = \frac{1}{k_{bl}} = \frac{d_{bl}}{D_{bl}} = \frac{d_{bl}}{D_{dl}} \qquad (19)$$

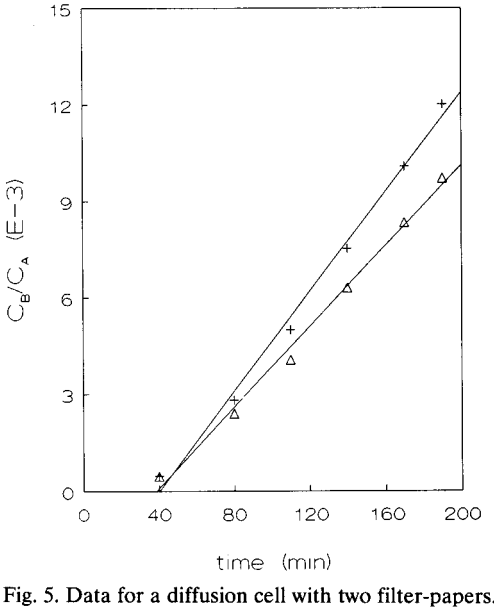

Fig. 5. Data for a diffusion cell with two filter-papers. C_B/C_A plotted against time for (+) hydroquinone and (△) glucose. T = 25°C.

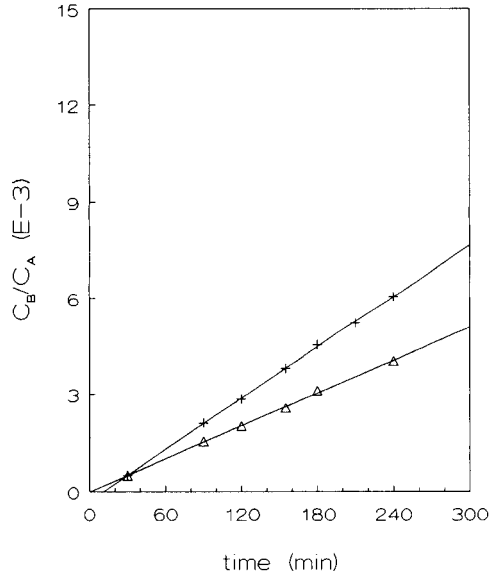

Fig. 6. Data for a diffusion cell with a hydrogel membrane and two filter-papers. C_B/C_A plotted against time for (+) hydroquinone and (△) glucose. T = 25°C.

where the subscript bl refers to the buffer solution layer.

As the diffusion coefficient of hydroquinone in 0.1 M phosphate buffer at 25°C is 0.89×10^{-9} m^2 s^{-1}, it can be calculated that the diffusion coefficient of glucose under the same conditions is 0.72×10^{-9} m^2 s^{-1}. Also, k_{bl} can be calculated for both compounds using the slopes of Fig. 5, as in this case $dC_B/dt = k_{bl}\Delta C A_f/V$ with $A_f = A_m = 3.46 \times 10^{-4}$ m^2 s^{-1}. For hydroquinone a value of $k_{bl} = 5.9 \times 10^{-7}$ m s^{-1} was found and for glucose $k_{bl} = 4.8 \times 10^{-7}$ m s^{-1}.

A gel C membrane, together with a filter-paper on each side, was placed between the two com-

TABLE 3

Diffusion coefficients in the buffer solution and effective diffusion coefficients in two gels with different degrees of cross-linking for hydroquinone and glucose at 25°C

Compound	Buffer:	Gel C		Gel D	
	D_{dl} (10^{-9} m^2 s^{-1})	D_{eff} (10^{-9} m^2 s^{-1})	$\frac{D_{eff}}{D_{dl}}$	D_{eff} (10^{-9} m^2 s^{-1})	$\frac{D_{eff}}{D_{dl}}$
Hydroquinone	0.89	0.25	0.28	0.18	0.20
Glucose	0.72	0.062	0.086	0.045	0.062

partments and also gave straight lines (Fig. 6). Now the slopes have a ratio of 0.63, which means that glucose is slowed by the membrane to a greater extent than hydroquinone. The ratio of 0.63 can also be seen as the ratio of the total mass transfer coefficients of hydroquinone and glucose, so

$$\frac{\left(\frac{1}{k_m}+\frac{1}{k_{bl}}\right)_{hydroquinone}}{\left(\frac{1}{k_m}+\frac{1}{k_{bl}}\right)_{glucose}} = 0.63 \qquad (20)$$

Inserting the value of k_{bl} for both glucose and hydroquinone, the ratio of the effective diffusion coefficients is found to be 0.25. $(D_{eff}/D_{dl})_{hydroquinone} = 0.28$ whereas $(D_{eff}/D_{dl})_{glucose} = 0.086$ (Table 3). For a second, extra cross-linked membrane (gel D), the same ratio of the slopes of 0.63 is found (Table 3). The ratio of the effective diffusion coefficients is 0.24, and $(D_{eff}/D_{dl})_{hydroquinone} = 0.20$ whereas $(D_{eff}/D_{dl})_{glucose} = 0.062$.

The conclusion can be drawn that glucose is slowed more than hydroquinone and also than oxygen and hydrogen peroxide, because of an interaction of glucose with the gel matrix. In both gels glucose is slowed 3.2 times more than hydroquinone (0.086 vs. 0.28 and 0.062 vs. 0.20). A size-exclusion effect can be excluded because, although gel D is far more cross-linked than gel C, this has evidently no influence.

The authors wish to acknowledge M.H. Kuijpers, M.W.C.M. Nieuwesteeg and G. Steeghs from Dräger Medical Electronics, Best, Netherlands, for their contribution to this work.

REFERENCES

1 S. Gernet, M. Koudelka and N.F. de Rooy, Sensors Actuators, 18 (1989) 59.
2 M.H. Kuijpers, US Pat., 4 492 622 (1985).
3 K. Mosbach, Methods Enzymol., 44 (1976) 263.
4 M. Lambrechts, PhD Thesis, Catholic University of Leuven, Leuven, 1989.
5 M. Shichiri, R. Kawamori, N. Hakui, N. Asakawa, Y. Yamasaki and H. Abe, Biomed. Biochim. Acta, 43 (1984) 561.
6 P. Janda and J. Weber, J. Electroanal. Chem., 300 (1991) 119.
7 D. Hale, H.L. Lan, L.I. Boguslavsky, H.I. Karan, Y. Okamoto and T.A. Skotheim, Anal. Chim. Acta, 251 (1991) 121.
8 P. Bianco, J. Haladjian and C. Bourdillon, J. Electroanal. Chem., 293 (1990) 151.
9 D.A. Gough and J.K. Leypoldt, Anal. Chem., 52 (1980) 1126.
10 C.A. Marrese, O. Miyawaki and L.B. Wingard, Jr., Anal. Chem., 59 (1987) 248.
11 V.G. Levich, Physicochemical Hydrodynamics, Prentice Hall, Englewood Cliffs, NJ, 1962.
12 E.W. Washburn, International Critical Tables, McGraw-Hill, New York, 1st edn., 1929.
13 M.L. Hitchman, Measurement of Dissolved Oxygen (Chemical Analysis, Vol. 49), Wiley, New York, 1978.
14 J.E. Middleton, Clin. Chim. Acta, 31 (1968) 433.

Analytica Chimica Acta, 273 (1993) 561–566
Elsevier Science Publishers B.V., Amsterdam

Quartz microbalance investigation of metal deposition from dilute solutions [a]

H.-J. Schmidt, U. Pittermann, H. Schneider and K.G. Weil

Institut für Physikalische Chemie, Technische Hochschule Darmstadt, Petersenstrasse 20, D(W)-6100 Darmstadt (Germany)

(Received 1st June 1992)

Abstract

A quartz microbalance was used to determine the cathodic deposition of lead (5.4 $\mu g\ l^{-1}$–0.3 $mg\ l^{-1}$) and copper (16 $\mu g\ l^{-1}$–0.7 $mg\ l^{-1}$) from dilute solutions. It was found that the removal of lead can be nearly complete when the total amount in the solution does not exceed the monolayer capacity of the electrode. Simultaneously with the formation of this monolayer, Au–Pb alloys are formed. These alloys also form when the electrode is held at a UPD (under potential deposition) potential. They were identified by electron diffraction as Au_2Pb, $AuPb_2$ and $AuPb_3$. The alloy formation can easily be detected from anodic stripping curves. With copper solutions, the deposition is quantitative throughout the examined range of concentrations. In contrast to the lead deposition, mainly bulk copper was formed in addition to Cu–Au alloys.

Keywords: Voltammetry; Copper; Lead; Metal deposition; Quartz crystal microbalance

In this paper it is shown that the in situ quartz crystal microbalance (QCM) is useful for determining trace metals in solution. Residual or background currents not associated with a mass change do not interfere with the in situ experiments, so measurements of the deposited mass as a function of time can be made. The determination of mass changes under controlled electrochemical conditions is possible. The extreme sensitivity of the QCM allows the measurement of monolayer and submonolayer masses at the quartz crystal electrode [1–5]. In addition, the QCM can be combined with other electrochemical methods, such as anodic stripping analysis, coulometry and voltammetry. In these experiments, the QCM was used in combination with anodic stripping analysis, which allowed us the frequency changes to be compared with the charge of dissolution of deposited metals.

Correspondence to: K.G. Weil, Institut für Physikalische Chemie, Technische Hochschule Darmstadt, Petersenstrasse 20, D(W)-6100 Darmstadt (Germany).

[a] Part of the Dissertation of H.-J. Schmidt.

EXPERIMENTAL

In all experiments 5-MHz AT-cut quartz crystals (KVG, Neckarbischofsheim), which were biplanar and circular with 15 mm diameter, were used. Gold films 200 nm thick were deposited on both sides of the crystals by standard thermal evaporation techniques (Edwards E306A coater). In order to improve the adhesion between the crystal and the deposit, a 5 nm thick chromium layer was evaporated on to the quartz prior to the deposition of gold. Only one of the polycrystalline gold films was in contact with the solution. The eigenfrequency of the quartz oscillator varies when material is deposited on or dissolved from this face. In such a way, mass changes can be

measured in situ during the deposition or dissolution period. The crystals were operated at their third harmonic, 15 MHz, which provides a greater mass sensitivity. The geometric area of the working electrode was 0.785 cm^2. The oscillator was a modified Pierce–Miller circuit [6] and the frequencies were measured with a Rohde and Schwarz FEG3 frequency counter. This gives a resolution of 1 Hz over 1 s. The BCD (binary coded decimal) data of the last three significant digits were converted to a 0–10 V analogue signal by a D/A converter and plotted with a two-channel *x–t* or *x–y* recorder. In addition, the frequency was recorded with an IBM-compatible PC. The QCM was calibrated by deposition of copper and lead under UPD (under potential deposition) conditions (UPD means that the electrode potential is more positive than the Nernst potential). A Wenking potentiostat with a ramp generator was used for the potentiodynamic and potentiostatic experiments. The counter electrode was a platinum wire and an Ag/AgCl (saturated KCl) electrode was used as a reference. All potentials are reported versus this electrode. For the deposition of lead a potential of −800 mV was applied and for copper a potential of −600 mV was applied. With the exception of the electrodes all parts in contact with the solution are coated with Teflon (TFE) because it is well known that the adsorption of metal ions on TFE surfaces is negligible. All solutions were deoxygenated by purging with purified nitrogen. During the measurements a nitrogen atmosphere was maintained over the solution. The solutions were stirred with a Teflon stirrer at a rate of 600 rpm. The volume of the solution was 15 cm^3, hence the ratio of electrode area to the volume of the solution was 5.2×10^{-2} cm^2 cm^{-3}. The base electrolyte for the lead deposition (0.1 M $NaClO_4$, pH 6.5) was prepared from perchloric acid (Suprapur, Merck) and sodium hydroxide (Suprapur, Merck); for UPD studies 0.02 M $Pb(ClO_4)_2$ (pro analysi, Merck) was added. The base electrolyte for the copper deposition was 0.01 M Na_2SO_4 (Suprapur, Merck); for UPD studies 0.02 M $CuSO_4 \cdot 5H_2O$ (pro analysi, Merck) was added. Working standard solutions of Pb^{2+} and Cu^{2+} were prepared from a stock standard solution. All solutions were prepared with triply distilled water.

The temperature during the measurements was 22 ± 2°C. The polycrystalline gold electrodes were electrochemically cleaned by repeated cycling (ca. 100 cycles) into the hydrogen evolution and oxide growth regions. The electrolyte solution was changed several times during this process. After the solution to be investigated had been filled into the cell, the desired potential was applied and maintained for the time of deposition, then the deposits were dissolved by anodic stripping. During the whole experiment the frequency of the QCM was recorded.

In a further experiment the UPD alloy formation of lead/gold alloys was investigated by electron diffraction (EM 9 S-2, Zeiss). For this purpose a gold film 20 nm thick was vapour deposited on to a glass plate and used as the cathode in the electrochemical cell. Lead was deposited for periods of 3–5 days. Then the gold films were removed from the glass substrate and investigated with an electron transmission microscope in the selected area diffraction mode.

RESULTS AND DISCUSSION

Figures 1 and 2 show the voltammograms and simultaneous frequency–potential curves of Pb^{2+} and Cu^{2+} solutions in the UPD range. Similar results of lead adsorption on gold, monitored with a QCM, are already reported by Melroy et al. [1]. The QCM was calibrated by determination of the desorption charge and corresponding frequency change. It is assumed that the electrochemical valency is 2 in both instances. For lead the calibration constant of the QCM is 5.9 ± 0.3 ng Hz^{-1} cm^{-2} and for copper it is 4.5 ± 1.1 ng Hz^{-1} cm^{-2}. Copper deposition from an acidic $CuSO_4$ solution under galvanostatic conditions, where the current efficiency is known to be 100%, gave the same value. For this reason, the calibration constant given above was used for the further calculations.

Lead deposition

The depositions were carried out in the overpotential range. Figure 3 shows the frequency

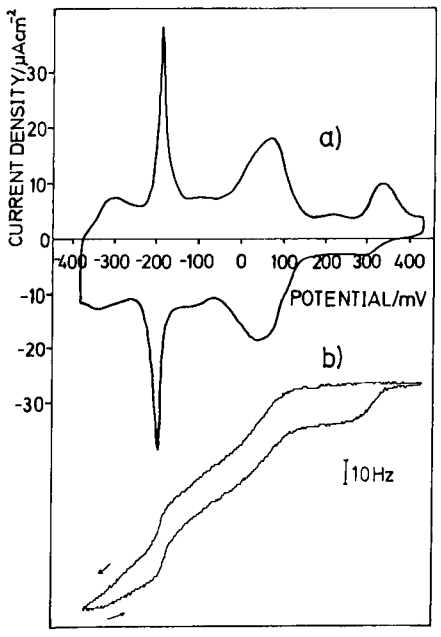

Fig. 1. (a) Cyclic voltammogram of Pb^{2+} on gold in the UPD range. System, 0.02 M $Pb(ClO_4)_2$; scan rate, 16 mV s^{-1}. (b) Frequency–potential curve. Scan rate, 1.6 mV s^{-1}.

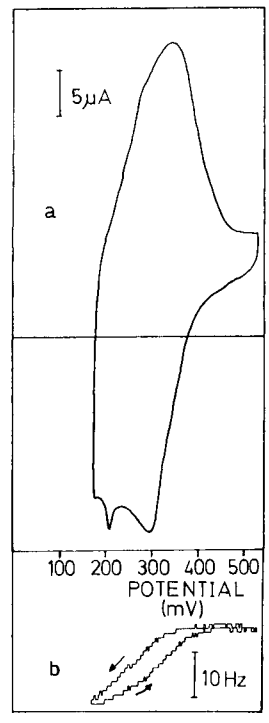

Fig. 2. (a) Cyclic voltammogram of Cu^{2+} on gold in the UPD range. System, 0.02 M $CuSO_4$; scan rate, 1.6 mV s^{-1}. (b) Frequency–potential curve. Scan rate, 1.6 mV s^{-1}.

changes as a function of the deposition time at various initial lead concentrations. The curves show a plateau after about 16 h of electrolysis. Figure 4 shows the percentage of deposition as a function of the initial amounts of lead. If the initial amount of lead is in the range of monolayer coverage, the percentage of deposition is about 98%. At higher initial amounts the percentage recovery of lead decreases. The first monolayer of lead on gold seems to be strongly bound but the formation of three-dimensional lead nuclei is inhibited, possibly by the simultaneous evolution of hydrogen.

Figure 5 shows a typical anodic stripping curve after a deposition time of 20 h at −800 mV. The initial concentration was 7.8×10^{-7} M. At these low concentrations, one always observes three anodic waves. The small peak appearing at the most positive potential is a typical UPD desorption peak (see Fig. 1a). Apparently the formation of a lead monolayer by charge transfer and the formation of alloys occur simultaneously. The very broad and structured peak at the most negative potential was reported previously by Schmidt and

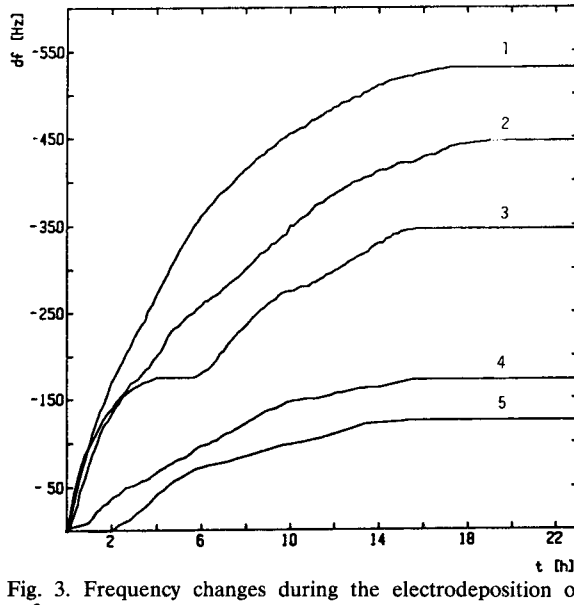

Fig. 3. Frequency changes during the electrodeposition of Pb^{2+} for different initial lead concentrations (c_0). Potential of deposition: −800 mV. c_0: (1) 1.3×10^{-6}; (2) 1.0×10^{-6}; (3) 7.8×10^{-7}; (4) 2.6×10^{-7}; (5) 7.8×10^{-8} mol l^{-1}.

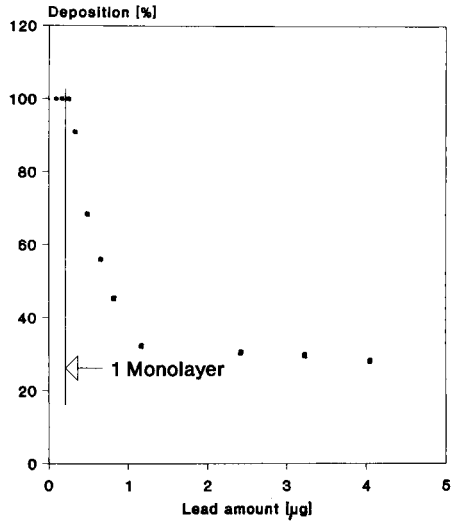

Fig. 4. Percentage of deposition as a function of the initial amounts of lead.

Gygax [7,8]. The second very sharp peak has not been observed before. The anodic stripping curves obtained after different deposition times never show any bulk dissolution of lead. It seems that the deposition of lead on the alloy surface is limited by the diffusion of gold into the alloy phase.

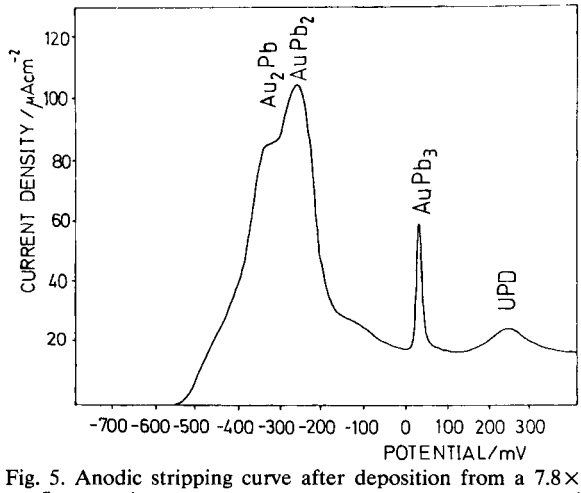

Fig. 5. Anodic stripping curve after deposition from a 7.8×10^{-7} mol l^{-1} lead solution. Base electrolyte, 0.01 mol l^{-1} $NaClO_4$; deposition time, 20 h; potential of deposition, −800 mV; scan rate, 16 mV s^{-1}.

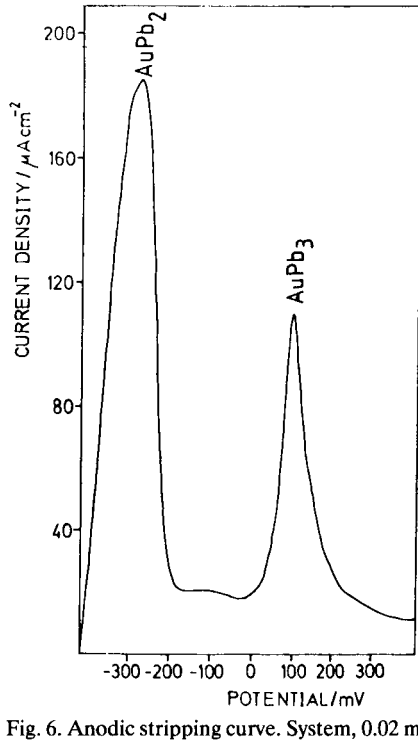

Fig. 6. Anodic stripping curve. System, 0.02 mol l^{-1} $Pb(ClO_4)_2$; deposition time, 2.5 h; potential of deposition, −410 mV (UPD range); scan rate, 16 mV s^{-1}.

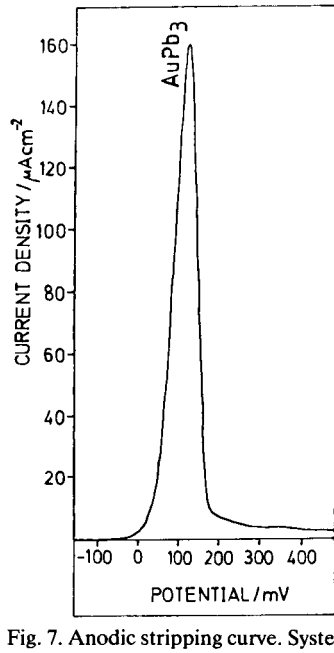

Fig. 7. Anodic stripping curve. System, 0.02 mol l^{-1} $Pb(ClO_4)_2$; deposition time, 41 h; potential of deposition, −160 mV (UPD range); scan rate, 1.6 mV s^{-1}.

In order to identify the alloys, the alloy formation in the underpotential range was studied. The formation of Au–Pb alloys in the underpotential range has not previously been observed [9,10], but thermodynamically stable alloys are well known [11]. Figure 1a shows a cyclic voltammogram of lead on gold in the UPD range. The peak observed at the most positive potentials is highly irreversible. This is in agreement with the experimental results of Hamelin [12], who studied the UPD deposition of lead on single crystal faces of gold. Figure 6 shows an anodic stripping curve after a waiting time of 2.5 h at a potential of −410 mV, a potential which definitely is more positive than the Nernst potential of lead in these solutions. Two anodic waves are observed, which are similar to those in Fig. 5, which were ascribed to alloy dissolution. With increasing polarization time at a fixed underpotential, the anodic stripping charge associated with these two peaks increases. This indicates the formation of two Au–Pb alloys on the electrode surface. Figure 7 shows an anodic stripping curve after a waiting time of 41 h at a potential of −160 mV. At this potential only the nobler alloy is formed. The sharp wave indicates that this intermetallic phase has a narrow range of homogeneity. Electron diffractograms from 20-nm gold films kept for 3–5 days in the presence of 0.02 M Pb^{2+} at a potential of −410 mV demonstrate the presence of two intermetallic phases. They could be identified as $AuPb_2$ and $AuPb_3$. At a potential of −160 mV only $AuPb_3$ is observed. If the potential is close to the Nernst potential, an Au_2Pb phase is additionally formed.

Copper deposition

Figure 8 shows the frequency changes as a function of the deposition time at various initial copper concentrations. In contrast to the deposi-

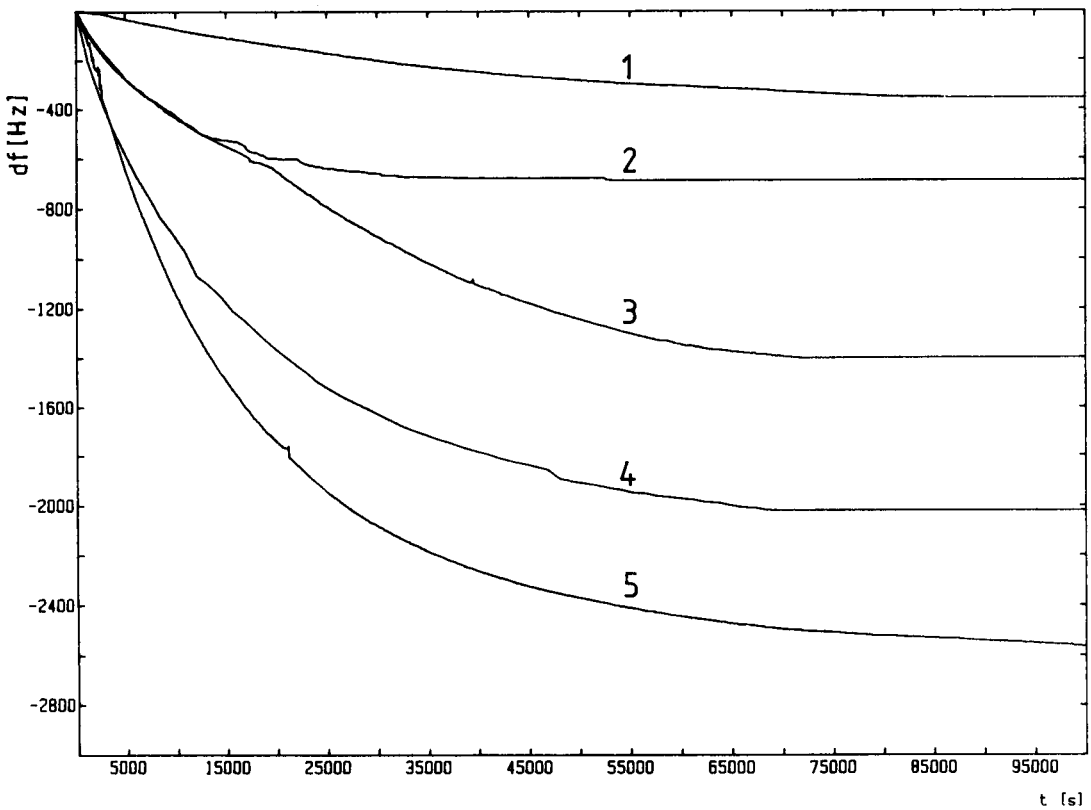

Fig. 8. Frequency changes during the electrodeposition of copper for different initial copper concentrations (c_0). Potential of deposition, −600 mV. c_0: (1) 1.3×10^{-6}; (2) 2.6×10^{-6}; (3) 5.2×10^{-6}; (4) 7.8×10^{-6}; (5) 1.0×10^{-5} mol l^{-1}.

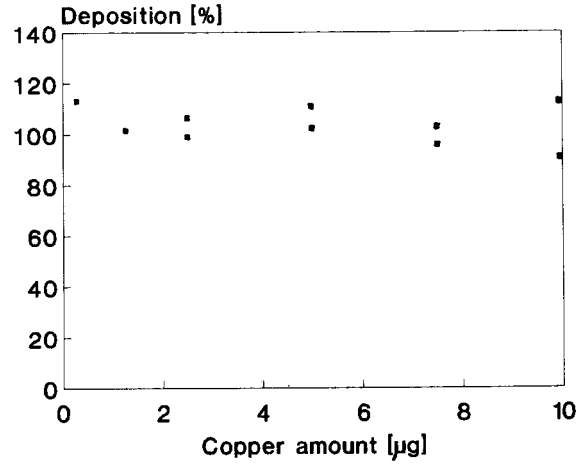

Fig. 9. Percentage of deposition as a function of the initial amounts of copper.

tion of lead, copper is deposited quantitatively throughout the range of concentrations (see Fig. 9). The formation of three-dimensional copper nuclei is not hindered, so in the whole copper concentration range bulk dissolution during the anodic stripping is observed. Because of the long periods of deposition, alloy formation is also observed (see Fig. 10).

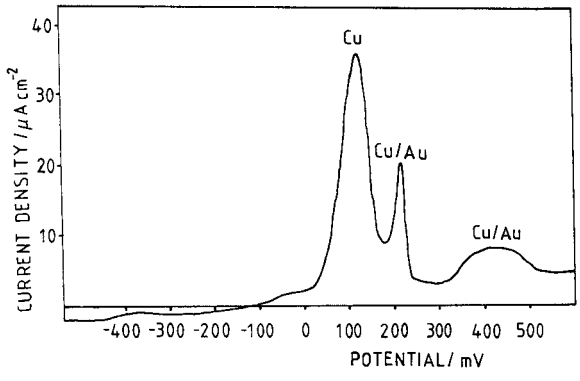

Fig. 10. Anodic stripping curve after deposition from a 1.3×10^{-6} mol l^{-1} copper solution. Base electrolyte, 0.01 mol l^{-1} Na_2SO_4; deposition time, 19 h; scan rate, 1.6 mV s^{-1}.

During the deposition of both lead and copper, the applied potential always remained more negative than the Nernst potential. For example, the electrode potential during copper deposition is over 400 mV more negative than the Nernst potential calculated for a 10^{-11} M copper solution. This concentration is reached when 99.9% of a 10^{-8} solution is deposited. In lead deposition, under the same conditions, the electrode potential is over 150 mV more negative than the corresponding Nernst potential.

Valuable support by the Fonds der Chemischen Industrie is greatly acknowledged.

REFERENCES

1 O. Melroy, K. Kanazawa, J.G. Gordon and D. Buttry, Langmuir, 2 (1986) 697.
2 M. Deakin and O. Melroy, J. Electroanal. Chem., 239 (1988) 321.
3 M. Hepel, K. Kanige and S. Bruckenstein, J. Electroanal. Chem., 266 (1989) 409.
4 W. Stöckel and R. Schumacher, Ber. Bunsenges. Phys. Chem., 93 (1989) 606.
5 H.-J. Schmidt and K.G. Weil, Electrochemical Lead Deposition from Highly Diluted Solutions, Dechema-Monographien 124, VCH, Weinheim, 1991, p. 249.
6 R.A. Heising, Quartz Crystals for Electric Circuits, Van Nostrand, New York, 1946.
7 E. Schmidt and H.R. Gygax, J. Electroanal. Chem., 13 (1967) 378.
8 E. Schmidt and H.R. Gygax, J. Electroanal. Chem., 14 (1967) 126.
9 K. Engelsmann, W.J. Lorenz and E. Schmidt, J. Electroanal. Chem., 114 (1980) 11.
10 H. Bort, K. Jüttner and W.J. Lorenz, Electrochim. Acta, 28 (1983) 993.
11 H. Okamoto and T.B. Massalski, The Au–Pb (Gold–Lead) System, in Bull. Alloy Phase Diagrams, 5 (1984) 276.
12 A. Hamelin, J. Electroanal. Chem., 165 (1984) 167.

ANALYTICA CHIMICA ACTA, VOL. 273 (1993)

AUTHOR INDEX

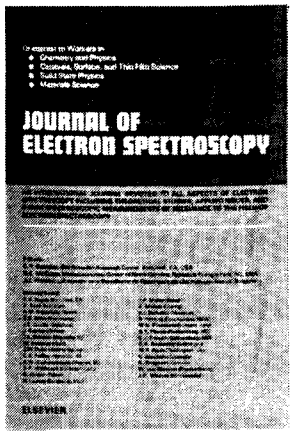

JOURNAL OF ELECTRON SPECTROSCOPY AND RELATED PHENOMENA

An International Journal Devoted to All Aspects, Fundamental or Applied, of Electron Spectroscopy - Including Theoretical Studies and Other Spectroscopic Measurements of Relevance to the Field of Electron Spectroscopy

AIMS AND SCOPE
This journal publishes experimental and theoretical work in the field of electron spectroscopy and all subjects relevant to it. Electron spectroscopy has a broad area of application and is the major technique in the study of solid surfaces. Work can be on free molecules, solids or surfaces. The individual techniques of electron spectroscopy include photoelectron spectroscopy of both outer and inner shells, both UV and X-ray induced; inverse photoemission; spin-polarized photoemission; Auger spectroscopy (including ion neutralization studies); synchrotron radiation studies in the area of photoemission and Auger electron emission; high resolution electron energy loss spectroscopy; electron scattering and resonance electron capture; electron spectroscopy in conjunction with microscopy; Penning ionization spectroscopy (including scanning tunnelling spectroscopy); theoretical treatments of the photoemission, Auger, energy loss and Penning ionization processes.

The journal welcomes papers on instruments and instrumental developments and is one of the major archival sources for work dealing with advances in quantitative analysis by electron spectroscopic techniques, particularly for surfaces and solids. Major topics within this area are ionization cross sections, angular distributions, mean free path lengths, standards, calibrations, deconvolution procedures, etc.

ABSTRACTED/INDEXED IN: Chemical Abstracts, Current Contents: Physical, Chemical & Earth Sciences, Mass Spectrometry Bulletin.

1993 SUBSCRIPTION INFORMATION
Volumes 60-63 in 16 issues
Dfl. 1432.00 / US $ 862.50 (including postage)
ISSN 0368-2048

I would like ☐ a free sample copy of Journal of Electron Spectroscopy and Related Phenomena.
☐ Instructions to Authors.
☐ to enter a subscription for 1993. Please send me a Proforma Invoice.

Name _____
Address _____

The Dutch Guilder price (Dfl.) is definitive. US$ prices are for your convenience only and are subject to exchange fluctuations. Customers in the European Community should add the appropriate VAT rate applicable in their country to the price(s).

Audience

Physicists, chemists, surface scientists and technologists using the techniques of electron spectroscopy in their work.

Elsevier Science Publishers
Attn. Eugene P.M. Wijnhoven
P.O. Box 330, 1000 AH Amsterdam
The Netherlands
Fax: (+31-20) 5862 845
In the USA & Canada
Attn. Judy Weislogel
P.O. Box 945, Madison Square Station
New York, NY 10160-0757, USA
Fax: (212) 633 3880

Multivariate Pattern Recognition in Chemometrics, Illustrated by Case Studies

edited by **R.G. Brereton**, University of Bristol, Bristol, UK

Data Handling in Science and Technology Volume 9

Chemometrics originated from multivariate statistics in chemistry, and this field is still the core of the subject. The increasing availability of user-friendly software in the laboratory has prompted the need to optimize it safely. This work comprises material presented in courses organized from 1987-1992, aimed mainly at professionals in industry.

The book covers approaches for pattern recognition as applied, primarily, to multivariate chemical data. These include data reduction and display techniques, principal components analysis and methods for classification and clustering. Comprehensive case studies illustrate the book, including numerical examples, and extensive problems are interspersed throughout the text. The book contains extensive cross-referencing between various chapters, comparing different notations and approaches, enabling readers from different backgrounds to benefit from it and to move around chapters at will. Worked examples and exercises are given, making the volume valuable for courses.

Tutorial versions of SPECTRAMAP and SIRIUS are optionally available as a Software Supplement, at a low price, to accompany the text.

Contents:

ELSEVIER
SCIENCE PUBLISHERS

1992 xii + 326 pages
Hardbound
Price: US $ 174.50 / Dfl. 305.00
ISBN 0-444-89783-6

Paperback
Price: US $ 85.50 / Dfl. 150.00
ISBN 0-444-89784-4

5 Pack Paperback + Software Supplement
Price: US $ 428.50 / Dfl. 750.00
ISBN 0-444-89786-0

Software Supplement
Price: US $ 100.00 / Dfl. 175.00
ISBN 0-444-89785-2

TO ORDER

Contact your regular supplier or:

ELSEVIER SCIENCE PUBLISHERS
P.O. Box 211
1000 AE Amsterdam
The Netherlands

Customers in the USA & Canada:
ELSEVIER SCIENCE PUBLISHERS
Attn. Judy Weislogel
P.O. Box 945
Madison Square Station
New York, NY 10160-0757, USA

No postage will be added to prepaid book orders. US $ book prices are valid only in the USA and Canada. In all other countries the Dutch guilder (Dfl.) price is definitive. Customers in The Netherlands please add 6% BTW. In New York State please add applicable sales tax. All prices are subject to change without prior notice.

PUBLICATION SCHEDULE FOR 1993

	S'92	O'92	N'92	D'92	J	F	M	A	M
Analytica Chimica Acta	267/1 267/2	268/1 268/2	269/1 269/2	270/1 270/2	271/1 271/2	272/1 272/2 273/1–2	274/1 274/2	275/1 275/2	276/1 276/2
Vibrational Spectroscopy		4/1			4/2		4/3		

INFORMATION FOR AUTHORS

Manuscripts. The language of the journal is English. English linguistic improvement is provided as part of the normal editorial processing. Authors should submit three copies of the manuscript in clear double-spaced typing on one side of the paper only. *Vibrational Spectroscopy* also accepts papers in English only.

Abstract. All papers and reviews begin with an Abstract (50–250 words) which should comprise a factual account of the contents of the paper, with emphasis on new information.

Figures. Figures should be prepared in black waterproof drawing ink on drawing or tracing paper of the same size as that on which the manuscript is typed. One original (or sharp glossy print) and two photostat (or other) copies are required. Attention should be given to line thickness, lettering (which should be kept to a minimum) and spacing on axes of graphs, to ensure suitability for reduction in size on printing. Axes of a graph should be clearly labelled, along the axes, outside the graph itself. All figures should be numbered with Arabic numerals, and require descriptive legends which should be typed on a separate sheet of paper. Simple straight-line graphs are not acceptable, because they can readily be described in the text by means of an equation or a sentence. Claims of linearity should be supported by regression data that include slope, intercept, standard deviations of the slope and intercept, standard error and the number of data points; correlation coefficients are optional.

Photographs should be glossy prints and be as rich in contrast as possible; colour photographs cannot be accepted. Line diagrams are generally preferred to photographs of equipment.

Computer outputs for reproduction as figures must be good quality on blank paper, and should preferably be submitted as glossy prints.

Nomenclature, abbreviations and symbols. In general, the recommendations of the International Union of Pure and Applied Chemistry (IUPAC) should be followed, and attention should be given to the recommendations of the Analytical Chemistry Division in the journal *Pure and Applied Chemistry* (see also *IUPAC Compendium of Analytical Nomenclature, Definitive Rules*, 1987).

References. The references should be collected at the end of the paper, numbered in the order of their appearance in the text (*not* alphabetically) and typed on a separate sheet.

Reprints. Fifty reprints will be supplied free of charge. Additional reprints (minimum 100) can be ordered. An order form containing price quotations will be sent to the authors together with the proofs of their article.

Papers dealing with vibrational spectroscopy should be sent to: Dr J.G. Grasselli, 150 Greentree Road, Chagrin Falls, OH 44022, U.S.A. Telefax: (+1-216) 2473360 (Americas, Canada, Australia and New Zealand) or Dr J.H. van der Maas, Department of Analytical Molecule Spectrometry, Faculty of Chemistry, University of Utrecht, P.O. Box 80083, 3508 TB Utrecht, The Netherlands. Telefax: (+31-30) 518219 (all other countries).

0003-2670/93/$06.00

This issue is printed on acid-free paper.

PRINTED IN THE NETHERLANDS

Data Handling in Science and Technology Volume 8

Design and Optimization in Organic Synthesis

by **R. Carlson**, Department of Organic Chemistry, Umeå University, Umeå, Sweden

This is the first general textbook on experimental design and optimization in organic synthesis. The book presents a unified methodology for carrying out systematic studies when the objective is to develop efficient and optimum synthetic methods. Strategies are included both for exploring the experimental conditions and for systematic studies of entire reaction systems (substrates, reagent(s) and solvents). The methodology is based on multivariate statistical techniques.

The following topics are treated in depth: classical two-level designs for screening experiments, gradient methods (steepest ascent, simplex methods) as well as response surface techniques for optimization, principal components analysis and PLS modelling.

The book is intended as a hands-on text for chemists and engineers engaged in developing synthetic methods in industrial research, e.g. in fine chemicals and pharmaceuticals production, as well as for advanced undergraduate students, graduate students, and researchers in an academic environment.

Contents:

1992 xvi + 536 pages

Price: US $ 169.00 / Dfl. 330.00

ISBN 0-444-89201-X

Elsevier Science Publishers

P.O. Box 211, 1000 AE Amsterdam, The Netherlands
P.O. Box 882, Madison Square Station, New York, NY 10159, USA